Development of Novel PARP Inhibitors Based on Phenanthridinones Using Computer-Aided Drug Design

by

Yuhua Fang

A Thesis submitted to the Faculty of Graduate Studies of
The University of Manitoba
in partial fulfillment of the requirements of the degree of

DOCTOR OF PHILOSOPHY

College of Pharmacy
Rady Faculty of Health Sciences
University of Manitoba
Winnipeg, Manitoba, Canada

Abstract

Poly(ADP-Ribose)Polymerase (PARP) is a family of 17 protein isomers that are involved in many cellular activities including DNA repair and apoptosis. Competitive inhibitors of the PARP family are used to mimic the endogenous substrate NAD^+ and disrupt PARylation. The inhibition of PARP is used for therapeutic purposes such as anticancer therapy. These inhibitors can be used as anticancer drugs individually or in combination with other treatments. PJ34 is a non-selective PARP inhibitor based on a 6-(5*H*)-phenanthridinone ring system with moderate potency that is widely used for studying PARP function. In this study, a new series of phenanthridinone-based PARP inhibitors have been successfully developed guided by *in silico* methods. Through *in silico* methods, we were able to design inhibitors with novel structures to interact with designated amino acid residues of the PARP enzyme. We present two scaffolds to produce novel and potent PARP inhibitors: The first scaffold docks into the nicotinamide binding site and the phosphate binding site while interacting with D766 or D770 using a hydroxyl arm. The second scaffold docks into the nicotinamide binding site and the adenine binding site while interacting with R878 D766 or D770 with warheads. *In vitro* enzymatic studies indicated that our potent PARP inhibitors that were ~10-fold more potent than the original benchmark PJ34 and similar in potency to the benchmark olaparib. Our enzymatic assay results also verified that designs of a pair of enantiomers, selectively interacting with D766 in PARP1 and E335 in PARP2 (based on the *in silico* prediction), were able to achieve PARP1/PARP2 preference with better PARP2-selectivity than PJ34/olaparib. Cellular assay results also suggested that 2 out of our top 3 inhibitors were able to have equivalent or better synergistic effects in combination with anticancer drug temozolomide (TMZ), when compared to olaparib/TMZ. We proposed that while our phenanthridinone-based inhibitors worked in the same manner as olaparib, our champion inhibitor based on thienoquinolinone with *de novo* design might be able to potentiate TMZ by both PARP-trapping and strong catalytic inhibition. Overall, using phenanthridinone and thienoquinolinone as core components, we were able to develop best-in-series PARP inhibitors which are promising for future development.

Acknowledgment

The research was inspired, guided, instructed, and comprehensively supported by my supervisor Dr. Geoff Tranmer. Together we achieved a lot in 7 years' research, from the M.Sc. program to the Ph.D. program. The research was also supported by a 2017 Research Manitoba New Investigator Operating grant and an NSERC Discovery Grant to Dr. Geoff Tranmer. The Ph.D. program was supported by the College of Pharmacy (including the 2019-2020 College of Pharmacy Endowment Fund Stipend) at the University of Manitoba. The dissertation would not have been possible without the support of my family.

Besides my supervisor, I would also like to thank the rest of my committee members, Dr. Ted Lakowski, Dr. John Sorensen for their comments and valuable advice. Special thanks to Dr. Ted Lakowski for maintaining the Pharmaceutical Analysis Laboratory (PAL) for the old mass spectrometry machine was the only analytical tool for me to identify the product conveniently.

Billy Vuong contributed to the research by providing statistical analysis for validating the optimized PARP1 enzymatic assay as well as help and guidance in the cell culture and MTS assay by instructing and performing some pilot studies. He also provided suggestions and supports in every aspect of the research, as well as proofreading the experiment part of the thesis. Similar, profound gratitude goes to other members of the Tranmer Research Group, Paul Szymanski, Nitesh Sanghai.

The support of CADD platform Schrodinger Maestro was from Dr. Raj Bhullar and Dr. Prashen Chelikani labs. Assistance was provided by Dr. Appalaraju Jaggupilli and Vikram Bhatia. The research also gained help from Dr. Sachin Katyal at the Department of Pharmacology and Therapeutics, University of Manitoba, Ramin Vakili, the NMR lab manager at the Chemistry Department, University of Winnipeg, Dr. David Davidson, the NMR lab manager at the Department of Chemistry, University of Manitoba, Xiao Feng, the Mass Spec technologist at Dalhousie University.

Table of Contents

List of Abbreviations

AD	Adenine binding site
ADDM	Azodicarboxylic dimorpholide
ADME	Absorption, distribution, metabolism, and excretion
ADP	Adenosine di-phosphate
AI	Artificial intelligence
ALC1	Amplification in liver cancer 1
Amino Acid A	Alanine
Amino Acid E	Glutamic acid
Amino Acid G	Glycine
Amino Acid H	Histidine
Amino Acid I	Isoleucine
Amino Acid L	Leucine
Amino Acid N	Asparagine
Amino Acid S	Serine
Amino Acid T	Threonine
Amino Acid V	Valine
Amino Acid Y	Tyrosine
ARCs	Ankyrin repeat clusters
ART	ADP-ribosyltransferase
AXIN	Axis inhibition protein
BER	Base excision repair
BRCA	Breast cancer gene
BRCT	BRCA1 C-terminal
CADD	Computer-aided drug design
CNN	Convolutional neural network
CREB	cAMP-response element-binding protein
CBP	CREB-binding protein
CPT	Camptothecin
DAG	Diacyl glycerol
DCM	Dichloromethane
DDR	DNA damage repair
DEN-1	Deneddylase 1
DIPEA	*N*,*N*-Diisopropylethylamine
D-loop	Donor loops
DNA	Deoxyribonucleic acid
DNAP	DNA-directed DNA polymerase
DNA-PKcs	DNA-dependent protein kinase catalytic subunit
ERK1/2	Extracellular signal-regulated kinase 1/2
FBDD	fragment-based drug discovery

FG	Functional group
HATU	1-[Bis(dimethylamino)methylene]-1*H*-1,2,3-triazolo[4,5-*b*]pyridinium 3-oxid hexafluorophosphate
HD	Helical domain
HOSA	Hydroxylamine-*O*-sulfonic acid
HPF1	Histone PARylation factor 1
HRR	Homologous recombination repair
HTS	High-throughput screening
IKKγ	IκB kinase gamma
IUPAC	International Union of Pure and Applied Chemistry
LBDD	Ligand-based drug discovery
MDC1	Mediator of DNA damage checkpoint protein 1
MEK1/2	Mitogen-activated protein kinase kinase 1/2
MeOH	Methanol
MERIT40	Mediator of RAP80 Interaction and Targeting 40
ML	Machine learning
MLDD	Machine learning drug design
MMR	Mismatch repair
MRE11	Meiotic recombination 11
NAD	Nicotinamide Adenine Dinucleotide
NEMO	NF-κB essential modifier
NER	Nucleotide excision repair
NF-κB	Nuclear factor kappa B
NHEJ	Non-homologous end-joining
NI	Nicotinamide binding site
NLS	Nuclear localization signal
P300	Histone acetyltransferase p300
PARPi	PARP inhibitor
PCNA	Proliferating cell nuclear antigen
PH	Phosphate-binding site
PI3K	Phosphoinositide 3-kinase
PK/PD	Pharmacokinetics/pharmacodynamics
PTIP	PAX transcription activation domain interacting protein
QSAR	Quantitative SAR
RP	Residue point
SAM	Sterile alpha motif
SAR	Structure–activity relationship
SBDD	Structure-based drug discovery
SSB	Single-strand break
TFA	Trifluoroacetic acid
TMZ	Temozolomide
TNFR1	Tumor necrosis factor receptor 1

TNFα	Tumor necrosis factor α
TNKS	Tankyrases
TOP	Topoisomerase
TPT	Topotecan
UV	Ultra violet
VSA	Van der Waals surface area
WGR	Tryptophan–glycine–arginine
Wnt	Wingless-related integration site
Xphos	2-Dicyclohexylphosphino-2′,4′,6′-triisopropylbiphenyl
XRCC1	X-ray cross complementing group 1 protein

List of Tables

List of Figures

Chapter 1: Introduction and Thesis Premise

Following research into the UV-mediated photocyclizations of phenanthridinones [1], we found that there were few studies on the development of phenanthridinones into Poly(ADP-Ribose)Polymerase (PARP) inhibitors. There is a commercially available inhibitor, PJ34, that is based on phenanthridinone, however, it is a non-selective inhibitor with moderate potency. Instead of exploring analogs of PJ34, we decided to employ *de novo* designs to develop potent and/or selective PARP inhibitors based on a core phenanthridinone ring system while exploring any patent space for novelty. To avoid shooting in the dark, we used computer-aided drug design (CADD) methods as a tool to expedite the design of novel PARP inhibitors that had improved potency and/or selectivity in comparison to PJ34 and olaparib, an FDA-approved PARP inhibitor. Our research pipelines include a) using benzamide as the core scaffold, which can be found among other commercially available PARP inhibitors and b) using a novel core scaffold, such as thienoquinolinone, to replace benzamide which has not been used ever before. Our procedure to develop the inhibitor is 1) studying small molecules that can be potentially used as PARP inhibitors, 2) exploring novel inhibitor scaffolds that occupied different parts of the protein binding pocket and 3) probing the potency of inhibitors with functional groups on novel scaffolds devised to enhance ligand-protein interactions. To cut the cost of performing this research, we plan to employ an in-house optimized enzymatic assay for screening. Promising inhibitors are sent for testing in cell assays. Meanwhile, based on computational- and knowledge-based analysis and prediction, combining *in silico* and *in vitro* experiments, we aim to present an R&D pathway towards the development of hit-to-lead PARP inhibitors. Furthermore, the purpose of the research is not limited to the development of a PARP inhibitor, but also on how we can use CADD as a guide and tool for drug development that is focused on a well-known biological target when traditional drug discovery is declining and drug design with artificial intelligence is growing [2].

Reference:

1. (a) Fang, Y., and G. K. Tranmer. "Continuous flow photochemistry as an enabling synthetic technology: synthesis of substituted-6-(5*H*)-phenanthridinones for use as poly (ADP-ribose) polymerase inhibitors." *MedChemComm*, vol. 7, no. 4, 2016, pp. 720–24, https://doi.org/10.1039/c5md00552c. (b) Fang, Y., and G. K. Tranmer. "Expedited access

to thieno [3, 2-*c*] quinolin-4 (5*H*)-ones and benzo [*h*]-1, 6-naphthyridin-5 (6*H*)-ones via a continuous flow photocyclization method." *Organic & Biomolecular Chemistry*, vol. 14, no. 46, 2016, pp. 10799–803, https://doi.org/10.1039/c6ob02279k.

2. Henstock, Peter V. “Artificial Intelligence for Pharma: Time for Internal Investment.” Trends in Pharmacological Sciences, vol. 40, no. 8, Aug. 2019, pp. 543–46, https://doi.org/10.1016/j.tips.2019.05.003.

Chapter 2: Review and Research Background

2.1. PARP Protein

2.1.1. A General Introduction to the PARP Family

Poly(ADP-Ribose) Polymerase (PARP) is a family of 17 protein members that are the only known proteins with the poly-ADP-ribosylation ability [1] [3]. The phylogenetic tree of the PARP protein shows that PARP isomers can be grouped into 6 different clades: PARP1-3 (Clade 1), PARP4 (Clade 5), PARP5a/b (Clade 4), PARP7, 9-15 (Clade 3), PARP6, 8, 16 (Clade 6) [2]. Clade 1 is the most fundamental and these enzymes are responsible for deoxyribonucleic acid (DNA) damage repair, chromatin regulation, and transcription. Clade 2 is for describing plant PARPs. Clade 3 includes miscellaneous proteins with different functions and structures. Clade 4 is made up of Tankyrases (TNKS) that include two isomers responsible for the Wnt/β-Catenin signalling pathway, regulating mitotic spindle formation as well as telomeres. Clade 5 proteins are PARP4 species that are located in vaults, the ribonucleoprotein organelle [3]. The major function of PARP is to produce poly(ADP-ribose), which is involved in signalling for some cellular bioactivity, including proliferation and apoptosis, via poly-ADP-ribosylation [1]. Mono-ADP-ribosylation is also found among PARP isomers excluding PARP1/2, TNKS, or those without poly-ADP-ribosylation ability, as a function to produce mono(ADP-ribose), and these enzymes act as transferases instead of polymerases because of the absence of catalytic glutamate [4, 5, 6, 7]. The endogenous substrate of PARP enzymes is NAD^+ (Nicotinamide Adenine Dinucleotide) [1]. For polymerases, the catalytic reaction where NAD^+ is converted into nicotinamide and an ADP-D-ribosyl component will build linear (such as TNKS) or branched (such as PARP1) ADP-ribose polymers on the target protein or target chromatin, the PARP enzyme itself, or, in some cases, DNA [1, 7, 8]. The ADP-ribose polymers are crucial for signalling pathways in response to inflammatory and DNA damage repair as the polymer acts as the scaffold for recruiting relative factors [1, 9, 10]. Even though PARP proteins can be categorized into 6 groups based on their protein sequence and structures [1], the catalytic domain is conserved [11]. The nicotinamide binding site (NI), where isomers share a conserved **H**(Y)G(A)S(T)-**Y**-SY(N)**E**(I/L/V) sequence are known as H-Y-E class of ADP-ribosyltransferase [12]. The donor loops (D-loop, the loop structure in the donor site of the

enzyme) share fewer similarities. PARP1-4 D-loops are longer and they create hydrophilic pockets, whereas those in TNKS1-2 (PARP5a/b) are shorter and hydrophobic [12].

As mentioned previously, the PARP protein is involved in DNA damage repair (DDR) pathways. The cause of DNA damage can be endogenous, such as oxygen radicals, or exogenous, such as chemotherapy (e.g. alkylating agents or topoisomerase 1 (TOP1) inhibitors), radiotherapy, or UV light [13, 14, 15, 16, 17]. For single-strand breaks (SSB) in DNA, base excision repair (BER), nucleotide excision repair (NER), and mismatch repair (MMR) are major DDR pathways. For double-strand breaks, which can also be a result of the accumulation of SSB and the collapse of the replication fork, homologous recombination repair (HRR) and non-homologous end-joining (NHEJ) are involved. PARP proteins are involved in BER, HRR, and NHEJ partnering with corresponding factors [18, 19, 20]. The proteins also take part in chromatin modification and transcriptional regulation [20]. The activation and the function of some of these proteins will be discussed below.

2.1.2. PARP1 Structure and Function

PARP1 is the most abundant and well-studied member of the PARP family [1]. It contains three major domains, including a DNA-binding domain, which has three zinc fingers (Zn1, Zn2, Zn3) and a nuclear localization signal (NLS) subdomain, a Breast Cancer gene 1 C-terminal (BRCT) automodification domain, a catalytic domain with a WGR (tryptophan–glycine–arginine) subdomain, and a catalytic subdomain [21]. The catalytic subdomain can be further divided into a helical domain (HD) and an ADP-ribosyltransferase (ART) domain [22]. The HD contains 6 α helices (αA - αF) [23]. The ART domain can be divided into a donor site and an acceptor site, and NAD will bind to the donor site while the acceptor side is used for protein ribosylation [23]. The ART domain contains the NI, which is the pocket the nicotinamide component of NAD would bind to, and it is highly conserved [23]. It is surrounded by G863, Y896, S904, Y907, and E988. The adenine component will bind to the adenine-binding site (AD) in the cleft between the end of the D-loop and the HD. It is surrounded by D770, H862, S864, G876, and R878 [23]. Another site between the NI and the AD is the phosphate-binding site (PH). It is near the α helix F subunit (αF) of the HD, neighbouring D766 and E763 [23].

Upon the detection of an exposed DNA base by both Zn1 and Zn2, Zn2 will first bind to the 3’ end and cast Zn1 to bind to the 5’ end. The binding site of Zn3 is on the surface of DNA

and Zn1. WGR will bind to the surface on DNA, Zn1, and Zn3. The order of Zn3 binding and WGR binding may differ. The catalytic domain will subsequently bind to the surface of WGR and Zn3 and initiate local unfolding of the HD [24, 25]. In general, the activation of PARP1 induces a conformational change (rearrangement) on the inactivated and extended PARP1 "beads-on-a-string structure", making independent Zn, BRCT and WGR domains collapse and fold [26, 27, 28]. The inactivation of PARP1 to release the protein from the DNA unfolds and resembles the protein structure to the status where each domain is independent [26]. Recognizing the DNA damage, PARP1 binds to the DNA break and recruits histone PARylation factor 1 (HPF1) [29]. Next, PARP1 protein mediates serine residues to react with the nucleophile which is the 2'-OH end of the terminal adenosine group of NAD to form Ser-ADPribose complex, to initiate the ADP-ribosylation [31]. Other amino acids that can be involved include glutamate [30], aspartate (especially for PARP3) [8], tyrosine [32], and lysine [33]. After ADP-ribosylation of the target proteins, itself, or DNA [34], the ribose polymer will be able to recruit factors such as X-ray cross-complementing group 1 protein (XRCC1), DNA ligase III, DNA ligase I, deneddylase 1 (DEN-1), Proliferating cell nuclear antigen (PCNA), and DNAP (DNA-directed DNA polymerase) for BER [19]. When DSB is present, PARP1 can also mediate HR and NHEJ by working along with meiotic recombination 11 (MRE11), breast cancer gene 1 (BRCA1) or Ku70/80, and DNA-dependent protein kinase catalytic subunit (DNA-PKcs), as well as DNA ligase IV for ligation [19].

The activation of PARP1 in the inflammatory pathway is independent of DNA damage. One example of the inducement of the activation is the PARP1 phosphorylation, which is a result of the activation of Mitogen-activated protein kinase 1/2 (MEK1/2) and extracellular signal-regulated kinase 1/2 (ERK1/2). There are several inducers of the MEK1/2 activation. When tumour necrosis factor α (TNFα) is bound to Tumor necrosis factor receptor 1 (TNFR1), it increases the influx of Ca^{2+}, as well as activates phosphotidyl choline-specific phospholipase. The former activates MEK1/2 directly, while the latter produces diacyl glycerol (DAG), which can upregulate MEK1/2 [35]. The result of the PARP1 activation in the inflammatory pathway is to activate Nuclear factor kappa B (NF-κB) transcription [35]. The NF-κB activation can also be mediated by the acetylation of PARP1 by Histone acetyltransferase p300 (P300) and CREB-binding protein (CBP) at lysine residues. Moreover, it can be a result of the DNA-damage-

induced PARP1 activation with the formation of IκB kinase gamma (IKKγ) (NF-κB essential modifier, NEMO) [36].

2.1.3. PARP2 Structure and Function

In general, PARP2 is smaller than PARP1 and PARP2 shares a 69% similarity with PARP1 [11]. It accounts for 10–15% of PARP activity upon becoming fully activated by DNA damage [11]. Compared to PARP1, PARP2 has a slightly longer D-loop, from L523 to Y528, which may be able to provide additional interaction with the acceptor site [37]. It is also discovered that PARP2 lacks zinc fingers, indicating that it can adopt a completely different method of detecting DNA damage from PARP1 [38]. PARP2 is previously found to target DNA gaps that are from DNase-I, instead of nick [1]. Further studies with crystal structures indicate that the WGR is crucial in DNA recognition as it can bridge nucleosomes by forming a PARP2-WGR-DNA complex and lining up DNA ends to create a WGR-shielded nick [39] [40]. In the case of SSB, the WGR domain from one PARP2 protein would attach to the broken strand. In the case of DSB, two WGR domains from two PARP2 proteins will hook the enzyme up onto two stands separately and introduce domain–domain signal transmitting [40]. During this procedure, the disordered N-terminus, the WGR domain, and the catalytic domain are contributing together to interact with the DNA damage, while the latter two are essential for connecting the protein to the damaged site [41].

As a Clade 1 PARP, the major job of PARP2 is to recruit DNA repair factors in response to DNA damage. Just as with PARP1, the activation of PARP2 requires HPF1 for the serine-based post-translational modification. The PARP2-HPF1 complex will bind to two nucleosomes, and upon activation, the protein will open the catalytic domain for substrate binding [42]. The activation of PARP2 brings about the conformational change, which is also similar to PARP1 [43]. During the BER, PARP2 is required to cooperate with PARP1 and XRCC1 [44].

The major difference between PARP1 and PARP2 inside the binding pocket is that, instead of D766 in PARP1, PARP2 has E335 in the analogous location [45]. This is will be discussed later. However, the difference between D766 and E335 will not influence PARP2 using NAD^+ as a substrate for poly-ADP-ribosylation.

2.1.4. TNKS Structure and Function

PARP5a/b (TNKS1/2) shares less similarity with PARP1. TNKS1 and TNKS2 share a >85% similarity, while TNKS2 does not have the His-Pro-Ser (HPS) motif [1]. TNKS1 has three major domains, namely, an Ankyrin Repeat Domain (ankyrin repeat clusters, ARCs) with 5 ankyrin clusters, a sterile alpha motif (SAM) domain, and a catalytic domain [46]. The ARCs are important for interacting with the target peptide. Each ankyrin cluster has its own preferred amino acid target, and together they construct a platform for contacting polymeric master scaffolding protein axis inhibition protein 1 (Axin1) [46, 47]. The SAM domain is required, collaborating with the ARCs, for polymerization in the Wnt/β-Catenin signalling pathway as well as for TNKS subcellular localization, enzymatic activity, and AXIN interaction [48]. A major difference between TNKS and PARP1 in the catalytic domain is that TNKS does not possess the regulatory domain, known as the HD [48]. The catalytic domain of TNKS also contains a zinc-binding motif, which may be related to the DNA-binding and PAR-binding [49] [50]. Despite the difference, TNKS protein also has conserved H-Y-E residues, implying its ability of poly-ADP-ribosylation with NAD^+ substrate [2]. Upon activation, the SAM domain will mediate oligomerization to increase the solubility of TNKS, including homodimerization and heterodimerization between TNKS1SAM-TNKS2SAM, and the catalytic domain will form the head-to-head dimer [51, 52].

Like PARP1, TNKS is also involved in DNA damage repair pathways. When dealing with the DNA damage, TNKS cooperates with proteins like a mediator of RAP80 interaction and targeting 40 (MERIT40), a mediator of DNA damage checkpoint protein 1 (MDC1), etc. It also plays a role in the ubiquitylation-associated events such as the Wnt/β-Catenin signalling pathway by the poly-ADP-ribosylation of AXIN1 and AXIN2 [53] to initiate the pathway. AXIN polymer components are consequently ubiquitinated and degraded [54]. TNKS is also responsible for telomere length regulation by releasing TRF1 endogenously and poly-ADP-ribosylation TRF1, and the overexpression of the TNKS induces telomere elongation [55]. Other functions include Golgi-related trafficking, such as the assembly of mitotic spindles [56, 57], and apoptosis without poly-ADP-ribosylation [58].

2.2. PARP inhibitor

2.2.1. General Introduction and Clinical Application

PARP inhibitors (PARPi) are used to inhibit PARP enzymes competitively. The starting point for PARPi is the discovery of the side product of the PARP ribosylation (PARylation) reaction, nicotinamide, in the 1970s [59]. Nicotinamide is also a weak PARPi. In the 1980s 3AB was used as a popular competitive PARPi ($K_i < 2\mu M$) and was a benchmark for studies on the cellular response to DNA damage. It is the first generation of PARPi based on benzamide, an analog of nicotinamide. [60, 61]. Olaparib, rucaparib, niraparib, and talazoparib are FDA-approved PARP inhibitors used as monotherapy agents used in treatment or maintenance therapy of germline BRCA 1/2 mutations or supplemental therapy following three or more rounds of chemotherapy for ovarian, breast, or pancreatic cancer. Rucaparib and olaparib can also be used for metastatic castration-resistant prostate cancer [62].

PARP enzymes are recruited for the DNA-repair procedure as previously discussed. Following the discovery of PARP's role in DNA repair, it is realized that PARPi could be used to enhance the therapeutic influence of chemo- and radiotherapy as the inhibition of polyADPribosylation interfered with the DNA damage repair process and induced apoptosis. Alkylating agents can induce cytotoxicity by reacting with DNA bases such as at the N7 position of guanine to creat alkyl adducts or cross-links on DNA bases and as a result prevent replication, transcription, or lead to mispairing or DNA fragmentation [14, 64]. Radiotherapy can cause DNA damage directly or generate free radicals, which would consequently induce DNA damage. Both pathways would lead to cell death [65]. Thus, PARP inhibitors, as anticancer agents and sensitizers, are sometimes used along with chemotherapy (DNA-alkylating agents, topoisomerase I poison) and radiotherapy to disrupt the DNA repair pathway and increase the cancer cell's sensitivity towards cytotoxic factors, due to PARP being involved in almost every DNA damage repair pathway [66, 67, 68, 69].

Synthetic lethality is used to describe a combined lethal effect [70]. The lethal effect only occurs when two deleterious, but non-fatal genetic variants are presented simultaneously [70]. Synthetic lethality is observed in BRCA1/2-associated cancer with a loss of PARP function: when PARP is inhibited (or absent), single-strand breaks (SSB) will further develop into the double-strand breaks (DSB) due to the suppression of the base excision repair (BER) and the collapse of the replication fork [71]. In BRCA1/2-associated cancer, homologous recombination repair (HRR)-deficient tumour cells are not able to repair the DSB when non-homologous end

joining (NHEJ) and alternative end-joining repair (ALT-EJ) are inhibited by PARPi [72, 73] and it induces cell death. Thus, BRCA1/2-mutated cancer patients are hypersensitive to PARPi, and consequently, inhibitors can be used as single agents treating BRCA-mutated ovarian or breast cancer patients [69, 74, 75, 76]. Additional endogenous proteins, such as Phosphoinositide 3-kinase (PI3K), are also identified and associated with synthetic lethality as PI3K inhibitors can enhance antitumor therapeutic effects when used together with PARPi [77].

As PARP is also involved in many other cellular activities, PARPi can be used in other therapies as well. For instance, a TNKS (PARP5) inhibitor can be multifunctional as the target protein TNKS is related to not only the DNA damage repair pathway but also the Wnt/β-Catenin signalling pathway and the regulation of telomere length [7]. A TNKS inhibitor is found to cause telomere shortening, which can be a potential treatment for gastric cancer and many other cancers [78, 80, 79]. In the meantime, a TNKS inhibitor could stabilize AXINs, which are key components in the Wnt/β-Catenin signalling pathway. Thus, a TNKS inhibitor prohibited the proliferation of lung adenocarcinoma cancer cells [53, 81]. A TNKS inhibitor is also revealed to work on, but is not limited to, hepatocellular carcinoma cells and colorectal cancer cells through the Wnt/β-Catenin signalling pathway [82, 83].

2.2.2. PARP-Trapping and PARP Trapper

In addition to catalytic inhibition, PARPi can undergo PARP-trapping to increase their potency and cytotoxicity [84]. PARP-trapping is discovered when olaparib and niraparib are found to be more cytotoxic during treatment of DT-40 lymphoma cells compared to veliparib, regardless of whether they had similar potency in inhibiting PARylation. However, the same level of cytotoxicity is not observed in PARP-deficient cells. Researchers also found PARP–DNA complexes after treating cells with PARPi [85]. Similar results are found in experiments with talazoparib [84]. Talazoparib is considered to have the greatest PARP-trapping ability among FDA-approved PARPi with a PARP-trapping potency 100-fold stronger than olaparib and 500-fold stronger than veliparib. The latter has very little PARP-trapping ability [86]. One proposed mechanism of action for PARP-trapping increasing cytotoxicity is that in addition to catalytic inhibition, the inhibitor allosterically forces the protein to be trapped at the DNA lesion (whether it appears endogenously or is induced by anticancer therapy) to form a PARP–DNA complex. The enzyme-DNA complex will stall the replication fork and could not be released

from the 5'-end of the DNA, which would also affect the HR [86]. Thus, a PARPi with a strong PARP-trapping ability may also be used as a single agent for anticancer therapy even if PARP trapping is reversible [85]. Meanwhile, when used as a combination therapy, a strong PARP trapper cannot create PARP–DNA complex onto the lesion induced by a Top1 inhibitor, indicating no PARP-trapping could be achieved with the Top1 inhibitor. In contrast, the lesion induced by alkylating agents with the 5'-dpr generated during BER is adequate for inducing PARP-trapping. In short, the synergy between a PARPi and a Top1 inhibitor (e.g., Camptothecin) mainly comes from the catalytic inhibition caused by the PARPi, while the synergy between a PARPi and an alkylating agent (e.g., Temozolomide) is a result of PARP-trapping [87, 88, 89]. In addition to alkylating agents, 5'-dpr is also caused by oxidative DNA damage. Similar to catalytic PARP inhibition, research suggests that PARP-trapping may contribute to synthetic lethality in HR-deficient cells, but it remains controversial because, compared to PARP-depletion with siRNA, HR-deficient cells are more sensitive to PARP inhibitors [74]. It is also found that, when the inhibitor with good PARP-trapping ability is used with alkylating agents, the tolerability decreases in a mouse model, suggesting that PARP-trapping has limited positive influence with alkylating agents clinically [92].

The mechanism of PARP-trapping is still unknown. The two leading theories are about whether the inhibitor influences the trapping allosterically, or whether the "trapping" itself is a cluster or an enhanced PARP-DNA binding. From previous research, it is noted that inhibitors with similar catalytic inhibition potency had dramatically different PARP-trapping abilities, such as talazoparib vs. olaparib, suggesting that the PARP-trapping capability is related to the structure/feature of the ligand and that it is not a result of the formation of the protein-ligand complex. Neither is it a pattern that correlated with a compound's inhibitory capability catalytically, which is mentioned several times by Murai et al. [84, 85, 86, 87, 88]. "Reverse allostery" is believed to be the mechanism, whereby the allosteric changes are transmitted from the catalytic site to DNA-binding domains [85]. Supportive reports also show that the allosteric effect of inhibitors drifted the WGR domain to stabilize DNA binding [90]. The allosteric theory is also backed by a structural study [91]. However, it remains controversial because the evidence is also found that talazoparib is able to stabilize the DNA binding by inhibiting automodification, and the PARP-trapping activity is not an allosteric effect from inhibitors [89, 92]. The common ground is that PARP-trapping was found to be independent of the cell cycle, with the DNA break

occurring during the S-phase and NEDD8/SCF machinery involved in the PARP-trapping activity by regulating chromatin retention [89]. In addition, PARP1 and PARP2 undergo different PARP-trapping pathways. The releasing of PARP1-trapping is a result of molecular arrangements and allostery, while the PARP2-trapping is manipulated by the chromatin remodeler amplification in liver cancer 1 (ALC1). As a recent finding in agreement with the allosteric-effect theory, Zandarashvili et al. found that the protein would present three types of configurations driven by different inhibitors using hydrogen/deuterium exchange mass spectrometry (HXMS) [94]. A slower HX in the ART domain could be observed when the protein bound to any ligand. However, when the protein was in a complex with a strong PARP trapper, like EB-47, a much slower HX was observed in most domains, indicating that the HD drifted away from the NI, which also caused the chain reaction in non-catalytic domains including the WGR domain and Zn1/3 domains. Under this configuration, there was strong SSB DNA retention, and it was positively related to the ligand concentration. When the protein was in a complex with talazoparib or olaparib, little or no difference in the HX was observed in the HD and non-catalytic region. In this case, there was no allosteric retention or there was mild allosteric retention. When the protein took in a weak or non-PARP trapper, like veliparib, a slower HX could be found in the HD but not in the WGR domain and zinc fingers, indicating that the HD travelled towards the ART domain with a shrinking binding pocket with an allosteric pro-release configuration. Corresponding to these three situations, the ability to trap PARP by a ligand could be determined by its influence on the binding pocket status. Even though the finding was in line with Murai et al., Zandarashvili mentioned that it was insufficient to explain why talazoparib and olaparib are strong PARP inhibitors, and he suggested that some other factors are regulating the PARP-trapping ability [94].

With the unclear PARP-trapping mechanism, it is difficult to find a shred of solid evidence showing what kind of design would generate a potent PARP trapper. After all, the compound size and the stereo configuration of the ligand would account for the trapping ability (or enhanced PARP-DNA binding) collaboratively. Murai et al. believed that talazoparib gained its outstanding PARP-trapping ability due to its two chiral centers [84]. In a similar case, pamiparib also shows great PARP-trapping ability and is a bulky pentacyclic compound with no rotatable side chains [95]. Due to this, the size of the compound may be attributable to its trapping ability. Zandarashvili et al. also mentions that interacting with the HD, especially with

D766/770, is critical to bring about an allosteric pro-retention configuration [94]. In addition, E763 can also be a potential site to interact with. For olaparib, the side chain extends into the AD site (groove between the D-loop and the helix αF of the HD), similar to EB-47 [94, 96]. The AD site is the groove between the D-loop and the helix αF of the HD. The PARP trapper UKTT15 also extends its side chain into the groove between the D-loop and the other side of the helix αF [94], implying that a certain spatial occupation inside the binding pocket can activate PARP-trapping. Mutation of D770/766 has been shown to directly decrease the efficacy of PARP inhibitors, suggesting it's role in PARP trapping [94]. Smaller ligands are less likely to trap PARP, due to them being less likely to interact with the binding pocket, with some examples including veliparib and PJ34 [85, 97]. Notably, while PARP trappers are much preferred in treating oncological diseases due to their superior cytotoxicity, inhibitors with strong or moderate PARP-trapping ability are not good candidates for cell-protecting purposes, especially in CNS diseases. PARP inhibitors are used to avoid NAD^+ depletion caused by PARP hyperactivation in some CNS diseases and other non-oncological diseases [97, 98]. In these cases, a strong PARP trapper would bring unwanted cytotoxicity. Under these circumstances, using PARP inhibitors without PARP-trapping properties to inhibit PARP activity without killing cells is rather important [98].

2.2.3. PARPi Design

As PARPi are often developed based on nicotinamide/benzamide, the PARP binding pocket, especially for PARP1, requires the benzamide-like motif to provide at least one H-bond donor, one H-bond acceptor, and one aromatic ring for the π-π stacking interaction with G863, S904, and Y907, respectively. It is commonly believed that the benzamide scaffold is necessary for developing potent inhibitors as the core structure inside the NI [99, 100]. The electron-rich aromatic ring of a benzamide analog attached directly to the carbonyl group is used for the π-π stacking interaction; the carbonyl group becomes the H-bond acceptor, and the primary or secondary amide NH becomes the H-bond donor. Due to the relative position among G863, S904, and the NI, a cis conformation is preferred for the carboxamide component [100]. To induce the cis conformation, the carboxamide component is always fused into a ring, which leads to the bicyclic isoquinolinone structure [99]. An application of the isoquinolinone core structure is olaparib, which has a phthalazinone core structure [101, 102]. A similar design can be found on

talazoparib, which has a tricyclic structure with the phthalazinone attached to the pyridine [103]. The benzene ring of isoquinolinone in olaparib is important: when switching it into bicyclo-heptane, the potency is decreased generally, on different cell lines [104]. In contrast, modification on the carboxamide ring may bring better potency. By turning the isoquinolinone into the quinazoline-dione, which possessed a pyrimidinedione component, Senaparib is believed to be 20-fold more potent compared to olaparib [105]. It is also possible to make the carboxamide into a heterocyclic ring like Rucaparib, which has a 7-member carboxamide ring [106]. Another strategy to achieve the cis conformation is to form a weak intramolecular H-bond from the carboxamide primary amine to the indole derivative. It can be seen as a "pseudo" ring, and examples are veliparib and niraparib as well as quinoline-8-carboxamides inhibitors (**Figure 1**) [102, 107, 108, 109].

While it is relatively difficult to strengthen the H-bonding, as the amino acid sites for H-bonds are already occupied by the carboxamide motif, researchers added more aromatic rings onto the ligand to increase the π-π stacking interaction with Y907. PJ34 is an example using phenanthridinone as the core structure with the carboxamide ring sandwiched by two benzene rings, making the carboxamide ring itself aromatic as well [110, 111]. The central aromatic ring can be beneficial and critical: the modification on Rucaparib turning the molecule into a phenanthridinone-like compound without the central aromatic component decreased the potency, compared to Rucaparib, if further structural optimization is not applied [112]. However, it is rare to see inhibitors with the phenanthridinone core structure compared to the most popular design with the bicyclic ring [113]. The modification of phenanthridinone is limited to changing small substituents. These modified phenanthridinone compounds usually have no functional groups occupying binding sites outside of the NI. [113]. Tetracyclic inhibitors can also be found. Except for indeno-isoquinolineones, these inhibitors consiste of both aromatic and non-aromatic rings [114]. The design with the mono-aromatic ring as the core component is able to deliver decent potency with IC_{50} = 3.1nM [115]. In these cases, the carboxamide ring itself is modified into the aromatic ring for π interaction. Interestingly, these designs are not further developed as well, probably due to the necessity of using more rotatable bonds to reach other binding regions in the protein.

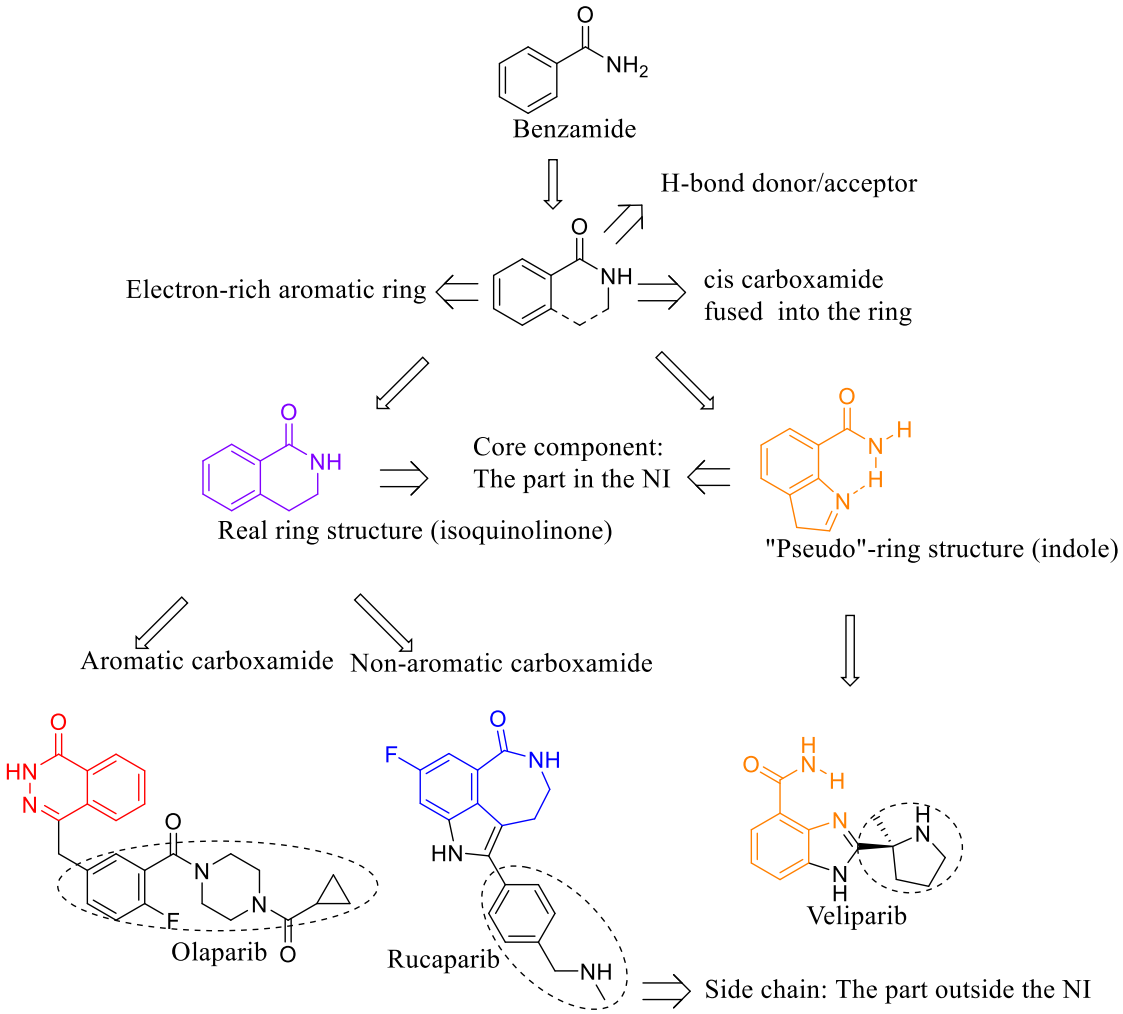

Figure 1 *The relationship between benzamide and PARP inhibitors. Derived from the original benzamide, a PARPi core structure is designed to fulfill some basic requirements including bearing an electron-rich aromatic ring, a combination of H-bond donor and acceptor and a cis-conformation. Based on these requirements, known PARP inhibitors could be divided into two major categories: The isoquinolinone analog (purple) has a fused carboxamide ring; The carboxamide ring could be either aromatic (olaparib, red) or non- aromatic (Rucaparib, blue); The indole analog (orange) has a weak intramolecular H-bond to form a pseudo-carboxamide ring. The benzamide analogue which will bind to the NI is identified as the core component and the component attached to the core component (circled) is identified as the side chain, which will bind to the region other than the NI.*

Conventionally, the binding pocket of PARP1 is divided into four parts, namely the NI, the AD, the phosphate-binding site, and the outer borders of NI (peripheral binding site) [116] (**Figure 2**). According to known complex crystal structures, PARP inhibitors show unity in the binding region (**Figure 3**). Based on the spatial occupancy, the design of the side chain can be classified into three categories: Small inhibitors such as PJ34, veliparib, or ones without a long side chain, such as talazoparib, majorly occupy the phosphate-binding site and a small part of the peripheral binding site when the molecule binds to the binding pocket [96, 111]. Longer inhibitors extend their chains into grooves between the D-loop and the HD, including the phosphate/peripheral binding site and the AD. For olaparib, it has its cyclopropyl group in the groove near R878, which is at the hydrophobic pocket of AD [96]. EB-47 also places its side chain in this position [94]. UKTT15, on the other hand, occupies the D-loop-HD gap near E763 [94]. For functional groups, there is no pattern in the side chain design. Nitrogen-bearing heteroaromatic saturated 4 & 5-membered nitrogen heterocycles and halogen-substituted rings are popular, especially in commercially available compounds. However, as the core component is meant to be more hydrophobic to be accommodated in the hydrophobic pocket, hydrophilic components are widely used for drug-ability. So far, it is difficult to determine if the size and molecular weight are related to potency and selectivity [12]. Generally, unselective inhibitors such as PJ34 tend to be smaller as they will only bind to the NI. PARP1/2-selective inhibitors such as olaparib are believed to be heavier with longer side chains that can interact with sites other than the NI [12]. However, veliparib, which is also small, is considered a PARP1/2 selective inhibitor against TNKS. Interestingly, highly TNKS-selective inhibitors such as IWR1 are designed to target another hydrophobic site adjacent to the AD without a carboxamide motif to interact with the NI, the conserved binding site [118]. Although a more popular TNKS-selective inhibitor XAV-939 keeps the carboxamide motif and interacted with the NI [119]. The chirality of the side chain may also influence the potency. Compared to its enantiomer, talazoparib has superior enzymatic and cellular potency than BMN-674 [103]. Ligand–residue interactions and their influence on potency will be discussed later in Chapter **2.3**.

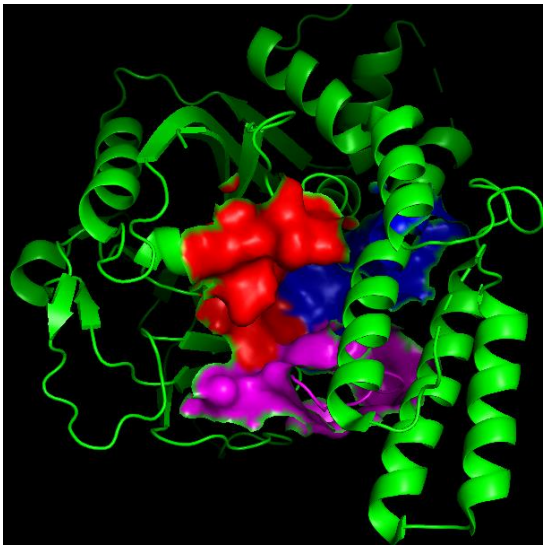

Figure 2 *Binding Sites of PARP Protein. Binding sites of a PARP protein include the NI (red), the AD (blue), the phosphate-binding site and the outer binding site (purple) [116, 117]. Binding sites are categorized according to* NAD^+ *occupation. The surface is generated by PyMol on selected residues.*

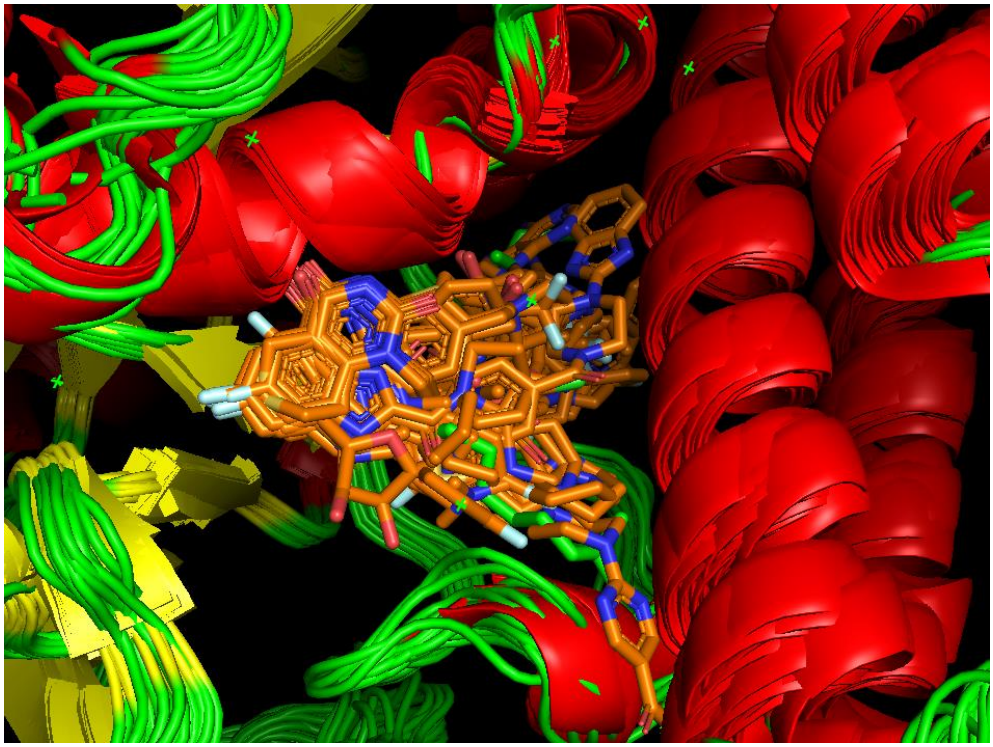

Figure 3 *Superposition of PARP1 inhibitors showing where ligands occupy in the PARP1 protein. Crystal structures are aligned using PyMol by aligning the sequence followed by*

*aligning the structure to minimize the RMSD between the aligned residues. Ligands are not aligned intentionally. RMSD is unavailable as crystal structures are aligned to PARP-PJ34 crystal structure complex (PDB ID **4UXB**) one by one. Superposition of all known homo-sapiens PARP1 crystal structures in complex with corresponding ligands. Proteins are shown in red (helix), yellow (sheet), and green (loop). Ligands are shown in orange (carbon), red (oxygen), and blue (nitrogen). The upper right part is the AD; the lower right part is the peripheral site with loops; the left part is the NI. The cluster of ligands stretches from the NI to the AD and the phosphate binding site and peripheral binding site, indicating the potential space occupancy inside the PARP1 protein, i.e. NI, AD and the groove between the D-loop and the HD.*

2.2.4. PARPi Resistance and Off-Target Effect

For PARPi drugs treating BRCA-mutation patients, the PARPi resistance mainly comes from the restoration of HRR and the stabilization of the replication fork as well as the enhancement of alternative repair pathways in some cases [120, 121, 122]. The restoration is the result of a secondary mutation on BRCA [123]. Somatic loss of 53BP1 is one example that could cause the restoration [124], as well as epigenetic re-expression of BRCA1 [125]. The stalled replication fork, which is usually mediated by BRCA, can be induced by the loss of PAX transcription activation domain interacting protein (PTIP) as it will recruit MRE11 [121]. The resistance can also come from other enhanced DNA damage repair pathways such as, in epithelial ovarian cancer cells, increased expression of aldehyde dehydrogenase A1 (ALDH1A1), which will introduce promoted ALDH activity that enhances microhomology-mediated end-joining activity [122]. The activation of the P53-dependent DNA damage repair pathway will weaken the sensitivity to olaparib, while the P53 stabilizer can overcome this PARPi resistance [126, 127, 128]. Other than the P53 stabilizer, several methods would also reverse the PARPi resistance, namely, mild hyperthermia, histone deacetylase inhibitors, heat shock protein-90 inhibitors, and BARD1 inhibitors [128]. Loss of PARP expression could eliminate PARP-trapping, which also contributes to resistance [129].

PARP inhibitors are observed with off-target effects on kinases, probably due to the high similarity between the NI and the kinase hinge region, which makes it easy for the carboxamide

group to bind. This off-target effect probably could not transfer into a synergistic effect clinically in most cases as only niraparib and rucaparib could significantly inhibit DYRK1s, CDK16, and PIM3 [130, 131]. Another related finding is that a vascular endothelial growth factor receptor (VEGFR) inhibitor can inhibit PARP, meaning PARP itself is suffered from off-target effects in clinical [132]

2.3. PARPi–Residue Interaction

2.3.1. General Introduction of PARPi–Residue Interaction Inside The NI

Herein we will review previous studies on PARP inhibitors with known PARP-inhibitor complex crystal structures published on the Protein Data Bank (PDB) [133]. The PDB provides a standardized platform to visualize possible protein-ligand interactions as cutoffs used for identifying interactions may varies in different software [133]. With these crystal structures, we can see what amino acid residues reported inhibitors interact with, which can be used for future inhibitor design. Compared to a conventional structure-activity relationship study (SAR), the studies of protein-ligand interactions can be more universal. SAR studies ignore why changing functional groups will influence the activity and how it works, i.e., the relationship of functional groups and the target. Thus, for structure-based drug discovery, a review of residues incorporated into the PARPi action from previous studies is necessary.

As previously discussed, the NI is the most important and conserved region for binding PARP inhibitors (especially PARP1 inhibitors). In the NI, the most conserved residues are G863, S907, Y907 as well as H862, which are identical among PARP1/2 and TNKS enzymes [134] (**Figure 4)**. These residues usually provide several important protein-ligand interactions, with either endogenous substrate NAD^+ or inhibitors with a benzamide motif (which is conserved for most known PARP inhibitors and some TNKS inhibitors) including two ligand-G863 H-bonds with G863 as both the H-bond acceptor and donor, one ligand-S904 H-bond with S904 as the H-bond donor, and π-π interaction with Y907 [12, 111, 136]. Inhibitor XAV-939 does not have a benzamide motif; instead, it forms a π-π interaction between its pyrimidinone and Y907, which can be the reason for its deficient potency inhibiting PARP1/2 [111]. Cation/π-π interaction can also be found between a ligand and H862 (**Table 1**). These are the most basic PARP-inhibitor interactions as most PARP1/2 and some TNKS inhibitors will interact with these residues [12]. There are additional amino acid residues inhibitors can target and they are possibly related to

inhibitor potency and selectivity. Based on previous studies and ligand-protein complex crystal structures, inhibitors can also interact with residues from the rest of the ART domain near the NI (S864, N868, G871), residues on the donor-loop (D-loop) (G876, R878, A880, G888, Y889, M890, G894, Y896), ones in the HD (E763, D766, D770), and residues from the acceptor-loop (A-loop) (E988). It is worth noting that even though studying the protein-ligand interaction will provide an insight into how PARP inhibitors work on the protein, it is not the only method for inhibitor design. As shown in **Table 1** aside from G863, S907, Y907, and H862, hot spots for potent inhibitors to directly interact with included D766, S864, R878, Y889, and Y896, of which interacting with facilitate binding affinity. Water-mediated H-bonds are also found in many scenarios while on the other hand, valuable targets inside the binding pocket are limited. No covalent contact is found in previous studies.

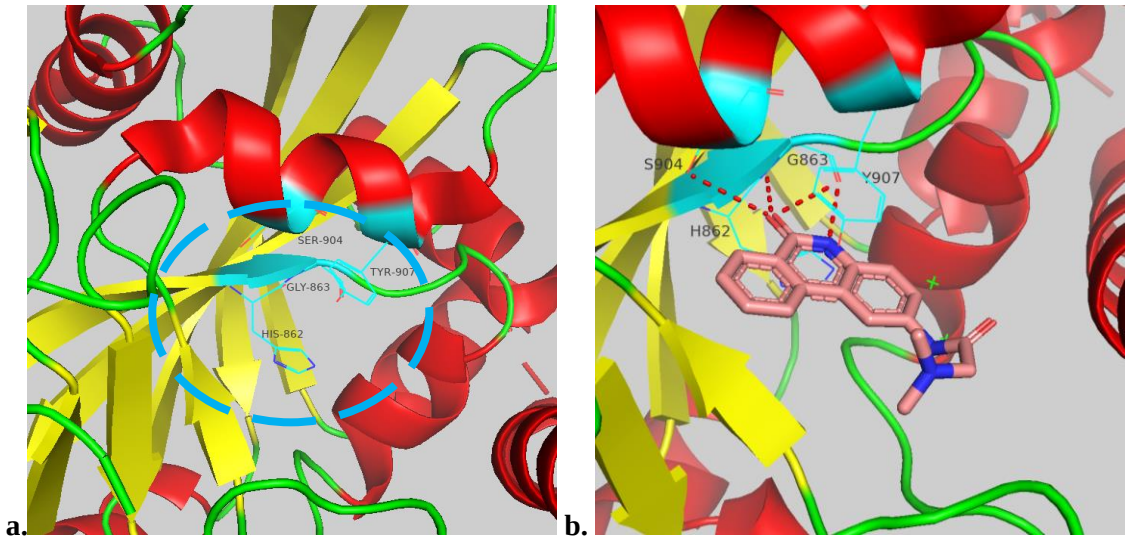

Figure 4 ***(a)****The NI of PARP enzyme. PDB ID* ***4UXB*** *[117]. Major residues include H862, G863, S904, Y907. The approximate area of the NI is circled above in blue.* ***(b)*** *PJ34 binds to the NI residues (cyan) (PDB ID* ***4UXB****). The H-bond are shown as the red dash.*

PDB[a] [133] [168]	Ligand	G863	S904	Y907	E763	D766	D770	H862	S864	N868	G876	R878
4UXB	PJ34	HH[b]	H	CP								
3GJW	GJW	HH	H	CPP				C	W			
3GN7	3GN	HH	H	CP				C				
2RCW	AAI	HH	H	CP				H				
2RD6	Veliparib	HH	H	CP				C				
3L3L	L3L	HH	H					C				
3L3M	A92	HH	H	HCCP		W		C				
4GV7	MEW	HH	H	CP								
4HHY	15R	HH	H					C				H
4HHZ	15S	HH	H	C								
4L6S	1WQ	HH	H	CP				C	W			
4UND		H	H	PP				CCP				
4PJT	Talazoparib	HW	H	CP				C				
4R5W	XAV939	H	H	CCP				C				
4R6E	Niraparib	HH	H	CCP		H		C				
4RV6	Rucaparib	HH	H	C				C				
5A00	D7N	HH	H	P				C				
4ZZZ	FSU	HH	H	CP				C				
5KPN	6WX	HHH	H	CP				C				HH
5KPP	6WZ	HHH	H	CP		W	W	C	W			
5KPQ	6X2	HHH	H	CP				C				
5WRQ	7TX	HHH	H	CP				C				H
5WRY	4YR	HHH	H	WCP				C				W
5WRZ	7U3	HH	H	CP				C				
5WS0	7U6	HH	H	CP		H		C				
5WS1	7U9	HH	H	CP		H		C				
5WTC	7UL	HHH	H	CP				C				
5XSR	8EC	HH	H	CP	H			C				
5XST	8E6	HH	H	CPP	H			C				
5XSU	8E3	HH	H	CCP	H			C				
6GHK	EZ2	HH	H	CCP				C				
6VKO	L1S	HH	H	CP	H	H		C				
6VKQ	UHB	HH	H	CP		Ct[c]	Ct	C	HH	H	H	
6XVW	O3H	HH	H	CP				C	W			
1UK0	FRM	HHH	H	CC								
1UK1	FRQ	HHHH		CP								
1WOK	CNQ	HH	H	C				C				
7KK4	Olaparib	HH	H	CP				C				HHH

Table 1 Pt1

PDB	Ligand	A880	G888	Y889	M890	Y894	Y896	E988	G871	IC_{50} (nM)[d]	k^d (nM)	Ref
4UXB	PJ34						C			135±150	110	[117][135]
3GJW	GJW									n/a	5.00	[137]
3GN7	3GN									n/a	5.00	[138]
2RCW	AAI			C						n/a	8.00	[139]
2RD6	Veliparib									9.30±11	3.90±1.6	[140]
3L3L	L3L		W	C			C			n/a	33.0	[141]
3L3M	A92									n/a	6.00	[142]
4GV7	MEW									3400±2200		[143]
4HHY	15R									1.92	n/a	
4HHZ	15S					H				19.0	n/a	[144]
4L6S	1WQ									n/a	3.00	[145]
4UND							P	W				
4PJT	Talazoparib			P	W		P	W		1.90±2.6	12.0	[111] [146] [172]
4R5W	XAV939									916±835	620	[111] [147]
4R6E	Niraparib			H						30.2±43	3.20	[117] [148]
4RV6	Rucaparib			C						102±160	1.40	[111] [149]
5A00	D7N									25.0±15	8.60	[150] [151]
4ZZZ	FSU									5300	87.0	[151]
5KPN	6WX						HP			n/a		[152]
5KPP	6WZ						HP			n/a		[153]
5KPQ	6X2						HP			n/a		[154]
5WRQ	7TX						H			n/a		[155]
5WRY	4YR					H	HP			n/a		[156]
5WRZ	7U3									n/a		[157]
5WS0	7U6						C			n/a		[158]
5WS1	7U9						C			n/a		[159]
5WTC	7UL						HP			n/a		[160]
5XSR	8EC			C						17.0	n/a	
5XST	8E6			C						27.0	n/a	
5XSU	8E3			C						244	n/a	[161]
6GHK	EZ2			P			W			n/a		[162]
6VKO	L1S			HC						n/a	20±5	[94]
6VKQ	UHB						C			45.0	n/a	[94] [163]
6XVW	O3H									n/a		[170]
1UK0	FRM									8.00	n/a	[164]
1UK1	FRQ									60.0	n/a	[165]
1WOK	CNQ									33.0	n/a	[166]
7KK4	Olaparib						HP			7.00±5.7	0.50±0.3	[167] [96]

Table 1 *Homo-sapiens PARP1 ligand–residue interactions. Potent inhibitors are highlighted. a. Representative homo-sapiens PARP1 crystal structures. b. Each letter represents one expected*

interaction. H: H-bond; W: Water-mediated H-Bond; C: Cation-π interaction; P: π-π interaction; Ct: Contact. c. "Contact" means that the interaction is found in the research and mutation of these residues influences drug potency, while the distance between the ligand and the corresponding residue in the crystal structure may be too long to be recognized by software as a direct bonding relationship d. Values written as mean±standard deviation are from PubChem database and corresponding pages are referenced. n/a: no corresponding record is found

2.3.2. Interaction with The Periphery Region

S864, N868, and G871 are in the ART domain between G863 and the D-loop. While only a few compounds are interecting with N868 and G871 [PDB ID **6BHV 6VKQ**] [169], H-bonding with S864 is more common as the amino acid (AA) is closer to the NI. A968427, an analog of PJ34, may have its tertiary amine form a water-mediated H-bond with S864, while the latter also interacts with N868 [PDB ID **3GJW**] [137]. The same water-mediated H-bond is also found for benzo[*1,4*]oxazin-3-one [PDB ID **4L6S**] [145] and MC2050 [PDB ID **6XVW**][170] with tertiary amines and 6wz with a carboxamide carbonyl group [PDB ID **5KPP**]; EB-47 may use its cyclopentane-1,2-diol hydroxyl groups to form H-bonds with S864 directly [PDB ID **6VKQ**] [94] [170]. (**Figure 5**)

2.3.3. Interaction with The D-loop

There are abundant AA targets on the D-loop **(Figure 6)** with the most common ones including G876, R878, A880, G888, Y889, M890, G894, and Y896 (although G876, R878, G894, and Y896 do not theoretically belong to the D-loop). The loop is responsible for communicating between ART and HD [25]. Two tyrosine residues are the most important ones on the D-loop as they are able to form both π interactions and H-bonds with ligand components. Among them, Y896 together with Y907 form a sandwich-type hydrophobic binding site, favouring compounds with larger hydrophobic contacts [171]. PJ34 can form a cation-π interaction with Y896 [PDB ID **4UXB**] [117] with its protonated tertiary amine. A similar cation-π interaction can be found on A906894 with its secondary amine [PDB ID **3L3L**] [141], EB-47, and benzoimidazoles with their tertiary amine [PDB ID **6VKQ 5WS0 5WS1**] [94]. Talazoparib interacts with Y896 through a T-shaped π-π interaction [PDB ID **4UND**] [117].

Talazoparib is also expected to interact with M890 with a water-mediated H-bond under a certain binding pose [PDB ID **4PJT**] [172]. Water-mediated H-bonds are expected for ME0527 with the backbone of the tyrosine [PDB ID **6GHK**]. Olaparib and its analog, quinazoline-2,4(1*H*,3*H*)-dione derivative **6wx,** interacts with the backbone of Y896 by H-bonding with its side-chain carbonyl group and the phenyl side chain of Y896 by π-π interaction [PDB ID **7KK4 5KPN**] [96]; quinazoline-2,4(1*H*,3*H*)-dione analogs **6wz**, **6x2**, **4yr**, and **7ul** are also found to have the same binding pattern [PDB ID **5KPP 5KPQ 5WRY 5WTC**]. In contrast, **7tx** is less likely to build a π-π interaction due to slight structural differences [PDB ID **5WRQ**]. Compared to Y896, Y889 is further away from the NI, however it may still interact with NAD^+ [169]. More cation-π interactions are presented with ligands such as A620223 (with its tertiary amine) and Rucaparib, A906894, tetrahydrothieno/tetrahydrofuro-pyridines (with their secondary amines) [PDB ID **2RCW 3L3L 4RV6 5XSR 5XST 5XSU**] [117, 141, 161]. Talazoparib and ME0527 are able to form a T-shaped π-π interaction with Y889 [PDB ID **4PJT 6GHK**] [172]. Apart from its phenyl ring, Y889 is able to form an H-bond target with its phenyl hydroxyl group, which is assumed to interact with niraparib's piperidine amine. A compound like UKTT15, which has a carboxamide component near Y889, is able to form both a cation-π interaction and an H-bond with the AA residue. Another very important AA target on the D-loop is R878 which is at the end of the D-loop near the AD, implying it may be involved in bioactivity when NAD^+ is bound to the protein. However, its function in PARP activity is not well-reviewed. It is only mentioned that H862, D770, S864, G876, and R878 might altogether stabilize NAD^+ in the AD [173], with ligands that interact with R878 having greater potency. (<10nM). Olaparib interacts with the residue through at most three H-bonds using its tertiary amine and carbonyl group of the cyclopropyl(piperazin-1-yl)methanone component, and it has an average IC_{50} value of 6.8nM [PDB ID **5DS3**] [25]. **15r** that interacted with the residue with its carbonyl group, which has an IC_{50} value of 1.92nM [PDB ID **4HHY**] [144]. In comparison, **15r**'s analog **15s** interacts with G894 instead of R878, and its inhibition capability is IC_{50}=19nM [PDB ID **4HHZ**] [144]. Other ligands like quinazoline-2,4(1*H*,3*H*)-dione analogs are likely to interact with the residue through direct H-bonding or water-mediated H-bonding [PDB ID **5KPN 5WRQ 5WRY**]. Since olaparib is a good PARP trapper, the ligand-R878 interaction may be crucial for the PARP-trapping ability [84].

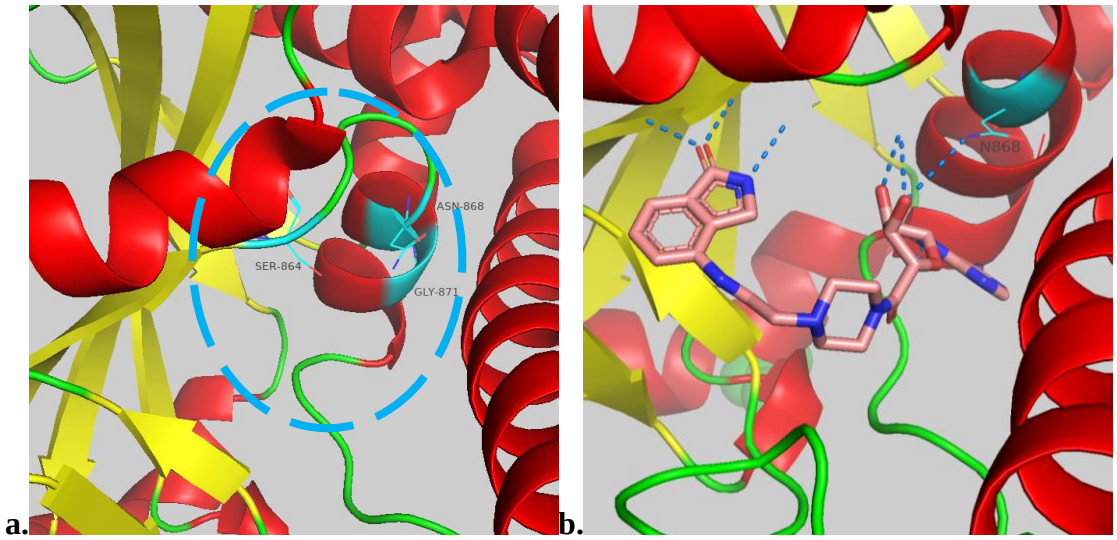

Figure 5 *(**a**)Residue targets around the NI-periphery region. Potential residue targets around the NI-periphery region are shown based on PDB ID **4UXB** [117]. The NI-periphery region is circled above and it is a part of the conventionally-believed phosphate binding site. Some important residues include S864, N868, G871. (**b**) The EB-47 interact with N868 (cyan) (PDB ID **6VKQ**) of the periphery region. The H-bond is shown as the blue dash.*

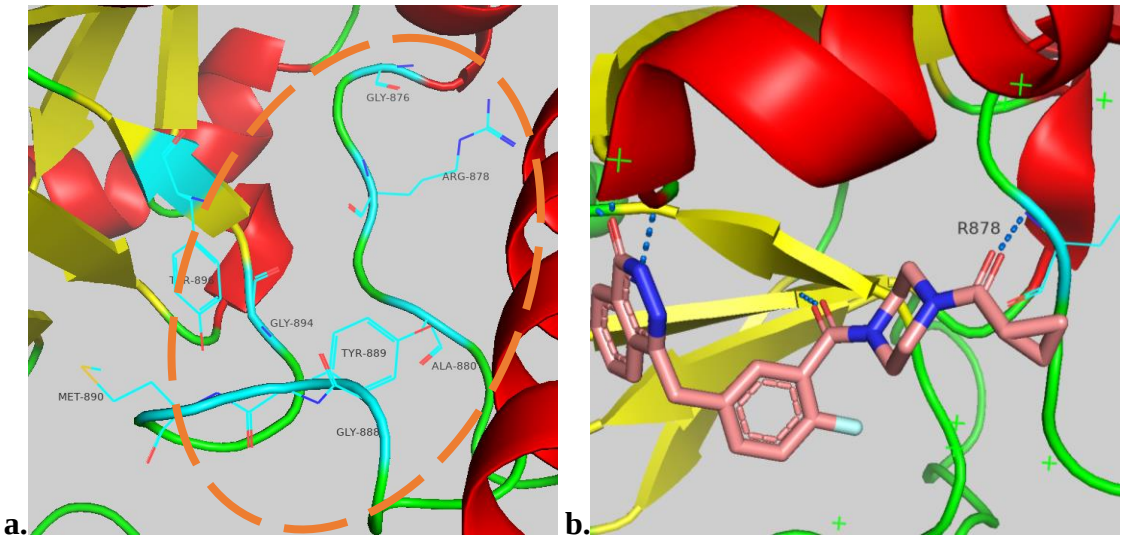

Figure 6 *(**a**) Residue targets on the D-loop (orange circle). Potential residue targets on the D-loop are shown based on PDB ID **4UXB** [117] including G876, R878, A880, G888, Y889, M890, G894 and Y896. They are distributed in the nicotinamide binding pocket and phosphate-binding pocket. (**b**) Olaparib interacts with R878 on the D-loop (PDB ID **5DS3**). The H-bond is shown as the blue dash.*

2.3.4. Interaction with The HD

Known ligand–residue interactions with residues in the HD are comparably simple(**Figure 7**). The residue targets include E763, D766, and D770, and they are believed to be associated with PARP-trapping caused by allosteric PARP-1 retention as the ligand may destabilize the HD, increasing the protein affinity for DNA [94]. The destabilization is caused by the ligand interacting with helix αF, where E763, D766, and D770 are located, and it triggered the allosteric chain reaction when the HD travels away from the ART domain [94]. Both double mutant D766/D770A and triple mutant E763/D766/D770A increased DNA-independent PARP1 activity and T_M when BAD (benzamide adenine dinucleotide) is presented, suggesting these residues are blocking BAD or NAD^+, from binding: D770 interferes in the binding of adenine base and E763, while D766 interferes the binding in the binding of phosphate groups [25, 94]. EB-47 is believed to contact with both D770 and D766 as the D766/770A mutant will prevent neither EB-47 nor DNA from binding. However, this kind of relationship is not reviewed in the crystal structure [PDB ID **6VKQ**] [94]. Another example of a ligand interacting with both D770 and D766 that is reviewed by the crystal structure is A927929; A927929 is predicted to participate in H-bonding with both residues through a water molecule [PDB ID **5KPP**]. Niraparib is expected to form an H-bond with D766 and is considered a weak PARP-trapper [PDB ID **4R6E**] [86, 117]. H-bonding with D766 is also found on benzoimidazole compounds [PDB ID **5WS0 5WS1**]. UKTT15 is able to interact with D766, probably forming an H-bond with the residue using its carbonyl group as an H-bond acceptor rather than using the secondary amine as an H-bond donor [PDB ID **6VKO**] [94]. UKTT15 may also form an H-bond with E763, but it is not proven in the previous study [PDB ID **6VKO**]. Tetrahydrothieno/tetrahydrofuro-pyridines may interact with E763 with secondary amines on the piperidine ring [PDB ID **5XSR 5XST 5XSU**] [161]. While the amines are able to interact with Y889 and E763 simultaneously, their IC_{50} values are about 90±65nM, which are comparably decent.

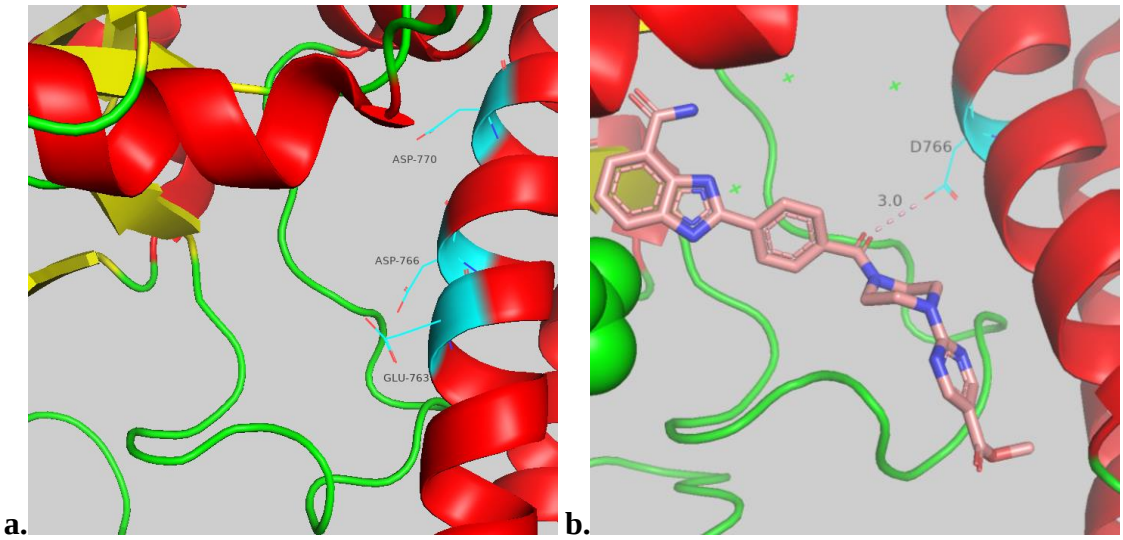

Figure 7 *(**a**) Potential residue targets in the HD. Potential residue targets in the HD are shown based on PDB ID **4UXB** [117] including E763, D766 and D770. (**b**) UKTT15's carbonyl group is 3.0Å (pink) away from D766 (cyan) in the HD (PDB ID **6VKO**).*

2.3.5. Other Targets and Covalent Bond Targets

E988 is located at the end of the acceptor-loop (A-loop) between the donor site and the acceptor site (**Figure 8**), and is a crucial catalytic residue in PARP1 for PAR elongation [1] [174]. Talazoparib may interact with E988 through water-mediated H-bonds with one water molecule [PDB ID **4UND**] [117], and **2us** can form a direct H-bond with the residue [PDB ID **4OQA**] [175]. It is unknown how the ligand–E988 interaction will affect the potency as **2us** is 300-fold less potent than talazoparib. Amino acid residue targets for covalent inhibitors include threonine, tyrosine, serine, lysine, cysteine, glutamate, aspartate, and histidine [176] [177]. Based on the PARP1 protein crystal structure, potential covalent-bonding targets in the binding pocket with accessible side chains include T887, Y689, Y889, Y896.

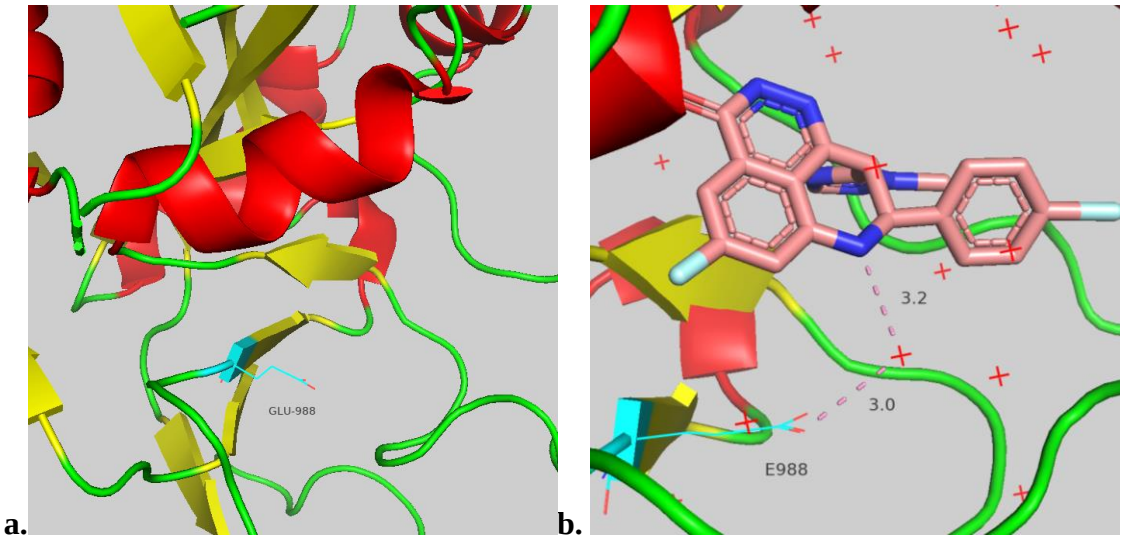

Figure 8 *(**a**) E988 on the acceptor site. E988 on the acceptor site is shown based on PDB ID **4UXB** [117]. The acceptor site is the region where the to-be ADP-ribosylated target or an ADP-ribose in a growing PAR scaffold is attached [178]. (**b**) Talazoparib may interact with E988 (cyan) (PDB ID **4UND**) through a water (red) mediated H-bond (red dash) as the distances are 3.0Å (E988-water molecule) and 3.2Å (talazoparib-water molecule).*

2.3.6. Amino Acid Residue Targets in PARP2

As mentioned previously, the structures of PARP2 and PARP1 share great similarities. By aligning the PARP2 sequence with PARP1, we find that, in addition to the NI, the D-loop is quite identical [45] between PARP2 and PARP1 as the major difference lies between isoleucine (PARP2) and valine (PARP1). The glutamic acid near the acceptor site in PARP1 (E988) can also be found in a similar place in PARP2. In comparison, there are more differences in the αF of the HD, implying that PARP2 selectivity may largely be related to the ligand–HD interaction. Among amino acid residues in PARP2 that are different from ones in PARP1, Q324, K325, S328, I331, E335, G338, and I342 may influence PARP2 selectivity as their residues are in the cavity of the binding pocket. A ligand could interact with them without clashing. Q332, E335, and D337 in PARP2 are in analogous positions to E763, D766, and D770 in PARP1. Among these residues, D770 is the same as D337. Q332 is neutral while E763 is negatively charged when they are similar in structure. E335 is longer than D766. Thus, Q332 and E335 can determine the selectivity for PARP2. Steffen et al. also mentioned it in their review and another residue

responsible for PARP2 selectivity may be Y455 [23]. However, based on the data from PubChem, veliparib in the review is not exactly a PARP2-selective inhibitor (which is also mentioned by Murai *et al.*): its IC_{50} value on PARP1 is 36.5±80nM, and the IC_{50} value on PARP2 is 21.2±37nM. Veliparib's potency inhibiting PARP2 is less than 2 folds compared to its potency inhibiting PARP1. It can be controversial to characterize veliparib as a PARP2-selective inhibitor [136]. Similar to veliparib, PARP2 inhibitor A-966492 is ~2-fold more selective for PARP2 over PARP1, which should not be considered as a PARP2-selective inhibitor either [179]. In fact, pure PARP-selective inhibitors are not well developed, which makes it difficult to identify more amino acid residues as targets for PARP2-selectivity. Another example is UPF1069, which is the only commercially available PARP2-selective inhibitor [180]. UPF-1069 has an IC_{50} of 300nM inhibiting PARP2, and its analogs have up to a 60-fold more selective over PARP1 [180a]. These compounds are believed to interact with E558 (E534 in the study) through a water-mediated H-bond and have the benzoyl moiety positioned near the HD near I331 and Q332 (Val307 and Lys308 in the Mus musculus protein). In this case, I331 and Q332 may also be involved in the determination of PARP2 selectivity. Quinoxaline analogs reported by Junya Ishida *et al.* have better overall potency and selectivity with IC_{50} of ~100nM inhibiting PARP1 and ~10nM inhibiting PARP2. These compounds are believed to interact with Q332, E335, and Y455 (Q308, E311, and Y431 in the study) in the αF of the HD with the R-phenyl group. In short, the PARP-2 selectivity of a compound relied on its interaction with unique residues in the HD of PARP2.

2.3.7. Amino Acid Residue Targets in TNKS (TNKS1)

There are three binding patterns for a ligand inside the TNKS protein. It can either bind to the NI, the AD, or both (like a dual-site inhibitor) (**Table 2**) [182] [183]. The AD is also referred to as the induced binding site. The amino acid residues inside the NI included H1184, G1185, S1221, and Y1224 (**Figure 9**), with Y1224/1213 forming a hydrophobic region for a benzamide-like aromatic ligand to stack in. However, Y1213 does not always form a π-stacking interaction with the ligand inside; instead, its backbone is often found to build an H-bond with an AD-binding ligand. Alternatively, H1184 can form a π-stacking interaction with the ligand in the NI. As the NI is almost identical between PARP1 and TNKS1, ligands that are primarily bound to the NI binding site in TNKS1 are more likely to have PARP1-inhibition ability as well. Thus,

their selectivity towards TNKS1 is not certain. Both PJ34 and XAV939 are bound to the NI in TNKS1 [PDB ID **3UH2 3UH4**] [184]. Although the crystal structure showed that PJ34 also appeared in the induced pocket, no ligand–residue interaction is assigned in that pocket for the PJ34 ligand. As a non-selective inhibitor, PJ34 is approximately 10-times less effective against TNKS1 compared to its potency against PARP1 [135]. In contrast, XAV939 is known to be a TNKS1-selective inhibitor with an IC_{50} around 40nM, which is 13-fold more effective on TNKS against PARP1 [147]. A NI-binding ligand is likely to interact with E1291 even though it belongs to the acceptor site [185].

Different from PARP1, there is no HD in the TNKS protein. The AD is composed of important residues such as H1201 and D1198. With the absence of the HD, the AD is exposed to the outside and allowed some small molecules to bind to this site directly [186]. As these molecules are not designed to interact with conserved residues in the NI, there is always a lack of carboxamide moieties. The TNKS1-selective inhibitors IWR1/2 have their quinoline components addressed inside the induced pocket [PDB ID **4DVI 4TKF**] [187, 188]. The quinoline moiety is able to form cation-π or π-π interactions with H1201 [188]. The carboxamide attached to the quinoline is able to interact with D1198. The inhibitors, including those dual-site inhibitors, that have functional groups inside the induced binding site always accepted nitrogen-containing bicyclic heterocycles such as quinoline, benzo-imidazolone [PDB ID **4K4E**] [189], and nicotinonitrile [PDB ID **5ECE**] [190] or benzenes such as benzene [PDB ID **4MSK**] [191], fluorobenzene [PDB ID **4LI7 4LI8**] [192], benzonitrile [PDB ID **4MT9**] [191], and anisole [PDB ID **3UDD**] [193].

PDB	Ligand	Type	H1184	G1185	D1198	H1201	Y1203	G1211	Y1213	S1221	Y1224	I1228	E1291	Ref
3UH2	PJ34	NI		H						H	P			
3UH4	XAV939	NI		H						H	P			[184]
4LI6	1XO	NI		H					H	H	CP			[192]
4W6E	3J5	NI		H						H	CPH		H	
4W5S	3J1	NI		H						H	CPH		H	[185]
6QXU	JKN	NI		H						H	CP			[194]
4K4E	K4E	AD			H	CP	W	H	H		Hal			
4K4F	K4F	AD			H	CP			H					[189]
4DVI	IWR2	AD			H	CP			H					[187]
3UDD	34M	AD				CP						H		[193]
4LI7	1XP	Dual			H	P					P			
4LI8	1XQ	Dual		H	H	P			H	H				[192]
4MT9	2D6	Dual		H		CP			H	H	CP			
4MSK	2C8	Dual		H		CP			H	H	CP			
4MSG	3C6	Dual		H					H	H	CP			[191]
4I9I	1DY	Dual		H	H				H	H	CP			[195]
5ECE	5N2	Dual	P	H		P			H	H				
5EBT	5N8	Dual	P	H	H				H	H				[190]

Table 2 *Representatives of TNKS1 ligand–residue interactions [168].* ***a.*** *Each letter represents one potential interaction.* ***H****: H-bond;* ***W****: Water-mediated H-bond;* ***C****: Cation-π interaction;* ***P****: π-π interaction;* ***Hal****: Halogen bond.*

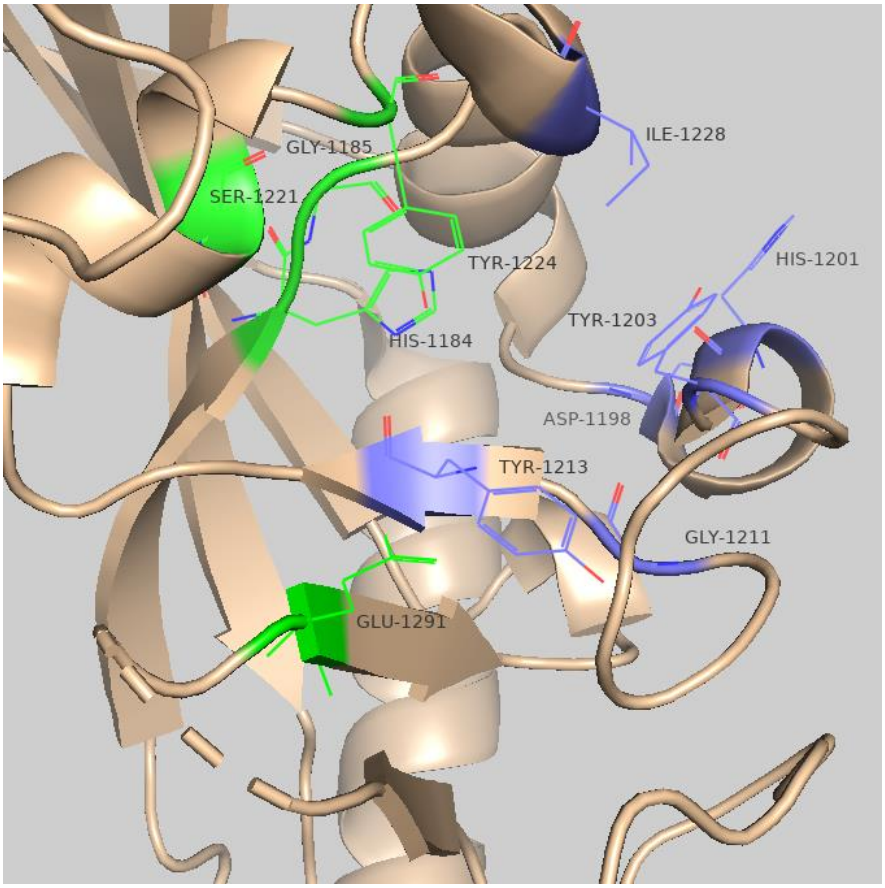

Figure 9 *Target residues in TNKS1. Target residues in TNKS1 (beige) are shown based on PDB ID* ***3UDD*** *[193]. H1184, G1185, S1221, Y1224, and E1291 (green) will interact with a NI-binding inhibitor or the NI-component of a dual-binding inhibitor; D1198, H1201, Y1203, G1211, Y1213, and I1228 (purple–blue) will interact with an AD-binding inhibitor or the AD-component of a dual-binding inhibitor.*

2.4. Drug Design

2.4.1. General Introduction to Drug Design and Drug Discovery

The term “drug design,” or “rational drug design,” refers to the innovative way of designing compounds with therapeutic effects, which could either be small organic compounds or macromolecules such as protein, based on a scientific rationale [196]. From a historical perspective, extracted products are found from plants and animals to treat certain diseases. With the understanding of the biological origin of diseases and the structural information of the active

component of a naturally occurring medicine, scientists are able to synthesize and modify these compounds for better therapeutic effects [196, 197]. However, modern drug design is closely related to target-based drug discovery. With molecular approaches, cell models and clinical samples are used for *in vitro* studies with a certain expression such as diseases, proteins, etc. With system approaches, *in vivo* studies focus on patients and animal models [197]. A conventional approach to initiate a drug design process is to search for bioactive hits using high-throughput screening (HTS) with a library of molecules that are used to discover hits that deliver a general idea of what a drug-like molecule/ligand behaves like [197, 198, 199]. A more efficient way, is using *in silico* drug design (computer-aided drug design, CADD), which is also used for hits discovery, which will be discussed later [198]. “Hit-to-lead” focuses on the optimization of hits to establish a structure-activity relationship (SAR) as well as preliminary pharmacological pharmacokinetics/pharmacodynamics (PK/PD) studies investigating "absorption, distribution, metabolism, and excretion" (ADME) properties. The “hit-to-lead” process can be achieved by direct modification of the hit molecule or by using a fragment-based approach (fragment-based drug discovery, FBDD) by linking, merging, or expanding hit fragments and evaluation by *in vitro* assays [198, 199]. Under the guidance of conventional, experience-based rules such as the “Rule of Five,” experimental results and *in silico* simulation, such as molecular docking or machine-learning/artificial-intelligence (ML/AI)-based structure optimization and potency prediction, leads are developed into candidates [199]. Candidates are further optimized and screened for better biological and physical properties to be developed into a good drug candidate for further development as an approved medicine [199].

2.4.2. The Methodology of Ligand-based Drug Discovery (LBDD)

Using a known molecule as a scaffold, researchers can make modifications to the scaffold and measure the experimental properties of these derivatives, which is known as LBDD [200]. The visual inspection of the relationship between structures and assayed results is determined and is known as SAR [201]. In general, the goal of LBDD is to optimize a mother molecule based on the pattern from SAR studies to achieve better bioactivity [201]. The accuracy of SAR is rather critical in LBDD, and the conventional SAR study would only present a trend. Quantitative SAR (QSAR) was introduced in the 1960s for more accurate analysis and prediction and will be discussed later. Another evolution in LBDD is the idea of a pharmacophore. The

pharmacophore was preliminarily defined as a molecular framework that carries the essential features responsible for a drug's biological activity and IUPAC later defined the term "pharmacophore" as "the ensemble of steric and electronic features that is necessary to ensure the optimal supramolecular interaction with a specific biological target structure and to trigger (or to block) its biological response" [202] [203]. A pharmacophore can be represented by 2D or 3D mapping with A (H-bond acceptor), D (H-bond donor), R (aromatic ring), H (hydrophobic fragment), N (negative ionized/ionizable), and P (positive ionized/ionizable). Collaborating with SBDD, a pharmacophore could also be modelled *in silico* if the target receptor crystal structure is available. A receptor-based pharmacophore model can be more accurate than mapping as long as key interactions between ligand candidates and the receptor are well-recognized. Moreover, it can be used for screening databases for similarly constructed molecules that may have better plausibility to be hit molecules [204]. A pharmacophore mapping can also be aligned with QSAR modelling to generate novel ligands [205]. On the other hand, further studies on SAR would update and optimize the pharmacophore (An example of SAR collaborating with the pharmacophore study is shown in [206]).

A classical application of the LBDD is bioisosterism, which is referred to as a group of chemical components sharing common physicochemical properties that contributed to similar biological activities [208]. Bioisosteres could be categorized as classical and nonclassical. Classical bioisosteres are defined by Grimm's Hydride Displacement Law and Erlenmeyer's Principle of the Number of Peripheral Electrons and included mono-/di-valent atoms and ring-equivalent replacements; Nonclassical bioisosteres are found using completely different components (e.g., a non-cyclic component and an aromatic component) sharing high similarity in electronic distribution, or different functional groups could serve similar biological roles (e.g., H-bond donor) [208]. However, changing pK_a and electron distribution during the modification would influence the protein-ligand relationship, such as ligand binding orientation [207]. Thus, how to choose a bioisostere correctly to ensure the resulting compound has expected features is important in the future study (rather than randomly screening)

QSAR study is an important and advanced method used in the LBDD. QSAR is developed from the SAR paradox: SAR is about the strong trend among different structures while in the meantime SAR details that similar structures would have similar properties.

However, it is not always true, as the deviation could emerge from a compound as a whole rather than individual fragments [209]. QSAR is the mathematical model based on the correlation that is significant statistically between chemical structures (in the active conformation) that are independent variables and biological activities. The model needs to be treated with an adequate number of molecules with appropriate biological features from the same assay so that it could be equivalently viable (i.e., these features could be either continuous such as Ki, Kd, IC_{50}, etc., or categorically binary, such as active/inactive, toxic/nontoxic, etc.) [209, 210]. Molecules used for the QSAR study should not be autocorrelated to avoid overfitting and internal or external validation should be applied. The strategy for 3D-QSAR included comparative molecular field analysis (CoMFA), comparative binding energy (COMBINE) analysis, comparative molecular surface analysis (CoMSA), etc. A general framework of 3D-QSAR protocols included structural alignment, data generation, data mining, model assessment, and predictions. 4D-, 5D-, and 6D-QSAR studies are also developed to integrate more features such as ligand conformation, ligand flexibility, and the influence of solvents (with the development of machine learning processes) for QSAR model optimization [201, 211, 212, 213].

2.4.3. The Methodology of Structure-based Drug Discovery (SBDD)

Structure-based drug design (SBDD) is used to design bio-active compounds targeting a specific druggable target with the available biologic structure [200]. The idea of SBDD originated in the 1970s when Beddell's group tried to design small molecules to fit in human deoxyhaemoglobin 2,3-diphosphoglycerate (DPG) receptor sites, which Klebe motioned was the only target with the crystal structure that has been studied pharmacologically [214] [215]. In that study, the residues and candidates are designed to interact based on the distances between them, and DPG functional groups are measured and used as the reference to design compound candidates. The size of DPG was also calculated and used as the reference to determine the size of candidates. Thus, for an SBDD project, the protein-ligand interaction and the ligand size (spatial occupancy) are two major concerns. Even though fragment-based NMR/X-Ray screening could be used for SBDD, it is still an auxiliary: it accurately advised the most-preferred binding site for a designated component, but it could be time-consuming and inconvenient; thus, computational *in silico* SBDD with virtual screening is more popular and efficient in the current stage [216]. From the perspective of methodology, compared to the

traditional methods such as HTS and even LBDD, SBDD tries to justify drug design by presenting ligand-protein interactions at the molecular level. Thus, SBDD can not be achieved without clear “ligand acceptor” structures, such as a protein structure of the binding site, which can either be determined by experimental approaches such as NMR or crystallography or *in silico* methods such as homologous modelling. To discover or innovate hit compounds that will interact with the target, the virtual screen with a library containing a significant number of small molecules or the *de novo* design are two major concepts. A molecular docking experiment is performed during the virtual screening or on the compounds from the *de novo* design. Through the molecular docking that accommodates a molecule into the target binding site within a proper orientation calculated by specific mechanisms, we are able to find/design the ligand that exhibits the desired ligand-protein interaction with minimum entropy [216] [217]. SBDD is more dependent on computational recourses to predict or analyze potential interactions as HTS and LBDD are more experiment-oriented [217].

The molecular docking experiment makes it possible to generate protein-ligand complexes based on fictitious binding action. However, in most scenarios, SBDD is used as a rationalizing method to analyze the significance of a certain design or functional group for its influence on drug potency. As mentioned by Ishida et al., quinazolinone derivatives were synthesized and evaluated on PARP1/2 assays. The authors analyzed the binding mode of compound **1e** (8-Methyl-2-{3-[4-(4-fluorophenyl)-3,6-dihydro-1(2*H*)-pyridinyl]propyl}-4(3*H*)-quinazolinone) in the PARP1/2 proteins using X-ray crystallography [181]. The result indicates that, while figuring out the binding orientation of the side chain, the shift from L769 in PARP1 to G314 in PARP2 reduces the hydrophobic region distribution and, as a result, decreases the potency of the compound **1e** inhibiting PARP2. While some PARP2-selective compounds are also reported, the SBDD study suggests that E335 (incorrectly numbered as E311 in the article) and Q332 (incorrectly numbered as Q308 in the article) contribute to the PARP2-selectivity against PARP1 [181]. In this case, SBDD is used more as a validation procedure, rather than an innovation technique.

A simple way to realize SBDD for *de novo* design is the superposition of target compounds for a consensus structure. When developing a novel TAK1 Type II inhibitor, Muraoka et al. superimposed a reported Type I inhibitor onto a known Type II inhibitor to

analyze components that could be remained or eliminated, based on expected ligand–residue interactions from crystal structures [218]. The new compounds employed some novel design, rather than straightforwardly "copy-and-pasting" from old ones, which could be found in traditional LBDD. In this way, the authors had a clear idea of where the functional groups would locate within the target structure or which region (e.g., the hinge region) a component would interact with. As "prototype" compounds, these novel compounds are relatively weak, but the authors argued that the converting methods could be used to develop novel inhibitors for other kinases as well [218].

SBDD should not be restricted as an approach for rationalizing the design of new drugs. With advances *in silico* drug design platforms, virtual screening and molecular docking coupled with scoring functions are more accurate than basic superposition. *In silico,* SBDD needs two major ingredients: a target and a ligand. The target, such as a druggable protein, contains the ligand binding site. A protein structure containing the binding site can be gained experimentally, such as through crystallography, NMR, Cryo-EM, etc., or computationally, such as homologous modelling or AI-based prediction. The ligand used for *in silico* SBDD can be designed by three strategies: (a) using the LBDD strategy to build a molecule based on the known bioactive molecule that could also be seen as a combination of LBDD and SBDD; (b) virtual screening of a small molecule library, which picks out promising fragments that would interact with the protein within the binding site, and these fragments are used as building blocks for the novel molecule; and (c) a *de novo* design from scratch. The ligand is then docked into the protein binding site. During the docking procedure, both the ligand and the protein can be flexible or rigid, or in between, based on the settings and the platform. The docking orientation, in some platforms, can be optimized based on forcefield or free energy perturbance (FEP). The scoring function is used to distinguish binders from non-binders. It relies on several approaches, namely, force field, empirical/knowledge-based, machine learning, etc. With free energy (of binding) calculations, researchers may also be able to tell the difference in potency when candidates share great similarities. The whole procedure can be repeated several times to find the promising compound by comparing *in silico* SBDD results with the experimental ones [219, 220, 221, 222]. A typical *in silico* SBDD to discover a drug candidate can be found from the case reported by the Jorgensen group [221, 223]. The virtual screening of drugs to inhibit SARS-COV-2 main protease brought 42 promising candidates. 17 of them are evaluated in a kinetic assay, and 14 out

of 17 showed good potency. A weak inhibitor perampanel was chosen for further development, guided by the molecular docking result, to generate three analogs with good inhibition capability. Further FEP calculations were performed to optimize the most promising one. As a result, the best candidate is at least 5000-fold more potent than perampanel.

2.4.4. CADD and ML/AIDD: The Perspective of Infrastructure and Technology

For academic users, there are open-source databases containing information on small molecules, proteins, and protein-ligand complexes, as shown in **Table 3**. Apart from the *de novo* design of small molecules, these databases are used for CADD and machine learning/artificial intelligence drug design (ML/AIDD) purposes, such as virtual screening or model training. The in-house database will not be discussed here. The platform for CADD can be either commercially available or open-source/free (for academic usage). Some popular platforms found in the literature are shown in **Table 4** [230]. For these platforms, common (and modern) docking methods include Monte Carlo and molecular dynamics simulations: These simulations use "force field calculations", which consists of different levels of empirical approximation, to achieve tasks such as energy minimization [224]. The types of interaction the force field calculation incorporates include bond vibration, angle vibration, torsion potentials, vdW interactions, and electrostatics [224]. For energy minimization, the algorithm is able to move the atom to decrease energy, which is based on Newton's equations of motion [224]. However, the procedure of energy minimization (especially when performed by the Monte Carlo method) could lead the conformation to an energy trap when it stops calculating at a local energy minimum **Figure 10**. Molecular dynamics simulations can achieve the most stable conformation [225]. Methods like molecular mechanics and quantum mechanics calculation will also improve the accuracy of energy minimization [225]. It is worth noting that the bioactive conformation for either the protein or the ligand, may not possess the minimum energy [225]. Some platforms with more advanced computing power and vast amounts of computing resources are able to achieve FEP for a more accurate prediction, especially for analogs, which would avoid false-positive results that are common in force field calculation [224] [226] [227] [228]. The underlying concept and the accuracy (statistical result) of FEP are shown in **Figure 11** and **Figure 12**. Compared to open-source/free ones, commercial platforms are kept updated. A recent study focused on docking accuracy by comparing top-rated docking results to experimental structures, indicated that

commercial platforms performed slightly better than free ones, especially when there are more rotatable bonds present [230] [231]. It is also mentioned that docking scores that are given by software are not reliable enough to indicate binding affinity [231].

Databases	Description	URL
Pubchem	Molecules with chemical, physical, biological, and other properties	https://pubchem.ncbi.nlm.nih.gov/
ZINC	Commercially available compounds	http://zinc.docking.org/
DrugBank	Molecules with chemical and biological information	https://www.drugbank.ca/
ChemDB	Commercially available compounds and isomers	http://cdb.ics.uci.edu/
CheMBL	Drug-like bioactive molecules with chemical, bioactivity, genomic data	https://ebi.ac.uk/chembl/
Protein Data Bank	Protein/protein–ligand complex crystal structure	https://www.rcsb.org/
PDBbind	Refined PDB files with experimental/ computational data, e.g., binding affinity data	http://www.pdbbind.org.cn/
PubMed	Gene/protein sequence	https://www.ncbi.nlm.nih.gov/
UniProt	Gene/protein sequence	https://www.uniprot.org/
BLAST	Protein alignment	https://blast.ncbi.nlm.nih.gov/Blast.cgi
GenBank	Gene sequecne	https://www.ncbi.nlm.nih.gov/genbank/

Table 3 *Examples of major databases used in CADD/MLDD*

Software and Algorithm	Docking Strategy	License	Last update
AutoDock [239]	Lamarckian genetic algorithm and empirical free energy scoring function	Open-source	2014.8
AutoDock Vina [240]		Open-source	2010.4
AutoDock Vina Extended [240]		Commercial	2021.4
DOCK [241]	Shape-based algorithm	Free	2007
FlexX [242][243]	Incremental construction	Commercial	2004
GOLD [244]	Genetic matching algorithm	Commercial	Unknown
Discovery Studio LigandFit [246]	Monte Carlo simulation	Commercial	Unknown
Schrodinger Maestro GLIDE [247]	Multiple strategies, including force-field-based method with OPLS3/4	Commercial	2020
Molecular Operating Environment (MOE) [248]	Multiple strategies, including force-field-based method with MM/GBVI.	Commercial	2020

Table 4 *Examples of popular CADD platforms.*

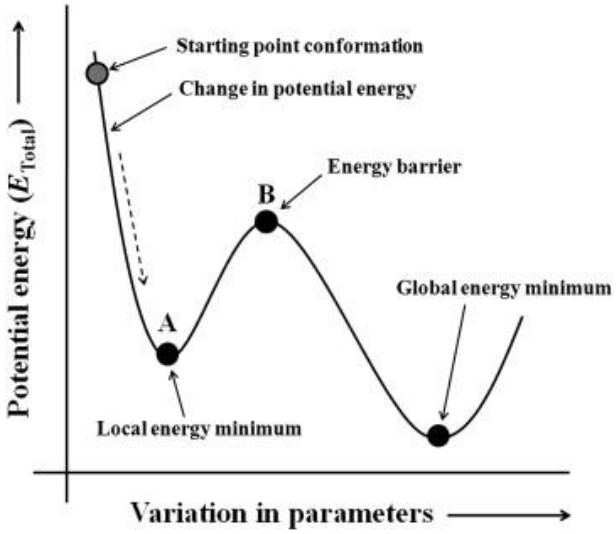

Figure 10 *The scheme of conventional energy minimization. Conventional energy minimization may stop at the local energy minimum closest to the starting molecular conformation, as the vibration will not make a further difference. The local energy minimum may not be the global energy minimum [225].*

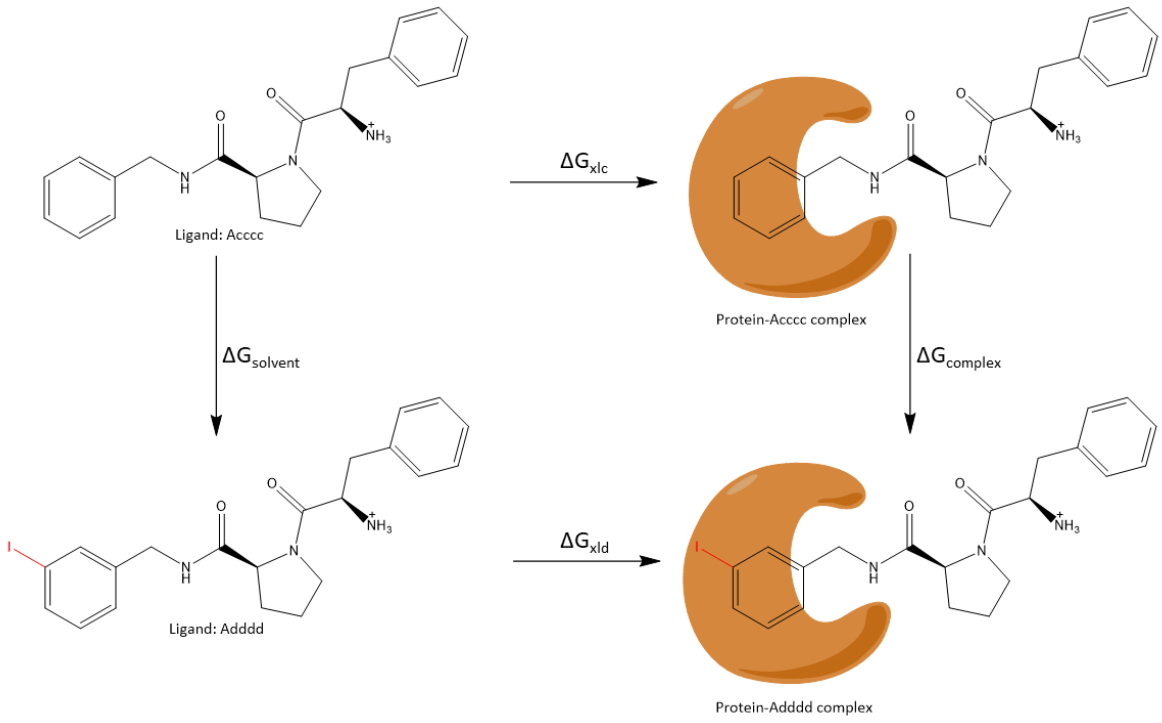

Figure 11 *Underlying concept of FEP calculation. $\Delta G_{solvent}$ is the free energy change when ligand Acccc is converted into Adddd. ΔG_{xlc} and ΔG_{xld} is the free energy change when ligands*

bind to the protein. $\Delta G_{complex}$ is the free energy change of the conversion from protein-Acccc complex to protein-Adddd conversion. By knowing the binding affinity of protein-Acccc complex, FEP can calculate and predict the binding affinity of protein-Adddd complex with this approach [228].

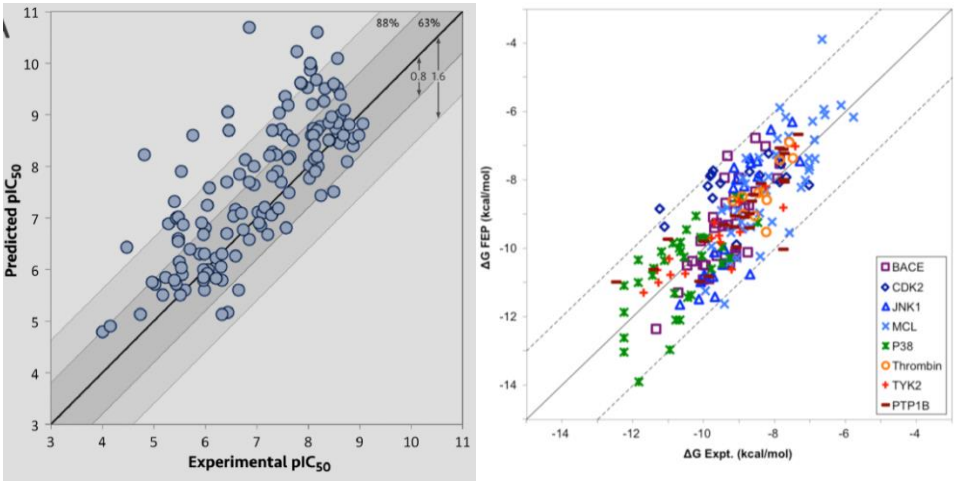

Figure 12 *A summary of the accuracy of the FEP+ prediction.* ***Left****: the correlation between predicted drug potency (pIC_{50}) by FEP+ from Schrodinger against experimental values. "…spanning 7 active drug discovery collaborations with industrial partners…the dark gray band represents 0.8 log unit of error in the predictions and the light gray band represents 1.6 log units of error in the predictions."* ***Right****: the correlation between predicted binding free energy and by FEP against experimental values. Quote "FEP-predicted binding free energies for most of the ligands are within 1.0 kcal/mol of their experimental values, and only nine of 199 studied ligands deviate from their experimental free energies by more than 2 kcal/mol" [228] [229].*

ML/AIDD methods are popular recently, especially after AlphaFold 2 impacted academia by predicting protein structures accurately [232] [233] [234]. It is still questionable whether and how MLDD will shape the pharmaceutical industrial world, as even though this state-of-the-art technology could be used in nearly all aspects of drug discovery and repurposing, we have not seen any report from major pharmaceutical companies of novel drug development mostly based on MLDD [235] [236]. The methodology involved in the MLDD includes the choice of datasets and the model to be constructed and trained. The datasets are open-source or in-house benchmarks with active and inactive molecules. The model uses neural network (NN) algorithms.

An example using a convolutional neural network (CNN) for LBDD is the GENTRL model introduced by InSilico Medicine [237]. It claimed to produce a novel kinase inhibitor with better potency for DDR1 in 46 days and was validated by experimental assays. However, generated molecules shared great similarities with the mother molecule in overall structures and key components, such as the trifluoromethyl group or indazole analogs. Another example of the combination of SBDD and MLDD is AtomNet, which applies CNN, along with benchmarks including the Directory of Useful Decoys Enhanced (DUDE), an in-house constructed ChEMBL-based DUDE-like benchmark and one with inactive molecules, for bioactivity prediction. Generally for SBDD purposes, a grid of 20Å is built in the binding site structure that can be retrieved from PDB, and it is translated into smaller vectorized grids containing features with 1Å-spacing so that each grid represents ligand and protein information in that specific location. The accuracy of the prediction is measured by receiver operating characteristic (ROC), the area under the curve (AUC), and logAUC over benchmarks [238].

2.5. The Conclusion from The Literature Review and Perspective of The Research

As discussed previously, PARP inhibitors can be used as a sensitizer when combined with chemo- or radiotherapy for cancer. By reviewing the PARP1/2 inhibitors, we divide some popular inhibitors that are commercially available or going through clinical trials into five types based on structure layouts (**Table 5**): Type I-III are compounds with carboxamide fused into the ring. Type I compounds are phenanthridinones with two aromatic rings attached to each side of the carboxamide to make tricyclic aromatic compounds; Type II compounds are tricyclic rings with a non-aromatic carboxamide; Type III compounds are bicyclic compounds with only one aromatic ring; Type IV compounds are ones with the carboxamide fused into the “pseudo”-ring; Type V are early generations of inhibitors that are benzamide derivatives. Type III compounds are the most popular ones and great similarity can be found especially in olaparib-like compounds such as olaparib, fluzoparib, and senaparib. Their analogs are widely studied and have superior abilities to inhibit PARP1. Some other inhibitors under this category are AZD2461 [260], XAV-939-like inhibitor MN64, which is also a TNKS-selective inhibitor [261], and DPQ-like inhibitor UPF-1069 [180b]. These compounds can be generally described as two components attached by a linker. rucaparib-like (Type II) and veliparib-like (Type IV) inhibitors are also popular and potent compounds. AG-14361 [262] and NMS-P118 [151] are the other two examples of Type II and Type IV inhibitors, respectively. These compounds majorly occupy the

NI and surrounding areas. According to the categorization, it is noticeable that there is homogeneity in PARP inhibitor drug design. In addition, there hasn’t been a pattern in Type I inhibitors. Thus, it would be interesting to make inhibitors based on phenanthridinone with a novel design, different from current layouts, to find something revolutionary.

I

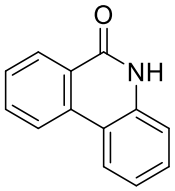

Phenanthridinone
IC_{50} = 377±93nM [249]

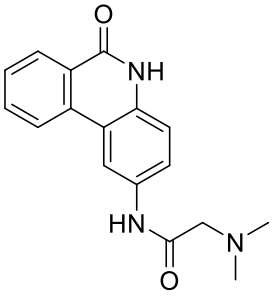

PJ34
IC_{50} = 135±150nM [135]

II

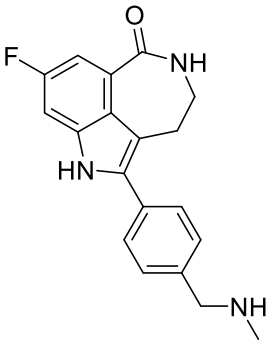

Rucaparib
IC_{50} = 102±160nM [149]

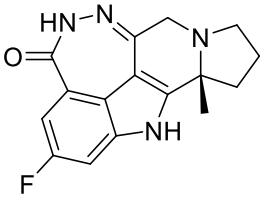

Pamiparib
IC_{50} = 0.900nM [95]

III

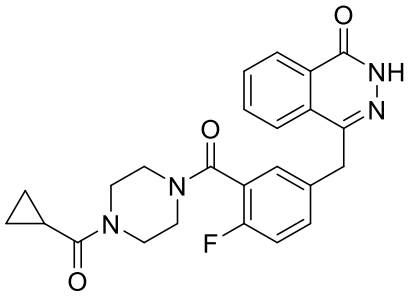

Olaparib
IC_{50} = 7.00±5.7nM [167]

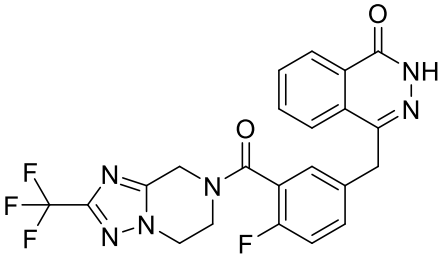

Fluzoparib
IC_{50} = 10.2nM [250]

IV

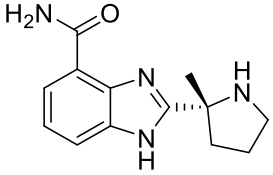

Veliparib
IC_{50} = 9.30±11nM [140a]

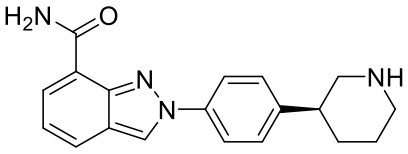

Niraparib
IC_{50} = 30.2±40nM [148]

V

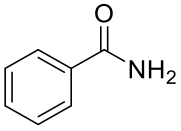

Benzamide
IC_{50} = 15800±7400nM [255]

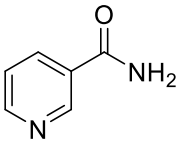

Nicotinamide
IC_{50} = 21000nM [256]

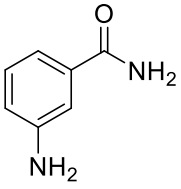

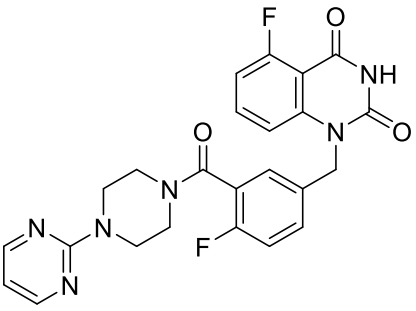

Senaparib
$IC_{50} \approx 0.350nM^{a}$ [251]

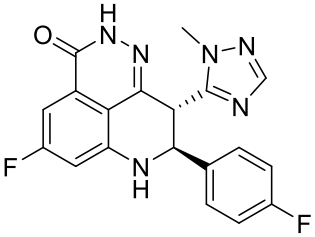

Talazoparib
IC_{50} = 1.90±2.6nM [146]

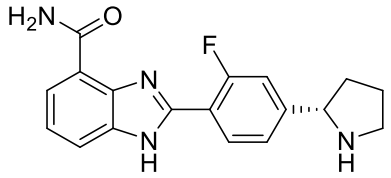

A-966492
IC_{50} = 1.00nM
[254]

3AB
IC_{50} = 20100±11000nM [257]

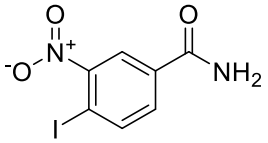

Iniparib
Not considered as a PARP inhibitor anymore [258]

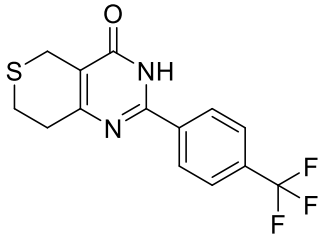

XAV-939
IC_{50} = 917±840nM [147]

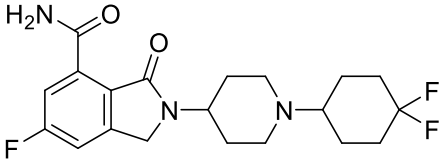

NMS-P118
25.0±15nM [150]

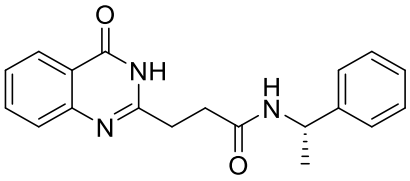

ME0328
IC_{50} = 3410±2200nM [252]

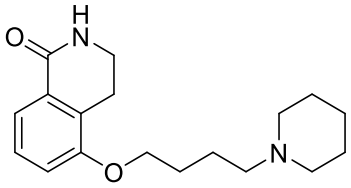

DPQ
IC_{50} = 46.6±6.6nM [253]

Table 5 *A brief outline of PARP inhibitors. This is a brief outline of PARP inhibitors that are FDA-approved, used in clinical trials, or popularly used in research, categorized by structural similarity [259]. (I) Tricyclic benzamide derivatives with a carboxamide ring and a 5H-phenanthridin-6-one motif; (II) Pairwise adjacent tricyclic benzamide derivatives with a carboxamide ring; (III) Bicyclic benzamide derivatives with a carboxamide ring; (IV) Bicyclic benzamide derivatives without a carboxamide ring; (V) Monocyclic benzamide derivatives; (a) Data is an approximation: only an abstract is found.*

The protein-ligand relationship will affect the potency and potentially the PARP-trapping/PARP-DNA binding ability. From crystal structure studies, Type III olaparib-like compounds occupy the NI and a portion of the AD, and Type II and Type IV inhibitors majorly occupy the NI. While the former one is bulky in size; the protein-ligand interaction differs among inhibitors. Meanwhile, both strong catalytic inhibition and PARP-trapping/tight PARP-DNA binding will benefit the cytotoxicity [85, 263]. From the previous review, the PARP-trapping ability, or PARP-DNA binding ability, possibly leads to severe cytotoxicity and is ranked as follows: Type II inhibitors > Type III inhibitors > Type IV inhibitors [85]. Cytotoxicity is particularly significant in the HR-deficient model [263]. As the mechanism is unknown, PARP-trapping or increased PARP-DNA binding ability cannot be predicted by a computational model so far. However, since only Type II and olaparib-like Type III inhibitors are considered as decent "PARP trappers," future PARP inhibitors should be designed in two similar approaches to increase the cytotoxicity, i.e., interacting with the AD or increasing the size of the component inside the NI. On the other hand, there are fewer reported attempts on phenanthridinone analogs even though phenanthridinone analogs are more likely to be promising candidates to achieve both approaches. (**Figure 13**): Some of the benefits of developing phenanthridinone analog can be summarized as follows: 1. Phenanthridinone has a rigid carboxamide ring that will increase the affinity inside the NI; 2. Phenanthridinone is larger in size, compared to benzamide-imidazole analogs and isoquinolinones; 3. The aromatic component attached to the amide NH of phenanthridinone is closer to the HD and the gulch between the D-loop and the HD, as well as important residues, which means a molecule may interact with critical residues a shorter side chain and less rotatable bonds. Thus, it is promising to develop potent PARP inhibitors based on phenanthridinones.

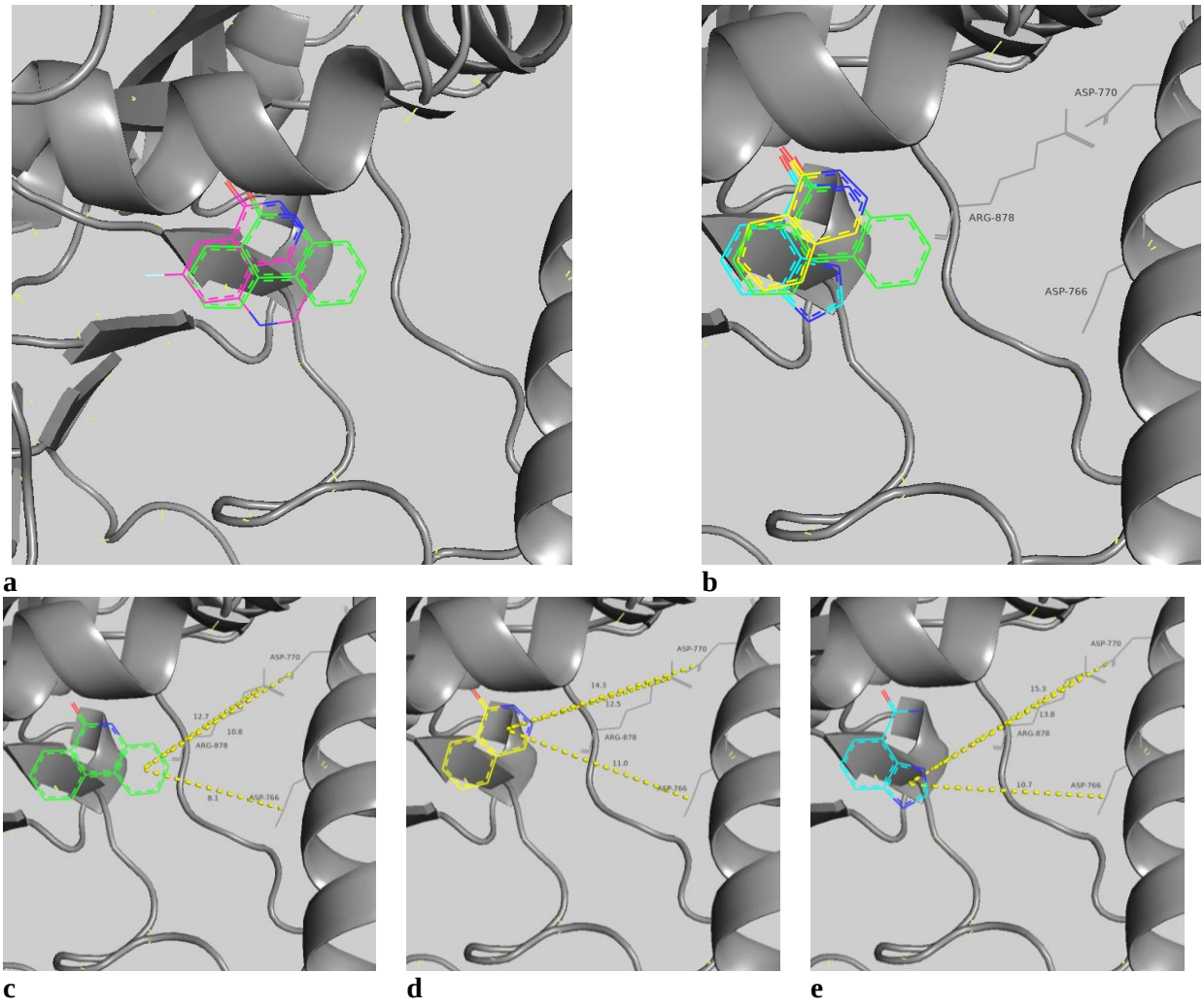

a **b** **c** **d** **e**

Figure 13 *Distances between ligands and interesting residue targets* ***(a)*** *Superposition of the phenanthridinone component of PJ34 (green, PDB ID* ***4UXB****) and the tricyclic component of talazoparib (purple, PDB ID* ***4UND****) as they are similar in size using PyMol. RMSD of two complexes is 0.707Å.* ***(b)*** *Superposition of the phenanthridinone component of PJ34, the benzo-imidazole component of veliparib (blue, PDB ID* ***2RD6****) and the isoquinolinone component of olaparib (yellow, PDB ID* ***7KK4****) as the phenanthridinone is larger.* ***(c)*** *The distances from the phenanthridinone component to D766/D770/R878 are 8.1Å, 10.8Å, and 12.7Å, respectively.* ***(d)*** *The distances from the isoquinolinone component to D766/D770/R878 are 11Å, 12.5Å, and 14.3Å, respectively.* ***(e)*** *The distances from the benzo-imidazole component to D766/D770/R878 are 10.7Å, 13.8Å, and 15.3Å, respectively. Irrelevant side chains are trimmed.*

There are some gaps we realizeD after reviewing current studies, One OF WHICH is whether PARP trapping is a “good” feature to have. For PARPi used for non-CNS disease, increased cytotoxicity with superior PARP-trapping/DNA-binding ability is beneficial for therapeutic effect. In contrast, when PARP inhibitors are used for NAD^+ depletion in the CNS that is common in Parkinson’s disease or brain tumours [264, 265], PARP-trapping is not preferred as the trapping will cause severe side effects due to cytotoxicity [97]. For example, in the development of pamiparib, a problem is a strong PARP trapper may not be a good choice when it is stated that the drug can be used for treating brain tumours [95]. However, the problem seems not to be considered and discussed. For comparison, a non- or weak-trapper such as veliparib can be a good candidate [266]. Furthermore, when designing the inhibitor for CNS treatment, a small molecule structure with a higher logP (e.g., a compound that is mainly composed of aromatic rings) and less efflux liability is preferred to pass the blood-brain barrier (BBB) and remain in the brain [267]. As the study on small PARP inhibitors has almost stopped even though these molecules can be better inhibitors for CNS diseases, it may be a breakthrough if we can figure out how to make novel small PARP inhibitors based on not only benzamide but other similar structures. Secondly, we find few examples where researchers have tried to develop PARP covalent inhibitors, except Iniparib which is a weak inhibitor [268], using warheads such as nitro and boronic acid groups. There are quite a few residues in the binding site that can be interacted with covalently, such as threonine on the middle section of the D-loop. Due to the mechanism of PARP action, a strong reversible covalent inhibitor may be able to enhance PARP-trapping by forming a tight ligand-protein–DNA complex. Using “temporary” covalent bonds with warheads such as a boron- or a nitro- group may strengthen the inhibition.

2.6. Reference

1. Amé et Al. The PARP Superfamily. *BioEssays*, vol. 26, no. 10, Sept. 2004, pp. 1148–48, https://doi.org/10.1002/bies.20142.
2. Haikarainen, Teemu, et al. “Tankyrases: Structure, Function and Therapeutic Implications in Cancer.” *Current Pharmaceutical Design*, vol. 20, no. 41, Oct. 2014, pp. 6472–88, https://doi.org/10.2174/1381612820666140630101525.
3. Perina, Dragutin, et al. “Distribution of Protein Poly(ADP-Ribosyl)Ation Systems across All Domains of Life.” *DNA Repair*, vol. 23, Nov. 2014, pp. 4–16, https://doi.org/10.1016/j.dnarep.2014.05.003.
4. Lu, Alvin Z., et al. "Enabling drug discovery for the PARP protein family through the detection of mono-ADP-ribosylation." *Biochemical Pharmacology*, vol. 167, Sept. 2019, pp. 97–106, https://doi.org/10.1016/j.bcp.2019.05.007.
5. Rasmussen, Marit, et al. "PARP7 and Mono-ADP-Ribosylation Negatively Regulate Estrogen Receptor α Signaling in Human Breast Cancer Cell-wis." *Cells*, vol. 10, no. 3, Mar. 2021, p. 623, https://doi.org/10.3390/cells10030623.
6. Kleine, Henning, et al. "Substrate-assisted catalysis by PARP10 limits its activity to mono-ADP-ribosylation." *Molecular Cell*, vol. 32, no. 1, Oct. 2008, pp. 57–69, https://doi.org/10.1016/j.molcel.2008.08.009.
7. Eisemann, Travis, and John M. Pascal. “Poly(ADP-Ribose) Polymerase Enzymes and the Maintenance of Genome Integrity.” *Cellular and Molecular Life Sciences*, vol. 77, no. 1, Nov. 2019, pp. 19–33, https://doi.org/10.1007/s00018-019-03366-0.
8. Vyas, Sejal, et al. “Family-Wide Analysis of Poly(ADP-Ribose) Polymerase Activity.” *Nature Communications*, vol. 5, no. 1, July 2014, https://doi.org/10.1038/ncomms5426.
9. Ba, Xueqing, and Nisha Jain Garg. "Signaling mechanism of poly (ADP-ribose) polymerase-1 (PARP-1) in inflammatory diseases." *The American Journal of Pathology*, vol. 178, no. 3, Mar. 2011, pp. 946–55, https://doi.org/10.1016/j.ajpath.2010.12.004.
10. Malanga, Maria, and Felix R. Althaus. "The role of poly (ADP-ribose) in the DNA damage signaling network." *Biochemistry and Cell Biology*, vol. 83, no. 3, June 2005, pp. 354–64, https://doi.org/10.1139/o05-038.

11. Huber, Aline, et al. "PARP-1, PARP-2 and ATM in the DNA damage response: functional synergy in mouse development." *DNA Repair*, vol. 3, no. 8–9, Aug. 2004, pp. 1103–08, https://doi.org/10.1016/j.dnarep.2004.06.002.
12. Wahlberg, Elisabet, et al. "Family-wide chemical profiling and structural analysis of PARP and tankyrase inhibitors." *Nature Biotechnology*, vol. 30, no. 3, Feb. 2012, pp. 283–88, https://doi.org/10.1038/nbt.2121.
13. Imlay, James A., and Stuart Linn. "DNA damage and oxygen radical toxicity." *Science*, vol. 240, no. 4857, June 1988, pp. 1302–09, https://doi.org/10.1126/science.3287616.
14. Fu, Dragony, et al."Balancing repair and tolerance of DNA damage caused by alkylating agents." *Nature Reviews Cancer*, vol. 12, no. 2, Jan. 2012, pp. 104–20, https://doi.org/10.1038/nrc3185.
15. Xu, Yang, and Chengtao Her. "Inhibition of topoisomerase (DNA) I (TOP1): DNA damage repair and anticancer therapy." *Biomolecules*, vol. 5, no. 3, July 2015, pp. 1652–70, https://doi.org/10.3390/biom5031652.
16. Lomax, M. E., et al. "Biological consequences of radiation-induced DNA damage: relevance to radiotherapy." *Clinical Oncology*, vol. 25, no. 10, Oct. 2013, pp. 578–85, https://doi.org/10.1016/j.clon.2013.06.007.
17. Sinha, Rajeshwar P., and Donat-P. Häder. "UV-induced DNA damage and repair: a review." *Photochemical & Photobiological Sciences*, vol. 1, no. 4, Mar. 2002, pp. 225–36, https://doi.org/10.1039/b201230h.
18. Toss, A., and L. Cortesi. "Molecular mechanisms of PARP inhibitors in BRCA-related ovarian cancer." *Journal of Cancer Science & Therapy*, vol. 05, no. 11, 2013, https://doi.org/10.4172/1948-5956.1000234.
19. Wei, Huiting, and Xiaochun Yu. "Functions of PARylation in DNA damage repair pathways." *Genomics, Proteomics & Bioinformatics*, vol. 14, no. 3, June 2016, pp. 131–39, https://doi.org/10.1016/j.gpb.2016.05.001.
20. Swindall, Amanda, et al. "PARP-1: Friend or Foe of DNA Damage and Repair in Tumorigenesis?" *Cancers*, vol. 5, no. 4, July 2013, pp. 943–58, https://doi.org/10.3390/cancers5030943.

21. Kouyama, Kenichi, et al. "Single-particle analysis of full-length human poly (ADP-ribose) polymerase 1." *Biophysics and Physicobiology*, vol. 16, 2019, pp. 59–67, https://doi.org/10.2142/biophysico.16.0_59.
22. Steffen, Jamin D., et al. " Fluorescent sensors of PARP-1 structural dynamics and allosteric regulation in response to DNA damage." *Nucleic Acids Research* vol. 44, no. 20, 2016, pp. 9771–9783, https://doi.org/10.1093/nar/gkw710.
23. Steffen, Jamin D., et al. "Structural implications for selective targeting of PARPs." *Frontiers in oncology*, vol. 3, no. 301, 2013, pp. 1–14, https://doi.org/10.3389/fonc.2013.00301.
24. Eustermann, Sebastian, et al. "Structural basis of detection and signaling of DNA single-strand breaks by human PARP-1." *Molecular Cell*, vol. 60, no. 5, Dec. 2015, pp. 742–54, https://doi.org/10.1016/j.molcel.2015.10.032.
25. Dawicki-McKenna, Jennine M., et al. "PARP-1 activation requires local unfolding of an autoinhibitory domain." *Molecular Cell*, vol. 60, no. 5, Dec. 2015, pp. 755–68, https://doi.org/10.1016/j.molcel.2015.10.013.
26. Pandey, Nootan, and Ben E. Black. "Rapid detection and signaling of DNA damage by PARP-1." *Trends in Biochemical Sciences*, vol. 46, no. 9, Sept. 2021, pp. 744–57, https://doi.org/10.1016/j.tibs.2021.01.014.
27. Lilyestrom, Wayne, et al. "Structural and biophysical studies of human PARP-1 in complex with damaged DNA." *Journal of Molecular Biology*, vol. 395, no. 5, Feb. 2010, pp. 983–94, https://doi.org/10.1016/j.jmb.2009.11.062.
28. Rudolph, Johannes, et al. "Probing the conformational changes associated with DNA binding to PARP1." *Biochemistry*, vol. 59, no. 21, May 2020, pp. 2003–11, https://doi.org/10.1021/acs.biochem.0c00256.
29. Gibbs-Seymour, Ian, et al. "HPF1/C4orf27 is a PARP-1-interacting protein that regulates PARP-1 ADP-ribosylation activity." *Molecular Cell*, vol. 62, no. 3, May 2016, pp. 432–42, https://doi.org/10.1016/j.molcel.2016.03.008.
30. Marsischky, Gerald T., et al. “Role of Glutamic Acid 988 of Human Poly-ADP-Ribose Polymerase in Polymer Formation.” *Journal of Biological Chemistry*, vol. 270, no. 7, Feb. 1995, pp. 3247–54, https://doi.org/10.1074/jbc.270.7.3247.

31. Bonfiglio, Juan José, et al. "Serine ADP-ribosylation depends on HPF1." *Molecular Cell*, vol. 65, no. 5, Mar. 2017, pp. 932-940.e6, https://doi.org/10.1016/j.molcel.2017.01.003.
32. Leslie Pedrioli, Deena M., et al. "Comprehensive ADP-ribosylome analysis identifies tyrosine as an ADP-ribose acceptor site." *EMBO Reports*, vol. 19, no. 8, June 2018, https://doi.org/10.15252/embr.201745310.
33. Messner, Simon, et al. "PARP1 ADP-ribosylates lysine residues of the core histone tails." *Nucleic Acids Research*, vol. 38, no. 19, June 2010, pp. 6350–62, https://doi.org/10.1093/nar/gkq463.
34. Talhaoui, Ibtissam, et al. "Poly (ADP-ribose) polymerases covalently modify strand break termini in DNA fragments in vitro." *Nucleic Acids Research*, vol. 44, no. 19, July 2016, pp. 9279–95, https://doi.org/10.1093/nar/gkw675.
35. Vuong, Billy, et al. "NF-κB transcriptional activation by TNFα requires phospholipase C, extracellular signal-regulated kinase 2 and poly (ADP-ribose) polymerase-1." *Journal of Neuroinflammation*, vol. 12, no. 1, Dec. 2015, https://doi.org/10.1186/s12974-015-0448-8.
36. Weaver, Alice N., and Eddy S. Yang. "Beyond DNA repair: additional functions of PARP-1 in cancer." *Frontiers in Oncology*, vol. 3, no. 290, 2013, pp. 1–11, https://doi.org/10.3389/fonc.2013.00290.
37. Bürkle, Alexander. *Poly (ADP-ribosyl) ation*. Springer Science & Business Media, 2008, pp. 13–19.
38. Amé, Jean-Christophe, et al. "PARP-2, A novel mammalian DNA damage-dependent poly (ADP-ribose) polymerase." *Journal of Biological Chemistry*, vol. 274, no. 25, June 1999, pp. 17860–68, https://doi.org/10.1074/jbc.274.25.17860.
39. Gaullier, Guillaume, et al. "Bridging of nucleosome-proximal DNA double-strand breaks by PARP2 enhances its interaction with HPF1." *PloS One*, vol. 15, no. 11, Nov. 2020, p. e0240932, https://doi.org/10.1371/journal.pone.0240932.
40. Obaji, Ezeogo, et al. “Structural Basis for DNA Break Recognition by ARTD2/PARP2.” *Nucleic Acids Research*, vol. 46, no. 22, Oct. 2018, pp. 12154–65, https://doi.org/10.1093/nar/gky927.
41. Riccio, Amanda A., et al. “PARP-2 Domain Requirements for DNA Damage-Dependent Activation and Localization to Sites of DNA Damage.” *Nucleic Acids Research*, vol. 44, no. 4, Dec. 2015, pp. 1691–702, https://doi.org/10.1093/nar/gkv1376.

42. (a) Bilokapic, Silvija, et al. "Bridging of DNA breaks activates PARP2–HPF1 to modify chromatin." *Nature*, vol. 585, no. 7826, Sept. 2020, pp. 609–13, https://doi.org/10.2210/pdb6wz9/pdb. (b) Kurgina, Tatyana A., et al. "Dual function of HPF1 in the modulation of PARP1 and PARP2 activities." *Communications Biology*, vol. 4, no. 1, Nov. 2021, pp. 1–11, https://doi.org/10.1038/s42003-021-02780-0.
43. Obaji, Ezeogo, et al. "Activation of PARP2/ARTD2 by DNA damage induces conformational changes relieving enzyme autoinhibition." *Nature Communications*, vol. 12, no. 1, June 2021, pp. 1–8, https://doi.org/10.1038/s41467-021-23800-x.
44. Schreiber, Valérie, et al. "Poly (ADP-ribose) polymerase-2 (PARP-2) is required for efficient base excision DNA repair in association with PARP-1 and XRCC1." *Journal of Biological Chemistry*, vol. 277, no. 25, June 2002, pp. 23028–36, https://doi.org/10.1074/jbc.m202390200.
45. Karlberg, Tobias, et al. "Crystal structure of the catalytic domain of human PARP2 in complex with PARP inhibitor ABT-888." *Biochemistry*, vol. 49, no. 6, Jan. 2010, pp. 1056–58, https://doi.org/10.1021/bi902079y.
46. Eisemann, Travis, et al. "Tankyrase-1 ankyrin repeats form an adaptable binding platform for targets of ADP-ribose modification." *Structure*, vol. 24, no. 10, Oct. 2016, pp. 1679–92, https://doi.org/10.1016/j.str.2016.07.014.
47. Guettler, Sebastian, et al. "Structural basis and sequence rules for substrate recognition by Tankyrase explain the basis for cherubism disease." *Cell*, vol. 147, no. 6, Dec. 2011, pp. 1340–54, https://doi.org/10.1016/j.cell.2011.10.046.
48. Mariotti, Laura, et al. "Tankyrase requires SAM domain-dependent polymerization to support Wnt-β-catenin signaling." *Molecular Cell*, vol. 63, no. 3, Aug. 2016, pp. 498–513, https://doi.org/10.1016/j.molcel.2016.06.019.
49. Lehtiö, Lari, et al. "Zinc binding catalytic domain of human tankyrase 1." *Journal of Molecular Biology*, vol. 379, no. 1, May 2008, pp. 136–45, https://doi.org/10.1016/j.jmb.2008.03.058.
50. Ahel, Ivan, et al. "Poly (ADP-ribose)-binding zinc finger motifs in DNA repair/checkpoint proteins." *Nature*, vol. 451, no. 7174, Jan. 2008, pp. 81–85, https://doi.org/10.1038/nature06420.

51. DaRosa, Paul A., et al. "Structural insights into SAM domain-mediated tankyrase oligomerization." *Protein Science*, vol. 25, no. 9, July 2016, pp. 1744–52, https://doi.org/10.1002/pro.2968.
52. Fan, Chen, et al. "Regulation of tankyrase activity by a catalytic domain dimer interface." *Biochemical and Biophysical Research Communications*, vol. 503, no. 3, Sept. 2018, pp. 1780–85, https://doi.org/10.1016/j.bbrc.2018.07.113.
53. Huang, Shih-Min A., et al. "Tankyrase inhibition stabilizes axin and antagonizes Wnt signalling." *Nature*, vol. 461, no. 7264, Sept. 2009, pp. 614–20, https://doi.org/10.1038/nature08356.
54. Zhang, Yue, et al. "RNF146 is a poly (ADP-ribose)-directed E3 ligase that regulates axin degradation and Wnt signalling." *Nature Cell Biology*, vol. 13, no. 5, Apr. 2011, pp. 623–29, https://doi.org/10.1038/ncb2222.
55. Cook, Brandoch D., et al. "Role for the related poly (ADP-Ribose) polymerases tankyrase 1 and 2 at human telomeres." *Molecular and Cellular Biology*, vol. 22, no. 1, Jan. 2002, pp. 332–42, https://doi.org/10.1128/mcb.22.1.332-342.2002.
56. Chang, Paul, et al. “Tankyrase-1 Polymerization of Poly(ADP-Ribose) Is Required for Spindle Structure and Function.” *Nature Cell Biology*, vol. 7, no. 11, Oct. 2005, pp. 1133–39, https://doi.org/10.1038/ncb1322.
57. Chang, William, et al. “NuMA Is a Major Acceptor of Poly(ADP-Ribosyl)Ation by Tankyrase 1 in Mitosis.” *Biochemical Journal*, vol. 391, no. 2, Oct. 2005, pp. 177–84, https://doi.org/10.1042/bj20050885.
58. Bae, Jeehyeon, et al. “Tankyrase 1 Interacts with Mcl-1 Proteins and Inhibits Their Regulation of Apoptosis.” *Journal of Biological Chemistry*, vol. 278, no. 7, Feb. 2003, pp. 5195–204, https://doi.org/10.1074/jbc.m201988200.
59. Brightwell, M., and S. Shall. “Poly(Adenosine Diphosphate Ribose) Polymerase InPhysarum Polycephalumnuclei.” *Biochemical Journal*, vol. 125, no. 3, Dec. 1971, p. 67P, https://doi.org/10.1042/bj1250067p.
60. Purnell, Michael R., and W. J. Whish. "Novel inhibitors of poly (ADP-ribose) synthetase." *Biochemical Journal*, vol. 185, no. 3, Mar. 1980, pp. 775–77, https://doi.org/10.1042/bj1850775.

61. Durkacz, Barbara W., et al. "(ADP-ribose) n participates in DNA excision repair." *Nature*, vol. 283, no. 5747, Feb. 1980, pp. 593–96, https://doi.org/10.1038/283593a0.
62. Center for Drug Evaluation and Research. “Drugs.” U.S. Food and Drug Administration, FDA, www.fda.gov/Drugs/.
63. Fu, Dragony, Jennifer A. Calvo, and Leona D. Samson. "Balancing repair and tolerance of DNA damage caused by alkylating agents." *Nature Reviews Cancer*, vol. 12, no. 2, Jan. 2012, pp. 104–20, https://doi.org/10.1038/nrc3185.
64. Ralhan, Ranju, and Jatinder Kaur. "Alkylating agents and cancer therapy." *Expert Opinion on Therapeutic Patents*, vol. 17, no. 9, Sept. 2007, pp. 1061–75, https://doi.org/10.1517/13543776.17.9.1061.
65. Baskar, Rajamanickam, et al. "Cancer and radiation therapy: current advances and future directions." *International Journal of Medical Sciences*, vol. 9, no. 3, 2012, pp. 193–99, https://doi.org/10.7150/ijms.3635.
66. Lesueur, Paul, et al. "Poly-(ADP-ribose)-polymerase inhibitors as radiosensitizers: a systematic review of pre-clinical and clinical human studies." *Oncotarget*, vol. 8, no. 40, July 2017, pp. 69105–24, https://doi.org/10.18632/oncotarget.19079.
67. Norris, Robin E., et al. "Preclinical evaluation of the PARP inhibitor, olaparib, in combination with cytotoxic chemotherapy in pediatric solid tumors." *Pediatric Blood & Cancer*, vol. 61, no. 1, Sept. 2013, pp. 145–50, https://doi.org/10.1002/pbc.24697.
68. Curtin, Nicola J. "PARP inhibitors for cancer therapy." *Expert Reviews in Molecular Medicine*, vol. 7, no. 4, Mar. 2005, pp. 1–20, https://doi.org/10.1017/s146239940500904x.
69. Ellisen, Leif W. "PARP inhibitors in cancer therapy: promise, progress, and puzzles." *Cancer Cell*, vol. 19, no. 2, Feb. 2011, pp. 165–67, https://doi.org/10.1016/j.ccr.2011.01.047.
70. O'Neil, Nigel J., Melanie L. Bailey, and Philip Hieter. "Synthetic lethality and cancer." *Nature Reviews Genetics*, vol. 18, no. 10, June 2017, pp. 613–23, https://doi.org/10.1038/nrg.2017.47.
71. Khodyreva, S. N., and O. I. Lavrik. "Poly (ADP-Ribose) polymerase 1 as a key regulator of DNA repair." *Molecular Biology*, vol. 50, no. 4, July 2016, pp. 580–95, https://doi.org/10.1134/s0026893316040038.

72. Gagne, Jean-Philippe, et al. "Proteome-wide identification of poly (ADP-ribose) binding proteins and poly (ADP-ribose)-associated protein complexes." *Nucleic Acids Research*, vol. 36, no. 22, Nov. 2008, pp. 6959–76, https://doi.org/10.1093/nar/gkn771.
73. Kötter, Annika, et al. "Inhibition of PARP1-dependent end-joining contributes to olaparib-mediated radiosensitization in tumor cells." *Molecular Oncology*, vol. 8, no. 8, July 2014, pp. 1616–25, https://doi.org/10.1016/j.molonc.2014.06.008.
74. Bryant, Helen E., et al. "Specific killing of BRCA2-deficient tumours with inhibitors of poly (ADP-ribose) polymerase." *Nature*, vol. 434, no. 7035, Apr. 2005, pp. 913–17, https://doi.org/10.1038/nature03443.
75. Burdak-Rothkamm, Susanne, and Kai Rothkamm. "DNA Damage Repair Deficiency and Synthetic Lethality for Cancer Treatment." *Trends in Molecular Medicine*, vol. 27, no. 1, Jan. 2021, pp. 91–92, https://doi.org/10.1016/j.molmed.2020.09.011.
76. Lord, Christopher J., and Alan Ashworth. "PARP inhibitors: Synthetic lethality in the clinic." *Science*, vol. 355, no. 6330, Mar. 2017, pp. 1152–58, https://doi.org/10.1126/science.aam7344.
77. Juvekar, Ashish, et al. "Combining a PI3K inhibitor with a PARP inhibitor provides an effective therapy for BRCA1-related breast cancer." *Cancer Discovery*, vol. 2, no. 11, Aug. 2012, pp. 1048–63, https://doi.org/10.1158/2159-8290.cd-11-0336.
78. Zhang, Hao, et al. "Inhibition of tankyrase 1 in human gastric cancer cells enhances telomere shortening by telomerase inhibitors." *Oncology Reports*, vol. 24, no. 4, Sept. 2010, pp. 1059–65, https://doi.org/10.3892/or.2010.1059.
79. Kulak, Ozlem, et al. "Disruption of Wnt/β-catenin signaling and telomeric shortening are inextricable consequences of tankyrase inhibition in human cells." *Molecular and Cellular Biology*, vol. 35, no. 14, May 2015, pp. 2425–35, https://doi.org/10.1128/mcb.00392-15.
80. Hodes, Richard. "Molecular targeting of cancer: telomeres as targets." *Proceedings of the National Academy of Sciences*, vol. 98, no. 14, July 2001, pp. 7649–51, https://doi.org/10.1073/pnas.151267698.
81. Li, Chong, et al. "XAV939 inhibits the proliferation and migration of lung adenocarcinoma A549 cells through the WNT pathway." *Oncology Letters*, vol. 15, no. 6, Apr. 2018, pp. 8973–82, https://doi.org/10.3892/ol.2018.8491.

82. Schatoff, Emma M., et al. “WNT Signaling and Colorectal Cancer.” Current Colorectal *Cancer Reports*, vol. 13, no. 2, Feb. 2017, pp. 101–10, https://doi.org/10.1007/s11888-017-0354-9.
83. Ma, Li, et al. “Tankyrase Inhibitors Attenuate WNT/β-Catenin Signaling and Inhibit Growth of Hepatocellular Carcinoma Cells.” *Oncotarget*, vol. 6, no. 28, June 2015, pp. 25390–401, https://doi.org/10.18632/oncotarget.4455.
84. Murai, Junko, et al. "Stereospecific PARP trapping by BMN 673 and comparison with olaparib and rucaparib." *Molecular Cancer Therapeutics*, vol. 13, no. 2, Dec. 2013, pp. 433–43, https://doi.org/10.1158/1535-7163.mct-13-0803.
85. Murai, Junko, et al. "Trapping of PARP1 and PARP2 by clinical PARP inhibitors." *Cancer Research*, vol. 72, no. 21, Oct. 2012, pp. 5588–99, https://doi.org/10.1158/0008-5472.can-12-2753.
86. Murai, Junko, and Yves Pommier. “Classification of PARP Inhibitors Based on PARP Trapping and Catalytic Inhibition, and Rationale for Combinations with Topoisomerase I Inhibitors and Alkylating Agents.” *Cancer Drug Discovery and Development*, Springer International Publishing, 2015, pp. 261–74, http://dx.doi.org/10.1007/978-3-319-14151-0_10.
87. Murai, Junko, et al. "Rationale for poly (ADP-ribose) polymerase (PARP) inhibitors in combination therapy with camptothecins or temozolomide based on PARP trapping versus catalytic inhibition." *Journal of Pharmacology and Experimental Therapeutics* 349.3 (2014): 408-416.
88. Murai, Junko, et al. "Tyrosyl-DNA phosphodiesterase 1 (TDP1) repairs DNA damage induced by topoisomerases I and II and base alkylation in vertebrate cells." *Journal of Biological Chemistry*, vol. 287, no. 16, Apr. 2012, pp. 12848–57, https://doi.org/10.1074/jbc.m111.333963.
89. Michelena, Jone, et al. "Analysis of PARP inhibitor toxicity by multidimensional fluorescence microscopy reveals mechanisms of sensitivity and resistance." *Nature Communications*, vol. 9, no. 1, July 2018, pp. 1–16, https://doi.org/10.1038/s41467-018-05031-9.
90. Marchand, Jean-Rémy, et al. "Investigating the allosteric reverse signalling of PARP inhibitors with microsecond molecular dynamic simulations and fluorescence

anisotropy." *Biochimica et Biophysica Acta (BBA)-Proteins and Proteomics*, vol. 1844, no. 10, Oct. 2014, pp. 1765–72, https://doi.org/10.1016/j.bbapap.2014.07.012

91. Aoyagi-Scharber, Mika, et al. "Structural basis for the inhibition of poly (ADP-ribose) polymerases 1 and 2 by BMN 673, a potent inhibitor derived from dihydropyridophthalazinone." *Acta Crystallographica Section F Structural Biology Communications*, vol. 70, no. 9, Aug. 2014, pp. 1143–49, https://doi.org/10.1107/s2053230x14015088.
92. Hopkins, Todd A., et al. "Mechanistic dissection of PARP1 trapping and the impact on in vivo tolerability and efficacy of PARP inhibitors." *Molecular Cancer Research*, vol. 13, no. 11, July 2015, pp. 1465–77, https://doi.org/10.1158/1541-7786.mcr-15-0191-t.
93. Blessing, Charlotte, et al. "The oncogenic helicase ALC1 regulates PARP inhibitor potency by trapping PARP2 at DNA breaks." *Molecular Cell*, vol. 80, no. 5, Dec. 2020, pp. 862-875.e6, https://doi.org/10.1016/j.molcel.2020.10.009.
94. Zandarashvili, Levani, et al. "Structural basis for allosteric PARP-1 retention on DNA breaks." *Science*, vol. 368, no. 6367, Apr. 2020, pp. 1–10, https://doi.org/10.1126/science.aax6367.
95. Xiong, Yao, et al. "Pamiparib is a potent and selective PARP inhibitor with unique potential for the treatment of brain tumor." *Neoplasia*, vol. 22, no. 9, Sept. 2020, pp. 431–40, https://doi.org/10.1016/j.neo.2020.06.009.
96. Ryan, Kevin, et al. "Dissecting the molecular determinants of clinical PARP1 inhibitor selectivity for tankyrase1." *Journal of Biological Chemistry*, vol. 296, no. 100251, Jan. 2021, pp. 1–13, https://doi.org/10.1074/jbc.ra120.016573.
97. Sinha, Asha, Sachin Katyal, and Tiina M. Kauppinen. "PARP-DNA trapping ability of PARP inhibitors jeopardizes astrocyte viability: Implications for CNS disease therapeutics." *Neuropharmacology*, vol. 187, no. 108502, Apr. 2021, pp. 1–13, https://doi.org/10.1016/j.neuropharm.2021.108502.
98. Kim, Chiho, Chuo Chen, and Yonghao Yu. "Avoid the trap: Targeting PARP1 beyond human malignancy." *Cell Chemical Biology*, vol. 28, no. 4, Apr. 2021, pp. 456–62, https://doi.org/10.1016/j.chembiol.2021.02.004.

99. Ferraris, Dana V. "Evolution of poly (ADP-ribose) polymerase-1 (PARP-1) inhibitors. From concept to clinic." *Journal of medicinal chemistry*, vol. 53, no. 12, Apr. 2010, pp. 4561–84, https://doi.org/10.1021/jm100012m.
100. Cepeda, Victoria, et al. "Poly (ADP-ribose) polymerase-1 (PARP-1) inhibitors in cancer chemotherapy." *Recent Patents on Anti-Cancer Drug Discovery*, vol. 1, no. 1, Jan. 2006, pp. 39–53, https://doi.org/10.2174/157489206775246430.
101. Chen, Ying, Lei Zhang, and Quan Hao. "Olaparib: a promising PARP inhibitor in ovarian cancer therapy." *Archives of Gynecology and Obstetrics*, vol. 288, no. 2, Apr. 2013, pp. 367–74, https://doi.org/10.1007/s00404-013-2856-2.
102. Hughes, David L. "Patent review of manufacturing routes to recently approved PARP inhibitors: olaparib, rucaparib, and niraparib." *Organic Process Research & Development*, vol. 21, no. 9, Aug. 2017, pp. 1227–44, https://doi.org/10.1021/acs.oprd.7b00235.
103. Shen, Yuqiao, et al. "BMN 673, a novel and highly potent PARP1/2 inhibitor for the treatment of human cancers with DNA repair deficiency." *Clinical Cancer Research*, vol. 19, no. 18, July 2013, pp. 5003–15, https://doi.org/10.1158/1078-0432.ccr-13-1391.
104. Lou, Xi-yu, et al. "Synthesis of olaparib derivatives and their antitumor activities." *Chemical Research in Chinese Universities*, vol. 29, no. 2, Mar. 2013, pp. 231–35, https://doi.org/10.1007/s40242-013-2448-5.
105. Abstract: Cao, Junning, et al. "Pooled analysis of phase I dose-escalation and dose cohort expansion studies of IMP4297, a novel PARP inhibitor, in Chinese and Australian patients with advanced solid tumors." *Journal of Clinical Oncology*, vol. 37, no. 15, May 2019, pp. 3059–3059, https://doi.org/10.1200/jco.2019.37.15_suppl.3059.
106. Colombo, Ilaria, Stephanie Lheureux, and Amit Manulal Oza. "Rucaparib: a novel PARP inhibitor for BRCA advanced ovarian cancer." *Drug Design, Development and Therapy*, vol. 12, Mar. 2018, pp. 605–17, https://doi.org/10.2147/dddt.s130809.
107. Li, Xiaofeng, et al. "Disposition and drug-drug interaction potential of veliparib (ABT-888), a novel and potent inhibitor of poly (ADP-ribose) polymerase." *Drug Metabolism and Disposition*, vol. 39, no. 7, Mar. 2011, pp. 1161–69, https://doi.org/10.1124/dmd.110.037820.

108. Bridges, Kathleen A., et al. "Niraparib (MK-4827), a novel poly (ADP-Ribose) polymerase inhibitor, radiosensitizes human lung and breast cancer cells." *Oncotarget*, vol. 5, no. 13, June 2014, pp. 5076–86, https://doi.org/10.18632/oncotarget.2083.

109. Lord, Anna-Marie, et al. "Design, synthesis, and evaluation in vitro of quinoline-8-carboxamides, a new class of poly (adenosine-diphosphate-ribose) polymerase-1 (PARP-1) inhibitor." *Journal of Medicinal Chemistry*, vol. 52, no. 3, Dec. 2008, pp. 868–77, https://doi.org/10.1021/jm8013629.

110. Abdelkarim, Galaleldin E., et al. "Protective effects of PJ34, a novel, potent inhibitor of poly (ADP-ribose) polymerase (PARP) in in vitro and in vivo models of stroke." *International Journal of Molecular Medicine*, vol. 7, no. 3, Mar. 2001, pp. 255–60, https://doi.org/10.3892/ijmm.7.3.255.

111. Thorsell, Ann-Gerd, et al. "Structural basis for potency and promiscuity in poly (ADP-ribose) polymerase (PARP) and tankyrase inhibitors." *Journal of Medicinal Chemistry*, vol. 60, no. 4, Dec. 2016, pp. 1262–71, https://doi.org/10.1021/acs.jmedchem.6b00990.

112. He, Xin, et al. "Design, synthesis and anticancer activities evaluation of novel 5H-dibenzo [b, e] azepine-6, 11-dione derivatives containing 1, 3, 4-oxadiazole units." *Bioorganic & Medicinal Chemistry Letters*, vol. 28, no. 5, Mar. 2018, pp. 847–52, https://doi.org/10.1016/j.bmcl.2018.02.008.

113. Examples of using 6(5*H*)-Phenanthridinone as the core structure: (a) Li, Jia-He, et al. "Synthesis of substituted 5-[*H*]-phenanthridin-6-ones as potent poly (ADP-ribose) polymerase-1 (PARP1) inhibitors." *Bioorganic & Medicinal Chemistry Letters*, vol. 11, no. 13, July 2001, pp. 1687–90, https://doi.org/10.1016/s0960-894x(01)00281-5. (b) Ferraris, Dana, et al. "Design and synthesis of poly ADP-ribose polymerase-1 inhibitors. 2. Biological evaluation of aza-5 [*H*]-phenanthridin-6-ones as potent, aqueous-soluble compounds for the treatment of ischemic injuries." *Journal of Medicinal Chemistry*, vol. 46, no. 14, June 2003, pp. 3138–51, https://doi.org/10.1021/jm030109s. (c) Ferraris, Dana, et al. "Design and synthesis of poly (ADP-ribose) polymerase-1 (PARP-1) inhibitors. Part 3: In vitro evaluation of 1, 3, 4, 5-tetrahydro-benzo [c][1,6]-and [c][1,7]-naphthyridin-6-ones." *Bioorganic & Medicinal Chemistry Letters*, vol. 13, no. 15, Aug. 2003, pp. 2513–18, https://doi.org/10.1016/s0960-894x(03)00465-7.

114. Some examples: (a) National Center for Biotechnology Information. "PubChem Compound Summary for CID 136242913, FC1=CC=2NC=3Cncc=4C3C2C(=C1)C(NN4)=O" *PubChem*, https://pubchem.ncbi.nlm.nih.gov/compound/136242913. Accessed 1 July, 2021. (b) National Center for Biotechnology Information. "PubChem Compound Summary for CID 687511" *PubChem*, https://pubchem.ncbi.nlm.nih.gov/compound/687511. Accessed 1 July, 2021. (c) National Center for Biotechnology Information. "PubChem Compound Summary for CID 44407525" *PubChem*, https://pubchem.ncbi.nlm.nih.gov/compound/44407525. Accessed 1 July, 2021. (d) National Center for Biotechnology Information. "PubChem Compound Summary for CID 25190931" *PubChem*, https://pubchem.ncbi.nlm.nih.gov/compound/25190931. Accessed 1 July, 2021.

115. Ferrigno, Federica, et al. "Development of substituted 6-[4-fluoro-3-(piperazin-1-ylcarbonyl) benzyl]-4, 5-dimethylpyridazin-3 (2H)-ones as potent poly (ADP–ribose) polymerase-1 (PARP-1) inhibitors active in BRCA deficient cells." *Bioorganic & Medicinal Chemistry Letters*, vol. 20, no. 3, Feb. 2010, pp. 1100–05, https://doi.org/10.1016/j.bmcl.2009.11.087.

116. Shen, Yuqiao, et al. "Trapping poly (ADP-ribose) polymerase." *Journal of Pharmacology and Experimental Therapeutics*, vol. 353, no. 3, Mar. 2015, pp. 446–57, https://doi.org/10.1124/jpet.114.222448.

117. PDB ID 4UXB; PDNB ID 4UND. Thorsell, Ann-Gerd, et al. "Structural basis for potency and promiscuity in poly (ADP-ribose) polymerase (PARP) and tankyrase inhibitors." *Journal of Medicinal Chemistry*, vol. 60, no. 4, Dec. 2016, pp. 1262–71, https://doi.org/10.1021/acs.jmedchem.6b00990.

118. Kirubakaran, Palani, et al. "Molecular insights on TNKS1/TNKS2 and inhibitor-IWR1 interactions." *Molecular BioSystems*, vol. 10, no. 2, 2014, pp. 281–93, https://doi.org/10.1039/c3mb70305c.

119. Tian, Xiao-Hong, et al. "XAV939, a tankyrase 1 inhibitior, promotes cell apoptosis in neuroblastoma cell lines by inhibiting Wnt/β-catenin signaling pathway." *Journal of Experimental & Clinical Cancer Research*, vol. 32, no. 1, Dec. 2013, https://doi.org/10.1186/1756-9966-32-100.

120. D'Andrea, Alan D. "Mechanisms of PARP inhibitor sensitivity and resistance." *DNA Repair*, vol. 71, Nov. 2018, pp. 172–76, https://doi.org/10.1016/j.dnarep.2018.08.021.
121. Chaudhuri, Arnab Ray, et al. "Replication fork stability confers chemoresistance in BRCA-deficient cells." *Nature*, vol. 535, no. 7612, July 2016, pp. 382–87, https://doi.org/10.1038/nature18325.
122. Liu, Lu, et al. "ALDH1A1 contributes to PARP inhibitor resistance via enhancing DNA repair in BRCA2−/− ovarian cancer cells." *Molecular Cancer Therapeutics*, vol. 19, no. 1, Sept. 2019, pp. 199–210, https://doi.org/10.1158/1535-7163.mct-19-0242.
123. Barber, Louise J., et al. "Secondary mutations in BRCA2 associated with clinical resistance to a PARP inhibitor." *The Journal of Pathology*, vol. 229, no. 3, Jan. 2013, pp. 422–29, https://doi.org/10.1002/path.4140.
124. Jaspers, Janneke E., et al. "Loss of 53BP1 causes PARP inhibitor resistance in Brca1-mutated mouse mammary tumors." *Cancer Discovery*, vol. 3, no. 1, Oct. 2012, pp. 68–81, https://doi.org/10.1158/2159-8290.cd-12-0049.
125. Ter Brugge, Petra, et al. "Mechanisms of therapy resistance in patient-derived xenograft models of BRCA1-deficient breast cancer." *Journal of the National Cancer Institute*, vol. 108, no. 11, July 2016, p. djw148, https://doi.org/10.1093/jnci/djw148.
126. Collot, Thomas, et al. "PARP inhibitor resistance and TP53 mutations in patients treated with olaparib for BRCA-mutated cancer: Four case reports." *Molecular Medicine Reports*,vol. 23, no. 75, Nov. 2020, pp. 1–8, https://doi.org/10.3892/mmr.2020.11713.
127. Zhang, Aili, et al. "The p53-binding protein 1-Tudor-interacting repair regulator complex participates in the DNA damage response." *Journal of Biological Chemistry*, vol. 292, no. 16, Apr. 2017, pp. 6461–67, https://doi.org/10.1074/jbc.m117.777474.
128. Kim, Yevgeniy, et al. "Reverse the resistance to PARP inhibitors." *International Journal of Biological Sciences*, vol. 13, no. 2, 2017, pp. 198–208, https://doi.org/10.7150/ijbs.17240.
129. Pettitt, Stephen J., et al. "Genome-wide and high-density CRISPR-Cas9 screens identify point mutations in PARP1 causing PARP inhibitor resistance." *Nature Communications*, vol. 9, no. 1, May 2018, https://doi.org/10.1038/s41467-018-03917-2.
130. Antolín, Albert A., and Jordi Mestres. "Linking off-target kinase pharmacology to the differential cellular effects observed among PARP inhibitors." *Oncotarget*, vol. 5, no. 10, Mar. 2014, pp. 3023–28, https://doi.org/10.18632/oncotarget.1814.

131. Antolin, Albert A., et al. "*The off-target kinase landscape of clinical PARP inhibitors*." Cold Spring Harbor Laboratory, 14 Jan. 2019, pp. 1–34, http://dx.doi.org/10.1101/520023.
132. Gohlke, Bjoern-Oliver, et al. "2D and 3D similarity landscape analysis identifies PARP as a novel off-target for the drug Vatalanib." *BMC Bioinformatics, vol. 16, no. 1, Sept. 2015, pp. 1–9, https://doi.org/10.1186/s12859-015-0730-x*.
133. Berman, Helen M., et al. "The protein data bank." *Nucleic Acids Research, vol. 28, no. 1, Jan. 2000, pp. 235–42, https://doi.org/10.1093/nar/28.1.235*.
134. Manasaryan, Garri, et al. "Bioinformatic Analysis of the Nicotinamide Binding Site in Poly (ADP-Ribose) Polymerase Family Proteins." *Cancers*,vol. 13, no. 6, Mar. 2021, pp. 1–16, https://doi.org/10.3390/cancers13061201.
135. National Center for Biotechnology Information. "PubChem Compound Summary for CID 4858" *PubChem*, https://pubchem.ncbi.nlm.nih.gov/compound/pj34. Accessed 14 July, 2021.
136. Canan, Stacie S. "*Structure Based Design of PARP Inhibitors.*" Cancer Drug Discovery and Development, Springer International Publishing, 2015, pp. 205–21, http://dx.doi.org/10.1007/978-3-319-14151-0_8.
137. Miyashiro, Julie, et al. "Synthesis and SAR of novel tricyclic quinoxalinone inhibitors of poly (ADP-ribose) polymerase-1 (PARP-1)." *Bioorganic & Medicinal Chemistry Letters*, vol. 19, no. 15, Aug. 2009, pp. 4050–54, https://doi.org/10.1016/j.bmcl.2009.06.016.
138. Penning, Thomas D., et al. "Discovery of the poly (ADP-ribose) polymerase (PARP) inhibitor 2-[(R)-2-methylpyrrolidin-2-yl±-1 H-benzimidazole-4-carboxamide (ABT-888) for the treatment of cancer." *Journal of Medicinal Chemistry*, vol. 52, no. 2, Dec. 2008, pp. 514–23, https://doi.org/10.1021/jm801171j.
139. Tong, Yunsong, et al. "Synthesis and evaluation of a new generation of orally efficacious benzimidazole-based poly (ADP-ribose) polymerase-1 (PARP-1) inhibitors as anticancer agents." *Journal of Medicinal Chemistry, vol. 52, no. 21, Oct. 2009, pp. 6803–13, https://doi.org/10.1021/jm900697r*.
140. (a) National Center for Biotechnology Information. "PubChem Compound Summary for CID 11960529, Veliparib" *PubChem*,

https://pubchem.ncbi.nlm.nih.gov/compound/Veliparib. Accessed 6 July, 2021. (b) Park, C.H. *PARP Complexed with A861695*. Sept. 2008, https://doi.org/10.2210/pdb2rd6/pdb b.

141. Gandhi, Viraj B., et al. "Discovery and SAR of substituted 3-oxoisoindoline-4-carboxamides as potent inhibitors of poly (ADP-ribose) polymerase (PARP) for the treatment of cancer." *Bioorganic & Medicinal Chemistry Letters*, vol. 20, no. 3, Feb. 2010, pp. 1023–26, https://doi.org/10.1016/j.bmcl.2009.12.042.
142. Penning, Thomas D., et al. "Optimization of phenyl-substituted benzimidazole carboxamide poly (ADP-ribose) polymerase inhibitors: identification of (S)-2-(2-fluoro-4-(pyrrolidin-2-yl) phenyl)-1 H-benzimidazole-4-carboxamide (A-966492), a highly potent and efficacious inhibitor." *Journal of Medicinal Chemistry*, vol. 53, no. 8, Mar. 2010, pp. 3142–53, https://doi.org/10.1021/jm901775.
143. (a) Lindgren, Anders EG, et al. "PARP inhibitor with selectivity toward ADP-ribosyltransferase ARTD3/PARP3." *ACS Chemical Biology*, vol. 8, no. 8, June 2013, pp. 1698–703, https://doi.org/10.1021/cb4002014. (b) National Center for Biotechnology Information. "PubChem Compound Summary for CID 135400457, 2-Methyl-4(3H)-quinazolinone" *PubChem*, https://pubchem.ncbi.nlm.nih.gov/compound/2-Methyl-4_3H_-quinazolinone. Accessed 6 July, 2021.
144. Ye, Na, et al. "Design, synthesis, and biological evaluation of a series of benzo [de±[1, 7± naphthyridin-7 (8 H)-ones bearing a functionalized longer chain appendage as novel PARP1 inhibitors." *Journal of Medicinal Chemistry*, vol. 56, no. 7, Mar. 2013, pp. 2885–903, https://doi.org/10.1021/jm301825t.
145. Gangloff, Anthony R., et al. "Discovery of novel benzo [b±[1, 4± oxazin-3 (4H)-ones as poly (ADP-ribose) polymerase inhibitors." *Bioorganic & Medicinal Chemistry Letters*, vol. 23, no. 16, Aug. 2013, pp. 4501–05, https://doi.org/10.1016/j.bmcl.2013.06.055
146. National Center for Biotechnology Information. "PubChem Compound Summary for CID 135565082, Talazoparib" *PubChem*, https://pubchem.ncbi.nlm.nih.gov/compound/Talazoparib. Accessed 6 July, 2021.
147. National Center for Biotechnology Information. "PubChem Compound Summary for CID 135418940" *PubChem*, https://pubchem.ncbi.nlm.nih.gov/compound/xav-939. Accessed 6 July, 2021.

148. National Center for Biotechnology Information. "PubChem Compound Summary for CID 24958200, Niraparib" *PubChem*, https://pubchem.ncbi.nlm.nih.gov/compound/Niraparib. Accessed 6 July, 2021.
149. National Center for Biotechnology Information. "PubChem Compound Summary for CID 9931954, Rucaparib" *PubChem*, https://pubchem.ncbi.nlm.nih.gov/compound/Rucaparib. Accessed 6 July, 2021.
150. National Center for Biotechnology Information. "PubChem Compound Summary for CID 49843531" *PubChem*, https://pubchem.ncbi.nlm.nih.gov/compound/nms-p118. Accessed 6 July, 2021.
151. Papeo, Gianluca, et al. "Discovery of 2-[1-(4, 4-difluorocyclohexyl) piperidin-4-yl±-6-fluoro-3-oxo-2, 3-dihydro-1 H-isoindole-4-carboxamide (NMS-P118): a potent, orally available, and highly selective parp-1 inhibitor for cancer therapy." *Journal of Medicinal Chemistry*, vol. 58, no. 17, Aug. 2015, pp. 6875–98, https://doi.org/10.1021/acs.jmedchem.5b00680.
152. Cao, R., et al. *Structure of Human PARP1 Catalytic Domain Bound to a Quinazoline-2,4(1H,3H)-Dione Inhibitor*. Dec. 2016, https://doi.org/10.2210/pdb5kpn/pdb..
153. Cao, R., et al. *Structure of Human PARP1 Catalytic Domain Bound to a Quinazoline-2,4(1H,3H)-Dione Inhibitor*. Dec. 2016, https://doi.org/10.2210/pdb5KPP/pdb.
154. Cao, R., et al. *Structure of Human PARP1 Catalytic Domain Bound to a Quinazoline-2,4(1H,3H)-Dione Inhibitor*. Dec. 2016, https://doi.org/10.2210/pdb5KPQ/pdb.
155. Cao, R., et al. *Structure of Human PARP1 Catalytic Domain Bound to a Quinazoline-2,4(1H,3H)-Dione Inhibitor*. Dec. 2016, https://doi.org/10.2210/pdb5WRQ/pdb.
156. Cao, R., et al. *Structure of Human PARP1 Catalytic Domain Bound to a Quinazoline-2,4(1H,3H)-Dione Inhibitor*. Dec. 2016, https://doi.org/10.2210/pdb5WRY/pdb.
157. Cao, R., et al. *Structure of Human PARP1 Catalytic Domain Bound to a Quinazoline-2,4(1H,3H)-Dione Inhibitor*. Dec. 2016, https://doi.org/10.2210/pdb5WRZ/pdb.
158. Cao, R., et al. *Structure of Human PARP1 Catalytic Domain Bound to a Quinazoline-2,4(1H,3H)-Dione Inhibitor*. Dec. 2016, https://doi.org/10.2210/pdb5WS0/pdb.
159. Cao, R., et al. *Structure of Human PARP1 Catalytic Domain Bound to a Quinazoline-2,4(1H,3H)-Dione Inhibitor*. Dec. 2016, https://doi.org/10.2210/pdb5WS1/pdb.

160. Cao, R., et al. *Structure of Human PARP1 Catalytic Domain Bound to a Quinazoline-2,4(1H,3H)-Dione Inhibitor*. Dec. 2016, https://doi.org/10.2210/pdb5WTC/pdb.

161. Chen, Xuxing, et al. "Design and synthesis of 2-(4, 5, 6, 7-tetrahydrothienopyridin-2-yl)-benzoimidazole carboxamides as novel orally efficacious Poly (ADP-ribose) polymerase (PARP) inhibitors." *European Journal of Medicinal Chemistry*, vol. 145, Feb. 2018, pp. 389–403, https://doi.org/10.1016/j.ejmech.2018.01.018.

162. Karlberg, T., et al. Human PARP1 (ARTD1) - Catalytic Domain in Complex with Inhibitor ME0527. May 2019, https://doi.org/10.2210/pdb6GHK/pdb.

163. Jagtap, Prakash G., et al. "The discovery and synthesis of novel adenosine substituted 2, 3-dihydro-1H-isoindol-1-ones: potent inhibitors of poly (ADP-ribose) polymerase-1 (PARP-1)." *Bioorganic & Medicinal Chemistry Letters, vol. 14, no. 1, Jan. 2004, pp. 81–85, https://doi.org/10.1016/j.bmcl.2003.10.007*.

164. Kinoshita, Takayoshi. "Inhibitor-induced structural change of the active site of human poly (ADP-ribose) polymerase." *Nihon Kessho Gakkaishi*, vol. 46, no. 6, 2004, pp. 421–25, https://doi.org/10.5940/jcrsj.46.421.

165. Hattori, Kouji, et al. "Rational approaches to discovery of orally active and brain-penetrable quinazolinone inhibitors of poly (ADP-ribose) polymerase." *Journal of Medicinal Chemistry*, vol. 47, no. 17, July 2004, pp. 4151–54, https://doi.org/10.1021/jm0499256.

166. Iishita, Akinori, et al. "Discovery of quinazolinone and quinoxaline derivatives as potent and selective poly (ADP-ribose) polymerase-1/2 inhibitors." *FEBS Letters*, vol. 579, no. 6, Jan. 2005, pp. 1389–93, https://doi.org/10.1016/j.febslet.2005.01.036.

167. National Center for Biotechnology Information. "PubChem Compound Summary for CID 23725625, olaparib" *PubChem*, https://pubchem.ncbi.nlm.nih.gov/compound/Olaparib. Accessed 6 July, 2021.

168. a) Corresponding PDB IDs and structure publications are cited for each case; b) Sehnal, David, et al. "Mol* Viewer: modern web app for 3D visualization and analysis of large biomolecular structures." *Nucleic Acids Research*, vol. 49, no. W1, May 2021, pp. W431–37, https://doi.org/10.1093/nar/gkab314.

169. Langelier, Marie-France, et al. "NAD+ analog reveals PARP-1 substrate-blocking mechanism and allosteric communication from catalytic center to DNA-binding

domains." *Nature Communications*, vol. 9, no. 1, Feb. 2018, pp. 1–13, https://doi.org/10.1038/s41467-018-03234-8.

170. Tomassi, Stefano, et al. "From PARP1 to TNKS2 inhibition: a structure-based approach." *ACS Medicinal Chemistry Letters*, vol. 11, no. 5, Feb. 2020, pp. 862–68, https://doi.org/10.1021/acsmedchemlett.9b00654
171. Romashov, Leonid V., et al. "Rational design and synthesis of new PARP1 inhibitors." *Mendeleev Communications*, vol. 22, no. 1, Jan. 2012, pp. 15–17, https://doi.org/10.1016/j.mencom.2012.01.005.
172. Aoyagi-Scharber, Mika, et al. "Structural basis for the inhibition of poly (ADP-ribose) polymerases 1 and 2 by BMN 673, a potent inhibitor derived from dihydropyridophthalazinone." *Acta Crystallographica Section F Structural Biology Communications*, vol. 70, no. 9, Aug. 2014, pp. 1143–49, https://doi.org/10.1107/s2053230x14015088.
173. Spiegel, Jacob O., Bennett Van Houten, and Jacob D. Durrant. "PARP1: Structural Insights and Pharmacological Targets for Inhibition." *DNA Repair*, vol. 103, no. 103125, July 2021, pp. 1–14, https://doi.org/10.1016/j.dnarep.2021.103125..
174. Yélamos, José, Valérie Schreiber, and Françoise Dantzer. "Toward specific functions of poly (ADP-ribose) polymerase-2." *Trends in Molecular Medicine*, vol. 14, no. 4, Apr. 2008, pp. 169–78, https://doi.org/10.1016/j.molmed.2008.02.003.
175. Patel, Maulik R., et al. "Discovery and Structure–Activity Relationship of Novel 2, 3-Dihydrobenzofuran-7-carboxamide and 2, 3-Dihydrobenzofuran-3 (2 H)-one-7-carboxamide Derivatives as Poly (ADP-ribose) polymerase-1 Inhibitors." *Journal of Medicinal Chemistry*, vol. 57, no. 13, June 2014, pp. 5579–601, https://doi.org/10.1021/jm5002502.
176. Sutanto, Fandi, Markella Konstantinidou, and Alexander Dömling. "Covalent inhibitors: a rational approach to drug discovery." *RSC Medicinal Chemistry*, vol. 11, no. 8, 2020, pp. 876–84, https://doi.org/10.1039/d0md00154f
177. Gehringer, Matthias, and Stefan A. Laufer. "Emerging and re-emerging warheads for targeted covalent inhibitors: applications in medicinal chemistry and chemical biology." *Journal of Medicinal Chemistry*, vol. 62, no. 12, Dec. 2018, pp. 5673–724, https://doi.org/10.1021/acs.jmedchem.8b01153

178. van Beek, Lotte, et al. "PARP Power: A Structural Perspective on PARP1, PARP2, and PARP3 in DNA Damage Repair and Nucleosome Remodelling." *International Journal of Molecular Sciences*, vol. 22, no. 5112, May 2021, pp. 1–23,, https://doi.org/10.3390/ijms22105112

179. Thorsell, Ann-Gerd, and Herwig Schüler. *Selectivity Profile of the Poly(ADP-Ribose) Polymerase (PARP) Inhibitor, A-966492*. Cold Spring Harbor Laboratory, 23 Mar. 2017, pp. 1–4, http://dx.doi.org/10.1101/119818..

180. (a) Pellicciari, Roberto, et al. "On the way to selective PARP-2 inhibitors. Design, synthesis, and preliminary evaluation of a series of isoquinolinone derivatives." *ChemMedChem*, vol. 3, no. 6, June 2008, pp. 914–23, https://doi.org/10.1002/cmdc.200800010. (b) Moroni, F., et al. "Selective PARP-2 inhibitors increase apoptosis in hippocampal slices but protect cortical cells in models of post-ischaemic brain damage." *British Journal of Pharmacology*, vol. 157, no. 5, July 2009, pp. 854–62, https://doi.org/10.1111/j.1476-5381.2009.00232.x

181. Ishida, Junya, et al. "Discovery of potent and selective PARP-1 and PARP-2 inhibitors: SBDD analysis via a combination of X-ray structural study and homology modeling." *Bioorganic & Medicinal Chemistry*, vol. 14, no. 5, Mar. 2006, pp. 1378–90, https://doi.org/10.1016/j.bmc.2005.09.061.

182. Nathubhai, Amit, et al. "Highly potent and isoform selective dual site binding Tankyrase/Wnt signaling inhibitors that increase cellular glucose uptake and have antiproliferative activity." *Journal of Medicinal Chemistry*, vol. 60, no. 2, Jan. 2017, pp. 814–20, https://doi.org/10.1021/acs.jmedchem.6b01574.

183. Lehtiö, Lari, Nai-Wen Chi, and Stefan Krauss. "Tankyrases as drug targets." *FEBS Journal*, vol. 280, no. 15, June 2013, pp. 3576–93, https://doi.org/10.1111/febs.12320

184. Kirby, Christina A., et al. "Structure of human tankyrase 1 in complex with small-molecule inhibitors PJ34 and XAV939." *Acta Crystallographica Section F Structural Biology and Crystallization Communications*, vol. 68, no. 2, Jan. 2012, pp. 115–18, https://doi.org/10.1107/s1744309111051219.

185. Johannes, Jeffrey W., et al. "Pyrimidinone nicotinamide mimetics as selective tankyrase and wnt pathway inhibitors suitable for in vivo pharmacology." *ACS medicinal chemistry letters*, vol. 6, no. 3, Jan. 2015, pp. 254–59, https://doi.org/10.1021/ml5003663.

186. Thorvaldsen, Tor Espen, et al. "Structure, dynamics, and functionality of tankyrase inhibitor-induced degradasomes." *Molecular Cancer Research*, vol. 13, no. 11, June 2015, pp. 1487–501, https://doi.org/10.1158/1541-7786.mcr-15-0125.

187. Gunaydin, Hakan, Yan Gu, and Xin Huang. "Novel binding mode of a potent and selective tankyrase inhibitor." *P LoS ONE, vol. 7, no. 3, Mar. 2012, pp. e33740 1–6, https://doi.org/10.1371/journal.pone.0033740*.

188. Qiu, Wei, et al. "Insights into the binding of PARP inhibitors to the catalytic domain of human tankyrase-2." *Acta Crystallographica Section D Biological Crystallography*, vol. 70, no. 10, Sept. 2014, pp. 2740–53, https://doi.org/10.1107/s1399004714017660.

189. Bregman, Howard, et al. "Discovery of novel, induced-pocket binding oxazolidinones as potent, selective, and orally bioavailable tankyrase inhibitors." *Journal of Medicinal Chemistry*, vol. 56, no. 11, May 2013, pp. 4320–42, https://doi.org/10.1021/jm4000038.

190. Johannes, Jeffrey W., et al. "Discovery of AZ0108, an orally bioavailable phthalazinone PARP inhibitor that blocks centrosome clustering." *Bioorganic & Medicinal Chemistry Letters*, vol. 25, no. 24, Dec. 2015, pp. 5743–47, https://doi.org/10.1016/j.bmcl.2015.10.079.

191. Hua, Zihao, et al. "Development of novel dual binders as potent, selective, and orally bioavailable tankyrase inhibitors." *Journal of Medicinal Chemistry, vol. 56, no. 24, Dec. 2013, pp. 10003–15, https://doi.org/10.1021/jm401317z*.

192. Shultz, Michael D., et al. "Identification of NVP-TNKS656: the use of structure–efficiency relationships to generate a highly potent, selective, and orally active tankyrase inhibitor." *Journal of Medicinal Chemistry*, vol. 56, no. 16, Aug. 2013, pp. 6495–511, https://doi.org/10.1021/jm400807n.

193. Shultz, Michael D., et al. "[1, 2, 4] triazol-3-ylsulfanylmethyl)-3-phenyl-[1, 2, 4] oxadiazoles: antagonists of the Wnt pathway that inhibit tankyrases 1 and 2 via novel adenosine pocket binding." *Journal of Medicinal Chemistry*, vol. 55, no. 3, Feb. 2012, pp. 1127–36, https://doi.org/10.1021/jm2011222.

194. Buchstaller, Hans-Peter, et al. "Discovery and optimization of 2-arylquinazolin-4-ones into a potent and selective tankyrase inhibitor modulating Wnt pathway activity." *Journal of Medicinal Chemistry*, vol. 62, no. 17, Aug. 2019, pp. 7897–909, https://doi.org/10.1021/acs.jmedchem.9b00656.

195. Bregman, Howard, et al. "Discovery of a class of novel tankyrase inhibitors that bind to both the nicotinamide pocket and the induced pocket." *Journal of Medicinal Chemistry*, vol. 56, no. 3, Jan. 2013, pp. 1341–45, https://doi.org/10.1021/jm301607v.

196. Klebe, Gerhard. "Introduction." *Drug Design*, Springer Berlin Heidelberg, 2013, pp. xi, http://dx.doi.org/10.1007/978-3-642-17907-5_3.

197. Stromgaard, Kristian, et al. "Introduction to Drug Design and Discovery." *Textbook of Drug Design and Discovery*, CRC Press, 2009, pp. 17–30, http://dx.doi.org/10.1201/9781439882405-5

198. Keserű, György M., and Gergely M. Makara. "Hit discovery and hit-to-lead approaches." *Drug Discovery Today*, vol. 11, no. 15–16, Aug. 2006, pp. 741–48, https://doi.org/10.1016/j.drudis.2006.06.016.

199. Anthony, D., and M. Lockey. "'Hit'to 'lead'and 'lead'to 'candidate'optimisation using multi-parametric principles." *Drug Discovery Today*, vol. 6, no. 7, Apr. 2001, pp. 347–56, https://doi.org/10.1016/s1359-6446(01)01713-5.

200. Merz, Kenneth M. Jr. "Ligand-Based Drug Design." *Drug Design*, Cambridge University Press, http://dx.doi.org/10.1017/cbo9780511730412.010.

201. Favia, Angelo D. "Theoretical and computational approaches to ligand-based drug discovery." F*rontiers in Bioscience*, vol. 16, no. 1, 2011, pp. 1276–90, https://doi.org/10.2741/3788.

202. Mannhold, Raimund, Hugo Kubinyi, and Gerd Folkers. *Pharmacophores and pharmacophore searches*. Vol. 32. John Wiley & Sons, 2006.

203. Güner, Osman F. *Pharmacophore perception, development, and use in drug design*. Vol. 2. Internat'l University Line, 2000.

204. Dixon, Steven L., Alexander M. Smondyrev, and Shashidhar N. Rao. "PHASE: a novel approach to pharmacophore modeling and 3D database searching." *Chemical Biology & Drug Design*, vol. 67, no. 5, May 2006, pp. 370–72, https://doi.org/10.1111/j.1747-0285.2006.00384.x.

205. Zou, Jun, et al. "Towards more accurate pharmacophore modeling: Multicomplex-based comprehensive pharmacophore map and most-frequent-feature pharmacophore model of

CDK2." *Journal of Molecular Graphics and Modelling*, vol. 27, no. 4, Nov. 2008, pp. 430–38, https://doi.org/10.1016/j.jmgm.2008.07.004.

206. Kumar, Gyanendra, et al. "SAR and pharmacophore models for the rhodanine inhibitors of Plasmodium falciparum enoyl-acyl carrier protein reductase." *IUBMB Life*, vol. 62, no. 3, Feb. 2010, pp. 204–13, https://doi.org/10.1002/iub.306.

207. Oebbeke, Matthias, et al. "Fragment Binding to Kinase Hinge: If Charge Distribution and Local pKa Shifts Mislead Popular Bioisosterism Concepts." *Angewandte Chemie International Edition*, vol. 60, no. 1, Oct. 2020, pp. 252–58, https://doi.org/10.1002/anie.202011295.

208. Patani, George A., and Edmond J. LaVoie. "Bioisosterism: a rational approach in drug design." *Chemical Reviews*, vol. 96, no. 8, Jan. 1996, pp. 3147–76, https://doi.org/10.1021/cr950066q.

209. Neves, Bruno J., et al. "QSAR-based virtual screening: advances and applications in drug discovery." *Frontiers in Pharmacology*, vol. 9, no. 1275, Nov. 2018, pp. 1–7, https://doi.org/10.3389/fphar.2018.01275

210. Cherkasov, Artem, et al. "QSAR modeling: where have you been? Where are you going to?." *Journal of Medicinal Chemistry*, vol. 57, no. 12, Jan. 2014, pp. 4977–5010, https://doi.org/10.1021/jm4004285.

211. Wang, Ting, and Rebecca C. Wade. "Comparative Binding Energy (COMBINE) analysis of OppA− peptide complexes to relate structure to binding thermodynamics." *Journal of Medicinal Chemistry*, vol. 45, no. 22, Sept. 2002, pp. 4828–37, https://doi.org/10.1021/jm020900.

212. Polanski, Jaroslaw, and B. Walczak. "The comparative molecular surface analysis (COMSA): a novel tool for molecular design." *Computers & Chemistry*, vol. 24, no. 5, July 2000, pp. 615–25, https://doi.org/10.1016/s0097-8485(00)00064-4.

213. Bacilieri, Magdalena, and Stefano Moro. "Ligand-based drug design methodologies in drug discovery process: an overview." *Current Drug Discovery Technologies*, vol. 3, no. 3, Sept. 2006, pp. 155–65, https://doi.org/10.2174/157016306780136781.

214. Beddell, C. R., et al. "Compounds designed to fit a site of known structure in human haemoglobin." *British Journal of Pharmacology*, vol. 57, no. 2, June 1976, pp. 201–09, https://doi.org/10.1111/j.1476-5381.1976.tb07468.x.

215. Klebe, Gerhard. "Recent developments in structure-based drug design." *Journal of Molecular Medicine*, vol. 78, no. 5, Feb. 2000, pp. 269–81, https://doi.org/10.1007/s001090000084

216. Jhoti, Harren, and Andrew R. Leach, eds. *S Structure-Based Drug Discovery. Springer Netherlands*, 2007, pp. 51–62, http://dx.doi.org/10.1007/1-4020-4407-0.

217. Batool, Maria, Bilal Ahmad, and Sangdun Choi. "A structure-based drug discovery paradigm." *International Journal of Molecular Sciences*, vol. 20, no. 11, June 2019, pp. 2783–90, https://doi.org/10.3390/ijms20112783..

218. Muraoka, Terushige, et al. "Development of a method for converting a TAK1 type I inhibitor into a type II or c-helix-out inhibitor by structure-based drug design (SBDD)." *Chemical and Pharmaceutical Bulletin* 64.11 (2016): 1622-1629.

219. Shechter, Sharon, David R. Thomas, and David A. Jans. "Application of In Silico and HTS Approaches to Identify Nuclear Import Inhibitors for Venezuelan Equine Encephalitis Virus Capsid Protein: A Case Study." *Frontiers in Chemistry*, vol. 8, no. 573121, Dec. 2020, pp. 1–9, https://doi.org/10.3389/fchem.2020.573121

220. Surabhi, Surabhi, and B. K. Singh. "Computer aided drug design: an overview." *Journal of Drug delivery and Therapeutics*, vol. 8, no. 5, Sept. 2018, pp. 504–09, https://doi.org/10.22270/jddt.v8i5.1894.

221. Zhang, Chun-Hui, et al. "Potent noncovalent inhibitors of the main protease of SARS-CoV-2 from molecular sculpting of the drug perampanel guided by free energy perturbation calculations." *ACS Central Science*, vol. 7, no. 3, Feb. 2021, pp. 467–75, https://doi.org/10.1021/acscentsci.1c00039.

222. El Hassab, Mahmoud A., et al. "Identification of a new potential SARS-COV-2 RNA-dependent RNA polymerase inhibitor via combining fragment-based drug design, docking, molecular dynamics, and MM-PBSA calculations." *Frontiers in Chemistry*, vol. 8, no. 584894, Oct. 2020, pp. 1–11, https://doi.org/10.3389/fchem.2020.584894.

223. Ghahremanpour, Mohammad M., et al. "Identification of 14 known drugs as inhibitors of the main protease of SARS-CoV-2." *ACS Medicinal Chemistry Letters*, vol. 11, no. 12, Oct. 2020, pp. 2526–33, https://doi.org/10.1021/acsmedchemlett.0c00521.

224. Kukol, Andreas. *Molecular Modeling of Proteins*. 2nd ed., vol. 443, Humana Press, 2008, pp. 5–20, http://dx.doi.org/10.1007/978-1-59745-177-2.

225. Roy, Kunal, et al. "Topological QSAR." *Understanding the Basics of QSAR for Applications in Pharmaceutical Sciences and Risk Assessment*, Elsevier, 2015, pp. 103–49, http://dx.doi.org/10.1016/b978-0-12-801505-6.00004-1.

226. Hu, Yuan, et al. "The importance of protonation and tautomerization in relative binding affinity prediction: a comparison of AMBER TI and Schrödinger FEP." *Journal of Computer-Aided Molecular Design*, vol. 30, no. 7, July 2016, pp. 533–39, https://doi.org/10.1007/s10822-016-9920-5.

227. Abel, Robert, et al. "Advancing drug discovery through enhanced free energy calculations." *Accounts of Chemical Research*, vol. 50, no. 7, July 2017, pp. 1625–32, https://doi.org/10.1021/acs.accounts.7b00083.

228. Wang, Lingle, et al. "Accurate and reliable prediction of relative ligand binding potency in prospective drug discovery by way of a modern free-energy calculation protocol and force field." *Journal of the American Chemical Society*, vol. 137, no. 7, Feb. 2015, pp. 2695–703, https://doi.org/10.1021/ja512751q.

229. "Free Energy Methods (FEP)." *Schrödinger*, http://www.schrodinger.com/science-articles/free-energy-methods-fep

230. Pagadala, Nataraj S., Khajamohiddin Syed, and Jack Tuszynski. "Software for molecular docking: a review." *Biophysical Reviews*, vol. 9, no. 2, Jan. 2017, pp. 91–102, https://doi.org/10.1007/s12551-016-0247-1.

231. Wang, Zhe, et al. "Comprehensive evaluation of ten docking programs on a diverse set of protein–ligand complexes: the prediction accuracy of sampling power and scoring power." *Physical Chemistry Chemical Physics*, vol. 18, no. 18, 2016, pp. 12964–75, https://doi.org/10.1039/c6cp01555g.

232. AlQuraishi, Mohammed. "AlphaFold at CASP13." *Bioinformatics*, vol. 35, no. 22, May 2019, pp. 4862–65, https://doi.org/10.1093/bioinformatics/btz422.

233. Jumper, John, et al. "Highly accurate protein structure prediction with AlphaFold." *Nature*, vol. 596, Jul. 2021, pp. 583–589, https://doi.org/10.1038/s41592-021-01362-6.
234. Fersht, Alan R. "AlphaFold–A personal perspective on the impact of Machine Learning." *Journal of Molecular Biology*, vol. 433, no. 20, Oct. 2021, pp. 167088–92, https://doi.org/10.1016/j.jmb.2021.167088.
235. Manne, Ravi. "Machine learning techniques in drug discovery and development." *International Journal of Applied Research*, vol. 7, no. 4, Apr. 2021, pp. 21–28, https://doi.org/10.22271/allresearch.2021.v7.i4a.8455.
236. Avram, Sorin, et al. "DrugCentral 2021 supports drug discovery and repositioning." *Nucleic Acids Research*, vol. 49, no. D1, Nov. 2020, pp. D1160–69, https://doi.org/10.1093/nar/gkaa997
237. Zhavoronkov, Alex, et al. "Deep learning enables rapid identification of potent DDR1 kinase inhibitors." *Nature Biotechnology*, vol. 37, no. 9, Sept. 2019, pp. 1038–40, https://doi.org/10.1038/s41587-019-0224-x.
238. Wallach, Izhar, Michael Dzamba, and Abraham Heifets. "AtomNet: a deep convolutional neural network for bioactivity prediction in structure-based drug discovery." *ArXiv.Org*, 10 Oct. 2015, https://arxiv.org/abs/1510.02855
239. Goodsell, David S., et al. "Automated Docking of Flexible Ligands: Applications of Autodock." *Journal of Molecular Recognition*, vol. 9, no. 1, Jan. 1996, pp. 1–5, https://doi.org/10.1002/(sici)1099-1352(199601)9:1<1::aid-jmr241>3.0.co;2-6
240. Trott, Oleg, and Arthur J. Olson. "AutoDock Vina: improving the speed and accuracy of docking with a new scoring function, efficient optimization, and multithreading." *Journal of Computational Chemistry*, vol. 31, no. 2, 2009, pp. 455–61, https://doi.org/10.1002/jcc.21334.
241. Lang, P. T., et al. "DOCK 6.1, University of California, San Francisco." 2007, http://dock.compbio.ucsf.edu/
242. Kramer, Bernd, Matthias Rarey, and Thomas Lengauer. "Evaluation of the FLEXX incremental construction algorithm for protein–ligand docking." *Proteins: Structure, Function, and Genetics*, vol. 37, no. 2, Nov. 1999, pp. 228–41, https://doi.org/10.1002/(sici)1097-0134(19991101)37:2<228::aid-prot8>3.0.co;2-8.

243. Cross, Simon SJ. "Improved FlexX docking using FlexS-determined base fragment placement." *Journal of Chemical Information and Modeling*, vol. 45, no. 4, July 2005, pp. 993–1001, https://doi.org/10.1021/ci050026f.

244. Verdonk, Marcel L., et al. "Improved protein–ligand docking using GOLD." *Proteins: Structure, Function, and Bioinformatics*, vol. 52, no. 4, Aug. 2003, pp. 609–23, https://doi.org/10.1002/prot.10465.

245. "Discovery Studio." Accelrys, 2008.

246. Venkatachalam, Cherayathumadom M., et al. "LigandFit: a novel method for the shape-directed rapid docking of ligands to protein active sites." *Journal of Molecular Graphics and Modelling*, vol. 21, no. 4, Jan. 2003, pp. 289–307, https://doi.org/10.1016/s1093-3263(02)00164-x.

247. (a) Friesner, Richard A., et al. "Extra precision glide: Docking and scoring incorporating a model of hydrophobic enclosure for protein− ligand complexes." *Journal of Medicinal Chemistry*, vol. 49, no. 21, Sept. 2006, pp. 6177–96, https://doi.org/10.1021/jm051256o. (b) Friesner, Richard A., et al. "Glide: a new approach for rapid, accurate docking and scoring. 1. Method and assessment of docking accuracy." *Journal of Medicinal Chemistry*, vol. 47, no. 7, Feb. 2004, pp. 1739–49, https://doi.org/10.1021/jm0306430. (c) Halgren, Thomas A., et al. "Glide: a new approach for rapid, accurate docking and scoring. 2. Enrichment factors in database screening." *Journal of Medicinal Chemistry*, vol. 47, no. 7, Feb. 2004, pp. 1750–59, https://doi.org/10.1021/jm030644s.

248. ChemicalComputingGroup, M. O. E. "Molecular Operating Environment." Chemical Computing Group Montreal, Quebec, Canada, 2008.

249. National Center for Biotechnology Information. "PubChem Compound Summary for CID 1853, 6(5H)-Phenanthridinone" *PubChem*, https://pubchem.ncbi.nlm.nih.gov/compound/6_5H_-Phenanthridinone. Accessed 30 July, 2021.

250. National Center for Biotechnology Information. "PubChem Compound Summary for CID 56649297, Fluzoparib" *PubChem*, https://pubchem.ncbi.nlm.nih.gov/compound/Fluzoparib. Accessed 30 July, 2021.

251. Xu, B., et al. "577P Updated analysis of phase I dose-escalation and dose cohort expansion studies of senaparib (IMP4297) in Chinese patients with advanced solid tumours." *Annals*

of Oncology, vol. 31, no. 1, Sept. 2020, pp. 491–94, https://doi.org/10.1016/j.annonc.2020.08.691.

252. National Center for Biotechnology Information. "PubChem Compound Summary for CID 135566764" *PubChem*, https://pubchem.ncbi.nlm.nih.gov/compound/me0328. Accessed 30 July, 2021.
253. (a) National Center for Biotechnology Information. "PubChem Compound Summary for CID 9948349" *PubChem*, https://pubchem.ncbi.nlm.nih.gov/compound/9948349. Accessed 30 July, 2021. (b) Costantino, Gabriele, et al. "Modeling of poly (ADP-ribose) polymerase (PARP) inhibitors. Docking of ligands and quantitative structure− activity relationship analysis." *Journal of Medicinal Chemistry*, vol. 44, no. 23, Oct. 2001, pp. 3786–94, https://doi.org/10.1021/jm010116l.
254. National Center for Biotechnology Information. "PubChem Compound Summary for CID 16666333" *PubChem*, https://pubchem.ncbi.nlm.nih.gov/compound/a-966492. Accessed 30 July, 2021.
255. National Center for Biotechnology Information. "PubChem Compound Summary for CID 2331, Benzamide" PubChem, https://pubchem.ncbi.nlm.nih.gov/compound/Benzamide. Accessed 30 July, 2021.
256. National Center for Biotechnology Information. "PubChem Compound Summary for CID 936, Nicotinamide" *PubChem*, https://pubchem.ncbi.nlm.nih.gov/compound/Nicotinamide. Accessed 30 July, 2021.
257. National Center for Biotechnology Information. "PubChem Compound Summary for CID 1645, 3-Aminobenzamide" *PubChem*, https://pubchem.ncbi.nlm.nih.gov/compound/3-Aminobenzamide. Accessed 30 July, 2021.
258. National Center for Biotechnology Information. "PubChem Compound Summary for CID 9796068, Iniparib" *PubChem*, https://pubchem.ncbi.nlm.nih.gov/compound/Iniparib. Accessed 30 July, 2021.
259. Sigorski, Dawid, Ewa Iżycka-Świeszewska, and Lubomir Bodnar. "Poly (ADP-ribose) polymerase inhibitors in prostate cancer: molecular mechanisms, and preclinical and clinical data." *Targeted Oncology*, vol. 15, no. 6, Oct. 2020, pp. 709–22, https://doi.org/10.1007/s11523-020-00756-4.

260. Oplustil O'Connor, Lenka, et al. "The PARP Inhibitor AZD2461 Provides Insights into the Role of PARP3 Inhibition for Both Synthetic Lethality and Tolerability with Chemotherapy in Preclinical Models." *Cancer Research*, vol. 76, no. 20, Aug. 2016, pp. 6084–94, https://doi.org/10.1158/0008-5472.can-15-3240.

261. Narwal, Mohit, et al. "Discovery of tankyrase inhibiting flavones with increased potency and isoenzyme selectivity." *Journal of Medicinal Chemistry*, vol. 56, no. 20, Oct. 2013, pp. 7880–89, https://doi.org/10.1021/jm401463y.

262. Curtin, Nicola J., et al. "Novel poly (ADP-ribose) polymerase-1 inhibitor, AG14361, restores sensitivity to temozolomide in mismatch repair-deficient cells." *Clinical Cancer Research*, vol. 10, no. 3, Feb. 2004, pp. 881–89, https://doi.org/10.1158/1078-0432.ccr-1144-3.

263. Chen, Hua-Dong, et al. "Increased PARP1-DNA binding due to autoPARylation inhibition of PARP1 on DNA rather than PARP1-DNA trapping is correlated with PARP1 inhibitor's cytotoxicity." *International Journal of Cancer*, vol. 145, no. 3, Jan. 2019, pp. 714–27, https://doi.org/10.1002/ijc.32131.

264. Leonetti, C., et al. "Targeted therapy for brain tumours: role of PARP inhibitors." *Current Cancer Drug Targets*, vol. 12, no. 3, Mar. 2012, pp. 218–36, https://doi.org/10.2174/156800912799277403.

265. Olsen, Abby L., and Mel B. Feany. "PARP inhibitors and Parkinson's disease." *New England Journal of Medicine*, vol. 380, no. 5, Jan. 2019, pp. 492–94, https://doi.org/10.1056/nejmcibr1814680.

266. Su, Jack M., et al. "A phase I trial of veliparib (ABT-888) and temozolomide in children with recurrent CNS tumors: a pediatric brain tumor consortium report." *Neuro-Oncology*, vol. 16, no. 12, June 2014, pp. 1661–68, https://doi.org/10.1093/neuonc/nou103.

267. Gupta, Shiv K., et al. "PARP inhibitors for sensitization of alkylation chemotherapy in glioblastoma: impact of blood-brain barrier and molecular heterogeneity." *Frontiers in Oncology*, vol. 8, no. 670, Jan. 2019, pp. 1–10, https://doi.org/10.3389/fonc.2018.00670.

268. Liu, Xuesong, et al. "Iniparib nonselectively modifies cysteine-containing proteins in tumor cells and is not a bona fide PARP inhibitor." *Clinical Cancer Research*, vol. 18, no. 2, Nov. 2011, pp. 510–23, https://doi.org/10.1158/1078-0432.ccr-11-1973.

Chapter 3: Research Objectives

The goal of the proposed research is to develop novel PARP inhibitors based on 6(5*H*)-phenanthridinone. We will start with building PARP protein (PARP1, PARP2, PARP5) homologous models. To develop a competitive inhibitor, an accurate protein model can help us understand the potential ligand-protein interactions inside the binding pocket, as well as recognize unusual binding sites that are rarely targeted. The protein model is fundamental to SBDD. The molecular docking experiments based on the protein model is the method to predict and visualize the ligand-protein relationship. The molecular docking method needs to be verified by redocking known ligands to corresponding known crystal structures and comparing the redocking results to experimental structures. For *de novo* design, a massive screen of different scaffolds is required. According to the molecular docking result, which shows the potential orientation of the ligand inside the protein, we expect to test ~100 compounds with different spatial occupancy and choose the best one(s) to develop potent and/or selective inhibitor candidates. To develop potent inhibitors, in addition to a novel scaffold, we are interested in using functional groups that are rarely used in previous studies. These functional groups include $-B(OH)_2$ and $-NO_2$ as these functional groups are with potential to form various interactions with protein residues, including H-bond, salt bridge and covalent bond, that are likely to benefit the affinity between a ligand and the protein. To develop PARP1-/PARP2-selective inhibitors, we want to achieve inhibitor selectivity through innovative structures. Champion compounds with superior potency should be tested in both enzymatic assay and cellular assay. The focus of the study in the cellular assay is whether the inhibitors can synergize with traditional chemotherapy drugs, as suggested by previous *in vitro* and clinical studies. Whether the inhibitor produces cytotoxicity can also be of interest. In conclusion, to achieve the goal of our research, the study objectives include:

1. To build computational models of PARP1, PARP2, TNKS1 proteins for *in silico* experiments including molecular docking and protein-ligand interaction analysis.
2. To design and synthesize inhibitor candidates based on 6(5*H*)-phenanthridinone, including designing and synthesizing PARP1-/PARP2-selective inhibitors and highly potent PARP1 inhibitors.
3. To explore the patent space by designing and synthesizing best-in-series PARP inhibitors.

4. To perform *in vitro* inhibition/cytotoxic studies in the PARP1/2 and TNKS1 enzymes and U251 cell lines.
5. To explore the structure-activity relationships and the relationship between protein-ligand interaction and inhibitor potency and selectivity and explore the possibility and accuracy of inhibitor potency guidance/prediction using *in silico* modelling.

The thesis is organized based on the R&D process of developing PARP inhibitors. **Chapter 1** provides a general background and an overview of the field as it relates to the proposed research. **Chapter 2** reviews the background of the proposed research, including PARP proteins, PARP inhibitors, PARP protein-ligand interactions, concepts in drug design, and a conclusion. **Chapter 4** demonstrates methods used during the research, including the *in silico* modelling, organic synthesis approaches, enzymatic assays, and cell culture. **Chapter 5** describes the results from each iteration taken during the R&D process. **Chapter 6** forms the conclusion and discussion in relation to the whole research project. **Chapter 7** provides supplemental information and contains detailed experimental results.

Chapter 4: Methods

4.1. Protein Homologous Modeling and Molecular Docking

PDB files of Homo Sapiens PARP-1 in complex with inhibitors were retrieved from the Protein Data Bank [1]. According to the literature review above, the structure of the human PARP1 catalytic domain bound to 2-[(3R)-3-azanylpyrrolidin-1-yl]carbonyl-1H-benzimidazole-4-carboxamide (PDB ID **5WS1**) and the structure of the human PARP1 catalytic domain bound to UKTT15 (PDB ID **6VKO**) were used as major templates to build homologous models respectively. PDB ID **5WS1** was used as the template for the Normal model; PDB ID **6VKO** was used as the template for the Open model. Protein sequences of Homo Sapiens PARP1 and PARP2 were retrieved from UniProt. Knowledge-based homologous models were prepared based on PARP1 or PARP2 gene sequences and templates from crystal structures of PDB ID **5WS1** and PDB ID **6VKO** in Schrodinger's Maestro Prime respectively to build the PARP1 Normal model, PARP1 Open model, PARP2 Normal model, PARP2 Open model. The protein was prepared using OPLS2005 force field. The pH was set at 8.0±1.0, in agreement with the condition of the enzymatic assay. The order of hydrogen bond was fixed, and steric clashes were eliminated; Missing side chains were fixed; non-conserved loops were refined, and all atoms were minimized; For the Normal model, the homologous model required a Ramachandra's plot with more than 85% residues in the preferred region. For the Open model, the percentage of residues in the preferred region would be discussed.

The hydrophobic/philic mapping was generated by Schrodinger's Maestro. A grid was generated containing the target active site with the grid spacing 1Å as the default setting. The OPLS-AA force field was used to calculate the van der Waals energies and the electrostatic parameters of atoms from the target protein. A probe oriented along the electric field was represented by a van der Waals sphere of radius 1.5Å and well depth 0.2 kcal/mol which had a 0.2 kcal/mol point dipole moment. The calculation was combined with a smoothing procedure. The hydrophobic and hydrophilic grid values were determined by equations: Hydrophilic: Grid_philic = vdW_energy + oriented-dipole_energy; Hydrophobic: Grid_phobic = vdW_energy − 0.15 oriented-dipole_energy. The values were read by Maestro to generate the surface.

For molecular modelling, all compounds were prepared in LigPrep using the same pH and treated with force-field OPLS2005. As shown in **Figure 14**, before the ligand docking, a grid

box was generated in the location of the theoretical binding pocket. The center of the grid was located in the center of the NI where the phenanthridinone component of PJ34 was near G863 and S904 and the length of the grid was 20Å. The grid should cover the cavity of the binding pocket, including the NI, the AD, the phosphate binding site, and the peripheral binding site. The molecular docking was performed with the XP algorithms generating at most 32 outcomes per ligand with flexible posing. Docking scores and ligand-protein interactions were analyzed manually after molecular docking. The docking pose with the highest docking score was considered as the most preferred binding orientation and the docking score was not used for comparing the ligand-protein affinity. The docking pose and the ligand-protein interaction were used for analysis and the ligand-protein interactions within 4.5Å were kept including the H-bond, the salt bridge, the π-interaction as well as the covalent bond. Superimposition of molecular docking results was done by showing two or more ligands together in the same homologous model.

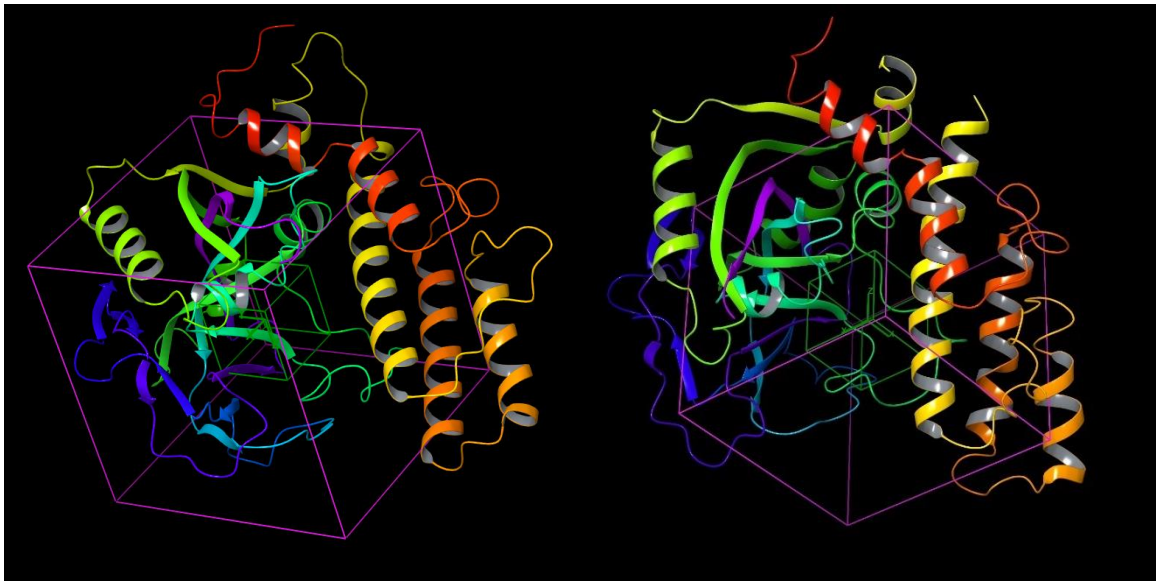

Figure 14 *PARP1 binding pocket and receptor grid. The left one is the Normal model mainly based on* ***5WS1*** *and the right one is the Open model mainly based on* ***6VKO****. The green grid is located in the center of the theoretical binding pocket. The purple grid defines the possible binding area for ligands.*

4.2. General Organic Synthesis Methods (**Figure 15**)

(Due to its size, specific compound characterization can be found in the supplemental info at the end of the thesis, following **Chapter 6**)

a. General amide coupling reaction: 1 equiv. of acyl chloride was added to the 1 equiv. of amine in acetonitrile dropwise at room temperature to make a 50mM solution. The mixture was stirred overnight. Acetonitrile was removed from the resulting mixture and the crude was dissolved in ethyl acetate. The resulting solution was washed with the equivalent amount of brine three times and dried by Na_2SO_4. The crude product was loaded to the silica gel, separated, and purified by the flash column (Hexane-Ethyl acetate gradients).

b. General UV-mediated photocyclization: The corresponding amide was dissolved in acetonitrile to make a 5mM solution. The solution was sonicated for 5min and pumped to the UV reactor using the Flow-UV machine (Vapourtec R2+/R4 system with (Vapourtec UV-150 ,10 mL coil). Whole wavelength UV was used with 60% of the lamp power (~ 112.5 watts). The total flow rate was set to 0.2mL/min and the reaction time was 50min for the solution to go through the 10mL reactor. The temperature was set to 21°C while the real temperature was ~60°C as the cooling module was not available. The pressure limit of the whole system was 12 Bar. The crude product was collected from the beginning of the reaction. For a small-scale reaction, the crude product was separated and purified directly by the flash column (Hexane-Ethyl acetate or DCM-MeOH gradient accordingly) after being loaded to the silica gel. For a large-scale reaction in which the product was used as the starting material for other reactions, the solvent was removed from the collected solution and the dry crude product was washed with methanol. The methanol was removed from the insoluble part after centrifuging the solution. After repeating the washing step three times, the remaining insoluble part was the desired product.

c. General one-pot amide coupling reaction and UV-mediated photocyclization: 1 equiv. of corresponding acyl chloride and 1 equiv. of the corresponding amine was pumped into the UV reactor simultaneously from two injectors with the same flow rate using a T-piece. The reaction condition and the work-up method were as same as **b**.

d. General HATU-mediated amide coupling reaction: 1 equiv. of carboxylic acid was dissolved into dry acetonitrile to make a 20mM solution, followed by the addition of 1.2 equiv. of HATU and 2 equiv. of DIPEA. The mixture was stirred at room temperature for 5min before adding the 1 equiv. of amine. The resulting mixture was stirred at room temperature overnight. The solvent was removed from the crude product and the crude product was dissolved in ethyl acetate and washed by the equivalent amount of brine three times. The resulting solution was dried by Na_2SO_4 and loaded onto the silica gel for separation and purification by the flash column (Hexane-Ethyl acetate or DCM-MeOH gradients accordingly). Products with phenanthridinone would contain yellowish by-products which could be removed after being washed with methanol that were as same as the corresponding steps described in **b**.

e. General Hydroxylamine-*O*-sulfonic acid (HOSA)-mediated synthesis of urea: To a flame-dried microwave vial 1 equiv. of amine, 1.2 equiv. of HATU, 2 equiv. of HOSA and 2 equiv. of DIPEA was added and dissolved in anhydrous acetonitrile. The mixture was sealed in the vial in which the air was replaced by argon. The solution was microwaved (130W) for 10min. The solvent was removed from the crude product before which was loaded onto the silica gel for separation and purification by the flash column (Hexane-Ethyl acetate gradients). The separated product would still need to be washed with methanol as described in **b**.

f. General deprotection of Boc-group: The protected amine was dissolved in DCM:TFA=1:1 as the solvent and stirred for 4 hours before no more bubbles were produced. The resulting crude product was ready to use after removing the solvent under the vacuum. Separation with the flash column (DCM-MeOH gradients) could also be employed to ensure purity.

g. General intramolecular Mitsunobu reaction [4]: 1 equiv. of the corresponding amide was dissolved in dry THF (0.1M) with 1.3 equiv. of PPh_3. 1.3 equiv. of azodicarboxylic dimorpholide (ADDM) was dissolved in dry THF (0.1M). The ADDM-THF solution was added into the amide solution drop-wise very slowly while stirring. The resulting solution was stirred overnight. THF was removed from the crude product after the reaction was completed and the solid product was dissolved in ethyl acetate to be washed by the equivalent amount of the brine, dried by Na_2SO_4 and loaded onto the silica gel. The crude

product was separated by the flash column (DCM-MeOH). The purified product was sent for deprotection **f**.

h. General Suzuki coupling reaction: The solvent DMF:H_2O=10:1 was degassed by being purged with argon and being sonicated repeatedly. 1 equiv. of 2-chlorophenanthridin-6(5*H*)-one (0.1M), 2 equiv. of 4-boronobenzoic acid, 3 equiv. of potassium acetate, 0.3 equiv. of XPhos, 0.1 equiv. of $Pd(OAc)_2$ were dissolved in the. The solution was purged with the argon again for 5min and sealed before being stirred at 140°C for overnight. The resulting mixture was absorbed by the silica gel and roughly separated by the flash column (DCM-MeOH gradients). The resulting product was a mixture of the target product and some unknown by-products. Dissolve ~1 equiv. of the resulting product in dry acetonitrile (~0.004M) along with 1.5 equiv. of HATU and 3 equiv. of DIPEA. The mixture solution was stirred for 2 min before adding 1.2 equiv. of the corresponding amine. The solution was stirred overnight. Acetonitrile was removed under argon from the crude product when the reaction was finished and the solid was dissolved in ethyl acetate and washed by the equivalent amount of the brine and dried by Na_2SO_4. The resulting solution was loaded onto the silica gel and separated by the flash column (DCM-MeOH gradients). Each portion from the chromatography separation was analyzed by LC-MS (LCMS-2020, Shimadzu) to locate the target product. The target product was collected and washed with methanol to ensure purity.

i. General reduction and synthesis of sulfinamide [5]: 1 equiv. of the corresponding amine (0.2M) was dissolved with 1.1 equiv. of PPh_3 and 10 equiv. of TEA in anhydrous. The mixed solution was injected into a flame-dried RB flask purged with argon. The reaction was kept in an ice bath. 1 equiv. of the corresponding chloride was dissolved in anhydrous DCM (0.2M) and the solution was injected into the RB flask drop-wise slowly. The reaction was stirred at 0°C for ~1h and loaded to the silica gel. The crude product was separated purified by the flash column (Hexane-Ethyl acetate gradients). The resulting product was still a mixture of sulfonamide and sulfinamide.

j. Suzuki coupling reaction: The resulting sulfonamide and sulfinamide was dissolved with K_2CO_3 in degassed DMF (~0.005M). The solution was purged with argon for 15min. $Pd(PPh_3)_4$ was added to the solution before the solution was stirred at 100°C oil bath for 24h. The crude reaction was absorbed by silica gel and loaded for the flash column

separation (Hexane-Ethyl acetate gradients). Each portion from the chromatography separation was analyzed by LC-MS (LCMS-2020, Shimadzu) to locate the target product which was collected eventually.

Synthesis of phenanthridinone analogs

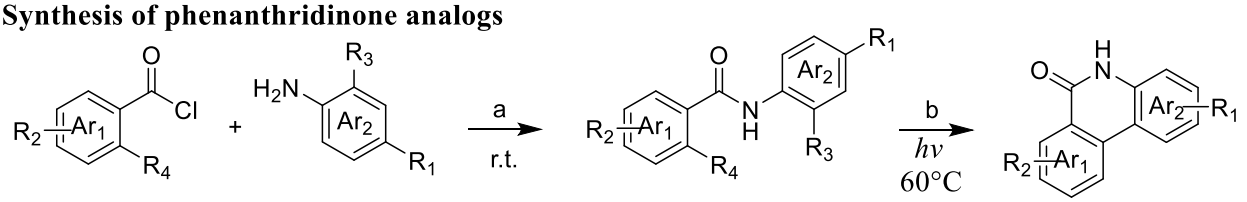

R_1: H, COOH, CH_2COOH, Halogen

R_2: H, Me, Halogen

R_3: H, Cl

R_4: H, Cl

Figure 15a *The synthesis of phenanthridinone analogs. Corresponding reaction conditions are listed in the text of* ***Chapter 4, Section 4.2****.*

Synthesis of phenanthridinone inhibitor compounds

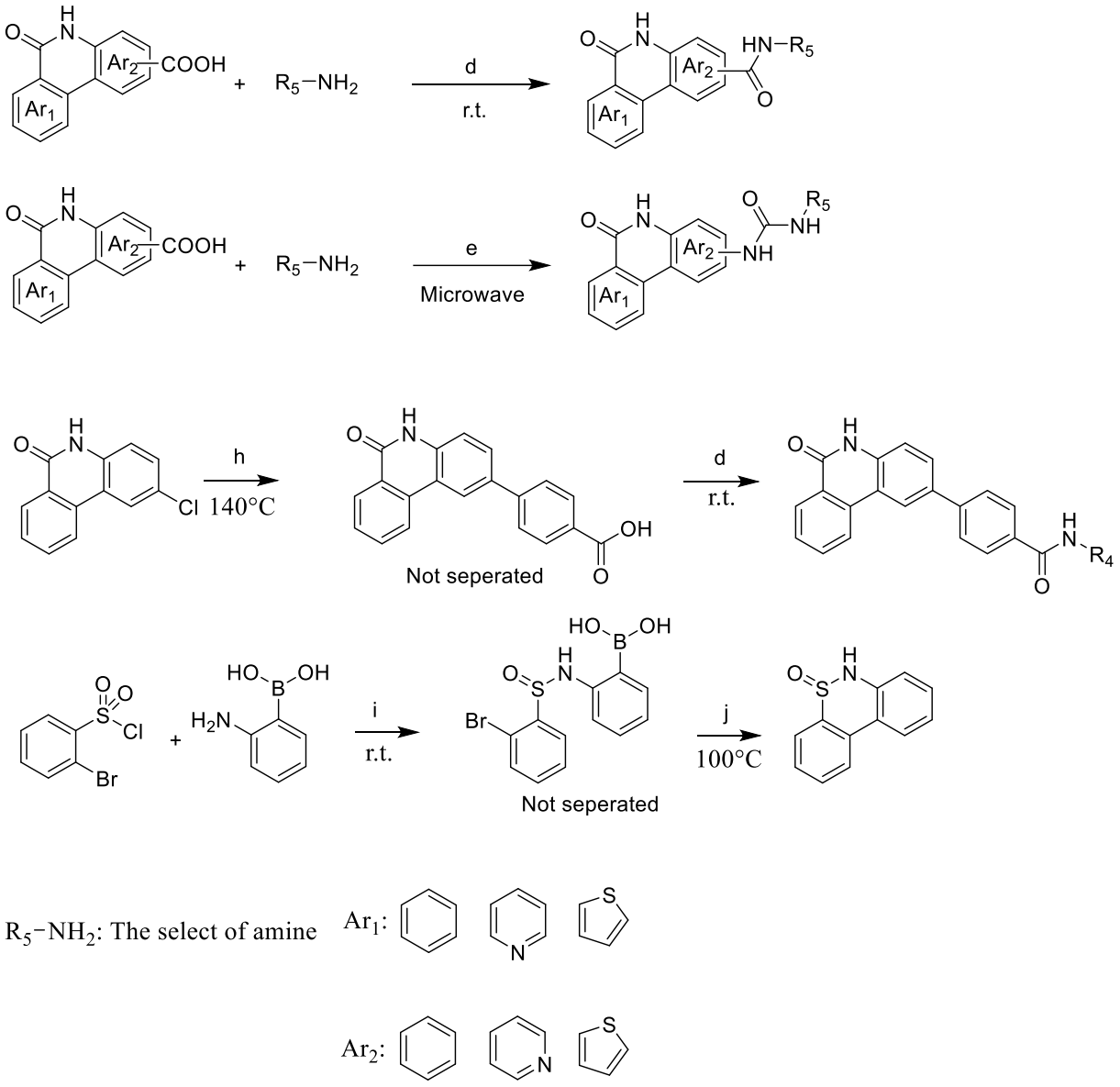

Figure 15b *The synthesis of phenanthridinone inhibitor compounds. Corresponding reaction conditions are listed in the text of* ***Chapter 4, Section 4.2***.

Synthesis of amines

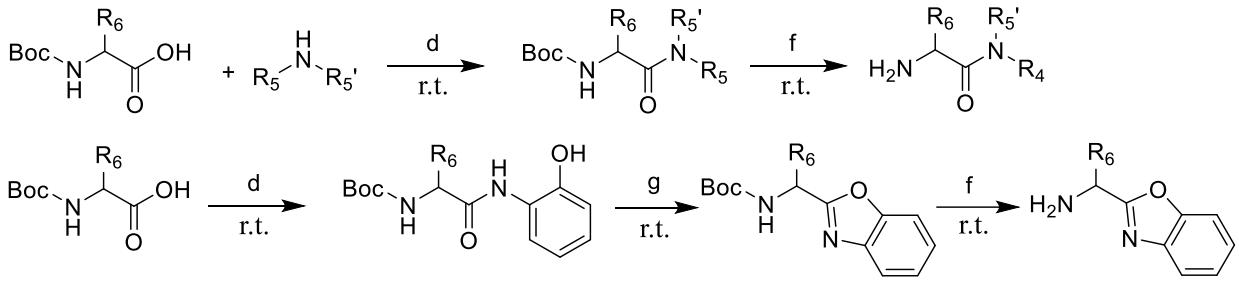

R_5−NH_2: The select of amine

R_6: The side chain of an amino acid

Figure 15c *The synthesis of amines that are not available commercially. Corresponding reaction conditions are listed in the text of* ***Chapter 4, Section 4.2****.*

4.3. Enzymatic Assay

4.3.1 Prepare materials: β-Nicotinamide adenine dinucleotide hydrate was purchased from Millipore Sigma, catalogue number N1636; Deoxyribonucleic acid from calf thymus was purchased from Millipore Sigma, catalogue number D4522; High specific activity PARP-1 enzyme was purchased from Bio-Techne, catalogue number 4668-500-01; Corning™ Black and White 96-Well Polypropylene Assay Plate was purchased from Fisher Scientific, catalogue number 07200762;

4.3.2 Prepare reagents: The NAD^+ stock was prepared at 50mM and the molarity was checked by measuring O.D. at 260nm of a 1/1000 dilution. It was diluted to 5000nM before use. The DNA stock was prepared at 1mg/mL and it was diluted to 0.25mg/mL before use. 5X Inhibitor solutions (10% DMSO) were prepared before use and. The PARP1 enzymatic buffer consisted of 50mM Tris hydrochloride (Sigma), 2mM $MgCl_2$ and RO water. pH=8.

4.3.3 Determination of excitation and emission wavelength: The fluorescent product with 150µL 1000nM ß-NAD solution using the development procedure (**4.3.6**); The fluorescence reading was measured using the Microplate Reader with different excitation/emission wavelength combinations around 370nm (excitation)/450nm (emission) to determine the best

wavelength combination. The optimal wavelength combination for FlexStation™ 3 Multi-Mode Microplate Reader was excitation wavelength 380 nm and emission wavelength 475 nm (475 nm cut-off). The optimal wavelength combination for BioTek™ Synergy™ 2 Multi-Mode Microplate Reader was excitation wavelength 372 nm and emission wavelength 444 nm;

4.3.4 Enzymatic assay cocktail: (Each vial) 30µL 5X enzyme solution, 30µL 5000nM NAD^+ solution, 30µL 0.25mg/mL DNA solution, 30µL inhibitor solution and 30µL enzymatic buffer.

4.3.5 Determining the activity of PARP1 enzyme (Determine PARP1 activity upon the arrival before being aliquoted): Dissolve the enzyme stock 10U/µL into the enzymatic assay buffer to make 5X enzyme solutions to make final gradients from 0.2 U/µL to 1.6U/µL. Mixed the reagents according to the enzymatic assay cocktail (**4.3.4**) with 60µL enzymatic buffer replacing 30µL and no inhibitor solution. The resulting solution was incubated for 90 min under 37 °C and treated with the Development Procedure (**4.3.6**), the Measurement Procedure (**4.3.7**) and the reading was analyzed by the Data Management Procedure (**4.3.8**). The concentration of PARP1 when NAD conversion ratio was around 70%-80% was taken for future experiments (Usually the PARP concentration we took for the enzymatic assay was 0.8U/µL, that was 8U/well or 24U/vial);

4.3.6 Development procedure: Add 30µL 20% acetophenone in EtOH and 30µL 2M KOH solution into the solution ready for fluorescent development. The solution was incubated at 4 °C for 15 min and treated with 135µL 100% formic acid. The mixture was incubated in the 110 °C oven for 5 min (the reported procedure), or in the microwave for 30s (10s microwaving + 5s resting for three times)

4.3.7 Measurement procedure: The solution was cooled down to room temperature and distributed to three wells (100µL/well). The fluorescent was measured on Multi-Mode Microplate Reader with determined excitation/emission wavelength;

4.3.8 Data management procedure: The data was processed using GraphPad Prism 8. IC_{50} curve was calculated using 4-parameter logistic regression. The data for the standard curve was processed using excel. Normalization was not necessary as the fluorescent reading was directly related to the ß-NAD concentration

4.3.9 The standard curve: 30μL different gradients of NAD^+ solution and 120μL enzymatic buffer were incubated for 90 min under 37 °C and treated with the Development Procedure (**4.3.6**), the Measurement Procedure (**4.3.7**) and the reading was analyzed by the excel.

4.3.10 The enzymatic assay for evaluating inhibitor IC_{50}: The enzymatic assay cocktail (**4.3.4**) with enzyme, inhibitor, NAD^+, DNA was incubated for 90 min under 37 °C and treated with the Development Procedure (**4.3.6**), the Measurement Procedure (**4.3.7**) and the reading was analyzed by the Data Management Procedure (**4.3.8**). For the Drug-Fluorescence Control group, the cocktail only contained 30μL corresponding inhibitor solution and 120μL enzymatic buffer. The concentration solution less than 1000nM would not influence the experiment according to experience;

4.3.10 Validation of the enzymatic assay (**Table 6**, **Table 7**, **Figure 16**, **Figure 17**, **Figure 18**)

The assay was optimized from the method reported by Putt *et al*. [3]. This assay detected the amount of NAD^+ that was consumed in the enzymatic assay to determine the activity of the PARP enzyme. We found the method was difficult to reproduce due to the unclear usage of the PARP1 enzyme as there was not a standard to measure the PARP1 enzyme activity from different vendors. Meanwhile, the enzymatic reaction condition, including the amount of the enzyme and the duration of the enzymatic reaction suggested in the literature, was not likely to consume an adequate amount of NAD^+ to a recognizable detection window. In addition, the reported reaction converting unreacted NAD^+ to the fluorescent product could be dangerous and cause errors as the organic solution could be evaporated in the oven and self-ignited.

The goal of the optimization was to standardize the amount of each reagent used in the enzymatic assay, especially the amount of the PARP1 enzyme, so that the assay could be performed with reagents from different vendors, under which condition we also needed to make sure that the enzymatic reaction would generate a recognizable detection window. Then, we tried to introduce a safe and accurate way to convert NAD^+ into the fluorescent product.

Followed by determining the concentration of DNA and reaction time used in the assay, we found that a 70%-80% conversion ratio (consumption of NAD) would be able to give a recognizable detection window when 1000nM NAD (final concentration) was used in the assay. Using PJ34 as a standard, when 70%-90% of NAD was consumed in the

enzymatic assay, the dose-response curve and data spots were meaningful, and the resulting IC_{50} values were reasonable (within 2 folds of the literature reported PJ34 IC_{50} = 110nM [6]) (**Figure 16**, **Table 6**). However, it was difficult to control the reaction progress to reach 90% of the conversion ratio, and the reaction rate might slow down after 90% of NAD^+ was consumed. Thus, we chose the amount of PARP1 enzyme to cause 70%-80% of NAD^+ consumption in 90min as the standard amount. The PARP1 standard amount was tested for every new purchase of the enzyme. Compared to the original method, with 1000nM we would have a larger detection window for better accuracy (100nM NAD^+ was used in the original assay).

We found using a benchtop microwave and microwave reactor were both able to convert NAD^+ to the target fluorescent product. The more convenient method with the benchtop microwave was able to complete the reaction within 30s with no noticeable heating on the enzymatic assay vials. Along with NAD standard curves (**Figure 17**), IC_{50} results and statistical results of 6-(5*H*)-phenanthridinone (Phe), PJ34, DPQ inhibiting PARP1 obtained from the microwave method and the oven method (**Figure 18**, **Table 7**), we argue that there was no significant difference between the two methods in producing the fluorescent product and both methods were able to measure inhibitors' IC_{50} values correctly. Thus, we believed that the microwave method was able to replace the oven method in producing the fluorescent product as it was more efficient and safer. We also found different excitation/emission wavelengths might be employed in different readers due to the difference in hardware.

In conclusion, we present an optimized enzymatic assay using a microwave for reaction/assay incubation and fluorescence development. The amount of PARP1 used in every entry was determined by the amount needed to induce 70%-80% of NAD^+ consumption, in this manner, the assay result remained consistent regardless of the original activity of the PARP enzyme. Overall, the optimized enzymatic assay was able to measure IC_{50} values correctly and it was cheaper than commercially available assay kits. It could be used for the massive screening and evaluation of PARP1 inhibitors.

4.3.11 PARP1, PARP2, TNK1 enzymatic assays using assay kits

PARP1, PARP2, TNK1 enzymatic assay kits were purchased from BPS Bioscience, including PARP1 Colorimetric Assay Kit Catalog #80580, PARP2 Colorimetric Assay Kit

Catalog #80581, TNKS1 Histone Ribosylation Colorimetric Assay Kit Catalog #80582. Assays were performed under the instruction recommended by assay kits.

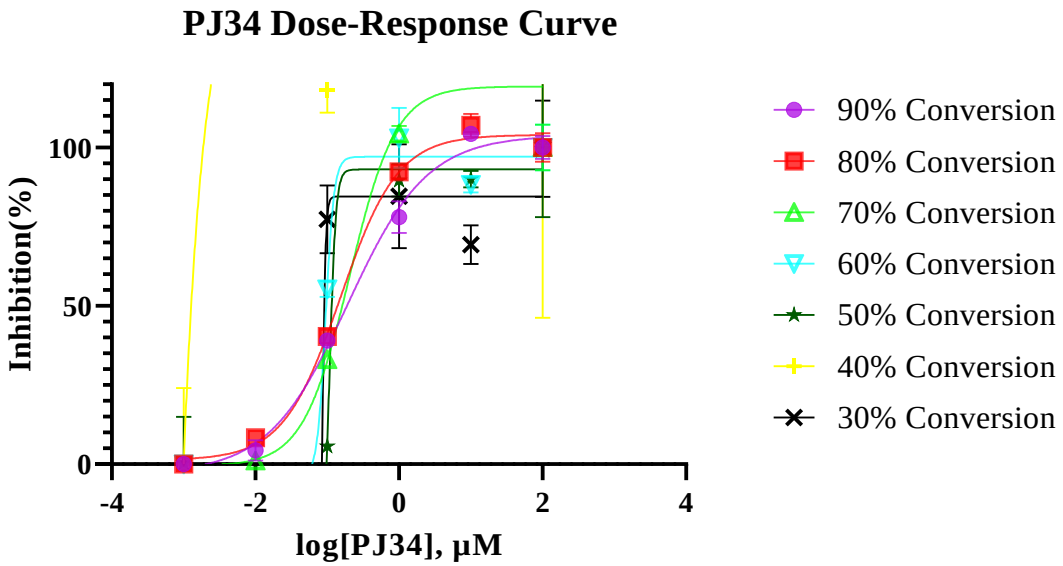

Figure 16 *PJ34 dose-response curves under different conversion rates. Experimental data were obtained from the enzymatic assay described in* ***Chapter 4, Section 4.3*** *but with different reaction times to achieve different conversions (approximately). Each experiment was plated in triplicate. Experimental data were processed with GraphPad 8.0.1. IC_{50} values were calculated using 4-parameter logistic regression. Data larger than 120% was not included.*

NAD^+ Conversion Ratio	Detection Window	PJ34 IC_{50}(nM)	Note
90%	1.14	0.193	
80%	1.11	0.153	
70%	1.21	0.205	
60%	0.772	0.095	Ambiguous
50%	0.581	0.108	Ambiguous
40%	0.626	0.000	Ambiguous
30%	0.482	0.086	Ambiguous

Table 6 *Supplemental info for* ***Figure 16****. PJ34 IC_{50} values under each NAD consumption ratio are listed. Detection window =* $\frac{\Delta Abs}{Maximum\ Abs - Blank\ Abs}$ *and. Abs: Fluorescent absorption reading.*

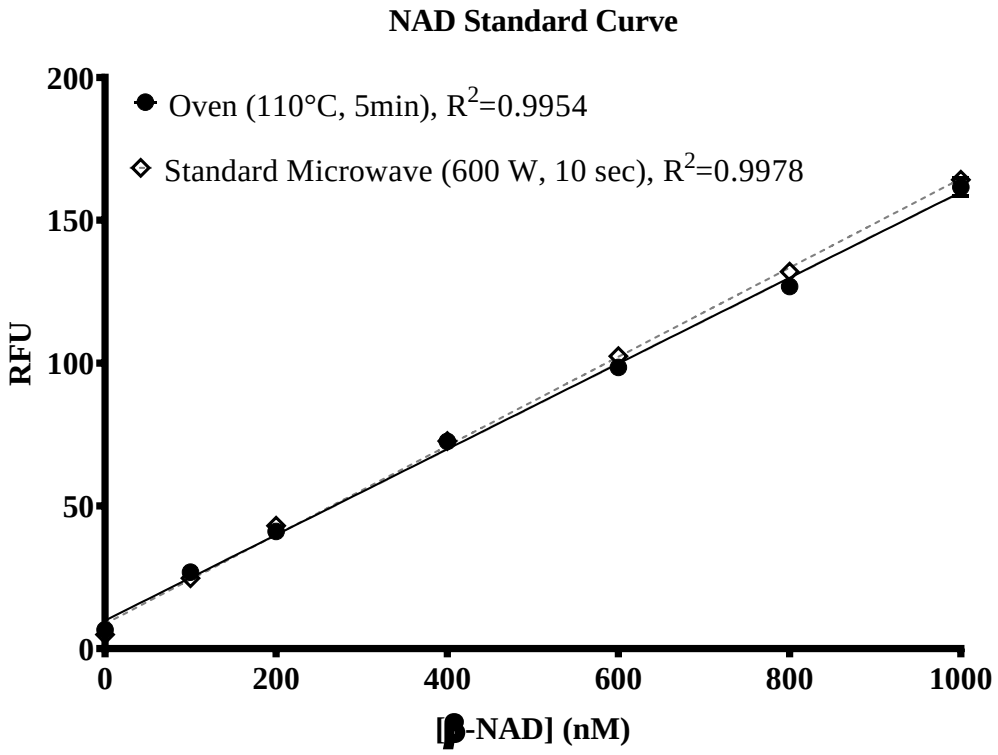

Figure 17 *NAD standard curves. NAD standard curve of using microwave and oven to convert NAD^+ to the fluorescent product respectively. RFU: Fluorescent reading of the final compound.*

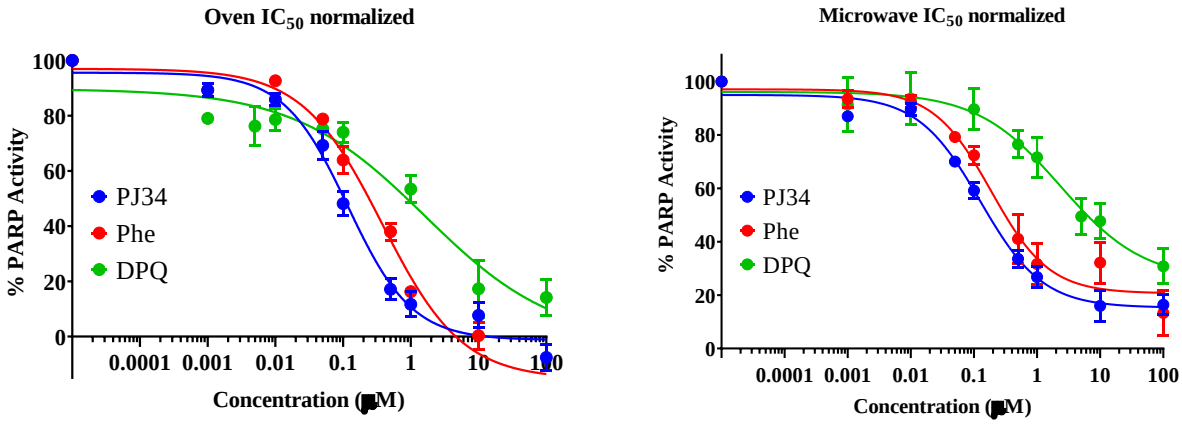

Figure 18 *IC_{50} curves of PJ34, Phe and DPQ inhibiting PARP1 obtained from the oven method and microwave method respectively. Experimental data was processed with GraphPad 8.0.1. IC_{50} values were calculated using 4-parameter logistic regression [7].*

$LogIC_{50}$ (nM)	PJ34		Phe		DPQ	
	Oven	Mw	Oven	Mw	Oven	Mw
	-1.04	-0.897	-0.524	-1.22	0.221	0.310
	-0.808	-0.746	-0.197	-0.688	0.282	0.583
	-0.875	-0.861	-0.491	-0.701	0.115	0.200
					-0.113	0.166
T-test (P values)	0.429		0.085		0.193	

IC_{50} (nM)	PJ34		Phe		DPQ	
	Oven	Mw	Oven	Mw	Oven	Mw
	92.3	127	299	59.1	1660	2040
	156	180	636	205	1920	3830
	133	138	323	199	1300	1580
					770	1470
T-test (P values)	0.441		0.089		0.223	
	Oven	Mw	Oven	Mw	Oven	Mw
Mean IC_{50} (nM)	127	148	419	154	1410	2230
stdev	32.2	27.7	188	82.5	496	1100
sem	18.6	16.0	109	47.7	248	547

Table 7 *IC_{50}s of PJ34, Phe, DPQ. IC_{50}s of three commercially available inhibitors PJ34, 6(5H)-Phe and DPQ were obtained using the oven method and the microwave method (MW) respectively and corresponding statistical results. Two-tailed two-sample T-test indicated no significant difference was found between the two methods (P>0.05).*

4.4. Cell Culture, Cell Viability Test and Combination Index

The MTS assay was performed to measure the cytotoxicity of PARP inhibitors on cells when used individually or in combination with other anticancer drugs. The cell line we choose was the human malignant glioblastoma U251 cell line, which was provided from the S. Katyal Lab, Max Rady College of Medicine Pharmacology and Therapeutics, Rady Faculty of Health Sciences, University of Manitoba. Cells were grown in Dulbecco's modified Eagle medium (DMEM) supplemented with 10% fetal bovine serum and 1X antibiotics including 100units/mL penicillin, 100µg/mL streptomycin, 0.25µg/mL fungizone, 1X glutamax supplement including 2mM *L*-alanyl-*L*-glutamine dipeptide. ~3000 cells/100µL DMEM media were distributed into each well and incubated at 37°C before being treated with drugs. Treated cells were incubated for 72h. Cell viability was tested using MTS protocol [8] by treating cells with MTS and incubating them for about 1 hour. Absorbance was measured by BioTek Gen 5 plate reader at OD 490nM. The dose-response curve of drugs including anticancer drugs or/and PARP inhibitors was measured in U251 cell lines. Anticancer drugs and PARP inhibitors were combined at a certain ratio which will be explained in **Chapter 5 Section 5.7**. The combination index (CI) was calculated to determine the synergistic effect using the equation (16) in reference [9]. The CI calculated using COMPUSYN software (http://www.combosyn.com/)[10] was used for comparison and reference.

4.5. References

1. Berman, Helen M., et al. "The protein data bank." *Nucleic Acids Research*, vol. 28, no. 1, Jan. 2000, pp. 235–42, https://doi.org/10.1093/nar/28.1.235.
2. UniProt Consortium. "UniProt: a hub for protein information." *Nucleic Acids Research*, vol. 43, no. D1, Oct. 2014, pp. D204–12, https://doi.org/10.1093/nar/gku989.
3. Putt, Karson S., and Paul J. Hergenrother. "An enzymatic assay for poly (ADP-ribose) polymerase-1 (PARP-1) via the chemical quantitation of NAD+: application to the high-throughput screening of small molecules as potential inhibitors." *Analytical Biochemistry*, vol. 326, no. 1, Mar. 2004, pp. 78–86, https://doi.org/10.1016/j.ab.2003.11.015
4. Yan, Yu, et al. "First Cascade Mitsunobu Reactions for the Synthesis of 2-Benzoxazole-N-Phenyl and 2-Benzimidazole-N-Phenyl Derivatives." *Molecular Diversity*, vol. 16, no. 1, Nov. 2011, pp. 157–62, https://doi.org/10.1007/s11030-011-9343-0.

5. Harmata, Michael, et al. "Expedient synthesis of sulfinamides from sulfonyl chlorides." *The Journal of Organic Chemistry*, vol. 72, no. 2, Dec. 2006, pp. 683–85, https://doi.org/10.1021/jo062296i.
6. Zhang, Wen-Ting, et al. "Design, synthesis, and cytoprotective effect of 2-aminothiazole analogues as potent poly (ADP-ribose) polymerase-1 inhibitors." *Journal of Medicinal Chemistry*, vol. 52, no. 3, Jan. 2009, pp. 718–25, https://doi.org/10.1021/jm800902t.
7. Beck, Benoit, et al. "Assay Operations for SAR Support." *Assay Guidance Manual*, edited by Sarine Markossian et. al., Eli Lilly & Company and the National Center for Advancing Translational Sciences, 1 May 2012, https://www.ncbi.nlm.nih.gov/books/NBK91994/#_NBK91994_pubdet_
8. Riss, Terry L., et al. "Cell Viability Assays." NCBI Bookshelf, 1 July 2016, https://www.ncbi.nlm.nih.gov/books/NBK144065/?report=reader#_NBK144065_pubdet_.
9. Chou, Ting-Chao. "Theoretical basis, experimental design, and computerized simulation of synergism and antagonism in drug combination studies." *Pharmacological Reviews*, vol. 58, no. 3, Sept. 2006, pp. 621–81, https://doi.org/10.1124/pr.58.3.10.
10. Chou, Ting-Chao. "Drug combination studies and their synergy quantification using the Chou-Talalay method." *Cancer Research*, vol. 70, no. 2, Jan. 2010, pp. 440–46, https://doi.org/10.1158/0008-5472.can-09-1947.

Chapter 5: Research Results

5.1. The General Results of CADD Study

5.1.1. Results and Conclusions

Based on PARP1-ligand crystal structures (PDB ID **5WS1** (Structure of human PARP1 catalytic domain bound to a benzoimidazole inhibitor) and **6VKO** (Crystal Structure of human PARP-1 CAT domain bound to inhibitor UKTT15)) [1, 2, 3], we have built two homologous models of the PARP1 catalytic domain. The model based on **5WS1** was named the Normal model, which reflected the status when the binding pocket was fully closed when a small inhibitor (e.g., benzoimidazole) was bound to the protein. The model based on **6VKO** was named the Open model, which reflected the status when the binding pocket was not fully closed led to a Pro-DNA-retention configuration [3]. It can also be seen as an intermediate state between a fully closed binding pocket and a fully opened binding pocket. The Ramachandran Plots [4] are shown. As residues with torsion angles (ϕ,ψ) within the disallowed region may have higher energy [5, 6], the open model had more amino acids in a higher-energy conformation than the Normal model, indicating the protein in this configuration was not likely in a minimum-energy conformation (**Figure 19**). We could also find this difference between the Open model and the Normal model when they were superimposed. The Open model had a larger binding pocket when the HD was away from the NI (**Figure 20**).

The Normal model reflected a general configuration of the PARP1 protein when a ligand was bound to the binding site. To find out the accuracy of our homologous models when used for docking purposes, we compared the homo-sapiens PARP1-ligand complex crystal structures to corresponding molecular docking results. As our goal was to compare the protein-ligand relationship instead of the overall structural similarity, we argued that conventional comparison using RMSD given by the software would not be accurate, as multiple factors were at play. The approach for judging accuracy involved two steps: 1. Whether the benzamide motif of a ligand was docked to the conventional NI and 2. whether a docking result shared a similar protein-ligand relationship to the corresponding crystal structure. Docking results that failed the first step were considered incorrect. A docking result showing the benzamide motif in the NI, showing conventional binding orientation was considered correct. For correct docking results, distances between a ligand and protein residues were measured (**Figure 21**). 4n pairs of distances could be

generated in total which were then be used to calculate RMSDs. A smaller RMSD indicated a higher similarity in the protein-ligand relative position, suggesting a better docking prediction closer to the experimental result (**Table 8**)

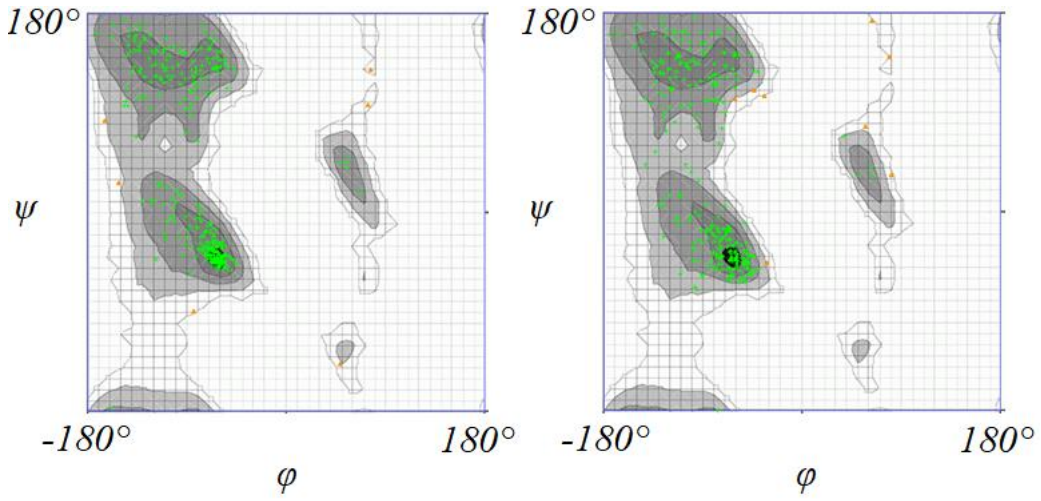

Figure 19 *The Ramachandran Plot of the Normal model (**left**) and the Open Model (**right**) [4]. For the Normal model, highly preferred observations are shown as green crosses: 308 (98.089%). Preferred observations are shown as brown triangles: 6 (1.911%). Questionable observations shown as red Circles: 0 (0.000%). Black, dark grey, grey, light grey represent highly preferred conformations (Delta ≥ -2). White with a black grid represents preferred conformations (-2 > Delta ≥ -4). White with a grey grid represents questionable conformations (Delta < -4). For the Open model, highly preferred observations are shown as green crosses: 289 (97.306%). Preferred observations are shown as brown triangles: 8 (2.694%). Questionable observations shown as red circles: 0 (0.000%). Black, dark grey, grey, light grey represent highly preferred conformations (Delta ≥ -2). White with a black grid represents preferred conformations (-2 > Delta ≥ -4). White with a grey grid represents questionable conformations (Delta < -4). Due to the difference in templates, some residues were trimmed when generating the homologous model.*

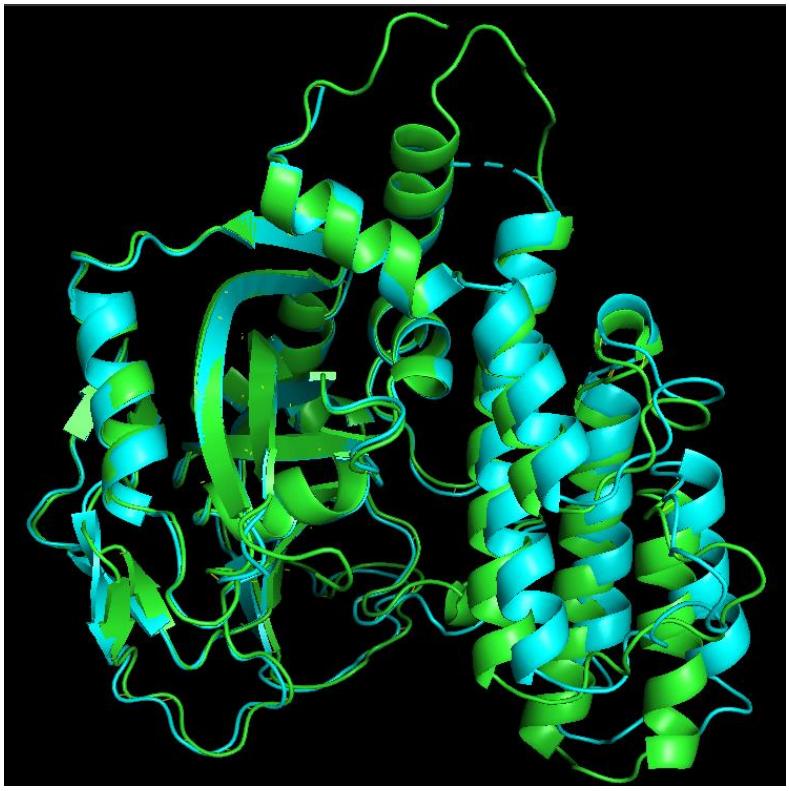

Figure 20 *Superimposition of the Normal model (green) and the Open model (cyan) using PyMol. The PARP1 Normal model was in green and the PARP1 Open model was in light blue. The HD of the Open model was away from the NI compared to the Normal model, indicating a half-opened status of the binding pocket. RMSD = 0.924Å*

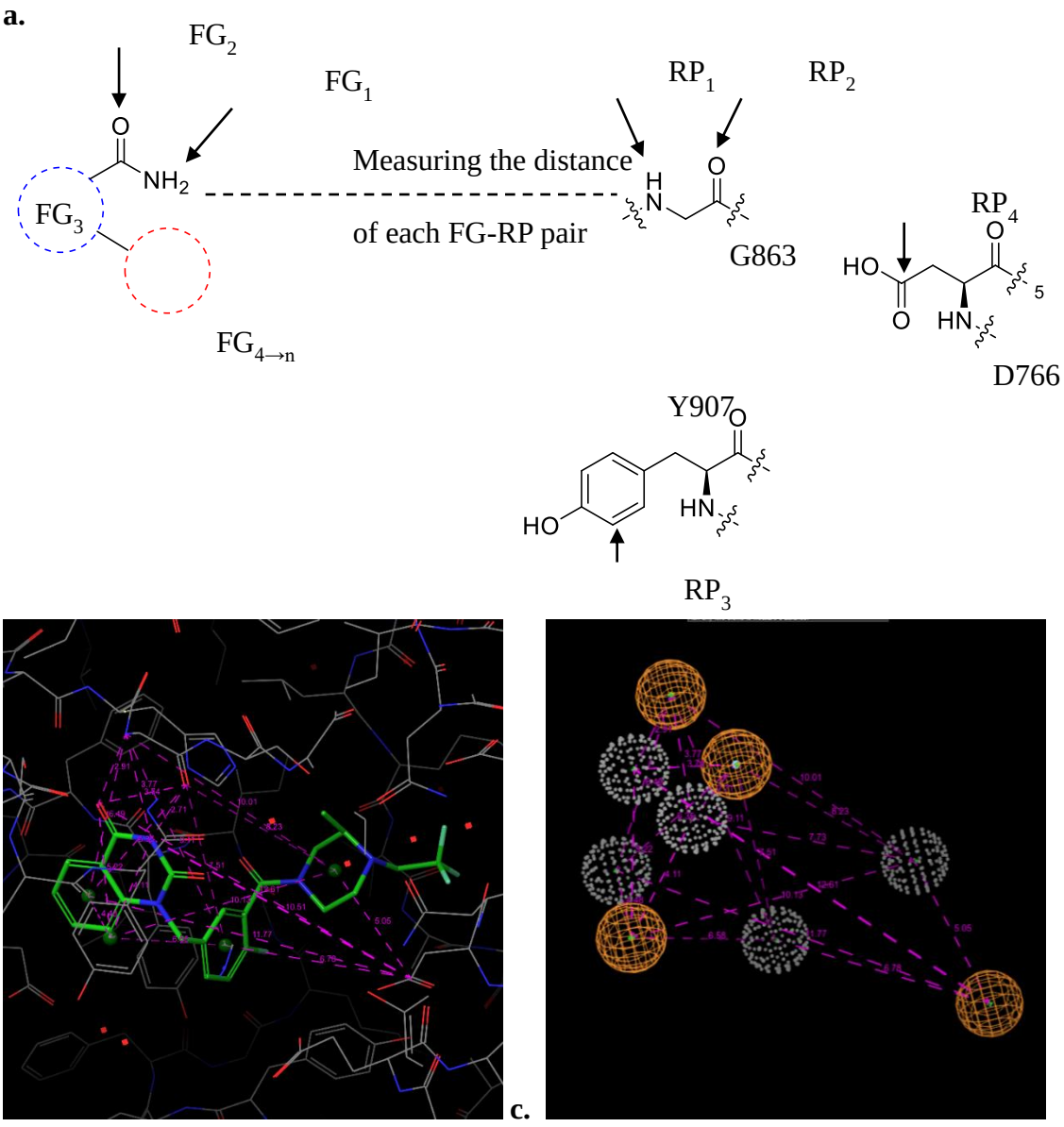

Figure 21 *Schemes of the method used to compare the accuracy of molecular re-docking results. Upper (panel* ***a****): For each compound, several functional groups (FG1→n) are selected based on a benzamide scaffold, including FG1(the amide nitrogen), FG2 (the amide oxygen), FG3(the ring connected to the carbonyl), FG4→n (other representative components). "Other representative components" can be rings or other functional groups that are usually treated as pharmacophores. For the PARP protein, four residue points (RP), including RP1(G863 amide nitrogen), RP2(G863 amide nitrogen), RP3(Y907 phenyl ring), RP4 (D766 carboxylic acid carbon), are used to ensure different molecule conformations/orientations would have different in FG-RP pair distances. RP is selected based on the residue's impotence in the binding pocket.*

*Lower left (panel **b**): The complex from PDB ID **5KPP** (Structure of human PARP1 catalytic domain bound to a quinazoline-2,4(1H,3H)-dione inhibitor) is used as an example showing how distances (purple) are calculated by Schrodinger Maestro "Measure" function. Green balls are centroids of rings. Lower right (panel **c**): The simplified model of **5KPP** complex. Grey balls with dots are FG on the ligand and orange mesh balls are RP on the protein.*

Excellent Docking		Good Docking		Moderate Docking		Poor Docking	
PDB ID	RMSD (Å)	PDB ID	RMSD (Å)	PDB ID	RMSD (Å)	PDB ID	RMSD (Å)
4GV7	0.112	5WS0	0.224	5KPO	0.502	4HHZ	0.885
		1UK1	0.228	3GN7	0.545	5WRY	1.043
		1UK0	0.241	6XVW	0.641	4ZZZ	1.457
		5KPQ	0.244	3GJW	0.658		
		1WOK	0.251	5WS1	0.659		
		5KPP	0.252	4R6E	0.689		
		4UXB	0.318	4PJT	0.717		
		4R5W	0.319	6GHK	0.723		
		5WRZ	0.349				
		6VKQ	0.371				
		5KPN	0.376				
		2RCW	0.412				
		5XSU	0.413				
		5XST	0.418				
		5WRQ	0.427				
		2RD6	0.428				
		5A00	0.450				
		5HA9	0.465				
		5XSR	0.488				
		3L3L	0.498				

Table 8 *RMSDs are calculated by comparing re-docking results and corresponding crystal structures. For these structures, limited by calculation capacity, at most 6 FG spots were selected and 24 pairs of FG-RP distances were calculated. However, more FG/RP spots would increase the accuracy of RMSD calculation. According to **Figure 22**, a docking result with RMSD<0.2Å was considered as an excellent docking; one with 0.2Å≤RMSD<0.5Å was considered good; one with 0.5Å≤RMSD<0.8Å was considered moderate; one with 0.8Å≤RMSD was considered poor.*

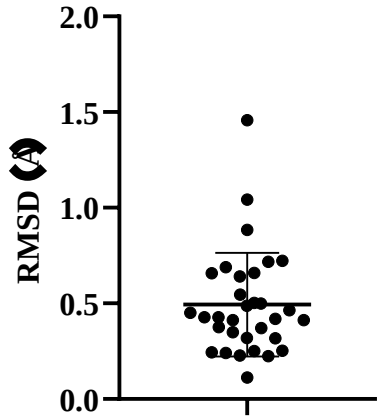

Figure 22 *RMSD distribution of correctly docked compounds with the data from **Table 8**. The vertical upper error is around 0.88Å and the vertical lower error is around 0.2Å. Thus, a docking result with RMSD<0.2Å was considered as an excellent docking; one with 0.2Å≤RMSD<0.5Å was considered good; one with 0.5Å≤RMSD<0.8Å was considered moderate; one with 0.8Å≤RMSD was considered poor.*

We tested 38 entries and 32 of them (**Table 8**) were correctly docked and more than half of them had RMSD less than the mean value (**Figure 22**). Among those that were not docked correctly, three of them were completely wrong as the benzamide component was not docked to the NI or neighbouring area (e.g., **4L6S**, **Figure 23a**) while the other three had the benzamide component in/near the NI but not correctly positioned, without aligning to G863 (e.g., **4HHY**, **Figure 23b**). Conventionally, when dealing with molecular docking results, we took results with RMSD $\leqslant$ 2.0 Å as good solutions [7]. Under this standard, all of our correct results could be considered good. To be more restricted, based on upper and error vertical error (**Figure 22**), we took a docking result with RMSD<0.2Å was considered as an excellent docking; one with 0.2Å≤RMSD<0.5Å was considered good; one with 0.5Å≤RMSD<0.8Å was considered moderate; one with 0.8Å≤RMSD was considered poor. According to this classification (**Table 8**), **4GV7** presented an excellent docking result; 20 out of 32 entries (e.g., **1WOK**, **2RCW**, **4UXB**)

presented good docking results; 8 out of 32 presented moderate docking results (e.g., **4R6E**, **6XVW**) and only 3 out of 32 were comparably worse (e.g., **5WRY**, **4HHZ**) (**Figure 23**). Excellent and good docking results were almost the same as original crystal structures while we could tell that some side-chain orientation outside of the NI from moderate and poor results were different from original crystal structures. 6 FGs from a ligand and 4 RPs from the protein limited the accuracy of this verification method. More spots taken into account would benefit the accuracy, which was difficult to achieve manually. For now, moderate results contained both molecules with correct side-chain orientation and incorrect ones, which could be separated visually. We found 3 examples from moderate results showing wrong side-chain orientation. Thus, 26 out of 32 (81%) docking results were well-predicted. In other words, when we could determine whether the benzamide component was in the NI, we had more than >80% success rate to predict molecular binding orientation correctly. We also found that accurate molecular docking was possible without the amide component (e.g., **5HA9**) (**Figure 24**). Thus, we concluded that the computational model and the *in-silico* docking method we used were accurate enough to predict ligand binding inside the PARP protein. In addition, smaller molecules were more likely to have more accurate docking results. It was reasonable that rotatable bonds, that were difficult to predict, increased the possibility of incorrect orientation.

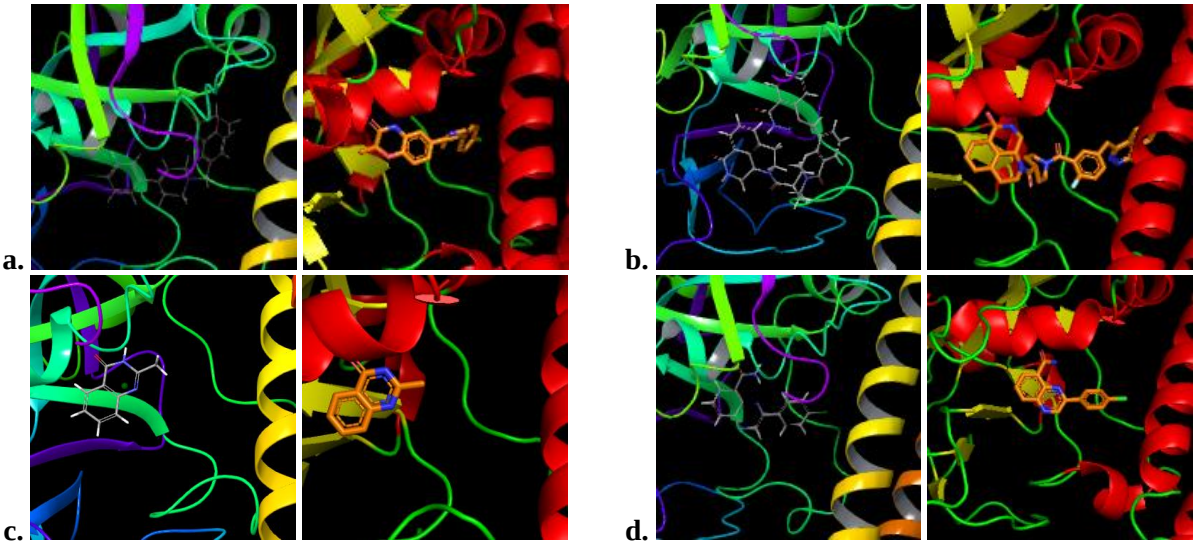

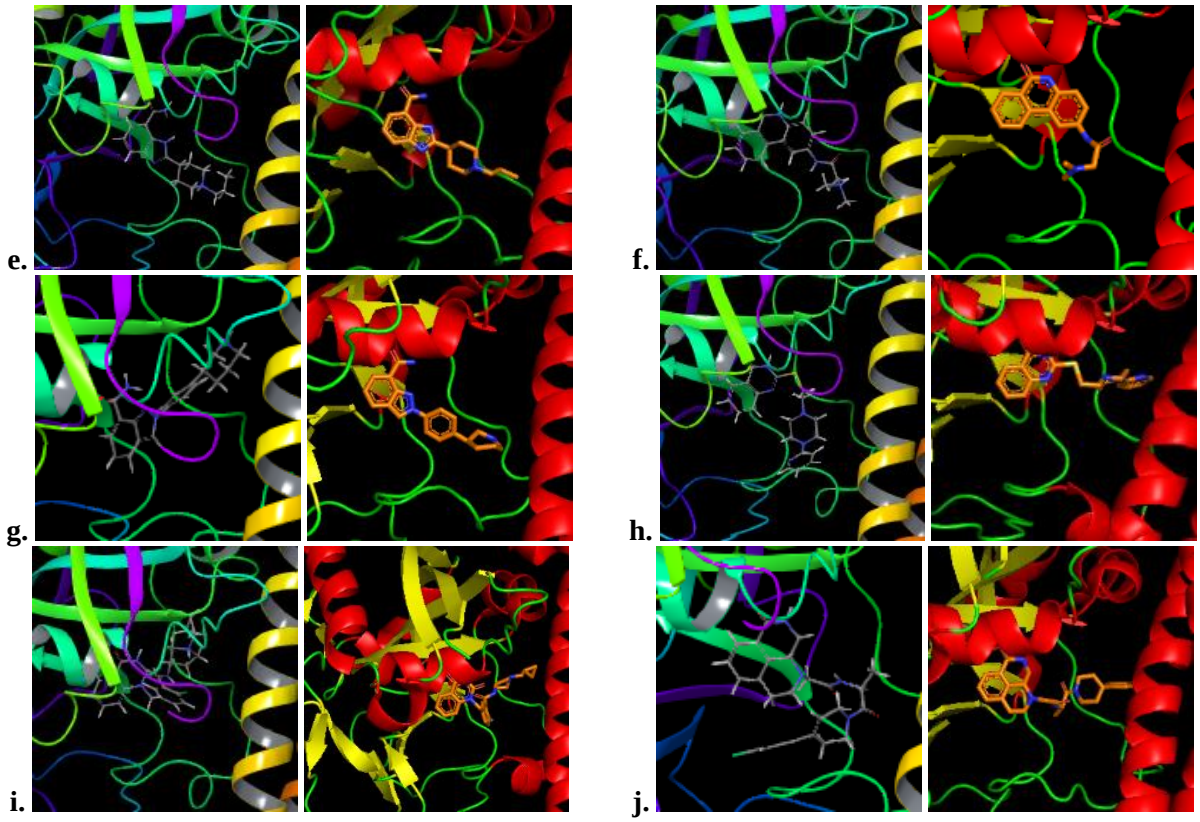

Figure 23 *Examples of pairs of re-docking results and crystal structures with different accuracy. Re-docking results were on the left of each sub-group and crystal structures were on the right. a. 4L6S; b. 4HHY; c.4GV7; d. 1WOK; e. 2RCW; f. 4UXB; g. 4R6E; h. 6XVW; i. 5WRY j. 4HHZ.*

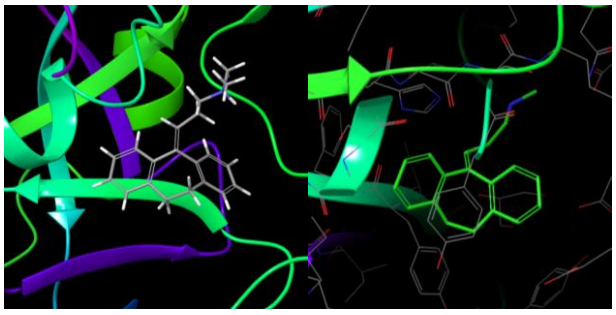

Figure 24 *5HA9 re-docking result (**left**) compared to the corresponding crystal structure (**right**).*

The difference in protein configuration might bring different hydrophobic regions inside the protein (**Figure 25** & **Figure 26**). We found that the Open model had a larger hydrophobic area (**Figure 26**), especially in the region near Q759. The region around the NI remained hydrophobic in both models, while there was some change both in the AD near R878 and the area around the middle section of the D-Loop near Q759 (**Figure 25 Figure 26**, highlighted in

blue circle). The comparison of the hydrophobic areas indicated that, apart from the NI, the physical environment did not change dramatically in the AD, suggesting the conformational change of the protein won't greatly affect the ligand binding in this area. In contrast, the hydrophobicity changed near Q759 with the closure of the binding pocket and influenced the ligand binding. If a ligand would bind to this site with good affinity when the binding pocket was not fully closed, it might lose the affinity gradually unless it could stop the HD from closing up.

By reviewing known crystal structures we believed that when introducing a ligand with a hydrophobic structure into the protein, the hydrophobic region and the hydrophobic component of the ligand complemented each other. We found that the orientation of the hydrophobic component would be directed by the hydrophobic region inside the binding pocket. For most PARP inhibitors, the carboxamide motif would locate in the NI hydrophobic pocket while the hydrophobic side chain would be attracted by the peripheral hydrophobic sites. Talazoparib (**Figure 27**) had its benzene substituent in the neighbouring hydrophobic region, leaving the hydrophilic triazole component in the non-hydrophobic part. Olaparib (**Figure 28**) as well had its benzene component positioned in the hydrophobic region, which had the piperazine component on it inserted into the groove between the D-Loop and the HD near R878. Thus, we had reasons to believe that the distribution of the hydrophobic region inside the binding pocket would affect the ligand configuration, especially the substituents connected by rotatable bonds. According to the hydrophobic mapping, we also believed that the hydrophobic region would attract and move the side chain to the groove between the D-Loop and the HD near Q759, or the one near R878. On the other hand, a ligand would achieve its best affinity if the free energy to adjust the torsion angle to fit the hydrophobic component into the hydrophobic region was minimum. It could also be seen from a previous study modifying the carbon-linker between the isoquinolinone component and the benzene component of olaparib: When the plain methane linker was turned into ketone or methanol, a general decrease in the inhibitory activity of olaparib could be observed [8]. In this case, a plain -CH- chain was easier to twist compared to the ketone or the methoxy component. The energy the compound took to adjust the torsion angle could increase when the methane chain converted to the carbonyl, decreasing the affinity. More overlapping between the protein's hydrophobic site and the ligand's hydrophobic component might induce better affinity. Thus, when designing the ligand, we need to not only consider the guidance effect

of the hydrophobic region inside the binding pocket but also less energy change during the ligand torques the side chain towards the hydrophobic site.

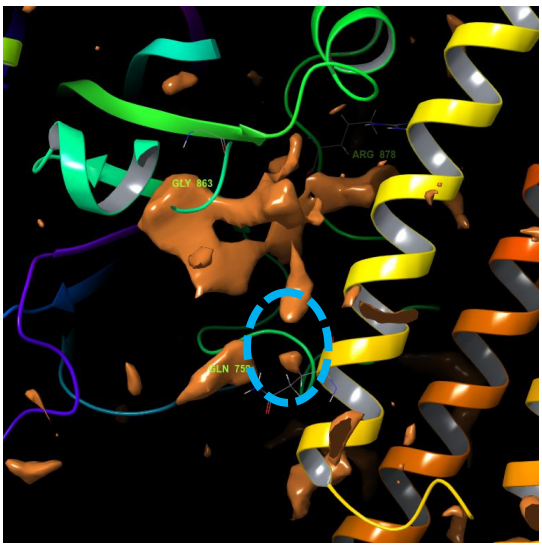

Figure 25 *The hydrophobic area inside the PARP1 Normal model. The hydrophobic region is shown in orange. The area that is different from the Open model is circled above in blue. The hydrophobic mapping was achieved by the Structural Analysis function of Schrodinger Maestro. The method was introduced in* ***Chapter 4***, ***Section 4.1***.

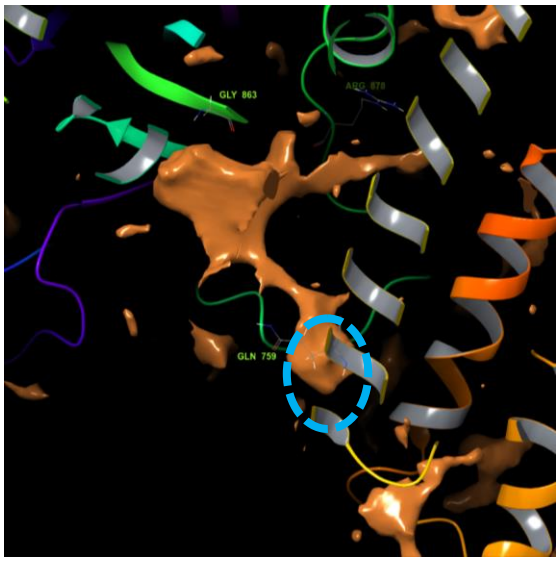

Figure 26 *The hydrophobic area inside the PARP1 Open model. The hydrophobic region is shown in orange. The area that is different from the Normal model is circled above in blue. The*

hydrophobic mapping was achieved by the Structural Analysis function of Schrodinger Maestro. The method was introduced in ***Chapter 4****,* ***Section 4.1****.*

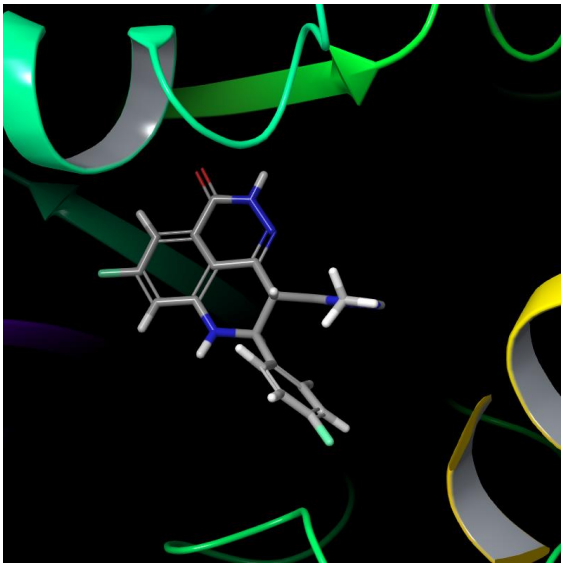

a. Without hydrophobic mapping

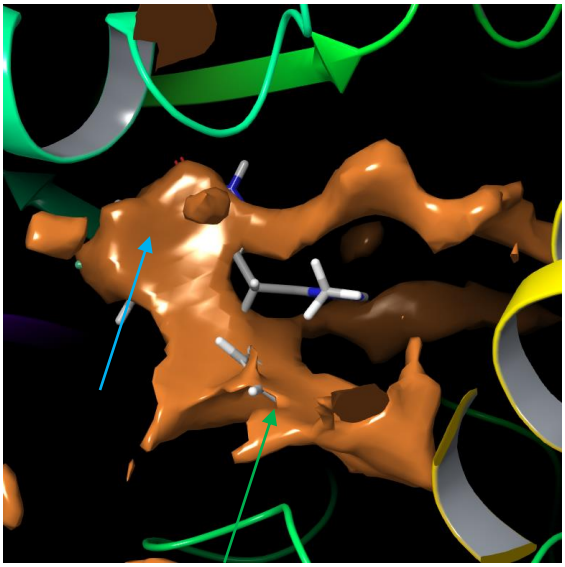

b. With hydrophobic mapping

Figure 27 *Hydrophobic mapping of PARP1-talazoparib complex. The hydrophobic region is in orange. The core component was in the hydrophobic pocket in the NI (blue arrow). The substituted benzene component was in the neighbouring hydrophobic region (green arrow) but the triazole component was not, as the benzene component was more hydrophobic than the triazole component. The hydrophobic mapping was achieved by the Structural Analysis function of Schrodinger Maestro. The method was introduced in* ***Chapter 4****,* ***Section 4.1****.*

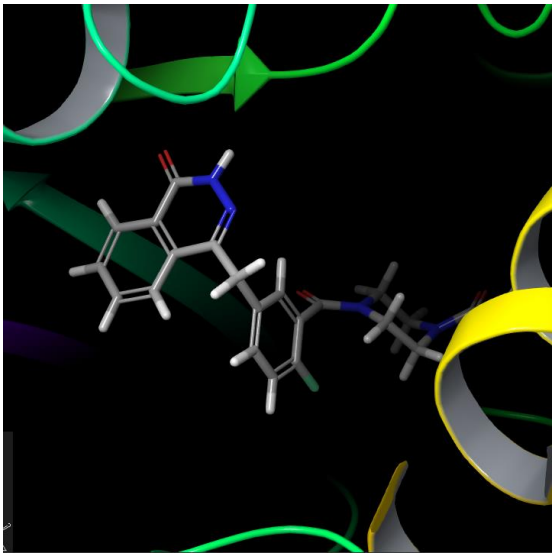

a. Without hydrophobic mapping

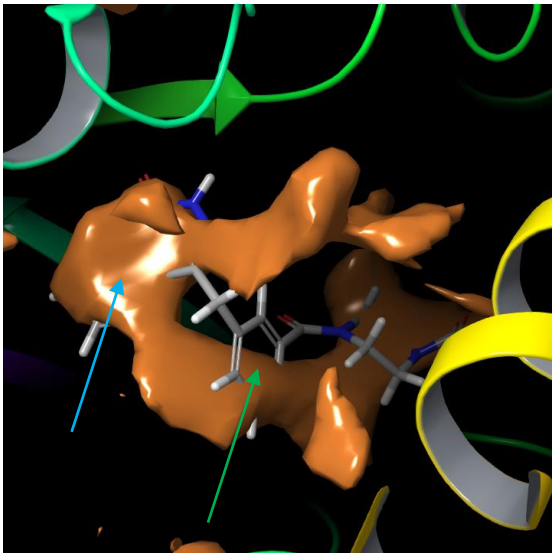

b. With hydrophobic mapping

Figure 28 *Hydrophobic mapping of PARP1-olaparib complex. The hydrophobic region is in orange. The core bicyclic component was completely in the hydrophobic pocket in the NI (blue arrow) while the benzene component was located in the neighbouring hydrophobic site (green arrow). Due to the orientation of the benzene ring, affected by the hydrophobic region, the following piperazine component was settled in the groove between the D-loop and the HD near R878. The hydrophobic mapping was achieved by the Structural Analysis function of Schrodinger Maestro. The method was introduced in* ***Chapter 4***, ***Section 4.1***.

5.2. Experiments on PJ34 Analogs

5.2.1. General Introduction

We started the development of novel inhibitors by investigating the analogs of our benchmark PJ34, since it is the only commercially available PARP inhibitor that is based on phenanthridin-6(5*H*)-one (Phe) and is widely used in related studies. As mentioned in the previous review (**Chapter 2**, **Section 2.5**), PJ34 was approximately 3-4 fold more potent than its precursor Phe. The PARP1-PJ34 complex crystal structure (PDB ID **4UXB**) suggested that PJ34 would form a cation-π interaction between the secondary amine and Y896 **Figure 29** [1, 9, 10]. Schrodinger Maestro did not show a similar interaction (**Figure 29**). It was unknown if the 2-(dimethylamino)acetamide side chain increased potency through the cation-π interaction with Y896. Thus, designing PJ34 analogs would be a method to figure out the influence of the amine side chain.

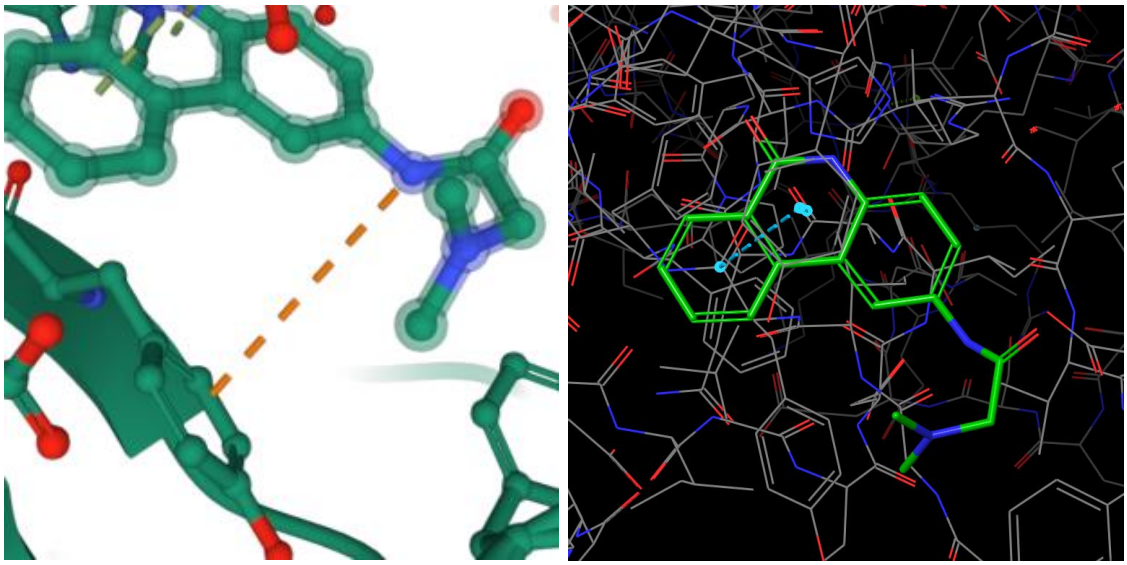

Figure 29 *The cation-π interaction between the ligand and Y896. Mol* indicated there was a cation-π interaction (orange) between the amide nitrogen and Y896 (**left**). However, Schrodinger Maestro indicated that cation-π interaction between the amide nitrogen did not exist (**right**).*

5.2.2. Results

PJ34 analogs were designed to study if the acetamide group influenced the potency by providing extra protein-ligand interaction. PJ34 is composed of three components: A phenanthridinone core structure, an amide linker, and a tertiary amine. Modifications were on the carbonyl-side benzene ring Ar, R_1 and R_2 positions respectively (**Figure 30**). The modification of the aromatic component converted the benzene ring to a thiophene ring. Analogs were composed of a tertiary or secondary amine that was similar to PJ34 and the amine was connected to the phenanthridinone or thienoquinolinone component with an amide or a urea linker. Examples of PJ34 analogs and corresponding IC_{50}s are shown in **Figure 31**.

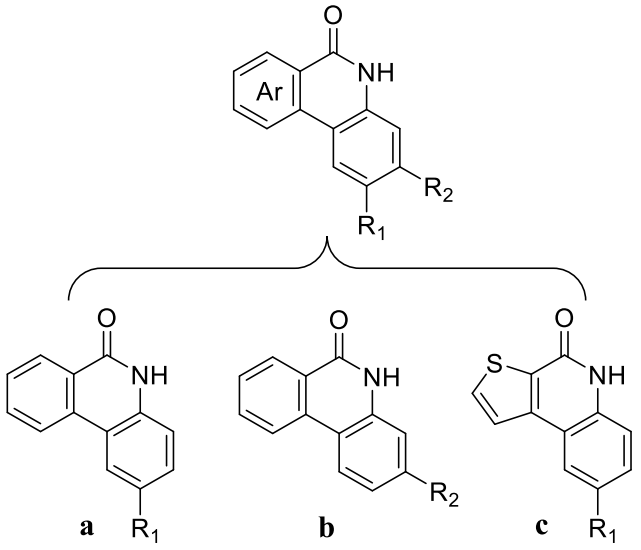

Figure 30 *Modifications to make PJ34 analogs. Ar: The benzene ring from the carbonyl component; R_1: 2'-substituent, para to the amine; R_2: 3'-substituent, meta to the amine*

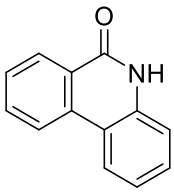

Phe IC_{50} = 419±53nM

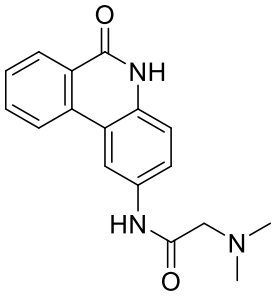

PJ34 IC_{50} = 148±28nM

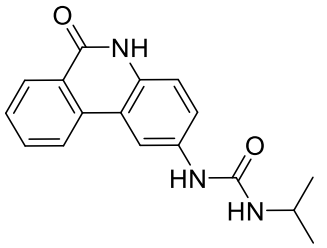

a1 IC_{50} = 93.4nM

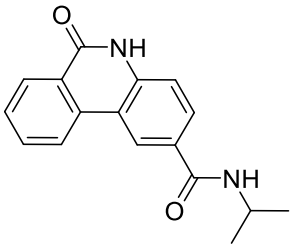

a2 IC_{50} = 39.4nM

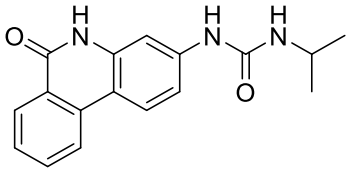

b1 IC_{50} = 219nM

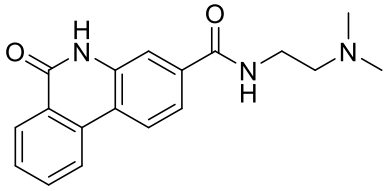

b2 IC_{50} = 443nM

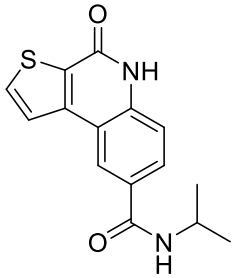

c1 IC_{50} = 1820nM

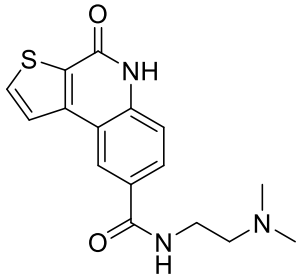

c2 IC_{50} = 10900nM

Figure 31 *PJ34, phenanthridinone and PJ34 analogs and their IC_{50}s. Experimental data were obtained from the enzymatic assay described in* ***Chapter 4, Section 4.3****. Each experiment was plated in triplicate. Data obtained from two or more experiments were shown as Mean±SD; otherwise, it was obtained from single measurements. Experimental data were processed with GraphPad 8.0.1. IC_{50} values were calculated using 4-parameter logistic regression.*

For *in silico* analysis, we docked PJ34 into the normal PARP1 homologous model to check the accuracy of the molecular docking by comparing the *in silico* docking result to the crystal structure. We found that the two configurations were very similar, as the phenanthridinone component and the amide nitrogens from the two complexes were in an analogous location. The deviation existed in direction of the carbonyl group and the position of the tertiary amine (**Figure 32**). Although PDB Mol* suggested there was the cation-π interaction, its molecular docking results suggested that the interaction might not exist. We also docked potent PJ34 analogs to the homologous model (**Figure 33**). We reviewed some orientations and none of them were expected to interact with Y896.

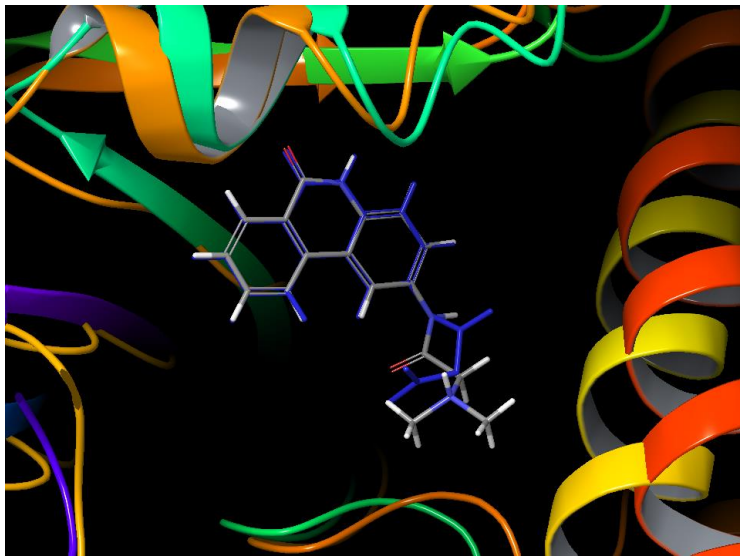

Figure 32 *Superposition of PARP1-PJ34 crystal structure and the molecular docking result. This is the superposition of the PARP1-PJ34 complex crystal structure (PDB ID* ***4UXB****) and the molecular docking result of PJ34 in the PARP1 Normal model. PJ34 from the crystal structure*

was shown in dark blue. The phenanthridinone structures were almost overlapping. Rotatable bonds connected to the amide group and the tertiary amine group caused deviation between molecular docking results and the crystal structure. The highest score orientation had RMSD=0.318Å calculated based on the method introduced in ***Chapter 5, Section 5.1****.*

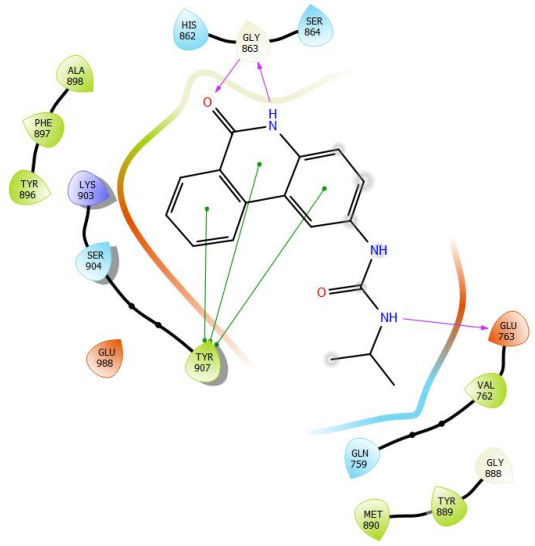

a. PARP1-**a1** interaction in the Normal model

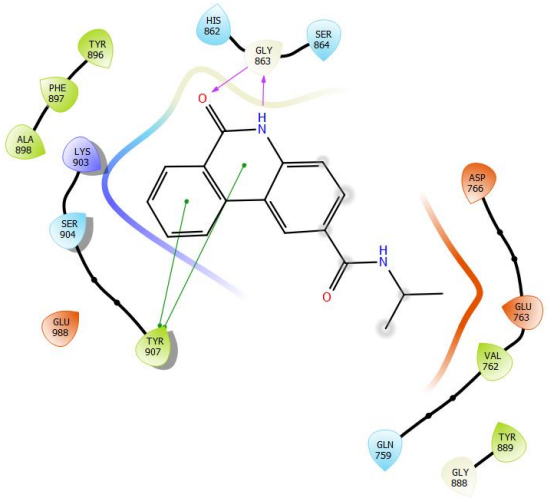

b. PARP1-**a2** interaction in the Normal model

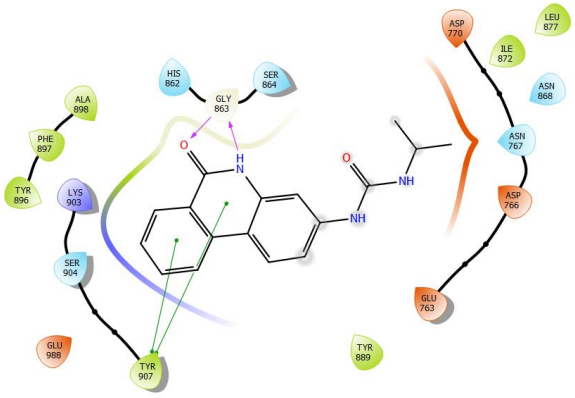

c. PARP1-**b1** interaction in the Normal model

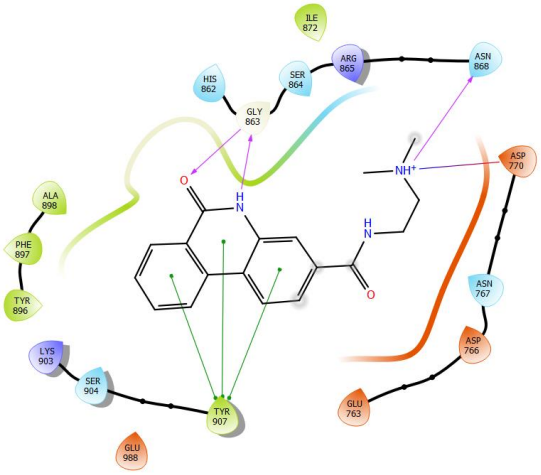

d. PARP1-**b2** interaction in the Normal model

Figure 33 *Potent PJ34 analogs docked to the PARP1 Normal model. Potential H-bonds were shown in purple and π interactions were shown in green. Grey circles indicated the components exposed to solvent.*

From the enzymatic assay, their overall potency ranked **a** compounds > **b** compounds > **c** compounds (**Figure 30 Figure 31**). As previously mentioned, **a** compounds were still able to form the cation-π interaction with the rotation of the amide or the urea bonds. In contrast, the amide structures from **b** compounds were too far for π interaction with Y896. Thus, the cation-π interaction with Y896 contributed to the affinity. **a1** was the most similar in structure to PJ34 and had similar potency. When the urea group was replaced by a simple amide (**a2**), the potency increased by over 2 fold, suggesting that the cation-π interaction with Y896 might not be limited to the amide NH attached directly to the aromatic ring. A layout with the amide carbonyl component attached to the aromatic ring might bring the secondary amine closer to Y896. This layout was more relative to the original crystal structure configuration of the PJ34-PARP1 complex (rather than the docking result) where there was a swap in position between the amide carbonyl and the amide nitrogen. When the urea substituent was on the R_2 position, **b1** was about 5-fold less active than **a1**. The dimethyl-amino group in the R_2 position of **b2** would further decrease the potency. As **b1 b2** were both compounds with flexible amide side chains, the influence could come from the spatial clash with the HD. Comparing **a** and **c** compounds, converting the phenanthridin-6(5*H*)-one component to the thieno[2,3-*c*]quinolin-4(5*H*)-one, the potency would be decreased significantly, therefore thieno[2,3-*c*]quinolin-4(5*H*)-one might not be a good core component. The loss of potency might be a result of decreased electron richness on the aromatic ring, leading to weakened π-interaction. We also noticed that **a1** might interact with E763 and **b2** might interact with D770 and N898. These two compounds both have a tertiary amine as an H-bond acceptor. In contrast, **a2** and **b1** didn't form any additional bond with any amino acid residue rather than conventional ones from the phenanthridinone component in the NI. Comparing **a1 b2** and **a2 b1**, we believed that interacting with D770 and N878 would not contribute to the potency when a compound majorly occupied the NI.

5.2.3. Conclusion

We tested PJ34 and its core component Phe, and PJ34 was found to be about 4-fold more potent than Phe. The structural difference between PJ34 and Phe was PJ34 had a dimethylamino acetamide side chain. To investigate the importance of dimethylamino acetamide side chain such as the potential cation-π interaction between the acetamide nitrogen and Y896 and the tertiary amine, we designed and synthesized some PJ34 analogs with modifications on the side chain

including the side-chain position as well as the carbonyl benzene component. These 6 compounds had different potency, ranging from 2-fold more potent to 100-fold less potent than PJ34. Although the molecular docking result suggested there might be no cation-π interaction, the comparison between **a** and **b** compounds implied that a secondary amine near Y896 would benefit the affinity. We took it as the evidence of the cation-π interaction that could not be predicted correctly by the molecular docking result and that this interaction would contribute to the potency. Hence, we kept the design with the amide attached to phenanthridinone. The potency of **a1** and **a2** suggested that the tertiary amine of PJ34 didn't contribute to the potency. In PJ34, the tertiary amine could only be used for the formation of the hydrochloride salt. As **a2** was more potent than **a1**, it implied that the layout of the amine group attached directly to the phenanthridinone might not benefit the binding affinity either. Using an amide carbonyl group attached to the phenanthridinone component might also produce potent inhibitors, equivalently or better. For an inhibitor that majorly binds to the NI, the R_2 position was not preferred for adding a large side chain. When the binding pocket was fully closed, there could be less room to accommodate compounds in the binding pocket near the R_2 position than the R_1 position, which was in line with what we saw from the shape of the binding pocket. Secondly, if the inhibitor only primarily occupied the NI, interacting with other residues aside from G863, S904 and Y907 could be meaningless, which we could see from the comparison between **a1/b2** and **a2/b1**. Thus, the importance of the amide nitrogen, which was thought to interact with Y896 might be limited. The function of the dimethylamino acetamide group might be limited to helping phenanthridinone compounds form HCl salts. The results of thieno[2,3-*c*]quinolin-4(5*H*)-one compounds suggested that the core component in the nicotinamide binding pocket would influence the potency greatly.

In conclusion, we argued that to develop novel PARP inhibitors, we could keep the phenanthridinone core component and the amide linker. Phenanthridinone was a good core component to start with, but it would be beneficial to figure out if there were any other small inhibitors, other than benzamide that would have a great affinity for the NI. We needed to figure out the potential mechanism of the ligand-protein interaction inside the NI, in addition to the conventional idea of "mimicking the nicotinamide". That was why a theinoquinolinone compound had a worse affinity. We also needed to review the relationship between the spatial

occupancy and the potency, as we saw different sizes/locations of side chains would have distinguished affinity.

5.3. Experiments on Small Phenanthridinone-type Inhibitor

5.3.1. Introduction

The design of the PARPi core structure, the benzamide motif, is very conserved, especially for commercial PARP inhibitors. This can be seen in newer generations of PARP inhibitors, such as Niraparib and olaparib, which are still using the benzamide motif. Few studies were attempted to develop novel PARP inhibitors based on a core structure other than benzamide. To search for an alternative structure, we need to understand the potential ligand-protein interaction inside the NI. Thus, we are looking back to small benzamide analogs to carry out a universal modification solution so that we can optimize the benzamide motif whenever it is used as a small PARP inhibitor or a part of a larger PARP inhibitor. The widely accepted concept of how benzamide interacts with the surrounding residues inside the NI has been discussed in the review chapter that the electron-rich aromatic ring and the amide provide the infrastructure for π-π interaction and H-bonding. But the study from Ferraris *et al*. [11, 12] hinted there could be other factors such as different electron density distribution influencing the potency of compounds. Even though they shared great similarities while the only difference was the position of N on the ring, benzo[*c*][1,8]naphthyridin-6(5*H*)-one analog delivered completely different potency. These compounds can be found in **Table 10** (**e1** compounds). These compounds do not have any substituents and they are rigid without any rotatable bonds, indicating the position of N leads to the diversity.

It is commonly known that π-π interaction is an interaction between the negatively charged region from the electron-rich π system above and below the aromatic ring and the positively charged region on the edge of the aromatic ring. According to Coulomb's Law, it was influenced by the electron richness and the distance. H-bonds between a ligand and amino acid residues were also important as discussed before. The essence of H-bonding is the interaction between a partial negative-charged component and a partial positive-positive charged component, mediated by δ^+ hydrogen. The relative electronegativity and the distance between two components determined the strength of H-bonding and the dipole charged distribution along with the bond axis limits the interaction being directional [13]. Thus, the H-bond is influenced by

three factors: electronegativity, distance, and bond angle. We asked if there was something on the benzamide structure that would influence the π-π interaction and the H-bond simultaneously and we found clues in the crystal structure shown in **Figure 34** [1, 10, 14]: While most inhibitors with known crystal structures had similar distances between the carboxamide component and G863 (which was why we were not taking the distance between the amide component and G863 into account), inhibitors like PJ34 and A968427 form different dihedral angles between the plane of the compound and the plane of G863. Even though PJ34 is further away from Y907 as a result of the 0° dihedral angle, A968427 was more parallel (comparing the distance ratio) to Y907 than PJ34. In short, if a ligand approaches the NI by different dihedral angles (with G863), the strength of the π-π interaction and the H-bonding, especially between G863 carbonyl group and NH from the molecule's carboxamide, would be different. Thus, we hypothesized that for a small PARP inhibitor, the major determinant of PARP inhibition potency was the binding pose. When the ligand reached the initial position in the NI, the initial strength was determined by the total electrostatic potential on the surface. However, since the surface electrostatic potential was not distributed evenly, the π interaction strength between each point on the ligand surface and Y907 differed. The uneven strength manipulated the ligand until it was balanced and consequently determined the final dihedral angle between the ligand and G863 (**Figure 35**). The dihedral angle between the ligand and G863 would influence the strength of ligand-G863 H-bonding. The center of the ligand might also move during this procedure.

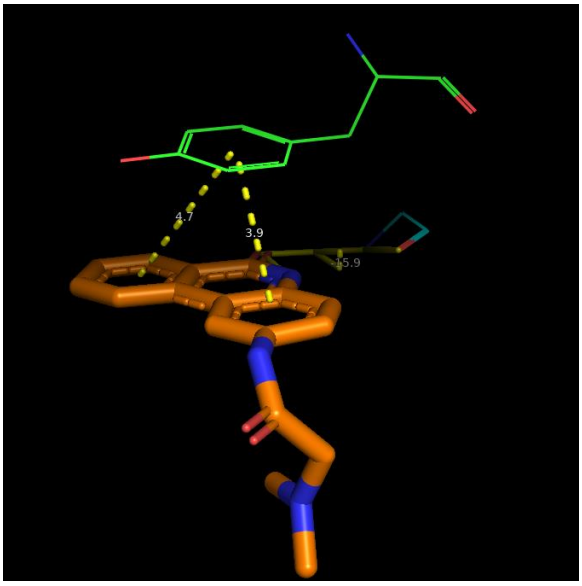

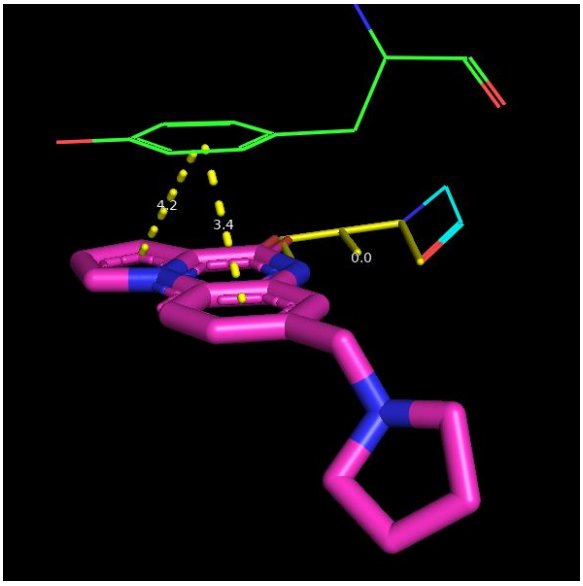

PJ34 A968427

Figure 34 *Dihedral angles of PJ34 and A968427 binding to G863 and Y907. These are dihedral angles of PJ34 (15.9°) and A968427 (0°) binding to G863 (blue) and Y907 (green). The distances between rings and Y907 of each compound were 4.7Å and 3.9Å (PJ34), 4.2Å and 3.4Å (A968427) (the distance between ring centroids). Our assumption was that the total electron richness of the ligand influenced the overall π interaction between the ligand and Y907, determining the initial distance between the ligand and the residue. To reach a balanced state, π interactions from each ring should be the same. Based on Columb's law, the aromatic ring with stronger electron potential would be pushed away from Y907 to obtain the same π-interaction strength as the aromatic ring with weaker electron potential. The swing of the ligand to balance the π-interaction strength led to different dihedral angles with G863, and influenced the H-bonding consequently.*

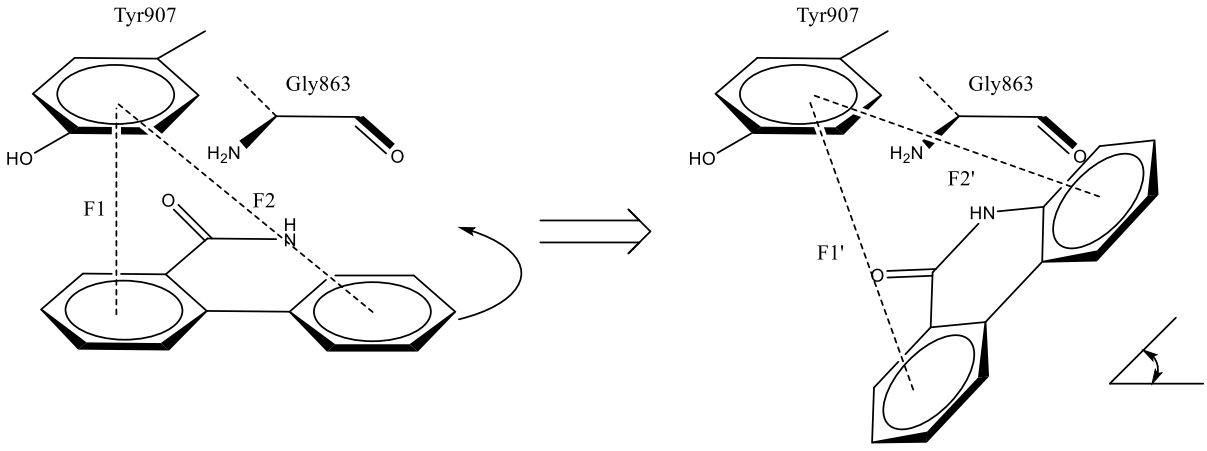

Figure 35 *An example of the proposed docking procedure. The docking begins at an initial position where F1≠F2. F1 and F2 are the π interaction strength between Y907 phenyl ring and ligand's ring attached to the carbonyl, ligands ring attached to the NH respectively. F1' and F2' were corresponding π interactions after rotation. Under the act of different forces, the ligand started to rotate until F1'=F2'≈* $F_{total\ \pi\ interaction}$ *and formed a dihedral angle between the ligand and G863.*

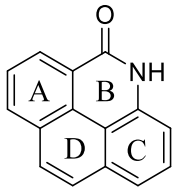

Figure 36 *Proposed pharmacophore of a simple PARP inhibitor. The pharmacophore consists of a tetracyclic system: ARing attaches to the carbonyl component; BRing is the carboxamide ring; CRing attaches to the amine component; DRing attaches to ARing and BRing.*

For a typical PARP inhibitor that only occupies the NI, its pharmacophore could be simplified as a tetracyclic system (**Figure 36**). We focused on bicyclic and tricyclic compounds. For further simplification, we made a few presumptions: 1. π interaction only came from the center of the ring; 2. ARing and CRing were considered; 3. The H-bond reached the maximum when the dihedral angle was 0; 4. We take a compound to reach the optimal position when there is no CRing as the competing π interaction does not exist; 5. The dihedral angle was positively related to the ratio between two distances ARing-Y907 vs. CRing-Y907 which would be defined in the equation (3)-(5) below; 6. The influence of the dihedral angle on the H-bond was not linear; as we didn't have a ready-to-use model to express this relationship, we used the sigmoid function for normalization as it was widely used for prediction purposes.

5.3.2. Results

We simply reviewed the importance of each component on a small PARP inhibitor: H-bond acceptor, H-bond donor, and aromatic rings (**Table 9**). From the results of tested small molecules, we believed that the H-bond acceptor served as a critical component as an on/off switch and it needed to be in a specific location where it could act as the H-bond acceptor when forming H-bonds with G863 and S904 simultaneously. Replacing the carbonyl group with the boronic acid or the sulfonyl/sulfinyl group would reduce the potency dramatically, even to zero (Phe vs. **s1 s5 s6 s7**). For the boronic group, it served as a much weaker H-bond acceptor but the hydroxyl group would be located in a similar position as the oxygen from the carbonyl group, its potency was 5000-fold less compared to phenanthridinone. However, the boronic compounds were at least 10-fold more potent than sulfonyl and sulfinyl compounds whose sulfonyl/sulfinyl

oxygen was not in the same plane of the compound, the dislocation od which might make it impossible to form the H-bond. The H-bond donor and aromatic rings also had an influence on the potency but the absence of these two features would not stop a ligand from being an inhibitor (Phe vs. **s10** & **s12**, **s10** vs. **s14**). In agreement with previous studies, an increase of electron richness of the aromatic ring would benefit the potency (**s10** vs. **s9**, **s12**vs. **s8** vs. **s19**, **s13** vs. **s15** vs. **s16**); a *cis* conformation of the carboxamide contributed to the inhibition as well (3AB vs. **s15**). Thus, we believed the prerequisite for a phenanthridinone-like compound to be a potent PARPi was to have a carbonyl group as an H-bond acceptor and the amine and aromatic components were influencing factors.

Name	Structure	IC_{50}(μM)	Name	Structure	IC_{50}(μM)
3AB	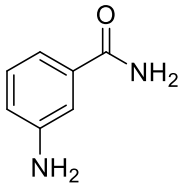	20.1 [16]	**s12**	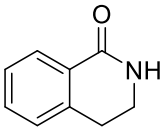	3.87±2.3
Phe	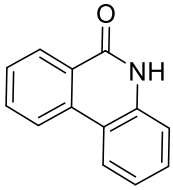	0.420 [17]	**s13**	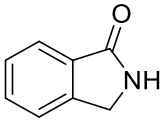	71.9*
s1	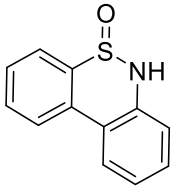	None	**s14**	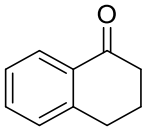	>100 (2400)
s5	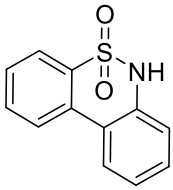	>100 (22100)	**s15**	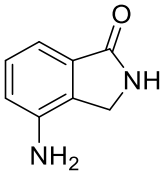	14.9±3.8
s6	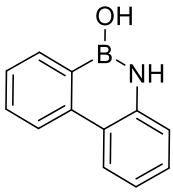	>100 (2070)	**s16**	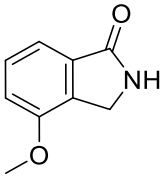	10.5±5.25

s7	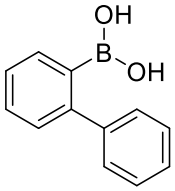	>100 (1170±43)	**s17**	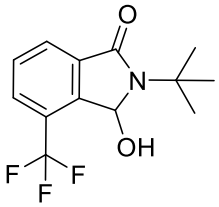	>100 (5950)
s8	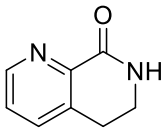	>100 (134±32)	**s18**	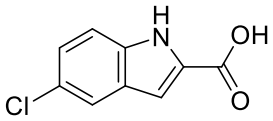	None
s9	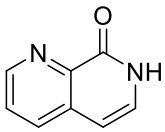	>100 (1130)	**s19**	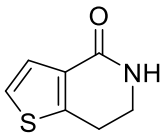	47.4
s10	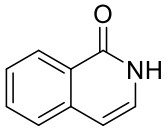	>100 229±140	**s20**	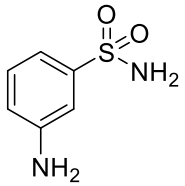	None
s11	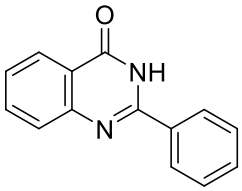	7.57±2.5			

Table 9 *Tested small molecules for PARP1 inhibition. Experimental data were obtained from the enzymatic assay described in* ***Chapter 4, Section 4.3****. Each experiment was plated in triplicate. Data obtained from two or more experiments were shown as Mean±SD; otherwise, it was obtained from single measurements. Experimental data were processed with GraphPad 8.0.1. IC_{50} values were calculated using 4-parameter logistic regression.3AB and Phe were used as a reference with IC_{50} data from literature [16] [17] (as we need them to adjust the equation parameters). Data in bracket were extrapolated. Data with * was* near the upper range (100000nM) used for the experiment.

Based on this understanding and the hypothesis, we proposed the equation to score these molecules (1)

$$E = E_{ARing} + E_{CRing} + E_H \quad (1)$$

where we only considered the interaction energy of aromatic components and the H-bond from amine. As the H-bond from the carbonyl group was a prerequisite, it was not taken into account. E was considered as the total binding energy. E_{ARing} was the π-π interaction energy of

the carbonyl aromatic ring and E_{CRing} was the π-π interaction energy of the amine aromatic ring. As both interact with Tyr907, the strength of the π-π interaction would be determined by the electrostatic potential of each ring. E_H represented the actual value of the amine H-bond energy which would also be represented by the electrostatic potential. E_H was a result of the theoretical H-bond energy E_{NH} subjected to the dihedral angle *f*(*t*) (2).

$$E_H = f(t)E_{NH} \tag{2}$$

f(*t*) was a function to describe the positive relationship between the dihedral angle and its influence on the H-bond. *t* is the ratio between the distance from Y907 to ARing and Y907 to CRing. The goal of *f*(*t*) is to convert the distance ratio to the dihedral angle. *f*(*t*) had two features. 1. It had limits: There would be an optimal angle the H-bond was perfectly formed and any increase or decrease of the angle value would reduce the strength. This feature suggested the function curve was asymmetric. 2. Due to the relationship of H-bond angle and H-bond strength according to the previous study [18], the influence of the angle on the strength was not linear. Since the accurate equation to express the influence with the above-mentioned two features was not yet known, we adopted the sigmoid function (3) as it was widely used for prediction purposes and presumed that the optimal angle was 0. The function could be changed in the future if there is a more suitable function that could convert ratio *t* to dihedral angle.

$$f(t) = 1 + \frac{c}{(1+\frac{t}{b})^a} \tag{3}$$

c was set as the difference between upper and lower limit (i.e. 0-1); *a* and *b* were constant. They were made heuristically. They were as well subjected to change according to different situations and tuning a and b can accommodate the function to different test subjects, e.g., ligands with different side chains. They were constant because they were not influenced by measured data. On the other hand, the interaction strength between the ligand and Tyr907 could be expressed by Coulomb's Law (4):

$$F = k\frac{q_a\, q_b}{r^2}, r = \sqrt{k\frac{q_a\, q_b}{F}} \tag{4}$$

where *F* was total the π-π interaction strength. When the ligand was considered as a whole, the strength distributed on each component should be the same, equaling to *F*. Thus, the ratio of two Tyr-Ring distances could be described as

$$t = \frac{r_{ARing}}{r_{CRing}} = \sqrt{\frac{q_{ARing}}{q_{CRing}}} \quad (5)$$

where r_{ARing} is the distance from the A-Ring to the Tyr and r_{CRing} was the distance from the C-Ring to the Tyr. q_{ARing} and q_{CRing} are electrostatic potentials of two rings respectively. In this case, the electrostatic potential of the center was used. *t* was the ratio of two distances and it was related to the dihedral angle.

We screened a series of purchased or synthesized candidates as listed using the same enzymatic assay. These candidates included bicyclic and tricyclic compounds. Electrostatic potentials were calculated by Gaussian 09W at Hartree–Fock level using the 3-21G basis set. Potential readings were taken from the surface of the amine hydrogen and the surface of the aromatic ring center. The scoring mechanism called FScore was carried out by magnifying the calculated *E* based on the equation above one hundred times for convenient and direct comparison with Schrodinger's docking score. Values of *a*, *b*, *c* were determined heuristically, as *a*=5, *b*=0.7, *c*=0.999.

Based on the prediction model, we scored phenanthridinone-like compounds to find the correlation between the prediction and the potency listed (**Table 9, Table 10, Table 11, Table 12**). We also compared our predicting results to the ones of Schrodinger's docking score [15]. According to the result, when scoring both bicyclic compounds and tricyclic compounds together, the prediction results from both methods were able to correlate to the drug potency; Schrodinger's docking score had a medium correlation while ours only had a low correlation. However, when the results of bicyclic compounds or tricyclic compounds were analyzed respectively, our prediction result had the same performance while Schrodinger's docking score lost the correlation between scores and drug potency. The result suggested our method had a similar prediction capability as Schrodinger's docking score when predicting compounds that had a significant difference in structure while we were able to outperform the latter one when objects were analogous to each other.

Name	Structure	IC_{50}(nM)	Name	Structure	IC_{50}(nM)
c34	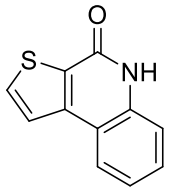	646	**e1**	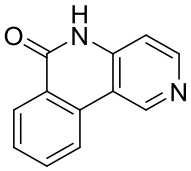	110
c35	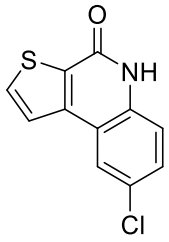	616	**e1-1**[a]	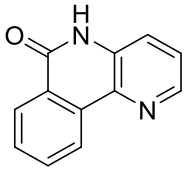	100
c38	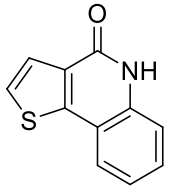	1480±480	**e1-2**[a]	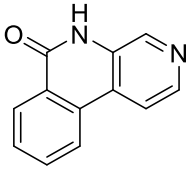	142
c39	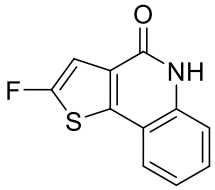	789±116	**e1-3**[a]	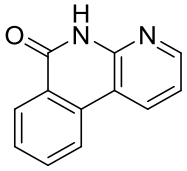	267
c40	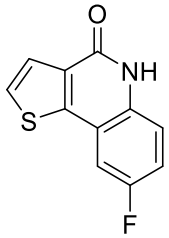	20300±12000	**e1-4**[a]	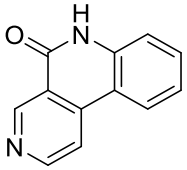	2230
d1	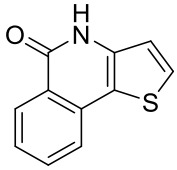	552±110	**e1-5**[a]	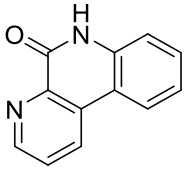	12000
d2	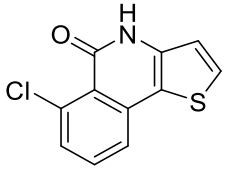	143±33	**e1-6**[a]	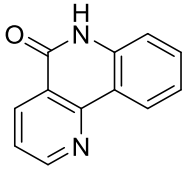	2490
e2	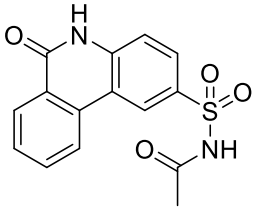	8290±1400	**s3**	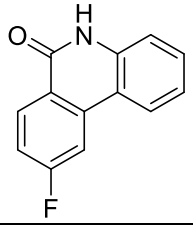	731±110

e3	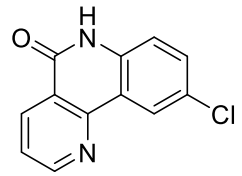	2160	**s4**	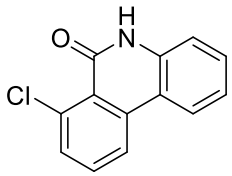	313±46
e4	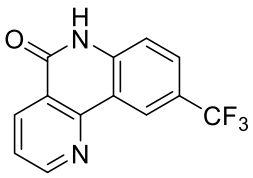	3970	PJ34	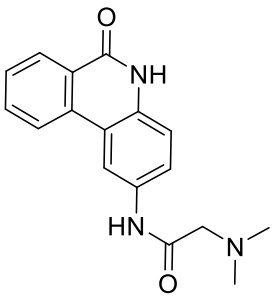	148±28
s2	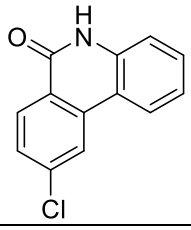	475±91			

Table 10 *IC_{50} values of more small PARP inhibitors. Experimental data were obtained from the enzymatic assay described in* ***Chapter 4, Section 4.3****. Each experiment was plated in triplicate. Data obtained from two or more experiments were shown as Mean±SD; otherwise, it was obtained from single measurements. Experimental data were processed with GraphPad 8.0.1. IC_{50} values were calculated using 4-parameter logistic regression (a) As* ***e1*** *and related compounds (****e1, e1-1, e1-2, e1-3, e1-4, e1-5, e1-6****) were tested by Ferraris et al. [11] [12], we only tested* ***e1*** *and used the experimental value to adjust the rest compounds using* ***e1*** *as the standard. Data in bracket were extrapolated. Data with * was* near the upper range used for the experiment.

Compound	Log (IC_{50})	FScore	Dscore
c34	2.81	7.58	8.29
c35	2.79	7.34	7.41
c38	3.17	8.16	7.60
c39	2.90	7.26	7.24
c40	4.31	7.69	7.73
d1	2.74	9.94	8.24
d2	2.15	8.70	8.30

e1	2.04	9.08	8.16
e1-1	2.00	9.65	8.51
e1-2	2.16	8.63	8.16
e1-3	2.43	6.53	8.85
e1-4	3.35	7.32	8.80
e1-5	4.08	6.41	8.76
e1-6	3.40	6.28	7.99
e2	3.92	0.61	6.25
e3	3.33	3.40	8.98
e4	3.60	2.67	8.29
s2	2.68	8.16	6.96
s3	2.86	8.07	7.90
s4	2.50	8.15	8.14
s8	5.13	5.51	7.11
s9	6.05	7.43	5.17
s10	5.36	8.72	5.88
s12	3.55	6.76	7.61
s13	5.86	7.61	5.04
s14	6.38	2.77	5.30
s15	4.17	8.01	5.43
s16	4.02	7.31	4.90
s17	6.77	0.60	6.33
s19	4.68	6.25	6.69
Phe	2.48	9.49	8.23
PJ34	2.17	9.83	10.5

Table 11 *Scorings of tested compounds. FScore is from our model and DScore is Schrodinger's docking score.*

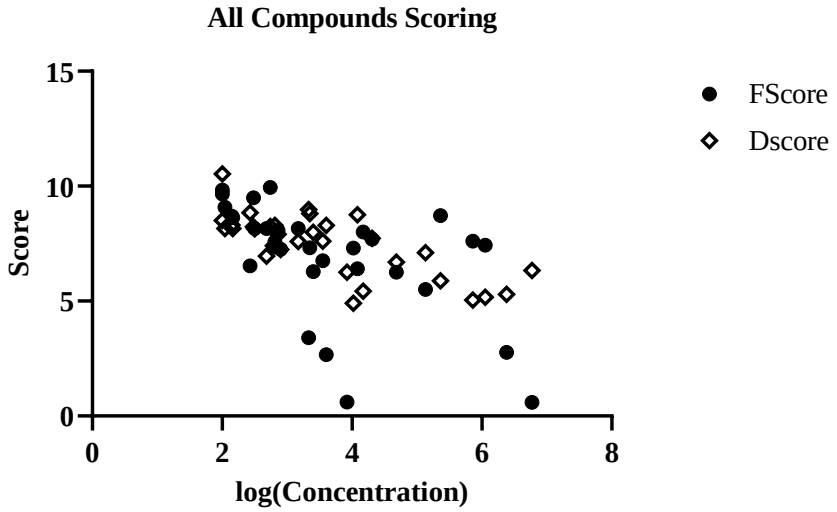

	log(Concentration) vs. FScore	log(Concentration) vs. Dscore
Pearson r		
r	-0.5444	-0.7383
95% confidence interval	-0.7506 to -0.2416	-0.8644 to -0.5246
R squared	0.2964	0.5451
P value		
P (two-tailed)	0.0013	<0.0001
P value summary	**	****
Significant? (alpha = 0.05)	Yes	Yes

Table 12a

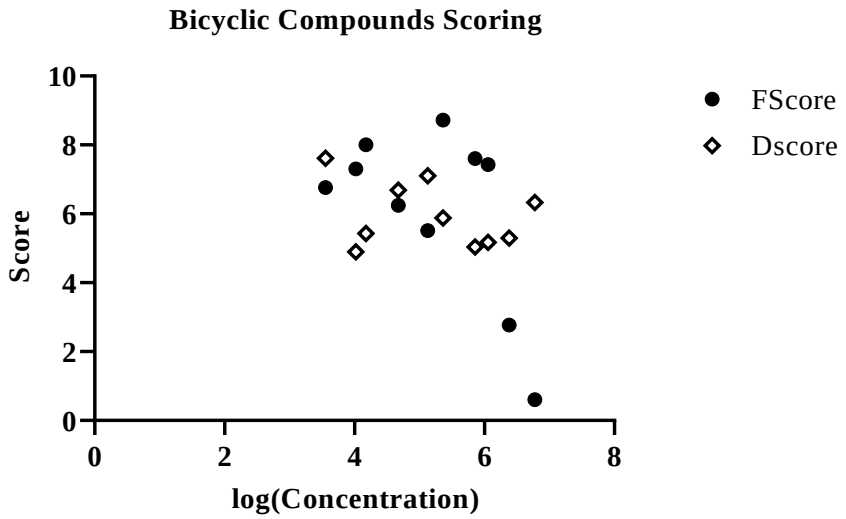

	log(Concentration) vs. FScore	log(Concentration) vs. Dscore
Pearson r		
r	-0.5890	-0.3133
95% confidence interval	-0.8889 to 0.06463	-0.7876 to 0.3941
R squared	0.3469	0.09815
P value		
P (two-tailed)	0.0732	0.3781
P value summary	ns	ns
Significant? (alpha = 0.05)	No	No
Number of XY Pairs	10	10

Table 12b

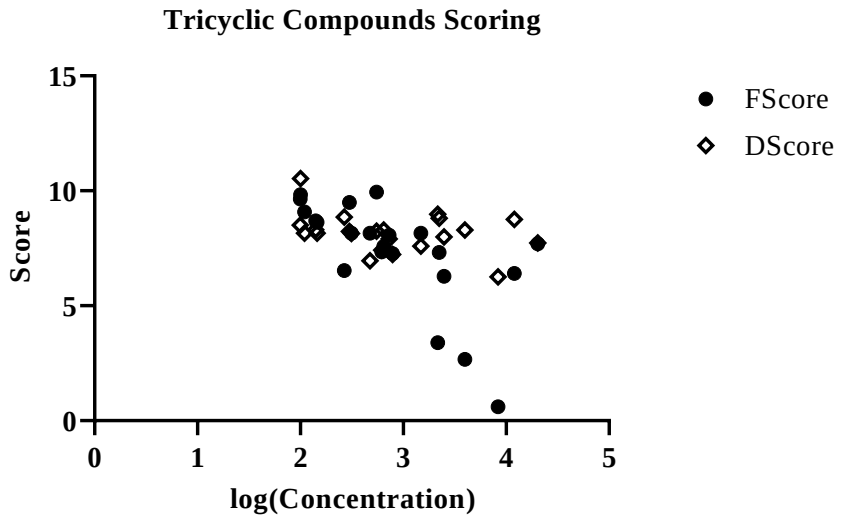

	log(Concentration) vs. FScore	log(Concentration) vs. DScore
Pearson r		
r	-0.6518	-0.3255
95% confidence interval	-0.8420 to -0.3174	-0.6570 to 0.1113
R squared	0.4248	0.1060
P value		
P (two-tailed)	0.0010	0.1393
P value summary	**	ns
Significant? (alpha = 0.05)	Yes	No

Table 12c *The comparison between DScore and FScore. PARPi potency $Log_{10}(IC_{50})$, prediction scores from our model and Schrodinger's docking score are shown above. When taking all compounds into account together, even though both predictions were significantly related to the potency ($P<0.05$), our prediction model showed a lower correlation compared to Schrodinger's docking score. However, when bicyclic or tricyclic compounds results were analyzed separately, our model showed superiority in correlation compared to Schrodinger's docking score. For bicyclic compounds, even though either method had no significant correlation, ours had a correlation $R^2=0.3469$ which was consistent with the overall scoring result while Schrodinger's docking score had no correlation $R^2=0.09815$. For tricyclic compounds, only our model showed significance and remained the correlation consistent with the overall scoring $R^2=0.4248$ result while Schrodinger's docking score had no significance with no correlation $R^2=0.106$.*

5.3.3. Conclusion

We have presented a knowledge-based model to predict the potency of small phenanthridinone-like bicyclic and tricyclic PARPi and produced a comparably reliable result, in which there was a trend that the prediction scores were positively related to inhibitor's IC_{50} values in general. This model was based on the hypothesis about how PARP1 inhibitors bound to the protein and what ligand-protein interactions were formed inside the binding pocket, which was summed up and supported by analyzing current experimental data and previous crystallographic studies: π-π interaction would initiate a cascade reaction starting from alternating the ligand's binding angle and ending up with turning the H-bond's binding angle, which would eventually determine the H-bond strength. The model was also built on the ligand surface electrostatic potential calculated by conventional quantum chemistry software Gaussian 09W. The surface electrostatic potential was used to represent the strength of the corresponding ligand-protein interaction, including the H-bond and the π-π interaction. The potential was also used for determining the ratio of the distance between two aromatic components and amino acid residues according to Coulomb's Law

The results suggested that, even though Schrodinger's docking function performed better in analyzing different compounds, our prediction method produced consistent results whenever it was used to predict bicyclic and tricyclic compounds separately or collectively. Particularly, our prediction method was able to produce correlated results among analogs while Schrodinger's docking score failed to do so. In conclusion, the negatively-related trend between our prediction result and the inhibitor's potency was strong circumstantial evidence implying the distinction in electron density distribution led to disparate ligand-protein interactions. To maximize a small inhibitor's potency, we need to not only increase the electron richness of aromatic components but also probe an optimized electron distribution to enlarge the strength of the H-bond. Methods that could be implemented included changing the position of elements on the heteroaromatic ring or adding an extra electron-donating/withdrawing substituent.

Our prediction method was better at predicting compounds sharing great similarities, compared to Schrodinger's scoring function. A popular method to predict analogs is using free energy perturbation (FEP). However, FEP requires a great computing resource which is not achievable by most medicinal chemistry labs. Our method provided an idea of calculating

representative protein-ligand interaction strength to predict the potency. By using the prediction model we proposed, more small PARP inhibitors based on different aromatic rings rather than benzamides could be developed. These molecules, that only bind to the NI, were believed to have only catalytic inhibition ability, rather than PARP trapping ability, which would benefit treating related CNS diseases. Meanwhile, for a larger PARP inhibitor, an alternative method to increase the potency was to fine-tune its core structure by slightly changing the electron density distribution with minor modification. It is worth noting that, the docking orientation of a larger molecule might be influenced by its considerable substituents. If the method was used to predict the potency of such larger inhibitors, the deviation would occur if the influence from substituents was not taken into account. A simplified explanation of this problem is shown in **Figure 37**. Testing two or more compounds with better and worse scores and relating prediction and experiment results could be used to adjust the prediction model. On the other hand, the existence of a side chain may force the core to move, making a theoretically deficient core become influential and preferred (if other conditions such as electron-richness remained the same). Hence, we were doing more experiments on thienoquinolinone (**c34**), even though it was a worse core concluded from either the experimental data (**Chapter 5, Section 5.2** & **5.3**) or the prediction score (**Chapter 5**, **Section 5.3**), to see if a side chain would bring about changes.

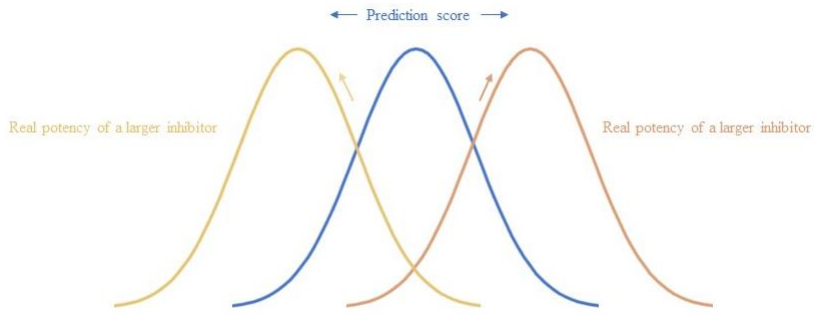

Figure 37 *Prediction on small molecules might not work on larger ones. This is a scheme showing why the prediction method introduced in this section might not be used for larger inhibitors with complicated side chains. The scheme is not related to any research data. The prediction model introduced in this study might not predict the potency of the core structure from a larger inhibitor as the side chain might influence the binding angle. The blue curve represented the prediction model used for small inhibitors when the binding angle was not*

influenced by any side chain. The orange and yellow curves represented the real potency of the larger inhibitor when the side chain would influence the binding angle. In this case, the prediction score was not related to the potency directly. A modification with either a better or a worse score could lead to a better potency. As we believed the pattern remained, evaluating the additional two or more compounds with a better and a worse score could determine the best optimization approach to take.

5.4. PARP Inhibitor's Spatial Occupancy Inside The Protein Binding Pocket and Its Influence on The Potency

5.4.1. General introduction

From the previous study, we noticed that adding a bulky side chain to the phenanthridinone core structure would decrease the inhibition potency. However, a PARP inhibitor must have additional functional components if it needs to reach the area outside of the NI. The binding pose and affinity of the inhibitor could be most affected by configurational entropy [19], hydrophobicity/hydrophilicity [20], and protein-ligand interaction [21]. These features determine what a ligand will be like, where it will be and how it will interact with residues in a protein. In addition to the NI which is the major and the largest hydrophobic region sandwiched by Y907 and Y896, there are two other major hydrophobic regions inside the PARP1 binding pocket (**Figure 38**). Both of them are in the gully between the D-loop and the HD. One is near the middle section of the D-loop and the end section of the HD αF helix, close to P885, while the other one is near the end section of the D-loop and the middle section of the HD αF helix close to R878. There are also some vacancies to accommodate bulky groups around the hydrophobic region. The region between R878 and R885 next to the αF helix was more hydrophilic (**Figure 38**). The protein-ligand interaction, such as H-bond and π-interaction, influenced the binding strength and induced the conformational change of the protein and the ligand.

5.4.2. Results

In this study, we explored phenanthridinone-based inhibitor candidates with bulky side chains and studied their binding patterns and potency. The theoretically correct binding pose of a compound was considered if 1. the phenanthridinone component was in the NI interacting with

S863, G904 and Y907 and 2. the pose had the highest docking score among molecular docking results. Poses with the phenanthridinone component not binding to the NI were considered as incorrect binding poses. The substituent was either on R_1 position or R_2 position (**Figure 39**). The design that converted the carbonyl benzene ring to the thiophene ring or the pyridine ring would also be studied. Different aromatic or heterocycle components were connected to the phenanthridinone analog core structure by the amide linker. Molecules in this study were shown in **Figure 40**. (**e** compounds were failed to be purified completely; Thus, their IC_{50} values were not as accurate)

a.

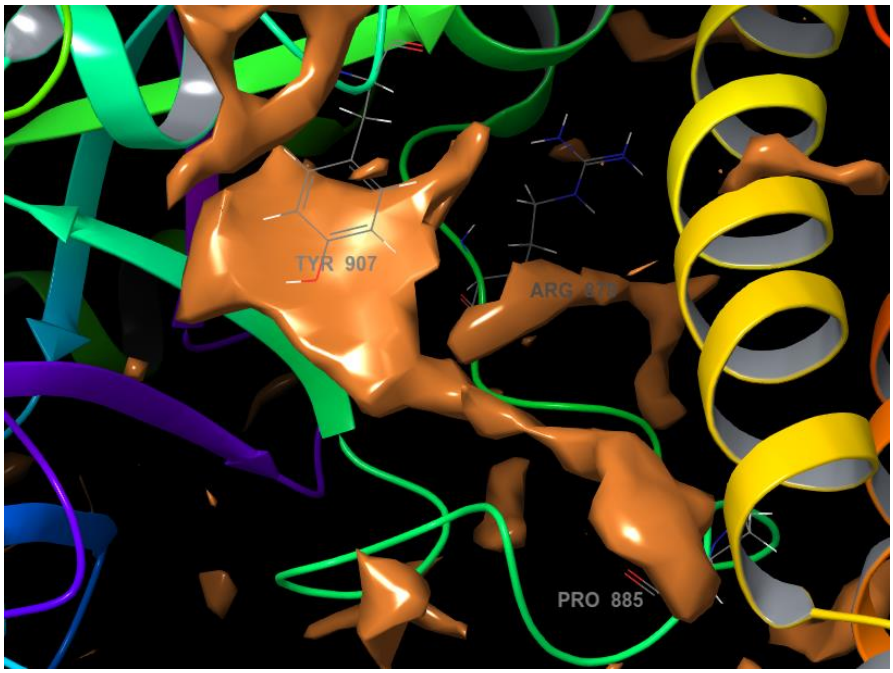

b.

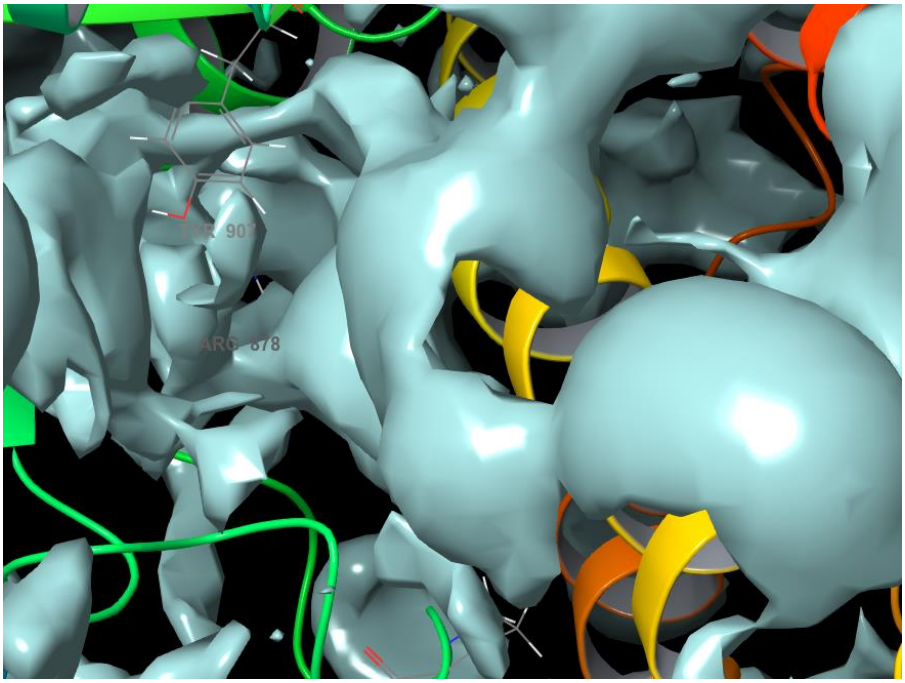

Figure 38 *The hydrophobic mapping. The hydrophobic (upper, orange) and hydrophilic (lower, cyan) regions in a PARP1 protein (PDB ID* ***6VKO****) binding pocket generated by Schrodinger Maestro Structure Analysis Hydrophobic/philic Surfaces. The major one was in the NI, near Y907. Two peripheral ones were located between the D-loop and the HD, including the one near P885 and the one near R878. The binding pocket was big enough to accommodate other*

components. The method to generate the hydrophobic/philic surface was introduced in ***Chapter 4***, ***Section 4.1***.

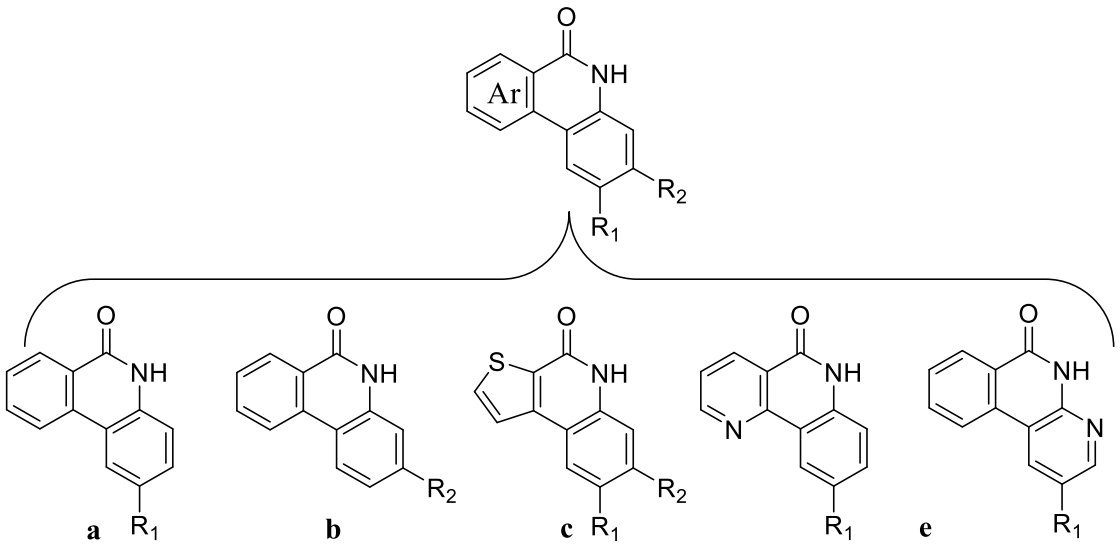

Figure 39 *Modification sites to make molecules for researching the binding site occupancy. Ar: The benzene ring from the carbonyl component; R_1: 2'-substituent, para to the amine; R_2: 3'-substituent, meta to the amine*

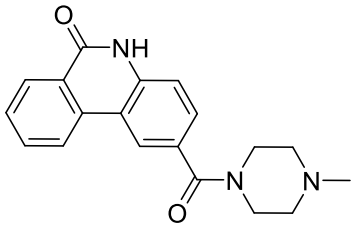

a3 IC_{50} = 627nM

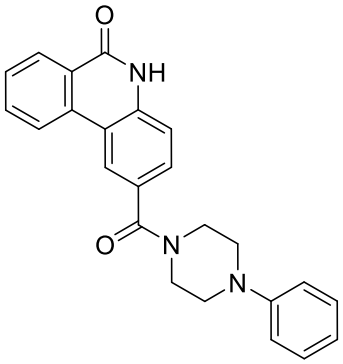

a4 IC_{50} = 21.9±0.11nM

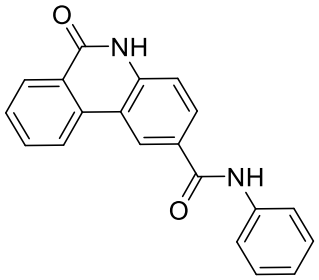

a5 IC_{50} = 272nM

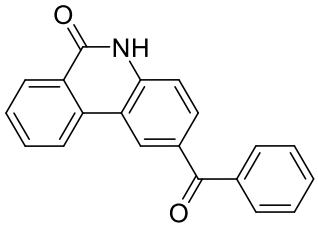

a6 IC_{50} = 1530nM

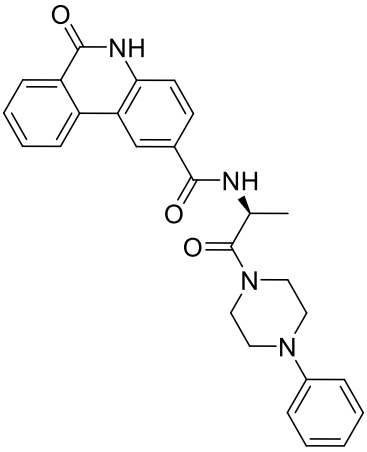

a7 IC_{50} = 2100±249nM

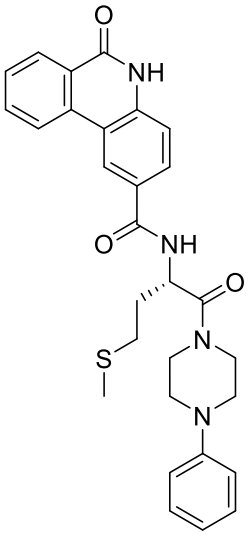

a8 IC_{50} = 275nM

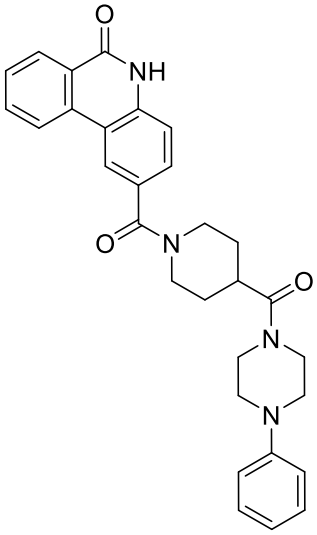

a9 IC_{50} = 324nM

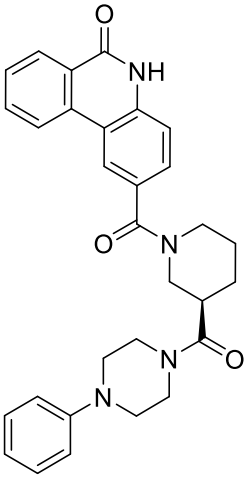

a10 IC_{50} = 915nM

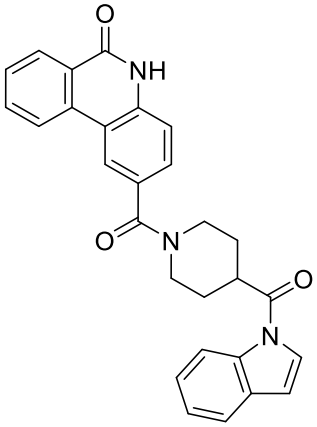

a11 IC_{50} = 917nM

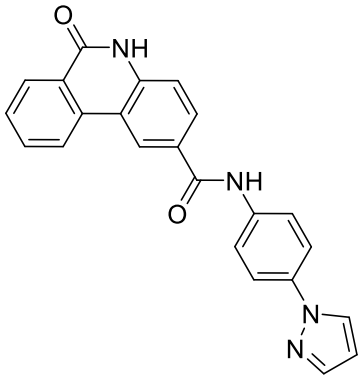

a12 IC_{50} = 1750nM

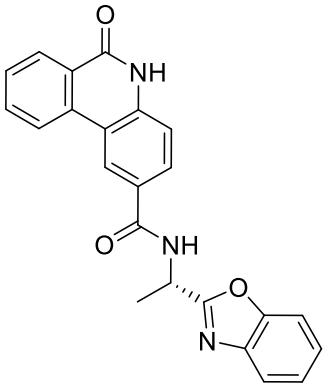

a13 IC_{50} = 3760nM

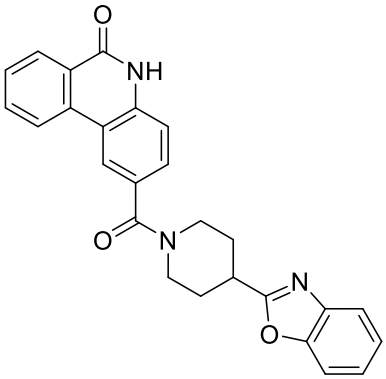

a14 IC_{50} = 213nM

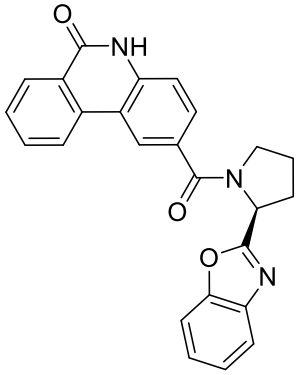

a15 IC_{50} = 791nM

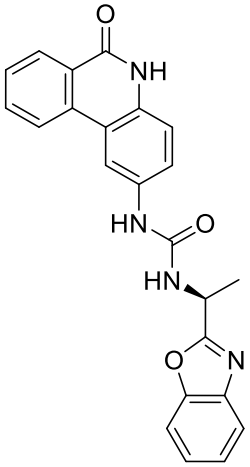

a16 IC_{50} = 53.0±2.3nM

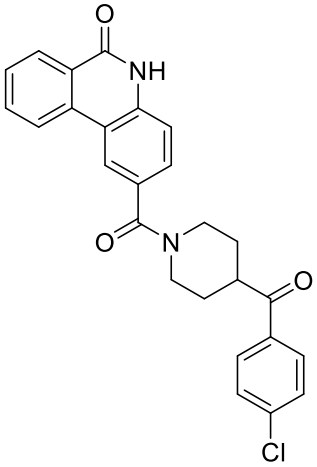

a17 IC_{50} = 1930±1400nM

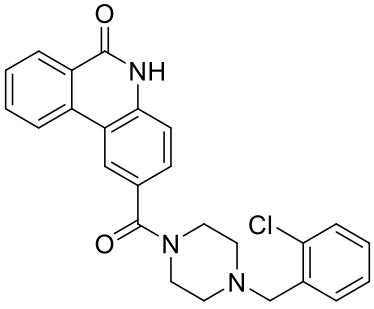

a18 IC_{50} = 941±620nM

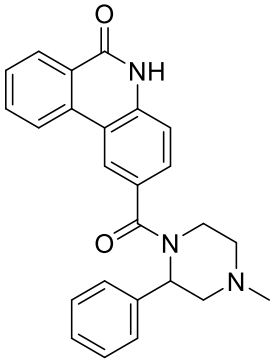

a19 IC_{50} = 809±400nM

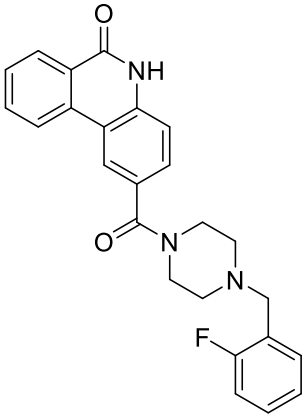

a20 IC_{50} = 1300±110nM

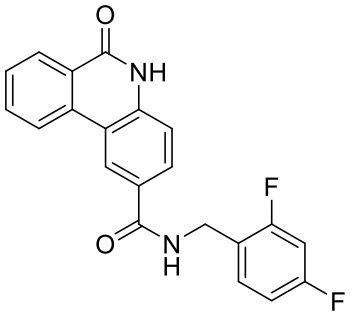

a21 IC_{50} = 13500±14000nM

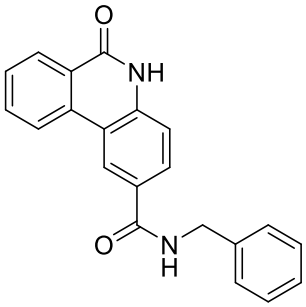

a22 IC_{50} = 10600nM

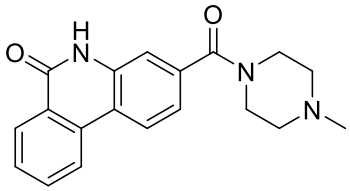

b3 IC_{50} = 301nM

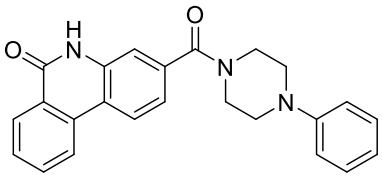

b4 IC_{50} = 72.9±35nM

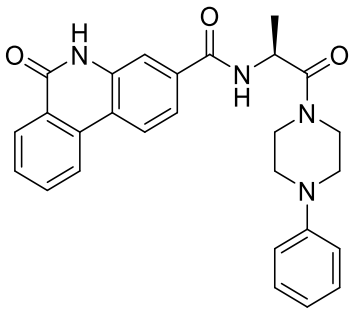

b5 IC_{50} = 96.3±12nM

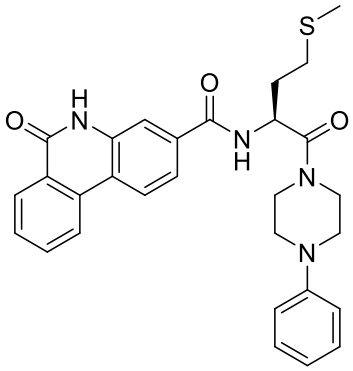

b6 IC_{50} = 483nM

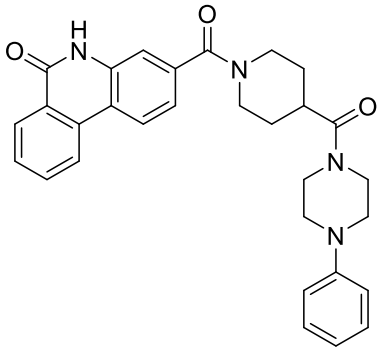

b7 IC_{50} = 74.6nM

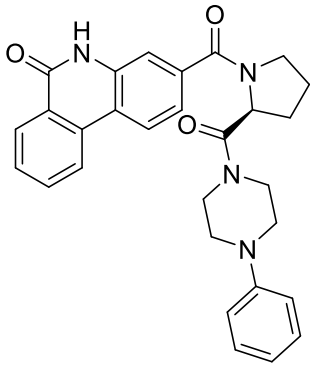

b8 IC_{50} = 327nM

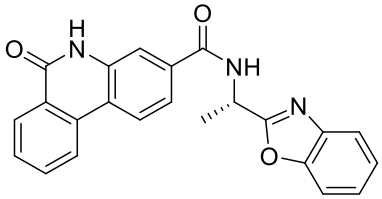

b9 IC_{50} = 212nM

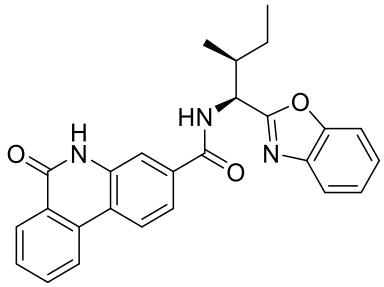

b10 IC_{50} = 1700nM

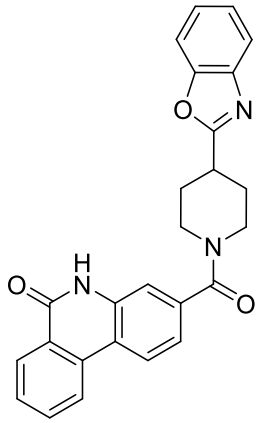

b11 IC_{50} = 143nM

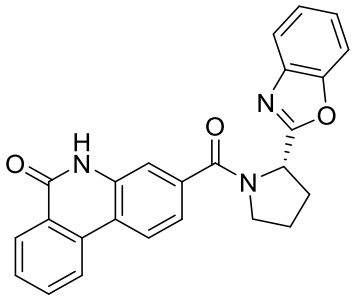

b12 IC_{50} = 225nM

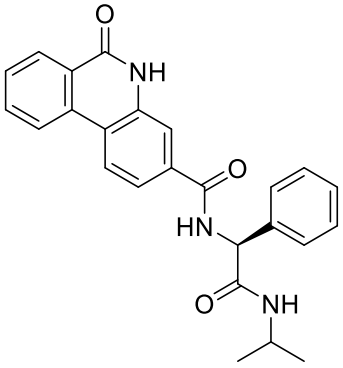

b13 IC_{50} = 1840nM

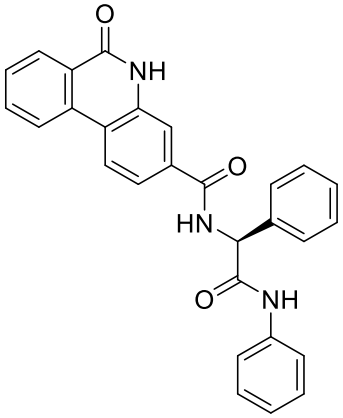

b14 IC_{50} = 12400nM

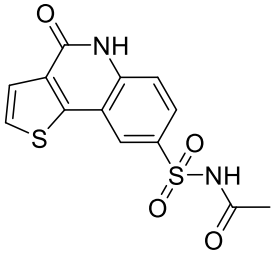

c3 IC_{50} = 8210nM

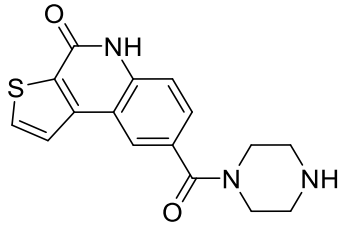

c4 IC_{50} = 105nM

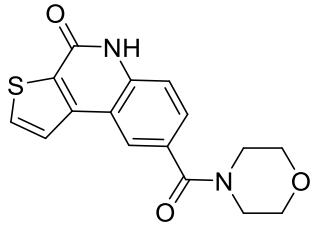

c5 IC_{50} = 566nM

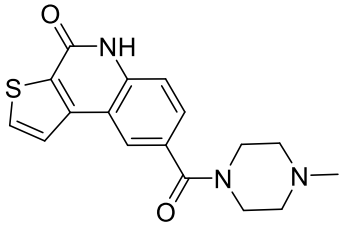

c6 IC_{50} = 1460nM

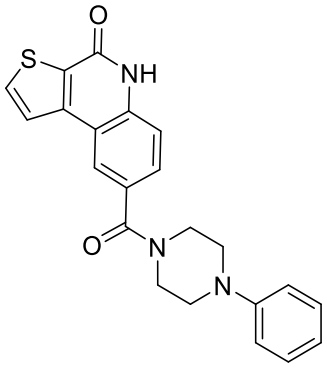

c7 IC_{50} = 385nM

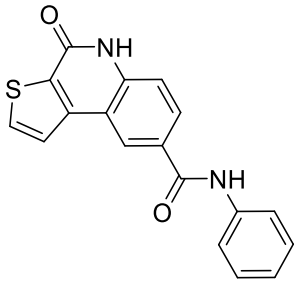

c8 IC_{50} = 692±62nM

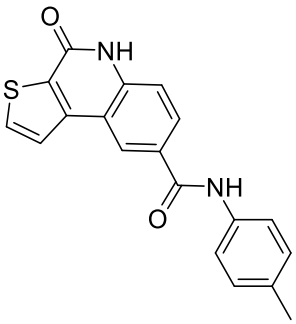

c9 IC_{50} = 27500nM

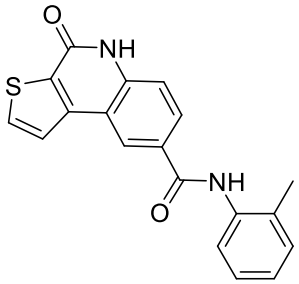

c10 IC_{50} = 6650nM

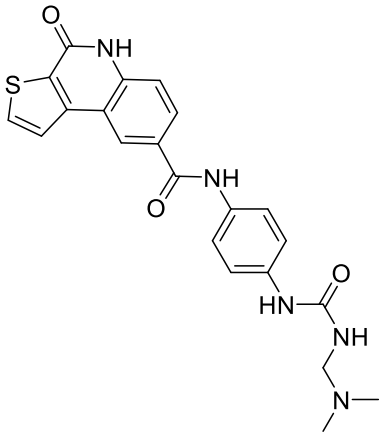

c11 IC_{50} = 16700±4200nM

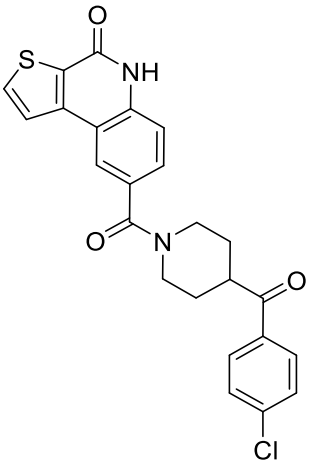

c12 IC_{50} = 1600±340nM

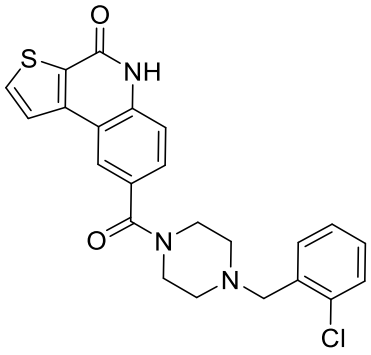

c13 IC_{50} = 2730nM

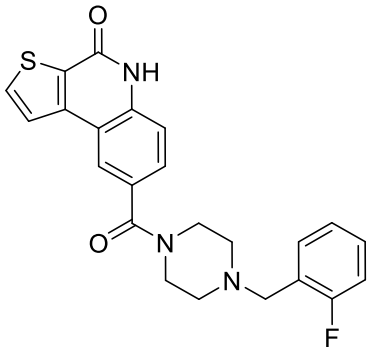

c14 IC_{50} = 1720nM

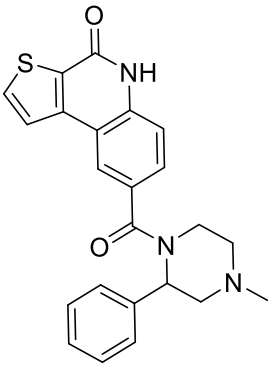

c15 IC_{50} = 3730nM

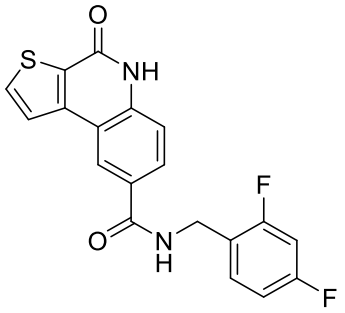

c16 IC_{50} = 2230±44nM

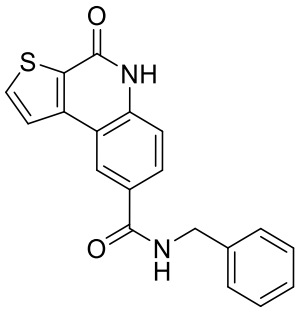

c17 IC_{50} = 1310±650nM

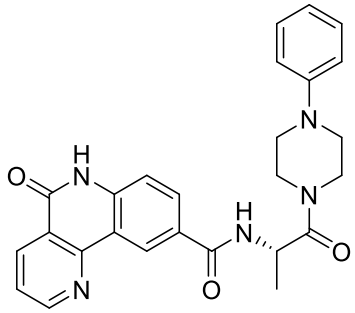

e5 IC_{50} = 9130±3900nM

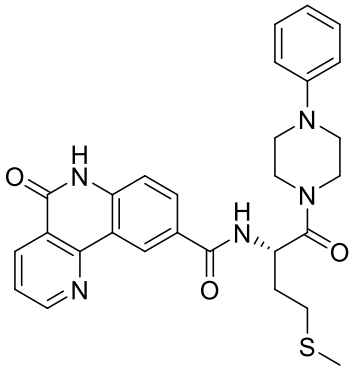

e6 IC_{50} = 38600±3100nM*

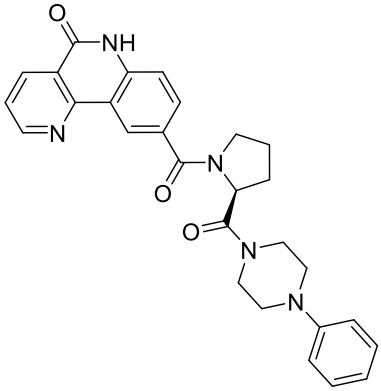

e7 IC_{50} = 34400nM*

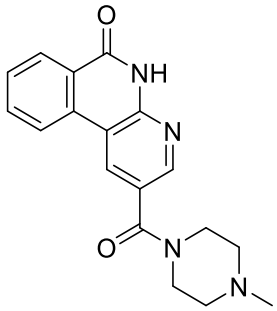

e8 IC_{50} = 44100nM*

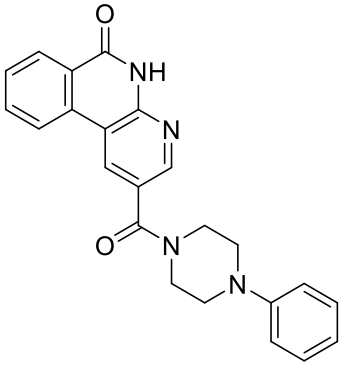

e9 IC_{50} = 139nM

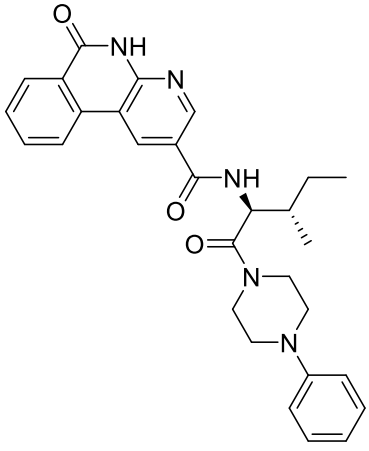

e10 IC_{50} = 89400nM*

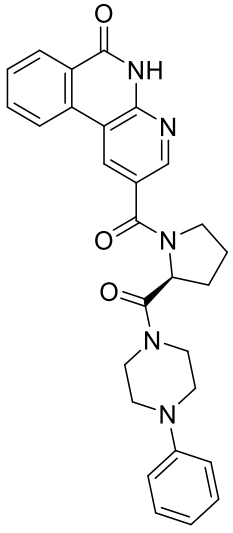

e11 IC_{50} = 34400nM*

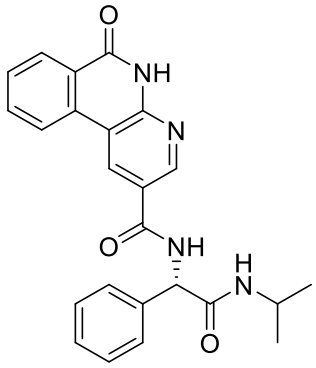

e12 IC_{50} = 36700nM*

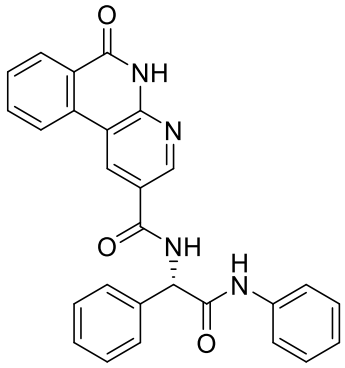

e13 IC_{50} = 66800nM*

Figure 40 *Molecules designed to study the space occupancy-potency relationship. Experimental data were obtained from the enzymatic assay described in* ***Chapter 4, Section 4.3****. Each experiment was plated in triplicate. Data obtained from two or more experiments were shown as Mean±SD; otherwise, it was obtained from single measurements. Experimental data were processed with GraphPad 8.0.1. IC_{50} values were calculated using 4-parameter logistic regression.* ***e5-e13*** *could not be purified completely and it would influence the inhibition (Thus, their IC_{50}s were considered as approximate values.) Compounds with IC_{50}s less than 150nM are highlighted. Data in bracket were extrapolated. Data with * was* near the upper range (100000nM) used for the experiment.

Not surprisingly, the overall potency for inhibitors with bulky and complex side chains was not as good as PJ34. The position of a substituent didn't make a significant difference comparing **a** and **b** compounds. The modification on the benzene ring might make a significant difference: Converting the benzene component to the thiophene component didn't decrease the potency significantly while using the pyridine might decrease the potency (**Figure 41**).

Approximately, we divided the binding pocket into four regions (**Figure 42**). These four regions were used to describe where side chains were occupied. Taking **a1** as an example: The phenanthridinone core component of the compound occupied the NI. Region A was where a small substituent like *N*-methyl-piperazine would occupy; Region B was near Y889 and G888 and a curled side chain such as **a4** (**Figure 43**) or **a13** (**Figure 44**) would occupy. Region C was the region sandwiched by the D-loop and the HD, between G888 and P885. Region D was

majorly the AD near R878. Details could be found in **Figure 42**. The substituent side-chain spatial occupancy of representative molecules (**a3-a22** and **b3-b14**) were listed in **Table 13**.

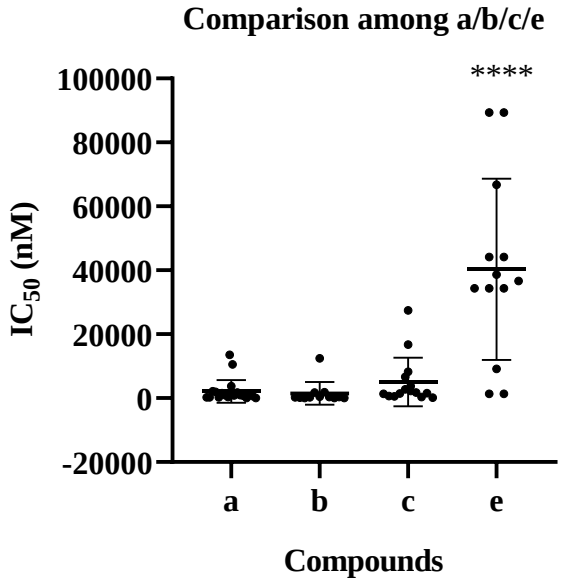

Figure 41 *Comparison of overall potency among different groups of inhibitors for researching the binding site occupancy. The data was analyzed by ordinary one-way ANOVA with a multiple comparisons test followed by Dunnett's post hoc analysis (GraphPad 8.0.1).* ***a*** *and* ***b*** *inhibitors didn't have a significant difference (P=0.9993) in potency;* ***a*** *and* ***c*** *inhibitors had no significant difference (P=0.9279) either.* ***c*** *and a trend to have higher* IC_{50}*s (less potent) compared to* ***a*** *and* ***b****.* ***e*** *inhibitors were significantly (P<0.0001) less potent than* ***a b c*** *compounds when compared to* ***a, b*** *or* ***c*** *compounds. However, due to the purity issue, the compounds* ***e*** *used here were not 100% pure and this could influence the inhibition. Thus, the conclusion about* ***e*** *was not certain.*

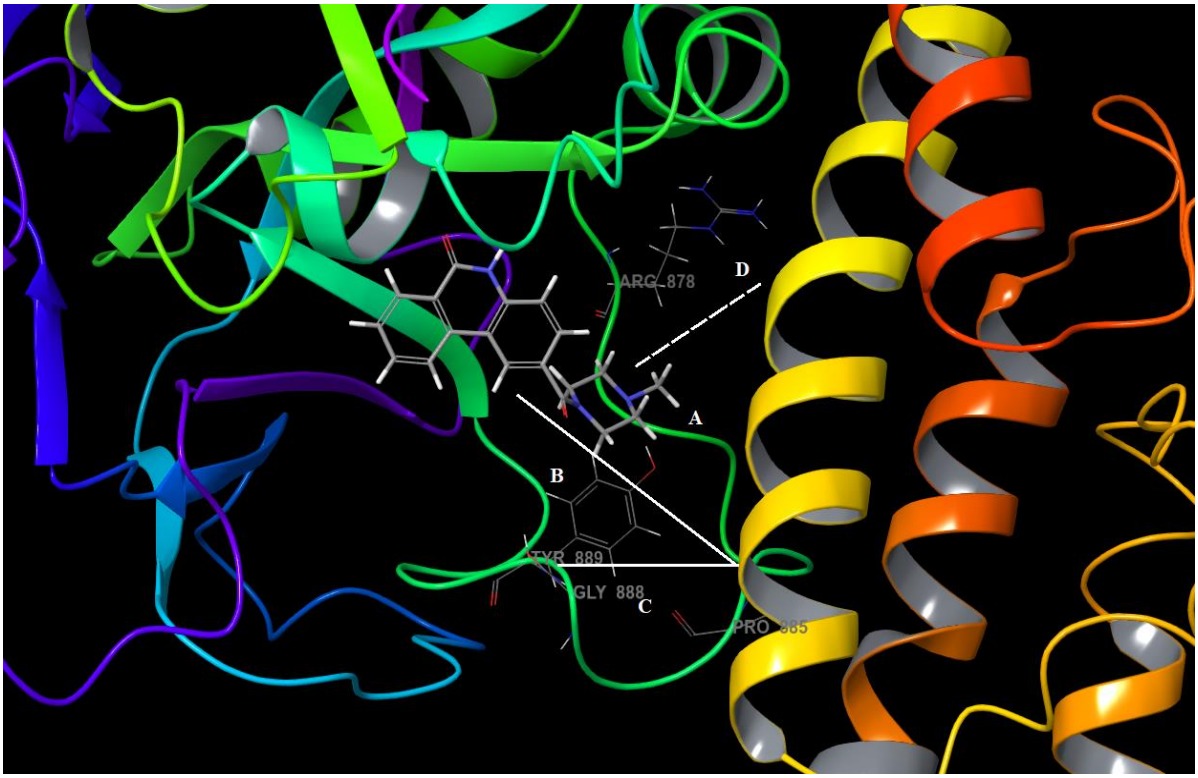

Figure 42 *The area division based on where a substituent side chain would occupy or end.* ***a3*** *docked into the Normal model is used as an example. Region A was near the NI majorly adopted by short components such as N-methyl-piperazine. Region B was "underneath" the NI and if a longer side chain was curled, it would majorly take this region adjacent to the starting end of the D-loop next to Y889 and G888. Region C referred to the gulch between the middle section of the D-loop and the HD, and it could be considered as between G888 and P885 as well. Region D was majorly the AD, near the end of the D-loop neighbouring R878 and it was also stacked between the D-loop and the HD*

a.

b.

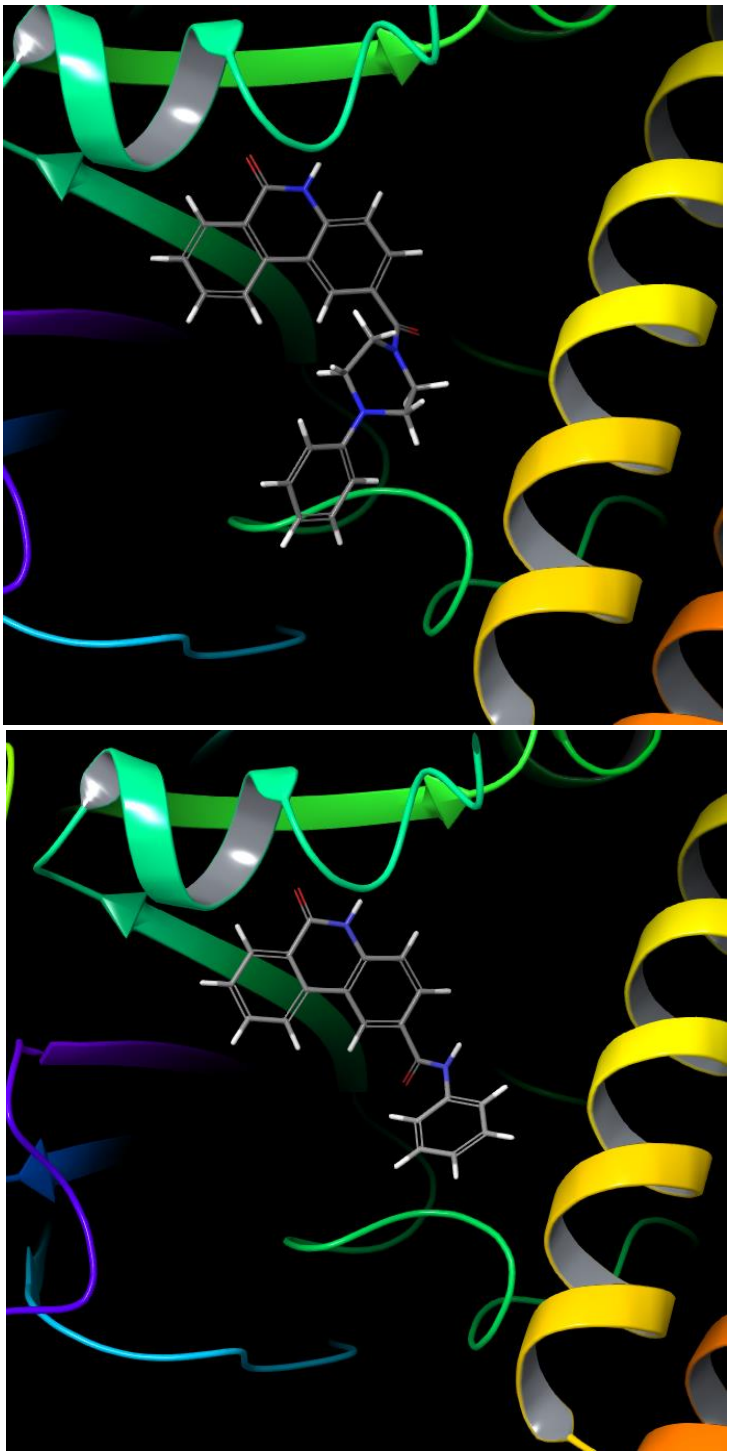

Figure 43 *Molecular docking of **a4** (panel **a**) and **a5** (panel **b**) into the Normal model.*

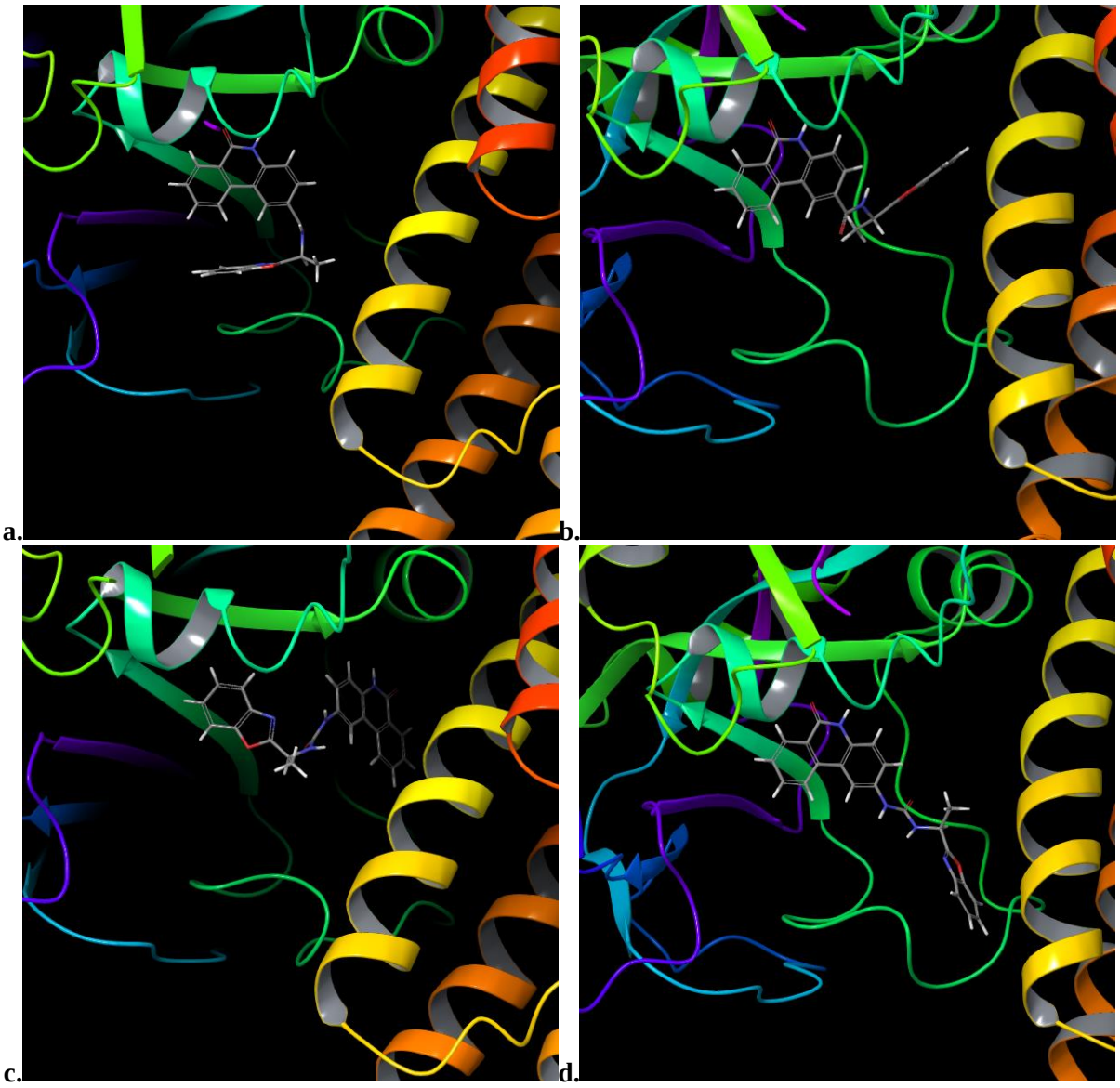

Figure 44 *Molecular docking of **a13** and **a16.** (**a**) **a13** docked to the Normal model; (**b**) **a13** docked to the Open model; (**c**) **a16** docked to the Normal model (docking score -8.7); (**d**) **a16** docked to the Open model (docking score -8.4). The only difference between the two compounds was **a13** had an amide linker and **a16** had a urea linker. The difference in the linker caused two molecular docking results: **a13** had a higher docking score in the Normal model compared to the Open model, indicating it was likely to have a higher affinity in the Normal model. In the Normal model, **a13**'s benzo-oxazole component was in the region between the D-loop and the NI. In contrast, even if **a16** had a higher docking score in the Normal model, the benzamide component was not inside the NI, indicating **a16** could not be docked into the Normal model correctly. In the*

*Open model, the benzo-oxazole component of **a16** was stacked into the groove between the D-loop and the HD, in which region **a16** might cause clashing.*

Cmp	Normal	Open	IC_{50}(nM)	Cmp	Normal	Open	IC_{50}(nM)
a3	A	A	62.0	**a19**	B	A	809
a4	B	D	21.9	**a20**	D	C	1300
a5	A	A	272	**a21**	B	D	13500
a6	A	A	1530	**a22**	B	A	10600
a7	*	C	2100	**b3**	D	A	301
a8	*	AD	275	**b4**	D	D	72.9
a9	B	B	324	**b5**	*	D	96.3
a10	*	*	915	**b6**	*	D	483
a11	B	C	917	**b7**	*	C	74.6
a12	B	C	1750	**b8**	*	D	327
a13	B	D	3760	**b9**	D	D	212
a14	B	*	213	**b10**	*	AD	1700
a15	A	*	791	**b11**	D	D	142
a16	*	C	53.0	**b12**	A	B	225
a17	B	C	1930	**b13**	*	AD	1840
a18	B	C	941	**b14**	*	AD	12500

Table 13 *The substituent side-chain spatial occupancy and corresponding IC_{50} values. IC_{50} values are from **Figure 40**. Normal: The Normal model. Open: The Open model. *: Failed docking, incorrect docking pose. A, B, C, D are regions categorized in **Figure 42***

In the Normal model, R_2-substituted compounds **b**, especially ones with long chains, were more likely to cause incorrect docking poses. The reason for this could be that R_2 was very close to the HD domain when the binding pocket was fully closed, and it caused inevitably steric hindrance or clashing. In contrast, most R_1-substituted compounds **a** could fit into the Normal model, in Region A and Region C. No compound could occupy Region C in the Normal model, suggesting that the space between the D-loop and the HD near P885 was inaccessible when the binding pocket was fully closed, making longer compounds such as **a7 a8** fail to dock. When the binding pocket was opened (in the Open model) which gave more space to the binding pocket, we found more successful docking cases. Larger compounds such as **a7** could enter Region C. **a8** could occupy both Region A and Region D due to its piperazine chain and methionine side chain. R_2-substituted compounds **b** were more likely to occupy the AD Region D. Unfortunately, there seems no direct relationship between potential spatial occupancy and potency.

R_1-substituted molecules were likely to extend the side chain towards the middle section of the D-loop. The side chain would be accommodated in the opening near the D-loop if the binding pocket was fully closed. Resulting from both space limitation and configuration entropy, when the side chain got longer, it would start to curl and extend to the region near the Acceptor site (**a5→a4→a13**), implying a functional group on such scaffold could potentially interact with residues in the Acceptor site (**Figure 43**, **Figure 44**). Otherwise, only the Open model could fit a longer ligand where it extended the side chain into the socket between the D-loop and the HD (**Figure 44**). E.g., in the Normal model, **a16** could not be docked into the protein correctly with the configuration where benzamide motif outside the NI. According to the knowledge that a molecule needs to bind to the NI to inhibit PARP1, one with such configuration was not expected to be a good inhibitor. Since **a16** was a decent inhibitor, it should have a more reasonable binding orientation. Meanwhile, in the Open model, the ligand was docked into the protein properly with the benzo-oxazole component stacked into the region between the D-loop and the HD, gaining more chances to interact with the two regions. This configuration in the Open model was more likely to be the docking pose of a strong PARP inhibitor like **a16**. Consequently, the real binding orientation of **a16** in the protein should be similar to the one in the Open model rather than the Normal model. A similar docking orientation happened to **a7** which had a much worse potency (**Figure 45**). When we compared the molecular docking result, we noticed that the piperazine component of **a7** could introduce clashing with G888 from the D-loop. None was found on **a16,** not only with G888 but also any other residues on the D-loop. The size and the configuration of **a7** could be a problem when it tried to stack into a narrow area like Region C. The phenyl-piperazine component of **a7** here was rigid and bulky while the amide-benzo-oxazole of **a16** was flexible. Instead of clashing, **a16** avoided the area around G888. The comparison suggested that, even though the loop was flexible, it was sensitive enough to decline ligand affinity when the bad contact happened.

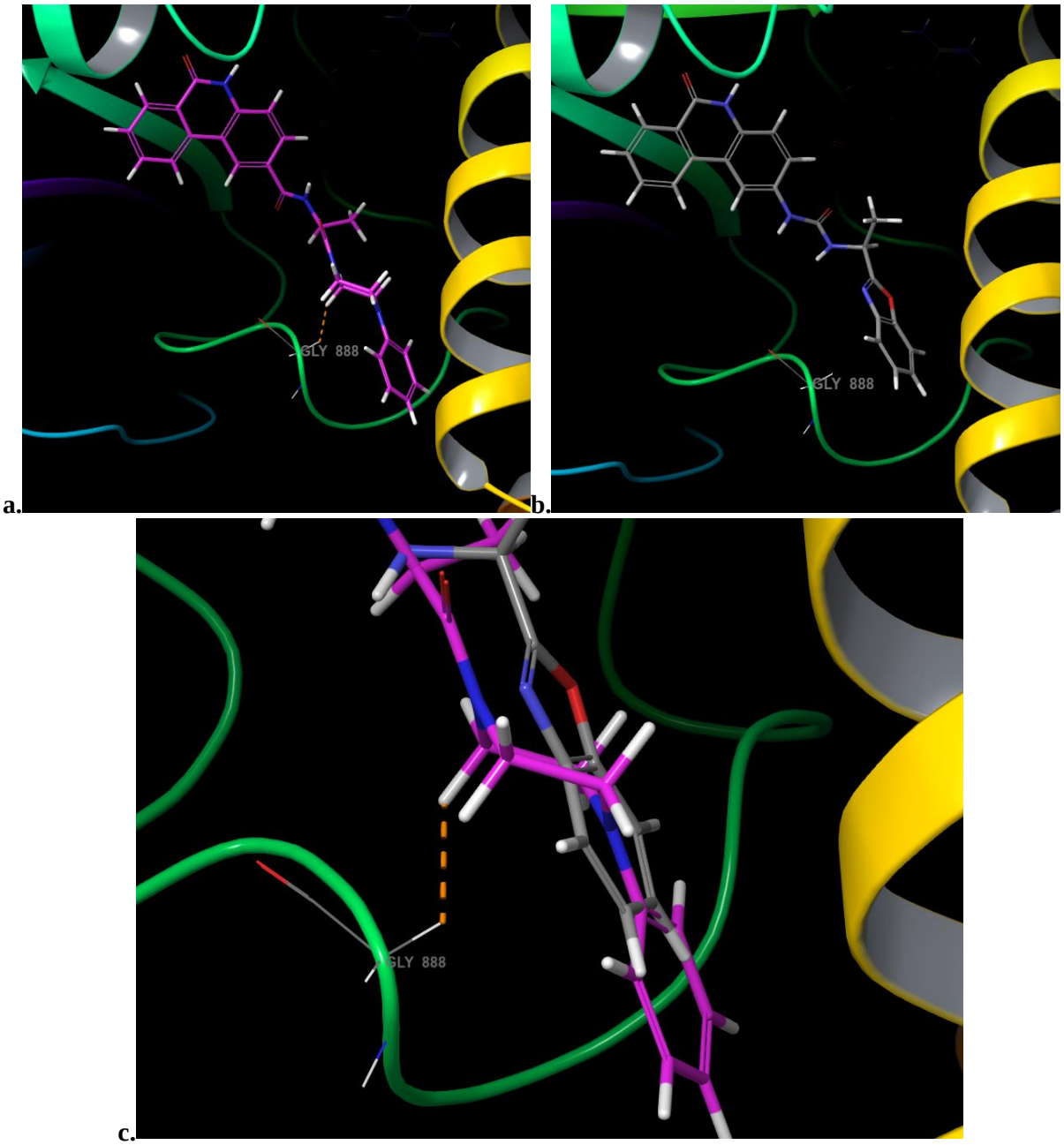

Figure 45 *Molecular docking of **a7** (**a**) and **a16** (**b**) in the Open model as well as superposition (**c**) of **a7 a16** focusing on the phenyl-piperazine and the benzo-oxazole components. The phenyl-piperazine component of **a7** was too close to G888 and caused bad contact (orange), such as clashing. The amide-benzo-oxazole component avoided this area.*

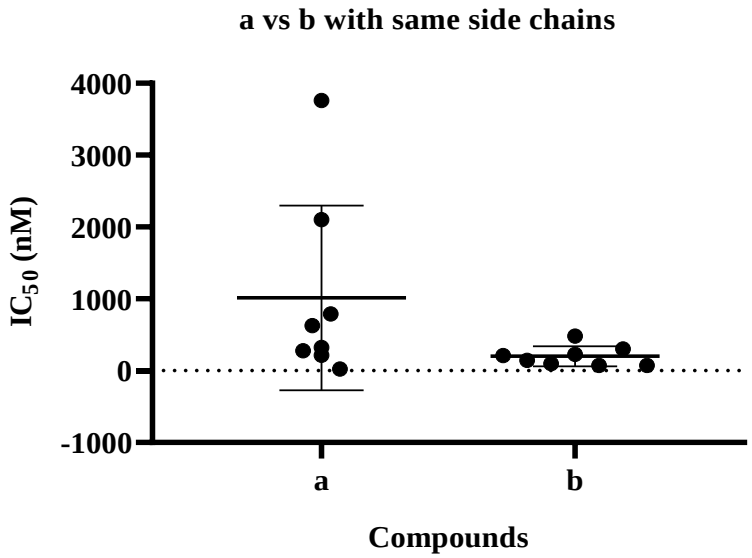

Figure 46 *Comparison between **a** and **b** compounds with same side chains. An unpaired t-test was used in GraphPad 8.0.1 to process the data. There was no significant difference (P=0.097) between the two types of compounds.*

As concluded previously, R_2-substituted molecules were likely to occupy Region D, the AD near R878. When the binding pocket was not fully closed, it gave side chains on the R_2 position adequate room to make a turn. **b** compounds were likely to have better and more consistent potency, although there was no significant difference (**Figure 46**). The potency might come from sufficient binding space when the pocket was not fully closed and less ligand conformational change, compared to curled compounds **a**. The consistency was also related to similar binding patterns as most of them entered Region D.

5.4.3. Conclusion

In this study we reviewed how molecules would orientate when they extended their side chains outside of the NI, what area would they occupy inside the binding pocket as well as the potential relationship between spatial occupancy and inhibition. As modification on the aromatic ring was yet to produce any superior result (**Figure 41**), compared to **a** compounds with plain phenanthridinone structure, we focused on the side chains and the spatial occupancy. When the R_1 position was substituted, the longer side chain started to bend and extend towards the Acceptor site when the pocket was fully closed and it could also intrude into the gully between the D-loop and the HD near G888/P885 when the pocket was not fully closed. The smaller side

chain would stay in Region A with the orientation possibly influenced by hydrophobicity. When there was a substituent at the R_2 position, most compounds accommodated into the binding pocket only when the pocket was not fully closed and lay their side chains into the AD near R878. These compounds did not have a huge difference in potency. The similar and consistent binding pattern made these compounds much easier to be predicted. Thus, with a specific area to occupy and a particular amino acid residue to interact with, we believed that R_2-substituted compounds were promising. In addition to target R878, a substituent extending from the R_2 position could also interact with D766 and D770, while one from the R_1 position could hardly reach R878. Secondly, as R_2-substituted compounds preferred the Open model, it implied that these compounds were more likely to induce "Pro-DNA-Retention" protein configuration which was a sign of PARP-trapping. To develop potent inhibitors based on R_2 substitution, we believed that phenyl-piperazine was the best scaffold to use. The phenyl-piperazine substituent delivered higher potency as **b4** was one of the most potent compounds in its category. Furthermore, the side chain could enter the AD directly without winding. When the side chain extended to the AD along the hydrophobic region, the phenyl group would be surrounded by important amino acid residues including R878, D770, D766. Modification on the phenyl ring with one or more functional groups would have better chances to interact with these residues. A functional group on the piperazine ring might also interact with R878 and D766. The maneuverability in modification made the phenyl-piperazine substituent a great scaffold (**Figure 47**).

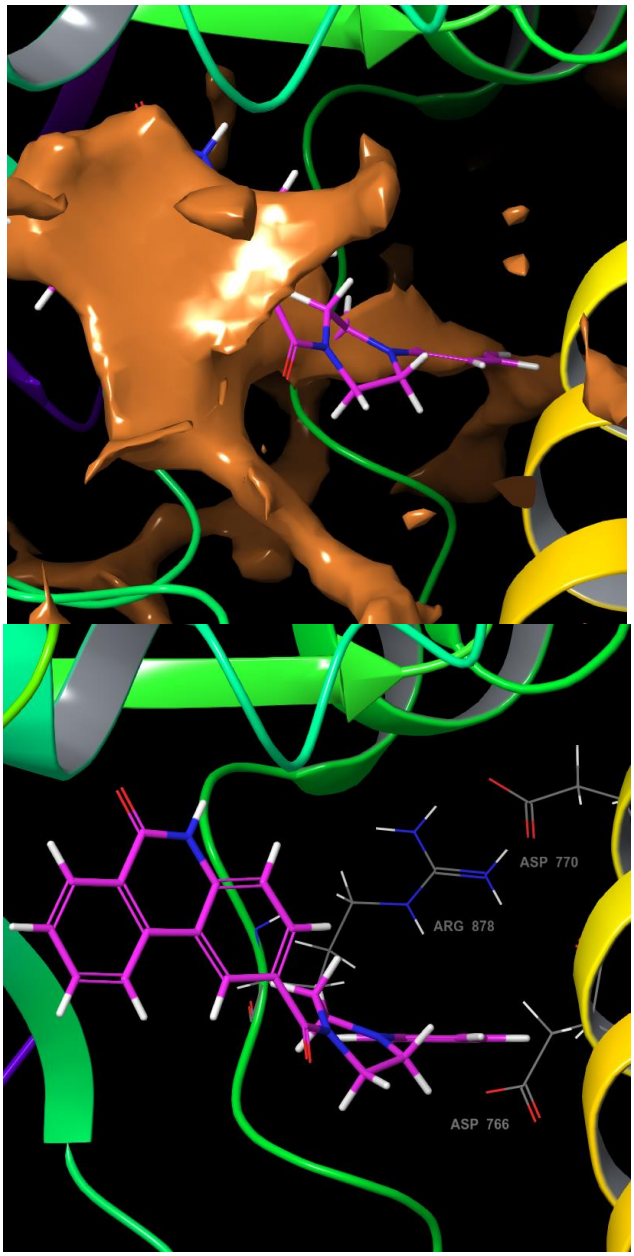

Figure 47 *Molecular docking of **b4. b4** (pink) extended the phenyl-piperazine side chain into the AD along the "boulevard" of the hydrophobic region (orange) which may facilitate the affinity. In the AD, the phenyl-piperazine moiety was surrounded by R878, D770, D766 closely, indicating functional group on two rings could easily interact with these residues. The method to generate the hydrophobic mapping was introduced in **Chapter 4**, **Section 4.1**.*

During the study, we were also looking for a scaffold that could be developed into a compound to interact with the HD only, especially D766/E763, to make it more PARP1/2-

selective versus TNKS proteins. This design would also lead to PARP1- or PARP2-selective inhibitors due to D766/E335 residue analogs. To guarantee the interaction, we were expecting a scaffold that would maintain a certain orientation in the protein. To achieve this goal, we were looking for a compound that was 1. small with less rotatable bonds, as rotatable bonds decreased the accuracy of binding orientation prediction and 2. whose binding pose was influenced and supported by physical interaction, such as hydrophobic interaction. Most larger molecules, even with good potency, did not meet the first requirement. We realized molecules such as **a3, a4, a5, a6** could be the starting point. When the phenyl group was attracted by the hydrophobic region (which could happen in the binding pocket), the side chain would be torqued and the orientation would be changed(**a3→a4**) (**Figure 48**). Smaller molecules such as **a5 a6** could also position their aromatic group near the hydrophobic region (**Figure 49**). This docking poses left the area near the HD (upper right area in **Figure 48** and **Figure 49**) vacant for additional functional groups to interact with residues such as D766/E763 in the HD. This kind of modification on the amide would make a "three-pointed star"-like **a** compounds with the phenanthridinone core structure, the phenyl component and the HD-interaction functional group as each end respectively.

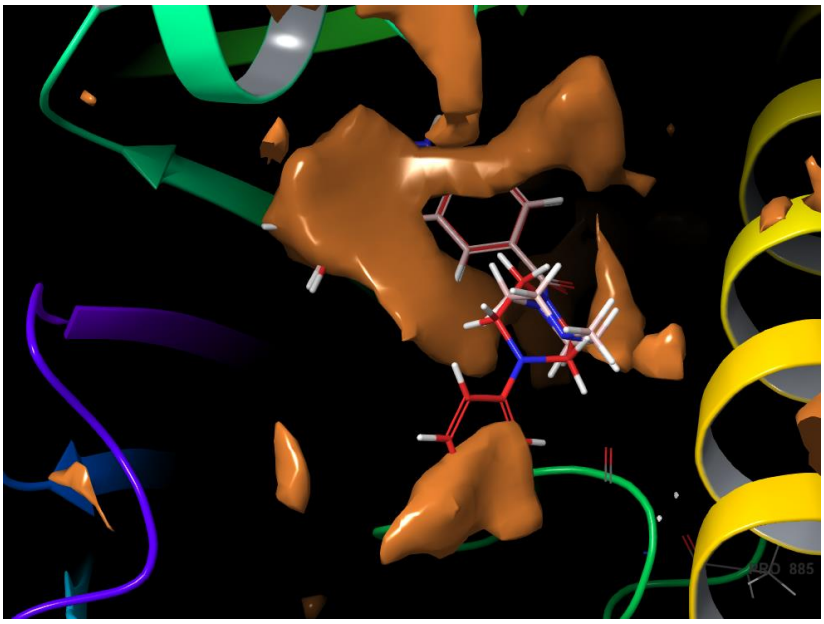

Figure 48 *Superposition of **a3** (pink) and **a4** (red) docked into the Normal model when the hydrophobic region (orange) was presented. The hydrophobic region is shown in orange. The method to generate the hydrophobic/philic surface was introduced in **Chapter 4**, **Section 4.1**.*

a. 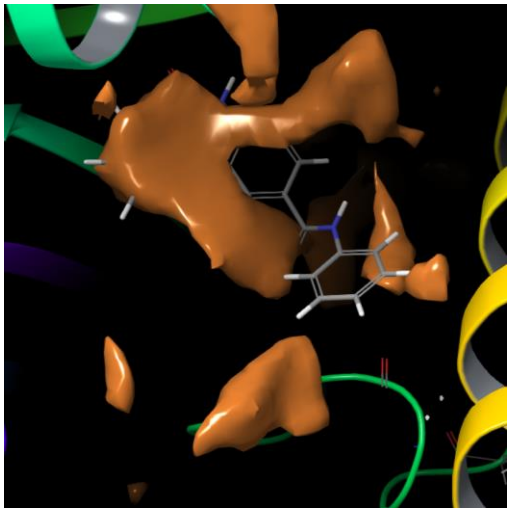 b. 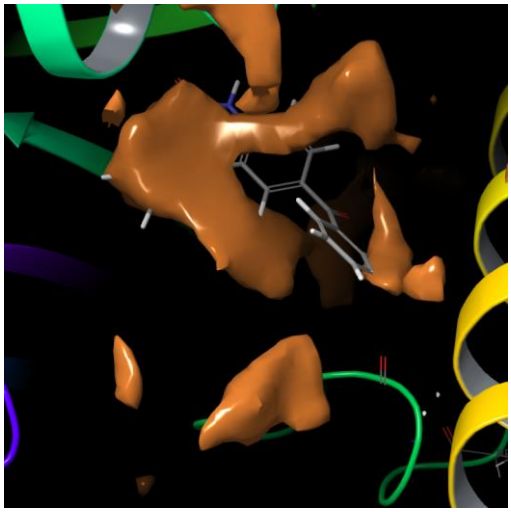

Figure 49 ***a5*** *(panel* ***a****) and* ***a6*** *(panel* ***b****) docked into the Normal model when the hydrophobic region (orange) was presented. The method to generate the hydrophobic/philic surface was introduced in* ***Chapter 4***, ***Section 4.1***.

We also considered the possibility of interaction with residues around Region D. We found that only larger molecules could stack the side chains in the area between the D-loop and the HD but these molecules, except **a16**, were less potent, and thus we believed that interfering with the D-loop would diminish the potency. However, even though **a16** was a good inhibitor, it was too short to reach further residues such as T887 which could be the target for both a covalent bond and H-bonds that would boost the inhibition by tightening the ligand-protein binding. Thus, we would need to redesign some larger molecules that could bypass the D-loop and reach target residues.

5.5. Experiments on Compounds Designed to Interact with The HD

5.5.1. Introduction

Some residues in the HD would influence the potency and selectivity of the PARP1 inhibitor. As we have discussed previously, D770 and D766 are considered critical residues involved in inducing a particular protein conformation in PARP1, called the “Pro-DNA-retention” conformation, and as a result, causing PARP-trapping that would increase the cytotoxicity of a PARP inhibitor [21]. Interacting with these residues in the HD especially in the Open model

would therefore increase the inhibitor potency [21]. E763 was also mentioned in the above paper that it might also play a part, although there was no solid evidence [21]. PARP1-selectivity against PARP2 could come from the interaction with D766 (PARP1) and E335 (PARP2). While these two residues are in the position analogous to each other, the difference in the side chain length would determine whether they can interact with the inhibitor. Previously in our study, we stated that while larger molecules might not have great capability in inhibiting PARP1, small molecules with an aromatic component on the R_1 (*para* to the amine of the phenanthridinone) could be developed into a "three-pointed star"-like molecule to guide a functional group to aim towards the HD when the aromatic component is attracted by the hydrophobic region. In this study, we would present compounds and their analogs designed under this concept trying to interact with the HD. Meanwhile, we would also combine the molecular docking method for prediction and analysis. As these molecules were designed to occupy not only the NI, both the Normal model and the Open model would be incorporated for research purposes.

5.5.2. Results

Generally, inhibitors used in this study were designed in the shape of "three-pointed stars". For each point of the star, the inhibitor consisted of the phenanthridinone core component, the benzene ring component, and the hydroxyl functional group as the H-bond donor. It was centred around the amide linker. The phenanthridinone core component was used as the anchor, which would provide basic inhibition ability by binding into the nicotinamide binding pocket competing with the endogenous substrate NAD^+. The benzene component was the guider and would be attracted by the hydrophobic region, rotating and pointing the hydroxyl arm towards the HD. The hydroxyl functional component was the H-bond donor and it would interact with D770/D766/E763 potentially (**Figure 50**). Analogs of this design included 1. converting the phenanthridinone component to the thienoquinolinone component; 2. changing the benzene component to alkyl components or cyclohexane components; 3. alternating the length of the amide linker and the hydroxyl arm; 4. using both R_1 and R_2 substitution respectively. Designed compounds with the corresponding potency are shown in **Figure 51**. As a result, we found that 1. the design did lead to some potent inhibitors such as **a48**; it was more potent compared to its scaffold **a5** from the last study; 2. R_1-substituted molecules were more potent than R_2-substituted ones and thienoquinolinone-based compounds were still low in potency; 3. the SAR study

suggested that the chirality would affect the potency and 4. the hydroxyl group was functioning as expected.

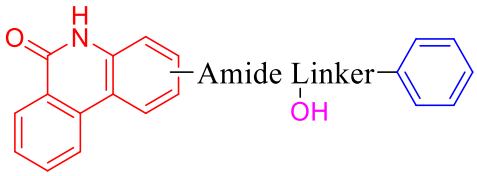

Figure 50 *The general design of inhibitors used in this study to interact with the HD through H-bonding. The inhibitor was centred around the amide linker, with the phenanthridinone component (red), the hydroxyl group (purple) and the benzene ring (blue) as three points. The phenanthridinone component was used as the anchor to bind to the NI. The hydroxyl functional group was to provide the H-bond with a residue on the αF of the HD and the benzene component was used as a guide, which would be attracted by the hydrophobic region, forcing the hydroxyl arm to point towards the HD.*

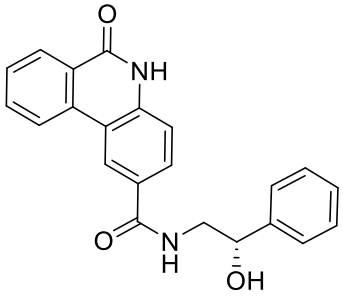

a23
IC_{50} = 1160±990nM

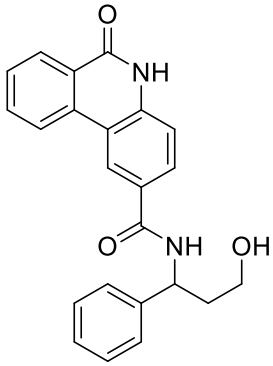

a24
IC_{50} = 159±18nM

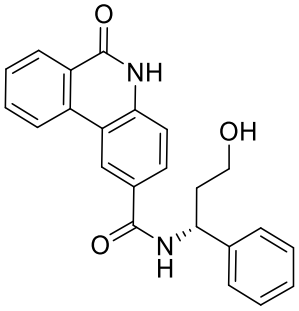

a25
IC_{50} = 2030±1100nM

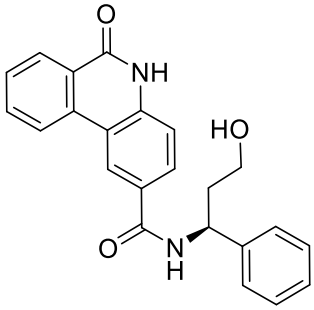

a26
IC_{50} = 124±68nM

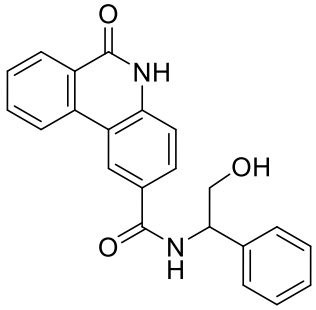

a27
IC_{50} = 545±330nM

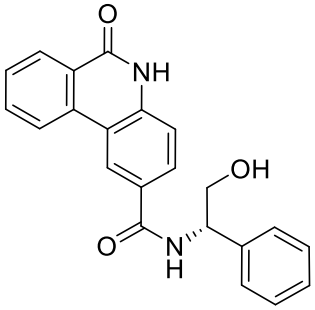

a28
IC_{50} =946±240nM

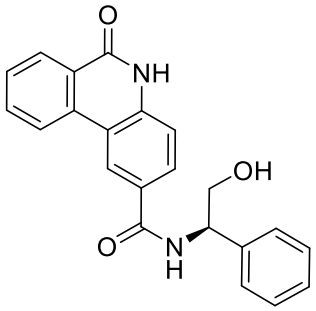

a29
IC_{50} = 108±6.3nM

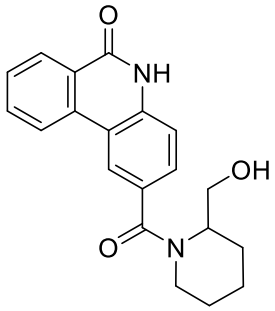

a30
IC_{50} = 141±33nM

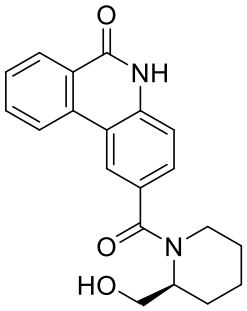

a31
IC_{50} = 243±14nM

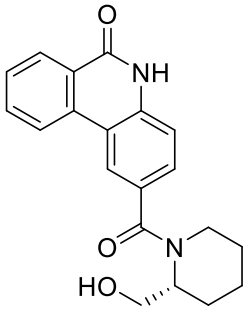

a32
IC_{50} = 149±25nM

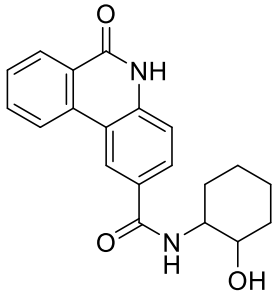

a33
IC_{50} = 312±39nM

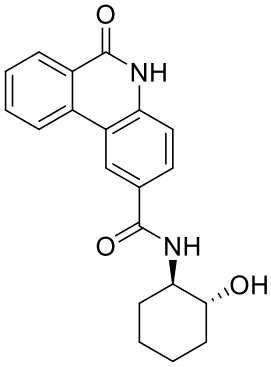

a34
IC_{50} = 473±160nM

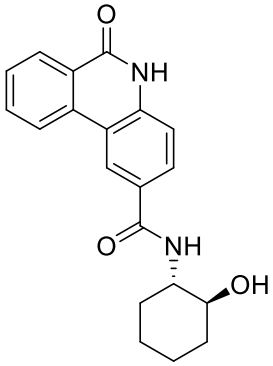

a35
IC_{50} = 276±47nM

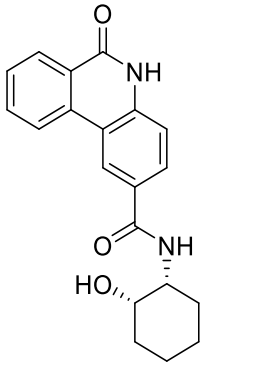

a36
IC_{50} = 330±110nM

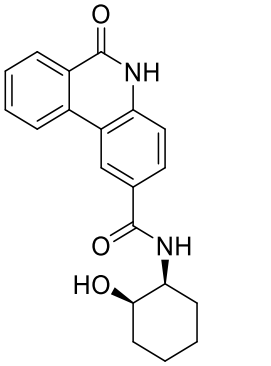

a37
IC_{50} = 382±97nM

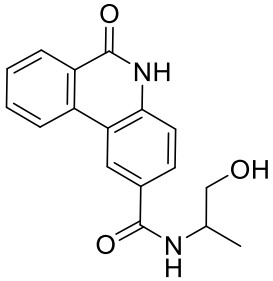

a38
IC_{50} =615±230nM

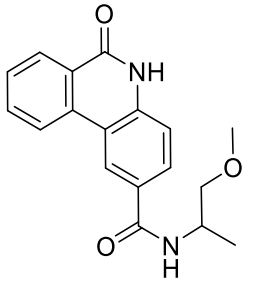

a39
IC_{50} = 690±630nM

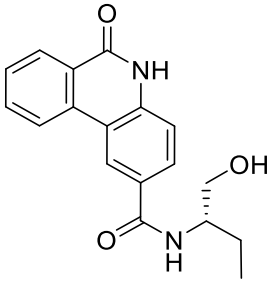

a40
IC_{50} = 566±230nM

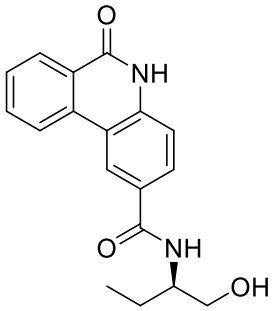

a41
IC_{50} = 12300±5500nM

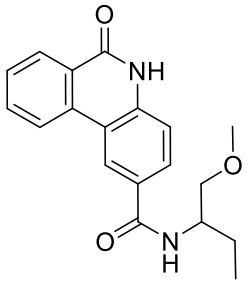

a42
IC_{50} = 552±380nM

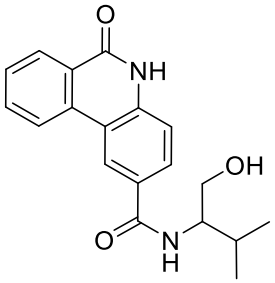

a43
IC_{50} = 277±120nM

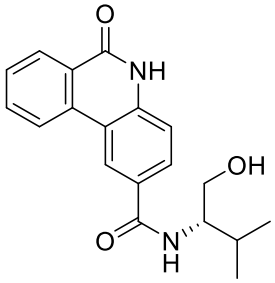

a44
IC_{50} = 693±220nM

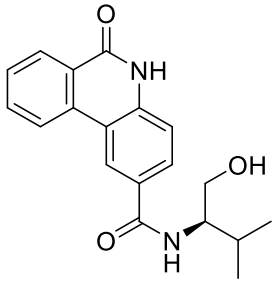

a45
IC_{50} = 179nM

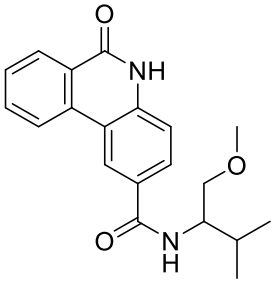

a46
IC_{50} >100000nM (213000nM)

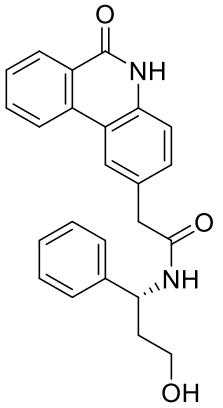

a47
IC_{50} = 746±390nM

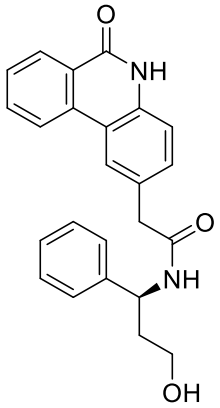

a48
IC_{50} = 35.0±19nM

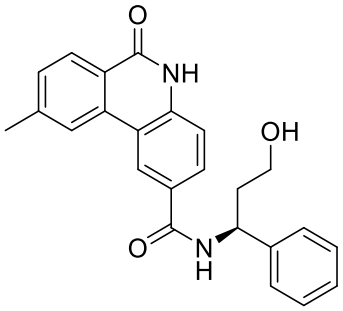

a51
IC_{50} = 38700±13000nM*

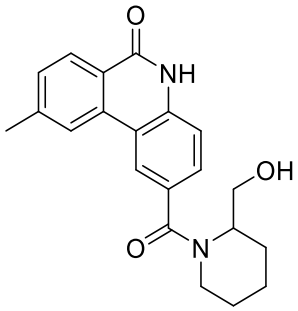

a52
IC_{50} = 783±83nM

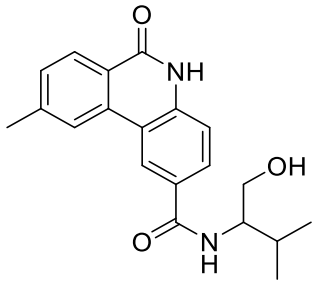

a53
IC_{50} = 40600±22000nM*

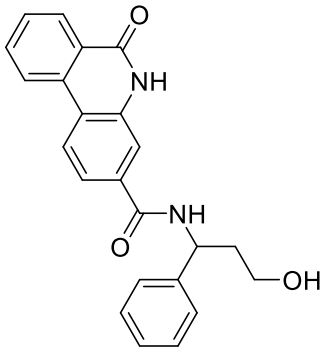

b15
IC_{50} = 450nM

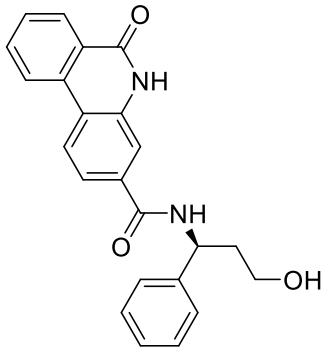

b16
IC_{50} = 803±110nM

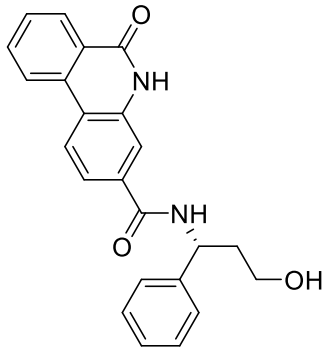

b17
IC_{50} = 496nM

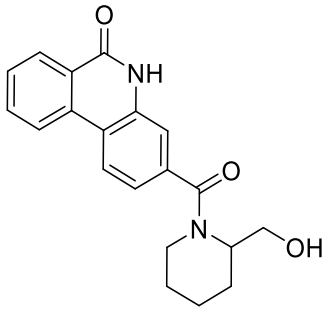

b18
IC_{50} = 143±0.60nM

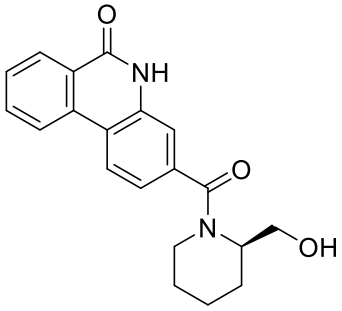

b19
IC_{50} =62.0±28nM

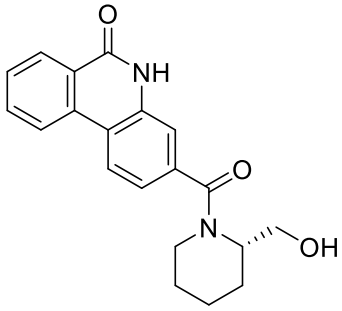

b20
IC_{50} =686nM

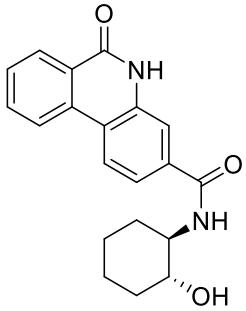

b21
IC_{50} = 685±54nM

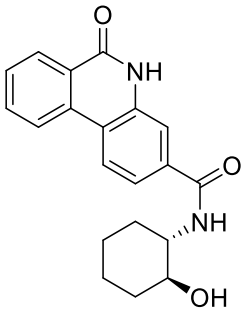

b22
IC_{50} = 524nM

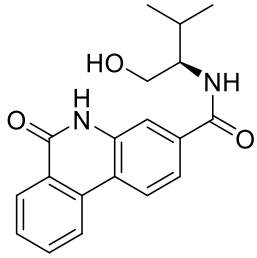

b23
IC_{50} = 506nM

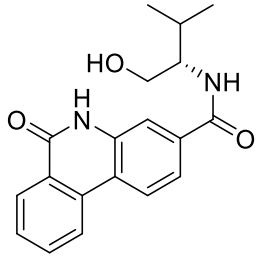

b24
IC_{50} = 7420nM

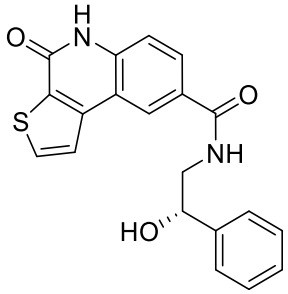

c18
IC_{50} = 512±74nM

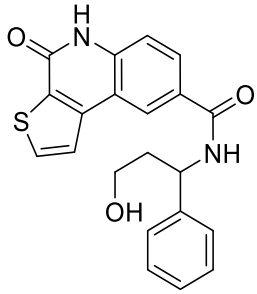

c19
IC_{50} = 519nM

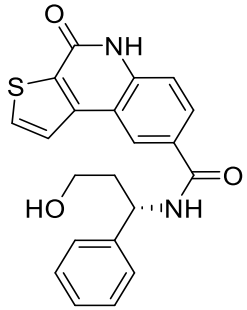

c20
IC_{50} = 406nM

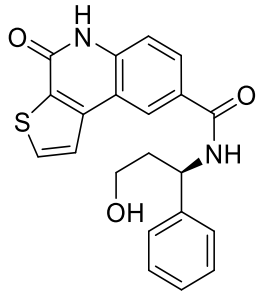

c21
IC_{50} = 931±520nM

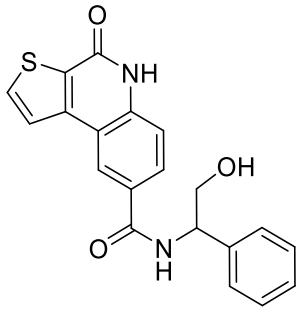

c22
IC_{50} = 1860±1000nM

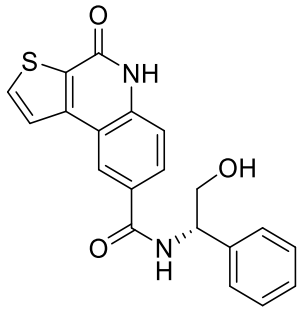

c23
IC_{50} = 2370±1500nM

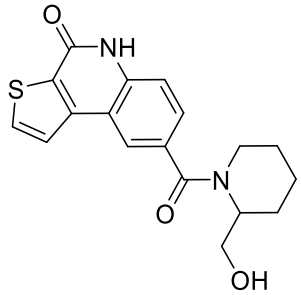

c24
IC_{50} = 311±12nM

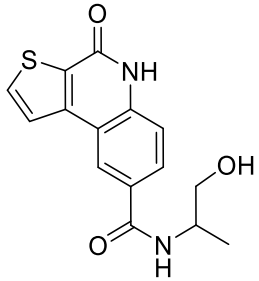

c25
IC_{50} = 2270nM

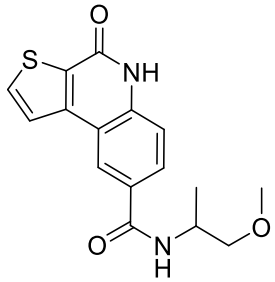

c26
IC_{50} = 3160±1600nM

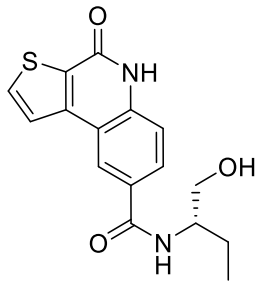

c27
IC_{50} = 722nM

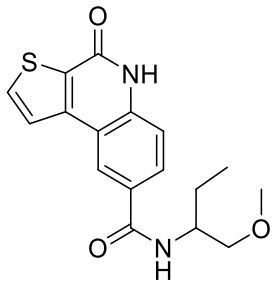

c28
IC_{50} = 3080nM

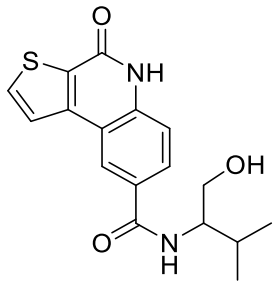

c29
IC_{50} = 1340nM

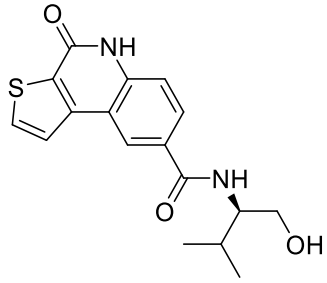

c30
IC_{50} = 1290nM

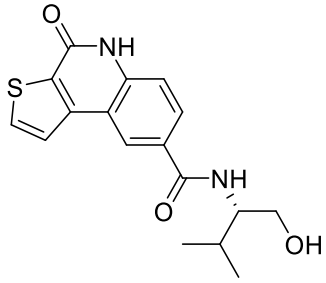

c31
IC_{50} = 1830nM

Figure 51 *Molecules with the "three-pointed star" design and IC_{50} values. Experimental data were obtained from the enzymatic assay described in* ***Chapter 4, Section 4.3****. Each experiment was plated in triplicate. Data obtained from two or more experiments were shown as Mean±SD; otherwise, it was obtained from single measurements. Experimental data were processed with*

*GraphPad 8.0.1. IC_{50} values were calculated using 4-parameter logistic regression. Data in bracket were extrapolated. Data with * was* near the upper range (100000nM) used for the experiment.

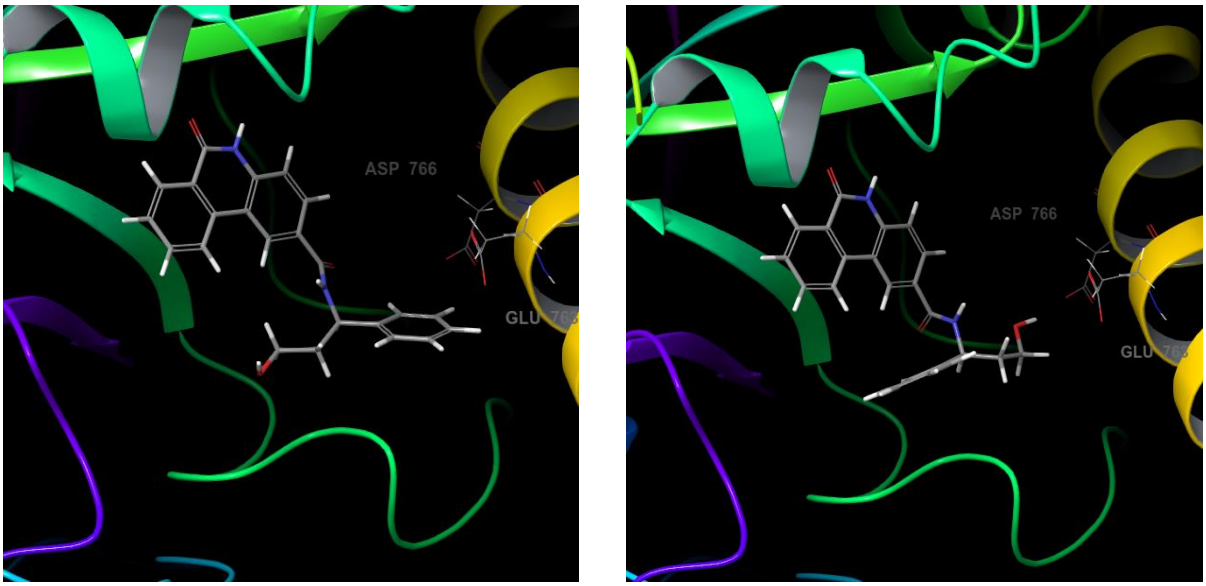

Figure 52 ***a25 (left)*** *and* ***a26 (right)*** *docked to the Open model.*

The first requirement for decent potency was to interact with the HD especially in the Open model as designed. **a26**, **a29, a33, a48** were the most potent ones in R_1-substituted compounds with IC_{50} values around or smaller than 100nM. **a26 a29** and **a48** were the design we were originally looking for, composed of the phenanthridinone core component in the NI and the benzene ring component in the region B that was attracted by the hydrophobic interaction to maintain the hydroxyl functional group arm around the HD to interact with D766 (**Figure 52**).

Changing the amide linker and the hydroxyl arm (**a29 → a23**) would greatly decrease the potency even if the total length were the same. Using the alkyl component to replace the aromatic ring was also likely to reduce the potency (**a27** vs. **a38**, **a29** vs. **a40/41/44/45**), which could be a result of increased hydrophobicity. The alkyl component was not as hydrophobic as the benzene ring. When the alkyl group became larger and more hydrophobic, the ligand gained better inhibition capability (**a38** vs. **a40/41** vs. **a43/44/45)**. When we changed the "three-pointed star" structure to the hexatomic ring (**a30-a37**), the ring might also be attracted by the hydrophobic region. Only with the correct configuration will the hydroxyl group interact with

D766 and the H-bond might also facilitate stabilizing the rotation (**Figure 53**). While **a24-a26** possessed decent potency, their analogs **b15-b17** were not as potent, which was the result of a different binding pose. R_2 position was close to the HD and therefore the hydroxyl arm was too long to form an H-bond with D766 (**Figure 54**). In contrast, a smaller molecule like **b18-b20** was just appropriate. Even though **b19** was potent, it was reacting with another critical residue R878. The position of the **b20** hexatomic ring was not covered by the hydrophobic region and thus it was not a powerful "guide" to maintain the right configuration for OH-D766 interaction, leading to worse potency (**Figure 55**). By comparing enantiomers' assay results, we found superior compounds, especially for R_1-position substituted ones, always shared the same stereo configuration (**Figure 56)**. This configuration would probably favour the OH-D766 interaction.

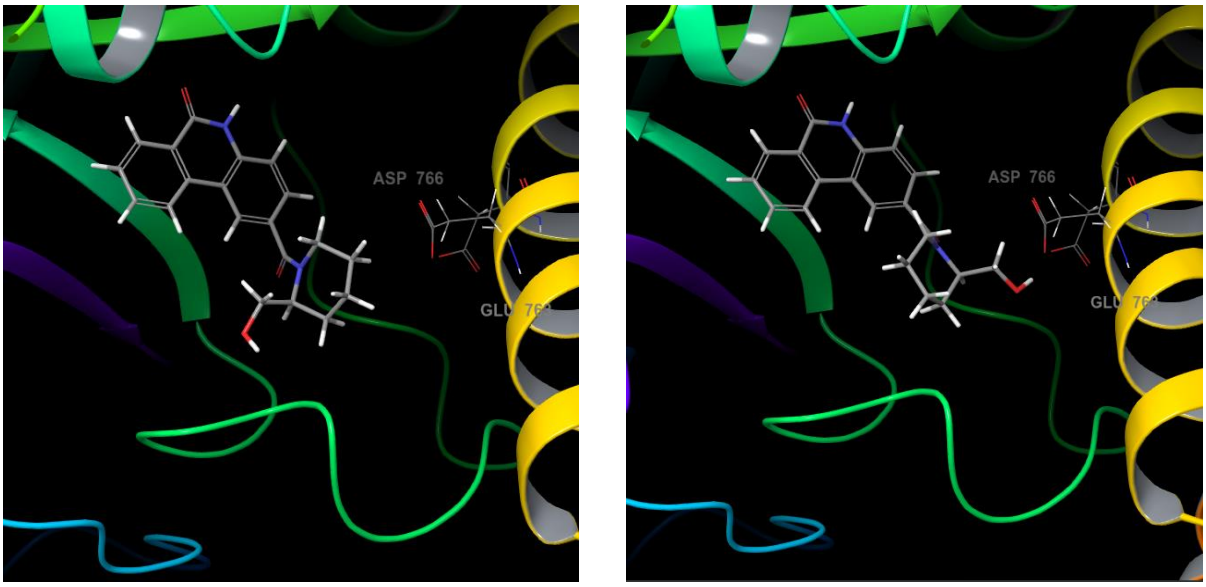

Figure 53 ***a31 (left)*** *and* ***a32*** *docked* ***(right)*** *to the Open model.*

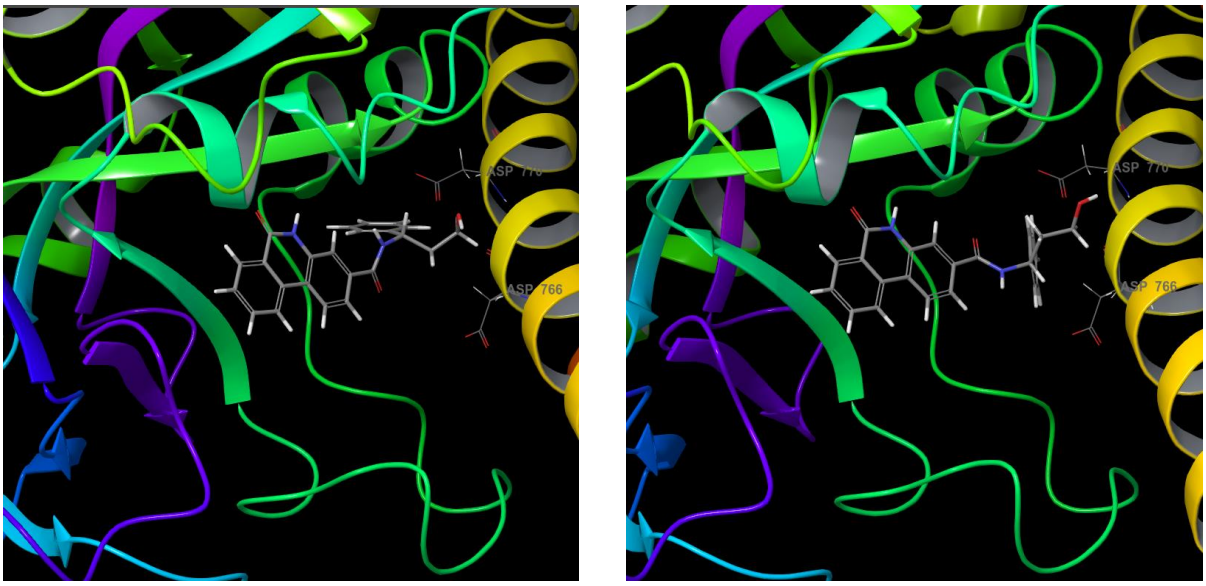

Figure 54 ***b16 (left)*** *and* ***b17 (right)*** *docked to the Open model.*

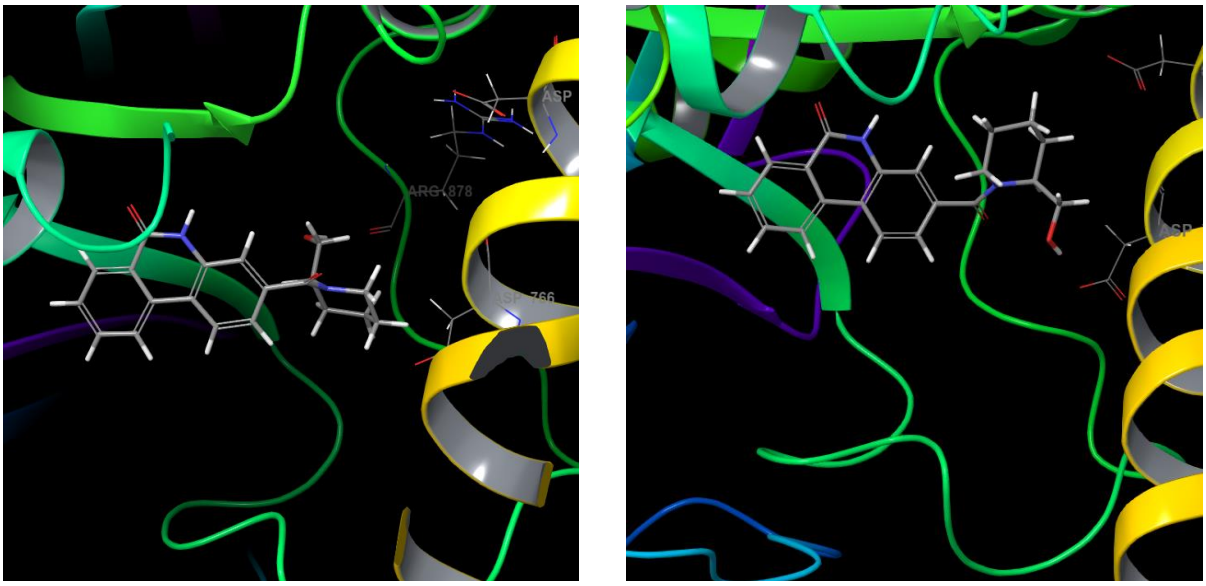

Figure 55 ***b19 (left)*** *and* ***b20 (right)*** *docked to the Open model.*

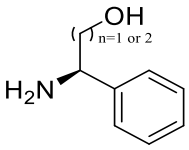

Figure 56 *The superior stereo configuration especially when the side chain was connected to the R1 position.*

According to the "Pro-DNA-Retention" theory, an inhibitor inducing the protein configuration with an opened binding pocket had a better chance to be a superior inhibitor. It implied that if a compound had interaction with the HD, or if it had a higher *in silico* affinity, in the Open model, it was likely to be superior in potency compared to its enantiomer (i.e., When predicting potency: HD-interaction in the Open model > higher affinity in the Open model > HD-interaction in the Normal model > other situations). The experimental results confirmed this assumption. For example, comparing **a25** and **a26**, **a26** was able to interact with D766 in the Open model in its best correct binding pose while **a25** couldn't, implying **a26** (IC_{50}=124nM) was a more promising inhibitor than **a25** (IC_{50}=2030nM), and the IC_{50} values were in line with the prediction (**Figure 57**).

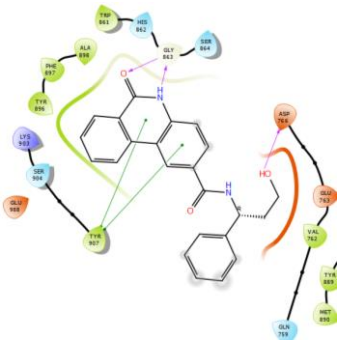

a25 in the Normal model, docking score -9.5

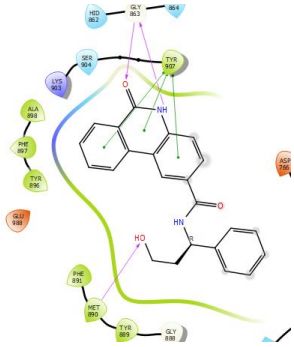

a25 in the Open model, docking score -8.5

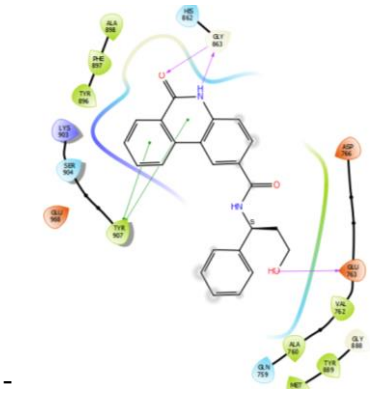

-

a26 in the Normal model, docking score -8.8

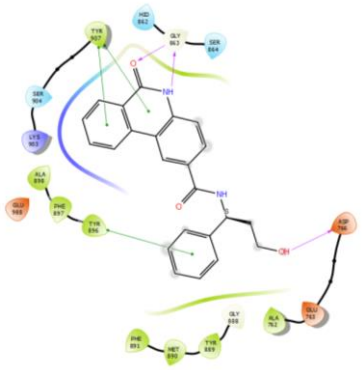

a26 in the Open model, docking score -8.7

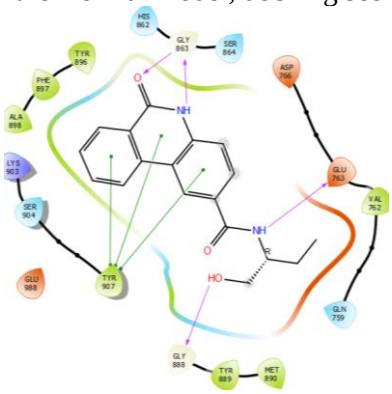

a40 in the Normal model, docking score -10.1

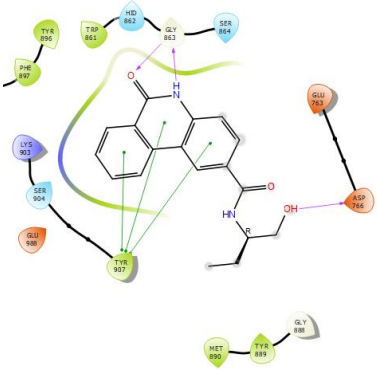

a40 in the Open model, docking score -8.1

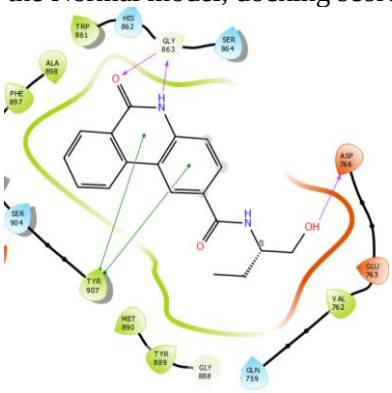

a41 in the Normal model, docking score -10.2

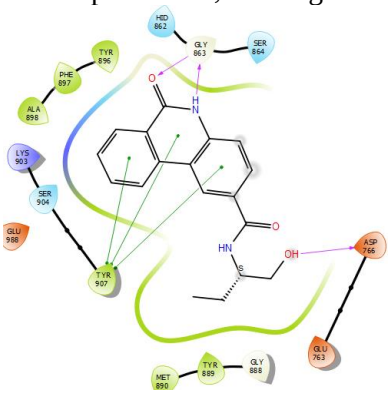

a40 in the Open model, docking score -8.1

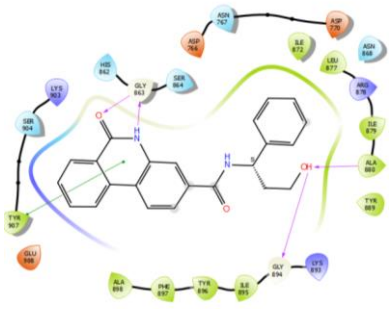

b16 in the Normal model, docking score -10.5

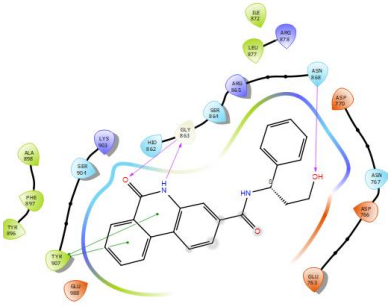

b16 in the Open model, docking score -8.8

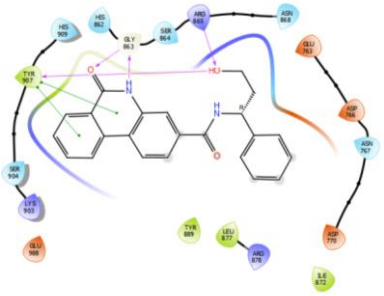

b17 in the Normal model, docking score -9.1

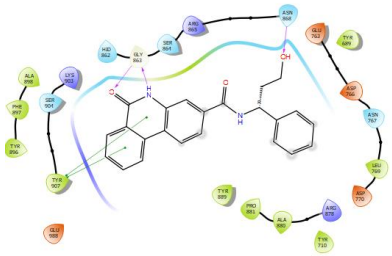

b17 in the Open model, docking score -8.2

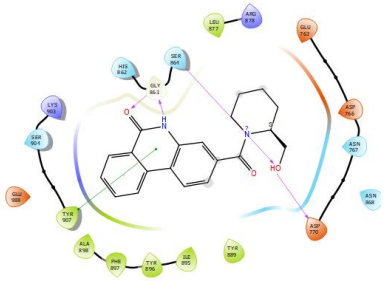

b19 in the Normal model, docking score -7.8

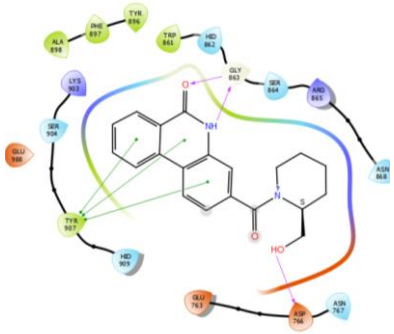

b19 in the Open model, docking score -8.0

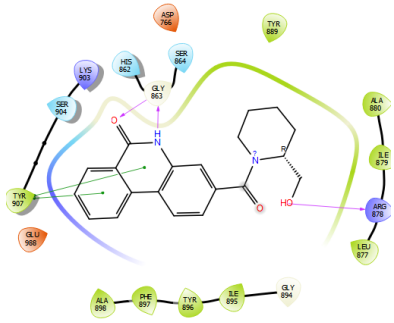

b20 in the Normal model, docking score -9.3

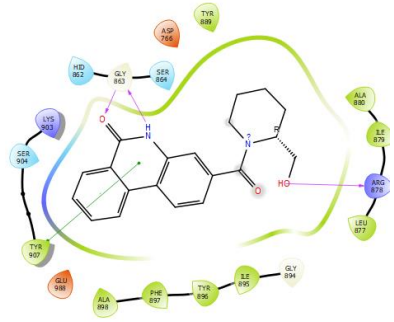

b20 in the Open model, docking score -7.9

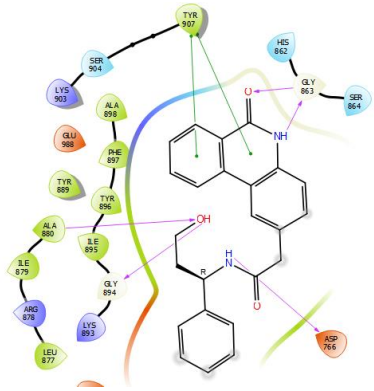

a47 in the Normal model, docking score -12.5

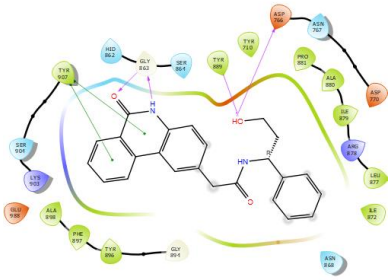

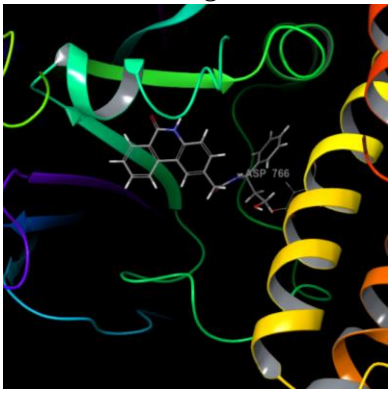

a47 in the Open model, docking score -8.9

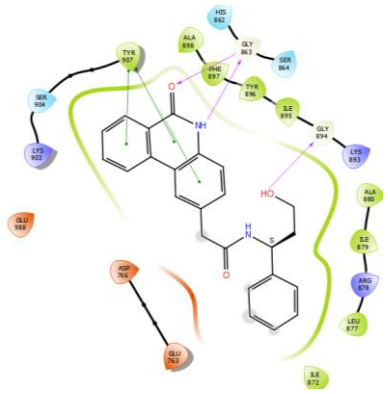

a48 in the Normal model, docking score -12.5

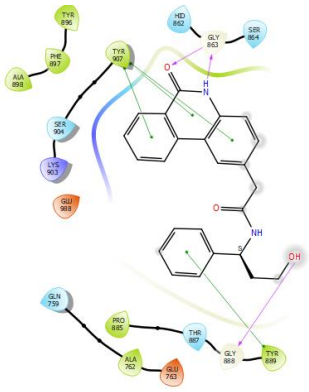

a48 in the Open model, docking score -8.9

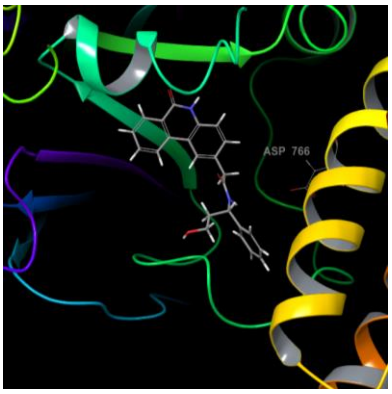

score -8.7

Figure 57 *Examples of "three-pointed star" inhibitor ligands docked to the Normal model and the Open model respectively. Purple arrow: From H-bond donor to H-bond acceptor. Green arrow: π interaction.*

This chirality-potency relationship applied to **a28**/**a29**, **a31**/**a32**, **a44**/**a45**, **a47**/**a48**, **b19**/**b20**, **b23/b24** and corresponding **c** compounds as well. For **a40/a41**, although two compounds almost shared the same binding orientation in both the Normal model and the Open model, the amide nitrogen was a worse H-bond donor compared to the hydroxyl group to interact with the D766 when the binding pocket was fully closed (which was shown in the Normal model). It resulted in less potency due to the weaker ligand-HD interaction. **b16**/**b17** also had similar binding poses but neither of them interacted with the HD; however, **b17** had an additional H-bond between the hydroxyl group and Tyr, explaining why **b17** was slightly more potent. An interesting finding on this topic came from comparing **a47**/**a48**. **a48** was the best inhibitor we found in this study. However, it did not exactly follow the above-mentioned SAR. Due to one additional carbon between the phenanthridinone and the amide, there was not enough room for the ligand to be docked as designed: the benzene was not in the favoured hydrophobic region and the amide was very much curled (possibly within a higher-energy conformation) (**Figure 57**). The binding pocket in the Open model might still be too small for the ligand. We introduced a larger homologous model and re-docked two isomers into the protein (**Figure 58**). In the new docking poses, the benzene ring went back to the hydrophobic region as designed. **a47** was not able to interact with the HD while **a48** formed an H-bond with E763, which could bring better potency**.** We argued that the complex made of the new homologous model and **a48** could be

closer to the real situation, implying **a48** could induce a wider opened protein configuration by interacting with E763 of the HD. This mechanism of action made **a48** the best PARP inhibitor so far.

a.

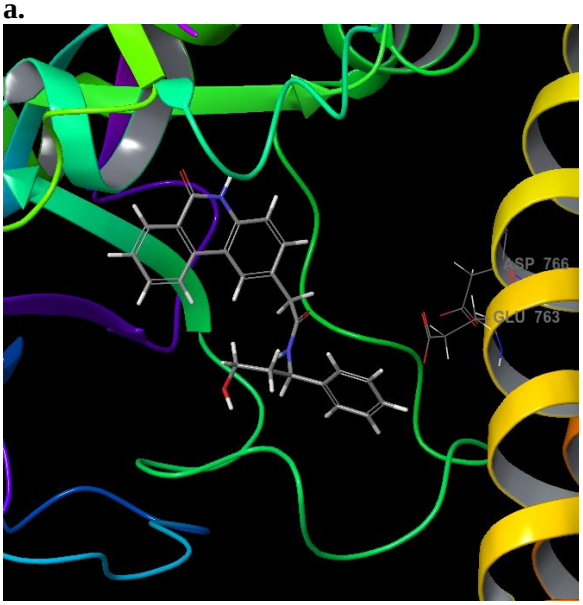

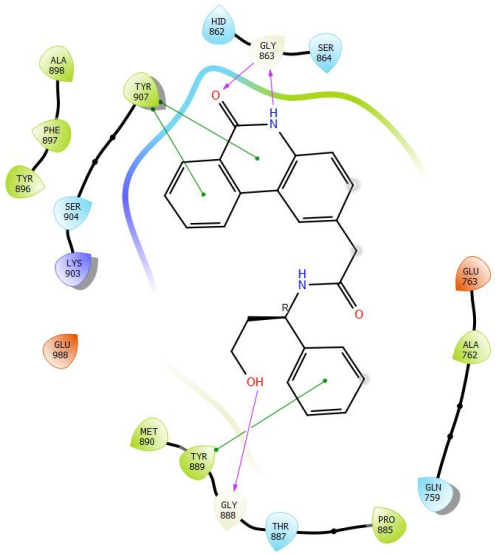

b.

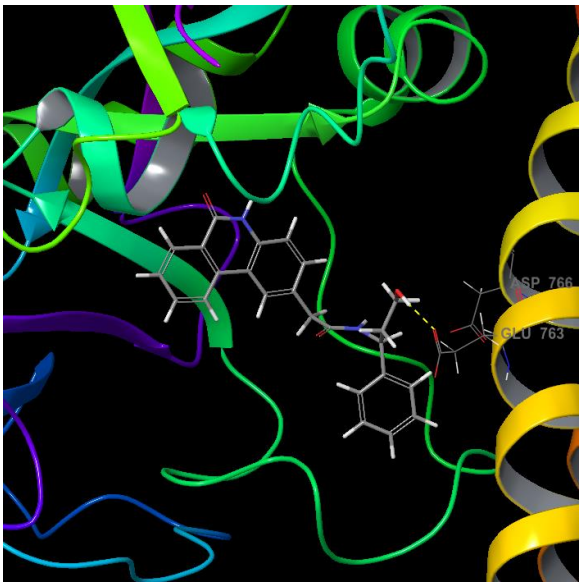

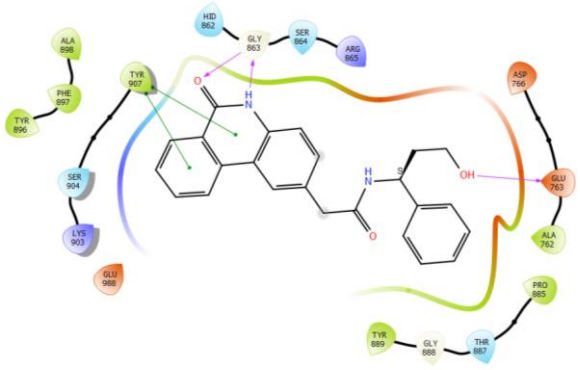

Figure 58 ***a47*** *(panel* ***a****)* ***a48*** *(panel* ***b****) docked to the new homologous model with a slightly wider binding pocket based on the protein crystal structure PDB ID* ***6VKO****. The RMSD comparing this model with the Open model was 0.23Å. Purple arrow: From H-bond donor to H-bond acceptor. Green arrow: π interaction. Yellow dash: H-bond.*

We also converted some hydroxyl components into methoxyl ones. We found in some cases there was a great impact on the potency (e.g., **a46**) while some didn't (e.g., **a42**). Considering the methoxyl group might also behave as an H-bond acceptor, it possibly disrupted some H-bonds while in other cases it acted as the acceptor with an appropriate pose. As the methoxyl group as the H-bond acceptor was not taken into account in the molecular docking, we didn't look deep into it. Another modification that decreased the potency was the methyl group on the phenanthridinone (**a51**-**a53**). Since the space in the carbonyl-half of the NI was narrow, an additional substituent such as the methyl group was likely to cause the steric clashing and subsequently weaken the binding affinity of the phenanthridinone core structure, diminishing the potency in consequence. Converting phenanthridinone (**a** compounds) to the thienoquinolinone (**c** compounds) also made poor inhibitors globally, indicating the latter one was a poor platform for developing PARP inhibitors.

Based on the molecular docking results, we predicted that chirality would lead to PARP1/PARP2 selectivity by selectively interacting with D766 or E335. As previously discussed, when compounds were designed to target the HD specifically, one was expected to gain better potency if the molecular docking result suggested it would interact with a residue in the HD such as D766 in the Open model with a better docking score. We presumed that it was the same for PARP2. if a compound had a higher affinity interacting with E335 in the PARP2 Open model, it would be a better PARP2 inhibitor. Meanwhile, if this compound was less potent in inhibiting PARP1 due to lower affinity interacting with D766, it would be more PARP2-selective against PARP1. When **a28 a29** were docked to the PARP2 Open model, two ligands showed similar binding poses and protein-ligand interactions (**Figure 59**). However, we believe **a29** was less PARP2-affinitive as it had a lower docking score and bad contact with E335. Hence, we predicted **a28** had better PARP2-selectivity than **a29**. Likewise, **a44** would be a good PARP2 inhibitor as well. To prove the point, we tested these compounds using a commercially available PARP2 assay kit (**Table 14**). The enzymatic assay result was partially in agreement with the prediction: Although **a28 a29** did not show significant selectivity towards PARP2 and PARP1 respectively, we found their preference on different proteins that were as stated in our prediction. Meanwhile, we argued that **a28** and **a44** were more PARP2-selective than PJ34 and olaparib**.**

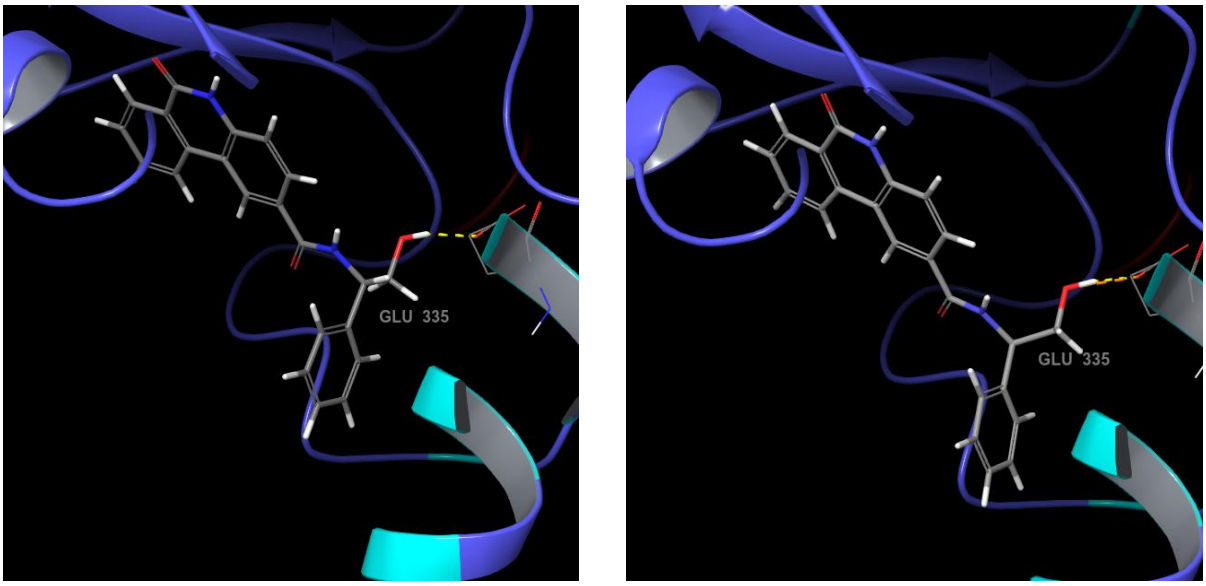

Figure 59 ***a28*** *(**left**, docking score -8.7)* ***a29*** *(**right**, docking score -8.4) docked to the PARP2 Open model. H-bond (yellow dash) and bad contact (orange) were also marked in the figure.*

Compounds	In-house PARP1 assay (nM) [a]	BPS PARP1 assay (nM) [b]	BPS PARP2 assay (nM) [b]	BPS PARP1/PARP2	BPS TNKS1(nM) [b]
Olaparib[c]	7.20	0.900	0.500	1.80	N/A
PJ34[d]	148±28	25.2	33[d]	0.76	2910
a28	946±240	132	62.8	2.10	474
a29	108±6.3	59.4	102	0.58	N/T
a44	693±230	136	35.6	3.81	N/T

Table 14 ***a28***, ***a29***, ***a44*** *inhibition potency against PARP2 and TNKS1. (a) Experimental data were obtained from the enzymatic assay described in* ***Chapter 4, Section 4.3****. Each experiment was plated in triplicate. Data obtained from two or more experiments were shown as Mean±SD. Experimental data were processed with GraphPad 8.0.1. IC_{50} values were calculated using 4-parameter logistic regression. (b) Experimental data were obtained from the BPS PARP1 or PARP2 or TNKS1 enzymatic assay. Each experiment was plated in triplicate. Data were from single measurements. Experimental data were processed with GraphPad 8.0.1. IC_{50} values were calculated using 4-parameter logistic regression. (c) The IC_{50} value of olaparib was from the reference of the BPS assay kit; (d) The IC_{50} value of PJ34 in PARP2 was literature value using a similar assay from the same vendor. N/A: Not available. N/T: Not tested.*

5.5.3. Conclusion

In this study, we presented some potent inhibitors that were designed to interact with the HD. Supported by the molecular docking results, we argued that the potency would come from their possibility of interacting with the HD when the binding pocket was not fully closed, which referred to their preference or affinity to be docked into the Open model and interacting with residues such as D770/D776/E763 *in silico*. By comparing molecular docking results and enzymatic assay results, we found that the design with (*R*)-2-amino-2-phenylethan-1-ol and (*S*)-3-amino-3-phenylpropan-1-ol were likely to produce more potent inhibitor as the stereo structure brought the hydroxyl group to a better position interacting with the HD. With **a48** becoming the most potent inhibitor in this study, it was highly possible that **a48** would reach the HD before other inhibitors such as **a29**, or it could induce a wider opened configuration favouring PARP-trapping or PARP-DNA binding. The early-stage interaction with the HD before the binding pocket was closed might either stall the conformational change of the protein to influence the catalytic reaction or constrain the protein structure to the open configuration which could relate to PARP-trapping. Combining *in silico* and *in vitro* results to analyze and predict the structure-activity relationship was more informative and accurate. In traditional SAR, (*R*)-2-amino-2-phenylethan-1-ol and (*S*)-3-amino-3-phenylpropan-1-ol might be considered as two chirality with two opposite stereo configurations. With a molecular modelling-based SAR study, we found that these two configurations led to the same spatial occupancy and it all related to the orientation of a compound, especially its side chain, which would interact with the target protein. The traditional SAR study would also find it difficult to explain.

We also demonstrated an example showing how molecular docking resulted and knowledge-based analysis could contribute to predicting the selectivity of inhibitors. By analyzing the docking result we predicted **a28** and **a44** were more PARP2-selective against PARP1 when **a29** was more PARP1-selective. The selectivity came from the relative position between D766/E335 and the hydroxyl arm. If the protein-ligand complex was rigid and fixed, spatial locations of the H-bond donors from the hydroxyl arms from **a28 a29** differed due to the chirality. Meanwhile, spatial locations of the H-bond acceptors from D766 and E335 also varied due to the residue lengths. The selectivity appeared with **a28**-E335 **a29**-D766 were more likely to form H-bonds. Unfortunately, the protein complex in the real world was flexible bringing **a28**-D766 and **a29**-E335 pairs as well decreased the selectivity of each compound: Due to the less-

rigid structure, the hydroxyl arm could “swing/vibrate” and rotate within a certain range allowing the compound such as **a28** to interact with D766 in PARP1 better than we predicted. A design to ensure the compound only interacted with E335 or D766 by restricting the side chain from vibrating or rotating might boost the selectivity. Decreasing the flexibility allows ligands to form **a28**-E335 **a29**-D766 interactions only, which would lead to better selectivity. Having said that, the PARP2-preference inhibitors had surpassed the benchmark inhibitors olaparib and PJ34. Through this case, we argued that structure-based prediction using molecular docking might facilitate the development of selective inhibitors targeting protein isomers. We also consider that designing a selective PARP inhibitor by modifying a chiral center in a proper position was promising and achievable. The modification of the chirality to produce PARP1/2 selective inhibitors would make these inhibitors approximately identical physically. Conventionally, if the PARP1/2 isomers needed to be inhibited respectively in a study, completely different compounds would be used. The influence from the structural distinction of different inhibitors might be an uncontrollable variable. PARP1/2-preference inhibitors **a28/a29** and **a44/a45** or future PARP1/2-selective isomer-inhibitors could be used without considering the variable.

5.6. Experiments on Compounds with Strong Functional Groups

5.6.1. Introduction

Previously in our research on the influence of the spatial occupancy of a PARP inhibitor’s side chain outside of the NI, we argued that the R_2-substituted side chain (*meta* to the phenanthridinone amine) was able to enter the AD which was surrounded by important amino acid residues such as R878, D770, D766. Interactions with these residues can be related to superior inhibition capability and cytotoxicity resulting from interrupted protein conformational change and enhanced PARP-trapping/ PARP-DNA binding ability. Designing functional groups in this area to form relatively strong bonds may benefit the inhibitor potency. In addition to H-bonding, ionic bonding and temporary covalent bonding are possible in this region with residues like Asp. The scaffold used in this study was 3-(4-phenylpiperazine-1-carbonyl)phenanthridin-6(5*H*)-one, which had been proved as a relatively potent inhibitor itself in our previous study. *Meta*-substituted phenyl-piperazine component was able to enter the AD easily, according to the molecular modelling result. Its rigid structure might also favour the potency, as well as the

accuracy of the molecular docking result. Thus, we were confident about the prediction result. Warheads such as -NO_2 and -$B(OH)_2$ can provide covalent bonding and H-bonding or ionic bonding simultaneously. Such interactions, especially covalent bonding, were stronger and the compound might be tightly bound to the protein and as a result, they would be better inhibitors.

A second choice was to interrupt the conformational change, or to induce the configuration of which the binding pocket can not fully close by stacking a functional group into the gully between the middle section of the D-loop and the αF of the HD, as UKTT15. In addition to avoiding steric clashing with the D-loop, the functional group may need to interact with both the helix and the D-loop to reinforce the stacking. There is a Thr residue (T887) in the middle section of D-loop which can be attacked by the warheads. UKTT15 showed a tight K_d (20±5nM) in the previous study while its IC_{50} was yet to know. Designing molecules similar to UKTT15 but with the warheads might give us a better PARP-trapper with the same mechanism of action.

5.6.2. Results

Molecules designed and synthesized for this experiments are shown in **Figure 60**. For this study, inhibitors were designed based on the scaffold 3-(4-phenylpiperazine-1-carbonyl)phenanthridin-6(5*H*)-one, guided by the molecular docking results. From the molecular modelling, we found that the distance between the phenyl component and residues R878, D770, D766 were less than 7.1Å (the distance between centers), which meant -$B(OH)_2$ and -NO_2 warheads could at least form H-bonds or ionic bonds with these residues (**Figure 61**). The relative position between the phenyl ring and residues into account, any substitution position on the benzene ring (*ortho, meta* or *para*) had a chance to interact with at least one amino acid residue (**Figure 61**). Having this in mind, we designed molecules **b25**-**b30** and the molecular docking result suggested that H-bonds and ionic bonds were possible between residues and the boron and nitro components. The prediction suggested, among these six molecules, **b26** was expected to be a good candidate as it could only be docked into the Open model properly, implying it had the best chance to induce the "Pro-DNA-Retention" protein configuration upon binding (**Figure 62-c**). **b30** had the best *in silico* affinity (docking score) while interacting with D766 and D770 simultaneously in the Open model hinting that **b30** could be a potent inhibitor as well (**Figure 62-i/j**). **b28** and **b29** were also good inhibitors potentially, as they could interact

with R878 through ionic bonds in the Open model (**Figure 62-e/f/g/h**). Interestingly, the presence of the fluorine was likely to influence the rotation angle of the benzene ring and thus made the nitro group close enough to D770 to build another ionic bond (**Figure 62-e/g**). Meanwhile, **b27** was likely to be the worst inhibitor, which could be only docked into the Normal model, implying it might not induce or form any solid protein-ligand interaction in the "Pro-DNA-Retention" protein configuration (**Figure 62-d**). **b25** might not be the best inhibitor either as ionic bonds were only available in the Normal model (**Figure 62-a/b**). Considering the binding configuration, the ligand-protein interaction and the docking score showed the prediction was **b30>b26**>**b28>b29>b25>b27**. Similarly, compounds **c33 c37** based on 8-(4-phenylpiperazine-1-carbonyl)thieno[2,3-*c*]quinolin-4(5*H*)-one were also designed. They should have a similar docking pose as **b28 b25**, indicating they could be more potent than the scaffold **c7**. They were attempts to build a novel inhibitor with even more novelty, avoiding any patent restriction.

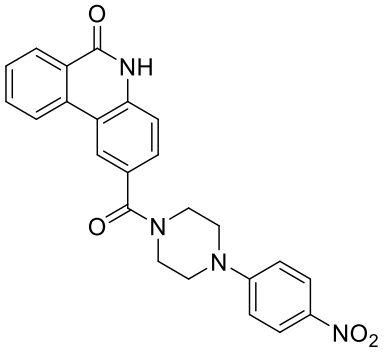

a49 IC_{50} = 30.4±29nM

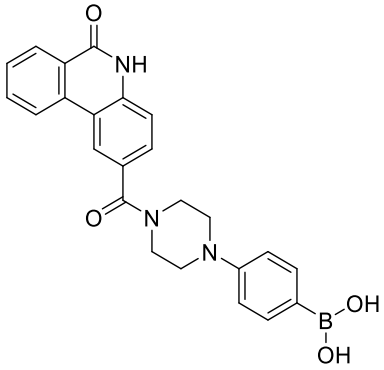

a50 IC_{50} = 133nM

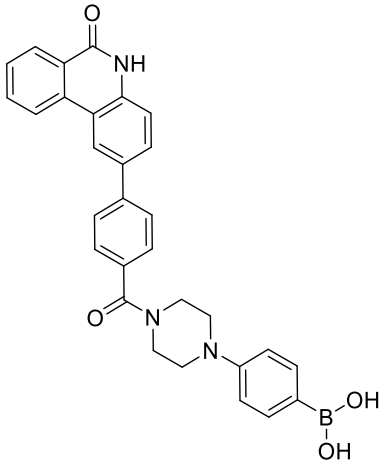

a55 IC_{50} = 2450nM

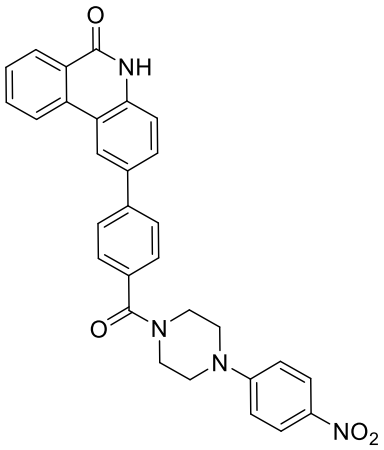

a56 IC_{50} = 919±197nM

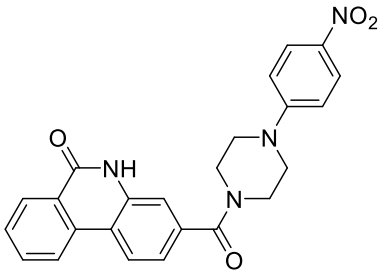

b25 IC_{50} = 17.8±9.4nM

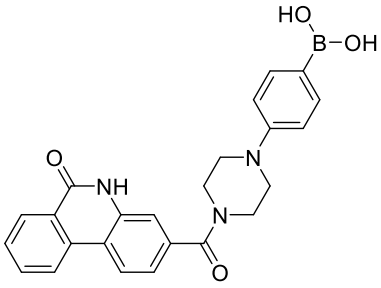

b26 IC_{50} = 15.8±1.9nM

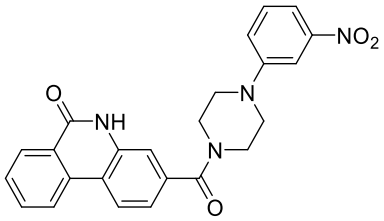

b27 IC_{50} = 43.0±2.3nM

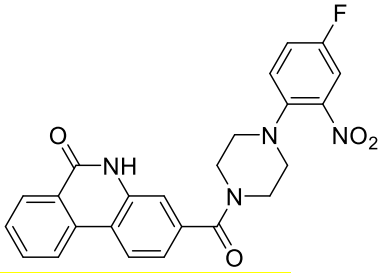

b28 IC_{50} = 10.7±0.19nM

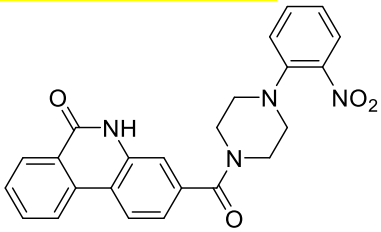

b29 IC_{50} = 14.1±5.3nM

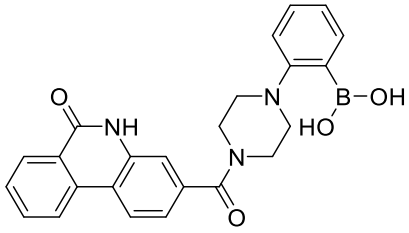

b30[a] IC_{50} = 38.4±3.9nM

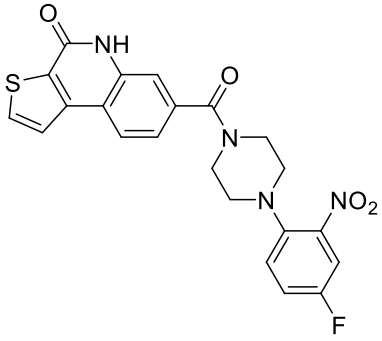

c33[b] IC_{50} = 135±0.70nM

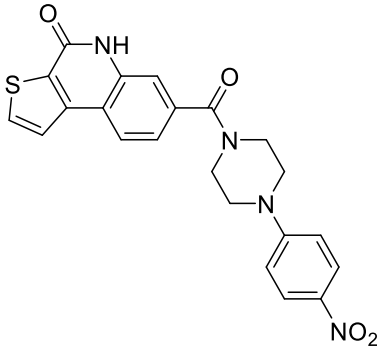

c37 IC_{50} = 9.51±0.36nM

Figure 60 *Inhibitors designed with -B(OH)$_2$ and -NO$_2$. Experimental data were obtained from the enzymatic assay described in* ***Chapter 4, Section 4.3****. Each experiment was plated in triplicate. Data obtained from two experiments were shown as Mean±SD; otherwise, it was obtained from single measurements. Experimental data were processed with GraphPad 8.0.1. IC_{50} values were calculated using 4-parameter logistic regression. (a)* ***b30*** *was not pure due to 3-(4-(2-hydroxyphenyl)piperazine-1-carbonyl)phenanthridin-6(5H)-one by-product which could not be separated completely from* ***b30****. (b)* ***c33*** *was not pure due to the unknown by-product formed during the photocyclization reaction. Compounds with IC_{50}s less than 150nM are highlighted.*

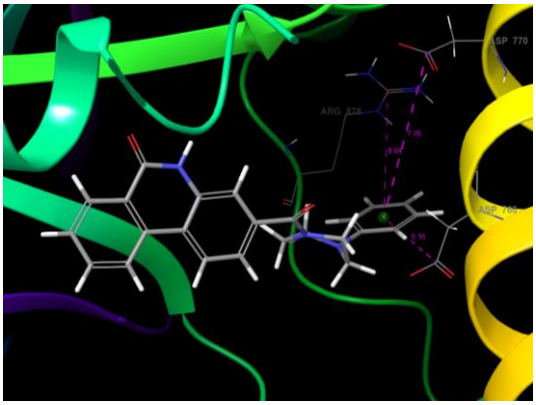

Figure 61 b4 *(grey) docked to the Open model. The phenyl group was surrounded by residues such as R878, D770, D766 within the distance of 7.05Å (from the center of the benzene ring to the carbonyl carbon). The Para and meta substituents would reach R878 and D770 while the ortho substituent would reach D766.*

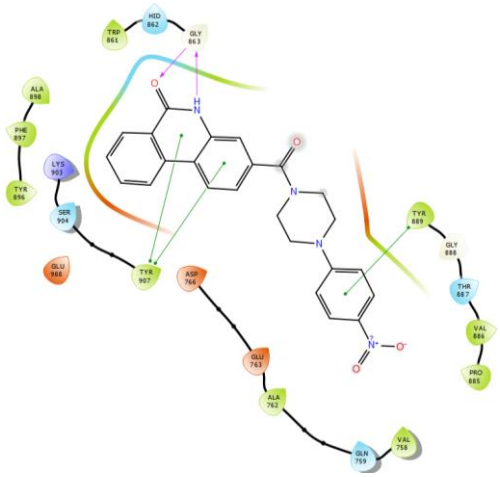

a. **b25** docked to the Open model, docking score -7.7

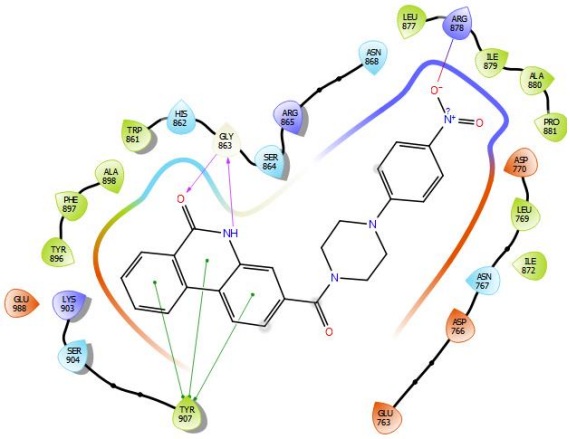

b. **b25** docked to the Normal model, docking score -9.2

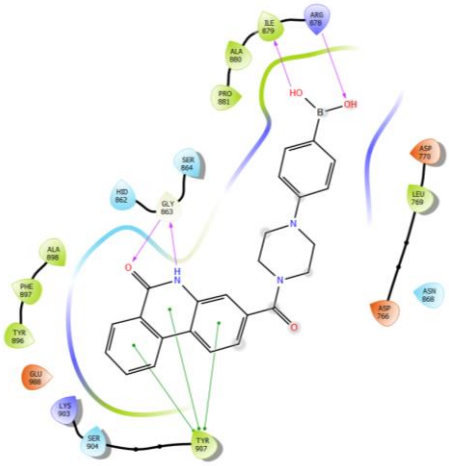

c. **b26** docked to the Open model, docking score -8.9

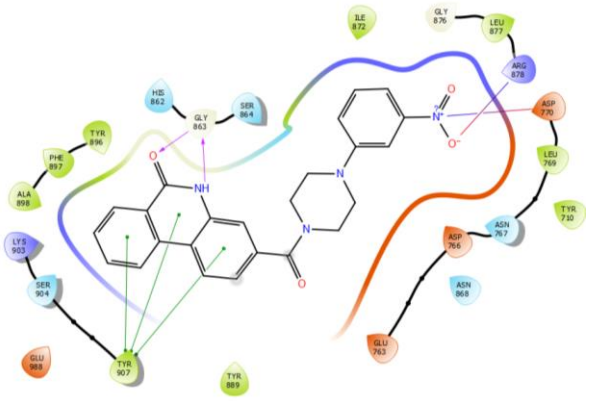

d. **b27** docked to the Normal model, docking score -9.2

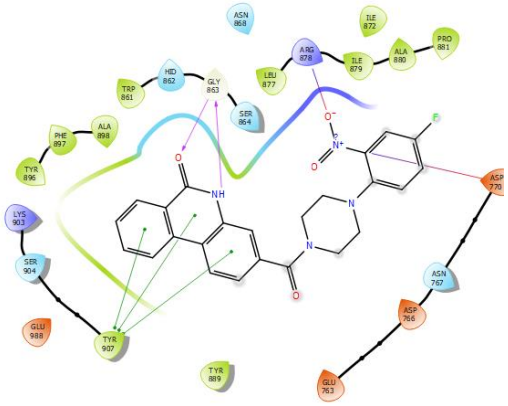

e. **b28** docked to the Open model, docking score -8.1

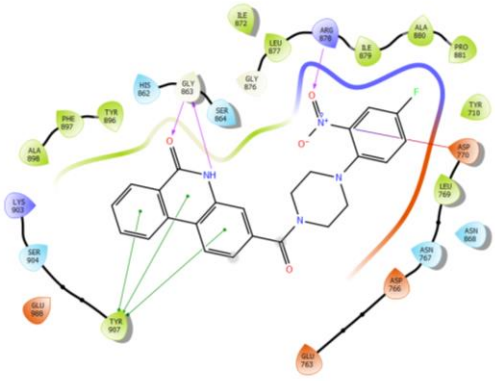

f. **b28** docked to the Normal model, docking score -10.4

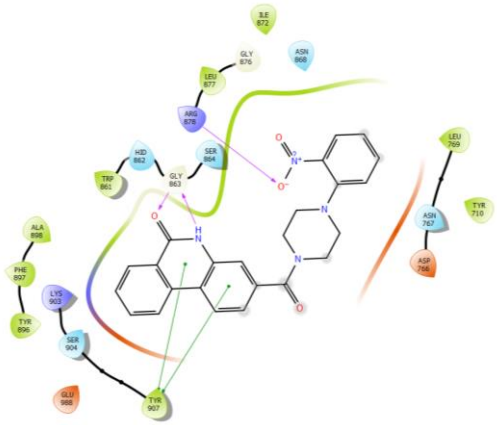

g. **b29** docked to the Open model, docking score -8.2

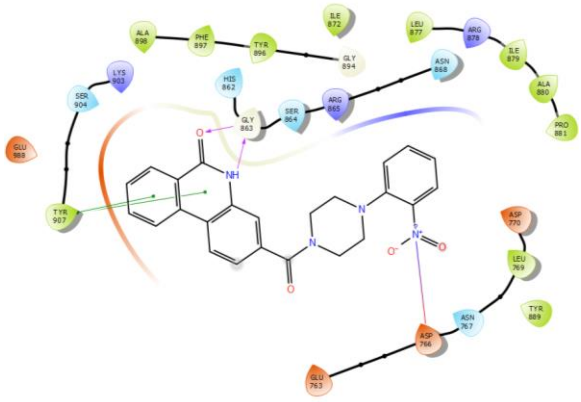

h. **b29** docked to the Normal model, docking score -10.3

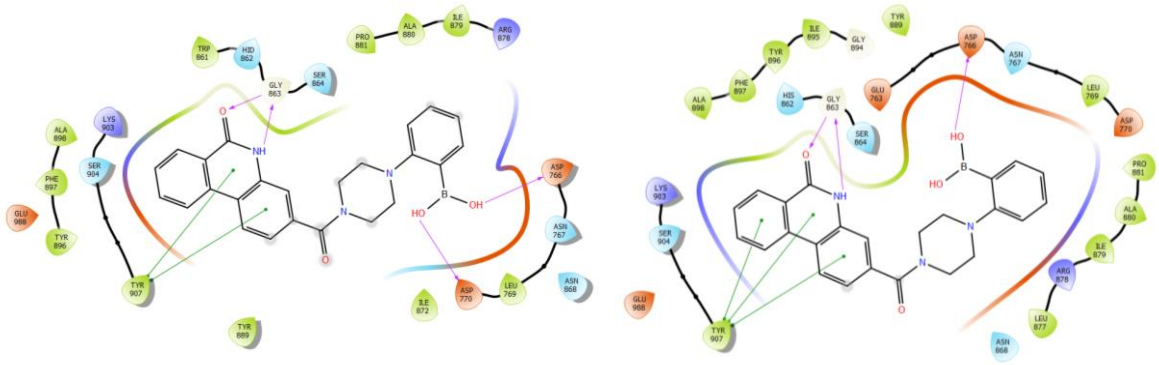

i. **b30** docked to the Open model, docking score -10.0

j. **b30** docked to the Normal model, docking score 12.7

Figure 62 *The protein-ligand interactions of compounds based on 3-(4-phenylpiperazine-1-carbonyl)phenanthridin-6(5H)-one in the Normal and the Open model respectively.* ***b26*** *can't be docked to the Normal model properly.* ***b27*** *couldn't be docked to the Open model properly.*

For comparison, 2-(4-phenylpiperazine-1-carbonyl)phenanthridin-6(5*H*)-one was also used as the scaffold to develop two compounds **a49 a50**. These compounds were most likely to occupy the area near the middle section of the D-loop and the molecular modelling suggested only **a50** might have extra interaction with residues on the D-loop (**Figure 63**). **a50** was predicted to interact with T887 through an H-bond, rather than a potential covalent bond. From the perspective of the docking pose, it was too far to build any covalent interaction (**Figure 63-c**). Thus, we predicted that compounds based on 2-(4-phenylpiperazine-1-carbonyl)phenanthridin-6(5*H*)-one were not likely to be more potent than the scaffold itself. To solve the steric clashing problem and to achieve the second choice of designing compounds following UKTT15, **a54** and **a55** were designed. Taking **a55** as an example (**Figure 64**), it was expected to form an analogous complex with PARP1 protein to UKTT15. In addition to interacting with D766 and E763, the piperazine would help the phenyl ring avoid clashing with the D-loop. An additional aromatic ring attached to the phenanthridinone core structure helped the nitro group on the second phenyl ring reach the neighbourhood of T887 to potentially form a covalent bond. We were also hoping the component could stack into the space between T887 of the D-loop and Q759 of the HD before the binding pocket closed, in which way the phenyl group might act as a physical hindrance to induce the "Pro-DNA-Retention" configuration by force.

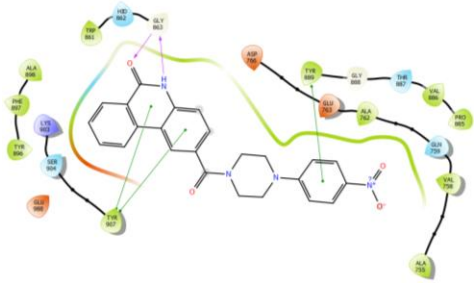

a. **a49** docked to the Open model; Docking Score 0.061

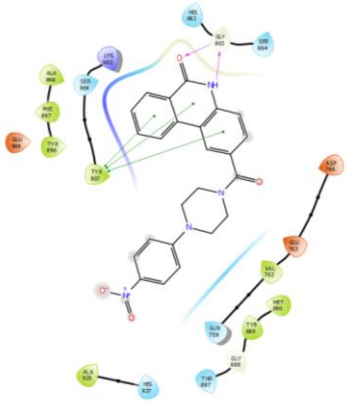

b. **a49** docked to the Normal model; Docking score: -10.167

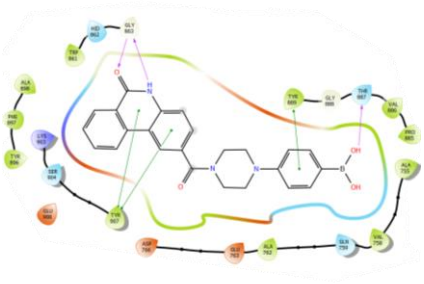

c. **a50** docked to the Open model; Docking score -7.917

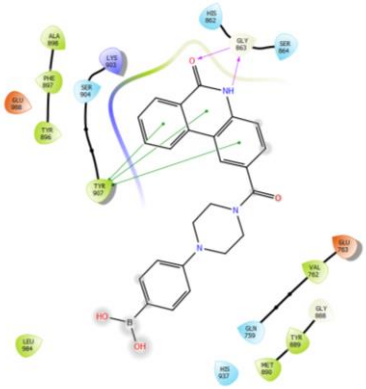

d. **a50** docked to the Normal model; Docking score: -9.567

Figure 63 *The protein-ligand interactions of compounds based on 2-(4-phenylpiperazine-1-carbonyl)phenanthridin-6(5H)-one in the Normal and the Open model respectively.*

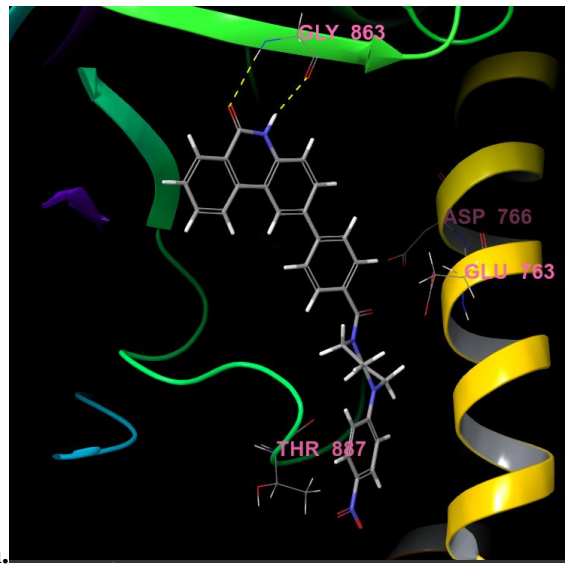

a.

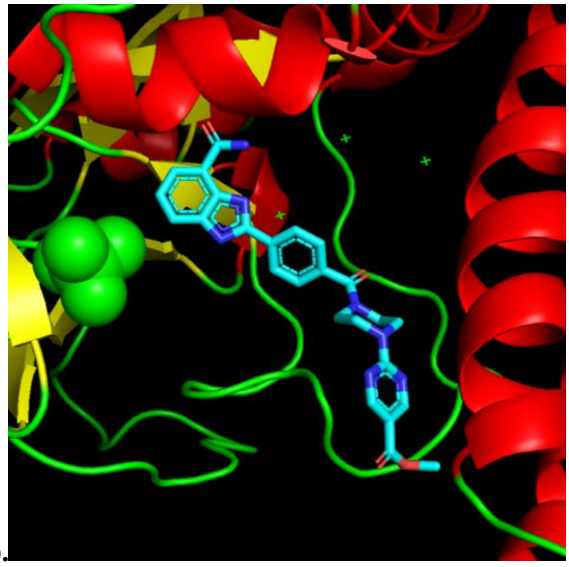

b.

Figure 64 ***a56*** *docked to the PARP1 Open model (**a**) compared to UKTT15-PARP1 complex crystal structure (**b**).* ***a56*** *was expected to be docked into the analogous position as UKTT15, in which position it would induce Pro-DNA-Retention conformation; The piperazine-aldehyde component was expected to interact with E763 and D766 and help the phenyl group stay away from the D-loop; The nitro warhead could be positioned near T887 for a potential covalent bond*.

The molecules were synthesized using the described route and evaluated using the in-house enzymatic assay as well as commercial enzymatic assay kits (**Figure 60 Table 14**). We only failed to get pure **b30** and **c33**. **b30** produced a hydroxyl-byproduct during work-up, and it was difficult to isolate from silica gel in the chromatography column. We were unable to separate **c33** from unknown by-products. Despite the purity issue, the result was in agreement with the prediction (**b28** > **b26** ≈ **b29** > **b25** > **b27**). With most compounds based on 3-(4-phenylpiperazine-1-carbonyl)phenanthridin-6(5*H*)-one showed superior potency against PARP1, **b28** was the most potent PARP1 inhibitor. **b28** was more potent than **b29** indicating that the fluorine did make an impact on the ligand-protein interaction, which could be a result of phenyl ring rotation as predicted. **b26** was slightly better than **b25**, implying H-bonds were more preferred than ionic bonds. The difference among **b25 b27 b29** mostly came from the substitution position and consequently their accessible amino acid residues. *Ortho* and *para* positions were more favoured. **c37** turned out to be the best inhibitor we have ever tested. It should share a similar binding pattern to its phenanthridinone analogs. Even though **b30** suffered from the purity issue, it still provided a comparably good potency. Better inhibition was expected when pure **b30** was used. Similarly, we could not determine whether **c33** was a bad inhibitor or not.

Compounds	In-house PARP1 (nM)	BPS PARP1 (nM) [b]	BPS PARP2 (nM) [b]	BPS TNKS1 (nM) [b]
Olaparib[a]	7.20	0.900	0.500	N/A
PJ34[d]	148±28	25.2	33.0[d]	2910
b4	72.9±35	N/T	N/T	198
b25	17.8±9.4	2.00	4.60	171
b26	15.8±1.9	3.20	6.90	104

Table 15 b4 b25 b26 *inhibition potency against PARP2 and TNKS1. (a) Experimental data were obtained from the enzymatic assay described in* ***Chapter 4, Section 4.3****. Each experiment was plated in triplicate. Data obtained from two or more experiments were shown as Mean±SD. Experimental data were processed with GraphPad 8.0.1. IC_{50} values were calculated using 4-parameter logistic regression. (b) Experimental data were obtained from the BPS PARP1 or PARP2 or TNKS1 enzymatic assay. Each experiment was plated in triplicate. Data were from single measurements. Experimental data were processed with GraphPad 8.0.1. IC_{50} values were calculated using 4-parameter logistic regression. (c) The IC_{50} value of olaparib was from the reference of the BPS assay kit; (d) The IC_{50} value of PJ34 in PARP2 was literature value using a similar assay from the same vendor. N/A: Not available.*

a49 and **a50** had worse potency than their scaffold **a4** as expected. Although **a49** could still be considered as a decent inhibitor, the bulkiness of the warheads, especially the boronic acid component, was likely to damage the ligand binding by causing clashing. Inhibitors designed after UKTT15, **a55 a56**, were poor PARP inhibitors. The potency suggested that they might fail to avoid spatial clashing or building covalent bonds.

Using BPS assay kits, we evaluated some inhibitors' potency inhibiting PARP1, PARP2, and TNKS1 for comparison. Comparing **b25 b26** with olaparib, we found that **b25 b26** was more PARP1-preferred, indicating that the ligand-protein interaction they had might be related to the structural difference between PARP1 and PARP2, that was between D766 (PARP1) and E335 (PARP2). The change from D766 to E335 could influence the binding negatively on **b25 b26** while having no or positive impact on olaparib. Comparing **b25 b26** with **b4**, they barely had any difference in inhibiting TNKS1, indicating the use of warheads did not form any beneficial interaction with critical residues in TNKS1.

5.6.3. Conclusion

In this study, we introduced some potent novel PARP1 inhibitors based on 3-(4-phenylpiperazine-1-carbonyl)phenanthridin-6(5*H*)-one (**b4**) and a best-in-series PARP1 inhibitor **c37** based on 8-(4-phenylpiperazine-1-carbonyl)thieno[2,3-*c*]quinolin-4(5*H*)-one (**c7**). These compounds were novelly designed and not analogous to any known potent PARP inhibitors.

They used the scaffold with phenanthridinones as the core structure binding to the NI and the phenylpiperazine as the side chain extending to the AD. They were equipped with functional groups -NO_2 or -$B(OH)_2$, usually known as warheads, that were good for H-bonding, ionic-bonding or covalent bonding. Evaluated with the in-house enzymatic assay, commercial enzymatic assay, these compounds outperformed the first benchmark PJ34 by nearly 10 folds and reached a similar level to the gold benchmark olaparib. These inhibitors were also able to inhibit PARP2 and TNKS1, making them potent broad-spectrum non-selective PARP inhibitors. They would be sent for further evaluation.

As our prediction on potency was in agreement with the following experimental results, we argued that *in silico* molecular docking results largely reflected the real situation that happened inside the protein. The mechanism of action was occupying the AD and strongly interacting with neighbouring critical amino acid residues such as R878, D770, D766 using not only H-bonding but also ionic bonding. These interactions built up the potency by more than 5 folds compared to the original scaffold. The presence of fluorine could slightly increase the potency, plausibly by rotating the phenyl group and consequently creating additional protein-ligand interaction between -NO_2 and D770. Different halogen groups might have similar effects, which could be predicted in the future by free energy perturbation *in silico* or verified with wet-lab experiments. Changing the halogen component could be used for optimization. From the current data, it was likely that H-bonding was preferred for compounds interacting with residues rather than ionic bonds, but it was yet to be proven. After all, the -NO_2 group could also form H-bonding in addition to ionic bonding, and there was a difference in size between the -NO_2 group and -$B(OH)_2$ group which would also change the affinity. *Para* and *ortho* substitution were preferred in these compounds, as they might have better access to R878 and D770, or D766 compared to *meta* ones, which could be estimated from **Figure 61**. We did not believe that the warheads were able to form any temporary covalent bonding with the residues illustrated. Compounds developed from **a4** as well as ones designed after UKTT15 aiming Thr on the D-loop had poor potency. **a50** was able to reach T887 according to the molecular modelling while it still delivered disappointing potency. The problem on **a55** and **a56** might still be the size of the inhibitor and spatial clashing with the D-loop. With an additional phenyl ring, **a55** and **a56** could be oversized to fit into the binding pocket.

We found that **b25** and **b26** showed different preferences towards PARP1 and PARP2 compared to olaparib. The diversity in preference could come from the structural difference between PARP1 and PARP2, which was D766 and E355. For olaparib, no component could interact with D766 in PARP1 or E763 in PARP2 [1] [10] [22]. The change between the two residues would not affect the ligand-protein interaction in olaparib. For **b25 b26**, some molecular docking results suggested their warheads in the *para* position could interact with D766 during the closure of the HD. The change from D766 to E355 would influence the binding negatively. This finding was also in agreement with our previous inhibitor design which used a chiral center to achieve the selectivity/preference between PARP1/PARP2 because of the residue difference.

While the rest of **c** compounds based on theinoquinolinone failed to produce great potency, ones with warheads (including **c33** which was not pure) were able to inhibit PARP1 very well. The first possibility was that warheads contributed to the ligand-binding incredibly. However, it might be overturned as **b** compounds with warheads only outperformed the scaffold **b4** by less than 10 folds while **c37** increased the number to 40 folds. It was also less possible that the warhead in **c37** had better interaction with the protein residue than the one in **b25** as the structure extending from the core carboxamide was identical between the two compounds. The last possibility, which was related to our previous study on small molecules and their potency prediction, was that the side chain influenced the docking orientation of the thienoquinolinone core structure inside the NI and somehow it ended up in a more advantageous orientation than a plain thienoquinolinone or one with other side chains would achieve. In this way, improved ligand binding was expected inside the NI. The more advantageous orientation provided additional affinity benefiting catalytic inhibition.

In summary, we proposed that we could design novel PARP inhibitors interacting with the AD with successful prediction. By interacting with the AD, we not only made inhibitors out of 6-(5*H*)-phenanthridinone, a potent platform that was barely studied but also a poor platform such as thienoquinolinone and turned it into the most potent inhibitor in our study. These inhibitors would be sent for further evaluation.

5.7. A Pilot Study of The Cytotoxicity of A Novel PARPi

5.7.1. Introduction

While perusing more potent PARP inhibitors with superb catalytic inhibition capability, we carried out a pilot study on the cytotoxicity of our novel PARP inhibitors, as well as how these PARP inhibitors would potentiate traditional anticancer drugs, such as alkylating agents and topoisomerase inhibitors. Drug combination exhibiting superior therapeutic effect to a single drug refers to synergism [23]. The term “synergism” is used to describe a mutual relationship between two or more drugs while the term “enhancement” is one-sided [24]. Furthermore, “enhancement” is affected by many other factors like drug concentration while synergism can be described by an objective index. In our case, synergism between PARP inhibitors and anticancer drugs describe how the former could potentiate the latter. The clinical significance here is to maximize the therapeutic effects of chemotherapy agents while minimizing the side effects [24]. In this study, we were using the Chou-Talalay method to study the synergism between a potent PARP inhibitor and a conventional anti-cancer drug [24]. The combination index (CI) was used to measure the synergism and the index at the highest fraction affected (Fa) ratio is the most meaningful for combination therapy. Having said that, we would also consider the overall CI values to judge the synergism.

The synergism between a PARP inhibitor and a chemotherapy drug comes from the ability of the PARP inhibitor to obstruct DNA repair and the ability of the chemotherapy drug to cause DNA damage [25]. The PARP inhibitor could potentiate the chemotherapy drug by preventing initiation of DNA repair by preventing PARylation and exacerbating DNA damage, formation of PARP-trapping complex that collapses the replication fork [25]. Previous studies suggested that PARP-trapping was a major inducer of the cytotoxicity when the inhibitor was used along with Temozolomide (TMZ) while topoisomerase I inhibitors such as camptothecin would be benefited from the catalytic inhibition [23]. To explore the capability of our novel PARP inhibitors, we designed the experiment to study the cytotoxicity as well as the synergetic effect when combining with Topotecan (TPT) and TMZ. We assumed that when PARP inhibitors were used collectively with TMZ, they will produce better cytotoxicity than ones used together with TPT. We also hypothesized that our novel PARP inhibitors would produce similar synergy to the benchmark drug olaparib when treated with anticancer drugs.

5.7.2. Results

By treating the human glioblastoma cell line (U251) with some of our potent PARP inhibitors individually we found that, not surprisingly, most PARP inhibitor candidates, including olaparib, didn't deliver strong cytotoxicity (**Figure 65**). **b25** had a clearer IC_{50} curve compared to other PARP inhibitors. Thus, we chose **b25** as our first inhibitor candidate to test the synergy with anticancer drugs including TMZ and TPT. For comparison, olaparib was used as a benchmark. The cytotoxicity of anticancer drugs and PARP inhibitors on U251 was shown in **Table 16**. TPT was the most potent drug in terms of cytotoxicity against the U251 cell line among four compounds while olaparib and **b25** were equally potent. For the following study in which the concentration ratio of an anticancer drug and a PARP inhibitor was constant, the ratio was determined considering both IC_{50} values and the previous study [25].

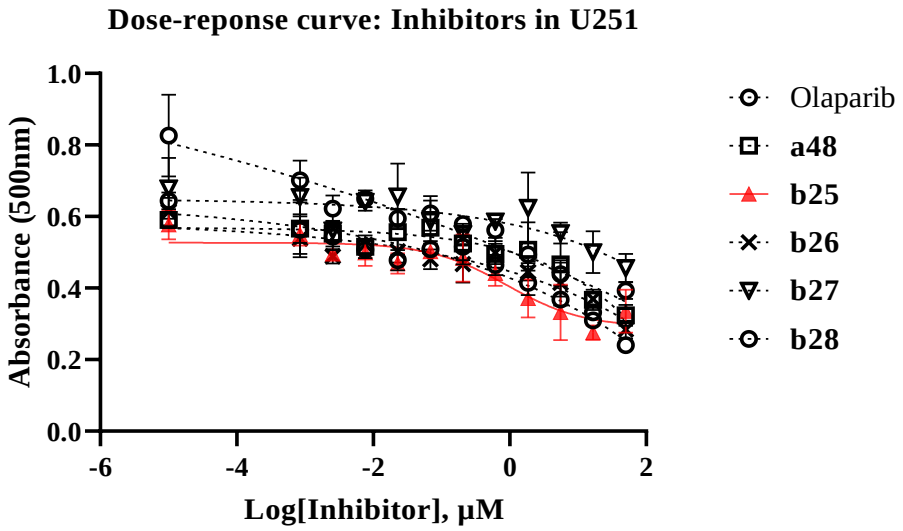

Figure 65 *Different PARP inhibitors' potency in the U251 cell line. Experimental data were obtained from the MTS assay described in* ***Chapter 4, Section 4.4****. Each experiment was plated in triplicate. Data obtained from two experiments were processed with GraphPad 8.0.1.* IC_{50} *curves were calculated using 4-parameter logistic regression.* ***b25*** *(red triangle) had a relatively clearer* IC_{50} *curve, compared to the rest compounds when concentration was below 100µM.*

Drug	TMZ	TPT	Olaparib	**b25**
IC_{50}(μM) [a]	595±110 [c]	0.080±0.03	41.1±0.22 [b]	82.0±0.09 [b]
Drug	TMZ	**b28**	**c37**	
IC_{50}(μM) [a]	566±170 [c]	180±110 [b]	248±140 [b]	

Table 16 *Drug potency treating U251 cells individually. Experimental data were obtained from the MTS assay described in* ***Chapter 4, Section 4.4****. Each experiment was plated in triplicate. Data obtained from three experiments were processed with GraphPad 8.0.1. IC_{50} curves were calculated using 4-parameter logistic regression. (a) Experiments were done in different generations of U251 cells. (b) At the highest concentration, the viability of cells was >50%; 2000μM TMZ was tested on each plate for ~100% growth inhibition. (c) Mean ± SD value from all plates in one experiment.*

We exposed the U251 cells to TMZ with or without PARP inhibitors. Anticancer drugs and PARP inhibitors were used in a constant ratio ([TMZ]:[PARPi] = 500:1) and non-constant ratios (fixed PARPi concentrations) respectively. We found that both PARP inhibitors were able to increase the cytotoxicity of TMZ which was consistent with previous studies [25] and TMZ was slightly more cytotoxic when combined with olaparib (**Figure 66 Figure 67**). Olaparib was able to potentiate TMZ by ~20 folds while **b25** was able to achieve ~15 folds when using the IC_{50}.value as a standard. The cytotoxicity was in a concentration-dependent manner (**Figure 66 Figure 67**). When TMZ was combined with 0.1μM, 1μM, and 10μM PARP inhibitors respectively, 10μM groups produced the most cytotoxicity (**Figure 67**).

Due to the solubility issue, U251 couldn't be treated with a high dose of the PARP inhibitor and it was difficult to reach a high percentage of viability reduction. The dose-effect curve for PARP inhibitors with inadequate plots without constraints could generate problematic data. Due to this concern instead of using COMPUSYN software to calculate the combination index to determine the synergism [24], we used GraphPad Prism to determine the dose-response curve first and then took the normalized data to calculate the combination index, based on the equation (16) in the reference [24c], to study the synergism between two drugs. By calculating

the CI value, we found that both PARP inhibitors synergistically sensitized U251 cells in a concentration-dependent manner as well; however, a high concentration of drug (which led to low viability) would have a high CI (low synergistic effect). Both PARP inhibitors would only have strong synergy with TMZ at a low concentration. **b25** showed lower overall synergy with TMZ compared to olaparib (**Figure 71, Table 17**).

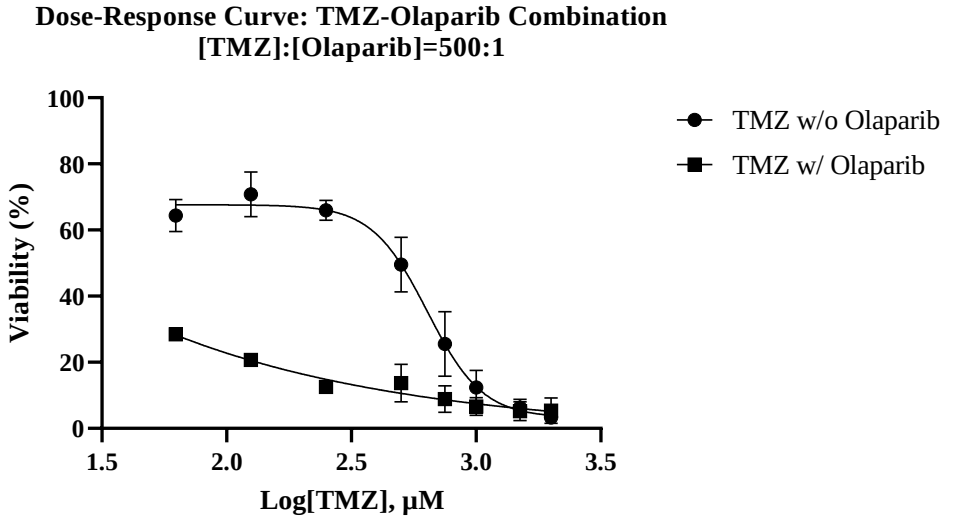

a.

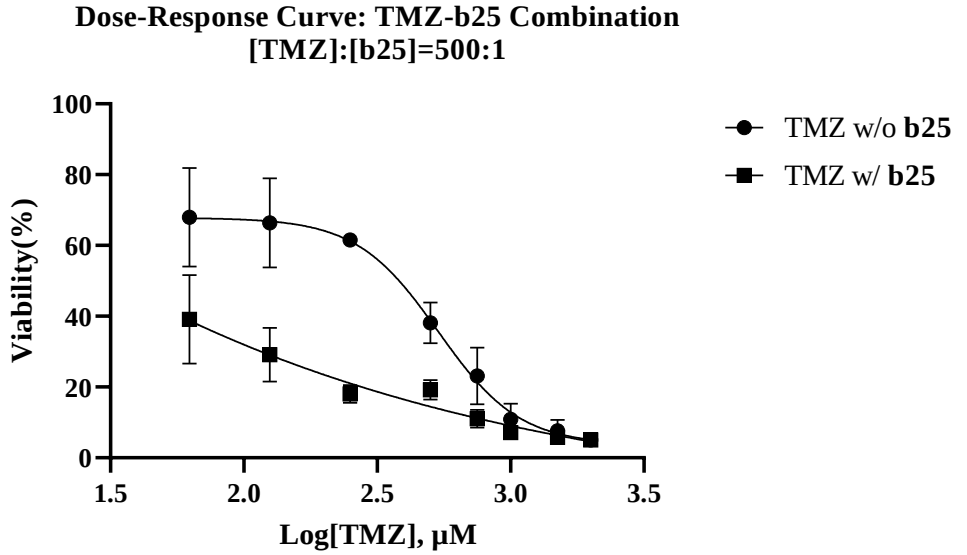

b.

Figure 66 *Dose-response curves of TMZ treating U251 cells in combination with olaparib (panel **a**) or **b25** (panel **b**) respectively with a constant ratio [TMZ]:[PARPi]=500:1 which was*

determined by the IC_{50} of drugs. Experimental data were obtained from the MTS assay described in ***Chapter 4, Section 4.4****. Each experiment was plated in triplicate. Data obtained from three experiments were processed with GraphPad 8.0.1. IC_{50} curves were calculated using 4-parameter logistic regression. PARP inhibitors were able to increase the cytotoxicity of TMZ comparably. The potting was a combined result based on three independent assay results done in triplicate.*

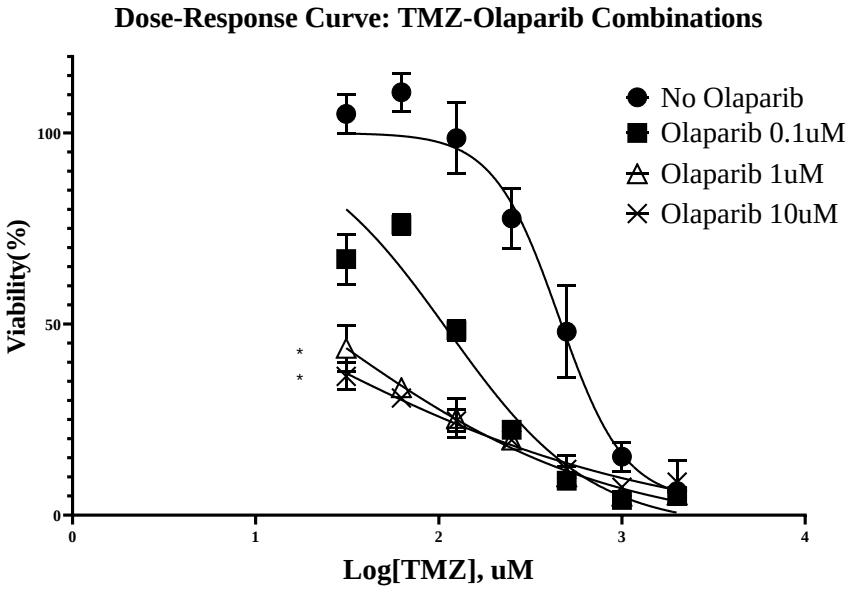

a.

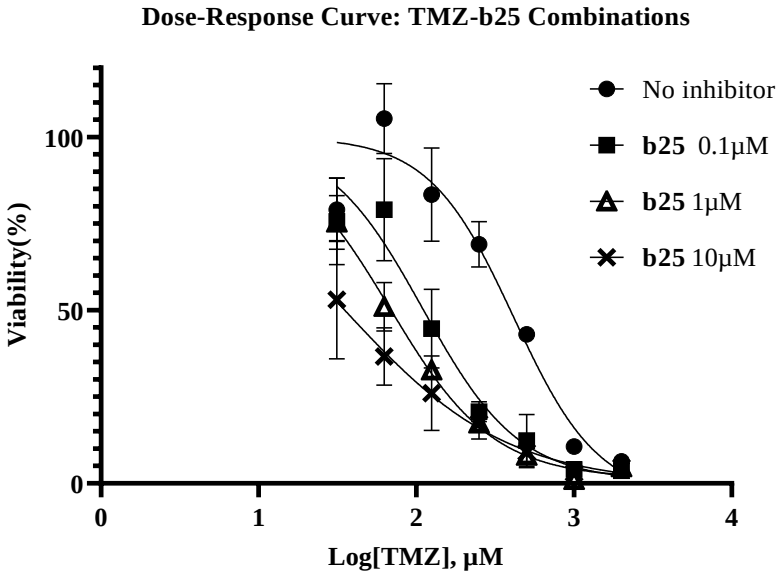

b.

Figure 67 *Dose-response curves of TMZ treating U251 cells in combination with 0.1μM, 1μM, 10μM of olaparib (panel* ***a****) and* ***b25*** *(panel* ***b****) respectively. Experimental data were obtained*

*from the MTS assay described in **Chapter 4, Section 4.4**. Each experiment was plated in triplicate. Data obtained from three experiments were processed with GraphPad 8.0.1. IC_{50} curves were calculated using 4-parameter logistic regression. Both PARP inhibitors contributed to the cytotoxicity of TMZ. Olaparib was able to increase the cytotoxicity significantly (*P<0.05) at 1 μM, 10μM while **b25** was not able to increase the cytotoxicity significantly. The potting was a combined result based on two independent assay results done in triplicate. Ordinary one-way ANOVA was used for statistical analysis.*

We subsequently employed TPT to treat the U251 cells with PARP inhibitors collectively. While both treatments showed enhanced cytotoxicity and the enhancement tended to be in a concentration-dependent manner as well, PARP inhibitors were not able to make a significant difference (**Figure 68 Figure 69**). Olaparib and **b25** were only able to potentiate TMZ by ~3 folds comparing IC_{50} values. Moreover, we found weaker synergy globally between TPT and PARP inhibitors when drugs were combined in a constant ratio. Still, olaparib showed a better synergistic effect with TPT compared to **b25**. Unlike the TMZ-PARP combination, the TPT-PARPi combination tended to have better synergy (lower CI value) at a higher dose (higher Fa) (**Figure 71**, **Table 17**). Due to the cytotoxicity being influenced by the drug concentration and combination, we could not directly compare which of the two, the TMZ-PARPi combination or the TPT-PARPi combination, was more cytotoxic. We only compared the synergism. Since the former combination had worse synergy than the latter one, which was also supported by the previous study [25], we chose to focus on the efficiency of the TMZ-PARPi combination.

Following experiments employed our top 2 inhibitors from the enzymatic assay, **b28** and **c37**. With a different generation of U251 cells, these two PARP inhibitors were less cytotoxic compared to olaparib and **b25**. Using TMZ as a standard, olaparib and **b25** were ~150 folds more potent than TMZ while **b28** and **c37** were about 2-3 folds more potent than TMZ (**Table 16**). These two less potent PARP inhibitors in the cell assay were not able to enhance the cytotoxicity as greatly as **b25** and olaparib when used in combination with TMZ. For U251 cells, the TMZ IC_{50} decreased from 566μM to 240μM and 172μM respectively when cooperating with **b28** and **c37**. Interestingly, two PARP inhibitors showed distinctive synergistic effects when combined with TMZ (**Figure 70**). Overall, **c37**, the champion inhibitor from the enzymatic assay, showed

strong to very strong synergy while **b28** only presented moderate synergy. When there was a 50% reduction of cell viability, olaparib (Fa = 50%, CI = 0.05) and **b25** (Fa = 50%, CI = 0.07) showed the best synergy in combination with TMZ. With the increase of the dose, **c37** started to become more synergistic with TMZ while the rest compounds showed less synergy. When comparing the synergy at the highest Fa, the order of synergism was **c37**-TMZ (Fa = 97%, CI = 0.08) > olaparib (Fa = 97%, CI = 0.20) > **b25**-TMZ (Fa = 97%, CI = 0.43) > **b28**-TMZ (Fa = 97%, CI = 0.85). **c37** had the highest average CI = 0.16 when there was 50% to 97% of affected cells, (**Figure 71**). From the perspective of synergism, **b28** was significantly weaker in synergy (P<0.0001) when combined with TMZ.

Fa (%)	[TMZ]:[Olaparib] = 500:1			[TMZ]:[**b25**] = 500:1		
	[TMZ] (μM)	CI	Synergy	[TMZ] (μM)	CI	Synergy
50	28.1	0.05	VSS	42.2	0.07	VSS
75	61.7	0.08	VSS	104	0.13	SS
90	135	0.12	SS	256	0.22	S
95	230	0.16	SS	472	0.33	S
97	337	0.20	SS	730	0.43	S
Fa (%)	[TPT]:[Olaparib] = 1:13.125			[TPT]:[**b25**] = 1:13.125		
	[TPT] (μM)	CI	Synergy	[TPT] (μM)	CI	Synergy
50	0.026	0.24	SS	0.023	0.34	S
75	0.063	0.21	SS	0.050	0.33	S
90	0.154	0.19	SS	0.113	0.30	S
95	0.283	0.18	SS	0.194	0.32	S
97	0.435	0.17	SS	0.287	0.32	S
Fa (%)	[TMZ]:[**b28**] = 500:1			[TMZ]:[**c37**] = 500:1		
	[TMZ] (μM)	CI	Synergy	[TMZ] (μM)	CI	Synergy
50	240	0.39	S	172	0.29	SS
75	612	0.50	S	314	0.20	SS
90	1560	0.64	S	572	0.13	SS
95	2950	0.75	WS	861	0.10	SS

97	4650	0.85	WS	1150	0.08	VSS

Table 17 *Calculated doses and combination indices (CI) and corresponding fraction affected (Fa) of treatments based on IC50 curves. The data were from* ***Figure 66*** **Figure 68.** *CI<0.1 (very strong synergistic, VSS), 0.1≤CI<0.3 (strong synergistic, SS), 0.3≤CI<0.7 (synergistic, S), 0.7≤CI<1 (weak synergistic, WS), CI=1 (additive), and CI>1 (antagonistic, A). Fa=100 means a 100% reduction of viability.*

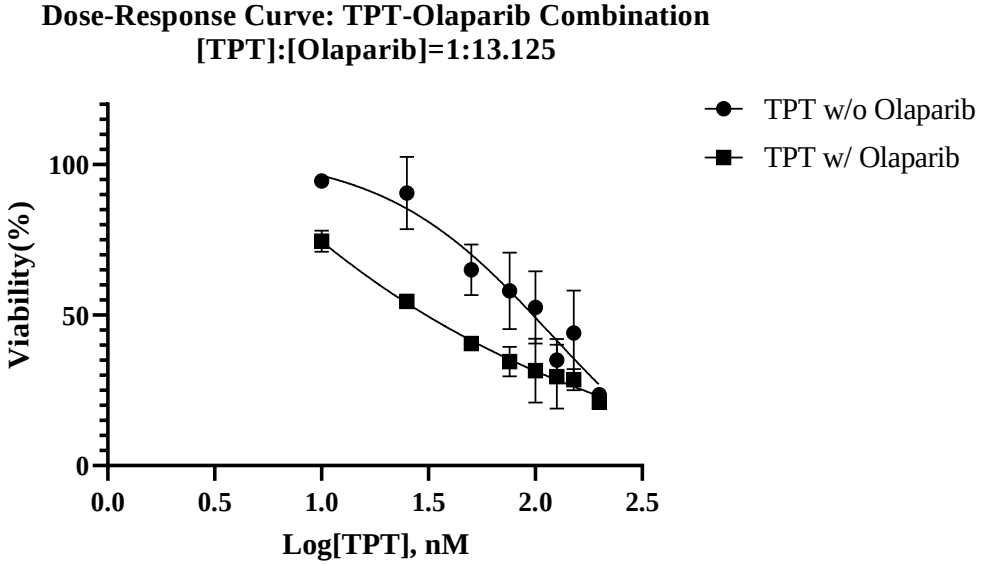

a.

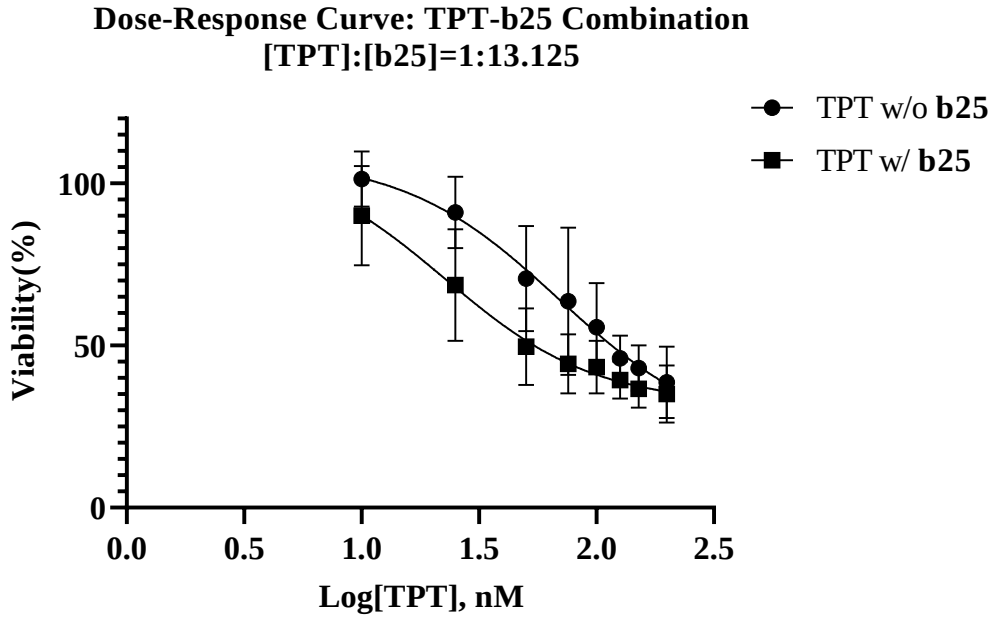

b.

Figure 68 *Dose-response curves of TPT treating U251 cells in combination with olaparib (panel **a**) or **b25** (panel **b**) respectively with a constant ratio [TMZ]:[PARPi]=1:13.125, which was determined by the IC_{50} of drugs. Experimental data were obtained from the MTS assay described in **Chapter 4, Section 4.4**. Each experiment was plated in triplicate. Data obtained from three experiments were processed with GraphPad 8.0.1. IC_{50} curves were calculated using 4-parameter logistic regression. PARP inhibitors were able to increase the cytotoxicity of TPT comparably. The potting was a combined result based on two independent assay results done in triplicate.*

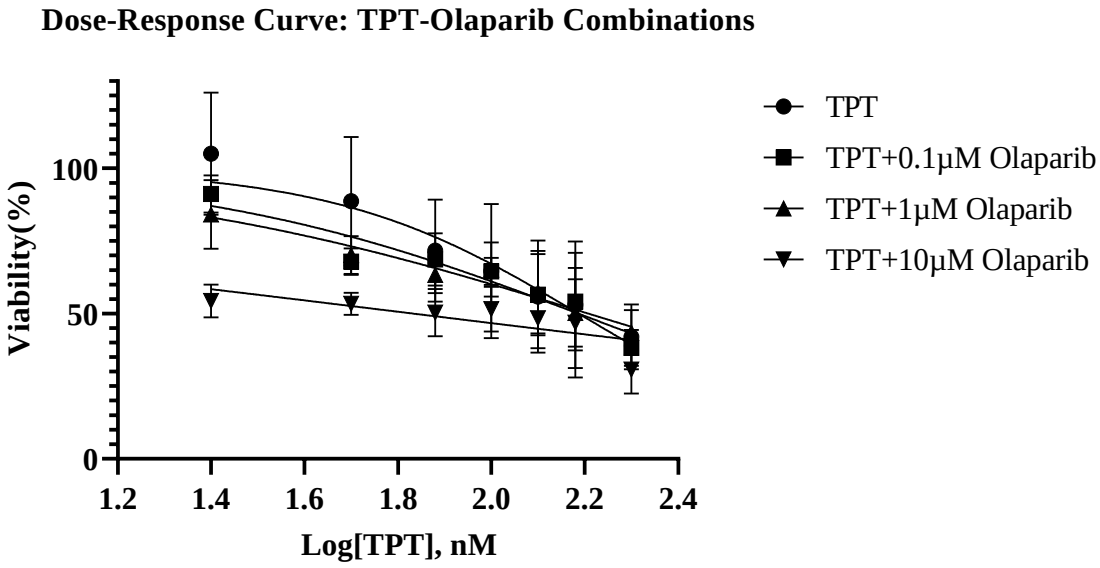

a.

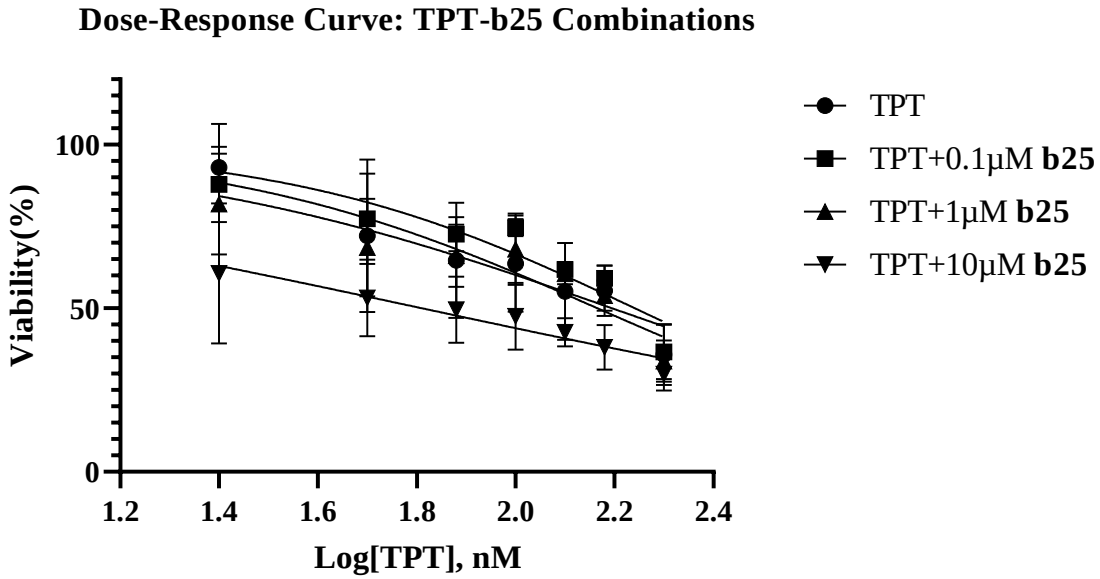

b.

Figure 69 *Dose-response curves of TPT treating U251 cells in combination with 0.1µM, 1µM, 10µM of olaparib (panel **a**) and **b25** (panel **b**) respectively. Experimental data were obtained from the MTS assay described in **Chapter 4, Section 4.4**. Each experiment was plated in triplicate. Data obtained from three experiments were processed with GraphPad 8.0.1. IC_{50} curves were calculated using 4-parameter logistic regression. PARP inhibitors were able to increase the cytotoxicity of TPT comparably, but not significantly. The potting was a combined result based on two independent assay results done in triplicate.*

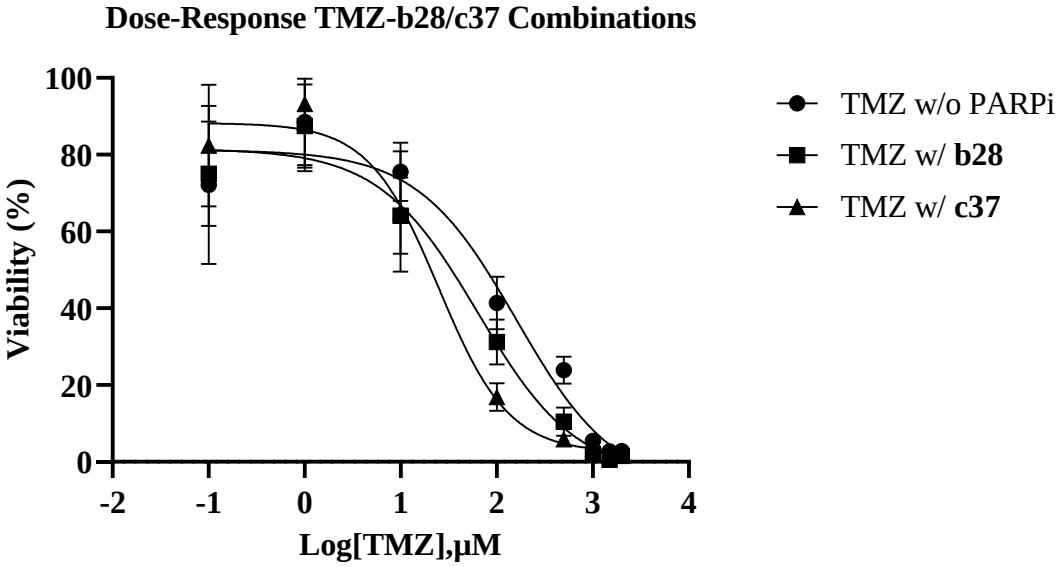

Figure 70 *Dose-response curves of TMZ treating U251 cells in combination with* ***b28*** *or* ***c37*** *respectively. For the consistency of the research, the ratio between two drugs was also set as [TMZ]:[PARPi]=500:1. Experimental data were obtained from the MTS assay described in* ***Chapter 4, Section 4.4****. Each experiment was plated in triplicate. Data obtained from three experiments were processed with GraphPad 8.0.1. IC_{50} curves were calculated using 4-parameter logistic regression. PARP inhibitors were able to increase the cytotoxicity of TMZ comparably, but not great. The potting was a combined result based on three independent assay results done in triplicate.*

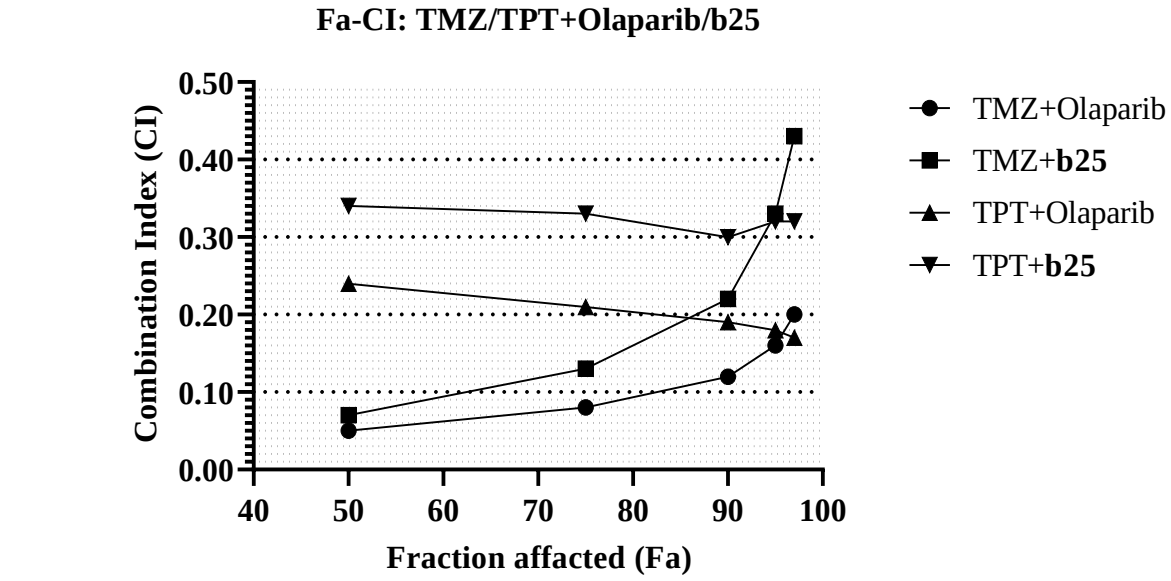

a.

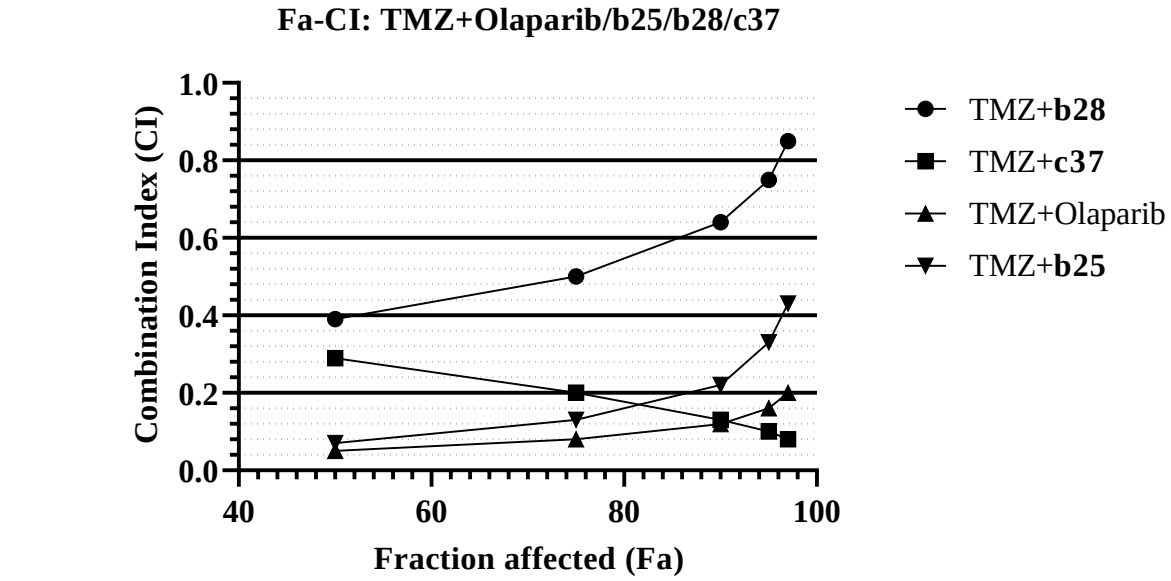

b.

Figure 71 *Fa-CI plots obtained from* ***Table 17*** *for TMZ or TPT in combination with olaparib and* ***b25 b28 c37*** *within a constant ratio. CI<0.1 (very strong synergistic, VSS), 0.1≤CI<0.3 (strong synergistic, SS), 0.3≤CI<0.7 (synergistic, S), 0.7≤CI<1 (weak synergistic, WS), CI=1 (additive), and CI>1 (antagonistic, A). Fa=100 means a 100% reduction of viability.*

5.7.3. Conclusion and Discussion

In summary, we explored the cytotoxicity and synergy when PARP inhibitors were used collectively with TMZ and TPT respectively. When they were used under the ratio [TMZ]:[PARPi] = 500:1 and [TPT]:[PARPi] = 1:13.125, all these combinations showed increase on cytotoxicity compared to using TMZ or TPT individually. The ratio was determined by IC_{50} values of anticancer drugs and PARP inhibitors, especially olaparib. We also referenced the recommendation from Murai's study where 1μM of PARP inhibitors were used for comparison [25]. Among them, we would see an obvious increase when TMZ was used with olaparib and **b25**, followed by the TPT-olaparib/**b25** pairs, and the TMZ-**c37/b28** pairs. The cytotoxicity of these combinations was in a concentration-dependent manner. However, as the cytotoxicity of these combinations could be affected by multiple factors, such as drug concentration, concentration ratio and viability of cells, *etc*., we introduced synergism to describe the ability of a PARP inhibitor to potentiate an anticancer drug. We found the synergism between PARP inhibitors and anticancer drugs was not directly related to the cytotoxicity of each component; meanwhile, the synergism was not fully related to the enhancement of the cytotoxicity due to the combination. The **c37**-TMZ combination had the best synergistic effect, either comparing the CI at the highest Fa, or comparing the global CI. However, it did not have great enhancement if only judged by the dose-response curve. The reason was, olaparib and **b25** were more cytotoxic individually compared to **c37**. As CI indeed was an indicator of the multiple of enhancement rather than the amount, and IC_{50} value was dropped off during the calculation and it won't influence the final calculation result, it was reasonable **c37** had better overall CI, especially at a higher dose.

We argued that the PARPi-TMZ combination had better synergy than the PARPi-TPT combination. The difference in synergy between the PARPi-TMZ and the PARPi-TPT combinations was in agreement with Murai's study [25]. The mechanism of different anticancer drugs would influence the cytotoxicity when combined with a PARP inhibitor. TMZ was able to expose 5'-deoxyribose phosphate (5'-dRP) groups when breaking the strand while TPT was only to produce 5'-phosphate ends. It was suggested that 5'-dRP was preferred for PARP1 to bind with, which was necessary for the formation of PARP-DNA complexes to cause PARP trapping at SSBs. In addition, the topoisomerase protein tended to bind covalently with the 3'-end. The

bulky topoisomerase-DNA complex with the less preferred 5'-end made it less possible to form the PARP-DNA complex. Thus, while the PARPi-TMZ combination would gain extra cytotoxicity from PARP trapping, the PARPi-TPT combination could only be benefited from the catalytic inhibition, making them less cytotoxic and synergistic. Conclusively, when combining with TPT, the PARP inhibitor was more likely to produce cytotoxicity through catalytic inhibition, which was why when the concentration of PARP increased, we were able to see a trend of rising synergistic effect; when combined with TMZ, the PARP inhibitor was more likely to produce cytotoxicity through PARP trapping, which might not be concentration-dependent, indicating with the accumulation of the PARP inhibitor, the cytotoxicity it contributed did not upsurge. For **c37**, we argued that it was both a good catalytic inhibitor and PARP-trapper; thus, we were able to see the lowest CI at the highest Fa, which could be a result of strong catalytic inhibition and PARP trapping.

One major issue here was the relationship between the dose and the synergism between the PARP inhibitor and the anticancer drug, especially TMZ. In our research, we found that only the **c37**-TMZ combination had the escalation in synergistic effect with the increasing dose; the rest of the tested groups were more likely to have better synergy at lower doses. The major difference in **c37** was the thiophene ring, replacing the benzene ring in the phenanthridinone. In Murai's paper [25], the strongest synergy appeared at the highest Fa. **Figure 72** showed a comparison between our result and Murai's result. We had a similar range of CI when 50%-97% of cells were affected but the curve was opposite to each other. In Cao's paper [26], the lowest CI was presented at the lowest Fa. Chou [24b] stated that "synergy at high effect levels is more relevant to therapy", implying a lower combination index was expected to be found at a higher dose range. The deviation could come from the different cell lines used in the research (Murai: chicken lymphoma DT40 and human prostate DU145; our study: human malignant glioblastoma U251). A high dose of TMZ was likely to induce resistance and as a result, less synergy was found at a high dose: Adaptive TMZ-resistance in U251 cells could be found within long-term TMZ treatment and it might be caused by an increased expression of O6-Methylguanine Methyltransferase, Signal Transducer and Activator of Transcription 3, upregulation of microRNA, and changes in mitochondria [27]. In our research, different PARP inhibitors were likely to influence the synergy differently. It could be related to their potency for catalytic inhibition, PARP-trapping, or simply enhanced PARP-DNA binding which might not be

concentration-dependent. Another issue that might bring concern was the antagonistic effect which was suggested by CI>1. We found that it was a common issue which was also found in the above-mentioned research [25] [26]. At a higher dose, the cytotoxicity of TMZ overwhelmed the synergistic effect of the PARP inhibitor and it became more of an additive effect (CI ≈ 1). When the deviation of the experiment occurred, the calculation probably brought CI > 1. However, judging by the scale of the "antagonistic" effect (1<CI<Infinity), CI > 1 won't necessarily mean an "obvious" antagonistic effect, but something close to an additive effect. It was also probably due to the Fa-CI curve being predicted by the plotting, which could be different from the real situation.

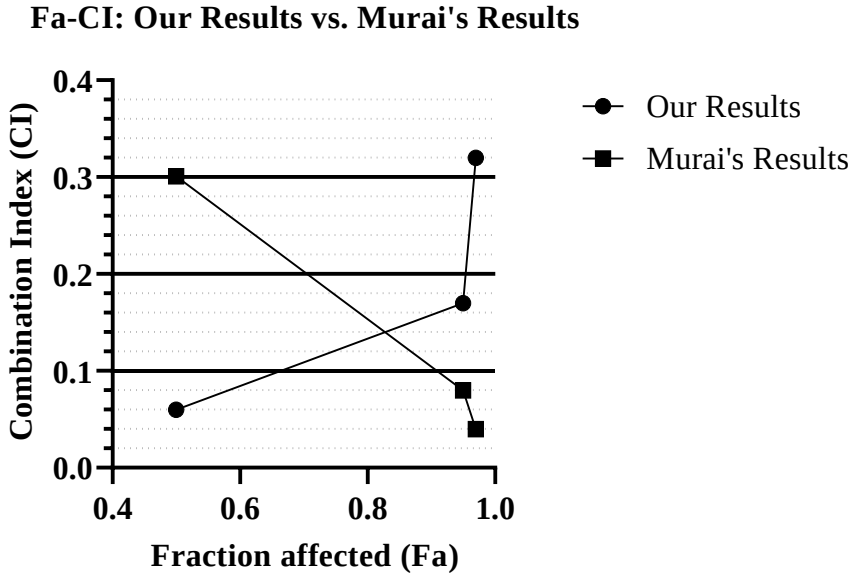

Figure 72 *A simple comparison between our results and Murai's result on the olaparib-TMZ combination. The CI at the highest Fa from Murai's result was an estimation based on their figure. Overall CI values were similar. However, it was worth noting that experiments were done in different cell lines. The comparison was only for reference*

In conclusion, we determined two of the three top inhibitors, **b25 c37**, from the enzymatic study were better or equivalent than/as the benchmark olaparib in terms of the enhancement in cytotoxicity or the synergistic effect when they were used with anticancer drugs. From the results between different anticancer drugs, our inhibitors probably had the same

mechanism as olaparib as the PARP-trapping was the major contributor to the cytotoxicity while **c37** would be benefited from both strong PARP trapping and PARP inhibition. The clinical significance came from the relationship between CI and Fa, as conventionally it was believed that CI at the highest Fa is the most meaningful for combination therapy [24] [25]. For the malignant glioblastoma tumour, when combining TPT with PARPi, it did generate better synergy at the higher dose, suggesting it was useful to use a high dosage in a single treatment. When TMZ was used with PARPi, except **c37**, we saw the better synergy at the lower dose, suggesting a low dosage in multiple treatments was the most efficient and it should be recommended clinically.

5.8. Reference

1. Berman, Helen M., et al. "The protein data bank." *Nucleic Acids Research*, vol. 28, no. 1, Jan. 2000, pp. 235–42, https://doi.org/10.1093/nar/28.1.235.
2. PDB ID: 5WS1. DOI Citation: Cao, R., et al. *Structure of Human PARP1 Catalytic Domain Bound to a Quinazoline-2,4(1H,3H)-Dione Inhibitor*. Dec. 2016, https://doi.org/10.2210/pdb5WS1/pdb
3. Zandarashvili, Levani, et al. "Structural basis for allosteric PARP-1 retention on DNA breaks." *Science*, vol. 368, no. 6367, Apr. 2020, pp. 1–10, https://doi.org/10.1126/science.aax6367.
4. The Ramachandran Plot was calculated by Zlab Ramachandran Plot server: https://zlab.umassmed.edu/bu/rama/. Anderson, Robert J., et al. “Main-Chain Conformational Tendencies of Amino Acids.” *Proteins: Structure, Function, and Bioinformatics*, vol. 60, no. 4, July 2005, pp. 679–89, https://doi.org/10.1002/prot.20530.
5. Ravikumar, Ashraya, et al. “Conformational Strain Indicated by Ramachandran Angles for the Protein Backbone Is Only Weakly Related to the Flexibility.” *The Journal of Physical Chemistry B*, vol. 125, no. 10, Mar. 2021, pp. 2597–606, https://doi.org/10.1021/acs.jpcb.1c00168.
6. Gunasekaran, K., et al. “Disallowed Ramachandran Conformations of Amino Acid Residues in Protein Structures.” *Journal of Molecular Biology*, vol. 264, no. 1, Nov. 1996, pp. 191–98, https://doi.org/10.1006/jmbi.1996.0633.

7. Ramírez, David, and Julio Caballero. "Is it reliable to take the molecular docking top scoring position as the best solution without considering available structural data?." *Molecules*, vol. 23, no. 5, Apr. 2018, pp. 1038–55, https://doi.org/10.3390/molecules23051038.
8. Lou, Xi-yu, et al. "Synthesis of olaparib derivatives and their antitumor activities." *Chemical Research in Chinese Universities*, vol. 29, no. 2, Mar. 2013, pp. 231–35, https://doi.org/10.1007/s40242-013-2448-5.
9. Sehnal, David, et al. "Mol* Viewer: modern web app for 3D visualization and analysis of large biomolecular structures." *Nucleic Acids Research*, vol. 49, no. W1, May 2021, pp. W431–37, https://doi.org/10.1093/nar/gkab314.
10. Thorsell, Ann-Gerd, et al. "Structural basis for potency and promiscuity in poly (ADP-ribose) polymerase (PARP) and tankyrase inhibitors." *Journal of Medicinal Chemistry*, vol. 60, no. 4, Dec. 2016, pp. 1262–71, https://doi.org/10.1021/acs.jmedchem.6b00990.
11. Ferraris, Dana, et al. "Design and synthesis of poly ADP-ribose polymerase-1 inhibitors. 2. Biological evaluation of aza-5 [*H*]-phenanthridin-6-ones as potent, aqueous-soluble compounds for the treatment of ischemic injuries." *Journal of Medicinal Chemistry*, vol. 46, no. 14, June 2003, pp. 3138–51, https://doi.org/10.1021/jm030109s.
12. Ferraris, Dana, et al. "Design and synthesis of poly (ADP-ribose) polymerase-1 (PARP-1) inhibitors. Part 3: In vitro evaluation of 1, 3, 4, 5-tetrahydro-benzo [c][1,6]-and [c][1,7]-naphthyridin-6-ones." *Bioorganic & Medicinal Chemistry Letters*, vol. 13, no. 15, Aug. 2003, pp. 2513–18, https://doi.org/10.1016/s0960-894x(03)00465-7.
13. Shahi, Abhishek, and Elangannan Arunan. "Why are hydrogen bonds directional?." *Journal of Chemical Sciences*, vol. 128, no. 10, Sept. 2016, pp. 1571–77, https://doi.org/10.1007/s12039-016-1156-3.
14. (a) PDB ID: 4UXB (b) PDB ID: 3GJW: Miyashiro, Julie, et al. "Synthesis and SAR of novel tricyclic quinoxalinone inhibitors of poly (ADP-ribose) polymerase-1 (PARP-1)." *Bioorganic & Medicinal Chemistry Letters*, vol. 19, no. 15, Aug. 2009, pp. 4050–54, https://doi.org/10.1016/j.bmcl.2009.06.016.
15. (a) Friesner, Richard A., et al. "Glide: a new approach for rapid, accurate docking and scoring. 1. Method and assessment of docking accuracy." *Journal of Medicinal Chemistry*, vol. 47, no. 7, Feb. 2004, pp. 1739–49, https://doi.org/10.1021/jm0306430. (b) Halgren,

Thomas A., et al. "Glide: a new approach for rapid, accurate docking and scoring. 2. Enrichment factors in database screening." *Journal of Medicinal Chemistry*, vol. 47, no. 7, Feb. 2004, pp. 1750–59, https://doi.org/10.1021/jm030644s. (c) Friesner, Richard A., et al. "Extra precision glide: Docking and scoring incorporating a model of hydrophobic enclosure for protein− ligand complexes." *Journal of Medicinal Chemistry*, vol. 49, no. 21, Sept. 2006, pp. 6177–96, https://doi.org/10.1021/jm051256o.

16. National Center for Biotechnology Information. "PubChem Compound Summary for CID 1645, 3-Aminobenzamide" *PubChem*, https://pubchem.ncbi.nlm.nih.gov/compound/3-Aminobenzamide. Accessed 16 June, 2021.
17. National Center for Biotechnology Information. "PubChem Compound Summary for CID 1853, 6(5H)-Phenanthridinone" *PubChem*, https://pubchem.ncbi.nlm.nih.gov/compound/6_5H_-Phenanthridinone. Accessed 16 June, 2021.
18. Hasegawa, Masami, and Haruhiko Noda. "Distribution of hydrogen bond angles in molecular crystals." *Nature*, vol. 254, no. 5497, Mar. 1975, pp. 212–212, https://doi.org/10.1038/254212a0.
19. Singh, Nidhi, and Arieh Warshel. "A comprehensive examination of the contributions to the binding entropy of protein–ligand complexes." *Proteins: Structure, Function, and Bioinformatics*, vol. 78, no. 7, Jan. 2010, pp. 1724–35, https://doi.org/10.1002/prot.22689.
20. Papaneophytou, Christos P., et al. "Quantification of the effects of ionic strength, viscosity, and hydrophobicity on protein–ligand binding affinity." *ACS Medicinal Chemistry Letters*, vol. 5, no. 8, July 2014, pp. 931–36, https://doi.org/10.1021/ml500204e.
21. Du, Xing, et al. "Insights into protein–ligand interactions: mechanisms, models, and methods." *International Journal of Molecular Sciences*, vol. 17, no. 2, Jan. 2016, p. 144, https://doi.org/10.3390/ijms17020144.
22. (a) PDB ID 4TVJ (b) PDB ID 7KK4, Ryan, Kevin, et al. "Dissecting the molecular determinants of clinical PARP1 inhibitor selectivity for tankyrase1." *Journal of Biological Chemistry*, vol. 296, no. 100251, Jan. 2021, pp. 1–13, https://doi.org/10.1074/jbc.ra120.016573.

23. Huang, Ruo-yue, et al. "Isobologram analysis: A comprehensive review of methodology and current research." *Frontiers in Pharmacology*, vol. 10, no. 1222, Oct. 2019, pp. 1–12, https://doi.org/10.3389/fphar.2019.01222.

24. (a) Zhang, Ning, et al. "Synergistic combination of microtubule targeting anticancer fludelone with cytoprotective panaxytriol derived from panax ginseng against MX-1 cells in vitro: experimental design and data analysis using the combination index method." *American Journal of Cancer Research*, vol. 6, no. 1, 2016, pp. 97–104. (b) Chou, Ting-Chao. "Drug combination studies and their synergy quantification using the Chou-Talalay method." *Cancer Research*, vol. 70, no. 2, Jan. 2010, pp. 440–46, https://doi.org/10.1158/0008-5472.can-09-1947. c. Chou, Ting-Chao. "Theoretical basis, experimental design, and computerized simulation of synergism and antagonism in drug combination studies." *Pharmacological Reviews*, vol. 58, no. 3, Sept. 2006, pp. 621–81, https://doi.org/10.1124/pr.58.3.10.

25. Murai, Junko, et al. "Rationale for poly (ADP-ribose) polymerase (PARP) inhibitors in combination therapy with camptothecins or temozolomide based on PARP trapping versus catalytic inhibition." *Journal of Pharmacology and Experimental Therapeutics* 349.3 (2014): 408-416.

26. Cao, Xiaoyu, et al. "Combination of PARP inhibitor and temozolomide to suppress chordoma progression." *Journal of Molecular Medicine*, vol. 97, no. 8, June 2019, pp. 1183–93, https://doi.org/10.1007/s00109-019-01802-z.

27. (a) Lee, Sang Y. "Temozolomide resistance in glioblastoma multiforme." *Genes & Diseases*, vol. 3, no. 3, Sept. 2016, pp. 198–210, https://doi.org/10.1016/j.gendis.2016.04.007. b. Pan, Qiang, et al. "Chemoresistance to temozolomide in human glioma cell line U251 is associated with increased activity of O 6-methylguanine-DNA methyltransferase and can be overcome by metronomic temozolomide regimen." *Cell Biochemistry and Biophysics*, vol. 62, no. 1, Sept. 2011, pp. 185–91, https://doi.org/10.1007/s12013-011-9280-7.

Chapter 6: Conclusion and Discussion

With specific reference to the objectives in **Chapter 3**, we have achieved the following:

1. For Objective 1, we accomplished building two protein models representing two different protein statuses that could be found in the PARP protein: One with a fully closed binding pocket and the other one with an open binding pocket. With two different models, we were able to reveal different protein-ligand relationships on one ligand, which helped us determine the most possible/accommodative protein-ligand relationship. In some cases, we were able to adjust the size of the binding pocket to accommodate the ligand. While using a dynamic protein model to dock ligands was still rare to see and difficult to achieve, using two or more models representing two or more protein conditions was the method to speculate the protein-ligand relationship more accurately. It was worth noting that this method was not found in previous studies. We also built similar models for PARP2 and TNKS1. Among them, PARP2 models, along with PARP1 models, were used to predict and design PARP2-selective inhibitors.
2. For Objective 2, we designed and synthesized approximately 130 molecules, and tested approximately 150 molecules in our in-house assay. We carried out a preliminary rationale for predicting the potency of the PARP inhibitor core structure or a small PARP inhibitor. Then we explored alternative inhibitor scaffolds by testing molecules that could occupy various parts of the binding pocket. And finally, we developed some potent PARP inhibitors, comparable to olaparib, using *de novo* designs with or without the benzamide core structure. The goal to develop PARP1 and PARP2-selective inhibitors was partially accomplished as we designed compounds to inhibit PARP1 and PARP2 selectively by switching chirality, which showed partial PARP1 or PARP2-preference rather than superior or obvious selectivity. We had difficulties preparing some interesting compounds based on pyridine (**e compounds**), due to purity issues and poor potency.
3. For Objective 3, we developed a decent PARP1 inhibitor **c37** as well as **d1, d2** based on thienoquinolinone that had not been patented or published before. Compounds based on **c37** would have the patent space we were looking for.

4. For Objective 4, we tested our compounds under dual enzymatic assay methods (in-house PARP1 assay for all compounds and PARP1, PARP2, TNKS1 commercial assay kit for some inhibitors) and *in vitro* studies involving U251 cell lines (for best inhibitors).
5. For objective 5, we found the consistency between the *in silico* models, along with knowledge-based prediction, and our *in vitro* results. In another word, *in vitro* results could be explained by our *in silico* modelling.

This research began with the idea of developing novel phenanthridinone-based PARP inhibitors that are more potent and selective than PJ34, a classic non-selective PARP inhibitor. We developed our own cost-efficient enzymatic assay, which was able to achieve high-throughput screening with decent accuracy. The design of inhibitors was based on an *in silico* prediction and rationale. To make the inhibitor different from those of previous studies, we explored different spatial occupations inside the PARP1-binding pocket looking for suitable scaffolds. Two kinds of inhibitors were further studied. The first one used the "three-point-star"-like structure with the phenanthridinone core structure, the hydrophobic component (like an aromatic ring), and the hydroxyl arm centred on the amide linker. The expected mechanism of these inhibitors was such that, with the phenanthridinone component locked to the NI, the hydrophobic component could be attracted by the hydrophobic region and push the hydroxyl arm to the HD. This type of inhibitor interacted with the HD using the hydroxyl functional group whose location in the protein might be influenced by the interaction between the hydrophobic component and the hydrophobic region as well as the chirality of the connecting amide. We found that a longer structure was more likely to bring superior potency. The hydroxyl arm helped the ligand contact with the HD before it fully closed. With a longer hydroxyl arm, a ligand could delay the binding pocket closure or maintain a larger binding pocket, which might be related to better catalytic inhibition or PARP-trapping. The relative location between the -OH group and an amino acid residue determined which amino acid residue the -OH group could form an H-bond with. Due to the difference between D766/E335 (mainly due to their location in PARP1 and PARP2 proteins), using a chiral center on the linker amide was predicted to change the PARP1/2 preference. However, the hydroxyl arm here was highly flexible so that it reduced PARP1- or PARP2-selectivity. The second type of PARP inhibitor employed the scaffold that was composed of "phenanthridinone-piperazine-phenyl" framework. The framework had an R_2-substituted (*meta* to the phenanthridinone amine) phenylpiperazine, which was positioned inside

the AD, with the phenyl ring surrounded by three critical amino amide residues D766, D770, and R878, which made any functional group on the phenyl ring have a chance to build one or more influential ligand-protein interactions. To maximally potentiate the ligand-protein interaction, we chose to put a warhead, i.e., a boron group or a nitro group, onto the phenyl ring, expecting basic H-bonding, as well as ionic-bonding and temporary covalent bonding. Compounds with this design provided great potency against PARP1, surpassing the first benchmark PJ34 by 10-fold and reaching the same level as the gold benchmark olaparib. Interestingly, with this scaffold, we were able to produce the most potent inhibitor in our research, based on thienoquinolinone, which nearly gave us no potent candidate.

We tested some of our PARP inhibitors in a cell-based assay, along with olaparib as a standard, to explore their cytotoxicity when they were used individually and collectively with TMZ and TPT. As expected, while all these PARP inhibitors, including olaparib, had limited cytotoxicity when used alone, they were able to enhance the cytotoxicity of TMZ or TPT in combination, respectively. PARP inhibitors enhanced TMZ and TPT in a concentration-dependent manner, where a higher concentration of the PARP inhibitor led to better cytotoxicity. The enhancement also differed between the PARPi-TMZ combination and the PARPi-TPT We found strong synergistic effects when PARP inhibitors were used collectively with TMZ, and olaparib showed a stronger but not significant synergy compared to **b25**. However, when PARP inhibitors were used along with TPT, we could only find weak synergism or no synergism at all, according to the CI results. The relationship between PARP inhibitors and TPT was more similar to an additive one. It is worth noting that the antagonism determined by CI does not necessarily suggest that a PARP inhibitor would decrease the efficacy of TPT as synergism scales from 0 to 1, and antagonism scales from 1 to infinity [1]. This finding was in agreement with Murai's conclusion that PARP inhibitors were only able to enhance the cytotoxicity of camptothecin instead of causing a great synergistic effect with camptothecin. Camptothecin and TPT are both topoisomerase-I inhibitors causing SSB with exposed 5'-phosphate and covalently topoisomerases-bonded 3'-ends. The 5'-deoxyribose phosphate (5'-dRP) group was believed to be crucial for PARP trapping, and it could be induced by TMZ. Thus, when PARP inhibitors were used in a combination with TMZ, in addition to conventional inhibition of PARylation for DNA repair, it could also cause PARP-trapping to induce stronger cytotoxicity and a better synergistic effect. In comparison, because the SSB caused by TPT did not have a 5'-dRP end, as

well as because the topoisomerase complex became a steric hindrance, it was less likely to form the PARP–DNA complex, and the contribution of PARP-trapping was minimal. The influence of the PARP inhibitor on TPT was restricted to catalytic inhibition. Consequently, we saw a weaker enhancement in cytotoxicity and no synergism when the PARP inhibitor was used together with TPT. We did find one conclusion contrary to previous research, according to the Fa–CI curve, PARP inhibitors should have a better synergistic effect at a higher dose when combined with anticancer drugs such as TMZ or TPT. However, in our study, better synergy was found at a lower dose. The clinical significance of this trend was that it is more beneficial to receive small-dose multiple treatments rather than a large dose in a short time.

The limitation of our research is we have not developed candidates that are significantly more effective than existing benchmark drugs. This is the case for two reasons: One is we haven't developed a superior compound. For compounds with the scaffold stacking into the AD, modification on the linker between the component in the AD and the core phenanthridinone component is necessary, especially the carboxamide structure between the piperazine component and the phenanthridinone component as the carboxamide structure is less flexible; for compounds with "three-pointed-star" structure, it is necessary to make it further rigid so that the functional group would only contact with D766 or E335, instead of both. We believe another method to increase general potency is related to the size of a compound which will be discussed later. Another reason is that phenanthridinone compounds are insoluble in water or most organic solvents. When phenanthridinone compounds are used for *in vitro* assays, invisible precipitation may cause lower observed IC_{50}. One method to solve the problem is to make organic salts of these compounds, which we haven't tried yet. However, we designed compounds with tertiary amine for future attempts. Further *in vitro* assays are also necessary to determine the potential of these compounds.

In terms of drug discovery, our research has presented some promising leads for novel PARP inhibitors. The future work will be focused on the "lead-to-candidate" progress. In addition to modifying compounds slightly to make them more potent, increasing the bioactivity of compounds, as well as modifying physical features such as LogP, downsizing a potent compound to a certain level may also benefit the potency. We have discussed the influence of different designs on drug potency from the perspective of the molecular structure including the

chirality, the potential spatial occupancy, and the ligand-protein interaction mediated by certain functional groups. The influence of the molecular surface was not mentioned in any previous study. It was mentioned in the review that there is the conformational change upon PARP enzyme activation [2], where the binding site is opened with the HD travelling away from the ART so that larger molecules could enter the binding site. Meanwhile, smaller molecules can bind to the pocket before it is widely opened. The timing for molecules with different sizes entering the protein binding pocket may be different. We asked whether the size of a molecule influences the binding activity and whether smaller molecules such as 3AB that have priority to enter the binding pocket become more competitive than larger molecules. The answer to the latter question was negative. The first-generation PARP inhibitor such as 3AB is poor in potency. To answer the first question, we looked back to some popular inhibitors that are reported or commercially available. As shown in **Table 18**, we listed out some important physical features, namely, the van der Waals surface area (VSA), the exact molecular weight (ExtMW), as well as VSA/ExtMW, and LogP, along with the experimental data IC_{50} and pIC_{50} values. A molecule's VSA is used to describe the surface area of a molecule as the summary of each atom's VSA. It is considered that the radius of each atom, like a sphere, is its van der Waals radius, and the available VSA of each atom is the area not overlapped [3]. Generally, it indicates the "size" of the molecule and can be calculated by MarvinSketch[4]. After analyzing the relationship between different descriptors, we argue that VSA has an interrelation with pIC_{50}, which can be described by a non-linear curve (**Figure 73**). It is a binomial equation, and the correlation R^2=0.7082 indicated a comparably strong relationship. According to the relevance curve, we believed that when a PARP inhibitor had a VSA of around, approximately, 525, it would have the best chance to be a potent candidate. Our potent candidates had VSAs ranging from 521 to 588 (**Figure 74**). Our study on popular PARP inhibitors and corresponding VSA values, as well as our further guess that compounds with VSA around 500 would have a better chance to be decent PARP inhibitors according to the curve, indicates that if we could downsize these compounds by 5% ~ 10% while maintaining current functional groups and overall layouts, they might be able to reach the best potency. Some modification ideas are listed in **Figure 75**.

Inhibitor	VSA	ExtMW	VSA/MW	LogP	IC_{50}(nM)	SD	pIC_{50}

Veliparib [5]	360	244	1.48	0.79	9.32	11	0.970
PJ34 [6]	426	295	1.44	1.87	135	150	2.13
Talazoparib [7]	459	380	1.21	2.11	1.90	2.6	0.280
Olaparib [8]	592	434	1.36	2.11	6.99	5.7	0.845
XAV-939 [9]	361	312	1.16	2.61	917	840	2.96
Rucaparib [10]	452	323	1.40	2.45	102	160	2.01
Niraparib [11]	464	320	1.45	2.47	30.2	43	1.48
ME0328 [12]	220	160	1.38	0.77	3410	2200	3.53
NMS-P118(D7N) [13]	554	395	1.40	1.33	25.0	15	1.40
A927929 [14]	468	388	1.20	2.75	6.00	0	0.778
A861696 [15]	360	244	1.47	0.79	4.00	1.0	0.602
A620223 [16]	454	287	1.58	1.6	5.50	2.5	0.740
eb47 [17]	696	537	1.30	-2.55	45.0	0	1.653
3ab [18]	194	136	1.42	-0.01	20100	11000	4.30
Fluzoparib [19]	567	472	1.20	3.07	10.2	0	1.01
Iniparib [20]	241	292	0.82	1.69	200	0	2.30
Pamiparib [21]	389	298	1.31	1.39	0.900	0	-0.045
Benzamide [22]	179	121	1.48	0.82	15800	7400	4.20
Phenanthridinone [23]	262	195	1.34	2.74	377	93	2.58
Nicotinamide [24]	171	122	1.41	-0.39	210000	0	5.32
DPQ [25]	506	302	1.67	2.38	46.6	6.6	1.67
A-966492 [26]	439	324	1.35	3.38	1.00	0	2.30
a4	537	383	1.40	3.69	21.9	0.11	1.34
a16	522	398	1.31	2.85	53.0	2.33	1.72
a48	547	386	1.41	2.87	35.0	19	1.54
a49	575	428	1.34	2.82	30.4	29	1.48
b25	575	428	1.34	2.82	17.8	9.4	1.25
b26	589	427	1.38	N/A	15.8	1.9	1.20
b28	580	446	1.30	2.95	10.7	0.19	1.03
b29	574	428	1.34	2.82	14.1	5.3	1.15

Table 18 *Popular PARP1 inhibitors and some of our candidates' physical and calculational features. VSA: Van der Waals surface area; ExtMW: Exact molecular weight; VSA, ExtMW and LogP values were calculated using ChemAxon MarvinSketch. IC_{50} and SD values of drugs with generic names were calculated from PubChem Database or corresponding literature while values of* ***a4-b29*** *were from experiments reported in previous chapters.*

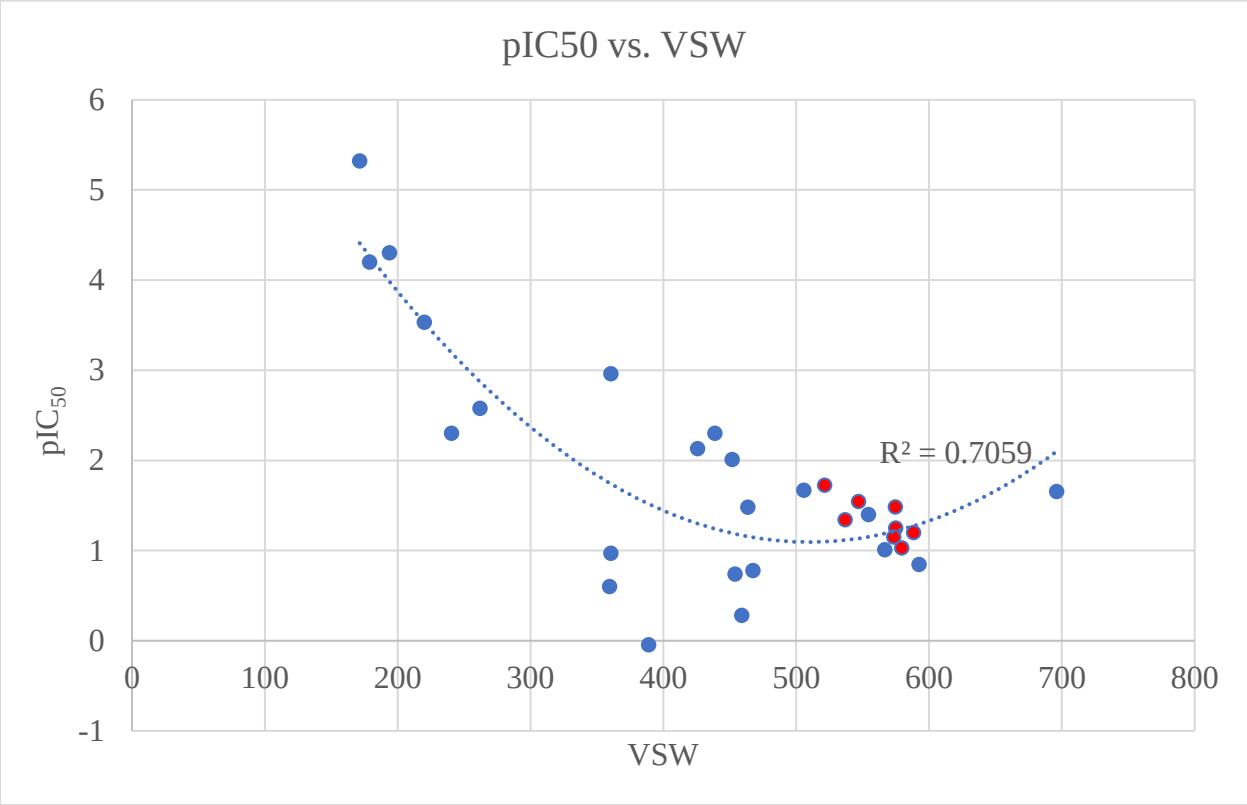

Figure 73 *pIC_{50}-VSA plotting. Values are from* ***Table 18****. Blue ones are popular inhibitors in the market. Red ones are some of our candidates. The relationship could be described with a binomial equation and the correlation R^2=0.7059, indicating a comparably strong relationship.*

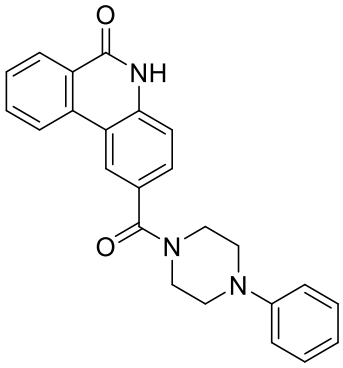

VSA = 537, IC_{50} = 21.9±0.11nM

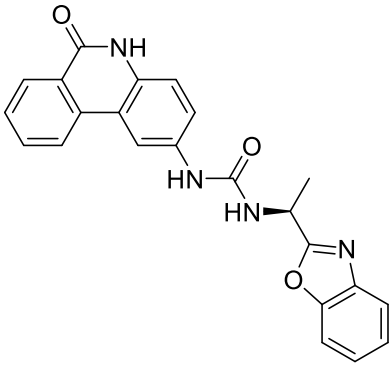

VSA = 522, IC_{50} = 53.0±2.3nM

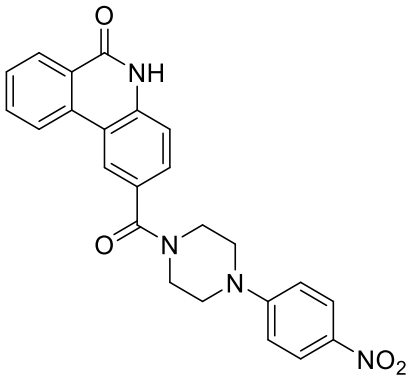

VSA=575, IC_{50} = 30.4±29nM

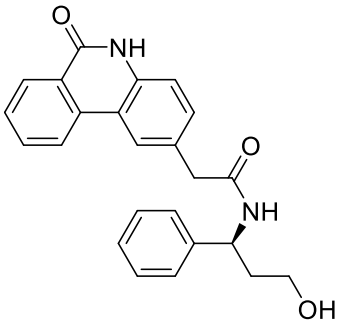

VSA = 547, IC_{50} = 35.0±19nM

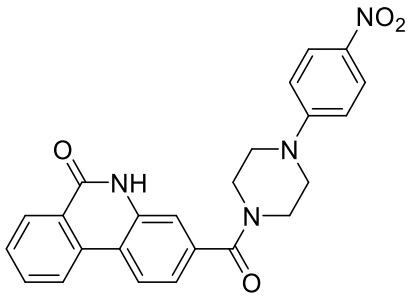

VSA = 575, IC_{50} = 17.8±9.4nM

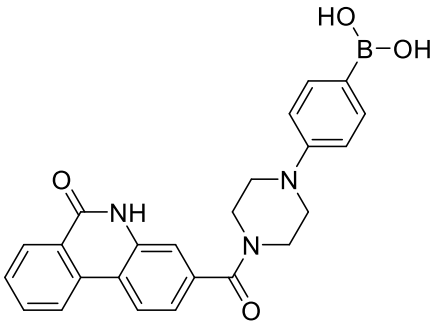

VSA = 589, IC_{50} = 15.8±1.9nM

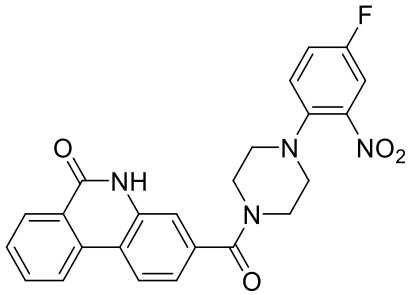

VSA = 580, IC_{50} = 10.7±0.19nM

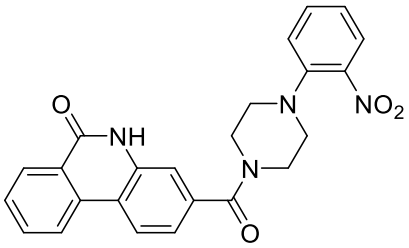

VSA = 574, IC_{50} = 14.1±5.3nM

Figure 74 *Our potent candidates from this study and their VSAs.*

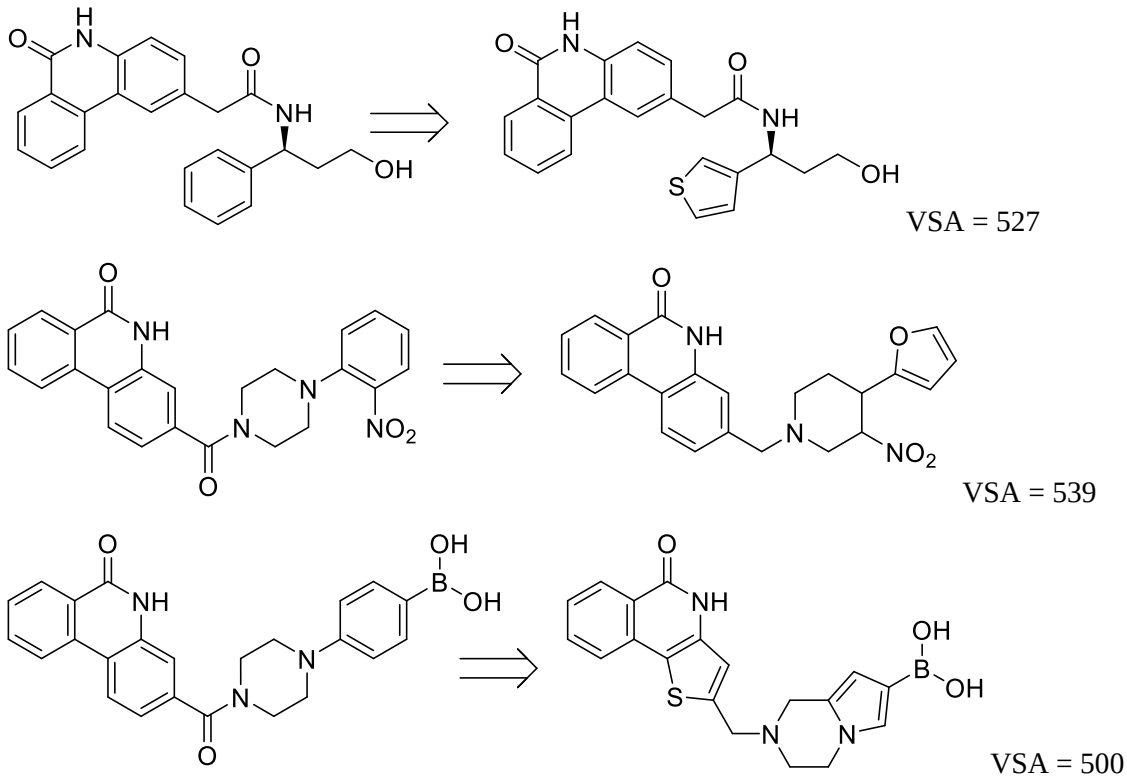

Figure 75 *Potential modifications to optimize VSA. Some types of possible modifications that could downsize molecules while maintaining current functional groups and layouts. VSA values were calculated using ChemAxon MarvinSketch.*

The method we took to discover *de novo* PARP inhibitors was a multi-discipline attempt to integrate *in silico* simulation and wet-lab experiments. We understood that a comprehensive knowledge of the potential protein-ligand relationship was necessary for an efficient drug design. The protein-ligand relationship referred to the binding pose of the ligand and any attractive interaction between the protein and the ligand. The efficiency was reflected in compounds sharing a similar protein-ligand relationship, which would produce a comparable inhibition ability or compounds designed under the same principle, which had a similar potency. While we were not able to build the crystal structure of each inhibitor-PARP complex, *in silico* modelling became an important tool for analysis and prediction. It was worth noting that we were not only using molecular modelling to rationalize the experimental results, as the modelling itself would

not 100% reproduce what occurred in the protein. For this reason, we counted on the structural orientation and the potential attractive interaction rather than the docking score. Additionally, this is why we required not only knowledge about each component of an inhibitor regarding the influence on the protein but also an accurate modelling and molecular docking method that would produce *in silico* results consistent with *in vitro* ones. For the first goal, on the basis of previous studies demonstrating possible protein-ligand interactions and their influences, we investigated every component to build a PARP inhibitor, from small compounds that were always used as core structures inside the NI and scaffolds developed on core structures for spatial occupancy, to larger PARP inhibitors by adding functional groups onto scaffolds for strong attractive interaction. The investigation helped us to develop our hypothesis about (1) the importance of known amino acid residues; (2) other promising residue targets; and (3) potential compound orientations inside the binding pocket and their impact. For the second goal, we continuously compared the molecular docking results to *in vitro* results and SAR studies to see if there was a pattern between *in silico* and *in vitro* results. Again, we expected ligands with similar protein-ligand relationships to have a similar potency. We concluded that our modelling and molecular docking method was accurate enough when we studied ligands interacting with the HD, as the molecular docking result was able to explain the experimental data and the SAR study, and it successfully predicted the PARP1/2-preference of pairs of enantiomers. Eventually, a batch of good inhibitors came from careful and rational design rather than random chance.

Creativity was also critical for the *de novo* design. It was commonly recognized that analogs of known potent inhibitors, compared to *de novo* designs or designs based on poor inhibitors, had a better chance to deliver decent results. That is why, as shown in our review in **Chapter 2**, inhibitors have undergone clinical trials that were very similar to each other, while the modification focused on bioavailability rather than drug potency. Although our research was based on a known core component, phenanthridinone, we designed novel structures on it to endow the inhibitor with different potency and selectivity. The creativeness mainly came from two steps we took: designing the scaffold on the core component and adding the functional component onto the scaffold. Compared to making analogs of a known inhibitor, our approach was more like designing a compound from scratch. The approach did not guarantee the potency if there was no accurate modelling, but it was easier for us to try new layouts. The creativity of a compound came from the idea of how we wanted to make a compound occupy the binding

pocket and interact with targeting residues. Hence, it was still a knowledge-based drug design. We understand that, as we mentioned in the review in **Chapter 2**, there are cutting-edge computational methods such as machine learning/artificial intelligence-based drug design and free energy perturbation calculation-based potency prediction, but they require advanced computational skills and resources that are not achievable in daily research. Our approach, integrating conventional molecular docking and *in vitro* studies for evaluating and verifying novel drug design can be more widely used. However, one that can influence the knowledge-based prediction is the accuracy of the *in silico* simulation platform itself. In general, different software would produce different molecular docking results, while the outdated one could be less accurate, which could lead to incorrect interpretations and mismatches between the SAR study and the molecular docking result.

We tried to develop best-in-series PARP inhibitors with a *de novo* design rather than use the existing hits and scaffolds for "decent results". Thus, two types of compounds were synthesized and tested in parallel. One was based on plain phenanthridinone, which has not been developed into a potent PARP inhibitor, partially because it is patented. Champion compounds based on phenanthridinone could be seen as "semi-novel" inhibitors, as their potency does not exactly come from phenanthridinone analogs. On the other hand, in this study, we also explored inhibitors with core structures that shared a similar layout to phenanthridinone that had not been patented. These core structures included thienoquinolinone with a thiophene ring and naphthridinone with a pyridine ring. Although we encountered problems in purifying the latter, we had evaluated several compounds based on thienoquinolinone and compared them to phenanthridinone-based inhibitors. As a matter of fact, there was no study using thienoquinolinone as a PARP inhibitor, and it was certainly not patented. Even though our study in small-molecule PARP inhibitors suggested that thienoquinolinone was not as potent as phenanthridinone as an inhibitor itself, and studies on the inhibitor's spatial occupancy and HD-interacted inhibitors actually supported the idea that thienoquinolinone was an ineffective platform to develop PARP inhibitors, we still took it as a potential breakthrough as the *in silico* modeling informed us that thienoquinolinone had a high rate of "correct" docking on different designs while some of them were synthesized and tested and some were not. The nicotinamide binding pocket was adjacent to the wall of the binding pocket, and we believed that a smaller carbonyl-half aromatic ring would increase the potency as long as, according to our assumption,

the plane of the core structure ligand could bind to the site within a proper dihedral angle with G863. Of course, due to the electron density distribution and electron richness, thienoquinolinone could not achieve the optimal binding pose to be a decent inhibitor. However, it was highly possible that the binding pose would be influenced by the side chain on the core structure. After we developed champion compounds based on phenanthridinone, we decided to provide thienoquinolinone with a final attempt, and we placed 4-nitro-*N*-phenylpiperazine and 2-nitro-4-fluoro-*N*-phenylpiperazine, two side chains that produced the most phenanthridinone-based inhibitor, onto thienoquinolinone. While the latter, **c33**, was only as potent as PJ34 in the enzymatic assay due to the purity issue as well as due to the fact that the final product could not completely be separated from the side product from the reaction synthesizing *meta*-COOH substituted thienoquinolinone, the former one, **c37**, became the best compound we had ever designed. It was not only as potent as the gold benchmark olaparib in the enzymatic assay, but it also delivered greater synergy than olaparib with the anticancer drug TMZ in the cell assay. As a result, we obtained a near best-in-series potent PARP inhibitor, using FDA-approved olaparib as a benchmark.

From our research, there are three pathways to move forward. The first pathway should focus on small PARP inhibitors. Using the proposed predicting method we should be able to design potent small inhibitors. Compared to larger ones, small inhibitors have a lower chance to cause PARP trapping, which made them promising inhibitors for CNS disease to prevent the depletion of NAD due to hyperactive PARP without inducing side effects due to PARP-trapping. The second pathway is to further characterize champion PARP inhibitors to evaluate their potency in different cell lines in combination with different anticancer drugs, as well as in BRCA-deficient cell lines individually. Further structural modification can be applied to optimize features such as solubility and VSA, among others. The third pathway is to develop TNKS-selective and PARP-2 selective inhibitors. Since the *in silico* modelling and analyzing method has proved useful and comparably accurate, it could be used to develop more selective inhibitors. For the TNKS-selective inhibitor, it is critical to pass the adenine-binding pocket to reach the wall of the ART domain. If champion compounds could maintain the protein with an open binding pocket (which could be evaluated by hydrogen/deuterium exchange-mass spectrometry (HXMS)), **b4** would be a great scaffold and starting point to build TNKS-selective

inhibitors. Meanwhile, we are confident that if ligand–D766/E335 interactions can be restricted, we can create PARP1- or PARP2-selective inhibitors.

In conclusion, we have presented our methods and results in developing novel, best-in-series PARP inhibitors that are designed with CADD methods and evaluated by enzymatic and cell-based assays. We have completed the "hit-to-lead" procedure with multidiscipline approaches and ~10% of our designed and synthesized compounds were 5–10-fold more potent than our original benchmark PJ34, and ~3% of compounds were equivalent to the gold benchmark olaparib. We have confirmed that with CADD we were able to convert a less potent inhibitor/core structure, phenanthiridinone, into potent and novel inhibitors.

References

1. Chou, Ting-Chao. "Drug combination studies and their synergy quantification using the Chou-Talalay method." *Cancer Research*, vol. 70, no. 2, Jan. 2010, pp. 440–46, https://doi.org/10.1158/0008-5472.can-09-1947.
2. Dawicki-McKenna, Jennine M., et al. "PARP-1 activation requires local unfolding of an autoinhibitory domain." *Molecular Cell*, vol. 60, no. 5, Dec. 2015, pp. 755–68, https://doi.org/10.1016/j.molcel.2015.10.013.
3. Ranganathan, Shoba, et al. *Encyclopedia of Bioinformatics and Computational Biology: ABC of Bioinformatics*. Elsevier, 2018, p. 524.
4. Marvin was used for drawing, displaying and characterizing chemical structures and calculating listed features including VSA, MW and LogP, Marvin 17.21.0, ChemAxon (https://www.chemaxon.com)
5. National Center for Biotechnology Information. "PubChem Compound Summary for CID 11960529, Veliparib" *PubChem*, https://pubchem.ncbi.nlm.nih.gov/compound/Veliparib. Accessed 6 October, 2021.
6. National Center for Biotechnology Information. "PubChem Compound Summary for CID 4858" *PubChem*, https://pubchem.ncbi.nlm.nih.gov/compound/pj34. Accessed 6 October, 2021.
7. National Center for Biotechnology Information. "PubChem Compound Summary for CID 135565082,

Talazoparib" *PubChem*, https://pubchem.ncbi.nlm.nih.gov/compound/Talazoparib. Accessed 6 October, 2021.

8. National Center for Biotechnology Information. "PubChem Compound Summary for CID 135565082, Talazoparib" *PubChem*, https://pubchem.ncbi.nlm.nih.gov/compound/Talazoparib. Accessed 6 October, 2021.
9. National Center for Biotechnology Information. "PubChem Compound Summary for CID 135418940" *PubChem*, https://pubchem.ncbi.nlm.nih.gov/compound/xav-939. Accessed 6 October, 2021.
10. National Center for Biotechnology Information. "PubChem Compound Summary for CID 9931954, Rucaparib" *PubChem*, https://pubchem.ncbi.nlm.nih.gov/compound/Rucaparib. Accessed 6 October, 2021.
11. National Center for Biotechnology Information. "PubChem Compound Summary for CID 24958200, Niraparib" *PubChem*, https://pubchem.ncbi.nlm.nih.gov/compound/Niraparib. Accessed 6 October, 2021.
12. National Center for Biotechnology Information. "PubChem Compound Summary for CID 135566764" *PubChem*, https://pubchem.ncbi.nlm.nih.gov/compound/me0328. Accessed 6 October, 2021.
13. National Center for Biotechnology Information. "PubChem Compound Summary for CID 49843531" *PubChem*, https://pubchem.ncbi.nlm.nih.gov/compound/nms-p118. Accessed 6 October, 2021.
14. Penning, Thomas D., et al. "Optimization of phenyl-substituted benzimidazole carboxamide poly (ADP-ribose) polymerase inhibitors: identification of (S)-2-(2-fluoro-4-(pyrrolidin-2-yl) phenyl)-1 H-benzimidazole-4-carboxamide (A-966492), a highly potent and efficacious inhibitor." *Journal of Medicinal Chemistry*, vol. 53, no. 8, Mar. 2010, pp. 3142–53, https://doi.org/10.1021/jm901775.
15. National Center for Biotechnology Information. "PubChem Compound Summary for CID 56587808, 1-(6-Bromopyridin-2-yl)-2,2,2-

trifluoroethanone" *PubChem*, https://pubchem.ncbi.nlm.nih.gov/compound/1-_6-Bromopyridin-2-yl_-2_2_2-trifluoroethanone. Accessed 6 October, 2021.

16. (a) Tong, Yunsong, et al. "Synthesis and evaluation of a new generation of orally efficacious benzimidazole-based poly (ADP-ribose) polymerase-1 (PARP-1) inhibitors as anticancer agents." *Journal of Medicinal Chemistry*, vol. 52, no. 21, Oct. 2009, pp. 6803–13, https://doi.org/10.1021/jm900697r. (b) Penning, Thomas D., et al. "Discovery and SAR of 2-(1-propylpiperidin-4-yl)-1H-benzimidazole-4-carboxamide: a potent inhibitor of poly (ADP-ribose) polymerase (PARP) for the treatment of cancer." *Bioorganic & Medicinal Chemistry Letters*, vol. 20, no. 3, Feb. 2010, pp. 1023–26, https://doi.org/10.1016/j.bmcl.2009.12.042.
17. Zandarashvili, Levani, et al. "Structural basis for allosteric PARP-1 retention on DNA breaks." *Science*, vol. 368, no. 6367, Apr. 2020, pp. 1–10, https://doi.org/10.1126/science.aax6367.
18. National Center for Biotechnology Information. "PubChem Compound Summary for CID 1645, 3-Aminobenzamide" *PubChem*, https://pubchem.ncbi.nlm.nih.gov/compound/3-Aminobenzamide. Accessed 6 October, 2021.
19. National Center for Biotechnology Information. "PubChem Compound Summary for CID 56649297, Fluzoparib" *PubChem*, https://pubchem.ncbi.nlm.nih.gov/compound/Fluzoparib. Accessed 6 October, 2021.
20. National Center for Biotechnology Information. "PubChem Compound Summary for CID 9796068, Iniparib" *PubChem*, https://pubchem.ncbi.nlm.nih.gov/compound/Iniparib. Accessed 6 October, 2021.
21. National Center for Biotechnology Information. "PubChem Compound Summary for CID 135565554, Pamiparib" *PubChem*, https://pubchem.ncbi.nlm.nih.gov/compound/Pamiparib. Accessed 6 October, 2021.
22. National Center for Biotechnology Information. "PubChem Compound Summary for CID 2331,

Benzamide" *PubChem*, https://pubchem.ncbi.nlm.nih.gov/compound/Benzamide. Accessed 6 October, 2021.

23. National Center for Biotechnology Information. "PubChem Compound Summary for CID 1853, 6(5H)-Phenanthridinone" *PubChem*, https://pubchem.ncbi.nlm.nih.gov/compound/6_5H_-Phenanthridinone. Accessed 6 October, 2021.
24. National Center for Biotechnology Information. "PubChem Compound Summary for CID 936, Nicotinamide" *PubChem*, https://pubchem.ncbi.nlm.nih.gov/compound/Nicotinamide. Accessed 6 October, 2021.
25. National Center for Biotechnology Information. "PubChem Compound Summary for CID 9948349" *PubChem*, https://pubchem.ncbi.nlm.nih.gov/compound/9948349. Accessed 6 October, 2021.
26. National Center for Biotechnology Information. "PubChem Compound Summary for CID 16666333" *PubChem*, https://pubchem.ncbi.nlm.nih.gov/compound/a-966492. Accessed 6 October, 2021.

Appendix

1. IC_{50} values of tested compounds using the PARP1 enzymatic assay described in Chapter 4, Section 4.3.

Each experiment was plated in triplicate. Data obtained from two or more experiments were shown as Mean±SD; otherwise, it was obtained from single measurements. Experimental data were processed with GraphPad 8.0.1. IC_{50} values were calculated using 4-parameter logistic regression.

Name	Structure	IC_{50} (nM)	n
Phe	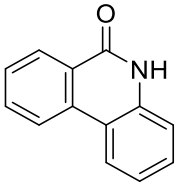	419±53	3
PJ34	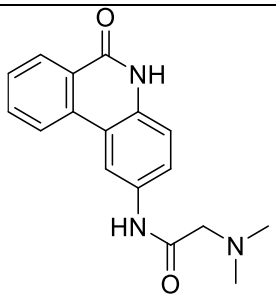	148±28	3
DPQ	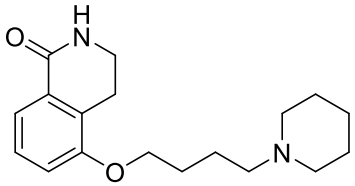	2230±1100	3
Olaparib	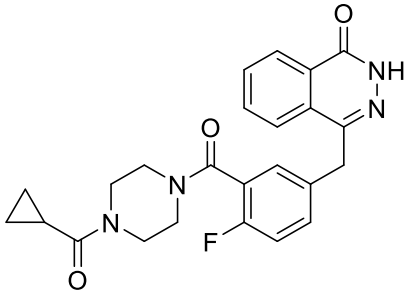	5.50	1

CPT	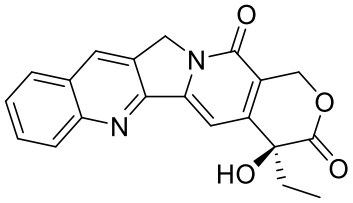	None	1
a1	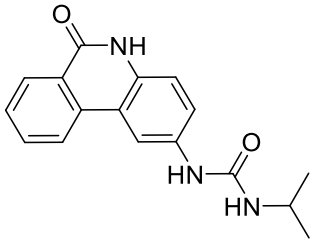	93.4	1
a2	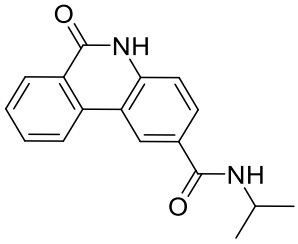	39.4	1
a3	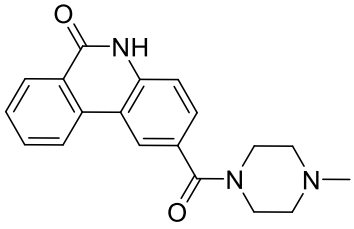	627	1
a4	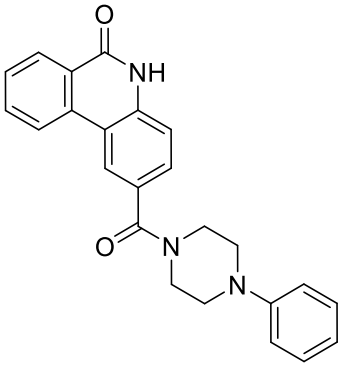	21.9±0.11	2
a5	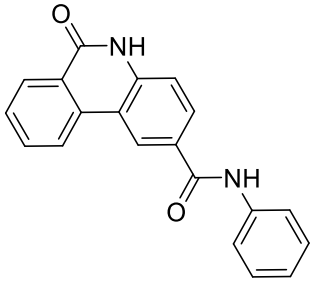	272	1

a6	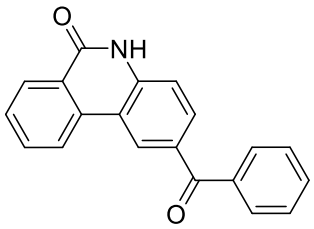	1530	1
a7	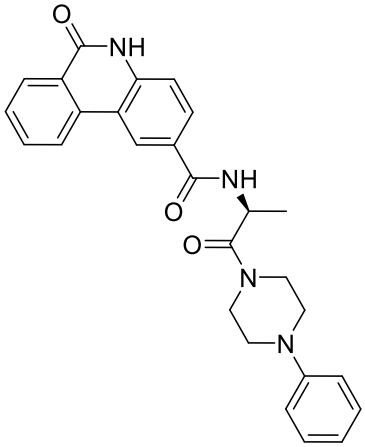	2100±250	2
a8	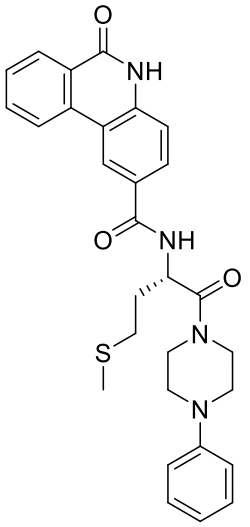	275	1

a9	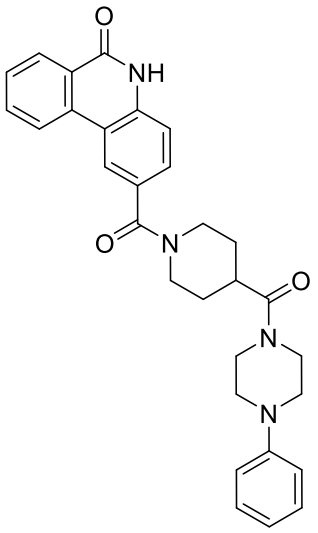	324	1
a10	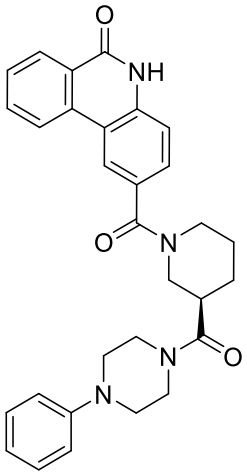	915	1
a11	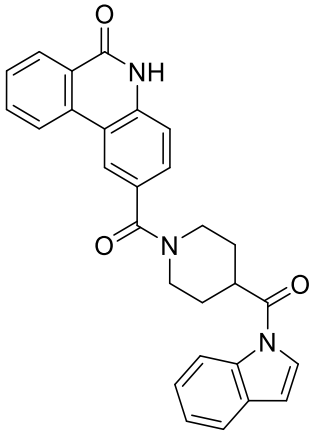	917	1

a12	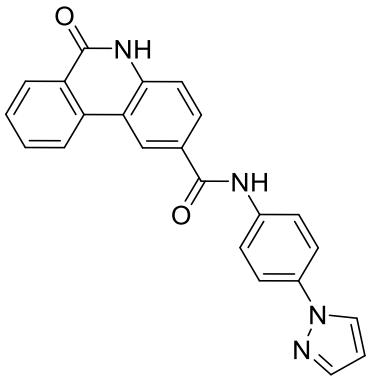	1750	1
a13	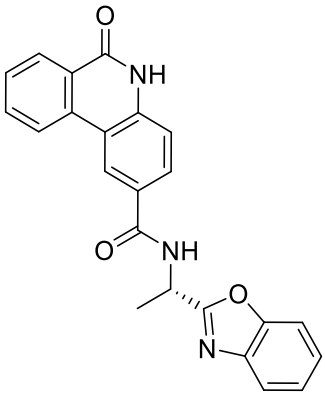	3760	1
a14	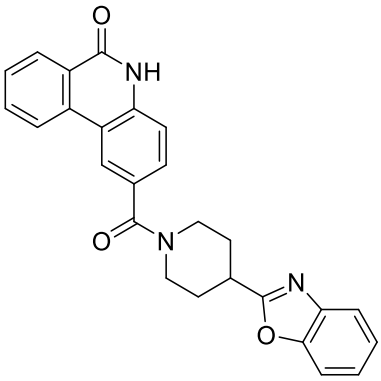	213	1
a15	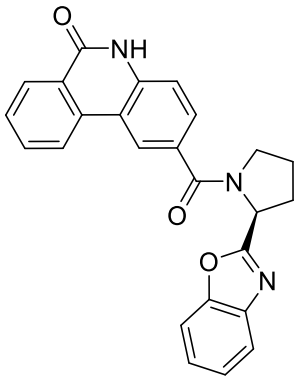	791	1

a16	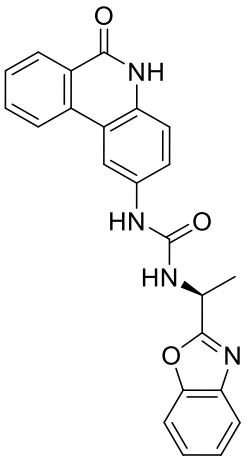	53.0±2.3	2
a17	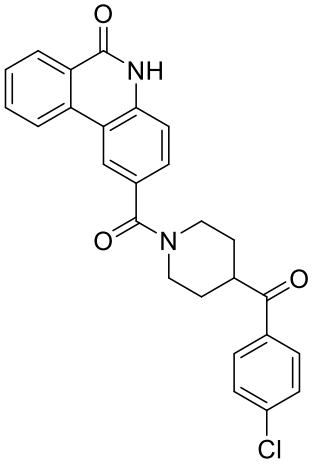	1930±1400	3
a18	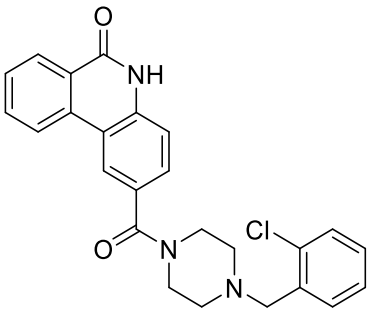	941±620	3
a19	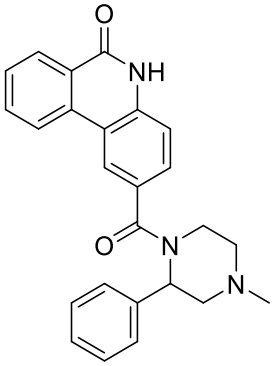	809±400	3

a20	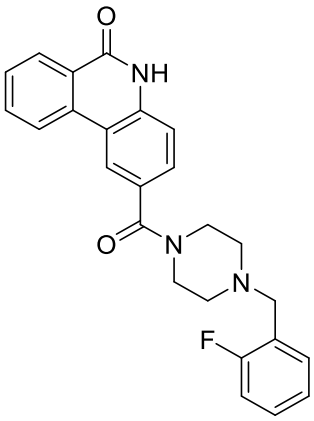	1300±110	3
a21	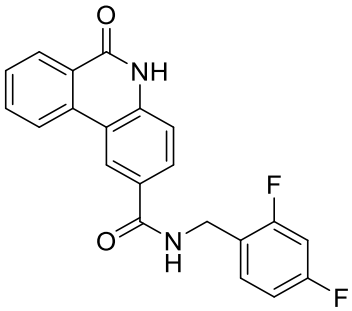	13500±14000	5
a22	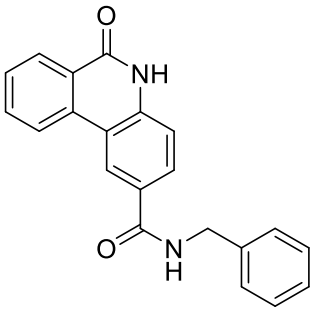	10600	1
a23	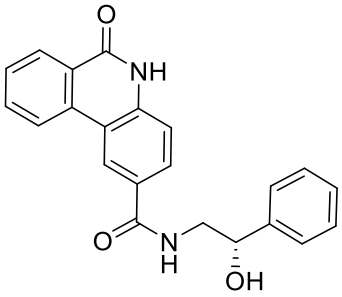	1160±990	7

a24	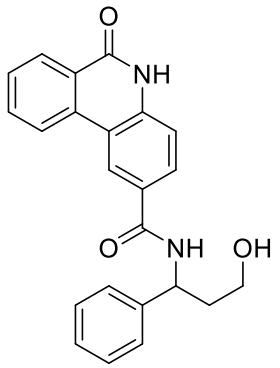	159±18	3
a25	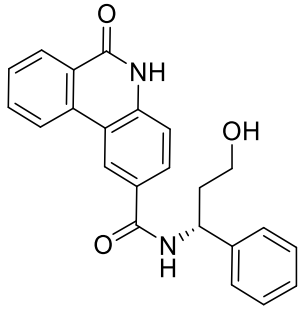	2030±1100	4
a26	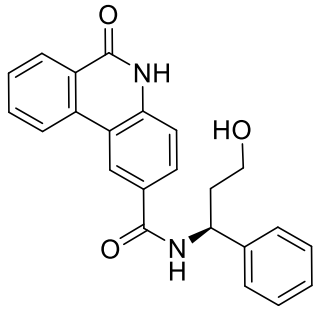	124±68	4
a27	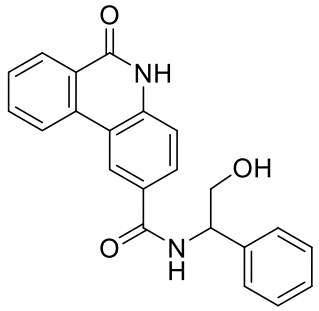	545±330	6

a28	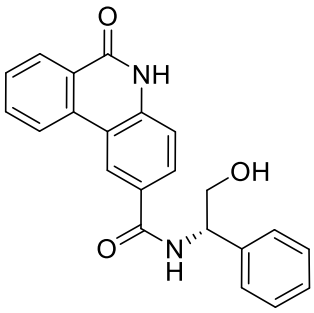	946±240	2
a29	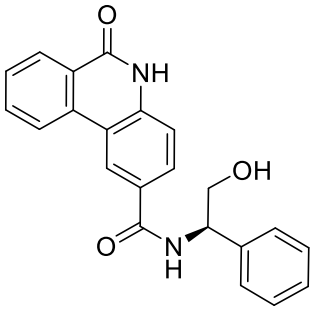	108±6.3	1
a30	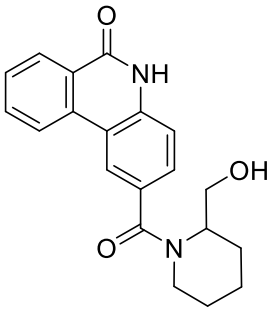	141±33	3
a31	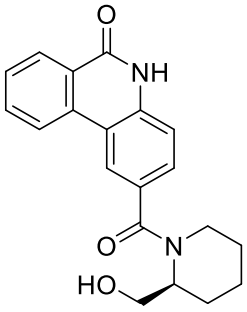	243±14	2
a32	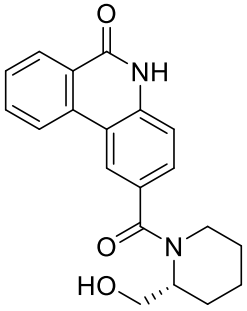	149±25	2

a33	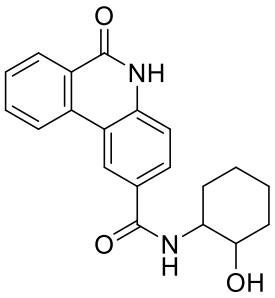	312±39	2
a34	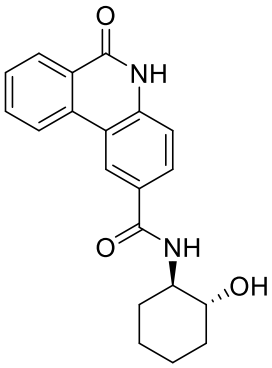	473±160	2
a35	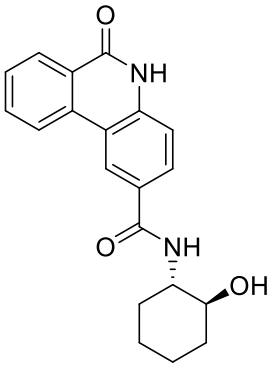	276±47	2
a36	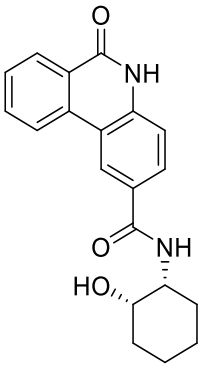	330±110	2

a37	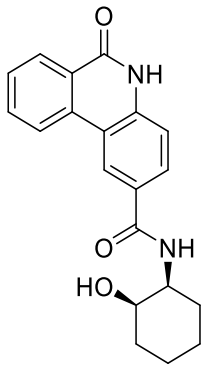	382±97	2
a38	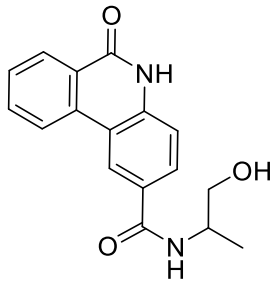	615±230	4
a39	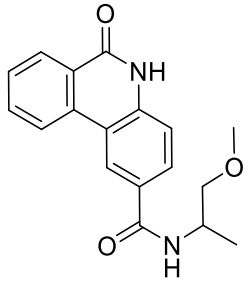	690±630	5
a40	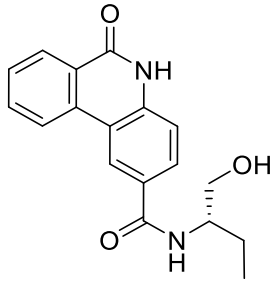	566±230	2
a41	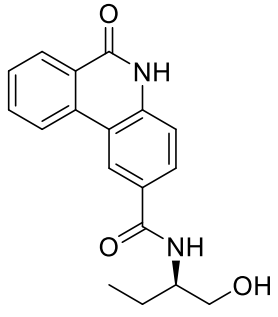	12300±5500	2

a42	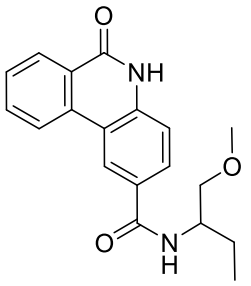	552±380	3
a43	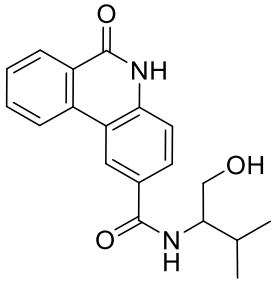	277±120	2
a44	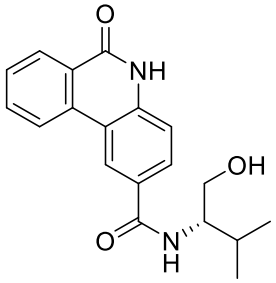	693±230	1
a45	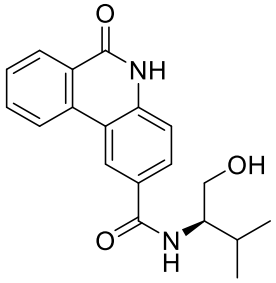	179	1
a46	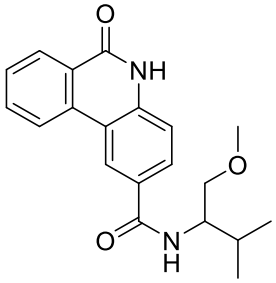	213000±70000	1

a47	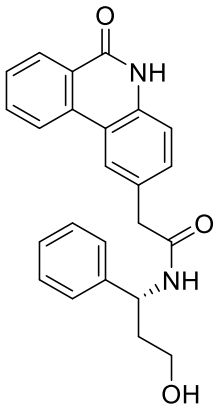	746±390	3
a48	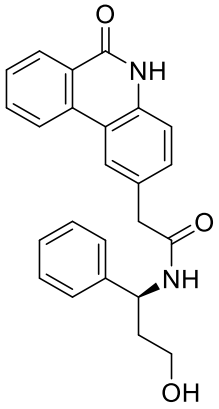	35.0±18	3
a49	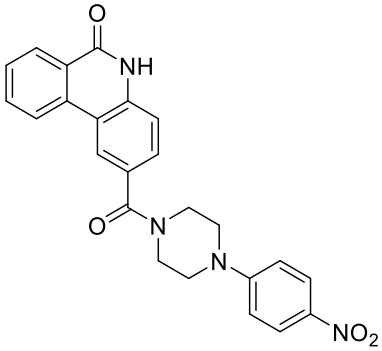	30.3±29	2
a50	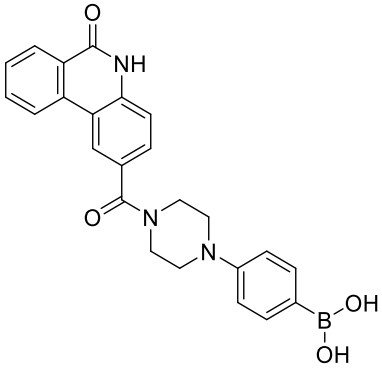	133	1

a51	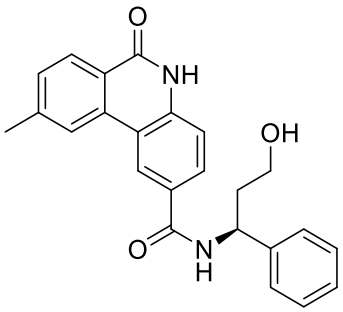	39000±13000	2
a52	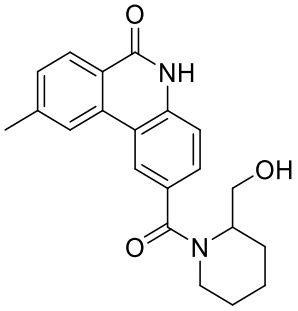	783±83	2
a53	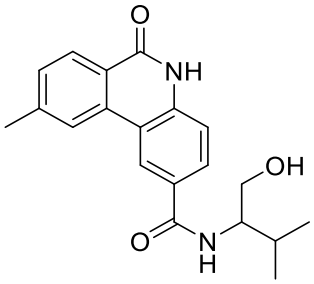	40600±22000	2
a54	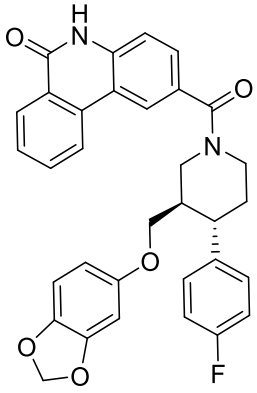	8830±2000	2

a55	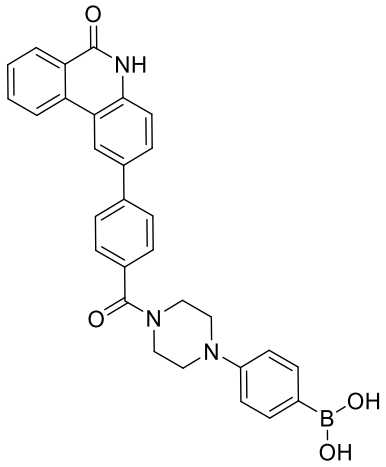	2450	1
a56	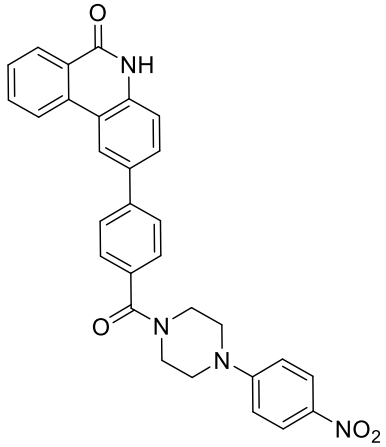	919±200	3
b1	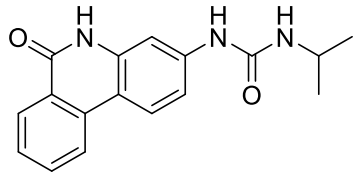	219	1
b2	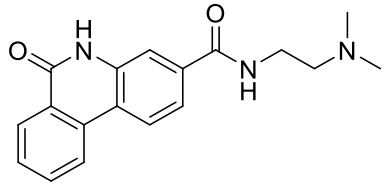	443	1
b3	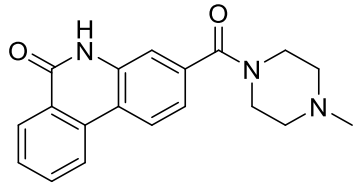	301	1

b4	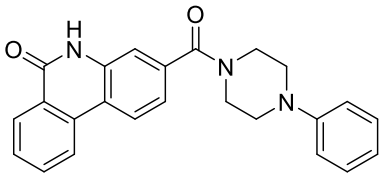	72.9±35	2
b5	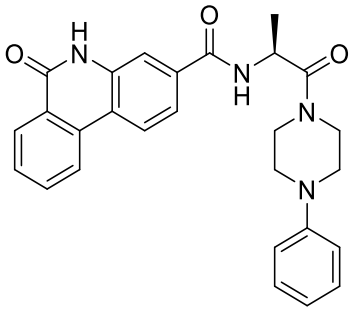	96.3±12	2
b6	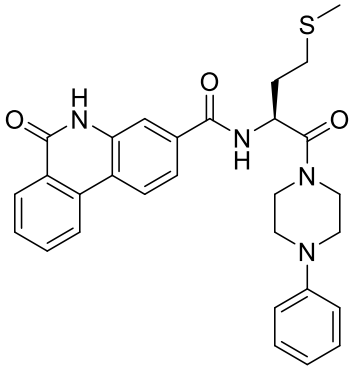	483	1
b7	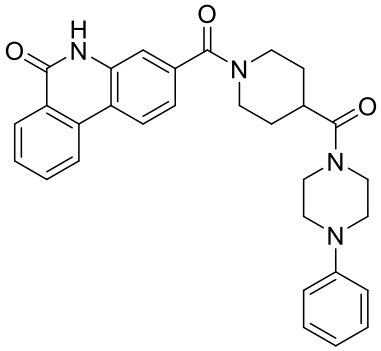	74.6	1
b8	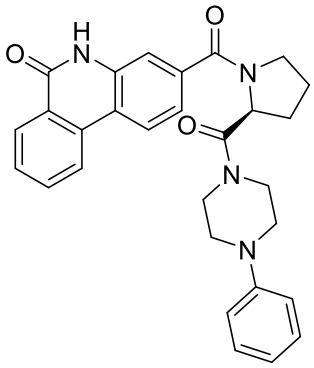	327	1

b9	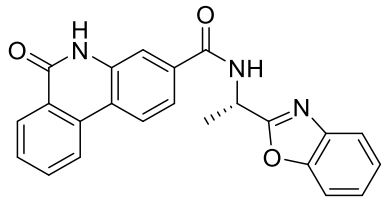	212	1
b10	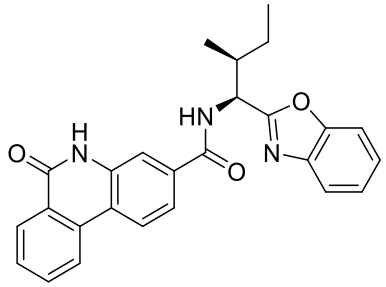	1700	1
b11	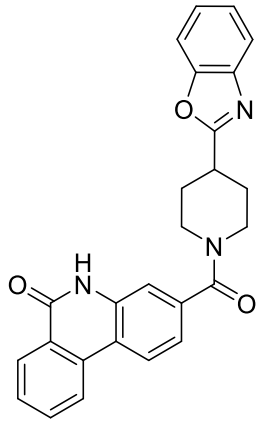	143	1
b12	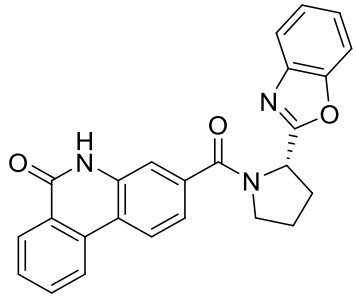	225	1
b13	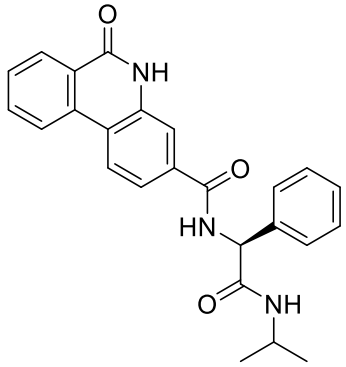	1840	1

b14	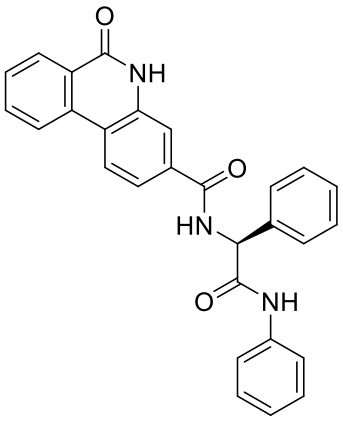	12500	1
b15	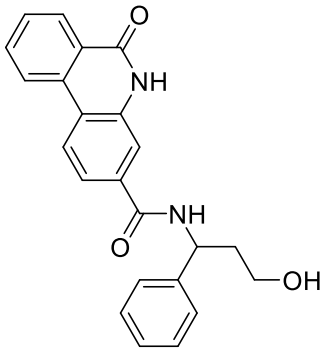	450	1
b16	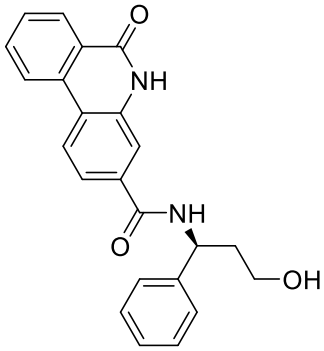	803±110	2
b17	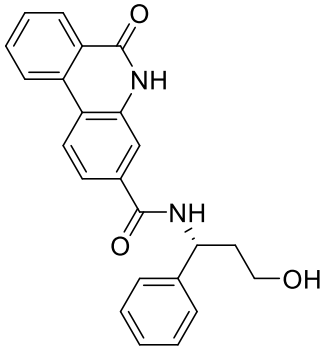	496	1

b18	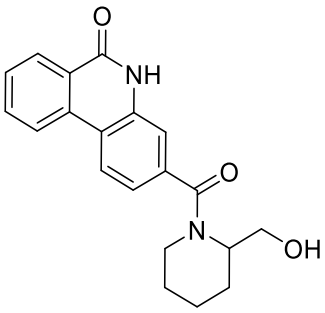	143±0.60	2
b19	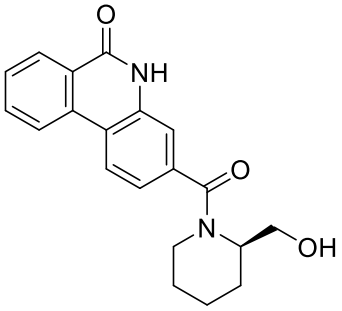	62.0±28	2
b20	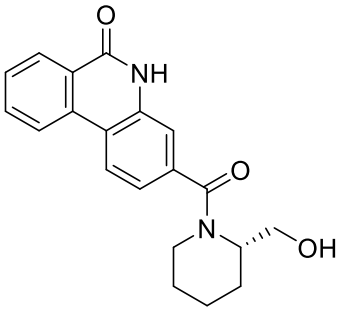	686	1
b21	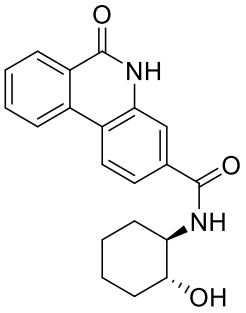	685±54	2
b22	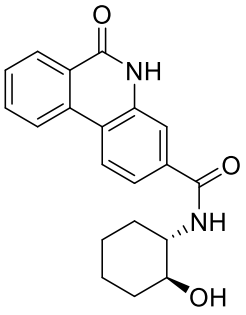	524	1

b23	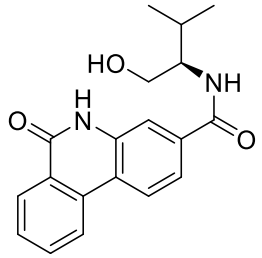	506	1
b24	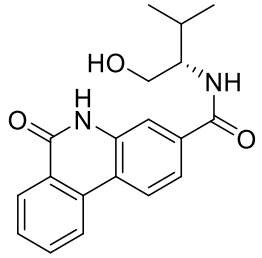	7420	1
b25	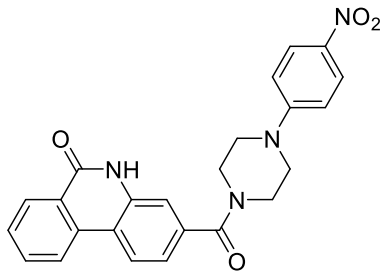	17.8±9.4	3
b26	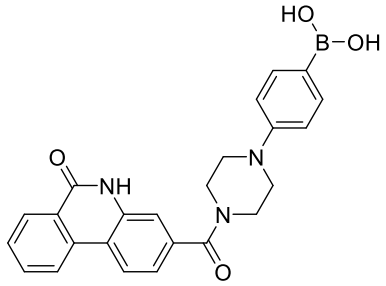	15.8±1.9	2
b27	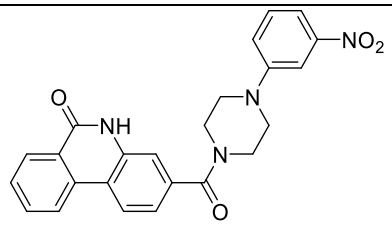	43.0±2.3	2
b28	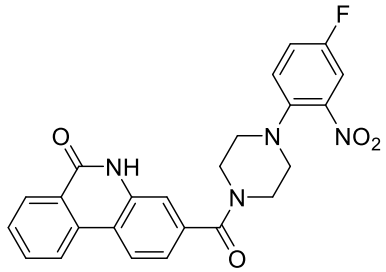	10.7±0.19	2

b29	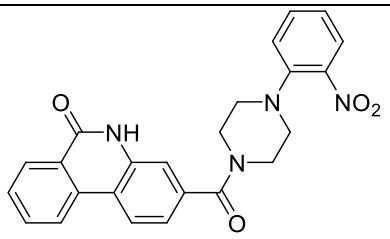	14.1±5.3	2
b30	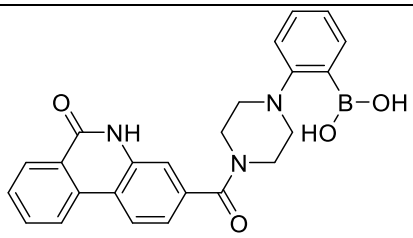	38.4±3.9	2
c1	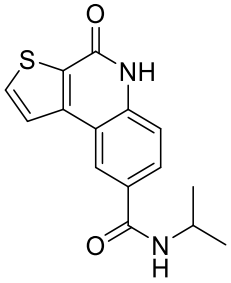	1820	1
c2	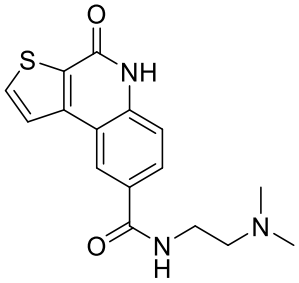	10900	1
c3	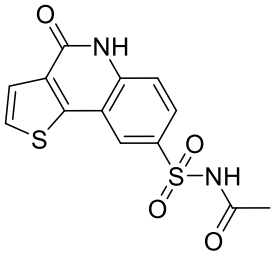	8210	1
c4	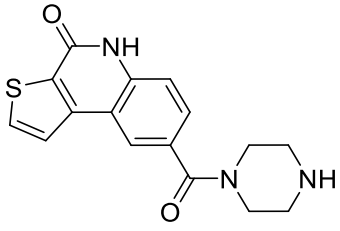	105	1

c5	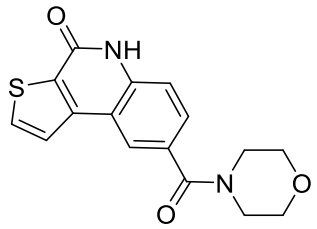	566	1
c6	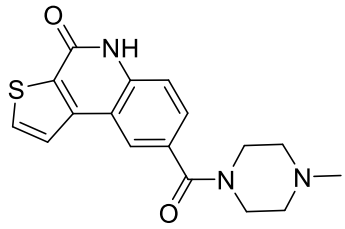	1460	1
c7	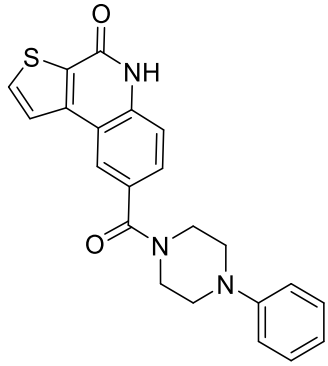	385	1
c8	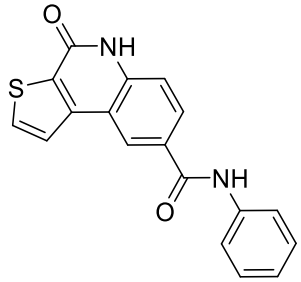	692±62	2
c9	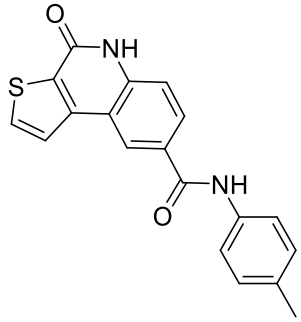	27500	1

c10	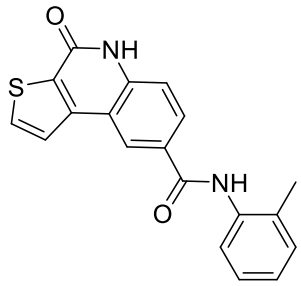	6650	1
c11	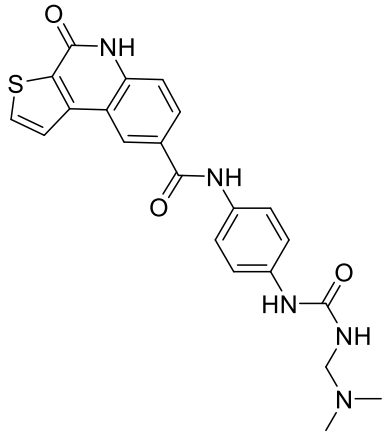	16700±4200	2
c12	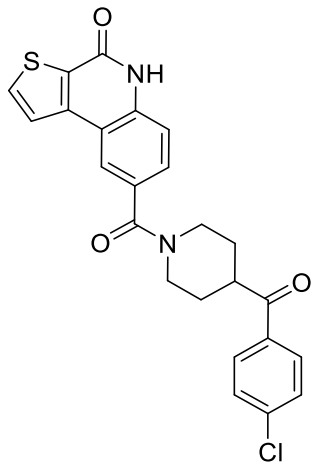	1600±340	2
c13	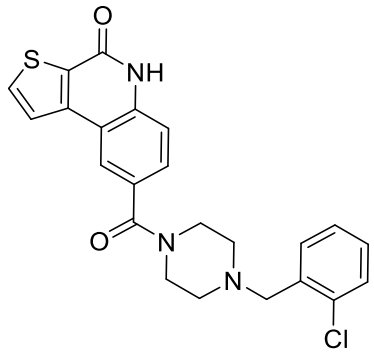	2730	1

c14	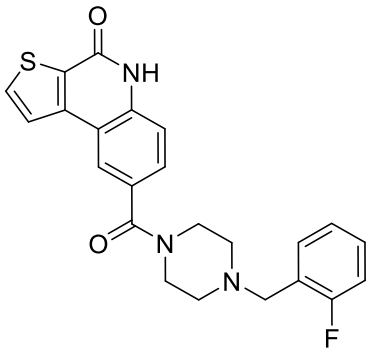	1720	1
c15	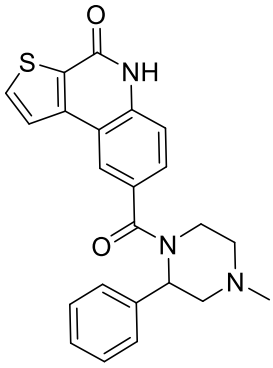	3730	
c16	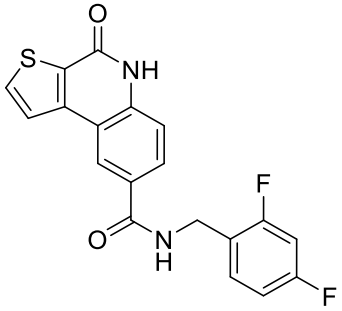	2230±44	2
c17	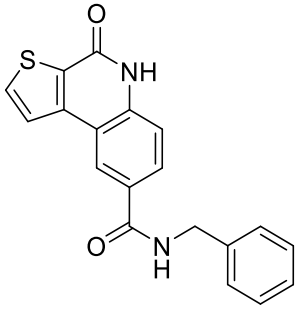	1310±650	2

c18	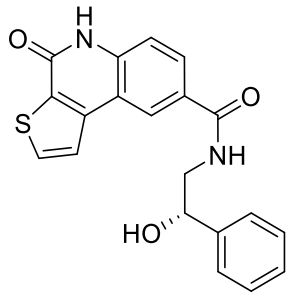	512±74	2
c19	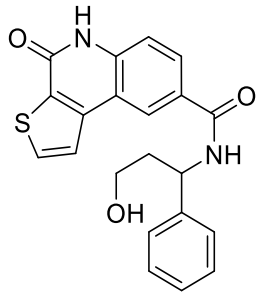	519	1
c20	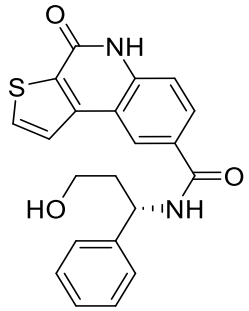	406	1
c21	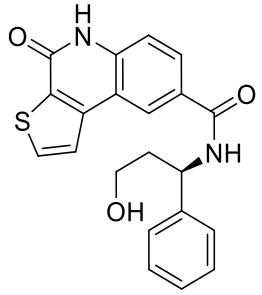	932±510	4
c22	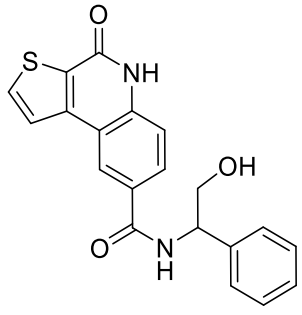	1860±1000	6

c23	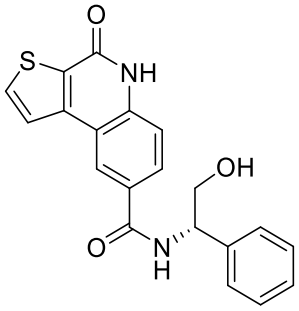	2370±1500	4
c24	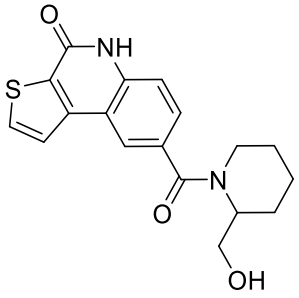	311±12	2
c25	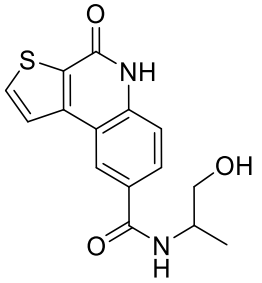	2270	1
c26	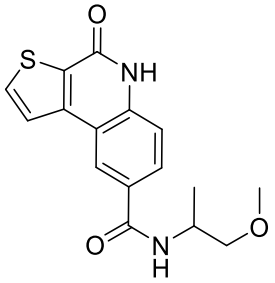	3160±1500	5
c27	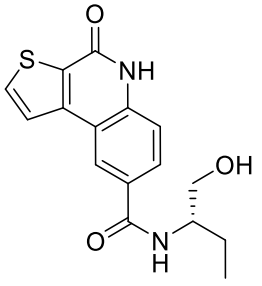	722	1

c28	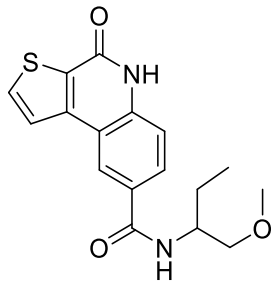	308	1
c29	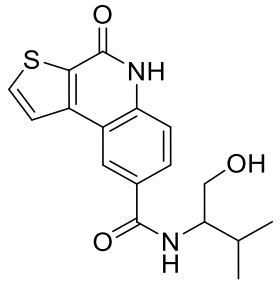	1340	1
c30	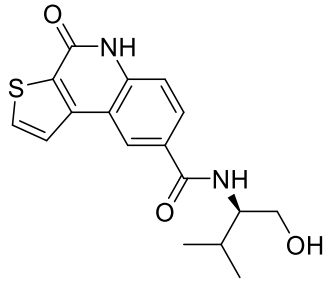	1290	1
c31	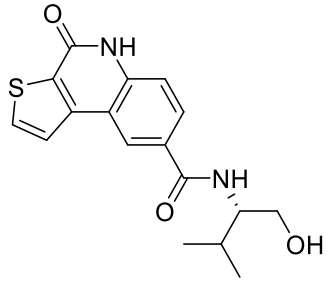	1830	1
c32	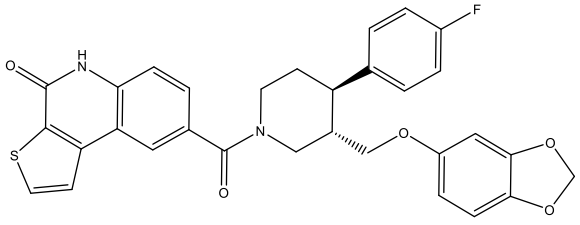	14900	1

c33	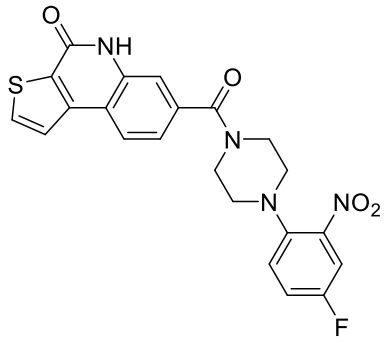	135±0.70	2
c34	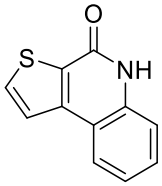	646±340	2
c35	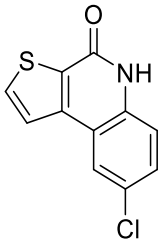	616±290	2
c36	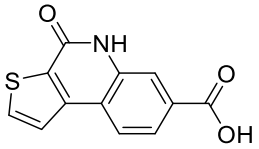	13400	1
c37	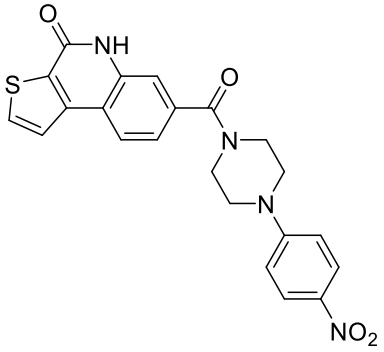	9.51±0.36	2
c38	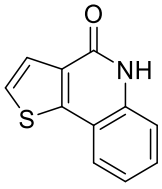	1480±480	3

c39	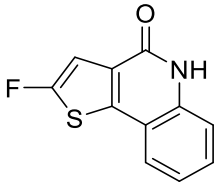	789±116	3
c40	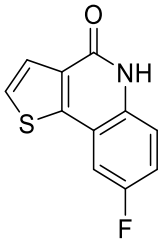	20300±12000	3
d1	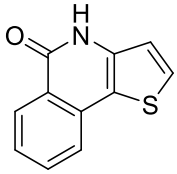	552±110	2
d2	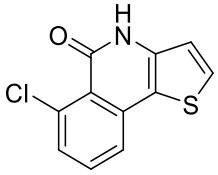	143±33	2
e1	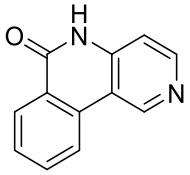	110	1
e2	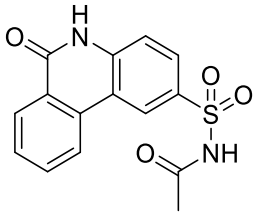	8290±1400	
e3	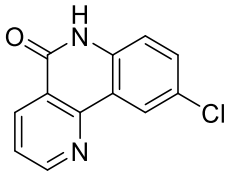	2160	1
e4	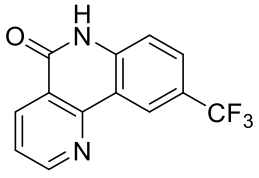	3970	1

e5	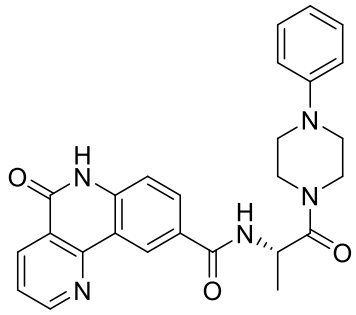	9130±3900	2
e6	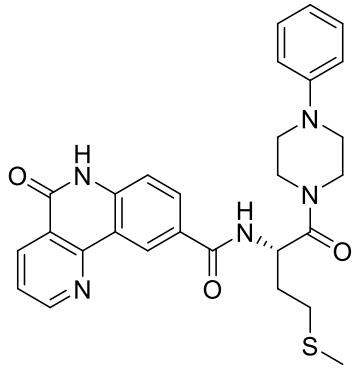	38600±3100	2
e7	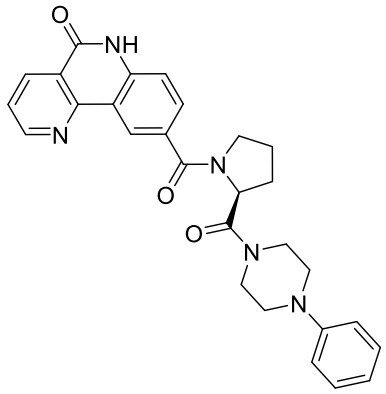	34400	0
e8	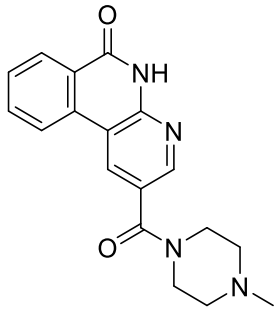	44100	1

e9	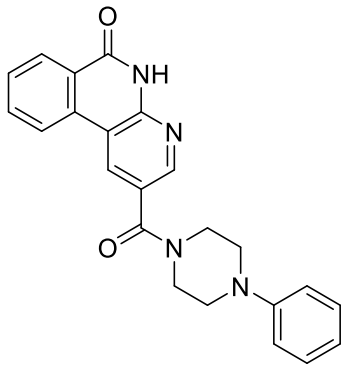	1390	1
e10	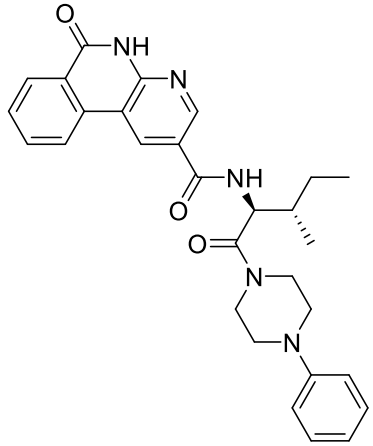	89400	1
e11	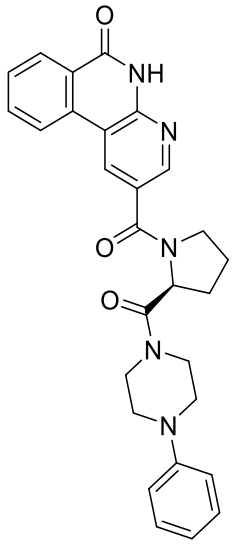	34400	1

e12	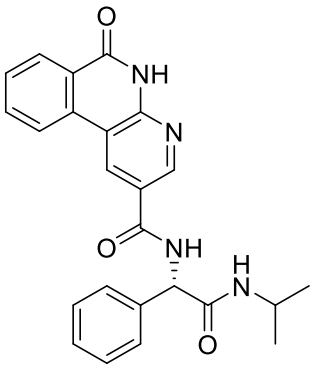	36700	1
e13	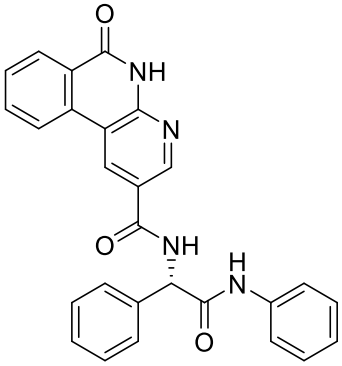	66800	1
s1	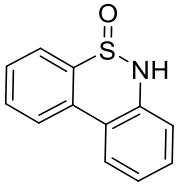	None	1
s2	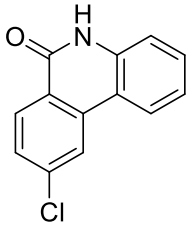	475±91	2
s3	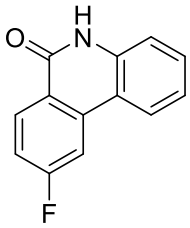	731±110	2
s4	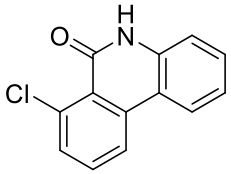	313±46	2

s5	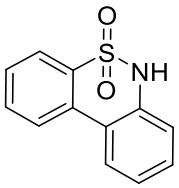	22100000	1
s6	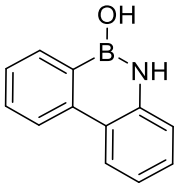	2070000	1
s7	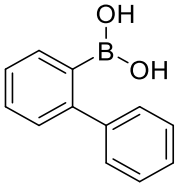	1170000±43000	2
s8	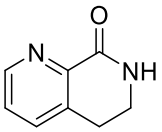	134000±32000	2
s9	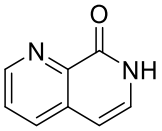	1130000	1
s10	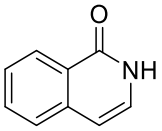	229000±140000	1
s11	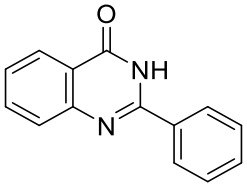	7570±2500	2
s12	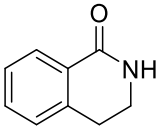	3870±2300	3
s13	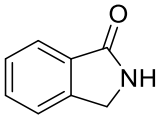	72000	1

s14	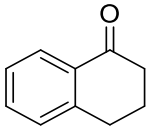	2400000	1
s15	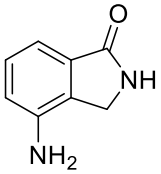	14900±3800	2
s16	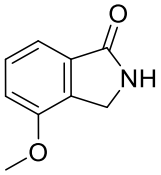	10400±5200	2
s17	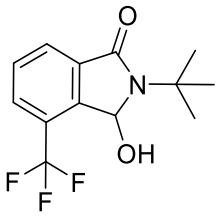	5950000	1
s18	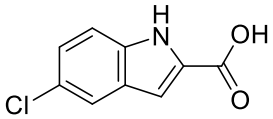	None	1
s19	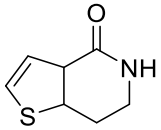	47400±18000	4
s20	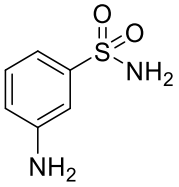	None	1
s21	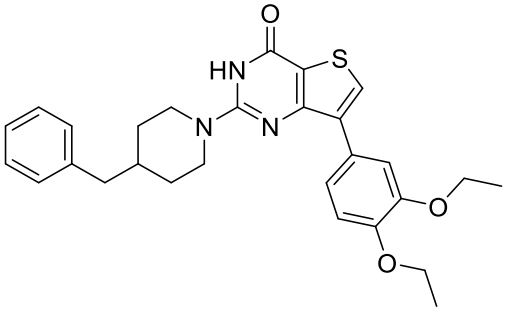	>100000	1

2. Characterization of molecules in the research

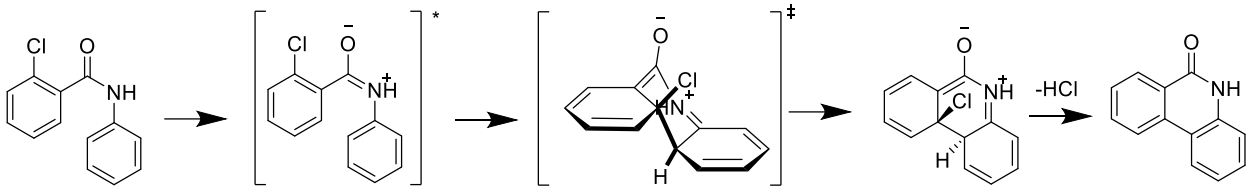

Figure S1 *Proposed photochemical cyclization to synthesize phenanthridinone compounds.*

Except as otherwise indicated, chemicals were ordered from Sigma-Aldrich, AK Scientific and Toronto Research Chemicals with the highest purity available. All solvent is purchased from Fisher Scientific. The instrument used for NMR analysis was the 7.05T Bruker Avance NMR Spectrometer equipped with 5 mm QNP probe for ^{1}H detection at 300 MHz and ^{13}C detection at 101MHz. The data was processed with Mnova 12.0.4. ^{1}H-NMR spectrum are reported relative to residual solvent: $CDCl_3$ (δ 7.26 ppm), DMSO-d_6 (δ 2.50 ppm), and they are reported as follows: chemical shift (δ/ ppm) (multiplicity, coupling constant (Hz), integration). Multiplicities are recognized and identified by Mnova software and reported as follows: s = singlet, d = doublet, t = triplet, q = quartet, m = multiplet. and ^{13}C-NMR spectrum are reported relative to residual solvent: $CDCl_3$ (δ 77.2 ppm), DMSO-d_6 (δ 39.5 ppm), and they are repoted as chemical shift (δ/ ppm) except otherwise stated (*e.g.* ^{13}C of C-F component). COSY and HSQC were used in the structural identification and reported for complicated compounds. The instrument used for high-resolution mass spectrometry (HRMS) analysis was the Bruker Daltonics Compact QTOF system. The ion source used for the measurement was ESI (electrospray ionization) and the source temperature was 180 °C. Samples were run in positive or negative mode. The spray voltages were + 3500V for the positive and - 3000V for the negative. The sheath gas flow was at 4 l/min and nebulizer gas was at 0.5 bar. Samples were introduced to the source by direct at 3 µl/min. HRMS was performed by a third-party service provider from the Dalhousie University. Theoretical molecular weight was calculated by ChemDraw 18.0. UV-mediated photochemical cyclization experiments were perfomed on a Vapourtec R-series system equipped with a UV-150 photochemical reactor. Chromatography was perfomed on a Teledyne ISCO Combiflash system.

6-(5*H*)-phenanthridinone, PJ34, olaparib, CPT, **s5-s21** are commercially available. **c3 e2 e3 e4 s2 s3 s4** was obtained from previous projects [(a) Fang, Y., and G. K. Tranmer. "Continuous flow photochemistry as an enabling synthetic technology: synthesis of substituted-6-(5*H*)-phenanthridinones for use as poly (ADP-ribose) polymerase inhibitors." *MedChemComm*, vol. 7, no. 4, 2016, pp. 720–24, https://doi.org/10.1039/c5md00552c. (b) Fang, Y., and G. K. Tranmer. "Expedited access to thieno [3, 2-*c*] quinolin-4 (5*H*)-ones and benzo [*h*]-1, 6-naphthyridin-5 (6*H*)-ones via a continuous flow photocyclization method." *Organic & Biomolecular Chemistry*, vol. 14, no. 46, 2016, pp. 10799–803, https://doi.org/10.1039/c6ob02279k.

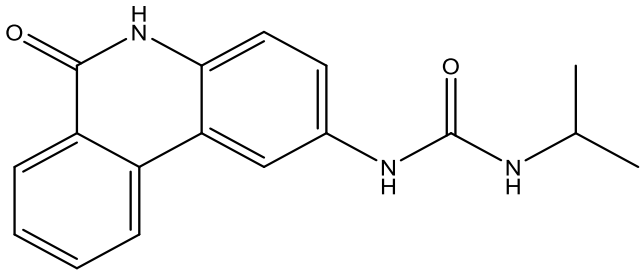

1-isopropyl-3-(6-oxo-5,6-dihydrophenanthridin-2-yl)urea (**a1**)

Using **Synthesis Method e**, 24mg (0.1mmol) **f2** was reacted with 6mg (0.1mmol) propan-2-amine to give 10.2mg **a1** (Yield: 35%) and the product was separated as yellowish white solid. ^{1}H NMR (400 MHz, DMSO-d_6) δ 11.54 (s, 1H), 8.45 (d, *J* = 1.7 Hz, 1H), 8.41 – 8.30 (m, 2H), 8.27 (d, *J* = 8.2 Hz, 1H), 7.91 – 7.83 (m, 1H), 7.64 (t, *J* = 7.5 Hz, 1H), 7.41 (dd, *J* = 8.7, 1.9 Hz, 1H), 7.26 (d, *J* = 8.7 Hz, 1H), 6.06 (d, *J* = 7.5 Hz, 1H), 3.87 – 3.74 (m, *J* = 6.5 Hz, 1H), 1.13 (d, *J* = 6.5 Hz, 6H).^{13}C NMR (101 MHz, DMSO) δ 160.8, 155.3, 136.0, 134.6, 133.2, 131.6, 128.3, 128.1, 126.4, 122.6, 121.4, 118.0, 116.9, 111.6, 41.5, 23.5. HRMS m/z (ESI-, M-H): Calcd for C17H17N3O2: 294.1248, (ESI-, M-H) found: 294.1242

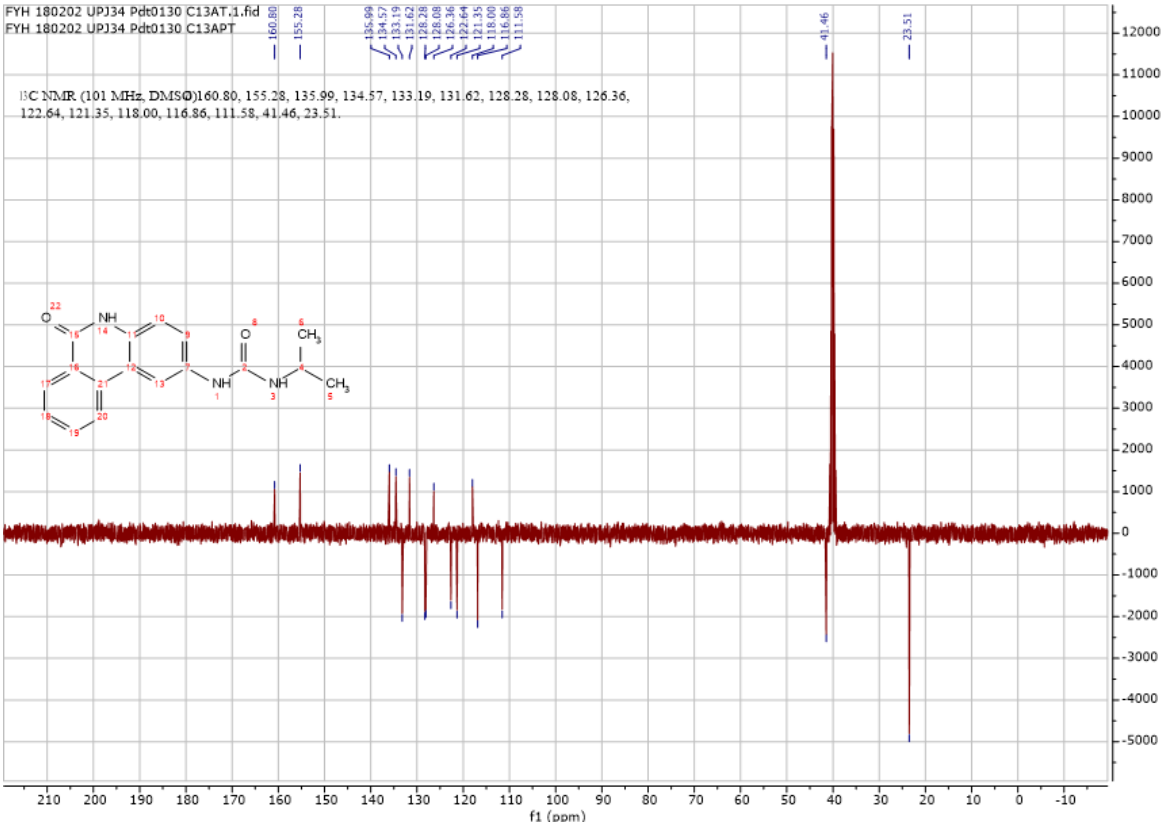
FYH 180202 UPJ34 Pdt0130 C13AT.1.fid
FYH 180202 UPJ34 Pdt0130 C13APT
160.80
155.28
135.99
134.57
133.19
131.62
128.28
128.08
126.36
122.64
121.35
118.00
116.86
111.58
41.46
23.51
13C NMR (101 MHz, DMSO) δ 160.80, 155.28, 135.99, 134.57, 133.19, 131.62, 128.28, 128.08, 126.36, 122.64, 121.35, 118.00, 116.86, 111.58, 41.46, 23.51.
f1 (ppm)

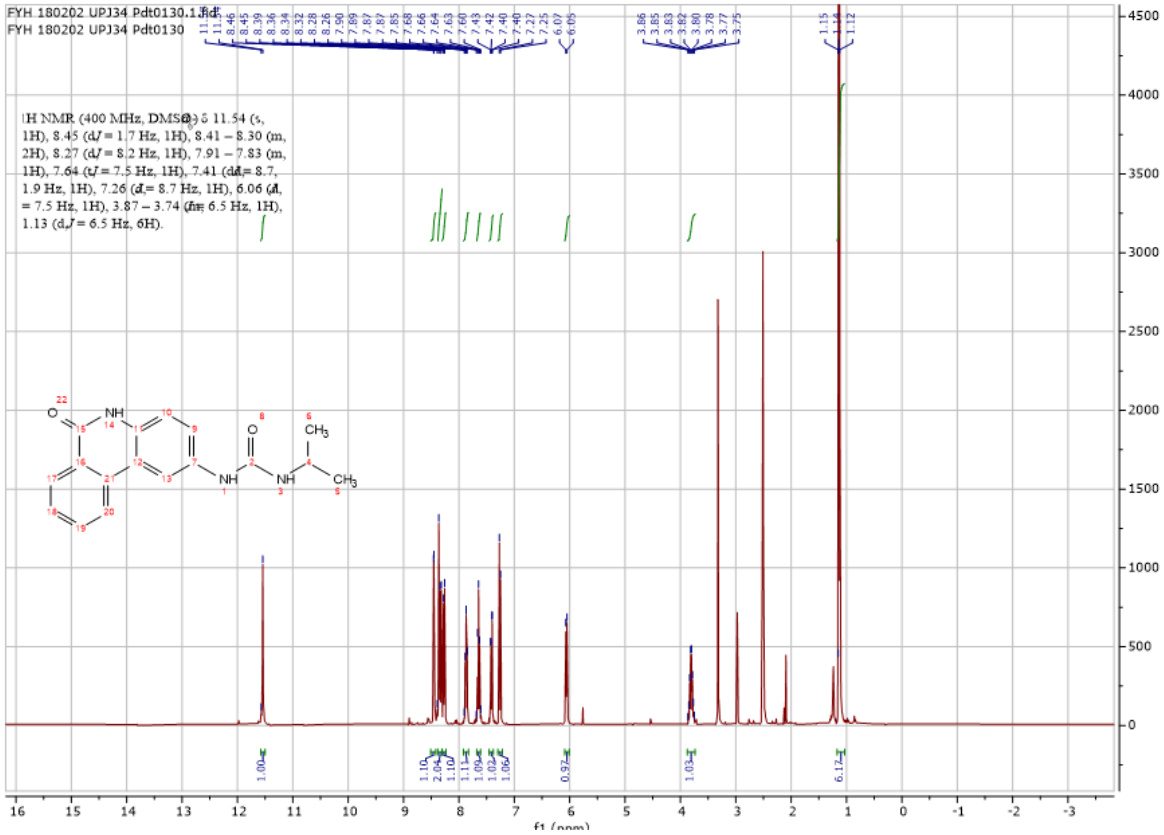
FYH 180202 UPJ34 Pdt0130.1.fid
FYH 180202 UPJ34 Pdt0130
1H NMR (400 MHz, DMSO-d6) δ 11.54 (s, 1H), 8.45 (d, J = 1.7 Hz, 1H), 8.41 – 8.30 (m, 2H), 8.27 (d, J = 8.2 Hz, 1H), 7.91 – 7.83 (m, 1H), 7.64 (t, J = 7.5 Hz, 1H), 7.41 (dd, J = 8.7, 1.9 Hz, 1H), 7.26 (d, J = 8.7 Hz, 1H), 6.06 (d, J = 7.5 Hz, 1H), 3.87 – 3.74 (m, 1H), 1.13 (d, J = 6.5 Hz, 6H).
f1 (ppm)

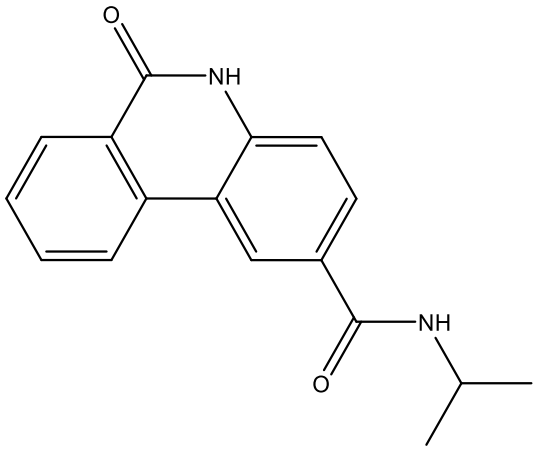

***N*-isopropyl-6-oxo-5,6-dihydrophenanthridine-2-carboxamide (a2)**

Using **Synthesis Method d**, 24mg (0.1mmol) **f2** was reacted with 6mg (0.1mmol) propan-2-amine to give 23.5mg **a2** (Yield: 84%) and the product was separated as yellowish white solid. ^{1}H NMR (300 MHz, DMSO-d_6) δ 11.87 (s, 1H), 8.85 (d, J = 1.9 Hz, 1H), 8.60 (d, J = 8.2 Hz, 1H), 8.34 (dd, J = 8.0, 1.6 Hz, 2H), 8.02 – 7.90 (m, 2H), 7.69 (t, J = 7.5 Hz, 1H), 7.40 (d, J = 8.5 Hz, 1H), 4.23 – 4.07 (m, 1H), 1.23 (d, J = 6.6 Hz, 6H). ^{13}C NMR (75 MHz, DMSO) δ 165.1, 161.3, 146.1, 138.6, 134.5, 133.4, 129.3, 128.9 128.8, 128.0, 126.1, 123.3, 122.6, 116.4, 41.6, 23.0. HRMS m/z (ESI-, M-H): Calcd for C17H16N2O2: 279.1139, (ESI-, M-H) found: 279.1143

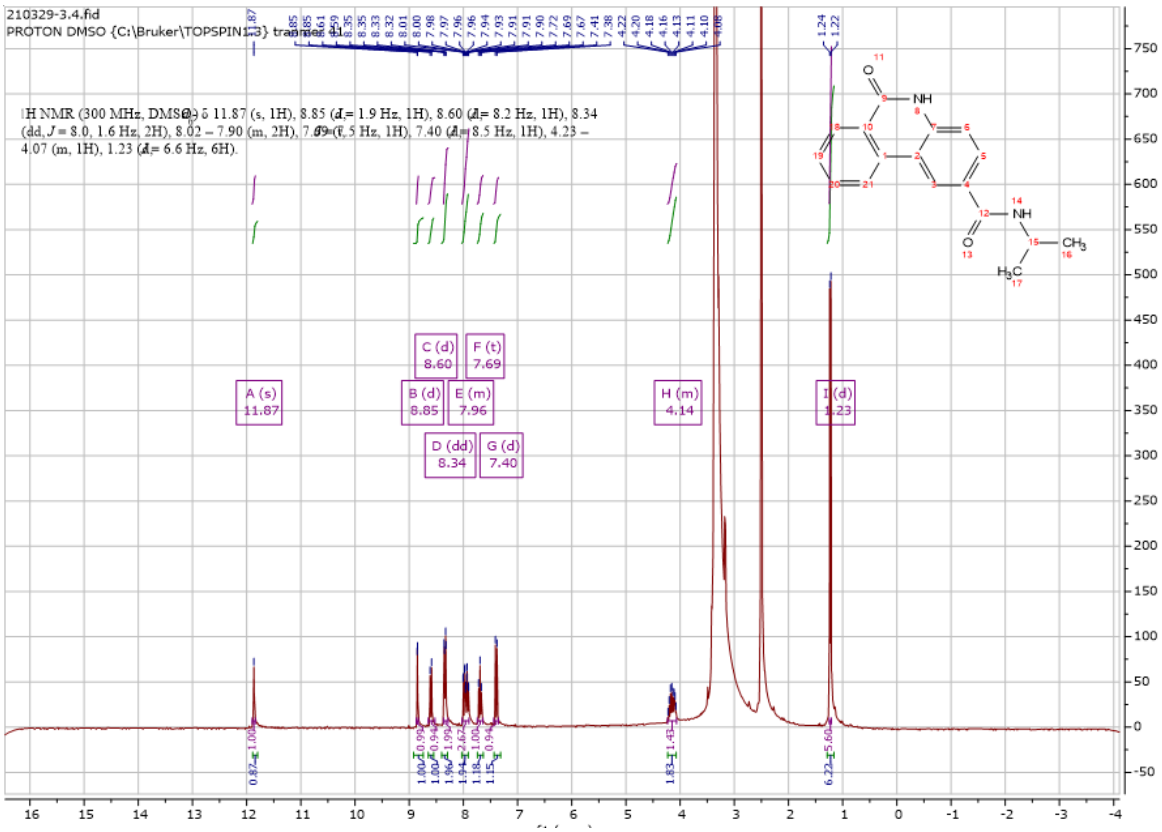
210329-3.4.fid
PROTON DMSO {C:\Bruker\TOPSPIN1.3} tranmer 41
1H NMR (300 MHz, DMSO) δ 11.87 (s, 1H), 8.85 (d, J = 1.9 Hz, 1H), 8.60 (d, J = 8.2 Hz, 1H), 8.34 (dd, J = 8.0, 1.6 Hz, 2H), 8.02 – 7.90 (m, 2H), 7.69 (t, J = 7.5 Hz, 1H), 7.40 (d, J = 8.5 Hz, 1H), 4.23 – 4.07 (m, 1H), 1.23 (d, J = 6.6 Hz, 6H).
A (s) 11.87
B (d) 8.85
C (d) 8.60
D (dd) 8.34
E (m) 7.96
F (t) 7.69
G (d) 7.40
H (m) 4.14
I (d) 1.23
f1 (ppm)

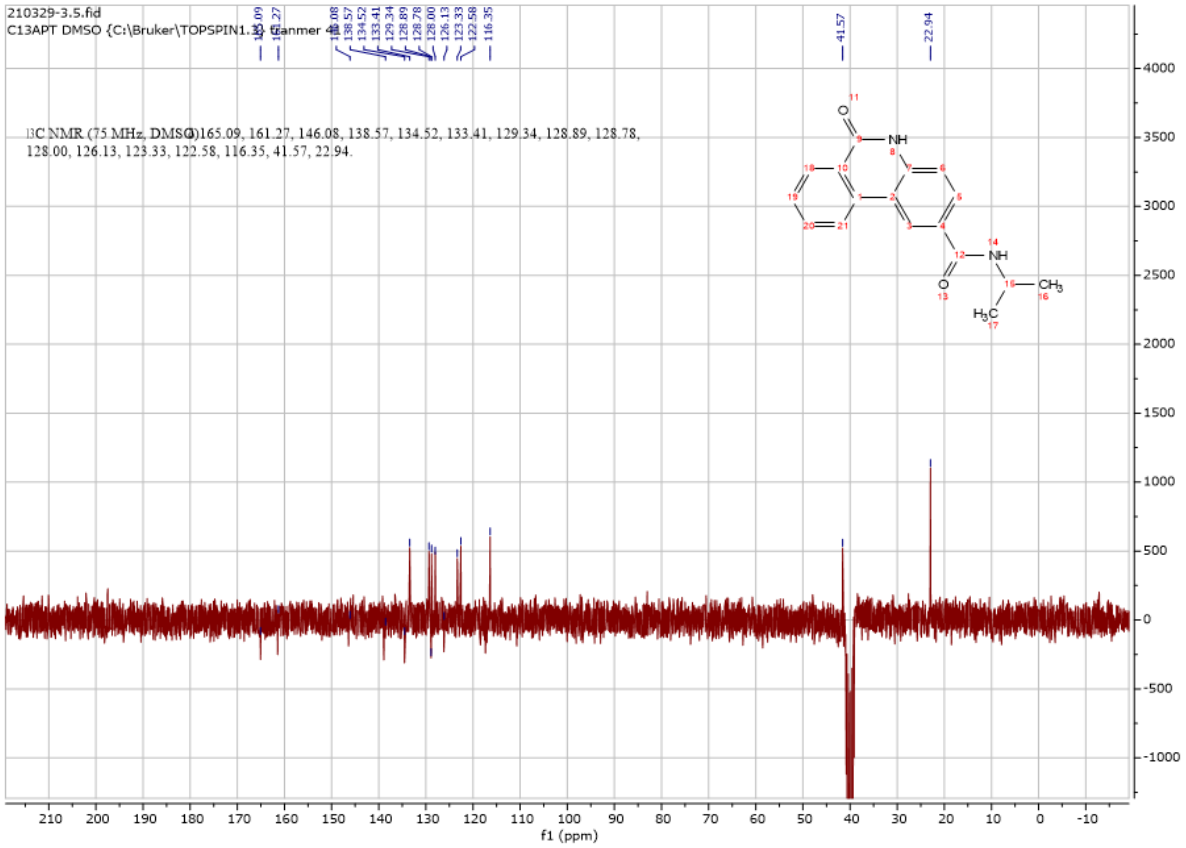
210329-3.5.fid
C13APT DMSO {C:\Bruker\TOPSPIN1.3} tranmer 41
13C NMR (75 MHz, DMSO) 165.09, 161.27, 146.08, 138.57, 134.52, 133.41, 129.34, 128.89, 128.78, 128.00, 126.13, 123.33, 122.58, 116.35, 41.57, 22.94.
f1 (ppm)

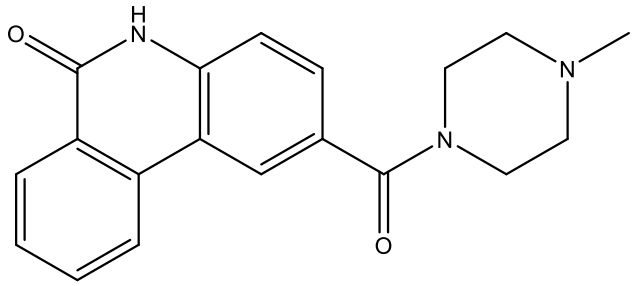

2-(4-methylpiperazine-1-carbonyl)phenanthridin-6(5*H*)-one (a3)

Using **Synthesis Method d**, 24mg (0.1mmol) **f2** was reacted with 10mg (0.1mmol) 4-methylpiperidine to give 19.9mg **a3** (Yield: 62%) and the product was separated as yellowish white solid. ^{1}H NMR (400 MHz, DMSO-d_6) δ 11.85 (s, 1H), 8.58 (d, *J* = 8.1 Hz, 1H), 8.40 (d, *J* = 1.5 Hz, 1H), 8.34 (dd, *J* = 7.9, 1.2 Hz, 1H), 7.92 – 7.83 (m, 1H), 7.72 – 7.64 (m, 1H), 7.52 (dd, *J* = 8.3, 1.7 Hz, 1H), 7.41 (d, *J* = 8.3 Hz, 1H), 3.47 (d, *J* = 46.6 Hz, 4H), 2.35 (s, 4H), 2.21 (s, 3H). ^{13}C NMR (101 MHz, DMSO) δ 169.2, 161.3, 137.8, 134.3, 133.5, 130.3, 128.9, 128.8, 128.0, 126.3, 123.4, 122.8, 117.7, 116.5, 61.3, 55.0, 46.1. HRMS m/z (ESI+, M+Na): HRMS m/z (ESI+, M+Na): Calcd for C19H19N3O2: 322.1550, (ESI+, M+Na) found: 322.1556

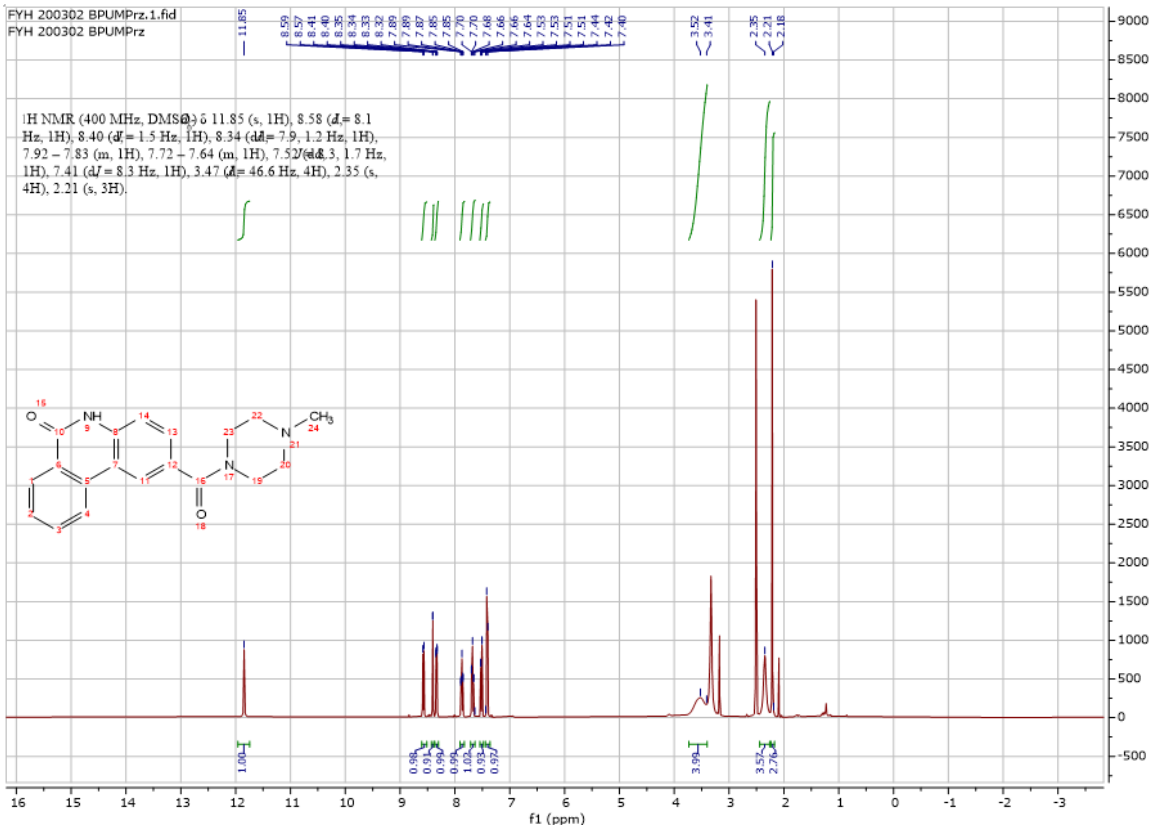
FYH 200302 BPUMPrz.1.fid
FYH 200302 BPUMPrz
1H NMR (400 MHz, DMSO) δ 11.85 (s, 1H), 8.58 (d, J = 8.1 Hz, 1H), 8.40 (d, J = 1.5 Hz, 1H), 8.34 (dd, J = 7.9, 1.2 Hz, 1H), 7.92 – 7.83 (m, 1H), 7.72 – 7.64 (m, 1H), 7.52 (dd, J = 8.3, 1.7 Hz, 1H), 7.41 (d, J = 8.3 Hz, 1H), 3.47 (s, 4H), 2.35 (s, 4H), 2.21 (s, 3H).
f1 (ppm)

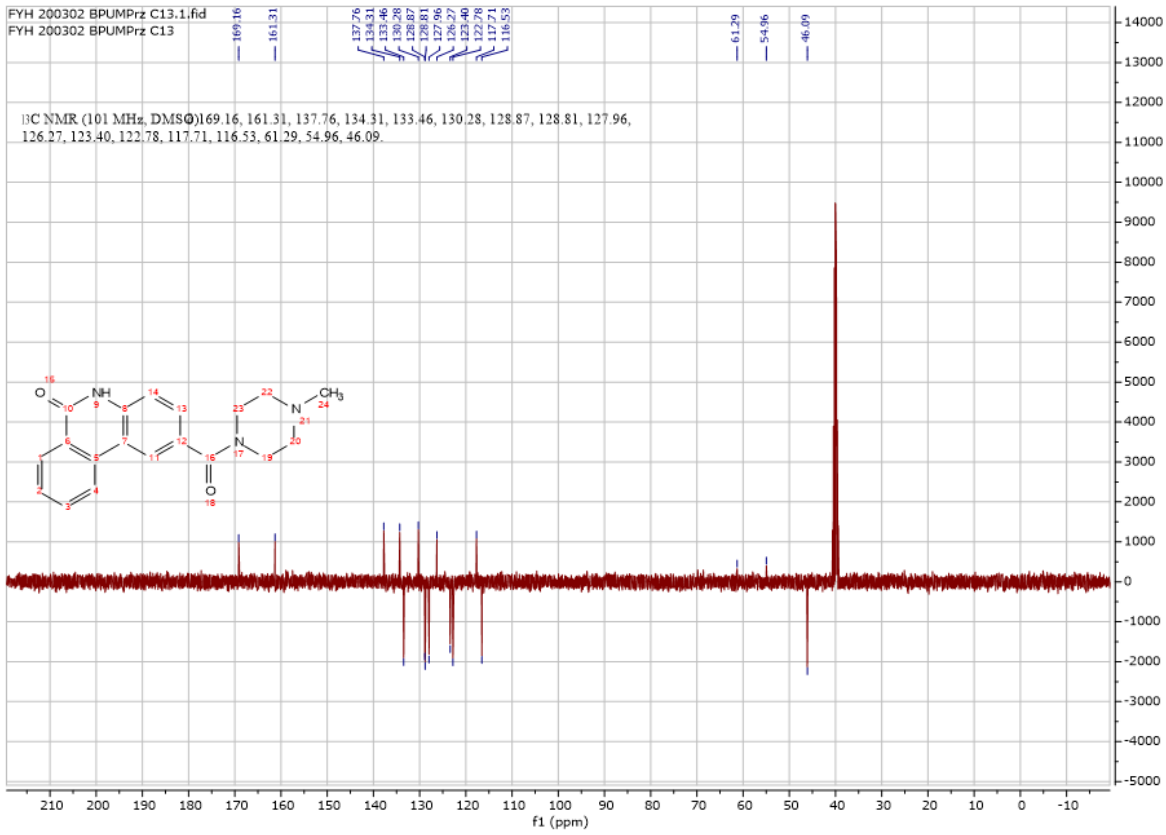
FYH 200302 BPUMPrz C13.1.fid
FYH 200302 BPUMPrz C13
13C NMR (101 MHz, DMSO) 169.16, 161.31, 137.76, 134.31, 133.46, 130.28, 128.87, 128.81, 127.96, 126.27, 123.40, 122.78, 117.71, 116.53, 61.29, 54.96, 46.09.
f1 (ppm)

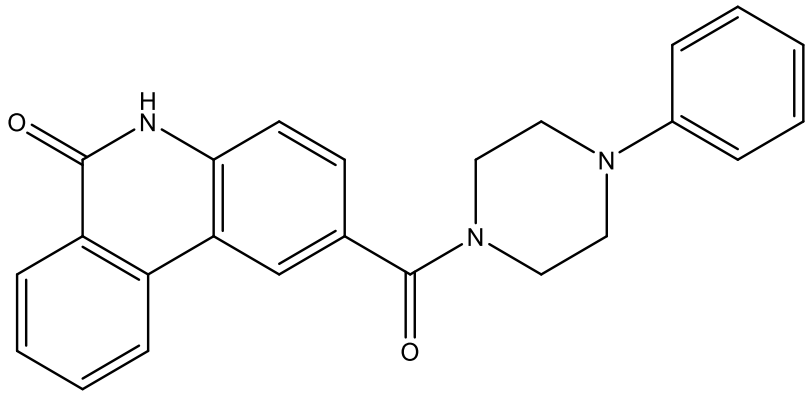

2-(4-phenylpiperazine-1-carbonyl)phenanthridin-6(5*H*)-one (a4)

Using **Synthesis Method d**, 24mg (0.1mmol) **f2** was reacted with 16mg (0.1mmol) 4-methylpiperidine to give 33mg **a4** (Yield: 86%) and the product was separated as yellow solid. ^{1}H NMR (300 MHz, DMSO-d_6) δ 11.86 (s, 1H), 8.59 (d, *J* = 8.1 Hz, 1H), 8.47 (d, *J* = 1.7 Hz, 1H), 8.34 (dd, *J* = 8.0, 1.4 Hz, 1H), 7.87 (td, *J* = 7.7, 1.5 Hz, 1H), 7.68 (t, *J* = 7.6 Hz, 1H), 7.58 (dd, *J* = 8.3, 1.7 Hz, 1H), 7.43 (d, *J* = 8.3 Hz, 1H), 7.29 – 7.18 (m, 2H), 6.97 (d, *J* = 8.2 Hz, 2H), 6.82 (t, *J* = 7.2 Hz, 1H), 3.69 (s, 4H), 3.22 (s, 4H). ^{13}C NMR (75 MHz, DMSO) δ 169.2, 161.3, 151.3, 137.8, 134.3, 133.5, 130.1, 129.5, 129.0, 128.8, 128.0, 126.3, 123.4, 122.9, 119.8, 117.7, 116.6, 116., 49.0. HRMS m/z (ESI+, M+Na): Calcd for C24H21N3O2: 406.1531, (ESI+, M+Na) found: 406.1531

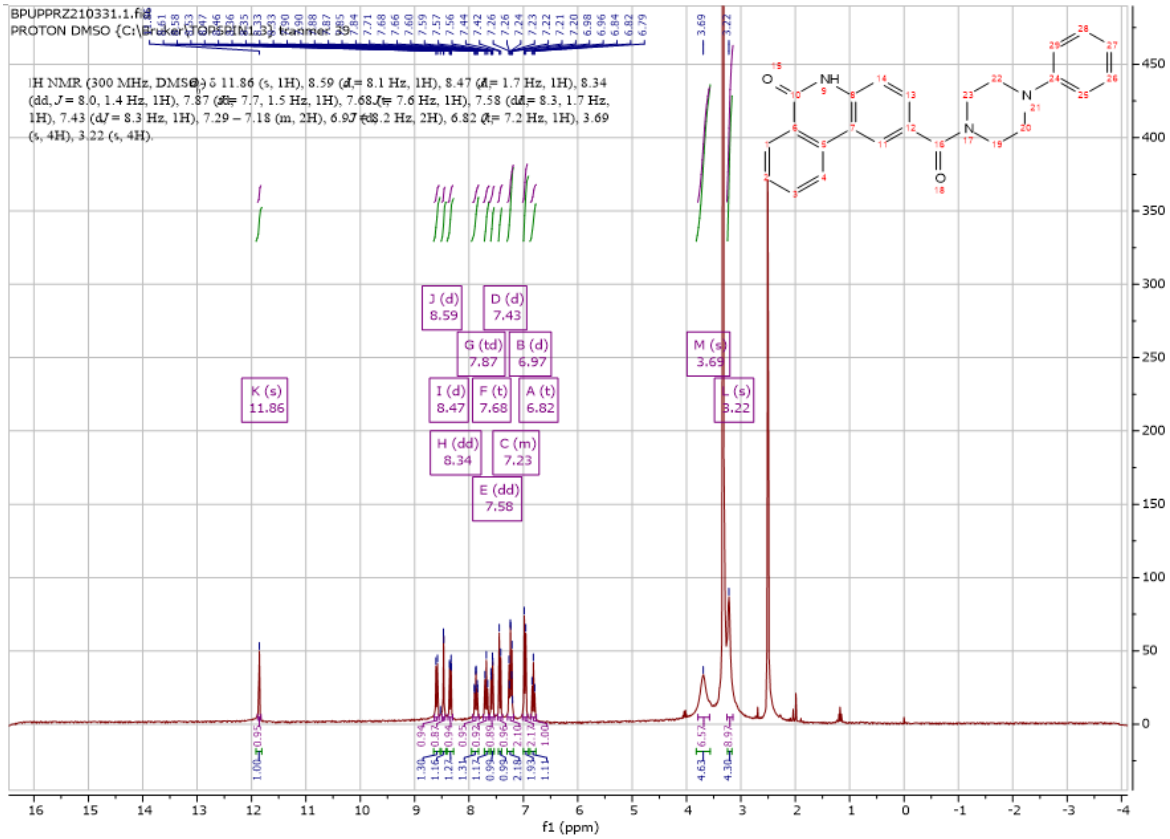
BPUPPRZ210331.1.fid
PROTON DMSO {C:\Bruker\TOPSPIN4.3} Eanmer 39
1H NMR (300 MHz, DMSO) δ 11.86 (s, 1H), 8.59 (d, J = 8.1 Hz, 1H), 8.47 (d, J = 1.7 Hz, 1H), 8.34 (dd, J = 8.0, 1.4 Hz, 1H), 7.87 (td, J = 7.7, 1.5 Hz, 1H), 7.68 (t, J = 7.6 Hz, 1H), 7.58 (dd, J = 8.3, 1.7 Hz, 1H), 7.43 (d, J = 8.3 Hz, 1H), 7.29 – 7.18 (m, 2H), 6.97 (d, J = 8.2 Hz, 2H), 6.82 (t, J = 7.2 Hz, 1H), 3.69 (s, 4H), 3.22 (s, 4H).
J (d) 8.59
D (d) 7.43
G (td) 7.87
B (d) 6.97
M (s) 3.69
K (s) 11.86
I (d) 8.47
F (t) 7.68
A (t) 6.82
L (s) 3.22
H (dd) 8.34
C (m) 7.23
E (dd) 7.58
f1 (ppm)

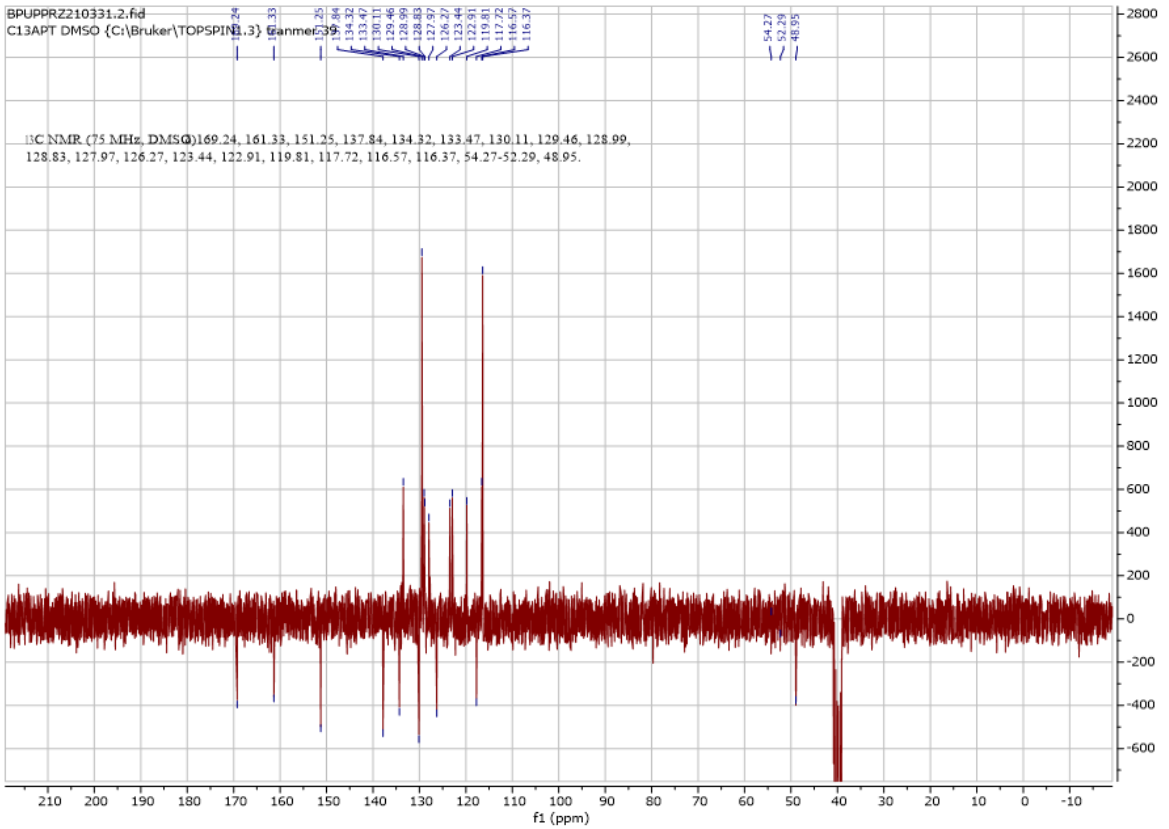
BPUPPRZ210331.2.fid
C13APT DMSO {C:\Bruker\TOPSPIN4.3} Eanmer 39
13C NMR (75 MHz, DMSO) 169.24, 161.33, 151.25, 137.84, 134.32, 133.47, 130.11, 129.46, 128.99, 128.83, 127.97, 126.27, 123.44, 122.91, 119.81, 117.72, 116.57, 116.37, 54.27-52.29, 48.95.
f1 (ppm)

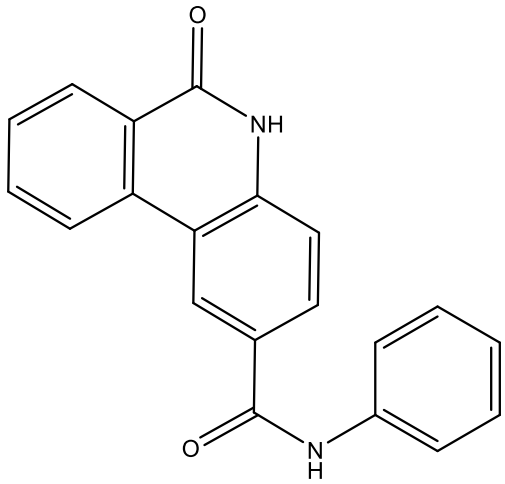

6-oxo-*N*-phenyl-5,6-dihydrophenanthridine-2-carboxamide (a5)

Using **Synthesis Method d**, 24mg (0.1mmol) **f2** was reacted with 9.4mg (0.1mmol) 4-methylpiperidine to give 29mg **a5** (Yield: 92%) and the product was separated as yellowish white solid. ^{1}H NMR (300 MHz, DMSO-d_6) δ 12.36 (s, 1H), 10.45 (s, 1H), 9.32 (d, J = 2.2 Hz, 1H), 9.04 (d, J = 2.1 Hz, 1H), 8.66 (d, J = 8.1 Hz, 1H), 8.37 (dd, J = 8.0, 1.4 Hz, 1H), 7.98 (td, J = 8.0, 7.6, 1.5 Hz, 1H), 7.85 – 7.71 (m, 4H), 7.47 – 7.35 (m, 2H), 7.15 (t, J = 7.2 Hz, 1H). ^{13}C NMR (75 MHz, DMSO) δ 164.0, 162.1, 149.7, 139.5, 139.3, 137.5, 133.7, 133.0, 131.8, 129.6, 129.6, 129.2, 128.1, 126.3, 124.4, 124.0, 121.0, 113.0. HRMS m/z (ESI-1, M-H): Calcd for C20H14N2O2: 313.0983, found 314.0937.

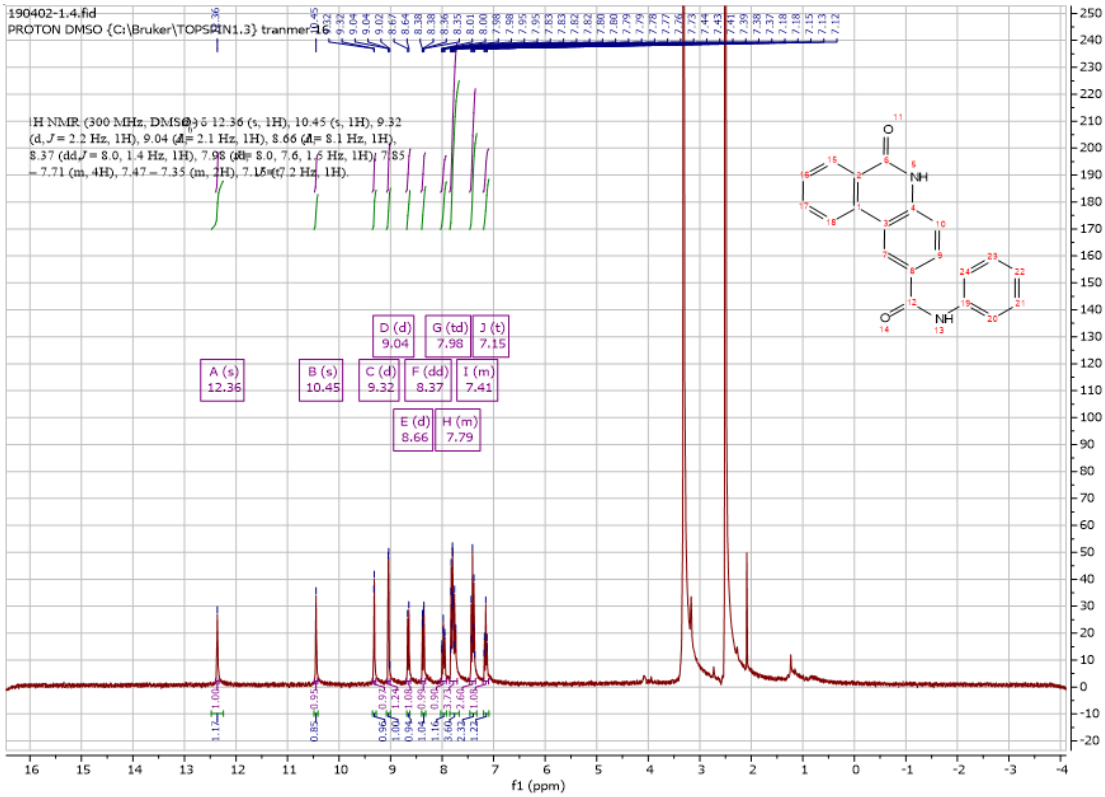
190402-1.4.fid
PROTON DMSO {C:\Bruker\TOPSPIN1.3} tranmer 16
H NMR (300 MHz, DMSO) δ 12.36 (s, 1H), 10.45 (s, 1H), 9.32 (d, J = 2.2 Hz, 1H), 9.04 (d, J = 2.1 Hz, 1H), 8.66 (d, J = 8.1 Hz, 1H), 8.37 (dd, J = 8.0, 1.4 Hz, 1H), 7.98 (td, J = 8.0, 7.6, 1.5 Hz, 1H), 7.85 – 7.71 (m, 4H), 7.47 – 7.35 (m, 2H), 7.15 (t, J = 7.2 Hz, 1H).
A (s) 12.36
B (s) 10.45
C (d) 9.32
D (d) 9.04
E (d) 8.66
F (dd) 8.37
G (td) 7.98
H (m) 7.79
I (m) 7.41
J (t) 7.15
f1 (ppm)

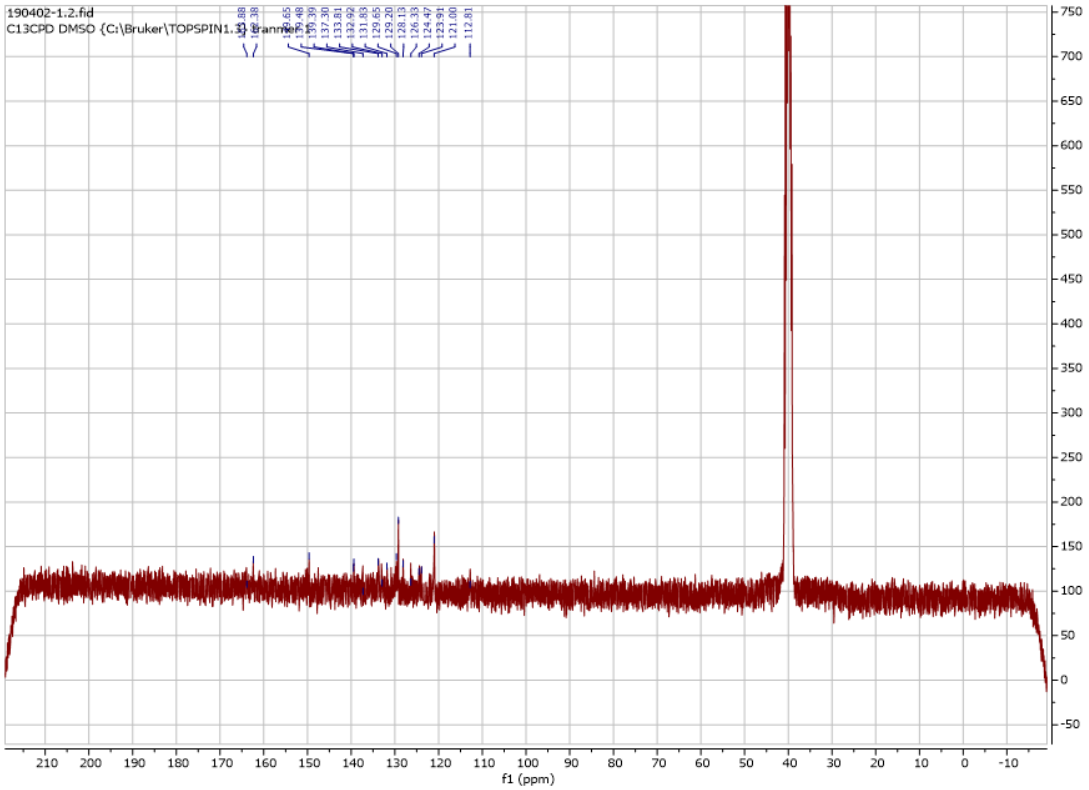
190402-1.2.fid
C13CPD DMSO {C:\Bruker\TOPSPIN1.3} tranmer 16
f1 (ppm)

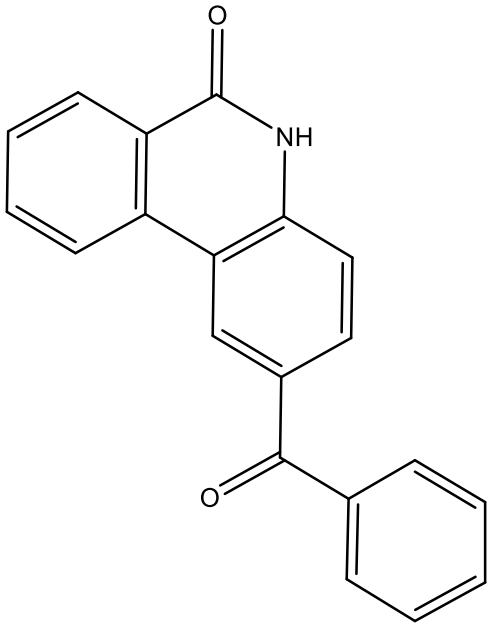

2-benzoylphenanthridin-6(5*H*)-one (a6)

Using **Synthesis Method c**, 176mg (1mmol) 2-chlorobenzoyl chloride was reacted with 196mg (1mmol) (4-aminophenyl)(phenyl)methanone to give 10.2mg (Yield: 3%) **a6** and the product was separated as yellow solid. ^{1}H NMR (300 MHz, DMSO-d_6) δ 8.72 (d, *J* = 1.9 Hz, 1H), 8.46 (d, *J* = 8.1 Hz, 1H), 8.35 (dd, *J* = 8.0, 1.5 Hz, 1H), 7.92 – 7.84 (m, 2H), 7.83 – 7.78 (m, 2H), 7.71 (ddt, *J* = 8.0, 4.7, 2.7 Hz, 3H), 7.60 (dd, *J* = 8.2, 6.7 Hz, 2H), 7.50 (d, *J* = 8.5 Hz, 1H). ^{13}C NMR (75 MHz, DMSO) δ 195.2, 161.5, 140.3, 140.3 137.9, 134.1, 133.8, 133.0, 133.0, 131.4, 130.1, 129.1, 128., 126.3, 125.9, 123.2, 117.6, 116.7. HRMS m/z (ESI+, M+Na): Calcd for C20H13NO2: 322.0844, (ESI+, M+Na) found: 322.0839

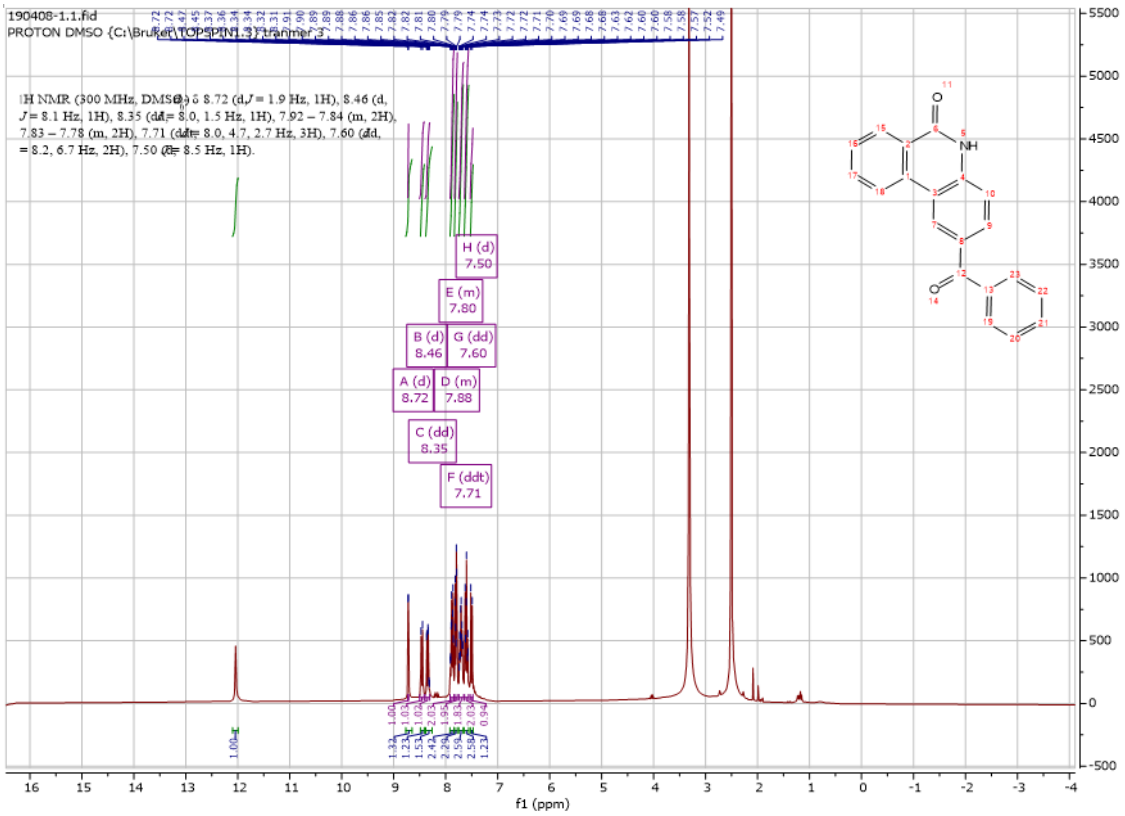
190408-1.1.fid
PROTON DMSO {C:\Bruker\TOPSPIN1.3} Tranmer 3
1H NMR (300 MHz, DMSO) δ 8.72 (d, J = 1.9 Hz, 1H), 8.46 (d, J = 8.1 Hz, 1H), 8.35 (dd, J = 8.0, 1.5 Hz, 1H), 7.92 – 7.84 (m, 2H), 7.83 – 7.78 (m, 2H), 7.71 (ddt, J = 8.0, 4.7, 2.7 Hz, 3H), 7.60 (dd, J = 8.2, 6.7 Hz, 2H), 7.50 (d, J = 8.5 Hz, 1H).
H (d) 7.50
E (m) 7.80
B (d) 8.46
G (dd) 7.60
A (d) 8.72
D (m) 7.88
C (dd) 8.35
F (ddt) 7.71
NH
f1 (ppm)

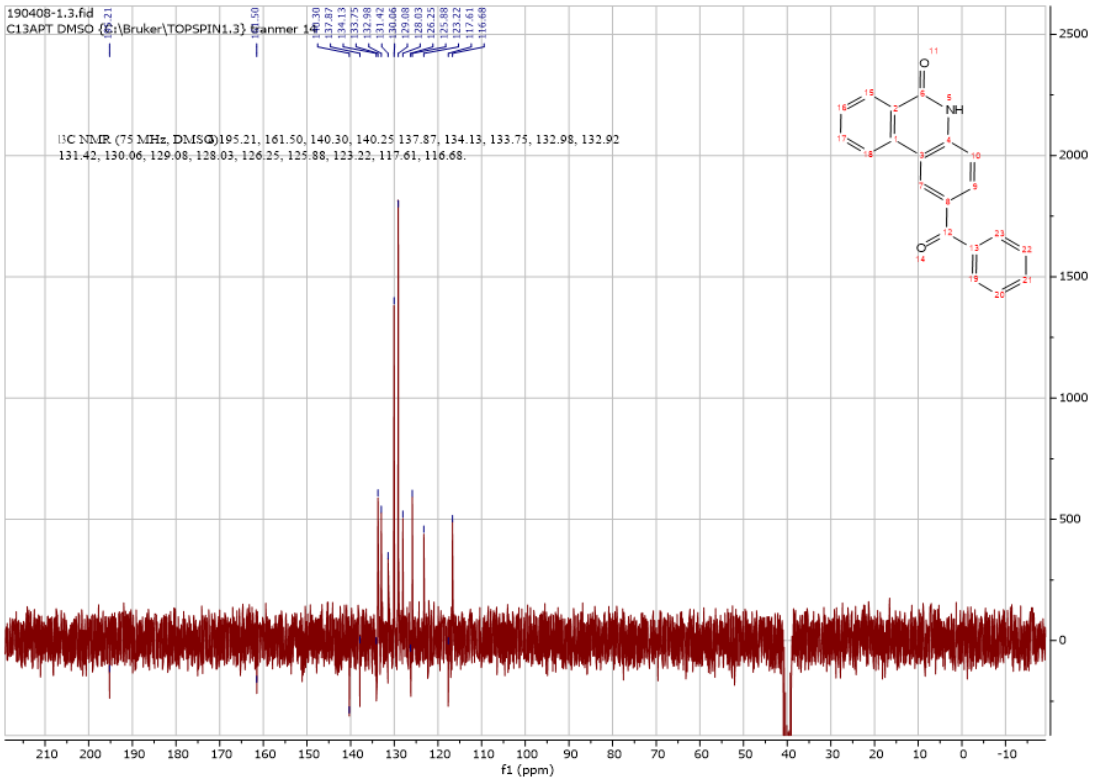
190408-1.3.fid
C13APT DMSO {C:\Bruker\TOPSPIN1.3} Tranmer 14
13C NMR (75 MHz, DMSO) δ 195.21, 161.50, 140.30, 140.25, 137.87, 134.13, 133.75, 132.98, 132.92, 131.42, 130.06, 129.08, 128.03, 126.25, 125.88, 123.22, 117.61, 116.68.
NH
f1 (ppm)

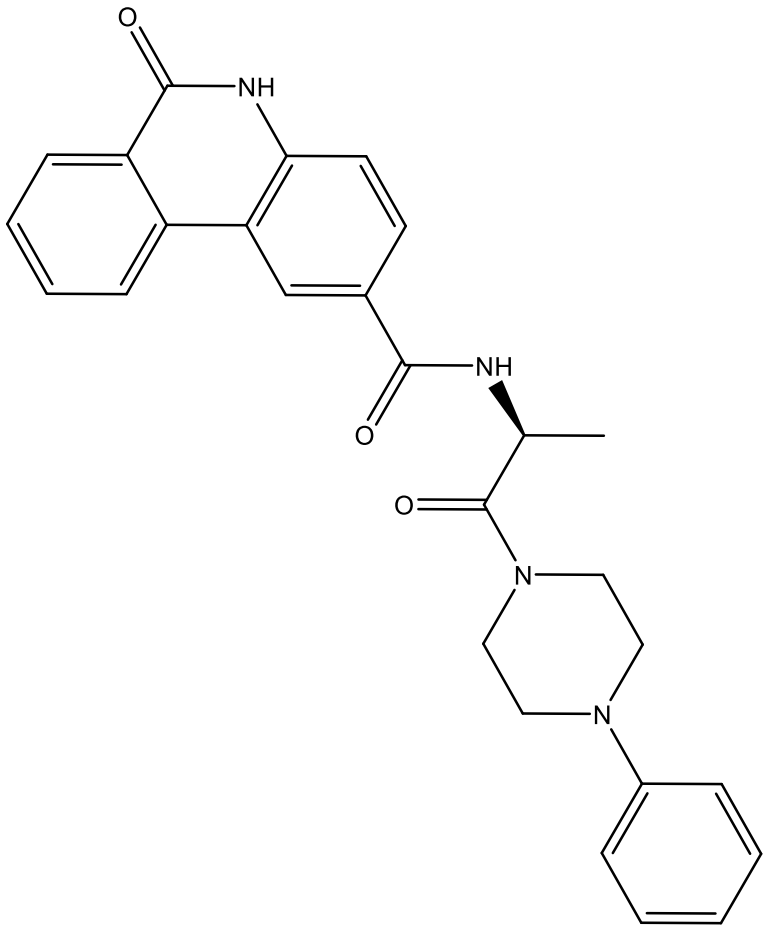

(*S*)-6-oxo-*N*-(1-oxo-1-(4-phenylpiperazin-1-yl)propan-2-yl)-5,6-dihydrophenanthridine-2-carboxamide (a7)

Using **Synthesis Method d**, 24mg (0.1mmol) **f2** was reacted with 24mg (0.1mmol) **f16** to give 36mg **a7** (Yield: 79%) and the product was separated as yellowish white solid. ^{1}H NMR (300 MHz, DMSO-d_6) δ 11.90 (s, 1H), 8.98 (s, 1H), 8.89 (d, *J* = 7.7 Hz, 1H), 8.62 (d, *J* = 8.1 Hz, 1H), 8.34 (d, *J* = 7.8 Hz, 1H), 8.04 (d, *J* = 8.6 Hz, 1H), 7.91 (q, *J* = 7.7 Hz, 1H), 7.69 (t, *J* = 7.4 Hz, 1H), 7.41 (d, *J* = 8.5 Hz, 1H), 7.21 (t, *J* = 7.9 Hz, 2H), 6.95 (d, *J* = 8.1 Hz, 2H), 6.80 (t, *J* = 7.2 Hz, 1H), 5.15 – 5.04 (m, 1H), 3.72 (m, 4H), 3.15 (m, 3H), 1.38 (d, *J* = 6.9 Hz, 2H), 1.18 (dd, *J* = 13.3, 8.0 Hz, 2H). ^{13}C NMR (75 MHz, DMSO) δ 170.9, 165.3, 161.4, 151.2, 139.2, 134.5, 133.4, 129.6, 129.4, 128.8, 128.0, 127.8, 126.2, 123.4, 123.0, 119.8, 117.4, 116.4, 116.3, 49.2, 48.8, 45.5, 45.1, 41.8, 18.0. HRMS m/z (ESI+, M+Na): Calcd for C27H26N4O3: 477.1903, (ESI+, M+Na) found: 477.1901

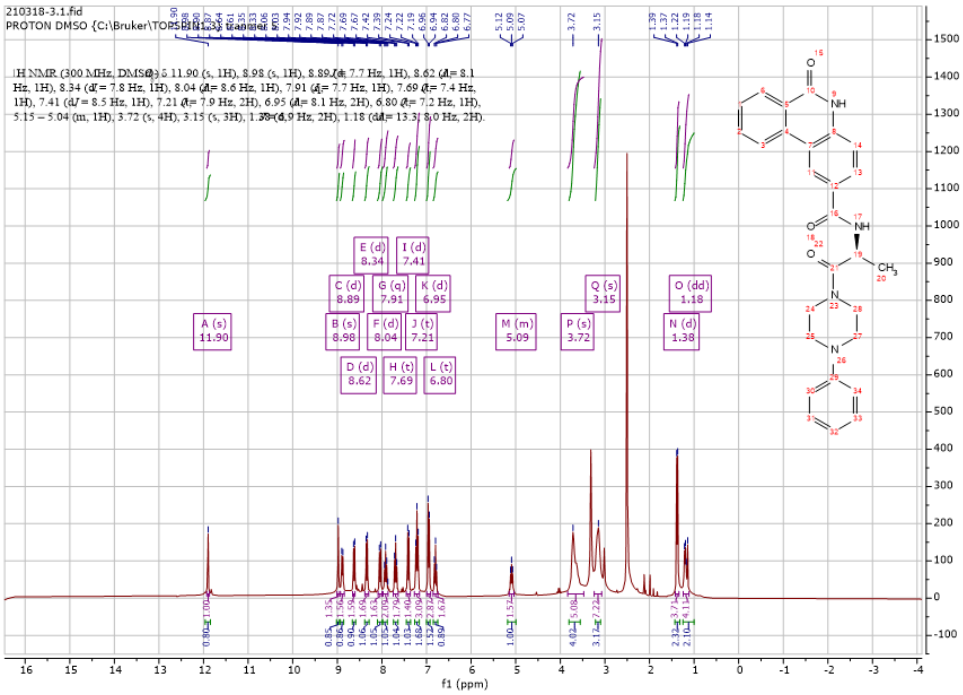
210318-3.1.fid
PROTON DMSO {C:\Bruker\TOPSPIN4.3.0_tranmer}
1H NMR (300 MHz, DMSO) δ 11.90 (s, 1H), 8.98 (s, 1H), 8.89 (d, J= 7.7 Hz, 1H), 8.62 (d, J= 8.1 Hz, 1H), 8.34 (d, J= 7.8 Hz, 1H), 8.04 (d, J= 8.6 Hz, 1H), 7.91 (d, J= 7.7 Hz, 1H), 7.69 (t, J= 7.4 Hz, 1H), 7.41 (d, J= 8.5 Hz, 1H), 7.21 (t, J= 7.9 Hz, 2H), 6.95 (d, J= 8.1 Hz, 2H), 6.80 (t, J= 7.2 Hz, 1H), 5.15 – 5.04 (m, 1H), 3.72 (s, 4H), 3.15 (s, 3H), 1.38 (d, J= 6.9 Hz, 2H), 1.18 (dd, J= 13.3, 8.0 Hz, 2H).
A (s) 11.90
B (s) 8.98
C (d) 8.89
D (d) 8.62
E (d) 8.34
F (d) 8.04
G (q) 7.91
H (t) 7.69
I (d) 7.41
J (t) 7.21
K (d) 6.95
L (t) 6.80
M (m) 5.09
P (s) 3.72
Q (s) 3.15
N (d) 1.38
O (dd) 1.18
f1 (ppm)

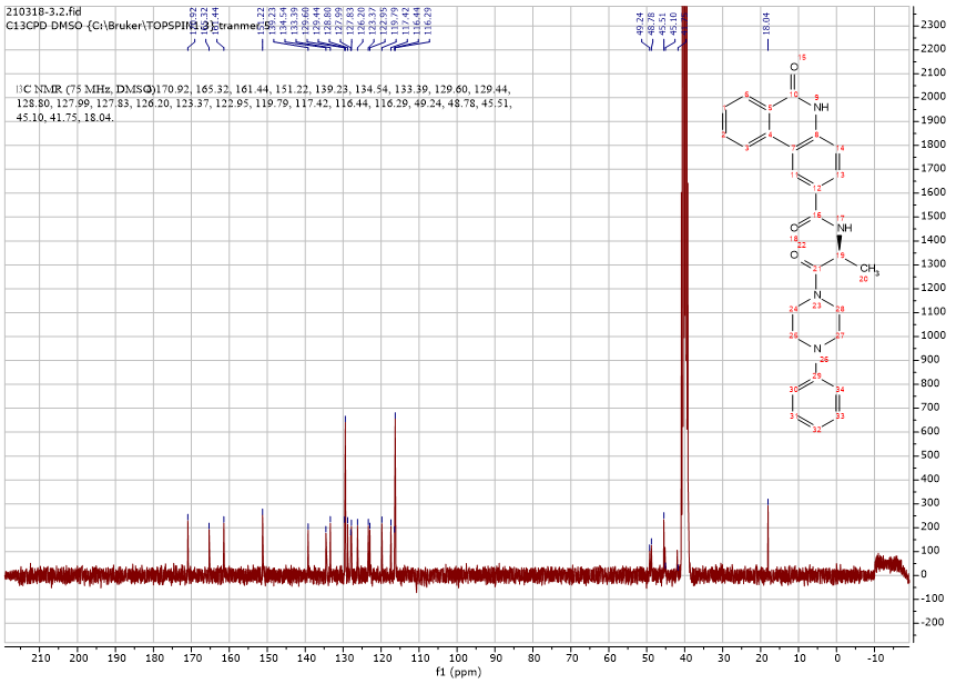
210318-3.2.fid
C13CPD DMSO {C:\Bruker\TOPSPIN4.3.0_tranmer}
13C NMR (75 MHz, DMSO) 170.92, 165.32, 161.44, 151.22, 139.23, 134.54, 133.39, 129.60, 129.44, 128.80, 127.99, 127.83, 126.20, 123.37, 122.95, 119.79, 117.42, 116.44, 116.29, 49.24, 48.78, 45.51, 45.10, 41.75, 18.04.
f1 (ppm)

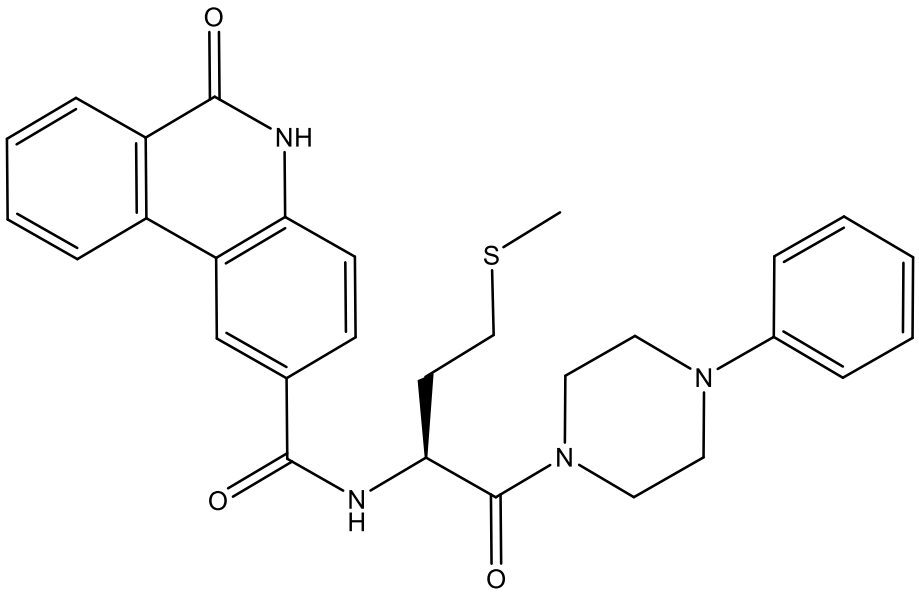

(*S*)-*N*-(4-(methylthio)-1-oxo-1-(4-phenylpiperazin-1-yl)butan-2-yl)-6-oxo-5,6-dihydrophenanthridine-2-carboxamide (a8)

Using **Synthesis Method d**, 24mg (0.1mmol) **f2** was reacted with 29.2mg (0.1mmol) **f20** to give 37mg **a8** (Yield: 72%) and the product was separated as yellowish white solid. ^{1}H NMR (300 MHz, DMSO-d_6) δ 11.90 (s, 1H), 8.98 (s, 1H), 8.90 (d, *J* = 8.1 Hz, 1H), 8.62 (d, *J* = 8.2 Hz, 1H), 8.34 (dd, *J* = 8.0, 1.4 Hz, 1H), 8.04 (dd, *J* = 8.5, 1.7 Hz, 1H), 7.98 – 7.87 (m, 1H), 7.69 (t, *J* = 7.5 Hz, 1H), 7.41 (d, *J* = 8.5 Hz, 1H), 7.21 (dd, *J* = 8.6, 7.1 Hz, 2H), 6.96 (d, *J* = 8.1 Hz, 2H), 6.80 (t, *J* = 7.2 Hz, 1H), 5.26 – 5.13 (m, 1H), 3.78 (m, 2H), 3.67 (m, 2H), 3.23 – 3.11 (m, 4H), 2.59 (m 2H), 2.08 – 1.96 (m, 5H). ^{13}C NMR (75 MHz, DMSO) δ 170.1, 165.9, 161.4, 151.2, 139.3, 134.5, 133.4, 129.7, 129.4, 128.8, 128.0, 127.7, 126.2, 123.4, 123.0, 119.8, 117.4, 116.5, 116.3, 49.3, 48.8, 48.7, 45.3, 40.8, 31.6, 30.5, 15.2. HRMS m/z (ESI+, M+Na): Calcd for C29H30N4O3S: 537.1936, (ESI+, M+Na) found: 537.1930

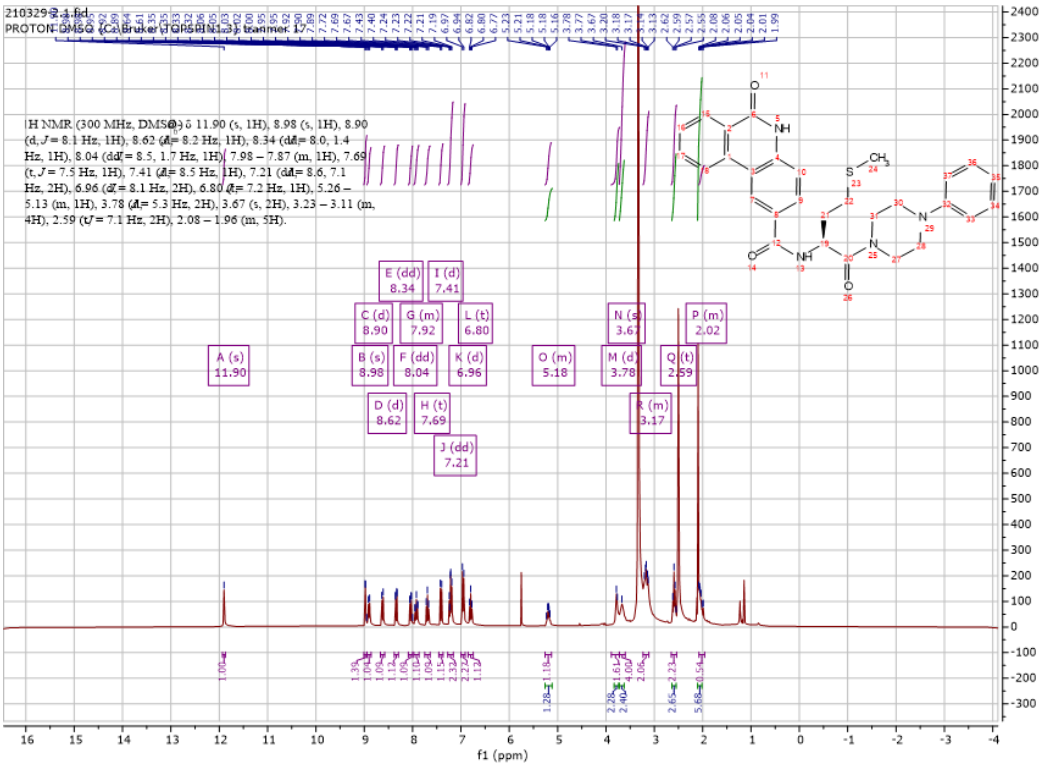
210329-2.1.fid
PROTON DMSO (C:\Bruker\TOPSPIN4.1.3) tranmer 1
1H NMR (300 MHz, DMSO) δ 11.90 (s, 1H), 8.98 (s, 1H), 8.90 (d, J = 8.1 Hz, 1H), 8.62 (dd, J = 8.2 Hz, 1H), 8.34 (dd, J = 8.0, 1.4 Hz, 1H), 8.04 (dd, J = 8.5, 1.7 Hz, 1H), 7.98 – 7.87 (m, 1H), 7.69 (t, J = 7.5 Hz, 1H), 7.41 (dd, J = 8.5 Hz, 1H), 7.21 (dd, J = 8.6, 7.1 Hz, 2H), 6.96 (dd, J = 8.1 Hz, 2H), 6.80 (d, J = 7.2 Hz, 1H), 5.26 – 5.13 (m, 1H), 3.78 (d, J = 5.3 Hz, 2H), 3.67 (s, 2H), 3.23 – 3.11 (m, 4H), 2.59 (t, J = 7.1 Hz, 2H), 2.08 – 1.96 (m, 5H).
A (s) 11.90
B (s) 8.98
C (d) 8.90
D (d) 8.62
E (dd) 8.34
F (dd) 8.04
G (m) 7.92
H (t) 7.69
I (d) 7.41
J (dd) 7.21
K (d) 6.96
L (t) 6.80
M (d) 3.78
N (s) 3.67
O (m) 5.18
P (m) 2.02
Q (t) 2.59
R (m) 3.17
f1 (ppm)

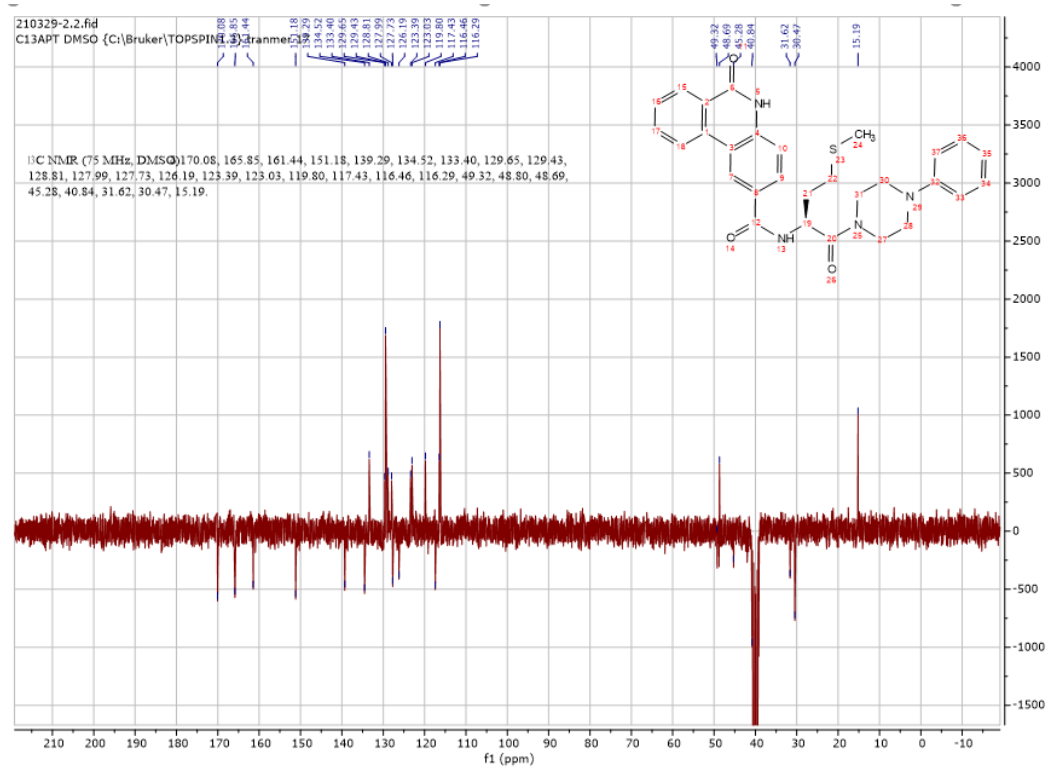
210329-2.2.fid
C13APT DMSO (C:\Bruker\TOPSPIN4.1.3) tranmer 1
13C NMR (75 MHz, DMSO) 170.08, 165.85, 161.44, 151.18, 139.29, 134.52, 133.40, 129.65, 129.43, 128.81, 127.99, 127.73, 126.19, 123.39, 123.03, 119.80, 117.43, 116.46, 116.29, 49.32, 48.80, 48.69, 45.28, 40.84, 31.62, 30.47, 15.19.
f1 (ppm)

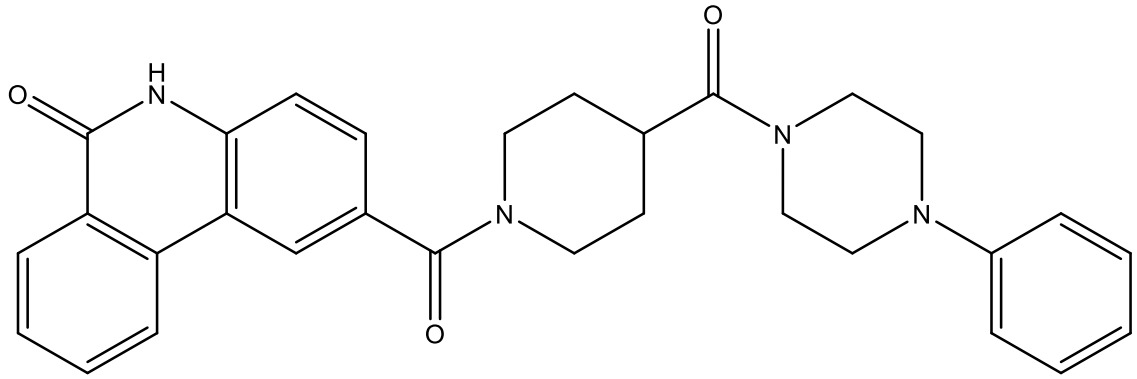

2-(4-(4-phenylpiperazine-1-carbonyl)piperidine-1-carbonyl)phenanthridin-6(5*H*)-one (a9)

Using **Synthesis Method d**, 24mg (0.1mmol) **f2** was reacted with 27.4mg (0.1mmol) **f18** to give 30.6mg **a9** (Yield: 62%) and the product was separated as yellowish white solid. ^{1}H NMR (400 MHz, DMSO-d_6) δ 11.86 (s, 1H), 8.60 (d, *J* = 8.2 Hz, 1H), 8.42 (d, *J* = 1.4 Hz, 1H), 8.33 (dd, *J* = 8.0, 1.2 Hz, 1H), 7.87 (ddd, *J* = 8.3, 7.3, 1.5 Hz, 1H), 7.72 – 7.64 (m, 1H), 7.53 (dd, *J* = 8.3, 1.7 Hz, 1H), 7.41 (d, *J* = 8.3 Hz, 1H), 7.23 (dd, *J* = 8.7, 7.3 Hz, 2H), 6.99 – 6.93 (m, 2H), 6.81 (t, *J* = 7.3 Hz, 1H), 3.65 (m, 5H), 3.26 – 2.90 (m, 7H), 1.86 – 1.52 (m, 5H). ^{13}C NMR (101 MHz, DMSO) δ 172.7, 169.2, 161.3, 151.3, 137.7, 134.3, 133.5, 130.6, 129.5, 128.8, 128.7, 128.0, 126.3, 122.7, 120.4, 119.8, 117.7, 116.5, 116.4, 53.3, 51.3, 45.1, 41.5, 37.5. HRMS m/z (ESI+, M+Na): Calcd for C30H30N4O3: 517.2216, (ESI+, M+Na) found: 517.2208

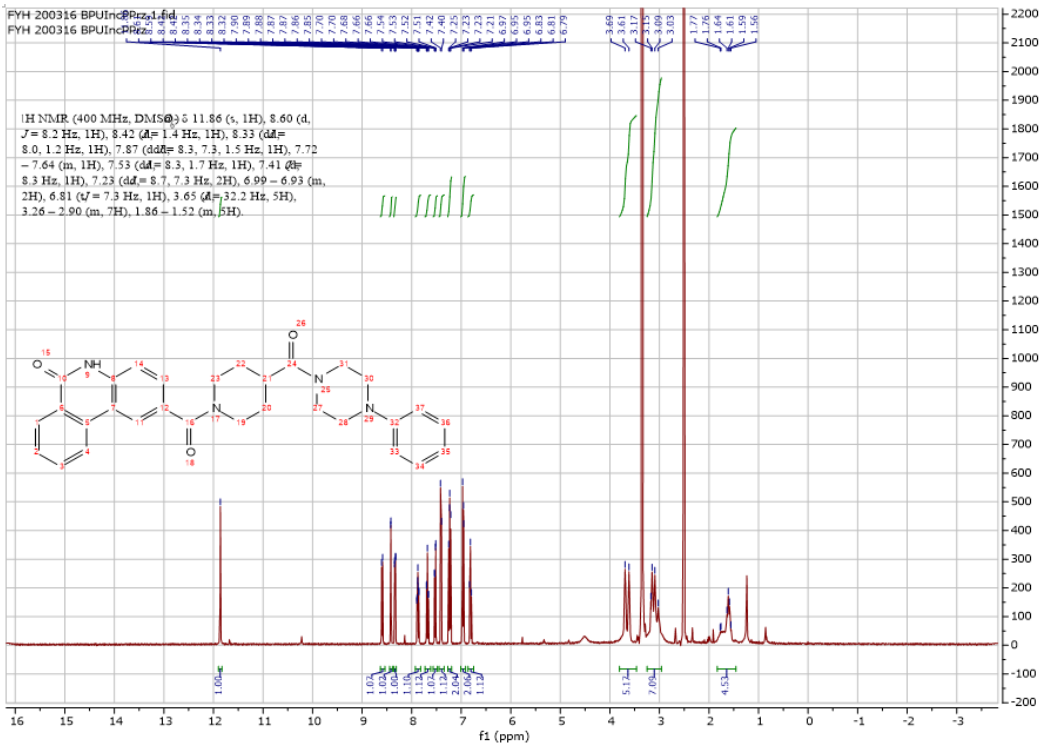
FYH 200316 BPUIncPPrz.1.fid
FYH 200316 BPUIncPPrz
1H NMR (400 MHz, DMSO) δ 11.86 (s, 1H), 8.60 (d, J = 8.2 Hz, 1H), 8.42 (d, J = 1.4 Hz, 1H), 8.33 (dd, J = 8.0, 1.2 Hz, 1H), 7.87 (ddd, J = 8.3, 7.3, 1.5 Hz, 1H), 7.72 – 7.64 (m, 1H), 7.53 (dd, J = 8.3, 1.7 Hz, 1H), 7.41 (d, J = 8.3 Hz, 1H), 7.23 (dd, J = 8.7, 7.3 Hz, 2H), 6.99 – 6.93 (m, 2H), 6.81 (t, J = 7.3 Hz, 1H), 3.65 (d, J = 32.2 Hz, 5H), 3.26 – 2.90 (m, 7H), 1.86 – 1.52 (m, 5H).
f1 (ppm)

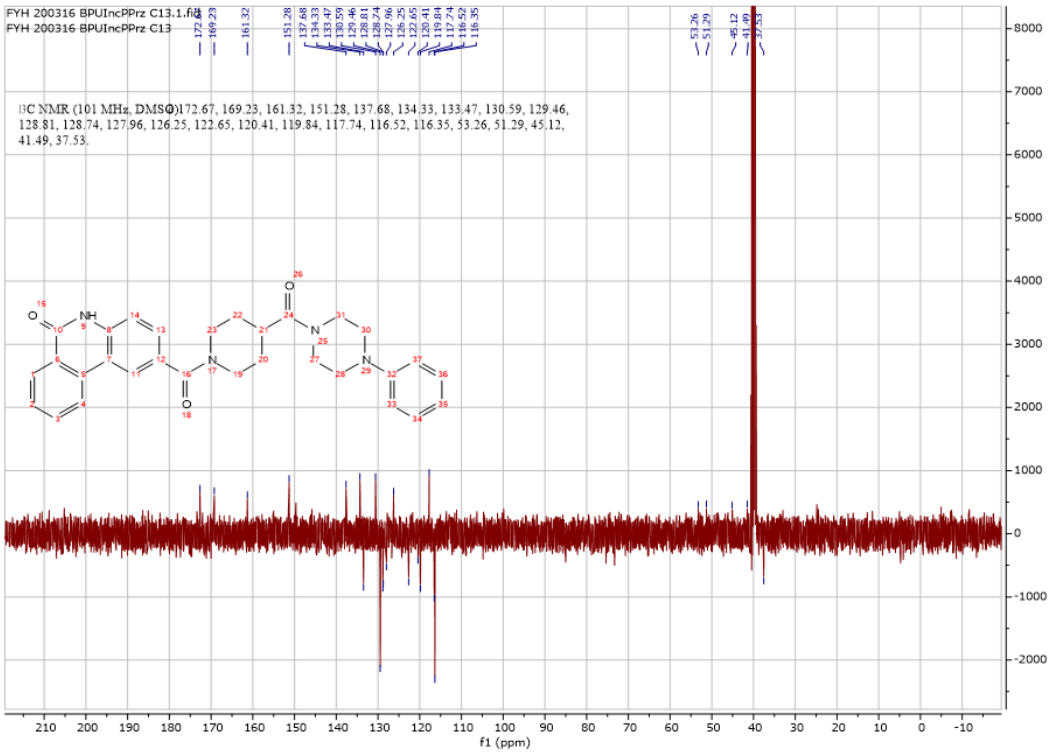
FYH 200316 BPUIncPPrz C13.1.fid
FYH 200316 BPUIncPPrz C13
13C NMR (101 MHz, DMSO) 172.67, 169.23, 161.32, 151.28, 137.68, 134.33, 133.47, 130.59, 129.46, 128.81, 128.74, 127.96, 126.25, 122.65, 120.41, 119.84, 117.74, 116.52, 116.35, 53.26, 51.29, 45.12, 41.49, 37.53.
f1 (ppm)

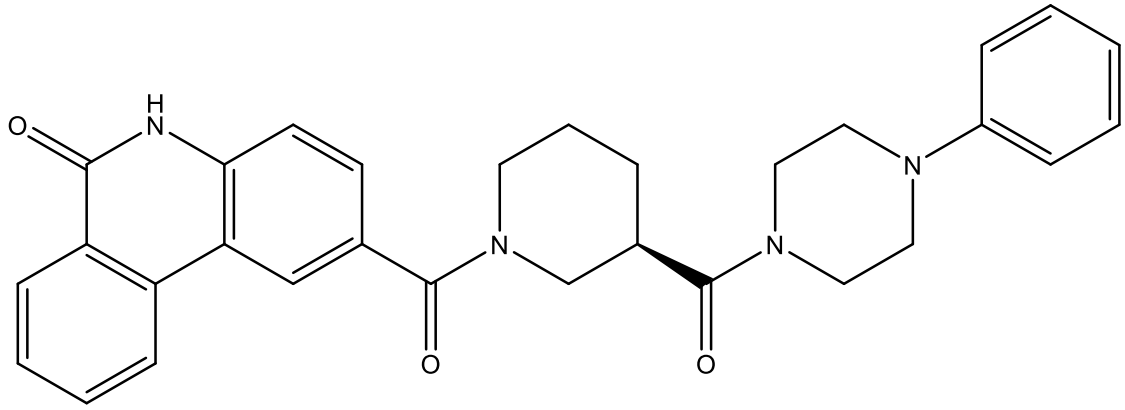

(R)-2-(3-(4-phenylpiperazine-1-carbonyl)piperidine-1-carbonyl)phenanthridin-6(5*H*)-one (a10)

Using **Synthesis Method d**, 24mg (0.1mmol) **f2** was reacted with 27.2mg (0.1mmol) **f21** to give 29.6mg **a10** (Yield: 60%) and the product was separated as yellowish white solid. ^{1}H NMR (300 MHz, DMSO-d_6) δ 11.87 (s, 1H), 8.66 (s, 1H), 8.50 (s, 1H), 8.37 (d, *J* = 7.8 Hz, 1H), 7.89 (t, 1H), 7.70 (t, *J* = 7.6 Hz, 1H), 7.53 (d, 1H), 7.43 (d, *J* = 8.3 Hz, 1H), 7.16 (s, 2H), 7.03 – 6.35 (m, 3H), 4.49 (m, 1H), 3.66 (m, 5H), 3.26 – 2.59 (m, 7H), 1.77 (m, 4H). 13C NMR (75 MHz, DMSO) δ 178.2, 169.5, 161.3, δ 137.6, 134.4, 123.4, 122.1, 128.0, 133.5, 128.9, 128.6, 116.6, 116.0, 126.4, 129.3, 119.9, 116.0, 42.4, 41.1, 44.7, 48.5, 50.5, 38.2, 27.5-24.3. C32 on the benzene attached to the piperazine was not found. HRMS m/z (ESI+, M+Na): Calcd for C30H30N4O3: 517.2216, (ESI+, M+Na) found: 517.2207

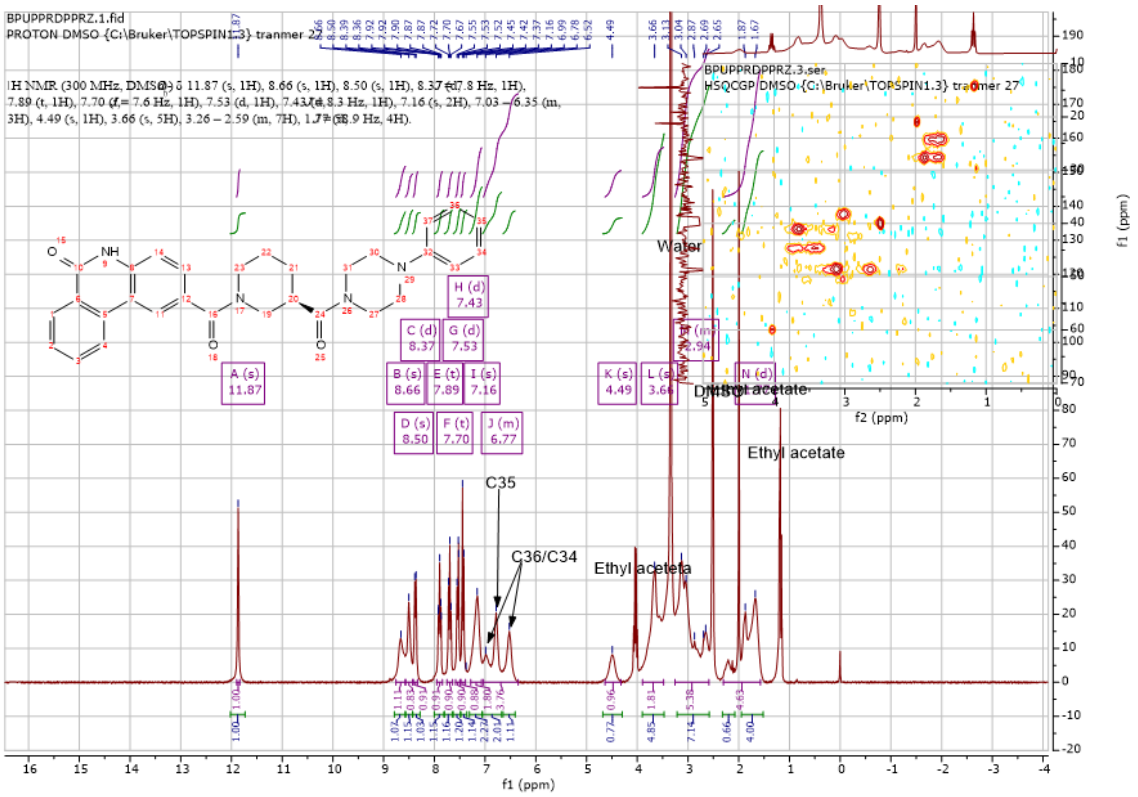
BPUPPRDPPRZ.1.fid
PROTON DMSO {C:\Bruker\TOPSPIN1.3} tranmer 27
BPUPPRDPPRZ.3.ser
HSQCGP DMSO {C:\Bruker\TOPSPIN1.3} tranmer 27
Water
DMSO
Ethyl acetate
C35
C36/C34
Ethyl acetate
f1 (ppm)
f2 (ppm)

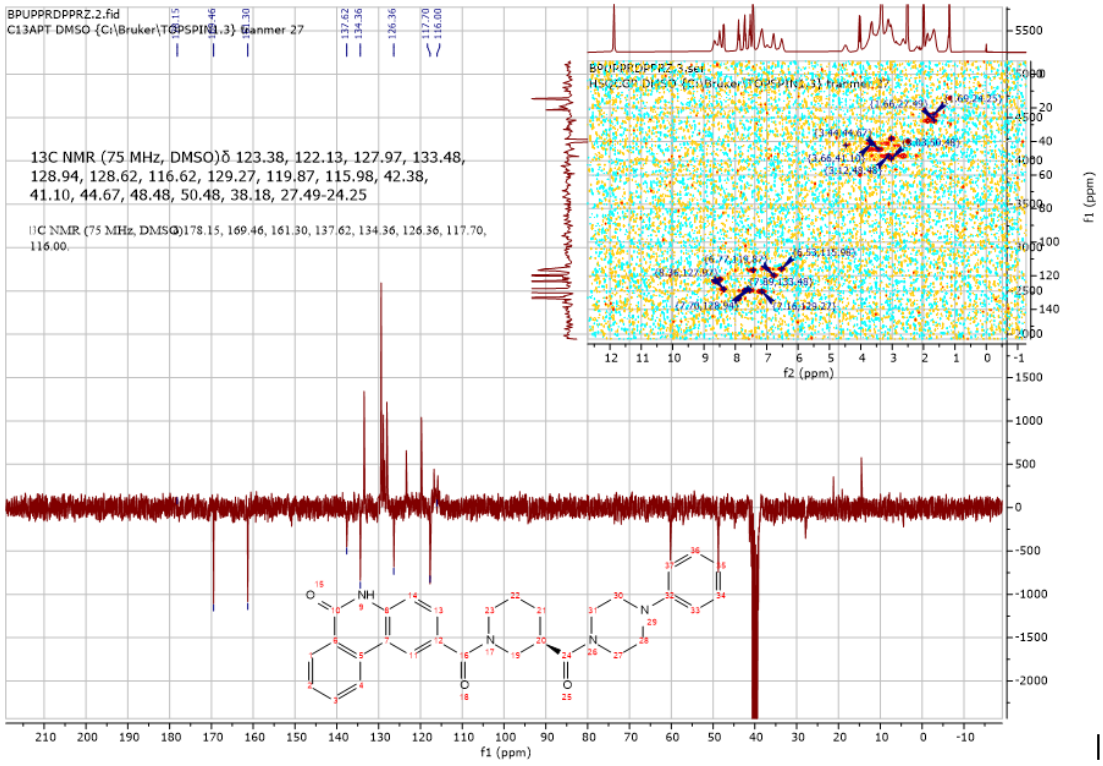
BPUPPRDPPRZ.2.fid
C13APT DMSO {C:\Bruker\TOPSPIN1.3} tranmer 27
13C NMR (75 MHz, DMSO)δ 123.38, 122.13, 127.97, 133.48, 128.94, 128.62, 116.62, 129.27, 119.87, 115.98, 42.38, 41.10, 44.67, 48.48, 50.48, 38.18, 27.49-24.25
13C NMR (75 MHz, DMSO)178.15, 169.46, 161.30, 137.62, 134.36, 126.36, 117.70, 116.00.
BPUPPRDPPRZ.3.ser
HSQCGP DMSO {C:\Bruker\TOPSPIN1.3} tranmer 27
f1 (ppm)
f2 (ppm)

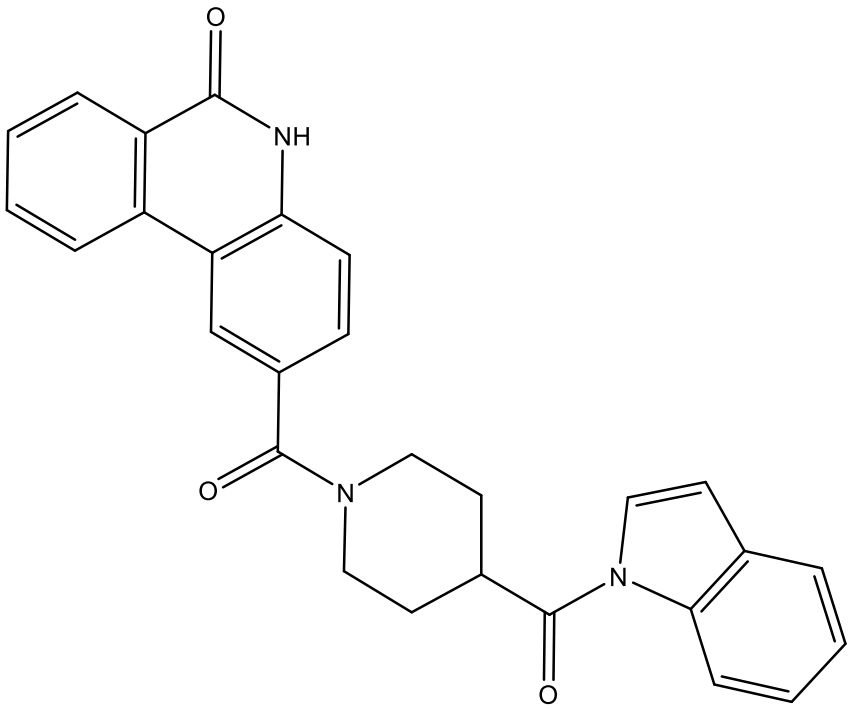

2-(4-(1H-indole-1-carbonyl)piperidine-1-carbonyl)phenanthridin-6(5*H*)-one (a11)

Using **Synthesis Method f**, 164mg (0.5mmol) **f23** was deprotected. Using **Synthesis Method d**, 24mg (0.1mmol) **f2** was reacted with 23mg (0.1mmol) deprotected **f23** to give 40mg **a11** (Yield: 89%) and the product was separated as yellowish white solid.^{1}H NMR (300 MHz, DMSO-d_6) δ 11.83 (s, 1H), 8.60 (d, *J* = 8.2 Hz, 1H), 8.45 (d, *J* = 1.7 Hz, 1H), 8.39 (d, *J* = 8.0 Hz, 1H), 8.34 (dd, *J* = 8.0, 1.4 Hz, 1H), 8.10 (d, *J* = 3.9 Hz, 1H), 7.93 – 7.82 (m, 1H), 7.68 (t, *J* = 7.5 Hz, 1H), 7.63 (dd, *J* = 7.1, 1.5 Hz, 1H), 7.56 (dd, *J* = 8.3, 1.7 Hz, 1H), 7.42 (d, *J* = 8.3 Hz, 1H), 7.37 – 7.23 (m, 2H), 6.79 (d, *J* = 3.8 Hz, 1H), 3.75 – 3.55 (m, 1H), 1.96 (m, 4H), 1.87 – 1.74 (m, 4H). ^{13}C NMR (75 MHz, DMSO) δ 174.3, 169.3, 161.3, 152.5, 146.1, 137.7, 133.5, 130.8, 130.5, 128.8, 128.8, 127.9, 126.9, 126.3, 125.2, 124.0, 123.5, 122.7, 121.3, 117.8, 116.6, 116.6, 109.1, 40.9, 29.0. HRMS m/z (ESI+, M+Na): Calcd for C28H23N3O3: 472.1637, (ESI+, M+Na) found: 472.1632

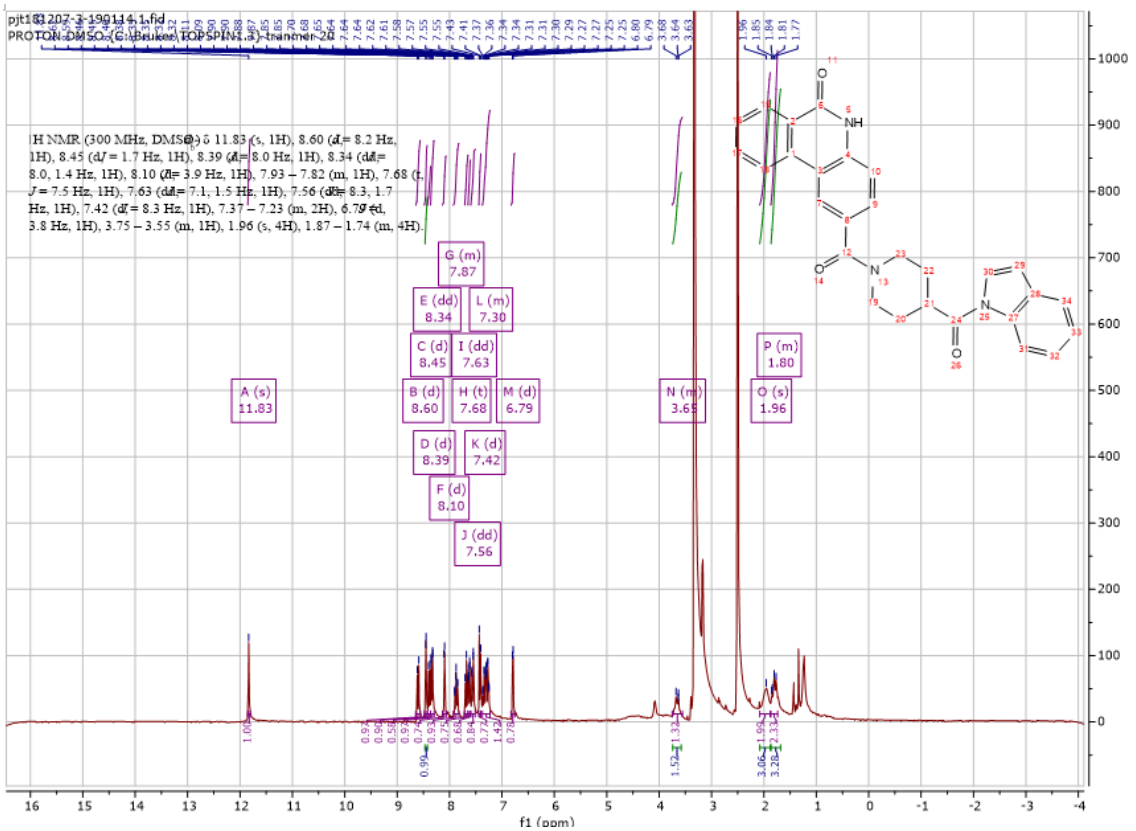
pjt181207-3-190114.1.fid
PROTON DMSO {C:\Bruker\TOPSPIN4.3} tranmer 20
H NMR (300 MHz, DMSO) δ 11.83 (s, 1H), 8.60 (d, J = 8.2 Hz, 1H), 8.45 (d, J = 1.7 Hz, 1H), 8.39 (d, J = 8.0 Hz, 1H), 8.34 (dd, J = 8.0, 1.4 Hz, 1H), 8.10 (d, J = 3.9 Hz, 1H), 7.93 – 7.82 (m, 1H), 7.68 (t, J = 7.5 Hz, 1H), 7.63 (dd, J = 7.1, 1.5 Hz, 1H), 7.56 (dd, J = 8.3, 1.7 Hz, 1H), 7.42 (d, J = 8.3 Hz, 1H), 7.37 – 7.23 (m, 2H), 6.79 (d, J = 3.8 Hz, 1H), 3.75 – 3.55 (m, 1H), 1.96 (s, 4H), 1.87 – 1.74 (m, 4H).
A (s) 11.83
B (d) 8.60
C (d) 8.45
D (d) 8.39
E (dd) 8.34
F (d) 8.10
G (m) 7.87
H (t) 7.68
I (dd) 7.63
J (dd) 7.56
K (d) 7.42
L (m) 7.30
M (d) 6.79
N (m) 3.65
O (s) 1.96
P (m) 1.80
f1 (ppm)

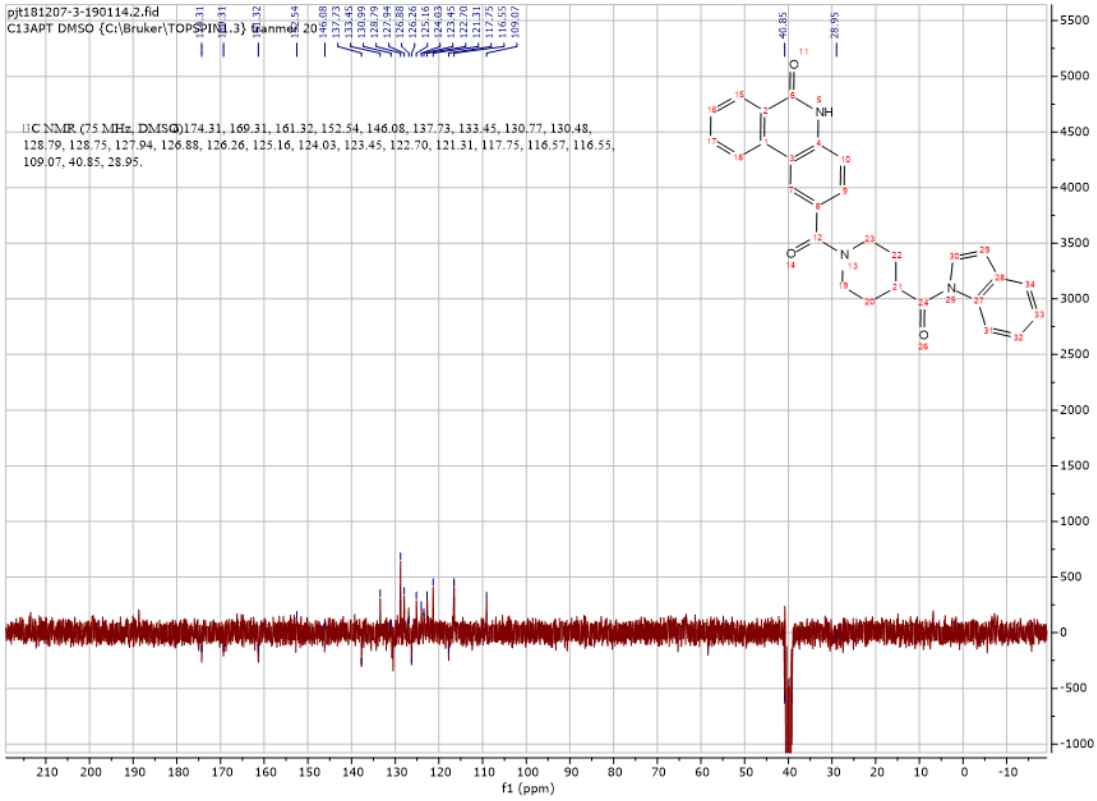
pjt181207-3-190114.2.fid
C13APT DMSO {C:\Bruker\TOPSPIN4.3} tranmer 20
C NMR (75 MHz, DMSO) 174.31, 169.31, 161.32, 152.54, 146.08, 137.73, 133.45, 130.77, 130.48, 128.79, 128.75, 127.94, 126.88, 126.26, 125.16, 124.03, 123.45, 122.70, 121.31, 117.75, 116.57, 116.55, 109.07, 40.85, 28.95.
f1 (ppm)

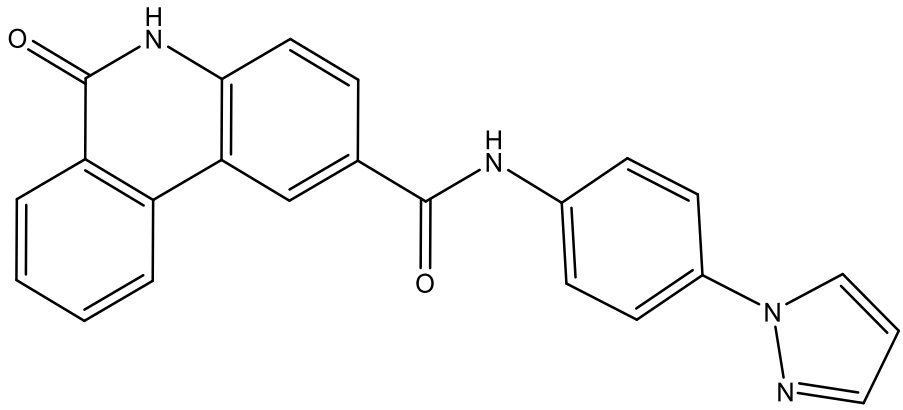

***N*-(4-(1H-pyrazol-1-yl)phenyl)-6-oxo-5,6-dihydrophenanthridine-2-carboxamide (a12)**

Using **Synthesis Method d**, 24mg (0.1mmol) **f2** was reacted with 16mg (0.1mmol) 4-(1*H*-pyrazol-1-yl)aniline to give 32.3mg **a12** (Yield: 85%) and the product was separated as yellowish white solid. ^{1}H NMR (300 MHz, DMSO-d_6) δ 11.96 (s, 1H), 10.49 (s, 1H), 9.02 (d, *J* = 1.9 Hz, 1H), 8.66 (d, *J* = 8.2 Hz, 1H), 8.36 (d, *J* = 7.9 Hz, 1H), 8.25 (s, 1H), 8.11 (dd, *J* = 8.6, 1.8 Hz, 1H), 7.95 (dd, *J* = 8.4, 4.2 Hz, 3H), 7.71 (dd, *J* = 14.2, 8.0 Hz, 4H), 7.48 (dd, *J* = 8.6, 3.8 Hz, 1H), 7.12 (s, 1H). ^{13}C NMR (75 MHz, DMSO) δ 165.3, 161.5, 139.5, 138.4, 135.8, 134.4, 133.5, 133.0, 130.2, 129.7, 128.9, 128.7, 128.0, 126.3, 123.5, 123.4, 122.0, 121.1, 118.4, 117.5, 116.6. HRMS m/z (ESI+, M+H): Calcd for C23H16N4O2: 380.1346, (ESI+, M+H) found: 381.1351

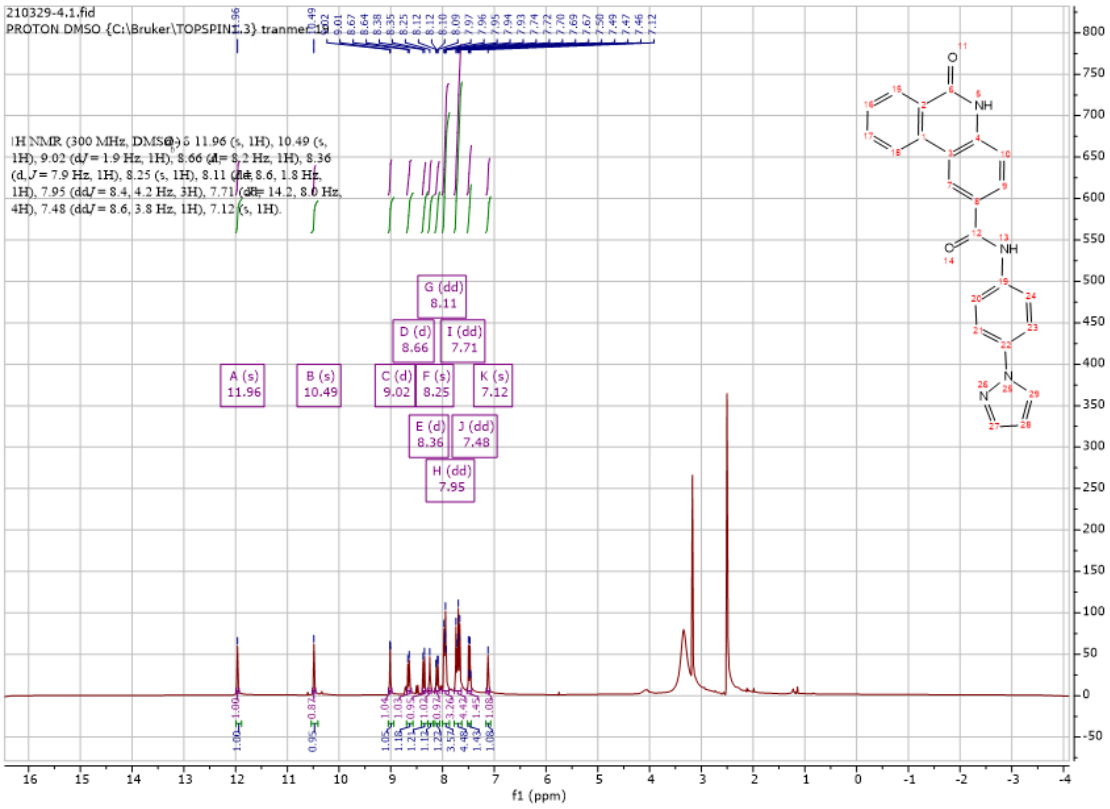
210329-4.1.fid
PROTON DMSO {C:\Bruker\TOPSPIN1.3} tranmet 13
1H NMR (300 MHz, DMSO) δ 11.96 (s, 1H), 10.49 (s, 1H), 9.02 (d, J = 1.9 Hz, 1H), 8.66 (d, J = 8.2 Hz, 1H), 8.36 (d, J = 7.9 Hz, 1H), 8.25 (s, 1H), 8.11 (dd, J = 8.6, 1.8 Hz, 1H), 7.95 (dd, J = 8.4, 4.2 Hz, 3H), 7.71 (dd, J = 14.2, 8.0 Hz, 4H), 7.48 (dd, J = 8.6, 3.8 Hz, 1H), 7.12 (s, 1H).
A (s) 11.96
B (s) 10.49
C (d) 9.02
D (d) 8.66
E (d) 8.36
F (s) 8.25
G (dd) 8.11
H (dd) 7.95
I (dd) 7.71
J (dd) 7.48
K (s) 7.12
f1 (ppm)

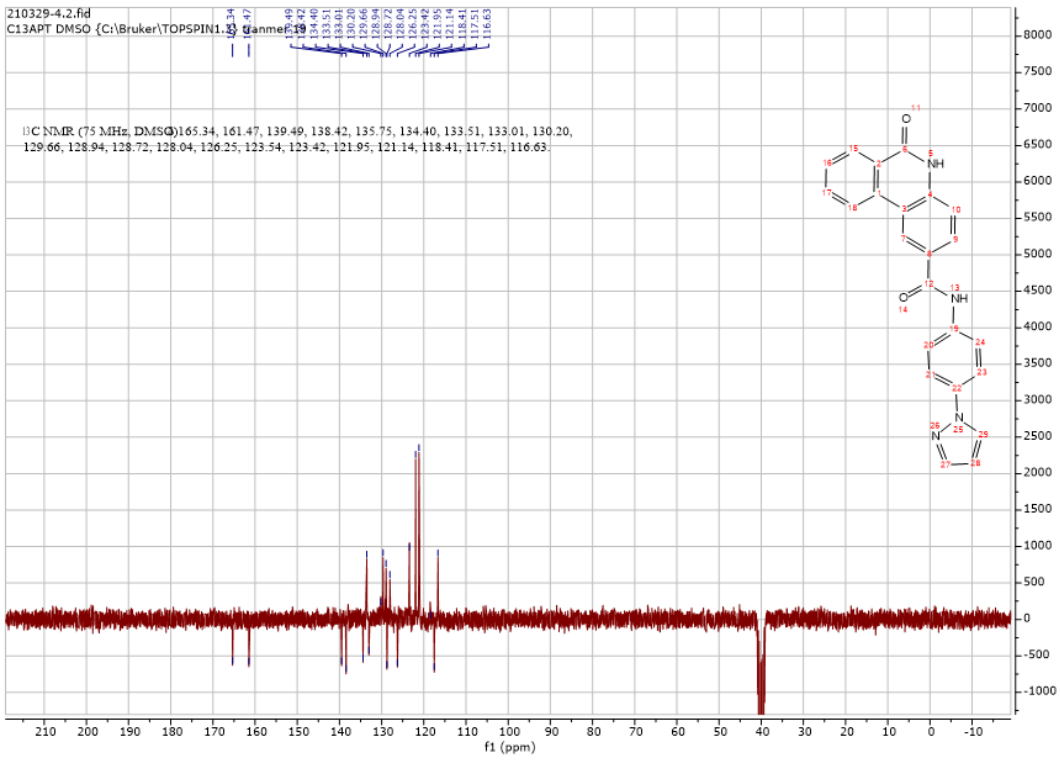
210329-4.2.fid
C13APT DMSO {C:\Bruker\TOPSPIN1.3} tranmet 19
13C NMR (75 MHz, DMSO) 165.34, 161.47, 139.49, 138.42, 135.75, 134.40, 133.51, 133.01, 130.20, 129.66, 128.94, 128.72, 128.04, 126.25, 123.54, 123.42, 121.95, 121.14, 118.41, 117.51, 116.63.
f1 (ppm)

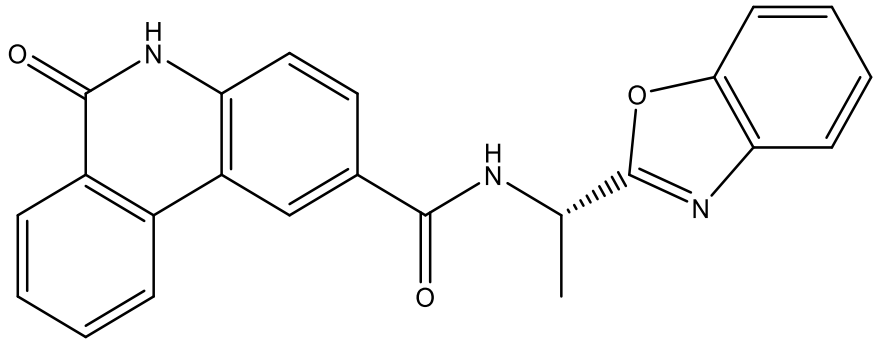

(*S*)-N-(1-(benzo[d]oxazol-2-yl)ethyl)-6-oxo-5,6-dihydrophenanthridine-2-carboxamide (a13)

Using **Synthesis Method d**, 24mg (0.1mmol) **f2** was reacted with 16.3mg (0.1mmol) **f8** to give 20.2mg **a13** (Yield: 53%) and the product was separated as yellowish white solid. ^{1}H NMR (300 MHz, DMSO-d_6) δ 11.93 (s, 1H), 9.28 (d, *J* = 7.6 Hz, 1H), 9.01 – 8.94 (m, 1H), 8.59 (d, *J* = 8.1 Hz, 1H), 8.35 (dd, *J* = 7.9, 1.1 Hz, 1H), 8.06 (dd, *J* = 8.5, 1.6 Hz, 1H), 7.98 – 7.87 (m, 1H), 7.78 – 7.65 (m, 3H), 7.43 (d, *J* = 8.5 Hz, 1H), 7.40 – 7.36 (m, 2H), 5.55 (q, *J* = 7.1 Hz, 1H), 1.75 (d, *J* = 7.1 Hz, 3H). ^{13}C NMR (75 MHz, DMSO) δ 167.6, 165.6, 161.5, 150.8, 141.1, 139.4, 134.5, 133.4, 129.6, 128.9, 128.0, 127.6, 126.2, 125.6, 124.9, 123.3, 123.0, 120.1, 117.5, 116.6, 111.3, 44.1, 19.0. HRMS m/z (ESI+, M+Na): Calcd for C23H17N3O3: 406.1168, (ESI+, M+Na) found: 406.1162

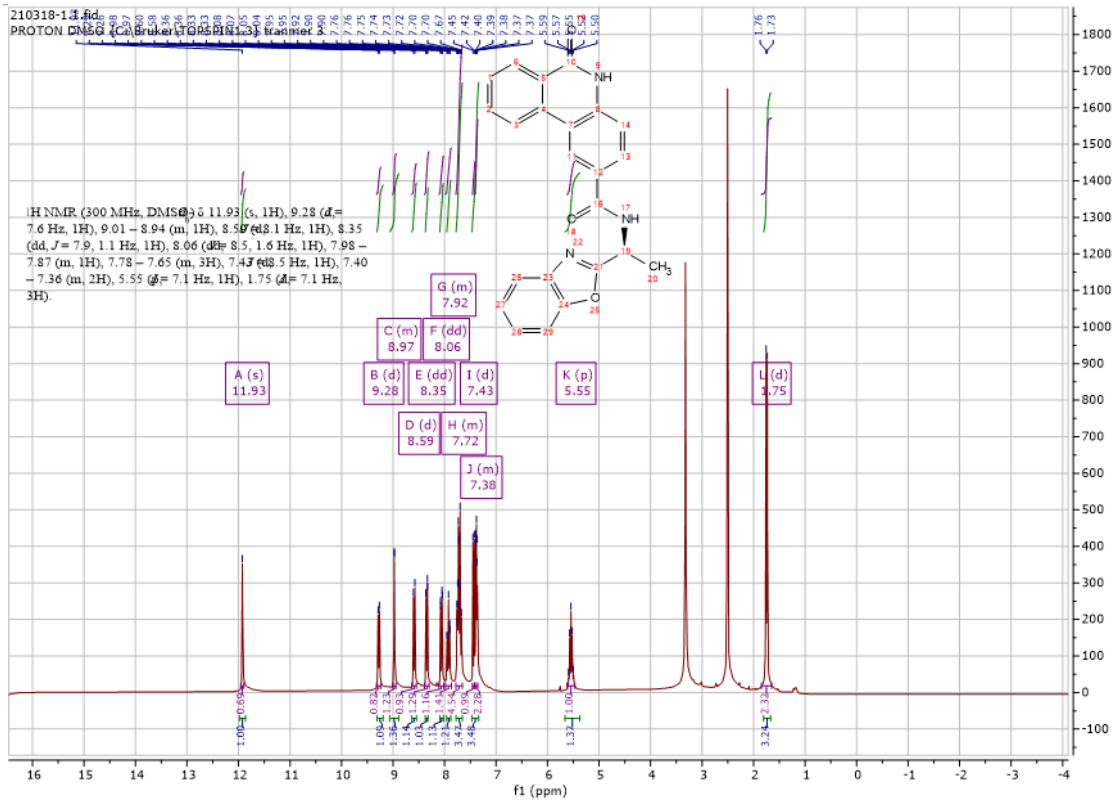
210318-1.1.fid
PROTON DMSO {C:\Bruker\TOPSPIN1.3} tranmer 3
1H NMR (300 MHz, DMSO) δ 11.93 (s, 1H), 9.28 (d, J = 7.6 Hz, 1H), 9.01 – 8.94 (m, 1H), 8.59 (d, J = 8.1 Hz, 1H), 8.35 (dd, J = 7.9, 1.1 Hz, 1H), 8.06 (dd, J = 8.5, 1.6 Hz, 1H), 7.98 – 7.87 (m, 1H), 7.78 – 7.65 (m, 3H), 7.43 (d, J = 8.5 Hz, 1H), 7.40 – 7.36 (m, 2H), 5.55 (p, J = 7.1 Hz, 1H), 1.75 (d, J = 7.1 Hz, 3H).
A (s) 11.93
B (d) 9.28
C (m) 8.97
D (d) 8.59
E (dd) 8.35
F (dd) 8.06
G (m) 7.92
H (m) 7.72
I (d) 7.43
J (m) 7.38
K (p) 5.55
L (d) 1.75
f1 (ppm)

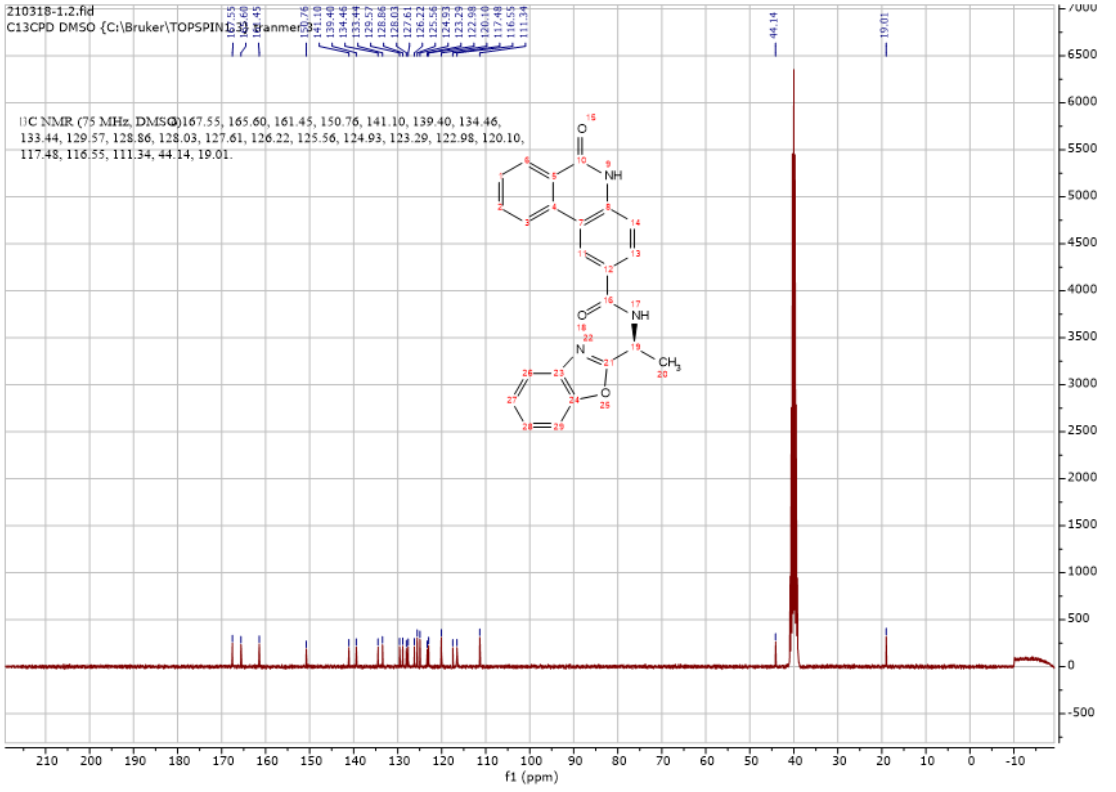
210318-1.2.fid
C13CPD DMSO {C:\Bruker\TOPSPIN1.3} tranmer3
13C NMR (75 MHz, DMSO) 167.55, 165.60, 161.45, 150.76, 141.10, 139.40, 134.46, 133.44, 129.57, 128.86, 128.03, 127.61, 126.22, 125.56, 124.93, 123.29, 122.98, 120.10, 117.48, 116.55, 111.34, 44.14, 19.01.
f1 (ppm)

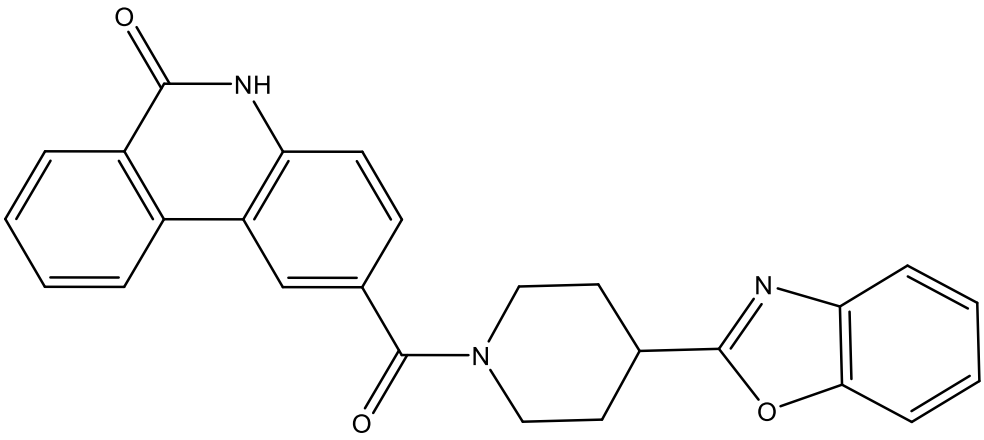

2-(4-(benzo[*d*]oxazol-2-yl)piperidine-1-carbonyl)phenanthridin-6(5*H*)-one (a14)

Using **Synthesis Method d**, 24mg (0.1mmol) **f2** was reacted with 20.1mg (0.1mmol) **f14** to give 20.2mg **a14** (Yield: 48%) and the product was separated as yellowish white solid. ^{1}H NMR (400 MHz, DMSO-d_6) δ 11.84 (s, 1H), 8.60 (d, *J* = 8.2 Hz, 1H), 8.48 – 8.43 (m, 1H), 8.34 (dd, *J* = 7.9, 1.2 Hz, 1H), 7.91 – 7.83 (m, 1H), 7.77 – 7.64 (m, 3H), 7.56 (dd, *J* = 8.3, 1.6 Hz, 1H), 7.46 – 7.31 (m, 3H), 4.77 – 3.55 (m, 2H), 3.39 (p, *J* = 6.0, Hz, 1H), 3.27 (m, 2H), 2.14 (m, 2H), 2.02 – 1.83 (m, 2H). ^{13}C NMR (101 MHz, DMSO) δ 169.4, 168.8, 161.3, 150.6, 141.2, 137.7, 134.4, 133.4, 130.5, 128.8, 128.8, 128.0, 126.3, 125.3, 124.8, 123.4, 122.7, 119.9, 117.8, 116.6, 111.1, 47.5, 35.4, 29.4. HRMS m/z (ESI+, M+Na): Calcd for C26H21N3O3: 423.1481, (ESI+, M+Na) found: 446.1479

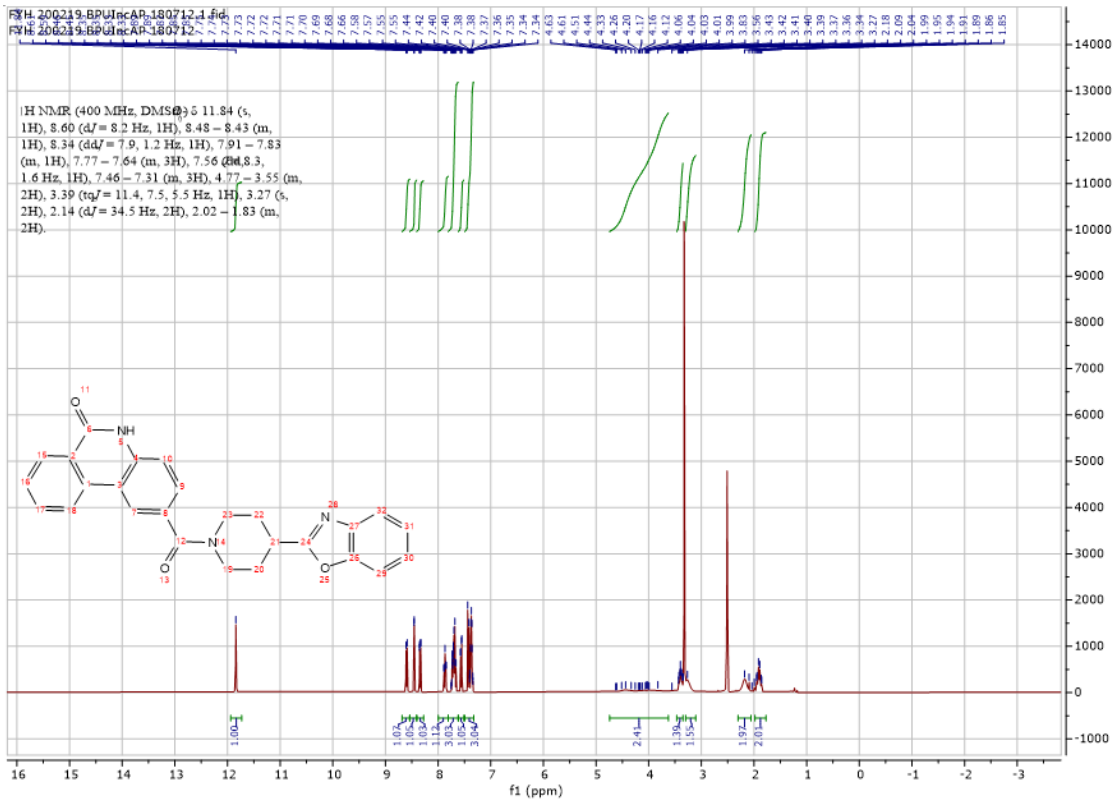
FYH 200219 BPUIncAP 180712 1 fid
FYH 200219 BPUIncAP 180712
1H NMR (400 MHz, DMSO) δ 11.84 (s, 1H), 8.60 (d, J = 8.2 Hz, 1H), 8.48 – 8.43 (m, 1H), 8.34 (dd, J = 7.9, 1.2 Hz, 1H), 7.91 – 7.83 (m, 1H), 7.77 – 7.64 (m, 3H), 7.56 (dd, J = 8.3, 1.6 Hz, 1H), 7.46 – 7.31 (m, 3H), 4.77 – 3.55 (m, 2H), 3.39 (tq, J = 11.4, 7.5, 5.5 Hz, 1H), 3.27 (s, 2H), 2.14 (d, J = 34.5 Hz, 2H), 2.02 – 1.83 (m, 2H).
f1 (ppm)

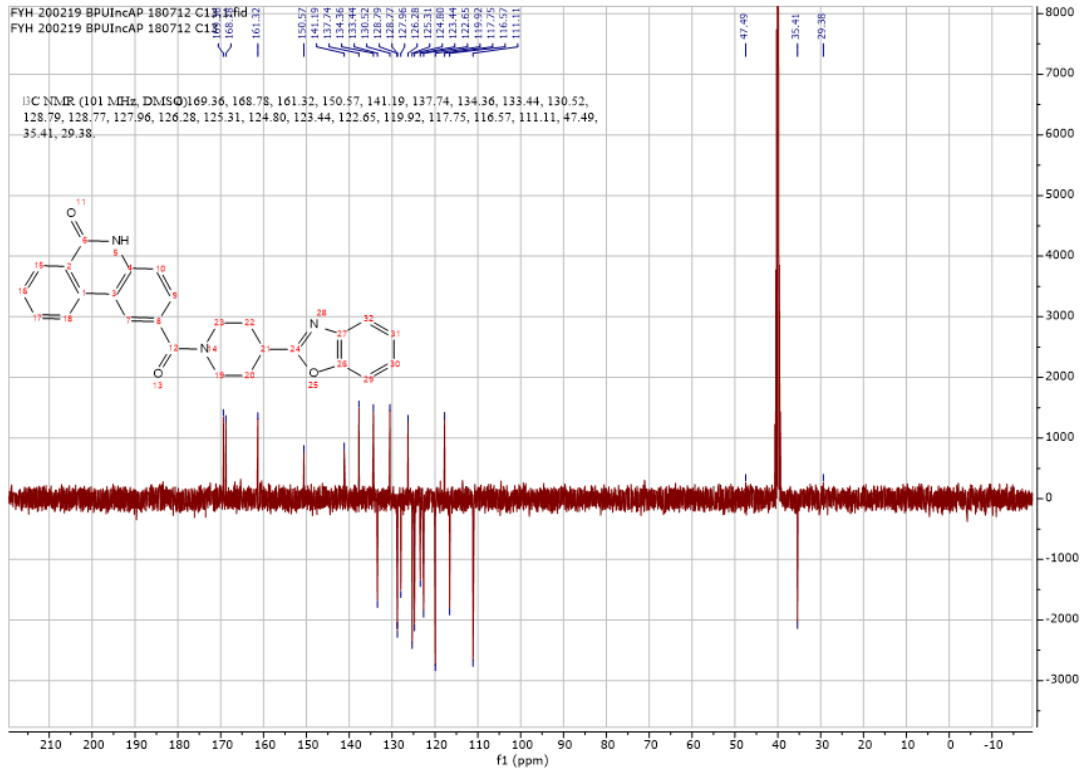
FYH 200219 BPUIncAP 180712 C13 1.fid
FYH 200219 BPUIncAP 180712 C13
13C NMR (101 MHz, DMSO) 169.36, 168.78, 161.32, 150.57, 141.19, 137.74, 134.36, 133.44, 130.52, 128.79, 128.77, 127.96, 126.28, 125.31, 124.80, 123.44, 122.65, 119.92, 117.75, 116.57, 111.11, 47.49, 35.41, 29.38.
f1 (ppm)

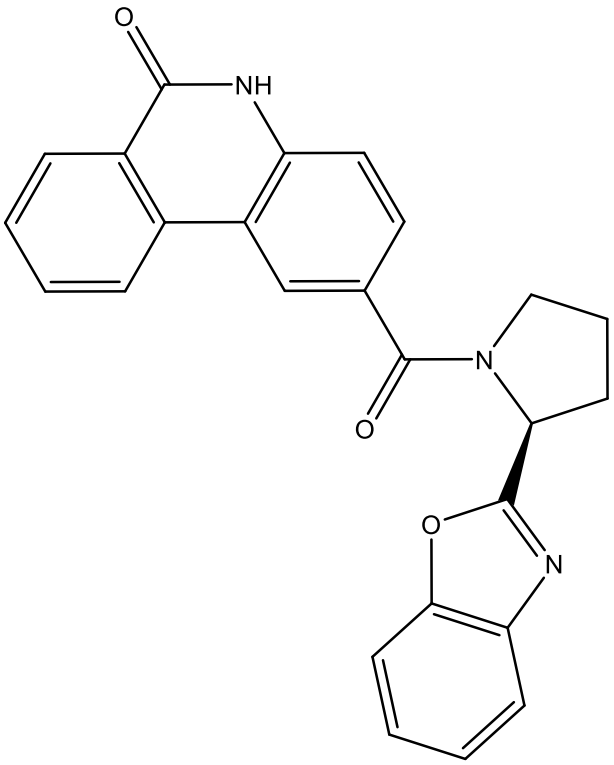

(*S*)-2-(2-(benzo[d]oxazol-2-yl)pyrrolidine-1-carbonyl)phenanthridin-6(5H)-one (a15)

Using **Synthesis Method d**, 24mg (0.1mmol) **f2** was reacted with 18.9mg (0.1mmol) **f12** to give 20.6mg **a15** (Yield: 42%) and the product was separated as yellowish transparent oil-like solid. Insufficient NMR Resolution. ^{1}H NMR (300 MHz, DMSO) δ 11.89 (s, 1H), 8.58 (m, 1H), 8.22 (m, 1H), 7.91-7.38 (m, 9H), 5.05 (m, 1H), 3.80 (m, 2H), 2.14 (m, 4H). ^{13}C NMR (75 MHz, DMSO) δ 150.5, 146.6, 143.7, 136.9, 134.0, 133.6, 129.5, 129.1, 128.6, 128.0, 126.2, 125.3, 124.9, 123.3, 120.0, 118.7, 116.5, 111.3, 110.1, 101.9, 55.6, 50.3, 31.8, 25.3. HRMS m/z (ESI+, M+Na): Calcd for C25H19N3O3: 432.1324, (ESI+, M+Na) found: 432.1321

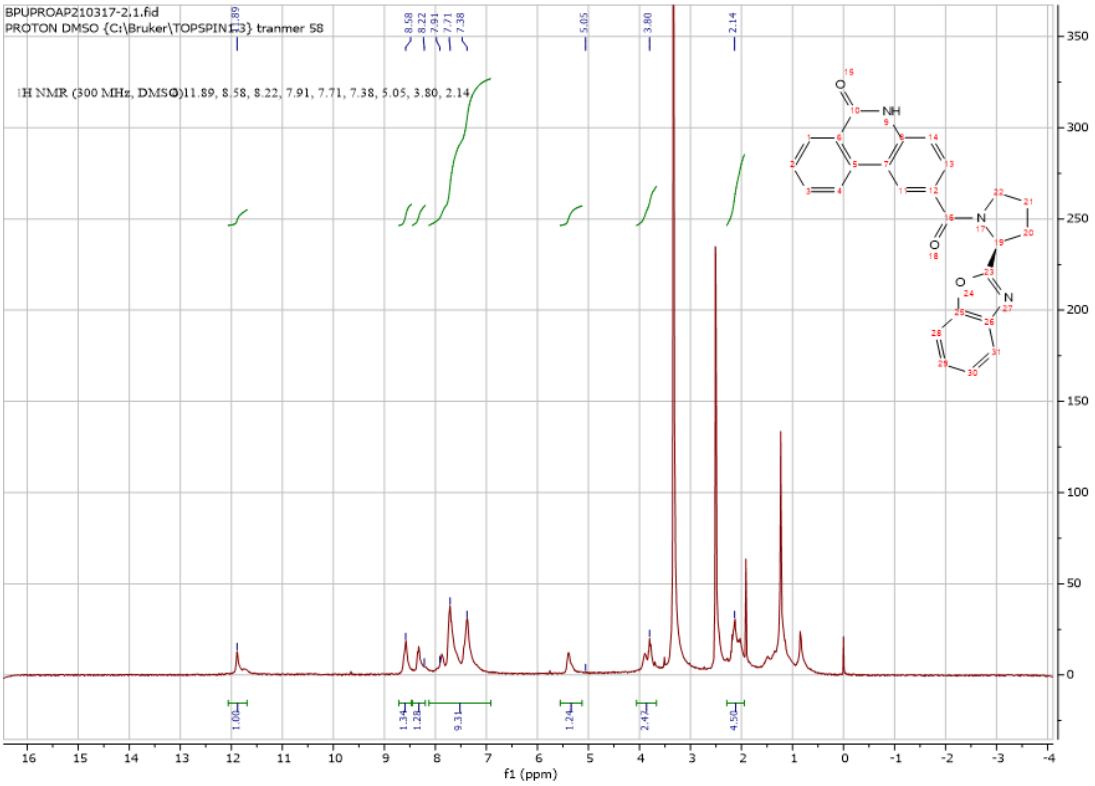
BPUPROAP210317-2,1.fid
PROTON DMSO {C:\Bruker\TOPSPIN1.3} tranmer 58
1H NMR (300 MHz, DMSO)11.89, 8.58, 8.22, 7.91, 7.71, 7.38, 5.05, 3.80, 2.14
f1 (ppm)

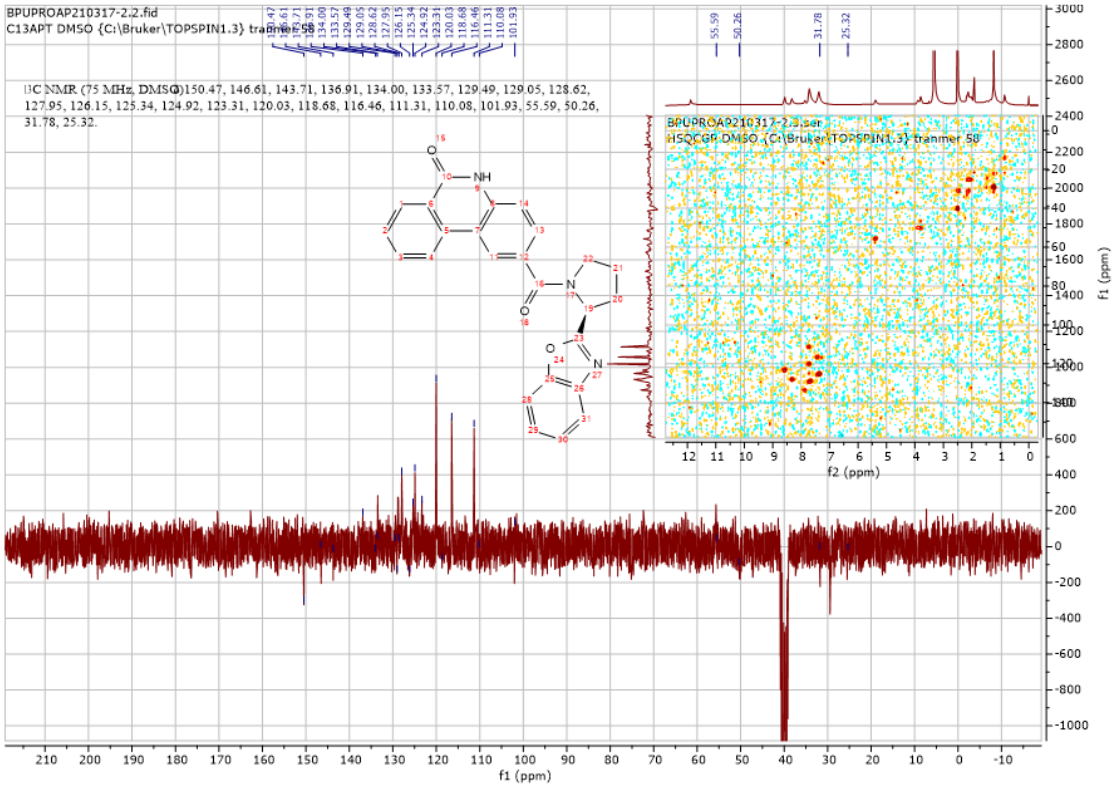
BPUPROAP210317-2,2.fid
C13APT DMSO {C:\Bruker\TOPSPIN1.3} tranmer 58
13C NMR (75 MHz, DMSO)150.47, 146.61, 143.71, 136.91, 134.00, 133.57, 129.49, 129.05, 128.62, 127.95, 126.15, 125.34, 124.92, 123.31, 120.03, 118.68, 116.46, 111.31, 110.08, 101.93, 55.59, 50.26, 31.78, 25.32.
BPUPROAP210317-2,3.ser
HSQCGP DMSO {C:\Bruker\TOPSPIN1.3} tranmer 58
f1 (ppm)
f2 (ppm)

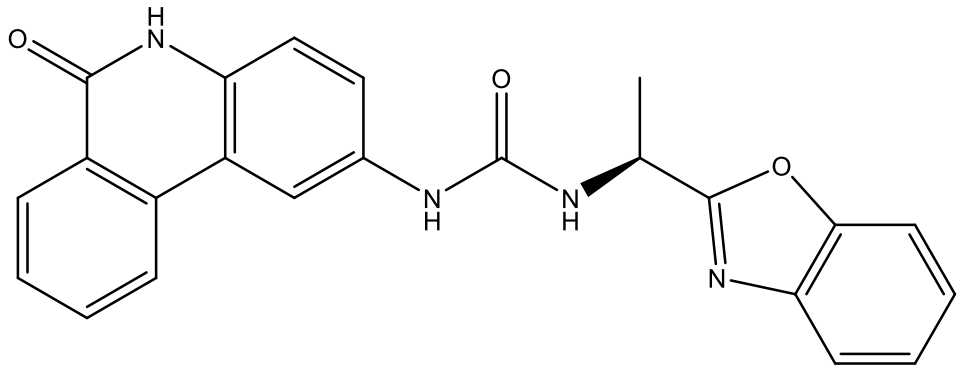

(*S*)-1-(1-(benzo[d]oxazol-2-yl)ethyl)-3-(6-oxo-5,6-dihydrophenanthridin-2-yl)urea (a16)

Using **Synthesis Method e**, 24mg (0.1mmol) **f2** was reacted with 16.2mg (0.1mmol) **f8** to give 12.1mg **a16** (Yield: 30%) and the product was separated as yellowish white solid. ^{1}H NMR (400 MHz, DMSO-d_6) δ 11.59 (s, 1H), 8.75 (s, 1H), 8.47 (d, *J* = 2.2 Hz, 1H), 8.32 (dd, *J* = 8.0, 1.2 Hz, 1H), 8.26 (d, *J* = 8.2 Hz, 1H), 7.85 (ddd, *J* = 8.3, 7.3, 1.5 Hz, 1H), 7.80 – 7.68 (m, 2H), 7.68 – 7.60 (m, 1H), 7.45 (dd, *J* = 8.8, 2.2 Hz, 1H), 7.41 – 7.32 (m, 2H), 7.27 (d, *J* = 8.8 Hz, 1H), 7.05 (d, *J* = 7.7 Hz, 1H), 5.19 (q, *J* = 7.1 Hz, 1H), 1.61 (d, *J* = 7.1 Hz, 3H). ^{13}C NMR (101 MHz, DMSO) δ 168.2, 160.8, 155.2, 141.1, 135.4, 134.5, 133.3, 131.9, 128.4, 128.1, 126.3, 125.5, 125.0, 122.7, 121.5, 120.1, 118.0, 116.9, 111.9, 111.3, 109.3, 44.4, 19.9. HRMS m/z (ESI+, M+Na): Calcd for C23H18N4O3: 421.1277, (ESI+, M+Na) found: 421.1270

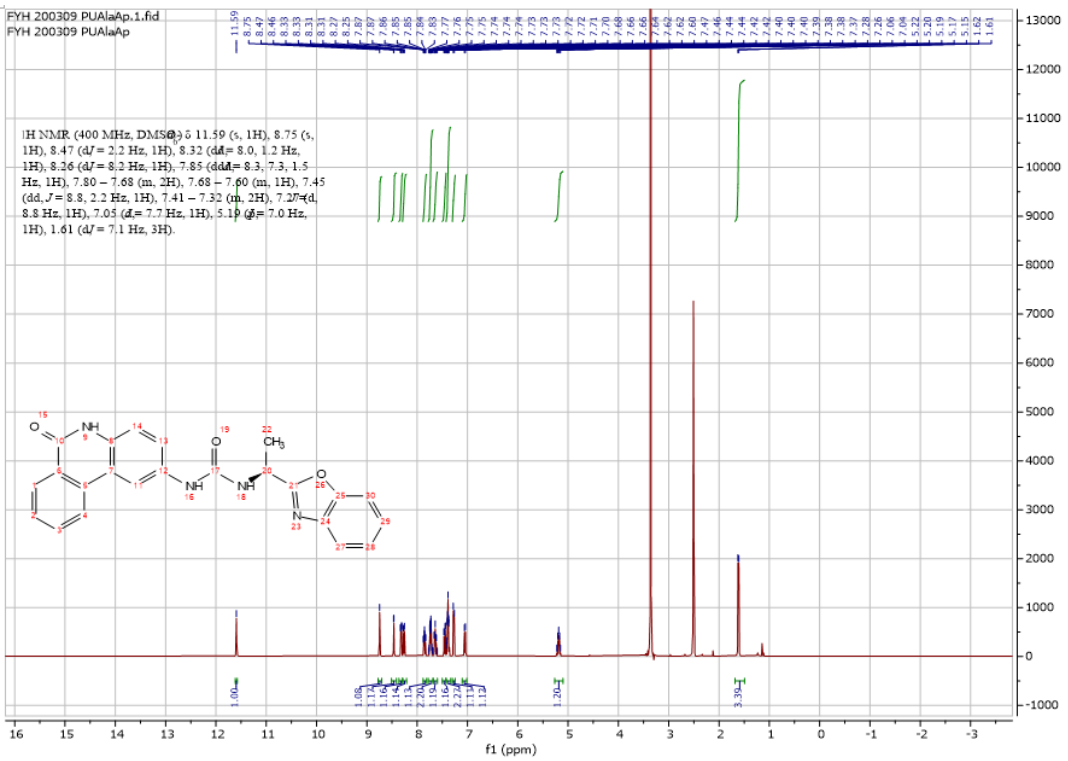
FYH 200309 PUAlaAp.1.fid
FYH 200309 PUAlaAp
1H NMR (400 MHz, DMSO) δ 11.59 (s, 1H), 8.75 (s, 1H), 8.47 (dd, J = 2.2 Hz, 1H), 8.32 (dd, J = 8.0, 1.2 Hz, 1H), 8.26 (dd, J = 8.2 Hz, 1H), 7.85 (ddd, J = 8.3, 7.3, 1.5 Hz, 1H), 7.80 – 7.68 (m, 2H), 7.68 – 7.60 (m, 1H), 7.45 (dd, J = 8.8, 2.2 Hz, 1H), 7.41 – 7.32 (m, 2H), 7.20 (d, J = 8.8 Hz, 1H), 7.05 (d, J = 7.7 Hz, 1H), 5.19 (d, J = 7.0 Hz, 1H), 1.61 (d, J = 7.1 Hz, 3H).
f1 (ppm)

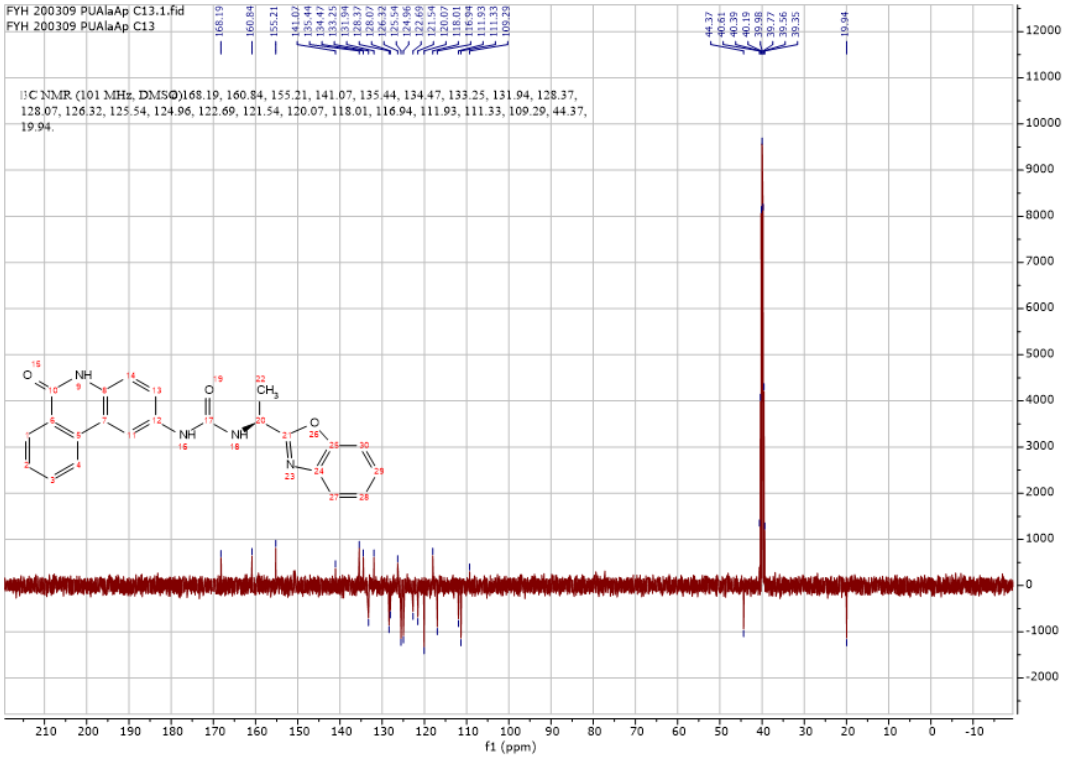
FYH 200309 PUAlaAp C13.1.fid
FYH 200309 PUAlaAp C13
13C NMR (101 MHz, DMSO) 168.19, 160.84, 155.21, 141.07, 135.44, 134.47, 133.25, 131.94, 128.37, 128.07, 126.32, 125.54, 124.96, 122.69, 121.54, 120.07, 118.01, 116.94, 111.93, 111.33, 109.29, 44.37, 19.94.
f1 (ppm)

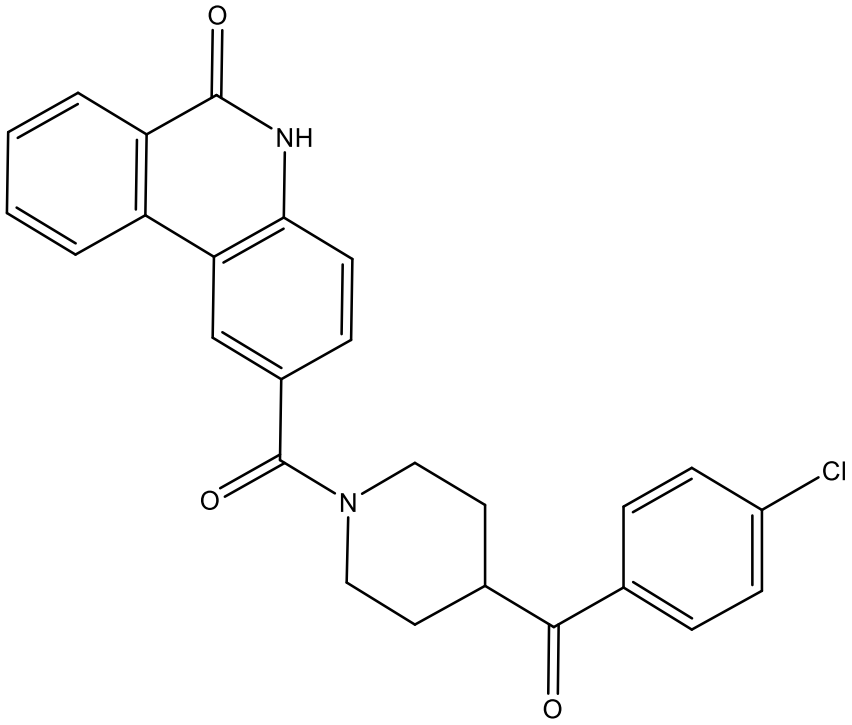

2-(4-(4-chlorobenzoyl)piperidine-1-carbonyl)phenanthridin-6(5*H*)-one (a17)

Using **Synthesis Method d**, 24mg (0.1mmol) **f2** was reacted with 22.4mg (0.1mmol) (4-chlorophenyl)(piperidin-4-yl)methanone to give 33.8mg **a17** (Yield: 76%) and the product was separated as yellowish white solid. ^{1}H NMR (300 MHz, DMSO-d_6) δ 11.82 (s, 1H), 8.59 (d, *J* = 8.2 Hz, 1H), 8.42 (d, *J* = 1.7 Hz, 1H), 8.33 (dd, *J* = 7.9, 1.4 Hz, 1H), 8.03 (dd, *J* = 9.0, 2.3 Hz, 2H), 7.87 (td, *J* = 8.1, 7.7, 1.5 Hz, 1H), 7.71 – 7.64 (m, 1H), 7.62 (d, *J* = 8.6 Hz, 2H), 7.53 (dd, *J* = 8.3, 1.7 Hz, 1H), 7.41 (d, *J* = 8.3 Hz, 1H), 3.74 (p, *J* = 6.0 Hz, 1H), 1.87 (m, 4H), 1.68 – 1.51 (m, 4H). ^{13}C NMR (75 MHz, DMSO) δ 201.43, 169.3, 161.3, 138.6, 137.7, 134.6, 134.3, 133.5, 130.7, 130.5, 129.4, 128.8, 128.7, 128.0, 126.2, 123.4, 122.7, 117.7, 116.5, 43.0, 28.6. HRMS m/z (ESI+, M+Na): Calcd for C26H21ClN2O3: 467.1138, (ESI+, M+Na) found: 467.1116

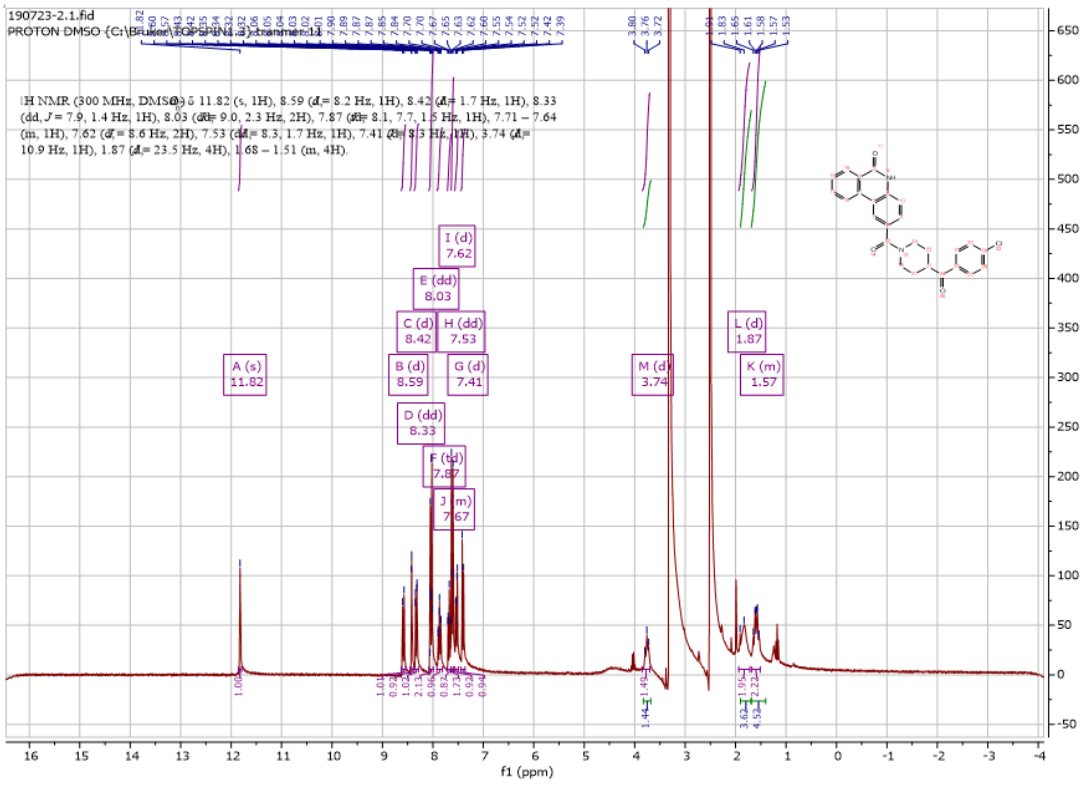
190723-2.1.fid
PROTON DMSO {C:\Bruker\TOPSPIN4.3} tranmer 11
¹H NMR (300 MHz, DMSO) δ 11.82 (s, 1H), 8.59 (d, J = 8.2 Hz, 1H), 8.42 (d, J = 1.7 Hz, 1H), 8.33 (dd, J = 7.9, 1.4 Hz, 1H), 8.03 (dd, J = 9.0, 2.3 Hz, 2H), 7.87 (td, J = 8.1, 7.7, 1.5 Hz, 1H), 7.71 – 7.64 (m, 1H), 7.62 (d, J = 8.6 Hz, 2H), 7.53 (dd, J = 8.3, 1.7 Hz, 1H), 7.41 (d, J = 8.3 Hz, 1H), 3.74 (d, J = 10.9 Hz, 1H), 1.87 (d, J = 23.5 Hz, 4H), 1.68 – 1.51 (m, 4H).
I (d) 7.62
E (dd) 8.03
C (d) 8.42
H (dd) 7.53
L (d) 1.87
A (s) 11.82
B (d) 8.59
G (d) 7.41
M (d) 3.74
K (m) 1.57
D (dd) 8.33
F (td) 7.87
J (m) 7.67
f1 (ppm)

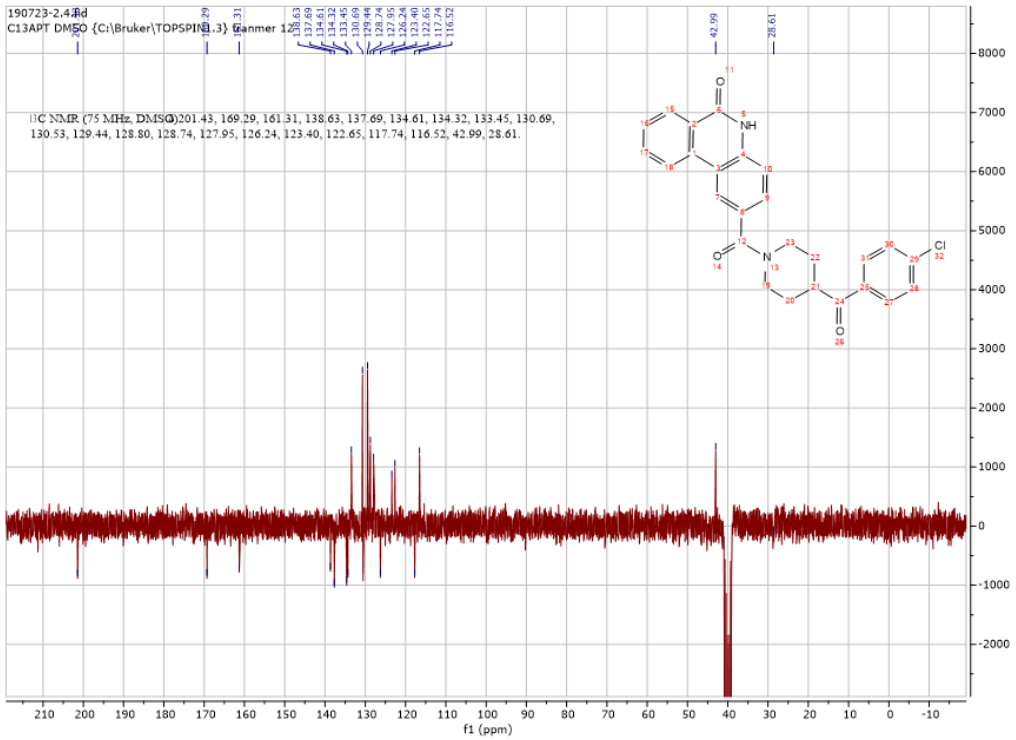
190723-2.4.fid
C13APT DMSO {C:\Bruker\TOPSPIN4.3} tranmer 12
¹³C NMR (75 MHz, DMSO) 201.43, 169.29, 161.31, 138.63, 137.69, 134.61, 134.32, 133.45, 130.69, 130.53, 129.44, 128.80, 128.74, 127.95, 126.24, 123.40, 122.65, 117.74, 116.52, 42.99, 28.61.
f1 (ppm)

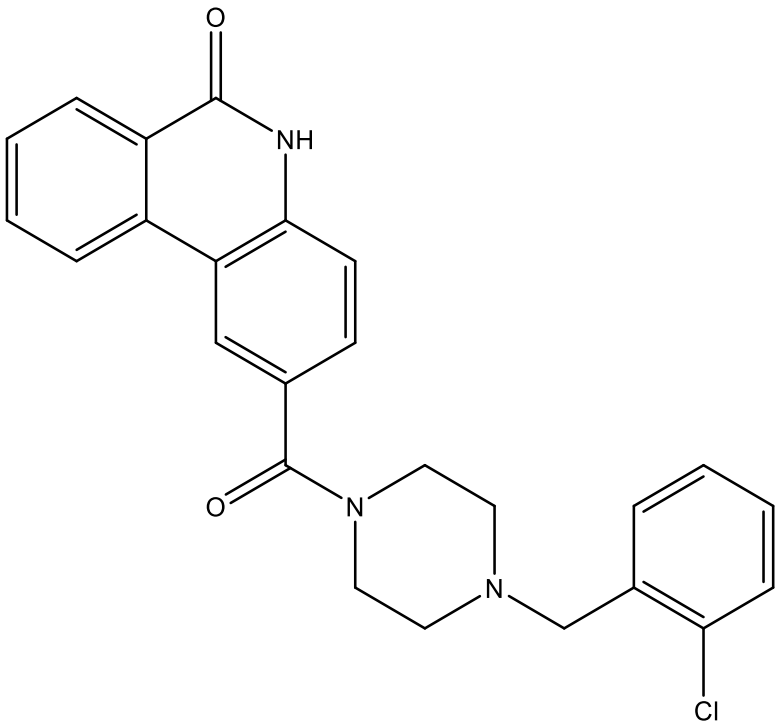

2-(4-(2-chlorobenzyl)piperazine-1-carbonyl)phenanthridin-6(5*H*)-one (a18)

Using **Synthesis Method d**, 24mg (0.1mmol) **f2** was reacted with 21mg (0.1mmol) 1-(2-chlorobenzyl)piperazine to give 27.2mg **a18** (Yield: 63%) and the product was separated as yellowish white solid. ^{1}H NMR (300 MHz, DMSO-d_6) δ 11.83 (s, 1H), 8.57 (d, J = 8.1 Hz, 1H), 8.41 (s, 1H), 8.38 – 8.29 (m, 1H), 7.93 – 7.81 (m, 1H), 7.67 (t, J = 7.4 Hz, 1H), 7.57 – 7.48 (m, 2H), 7.47 – 7.38 (m, 2H), 7.31 (dtd, J = 14.6, 7.3, 1.8 Hz, 2H), 3.62 (m, 8H), 2.50 (d, J = 1.8 Hz, 2H). ^{13}C NMR (75 MHz, DMSO) δ 169.1, 161.3, 137.8, 135.8, 134.3, 133.8, 133.4, 131.4, 130.2, 129.8, 129.2, 128.9, 128.8, 128.0, 127.5, 126.3, 123.4, 122.9, 117.7, 116.5, 58.9, 53.0. HRMS m/z (ESI+, M+H): Calcd for C25H22ClN3O2: 432.1473, (ESI+, M+H) found: 432.1474

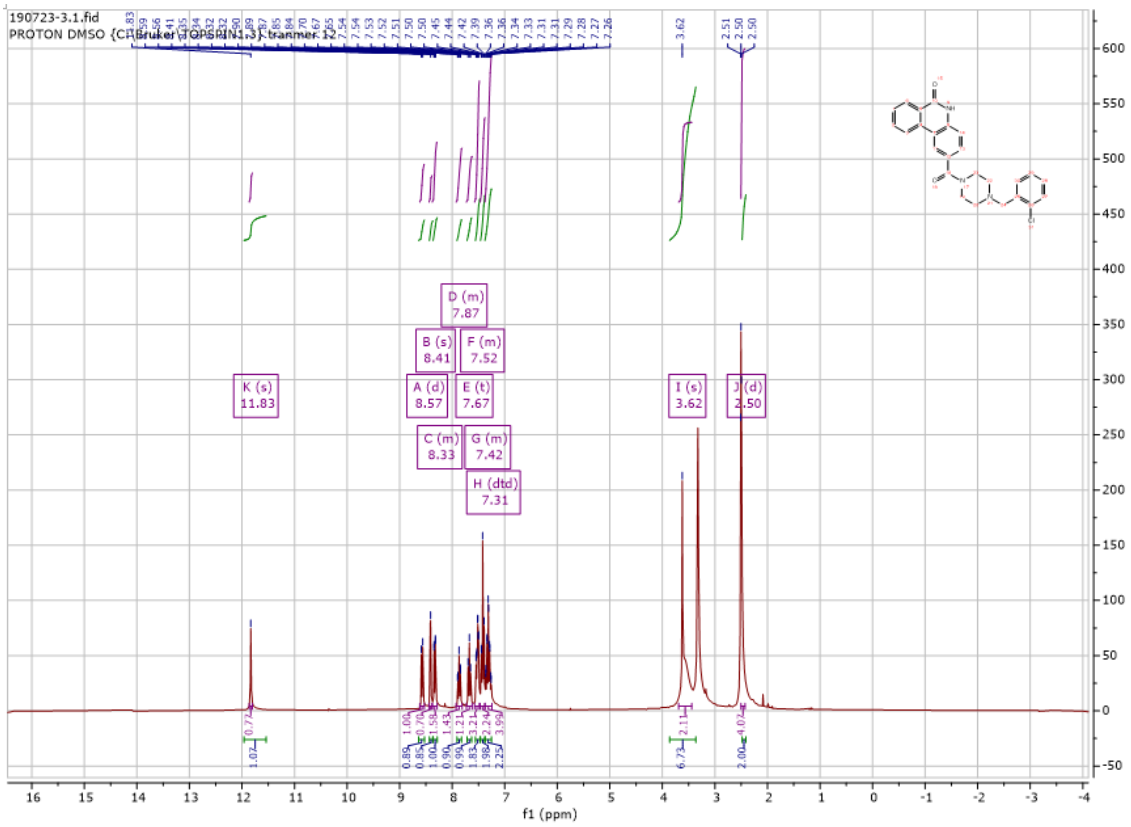
190723-3.1.fid
PROTON DMSO {C:\Bruker\TOPSPIN1.3} tranmer
D (m) 7.87
B (s) 8.41
F (m) 7.52
K (s) 11.83
A (d) 8.57
E (t) 7.67
I (s) 3.62
J (d) 2.50
C (m) 8.33
G (m) 7.42
H (dtd) 7.31
f1 (ppm)

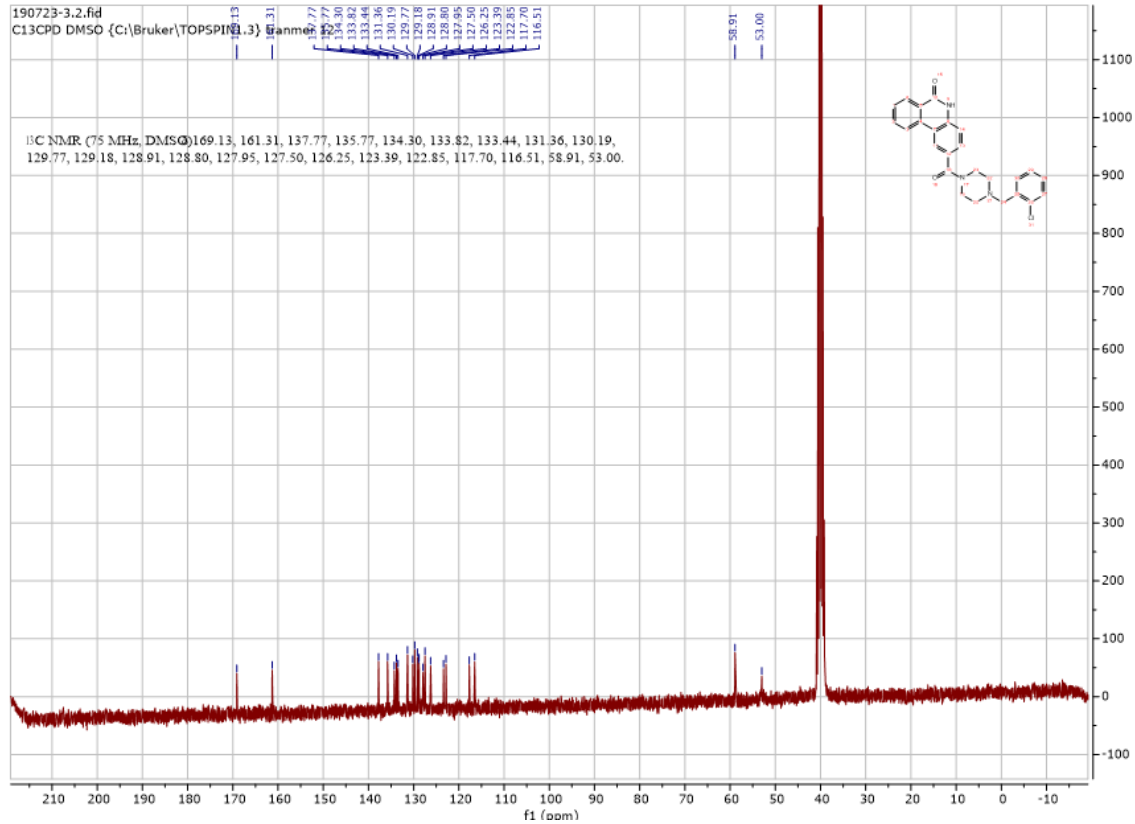
190723-3.2.fid
C13CPD DMSO {C:\Bruker\TOPSPIN1.3} tranmer
13C NMR (75 MHz, DMSO) 169.13, 161.31, 137.77, 135.77, 134.30, 133.82, 133.44, 131.36, 130.19, 129.77, 129.18, 128.91, 128.80, 127.95, 127.50, 126.25, 123.39, 122.85, 117.70, 116.51, 58.91, 53.00.
f1 (ppm)

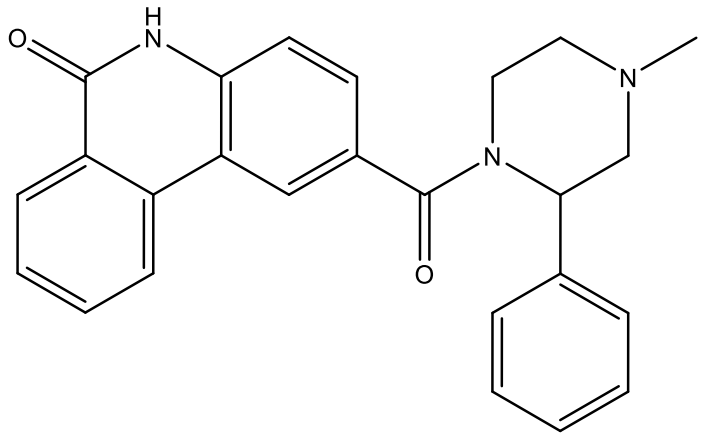

2-(4-methyl-2-phenylpiperazine-1-carbonyl)phenanthridin-6(5*H*)-one (a19)

Using **Synthesis Method d**, 24mg (0.1mmol) **f2** was reacted with 17.7mg (0.1mmol) 1-methyl-3-phenylpiperazine to give 21.4mg **a19** (Yield: 54%) and the product was separated as yellowish white solid. ^{1}H NMR (300 MHz, DMSO-d_6) δ 11.83 (s, 1H), 8.40 (s, 2H), 8.32 (d, *J* = 7.9 Hz, 1H), 7.85 (t, *J* = 7.2 Hz, 1H), 7.67 (t, *J* = 7.5 Hz, 1H), 7.55 (dd, *J* = 8.3, 1.5 Hz, 1H), 7.48 (d, *J* = 7.4 Hz, 2H), 7.44 – 7.35 (m, 3H), 7.28 (t, *J* = 7.2 Hz, 1H), 3.14 (t, *J* = 6.0 Hz, 1H), 2.712.42 (m, 2H), 2.22 (s, 3H), 2.15 − 1.23 (m, 2H), 1.21 (s, 2H). ^{13}C NMR (75 MHz, DMSO) δ 170.1, 161.3, 140.3, 137.8, 134.2, 133.4, 130.2, 128.8, 128.7, 128.6, 128.0, 127.7, 127.1, 126.3, 123.3, 122.4, 117.8, 116.6, 57.4, 55.1, 46.2, 29.2, 18.0. HRMS m/z (ESI+, M+H): Calcd for C25H23N3O2: 398.1790, (ESI+, M+H) found: 398.1869

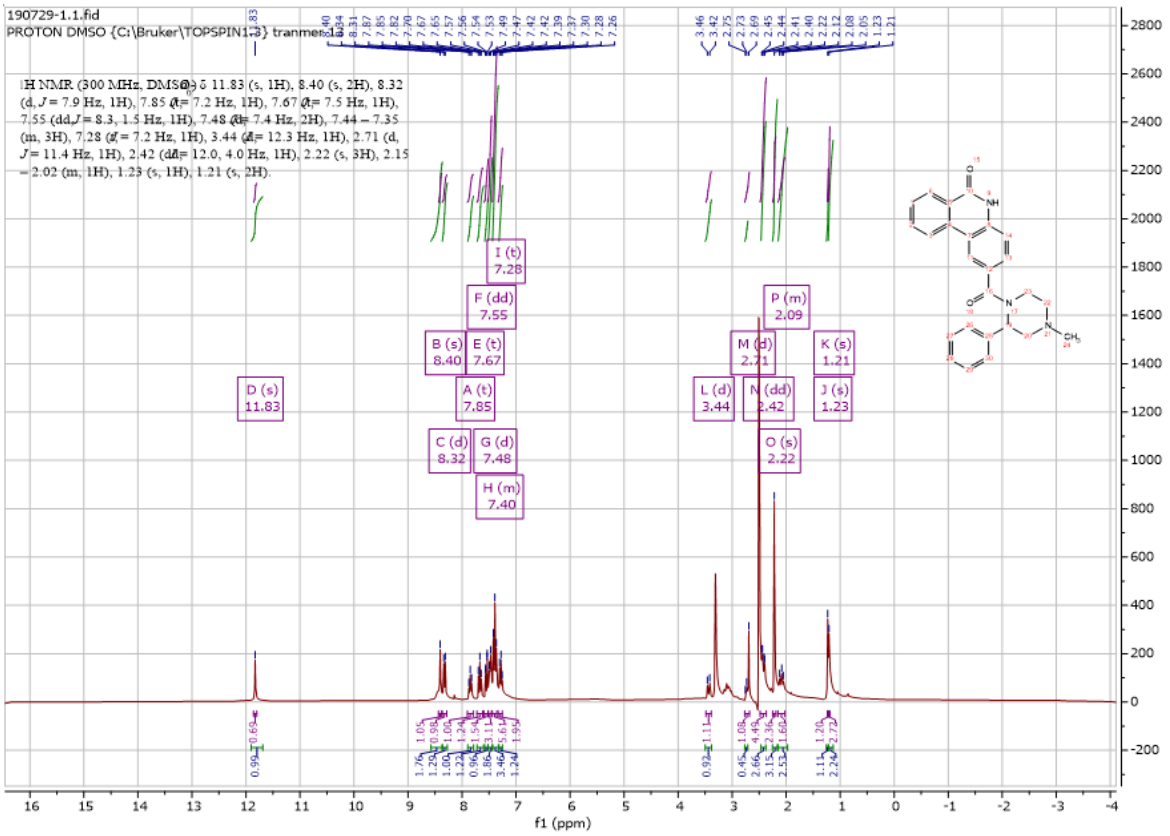
190729-1.1.fid
PROTON DMSO {C:\Bruker\TOPSPIN1.3} tranmenta
1H NMR (300 MHz, DMSO) δ 11.83 (s, 1H), 8.40 (s, 2H), 8.32 (d, J = 7.9 Hz, 1H), 7.85 (t, J = 7.2 Hz, 1H), 7.67 (t, J = 7.5 Hz, 1H), 7.55 (dd, J = 8.3, 1.5 Hz, 1H), 7.48 (d, J = 7.4 Hz, 2H), 7.44 – 7.35 (m, 3H), 7.28 (t, J = 7.2 Hz, 1H), 3.44 (d, J = 12.3 Hz, 1H), 2.71 (d, J = 11.4 Hz, 1H), 2.42 (dd, J = 12.0, 4.0 Hz, 1H), 2.22 (s, 3H), 2.15 – 2.02 (m, 1H), 1.23 (s, 1H), 1.21 (s, 2H).
I (t) 7.28
F (dd) 7.55
B (s) 8.40
E (t) 7.67
A (t) 7.85
D (s) 11.83
C (d) 8.32
G (d) 7.48
H (m) 7.40
P (m) 2.09
M (d) 2.71
K (s) 1.21
L (d) 3.44
N (dd) 2.42
J (s) 1.23
O (s) 2.22
f1 (ppm)

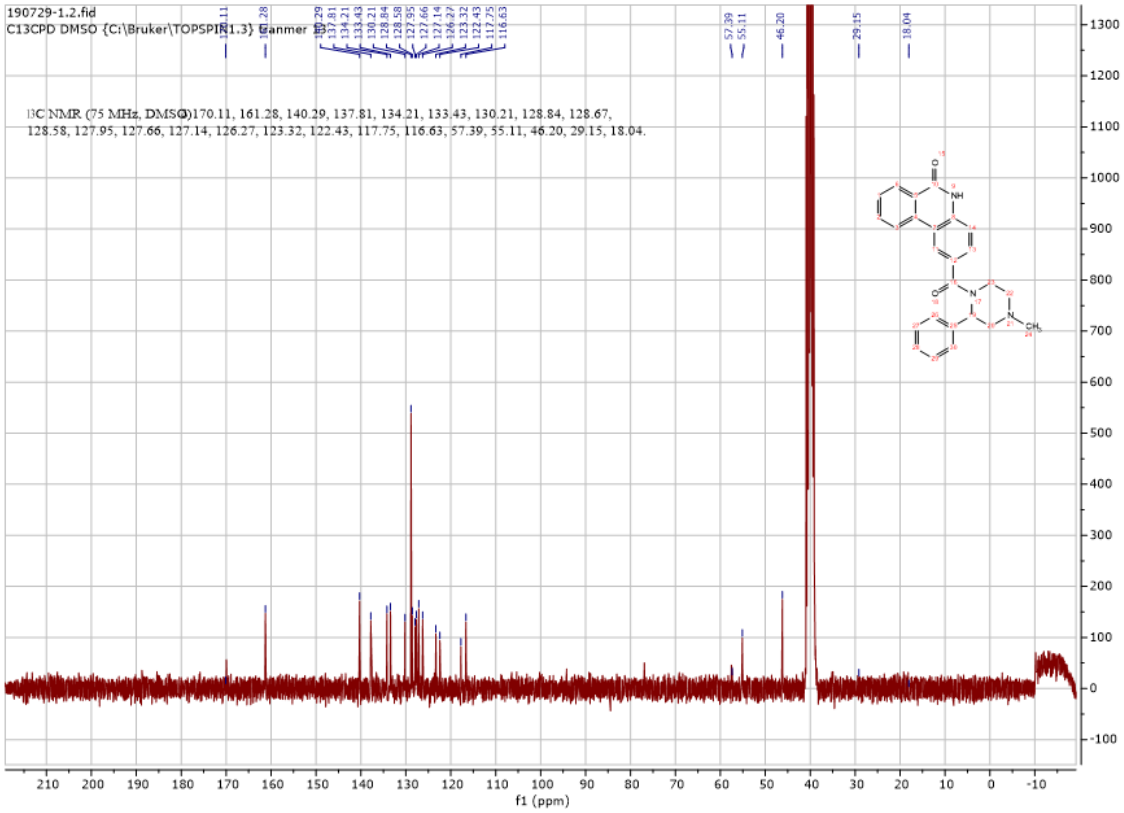
190729-1.2.fid
C13CPD DMSO {C:\Bruker\TOPSPIN1.3} tanmer 13
13C NMR (75 MHz, DMSO) 170.11, 161.28, 140.29, 137.81, 134.21, 133.43, 130.21, 128.84, 128.67, 128.58, 127.95, 127.66, 127.14, 126.27, 123.32, 122.43, 117.75, 116.63, 57.39, 55.11, 46.20, 29.15, 18.04.
f1 (ppm)

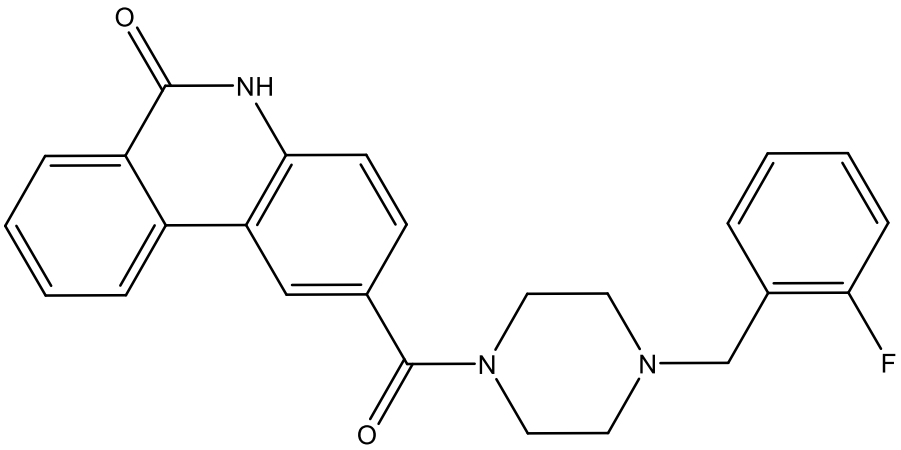

2-(4-(2-fluorobenzyl)piperazine-1-carbonyl)phenanthridin-6(5*H*)-one (a20)

Using **Synthesis Method d**, 24mg (0.1mmol) **f2** was reacted with 19.6mg (0.1mmol) 1-(2-fluorobenzyl)piperazine to give 23.2mg **a20** (Yield: 56%) and the product was separated as yellowish white solid. ^{1}H NMR (300 MHz, DMSO-d_6) δ 11.83 (s, 1H), 8.56 (d, J = 8.1 Hz, 1H), 8.40 (s, 1H), 8.37 – 8.29 (m, 1H), 7.92 – 7.81 (m, 1H), 7.67 (t, J = 7.5 Hz, 1H), 7.51 (dd, J = 8.3, 1.5 Hz, 1H), 7.47 – 7.35 (m, 2H), 7.35 – 7.28 (m, 1H), 7.23 – 7.10 (m, 2H), 3.58 (m, 6H), 2.45 (m, 4H). ^{13}C NMR (75 MHz, DMSO-d_6) δ 169.1, 161.3, 161.3 (d, J = 244.1 Hz), 137.8, 134.3, 133.4, 132.0 (d, J = 4.5 Hz), 130.2, 129.7 (d, J = 8.2 Hz), 128.9, 128.8, 127.9, 126.3, 124.7 (d, J = 7.9 Hz), 124.6 (d, J = 3.6 Hz), 123.4, 122.9, 117.7, 116.5, 115.7 (d, J = 22.0 Hz), 54.9, 52.7. HRMS m/z (ESI+, M+H): Calcd for C25H22FN3O2: 416.1769, (ESI+, M+H) found: 416.1769

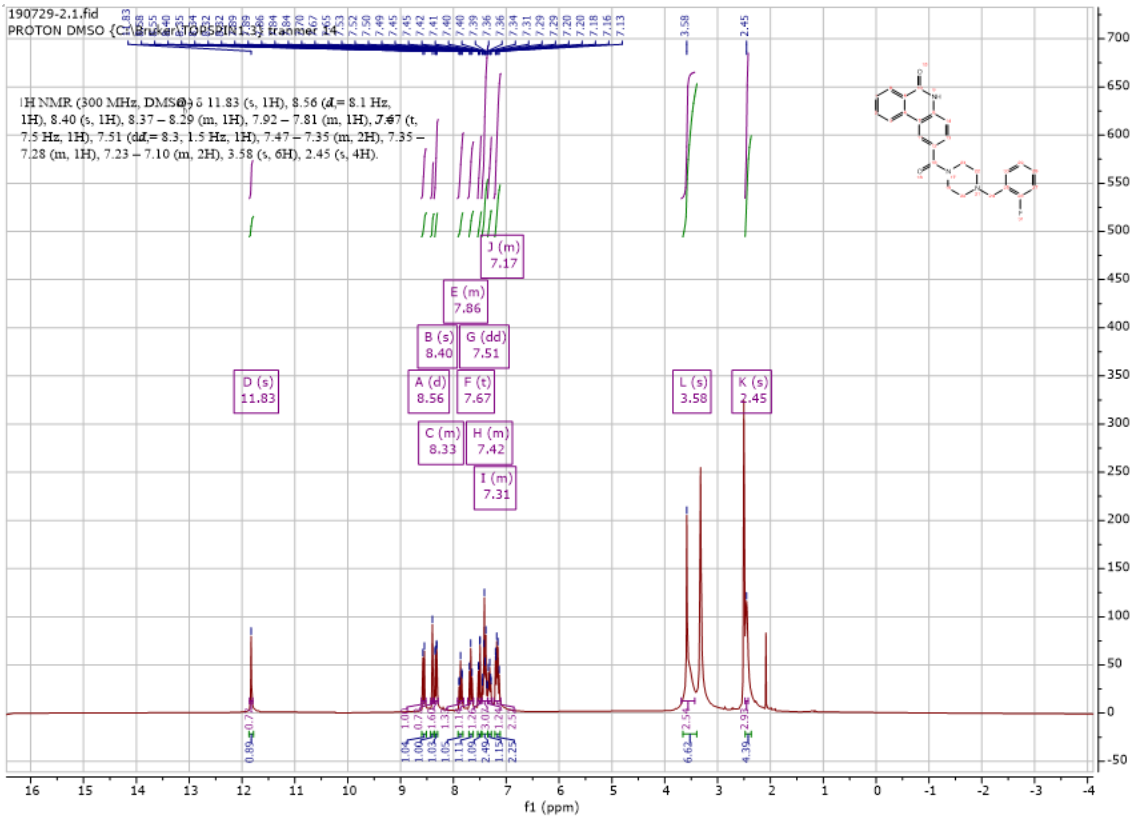
190729-2.1.fid
PROTON DMSO {C:\Bruker\TOPSPIN1.3} tranmer 14
¹H NMR (300 MHz, DMSO-d6) δ 11.83 (s, 1H), 8.56 (d, J = 8.1 Hz, 1H), 8.40 (s, 1H), 8.37 – 8.29 (m, 1H), 7.92 – 7.81 (m, 1H), 7.67 (t, J = 7.5 Hz, 1H), 7.51 (dd, J = 8.3, 1.5 Hz, 1H), 7.47 – 7.35 (m, 2H), 7.35 – 7.28 (m, 1H), 7.23 – 7.10 (m, 2H), 3.58 (s, 6H), 2.45 (s, 4H).
J (m) 7.17
E (m) 7.86
B (s) 8.40
G (dd) 7.51
D (s) 11.83
A (d) 8.56
F (t) 7.67
L (s) 3.58
K (s) 2.45
C (m) 8.33
H (m) 7.42
I (m) 7.31
f1 (ppm)

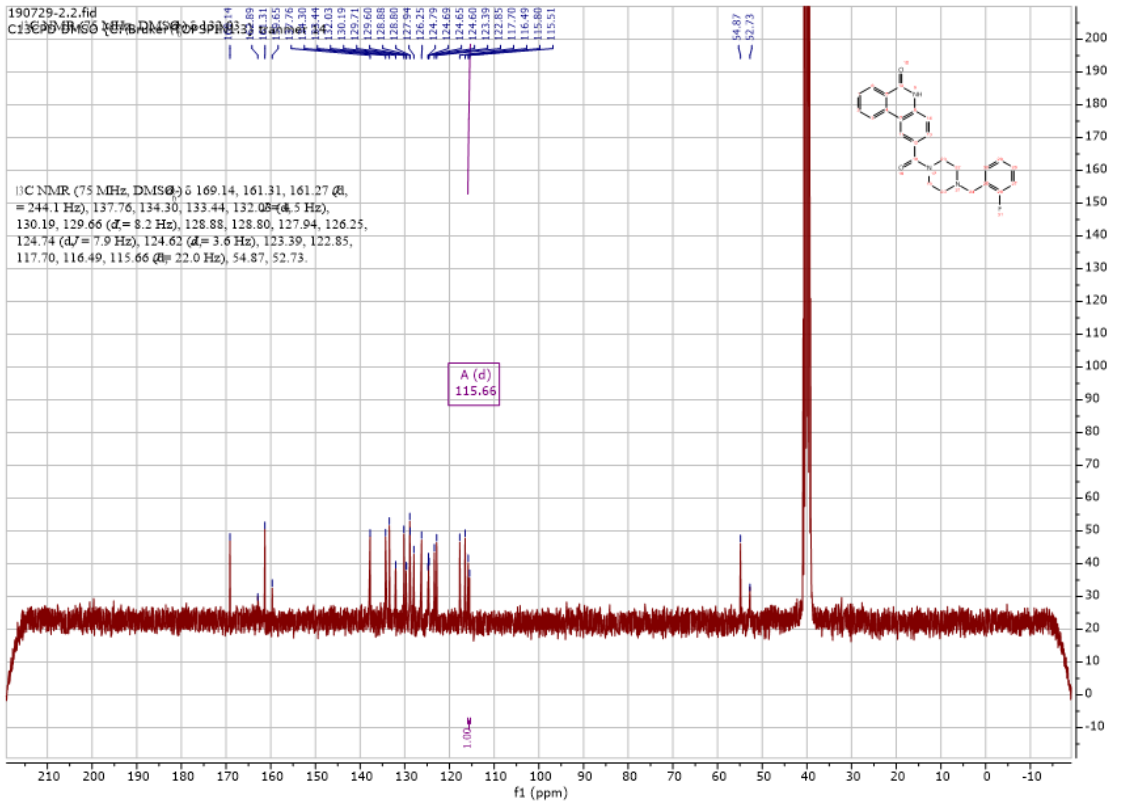
190729-2.2.fid
¹³C NMR (75 MHz, DMSO-d6) δ 169.14, 161.31, 161.27 (d, J = 244.1 Hz), 137.76, 134.30, 133.44, 132.03 (d, J = 4.5 Hz), 130.19, 129.66 (d, J = 8.2 Hz), 128.88, 128.80, 127.94, 126.25, 124.74 (d, J = 7.9 Hz), 124.62 (d, J = 3.6 Hz), 123.39, 122.85, 117.70, 116.49, 115.66 (d, J = 22.0 Hz), 54.87, 52.73.
A (d) 115.66
f1 (ppm)

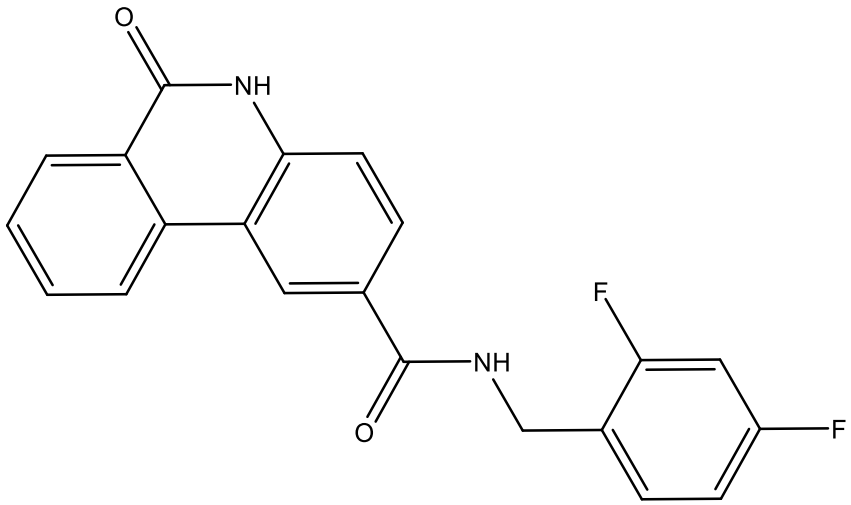

***N*-(2,4-difluorobenzyl)-6-oxo-5,6-dihydrophenanthridine-2-carboxamide (a21)**

Using **Synthesis Method d**, 24mg (0.1mmol) **f2** was reacted with 14.4mg (0.1mmol) (2,4-difluorophenyl)methanamine to give 29.8mg **a21** (Yield: 82%) and the product was separated as yellowish white solid. ^{1}H NMR (300 MHz, DMSO-d_6) δ 11.90 (s, 1H), 9.14 (t, *J* = 5.6 Hz, 1H), 8.94 (d, *J* = 1.4 Hz, 1H), 8.57 (d, *J* = 8.1 Hz, 1H), 8.34 (dd, *J* = 7.9, 1.1 Hz, 1H), 8.03 (dd, *J* = 8.5, 1.7 Hz, 1H), 7.98 – 7.86 (m, 1H), 7.69 (t, *J* = 7.5 Hz, 1H), 7.54 – 7.44 (m, 1H), 7.42 (d, *J* = 8.5 Hz, 1H), 7.24 (td, *J* = 10.5, 2.5 Hz, 1H), 7.14 – 7.02 (m, 1H), 4.56 (d, *J* = 5.4 Hz, 2H). ^{13}C NMR (75 MHz, DMSO-d_6) δ 166.1, 161.4, 159.5 (dd, *J* = 114.1 Hz, *J* = 12 Hz), 139.2, 134.5, 133.4, 131.4 (*J* = 9.75 Hz, *J* = 6.075 Hz), 129.4, 128.8, 128.1, 128.0, 126.2, 123.3, 123.1 (*J* = 15.225 Hz, *J* = 3.75 Hz), 122.8, 117.5, 116.5, 111.8 (d, *J* = 21.1 Hz, *J* = 4.05 Hz), 104.1 (t, *J* = 25.9 Hz), 36.7. HRMS m/z (ESI+, M+Na): Calcd for C21H14F2N2O2: 387.0921, (ESI+, M+Na) found: 387.0917

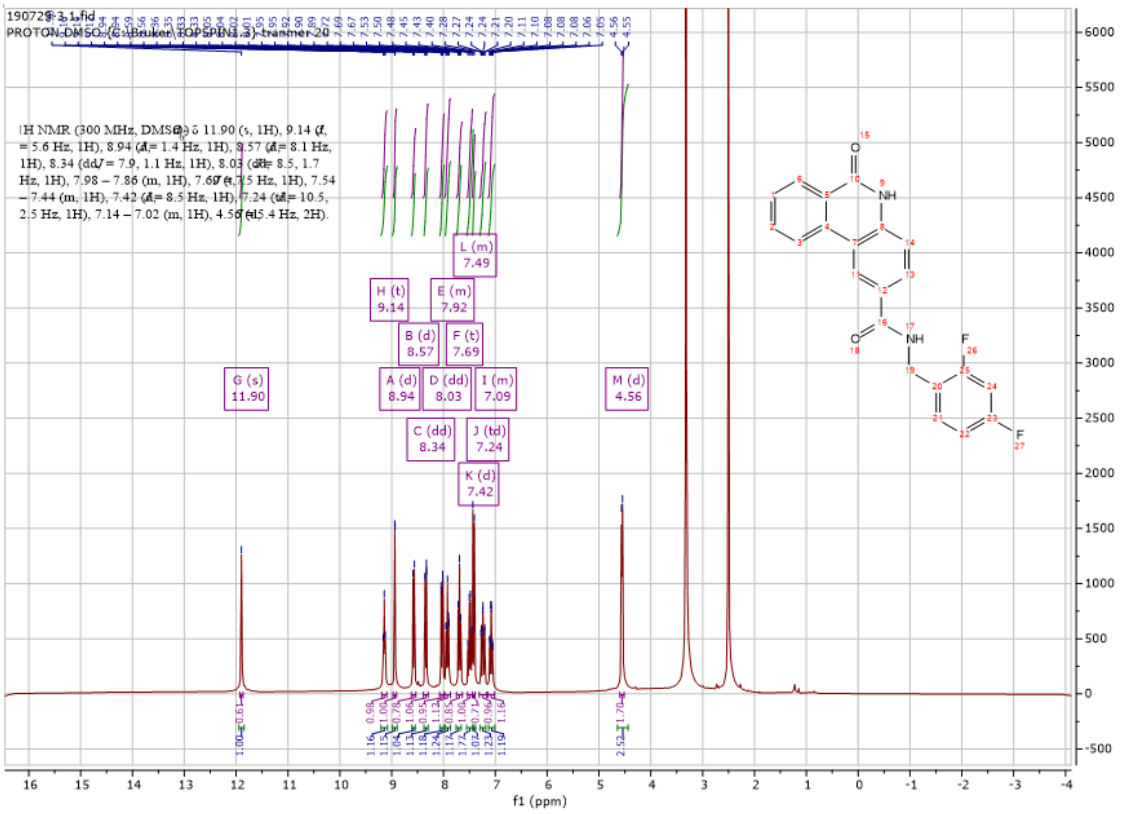
190729-3.1.fid
PROTON-DMSO {C:\Bruker\TOPSPIN3.5} tranmer-20
¹H NMR (300 MHz, DMSO-d6) δ 11.90 (s, 1H), 9.14 (t, J = 5.6 Hz, 1H), 8.94 (d, J = 1.4 Hz, 1H), 8.57 (d, J = 8.1 Hz, 1H), 8.34 (dd, J = 7.9, 1.1 Hz, 1H), 8.03 (dd, J = 8.5, 1.7 Hz, 1H), 7.98 – 7.86 (m, 1H), 7.69 (t, J = 7.5 Hz, 1H), 7.54 – 7.44 (m, 1H), 7.42 (d, J = 8.5 Hz, 1H), 7.24 (td, J = 10.5, 2.5 Hz, 1H), 7.14 – 7.02 (m, 1H), 4.56 (d, J = 5.4 Hz, 2H).
L (m) 7.49
H (t) 9.14
E (m) 7.92
B (d) 8.57
F (t) 7.69
G (s) 11.90
A (d) 8.94
D (dd) 8.03
I (m) 7.09
M (d) 4.56
C (dd) 8.34
J (td) 7.24
K (d) 7.42
f1 (ppm)

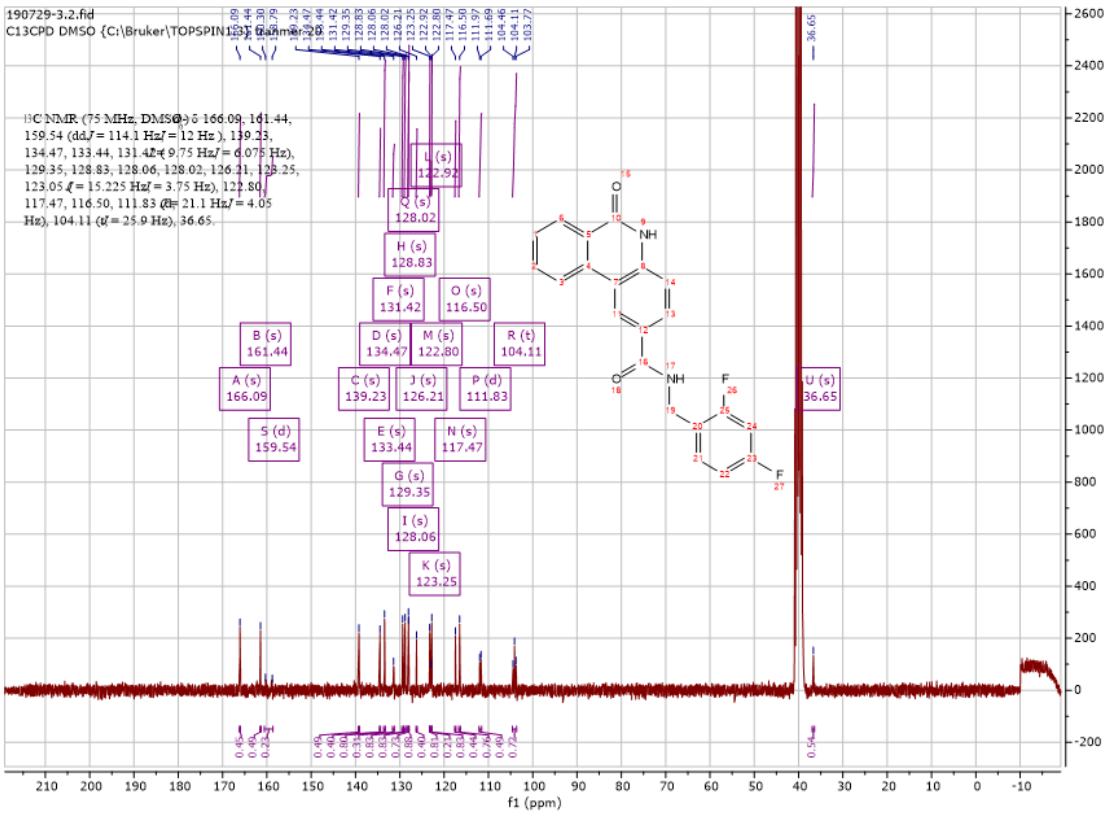
190729-3.2.fid
C13CPD DMSO {C:\Bruker\TOPSPIN3.5} tranmer-26
¹³C NMR (75 MHz, DMSO-d6) δ 166.09, 161.44, 159.54 (dd, J = 114.1 Hz, J = 12 Hz), 139.23, 134.47, 133.44, 131.42 (t, J = 9.75 Hz, J = 6.075 Hz), 129.35, 128.83, 128.06, 128.02, 126.21, 123.25, 123.05 (t, J = 15.225 Hz, J = 3.75 Hz), 122.80, 117.47, 116.50, 111.83 (d, J = 21.1 Hz, J = 4.05 Hz), 104.11 (d, J = 25.9 Hz), 36.65.
L (s) 122.92
Q (s) 128.02
H (s) 128.83
F (s) 131.42
O (s) 116.50
B (s) 161.44
D (s) 134.47
M (s) 122.80
R (t) 104.11
A (s) 166.09
C (s) 139.23
J (s) 126.21
P (d) 111.83
U (s) 36.65
S (d) 159.54
E (s) 133.44
N (s) 117.47
G (s) 129.35
I (s) 128.06
K (s) 123.25
f1 (ppm)

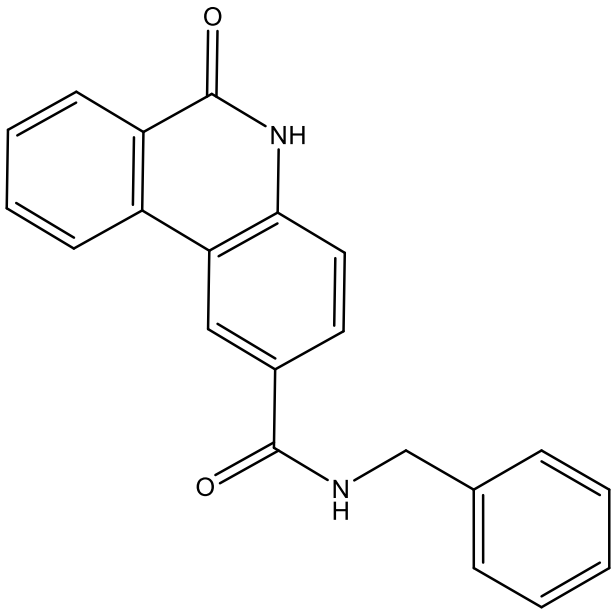

***N*-benzyl-6-oxo-5,6-dihydrophenanthridine-2-carboxamide (a22)**

Using **Synthesis Method d**, 24mg (0.1mmol) **f2** was reacted with 10.7mg (0.1mmol) phenylmethanamine to give 26.9mg **a22** (Yield: 82%) and the product was separated as yellowish white solid. ^{1}H NMR (300 MHz, DMSO-d_6) δ 12.30 (s, 1H), 9.26 (dd, *J* = 6.7, 4.1 Hz, 2H), 9.00 (d, *J* = 2.1 Hz, 1H), 8.57 (d, *J* = 8.1 Hz, 1H), 8.35 (dd, *J* = 8.0, 1.4 Hz, 1H), 7.95 (ddd, *J* = 8.3, 7.2, 1.5 Hz, 1H), 7.79 – 7.68 (m, 1H), 7.45 – 7.30 (m, 5H), 7.27 (ddt, *J* = 8.5, 5.6, 2.0 Hz, 1H), 4.58 (d, *J* = 5.8 Hz, 2H). ^{13}C NMR (75 MHz, DMSO) δ 164.7, 162.4, 150.3, 149.4, 139.8, 133.7, 133.1, 131.2, 129.6, 128.8, 128.0, 128.1, 127.9, 127.4, 126.4, 124.8, 123.7, 112.8, 43.2. HRMS m/z (ESI-, M-H): Calcd for C21H16N2O2: 327.1139, (ESI-,M-H) found 328.1085.

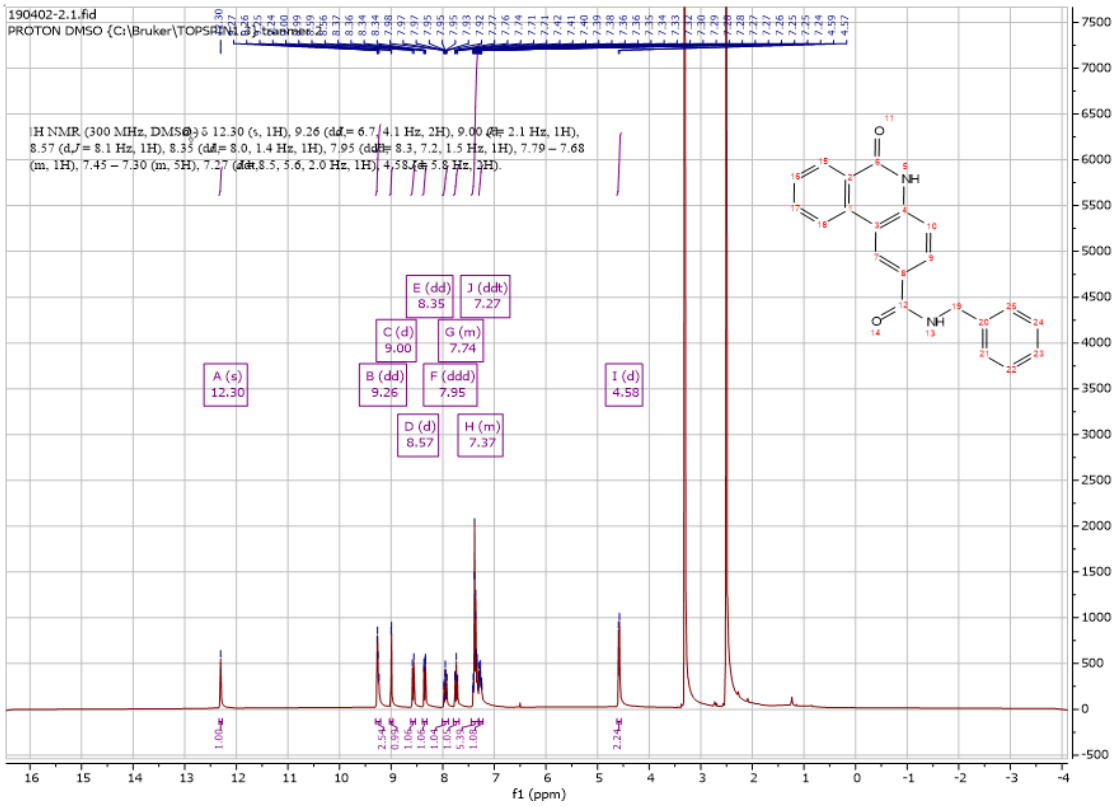
190402-2.1.fid
PROTON DMSO {C:\Bruker\TOPSPIN1.3 pl 7\nmrdata} 8
1H NMR (300 MHz, DMSO) δ 12.30 (s, 1H), 9.26 (dd, J = 6.7, 4.1 Hz, 2H), 9.00 (d, J = 2.1 Hz, 1H), 8.57 (d, J = 8.1 Hz, 1H), 8.35 (dd, J = 8.0, 1.4 Hz, 1H), 7.95 (ddd, J = 8.3, 7.2, 1.5 Hz, 1H), 7.79 – 7.68 (m, 1H), 7.45 – 7.30 (m, 5H), 7.27 (ddt, J = 8.5, 5.6, 2.0 Hz, 1H), 4.58 (d, J = 5.8 Hz, 2H).
A (s) 12.30
B (dd) 9.26
C (d) 9.00
D (d) 8.57
E (dd) 8.35
F (ddd) 7.95
G (m) 7.74
H (m) 7.37
J (ddt) 7.27
I (d) 4.58
f1 (ppm)

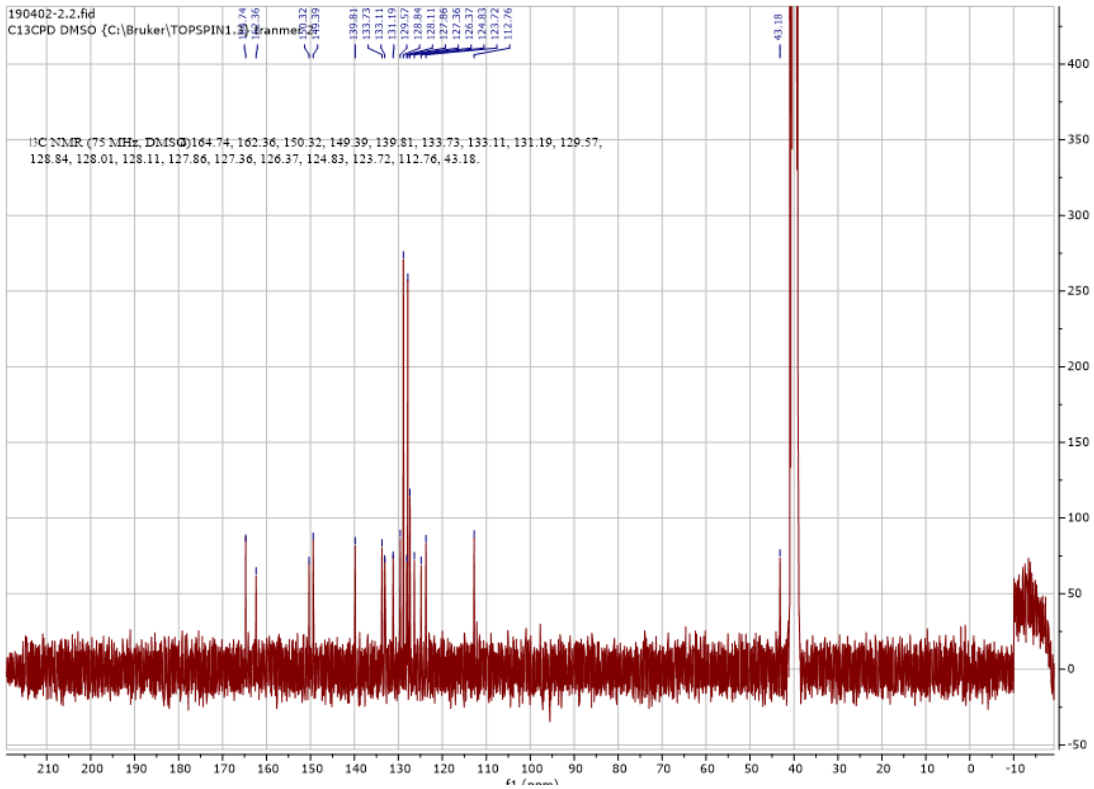
190402-2.2.fid
C13CPD DMSO {C:\Bruker\TOPSPIN1.3 pl 7\nmrdata} 8
13C NMR (75 MHz, DMSO) 164.74, 162.36, 150.32, 149.39, 139.81, 133.73, 133.11, 131.19, 129.57, 128.84, 128.01, 128.11, 127.86, 127.36, 126.37, 124.83, 123.72, 112.76, 43.18.
f1 (ppm)

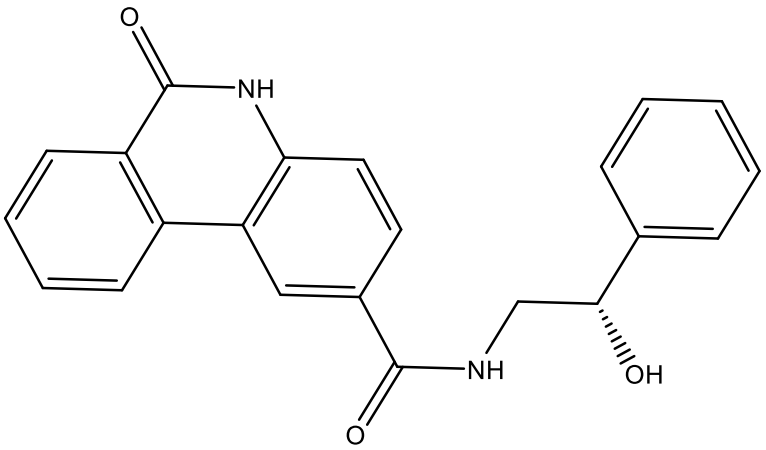

(*S*)-N-(2-hydroxy-2-phenylethyl)-6-oxo-5,6-dihydrophenanthridine-2-carboxamide (a23)

Using **Synthesis Method d**, 24mg (0.1mmol) **f2** was reacted with 13.7mg (0.1mmol) (*S*)-2-amino-1-phenylethan-1-ol to give 27.1mg **a23** (Yield: 76%) and the product was separated as yellowish white solid. ^{1}H NMR (400 MHz, DMSO-d_6) δ 11.91 (s, 1H), 8.91 (d, *J* = 1.4 Hz, 1H), 8.77 (t, *J* = 5.7 Hz, 1H), 8.59 (d, *J* = 8.1 Hz, 1H), 8.34 (dd, *J* = 7.9, 1.2 Hz, 1H), 8.00 (dd, *J* = 8.5, 1.8 Hz, 1H), 7.97 – 7.89 (m, 1H), 7.70 (t, *J* = 7.6 Hz, 1H), 7.44 – 7.32 (m, 6H), 7.30 – 7.19 (m, 1H), 5.59 (d, *J* = 4.4 Hz, 1H), 4.82 (dd, *J* = 8.5, 4.4 Hz, 1H), 3.62 – 3.51 (m, 1H). ^{13}C NMR (101 MHz, DMSO) δ 166.2, 161.6, 144.3, 139.0, 134.6, 133.5, 129.3, 128.8, 128.6, 128.6, 128.0, 127.5, 127.5, 126.4, 126.2, 122.8, 117.4, 116.4, 71.8, 48.3. HRMS m/z (ESI+, M+Na): Calcd for C22H18N2O3: 381.1215, (ESI+, M+Na) found: 381.1213

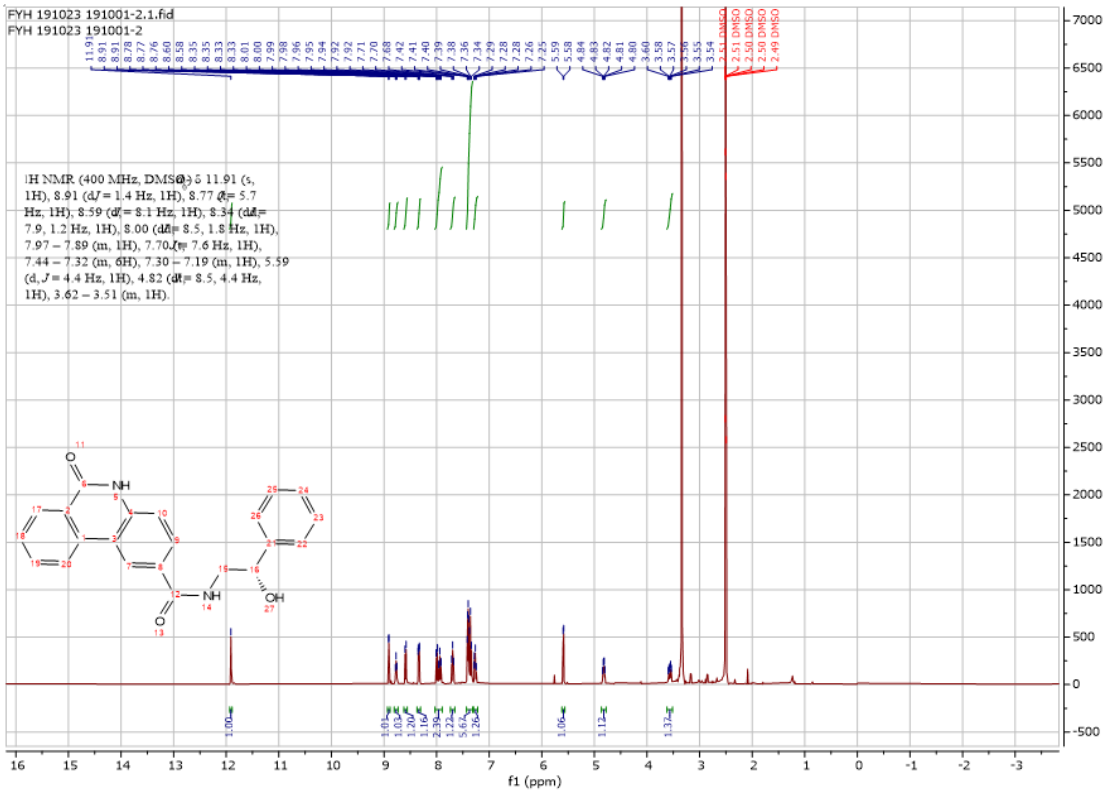
FYH 191023 191001-2.1.fid
FYH 191023 191001-2
1H NMR (400 MHz, DMSO) δ 11.91 (s, 1H), 8.91 (d, J = 1.4 Hz, 1H), 8.77 (d, J = 5.7 Hz, 1H), 8.59 (d, J = 8.1 Hz, 1H), 8.34 (dd, J = 7.9, 1.2 Hz, 1H), 8.00 (dd, J = 8.5, 1.8 Hz, 1H), 7.97 – 7.89 (m, 1H), 7.70 (d, J = 7.6 Hz, 1H), 7.44 – 7.32 (m, 6H), 7.30 – 7.19 (m, 1H), 5.59 (d, J = 4.4 Hz, 1H), 4.82 (dt, J = 8.5, 4.4 Hz, 1H), 3.62 – 3.51 (m, 1H).
f1 (ppm)

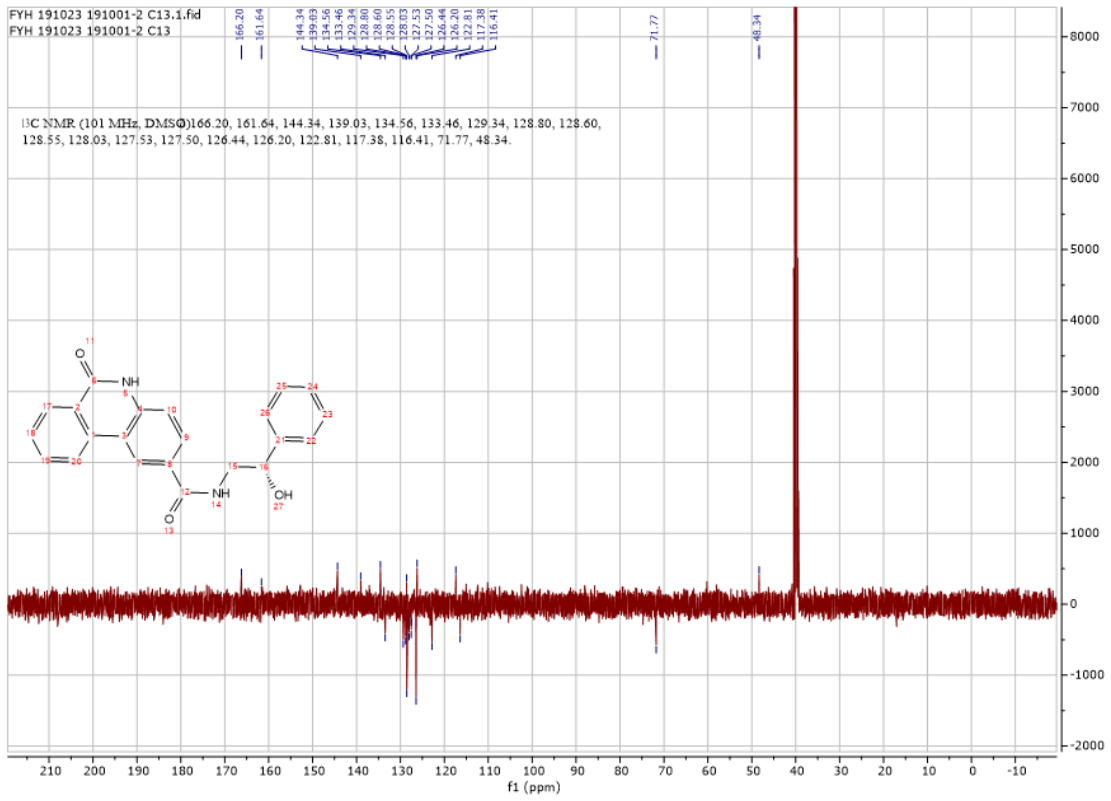
FYH 191023 191001-2 C13.1.fid
FYH 191023 191001-2 C13
13C NMR (101 MHz, DMSO) δ 166.20, 161.64, 144.34, 139.03, 134.56, 133.46, 129.34, 128.80, 128.60, 128.55, 128.03, 127.53, 127.50, 126.44, 126.20, 122.81, 117.38, 116.41, 71.77, 48.34.
f1 (ppm)

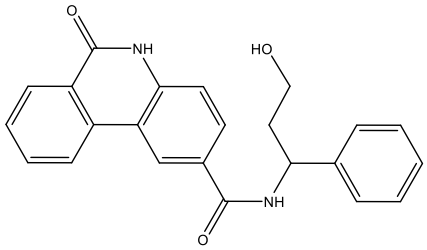

***N*-(3-hydroxy-1-phenylpropyl)-6-oxo-5,6-dihydrophenanthridine-2-carboxamide (a24)**

Using **Synthesis Method d**, 24mg (0.1mmol) **f2** was reacted with 15.1mg (0.1mmol) 3-amino-3-phenylpropan-1-ol to give 29.8mg **a24** (Yield: 80%) and the product was separated as yellowish white solid. ^{1}H NMR (300 MHz, DMSO-d_6) δ 11.89 (s, 1H), 8.93 – 8.84 (m, 2H), 8.60 (d, *J* = 8.2 Hz, 1H), 8.35 (dd, *J* = 8.0, 1.4 Hz, 1H), 8.00 (dd, *J* = 8.5, 1.8 Hz, 1H), 7.94 (td, *J* = 8.2, 7.7, 1.5 Hz, 1H), 7.70 (t, *J* = 7.5 Hz, 1H), 7.43 (ddd, *J* = 8.3, 5.1, 2.8 Hz, 3H), 7.34 (dd, *J* = 8.5, 6.7 Hz, 2H), 7.28 – 7.18 (m, 1H), 5.24 (dd, *J* = 8.5, 5.9 Hz, 1H), 4.60 (s, 1H), 3.49 (m, 2H), 2.20 – 1.89 (m, 2H). ^{13}C NMR (75 MHz, DMSO) δ 165.5, 161.4, 144.7, 139.2, 134.5, 133.4, 129.4, 128.8, 128.7, 128.7, 128.0, 127.1, 127.0, 126.2, 123.3, 122.7, 117.4, 116.4, 58.4, 50.8, 39.6. HRMS m/z (ESI+, M+Na): Calcd for C23H20N2O3: 395.1372, (ESI+, M+Na) found: 395.1364

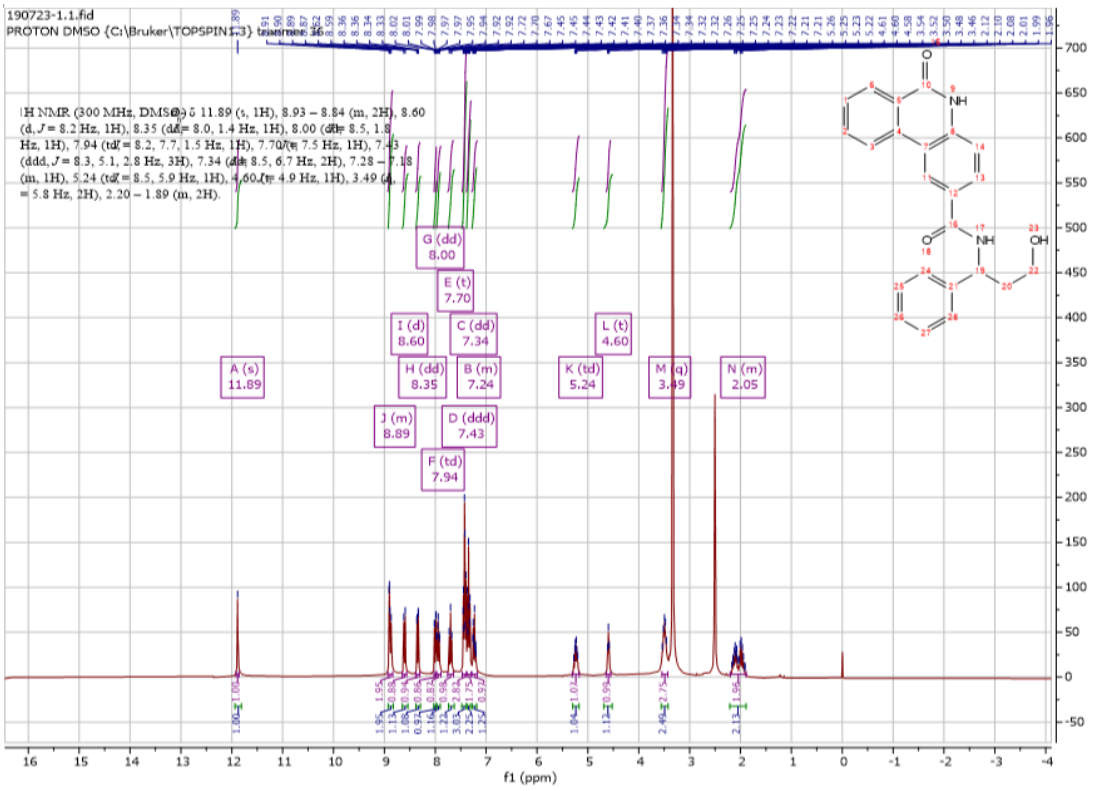
190723-1.1.fid
PROTON DMSO {C:\Bruker\TOPSPIN1...3} tranmet 36
¹H NMR (300 MHz, DMSO) δ 11.89 (s, 1H), 8.93 – 8.84 (m, 2H), 8.60 (d, J = 8.2 Hz, 1H), 8.35 (dd, J = 8.0, 1.4 Hz, 1H), 8.00 (dd, J = 8.5, 1.8 Hz, 1H), 7.94 (td, J = 8.2, 7.7, 1.5 Hz, 1H), 7.70 (t, J = 7.5 Hz, 1H), 7.43 (ddd, J = 8.3, 5.1, 2.8 Hz, 3H), 7.34 (dd, J = 8.5, 6.7 Hz, 2H), 7.28 – 7.18 (m, 1H), 5.24 (td, J = 8.5, 5.9 Hz, 1H), 4.60 (t, J = 4.9 Hz, 1H), 3.49 (q, J = 5.8 Hz, 2H), 2.20 – 1.89 (m, 2H).
A (s) 11.89
G (dd) 8.00
E (t) 7.70
I (d) 8.60
C (dd) 7.34
L (t) 4.60
H (dd) 8.35
B (m) 7.24
K (td) 5.24
M (q) 3.49
N (m) 2.05
J (m) 8.89
D (ddd) 7.43
F (td) 7.94
f1 (ppm)

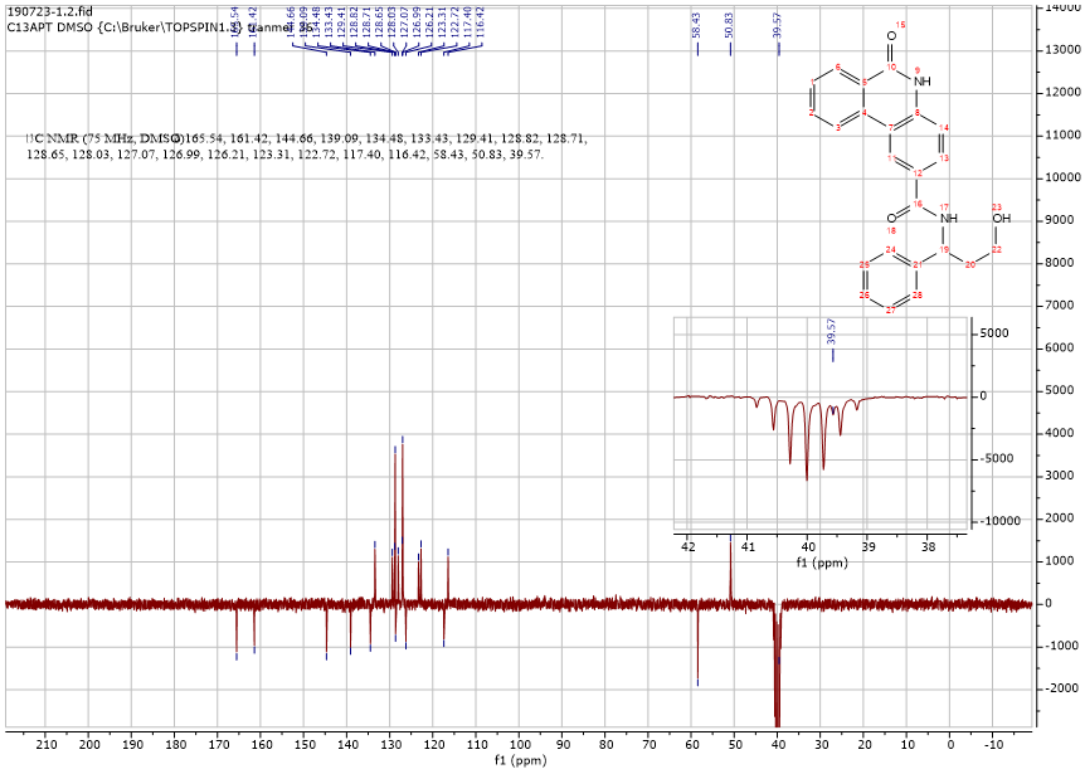
190723-1.2.fid
C13APT DMSO {C:\Bruker\TOPSPIN1...3} tranmet 36
¹³C NMR (75 MHz, DMSO) 165.54, 161.42, 144.66, 139.09, 134.48, 133.43, 129.41, 128.82, 128.71, 128.65, 128.03, 127.07, 126.99, 126.21, 123.31, 122.72, 117.40, 116.42, 58.43, 50.83, 39.57.
39.57
f1 (ppm)

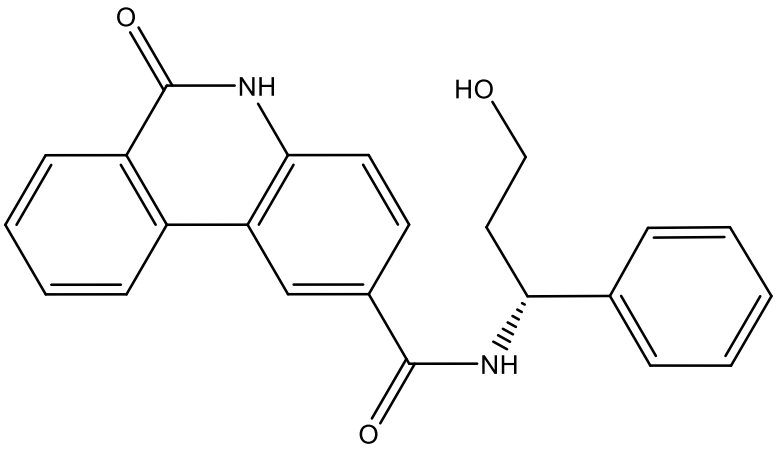

(*R*)-N-(3-hydroxy-1-phenylpropyl)-6-oxo-5,6-dihydrophenanthridine-2-carboxamide (a25)

Using **Synthesis Method d**, 24mg (0.1mmol) **f2** was reacted with 15.1mg (0.1mmol) (*R*)-3-amino-3-phenylpropan-1-ol to give 30.3mg **a25** (Yield: 81%) and the product was separated as yellowish white solid. ^{1}H NMR (400 MHz, DMSO-d_6) δ 11.92 (s, 1H), 8.94 – 8.87 (m, 2H), 8.61 (d, *J* = 8.2 Hz, 1H), 8.34 (dd, *J* = 8.0, 1.4 Hz, 1H), 8.00 (dd, *J* = 8.5, 1.8 Hz, 1H), 7.95 (ddd, *J* = 8.4, 7.2, 1.5 Hz, 1H), 7.70 (ddd, *J* = 8.1, 7.1, 1.0 Hz, 1H), 7.47 – 7.38 (m, 3H), 7.34 (dd, *J* = 8.4, 6.9 Hz, 2H), 7.27 – 7.19 (m, 1H), 5.23 (dd, *J* = 8.6, 6.0 Hz, 1H), 4.62 (s, 1H), 3.49 (m, 2H), 2.18 – 1.88 (m, 2H). ^{13}C NMR (101 MHz, DMSO) δ 165.5, 161.4, 144.7, 139.1, 134.5, 133.5, 129.4, 128.8, 128.7, 128.6, 128.0, 127.1, 127.0, 126.2, 123.3, 122.7, 117.4, 116.4, 58.4, 50.8, 39.6. HRMS m/z (ESI+, M+Na): Calcd for C23H20N2O3: 395.1372, (ESI+, M+Na) found: 395.1364

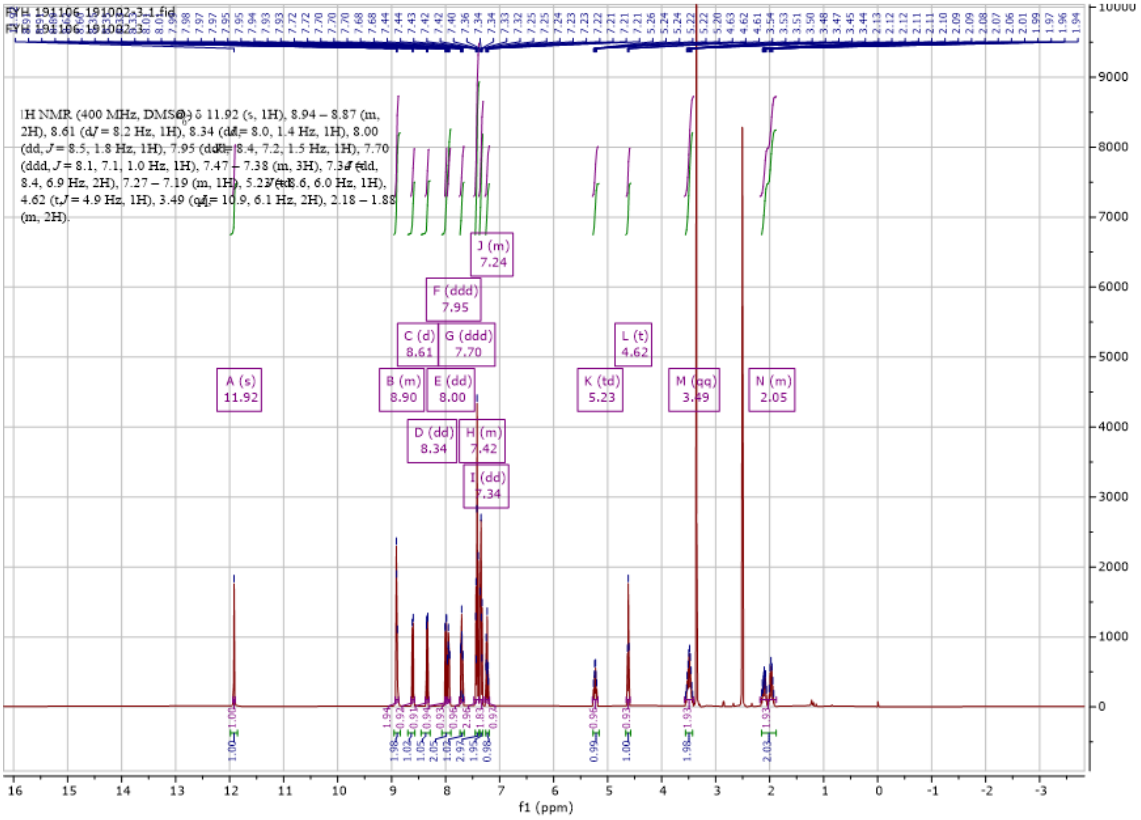
FYH 191106 191002-3 1.fid
1H NMR (400 MHz, DMSO) δ 11.92 (s, 1H), 8.94 – 8.87 (m, 2H), 8.61 (d, J = 8.2 Hz, 1H), 8.34 (dd, J = 8.0, 1.4 Hz, 1H), 8.00 (dd, J = 8.5, 1.8 Hz, 1H), 7.95 (ddd, J = 8.4, 7.2, 1.5 Hz, 1H), 7.70 (ddd, J = 8.1, 7.1, 1.0 Hz, 1H), 7.47 – 7.38 (m, 3H), 7.34 (dd, J = 8.4, 6.9 Hz, 2H), 7.27 – 7.19 (m, 1H), 5.23 (td, J = 8.6, 6.0 Hz, 1H), 4.62 (t, J = 4.9 Hz, 1H), 3.49 (qq, J = 10.9, 6.1 Hz, 2H), 2.18 – 1.88 (m, 2H).
J (m) 7.24
F (ddd) 7.95
C (d) 8.61
G (ddd) 7.70
L (t) 4.62
A (s) 11.92
B (m) 8.90
E (dd) 8.00
K (td) 5.23
M (qq) 3.49
N (m) 2.05
D (dd) 8.34
H (m) 7.42
I (dd) 7.34
f1 (ppm)

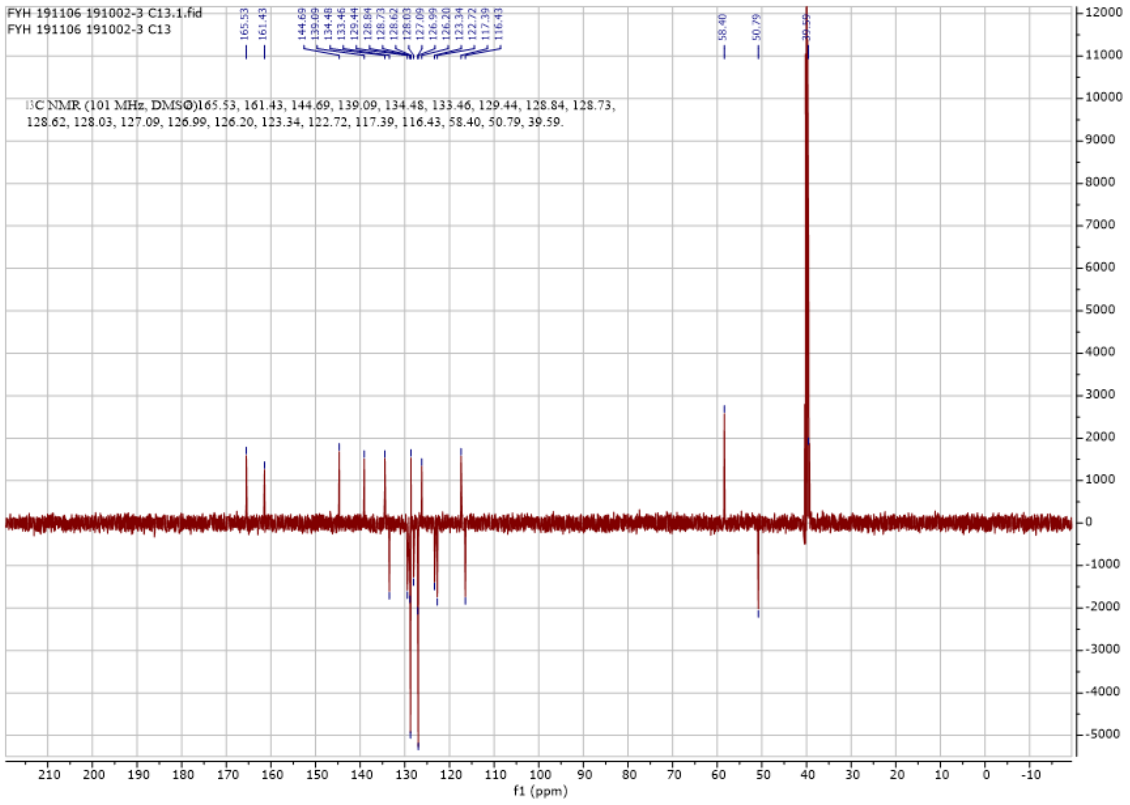
FYH 191106 191002-3 C13.1.fid
FYH 191106 191002-3 C13
13C NMR (101 MHz, DMSO) 165.53, 161.43, 144.69, 139.09, 134.48, 133.46, 129.44, 128.84, 128.73, 128.62, 128.03, 127.09, 126.99, 126.20, 123.34, 122.72, 117.39, 116.43, 58.40, 50.79, 39.59.
f1 (ppm)

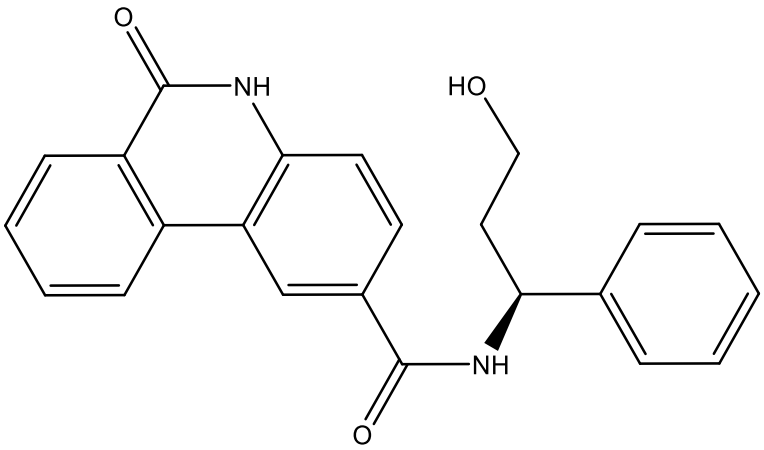

(*S*)-N-(3-hydroxy-1-phenylpropyl)-6-oxo-5,6-dihydrophenanthridine-2-carboxamide (a26)

Using **Synthesis Method d**, 24mg (0.1mmol) **f2** was reacted with 15.1mg (0.1mmol) (*S*)-3-amino-3-phenylpropan-1-ol to give 29.9mg **a26** (Yield: 80%) and the product was separated as yellowish white solid. ^{1}H NMR (400 MHz, DMSO-d_6) δ 11.92 (s, 1H), 8.90 (d, *J* = 7.5 Hz, 2H), 8.61 (d, *J* = 8.2 Hz, 1H), 8.37 – 8.31 (m, 1H), 8.00 (dd, *J* = 8.5, 1.6 Hz, 1H), 7.97 – 7.91 (m, 1H), 7.70 (t, *J* = 7.5 Hz, 1H), 7.42 (t, *J* = 8.4 Hz, 3H), 7.34 (t, *J* = 7.6 Hz, 2H), 7.23 (t, *J* = 7.3 Hz, 1H), 5.23 (dd, *J* = 8.4, 6.0 Hz, 1H), 4.62 (s, 1H), 3.48 (m, 2H), 2.10 – 1.96 (m, 2H). ^{13}C NMR (101 MHz, DMSO) δ 165.5, 161.4, 144.7, 139.1, 134.5, 133.5, 129.4, 128.8, 128.7, 128.6, 128.0, 127.1, 127.0, 126.2, 123.3, 122.7, 117.4, 116.4, 58.4, 50.8, 39.6. HRMS m/z (ESI+, M+Na): Calcd for C23H20N2O3: 395.1372, (ESI+, M+Na) found: 395.1364

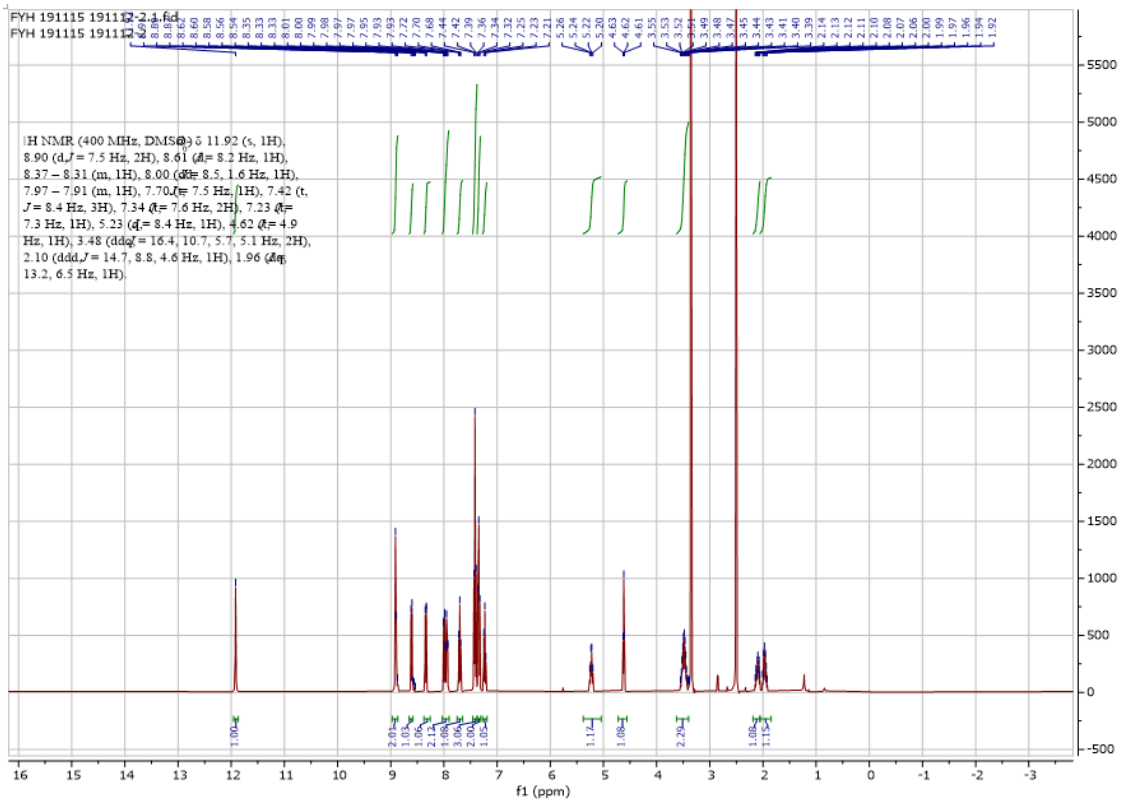
FYH 191115 191112-2 1.1.fid
FYH 191115 191112-2 1
1H NMR (400 MHz, DMSO-d6) δ 11.92 (s, 1H), 8.90 (d, J = 7.5 Hz, 2H), 8.61 (d, J = 8.2 Hz, 1H), 8.37 – 8.31 (m, 1H), 8.00 (dd, J = 8.5, 1.6 Hz, 1H), 7.97 – 7.91 (m, 1H), 7.70 (t, J = 7.5 Hz, 1H), 7.42 (t, J = 8.4 Hz, 3H), 7.34 (t, J = 7.6 Hz, 2H), 7.23 (t, J = 7.3 Hz, 1H), 5.23 (d, J = 8.4 Hz, 1H), 4.62 (t, J = 4.9 Hz, 1H), 3.48 (ddq, J = 16.4, 10.7, 5.7, 5.1 Hz, 2H), 2.10 (ddd, J = 14.7, 8.8, 4.6 Hz, 1H), 1.96 (dq, J = 13.2, 6.5 Hz, 1H).
f1 (ppm)

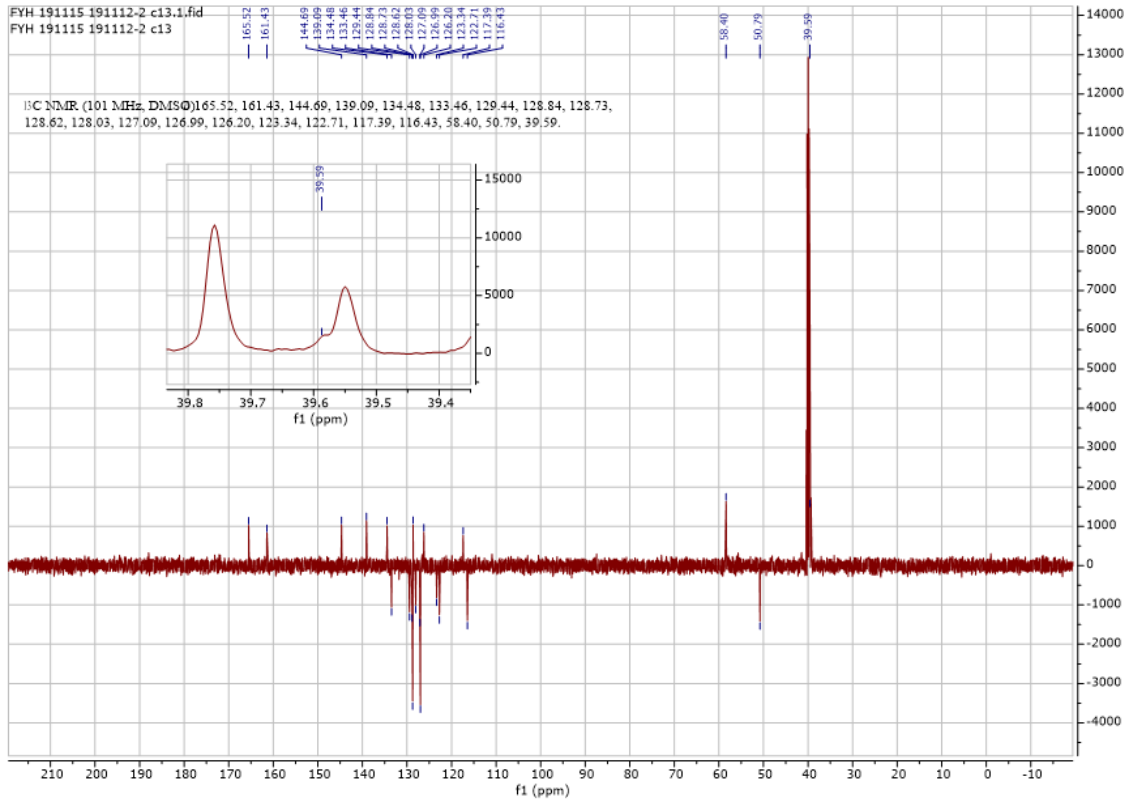
FYH 191115 191112-2 c13.1.fid
FYH 191115 191112-2 c13
13C NMR (101 MHz, DMSO-d6) 165.52, 161.43, 144.69, 139.09, 134.48, 133.46, 129.44, 128.84, 128.73, 128.62, 128.03, 127.09, 126.99, 126.20, 123.34, 122.71, 117.39, 116.43, 58.40, 50.79, 39.59.
f1 (ppm)

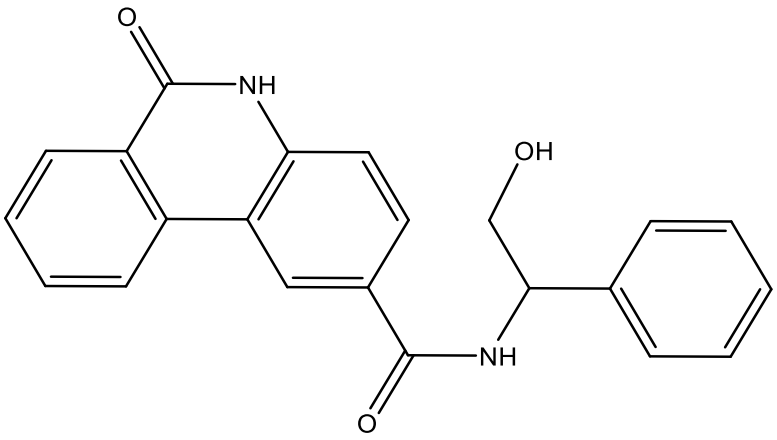

***N*-(2-hydroxy-1-phenylethyl)-6-oxo-4a,5,6,10b-tetrahydrophenanthridine-2-carboxamide (a27)**

Using **Synthesis Method d**, 24mg (0.1mmol) **f2** was reacted with 13.7mg (0.1mmol) 2-amino-2-phenylethan-1-ol to give 29.4mg **a27** (Yield: 82%) and the product was separated as yellowish white solid. ^{1}H NMR (400 MHz, DMSO-d_6) δ 11.92 (s, 1H), 8.97 (d, *J* = 1.7 Hz, 1H), 8.88 (d, *J* = 8.0 Hz, 1H), 8.64 (d, *J* = 8.2 Hz, 1H), 8.35 (dd, *J* = 8.0, 1.2 Hz, 1H), 8.06 – 7.97 (m, 1H), 7.94 (dd, *J* = 8.2, 1.3 Hz, 1H), 7.75 – 7.66 (m, 1H), 7.48 – 7.37 (m, 3H), 7.34 (t, *J* = 7.6 Hz, 2H), 7.29 – 7.20 (m, 1H), 5.16 (m, 1H), 5.05 (s, 1H), 3.76 (dd, *J* = 10.9, 5.1 Hz, 1H) 3.73 (dd, *J* = 10.9, 5.1 Hz, 1H). ^{13}C NMR (101 MHz, DMSO) δ 165.9, 161.5, 141.9, 139.1, 134.5, 133.4, 129.5, 128.8, 128.7, 128.6, 128.0, 127.5, 127.3, 126.2, 123.4, 122.9, 117.4, 116.4, 65.1, 56.5. HRMS m/z (ESI+, M+Na): Calcd for C22H18N2O3: 381.1215, (ESI+, M+Na) found: 381.1208

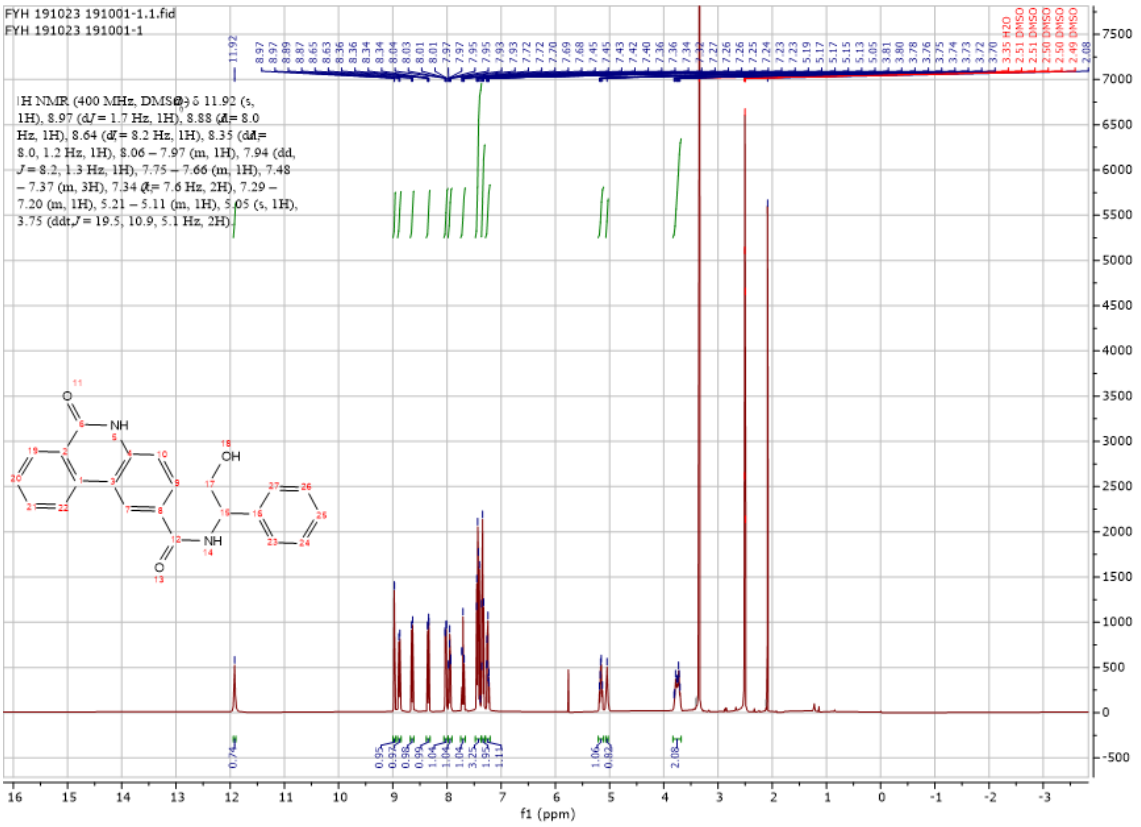
FYH 191023 191001-1.1.fid
FYH 191023 191001-1
1H NMR (400 MHz, DMSO) δ 11.92 (s, 1H), 8.97 (d, J = 1.7 Hz, 1H), 8.88 (d, J = 8.0 Hz, 1H), 8.64 (d, J = 8.2 Hz, 1H), 8.35 (dd, J = 8.0, 1.2 Hz, 1H), 8.06 – 7.97 (m, 1H), 7.94 (dd, J = 8.2, 1.3 Hz, 1H), 7.75 – 7.66 (m, 1H), 7.48 – 7.37 (m, 3H), 7.34 (d, J = 7.6 Hz, 2H), 7.29 – 7.20 (m, 1H), 5.21 – 5.11 (m, 1H), 5.05 (s, 1H), 3.75 (ddt, J = 19.5, 10.9, 5.1 Hz, 2H).
f1 (ppm)

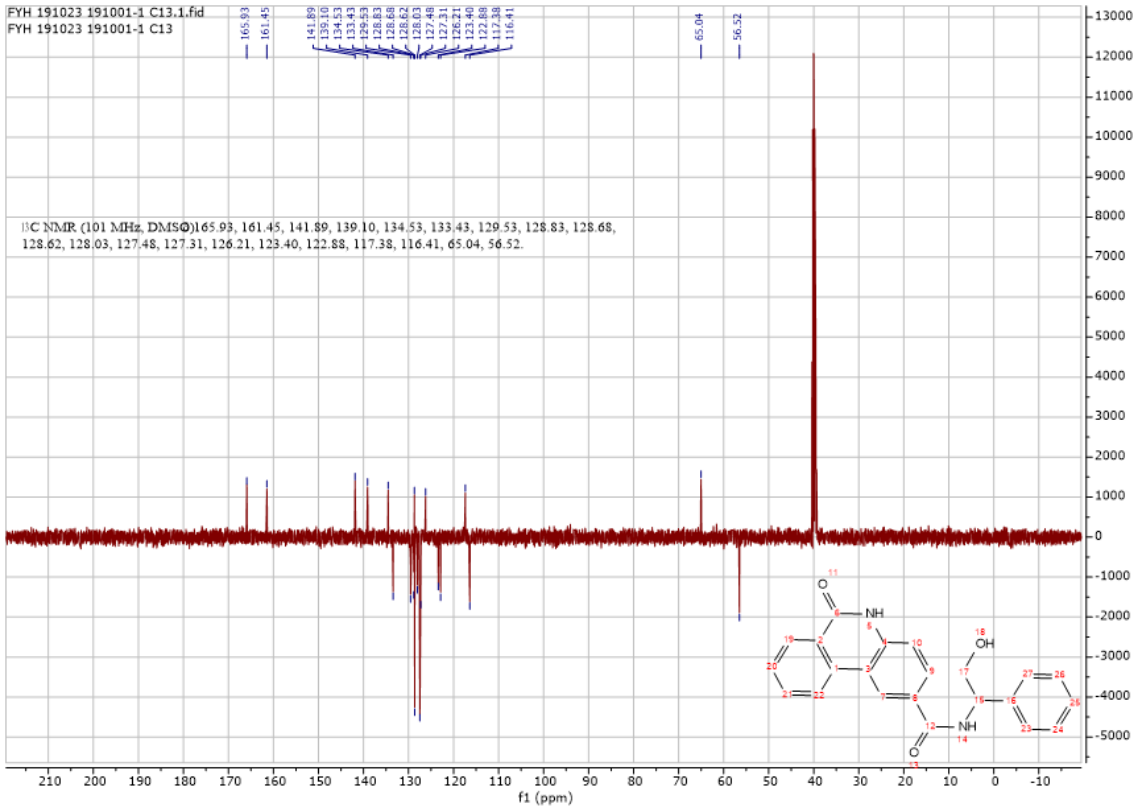
FYH 191023 191001-1 C13.1.fid
FYH 191023 191001-1 C13
13C NMR (101 MHz, DMSO) 165.93, 161.45, 141.89, 139.10, 134.53, 133.43, 129.53, 128.83, 128.68, 128.62, 128.03, 127.48, 127.31, 126.21, 123.40, 122.88, 117.38, 116.41, 65.04, 56.52.
f1 (ppm)

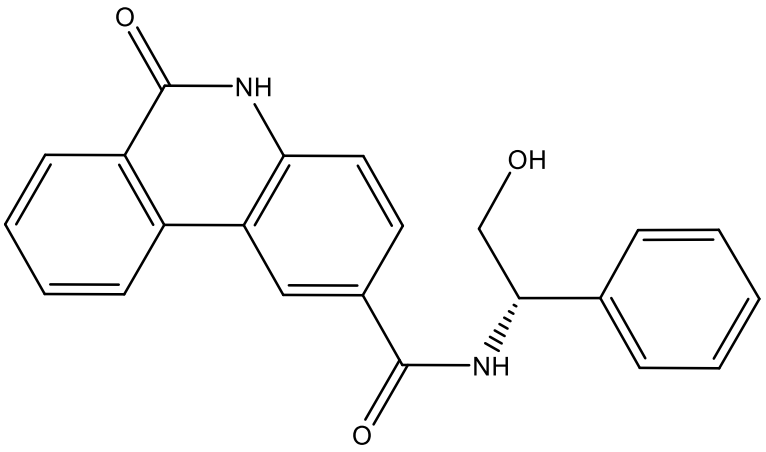

(*S*)-N-(2-hydroxy-1-phenylethyl)-6-oxo-5,6-dihydrophenanthridine-2-carboxamide (a28)

Using **Synthesis Method d**, 24mg (0.1mmol) **f2** was reacted with 13.7mg (0.1mmol) (*S*)-2-amino-2-phenylethan-1-ol to give 30mg **a28** (Yield: 84%) and the product was separated as yellowish white solid. ^{1}H NMR (400 MHz, DMSO-d_6) δ 11.93 (s, 1H), 8.97 (d, *J* = 1.7 Hz, 1H), 8.88 (d, *J* = 8.0 Hz, 1H), 8.64 (d, *J* = 8.2 Hz, 1H), 8.35 (dd, *J* = 8.0, 1.2 Hz, 1H), 8.02 (dd, *J* = 8.5, 1.8 Hz, 1H), 7.95 (ddd, *J* = 8.4, 7.3, 1.4 Hz, 1H), 7.75 – 7.64 (m, 1H), 7.48 – 7.38 (m, 3H), 7.34 (t, *J* = 7.5 Hz, 2H), 7.28 – 7.19 (m, 1H), 5.16 (m, 1H), 5.04 (s, 1H), 3.83 – 3.66 (m, 2H). ^{13}C NMR (101 MHz, DMSO) δ 165.9, 161.4, 141.9, 139.1, 134.5, 133.4, 129.5, 128.8, 128.7, 128.6, 128.0, 127.5, 127.3, 126.2, 123.4, 122.9, 117.4, 116.4, 65.0, 56.5. HRMS m/z (ESI+, M+Na): Calcd for C22H18N2O3: 381.1215, (ESI+, M+Na) found: 381.1209

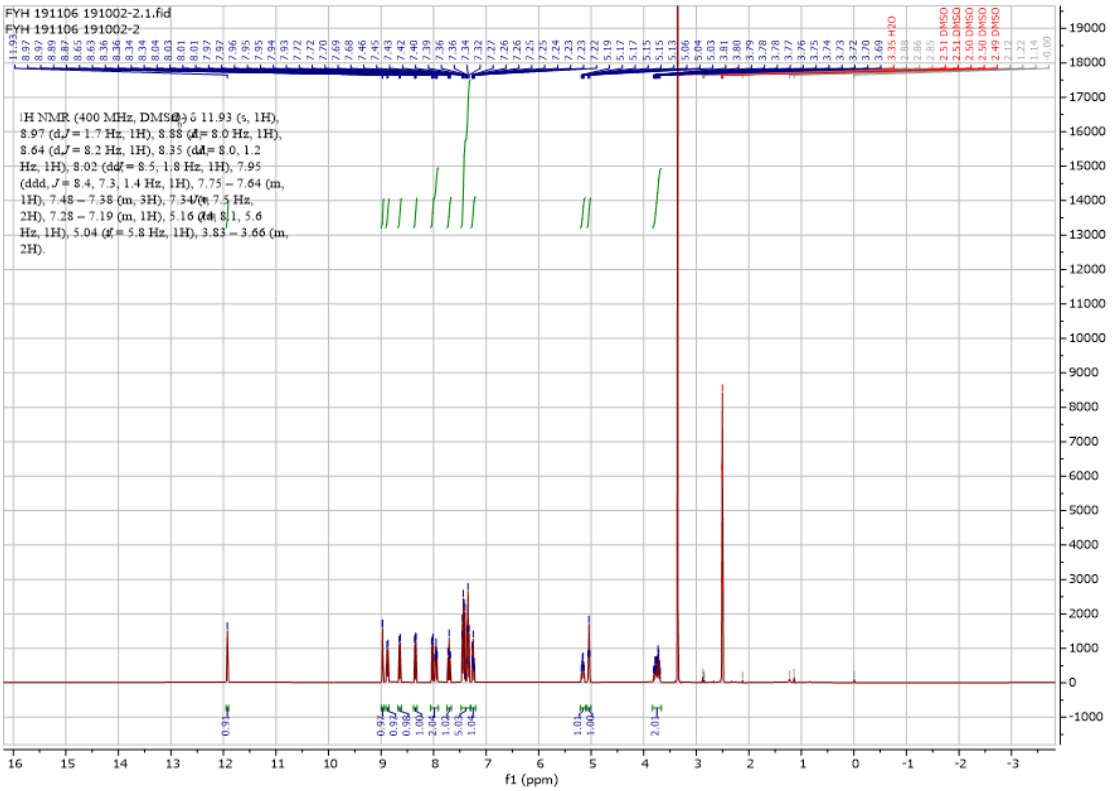
FYH 191106 191002-2.1.fid
FYH 191106 191002-2
1H NMR (400 MHz, DMSO-d6) δ 11.93 (s, 1H), 8.97 (d, J = 1.7 Hz, 1H), 8.88 (dd, J = 8.0 Hz, 1H), 8.64 (d, J = 8.2 Hz, 1H), 8.35 (dd, J = 8.0, 1.2 Hz, 1H), 8.02 (dd, J = 8.5, 1.8 Hz, 1H), 7.95 (ddd, J = 8.4, 7.3, 1.4 Hz, 1H), 7.75 – 7.64 (m, 1H), 7.48 – 7.38 (m, 3H), 7.34 (t, J = 7.5 Hz, 2H), 7.28 – 7.19 (m, 1H), 5.16 (td, J = 8.1, 5.6 Hz, 1H), 5.04 (d, J = 5.8 Hz, 1H), 3.83 – 3.66 (m, 2H).
f1 (ppm)

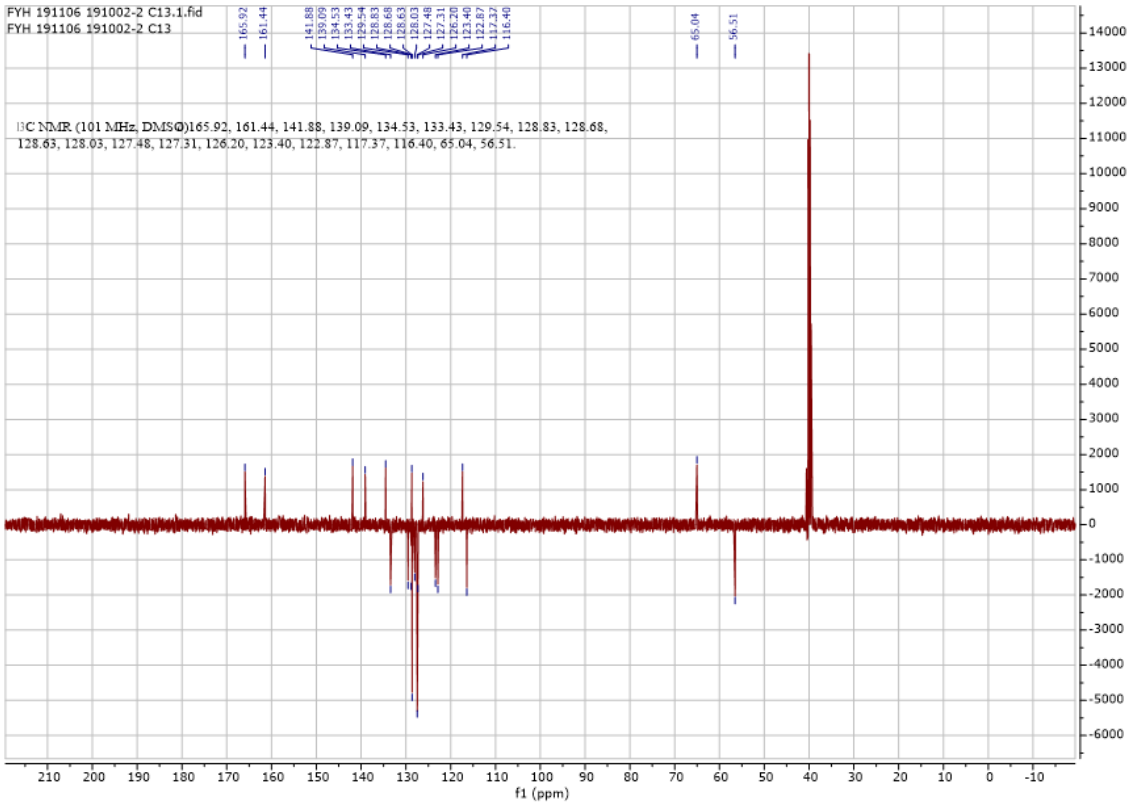
FYH 191106 191002-2 C13.1.fid
FYH 191106 191002-2 C13
13C NMR (101 MHz, DMSO-d6) 165.92, 161.44, 141.88, 139.09, 134.53, 133.43, 129.54, 128.83, 128.68, 128.63, 128.03, 127.48, 127.31, 126.20, 123.40, 122.87, 117.37, 116.40, 65.04, 56.51.
f1 (ppm)

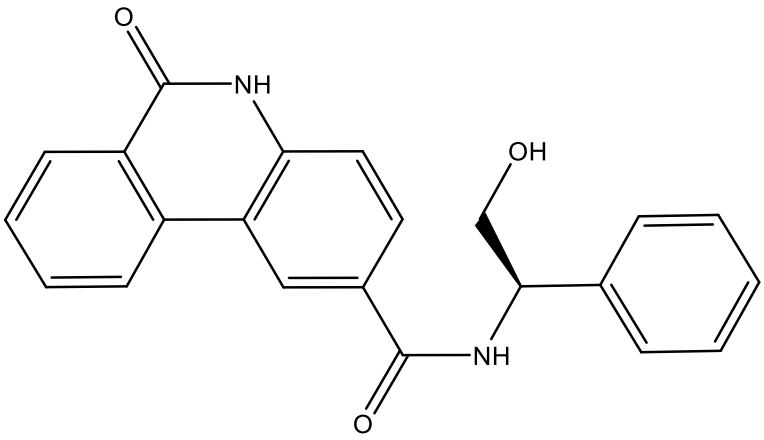

(*R*)-N-(2-hydroxy-1-phenylethyl)-6-oxo-5,6-dihydrophenanthridine-2-carboxamide (a29)

Using **Synthesis Method d**, 24mg (0.1mmol) **f2** was reacted with 13.7mg (0.1mmol) (*R*)-2-amino-2-phenylethan-1-ol to give 31mg **a29** (Yield: 87%) and the product was separated as yellowish white solid. ^{1}H NMR (300 MHz, DMSO-d_6) δ 11.89 (s, 1H), 8.96 (s, 1H), 8.85 (d, *J* = 8.1 Hz, 1H), 8.64 (d, *J* = 8.2 Hz, 1H), 8.35 (dd, *J* = 8.0, 1.4 Hz, 1H), 8.02 (dd, *J* = 8.5, 1.8 Hz, 1H), 7.95 (ddd, *J* = 8.4, 7.2, 1.5 Hz, 1H), 7.70 (t, *J* = 7.5 Hz, 1H), 7.47 – 7.39 (m, 3H), 7.34 (t, *J* = 7.5 Hz, 2H), 7.28 – 7.19 (m, 1H), 5.16 (dt, *J* = 7.9, 7.9 Hz, 1H), 5.01 (s, 1H), 3.75 (m, 2H). ^{13}C NMR (75 MHz, DMSO) δ 165.9, 161.4, 141.9, 139.1, 134.5, 133.4, 129.5, 128.8, 128.7, 128.6, 128.0, 127.5, 127.3, 126.2, 123.4, 122.9, 117.4, 116.4, 65.0, 56.5. HRMS m/z (ESI+, M+Na): Calcd for C22H18N2O3: 381.1215, (ESI+, M+Na) found: 381.1211

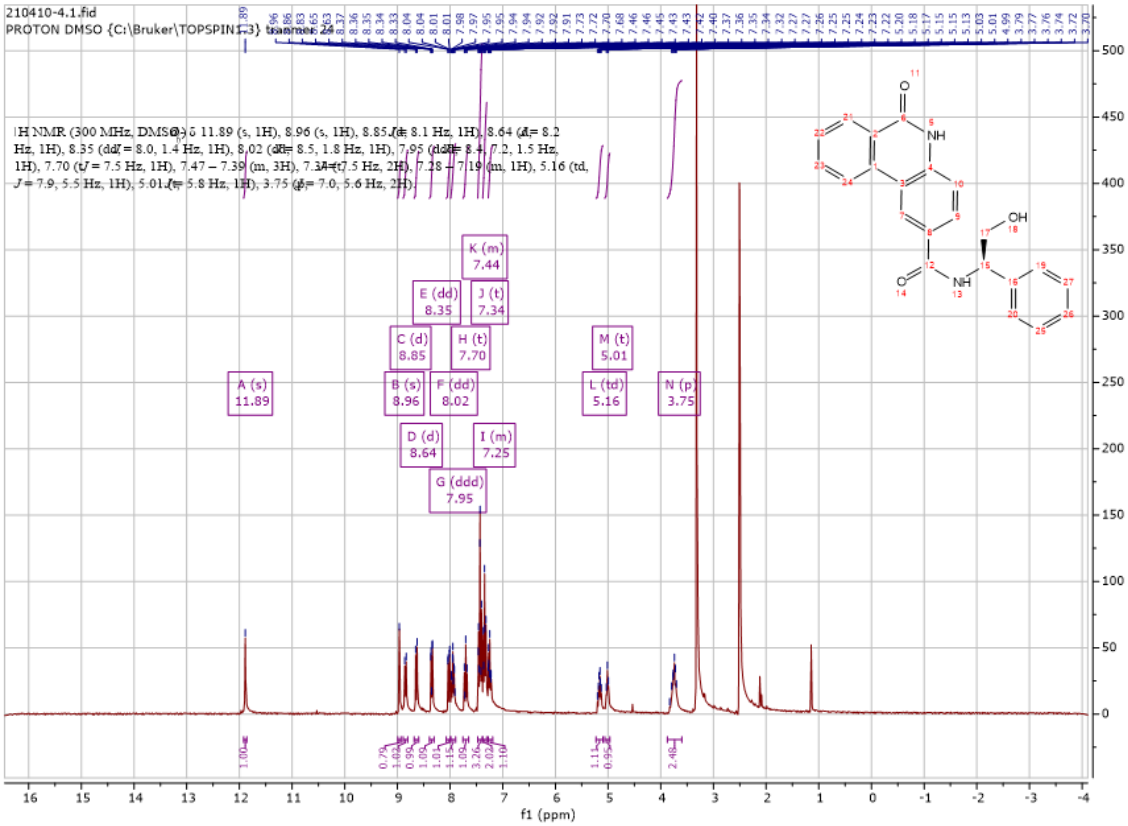
210410-4.1.fid
PROTON DMSO {C:\Bruker\TOPSPIN1.3} tranmer 24
1H NMR (300 MHz, DMSO) δ 11.89 (s, 1H), 8.96 (s, 1H), 8.85 (d, J = 8.1 Hz, 1H), 8.64 (d, J = 8.2 Hz, 1H), 8.35 (dd, J = 8.0, 1.4 Hz, 1H), 8.02 (dd, J = 8.5, 1.8 Hz, 1H), 7.95 (ddd, J = 8.4, 7.2, 1.5 Hz, 1H), 7.70 (t, J = 7.5 Hz, 1H), 7.47 – 7.39 (m, 3H), 7.34 (t, J = 7.5 Hz, 2H), 7.28 – 7.19 (m, 1H), 5.16 (td, J = 7.9, 5.5 Hz, 1H), 5.01 (t, J = 5.8 Hz, 1H), 3.75 (p, J = 7.0, 5.6 Hz, 2H).
A (s) 11.89
B (s) 8.96
C (d) 8.85
D (d) 8.64
E (dd) 8.35
F (dd) 8.02
G (ddd) 7.95
H (t) 7.70
I (m) 7.25
J (t) 7.34
K (m) 7.44
L (td) 5.16
M (t) 5.01
N (p) 3.75
f1 (ppm)

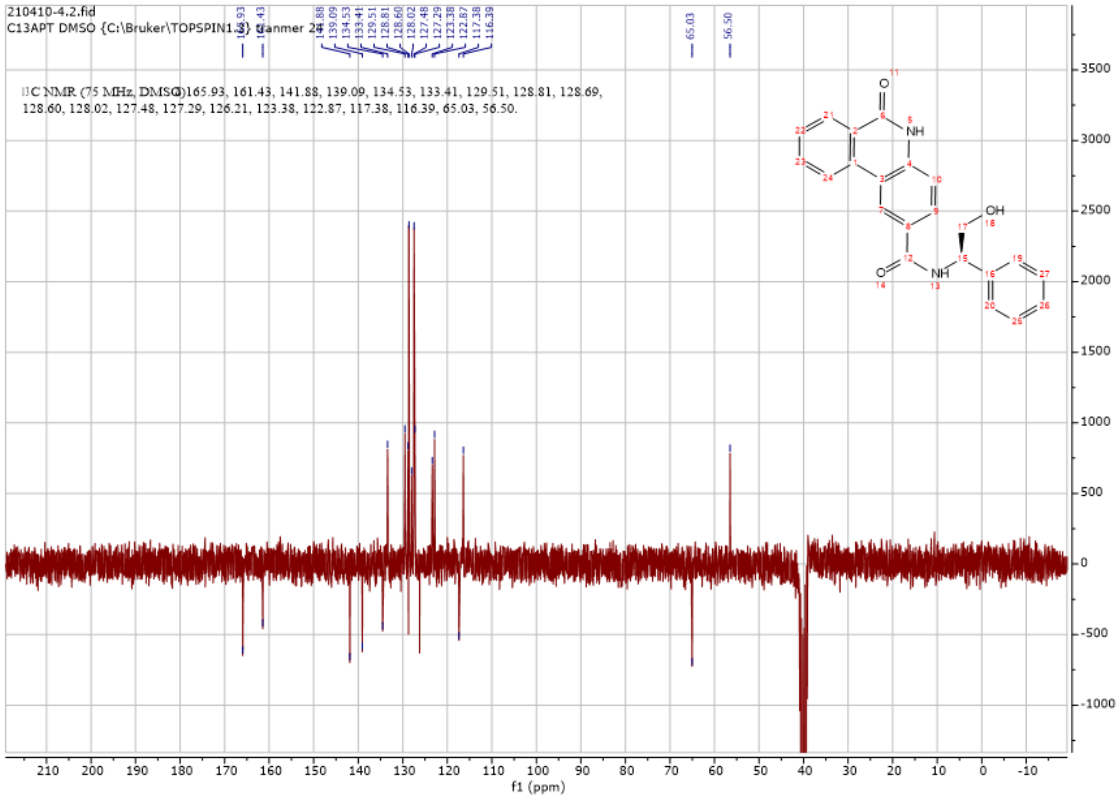
210410-4.2.fid
C13APT DMSO {C:\Bruker\TOPSPIN1.3} tranmer 24
13C NMR (75 MHz, DMSO) δ 165.93, 161.43, 141.88, 139.09, 134.53, 133.41, 129.51, 128.81, 128.69, 128.60, 128.02, 127.48, 127.29, 126.21, 123.38, 122.87, 117.38, 116.39, 65.03, 56.50.
f1 (ppm)

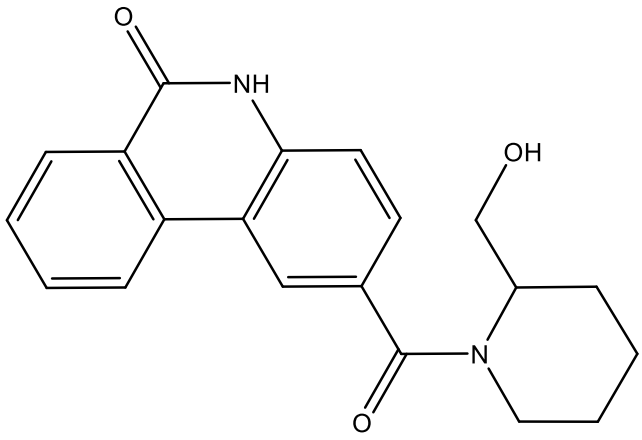

2-(2-(hydroxymethyl)piperidine-1-carbonyl)phenanthridin-6(5*H*)-one (a30)

Using **Synthesis Method d**, 24mg (0.1mmol) **f2** was reacted with 11.5mg (0.1mmol) piperidin-2-ylmethanol to give 22.2mg **a30** (Yield: 66%) and the product was separated as yellowish white solid. ^{1}H NMR (300 MHz, DMSO-d_6) δ 11.81 (s, 1H), 8.53 (d, J = 8.2 Hz, 1H), 8.43 (s, 1H), 8.34 (dd, J = 7.9, 1.4 Hz, 1H), 7.87 (td, 1H), 7.68 (t, J = 7.5 Hz, 1H), 7.53 (dd, J = 8.4, 1.6 Hz, 1H), 7.40 (d, J = 8.4 Hz, 1H), 4.83 (s, 1H), 3.33 (m, 5H), 1.77 – 1.32 (m, 6H). ^{13}C NMR (75 MHz, DMSO) δ 170.1, 161.3, 137.4, 134.4, 133.4, 131.3, 128.9, 128.7, 128.0, 126.3, 123.3, 122.5, 117.5, 116.4, 59.2, 57.4(C23), 44.6 – 37.3 (C19), 25.7, 19.5. HRMS m/z (ESI+, M+Na): Calcd for C20H20N2O3: 359.1372, (ESI+, M+Na) found: 359.1365

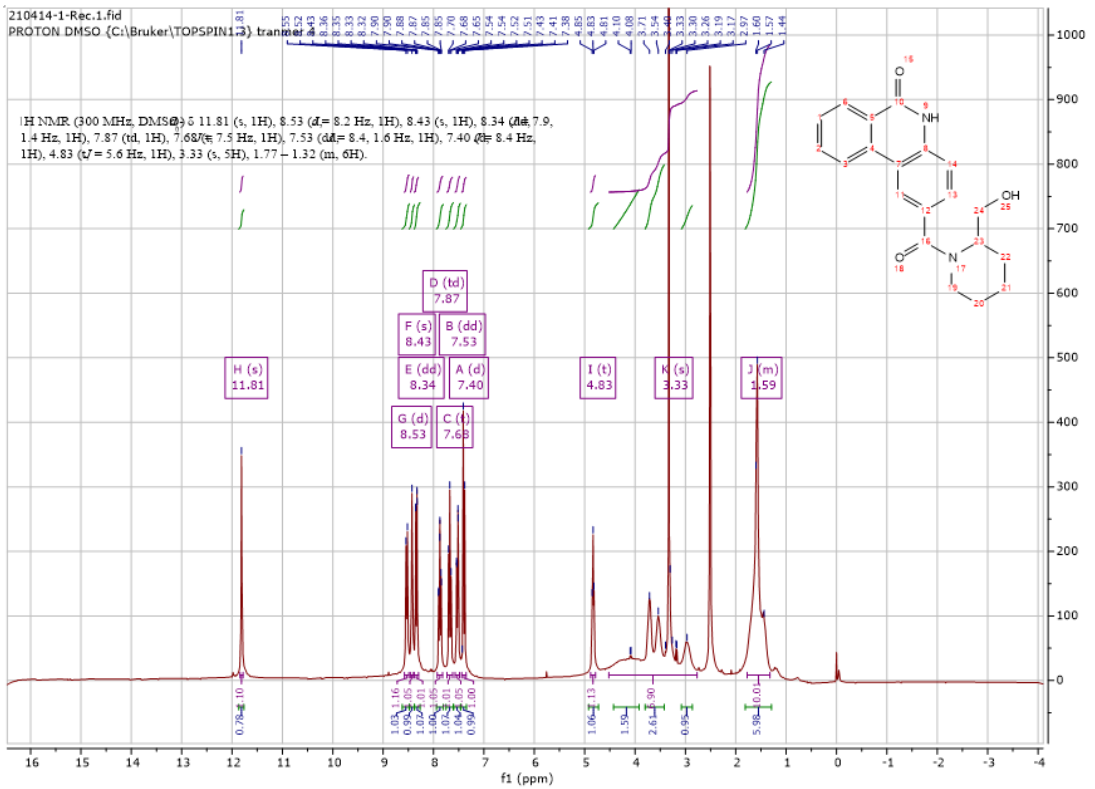
210414-1-Rec.1.fid
PROTON DMSO {C:\Bruker\TOPSPIN1.3} tranmer 4
1H NMR (300 MHz, DMSO) δ 11.81 (s, 1H), 8.53 (d, J = 8.2 Hz, 1H), 8.43 (s, 1H), 8.34 (dd, J = 7.9, 1.4 Hz, 1H), 7.87 (td, J = 7.7, 1.6 Hz, 1H), 7.68 (t, J = 7.5 Hz, 1H), 7.53 (dd, J = 8.4, 1.6 Hz, 1H), 7.40 (d, J = 8.4 Hz, 1H), 4.83 (t, J = 5.6 Hz, 1H), 3.33 (s, 5H), 1.77 – 1.32 (m, 6H).
H (s) 11.81
D (td) 7.87
F (s) 8.43
B (dd) 7.53
E (dd) 8.34
A (d) 7.40
G (d) 8.53
C (t) 7.68
I (t) 4.83
K (s) 3.33
J (m) 1.59
f1 (ppm)

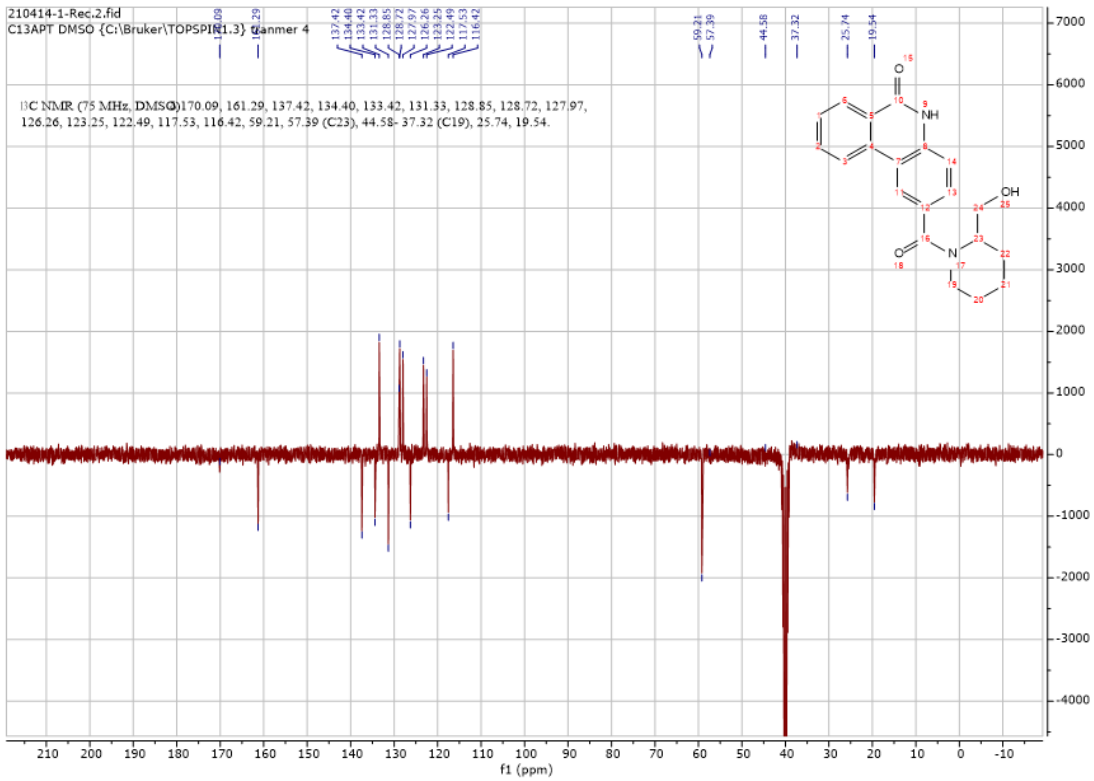
210414-1-Rec.2.fid
C13APT DMSO {C:\Bruker\TOPSPIN1.3} tranmer 4
13C NMR (75 MHz, DMSO) 170.09, 161.29, 137.42, 134.40, 133.42, 131.33, 128.85, 128.72, 127.97, 126.26, 123.25, 122.49, 117.53, 116.42, 59.21, 57.39 (C23), 44.58- 37.32 (C19), 25.74, 19.54.
f1 (ppm)

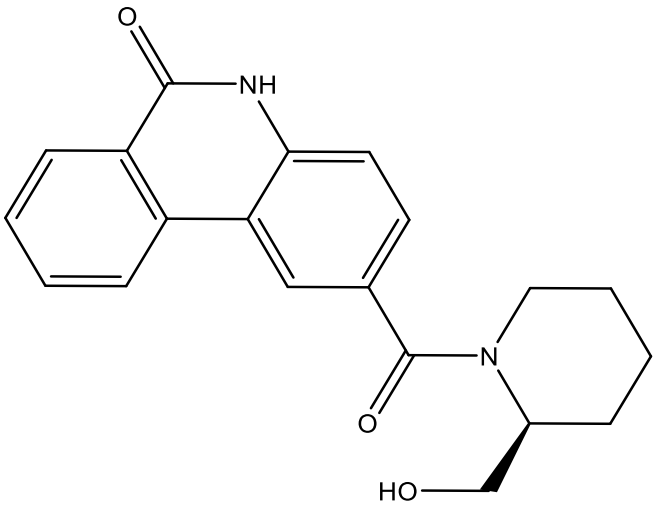

(*S*)-2-(2-(hydroxymethyl)piperidine-1-carbonyl)phenanthridin-6(5H)-one (a31)

Using **Synthesis Method d**, 24mg (0.1mmol) **f2** was reacted with 11.5mg (0.1mmol) (*S*)-piperidin-2-ylmethanol to give 21.5mg **a31** (Yield: 64%) and the product was separated as yellowish white solid. ^{1}H NMR (300 MHz, DMSO-d_6) δ 11.81 (s, 1H), 8.53 (d, *J* = 8.1 Hz, 1H), 8.43 (s, 1H), 8.34 (dd, *J* = 7.9, 1.4 Hz, 1H), 7.87 (ddd, *J* = 8.3, 7.2, 1.5 Hz, 1H), 7.73 – 7.62 (m, 1H), 7.52 (dd, *J* = 8.3, 1.7 Hz, 1H), 7.39 (d, *J* = 8.3 Hz, 1H), 4.83 (s, 1H), 3.75 – 2.75 (m, 5H), 1.56 (m, 6H) ^{13}C NMR (75 MHz, DMSO) δ 170.1, 161.3, 137.4, 134.4, 133.4, 131.3, 128.9, 128.7, 128.0, 126.3, 123.3, 122.5, 117.5, 116.4, 59.2, 57.2(C19), 44.7-37.2 (C23), 25.7, 19.5. HRMS m/z (ESI+, M+Na): Calcd for C20H20N2O3: 359.1372, (ESI+, M+Na) found: 359.1364

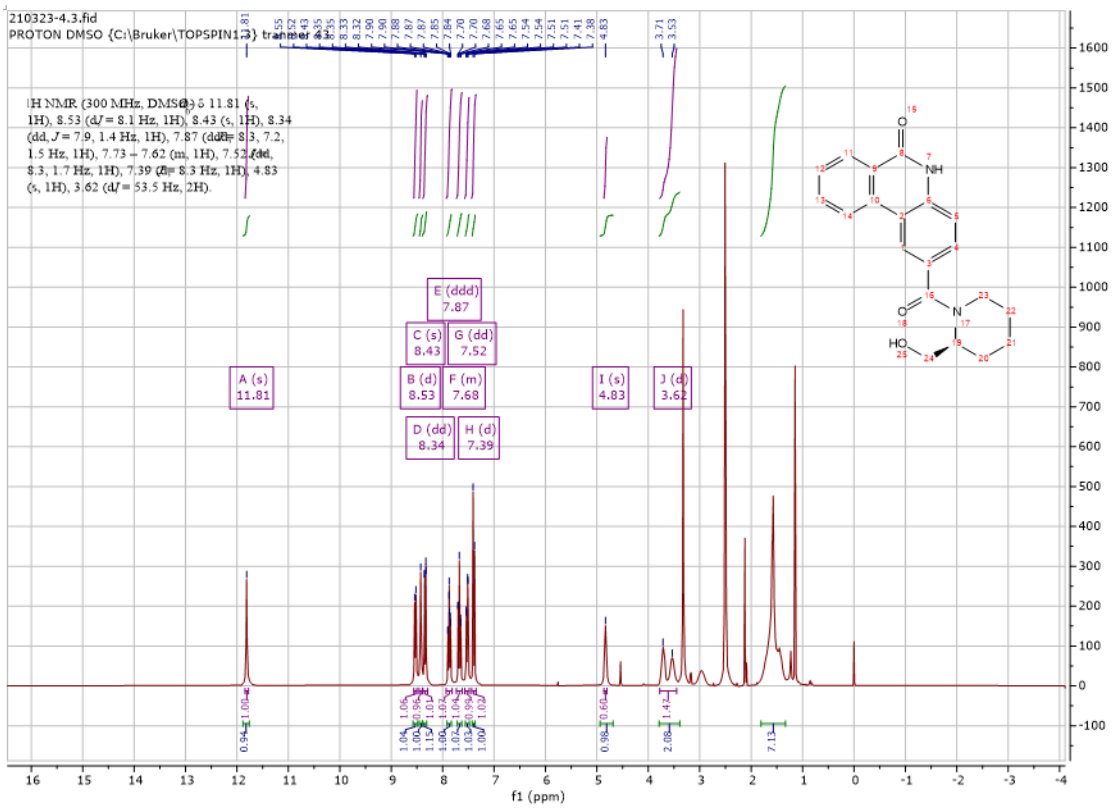
210323-4.3.fid
PROTON DMSO {C:\Bruker\TOPSPIN1.3} tranmer 43
1H NMR (300 MHz, DMSO) δ 11.81 (s, 1H), 8.53 (d, J = 8.1 Hz, 1H), 8.43 (s, 1H), 8.34 (dd, J = 7.9, 1.4 Hz, 1H), 7.87 (ddd, J = 8.3, 7.2, 1.5 Hz, 1H), 7.73 – 7.62 (m, 1H), 7.52 (ddd, J = 8.3, 1.7 Hz, 1H), 7.39 (d, J = 8.3 Hz, 1H), 4.83 (s, 1H), 3.62 (d, J = 53.5 Hz, 2H).
A (s) 11.81
B (d) 8.53
C (s) 8.43
D (dd) 8.34
E (ddd) 7.87
F (m) 7.68
G (dd) 7.52
H (d) 7.39
I (s) 4.83
J (d) 3.62
f1 (ppm)

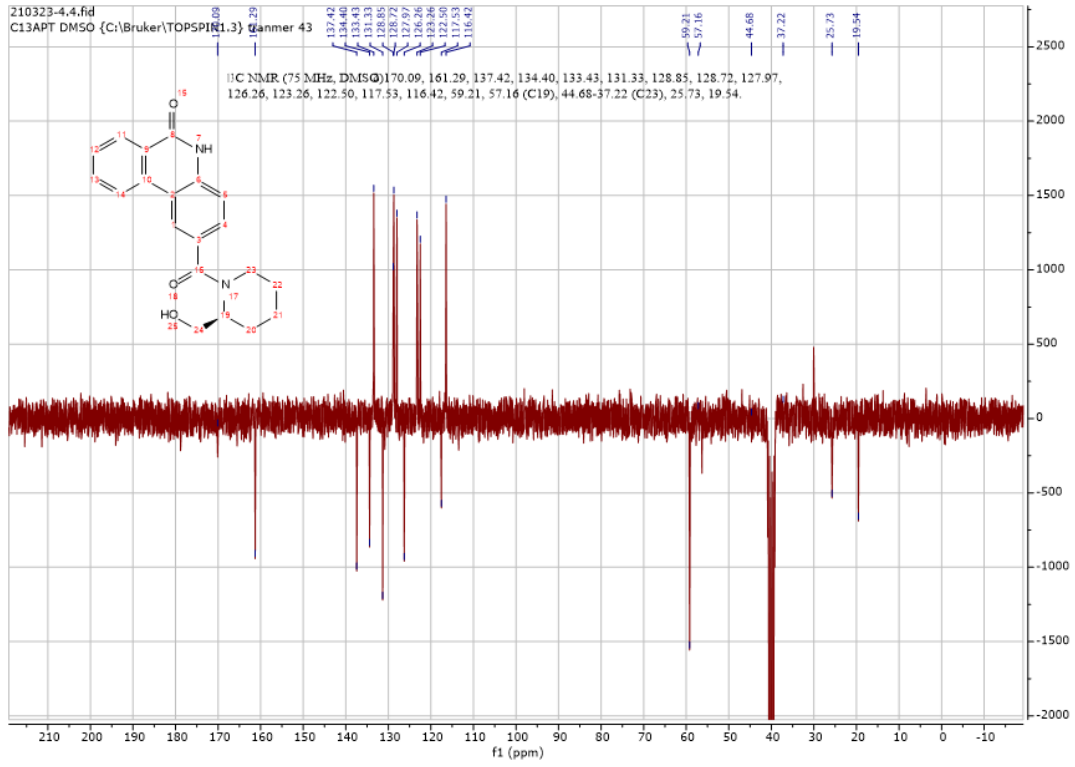
210323-4.4.fid
C13APT DMSO {C:\Bruker\TOPSPIN1.3} tranmer 43
13C NMR (75 MHz, DMSO) 170.09, 161.29, 137.42, 134.40, 133.43, 131.33, 128.85, 128.72, 127.97, 126.26, 123.26, 122.50, 117.53, 116.42, 59.21, 57.16 (C19), 44.68-37.22 (C23), 25.73, 19.54.
f1 (ppm)

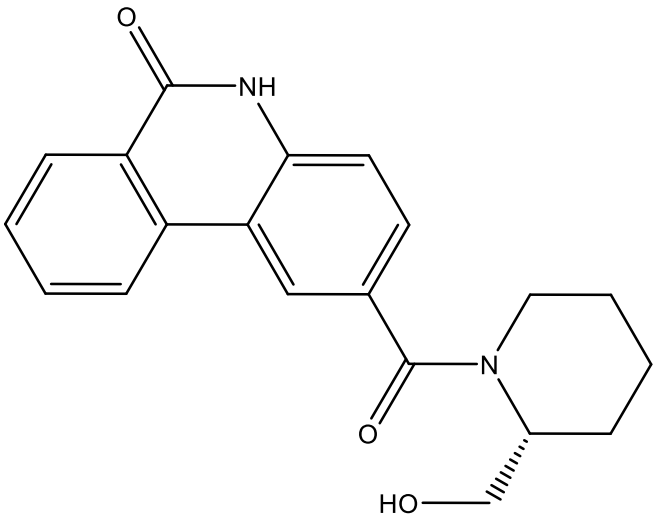

(*R*)-2-(2-(hydroxymethyl)piperidine-1-carbonyl)phenanthridin-6(5H)-one (a32)

Using **Synthesis Method d**, 24mg (0.1mmol) **f2** was reacted with 11.5mg (0.1mmol) (*R*)-piperidin-2-ylmethanol to give 20.8mg **a32** (Yield: 62%) and the product was separated as yellowish white solid. ^{1}H NMR (300 MHz, DMSO-d_6) δ 11.82 (s, 1H), 8.54 (d, *J* = 8.2 Hz, 1H), 8.43 (s, 1H), 8.34 (dd, *J* = 8.1, 1.9 Hz, 1H), 7.93 – 7.82 (m, 1H), 7.73 – 7.63 (m, 1H), 7.53 (d, *J* = 8.3 Hz, 1H), 7.40 (dd, *J* = 8.4, 2.1 Hz, 1H), 4.82 (s, 1H), 4.59 – 2.99 (m, 5H), 1.86 – 1.33 (m, 6H). ^{13}C NMR (75 MHz, DMSO) δ 170.6, 161.3, 137.4, 134.4, 133.4, 131.3, 128.8, 128.7, 128.0, 126.3, 123.3, 122.5, 117.5, 116.4, 59.2, 55.1 (C23), 44.9-37.1 (C19), 25.7, 19.5. HRMS m/z (ESI+, M+H): Calcd for C20H20N2O3: 337.1547, (ESI+, M+H) found: 337.1545

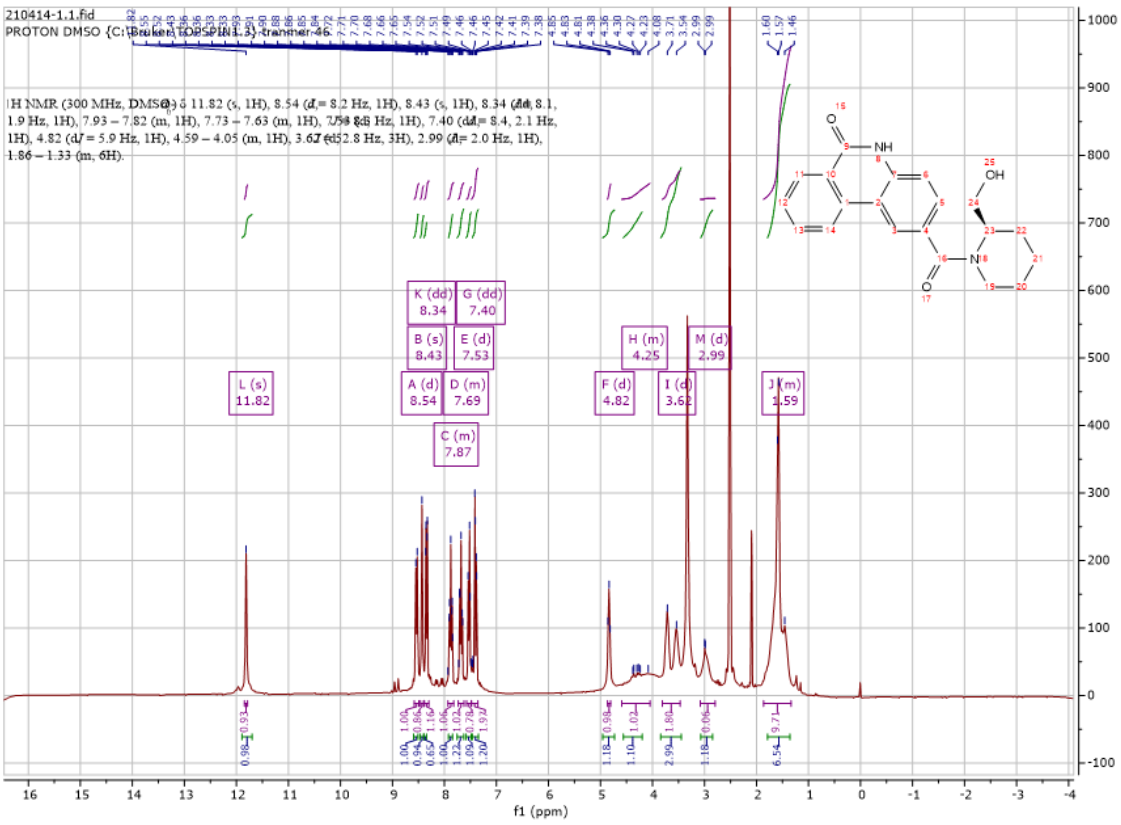
210414-1.1.fid
PROTON DMSO {C:\Bruker\TOPSPIN1.3} tanmer 46
1H NMR (300 MHz, DMSO) δ 11.82 (s, 1H), 8.54 (d, J = 8.2 Hz, 1H), 8.43 (s, 1H), 8.34 (dd, J = 8.1, 1.9 Hz, 1H), 7.93 – 7.82 (m, 1H), 7.73 – 7.63 (m, 1H), 7.58 (d, J = 8.8 Hz, 1H), 7.40 (dd, J = 8.4, 2.1 Hz, 1H), 4.82 (d, J = 5.9 Hz, 1H), 4.59 – 4.05 (m, 1H), 3.67 (d, J = 2.8 Hz, 3H), 2.99 (d, J = 2.0 Hz, 1H), 1.86 – 1.33 (m, 6H).
K (dd) 8.34
G (dd) 7.40
B (s) 8.43
E (d) 7.53
H (m) 4.25
M (d) 2.99
L (s) 11.82
A (d) 8.54
D (m) 7.69
F (d) 4.82
I (d) 3.62
J (m) 2.59
C (m) 7.87
f1 (ppm)

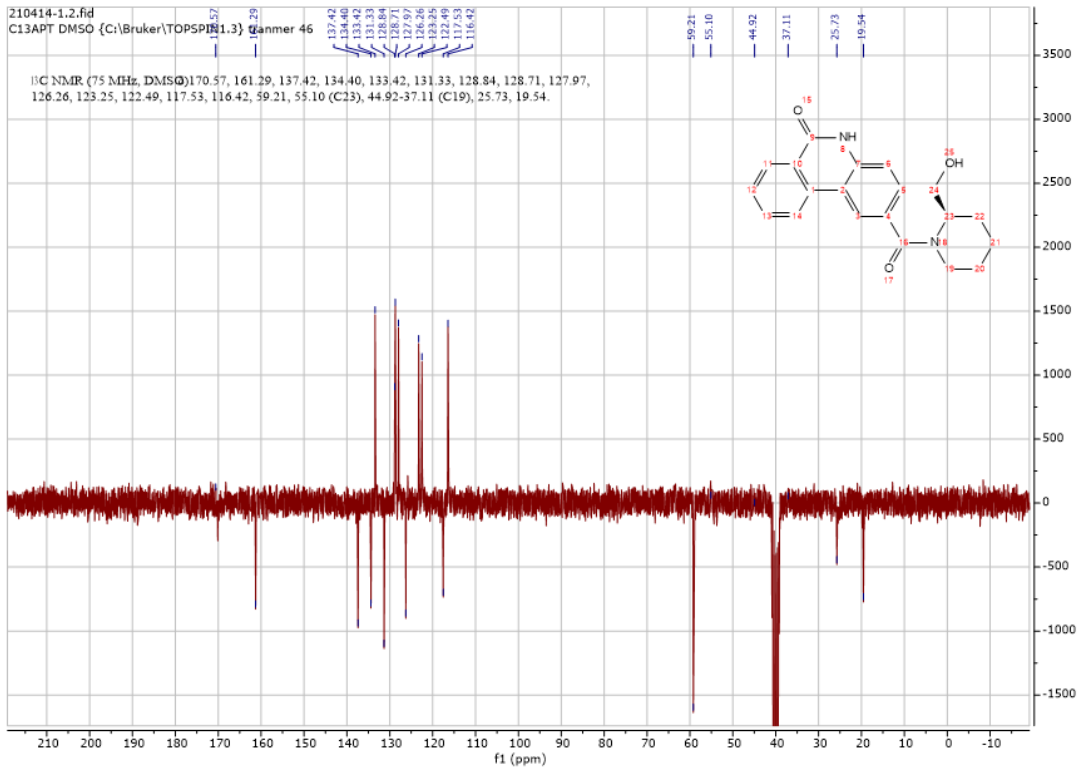
210414-1.2.fid
C13APT DMSO {C:\Bruker\TOPSPIN1.3} tanmer 46
13C NMR (75 MHz, DMSO) 170.57, 161.29, 137.42, 134.40, 133.42, 131.33, 128.84, 128.71, 127.97, 126.26, 123.25, 122.49, 117.53, 116.42, 59.21, 55.10 (C23), 44.92-37.11 (C19), 25.73, 19.54.
f1 (ppm)

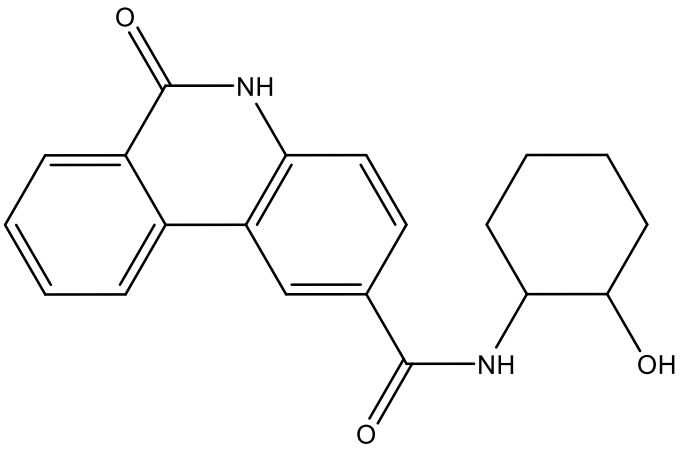

***N*-(2-hydroxycyclohexyl)-6-oxo-5,6-dihydrophenanthridine-2-carboxamide (a33)**

Using **Synthesis Method d**, 24mg (0.1mmol) **f2** was reacted with 11.5mg (0.1mmol) 2-aminocyclohexan-1-ol to give 24.2mg **a33** (Yield: 72%) and the product was separated as yellowish white solid. ^{1}H NMR (300 MHz, DMSO-d_6) δ 11.86 (s, 1H), 8.91 – 8.85 (m, 1H), 8.62 (d, J = 8.1 Hz, 1H), 8.34 (dd, J = 7.9, 1.1 Hz, 1H), 8.24 (d, J = 8.0 Hz, 1H), 8.00 (dd, J = 8.5, 1.6 Hz, 1H), 7.97 – 7.89 (m, 1H), 7.70 (t, J = 7.5 Hz, 1H), 7.40 (d, J = 8.5 Hz, 1H), 4.66 (s, 1H), 3.70 (m, 2H), 3.54 – 3.41 (m, 2H), 1.91 (m, 3H), 1.67 (m, 3H). ^{13}C NMR (75 MHz, DMSO) δ 165.8, 161.4, 138.9, 134.6, 133.4, 129.5, 129.2, 128.7, 128.0, 126.2, 123.34, 122.7, 117.3, 116.3, 71.8, 55.8, 35.1, 32.0, 25.0, 24.7. HRMS m/z (ESI+, M+Na): Calcd for C20H20N2O3: 359.1372, (ESI+, M+Na) found: 359.1363

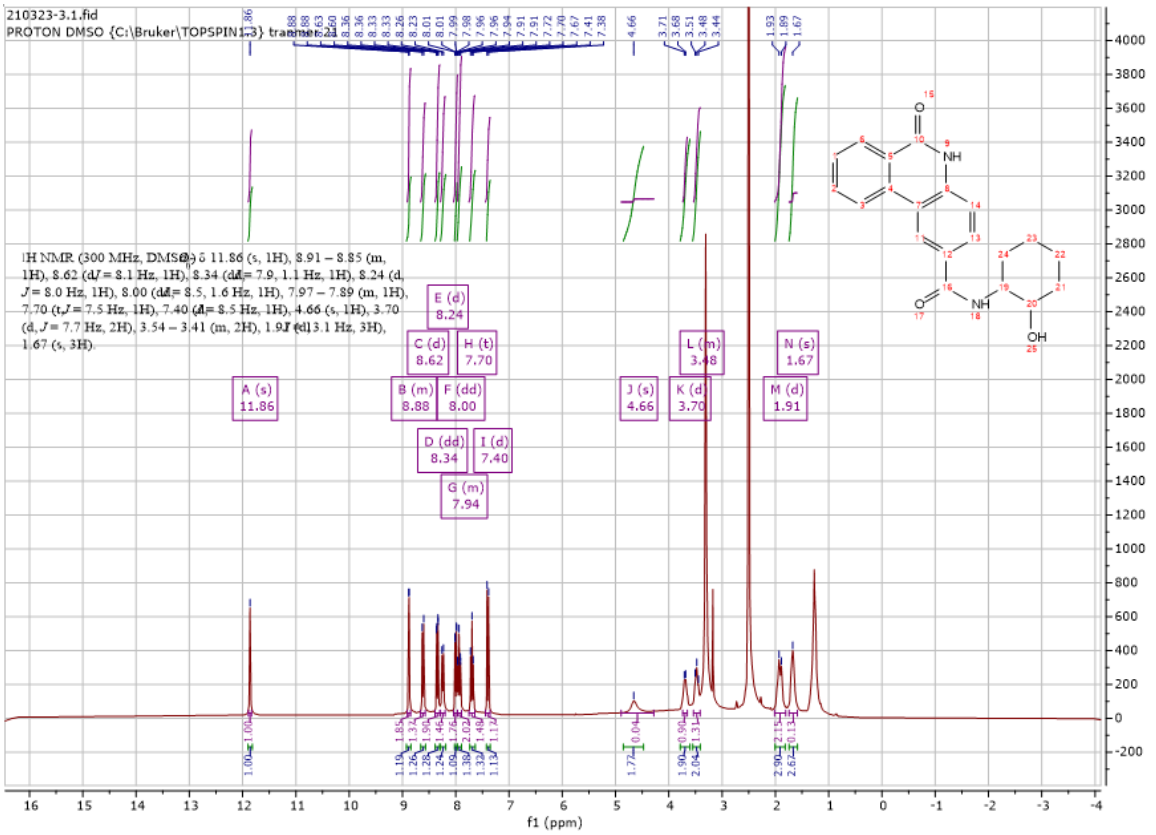
210323-3.1.fid
PROTON DMSO {C:\Bruker\TOPSPIN1.3} tranmer 21
1H NMR (300 MHz, DMSO) δ 11.86 (s, 1H), 8.91 – 8.85 (m, 1H), 8.62 (d, J = 8.1 Hz, 1H), 8.34 (dd, J = 7.9, 1.1 Hz, 1H), 8.24 (d, J = 8.0 Hz, 1H), 8.00 (dd, J = 8.5, 1.6 Hz, 1H), 7.97 – 7.89 (m, 1H), 7.70 (t, J = 7.5 Hz, 1H), 7.40 (d, J = 8.5 Hz, 1H), 4.66 (s, 1H), 3.70 (d, J = 7.7 Hz, 2H), 3.54 – 3.41 (m, 2H), 1.91 (d, J = 3.1 Hz, 3H), 1.67 (s, 3H).
A (s) 11.86
B (m) 8.88
C (d) 8.62
D (dd) 8.34
E (d) 8.24
F (dd) 8.00
G (m) 7.94
H (t) 7.70
I (d) 7.40
J (s) 4.66
K (d) 3.70
L (m) 3.48
M (d) 1.91
N (s) 1.67
f1 (ppm)

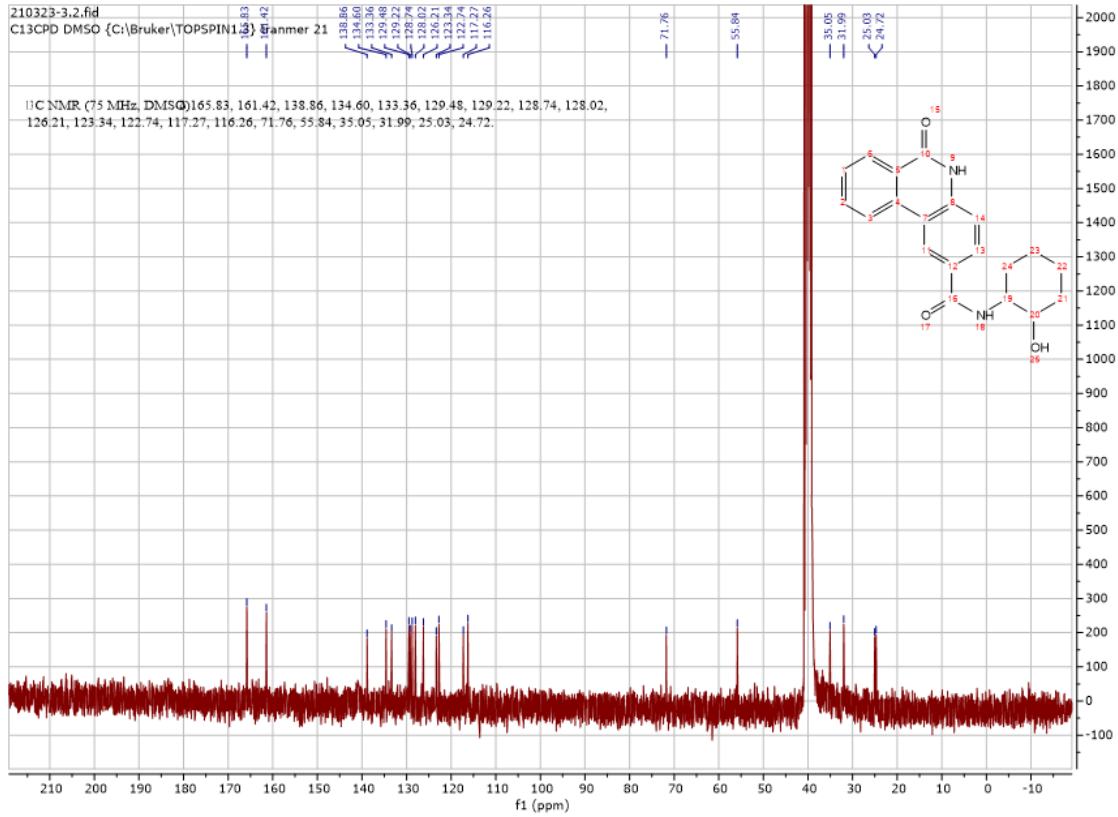
210323-3.2.fid
C13CPD DMSO {C:\Bruker\TOPSPIN1.3} tranmer 21
13C NMR (75 MHz, DMSO) 165.83, 161.42, 138.86, 134.60, 133.36, 129.48, 129.22, 128.74, 128.02, 126.21, 123.34, 122.74, 117.27, 116.26, 71.76, 55.84, 35.05, 31.99, 25.03, 24.72.
f1 (ppm)

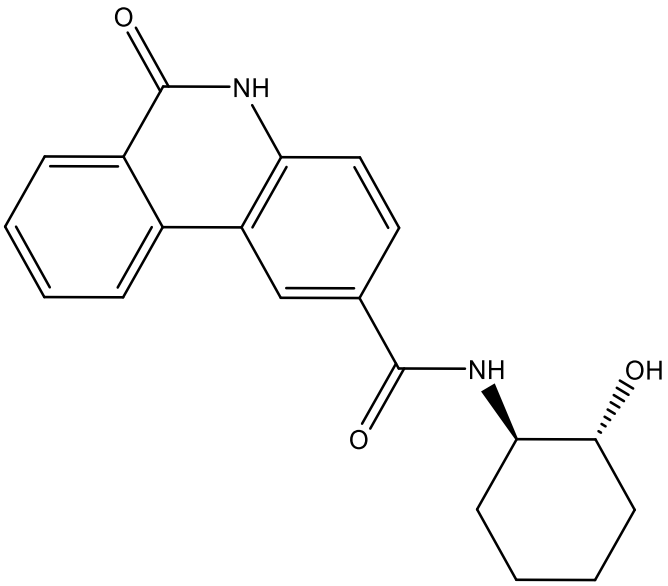

***N*-((1*R*,2*R*)-2-hydroxycyclohexyl)-6-oxo-5,6-dihydrophenanthridine-2-carboxamide (a34)**

Using **Synthesis Method d**, 24mg (0.1mmol) **f2** was reacted with 11.5mg (0.1mmol) (1*R*,2*R*)-2-aminocyclohexan-1-ol to give 24.4mg **a34** (Yield: 73%) and the product was separated as yellowish white solid. ^{1}H NMR (300 MHz, DMSO-d_6) δ 11.87 (s, 1H), 8.88 (d, *J* = 1.9 Hz, 1H), 8.62 (d, *J* = 8.2 Hz, 1H), 8.34 (dd, *J* = 8.0, 1.4 Hz, 1H), 8.26 (d, *J* = 8.0 Hz, 1H), 8.00 (dd, *J* = 8.5, 1.8 Hz, 1H), 7.93 (ddd, *J* = 8.3, 7.2, 1.5 Hz, 1H), 7.70 (td, 1H), 7.40 (d, *J* = 8.5 Hz, 1H), 4.69 (s, 1H), 3.70 (m, 1H), 3.49 (m, 1H), 2.02 – 1.57 (m, 4H), 1.26 (m, 4H). ^{13}C NMR (75 MHz, DMSO) δ 165.8, 161.4, 138.9, 134.6, 133.4, 129.5, 129.2, 128.7, 128.0, 126.2, 123.3, 122.7, 117.3, 116.3, 71.8, 55.9, 35.1, 32.0, 25.0, 24.7. HRMS m/z (ESI+, M+Na): Calcd for C20H20N2O3: 359.1372, (ESI+, M+Na) found: 359.1672

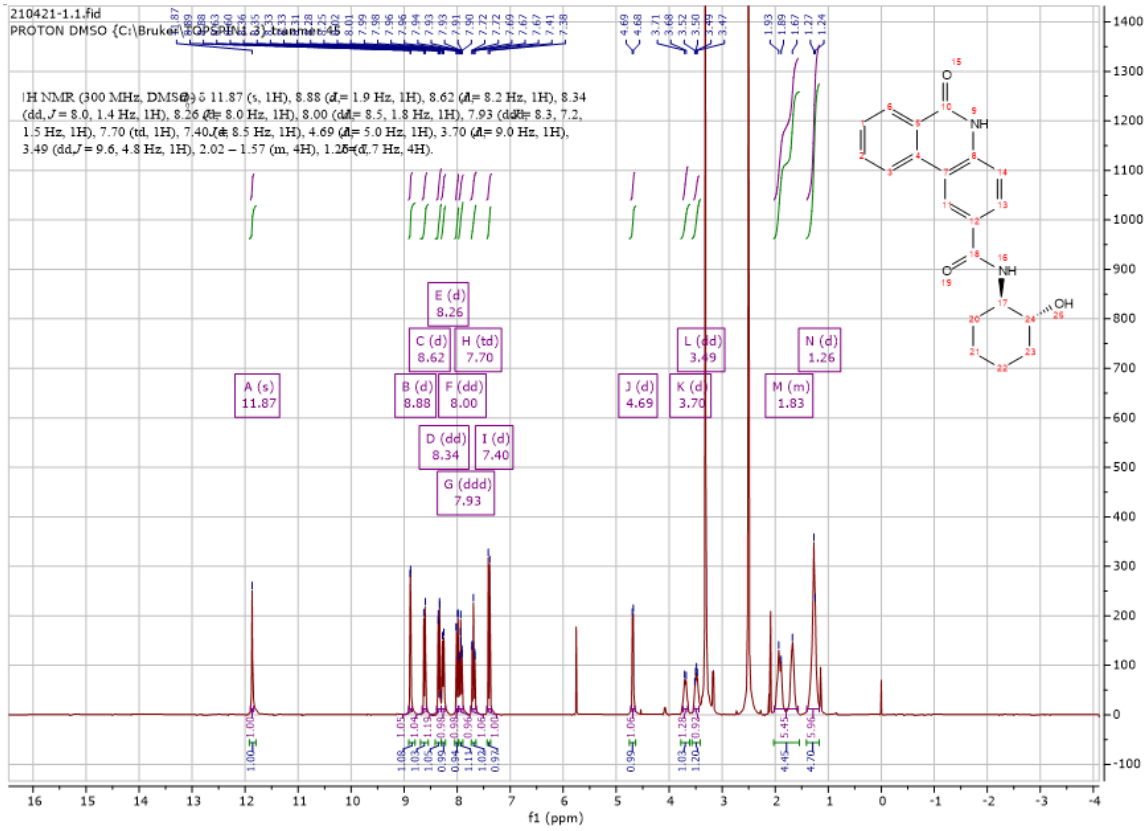
210421-1.1.fid
PROTON DMSO {C:\Bruker\TOPSPIN1.3} Eanmer 45
1H NMR (300 MHz, DMSO) δ 11.87 (s, 1H), 8.88 (d, J = 1.9 Hz, 1H), 8.62 (d, J = 8.2 Hz, 1H), 8.34 (dd, J = 8.0, 1.4 Hz, 1H), 8.26 (d, J = 8.0 Hz, 1H), 8.00 (dd, J = 8.5, 1.8 Hz, 1H), 7.93 (ddd, J = 8.3, 7.2, 1.5 Hz, 1H), 7.70 (td, J = 8.5 Hz, 1H), 7.40 (d, J = 8.5 Hz, 1H), 4.69 (d, J = 5.0 Hz, 1H), 3.70 (d, J = 9.0 Hz, 1H), 3.49 (dd, J = 9.6, 4.8 Hz, 1H), 2.02 – 1.57 (m, 4H), 1.26 (d, J = 7 Hz, 4H).
A (s) 11.87
B (d) 8.88
C (d) 8.62
D (dd) 8.34
E (d) 8.26
F (dd) 8.00
G (ddd) 7.93
H (td) 7.70
I (d) 7.40
J (d) 4.69
K (d) 3.70
L (dd) 3.49
M (m) 1.83
N (d) 1.26
f1 (ppm)

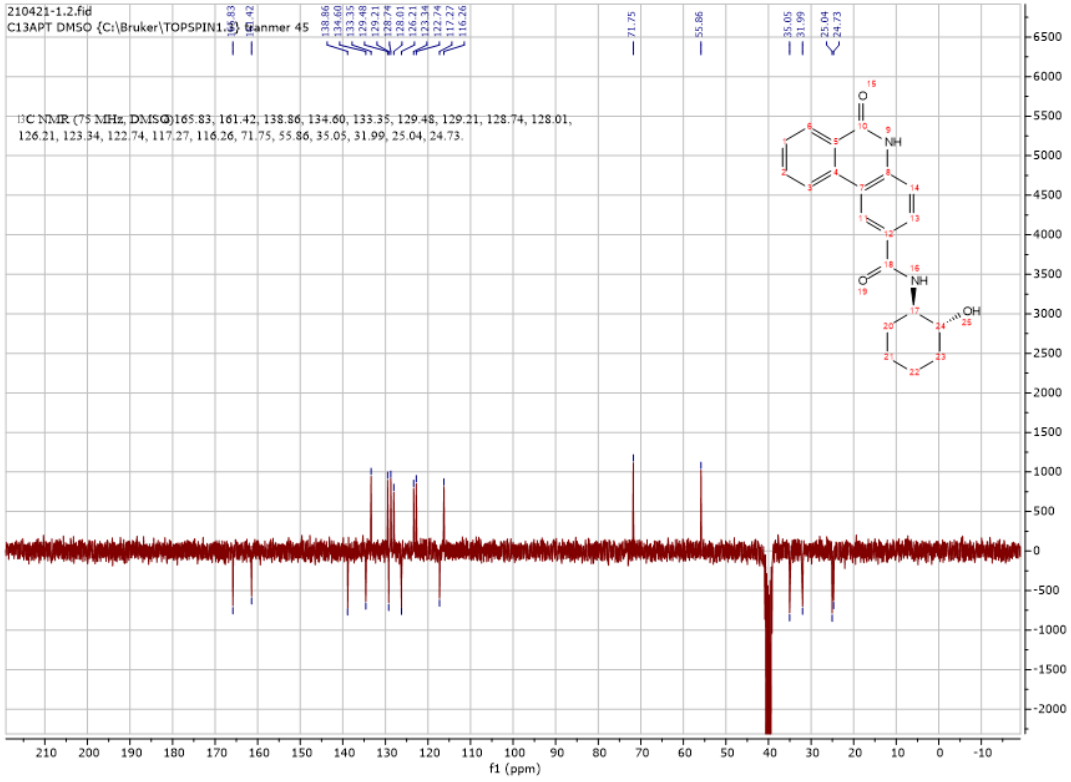
210421-1.2.fid
C13APT DMSO {C:\Bruker\TOPSPIN1.3} Eanmer 45
13C NMR (75 MHz, DMSO) 165.83, 161.42, 138.86, 134.60, 133.35, 129.48, 129.21, 128.74, 128.01, 126.21, 123.34, 122.74, 117.27, 116.26, 71.75, 55.86, 35.05, 31.99, 25.04, 24.73.
f1 (ppm)

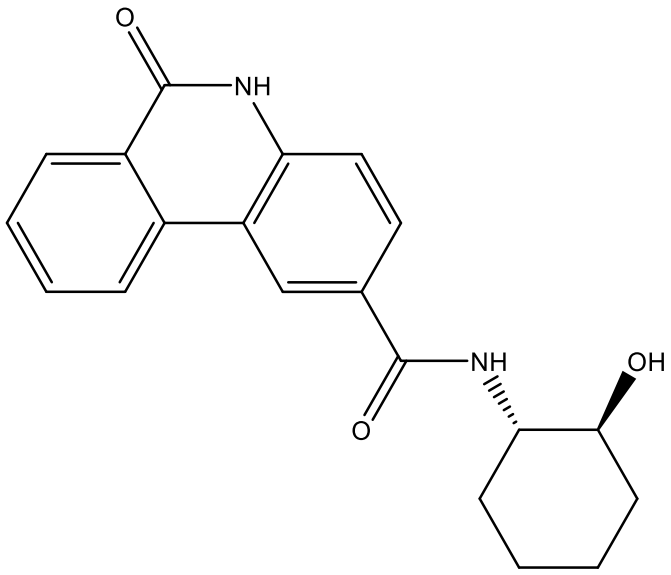

***N*-((1*S*,2*S*)-2-hydroxycyclohexyl)-6-oxo-5,6-dihydrophenanthridine-2-carboxamide (a35)**

Using **Synthesis Method d**, 24mg (0.1mmol) **f2** was reacted with 11.5mg (0.1mmol) (1*S*,2*S*)-2-aminocyclohexan-1-ol to give 23.5mg **a35** (Yield: 70%) and the product was separated as yellowish white solid. ^{1}H NMR (300 MHz, DMSO-d_6) δ 11.87 (s, 1H), 8.88 (d, *J* = 1.9 Hz, 1H), 8.62 (d, *J* = 8.1 Hz, 1H), 8.35 (dd, *J* = 8.0, 1.4 Hz, 1H), 8.26 (d, *J* = 8.0 Hz, 1H), 8.00 (dd, *J* = 8.5, 1.8 Hz, 1H), 7.94 (ddd, *J* = 8.4, 7.2, 1.5 Hz, 1H), 7.75 – 7.64 (m, 1H), 7.40 (d, *J* = 8.5 Hz, 1H), 4.68 (s, 1H), 3.70 (m, 1H), 3.53 – 3.45 (m, 1H), 1.91 (m, 2H), 1.67 (m, 2H), 1.27 (m, 4H). ^{13}C NMR (75 MHz, DMSO) δ 165.9, 161.4, 138.9, 134.6, 133.4, 129.5, 129.2, 128.8, 128.0, 126.2, 123.3, 122.7, 117.3, 116.3, 71.8, 55.8, 35.1, 32.0, 25.0, 24.7. HRMS m/z (ESI+, M+Na): Calcd for C20H20N2O3: 359.1372, (ESI+, M+Na) found: 359.1365

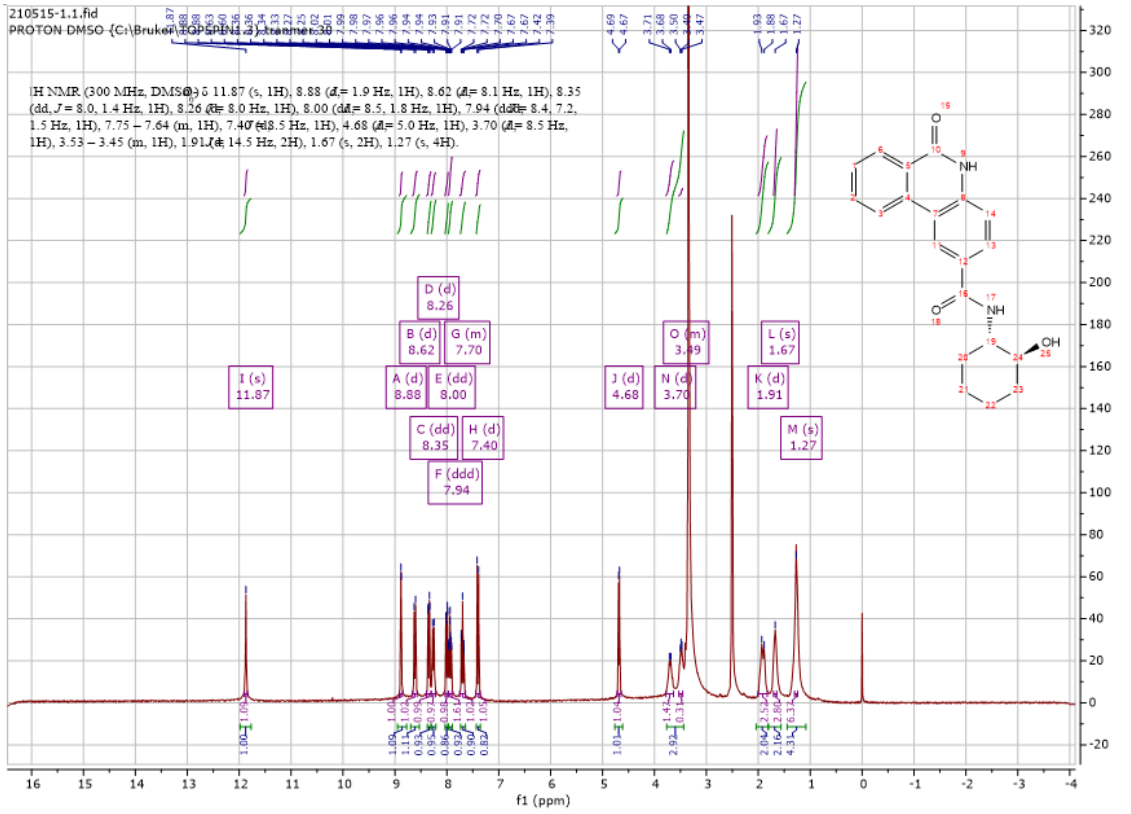
210515-1.1.fid
PROTON DMSO (C:\Bruker\TOPSPIN1.3) Tranmer 30
1H NMR (300 MHz, DMSO) δ 11.87 (s, 1H), 8.88 (d, J = 1.9 Hz, 1H), 8.62 (d, J = 8.1 Hz, 1H), 8.35 (dd, J = 8.0, 1.4 Hz, 1H), 8.26 (d, J = 8.0 Hz, 1H), 8.00 (dd, J = 8.5, 1.8 Hz, 1H), 7.94 (ddd, J = 8.4, 7.2, 1.5 Hz, 1H), 7.75 – 7.64 (m, 1H), 7.40 (d, J = 8.5 Hz, 1H), 4.68 (d, J = 5.0 Hz, 1H), 3.70 (d, J = 8.5 Hz, 1H), 3.53 – 3.45 (m, 1H), 1.91 (d, J = 14.5 Hz, 2H), 1.67 (s, 2H), 1.27 (s, 4H).
I (s) 11.87
A (d) 8.88
B (d) 8.62
C (dd) 8.35
D (d) 8.26
E (dd) 8.00
F (ddd) 7.94
G (m) 7.70
H (d) 7.40
J (d) 4.68
N (d) 3.70
O (m) 3.49
K (d) 1.91
L (s) 1.67
M (s) 1.27
f1 (ppm)

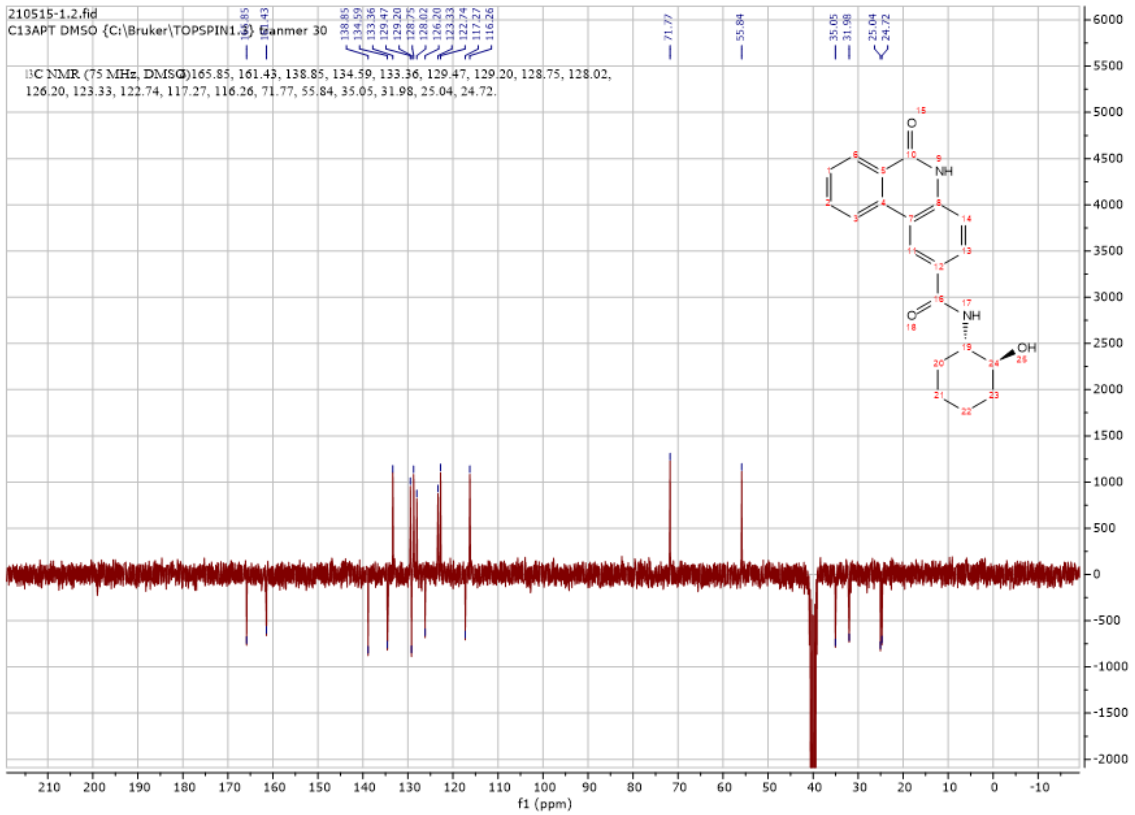
210515-1.2.fid
C13APT DMSO (C:\Bruker\TOPSPIN1.3) Tranmer 30
13C NMR (75 MHz, DMSO) 165.85, 161.43, 138.85, 134.59, 133.36, 129.47, 129.20, 128.75, 128.02, 126.20, 123.33, 122.74, 117.27, 116.26, 71.77, 55.84, 35.05, 31.98, 25.04, 24.72.
f1 (ppm)

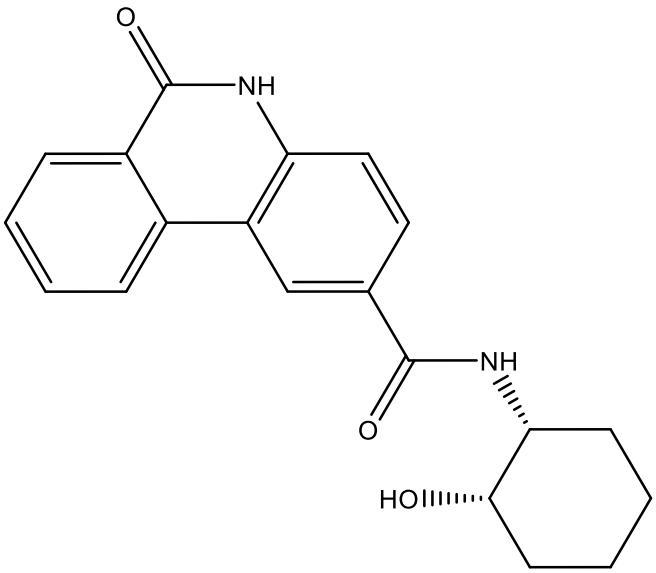

***N*-((1*R*,2*S*)-2-hydroxycyclohexyl)-6-oxo-5,6-dihydrophenanthridine-2-carboxamide (a36)**

Using **Synthesis Method d**, 24mg (0.1mmol) **f2** was reacted with 11.5mg (0.1mmol) (1*R*,2*S*)-2-aminocyclohexan-1-ol to give 24.6mg **a36** (Yield: 73%) and the product was separated as yellowish white solid. ^{1}H NMR (300 MHz, DMSO-d_6) δ 11.87 (s, 1H), 8.90 (d, *J* = 1.9 Hz, 1H), 8.65 (d, *J* = 8.1 Hz, 1H), 8.34 (dd, *J* = 7.9, 1.4 Hz, 1H), 8.09 (d, *J* = 7.8 Hz, 1H), 8.00 (dd, *J* = 8.5, 1.8 Hz, 1H), 7.93 (ddd, *J* = 8.4, 7.2, 1.5 Hz, 1H), 7.70 (t, 1H), 7.40 (d, *J* = 8.6 Hz, 1H), 4.71 (s, 1H), 4.00 – 3.77 (m, 2H), 1.95 – 1.21 (m, 8H). ^{13}C NMR (75 MHz, DMSO) δ 165.4, 161.4, 138.9, 134.6, 133.4, 129.5, 129.0, 128.7, 128.0, 126.2, 123.5, 123.0, 117.3, 116.3, 67.1, 52.4, 32.4, 26.7, 25.0, 19.7. HRMS m/z (ESI+, M+Na): Calcd for C20H20N2O3: 359.1372, (ESI+, M+Na) found: 359.1365

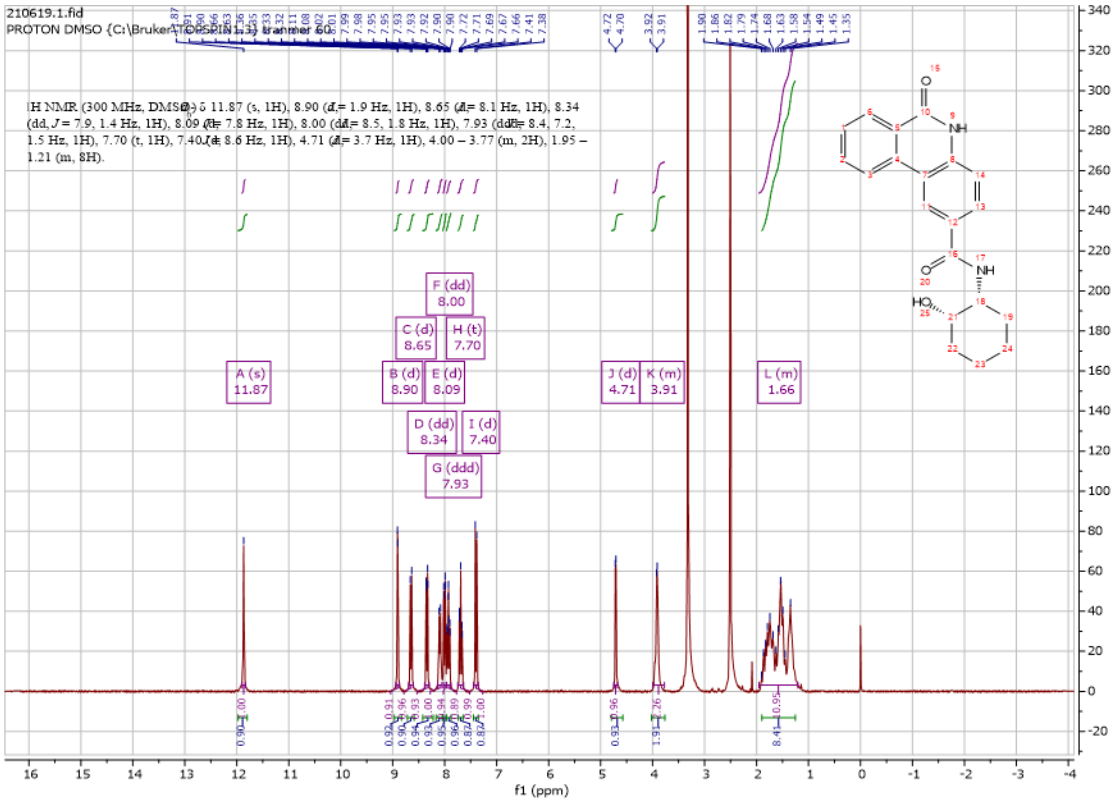
210619.1.fid
PROTON DMSO {C:\Bruker\TOPSPIN1.3} Ganmer 60
1H NMR (300 MHz, DMSO) δ 11.87 (s, 1H), 8.90 (d, J = 1.9 Hz, 1H), 8.65 (d, J = 8.1 Hz, 1H), 8.34 (dd, J = 7.9, 1.4 Hz, 1H), 8.09 (d, J = 7.8 Hz, 1H), 8.00 (dd, J = 8.5, 1.8 Hz, 1H), 7.93 (ddd, J = 8.4, 7.2, 1.5 Hz, 1H), 7.70 (t, 1H), 7.40 (d, J = 8.6 Hz, 1H), 4.71 (d, J = 3.7 Hz, 1H), 4.00 – 3.77 (m, 2H), 1.95 – 1.21 (m, 8H).
A (s) 11.87
B (d) 8.90
C (d) 8.65
D (dd) 8.34
E (d) 8.09
F (dd) 8.00
G (ddd) 7.93
H (t) 7.70
I (d) 7.40
J (d) 4.71
K (m) 3.91
L (m) 1.66
f1 (ppm)

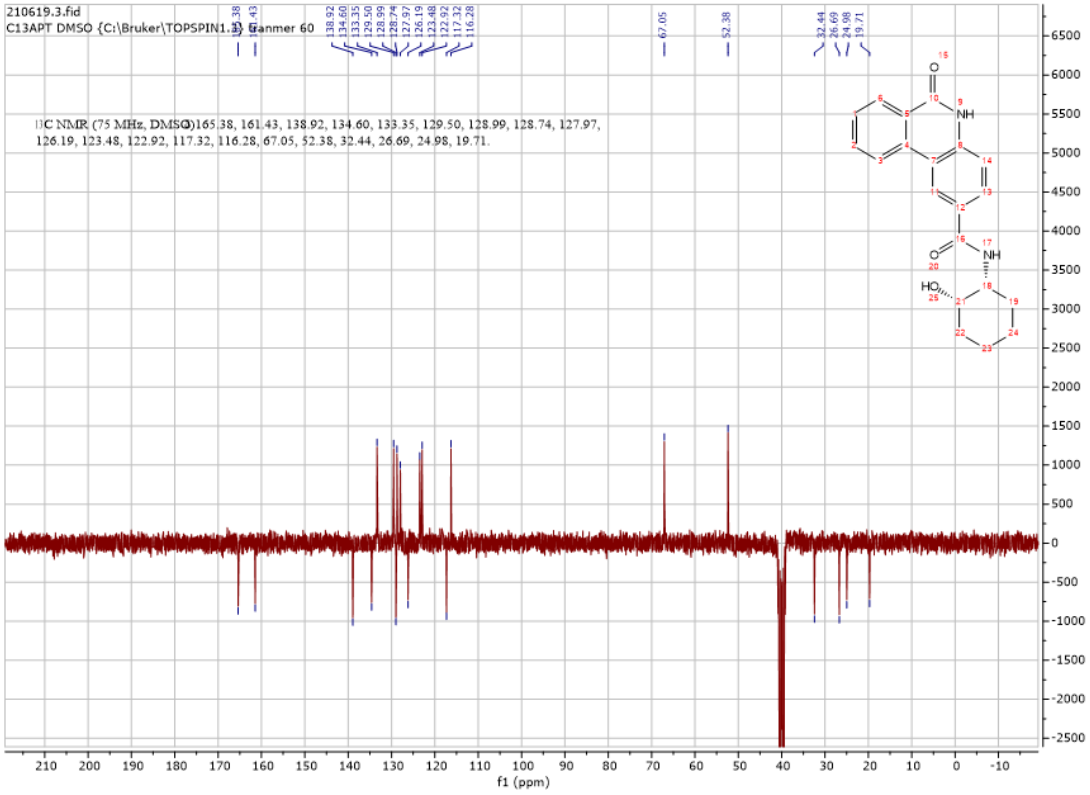
210619.3.fid
C13APT DMSO {C:\Bruker\TOPSPIN1.3} Ganmer 60
13C NMR (75 MHz, DMSO) 165.38, 161.43, 138.92, 134.60, 133.35, 129.50, 128.99, 128.74, 127.97, 126.19, 123.48, 122.92, 117.32, 116.28, 67.05, 52.38, 32.44, 26.69, 24.98, 19.71.
f1 (ppm)

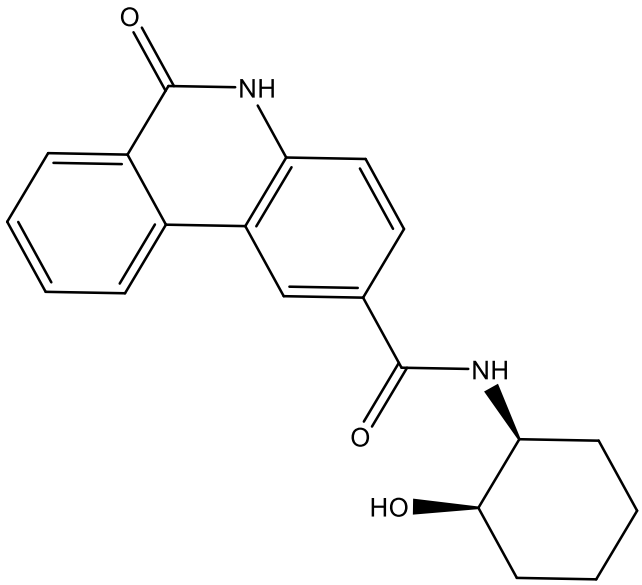

***N*-((1*S*,2*R*)-2-hydroxycyclohexyl)-6-oxo-5,6-dihydrophenanthridine-2-carboxamide (a37)**

Using **Synthesis Method d**, 24mg (0.1mmol) **f2** was reacted with 11.5mg (0.1mmol) (1*S*,2*R*)-2-aminocyclohexan-1-ol to give 24.3mg **a37** (Yield: 72%) and the product was separated as yellowish white solid. ^{1}H NMR (300 MHz, DMSO-d_6) δ 11.88 (s, 1H), 8.91 (d, *J* = 1.9 Hz, 1H), 8.65 (d, *J* = 8.2 Hz, 1H), 8.34 (dd, *J* = 8.0, 1.4 Hz, 1H), 8.11 (d, *J* = 7.8 Hz, 1H), 8.01 (dd, *J* = 8.5, 1.8 Hz, 1H), 7.93 (ddd, *J* = 8.4, 7.1, 1.5 Hz, 1H), 7.70 (t, 1H), 7.40 (d, *J* = 8.5 Hz, 1H), 4.72 (s, 1H), 3.98 – 3.82 (m, 2H), 1.94 – 1.23 (m, 8H). ^{13}C NMR (75 MHz, DMSO) δ 165.4, 161.4, 138.9, 134.6, 133.4, 129.5, 129.0, 128.7, 128.0, 126.2, 123.5, 122.9, 117.3, 116.3, 67.1, 52.4, 32.4, 26.7, 25.0, 19.7. HRMS m/z (ESI+, M+Na): Calcd for C20H20N2O3: 359.1372, (ESI+, M+Na) found: 359.1365

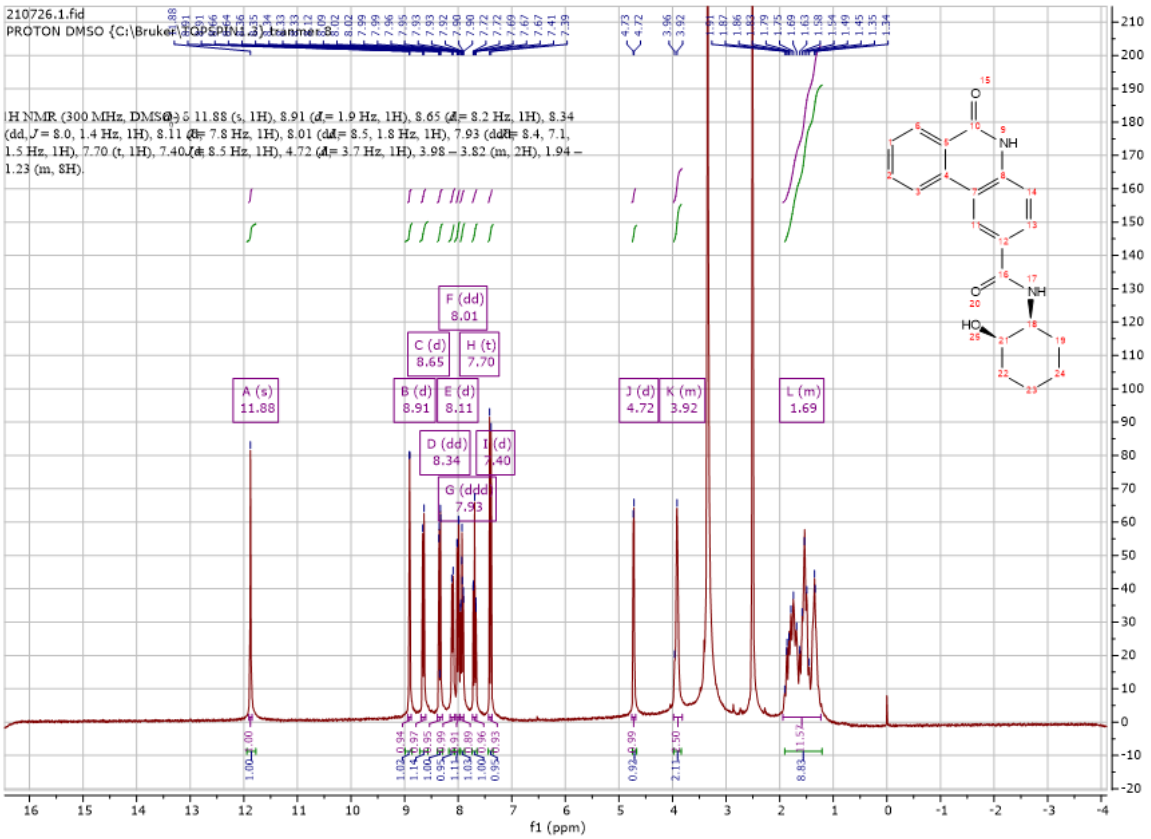
210726.1.fid
PROTON DMSO {C:\Bruker\TOPSPIN1.3} tranmer 8
1H NMR (300 MHz, DMSO) δ 11.88 (s, 1H), 8.91 (d, J = 1.9 Hz, 1H), 8.65 (d, J = 8.2 Hz, 1H), 8.34 (dd, J = 8.0, 1.4 Hz, 1H), 8.11 (d, J = 7.8 Hz, 1H), 8.01 (dd, J = 8.5, 1.8 Hz, 1H), 7.93 (ddd, J = 8.4, 7.1, 1.5 Hz, 1H), 7.70 (t, 1H), 7.40 (d, J = 8.5 Hz, 1H), 4.72 (d, J = 3.7 Hz, 1H), 3.98 – 3.82 (m, 2H), 1.94 – 1.23 (m, 8H).
A (s) 11.88
B (d) 8.91
C (d) 8.65
D (dd) 8.34
E (d) 8.11
F (dd) 8.01
G (ddd) 7.93
H (t) 7.70
I (d) 7.40
J (d) 4.72
K (m) 3.92
L (m) 1.69
f1 (ppm)

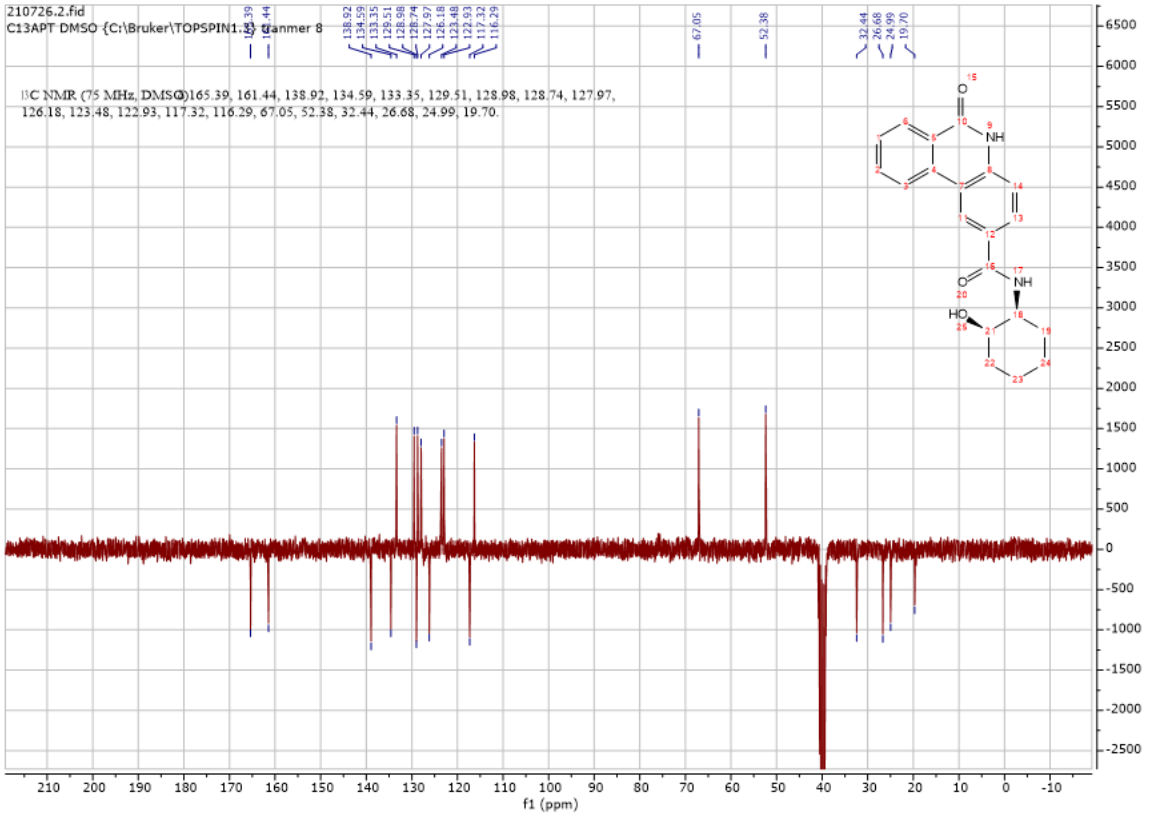
210726.2.fid
C13APT DMSO {C:\Bruker\TOPSPIN1.3} tranmer 8
13C NMR (75 MHz, DMSO) δ 165.39, 161.44, 138.92, 134.59, 133.35, 129.51, 128.98, 128.74, 127.97, 126.18, 123.48, 122.93, 117.32, 116.29, 67.05, 52.38, 32.44, 26.68, 24.99, 19.70.
f1 (ppm)

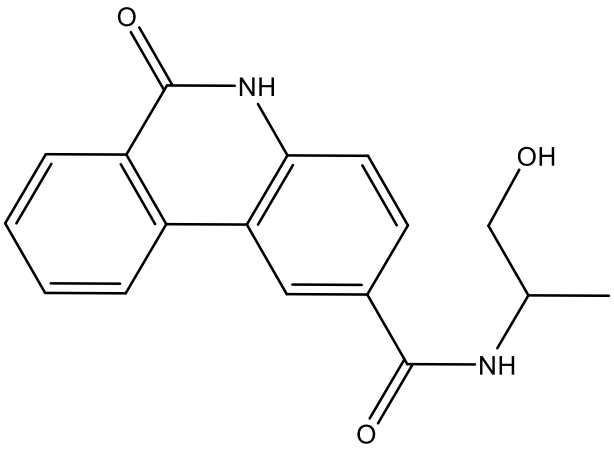

***N*-(1-hydroxypropan-2-yl)-6-oxo-5,6-dihydrophenanthridine-2-carboxamide (a38)**

Using **Synthesis Method d**, 24mg (0.1mmol) **f2** was reacted with 7.5mg (0.1mmol) 2-aminopropan-1-ol to give 23.7mg **a38** (Yield: 80%) and the product was separated as yellowish white solid. ^{1}H NMR (400 MHz, DMSO-d_6) δ 11.91 (s, 1H), 8.88 (d, *J* = 1.7 Hz, 1H), 8.62 (d, *J* = 8.1 Hz, 1H), 8.34 (dd, *J* = 8.0, 1.2 Hz, 1H), 8.28 (d, *J* = 8.0 Hz, 1H), 8.00 (dd, *J* = 8.5, 1.8 Hz, 1H), 7.93 (ddd, *J* = 8.3, 7.2, 1.4 Hz, 1H), 7.74 – 7.65 (m, 1H), 7.39 (d, *J* = 8.5 Hz, 1H), 4.80 (t, *J* = 5.8 Hz, 1H), 4.09 (s, 1H), 3.52 – 3.40 (m, 2H), 1.19 (d, *J* = 6.7 Hz, 3 H) ^{13}C NMR (101 MHz, DMSO) δ 169.9, 161.3, 137.4, 134.4, 133.5, 131.3, 128.9, 128.7, 128.0, 126.2, 123.3, 122.52, 117.5, 116.4, 59.2, 25.6, 19.5. HRMS m/z (ESI+, M+Na): Calcd for C17H16N2O3: 319.1059, (ESI+, M+Na) found: 319.1053

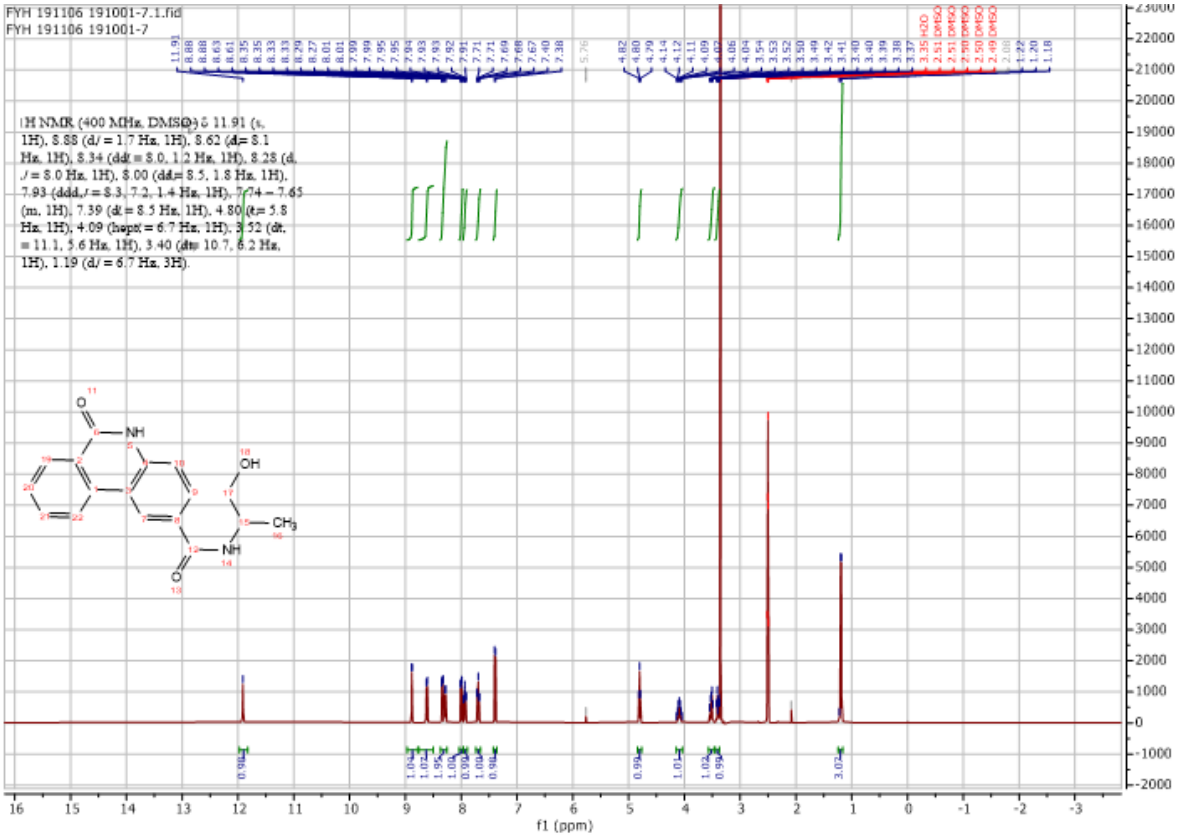
FYH 191106 191001-7.1.fid
FYH 191106 191001-7
1H NMR (400 MHz, DMSO) δ 11.91 (s, 1H), 8.88 (d, J = 1.7 Hz, 1H), 8.62 (d, J = 8.1 Hz, 1H), 8.34 (dd, J = 8.0, 1.2 Hz, 1H), 8.28 (d, J = 8.0 Hz, 1H), 8.00 (dd, J = 8.5, 1.8 Hz, 1H), 7.93 (ddd, J = 8.3, 7.2, 1.4 Hz, 1H), 7.74 – 7.65 (m, 1H), 7.39 (d, J = 8.5 Hz, 1H), 4.80 (t, J = 5.8 Hz, 1H), 4.09 (hept, J = 6.7 Hz, 1H), 3.52 (dt, J = 11.1, 5.6 Hz, 1H), 3.40 (dt, J = 10.7, 6.2 Hz, 1H), 1.19 (d, J = 6.7 Hz, 3H).
f1 (ppm)

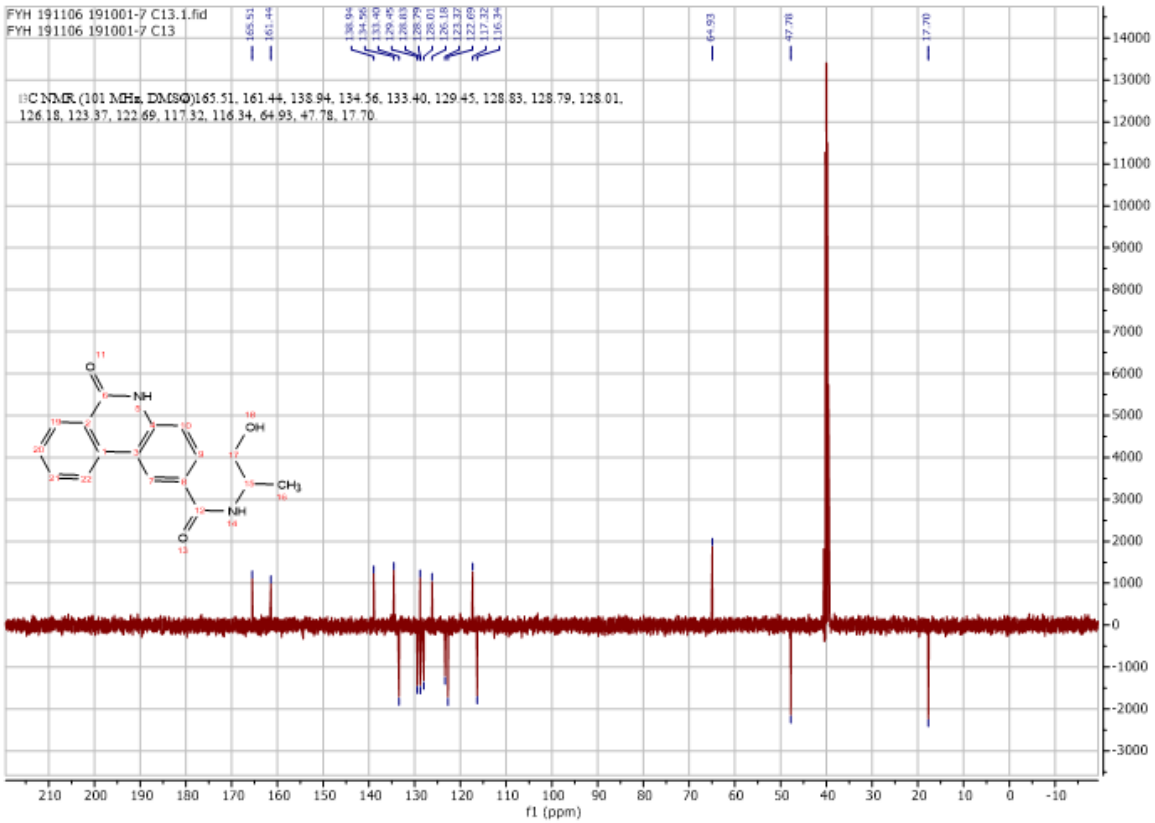
FYH 191106 191001-7 C13.1.fid
FYH 191106 191001-7 C13
13C NMR (101 MHz, DMSO) δ 165.51, 161.44, 138.94, 134.56, 133.40, 129.45, 128.83, 128.79, 128.01, 126.18, 123.37, 122.69, 117.32, 116.34, 64.93, 47.78, 17.70.
f1 (ppm)

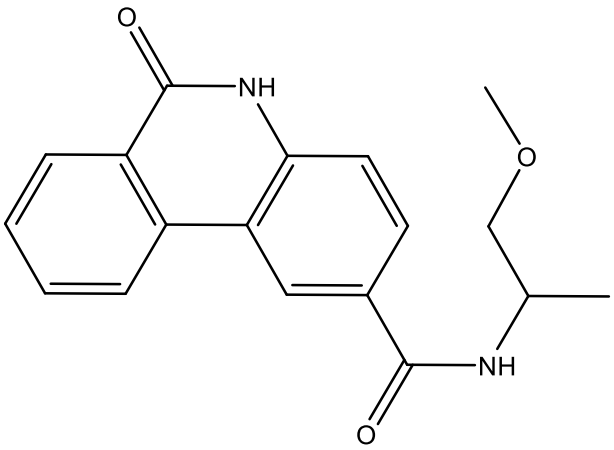

***N*-(1-methoxypropan-2-yl)-6-oxo-5,6-dihydrophenanthridine-2-carboxamide (a39)**

Using **Synthesis Method d**, 24mg (0.1mmol) **f2** was reacted with 8.9mg (0.1mmol) 1-methoxypropan-2-amine to give 26.3mg **a39** (Yield: 85%) and the product was separated as yellowish white solid. ^{1}H NMR (400 MHz, DMSO-d_6) δ 11.92 (s, 1H), 8.87 (d, *J* = 1.7 Hz, 1H), 8.60 (d, *J* = 8.1 Hz, 1H), 8.39 (d, *J* = 8.0 Hz, 1H), 8.34 (dd, *J* = 8.0, 1.1 Hz, 1H), 8.00 (dd, *J* = 8.5, 1.8 Hz, 1H), 7.94 (ddd, *J* = 8.3, 7.2, 1.4 Hz, 1H), 7.73 – 7.65 (m, 1H), 7.40 (d, *J* = 8.5 Hz, 1H), 4.33 – 4.22 (m, 1H), 3.46(dd, *J* = 9.5, 6.2 Hz, 1H), 3.35 (m, 4H), 1.20 (d, *J* = 6.8 Hz, 3H). ^{13}C NMR (101 MHz, DMSO) δ 165.4, 161.4, 139.0, 134.5, 133.4, 129.4, 128.8, 128.6, 128.0, 126.2, 123.4, 122.7, 117.4, 116.4, 75.6, 58.6, 45.0, 18.0. HRMS m/z (ESI+, M+Na): Calcd for C18H18N2O3: 333.1215, (ESI+, M+Na) found: 333.1206

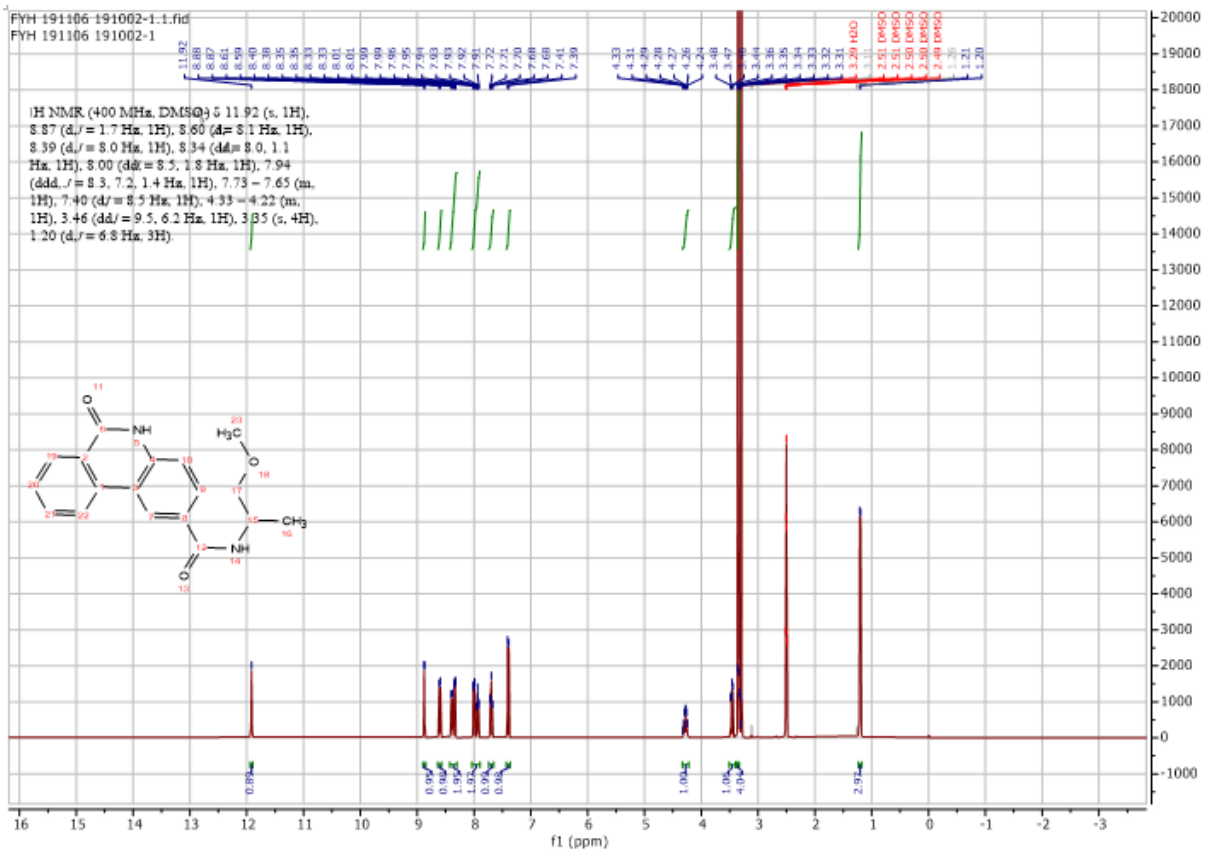
FYH 191106 191002-1.1.fid
FYH 191106 191002-1
¹H NMR (400 MHz, DMSO) δ 11.92 (s, 1H), 8.87 (d, J = 1.7 Hz, 1H), 8.60 (d, J = 8.1 Hz, 1H), 8.39 (d, J = 8.0 Hz, 1H), 8.34 (dd, J = 8.0, 1.1 Hz, 1H), 8.00 (dd, J = 8.5, 1.8 Hz, 1H), 7.94 (ddd, J = 8.3, 7.2, 1.4 Hz, 1H), 7.73 – 7.65 (m, 1H), 7.40 (d, J = 8.5 Hz, 1H), 4.33 – 4.22 (m, 1H), 3.46 (dd, J = 9.5, 6.2 Hz, 1H), 3.35 (s, 4H), 1.20 (d, J = 6.8 Hz, 3H).
f1 (ppm)

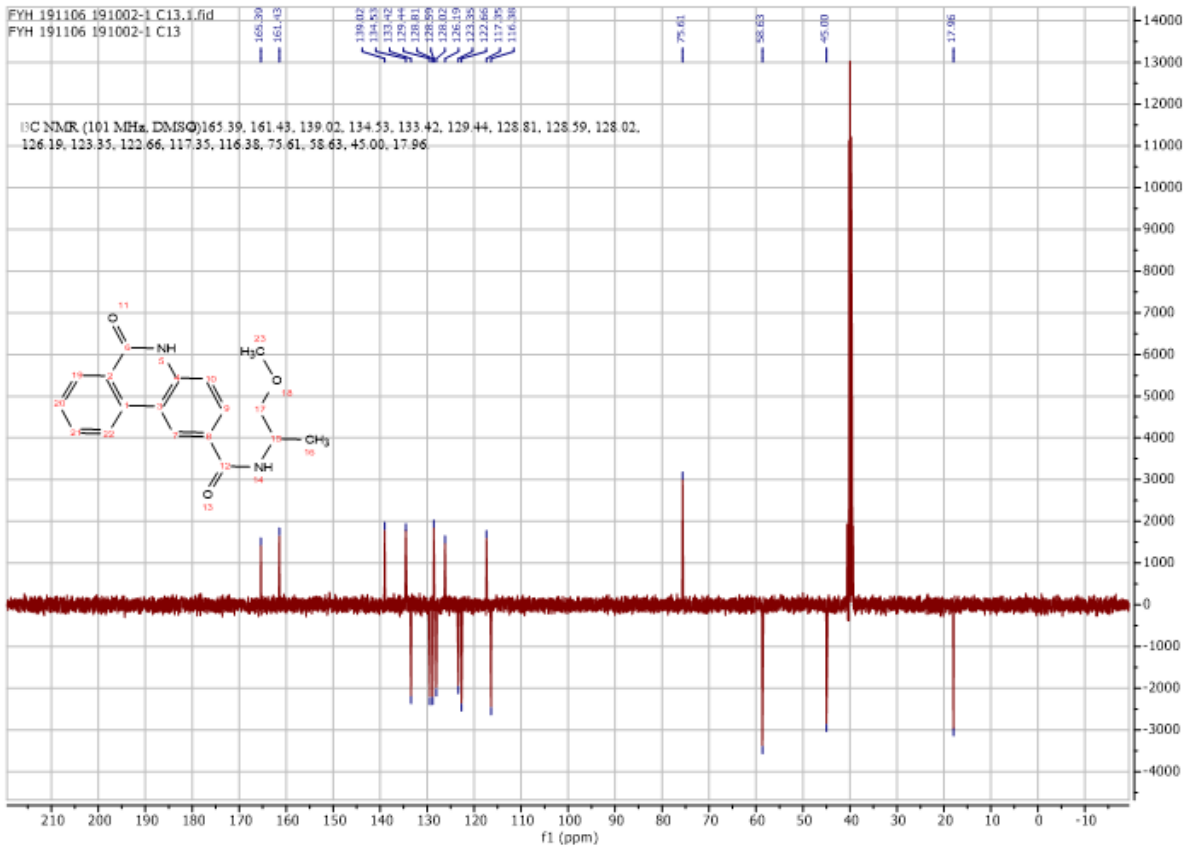
FYH 191106 191002-1 C13.1.fid
FYH 191106 191002-1 C13
¹³C NMR (101 MHz, DMSO) 165.39, 161.43, 139.02, 134.53, 133.42, 129.44, 128.81, 128.59, 128.02, 126.19, 123.35, 122.66, 117.35, 116.38, 75.61, 58.63, 45.00, 17.96.
f1 (ppm)

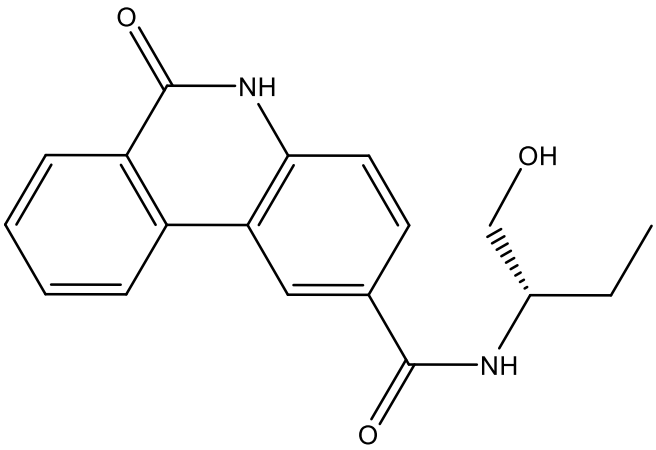

(*S*)-N-(1-hydroxybutan-2-yl)-6-oxo-5,6-dihydrophenanthridine-2-carboxamide (a40)

Using **Synthesis Method d**, 24mg (0.1mmol) **f2** was reacted with 8.9mg (0.1mmol) (*S*)-2-aminobutan-1-ol to give 26mg **a40** (Yield: 84%) and the product was separated as yellowish white solid. ^{1}H NMR (400 MHz, DMSO-d_6) δ 11.91 (s, 1H), 8.90 (d, *J* = 1.7 Hz, 1H), 8.62 (d, *J* = 8.2 Hz, 1H), 8.34 (dd, *J* = 8.0, 1.2 Hz, 1H), 8.20 (d, *J* = 8.4 Hz, 1H), 8.01 (dd, *J* = 8.5, 1.8 Hz, 1H), 7.98 – 7.82 (m, 1H), 7.70 (t, *J* = 7.6 Hz, 1H), 7.40 (d, *J* = 8.5 Hz, 1H), 4.75 (s, 1H), 3.93 (dp, *J* = 10.0, 5.1, 4.5 Hz, 1H), 3.48 (ddd, *J* = 29.7, 10.9, 5.6 Hz, 2H), 1.80 – 1.43 (m, 1H), 0.91 (t, *J* = 7.4 Hz, 3H). ^{13}C NMR (101 MHz, DMSO) δ 165.9, 161.4, 138.9, 134.6, 133.4, 129.5, 128.9, 128.8, 128.0, 126.2, 123.4, 122.7, 117.3, 116.3, 63.6, 53.6, 24.2, 11.2. HRMS m/z (ESI+, M+Na): Calcd for C18H18N2O3: 333.1215, (ESI+, M+Na) found: 333.1214

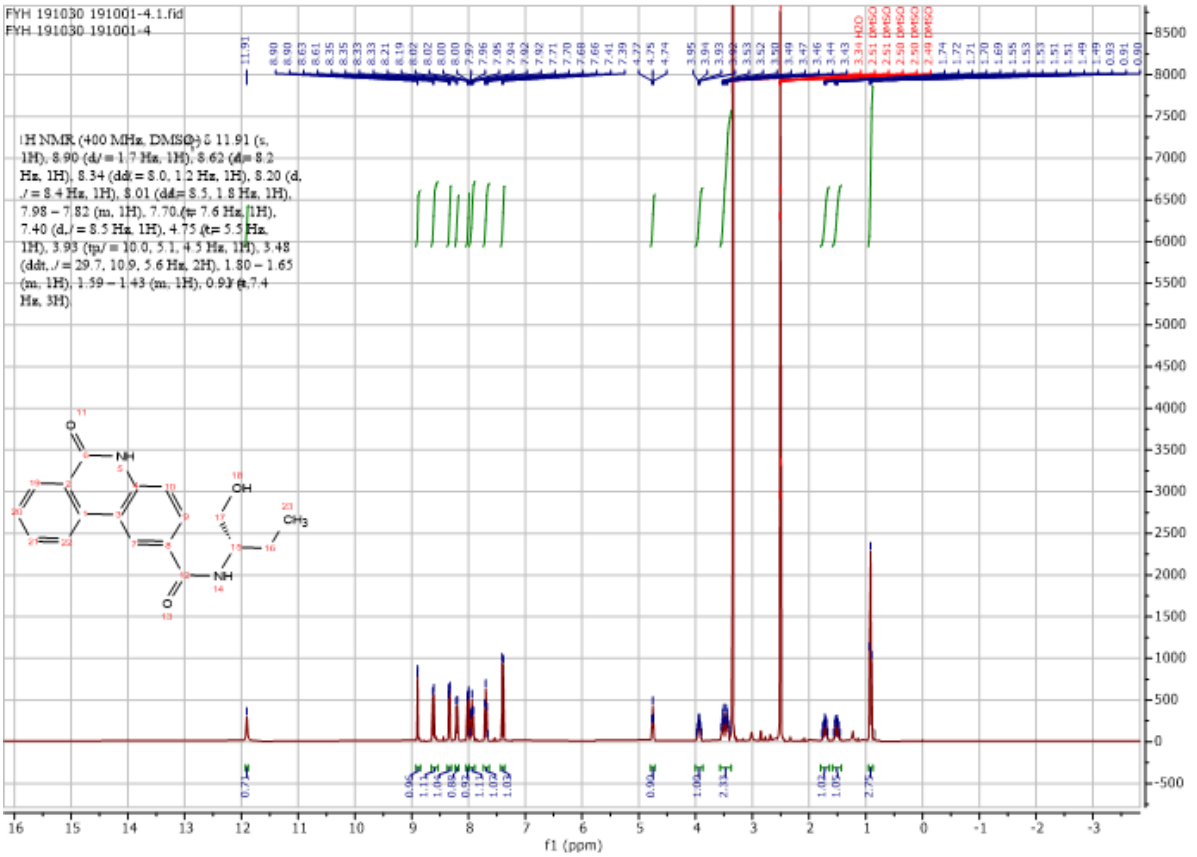

^{1}H NMR (400 MHz, DMSO-d_6) δ 11.91 (s, 1H), 8.90 (d, J = 1.7 Hz, 1H), 8.62 (d, J = 8.2 Hz, 1H), 8.34 (dd, J = 8.0, 1.2 Hz, 1H), 8.20 (d, J = 8.4 Hz, 1H), 8.01 (dd, J = 8.5, 1.8 Hz, 1H), 7.98 – 7.82 (m, 1H), 7.70 (t, J = 7.6 Hz, 1H), 7.40 (d, J = 8.5 Hz, 1H), 4.75 (t, J = 5.5 Hz, 1H), 3.93 (tq, J = 10.0, 5.1, 4.5 Hz, 1H), 3.48 (ddt, J = 29.7, 10.9, 5.6 Hz, 2H), 1.80 – 1.65 (m, 1H), 1.59 – 1.43 (m, 1H), 0.93 (t, J = 7.4 Hz, 3H).

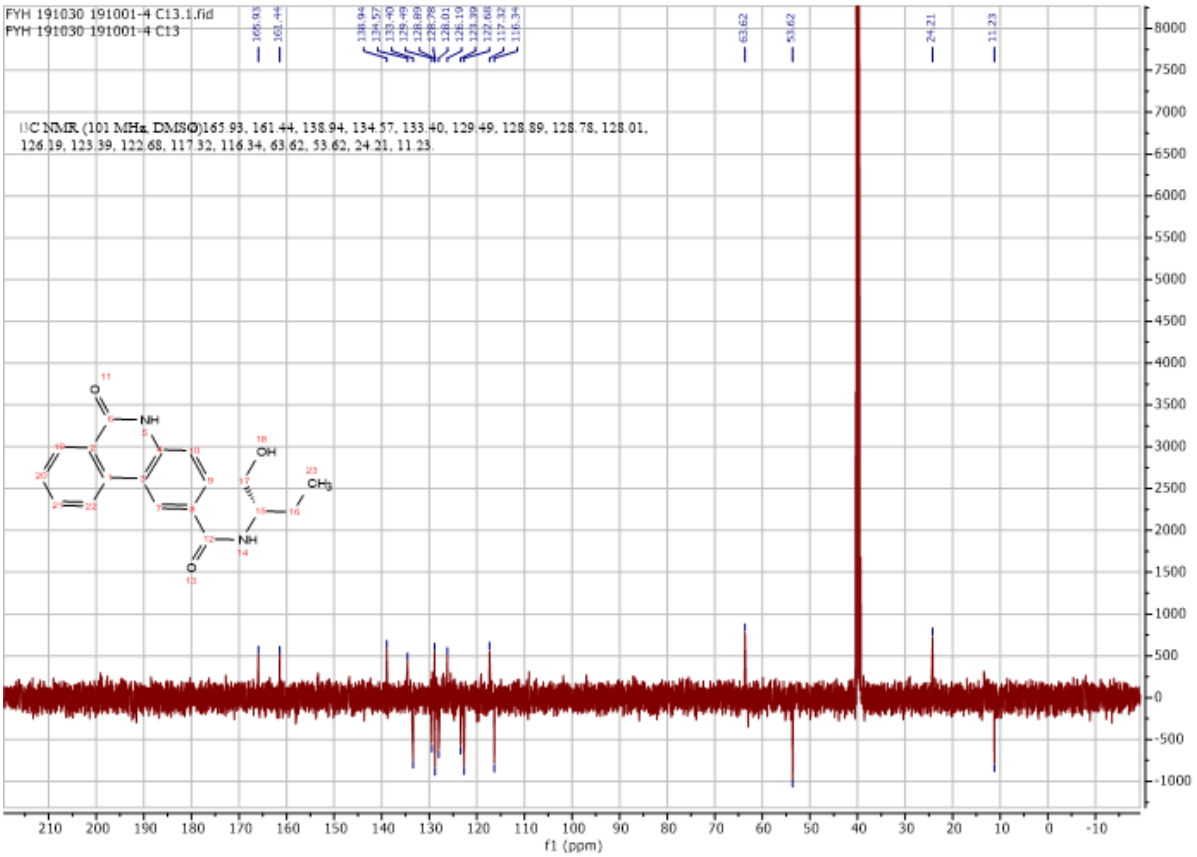

^{13}C NMR (101 MHz, DMSO-d_6) 165.93, 161.44, 138.94, 134.57, 133.40, 129.49, 128.89, 128.78, 128.01, 126.19, 123.39, 122.68, 117.32, 116.34, 63.62, 53.62, 24.21, 11.23.

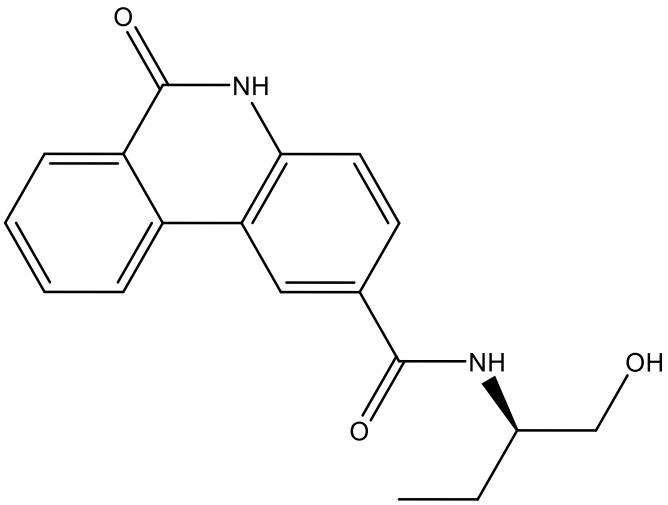

(*R*)-N-(1-hydroxybutan-2-yl)-6-oxo-5,6-dihydrophenanthridine-2-carboxamide (a41)

Using **Synthesis Method d**, 24mg (0.1mmol) **f2** was reacted with 8.9mg (0.1mmol) (*R*)-2-aminobutan-1-ol to give 25.7mg **a41** (Yield: 83%) and the product was separated as yellowish white solid. ^{1}H NMR (300 MHz, DMSO-d_6) δ 11.87 (s, 1H), 8.89 (d, *J* = 1.9 Hz, 1H), 8.62 (d, *J* = 8.1 Hz, 1H), 8.34 (dd, *J* = 8.0, 1.4 Hz, 1H), 8.17 (d, *J* = 8.4 Hz, 1H), 8.01 (dd, *J* = 8.5, 1.8 Hz, 1H), 7.93 (ddd, *J* = 8.4, 7.2, 1.5 Hz, 1H), 7.70 (td, 1H), 7.40 (d, *J* = 8.5 Hz, 1H), 4.72 (s, 1H), 3.94 (m, 1H), 3.49 (m, 2H), 1.80 – 1.36 (m, 2H), 0.92 (t, *J* = 7.4 Hz, 3H). ^{13}C NMR (75 MHz, DMSO) δ 166.0, 161.4, 138.9, 134.6, 133.4, 129.5, 128.9, 128.8, 128.0, 126.2, 123.4, 122.7, 117.3, 116.3, 63.6, 53.6, 24.2, 11.2. HRMS m/z (ESI+, M+Na): Calcd for C18H18N2O3: 333.1215, (ESI+, M+Na) found: 333.1210

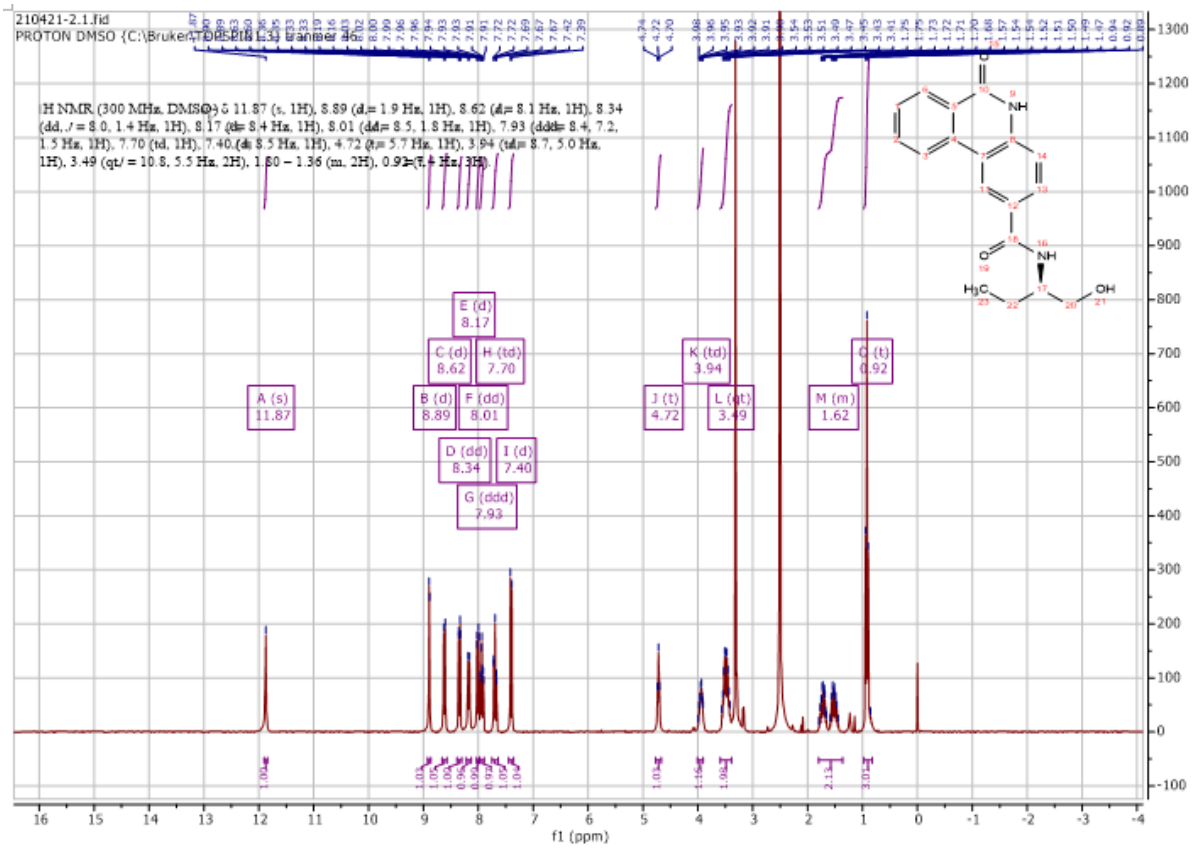
210421-2.1.fid
PROTON DMSO (C:\Bruker\TOPSPIN1.3) tranmer 46
1H NMR (300 MHz, DMSO) δ 11.87 (s, 1H), 8.89 (d, J = 1.9 Hz, 1H), 8.62 (d, J = 8.1 Hz, 1H), 8.34 (dd, J = 8.0, 1.4 Hz, 1H), 8.17 (d, J = 8.4 Hz, 1H), 8.01 (dd, J = 8.5, 1.8 Hz, 1H), 7.93 (ddd, J = 8.4, 7.2, 1.5 Hz, 1H), 7.70 (td, J = 7.4, 1.4 Hz, 1H), 7.40 (d, J = 8.5 Hz, 1H), 4.72 (t, J = 5.7 Hz, 1H), 3.94 (td, J = 8.7, 5.0 Hz, 1H), 3.49 (qt, J = 10.8, 5.5 Hz, 2H), 1.80 – 1.36 (m, 2H), 0.92 (t, J = 7.4 Hz, 3H).
A (s) 11.87
B (d) 8.89
C (d) 8.62
D (dd) 8.34
E (d) 8.17
F (dd) 8.01
G (ddd) 7.93
H (td) 7.70
I (d) 7.40
J (t) 4.72
K (td) 3.94
L (qt) 3.49
M (m) 1.62
O (t) 0.92
f1 (ppm)

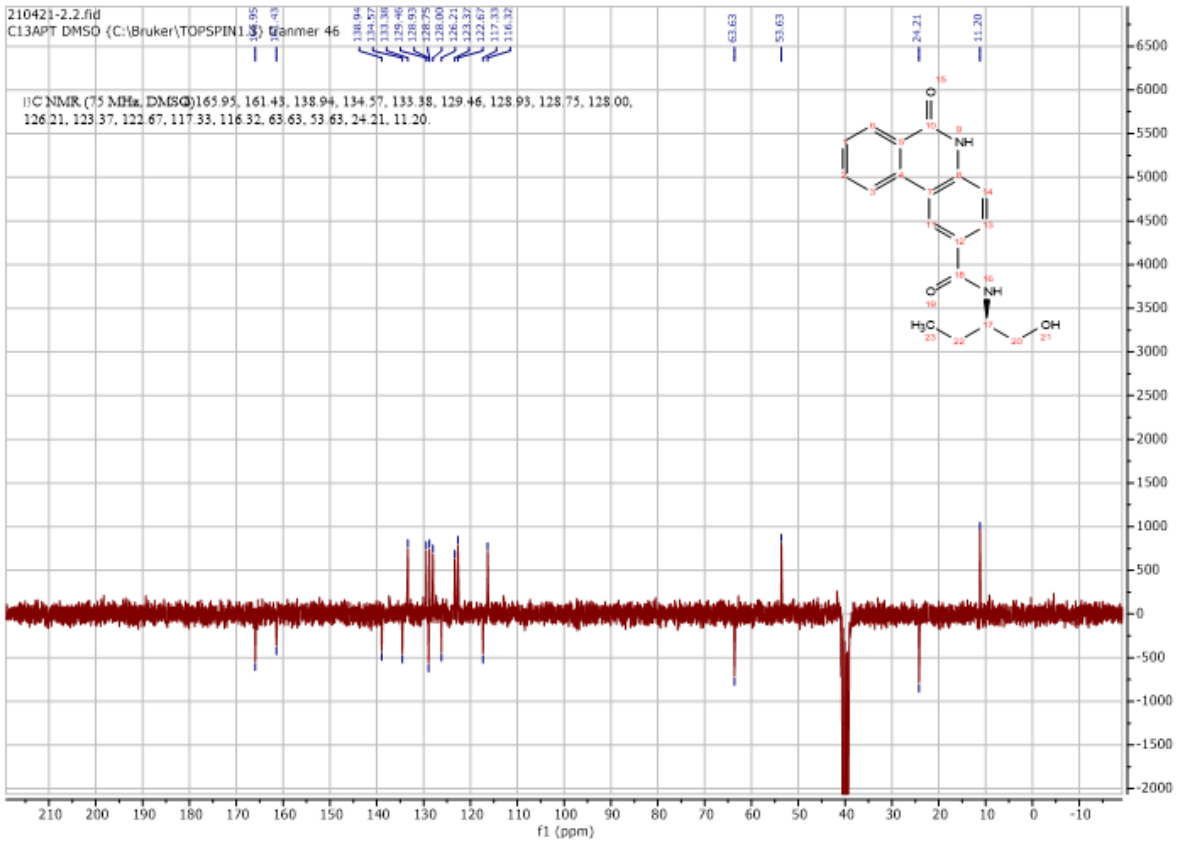
210421-2.2.fid
C13APT DMSO (C:\Bruker\TOPSPIN1.3) tranmer 46
13C NMR (75 MHz, DMSO) δ 165.95, 161.43, 138.94, 134.57, 133.38, 129.46, 128.93, 128.75, 128.00, 126.21, 123.37, 122.67, 117.33, 116.32, 63.63, 53.63, 24.21, 11.20.
f1 (ppm)

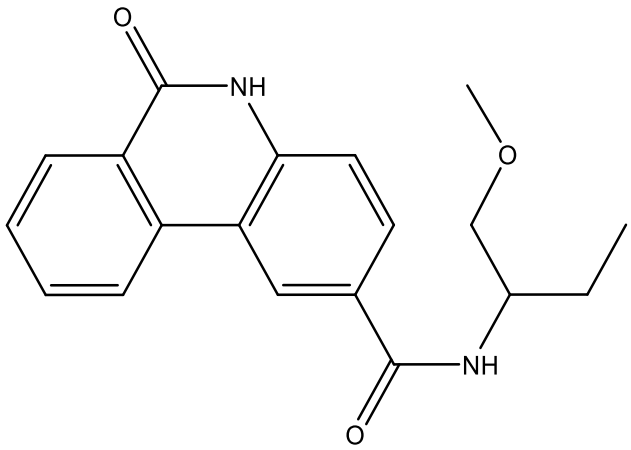

N-(1-methoxybutan-2-yl)-6-oxo-5,6-dihydrophenanthridine-2-carboxamide (a42)

Using **Synthesis Method d**, 24mg (0.1mmol) **f2** was reacted with 10.4mg (0.1mmol) 1-methoxybutan-2-amine to give 26.9mg **a42** (Yield: 83%) and the product was separated as yellowish white solid. ^{1}H NMR (400 MHz, DMSO-d_6) δ 11.91 (s, 1H), 8.89 (d, J = 1.6 Hz, 1H), 8.61 (d, J = 8.1 Hz, 1H), 8.34 (dd, J = 8.0, 1.2 Hz, 1H), 8.31 (d, J = 8.4 Hz, 1H), 8.01 (dd, J = 8.5, 1.8 Hz, 1H), 7.94 (ddd, J = 8.3, 7.2, 1.4 Hz, 1H), 7.74 – 7.65 (m, 1H), 7.40 (d, J = 8.5 Hz, 1H), 4.18 – 4.05 (m, 1H), 3.46 (dd, J = 9.7, 6.2 Hz, 1H), 3.38 (dd, J = 9.7, 5.7 Hz, 1H), 3.28 (s, 3H), 1.67 (m, 1H), 1.61 – 1.46 (m, 1H), 0.92 (t, J = 7.4 Hz, 3H). ^{13}C NMR (101 MHz, DMSO) δ 165.8, 161.4, 139.0, 134.5, 133.4, 129.5, 128.8, 128.6, 128.0, 126.2, 123.4, 122.6, 117.4, 116.4, 74.5, 58.7, 50.8, 24.6, 11.1. HRMS m/z (ESI+, M+Na): Calcd for C19H20N2O3: 347.1372, (ESI+, M+Na) found: 347.1367

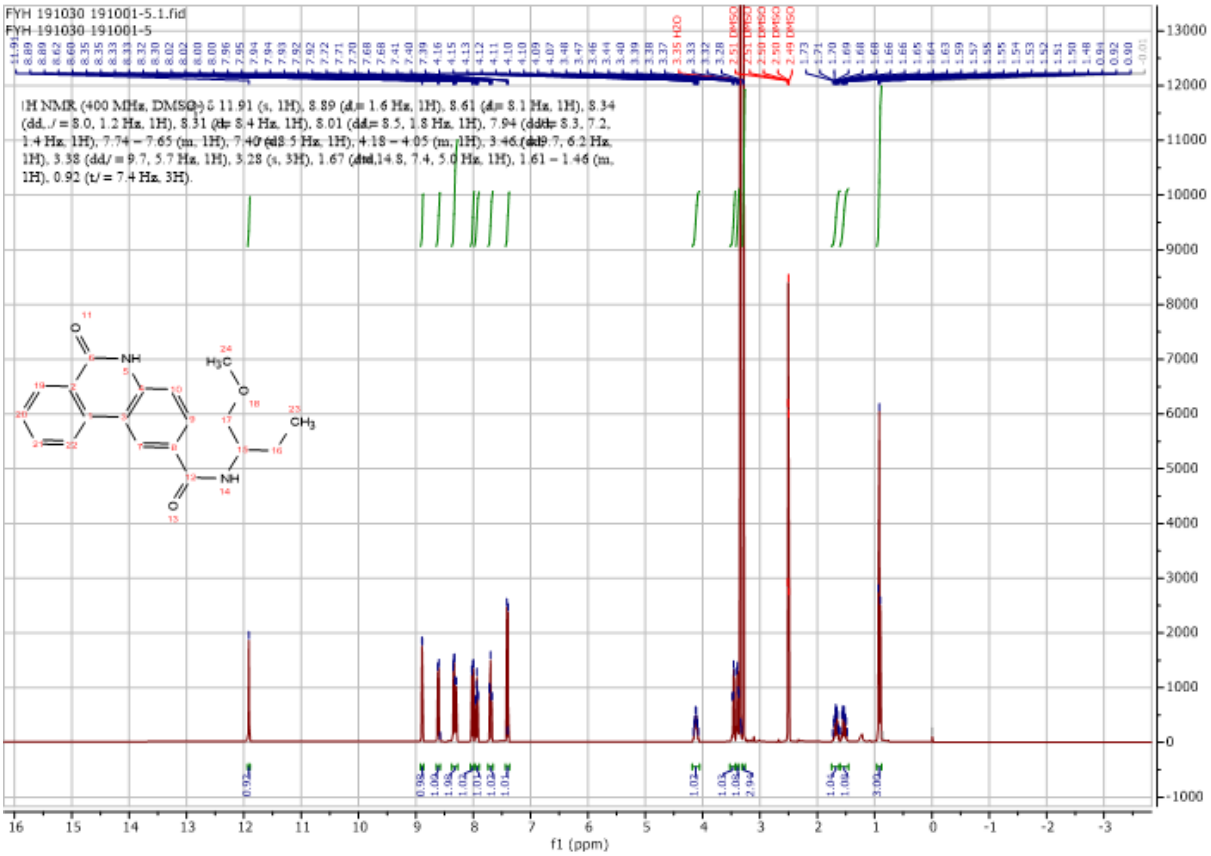
FYH 191030 191001-5.1.fid
FYH 191030 191001-5
1H NMR (400 MHz, DMSO-d6) δ 11.91 (s, 1H), 8.89 (d, J = 1.6 Hz, 1H), 8.61 (d, J = 8.1 Hz, 1H), 8.34 (dd, J = 8.0, 1.2 Hz, 1H), 8.31 (dt, J = 8.4 Hz, 1H), 8.01 (dd, J = 8.5, 1.8 Hz, 1H), 7.94 (ddd, J = 8.3, 7.2, 1.4 Hz, 1H), 7.74 – 7.65 (m, 1H), 7.40 (d, J = 8.5 Hz, 1H), 4.18 – 4.05 (m, 1H), 3.46 (dd, J = 9.7, 6.2 Hz, 1H), 3.38 (dd, J = 9.7, 5.7 Hz, 1H), 3.28 (s, 3H), 1.67 (dtd, J = 14.8, 7.4, 5.0 Hz, 1H), 1.61 – 1.46 (m, 1H), 0.92 (t, J = 7.4 Hz, 3H).
f1 (ppm)

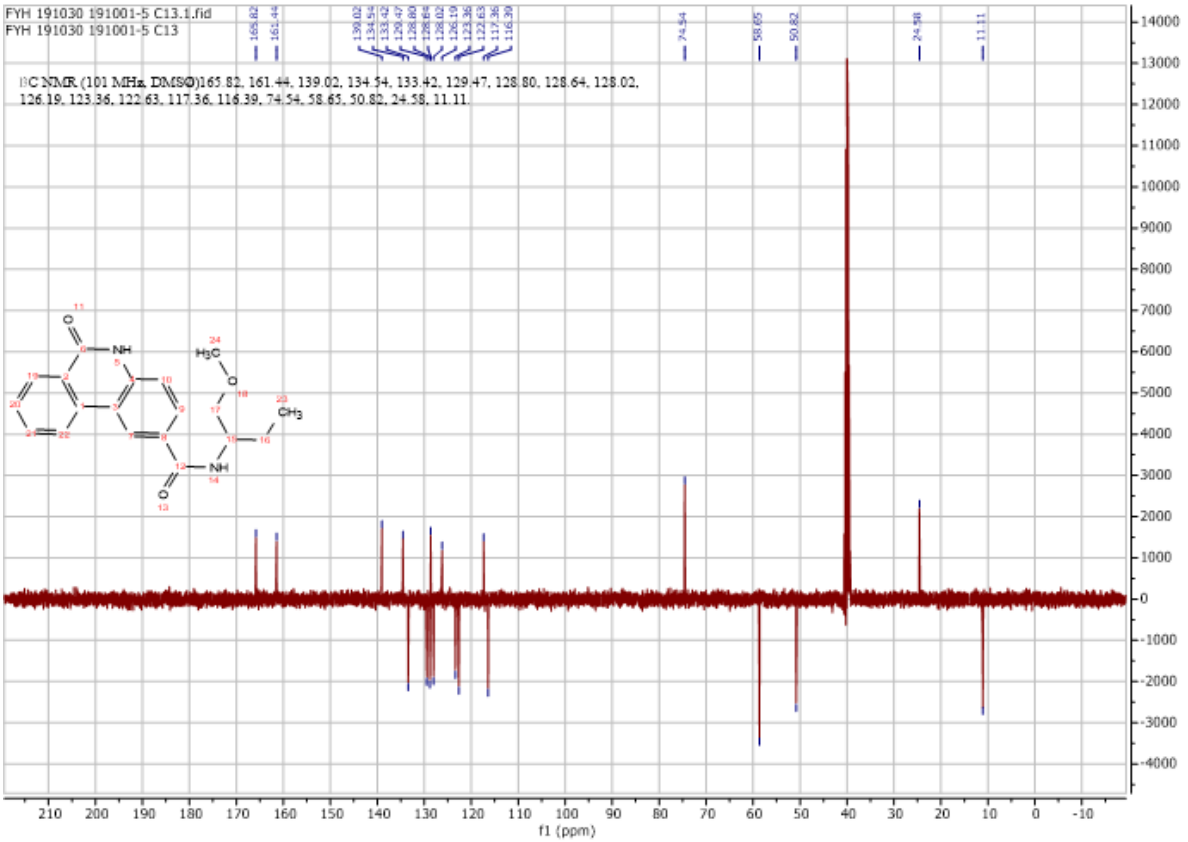
FYH 191030 191001-5 C13.1.fid
FYH 191030 191001-5 C13
13C NMR (101 MHz, DMSO) δ 165.82, 161.44, 139.02, 134.54, 133.42, 129.47, 128.80, 128.64, 128.02, 126.19, 123.36, 122.63, 117.36, 116.39, 74.54, 58.65, 50.82, 24.58, 11.11.
f1 (ppm)

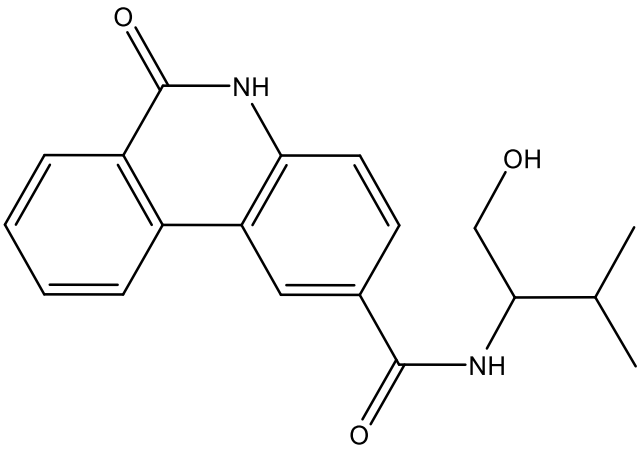

***N*-(1-hydroxy-3-methylbutan-2-yl)-6-oxo-5,6-dihydrophenanthridine-2-carboxamide (a43)**

Using **Synthesis Method d**, 24mg (0.1mmol) **f2** was reacted with 10.2mg (0.1mmol) 2-amino-3-methylbutan-1-ol to give 25.6mg **a43** (Yield: 79%) and the product was separated as yellowish white solid. ^{1}H NMR (400 MHz, DMSO-d_6) δ 11.90 (s, 1H), 8.91 (d, *J* = 1.7 Hz, 1H), 8.63 (d, *J* = 8.2 Hz, 1H), 8.34 (dd, *J* = 8.0, 1.2 Hz, 1H), 8.18 (d, *J* = 8.8 Hz, 1H), 8.01 (dd, *J* = 8.5, 1.8 Hz, 1H), 7.94 (ddd, *J* = 8.4, 7.3, 1.4 Hz, 1H), 7.74 – 7.65 (m, 1H), 7.40 (d, *J* = 8.5 Hz, 1H), 4.66 (s, 1H), 3.86 (ddd, *J* = 8.7, 7.1, 4.1 Hz, 1H), 3.57 (m, 2H), 2.07 – 1.90 (m, *J* = 6.8 Hz, 1H), 0.95 (d, *J* = 6.9 Hz, 3H), 0.93 (d, *J* = 6.9 Hz, 3H).^{13}C NMR (101 MHz, DMSO) δ 166.1, 161.4, 138.9, 134.6, 133.4, 129.6, 129.1, 128.8, 128.0, 126.2, 123.4, 122.8, 117.3, 116.3, 61.8, 57.3, 29.1, 20.2, 19.4. HRMS m/z (ESI+, M+Na): Calcd for C19H20N2O3: 347.1372, (ESI+, M+Na) found: 347.1365

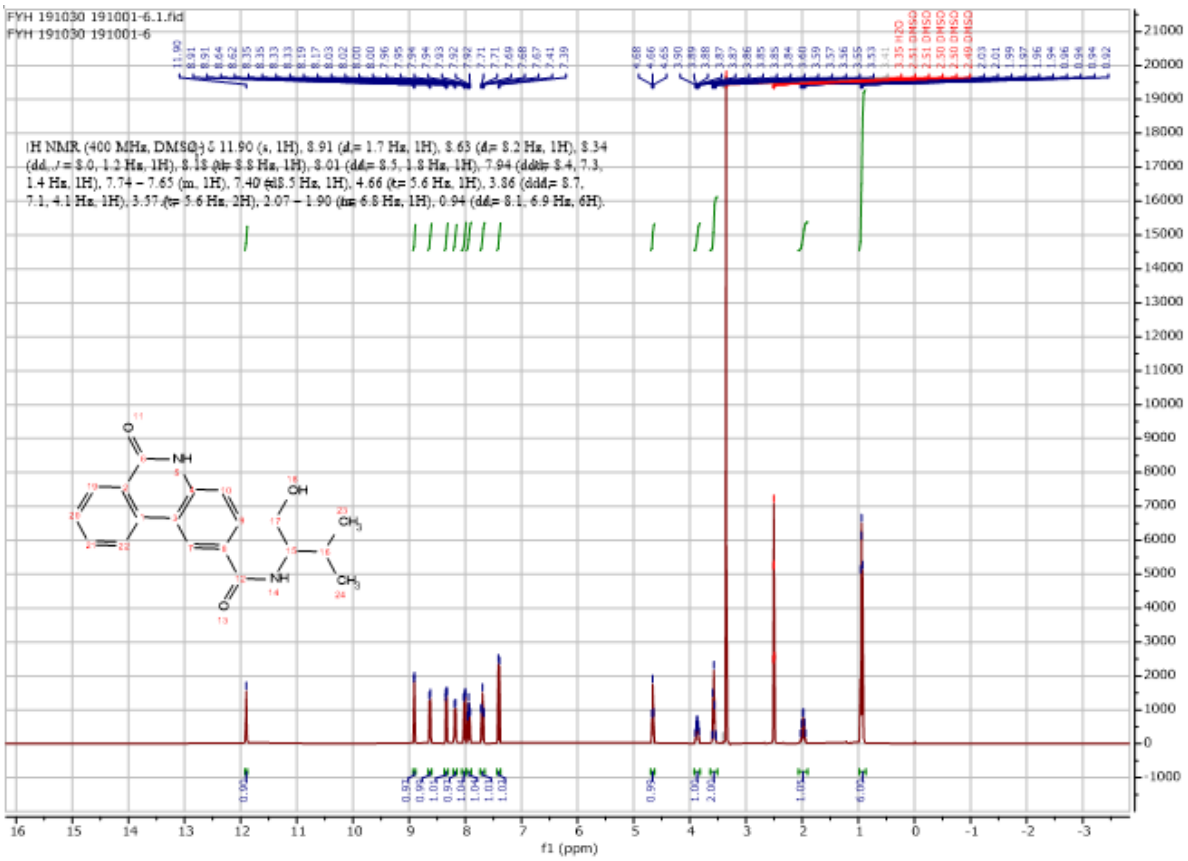
FYH 191030 191001-6.1.fid
FYH 191030 191001-6
f1 (ppm)

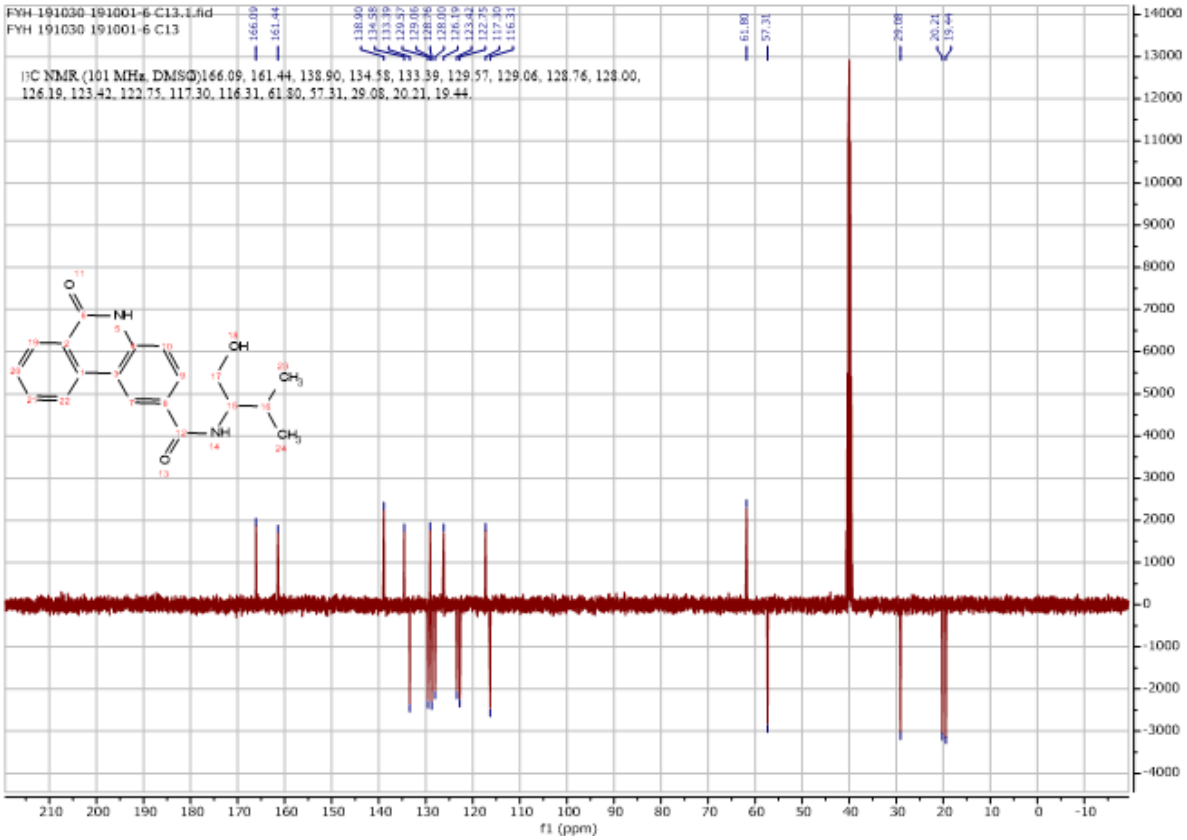
FYH 191030 191001-6 C13.1.fid
FYH 191030 191001-6 C13
f1 (ppm)

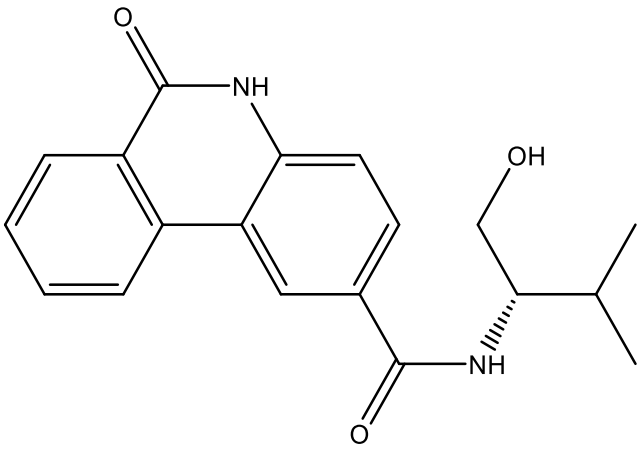

(*S*)-N-(1-hydroxy-3-methylbutan-2-yl)-6-oxo-5,6-dihydrophenanthridine-2-carboxamide (a44)

Using **Synthesis Method d**, 24mg (0.1mmol) **f2** was reacted with 10.3mg (0.1mmol) (*S*)-2-amino-3-methylbutan-1-ol to give 25mg **a44** (Yield: 77%) and the product was separated as yellowish white solid. ^{1}H NMR (300 MHz, DMSO-d_6) δ 11.86 (s, 1H), 8.93 – 8.87 (m, 1H), 8.62 (d, *J* = 8.1 Hz, 1H), 8.39 – 8.30 (m, 1H), 8.15 (d, *J* = 8.8 Hz, 1H), 8.01 (dd, *J* = 8.5, 1.6 Hz, 1H), 7.98 – 7.88 (m, 1H), 7.69 (t, *J* = 7.5 Hz, 1H), 7.41 (d, *J* = 8.5 Hz, 1H), 4.63 (s, 1H), 3.88 (m, 1H), 3.58 (m, 2H), 1.98 (dq, *J* = 13.5, 6.8 Hz, 1H), 0.96 (d, *J* = 6.4 Hz, 3H), 0.94 (d, *J* = 6.4 Hz, 3H). ^{13}C NMR (75 MHz, DMSO) δ 166.1, 161.4, 138.9, 134.6, 133.4, 129.5, 129.1, 128.7, 128.0, 126.2, 123.39, 122.8, 117.3, 116.3, 61.8, 57.3, 29.1, 20.2, 19.4. HRMS m/z (ESI+, M+Na): Calcd for C19H20N2O3: 347.1372, (ESI+, M+Na) found: 347.1367

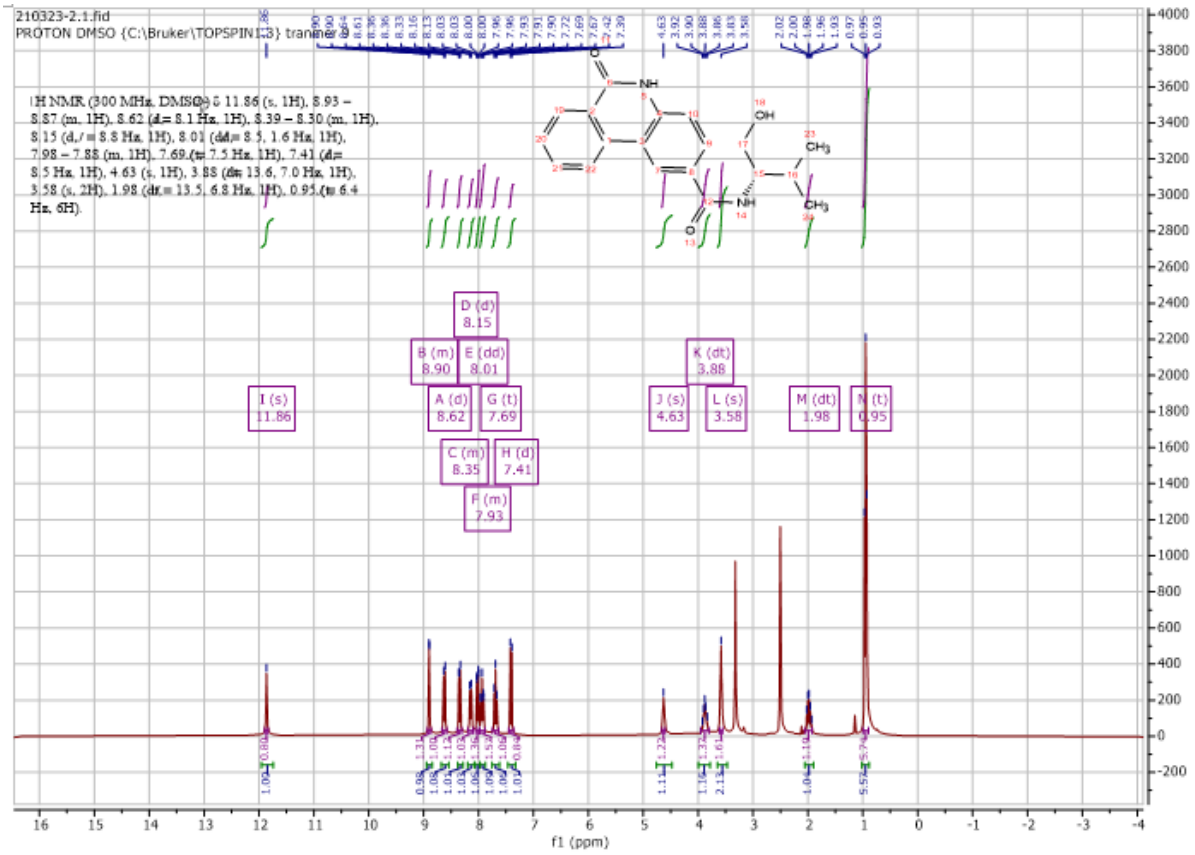
210323-2.1.fid
PROTON DMSO {C:\Bruker\TOPSPIN1.3} tranmer 9
¹H NMR (300 MHz, DMSO) δ 11.86 (s, 1H), 8.93 – 8.87 (m, 1H), 8.62 (d, J = 8.1 Hz, 1H), 8.39 – 8.30 (m, 1H), 8.15 (d, J = 8.8 Hz, 1H), 8.01 (dd, J = 8.5, 1.6 Hz, 1H), 7.98 – 7.88 (m, 1H), 7.69 (t, J = 7.5 Hz, 1H), 7.41 (d, J = 8.5 Hz, 1H), 4.63 (s, 1H), 3.88 (dt, J = 13.6, 7.0 Hz, 1H), 3.58 (s, 2H), 1.98 (dt, J = 13.5, 6.8 Hz, 1H), 0.95 (t, J = 6.4 Hz, 6H).
D (d) 8.15
B (m) 8.90
E (dd) 8.01
K (dt) 3.88
I (s) 11.86
A (d) 8.62
G (t) 7.69
J (s) 4.63
L (s) 3.58
M (dt) 1.98
N (t) 0.95
C (m) 8.35
H (d) 7.41
F (m) 7.93
f1 (ppm)

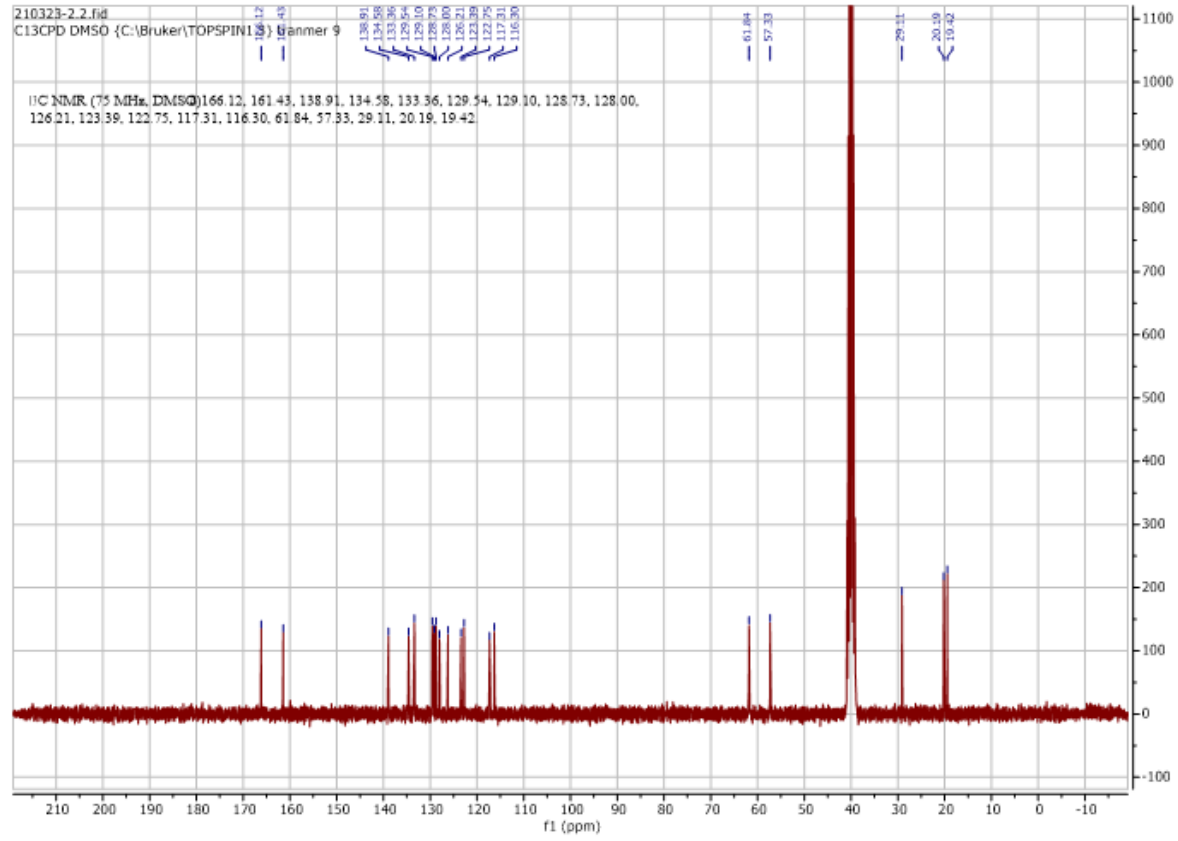
210323-2.2.fid
C13CPD DMSO {C:\Bruker\TOPSPIN1.3} tranmer 9
¹³C NMR (75 MHz, DMSO) δ 166.12, 161.43, 138.91, 134.58, 133.36, 129.54, 129.10, 128.73, 128.00, 126.21, 123.39, 122.75, 117.31, 116.30, 61.84, 57.33, 29.11, 20.19, 19.42
f1 (ppm)

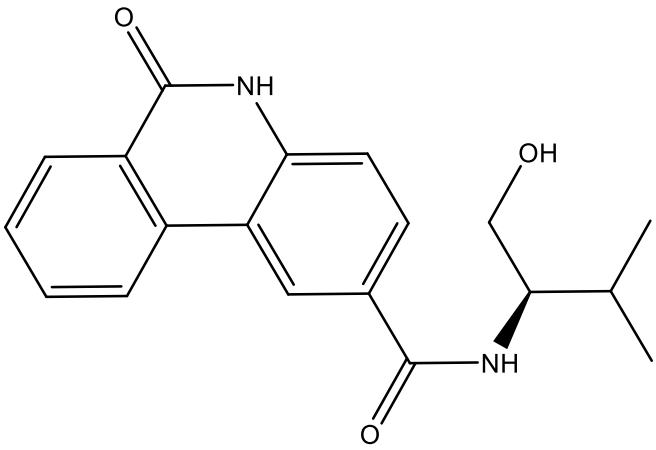

(*R*)-N-(1-hydroxy-3-methylbutan-2-yl)-6-oxo-5,6-dihydrophenanthridine-2-carboxamide (a45)

Using **Synthesis Method d**, 24mg (0.1mmol) **f2** was reacted with 10.3mg (0.1mmol) (*R*)-2-amino-3-methylbutan-1-ol to give 24.6mg **a45** (Yield: 76%) and the product was separated as yellowish white solid. ^{1}H NMR (300 MHz, DMSO-d_6) δ 11.87 (s, 1H), 8.90 (d, *J* = 1.9 Hz, 1H), 8.63 (d, *J* = 8.1 Hz, 1H), 8.34 (dd, *J* = 8.0, 1.4 Hz, 1H), 8.15 (d, *J* = 8.7 Hz, 1H), 8.01 (dd, *J* = 8.5, 1.8 Hz, 1H), 7.98 – 7.89 (m, 1H), 7.69 (t, *J* = 7.6 Hz, 1H), 7.41 (d, *J* = 8.5 Hz, 1H), 4.63 (s, 1H), 3.87 (ddd, *J* = 12, 8.0 Hz, 1H), 3.58 (m, 2H), 1.99 (m, 1H), 0.96 (d, *J* = 6.5 Hz, 6H), 0.94 (d, *J* = 6.5 Hz, 3H). ^{13}C NMR (75 MHz, DMSO) δ 166.1, 161.4, 138.9, 134.6, 133.4, 129.5, 129.1, 128.7, 128.0, 126.2, 123.4, 122.7, 117.3, 116.3, 61.8, 57.3, 29.1, 20.2, 19.4. HRMS m/z (ESI+, M+Na): Calcd for C19H20N2O3: 347.1372, (ESI+, M+Na) found: 347.1366

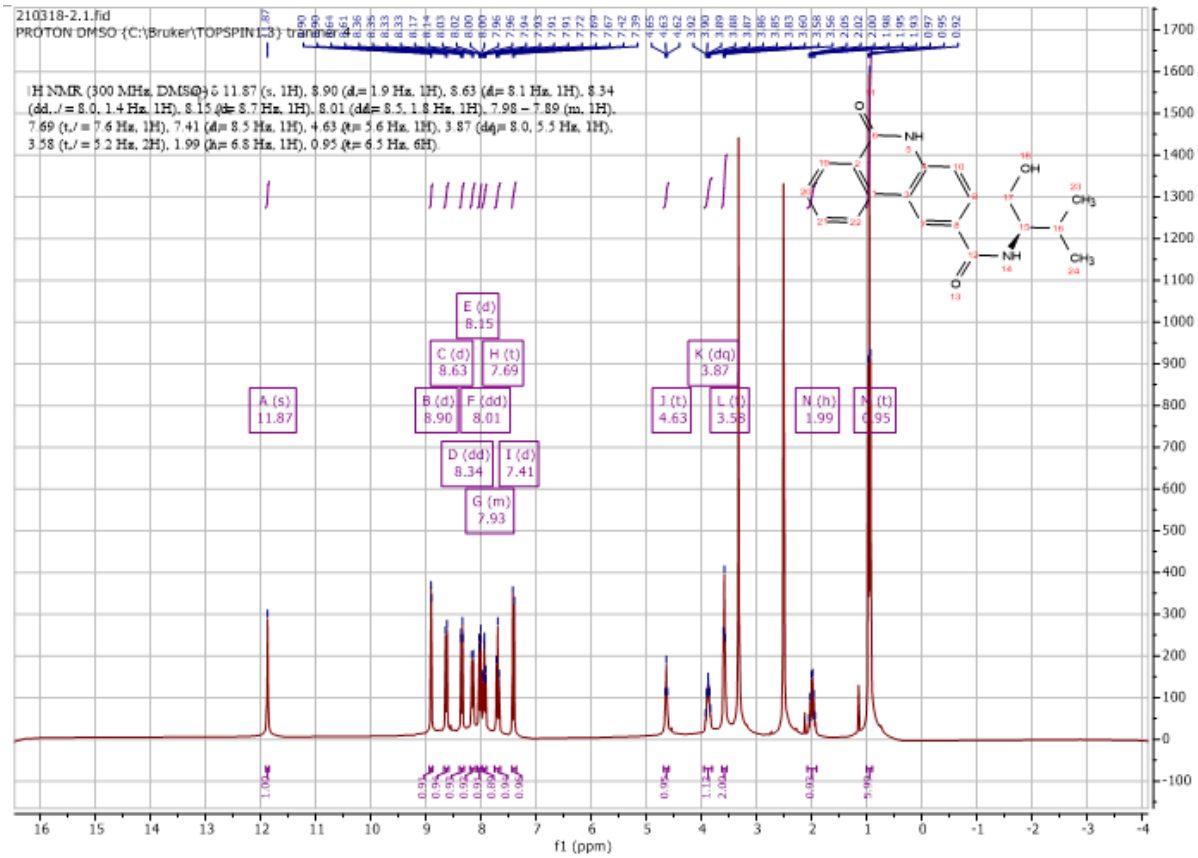
210318-2.1.fid
PROTON DMSO {C:\Bruker\TOPSPIN1.3} tranmer 4
1H NMR (300 MHz, DMSO) δ 11.87 (s, 1H), 8.90 (d, J= 1.9 Hz, 1H), 8.63 (d, J= 8.1 Hz, 1H), 8.34 (dd, J = 8.0, 1.4 Hz, 1H), 8.15 (d, J= 8.7 Hz, 1H), 8.01 (dd, J= 8.5, 1.8 Hz, 1H), 7.98 – 7.89 (m, 1H), 7.69 (t, J = 7.6 Hz, 1H), 7.41 (d, J= 8.5 Hz, 1H), 4.63 (t, J= 5.6 Hz, 1H), 3.87 (dq, J= 8.0, 5.5 Hz, 1H), 3.58 (t, J = 5.2 Hz, 2H), 1.99 (h, J= 6.8 Hz, 1H), 0.95 (t, J= 6.5 Hz, 6H).
A (s) 11.87
B (d) 8.90
C (d) 8.63
D (dd) 8.34
E (d) 8.15
F (dd) 8.01
G (m) 7.93
H (t) 7.69
I (d) 7.41
J (t) 4.63
K (dq) 3.87
L (t) 3.58
N (h) 1.99
M (t) 0.95
f1 (ppm)

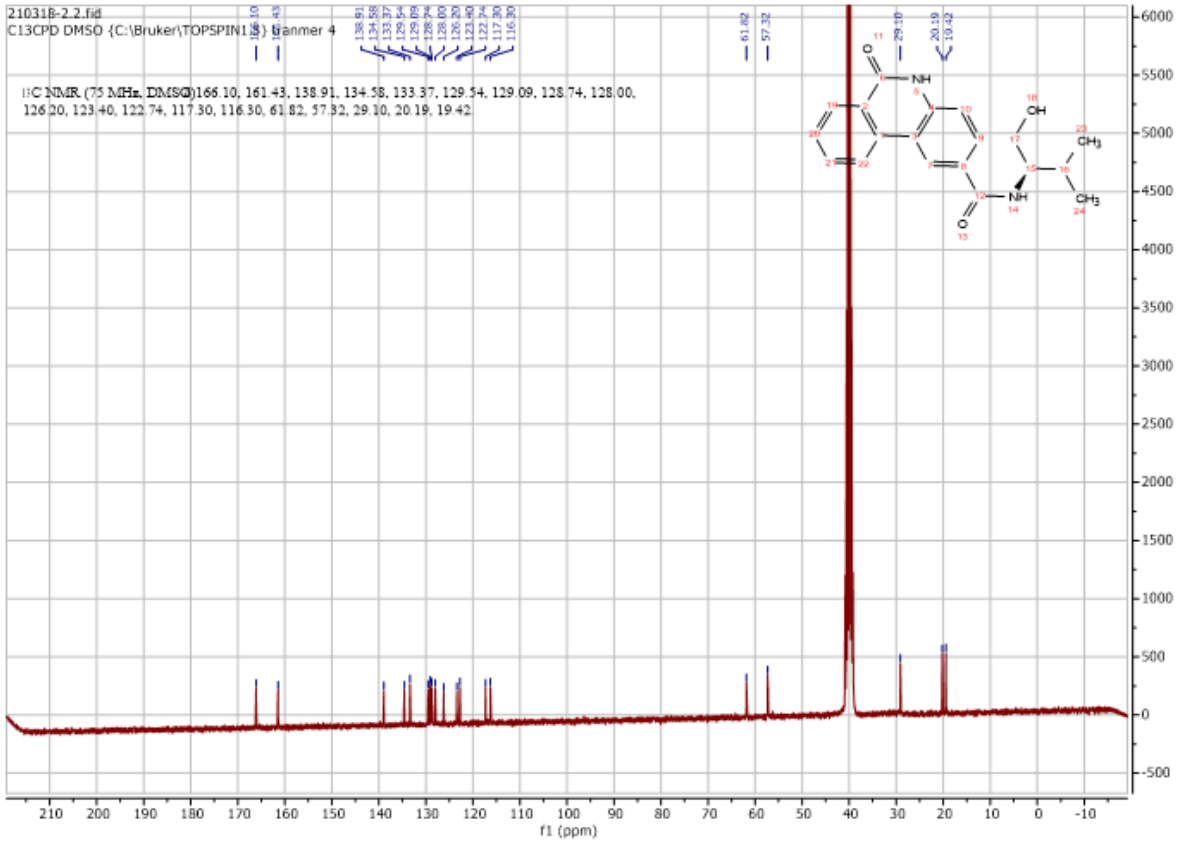
210318-2.2.fid
C13CPD DMSO {C:\Bruker\TOPSPIN1.3} tranmer 4
13C NMR (75 MHz, DMSO) δ 166.10, 161.43, 138.91, 134.58, 133.37, 129.54, 129.09, 128.74, 128.00, 126.20, 123.40, 122.74, 117.30, 116.30, 61.82, 57.32, 29.10, 20.19, 19.42
f1 (ppm)

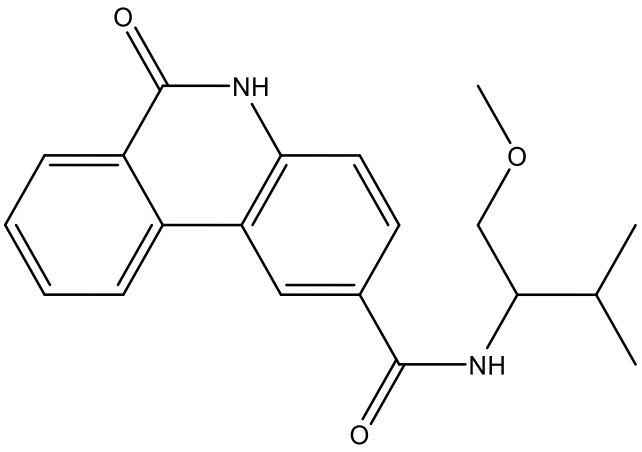

N-(1-methoxy-3-methylbutan-2-yl)-6-oxo-5,6-dihydrophenanthridine-2-carboxamide (a46)

Using **Synthesis Method d**, 24mg (0.1mmol) **f2** was reacted with 11.8mg (0.1mmol) 1-methoxy-3-methylbutan-2-amine to give 26.7mg **a46** (Yield: 79%) and the product was separated as yellowish white solid. ^{1}H NMR (300 MHz, DMSO-d_6) δ 11.87 (s, 1H), 8.92 – 8.86 (m, 1H), 8.61 (d, *J* = 8.1 Hz, 1H), 8.35 (dd, *J* = 7.9, 1.1 Hz, 1H), 8.26 (d, *J* = 8.7 Hz, 1H), 8.01 (dd, *J* = 8.5, 1.6 Hz, 1H), 7.97 – 7.90 (m, 1H), 7.70 (t, *J* = 7.5 Hz, 1H), 7.41 (d, *J* = 8.5 Hz, 1H), 4.11 – 3.96 (m, 1H), 3.51 (m, 2H), 3.28 (s, 3H), 1.95 (dq, *J* = 13.6, 6.8 Hz, 1H), 0.95 (dd, *J* = 6.7, 4.9 Hz, 6H). ^{13}C NMR (75 MHz, DMSO) δ 165.9, 161.4, 139.0, 134.6, 133.4, 129.5, 128.8, 128.8, 128.0, 126.2, 123.4, 122.7, 117.3, 116.4, 72.9, 58.6, 54.6, 29.7, 20.0, 19.5. HRMS m/z (ESI+, M+Na): Calcd for C20H22N2O3: 361.1528, (ESI+, M+Na) found: 361.1520

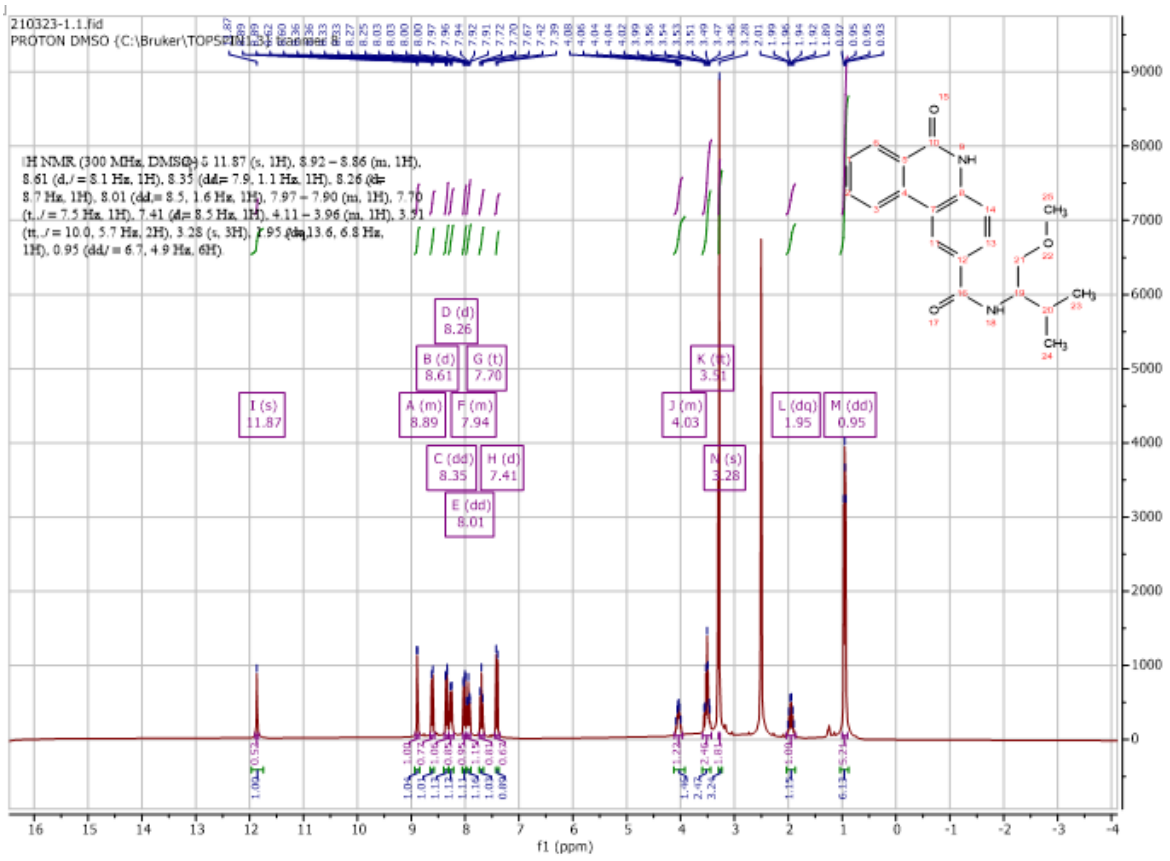
210323-1.1.fid
PROTON DMSO {C:\Bruker\TOPSPIN1.3} tianmer 8
1H NMR (300 MHz, DMSO) δ 11.87 (s, 1H), 8.92 – 8.86 (m, 1H), 8.61 (d, J = 8.1 Hz, 1H), 8.35 (dd, J = 7.9, 1.1 Hz, 1H), 8.26 (d, J = 8.7 Hz, 1H), 8.01 (dd, J = 8.5, 1.6 Hz, 1H), 7.97 – 7.90 (m, 1H), 7.70 (t, J = 7.5 Hz, 1H), 7.41 (d, J = 8.5 Hz, 1H), 4.11 – 3.96 (m, 1H), 3.51 (tt, J = 10.0, 5.7 Hz, 2H), 3.28 (s, 3H), 1.95 (dq, J = 13.6, 6.8 Hz, 1H), 0.95 (dd, J = 6.7, 4.9 Hz, 6H).
I (s) 11.87
A (m) 8.89
B (d) 8.61
C (dd) 8.35
D (d) 8.26
E (dd) 8.01
F (m) 7.94
G (t) 7.70
H (d) 7.41
J (m) 4.03
K (tt) 3.51
N (s) 3.28
L (dq) 1.95
M (dd) 0.95
f1 (ppm)

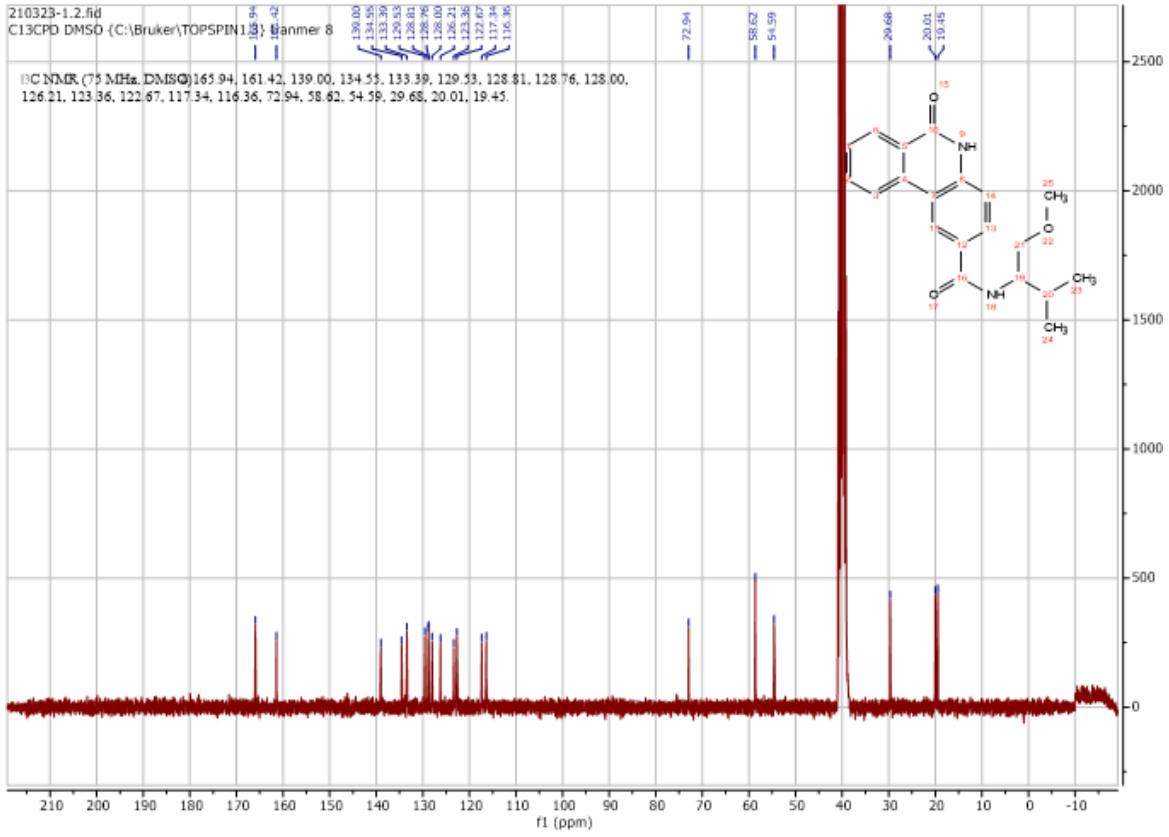
210323-1.2.fid
C13CPD DMSO {C:\Bruker\TOPSPIN1.3} tianmer 8
13C NMR (75 MHz, DMSO) δ 165.94, 161.42, 139.00, 134.55, 133.39, 129.53, 128.81, 128.76, 128.00, 126.21, 123.36, 122.67, 117.34, 116.36, 72.94, 58.62, 54.59, 29.68, 20.01, 19.45.
f1 (ppm)

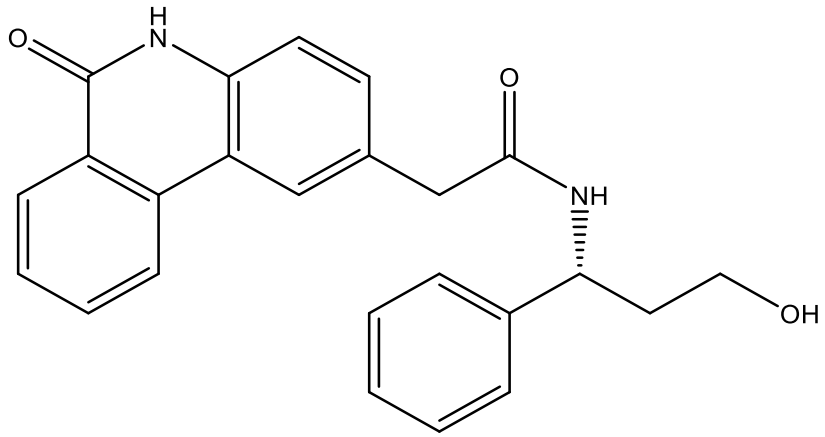

(*R*)-N-(3-hydroxy-1-phenylpropyl)-2-(6-oxo-5,6-dihydrophenanthridin-2-yl)acetamide (a47)

Using **Synthesis Method d**, 25.4mg (0.1mmol) **f5** was reacted with 15.1mg (0.1mmol) (*R*)-3-amino-3-phenylpropan-1-ol to give 32.1mg **a47** (Yield: 83%) and the product was separated as yellowish white solid. ^{1}H NMR (400 MHz, DMSO-d_6) δ 11.66 (s, 1H), 8.58 (d, *J* = 8.3 Hz, 1H), 8.38 – 8.29 (m, 2H), 8.21 (d, *J* = 1.8 Hz, 1H), 7.87 (ddd, *J* = 8.3, 7.2, 1.5 Hz, 1H), 7.65 (ddd, *J* = 8.1, 7.1, 1.0 Hz, 1H), 7.39 – 7.25 (m, 6H), 7.24 – 7.16 (m, 1H), 4.93 (dd, *J* = 8.5, 6.0 Hz, 1H), 4.51 (s, 1H), 3.57 (m, 2H), 3.45 – 3.36 (m, 2H), 1.95 – 1.74 (m, 2H). ^{13}C NMR (101 MHz, DMSO) δ 170.0, 161.2, 144.4, 135.6, 134.6, 133.3, 130.9, 130.9, 128.7, 128.4, 128.0, 127.1, 126.8, 126.2, 123.7, 122.7, 117.7, 116.4, 58.2, 58.2, 50.2, 42.5, 39.9. HRMS m/z (ESI+, M+Na): Calcd for C24H22N2O3: 409.1528, (ESI+, M+Na) found: 409.1523

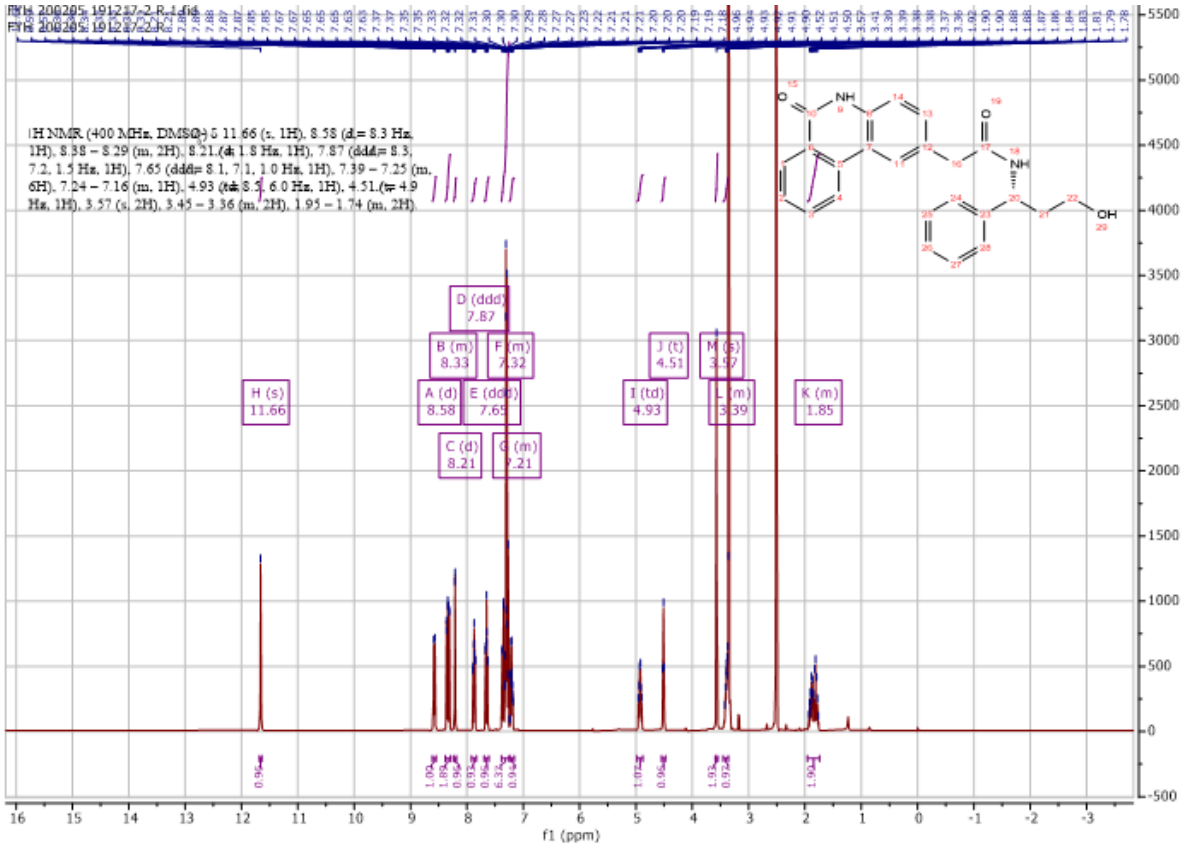
FYH 200205 191217-2 R 1.fid
FYH 200205 191217-2 R
1H NMR (400 MHz, DMSO-d6) δ 11.66 (s, 1H), 8.58 (d, J = 8.3 Hz, 1H), 8.38 – 8.29 (m, 2H), 8.21 (dd, J = 1.8 Hz, 1H), 7.87 (ddd, J = 8.3, 7.2, 1.5 Hz, 1H), 7.65 (ddd, J = 8.1, 7.1, 1.0 Hz, 1H), 7.39 – 7.25 (m, 6H), 7.24 – 7.16 (m, 1H), 4.93 (td, J = 8.5, 6.0 Hz, 1H), 4.51 (t, J = 4.9 Hz, 1H), 3.57 (s, 2H), 3.45 – 3.36 (m, 2H), 1.95 – 1.74 (m, 2H).
D (ddd) 7.87
B (m) 8.33
F (m) 7.32
J (t) 4.51
M (s) 3.57
H (s) 11.66
A (d) 8.58
E (ddd) 7.65
I (td) 4.93
L (m) 3.39
K (m) 1.85
C (d) 8.21
G (m) 7.21
f1 (ppm)

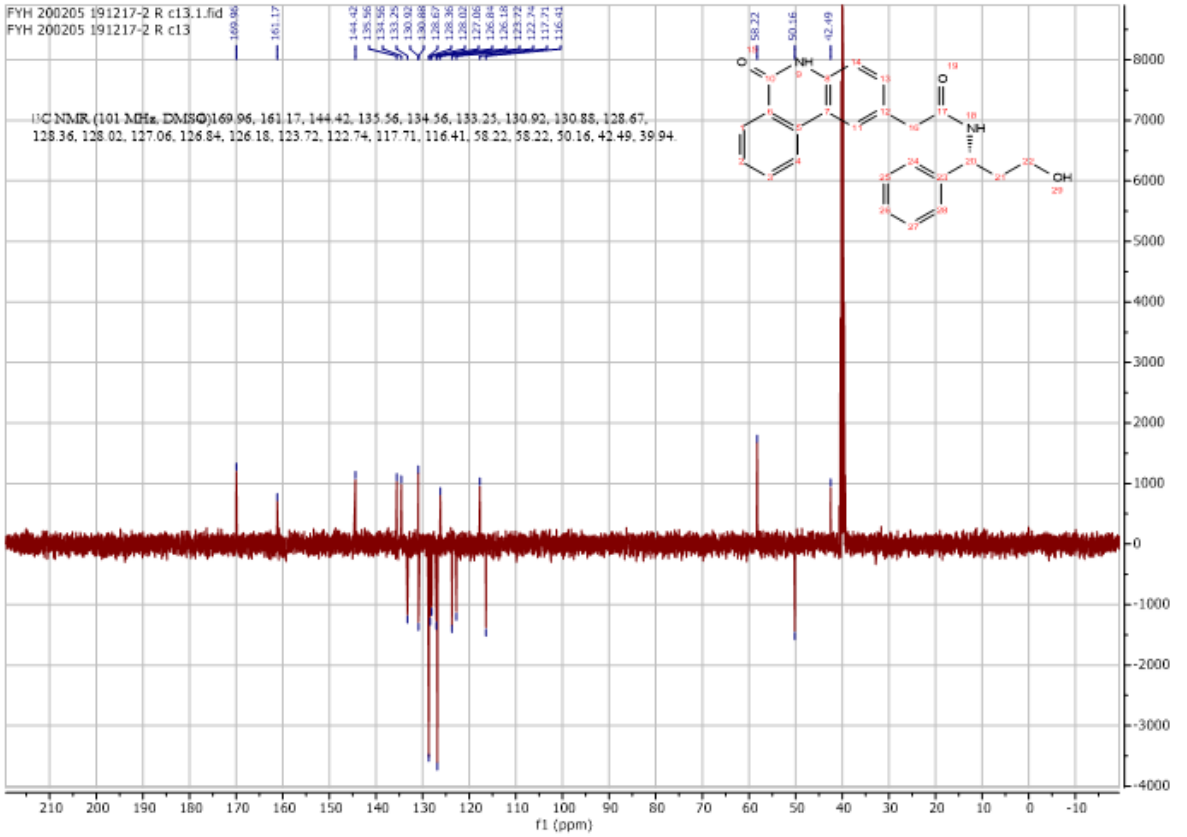
FYH 200205 191217-2 R c13.1.fid
FYH 200205 191217-2 R c13
13C NMR (101 MHz, DMSO) 169.96, 161.17, 144.42, 135.56, 134.56, 133.25, 130.92, 130.88, 128.67, 128.36, 128.02, 127.06, 126.84, 126.18, 123.72, 122.74, 117.71, 116.41, 58.22, 58.22, 50.16, 42.49, 39.94.
f1 (ppm)

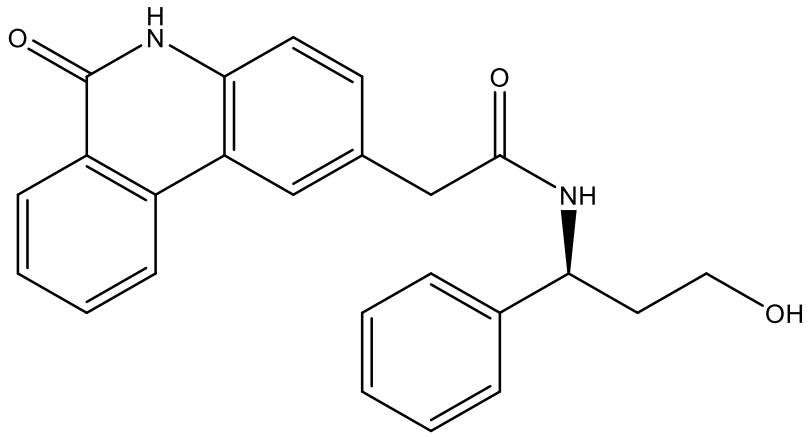

(*S*)-N-(3-hydroxy-1-phenylpropyl)-2-(6-oxo-5,6-dihydrophenanthridin-2-yl)acetamide (a48)

Using **Synthesis Method d**, 25.4mg (0.1mmol) **f5** was reacted with 15.1mg (0.1mmol) (*S*)-3-amino-3-phenylpropan-1-ol to give 33mg **a48** (Yield: 85%) and the product was separated as yellowish white solid. ^{1}H NMR (400 MHz, DMSO-d_6) δ 11.66 (s, 1H), 8.58 (d, *J* = 8.4 Hz, 1H), 8.38 – 8.29 (m, 2H), 8.23 – 8.19 (m, 1H), 7.87 (ddd, *J* = 8.3, 7.2, 1.5 Hz, 1H), 7.69 – 7.61 (m, 1H), 7.41 – 7.16 (m, 7H), 4.93 (dd, *J* = 8.5, 6.2 Hz, 1H), 4.51 (s, 1H), 3.57 (m, 2H), 3.45 – 3.36 (m, 2H), 1.95 – 1.74 (m, 2H). ^{13}C NMR (101 MHz, DMSO) δ 170.0, 161.2, 144.4, 135.6, 134.6, 133.3, 130.9, 130.9, 128.7, 128.4, 128.0, 127.1, 126.8, 126.2, 123.7, 122.7, 117.7, 116.4, 58.2, 50.2, 42.5, 39.9. HRMS m/z (ESI+, M+Na): Calcd for C24H22N2O3: 409.1528, (ESI+, M+Na) found: 409.1521

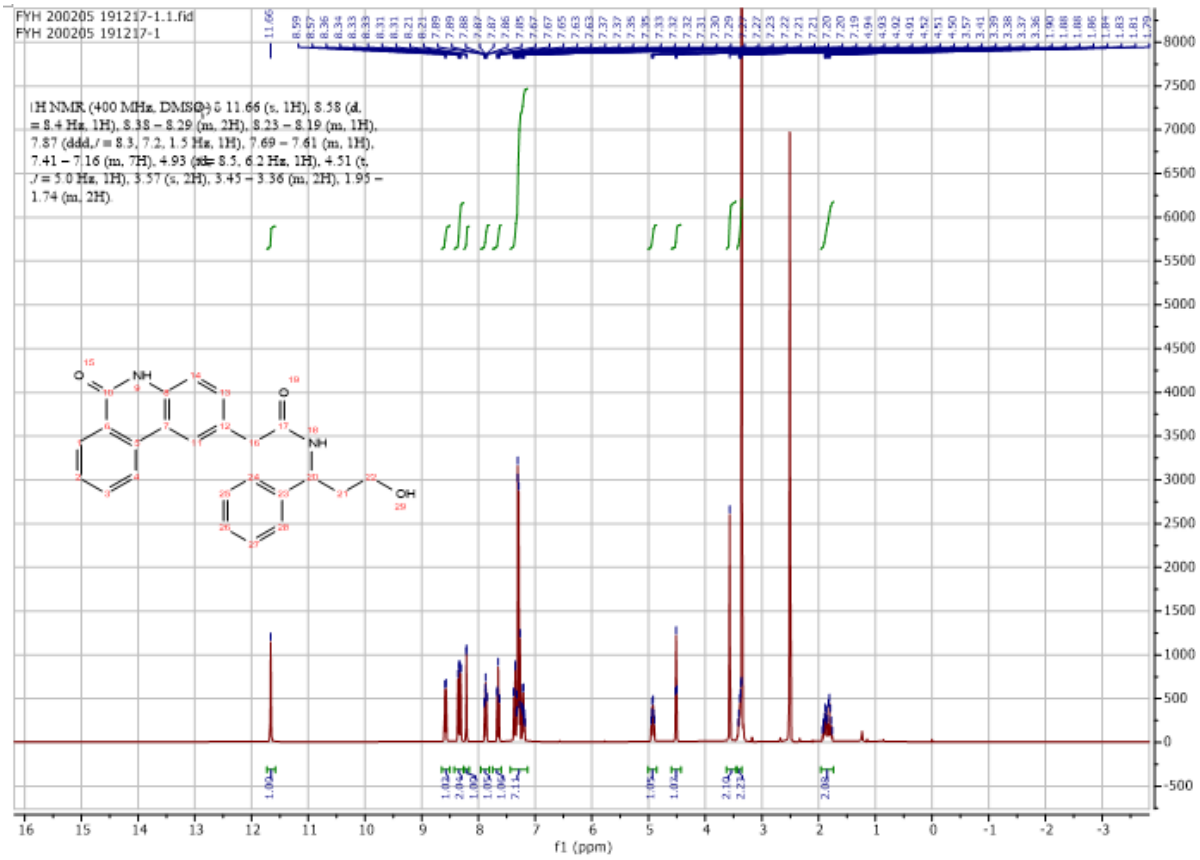
FYH 200205 191217-1.1.fid
FYH 200205 191217-1
¹H NMR (400 MHz, DMSO-d6) δ 11.66 (s, 1H), 8.58 (d, J = 8.4 Hz, 1H), 8.38 – 8.29 (m, 2H), 8.23 – 8.19 (m, 1H), 7.87 (ddd, J = 8.3, 7.2, 1.5 Hz, 1H), 7.69 – 7.61 (m, 1H), 7.41 – 7.16 (m, 7H), 4.93 (td, J = 8.5, 6.2 Hz, 1H), 4.51 (t, J = 5.0 Hz, 1H), 3.57 (s, 2H), 3.45 – 3.36 (m, 2H), 1.95 – 1.74 (m, 2H).
f1 (ppm)

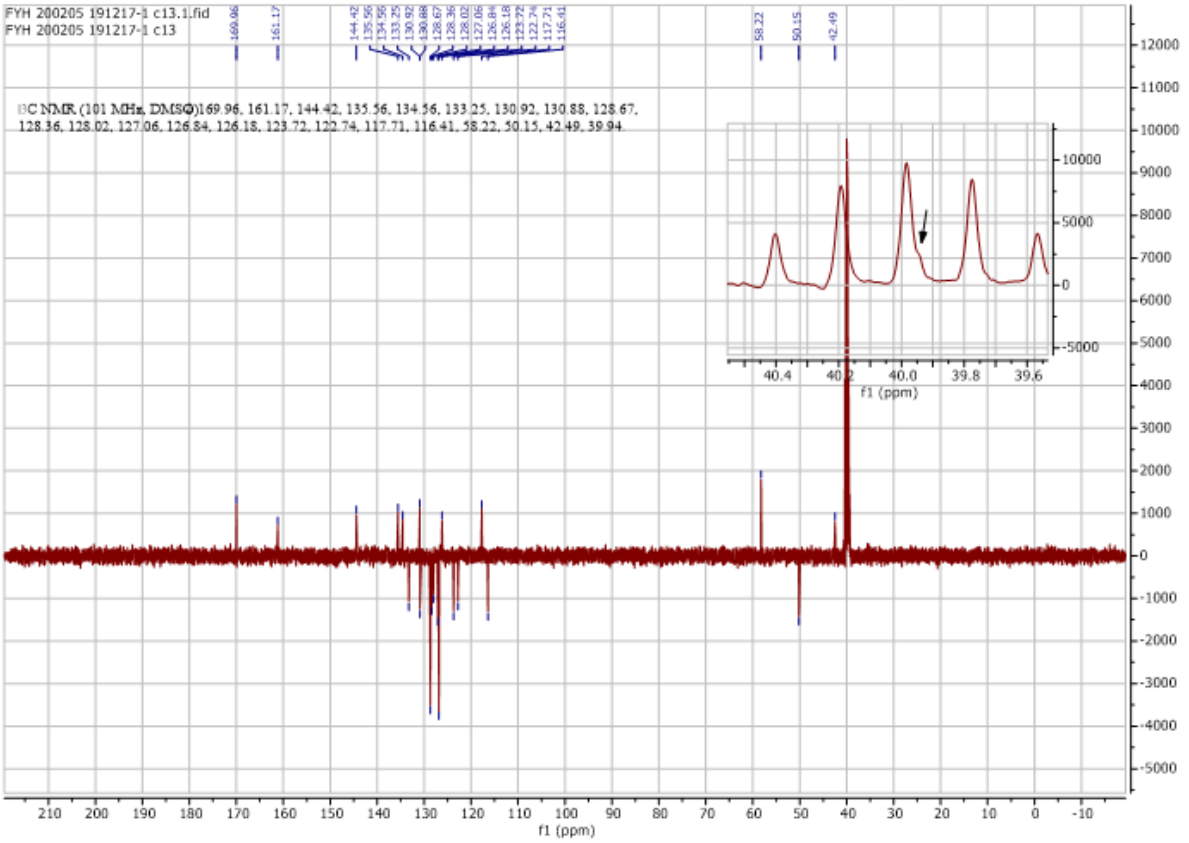
FYH 200205 191217-1 c13.1.fid
FYH 200205 191217-1 c13
¹³C NMR (101 MHz, DMSO-d6) 169.96, 161.17, 144.42, 135.56, 134.56, 133.25, 130.92, 130.88, 128.67, 128.36, 128.02, 127.06, 126.84, 126.18, 123.72, 122.74, 117.71, 116.41, 58.22, 50.15, 42.49, 39.94.
f1 (ppm)

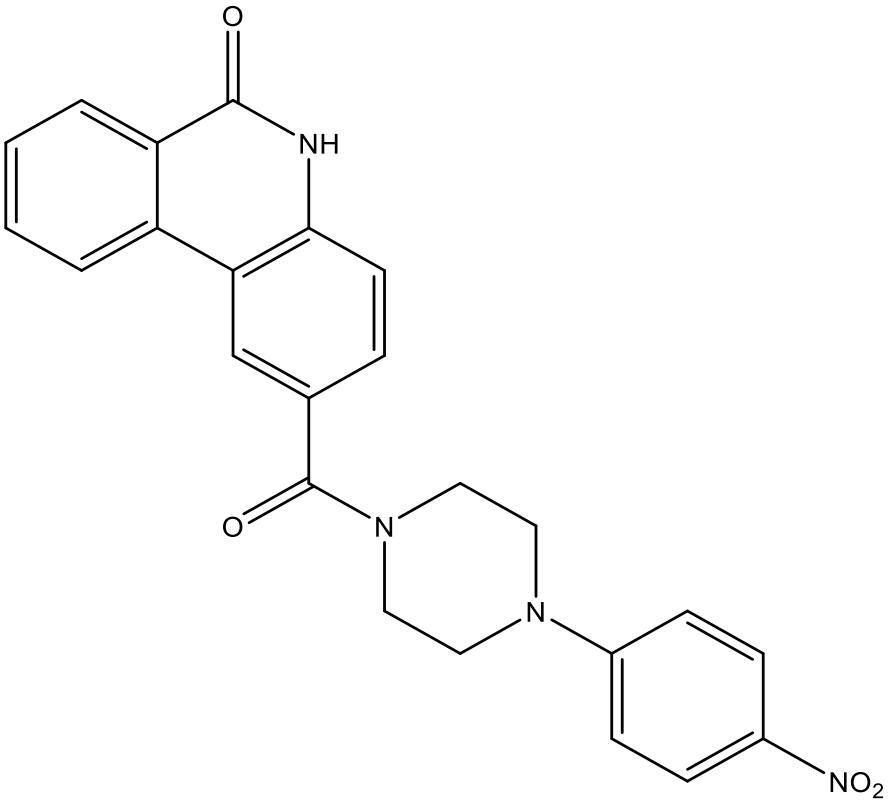

2-(4-(4-nitrophenyl)piperazine-1-carbonyl)phenanthridin-6(5H)-one (a49)

Using **Synthesis Method d**, 24mg (0.1mmol) **f2** was reacted with 20.7mg (0.1mmol) 1-(4-nitrophenyl)piperazine to give 28.5mg **a55** (Yield: 57%) and the product was separated as yellow solid. ^{1}H NMR (300 MHz, DMSO-d_6) δ 11.86 (s, 1H), 8.59 (d, J = 8.2 Hz, 1H), 8.49 (d, J = 1.7 Hz, 1H), 8.34 (dd, J = 8.0, 1.4 Hz, 1H), 8.13 – 8.04 (m, 2H), 7.93 – 7.82 (m, 1H), 7.74 – 7.64 (m, 1H), 7.60 (dd, J = 8.4, 1.7 Hz, 1H), 7.43 (d, J = 8.3 Hz, 1H), 7.08 – 6.99 (m, 2H), 3.66 (d, J = 31.7 Hz, 8H). ^{13}C NMR (75 MHz, DMSO) δ 169.4, 161.3, 154.9, 137.9, 137.6, 134.3, 133.5, 129.9, 129.1, 128.9, 128.0, 126.3, 126.2, 123.4, 123.0, 117.7, 116.6, 113.1, 46.6, 46.5. HRMS m/z (ESI+, M+Na): Calcd for C24H20N4O4: 451.1382, (ESI+, M+Na) found: 451.1381

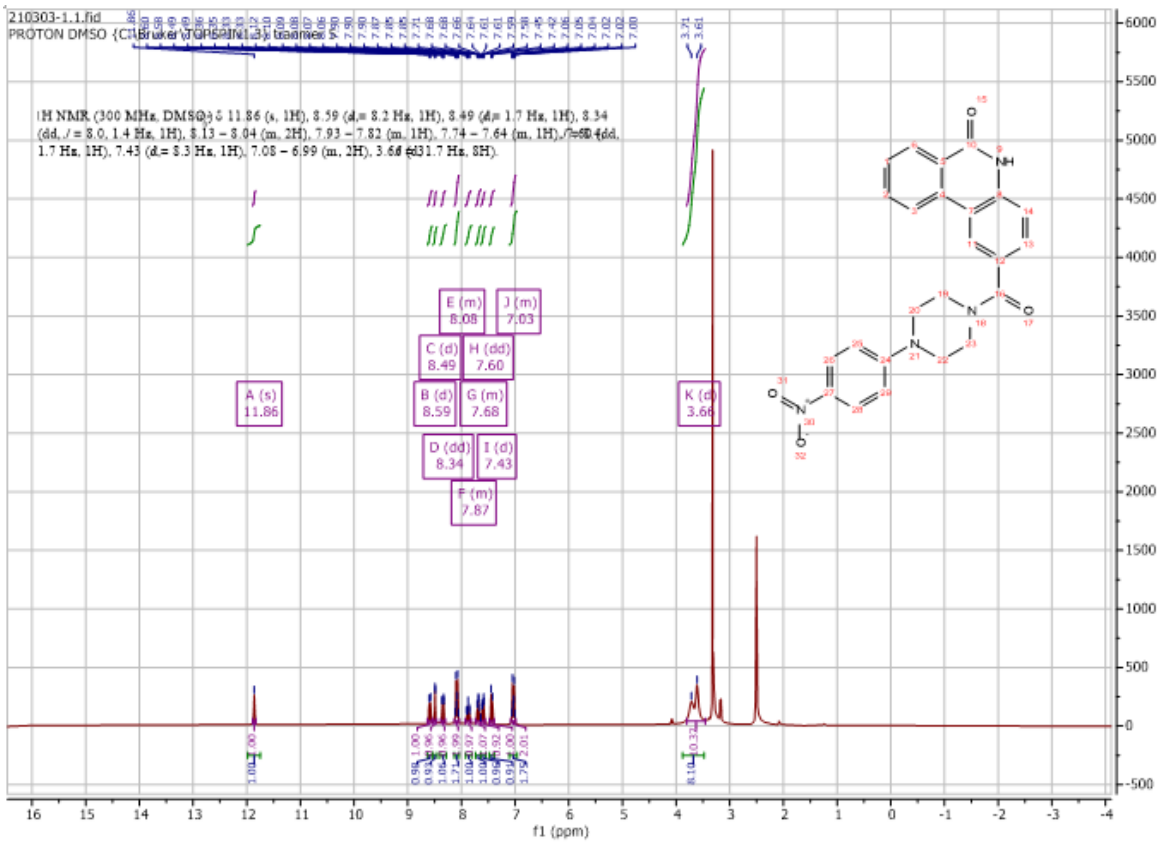
210303-1.1.fid
PROTON DMSO {C:\Bruker\TOPSPIN1.3} Bruker 5
1H NMR (300 MHz, DMSO) δ 11.86 (s, 1H), 8.59 (d, J = 8.2 Hz, 1H), 8.49 (d, J = 1.7 Hz, 1H), 8.34 (dd, J = 8.0, 1.4 Hz, 1H), 8.13 – 8.04 (m, 2H), 7.93 – 7.82 (m, 1H), 7.74 – 7.64 (m, 1H), 7.60 (dd, J = 8.4, 1.7 Hz, 1H), 7.43 (d, J = 8.3 Hz, 1H), 7.08 – 6.99 (m, 2H), 3.66 (d, J = 31.7 Hz, 8H).
A (s) 11.86
B (d) 8.59
C (d) 8.49
D (dd) 8.34
E (m) 8.08
F (m) 7.87
G (m) 7.68
H (dd) 7.60
I (d) 7.43
J (m) 7.03
K (d) 3.66
f1 (ppm)

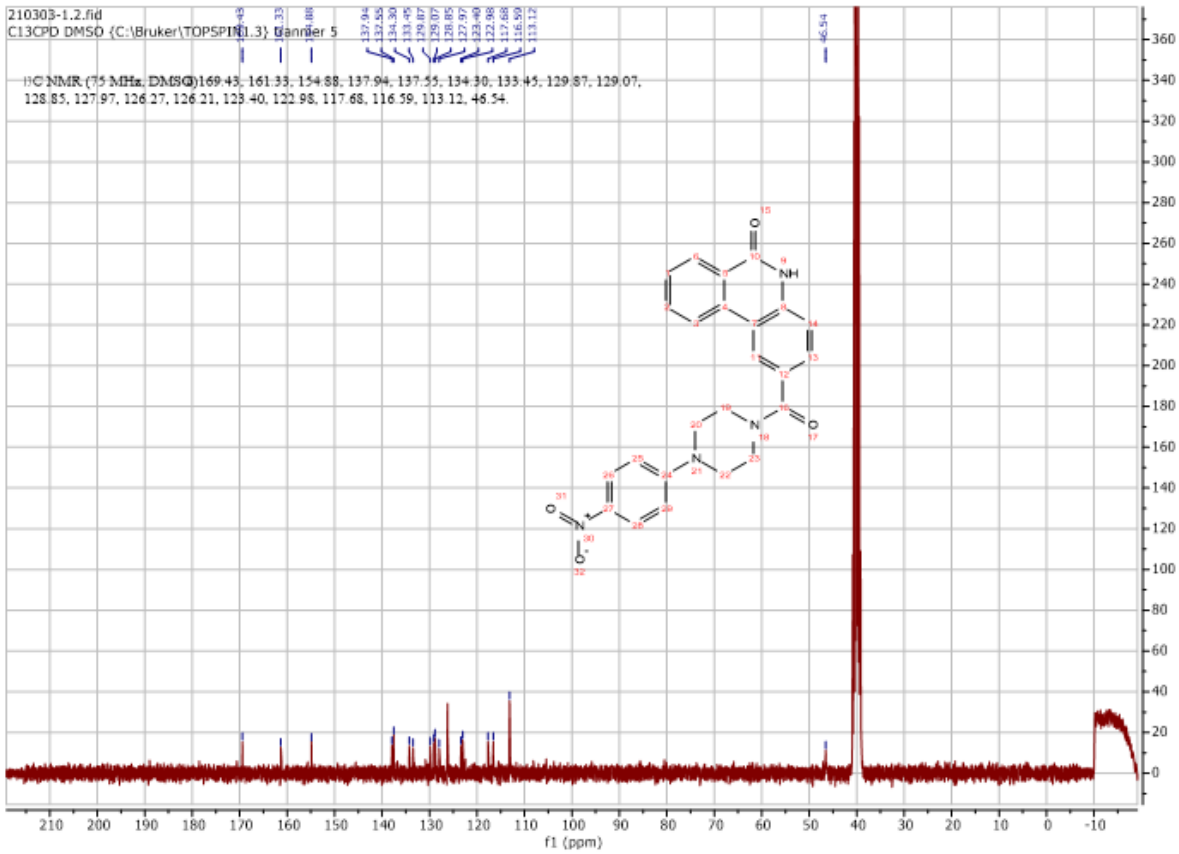
210303-1.2.fid
C13CPD DMSO {C:\Bruker\TOPSPIN1.3} Bruker 5
13C NMR (75 MHz, DMSO) 169.43, 161.33, 154.88, 137.94, 137.55, 134.30, 133.45, 129.87, 129.07, 128.85, 127.97, 126.27, 126.21, 123.40, 122.98, 117.68, 116.59, 113.12, 46.54.
f1 (ppm)

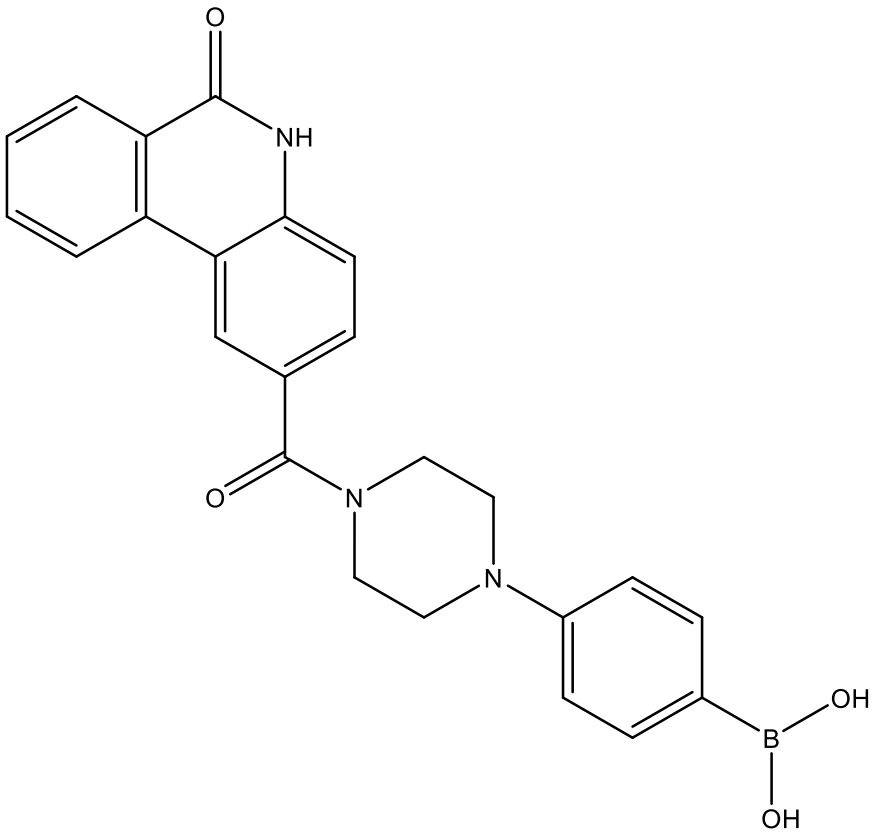

(4-(4-(6-oxo-5,6-dihydrophenanthridine-2-carbonyl)piperazin-1-yl)phenyl)boronic acid (a50)

Using **Synthesis Method d**, 24mg (0.1mmol) **f2** was reacted with 20.6mg (0.1mmol) (4-(piperazin-1-yl)phenyl)boronic acid to give 27.2mg **a55** (Yield: 54%) and the product was separated as yellow solid. ^{1}H NMR (300 MHz, DMSO-d_6) δ 11.85 (s, 1H), 8.63 – 8.55 (m, 1H), 8.50 – 8.44 (m, 1H), 8.34 (dd, *J* = 7.9, 1.4 Hz, 1H), 7.92 – 7.81 (m, 1H), 7.72 – 7.63 (m, 5H), 7.58 (dd, *J* = 8.3, 1.6 Hz, 1H), 7.43 (d, *J* = 8.3 Hz, 1H), 6.91 (d, *J* = 8.2 Hz, 2H), 3.64 (d, *J* = 29.6 Hz, 6H), 3.29 (s, 2H). ^{13}C NMR (75 MHz, DMSO) δ 169.3, 161.3, 152.4, 137.9, 135.9, 134.3, 133.5, 130.1, 129.0, 128.8, 128.0, 126.3, 123.4, 122.9, 117.7, 116.6, 114.6, 49.1. HRMS m/z (ESI-, M-H): Calcd for C24H22BN3O4: 426.1631, (ESI-, M-H) found: 426.1632

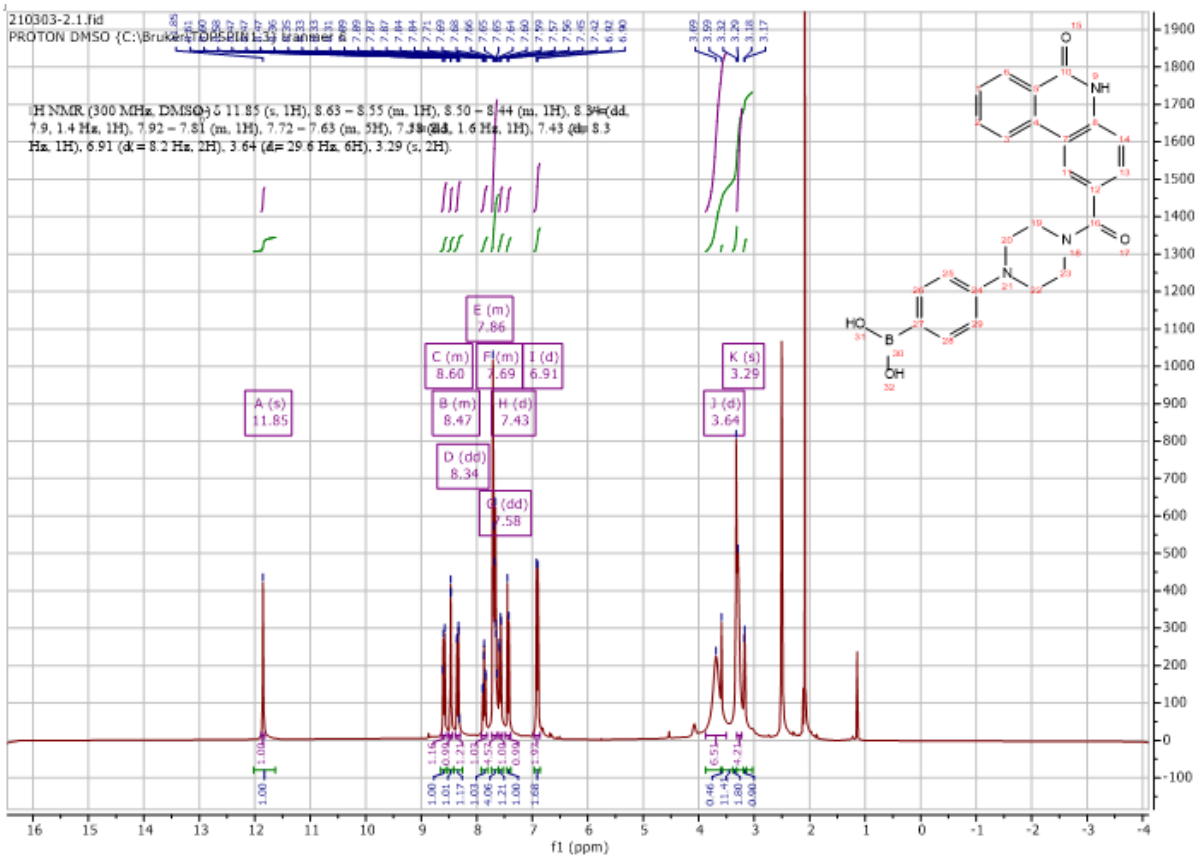
210303-2.1.fid
PROTON DMSO {C:\Bruker\TOPSPIN3.3} tianmei 6
A (s) 11.85
B (m) 8.47
C (m) 8.60
D (dd) 8.34
E (m) 7.86
F (m) 7.69
G (dd) 7.58
H (d) 7.43
I (d) 6.91
J (d) 3.64
K (s) 3.29
f1 (ppm)

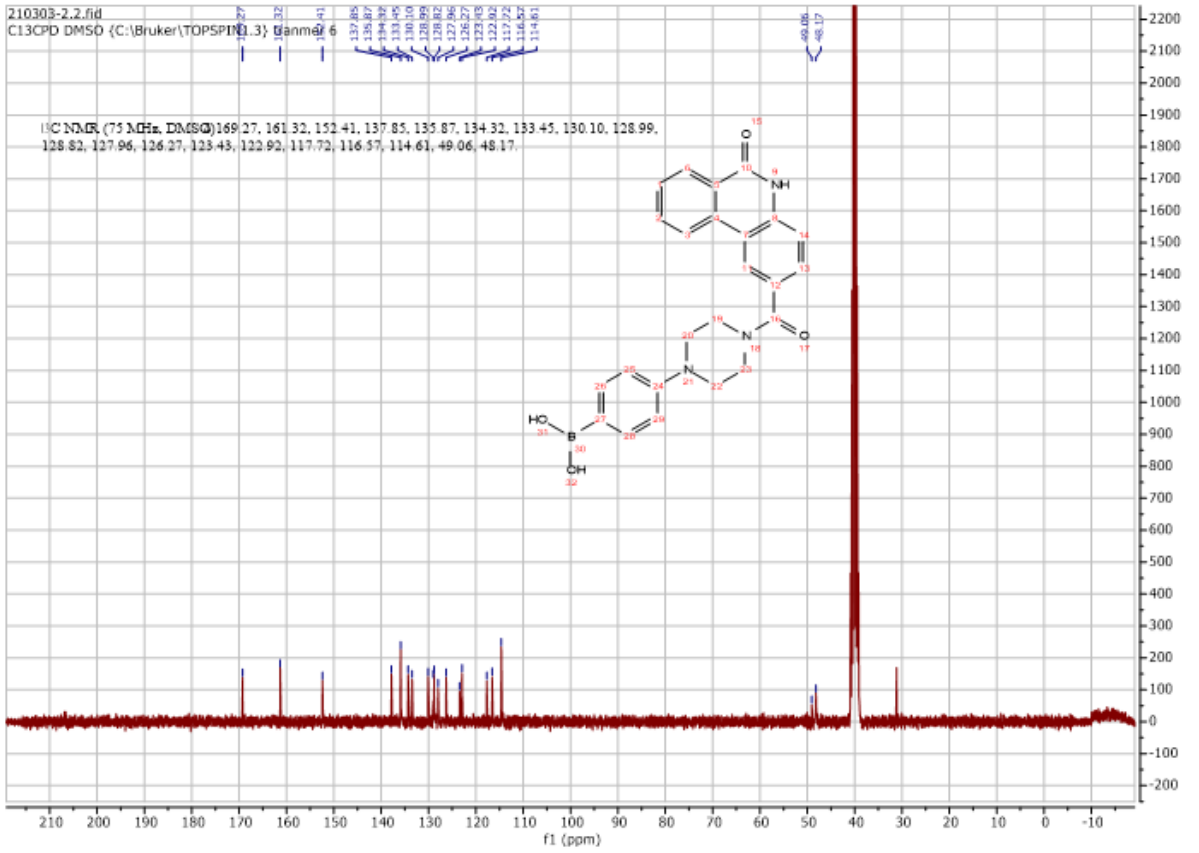
210303-2.2.fid
C13CPD DMSO {C:\Bruker\TOPSPIN3.3} tianmei 6
f1 (ppm)

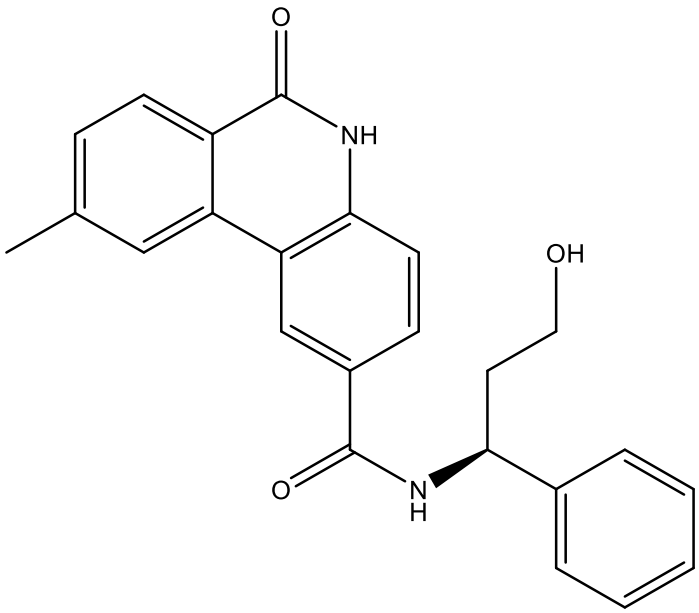

(*S*)-N-(3-hydroxy-1-phenylpropyl)-9-methyl-6-oxo-5,6-dihydrophenanthridine-2-carboxamide (a51)

Using **Synthesis Method d**, 25.4mg (0.1mmol) **f6** was reacted with 15.1mg (0.1mmol) (*S*)-3-amino-3-phenylpropan-1-ol to give 34.2mg **a51** (Yield: 89%) and the product was separated as yellowish white solid. ^{1}H NMR (400 MHz, DMSO-d_6) δ 11.79 (s, 1H), 8.85 (d, J = 8.1 Hz, 2H), 8.37 (s, 1H), 8.23 (d, J = 8.1 Hz, 1H), 8.06 – 7.96 (m, 1H), 7.55 – 7.48 (m, 1H), 7.47 – 7.31 (m, 5H), 7.28 – 7.19 (m, 1H), 5.29 – 5.19 (m, 1H), 4.60 (s, 1H), 3.49 (m, 2H), 2.59 (s, 3H), 2.20 – 2.06 (m, 1H), 1.99 (m, 1H). ^{13}C NMR (101 MHz, DMSO) δ 165.7, 161.4, 144.6, 143.8, 139.3, 134.5, 130.1, 129.2, 128.7, 128.7, 128.1, 127.1, 127.1, 124.0, 123.0, 122.8, 117.4, 116.3, 58.5, 50.9, 39.5, 22.1. HRMS m/z (ESI+, M+Na): Calcd for C24H22N2O3: 409.1528, (ESI+, M+Na) found: 409.1521

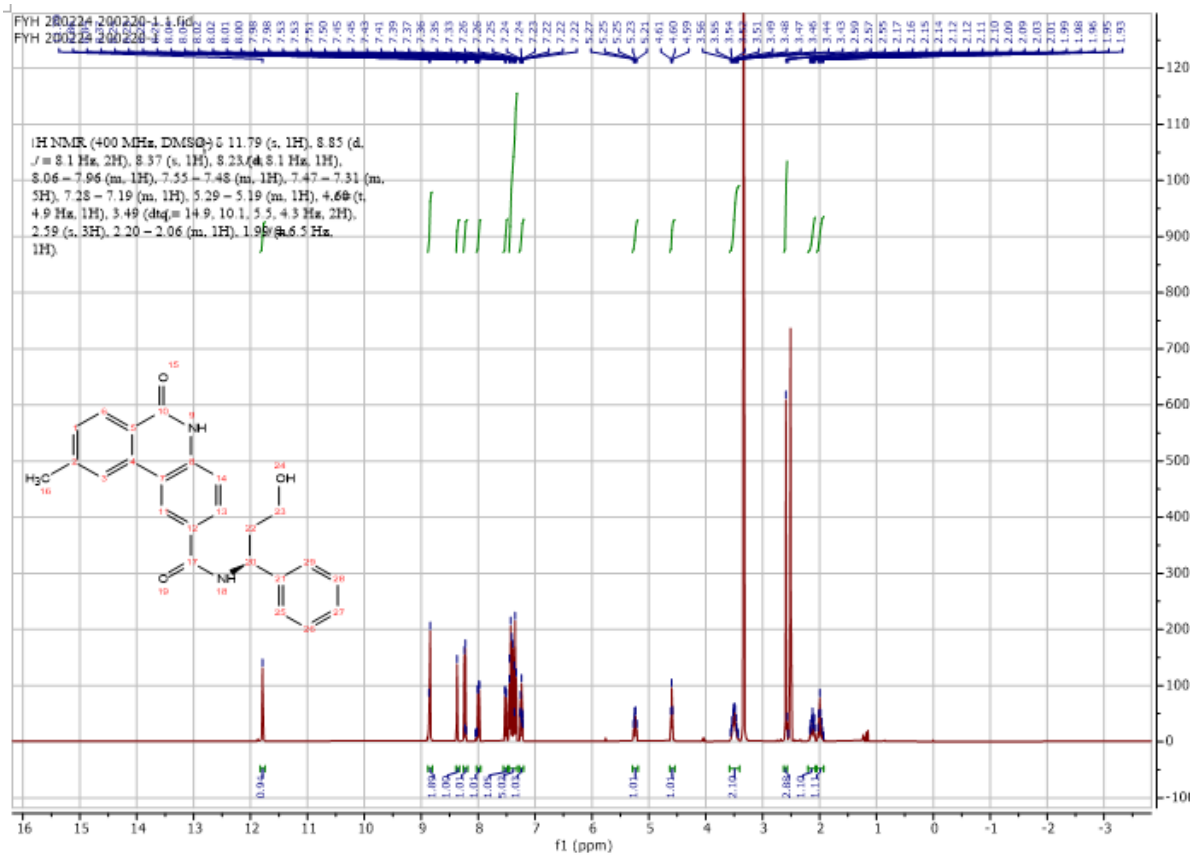
FYH 200224 200220-1 1.fid
FYH 200224 200220-1
1H NMR (400 MHz, DMSO) δ 11.79 (s, 1H), 8.85 (d, J = 8.1 Hz, 2H), 8.37 (s, 1H), 8.23 (d, J = 8.1 Hz, 1H), 8.06 – 7.96 (m, 1H), 7.55 – 7.48 (m, 1H), 7.47 – 7.31 (m, 5H), 7.28 – 7.19 (m, 1H), 5.29 – 5.19 (m, 1H), 4.60 (t, J = 4.9 Hz, 1H), 3.49 (dtq, J = 14.9, 10.1, 5.5, 4.3 Hz, 2H), 2.59 (s, 3H), 2.20 – 2.06 (m, 1H), 1.95 (q, J = 6.5 Hz, 1H).
f1 (ppm)

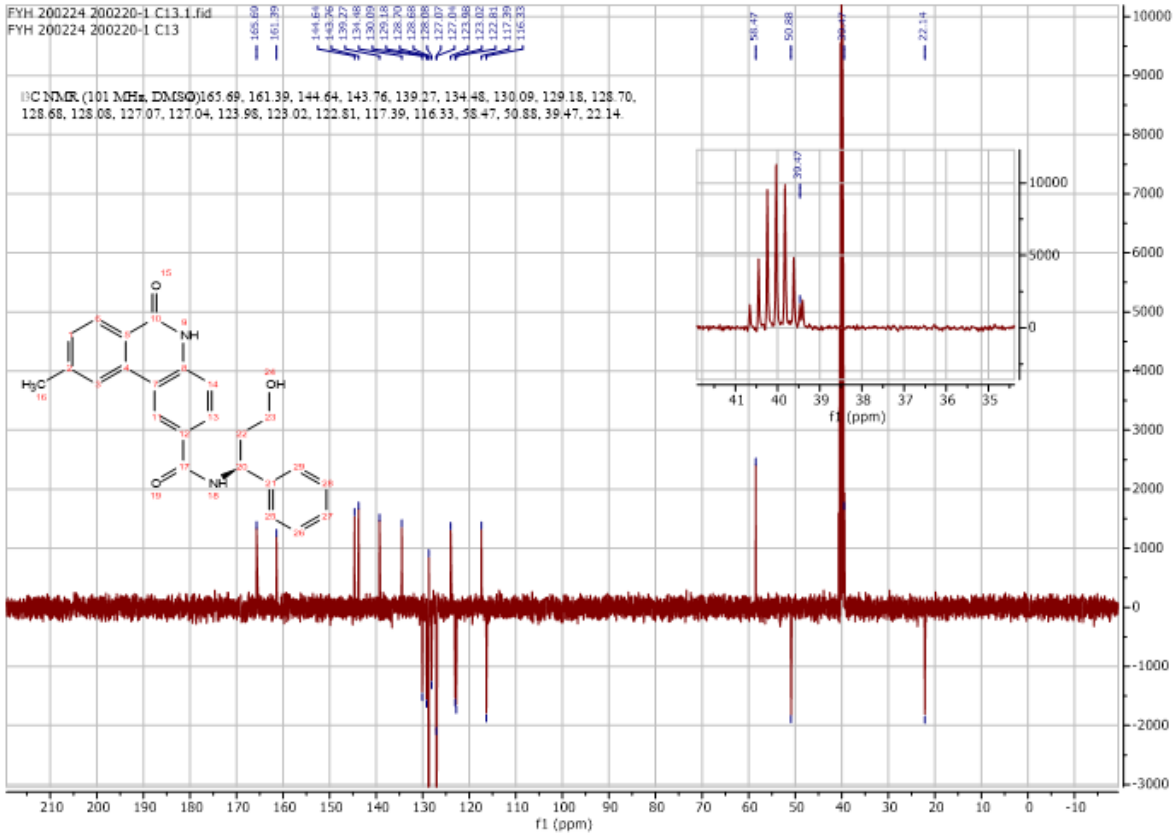
FYH 200224 200220-1 C13.1.fid
FYH 200224 200220-1 C13
13C NMR (101 MHz, DMSO) δ 165.69, 161.39, 144.64, 143.76, 139.27, 134.48, 130.09, 129.18, 128.70, 128.68, 128.08, 127.07, 127.04, 123.98, 123.02, 122.81, 117.39, 116.33, 58.47, 50.88, 39.47, 22.14.
f1 (ppm)

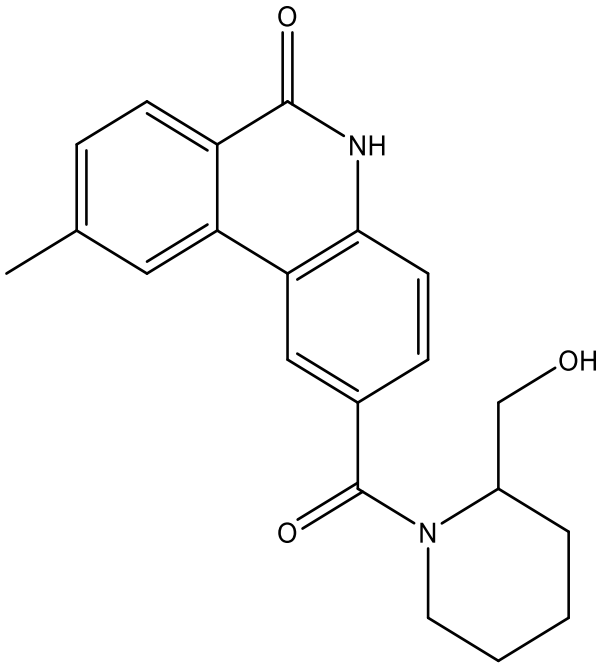

2-(2-(hydroxymethyl)piperidine-1-carbonyl)-9-methylphenanthridin-6(5*H*)-one (a52)

Using **Synthesis Method d**, 25.4mg (0.1mmol) **f6** was reacted with 11.5mg (0.1mmol) piperidin-2-ylmethanol to give 26.6mg **a52** (Yield: 76%) and the product was separated as yellowish white solid. ^{1}H NMR (400 MHz, DMSO-d_6) δ 11.71 (s, 1H), 8.38 (d, J = 21.1 Hz, 2H), 8.22 (d, J = 8.1 Hz, 1H), 7.54 – 7.46 (m, 2H), 7.37 (d, J = 8.3 Hz, 1H), 4.83 (s, 1H), 4.68 – 3.44 (m, 4H), 2.96 (m, 1H), 2.55 (s, 3H), 1.99 – 1.32 (m, 6H). ^{13}C NMR (101 MHz, DMSO) δ 169.7, 161.3, 143.7, 137.6, 134.4, 131.3, 130.0, 128.6, 127.98, 124.0, 123.2, 122.5, 117.6, 116.3, 59.2, 56.8, 46.9-36.3 (C20), 25.6, 22.0, 19.5. HRMS m/z (ESI+, M+Na): Calcd for C21H22N2O3: 373.1528, (ESI+, M+Na) found: 373.1522

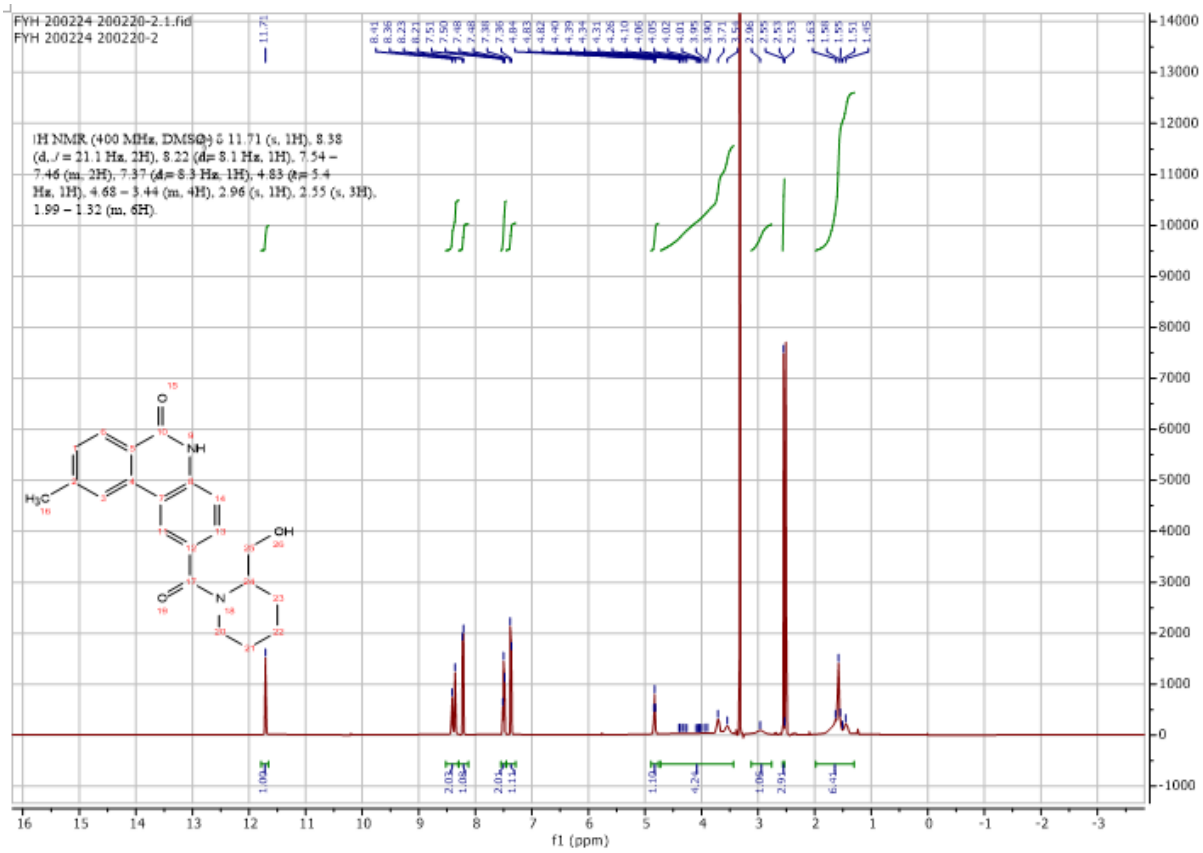
FYH 200224 200220-2.1.fid
FYH 200224 200220-2
1H NMR (400 MHz, DMSO) δ 11.71 (s, 1H), 8.38 (d, J = 21.1 Hz, 2H), 8.22 (d= 8.1 Hz, 1H), 7.54 – 7.46 (m, 2H), 7.37 (d= 8.3 Hz, 1H), 4.83 (t= 5.4 Hz, 1H), 4.68 – 3.44 (m, 4H), 2.96 (s, 1H), 2.55 (s, 3H), 1.99 – 1.32 (m, 6H).
f1 (ppm)

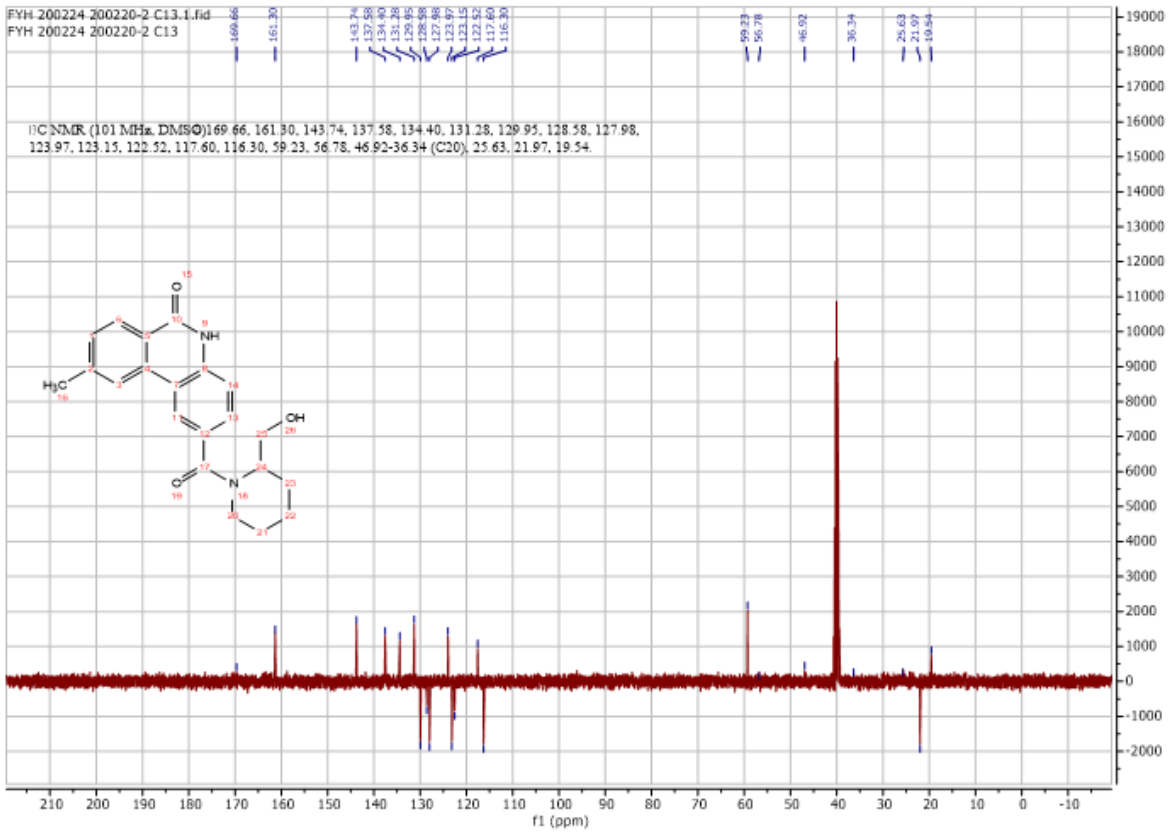
FYH 200224 200220-2 C13.1.fid
FYH 200224 200220-2 C13
13C NMR (101 MHz, DMSO)169.66, 161.30, 143.74, 137.58, 134.40, 131.28, 129.95, 128.58, 127.98, 123.97, 123.15, 122.52, 117.60, 116.30, 59.23, 56.78, 46.92-36.34 (C20), 25.63, 21.97, 19.54.
f1 (ppm)

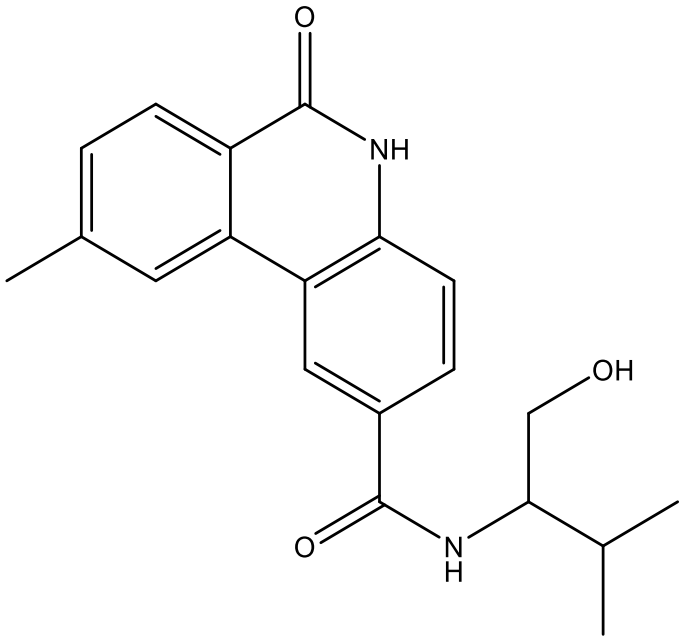

***N*-(1-hydroxy-3-methylbutan-2-yl)-9-methyl-6-oxo-5,6-dihydrophenanthridine-2-carboxamide (a53)**

Using **Synthesis Method d**, 25.4mg (0.1mmol) **f6** was reacted with 10.3mg (0.1mmol) 2-amino-3-methylbutan-1-ol to give 27mg **a53** (Yield: 80%) and the product was separated as yellowish white solid. ^{1}H NMR (400 MHz, DMSO-d_6) δ 11.77 (s, 1H), 8.85 (d, *J* = 1.7 Hz, 1H), 8.39 (s, 1H), 8.23 (d, *J* = 8.1 Hz, 1H), 8.11 (d, *J* = 8.8 Hz, 1H), 8.00 (dd, *J* = 8.5, 1.8 Hz, 1H), 7.55 – 7.48 (m, 1H), 7.39 (d, *J* = 8.5 Hz, 1H), 4.64 (s, 1H), 3.93 – 3.82 (m, 1H), 3.59 (m, 2H), 2.59 (s, 3H), 2.06 – 1.93 (m, *J* = 6.8 Hz, 1H), 0.95 (dd, *J* = 9.8, 6.8 Hz, 6H).^{13}C NMR (101 MHz, DMSO) δ 166.2, 161.4, 143.7, 139.1, 134.6, 130.0, 129.3, 129.1, 128.1, 124.0, 123.1, 122.8, 117.3, 116.2, 61.9, 57.4, 29.1, 22.2, 20.2, 19.5. HRMS m/z (ESI+, M+Na): Calcd for C20H22N2O3: 361.1528, (ESI+, M+Na) found: 361.1521

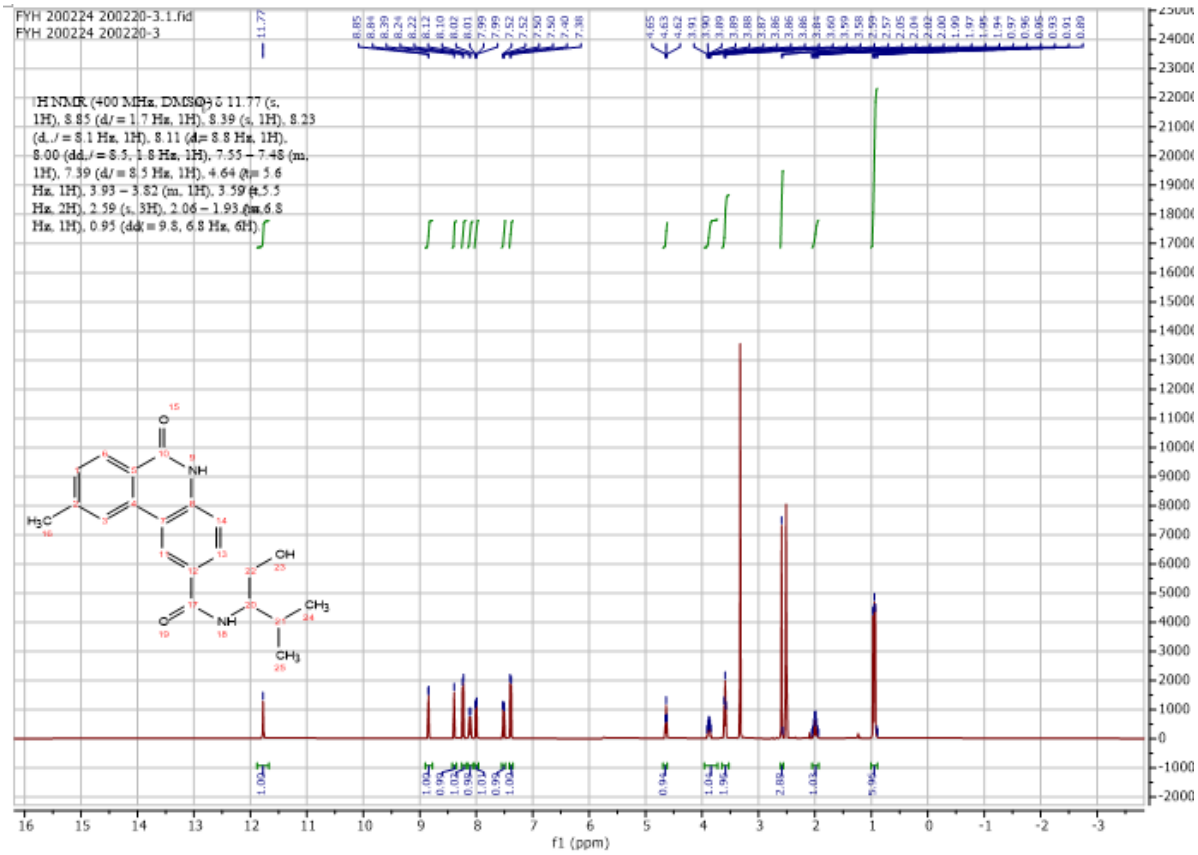
FYH 200224 200220-3.1.fid
FYH 200224 200220-3
¹H NMR (400 MHz, DMSO) δ 11.77 (s, 1H), 8.85 (d, J = 1.7 Hz, 1H), 8.39 (s, 1H), 8.23 (d, J = 8.1 Hz, 1H), 8.11 (d, J = 8.8 Hz, 1H), 8.00 (dd, J = 8.5, 1.8 Hz, 1H), 7.55 – 7.48 (m, 1H), 7.39 (d, J = 8.5 Hz, 1H), 4.64 (t, J = 5.6 Hz, 1H), 3.93 – 3.82 (m, 1H), 3.59 (t, J = 5.5 Hz, 2H), 2.59 (s, 3H), 2.06 – 1.93 (m, 1H), 0.95 (dd, J = 9.8, 6.8 Hz, 6H)
f1 (ppm)

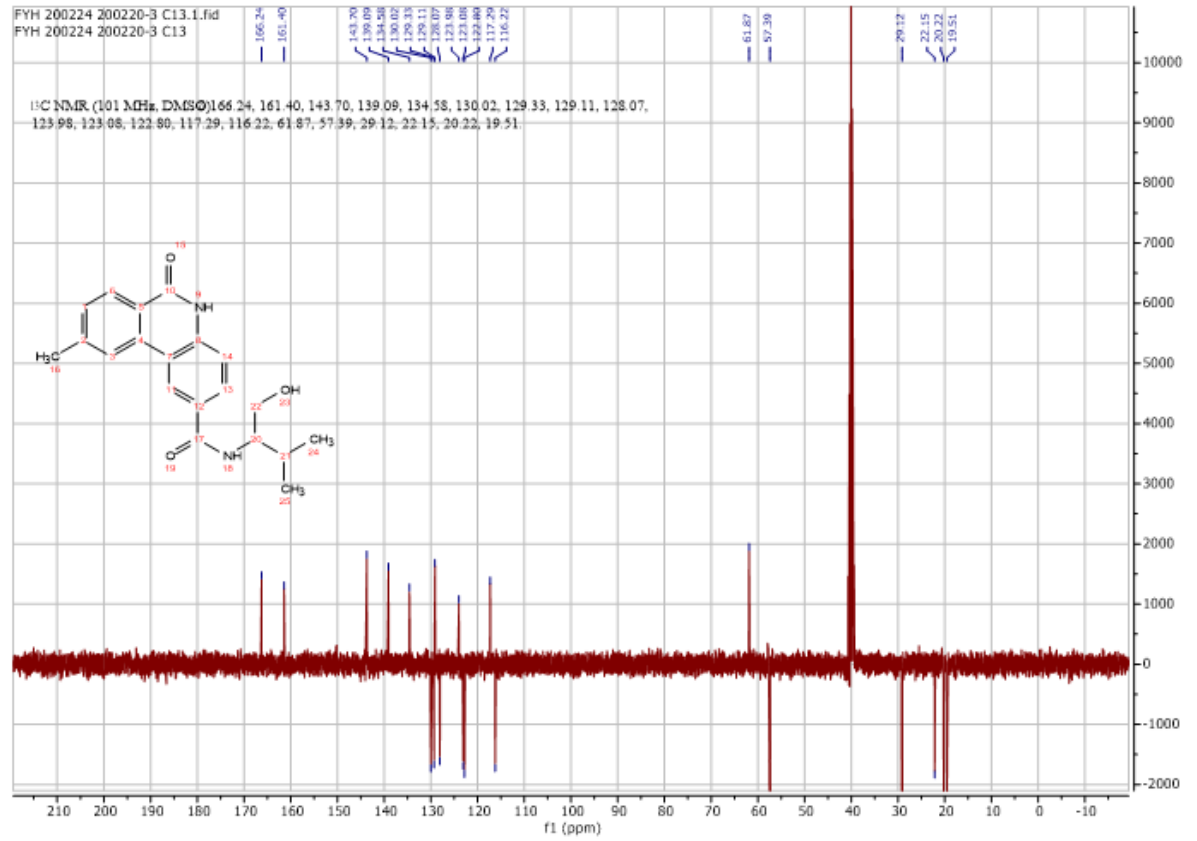
FYH 200224 200220-3 C13.1.fid
FYH 200224 200220-3 C13
¹³C NMR (101 MHz, DMSO) 166.24, 161.40, 143.70, 139.09, 134.58, 130.02, 129.33, 129.11, 128.07, 123.98, 123.08, 122.80, 117.29, 116.22, 61.87, 57.39, 29.12, 22.15, 20.22, 19.51
f1 (ppm)

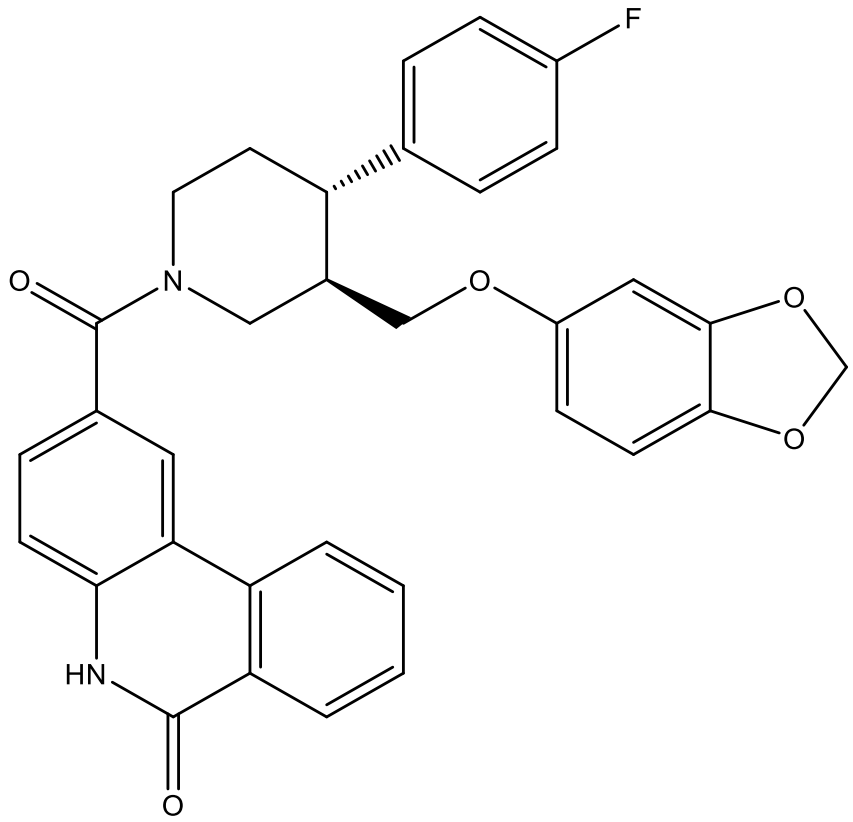

2-((3*R*,4*S*)-3-((benzo[*d*][1,3]dioxol-5-yloxy)methyl)-4-(4-fluorophenyl)piperidine-1-carbonyl)phenanthridin-6(5H)-one (a54)

Using **Synthesis Method d**, 24mg (0.1mmol) **f2** was reacted with 32.9mg (0.1mmol) (3*R*,4*S*)-3-((benzo[*d*][1,3]dioxol-5-yloxy)methyl)-4-(4-fluorophenyl)piperidine to give 25.3mg **a54** (Yield: 46%) and the product was separated as yellowish white solid. ^{1}H NMR (400 MHz, DMSO-d_6) δ 11.87 (s, 1H), 8.60 (d, *J* = 8.2 Hz, 1H), 8.51 (s, 1H), 8.38 – 8.30 (m, 1H), 7.88 (t, *J* = 7.5 Hz, 1H), 7.68 (t, *J* = 7.6 Hz, 1H), 7.61 (d, *J* = 8.3 Hz, 1H), 7.41 (dd, *J* = 16.3, 7.1 Hz, 3H), 7.15 (t, *J* = 8.7 Hz, 2H), 6.87 – 5.77 (m, 5H), 5.06 – 4.54 (m, 1H), 3.88 – 3.39 (m, 3H), 3.27 – 2.99 (m, 1H), 2.82 (m, 2H), 2.69 (s, 1H), 2.43 – 2.19 (m, 1H), 1.85 (m, 1H). (impurity: Hexane, Ethyl acetate) ^{13}C NMR (101 MHz, DMSO) δ 169.2(-CF), 162.6, 161.3, 160.2(-CF), 159.2, 141.6, 140.1, 140.1, 137.7, 134.4, 133.5, 131.5, 129.8, 129.8, 128.9, 128.8, 128.0, 126.3, 123.4, 122.7, 122.6, 117.7, 116.5, 115.8, 115.6, 101.4, 69.6, 54.0, 47.4, 44.0, 38.7, 34.8. HRMS m/z (ESI+, M+Na): Calcd for C33H27FN2O5: 573.1802, (ESI+, M+Na) found: 573.1785

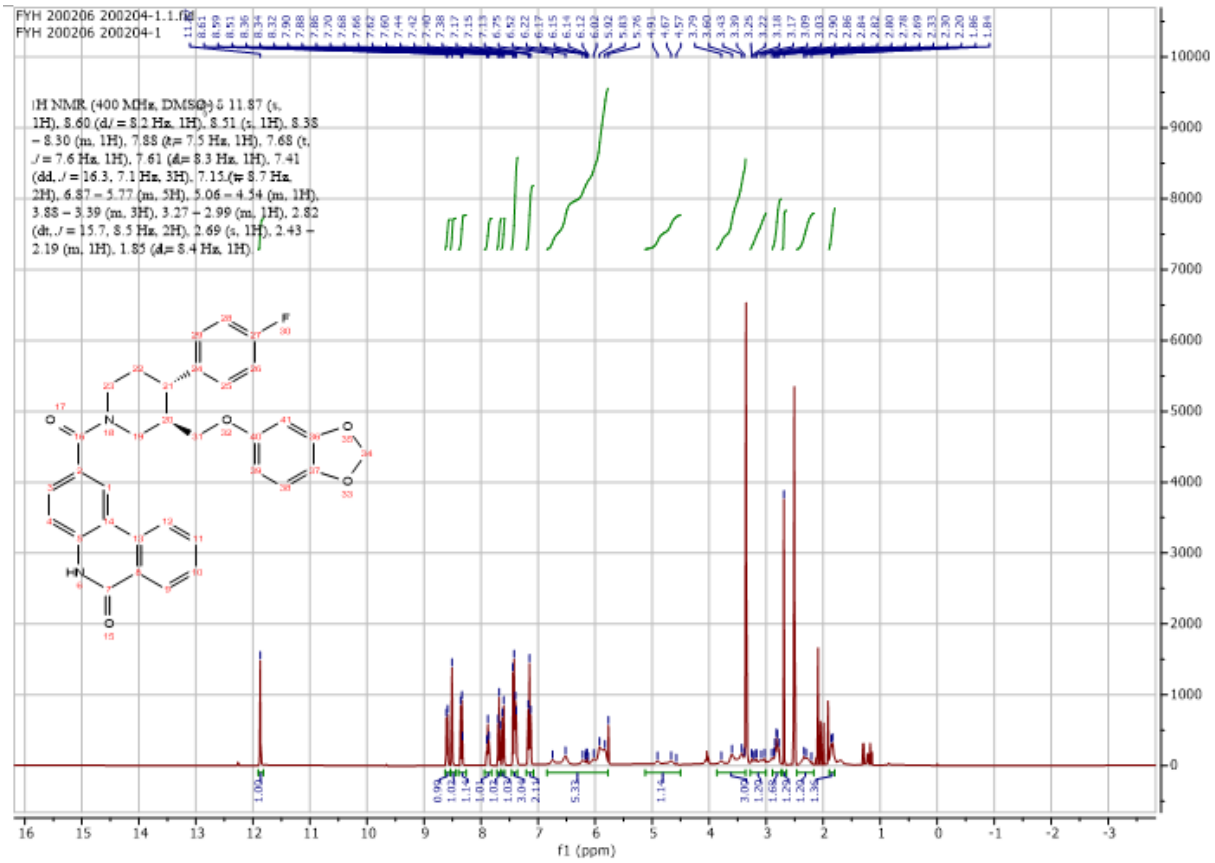
FYH 200206 200204-1.1.fid
FYH 200206 200204-1
¹H NMR (400 MHz, DMSO-d6) δ 11.87 (s, 1H), 8.60 (d, J = 8.2 Hz, 1H), 8.51 (s, 1H), 8.38 – 8.30 (m, 1H), 7.88 (t, J = 7.5 Hz, 1H), 7.68 (t, J = 7.6 Hz, 1H), 7.61 (d, J = 8.3 Hz, 1H), 7.41 (dd, J = 16.3, 7.1 Hz, 3H), 7.15 (d, J = 8.7 Hz, 2H), 6.87 – 5.77 (m, 5H), 5.06 – 4.54 (m, 1H), 3.88 – 3.39 (m, 3H), 3.27 – 2.99 (m, 1H), 2.82 (dt, J = 15.7, 8.5 Hz, 2H), 2.69 (s, 1H), 2.43 – 2.19 (m, 1H), 1.85 (d, J = 8.4 Hz, 1H).
f1 (ppm)

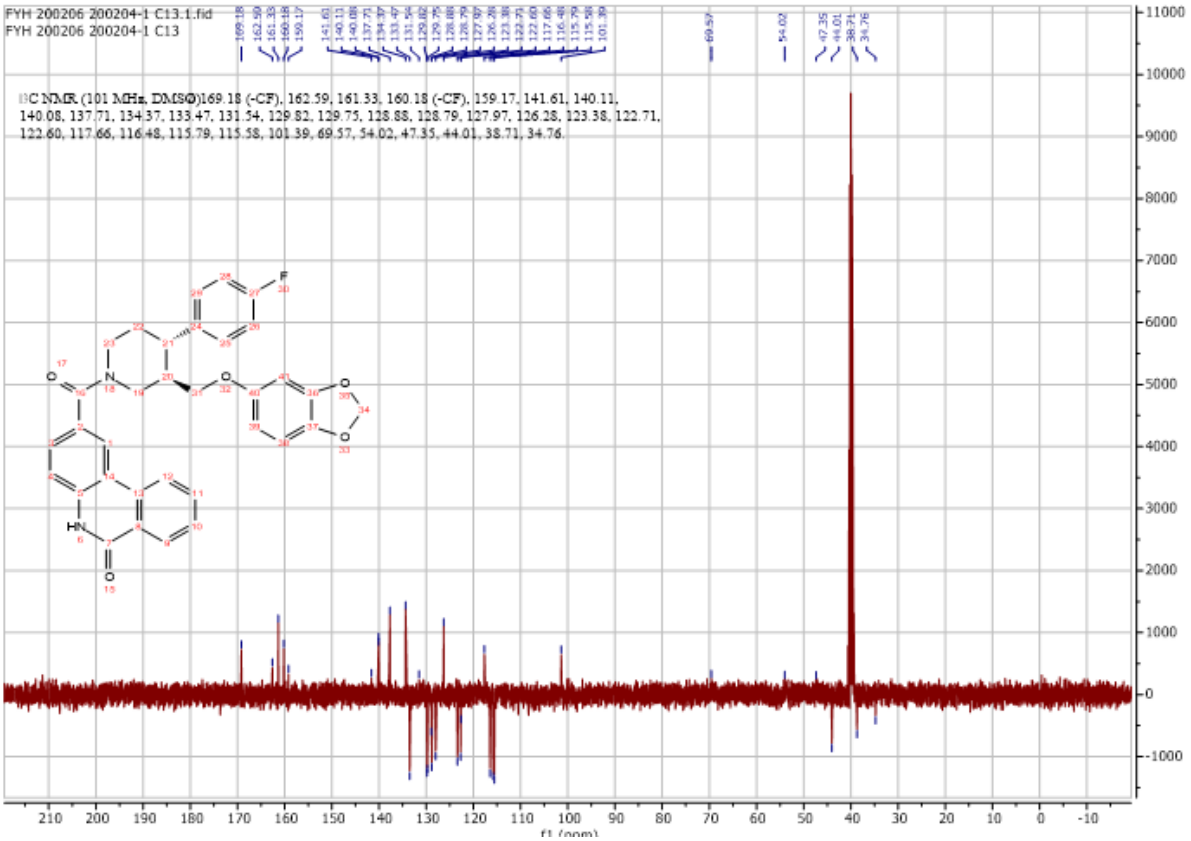
FYH 200206 200204-1 C13.1.fid
FYH 200206 200204-1 C13
¹³C NMR (101 MHz, DMSO) δ 169.18 (-CF), 162.59, 161.33, 160.18 (-CF), 159.17, 141.61, 140.11, 140.08, 137.71, 134.37, 133.47, 131.54, 129.82, 129.75, 128.88, 128.79, 127.97, 126.28, 123.38, 122.71, 122.60, 117.66, 116.48, 115.79, 115.58, 101.39, 69.57, 54.02, 47.35, 44.01, 38.71, 34.76.
f1 (ppm)

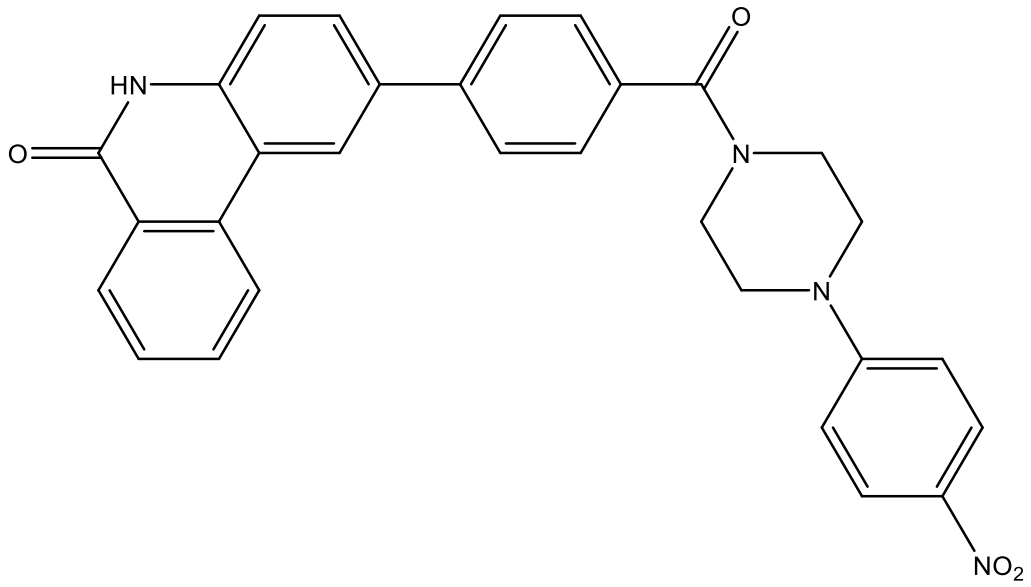

2-(4-(4-(4-nitrophenyl)piperazine-1-carbonyl)phenyl)phenanthridin-6(5H)-one (a55)

1750mg (10mmol) 2-chlorobenzoyl was reacted with 1276mg (10mmol) chloride 4-chloroaniline using **Synthesis Method a** to produce ~1502mg (Yield: 56%) 2-chloro-*N*-(4-chlorophenyl)benzamide, which was able to produce ~987mg (Yield: 77%) 2-chlorophenanthridin-6(5*H*)-one using **Synthesis Method b**. 45.8mg chlorophenanthridin-6(5*H*)-one was reacted 4-boronobenzoic acid with using **Synthesis Method h** to produce 4-(6-oxo-5,6-dihydrophenanthridin-2-yl)benzoic acid which could not be purified completely. 4-(6-oxo-5,6-dihydrophenanthridin-2-yl)benzoic acid was carried on to react with 1-(4-nitrophenyl)piperazine using **Synthesis Method d** to give 10.3mg (Yield: 12%) **a49** as yellow solid. ^{1}H NMR (300 MHz, DMSO-d_6) δ 11.84 (s, 1H), 8.97 – 8.62 (m, 2H), 8.14 – 8.05 (m, 2H), 7.99 – 7.85 (m, 4H), 7.69 (t, *J* = 7.6 Hz, 1H), 7.62 – 7.56 (m, 2H), 7.48 (d, *J* = 8.5 Hz, 1H), 7.09 – 7.00 (m, 2H), 3.68 (m, *J* = 50.5 Hz, 8H). ^{13}C NMR (75 MHz, DMSO) δ 169.5, 161.3, 154.9, 141.4, 137.5, 134.7, 133.8, 133.3, 128.7, 128.3, 127.1, 126.3, 121.9, 118.5, 117.3, 113.2, 46.5. HRMS m/z (ESI-, M-H): Calcd for C30H24N4O4: 503.1725, (ESI-, M-H) found: 503.1727

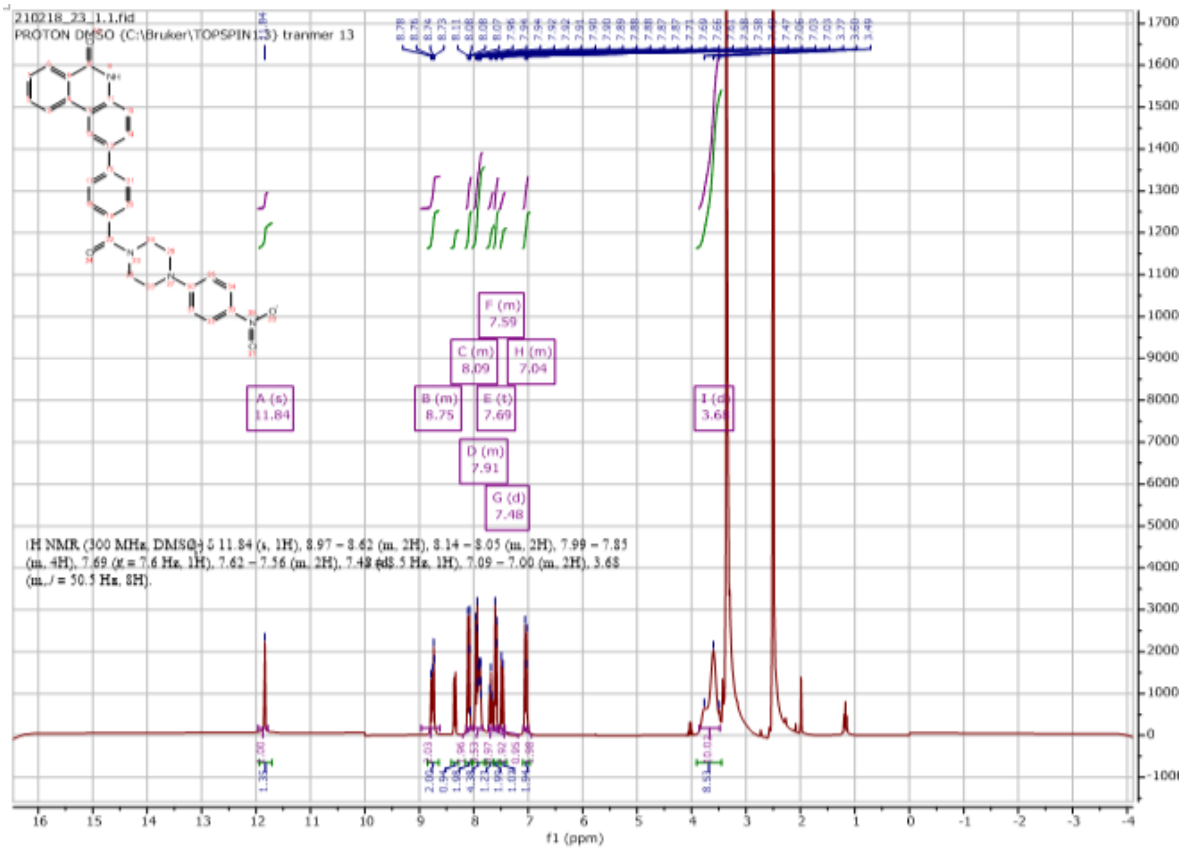
210218_23_1.1.fid
PROTON DMSO (C:\Bruker\TOPSPIN1.3) tranmer 13
F (m) 7.59
C (m) 8.09
H (m) 7.04
A (s) 11.84
B (m) 8.75
E (t) 7.69
I (d) 3.66
D (m) 7.91
G (d) 7.48
¹H NMR (300 MHz, DMSO) δ 11.84 (s, 1H), 8.97 – 8.62 (m, 2H), 8.14 – 8.05 (m, 2H), 7.99 – 7.85 (m, 4H), 7.69 (t, J = 7.6 Hz, 1H), 7.62 – 7.56 (m, 2H), 7.48 (d, J = 8.5 Hz, 1H), 7.09 – 7.00 (m, 2H), 3.68 (m, J = 50.5 Hz, 8H).
f1 (ppm)

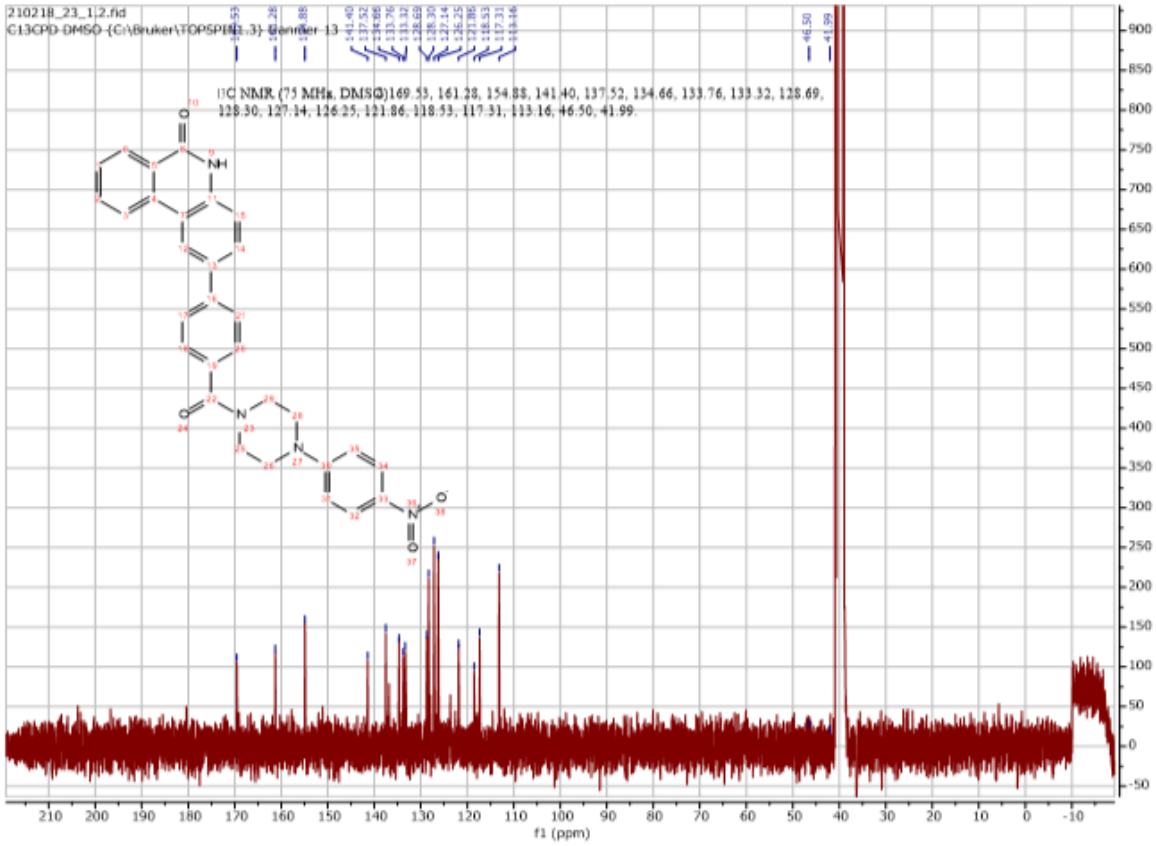
210218_23_1.2.fid
C13CPD DMSO (C:\Bruker\TOPSPIN1.3) tranmer 13
¹³C NMR (75 MHz, DMSO) 169.53, 161.28, 154.88, 141.40, 137.52, 134.66, 133.76, 133.32, 128.69, 128.30, 127.14, 126.25, 121.86, 118.53, 117.31, 113.16, 46.50, 41.99.
f1 (ppm)

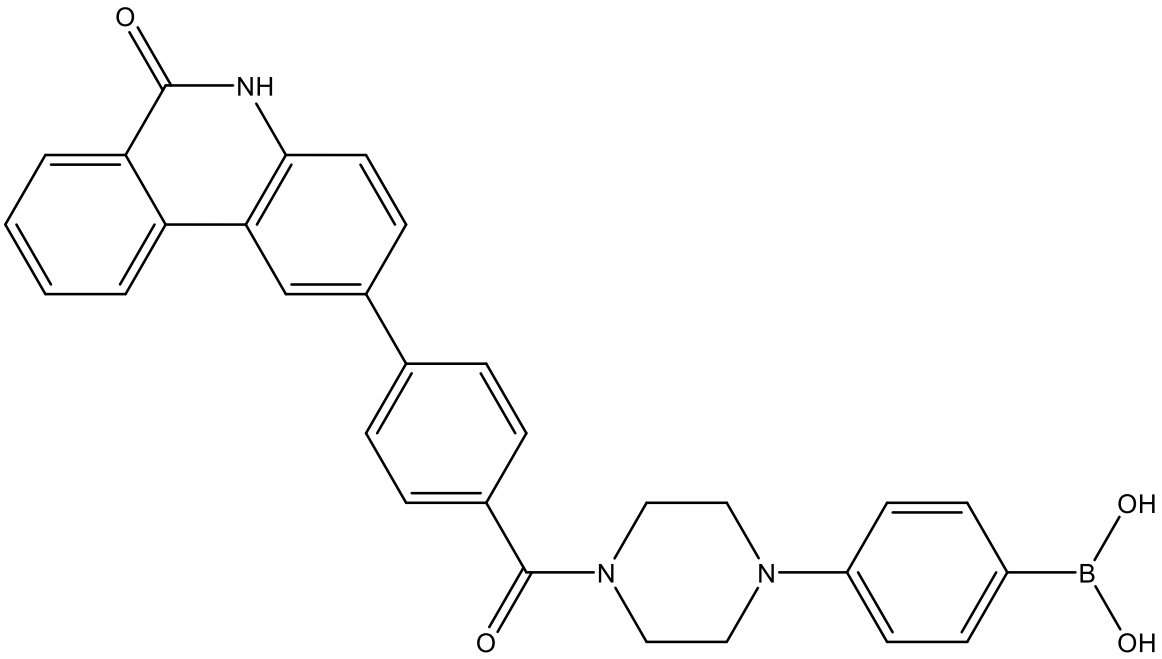

(4-(4-(4-(6-oxo-5,6-dihydrophenanthridin-2-yl)benzoyl)piperazin-1-yl)phenyl)boronic acid (a56)

1750mg (10mmol) 2-chlorobenzoyl was reacted with 1276mg (10mmol) chloride 4-chloroaniline using **Synthesis Method a** to produce ~1502mg (Yield: 56%) 2-chloro-*N*-(4-chlorophenyl)benzamide, which was able to produce ~987mg (Yield: 77%) 2-chlorophenanthridin-6(5*H*)-one using **Synthesis Method b**. 45.8mg chlorophenanthridin-6(5*H*)-one was reacted 4-boronobenzoic acid with using **Synthesis Method h** to produce 4-(6-oxo-5,6-dihydrophenanthridin-2-yl)benzoic acid which could not be purified completely. 4-(6-oxo-5,6-dihydrophenanthridin-2-yl)benzoic acid was carried on to react with (4-(piperazin-1-yl)phenyl)boronic acid using **Synthesis Method d** to give 9.2mg (Yield: 11%) **a50** as yellow solid. ^{1}H NMR (300 MHz, DMSO-d_6) δ 11.80 (s, 1H), 8.81 – 8.70 (m, 2H), 8.35 (dd, *J* = 7.9, 1.4 Hz, 1H), 7.97 – 7.83 (m, 4H), 7.75 – 7.61 (m, 5H), 7.57 (d, *J* = 8.1 Hz, 2H), 7.48 (d, *J* = 8.5 Hz, 1H), 6.92 (d, *J* = 8.2 Hz, 2H), 3.66 (s, 4H), 3.30 (s, 4H). ^{13}C NMR (75 MHz, DMSO) δ 169.4, 161.3, 152.4, 141.3, 136.8, 135.9, 134.9, 134.7, 133.8, 133.3, 128.7, 128.6, 128.2, 128.0, 127.1, 126.3, 123.6, 121.9, 118.5, 117.3, 114.7, 47.9, 41.5. HRMS m/z (ESI-, M-H): Calcd for C30H26BN3O4: 502.1944, (ESI-, M-H) found: 502.1934

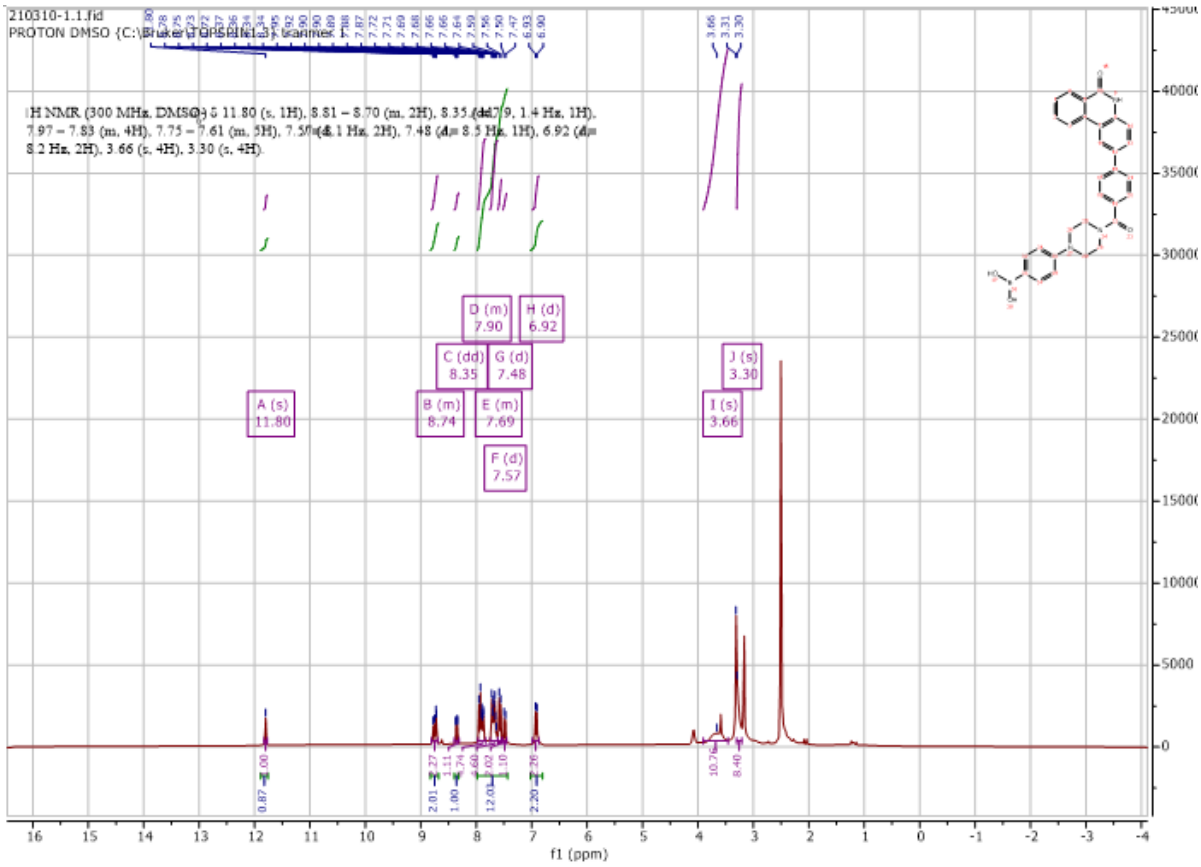
210310-1-1.fid
PROTON DMSO {C:\Bruker\TOPSPIN3.3} tanmei
A (s) 11.80
B (m) 8.74
C (dd) 8.35
D (m) 7.90
E (m) 7.69
F (d) 7.57
G (d) 7.48
H (d) 6.92
I (s) 3.66
J (s) 3.30
f1 (ppm)

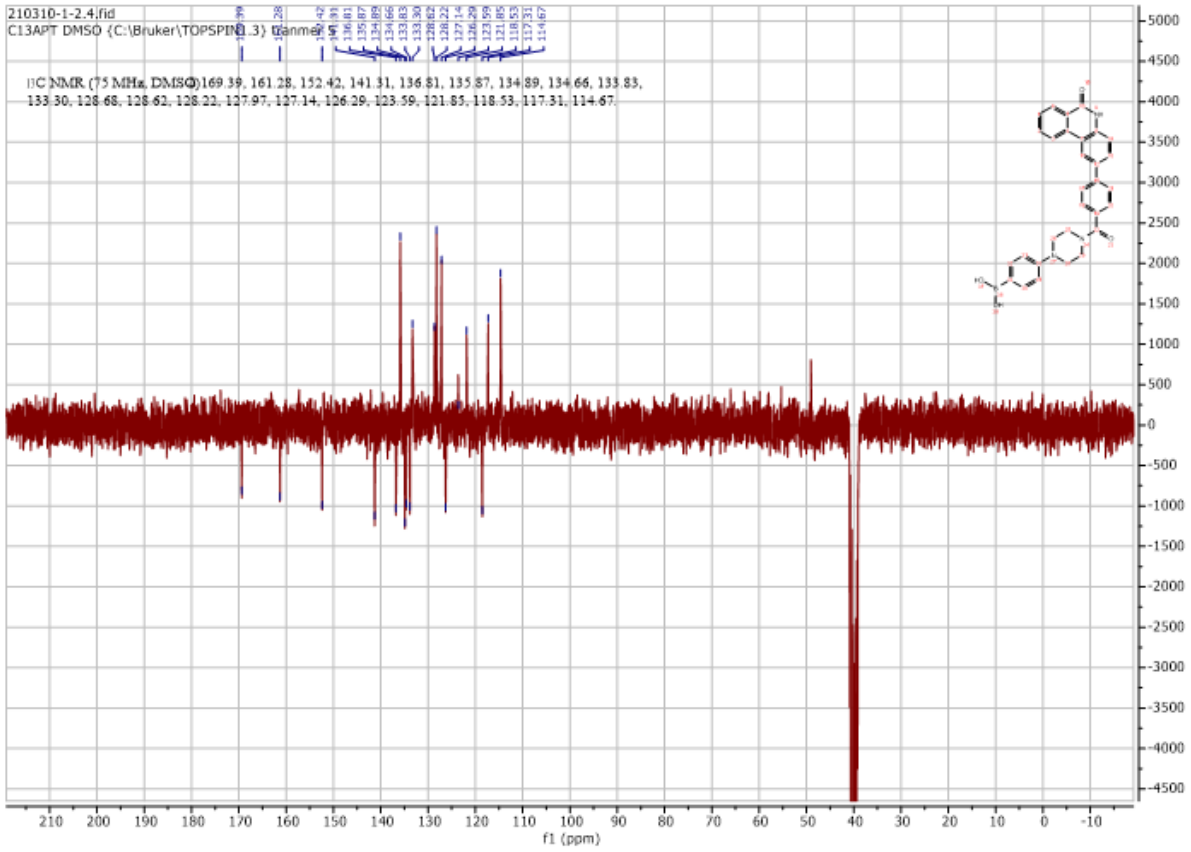
210310-1-2.4.fid
C13APT DMSO {C:\Bruker\TOPSPIN3.3} tanmei
f1 (ppm)

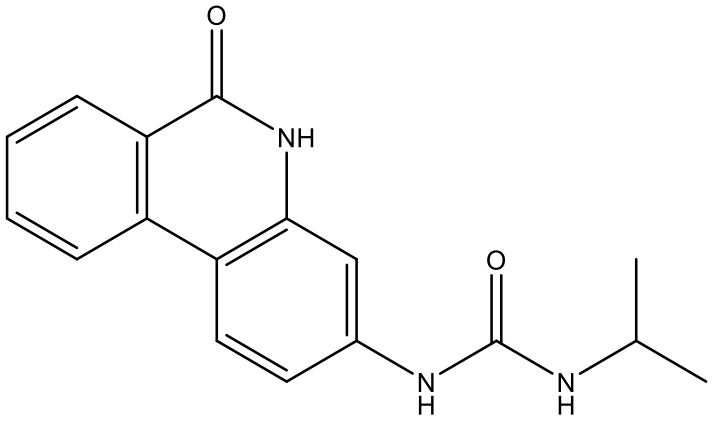

1-isopropyl-3-(6-oxo-5,6-dihydrophenanthridin-3-yl)urea (b1)

Using **Synthesis Method e**, 24mg (0.1mmol) **f3** was reacted with 6mg (0.1mmol) propan-2-amine to give 9.4mg **b1** (Yield: 32%) and the product was separated as yellowish white solid. ^{1}H NMR (400 MHz, DMSO-d_6) δ 11.53 (s, 1H), 8.63 (s, 1H), 8.34 (d, *J* = 8.2 Hz, 1H), 8.26 (dd, *J* = 8.0, 1.2 Hz, 1H), 8.20 (d, *J* = 8.9 Hz, 1H), 7.79 (ddd, *J* = 8.3, 7.2, 1.5 Hz, 1H), 7.57 – 7.49 (m, 2H), 7.25 (dd, *J* = 8.8, 2.1 Hz, 1H), 6.06 (d, *J* = 7.5 Hz, 1H), 3.87 – 3.71 (m, *J* = 6.6 Hz, 1H), 1.13 (d, *J* = 6.5 Hz, 6H). ^{13}C NMR (101 MHz, DMSO) δ 161.6, 154.7, 142.4, 137.9, 135.1, 133.1, 127.9, 127.0, 125.0, 124.3, 122.3, 113.1, 111.8, 103.8, 41.5, 23.4. HRMS m/z (ESI+, M+Na): Calcd for C17H17N3O2: 318.1218, (ESI+, M+Na) found: 318.1211

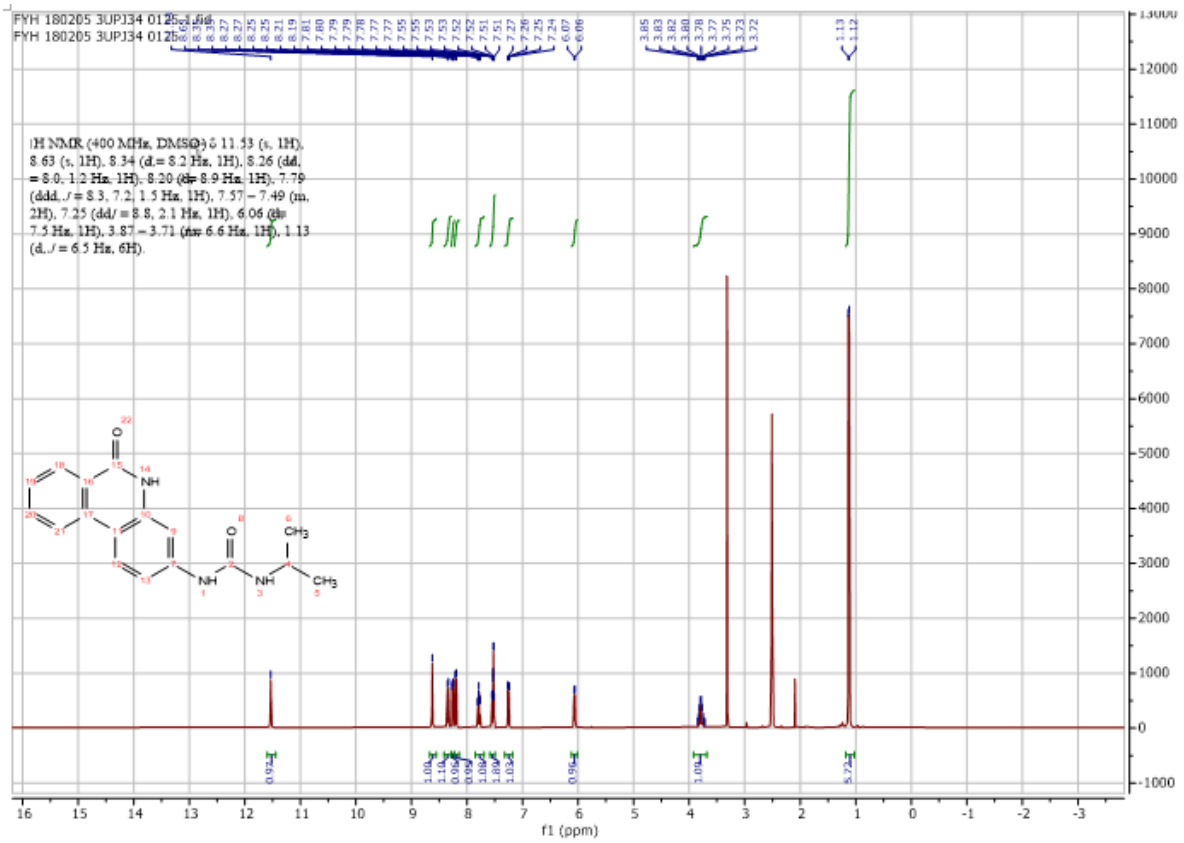
FYH 180205 3UP334 0125_1.fid
FYH 180205 3UP334 0125
1H NMR (400 MHz, DMSO) δ 11.53 (s, 1H), 8.63 (s, 1H), 8.34 (d, J = 8.2 Hz, 1H), 8.26 (dd, J = 8.0, 1.2 Hz, 1H), 8.20 (dt, J = 8.9 Hz, 1H), 7.79 (ddd, J = 8.3, 7.2, 1.5 Hz, 1H), 7.57 – 7.49 (m, 2H), 7.25 (dd, J = 8.8, 2.1 Hz, 1H), 6.06 (dt, J = 7.5 Hz, 1H), 3.87 – 3.71 (m, 6H), 1.13 (d, J = 6.5 Hz, 6H).
f1 (ppm)

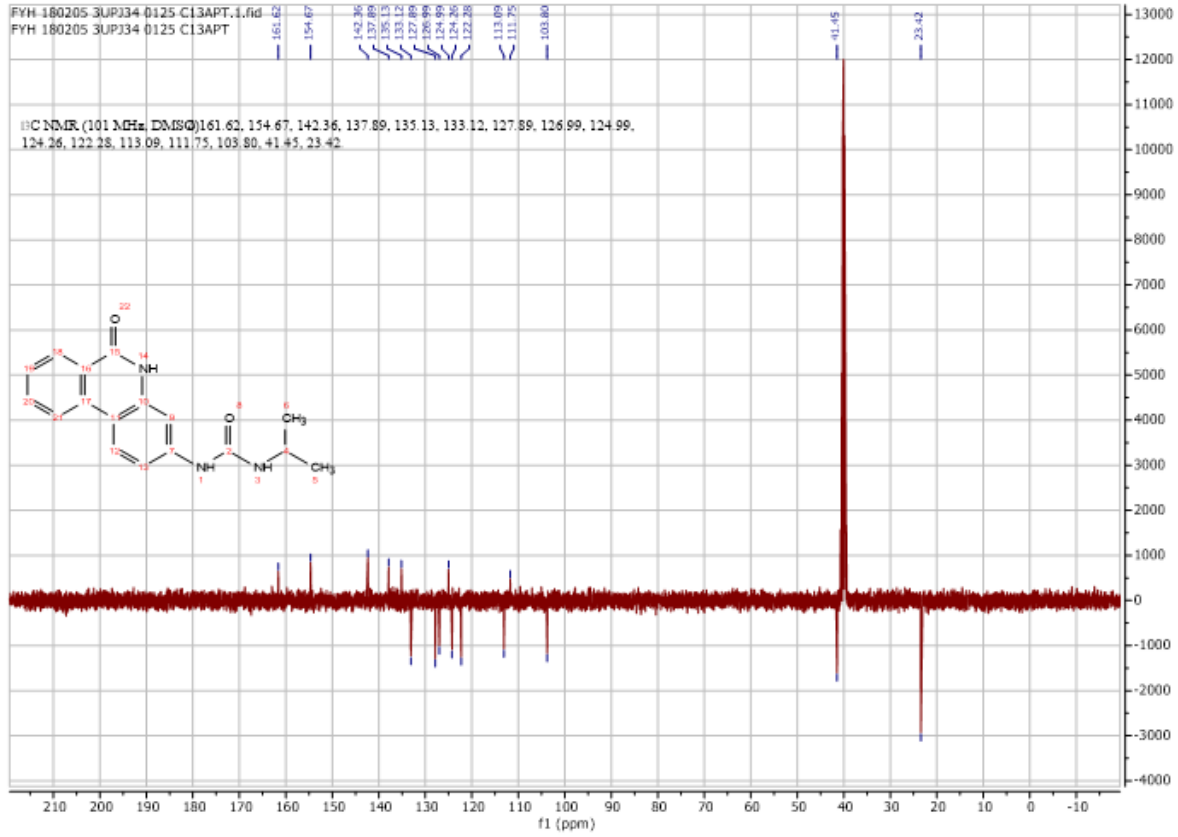
FYH 180205 3UP334 0125 C13APT.1.fid
FYH 180205 3UP334 0125 C13APT
13C NMR (101 MHz, DMSO) 161.62, 154.67, 142.36, 137.89, 135.13, 133.12, 127.89, 126.99, 124.99, 124.26, 122.28, 113.09, 111.75, 103.80, 41.45, 23.42
f1 (ppm)

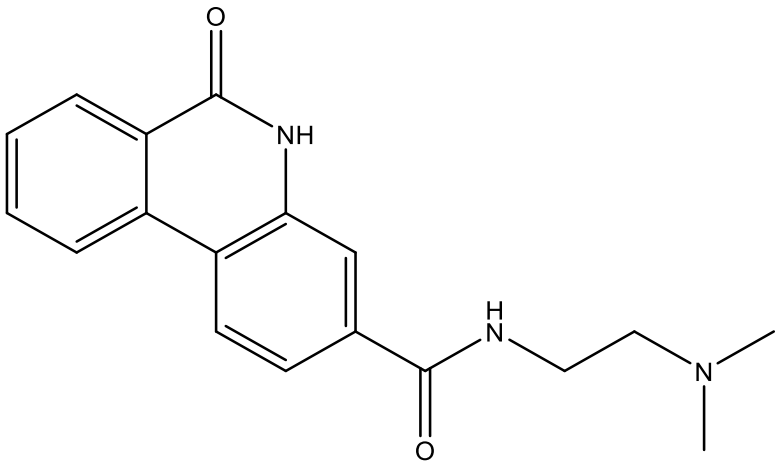

***N*-(2-(dimethylamino)ethyl)-6-oxo-5,6-dihydrophenanthridine-3-carboxamide (b2)**

Using **Synthesis Method d**, 24mg (0.1mmol) **f3** was reacted with 8.8mg (0.1mmol) *N*1,*N*1-dimethylethane-1,2-diamine to give 27.3mg **b2** (Yield: 88%) and the product was separated as yellow solid. ^{1}H NMR (400 MHz, DMSO-d_6) δ 11.80 (s, 1H), 8.58 (d, *J* = 8.1 Hz, 1H), 8.54 – 8.45 (m, 2H), 8.35 (dd, *J* = 8.0, 1.2 Hz, 1H), 7.89 (ddd, *J* = 8.3, 7.2, 1.4 Hz, 1H), 7.84 (d, *J* = 1.6 Hz, 1H), 7.74 – 7.66 (m, 2H), 3.39 (dt, *J* = 15.5, 7.8 Hz, 2H), 2.44 (t, *J* = 6.8 Hz, 2H), 2.21 (s, 6H). ^{13}C NMR (101 MHz, DMSO) δ 166.0, 161.3, 136.9, 136.0, 134.1, 133.4, 129.1, 128.0, 126.6, 123.8, 123.7, 120.8, 120.1, 116.1, 58.6, 45.7, 38.0. HRMS m/z (ESI+, M+H): Calcd for C18H19N3O2: 310.1550, (ESI+, M+H) found: 310.1554

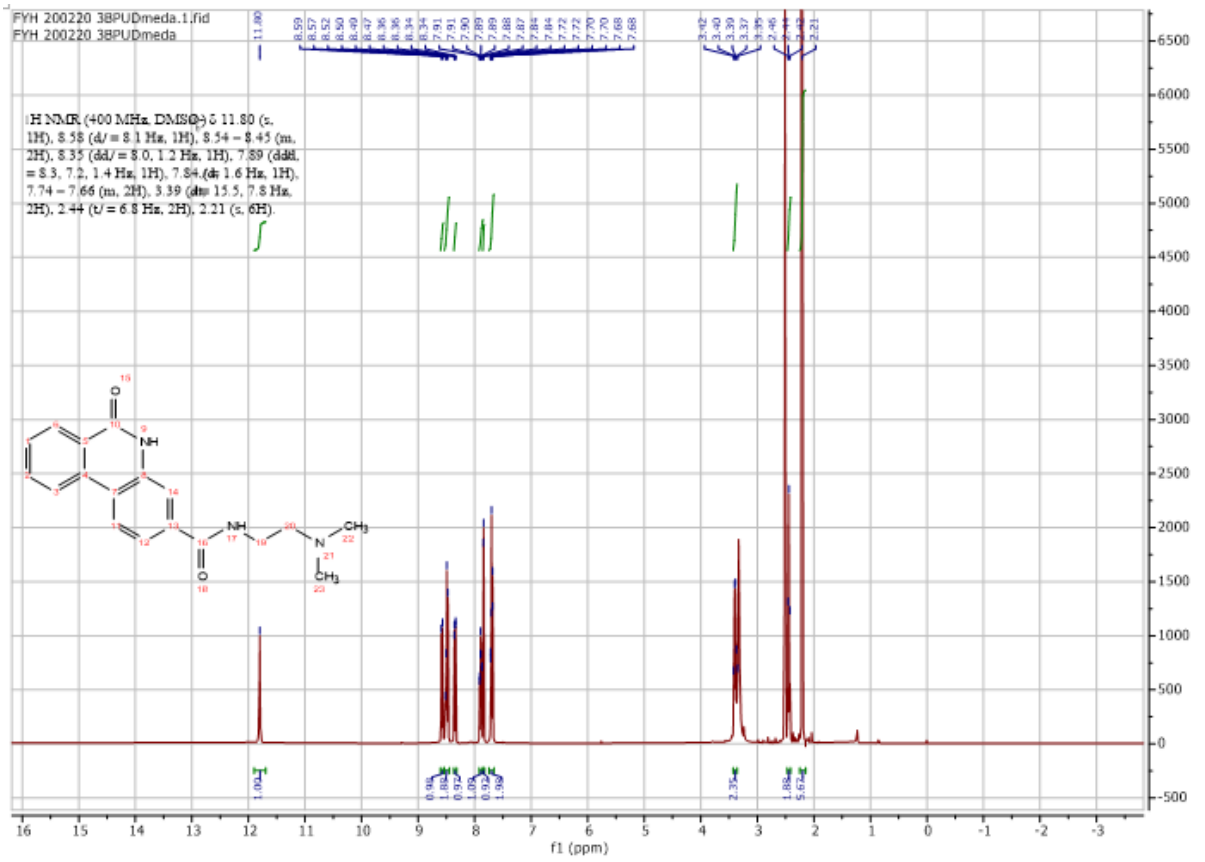
FYH 200220 3BPUDmeda.1.fid
FYH 200220 3BPUDmeda
f1 (ppm)

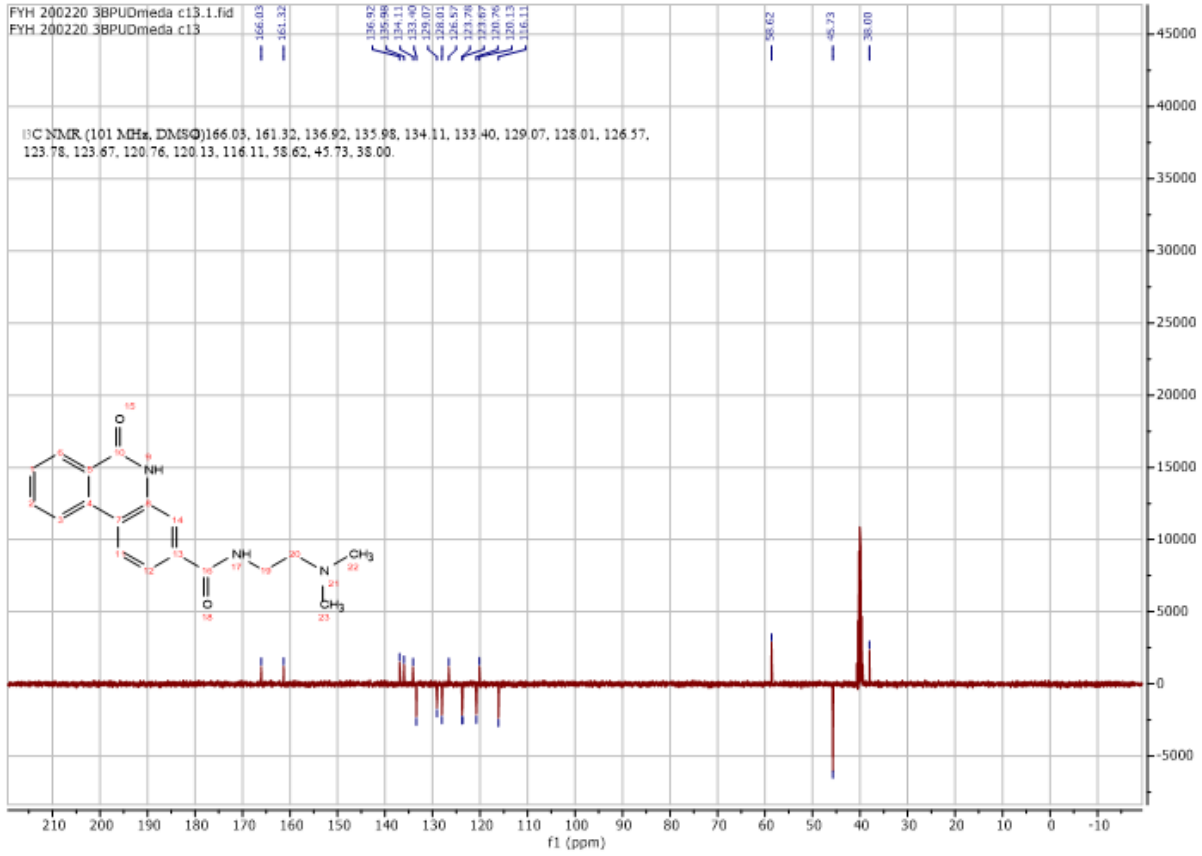
FYH 200220 3BPUDmeda c13.1.fid
FYH 200220 3BPUDmeda c13
f1 (ppm)

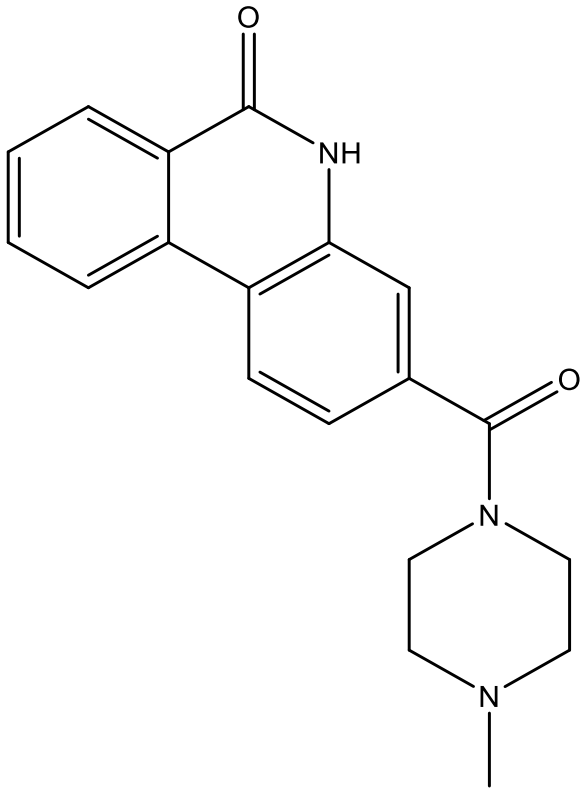

3-(4-methylpiperazine-1-carbonyl)phenanthridin-6(5H)-one (b3)

Using **Synthesis Method d**, 24mg (0.1mmol) **f3** was reacted with 10mg (0.1mmol) 1-methylpiperazine to give 21.3mg **b3** (Yield: 66%) and the product was separated as yellow solid. ^{1}H NMR (300 MHz, DMSO-d_6) δ 11.77 (s, 1H), 8.53 (d, J = 8.1 Hz, 1H), 8.45 (d, J = 8.3 Hz, 1H), 8.34 (dd, J = 8.0, 1.5 Hz, 1H), 7.88 (ddd, J = 8.3, 7.1, 1.5 Hz, 1H), 7.74 – 7.63 (m, 1H), 7.37 (d, J = 1.6 Hz, 1H), 7.25 (dd, J = 8.2, 1.7 Hz, 1H), 3.61 (s, 4H), 2.34 (s, 4H), 2.21 (s, 3H). ^{13}C NMR (75 MHz, DMSO) δ 168.6, 161.3, 137.2, 136.9, 134.1, 133.5, 128.9, 128.0, 126.4, 124.0, 123.4, 121.1, 118.9, 115.1, 55.0, 47.4, 46.1, 41.3. HRMS m/z (ESI+, M+H): Calcd for C19H19N3O2: 322.1550, (ESI+, M+H) found: 322.1552

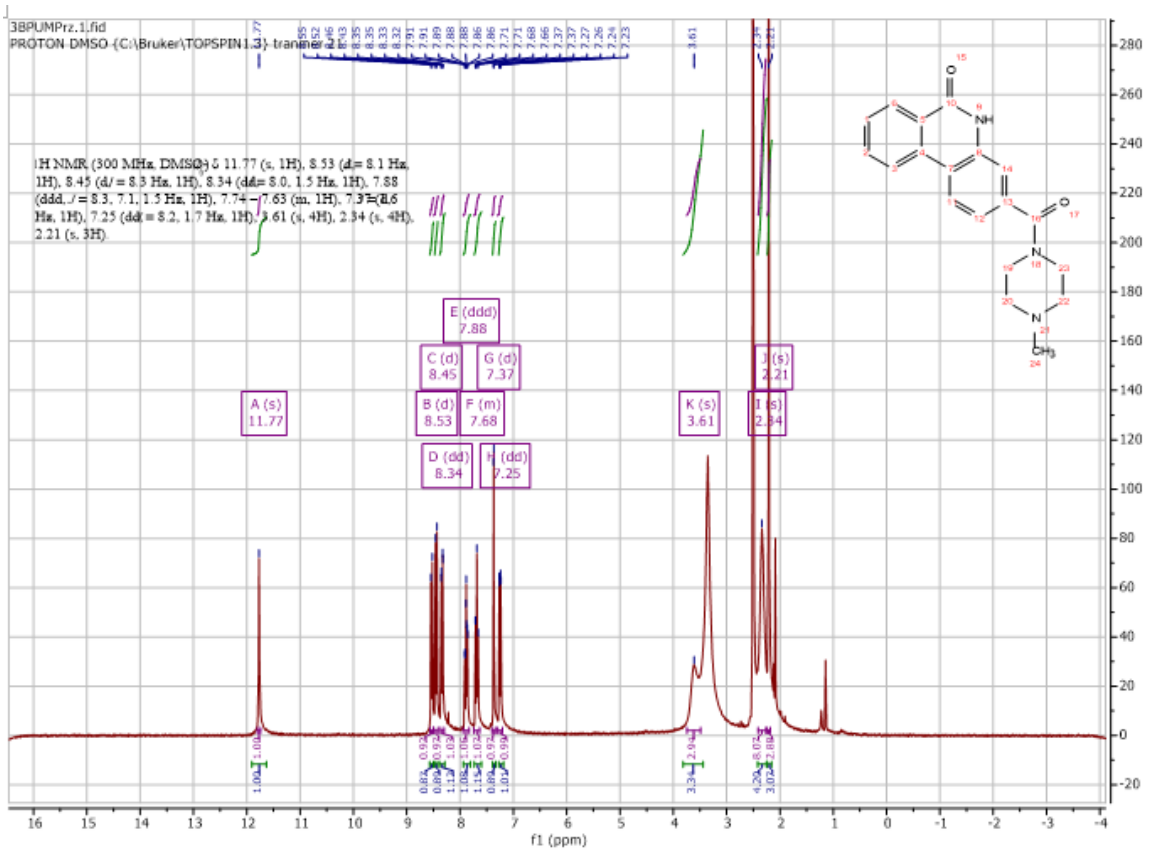
3BPUMPrz.1.fid
PROTON DMSO {C:\Bruker\TOPSPIN1.3} tranmer 21
1H NMR (300 MHz, DMSO) δ 11.77 (s, 1H), 8.53 (d, J = 8.1 Hz, 1H), 8.45 (d, J = 8.3 Hz, 1H), 8.34 (dd, J = 8.0, 1.5 Hz, 1H), 7.88 (ddd, J = 8.3, 7.1, 1.5 Hz, 1H), 7.74 – 7.63 (m, 1H), 7.37 (d, J = 8.6 Hz, 1H), 7.25 (dd, J = 8.2, 1.7 Hz, 1H), 3.61 (s, 4H), 2.34 (s, 4H), 2.21 (s, 3H).
A (s) 11.77
B (d) 8.53
C (d) 8.45
D (dd) 8.34
E (ddd) 7.88
F (m) 7.68
G (d) 7.37
H (dd) 7.25
K (s) 3.61
L (s) 2.34
J (s) 2.21
f1 (ppm)

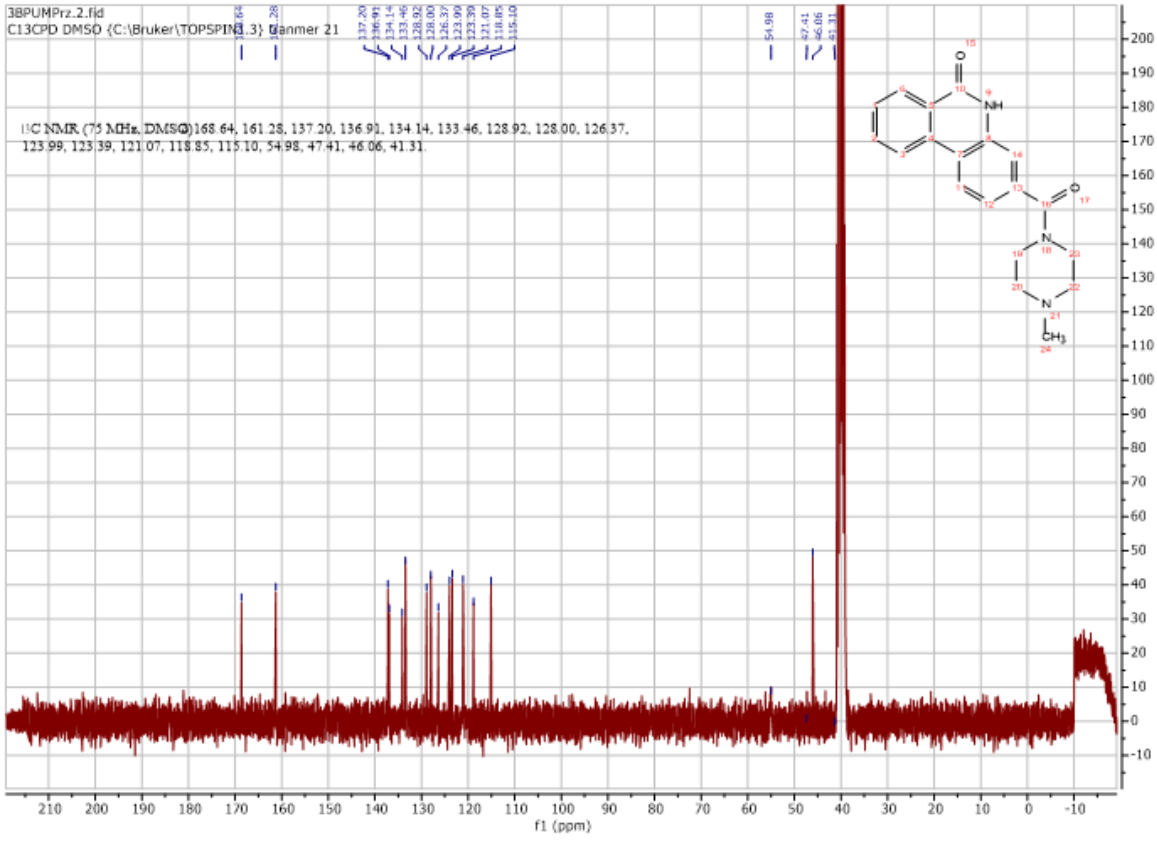
3BPUMPrz.2.fid
C13CPD DMSO {C:\Bruker\TOPSPIN1.3} tranmer 21
13C NMR (75 MHz, DMSO) 168.64, 161.28, 137.20, 136.91, 134.14, 133.46, 128.92, 128.00, 126.37, 123.99, 123.39, 121.07, 118.85, 115.10, 54.98, 47.41, 46.06, 41.31.
f1 (ppm)

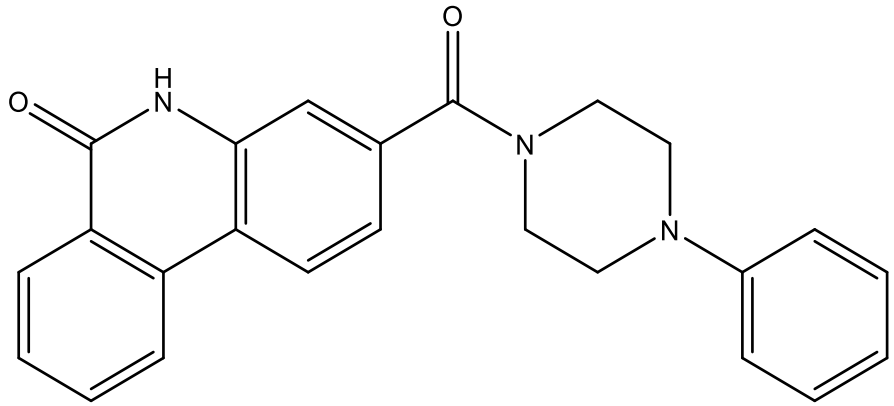

3-(4-phenylpiperazine-1-carbonyl)phenanthridin-6(5*H*)-one (b4)

Using **Synthesis Method d**, 24mg (0.1mmol) **f3** was reacted with 16mg (0.1mmol) 1-phenylpiperazine to give 27.6mg **b4** (Yield: 72%) and the product was separated as yellow solid. ^{1}H NMR (400 MHz, DMSO-d_6) δ 11.79 (s, 1H), 8.56 (d, *J* = 8.2 Hz, 1H), 8.48 (d, *J* = 8.3 Hz, 1H), 8.35 (dd, *J* = 8.0, 1.2 Hz, 1H), 7.90 (td, *J* = 8.3, 7.8, 1.4 Hz, 1H), 7.74 – 7.65 (m, 1H), 7.42 (d, *J* = 1.6 Hz, 1H), 7.32 (dd, *J* = 8.2, 1.6 Hz, 1H), 7.28 – 7.20 (m, 2H), 7.01 – 6.94 (m, 2H), 6.82 (t, *J* = 7.3 Hz, 1H), 3.92 – 3.43 (m, 4H), 3.23 – 3.15 (m, 4H). ^{13}C NMR (101 MHz, DMSO) δ 168.7, 161.3, 151.2, 137.0, 137.0, 134.2, 133.5, 129.5, 129.0, 128.0, 126.4, 124.0, 123.4, 121.2, 120.0, 119.0, 116.4, 115.3, 73.6, 61.9. HRMS m/z (ESI-, M-H): Calcd for C24H21N3O2: 382.1550, (ESI-, M-H) found: 382.1552

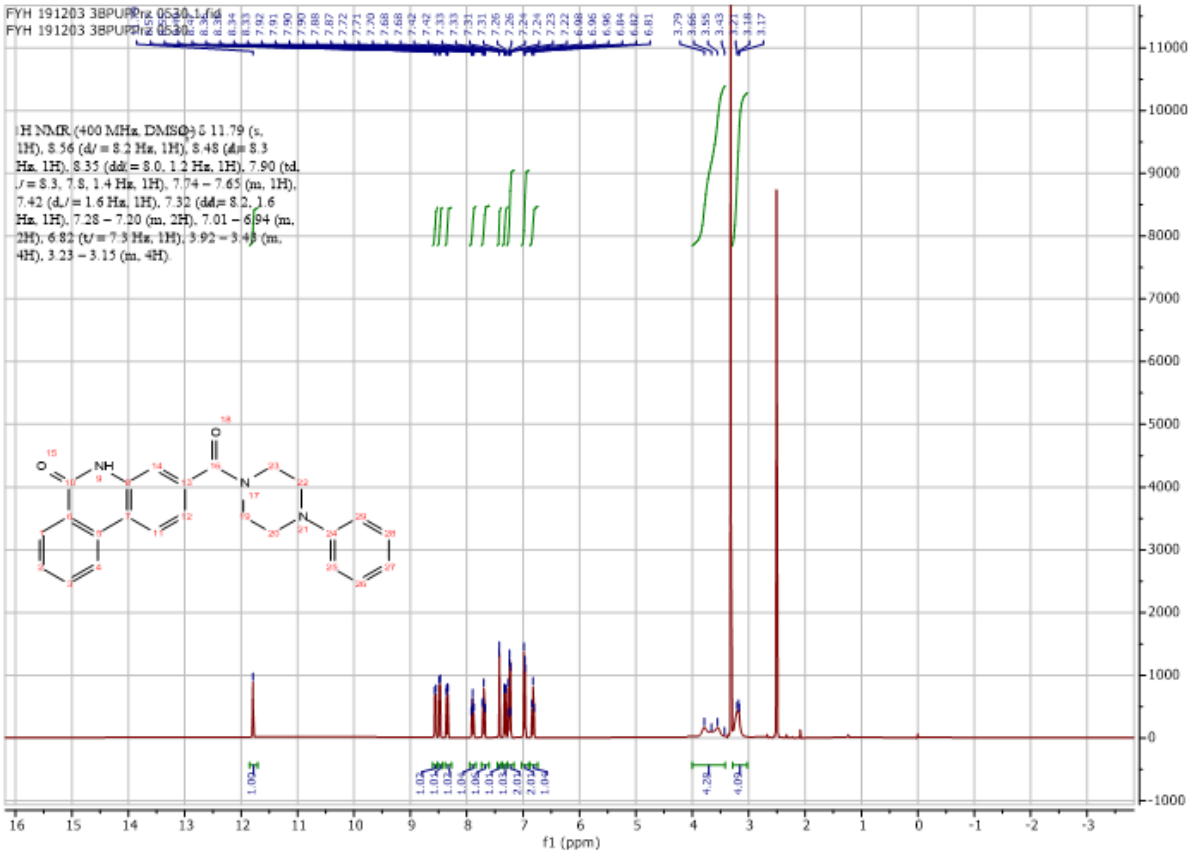
FYH 191203 3BPUPPrz 0530 1.fid
FYH 191203 3BPUPPrz 0530
¹H NMR (400 MHz, DMSO-d6) δ 11.79 (s, 1H), 8.56 (d, J = 8.2 Hz, 1H), 8.48 (d, J = 8.3 Hz, 1H), 8.35 (dd, J = 8.0, 1.2 Hz, 1H), 7.90 (td, J = 8.3, 7.8, 1.4 Hz, 1H), 7.74 – 7.65 (m, 1H), 7.42 (d, J = 1.6 Hz, 1H), 7.32 (dd, J = 8.2, 1.6 Hz, 1H), 7.28 – 7.20 (m, 2H), 7.01 – 6.94 (m, 2H), 6.82 (t, J = 7.3 Hz, 1H), 3.92 – 3.43 (m, 4H), 3.23 – 3.15 (m, 4H).
f1 (ppm)

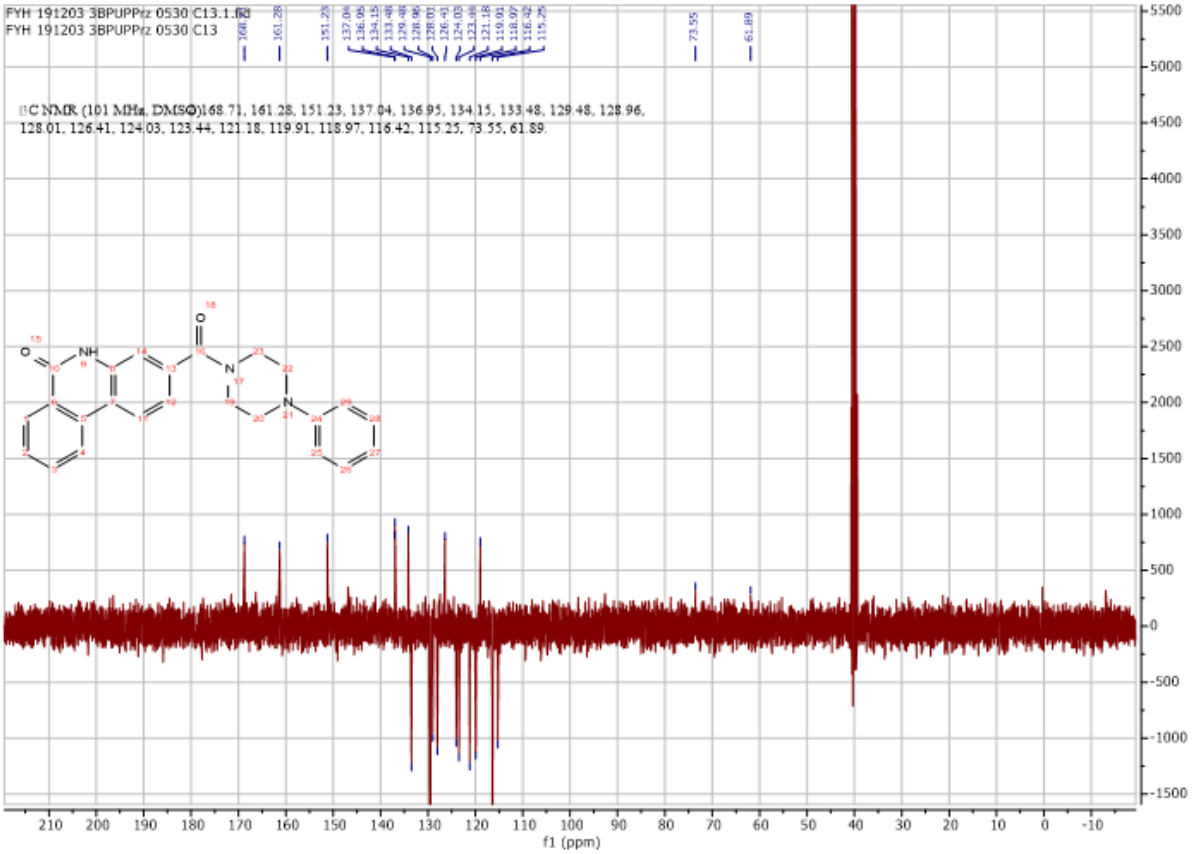
FYH 191203 3BPUPPrz 0530 C13 1.fid
FYH 191203 3BPUPPrz 0530 C13
¹³C NMR (101 MHz, DMSO-d6) δ 168.71, 161.28, 151.23, 137.04, 136.95, 134.15, 133.48, 129.48, 128.96, 128.01, 126.41, 124.03, 123.44, 121.18, 119.91, 118.97, 116.42, 115.25, 73.55, 61.89.
f1 (ppm)

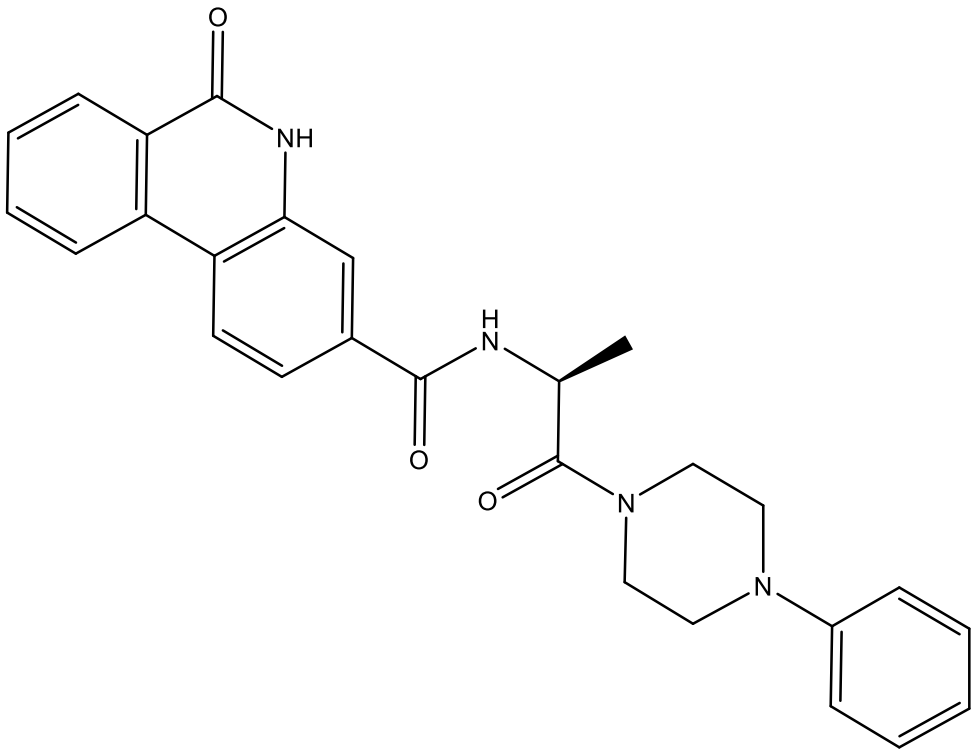

(*S*)-6-oxo-N-(1-oxo-1-(4-phenylpiperazin-1-yl)propan-2-yl)-5,6-dihydrophenanthridine-3-carboxamide (b5)

Using **Synthesis Method d**, 24mg (0.1mmol) **f3** was reacted with 23.5mg (0.1mmol) **f16** to give 31.3mg **b5** (Yield: 69%) and the product was separated as yellow solid. ^{1}H NMR (300 MHz, DMSO-d_6) δ 11.80 (s, 1H), 8.81 (d, *J* = 7.5 Hz, 1H), 8.58 (d, *J* = 8.2 Hz, 1H), 8.48 (d, *J* = 8.5 Hz, 1H), 8.34 (dd, *J* = 7.9, 1.4 Hz, 1H), 7.91 (d, 1H), 7.85 (d, *J* = 1.7 Hz, 1H), 7.78 (dd, *J* = 8.4, 1.7 Hz, 1H), 7.70 (t, *J* = 7.5 Hz, 1H), 7.22 (t, 2H), 6.96 (d, *J* = 8.1 Hz, 2H), 6.81 (t, *J* = 7.2 Hz, 1H), 5.03 (q, *J* = 7.1 Hz, 1H), 3.66 (m, 4H), 3.17 (m, 4H), 1.35 (d, *J* = 6.9 Hz, 3H). ^{13}C NMR (75 MHz, DMSO) δ 170.7, 165.7, 161.3, 151.2, 136.9, 135.3, 134.1, 133.4, 129.5, 129.1, 128.0, 126.6, 123.8, 123.7, 121.1, 120.3, 119.8, 116.3, 116.3, 49.3, 48.8, 45.7, 45.3, 41.9, 17.9. HRMS m/z (ESI-, M-H): Calcd for C27H26N4O3: 453.1932, (ESI-, M-H) found: 453.1926

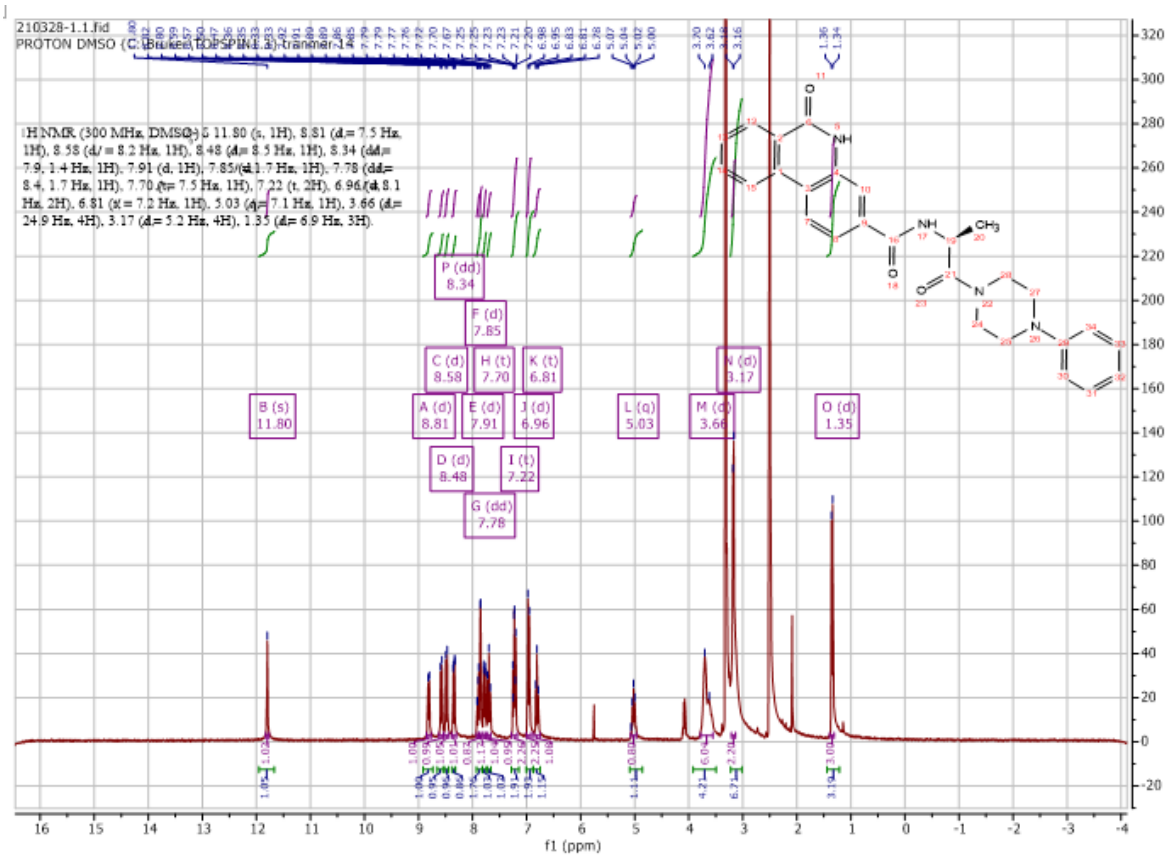
210328-1.1.fid
PROTON DMSO {C:\Bruker\TOPSPIN4.1.3}-tranmer-14
1H NMR (300 MHz, DMSO) δ 11.80 (s, 1H), 8.81 (d, J = 7.5 Hz, 1H), 8.58 (d, J = 8.2 Hz, 1H), 8.48 (d, J = 8.5 Hz, 1H), 8.34 (dd, J = 7.9, 1.4 Hz, 1H), 7.91 (d, 1H), 7.85 (d, J = 1.7 Hz, 1H), 7.78 (dd, J = 8.4, 1.7 Hz, 1H), 7.70 (t, J = 7.5 Hz, 1H), 7.22 (t, 2H), 6.96 (d, J = 8.1 Hz, 2H), 6.81 (t, J = 7.2 Hz, 1H), 5.03 (q, J = 7.1 Hz, 1H), 3.66 (d, J = 24.9 Hz, 4H), 3.17 (d, J = 5.2 Hz, 4H), 1.35 (d, J = 6.9 Hz, 3H).
P (dd) 8.34
F (d) 7.85
C (d) 8.58
H (t) 7.70
K (t) 6.81
N (d) 3.17
B (s) 11.80
A (d) 8.81
E (d) 7.91
J (d) 6.96
L (q) 5.03
M (d) 3.66
O (d) 1.35
D (d) 8.48
I (t) 7.22
G (dd) 7.78
f1 (ppm)

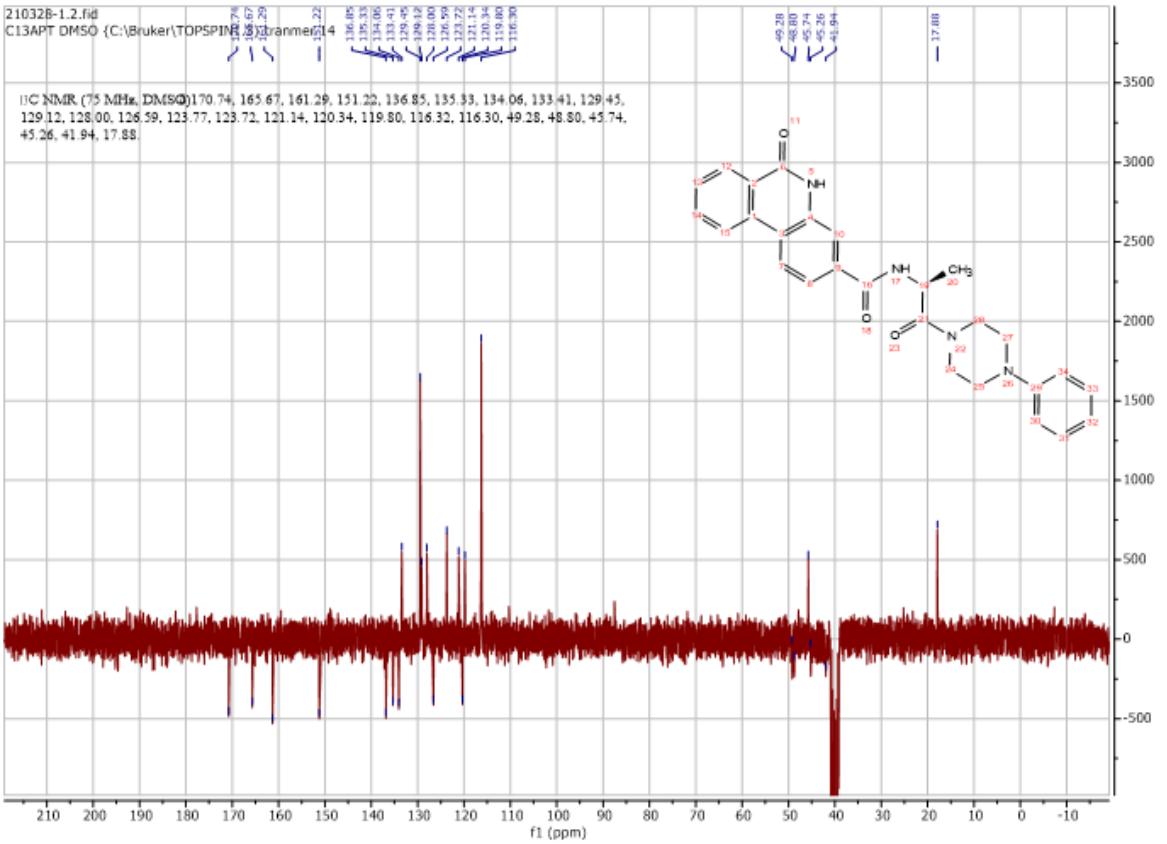
210328-1.2.fid
C13APT DMSO {C:\Bruker\TOPSPIN4.1.3}-tranmer-14
13C NMR (75 MHz, DMSO) 170.74, 165.67, 161.29, 151.22, 136.85, 135.33, 134.06, 133.41, 129.45, 129.12, 128.00, 126.59, 123.77, 123.72, 121.14, 120.34, 119.80, 116.32, 116.30, 49.28, 48.80, 45.74, 45.26, 41.94, 17.88.
f1 (ppm)

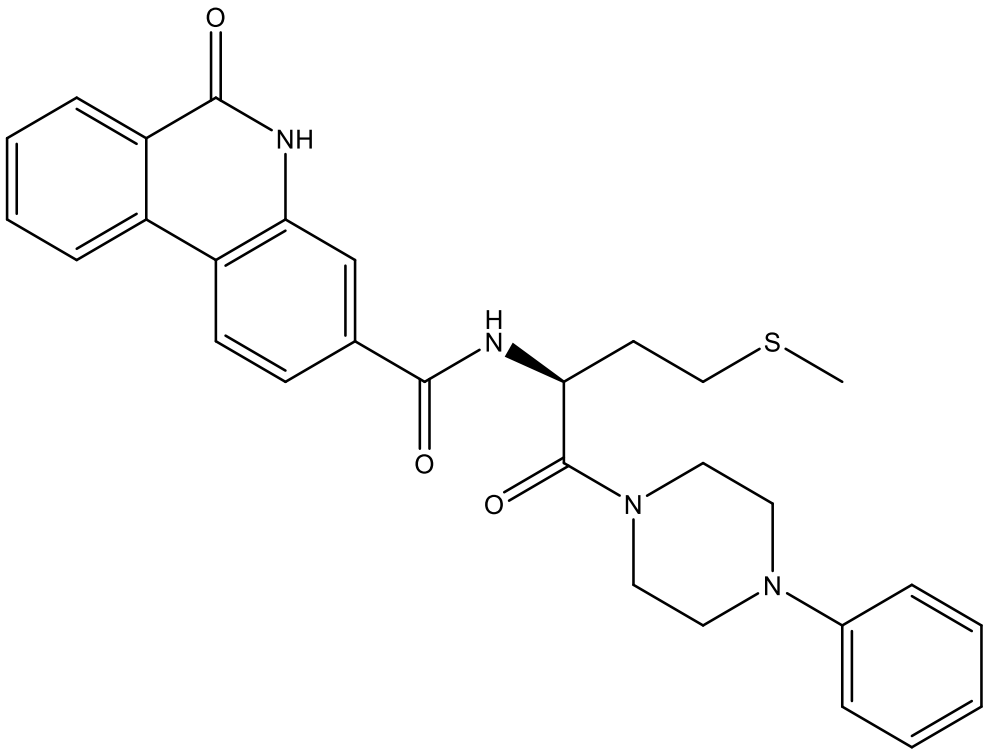

(*S*)-N-(4-(methylthio)-1-oxo-1-(4-phenylpiperazin-1-yl)butan-2-yl)-6-oxo-5,6-dihydrophenanthridine-3-carboxamide (b6)

Using **Synthesis Method d**, 24mg (0.1mmol) **f3** was reacted with 27.5mg (0.1mmol) **f17** to give 34.3mg **b6** (Yield: 67%) and the product was separated as yellow solid. ^{1}H NMR (300 MHz, DMSO-d_6) δ 11.80 (s, 1H), 8.86 (d, J = 7.9 Hz, 1H), 8.58 (d, J = 8.2 Hz, 1H), 8.48 (d, J = 8.5 Hz, 1H), 8.34 (dd, J = 8.0, 1.4 Hz, 1H), 7.93 – 7.84 (m, 2H), 7.79 (dd, J = 8.4, 1.7 Hz, 1H), 7.70 (t, 1H), 7.22 (t, 2H), 6.97 (t, 2H), 6.81 (t, J = 7.2 Hz, 1H), 5.12 (m, 1H), 3.83 – 3.52 (m, 4H), 3.18 (dt, J = 9.8, 4.7 Hz, 4H), 2.58 (m, 2H), 2.09 (m, 5H). HRMS m/z (ESI+, M+H): Calcd for C29H30N4O3S: 515.2111, (ESI+, M+H) found: 515.2124

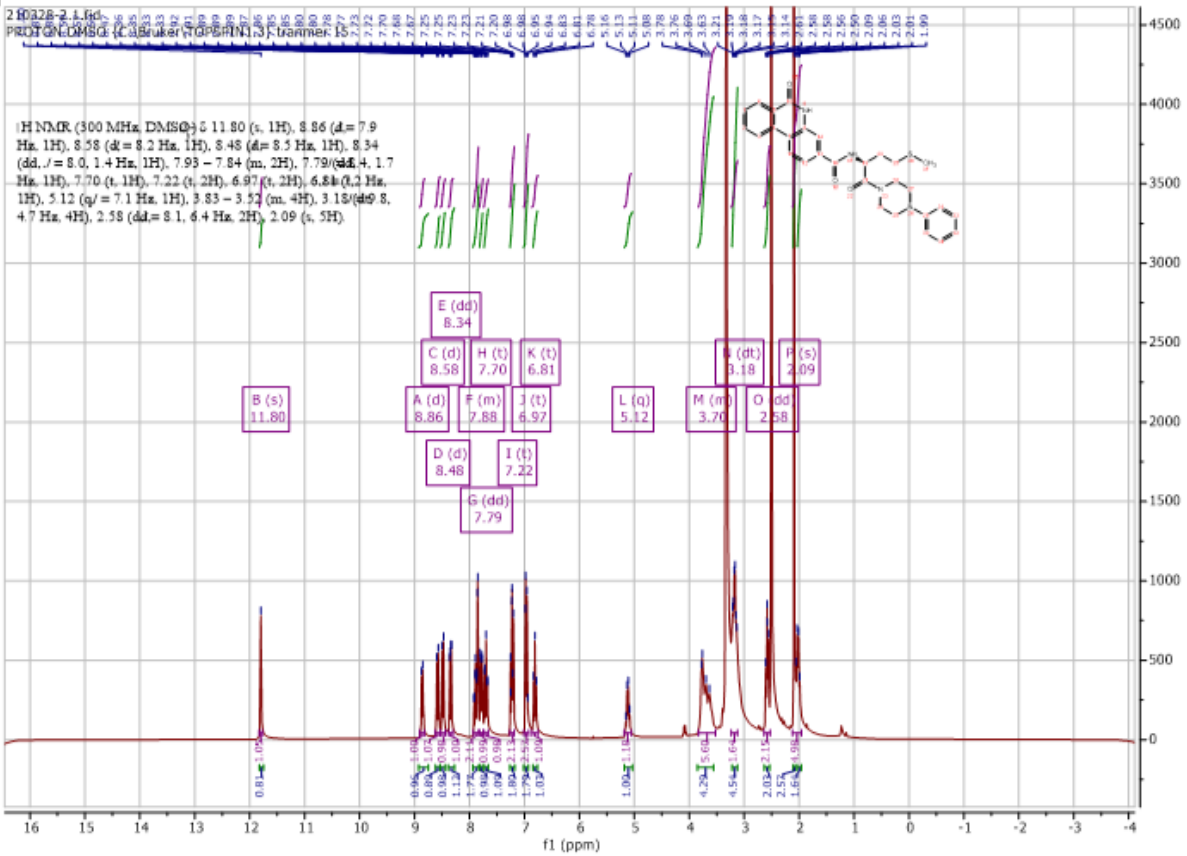
210328-2.1.fid
PROTON DMSO (C:\Bruker\TOPSPIN4.1.3) tranmer 15
¹H NMR (300 MHz, DMSO) δ 11.80 (s, 1H), 8.86 (d, J = 7.9 Hz, 1H), 8.58 (d, J = 8.2 Hz, 1H), 8.48 (d, J = 8.5 Hz, 1H), 8.34 (dd, J = 8.0, 1.4 Hz, 1H), 7.93 – 7.84 (m, 2H), 7.79 (dd, J = 8.4, 1.7 Hz, 1H), 7.70 (t, J = 7.8 Hz, 1H), 7.22 (t, J = 7.6 Hz, 2H), 6.97 (t, J = 7.2 Hz, 2H), 6.81 (d, J = 8.2 Hz, 1H), 5.12 (q, J = 7.1 Hz, 1H), 3.83 – 3.52 (m, 4H), 3.18 (dt, J = 9.8, 4.7 Hz, 4H), 2.58 (dd, J = 8.1, 6.4 Hz, 2H), 2.09 (s, 5H).
E (dd) 8.34
C (d) 8.58
H (t) 7.70
K (t) 6.81
B (s) 11.80
A (d) 8.86
F (m) 7.88
J (t) 6.97
L (q) 5.12
M (m) 3.70
O (dd) 2.58
D (d) 8.48
I (t) 7.22
G (dd) 7.79
f1 (ppm)

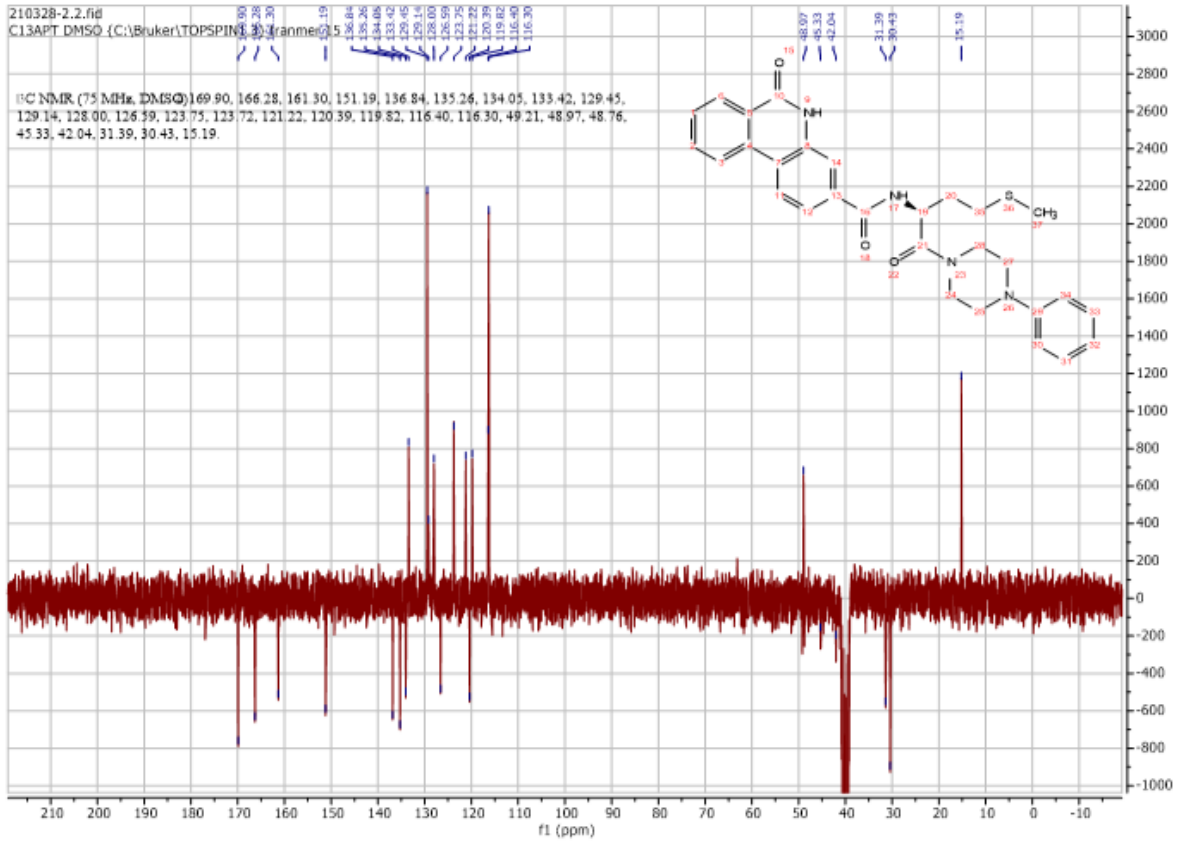
210328-2.2.fid
C13APT DMSO (C:\Bruker\TOPSPIN4.1.3) tranmer 15
¹³C NMR (75 MHz, DMSO) 169.90, 166.28, 161.30, 151.19, 136.84, 135.26, 134.05, 133.42, 129.45, 129.14, 128.00, 126.59, 123.75, 123.72, 121.22, 120.39, 119.82, 116.40, 116.30, 49.21, 48.97, 48.76, 45.33, 42.04, 31.39, 30.43, 15.19.
f1 (ppm)

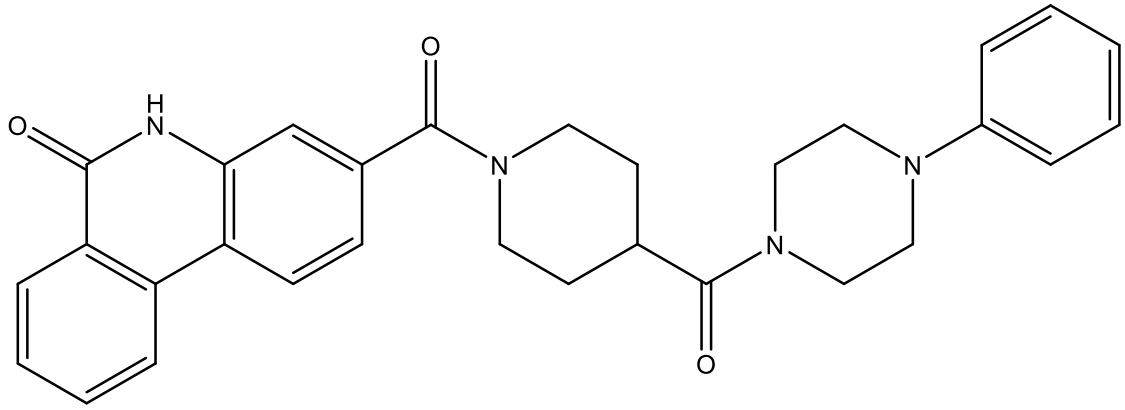

3-(4-(4-phenylpiperazine-1-carbonyl)piperidine-1-carbonyl)phenanthridin-6(5*H*)-one (b7)

Using **Synthesis Method d**, 24mg (0.1mmol) **f3** was reacted with 27.5mg (0.1mmol) **f18** to give 36.1mg **b7** (Yield: 73%) and the product was separated as yellow solid. ^{1}H NMR (400 MHz, DMSO-d_6) δ 11.78 (s, 1H), 8.54 (d, *J* = 8.2 Hz, 1H), 8.46 (d, *J* = 8.2 Hz, 1H), 8.34 (d, *J* = 7.9 Hz, 1H), 7.89 (t, *J* = 7.6 Hz, 1H), 7.69 (t, *J* = 7.5 Hz, 1H), 7.39 (s, 1H), 7.30 – 7.14 (m, 3H), 6.96 (d, *J* = 8.0 Hz, 2H), 6.81 (t, *J* = 7.2 Hz, 1H), 4.50 (s, 1H), 3.66 (d, *J* = 30.2 Hz, 5H), 3.23 – 2.85 (m, 7H), 1.90 – 1.30 (m, 4H). ^{13}C NMR (101 MHz, DMSO) δ 172.7, 168.7, 161.3, 151.3, 137.5, 136.9, 134.2, 133.5, 129.5, 128.9, 128.0, 126.4, 124.1, 123.4, 121.0, 119.8, 118.8, 116.3, 114.8, 49.5, 48.9, 45.1, 41.5, 37.5. HRMS m/z (ESI+, M+Na): Calcd for C30H30N4O3: 517.2216, (ESI+, M+Na) found: 517.2209

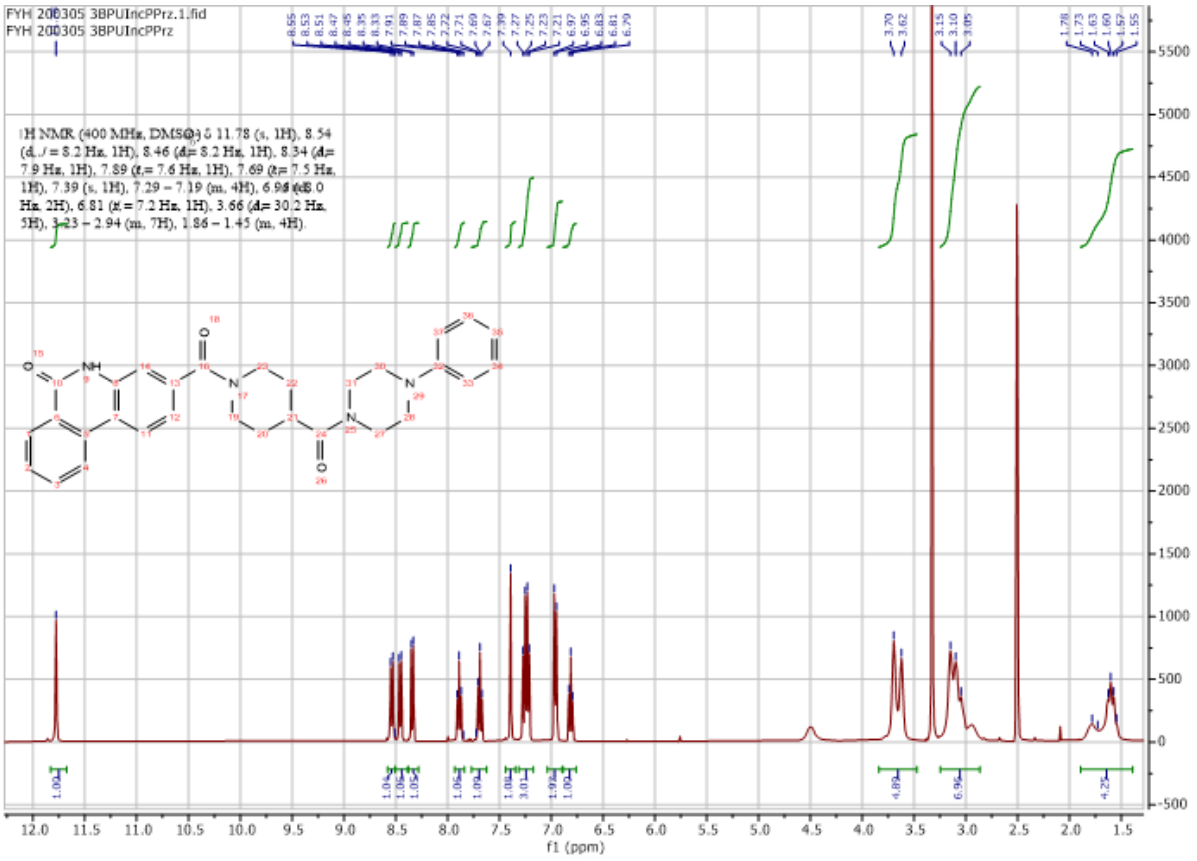
FYH 200305 3BPUIncPPrz.1.fid
FYH 200305 3BPUIncPPrz
f1 (ppm)

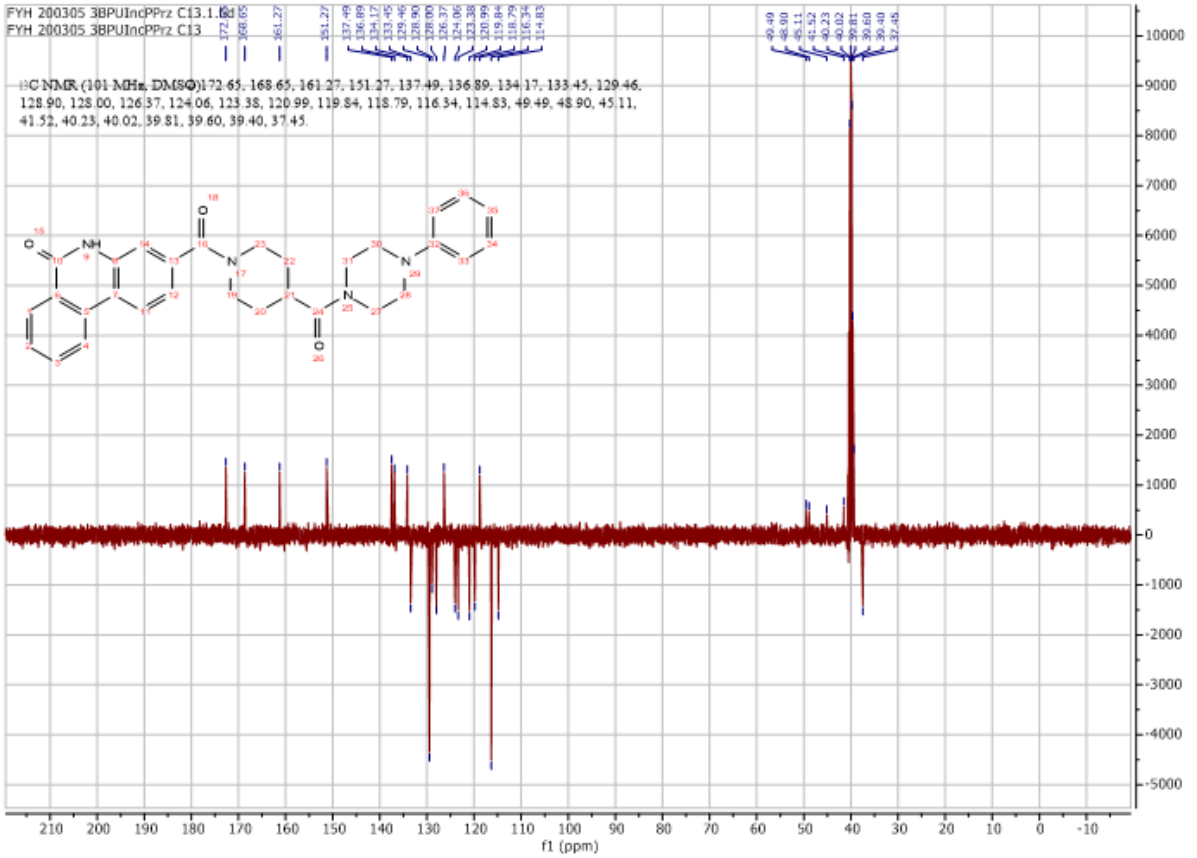
FYH 200305 3BPUIncPPrz C13.1.fid
FYH 200305 3BPUIncPPrz C13
f1 (ppm)

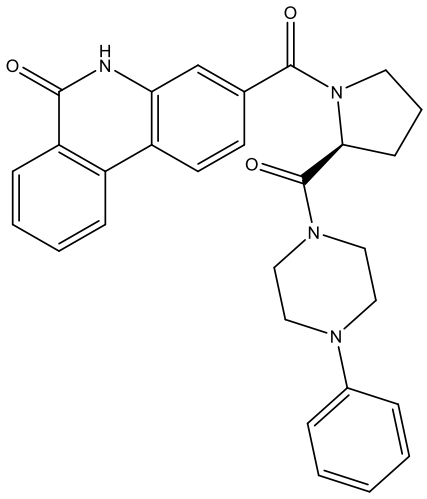

(*S*)-3-(2-(4-phenylpiperazine-1-carbonyl)pyrrolidine-1-carbonyl)phenanthridin-6(5H)-one (b8)

Using **Synthesis Method d**, 24mg (0.1mmol) **f3** was reacted with 26mg (0.1mmol) **f19** to give 28.2mg **b8** (Yield: 59%) and the product was separated as yellow solid. Failed to get clean NMR spectra but the MASS spectra was recognizable. HRMS m/z (ESI+, M+Na): Calcd for C29H28N4O3: 503.2059, (ESI+, M+Na) found: 503.2053

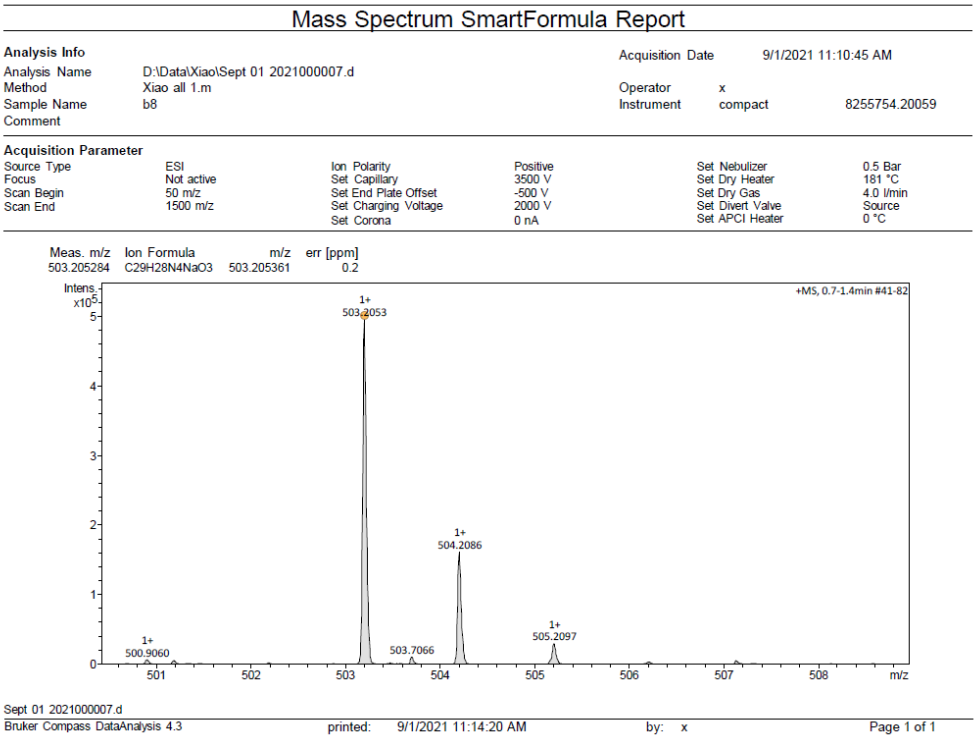

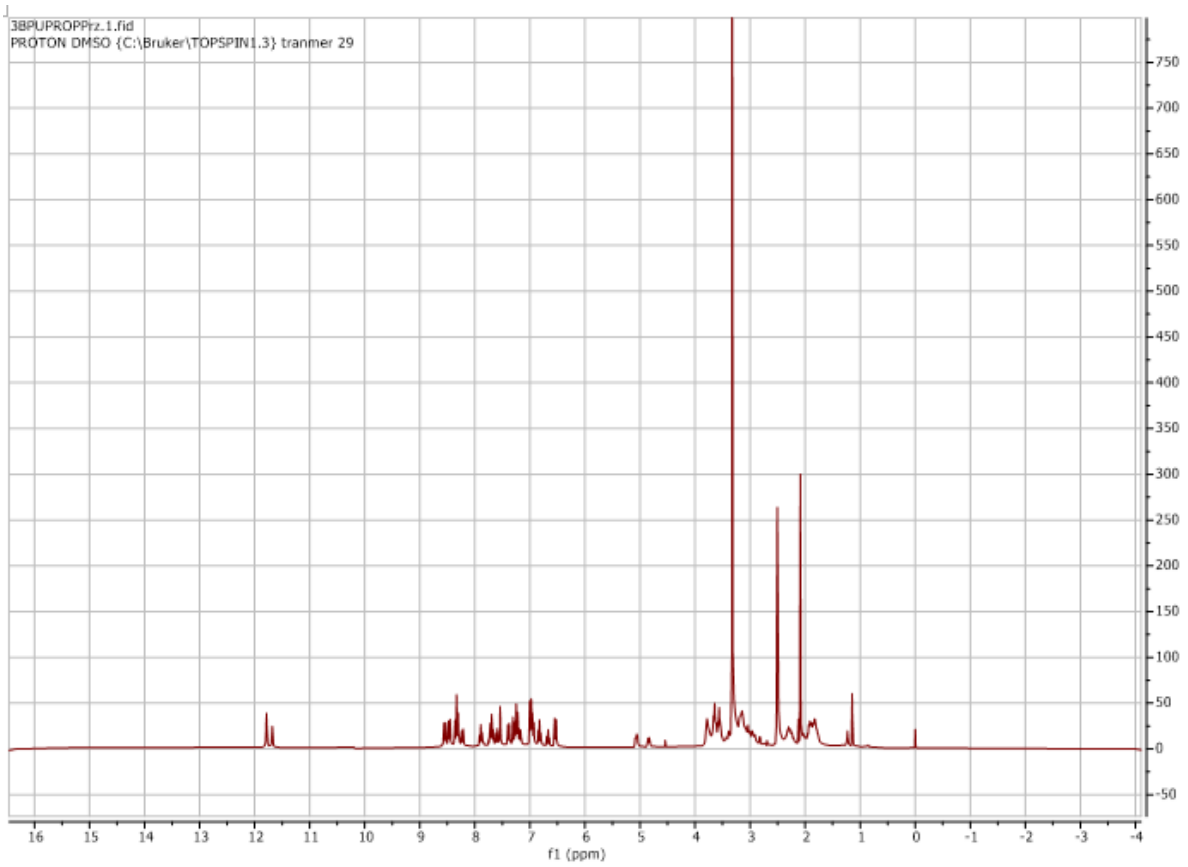
3BPUPROPPrz.1.fid
PROTON DMSO {C:\Bruker\TOPSPIN1.3} tranmer 29
f1 (ppm)

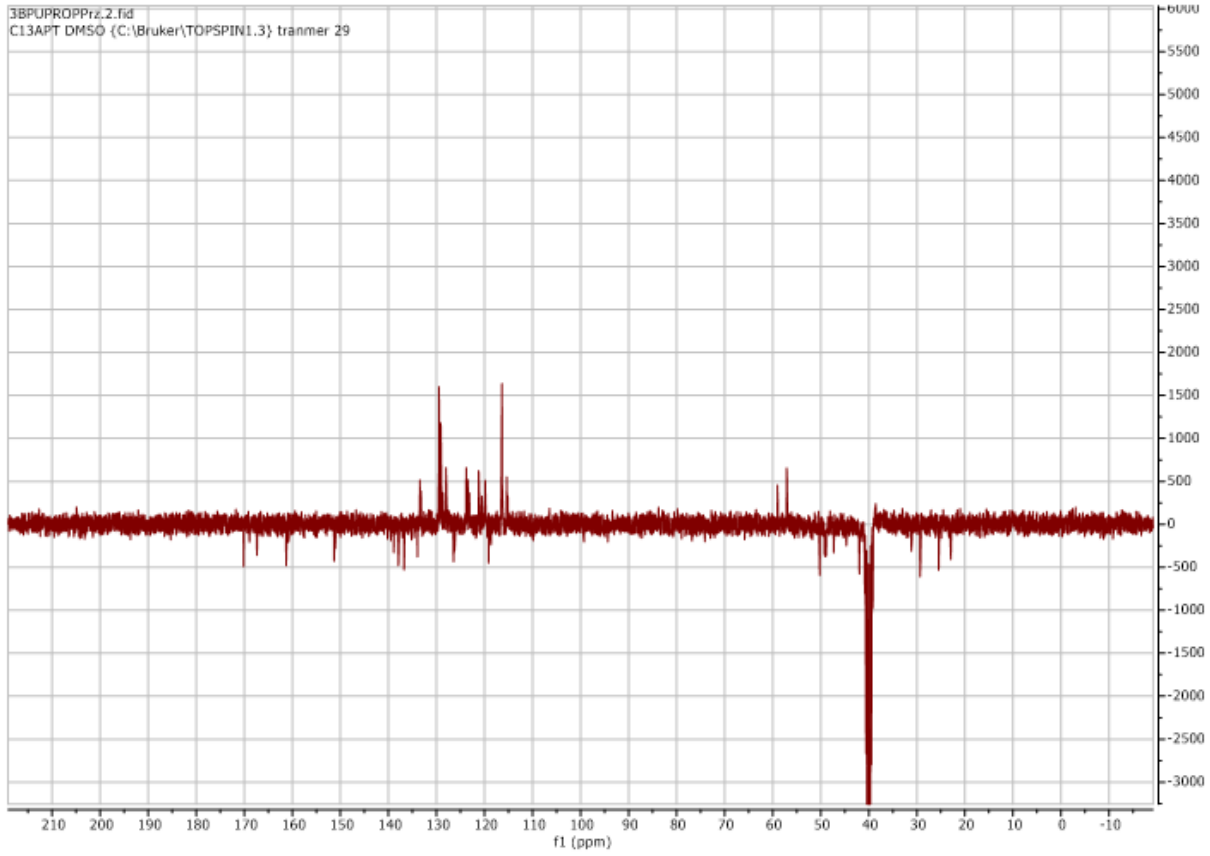
3BPUPROPPrz.2.fid
C13APT DMSO {C:\Bruker\TOPSPIN1.3} tranmer 29
f1 (ppm)

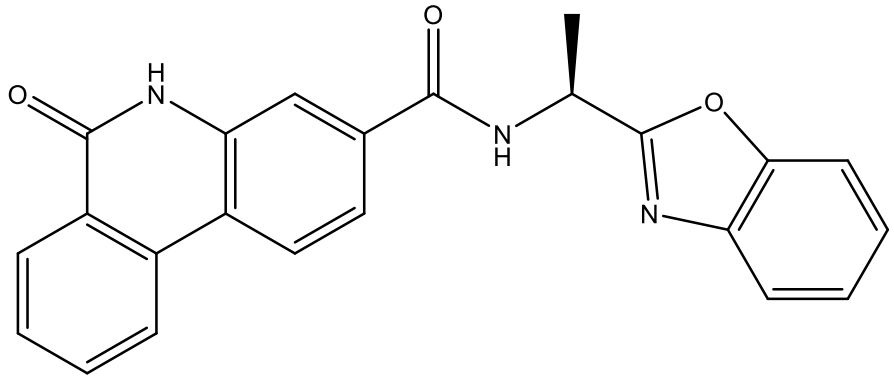

(*S*)-N-(1-(benzo[d]oxazol-2-yl)ethyl)-6-oxo-5,6-dihydrophenanthridine-3-carboxamide (b9)

Using **Synthesis Method d**, 24mg (0.1mmol) **f3** was reacted with 16.4mg (0.1mmol) **f8** to give 35.5mg **b9** (Yield: 93%) and the product was separated as yellow solid. ^{1}H NMR (400 MHz, DMSO-d_6) δ 11.82 (s, 1H), 9.31 (d, J = 7.6 Hz, 1H), 8.60 (d, J = 8.2 Hz, 1H), 8.52 (d, J = 8.4 Hz, 1H), 8.35 (dd, 1H), 7.94 – 7.87 (m, 2H), 7.81 (dd, J = 8.4, 1.8 Hz, 1H), 7.79 – 7.68 (m, 3H), 7.45 – 7.34 (m, 2H), 5.57 – 5.37 (m, 1H), 1.71 (d, J = 7.1 Hz, 3H).^{13}C NMR (101 MHz, DMSO) δ 167.4, 166.0, 161.3, 152.3, 137.0, 135.1, 134.0, 133.4, 129.2, 128.0, 126.7, 125.6, 124.9, 123.9, 123.8, 121.1, 120.5, 120.1, 116.5, 111.3, 100.5, 44.3, 18.8. HRMS m/z (ESI+, M+Na): Calcd for C23H17N3O3: 406.1168, (ESI+, M+Na) found: 406.1162

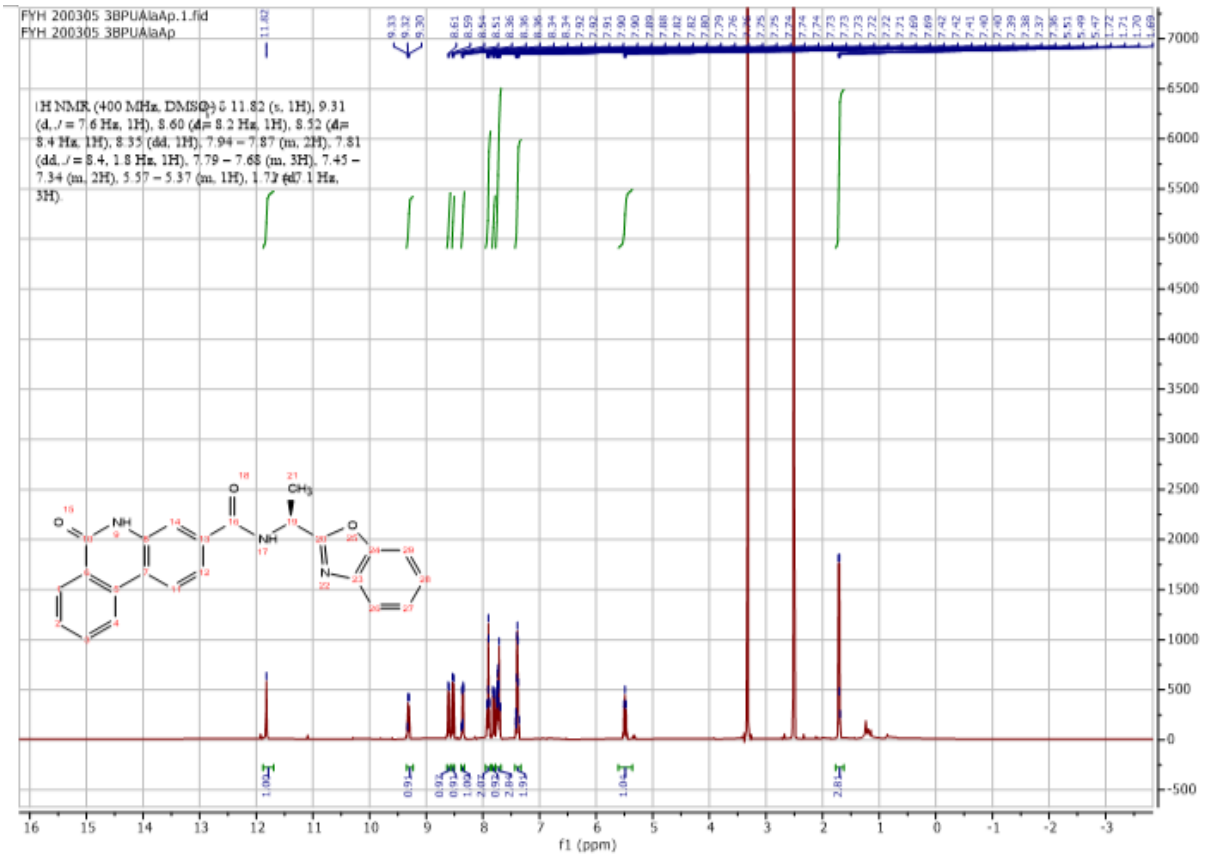

^{1}H NMR (400 MHz, DMSO-d_6) δ 11.82 (s, 1H), 9.31 (d, J = 7.6 Hz, 1H), 8.60 (d, J = 8.2 Hz, 1H), 8.52 (d, J = 8.4 Hz, 1H), 8.35 (dd, 1H), 7.94 – 7.87 (m, 2H), 7.81 (dd, J = 8.4, 1.8 Hz, 1H), 7.79 – 7.68 (m, 3H), 7.45 – 7.34 (m, 2H), 5.57 – 5.37 (m, 1H), 1.72 (d, J = 7.1 Hz, 3H).

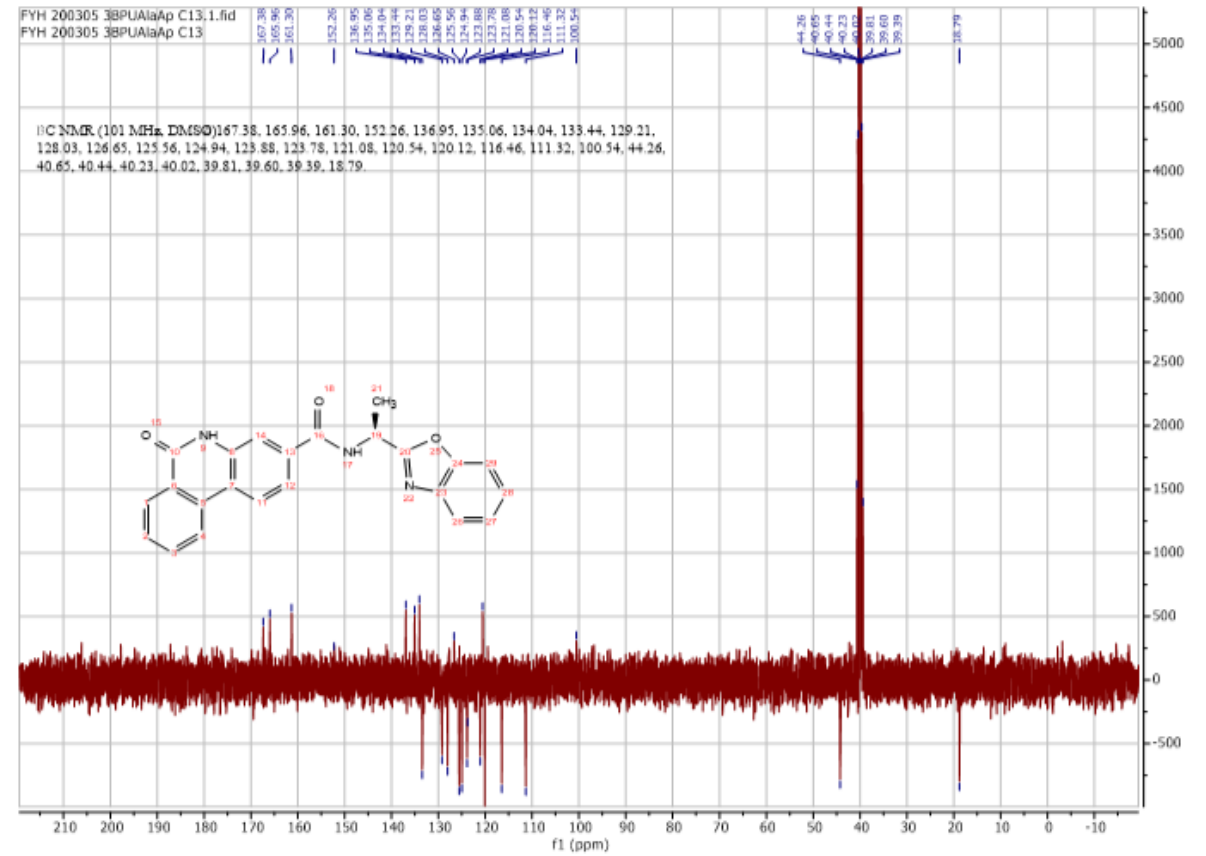

^{13}C NMR (101 MHz, DMSO) 167.38, 165.96, 161.30, 152.26, 136.95, 135.06, 134.04, 133.44, 129.21, 128.03, 126.65, 125.56, 124.94, 123.88, 123.78, 121.08, 120.54, 120.12, 116.46, 111.32, 100.54, 44.26, 40.65, 40.44, 40.23, 40.02, 39.81, 39.60, 39.39, 18.79.

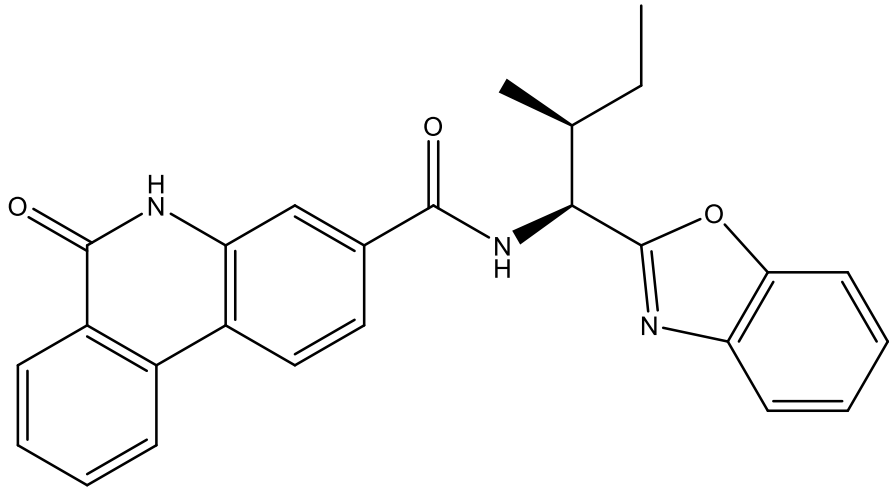

_N_-((1_S_,2_S_)-1-(benzo[d]oxazol-2-yl)-2-methylbutyl)-6-oxo-5,6-dihydrophenanthridine-3-carboxamide (b10)

Using **Synthesis Method d**, 24mg (0.1mmol) **f3** was reacted with 20.5mg (0.1mmol) **f10** to give 34.6mg **b10** (Yield: 81%) and the product was separated as yellow solid. ^{1}H NMR (300 MHz, DMSO-d_6) δ 11.81 (s, 1H), 9.21 (d, J = 8.1 Hz, 1H), 8.59 (d, J = 8.2 Hz, 1H), 8.50 (d, J = 8.5 Hz, 1H), 8.35 (d, J = 7.9 Hz, 1H), 7.94 – 7.85 (m, 2H), 7.80 (d, J = 8.4 Hz, 1H), 7.77 – 7.68 (m, 2H), 7.43 – 7.36 (m, 2H), 5.23 (t, J = 8.2 Hz, 1H), 1.75 – 1.31 (m, 2H), 0.92 (m, 6H). ^{13}C NMR (75 MHz, DMSO) δ 166.7, 166.2, 161.3, 150.4, 141.0, 136.9, 135.2, 134.0, 133.4, 129.2, 128.0, 126.6, 125.6, 125.0, 123.7, 121.3, 120.6, 120.2, 116.5, 115.5, 111.3, 53.0, 37.1, 25.6, 16.1, 11.2. HRMS m/z (ESI+, M+Na): Calcd for C26H23N3O3: 448.1637, (ESI+, M+Na) found: 448.1629

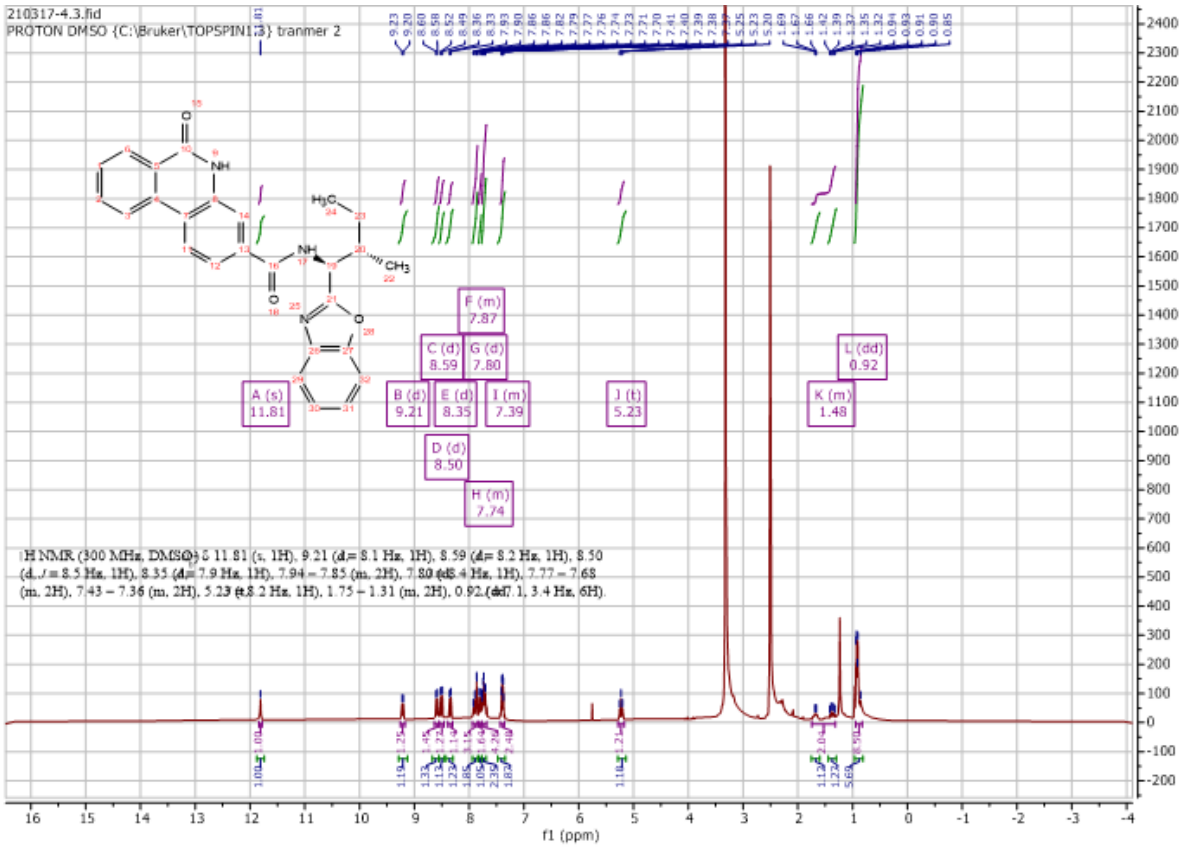

^{1}H NMR (300 MHz, DMSO) δ 11.81 (s, 1H), 9.21 (d, J = 8.1 Hz, 1H), 8.59 (d, J = 8.2 Hz, 1H), 8.50 (d, J = 8.5 Hz, 1H), 8.35 (d, J = 7.9 Hz, 1H), 7.94 – 7.85 (m, 2H), 7.80 (d, J = 8.4 Hz, 1H), 7.77 – 7.68 (m, 2H), 7.43 – 7.36 (m, 2H), 5.23 (t, J = 8.2 Hz, 1H), 1.75 – 1.31 (m, 2H), 0.92 (dd, J = 7.1, 3.4 Hz, 6H).

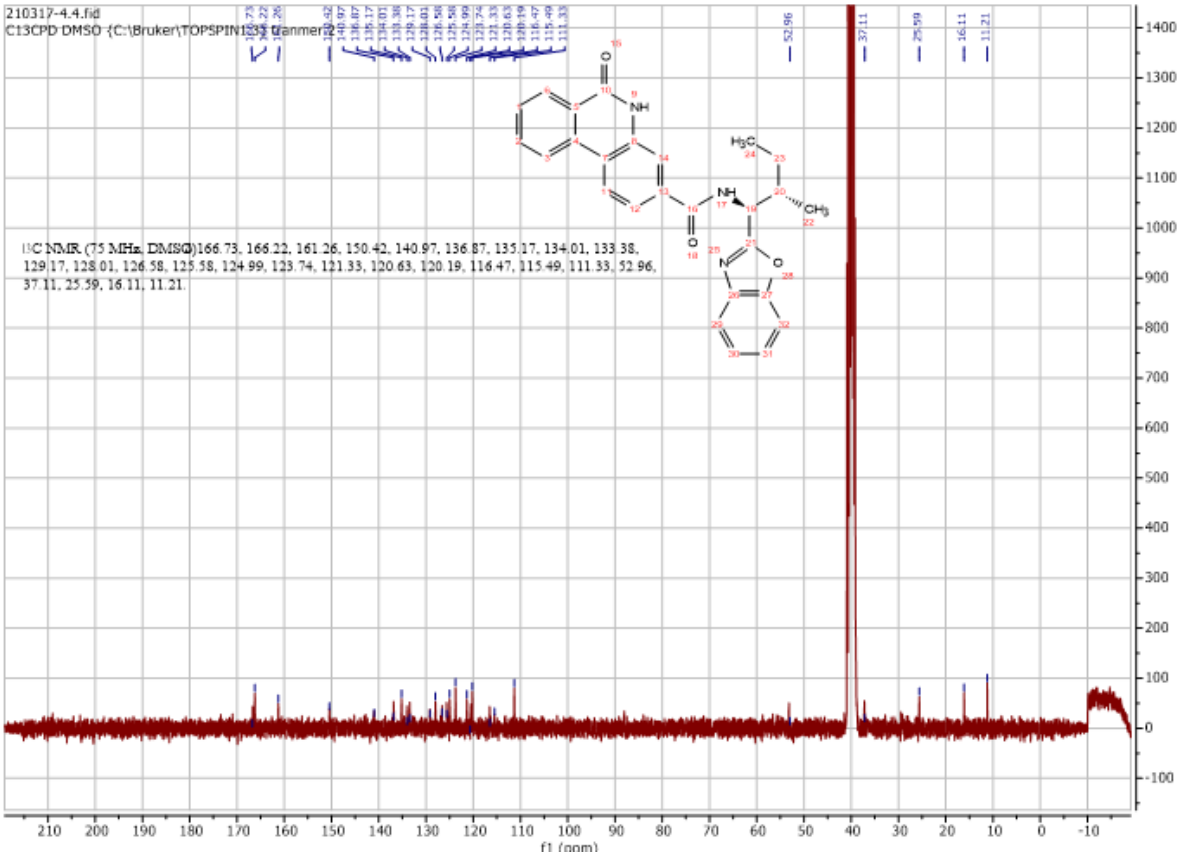

^{13}C NMR (75 MHz, DMSO) δ 166.73, 166.22, 161.26, 150.42, 140.97, 136.87, 135.17, 134.01, 133.38, 129.17, 128.01, 126.58, 125.58, 124.99, 123.74, 121.33, 120.63, 120.19, 116.47, 115.49, 111.33, 52.96, 37.11, 25.59, 16.11, 11.21.

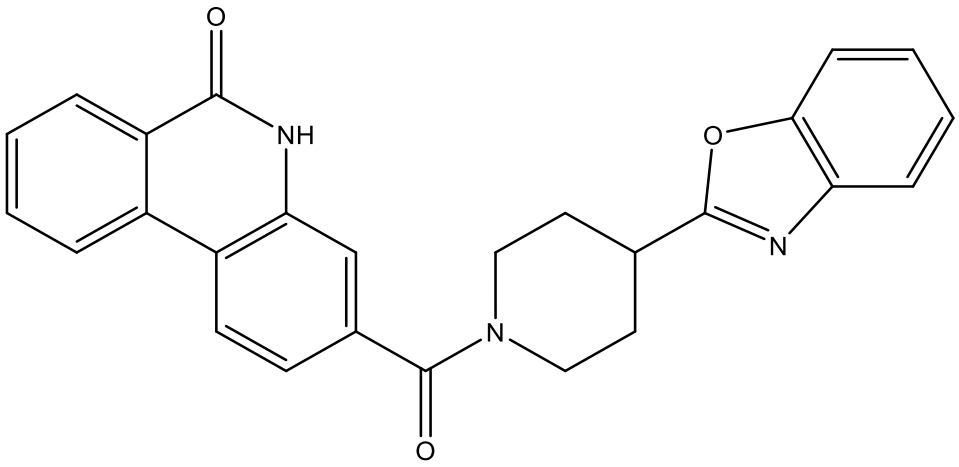

3-(4-(benzo[*d*]oxazol-2-yl)piperidine-1-carbonyl)phenanthridin-6(5*H*)-one (b11)

Using **Synthesis Method d**, 24mg (0.1mmol) **f3** was reacted with 20.3mg (0.1mmol) **f14** to give 32.8mg **b11** (Yield: 78%) and the product was separated as yellow solid. ^{1}H NMR (400 MHz, DMSO-d_6) δ 11.78 (s, 1H), 8.55 (d, *J* = 8.1 Hz, 1H), 8.47 (d, *J* = 8.4 Hz, 1H), 8.35 (dd, *J* = 8.0, 1.2 Hz, 1H), 7.89 (ddd, *J* = 8.3, 7.3, 1.4 Hz, 1H), 7.78 – 7.65 (m, 3H), 7.42 (d, *J* = 1.5 Hz, 1H), 7.41 – 7.33 (m, 2H), 7.31 (dd, *J* = 8.2, 1.6 Hz, 1H), 4.47 – 3.76 (m, 2H), 3.41 (tdt, *J* = 12.8, 8.9, 3.7 Hz, 1H), 3.28 – 3.07 (m, 2H), 2.32 – 2.04 (m, 2H), 1.86 (qd, *J* = 11.5, 4.1 Hz, 2H). ^{13}C NMR (101 MHz, DMSO) δ 168.8, 168.7, 161.3, 150.6, 141.2, 137.4, 136.9, 134.2, 133.5, 128.9, 128.0, 126.4, 125.3, 124.8, 124.1, 123.4, 121.0, 119.9, 118.9, 114.9, 111.1, 51.3, 35.4, 28.7. HRMS m/z (ESI+, M+Na): Calcd for C26H21N3O3: 446.1481, (ESI+, M+Na) found: 446.1475

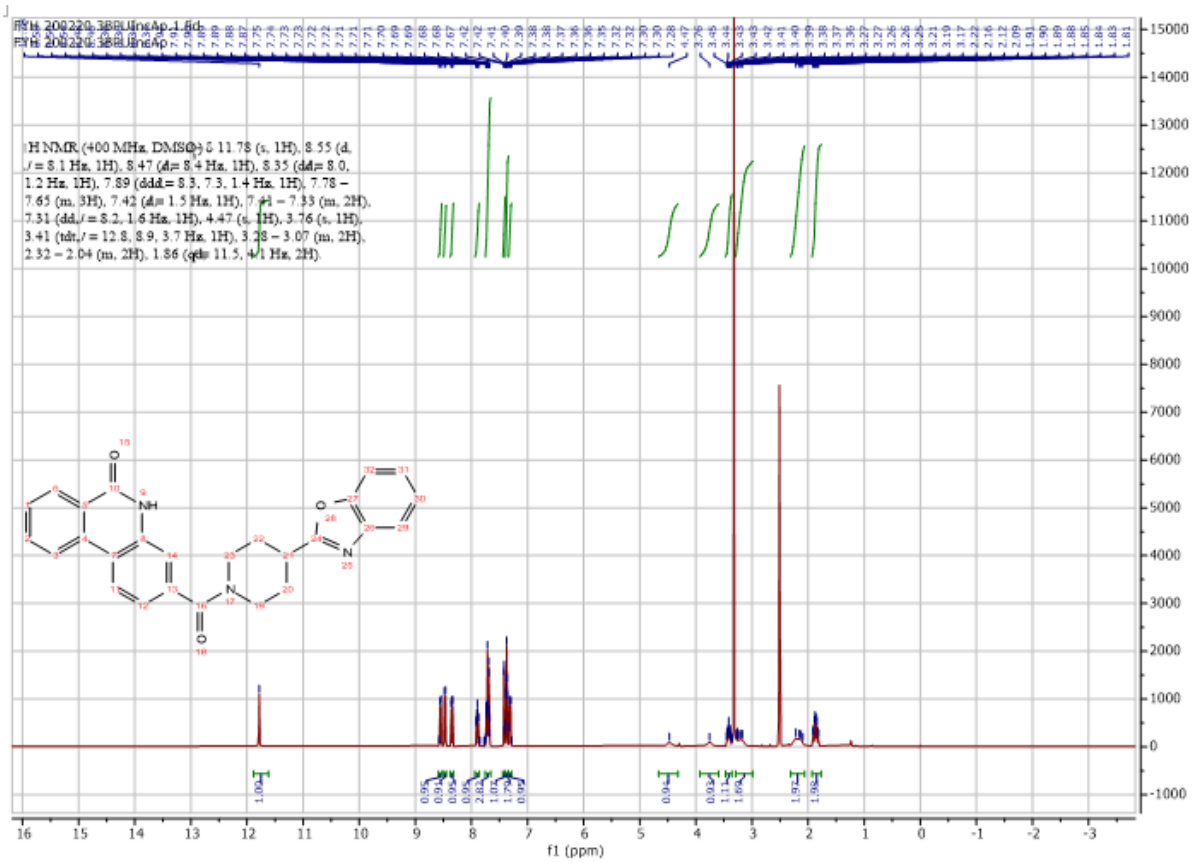
FYH 200220 3BPUIncAp_1.fid
FYH 200220 3BPUIncAp
¹H NMR (400 MHz, DMSO-d6) δ 11.78 (s, 1H), 8.55 (d, J = 8.1 Hz, 1H), 8.47 (d, J = 8.4 Hz, 1H), 8.35 (dd, J = 8.0, 1.2 Hz, 1H), 7.89 (ddd, J = 8.3, 7.3, 1.4 Hz, 1H), 7.78 – 7.65 (m, 3H), 7.42 (d, J = 1.5 Hz, 1H), 7.41 – 7.33 (m, 2H), 7.31 (dd, J = 8.2, 1.6 Hz, 1H), 4.47 (s, 1H), 3.76 (s, 1H), 3.41 (tdt, J = 12.8, 8.9, 3.7 Hz, 1H), 3.28 – 3.07 (m, 2H), 2.32 – 2.04 (m, 2H), 1.86 (qdt, J = 11.5, 4.1 Hz, 2H).
f1 (ppm)

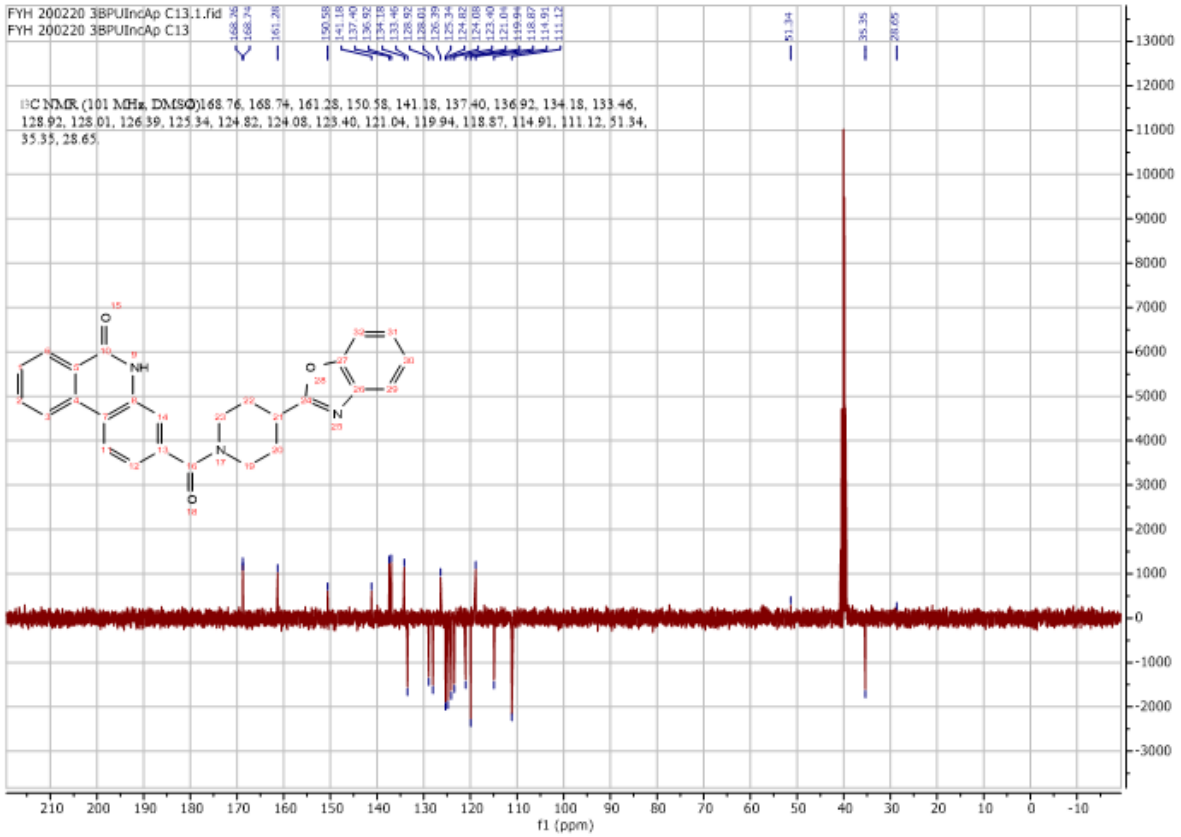
FYH 200220 3BPUIncAp C13.1.fid
FYH 200220 3BPUIncAp C13
¹³C NMR (101 MHz, DMSO-d6) δ 168.76, 168.74, 161.28, 150.58, 141.18, 137.40, 136.92, 134.18, 133.46, 128.92, 128.01, 126.39, 125.34, 124.82, 124.08, 123.40, 121.04, 119.94, 118.87, 114.91, 111.12, 51.34, 35.35, 28.65.
f1 (ppm)

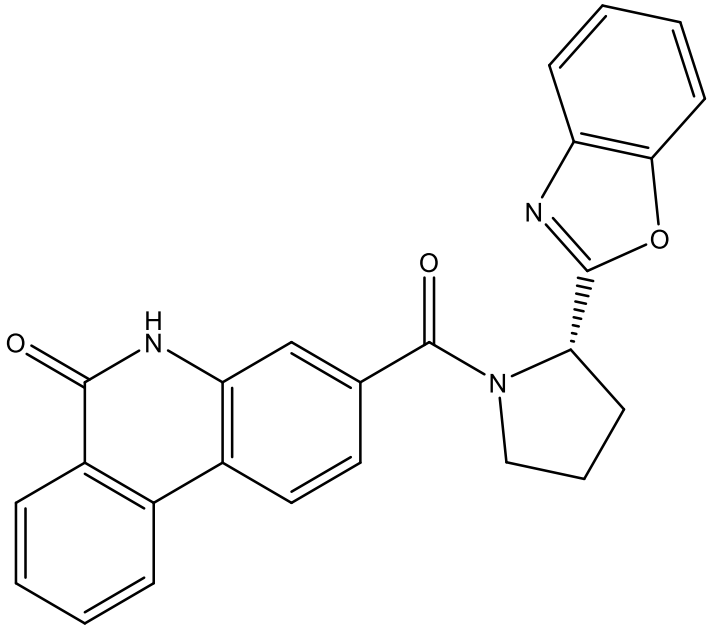

(*S*)-3-(2-(benzo[d]oxazol-2-yl)pyrrolidine-1-carbonyl)phenanthridin-6(5*H*)-one (b12)

Using **Synthesis Method d**, 24mg (0.1mmol) **f3** was reacted with 19mg (0.1mmol) **f12** to give 30.7mg **b12** (Yield: 75%) and the product was separated as yellow solid. ^{1}H NMR (300 MHz, DMSO-d_6) δ 11.77 (s, 1H), 8.56 (d, *J* = 8.1 Hz, 1H), 8.48 (d, *J* = 6.5 Hz, 1H), 8.35 (d, *J* = 7.9 Hz, 1H), 7.90 (t, *J* = 7.7 Hz, 1H), 7.76 – 7.65 (m, 3H), 7.59 (s, 1H), 7.46 (d, *J* = 8.3 Hz, 1H), 7.40 (dd, *J* = 6.6, 2.9 Hz, 2H), 5.40 (dd, *J* = 8.1, 4.6 Hz, 1H), 3.86 – 3.58 (m, 2H), 2.19 – 1.92 (m, 4H). ^{13}C NMR (75 MHz, DMSO) δ 168.2, 161.5, 153.7, 150.5, 137.2, 136.8, 134.1, 133.5, 129.1, 128.0, 126.5, 125.4, 125.0, 123.9, 123.5, 121.3, 120.1, 119.5, 118.7, 115.6, 111.3, 55.5, 50.5, 31.2, 25.5. HRMS m/z (ESI+, M+Na): Calcd for C25H19N3O3: 432.1324, (ESI+, M+Na) found: 432.1311

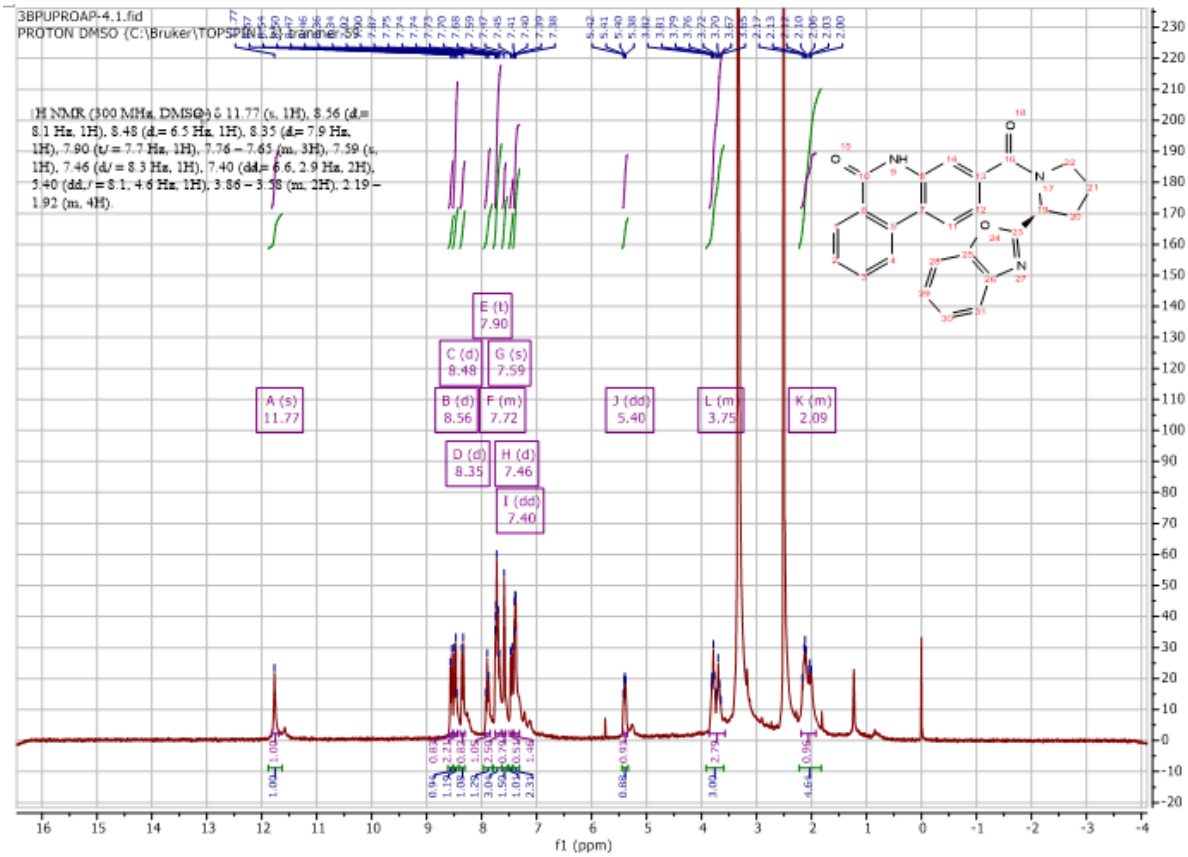
3BPUPROAP-4.1.fid
PROTON DMSO (C:\Bruker\TOPSPIN4.1.3) Gianmario 39
¹H NMR (300 MHz, DMSO) δ 11.77 (s, 1H), 8.56 (d, J = 8.1 Hz, 1H), 8.48 (d, J = 6.5 Hz, 1H), 8.35 (d, J = 7.9 Hz, 1H), 7.90 (t, J = 7.7 Hz, 1H), 7.76 – 7.65 (m, 3H), 7.59 (s, 1H), 7.46 (d, J = 8.3 Hz, 1H), 7.40 (dd, J = 6.6, 2.9 Hz, 2H), 5.40 (dd, J = 8.1, 4.6 Hz, 1H), 3.86 – 3.58 (m, 2H), 2.19 – 1.92 (m, 4H).
A (s) 11.77
B (d) 8.56
C (d) 8.48
D (d) 8.35
E (t) 7.90
F (m) 7.72
G (s) 7.59
H (d) 7.46
I (dd) 7.40
J (dd) 5.40
L (m) 3.75
K (m) 2.09
f1 (ppm)

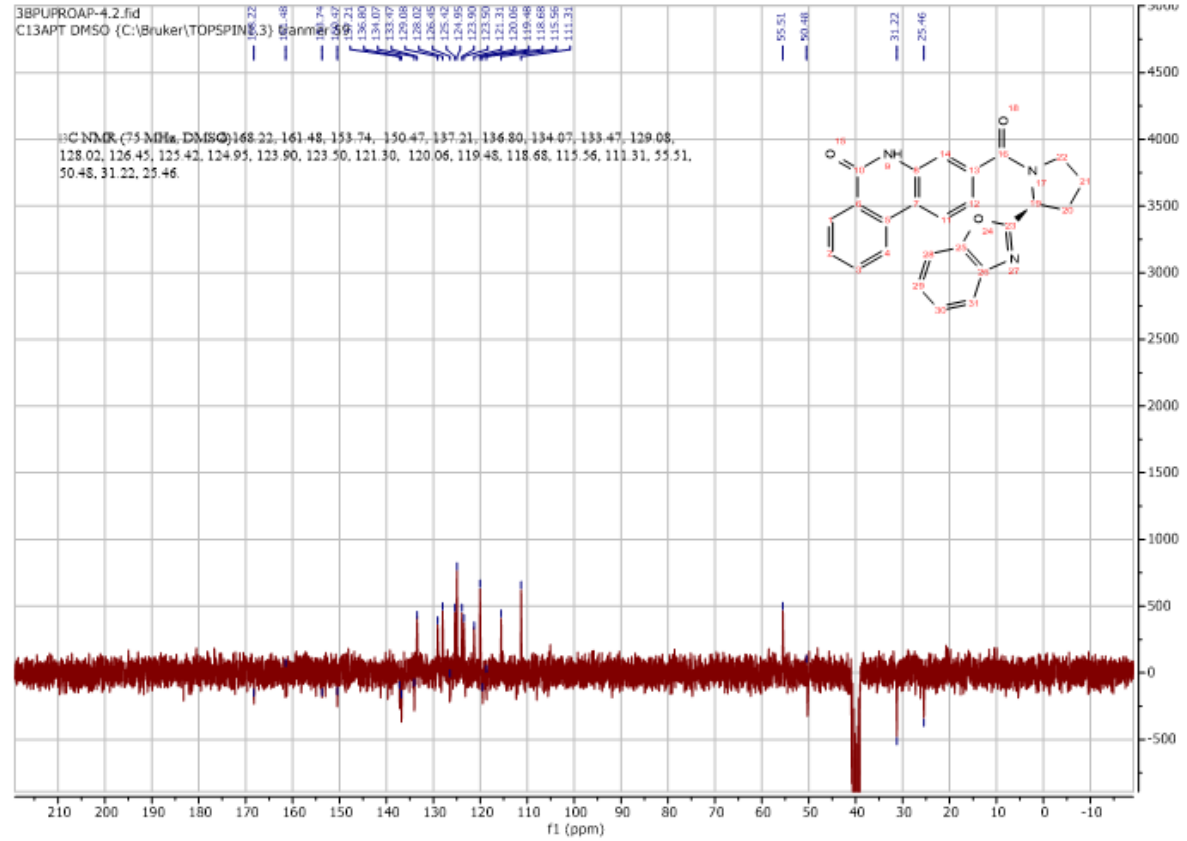
3BPUPROAP-4.2.fid
C13APT DMSO (C:\Bruker\TOPSPIN4.1.3) Gianmario 39
¹³C NMR (75 MHz, DMSO) 168.22, 161.48, 153.74, 150.47, 137.21, 136.80, 134.07, 133.47, 129.08, 128.02, 126.45, 125.42, 124.95, 123.90, 123.50, 121.30, 120.06, 119.48, 118.68, 115.56, 111.31, 55.51, 50.48, 31.22, 25.46.
f1 (ppm)

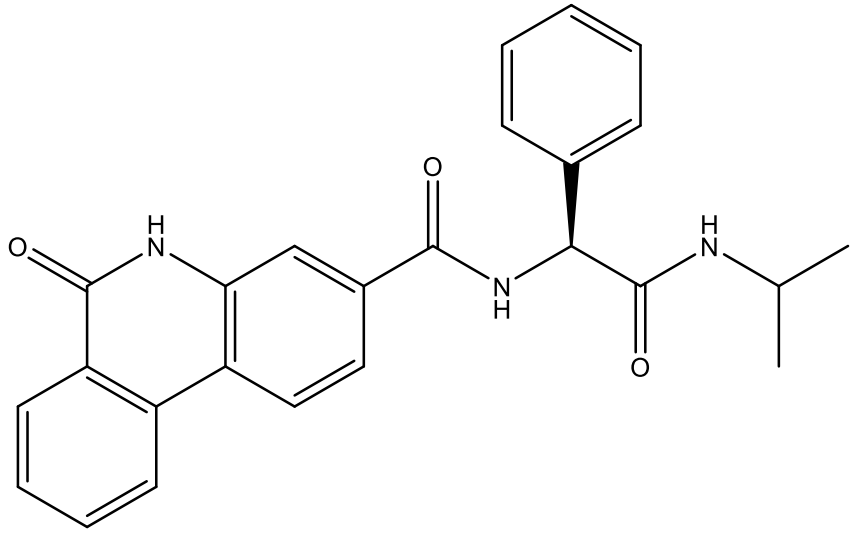

(*S*)-N-(2-(isopropylamino)-2-oxo-1-phenylethyl)-6-oxo-5,6-dihydrophenanthridine-3-carboxamide (b13)

Using **Synthesis Method d**, 25mg (0.1mmol) (*S*)-2-((tert-butoxycarbonyl)amino)-2-phenylacetic acid was reacted with 6mg (0.1mmol) propan-2-amine and the crude product was deprotected using **Synthesis Method f**. The crude product was reacted with 24mg (0.1mmol) **f3** to give 22.3mg **b13** (Yield: 54%) and the product was separated as yellow solid. ^{1}H NMR (400 MHz, DMSO-d_6) δ 11.77 (s, 1H), 8.83 (d, *J* = 8.1 Hz, 1H), 8.58 (d, *J* = 8.2 Hz, 1H), 8.48 (d, *J* = 8.5 Hz, 1H), 8.35 (dd, *J* = 8.0, 1.2 Hz, 1H), 8.21 (d, *J* = 7.6 Hz, 1H), 7.94 – 7.84 (m, 2H), 7.79 (dd, *J* = 8.4, 1.7 Hz, 1H), 7.74 – 7.66 (m, 1H), 7.55 – 7.48 (m, 2H), 7.42 – 7.34 (m, 2H), 7.34 – 7.27 (m, 1H), 5.68 (d, *J* = 8.1 Hz, 1H), 3.95 – 3.79 (m, 1H), 1.12 (d, *J* = 6.6 Hz, 3H), 1.01 (d, *J* = 6.5 Hz, 3H). ^{13}C NMR (101 MHz, DMSO) δ 169.1, 165.9, 161.3, 139.3, 136.8, 135.3, 134.1, 133.4, 129.2, 128.8, 128.0, 128.0, 127.8, 126.6, 123.7, 123.7, 121.5, 120.4, 116.4, 57.3, 41.2, 22.7. HRMS m/z (ESI+, M+Na): Calcd for C25H23N3O3: 436.1637, (ESI+, M+Na) found: 436.1629

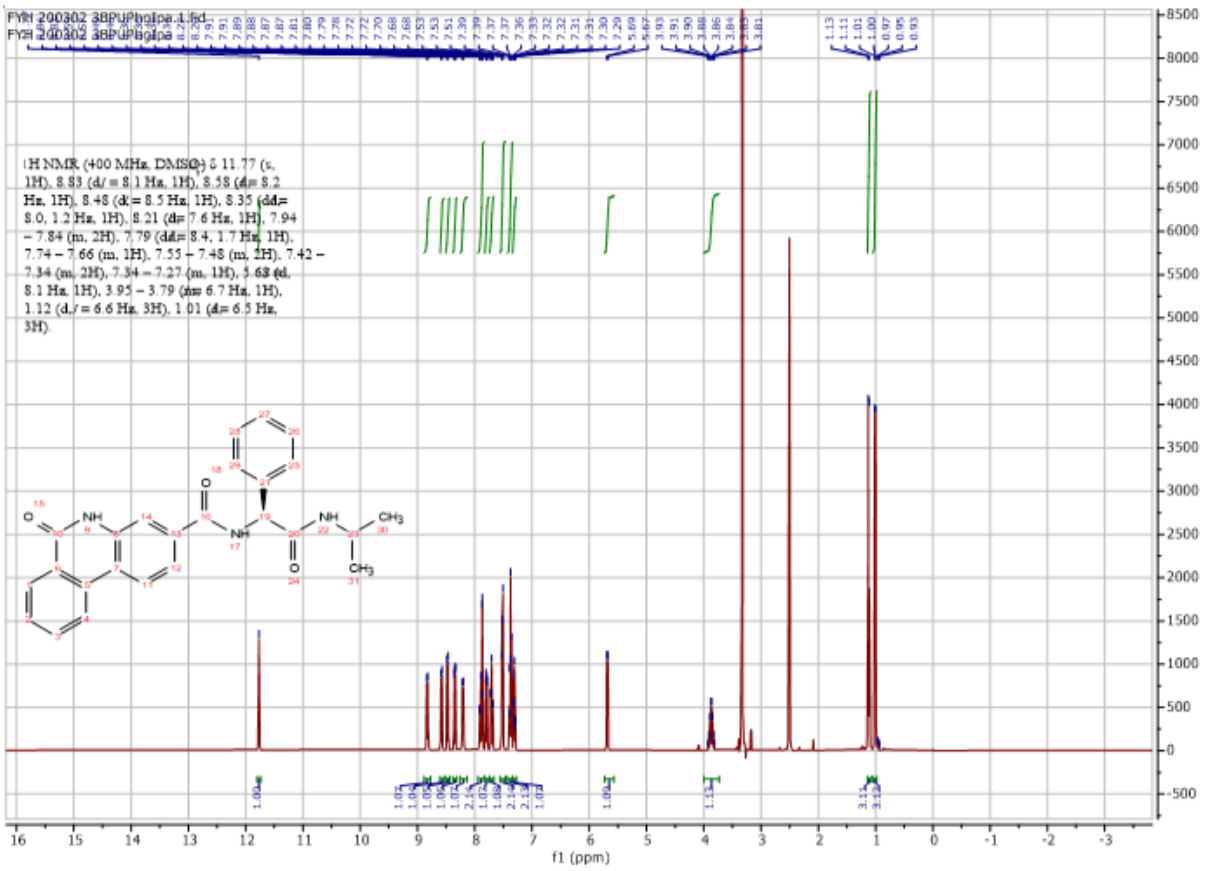
FYH 200302 3BPUPhgIpa 1.fid
FYH 200302 3BPUPhgIpa
1H NMR (400 MHz, DMSO) δ 11.77 (s, 1H), 8.83 (d, J = 8.1 Hz, 1H), 8.58 (d, J = 8.2 Hz, 1H), 8.48 (d, J = 8.5 Hz, 1H), 8.35 (dd, J = 8.0, 1.2 Hz, 1H), 8.21 (d, J = 7.6 Hz, 1H), 7.94 – 7.84 (m, 2H), 7.79 (dd, J = 8.4, 1.7 Hz, 1H), 7.74 – 7.66 (m, 1H), 7.55 – 7.48 (m, 2H), 7.42 – 7.34 (m, 2H), 7.34 – 7.27 (m, 1H), 5.68 (d, J = 8.1 Hz, 1H), 3.95 – 3.79 (m, J = 6.7 Hz, 1H), 1.12 (d, J = 6.6 Hz, 3H), 1.01 (d, J = 6.5 Hz, 3H).
f1 (ppm)

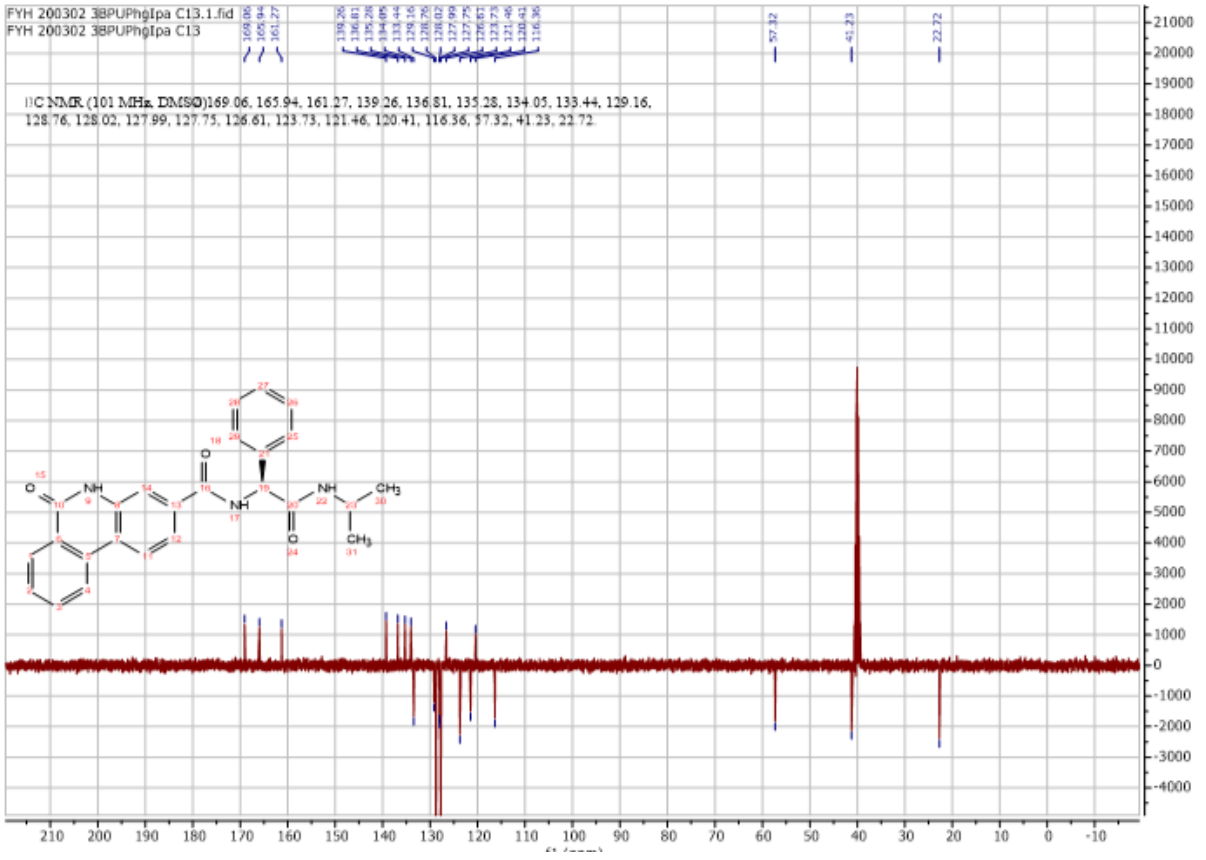
FYH 200302 3BPUPhgIpa C13.1.fid
FYH 200302 3BPUPhgIpa C13
13C NMR (101 MHz, DMSO) 169.06, 165.94, 161.27, 139.26, 136.81, 135.28, 134.05, 133.44, 129.16, 128.76, 128.02, 127.99, 127.75, 126.61, 123.73, 121.46, 120.41, 116.36, 57.32, 41.23, 22.72.

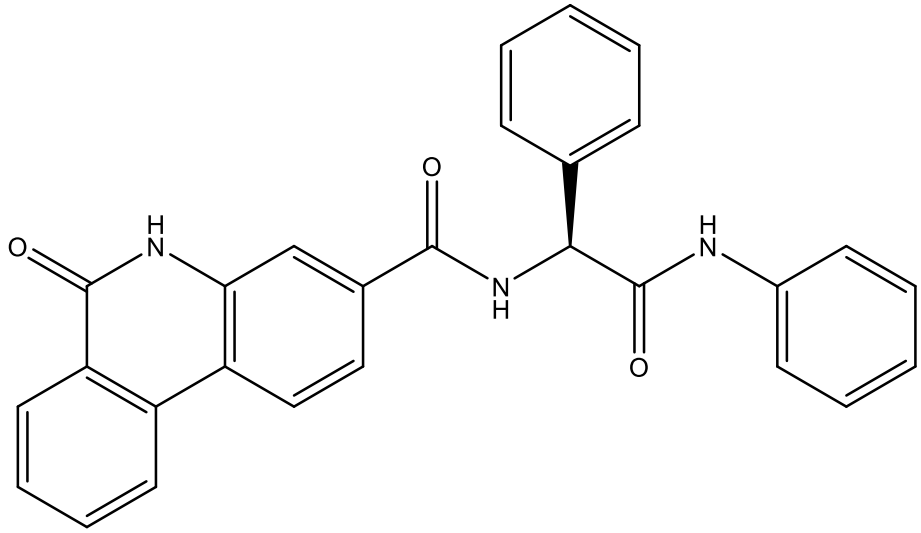

(*S*)-6-oxo-N-(2-oxo-1-phenyl-2-(phenylamino)ethyl)-5,6-dihydrophenanthridine-3-carboxamide (b14)

Using **Synthesis Method d**, 24mg (0.1mmol) **f3** was reacted with 22.8mg (0.1mmol) **f22** to give 38.2mg **b14** (Yield: 85%) and the product was separated as yellow solid. ^{1}H NMR (400 MHz, DMSO-d_6) δ 11.80 (s, 1H), 10.41 (s, 1H), 9.13 (d, J = 7.5 Hz, 1H), 8.60 (d, J = 8.2 Hz, 1H), 8.49 (d, J = 8.6 Hz, 1H), 8.35 (d, J = 7.9 Hz, 1H), 7.94 – 7.86 (m, 2H), 7.84 (dd, J = 8.4, 2.0 Hz, 1H), 7.71 (t, J = 7.5 Hz, 1H), 7.62 (dd, J = 7.7, 5.3 Hz, 4H), 7.47 – 7.38 (m, 2H), 7.38 – 7.28 (m, 3H), 7.07 (t, J = 7.4 Hz, 1H), 5.88 (d, J = 7.6 Hz, 1H). ^{13}C NMR (101 MHz, DMSO) δ 169.1, 166.5, 161.3, 158.1, 139.3, 138.2, 136.8, 135.2, 134.1, 133.4, 129.3, 129.0, 128.4, 128.3, 128.0, 126.6, 124.0, 123.8, 123.7, 121.6, 120.4, 119.7, 116.6, 58.5. HRMS m/z (ESI+, M+Na): Calcd for C28H21N3O3: 470.1481, (ESI+, M+Na) found: 470.1472

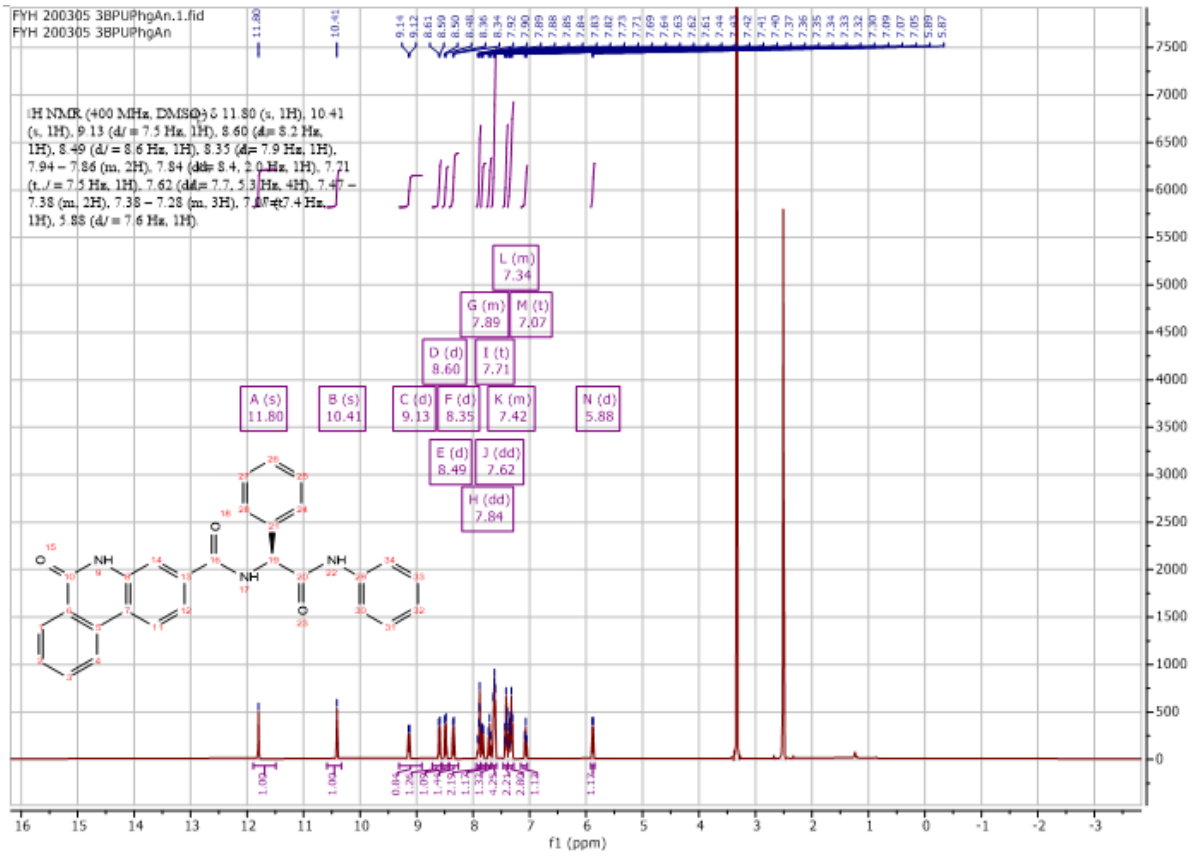
FYH 200305 3BPUPhgAn.1.fid
FYH 200305 3BPUPhgAn
¹H NMR (400 MHz, DMSO-d6) δ 11.80 (s, 1H), 10.41 (s, 1H), 9.13 (d, J = 7.5 Hz, 1H), 8.60 (d, J = 8.2 Hz, 1H), 8.49 (d, J = 8.6 Hz, 1H), 8.35 (d, J = 7.9 Hz, 1H), 7.94 – 7.86 (m, 2H), 7.84 (dd, J = 8.4, 2.0 Hz, 1H), 7.71 (t, J = 7.5 Hz, 1H), 7.62 (dd, J = 7.7, 5.3 Hz, 4H), 7.47 – 7.38 (m, 2H), 7.38 – 7.28 (m, 3H), 7.07 (t, J = 7.4 Hz, 1H), 5.88 (d, J = 7.6 Hz, 1H).
A (s) 11.80
B (s) 10.41
C (d) 9.13
D (d) 8.60
E (d) 8.49
F (d) 8.35
G (m) 7.89
H (dd) 7.84
I (t) 7.71
J (dd) 7.62
K (m) 7.42
L (m) 7.34
M (t) 7.07
N (d) 5.88
f1 (ppm)

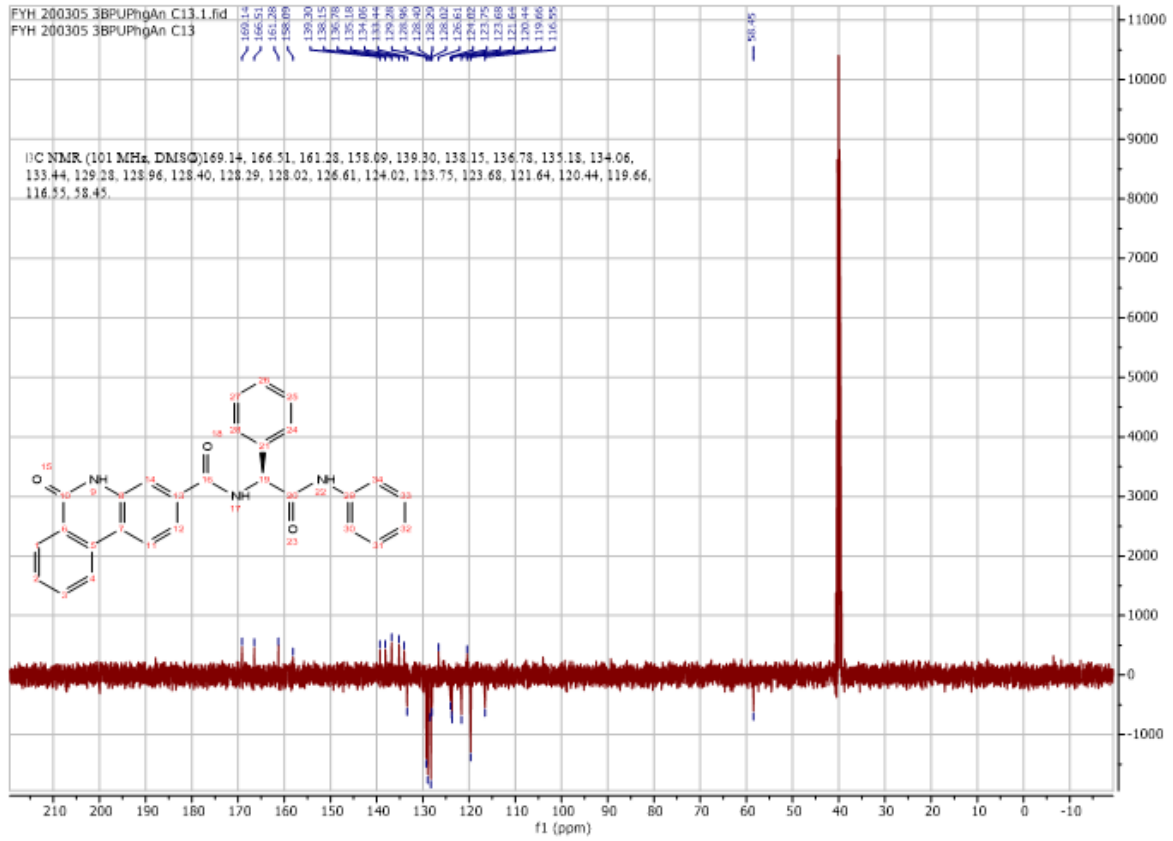
FYH 200305 3BPUPhgAn C13.1.fid
FYH 200305 3BPUPhgAn C13
¹³C NMR (101 MHz, DMSO-d6) 169.14, 166.51, 161.28, 158.09, 139.30, 138.15, 136.78, 135.18, 134.06, 133.44, 129.28, 128.96, 128.40, 128.29, 128.02, 126.61, 124.02, 123.75, 123.68, 121.64, 120.44, 119.66, 116.55, 58.45.
f1 (ppm)

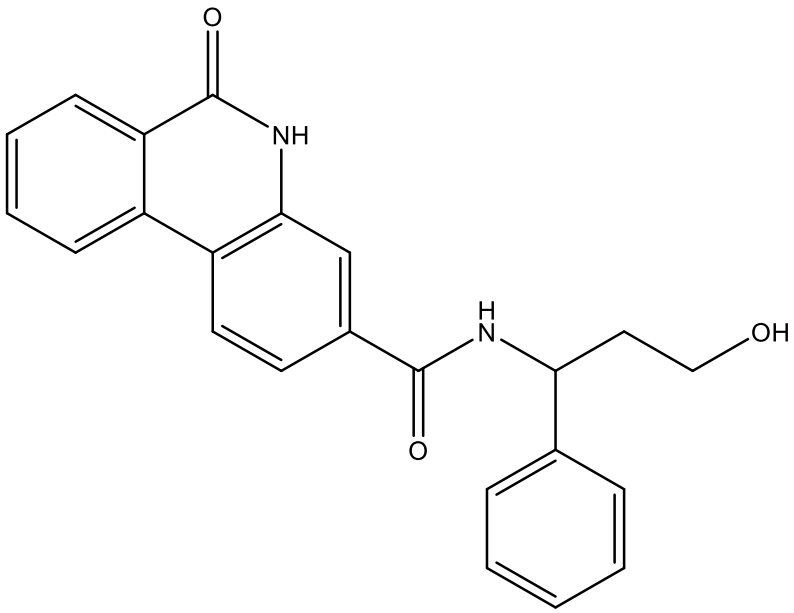

***N*-(3-hydroxy-1-phenylpropyl)-6-oxo-5,6-dihydrophenanthridine-3-carboxamide (b15)**

Using **Synthesis Method d**, 24mg (0.1mmol) **f3** was reacted with 15.1mg (0.1mmol) 3-amino-3-phenylpropan-1-ol to give 31.2mg **b15** (Yield: 84%) and the product was separated as white solid. ^{1}H NMR (300 MHz, DMSO-d_6) δ 11.79 (s, 1H), 8.93 (d, J = 8.2 Hz, 1H), 8.58 (d, J = 8.2 Hz, 1H), 8.49 (d, 1H), 8.34 (dd, J = 7.9, 1.4 Hz, 1H), 7.89 (td, J = 8.2, 7.7, 1.5 Hz, 1H), 7.82 (d, J = 1.7 Hz, 1H), 7.75 (dd, J = 8.4, 1.8 Hz, 1H), 7.73 – 7.66 (m, 1H), 7.46 – 7.38 (m, 2H), 7.34 (t, J = 7.6 Hz, 2H), 7.29 – 7.18 (m, 1H), 5.19 (dd, J = 8.5, 5.8 Hz, 1H), 4.59 (s, 1H), 3.46 (m, 2H), 1.99 (m, 2H). ^{13}C NMR (75 MHz, DMSO) δ 165.8, 161.3, 144.5, 136.9, 136.1, 134.1, 133.4, 129.1, 128.7, 128.0, 127.1, 127.0, 126.6, 123.7, 123.7, 121.0, 120.2, 116.3, 58.4, 51.0, 39.2. HRMS m/z (ESI+, M+Na): Calcd for C23H20N2O3: 395.1372, (ESI+, M+Na) found: 395.1362

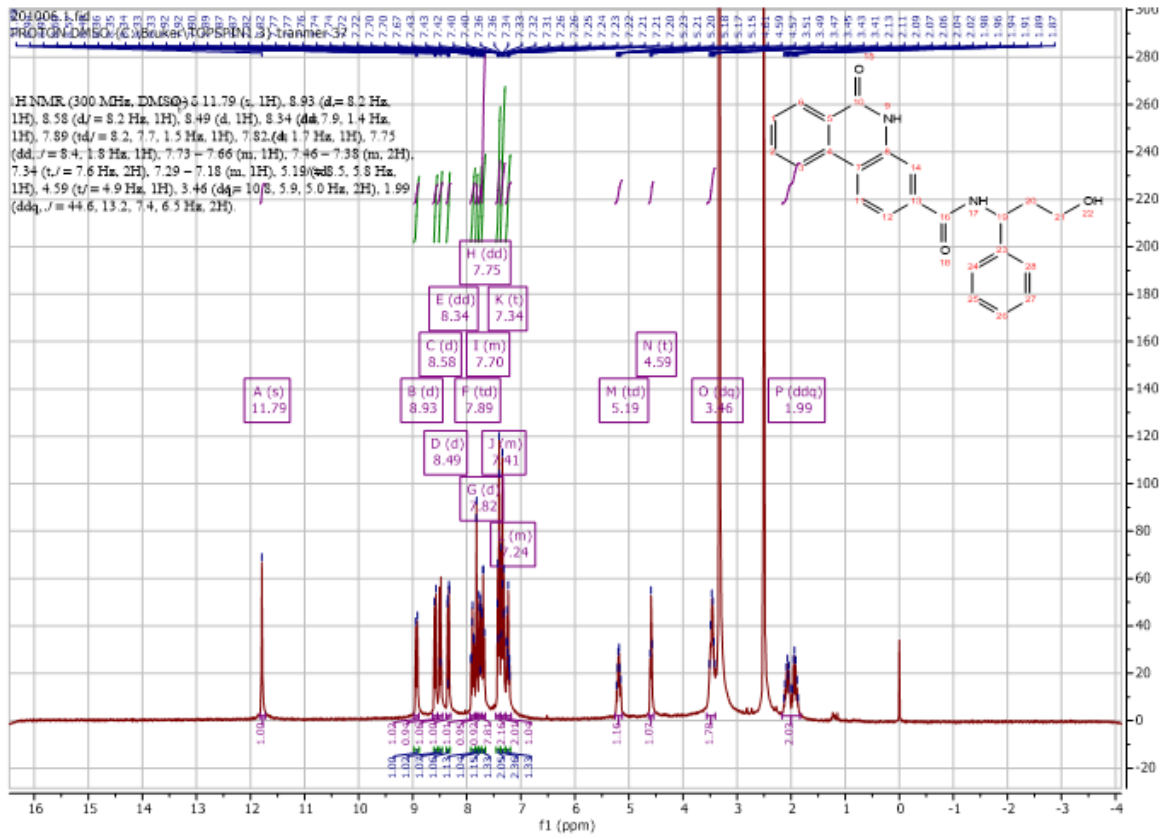
201006.1.fid
PROTON DMSO (C:\Bruker\TOPSPIN1.3) tranmer 37
¹H NMR (300 MHz, DMSO) δ 11.79 (s, 1H), 8.93 (d, J = 8.2 Hz, 1H), 8.58 (d, J = 8.2 Hz, 1H), 8.49 (d, 1H), 8.34 (dd, J = 7.9, 1.4 Hz, 1H), 7.89 (td, J = 8.2, 7.7, 1.5 Hz, 1H), 7.82 (dd, J = 1.7 Hz, 1H), 7.75 (dd, J = 8.4, 1.8 Hz, 1H), 7.73 – 7.66 (m, 1H), 7.46 – 7.38 (m, 2H), 7.34 (t, J = 7.6 Hz, 2H), 7.29 – 7.18 (m, 1H), 5.19 (td, J = 8.5, 5.8 Hz, 1H), 4.59 (t, J = 4.9 Hz, 1H), 3.46 (dq, J = 10.8, 5.9, 5.0 Hz, 2H), 1.99 (ddq, J = 44.6, 13.2, 7.4, 6.5 Hz, 2H).
H (dd) 7.75
E (dd) 8.34
K (t) 7.34
C (d) 8.58
I (m) 7.70
N (t) 4.59
A (s) 11.79
B (d) 8.93
F (td) 7.89
M (td) 5.19
O (dq) 3.46
P (ddq) 1.99
D (d) 8.49
J (m) 7.41
G (d) 7.82
(m) 7.24
f1 (ppm)

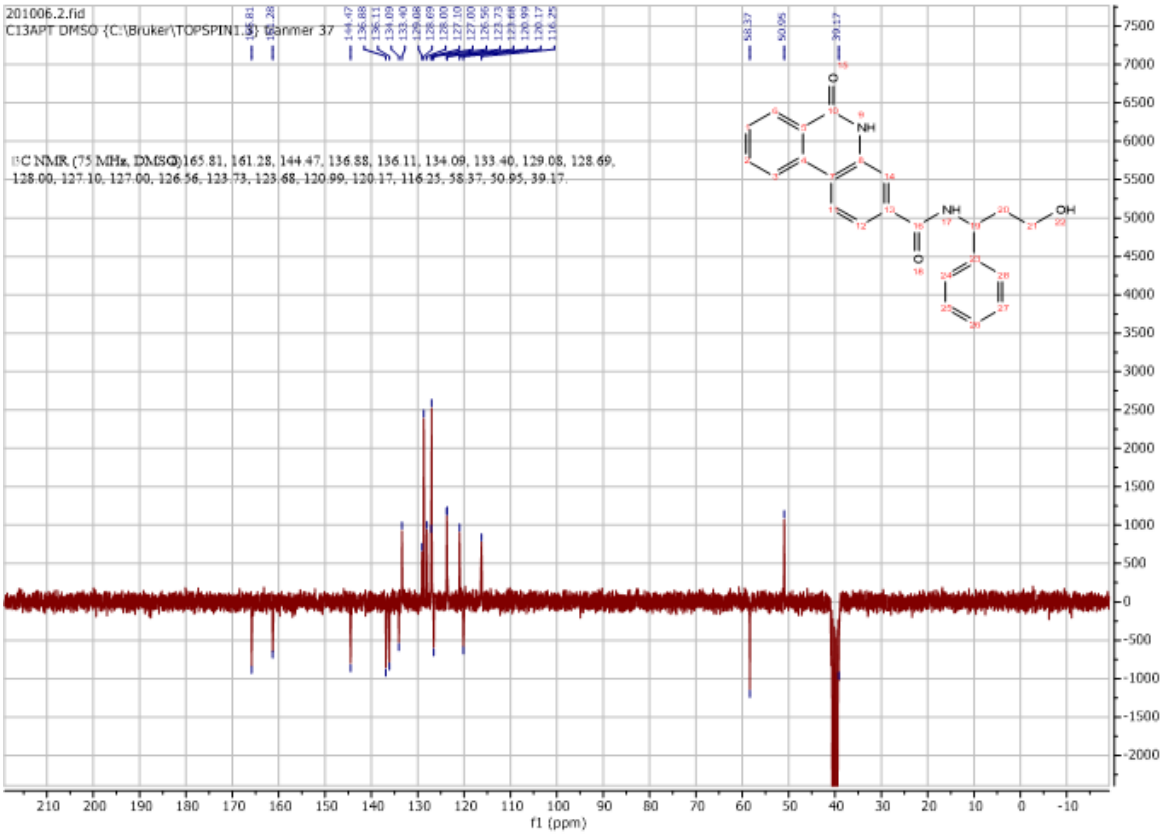
201006.2.fid
C13APT DMSO (C:\Bruker\TOPSPIN1.3) tranmer 37
¹³C NMR (75 MHz, DMSO) 165.81, 161.28, 144.47, 136.88, 136.11, 134.09, 133.40, 129.08, 128.69, 128.00, 127.10, 127.00, 126.56, 123.73, 123.68, 120.99, 120.17, 116.25, 58.37, 50.95, 39.17.
f1 (ppm)

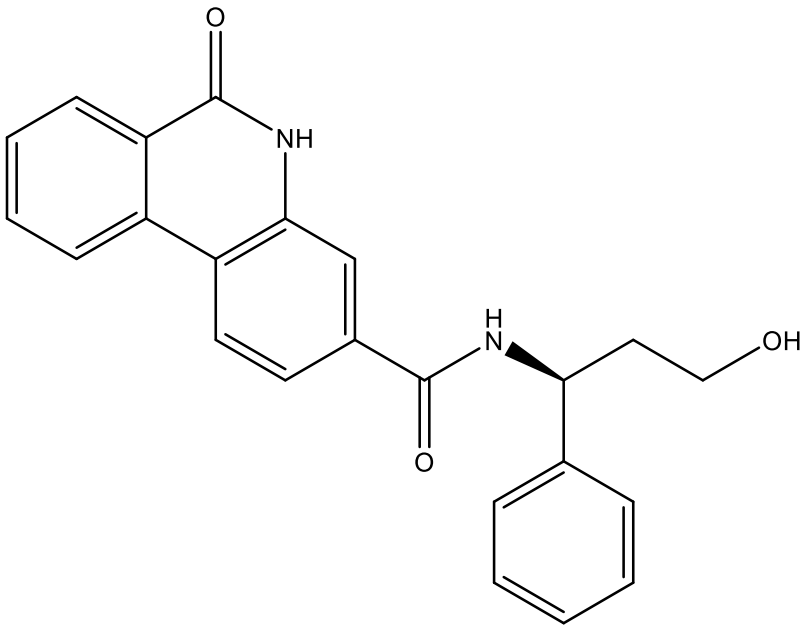

(*S*)-*N*-(3-hydroxy-1-phenylpropyl)-6-oxo-5,6-dihydrophenanthridine-3-carboxamide (b16)

Using **Synthesis Method d**, 24mg (0.1mmol) **f3** was reacted with 15.1mg (0.1mmol) (*S*)-3-amino-3-phenylpropan-1-ol to give 31.6mg **b16** (Yield: 85%) and the product was separated as white solid. ^{1}H NMR (300 MHz, DMSO-d_6) δ 11.79 (s, 1H), 8.93 (d, *J* = 8.1 Hz, 1H), 8.58 (d, *J* = 8.1 Hz, 1H), 8.49 (d, *J* = 8.5 Hz, 1H), 8.39 – 8.30 (m, 1H), 7.93 – 7.85 (m, 1H), 7.83 (d, *J* = 1.4 Hz, 1H), 7.76 (dd, *J* = 8.4, 1.5 Hz, 1H), 7.70 (t, *J* = 7.5 Hz, 1H), 7.42 (d, *J* = 7.1 Hz, 2H), 7.34 (t, *J* = 7.5 Hz, 2H), 7.23 (t, *J* = 7.2 Hz, 1H), 5.19 (dt, *J* = 8.5, 6.0 Hz, 1H), 4.59 (s, 1H), 3.46 (m, 2H), 2.00 (m, 6.5 Hz, 2H). ^{13}C NMR (75 MHz, DMSO) δ 165.8, 161.3, 144.5, 136.9, 136.1, 134.1, 133.4, 129.1, 128.7, 128.0, 127.1, 127.0, 126.6, 123.7, 123.7, 121.0, 120.2, 116.2, 58.4, 51.0, 39.2. HRMS m/z (ESI+, M+Na): Calcd for C23H20N2O3: 395.1372, (ESI+, M+Na) found: 395.1369

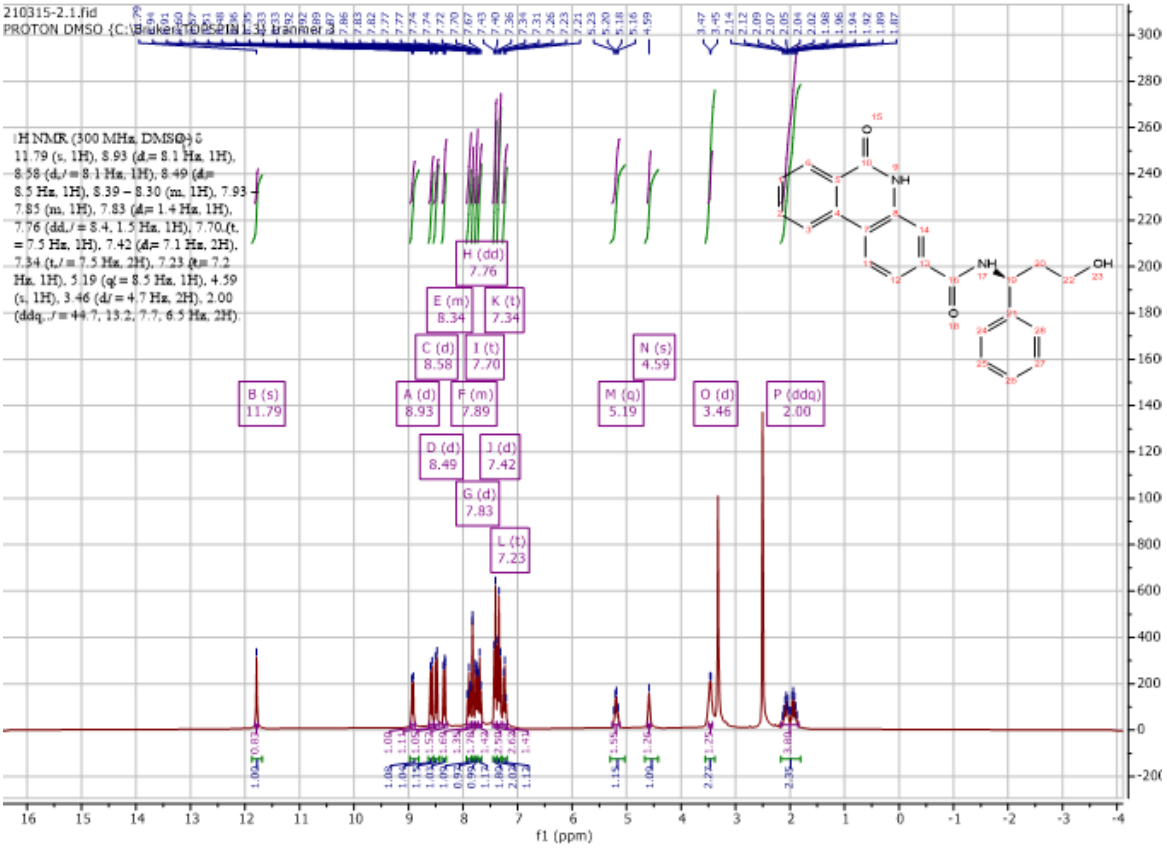
210315-2.1.fid
PROTON DMSO {C:\Bruker\TOPSPIN1.3} tranmer 7
1H NMR (300 MHz, DMSO) δ 11.79 (s, 1H), 8.93 (d, J = 8.1 Hz, 1H), 8.58 (d, J = 8.1 Hz, 1H), 8.49 (d, J = 8.5 Hz, 1H), 8.39 – 8.30 (m, 1H), 7.93 – 7.85 (m, 1H), 7.83 (d, J = 1.4 Hz, 1H), 7.76 (dd, J = 8.4, 1.5 Hz, 1H), 7.70 (t, J = 7.5 Hz, 1H), 7.42 (d, J = 7.1 Hz, 2H), 7.34 (t, J = 7.5 Hz, 2H), 7.23 (t, J = 7.2 Hz, 1H), 5.19 (q, J = 8.5 Hz, 1H), 4.59 (s, 1H), 3.46 (d, J = 4.7 Hz, 2H), 2.00 (ddq, J = 44.7, 13.2, 7.7, 6.5 Hz, 2H).
H (dd) 7.76
E (m) 8.34
K (t) 7.34
C (d) 8.58
I (t) 7.70
N (s) 4.59
B (s) 11.79
A (d) 8.93
F (m) 7.89
M (q) 5.19
O (d) 3.46
P (ddq) 2.00
D (d) 8.49
J (d) 7.42
G (d) 7.83
L (t) 7.23
f1 (ppm)

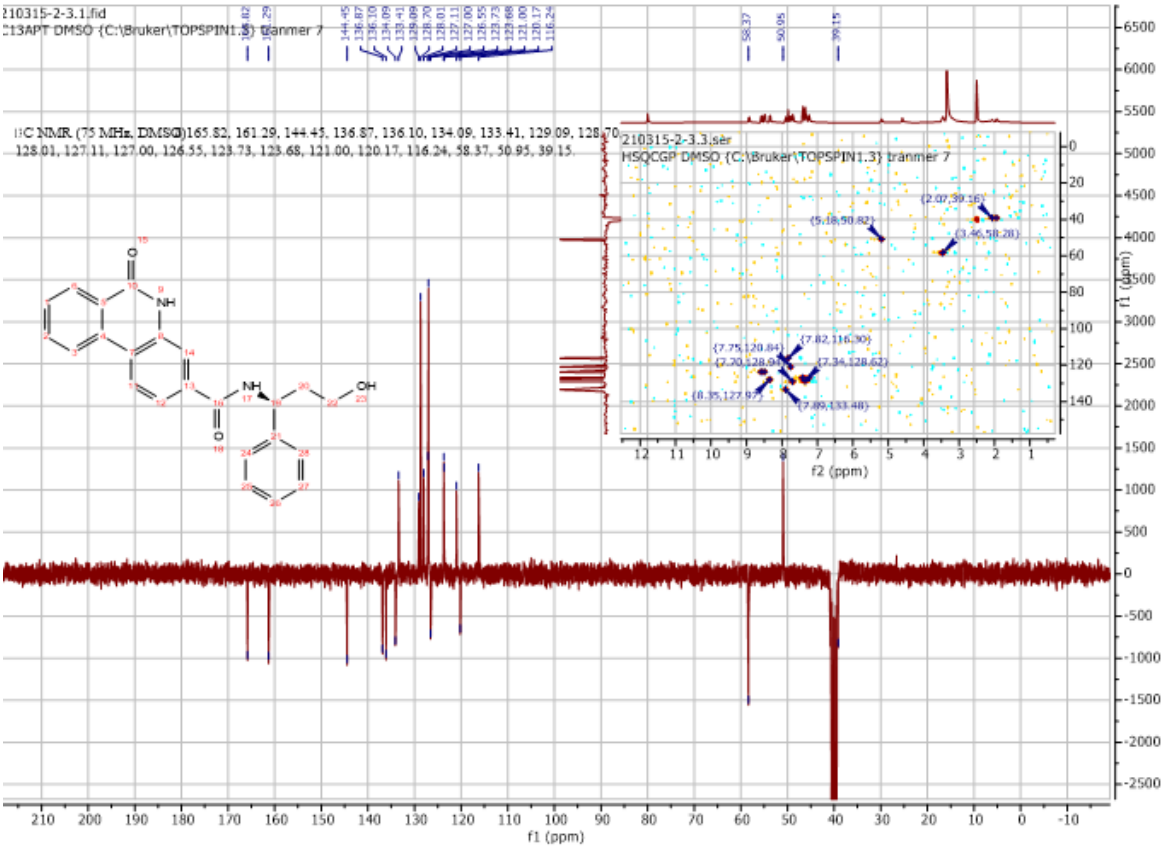
210315-2-3.1.fid
13APT DMSO {C:\Bruker\TOPSPIN1.3} tranmer 7
13C NMR (75 MHz, DMSO) 165.82, 161.29, 144.45, 136.87, 136.10, 134.09, 133.41, 129.09, 128.70, 128.01, 127.11, 127.00, 126.55, 123.73, 123.68, 121.00, 120.17, 116.24, 58.37, 50.95, 39.15.
210315-2-3.3.ser
HSQCGP DMSO {C:\Bruker\TOPSPIN1.3} tranmer 7
(2.07,39.16)
(5.18,50.82)
(3.46,58.28)
(7.82,116.30)
(7.75,120.84)
(7.70,128.94)
(7.34,128.62)
(8.35,127.97)
(7.89,133.48)
f2 (ppm)
f1 (ppm)

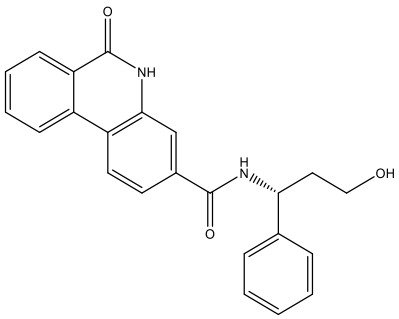

(*R*)-*N*-(3-hydroxy-1-phenylpropyl)-6-oxo-5,6-dihydrophenanthridine-3-carboxamide (b17)

Using **Synthesis Method d**, 24mg (0.1mmol) **f3** was reacted with 15.1mg (0.1mmol) (*R*)-3-amino-3-phenylpropan-1-ol to give 30.9mg **b17** (Yield: 83%) and the product was separated as white solid. ^{1}H NMR (300 MHz, DMSO-d_6) δ 11.79 (s, 1H), 8.93 (d, *J* = 8.2 Hz, 1H), 8.58 (d, *J* = 8.2 Hz, 1H), 8.49 (d, *J* = 8.5 Hz, 1H), 8.34 (dd, *J* = 8.0, 1.4 Hz, 1H), 7.89 (td, *J* = 8.2, 7.7, 1.5 Hz, 1H), 7.83 (d, *J* = 1.7 Hz, 1H), 7.76 (dd, *J* = 8.4, 1.8 Hz, 1H), 7.70 (t, *J* = 7.6 Hz, 1H), 7.45 – 7.38 (m, 2H), 7.34 (dd, *J* = 8.5, 6.7 Hz, 2H), 7.28 – 7.20 (m, 1H), 5.19 (dd, *J* = 8.6, 5.8 Hz, 1H), 4.59 (s, 1H), 3.47 (m, 2H), 2.16 – 1.84 (m, 2H). ^{13}C NMR (75 MHz, DMSO) δ 165.8, 161.3, 144.5, 136.9, 136.1, 134.1, 133.4, 129.1, 128.7, 128.0, 127.1, 127.0, 126.5, 123.7, 123.7, 121.0, 120.2, 116.2, 58.4, 51.0, 39.2. HRMS m/z (ESI+, M+Na): Calcd for C23H20N2O3: 395.1372, (ESI+, M+Na) found: 395.1357

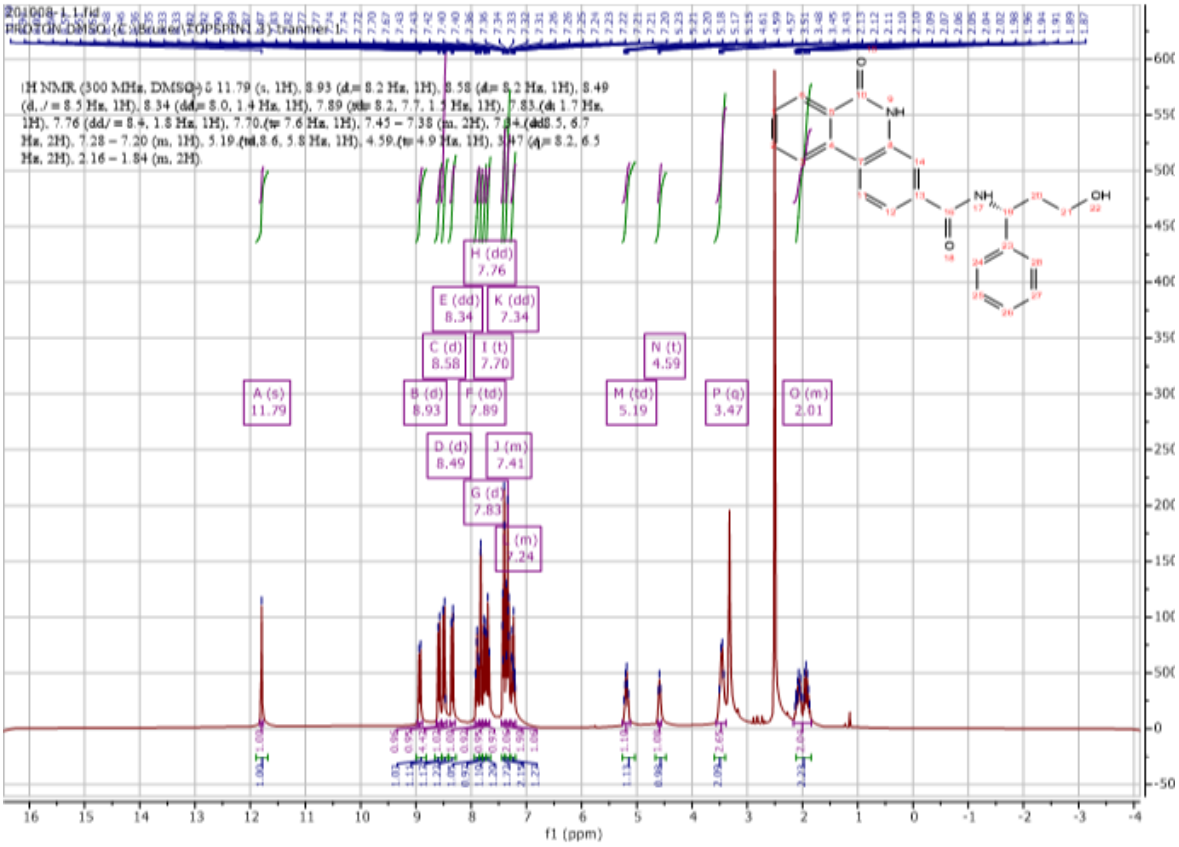
A (s) 11.79
B (d) 8.93
C (d) 8.58
D (d) 8.49
E (dd) 8.34
F (td) 7.89
G (d) 7.83
H (dd) 7.76
I (t) 7.70
J (m) 7.41
K (dd) 7.34
M (td) 5.19
N (t) 4.59
O (m) 2.01
P (q) 3.47
f1 (ppm)

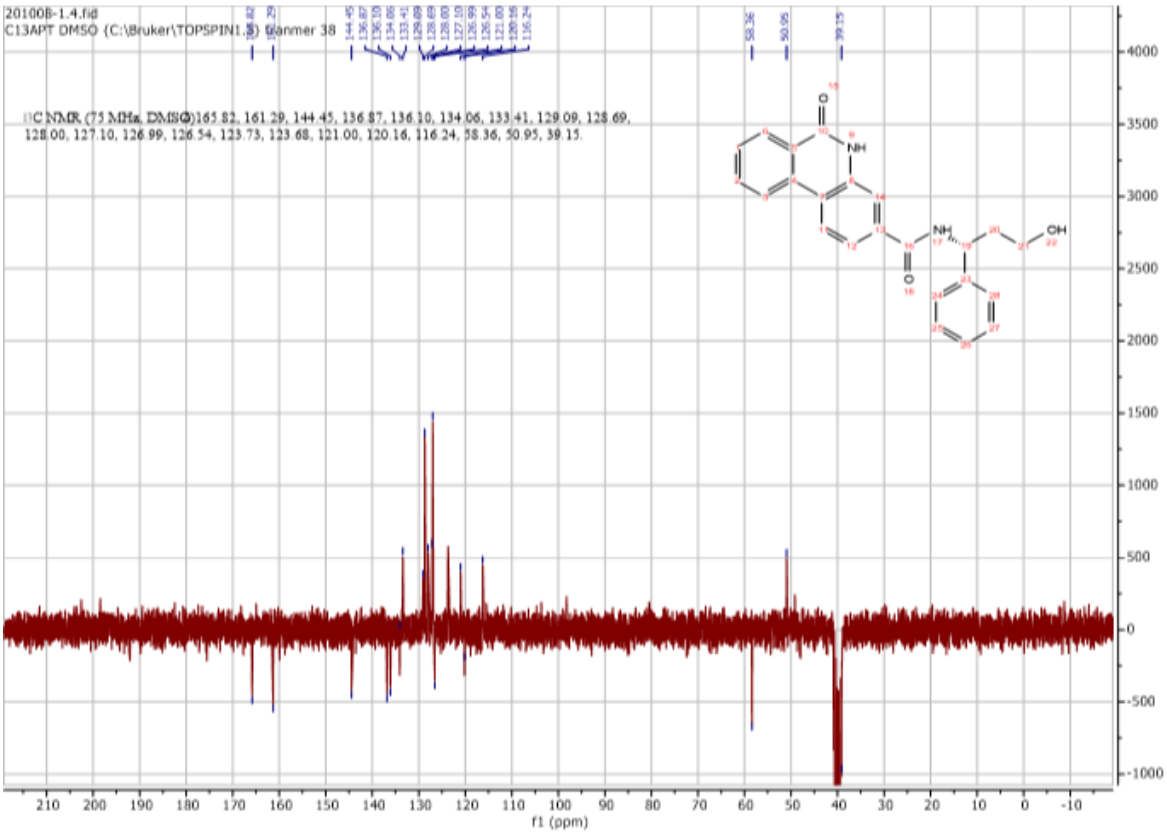
f1 (ppm)

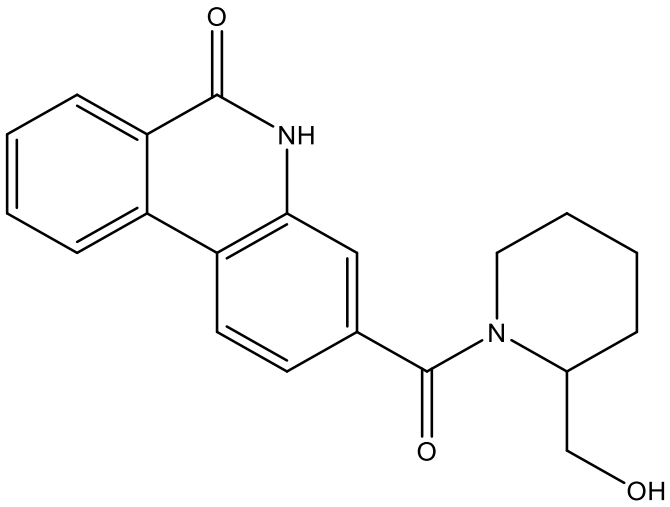

3-(2-(hydroxymethyl)piperidine-1-carbonyl)phenanthridin-6(5*H*)-one (b18)

Using **Synthesis Method d**, 24mg (0.1mmol) **f3** was reacted 11.5mg (0.1mmol) piperidin-2-ylmethanol to give 25.2mg **b18** (Yield: 75%) and the product was separated as white solid. ^{1}H NMR (300 MHz, DMSO-d_6) δ 11.77 (s, 1H), 8.53 (d, *J* = 8.1 Hz, 1H), 8.43 (d, *J* = 8.3 Hz, 1H), 8.35 (dd, *J* = 8.0, 1.4 Hz, 1H), 7.89 (ddd, *J* = 8.3, 7.1, 1.5 Hz, 1H), 7.74 – 7.63 (m, 1H), 7.38 (d, *J* = 1.6 Hz, 1H), 7.27 (dd, *J* = 8.2, 1.6 Hz, 1H), 4.80 (s, 1H), 4.59 – 2.66 (m, 5H), 1.95 – 1.27 (m, 6H). ^{13}C NMR (126 MHz, DMSO) δ 169.7, 161.3, 138.5, 136.9, 134.2, 133.4, 128.8, 128.0, 126.3, 123.8, 123.3, 120.9, 118.4, 114.9, 59.1, 55.1 – 50.2 (C19), 44.1-37.5 (C22), 25.7 (C22&C20), 19.5(C21). HRMS m/z (ESI+, M+Na): Calcd for C20H20N2O3: 359.1372, (ESI+, M+Na) found: 359.1367

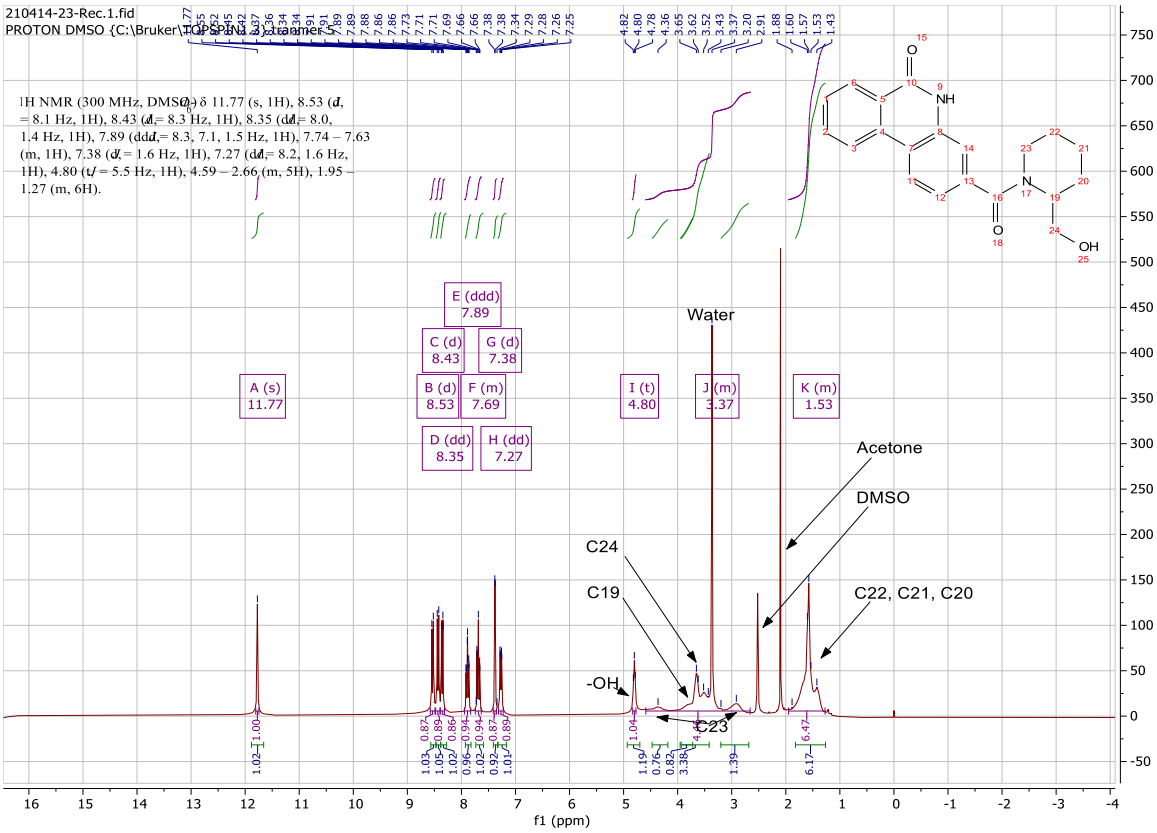
210414-23-Rec.1.fid
PROTON DMSO {C:\Bruker\TOPSPIN3} trammer 5
1H NMR (300 MHz, DMSO) δ 11.77 (s, 1H), 8.53 (d, = 8.1 Hz, 1H), 8.43 (d, = 8.3 Hz, 1H), 8.35 (dd, = 8.0, 1.4 Hz, 1H), 7.89 (ddd, = 8.3, 7.1, 1.5 Hz, 1H), 7.74 – 7.63 (m, 1H), 7.38 (d, = 1.6 Hz, 1H), 7.27 (dd, = 8.2, 1.6 Hz, 1H), 4.80 (t, = 5.5 Hz, 1H), 4.59 – 2.66 (m, 5H), 1.95 – 1.27 (m, 6H).
A (s) 11.77
B (d) 8.53
C (d) 8.43
D (dd) 8.35
E (ddd) 7.89
F (m) 7.69
G (d) 7.38
H (dd) 7.27
I (t) 4.80
J (m) 3.37
K (m) 1.53
Water
Acetone
DMSO
C24
C19
-OH
C23
C22, C21, C20
f1 (ppm)

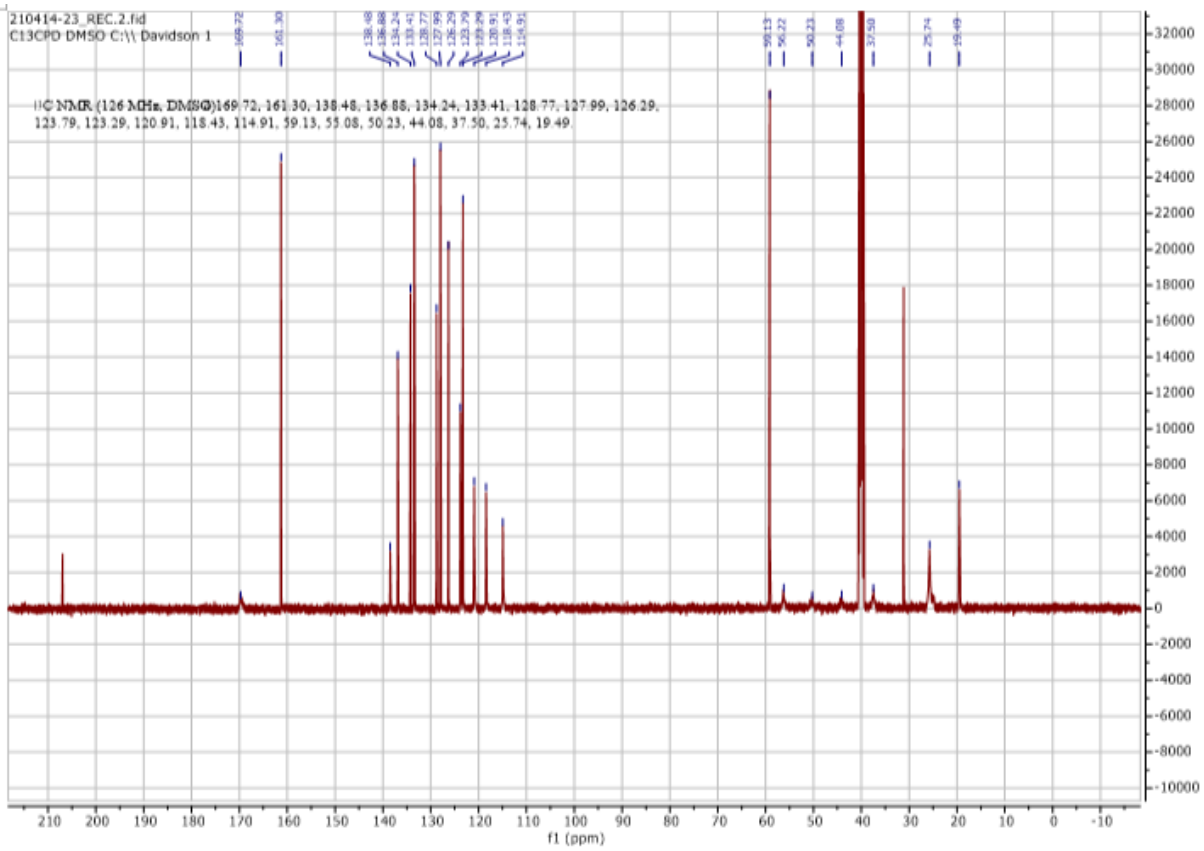
210414-23_REC.2.fid
C13CPD DMSO C:\\ Davidson 1
169.72
161.30
138.48
136.88
134.24
133.41
128.77
127.99
126.29
123.79
123.29
120.91
118.43
114.91
59.13
56.22
50.23
44.08
37.50
25.74
19.49
f1 (ppm)

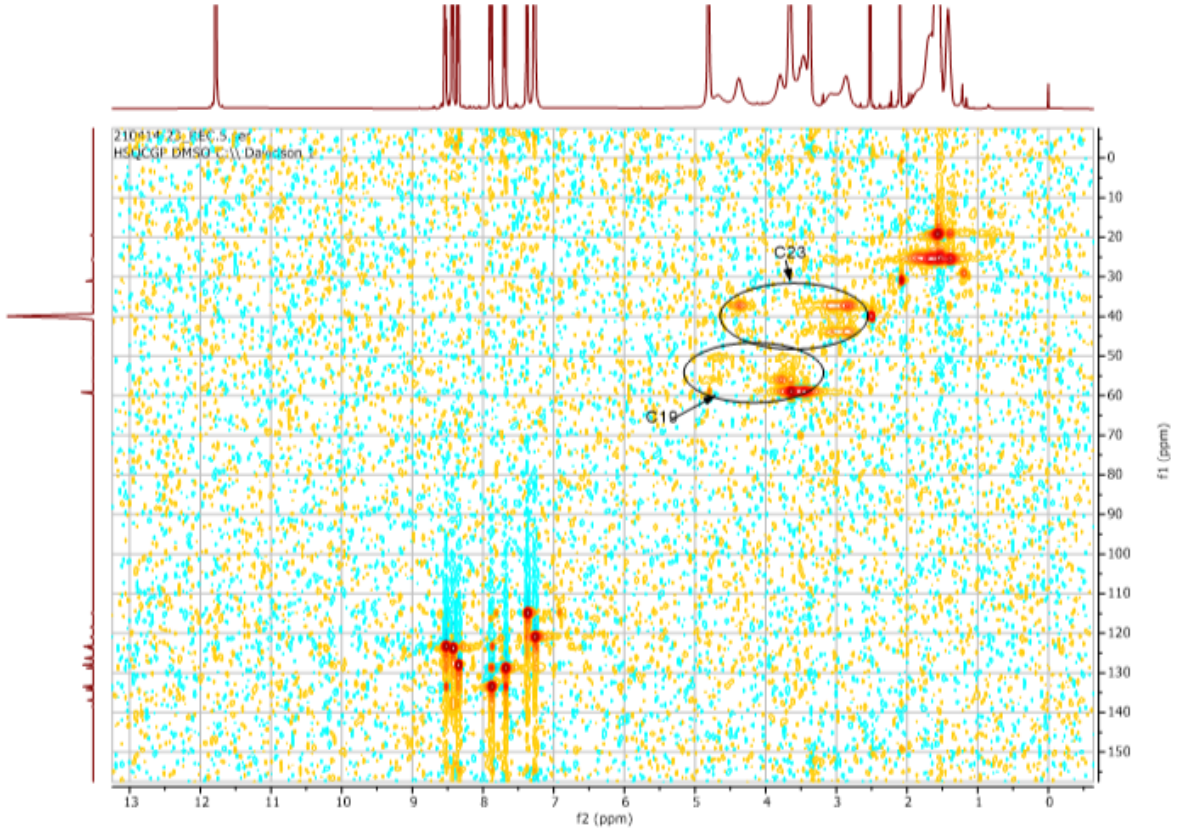
210414-23_REC.5.ser
HSQCGP DMSO C:\\ Davidson 1
C23
C19
f2 (ppm)
f1 (ppm)

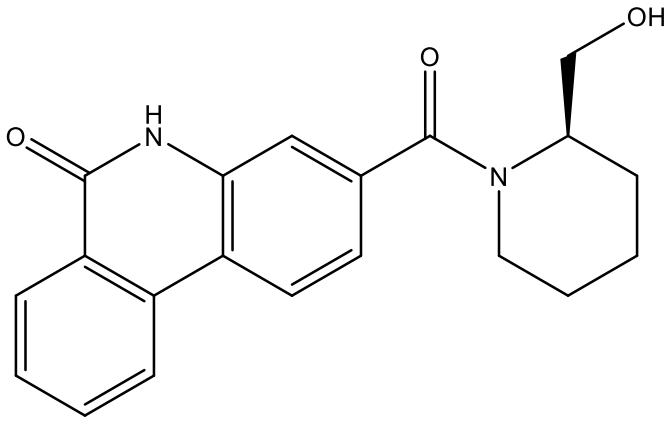

(*R*)-3-(2-(hydroxymethyl)piperidine-1-carbonyl)phenanthridin-6(5H)-one (b19)

Using **Synthesis Method d**, 24mg (0.1mmol) **f3** was reacted 11.5mg (0.1mmol) (*R*)-piperidin-2-ylmethanol to give 25.6mg **b19** (Yield: 76%) and the product was separated as white solid. ^{1}H NMR (300 MHz, DMSO-d_6) δ 11.75 (s, 1H), 8.53 (d, *J* = 8.2 Hz, 1H), 8.43 (d, *J* = 8.3 Hz, 1H), 8.34 (dd, *J* = 7.9, 1.4 Hz, 1H), 7.88 (ddd, *J* = 8.3, 7.1, 1.5 Hz, 1H), 7.68 (t, *J* = 7.7 Hz, 1H), 7.36 (d, *J* = 1.6 Hz, 1H), 7.25 (d, *J* = 8.2 Hz, 1H), 4.76 (s, 1H), 4.34 – 2.88 (m, 5H), 1.58 (m, 6H). ^{13}C NMR (75 MHz, DMSO) δ 169.7, 161.3, 138.4, 136.9, 134.2, 133.4, 128.8, 128.0, 126.3, 123.8, 123.3, 120.9, 118.4, 114.9, 59.1, 56.7 (C10), 44.9 – 36.4 (C14), 25.7, 19.5. HRMS m/z (ESI+, M+Na): Calcd for C20H20N2O3: 359.1372, (ESI+, M+Na) found: 359.1362

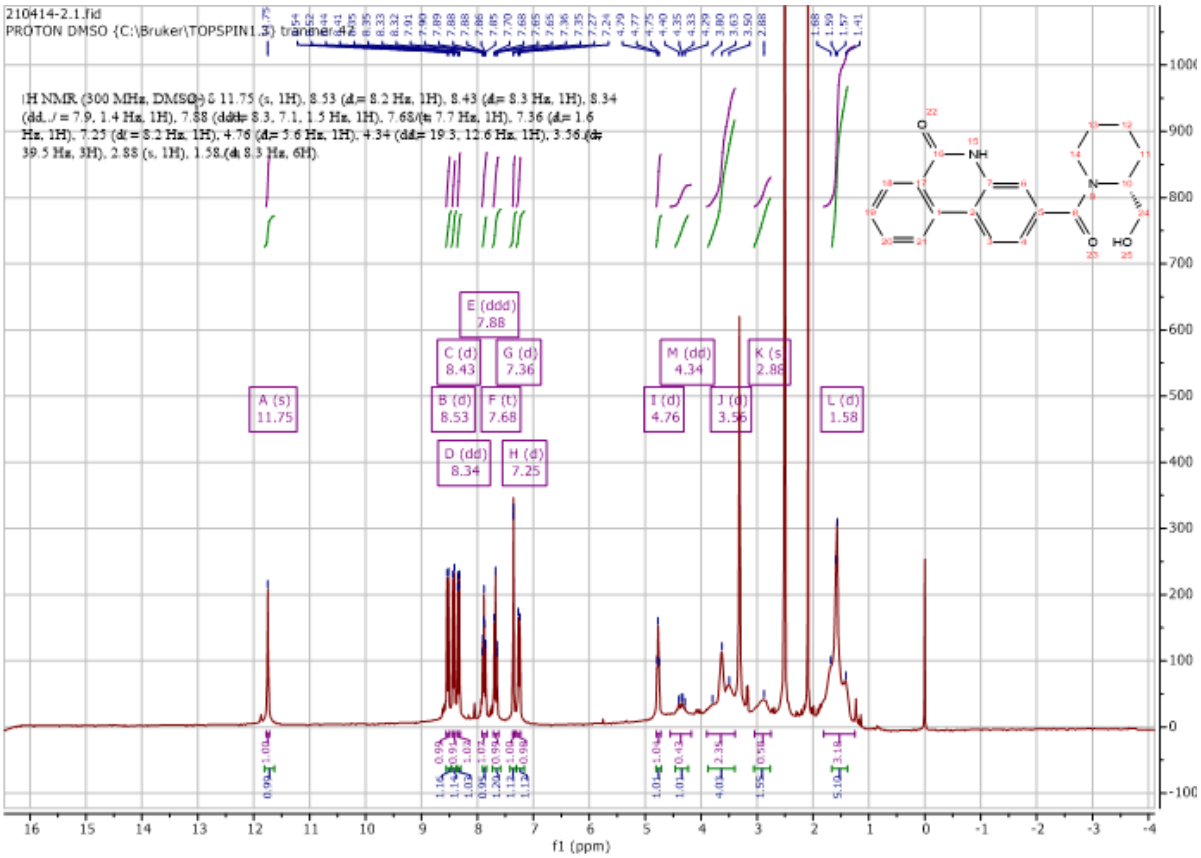
210414-2.1.fid
PROTON DMSO {C:\Bruker\TOPSPIN1.3} tranmer 42
A (s) 11.75
B (d) 8.53
C (d) 8.43
D (dd) 8.34
E (ddd) 7.88
F (t) 7.68
G (d) 7.36
H (d) 7.25
I (d) 4.76
J (d) 3.56
K (s) 2.88
L (d) 1.58
f1 (ppm)

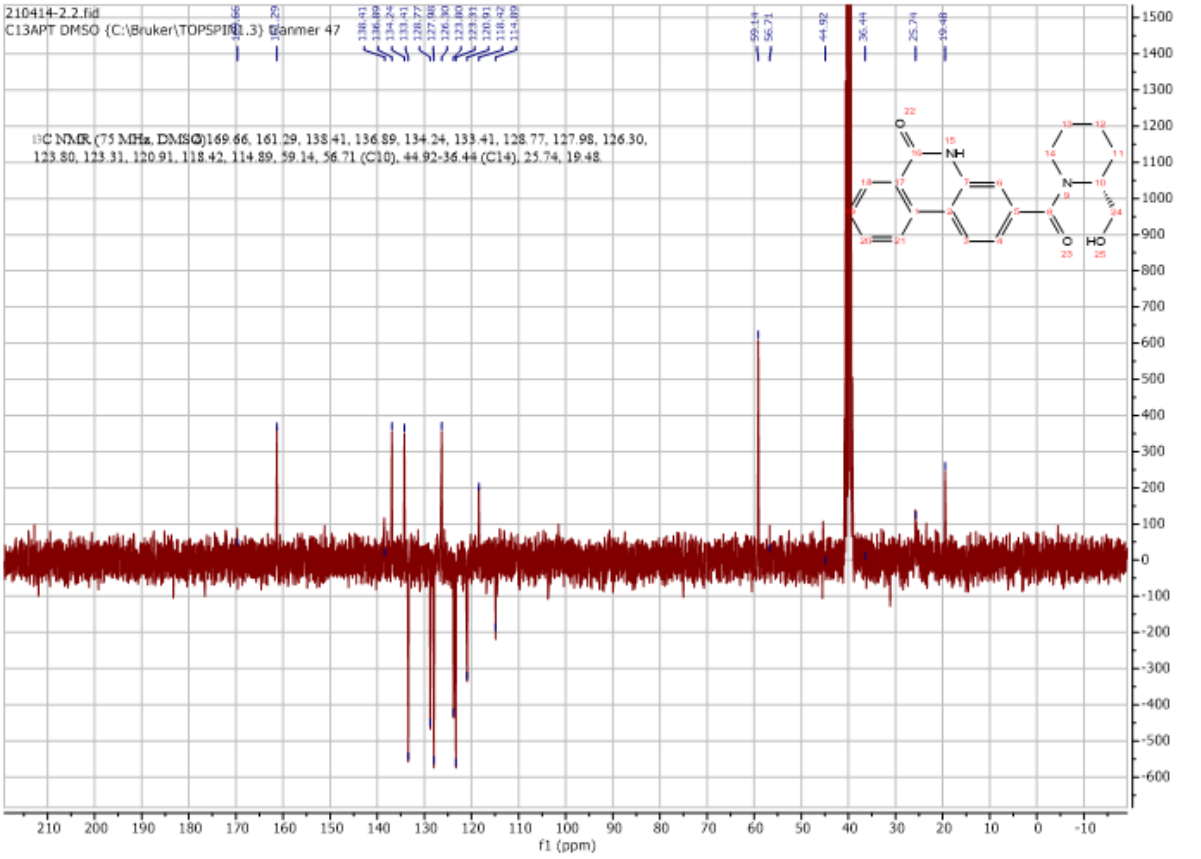
210414-2.2.fid
C13APT DMSO {C:\Bruker\TOPSPIN1.3} tranmer 47
f1 (ppm)

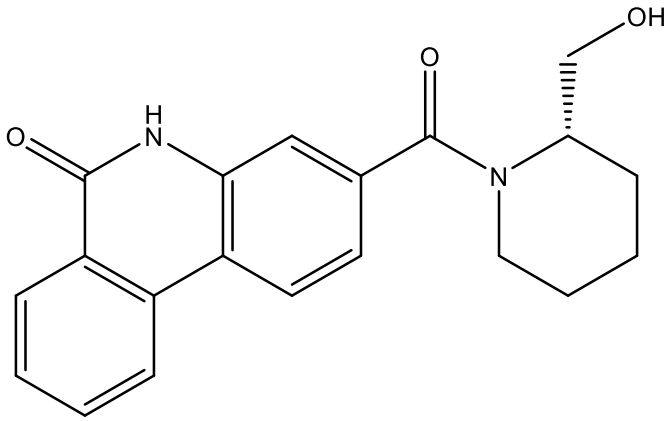

(*S*)-3-(2-(hydroxymethyl)piperidine-1-carbonyl)phenanthridin-6(5H)-one (b20)

Using **Synthesis Method d**, 24mg (0.1mmol) **f3** was reacted 11.5mg (0.1mmol) (*S*)-piperidin-2-ylmethanol to give 24.9mg **b20** (Yield: 74%) and the product was separated as white solid. ^{1}H NMR (300 MHz, DMSO-d_6) δ 11.75 (s, 1H), 8.53 (d, *J* = 8.2 Hz, 1H), 8.43 (d, *J* = 8.3 Hz, 1H), 8.34 (dd, *J* = 7.9, 1.4 Hz, 1H), 7.88 (ddd, *J* = 8.3, 7.2, 1.5 Hz, 1H), 7.71 – 7.65 (m, 1H), 7.36 (d, *J* = 1.6 Hz, 1H), 7.26 (dd, *J* = 8.1, 1.6 Hz, 1H), 4.77 (s, 1H), 4.36 – 2.90 (m, 5H), 1.49 (d, *J* = 48.6 Hz, 6H).^{13}C NMR (75 MHz, DMSO) δ 169.5, 161.3, 138.4, 136.9, 134.3, 133.4, 128.8, 128.0, 126.3, 123.8, 123.3, 120.9, 118.4, 114.9, 59.1, 56.0 (C10), 44.5-37.6(C14), 25.9, 19.5. HRMS m/z (ESI+, M+Na): Calcd for C20H20N2O3: 337.1547, (ESI+, M+H) found: 337.1545

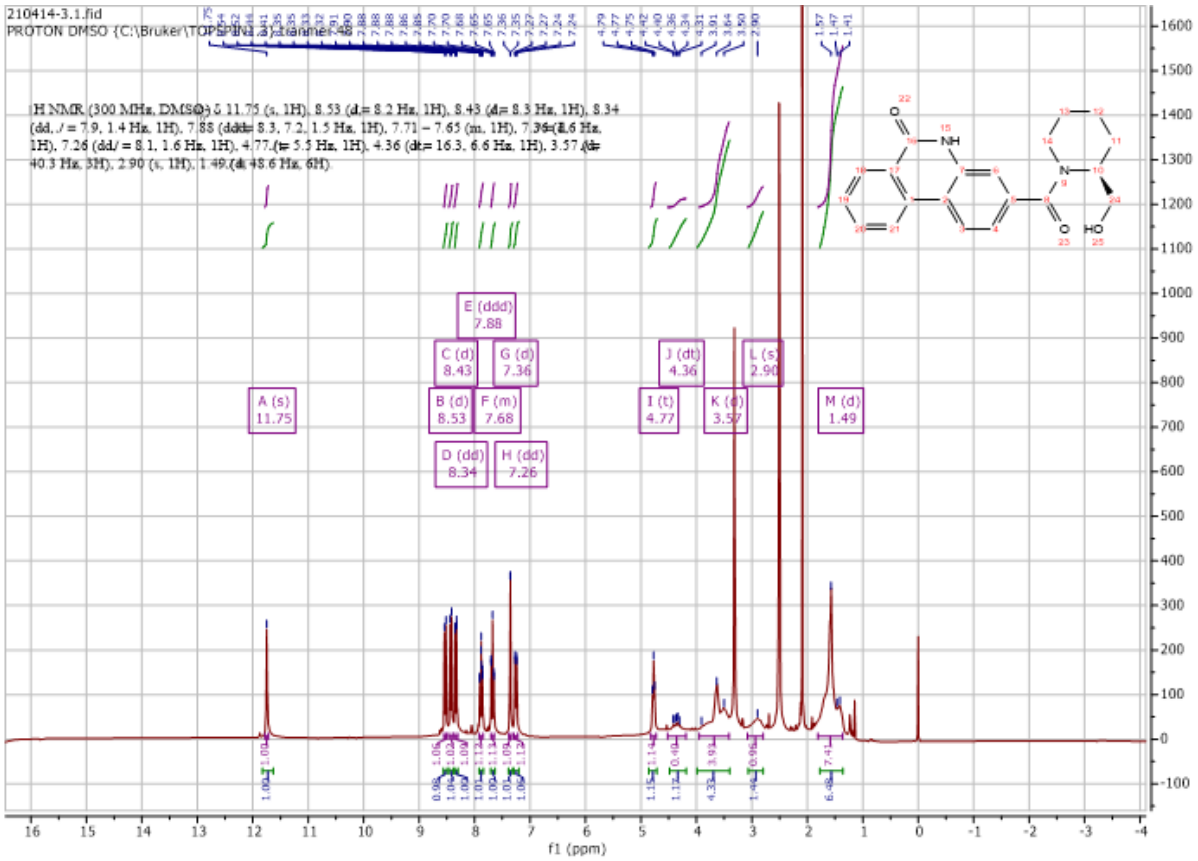
210414-3.1.fid
PROTON DMSO (C:\Bruker\TOPSPIN4.3) zg1anmer 48
¹H NMR (300 MHz, DMSO) δ 11.75 (s, 1H), 8.53 (d, J = 8.2 Hz, 1H), 8.43 (d, J = 8.3 Hz, 1H), 8.34 (dd, J = 7.9, 1.4 Hz, 1H), 7.88 (ddd, J = 8.3, 7.2, 1.5 Hz, 1H), 7.71 – 7.65 (m, 1H), 7.36 (d, J = 8.6 Hz, 1H), 7.26 (dd, J = 8.1, 1.6 Hz, 1H), 4.77 (t, J = 5.5 Hz, 1H), 4.36 (dt, J = 16.3, 6.6 Hz, 1H), 3.57 (dt, J = 40.3 Hz, 3H), 2.90 (s, 1H), 1.49 (d, J = 48.6 Hz, 6H).
A (s) 11.75
B (d) 8.53
C (d) 8.43
D (dd) 8.34
E (ddd) 7.88
F (m) 7.68
G (d) 7.36
H (dd) 7.26
I (t) 4.77
J (dt) 4.36
K (d) 3.57
L (s) 2.90
M (d) 1.49
f1 (ppm)

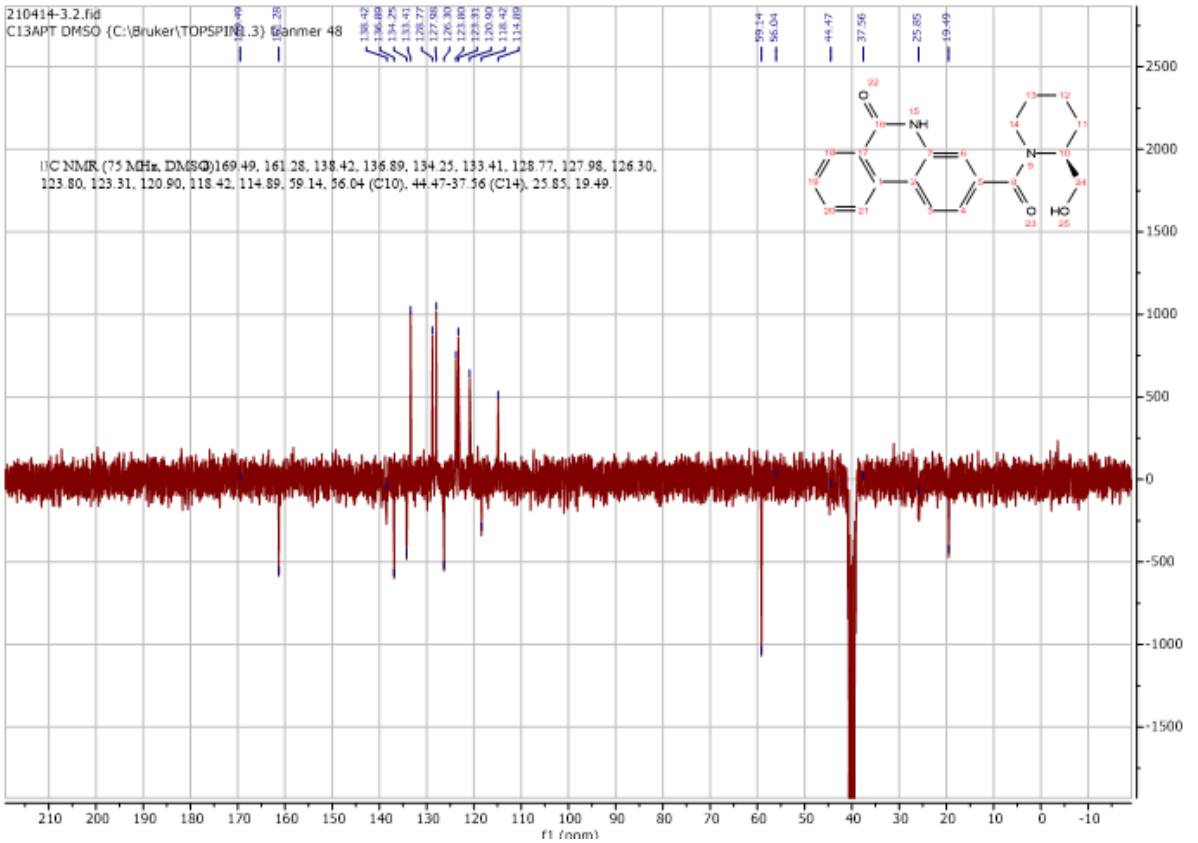
210414-3.2.fid
C13APT DMSO (C:\Bruker\TOPSPIN4.3) zganmer 48
¹³C NMR (75 MHz, DMSO) δ 169.49, 161.28, 138.42, 136.89, 134.25, 133.41, 128.77, 127.98, 126.30, 123.80, 123.31, 120.90, 118.42, 114.89, 59.14, 56.04 (C10), 44.47-37.56 (C14), 25.85, 19.49.
f1 (ppm)

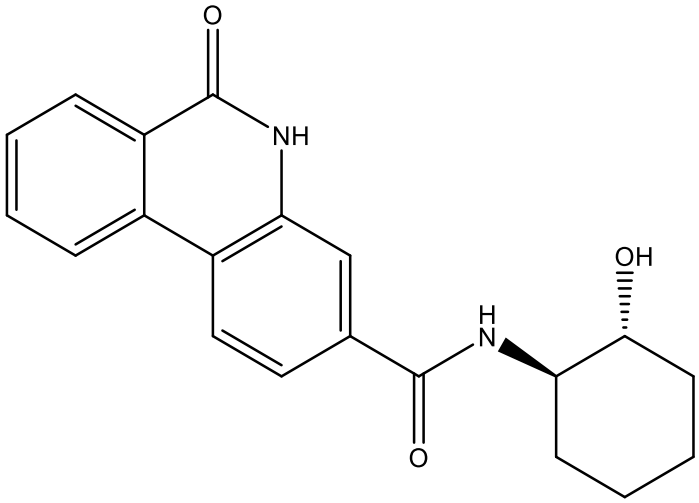

***N*-((1*R*,2*R*)-2-hydroxycyclohexyl)-6-oxo-5,6-dihydrophenanthridine-3-carboxamide (b21)**

Using **Synthesis Method d**, 24mg (0.1mmol) **f3** was with 11.5mg (0.1mmol) (1*R*,2*R*)-2-aminocyclohexan-1-ol to give 28.3mg **b21** (Yield: 84%) and the product was separated as white solid. ^{1}H NMR (300 MHz, DMSO-d_6) δ 11.76 (s, 1H), 8.59 (d, *J* = 8.2 Hz, 1H), 8.46 (s, 1H), 8.35 (dd, *J* = 8.0, 1.4 Hz, 1H), 8.23 (d, *J* = 8.0 Hz, 1H), 7.94 – 7.82 (m, 2H), 7.75 (dd, *J* = 8.4, 1.7 Hz, 1H), 7.69 (t, *J* = 7.5 Hz, 1H), 4.62 (s, 1H), 3.70 – 3.62 (m, 1H), 3.45 (m, 1H), 1.89 (m, 2H), 1.67 (m, 2H), 1.28 – 1.22 (m, 4H). ^{13}C NMR (75 MHz, DMSO) δ 166.0, 161.3, 136.8, 136.6, 134.1, 133.4, 129.0, 128.0, 126.5, 123.7, 123.5, 121.1, 120.0, 116.3, 71.5, 55.9, 35.0, 31.7, 24.9, 24.6. HRMS m/z (ESI+, M+Na): Calcd for C20H20N2O3: 359.1372, (ESI+, M+Na) found: 359.1365

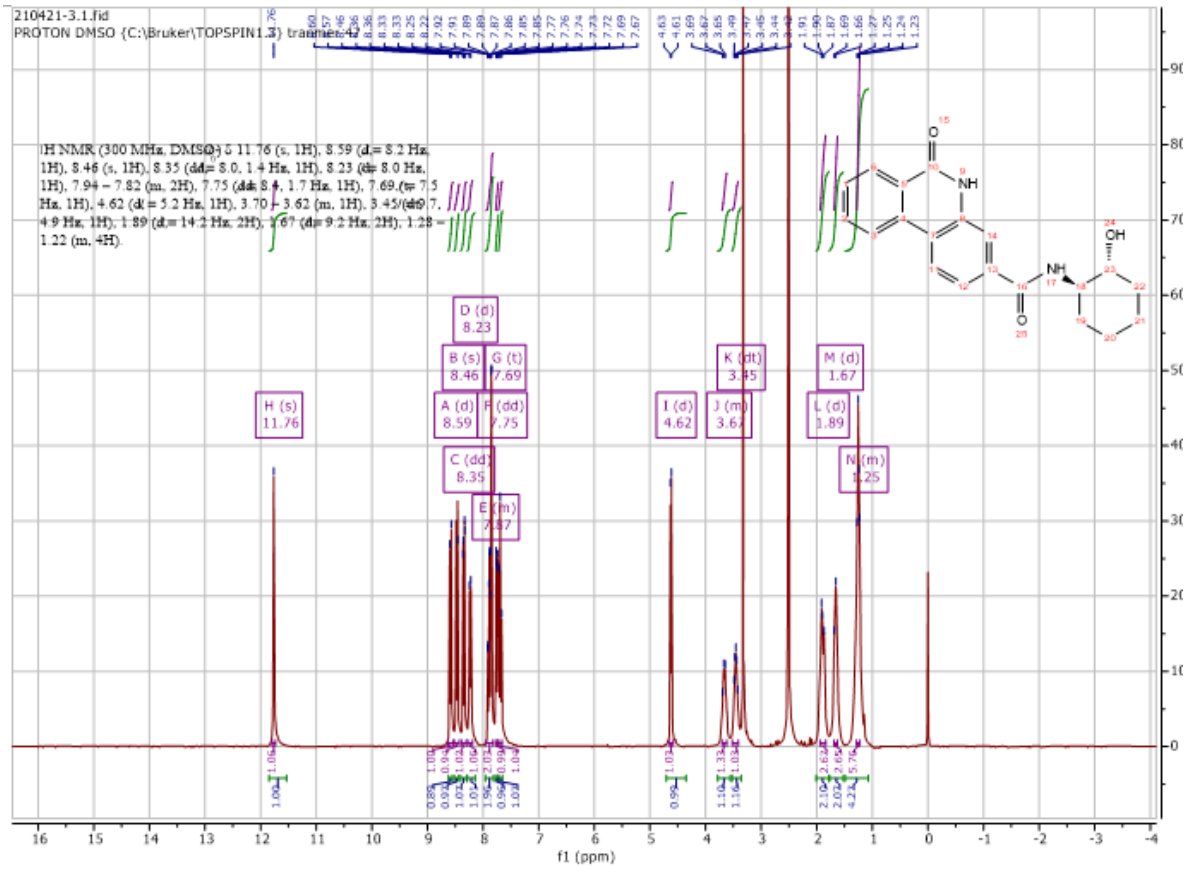
210421-3.1.fid
PROTON DMSO (C:\Bruker\TOPSPIN1.3) tranmer 42
1H NMR (300 MHz, DMSO) δ 11.76 (s, 1H), 8.59 (d, J = 8.2 Hz, 1H), 8.46 (s, 1H), 8.35 (dd, J = 8.0, 1.4 Hz, 1H), 8.23 (d, J = 8.0 Hz, 1H), 7.94 – 7.82 (m, 2H), 7.75 (dd, J = 8.4, 1.7 Hz, 1H), 7.69 (t, J = 7.5 Hz, 1H), 4.62 (d, J = 5.2 Hz, 1H), 3.70 – 3.62 (m, 1H), 3.45 (dd, J = 9.7, 4.9 Hz, 1H), 1.89 (dt, J = 14.2 Hz, 2H), 1.67 (d, J = 9.2 Hz, 2H), 1.28 – 1.22 (m, 4H).
D (d) 8.23
B (s) 8.46
G (t) 7.69
K (dt) 3.45
M (d) 1.67
H (s) 11.76
A (d) 8.59
F (dd) 7.75
I (d) 4.62
J (m) 3.62
L (d) 1.89
C (dd) 8.35
N (m) 1.25
E (m) 7.87
f1 (ppm)

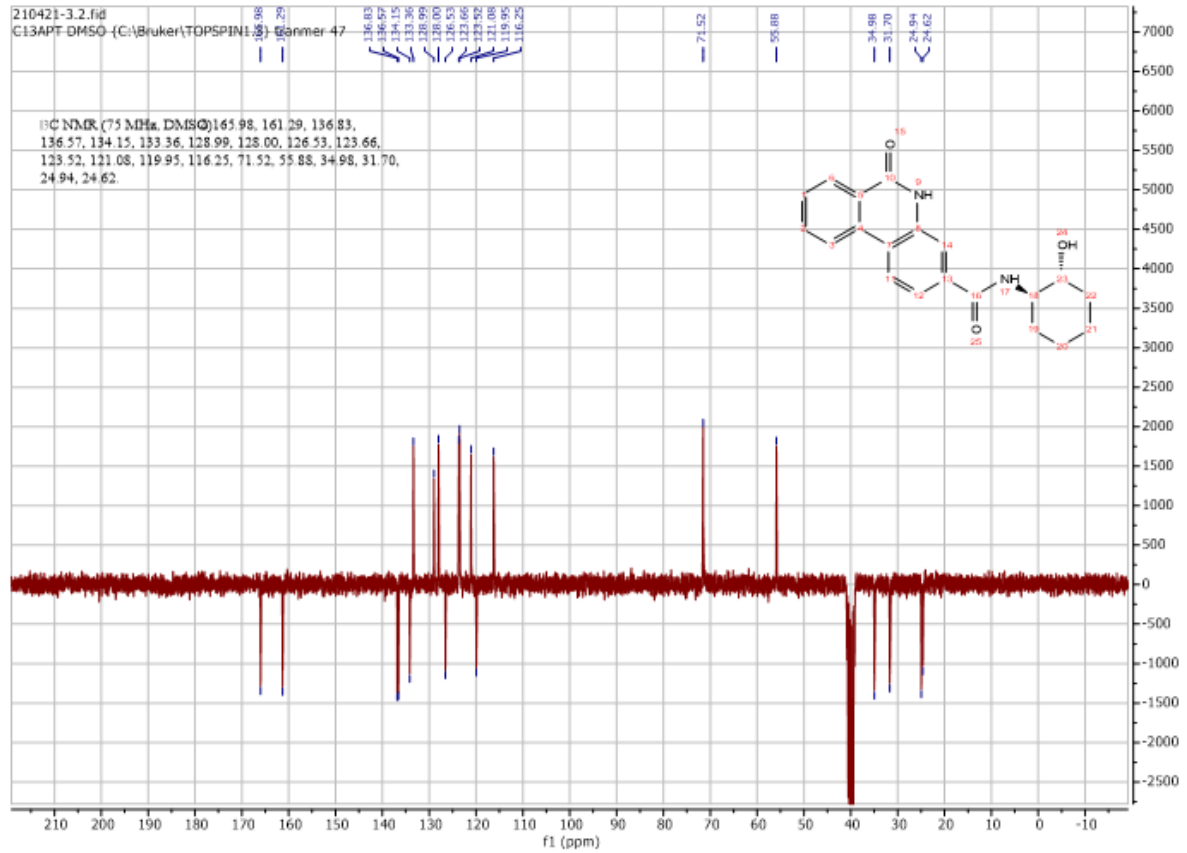
210421-3.2.fid
C13APT DMSO (C:\Bruker\TOPSPIN1.3) tranmer 47
13C NMR (75 MHz, DMSO) 165.98, 161.29, 136.83, 136.57, 134.15, 133.36, 128.99, 128.00, 126.53, 123.66, 123.52, 121.08, 119.95, 116.25, 71.52, 55.88, 34.98, 31.70, 24.94, 24.62.
f1 (ppm)

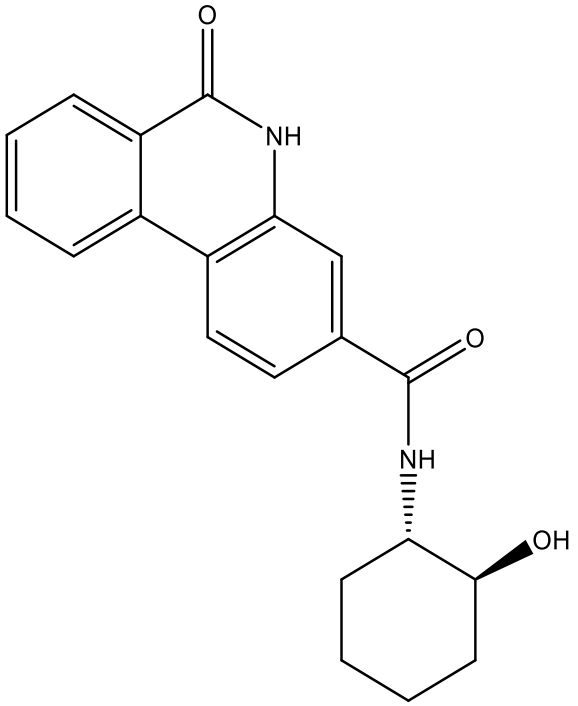

***N*-((1*S*,2*S*)-2-hydroxycyclohexyl)-6-oxo-5,6-dihydrophenanthridine-3-carboxamide (b22)**

Using **Synthesis Method d**, 24mg (0.1mmol) **f3** was with 11.5mg (0.1mmol) (1*S*,2*S*)-2-aminocyclohexan-1-ol to give 28.6mg **b22** (Yield: 85%) and the product was separated as white solid. ^{1}H NMR (300 MHz, DMSO-d_6) δ 11.77 (s, 1H), 8.59 (d, J = 8.2 Hz, 1H), 8.47 (d, J = 8.5 Hz, 1H), 8.35 (dd, J = 7.9, 1.4 Hz, 1H), 8.24 (d, J = 8.0 Hz, 1H), 7.94 – 7.82 (m, 2H), 7.80 – 7.64 (m, 2H), 4.63 (s, 1H), 3.70 – 3.62 (m, 1H), 3.50 – 3.37 (m, 1H), 1.89 (m, 2H), 1.65 (m, 2H), 1.24 (d, J = 7.1 Hz, 4H). ^{13}C NMR (75 MHz, DMSO) δ 166.0, 161.3, 136.8, 136.6, 134.2, 133.4, 129.0, 128.0, 126.5, 123.7, 123.5, 121.1, 120.0, 116.2, 71.5, 55.9, 35.0, 31.7, 24.9, 24.6. HRMS m/z (ESI+, M+Na): Calcd for C20H20N2O3: 359.1372, (ESI+, M+Na) found: 359.1364

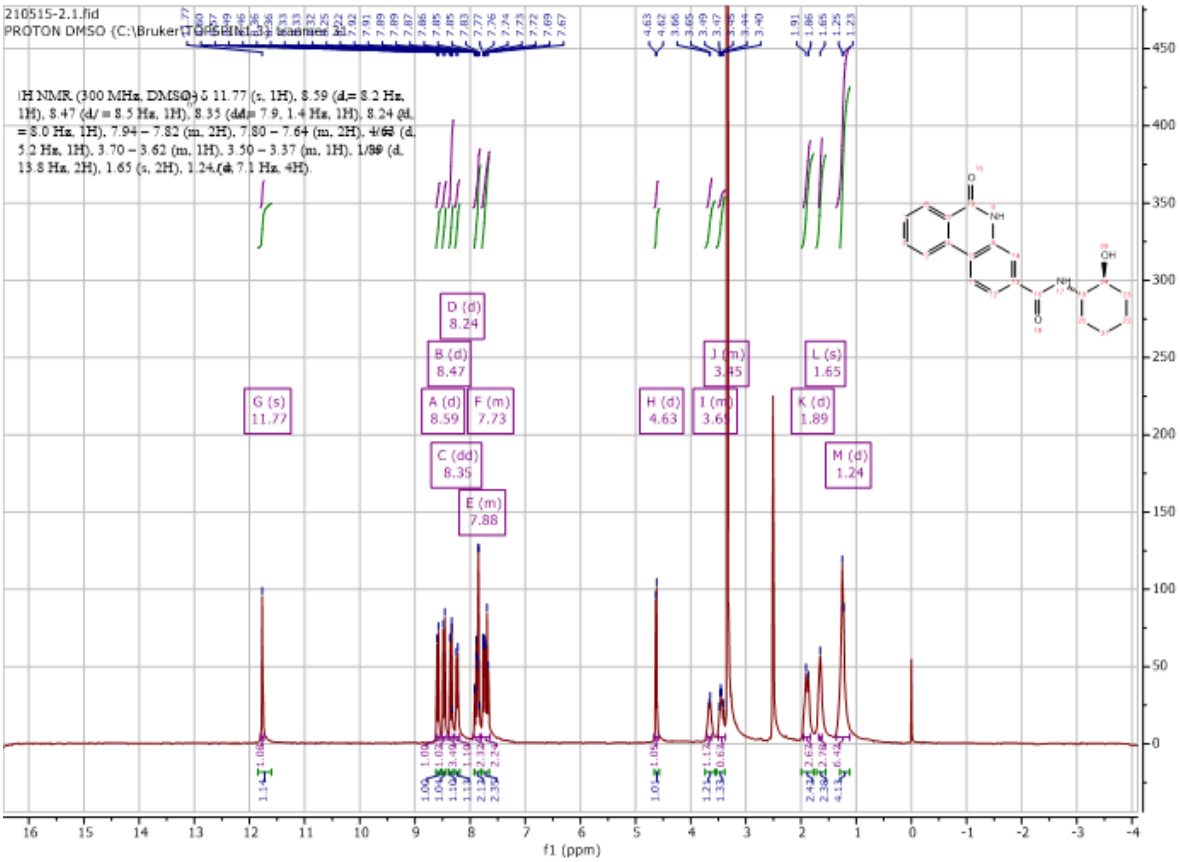
210515-2.1.fid
PROTON DMSO (C:\Bruker\TOPSPIN1.3) Tanmer 31
1H NMR (300 MHz, DMSO) δ 11.77 (s, 1H), 8.59 (d, J = 8.2 Hz, 1H), 8.47 (d, J = 8.5 Hz, 1H), 8.35 (dd, J = 7.9, 1.4 Hz, 1H), 8.24 (d, J = 8.0 Hz, 1H), 7.94 – 7.82 (m, 2H), 7.80 – 7.64 (m, 2H), 4.63 (d, J = 5.2 Hz, 1H), 3.70 – 3.62 (m, 1H), 3.50 – 3.37 (m, 1H), 1.89 (d, J = 13.8 Hz, 2H), 1.65 (s, 2H), 1.24 (d, J = 7.1 Hz, 4H).
D (d) 8.24
B (d) 8.47
J (m) 3.45
L (s) 1.65
G (s) 11.77
A (d) 8.59
F (m) 7.73
H (d) 4.63
I (m) 3.65
K (d) 1.89
C (dd) 8.35
M (d) 1.24
E (m) 7.88
f1 (ppm)

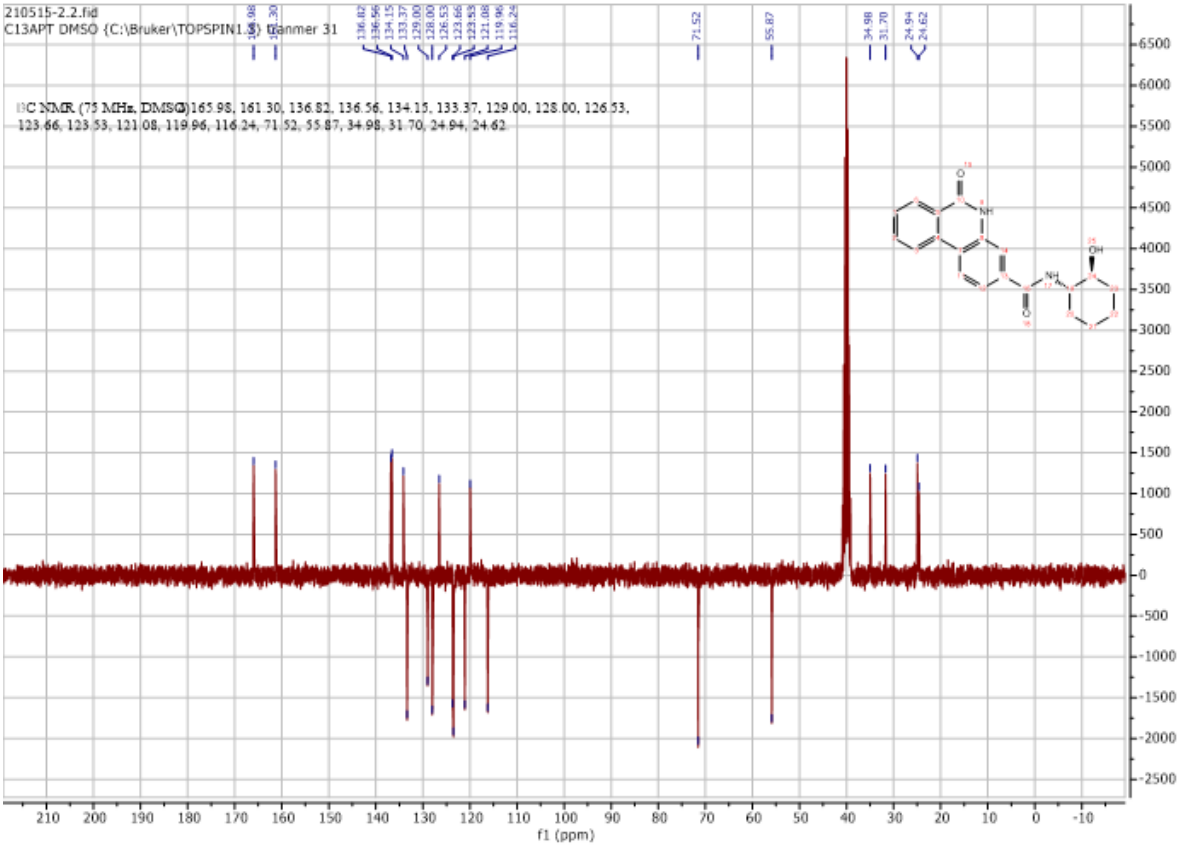
210515-2.2.fid
C13APT DMSO (C:\Bruker\TOPSPIN1.3) Tanmer 31
13C NMR (75 MHz, DMSO) δ 165.98, 161.30, 136.82, 136.56, 134.15, 133.37, 129.00, 128.00, 126.53, 123.66, 123.53, 121.08, 119.96, 116.24, 71.52, 55.87, 34.98, 31.70, 24.94, 24.62.
f1 (ppm)

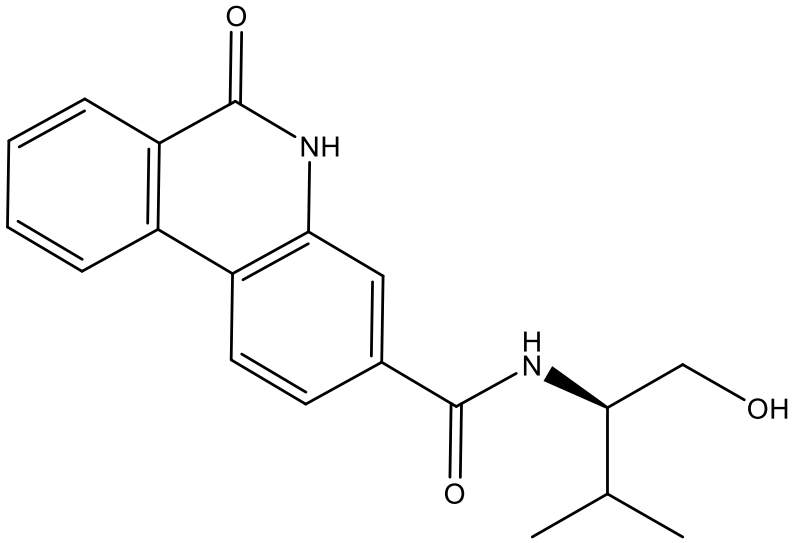

(*R*)-*N*-(1-hydroxy-3-methylbutan-2-yl)-6-oxo-5,6-dihydrophenanthridine-3-carboxamide (b23)

Using **Synthesis Method d**, 24mg (0.1mmol) **f3** was with 10.3mg (0.1mmol) (*R*)-2-amino-3-methylbutan-1-ol to give 23.7mg **b23** (Yield: 73%) and the product was separated as white solid. ^{1}H NMR (300 MHz, DMSO-d_6) δ 11.53 (s, 1H), 8.34 (d, *J* = 8.2 Hz, 1H), 8.23 (d, *J* = 8.4 Hz, 1H), 8.10 (dd, *J* = 7.9, 1.4 Hz, 1H), 7.84 (d, *J* = 8.9 Hz, 1H), 7.65 (ddd, *J* = 8.3, 7.2, 1.5 Hz, 1H), 7.60 (d, *J* = 1.7 Hz, 1H), 7.50 (dd, *J* = 8.5, 1.8 Hz, 1H), 7.48 – 7.42 (m, 1H), 4.35 (s, 1H), 3.61 (dq, *J* = 21.0, 6.2 Hz, 1H), 3.35 – 3.25 (m, 2H), 1.71 (dq, *J* = 16.5, 6.7 Hz, 1H), 0.70 (d, *J* = 6.9 Hz, 3H), 0.68 (d, *J* = 6.9 Hz, 3H). ^{13}C NMR (75 MHz, DMSO) δ 166.4, 161.3, 136.8, 136.6, 134.2, 133.4, 129.0, 128.0, 126.5, 123.7, 123.6, 121.1, 120.0, 116.2, 61.8, 57.2, 29.1, 20.2, 19.1. HRMS m/z (ESI+, M+Na): Calcd for C19H20N2O3: 347.1372, (ESI+, M+Na) found: 347.1365

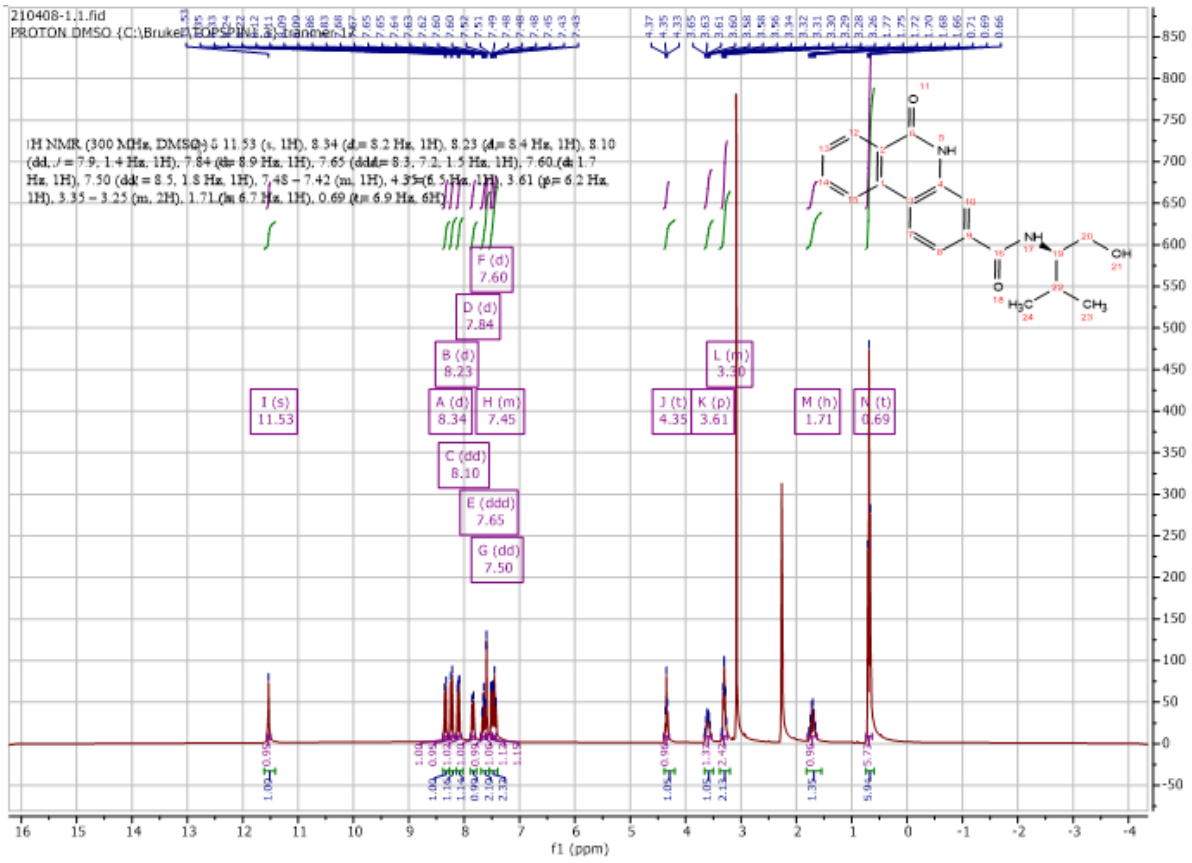
210408-1.1.fid
PROTON DMSO (C:\Bruker\TOPSPIN4.3) Banmer 17
F (d) 7.60
D (d) 7.84
B (d) 8.23
L (m) 3.30
I (s) 11.53
A (d) 8.34
H (m) 7.45
J (t) 4.35
K (p) 3.61
M (h) 1.71
N (t) 0.69
C (dd) 8.10
E (dddd) 7.65
G (dd) 7.50
f1 (ppm)

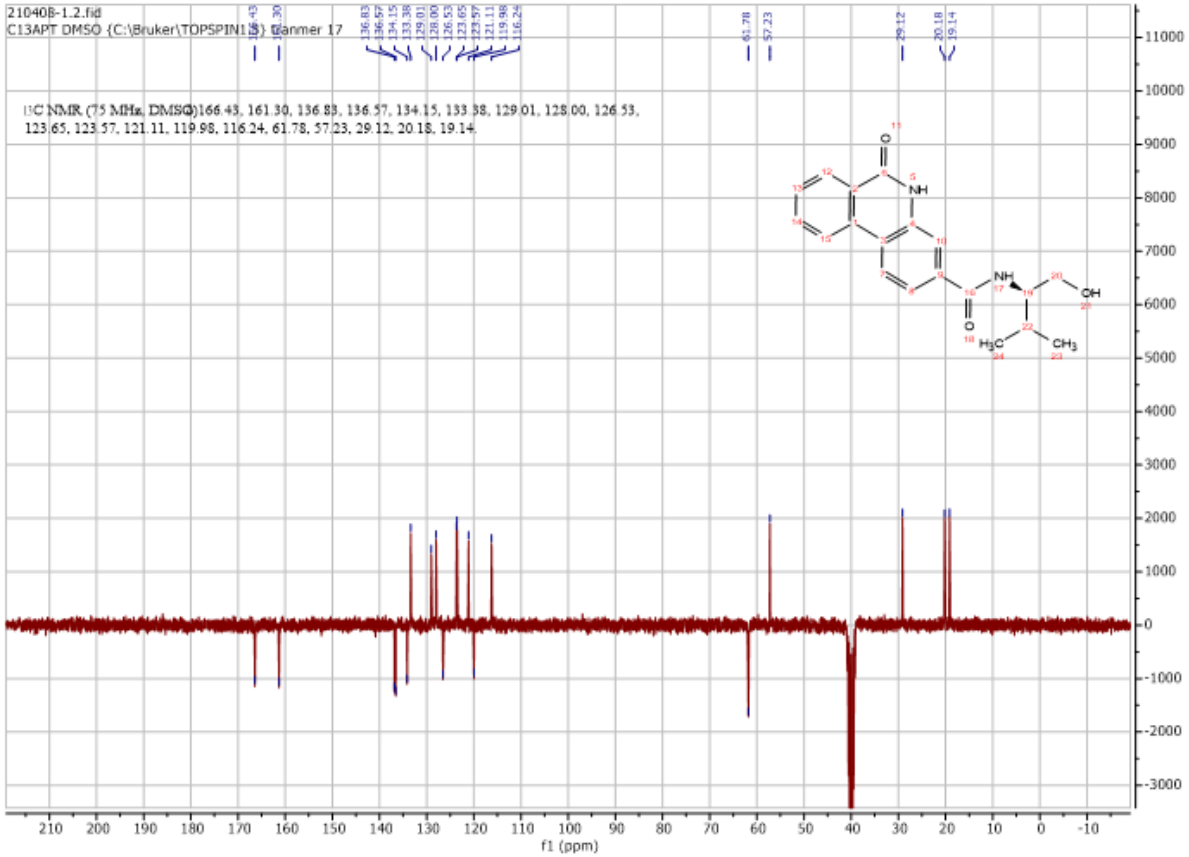
210408-1.2.fid
C13APT DMSO (C:\Bruker\TOPSPIN4.3) Banmer 17
f1 (ppm)

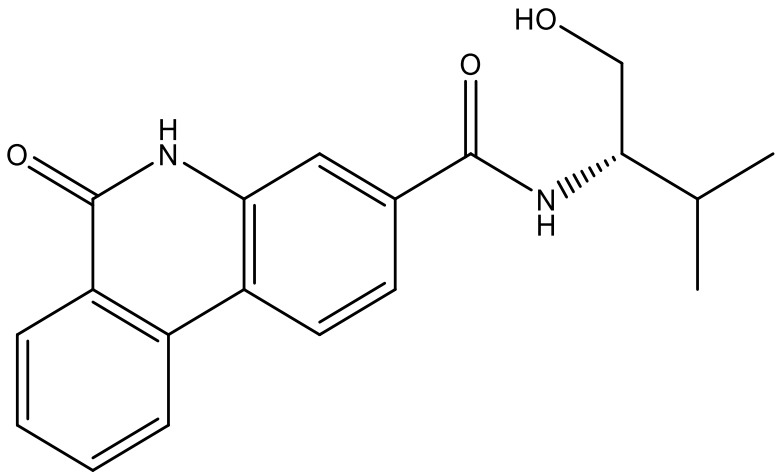

(*S*)-*N*-(1-hydroxy-3-methylbutan-2-yl)-6-oxo-5,6-dihydrophenanthridine-3-carboxamide (b24)

Using **Synthesis Method d**, 24mg (0.1mmol) **f3** was with 10.3mg (0.1mmol) (*S*)-2-amino-3-methylbutan-1-ol to give 24mg **b24** (Yield: 74%) and the product was separated as white solid. ^{1}H NMR (300 MHz, DMSO-d_6) δ 11.77 (s, 1H), 8.58 (d, *J* = 8.1 Hz, 1H), 8.48 (s, 1H), 8.34 (dd, *J* = 7.9, 1.4 Hz, 1H), 8.08 (d, *J* = 8.9 Hz, 1H), 7.95 – 7.80 (m, 2H), 7.78 (s, 2H), 4.50 (s, 1H), 3.75 (m, 1H), 3.48 (m, 2H), 1.98 (m, 1H), 0.87 (dd, *J* = 7.5, 6.9 Hz, 6H). ^{13}C NMR (75 MHz, DMSO) δ 166.8, 161.3, 136.8, 136.6, 134.2, 133.4, 129.0, 128.0, 126.5, 123.7, 123.6, 121.1, 120.0, 116.2, 61.8, 57.2, 29.1, 20.2, 19.1. HRMS m/z (ESI+, M+Na): Calcd for C19H20N2O3: 347.1372, (ESI+, M+Na) found: 347.1363

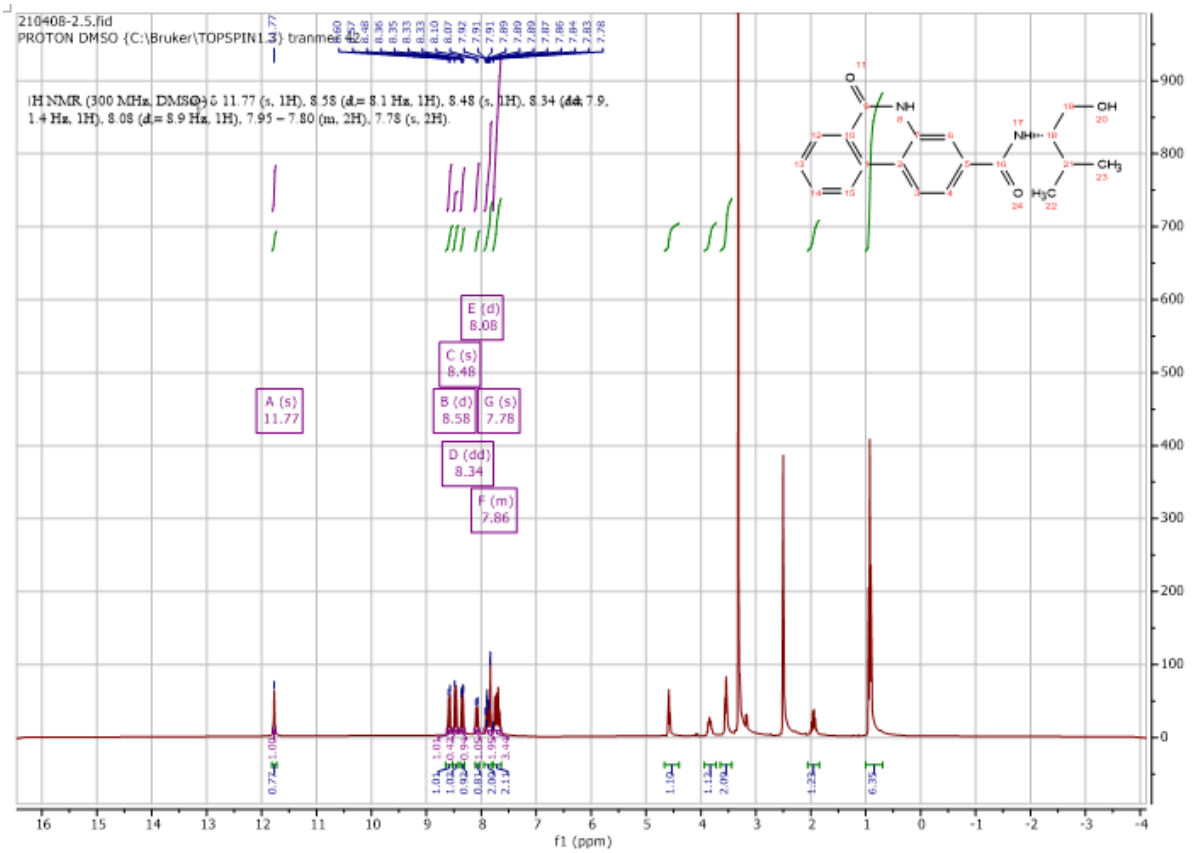
210408-2.5.fid
PROTON DMSO {C:\Bruker\TOPSPIN1.3} tranmer 42
1H NMR (300 MHz, DMSO) δ 11.77 (s, 1H), 8.58 (d, J = 8.1 Hz, 1H), 8.48 (s, 1H), 8.34 (dd, J = 7.9, 1.4 Hz, 1H), 8.08 (d, J = 8.9 Hz, 1H), 7.95 – 7.80 (m, 2H), 7.78 (s, 2H).
A (s) 11.77
B (d) 8.58
C (s) 8.48
D (dd) 8.34
E (d) 8.08
F (m) 7.86
G (s) 7.78
f1 (ppm)

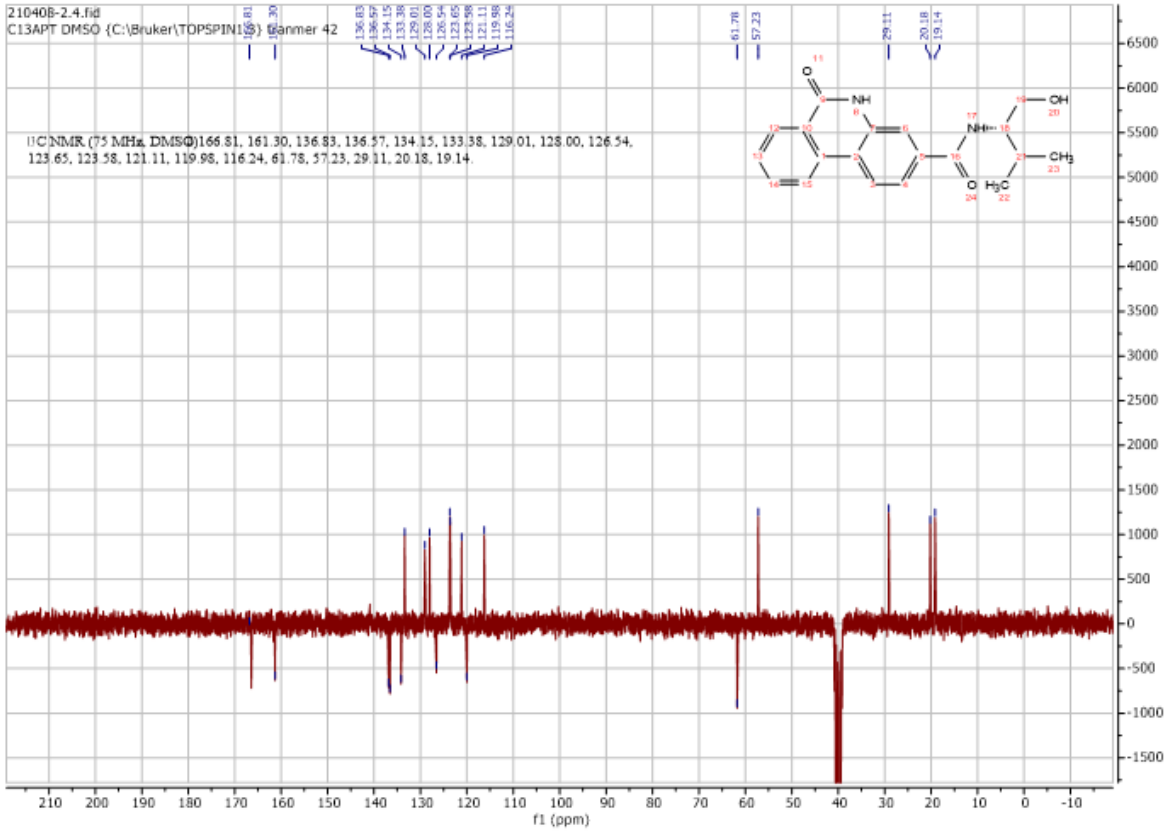
210408-2.4.fid
C13APT DMSO {C:\Bruker\TOPSPIN1.3} tranmer 42
13C NMR (75 MHz, DMSO) 166.81, 161.30, 136.83, 136.57, 134.15, 133.38, 129.01, 128.00, 126.54, 123.65, 123.58, 121.11, 119.98, 116.24, 61.78, 57.23, 29.11, 20.18, 19.14.
f1 (ppm)

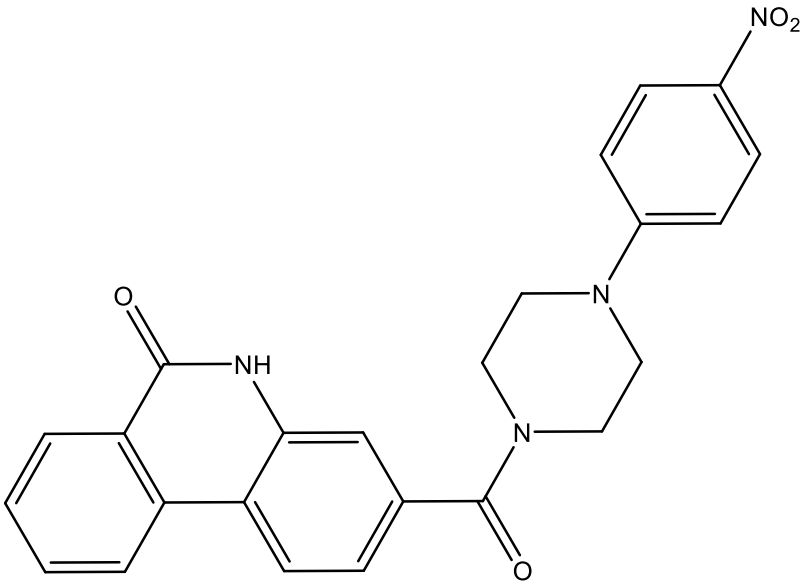

3-(4-(4-nitrophenyl)piperazine-1-carbonyl)phenanthridin-6(5*H*)-one (b25)

Using **Synthesis Method d**, 24mg (0.1mmol) **f3** was reacted with 20.7mg (0.1mmol) 1-(4-nitrophenyl)piperazine to give 25.7mg **b25** (Yield: 60%) and the product was separated as yellow solid. ^{1}H NMR (300 MHz, DMSO-d_6) δ 11.81 (s, 1H), 8.56 (d, *J* = 7.9 Hz, 1H), 8.48 (d, *J* = 8.3 Hz, 1H), 8.35 (d, *J* = 7.9 Hz, 1H), 8.09 (d, *J* = 9.0 Hz, 2H), 7.90 (t, *J* = 7.6 Hz, 1H), 7.70 (t, *J* = 7.5 Hz, 1H), 7.44 (s, 1H), 7.34 (d, *J* = 8.2 Hz, 1H), 7.04 (d, *J* = 9.2 Hz, 2H), 3.59 (m, 8H). ^{13}C NMR (75 MHz, DMSO) δ ^{13}C NMR (75 MHz, DMSO) δ 168.9, 161.3, 154.9, 137.6, 137.0, 136.8, 134.1, 133.5, 129.0, 128.0, 126.4, 126.2, 124.0, 123.4, 121.2, 119.0, 115.4, 113.2, 44.8, 42.5. HRMS m/z (ESI+, M+Na): Calcd for C24H20N4O4: 451.1382, (ESI+, M+Na) found: 451.1379

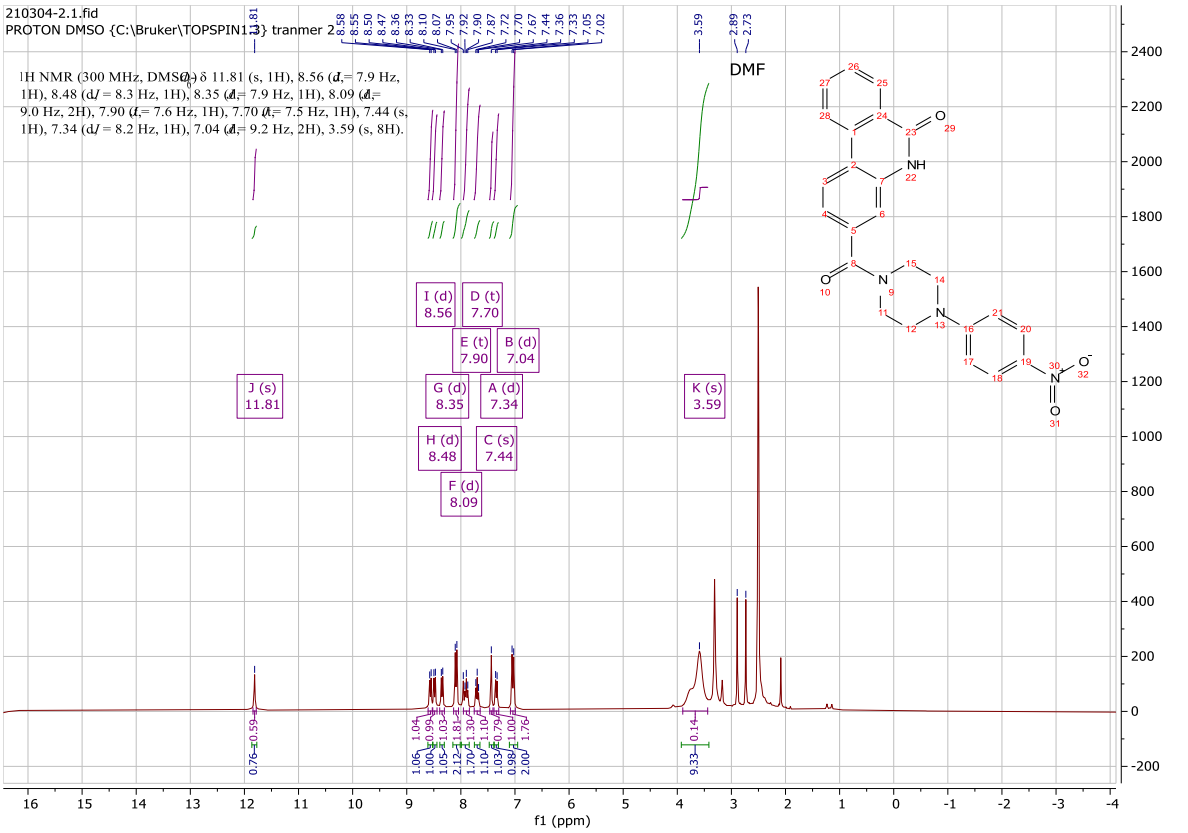
210304-2.1.fid
PROTON DMSO {C:\Bruker\TOPSPIN1.3} tranmer 2
¹H NMR (300 MHz, DMSO) δ 11.81 (s, 1H), 8.56 (d, J = 7.9 Hz, 1H), 8.48 (d, J = 8.3 Hz, 1H), 8.35 (d, J = 7.9 Hz, 1H), 8.09 (d, J = 9.0 Hz, 2H), 7.90 (t, J = 7.6 Hz, 1H), 7.70 (t, J = 7.5 Hz, 1H), 7.44 (s, 1H), 7.34 (d, J = 8.2 Hz, 1H), 7.04 (d, J = 9.2 Hz, 2H), 3.59 (s, 8H).
DMF
I (d) 8.56
D (t) 7.70
E (t) 7.90
B (d) 7.04
J (s) 11.81
G (d) 8.35
A (d) 7.34
K (s) 3.59
H (d) 8.48
C (s) 7.44
F (d) 8.09
f1 (ppm)

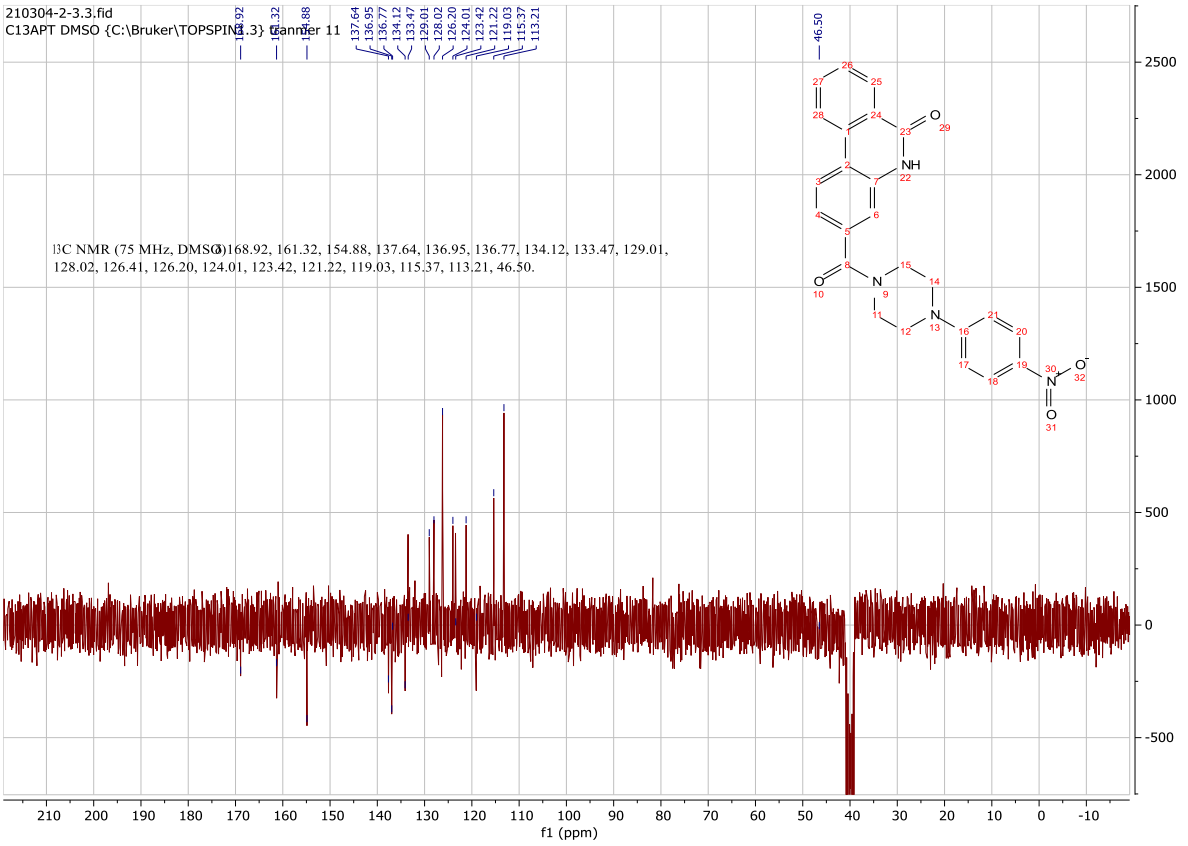
210304-2-3.3.fid
C13APT DMSO {C:\Bruker\TOPSPIN1.3} tranmer 11
¹³C NMR (75 MHz, DMSO) 168.92, 161.32, 154.88, 137.64, 136.95, 136.77, 134.12, 133.47, 129.01, 128.02, 126.41, 126.20, 124.01, 123.42, 121.22, 119.03, 115.37, 113.21, 46.50.
f1 (ppm)

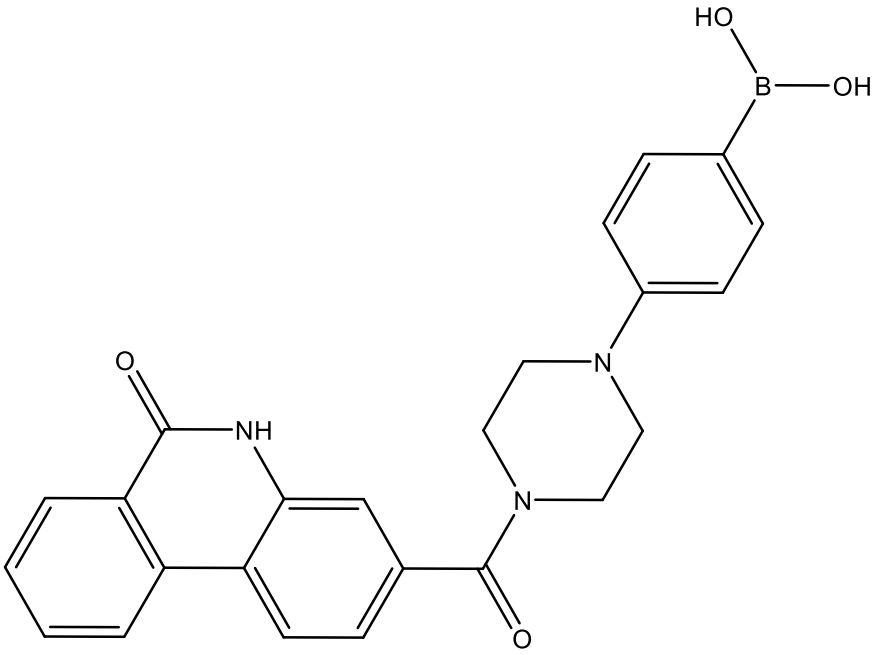

(4-(4-(6-oxo-5,6-dihydrophenanthridine-3-carbonyl)piperazin-1-yl)phenyl)boronic acid (b26)

Using **Synthesis Method d**, 24mg (0.1mmol) **f3** was reacted with 20.6mg (0.1mmol) (4-(piperazin-1-yl)phenyl)boronic acid to give 26.9mg **b26** (Yield: 63%) and the product was separated as yellow solid. ^{1}H NMR (300 MHz, DMSO-d_6) δ 11.79 (s, 1H), 8.56 (d, J = 8.0 Hz, 1H), 8.48 (d, J = 8.3 Hz, 1H), 8.35 (d, J = 7.8 Hz, 1H), 7.90 (t, J = 7.6 Hz, 1H), 7.76 – 7.64 (m, 5H), 7.42 (s, 1H), 7.32 (d, J = 8.0 Hz, 1H), 6.91 (d, J = 8.1 Hz, 2H), 3.67 (m, 6H), 3.17 (m, 2H).^{13}C NMR (75 MHz, DMSO) δ 168.7, 161.3, 152.4, 137.0, 136.9, 135.9, 134.1, 133.5, 130.4, 129.0, 128.0, 126.4, 124.0, 123.4, 121.2, 119.0, 115.3, 114.7, 56.6, 48.9. HRMS m/z (ESI-, M-H): Calcd for C24H22BN3O4: 426.1631, (ESI-, M-H) found: 426.1635

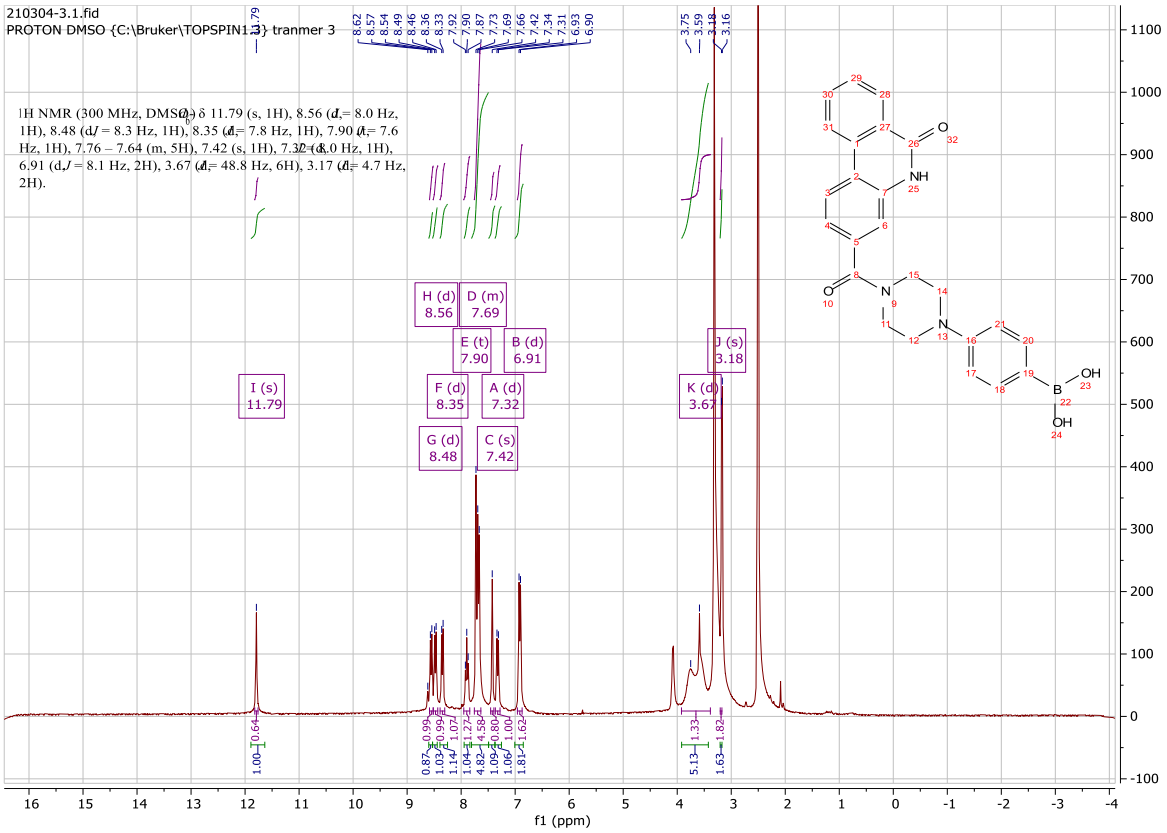
210304-3.1.fid
PROTON DMSO {C:\Bruker\TOPSPIN1.3} tranmer 3
1H NMR (300 MHz, DMSO-d6) δ 11.79 (s, 1H), 8.56 (d, J = 8.0 Hz, 1H), 8.48 (d, J = 8.3 Hz, 1H), 8.35 (d, J = 7.8 Hz, 1H), 7.90 (t, J = 7.6 Hz, 1H), 7.76 – 7.64 (m, 5H), 7.42 (s, 1H), 7.32 (d, J = 8.0 Hz, 1H), 6.91 (d, J = 8.1 Hz, 2H), 3.67 (d, J = 48.8 Hz, 6H), 3.17 (d, J = 4.7 Hz, 2H).
H (d) 8.56
D (m) 7.69
E (t) 7.90
B (d) 6.91
J (s) 3.18
I (s) 11.79
F (d) 8.35
A (d) 7.32
K (d) 3.67
G (d) 8.48
C (s) 7.42
f1 (ppm)

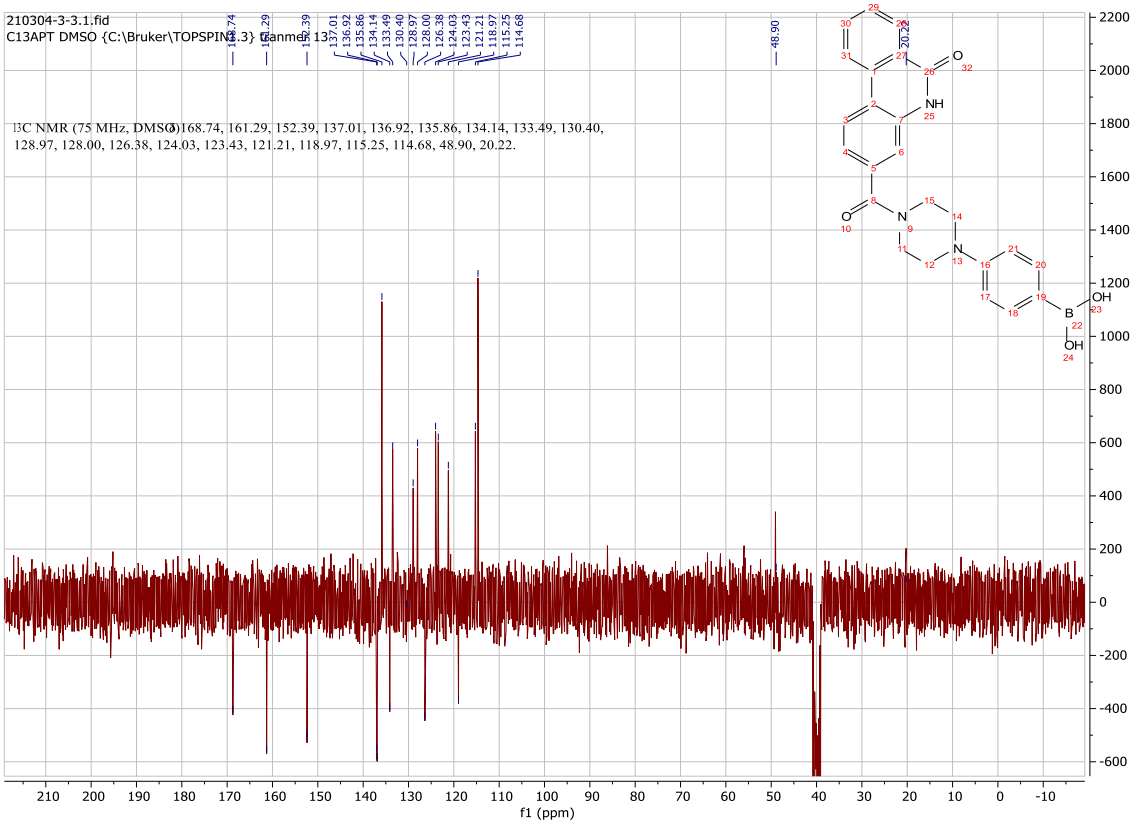
210304-3-3.1.fid
C13APT DMSO {C:\Bruker\TOPSPIN1.3} tranmer 13
13C NMR (75 MHz, DMSO) 168.74, 161.29, 152.39, 137.01, 136.92, 135.86, 134.14, 133.49, 130.40, 128.97, 128.00, 126.38, 124.03, 123.43, 121.21, 118.97, 115.25, 114.68, 48.90, 20.22.
f1 (ppm)

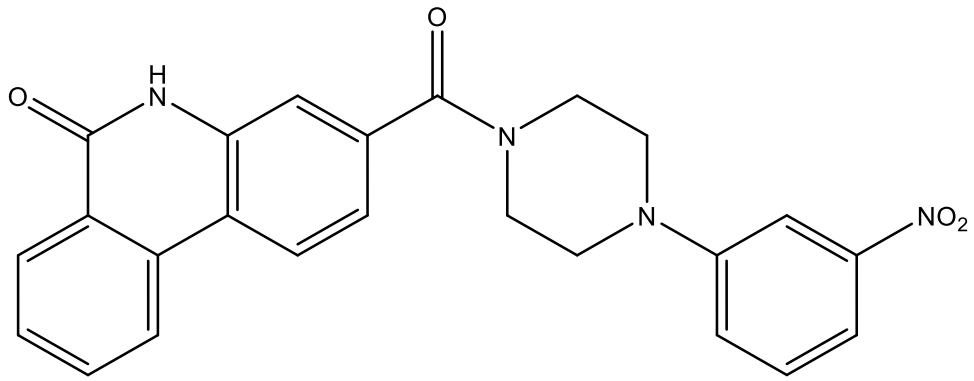

3-(4-(3-nitrophenyl)piperazine-1-carbonyl)phenanthridin-6(5*H*)-one (b27)

Using **Synthesis Method d**, 24mg (0.1mmol) **f3** was reacted with 20.8mg (0.1mmol) 1-(3-nitrophenyl)piperazine to give 27.8mg **b27** (Yield: 65%) and the product was separated as yellow solid. ^{1}H NMR (300 MHz, DMSO-d_6) δ 11.81 (s, 1H), 8.56 (d, *J* = 8.2 Hz, 1H), 8.48 (d, *J* = 8.3 Hz, 1H), 8.35 (dd, *J* = 8.0, 1.4 Hz, 1H), 7.95 – 7.85 (m, 1H), 7.75 – 7.67 (m, 2H), 7.63 (dt, *J* = 7.5, 1.2 Hz, 1H), 7.51 (t, *J* = 8.1 Hz, 1H), 7.46 – 7.39 (m, 2H), 7.34 (dd, *J* = 8.3, 1.6 Hz, 1H), 3.96 – 3.35 (m, 8H). ^{13}C NMR (75 MHz, DMSO) δ 168.8, 161.3, 151.8, 149.3, 137.0, 136.9, 134.1, 133.5, 130.7, 129.0, 128.0, 126.4, 124.0, 123.4, 122.2, 121.2, 119.0, 115.3, 113.6, 109.3, 53.9, 48.1. HRMS m/z (ESI+, M+Na): Calcd for C24H20N4O4: 451.1631, (ESI+, M+Na) found: 451.1367

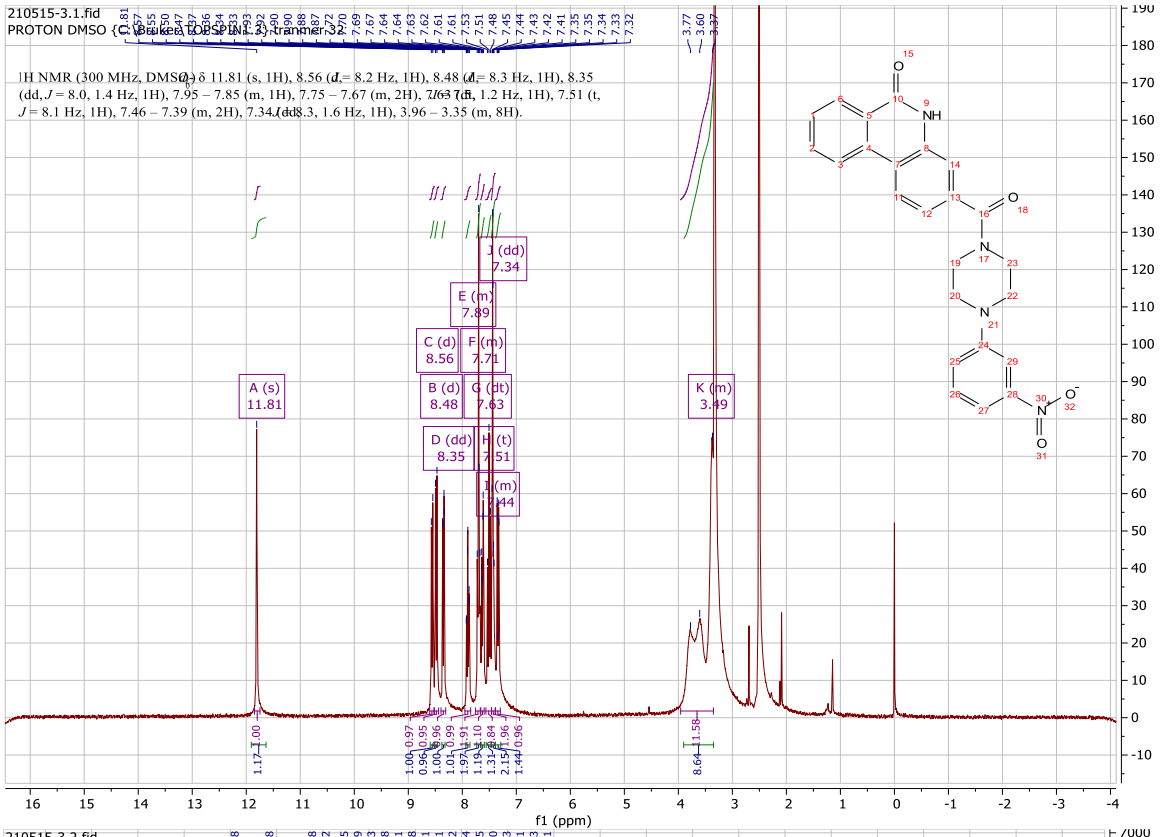
210515-3.1.fid
PROTON DMSO {C:\Bruker\TOPSPIN4.3} tranmer 32
A (s) 11.81
B (d) 8.48
C (d) 8.56
D (dd) 8.35
E (m) 7.89
F (m) 7.71
G (dt) 7.63
H (t) 7.51
I (m) 7.44
J (dd) 7.34
K (m) 3.49
f1 (ppm)

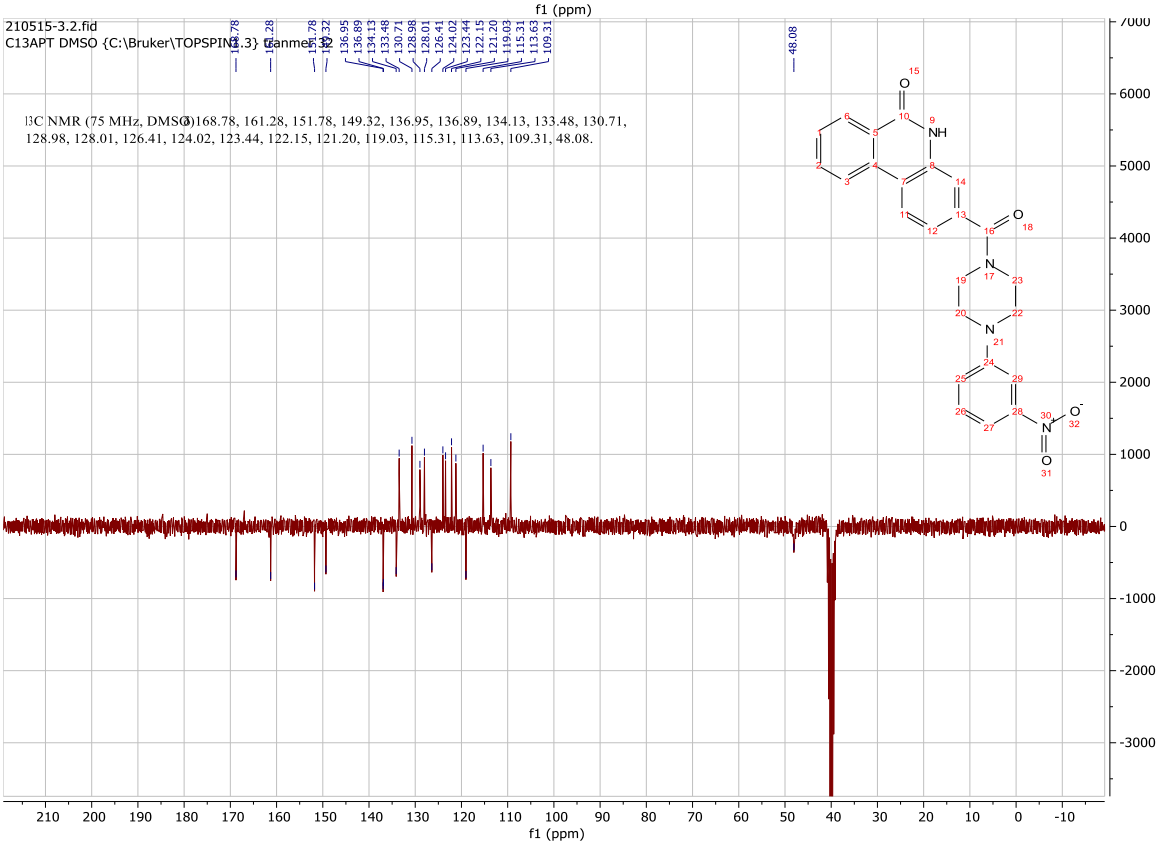
210515-3.2.fid
C13APT DMSO {C:\Bruker\TOPSPIN4.3} tranmer 32
f1 (ppm)

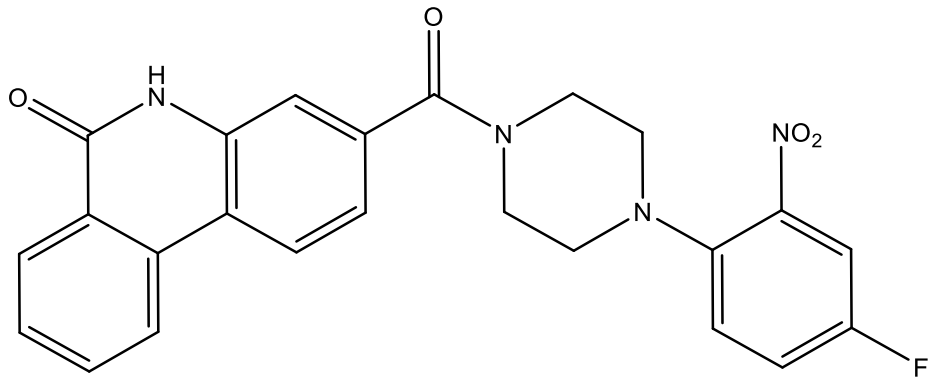

3-(4-(4-fluoro-2-nitrophenyl)piperazine-1-carbonyl)phenanthridin-6(5*H*)-one (b28)

Using **Synthesis Method d**, 24mg (0.1mmol) **f3** was reacted with 22.6mg (0.1mmol) 1-(4-fluoro-2-nitrophenyl)piperazine to give 12.9mg **b28** (Yield: 29%) and the product was separated as yellow solid. ^{1}H NMR (300 MHz, DMSO-d_6) δ 11.80 (s, 1H), 8.55 (d, J = 8.2 Hz, 1H), 8.48 (s, 1H), 8.34 (dd, J = 7.9, 1.4 Hz, 1H), 7.95 – 7.81 (m, 2H), 7.75 – 7.64 (m, 1H), 7.63 – 7.47 (m, 2H), 7.42 (d, J = 1.6 Hz, 1H), 7.33 (dd, J = 8.2, 1.6 Hz, 1H), 3.63 (m, 4H), 3.01 (m, 4H). ^{13}C NMR (75 MHz, DMSO) δ 168.7, 161.3, 160.4 (d, J = 233.8 Hz) 159.1, 155.9, 145.3, 142.1, 137.0, 134.1, 133.5, 129.0, 128.0, 126.4, 125.4 (d, J = 8.3 Hz), 124.0, 123.4, 121.2, 121.1 (d, J = 21.9 Hz), 119.0, 115.3, 112.5(d, J = 27.6 Hz), 52.5, 46.3. HRMS m/z (ESI+, M+Na): Calcd for C24H19FN4O4: 469.1288, (ESI+, M+Na) found: 469.1288

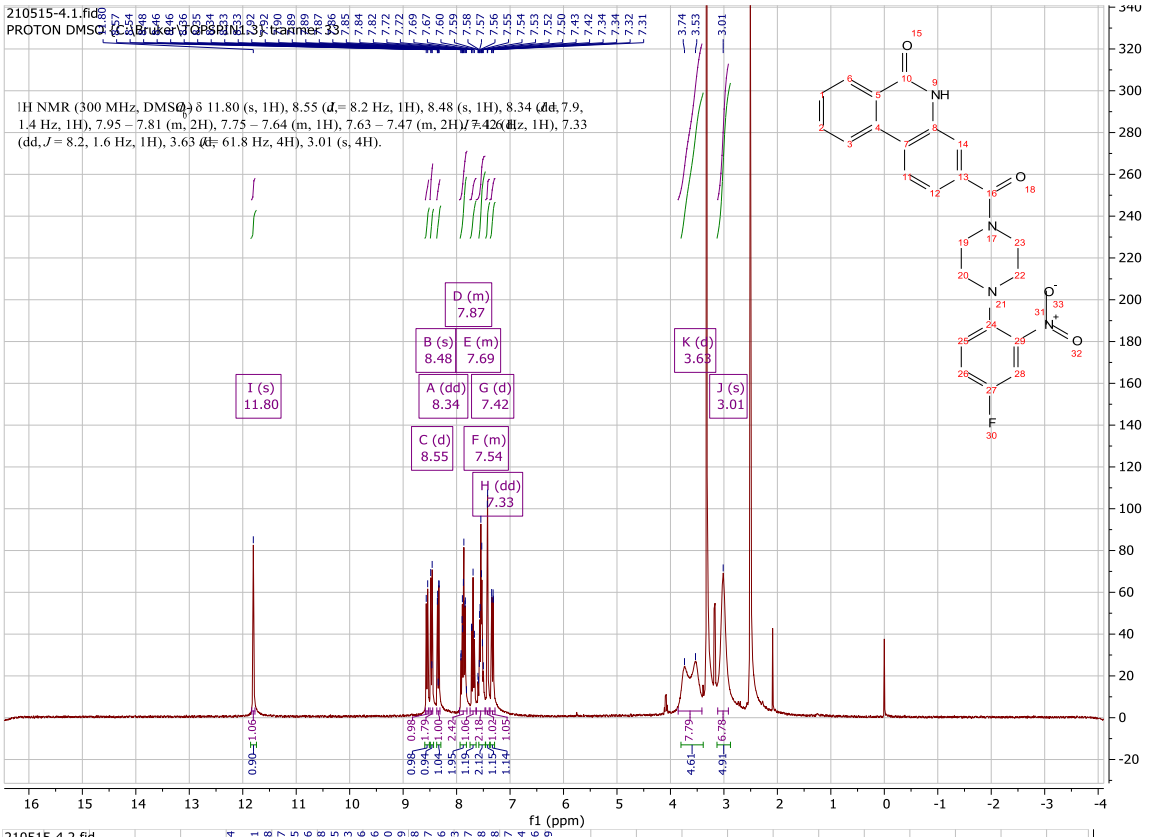
210515-4.1.fid
PROTON DMSO {C:\Bruker\TOPSPIN4.1.3} tramer 33
I (s) 11.80
B (s) 8.48
E (m) 7.69
D (m) 7.87
A (dd) 8.34
G (d) 7.42
C (d) 8.55
F (m) 7.54
H (dd) 7.33
K (d) 3.63
J (s) 3.01
f1 (ppm)

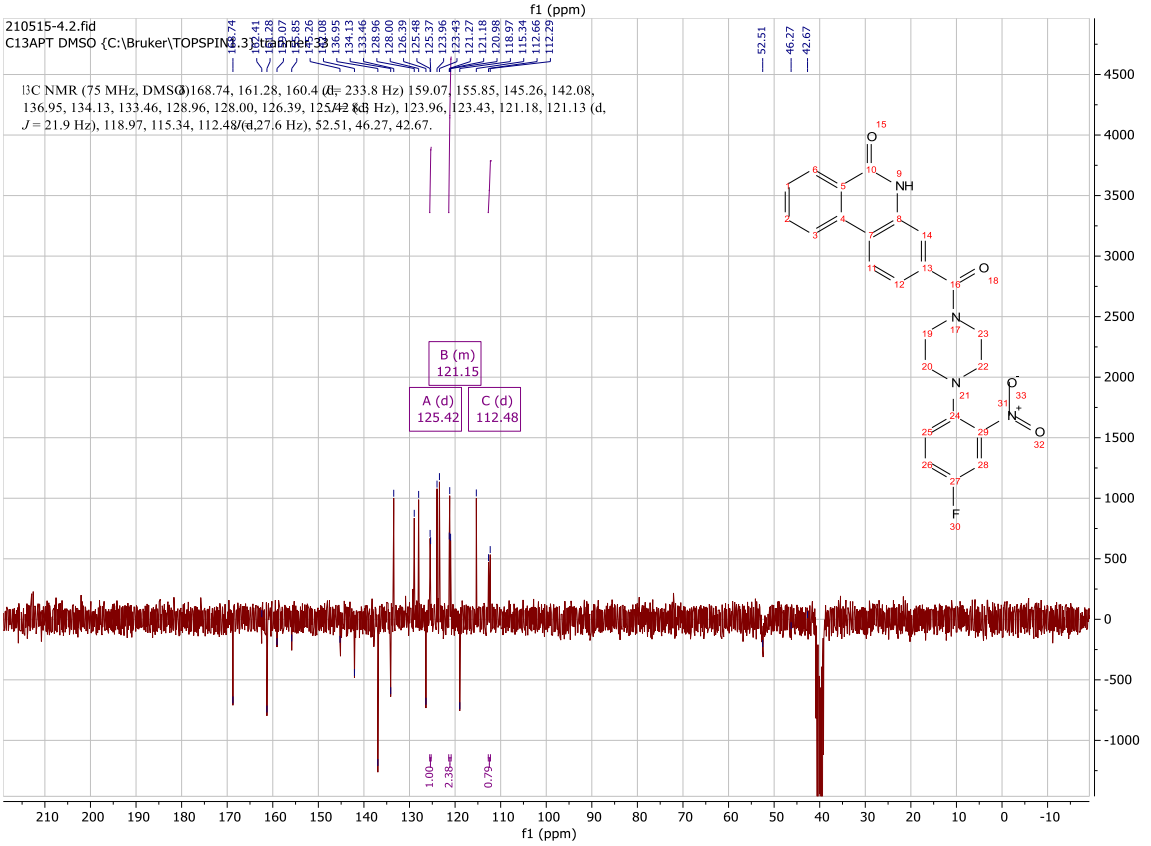
210515-4.2.fid
C13APT DMSO {C:\Bruker\TOPSPIN4.1.3} tramer 33
B (m) 121.15
A (d) 125.42
C (d) 112.48
f1 (ppm)

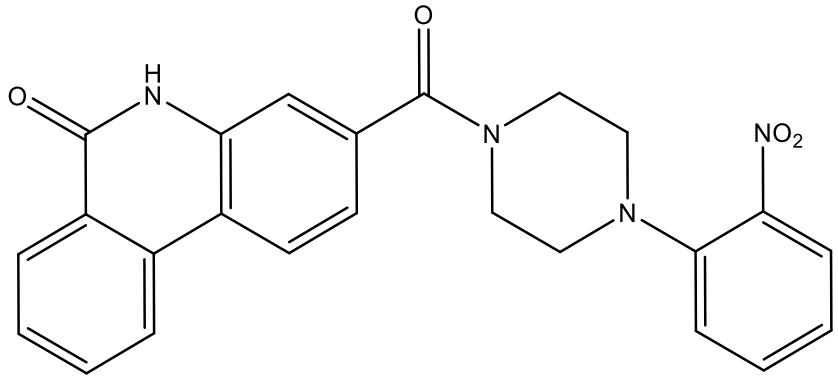

3-(4-(2-nitrophenyl)piperazine-1-carbonyl)phenanthridin-6(5*H*)-one (b29)

Using **Synthesis Method d**, 24mg (0.1mmol) **f3** was reacted with 20.6mg (0.1mmol) 1-(2-nitrophenyl)piperazineto give 25.3mg **b29** (Yield: 59%) and the product was separated as yellow solid. ^{1}H NMR (300 MHz, DMSO-d_6) δ 8.55 (d, J = 8.2 Hz, 1H), 8.47 (d, J = 8.3 Hz, 1H), 8.35 (dd, J = 7.9, 1.4 Hz, 1H), 7.90 (td, 1H), 7.86 (dd, 1H), 7.70 (t, J = 7.6 Hz, 1H), 7.63 (td, J = 8.5, 7.4, 1.6 Hz, 1H), 7.43 (d, J = 1.6 Hz, 1H), 7.39 (dd, J = 8.3, 1.2 Hz, 1H), 7.34 (dd, J = 8.2, 1.6 Hz, 1H), 7.21 (td, 1H), 3.76 (m, 4H), 3.07 (m, 4H). ^{13}C NMR (75 MHz, DMSO) δ 168.8, 161.3, 155.1, 145.4, 143.9, 136.9, 134.3, 134.1, 133.5, 129.0, 128.0, 126.4, 126.0, 124.0, 123.42, 123.3, 122.6, 121.2, 119.0, 115.3, 51.9, 47.2. HRMS m/z (ESI+, M+Na): Calcd for C24H20N4O4: 451.1382, (ESI+, M+Na) found: 451.1376

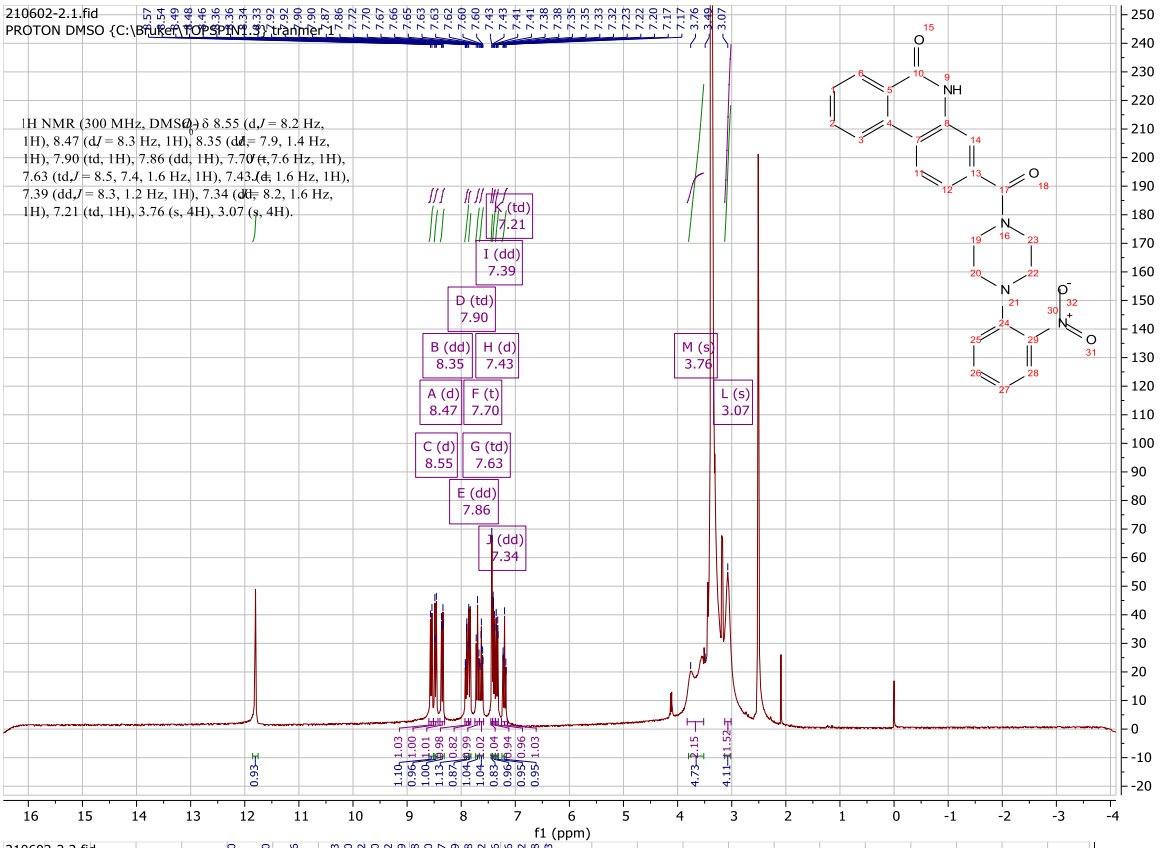
210602-2.1.fid
PROTON DMSO {C:\Bruker\TOPSPIN4.3} Tranmer 1
1H NMR (300 MHz, DMSO) δ 8.55 (d, J = 8.2 Hz, 1H), 8.47 (d, J = 8.3 Hz, 1H), 8.35 (dd, J = 7.9, 1.4 Hz, 1H), 7.90 (td, 1H), 7.86 (dd, 1H), 7.70 (t, 7.6 Hz, 1H), 7.63 (td, J = 8.5, 7.4, 1.6 Hz, 1H), 7.43 (d, 1.6 Hz, 1H), 7.39 (dd, J = 8.3, 1.2 Hz, 1H), 7.34 (dd, 8.2, 1.6 Hz, 1H), 7.21 (td, 1H), 3.76 (s, 4H), 3.07 (s, 4H).
K (td) 7.21
I (dd) 7.39
D (td) 7.90
B (dd) 8.35
H (d) 7.43
A (d) 8.47
F (t) 7.70
C (d) 8.55
G (td) 7.63
E (dd) 7.86
J (dd) 7.34
M (s) 3.76
L (s) 3.07
f1 (ppm)

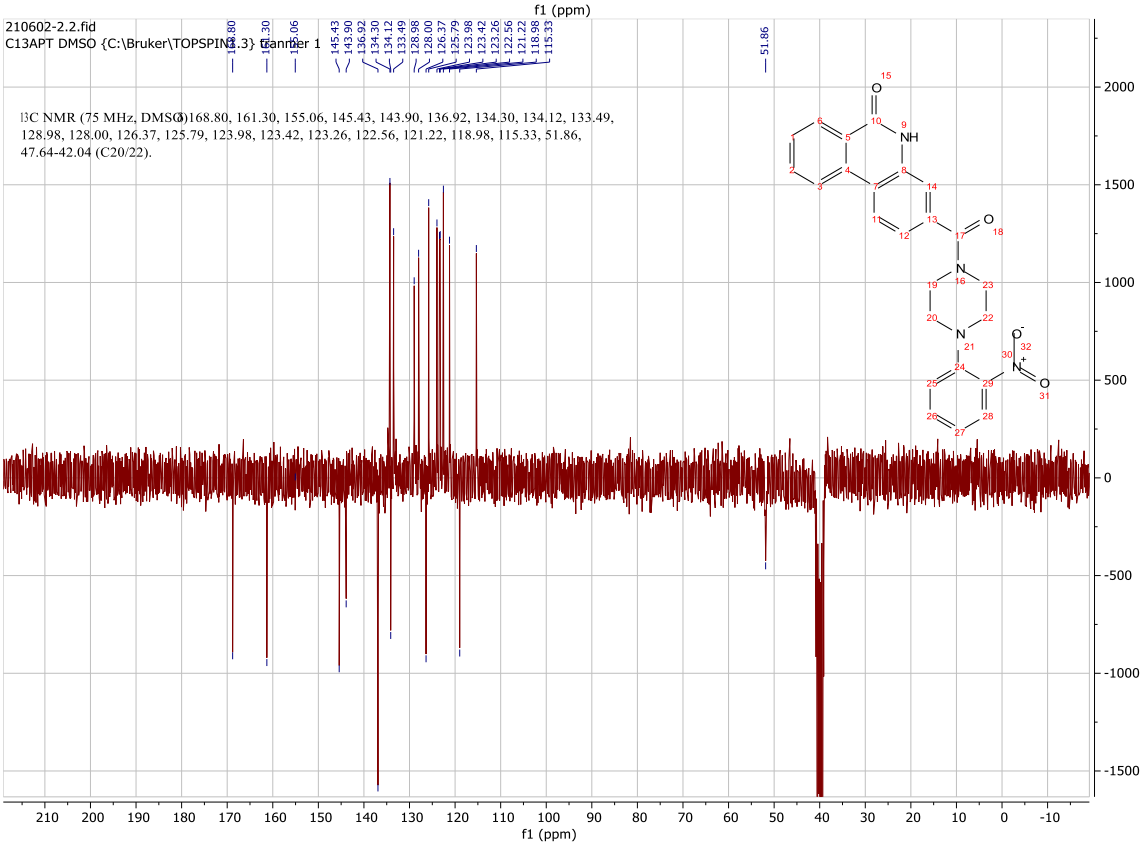
210602-2.2.fid
C13APT DMSO {C:\Bruker\TOPSPIN4.3} Tranmer 1
13C NMR (75 MHz, DMSO) 168.80, 161.30, 155.06, 145.43, 143.90, 136.92, 134.30, 134.12, 133.49, 128.98, 128.00, 126.37, 125.79, 123.98, 123.42, 123.26, 122.56, 121.22, 118.98, 115.33, 51.86, 47.64-42.04 (C20/22).
f1 (ppm)

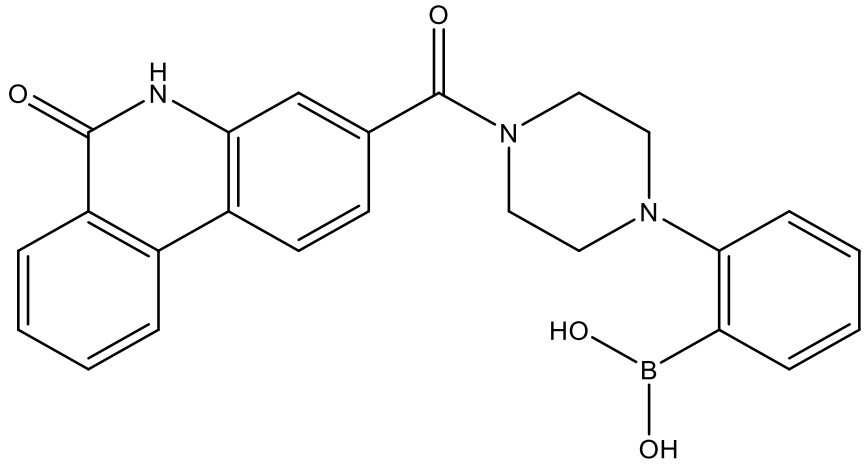

(2-(4-(6-oxo-5,6-dihydrophenanthridine-3-carbonyl)piperazin-1-yl)phenyl)boronic acid (b30)

Using **Synthesis Method d**, 24mg (0.1mmol) **f3** was reacted with 20.6mg (0.1mmol) (2-(piperazin-1-yl)phenyl)boronic. Failed to get clean product. The purity was about 50% depending on NMR. NMR was for reference.^{1}H NMR (300 MHz, DMSO-d_6) δ 11.84 (s, 1H), 8.94 (s, 2H), 8.48 (d, J = 8.3 Hz, 1H), 8.44 (d, J = 4.5 Hz, 1H), 8.35 (d, J = 7.9 Hz, 1H), 7.90 (t, J = 7.6 Hz, 1H), 7.74 (dq, J = 14.0, 7.6 Hz, 2H), 7.44 (d, J = 10.4 Hz, 2H), 7.37 (d, J = 7.4 Hz, 1H), 7.28 (dd, J = 8.4, 4.2 Hz, 1H), 7.19 (t, J = 7.2 Hz, 1H), 3.50 (m, 4H), 3.21 – 3.02 (m, 4H). ^{13}C NMR (75 MHz, DMSO) δ 168.8, 161.3, 158.3, 139.9, 136.9, 135.8, 134.1, 133.5, 131.8, 129.0, 127.9, 126.3, 125.2, 124.0, 121.3, 121.0, 119.7, 119.0, 115.3, 53.8, 42.0. HRMS m/z (ESI+, M+Na): Calcd for C24H22BN3O4: 450.1601, (ESI+, M+Na) found: 450.1604

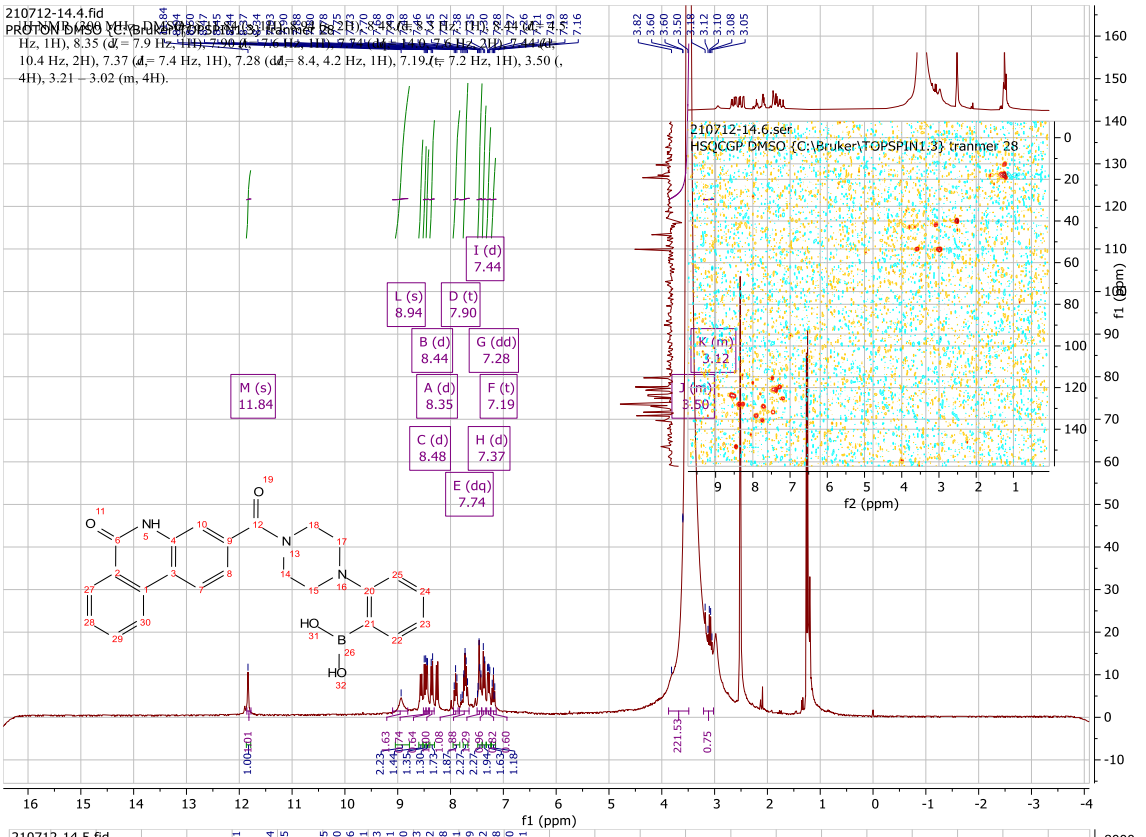
210712-14.4.fid
PROTON DMSO {C:\Bruker\TOPSPIN1.3} tranner 28
210712-14.6.ser
HSQCGP DMSO {C:\Bruker\TOPSPIN1.3} tranner 28
I (d) 7.44
L (s) 8.94
D (t) 7.90
B (d) 8.44
G (dd) 7.28
M (s) 11.84
A (d) 8.35
F (t) 7.19
C (d) 8.48
H (d) 7.37
E (dq) 7.74
K (m) 3.12
J (m) 3.50
f1 (ppm)
f2 (ppm)

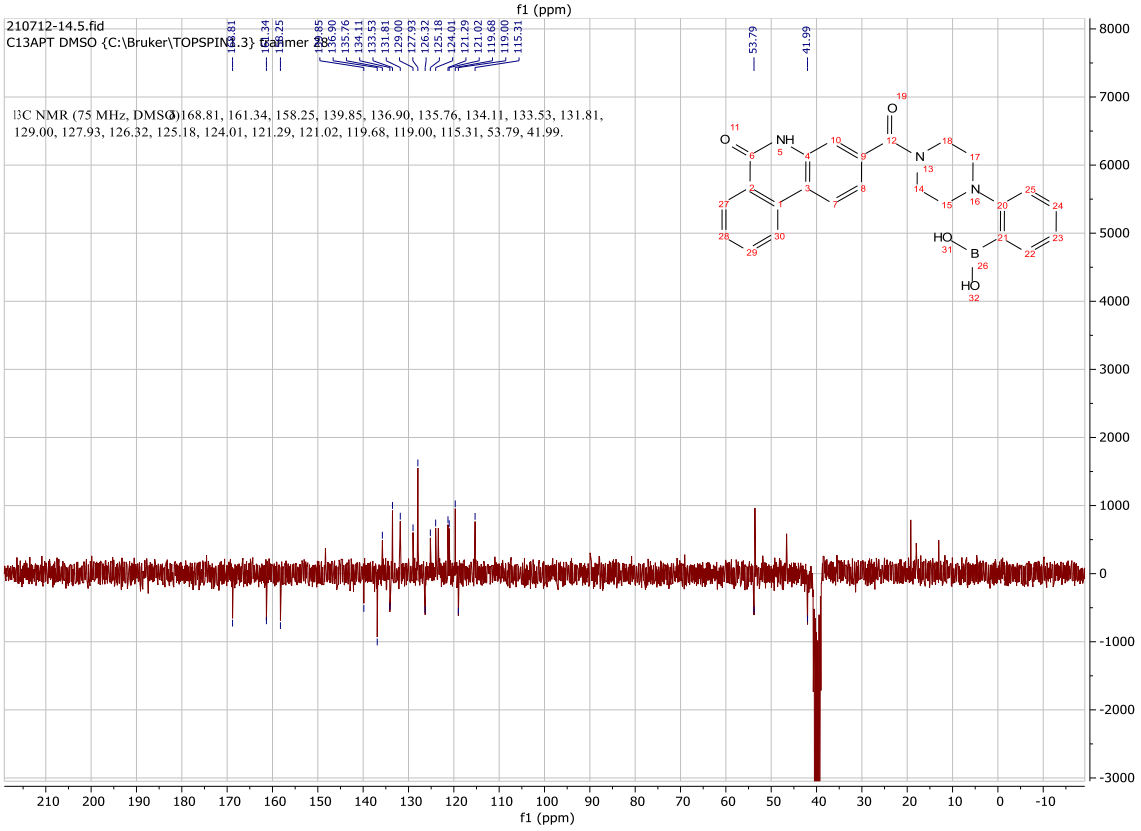
210712-14.5.fid
C13APT DMSO {C:\Bruker\TOPSPIN1.3} tranner 28
13C NMR (75 MHz, DMSO) 168.81, 161.34, 158.25, 139.85, 136.90, 135.76, 134.11, 133.53, 131.81, 129.00, 127.93, 126.32, 125.18, 124.01, 121.29, 121.02, 119.68, 119.00, 115.31, 53.79, 41.99.
f1 (ppm)

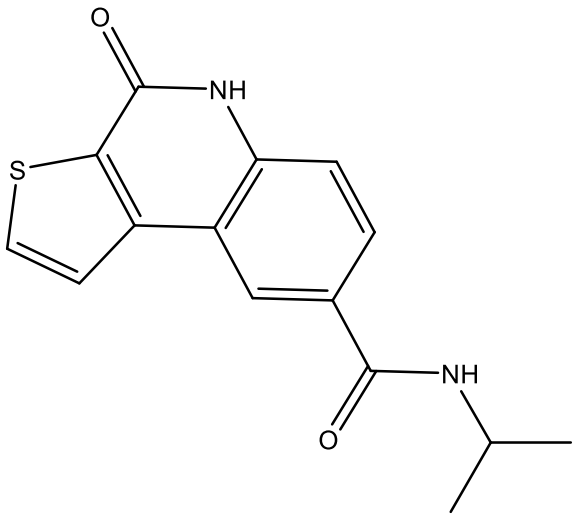

***N*-isopropyl-4-oxo-4,5-dihydrothieno[2,3-*c*]quinoline-8-carboxamide (c1)**

Using **Synthesis Method d**, 24.5mg (0.1mmol) **c36** was reacted with 5.9mg (0.1mmol) propan-2-amine to give 25.2mg **c1** (Yield: 88%) and the product was separated as yellowish white solid. ^{1}H NMR (400 MHz, DMSO-d_6) δ 12.04 (s, 1H), 8.68 – 8.59 (m, 1H), 8.29 – 8.20 (m, 2H), 8.09 (d, *J* = 5.2 Hz, 1H), 7.97 (dd, *J* = 8.6, 1.7 Hz, 1H), 7.46 (d, *J* = 8.6 Hz, 1H), 4.21 – 4.06 (m, *J* = 6.8 Hz, 1H), 1.21 (d, *J* = 6.6 Hz, 6H). ^{13}C NMR (101 MHz, DMSO) δ 165.1, 158.3, 143.5, 139.6, 135.1, 130.8, 128.9, 128.6, 123.9, 123.7, 116.7, 116.3, 41.6, 22.9. HRMS m/z (ESI+, M+Na): Calcd for C15H14N2O2S: 309.0674, (ESI+, M+Na) found: 309.0669

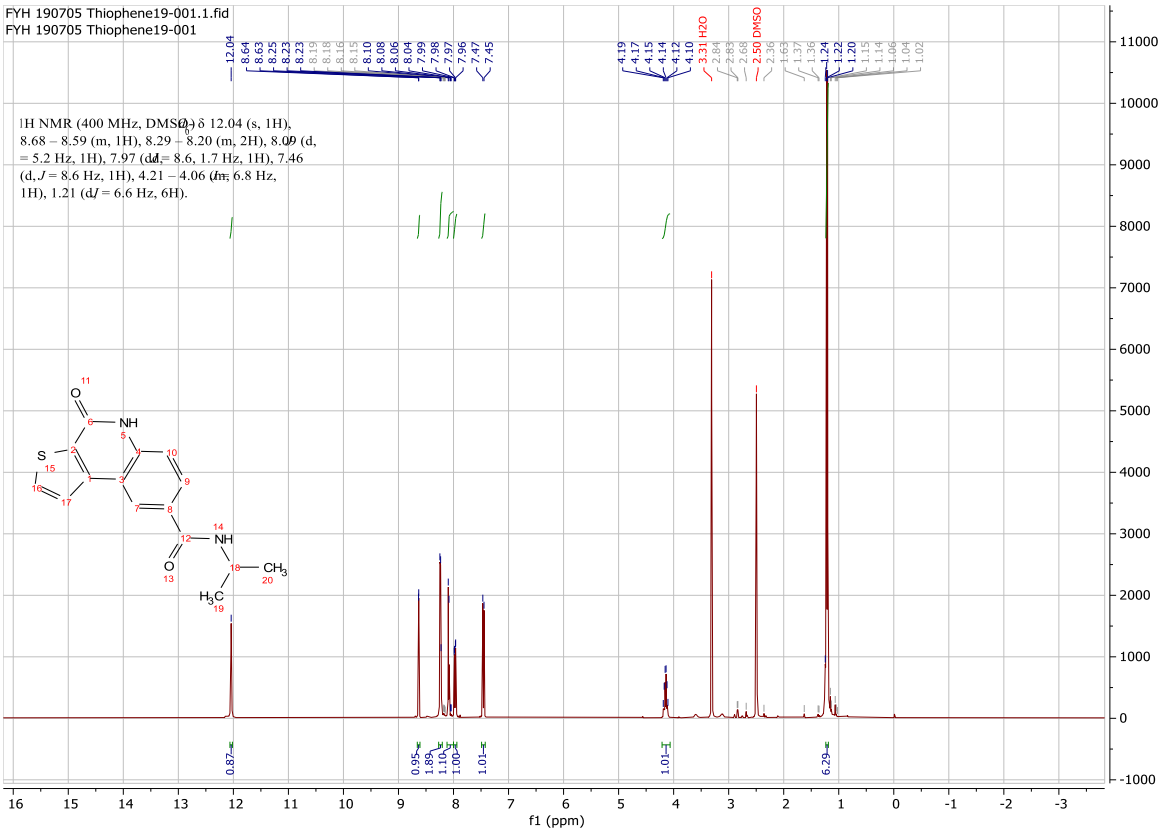
FYH 190705 Thiophene19-001.1.fid
FYH 190705 Thiophene19-001
1H NMR (400 MHz, DMSO-d6) δ 12.04 (s, 1H), 8.68 – 8.59 (m, 1H), 8.29 – 8.20 (m, 2H), 8.09 (d, J = 5.2 Hz, 1H), 7.97 (dd, J = 8.6, 1.7 Hz, 1H), 7.46 (d, J = 8.6 Hz, 1H), 4.21 – 4.06 (m, 1H), 1.21 (d, J = 6.6 Hz, 6H).
f1 (ppm)

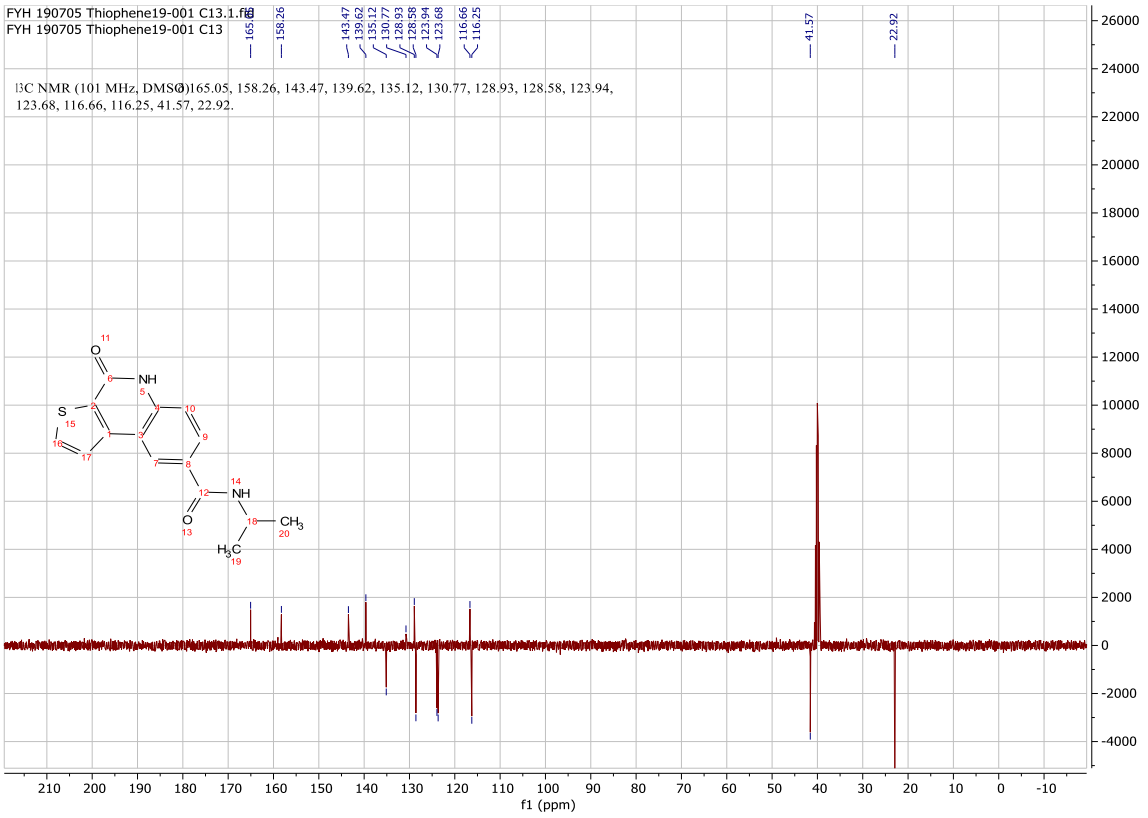
FYH 190705 Thiophene19-001 C13.1.fid
FYH 190705 Thiophene19-001 C13
13C NMR (101 MHz, DMSO-d6) 165.05, 158.26, 143.47, 139.62, 135.12, 130.77, 128.93, 128.58, 123.94, 123.68, 116.66, 116.25, 41.57, 22.92.
f1 (ppm)

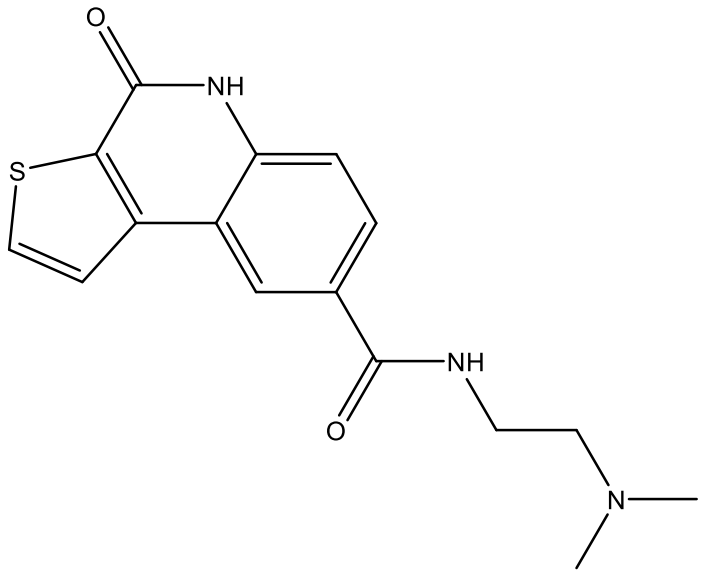

***N*-(2-(dimethylamino)ethyl)-4-oxo-4,5-dihydrothieno[2,3-*c*]quinoline-8-carboxamide (c2)**

Using **Synthesis Method d**, 24.5mg (0.1mmol) **c36** was reacted with 8.9mg (0.1mmol) *N*1,*N*1-dimethylethane-1,2-diamine to give 25.8mg **c2** (Yield: 82%) and the product was separated as yellowish white solid. ^{1}H NMR (300 MHz, DMSO-d_6) δ 12.07 (s, 1H), 8.72 (d, *J* = 1.8 Hz, 1H), 8.58 (t, *J* = 5.5 Hz, 1H), 8.25 (dd, *J* = 5.2, 1.5 Hz, 1H), 8.11 (dd, *J* = 5.2, 1.5 Hz, 1H), 7.98 (dt, *J* = 8.6, 1.7 Hz, 1H), 7.48 (dd, *J* = 8.6, 1.5 Hz, 1H), 3.44 (q, *J* = 7.1, 6.5 Hz, 2H), 2.55 (d, *J* = 7.1 Hz, 2H), 2.27 (d, *J* = 1.5 Hz, 6H). ^{13}C NMR (75 MHz, DMSO) δ 165.9, 158.1, 143.5, 139.7, 135.2, 130.8, 129.0, 128.5, 123.9, 123.8, 116.7, 116.3, 58.6, 45.5, 37.1. HRMS m/z (ESI+, M+H): Calcd for C16H17N3O2S: 316.1114, (ESI+, M+H) found: 316.1114

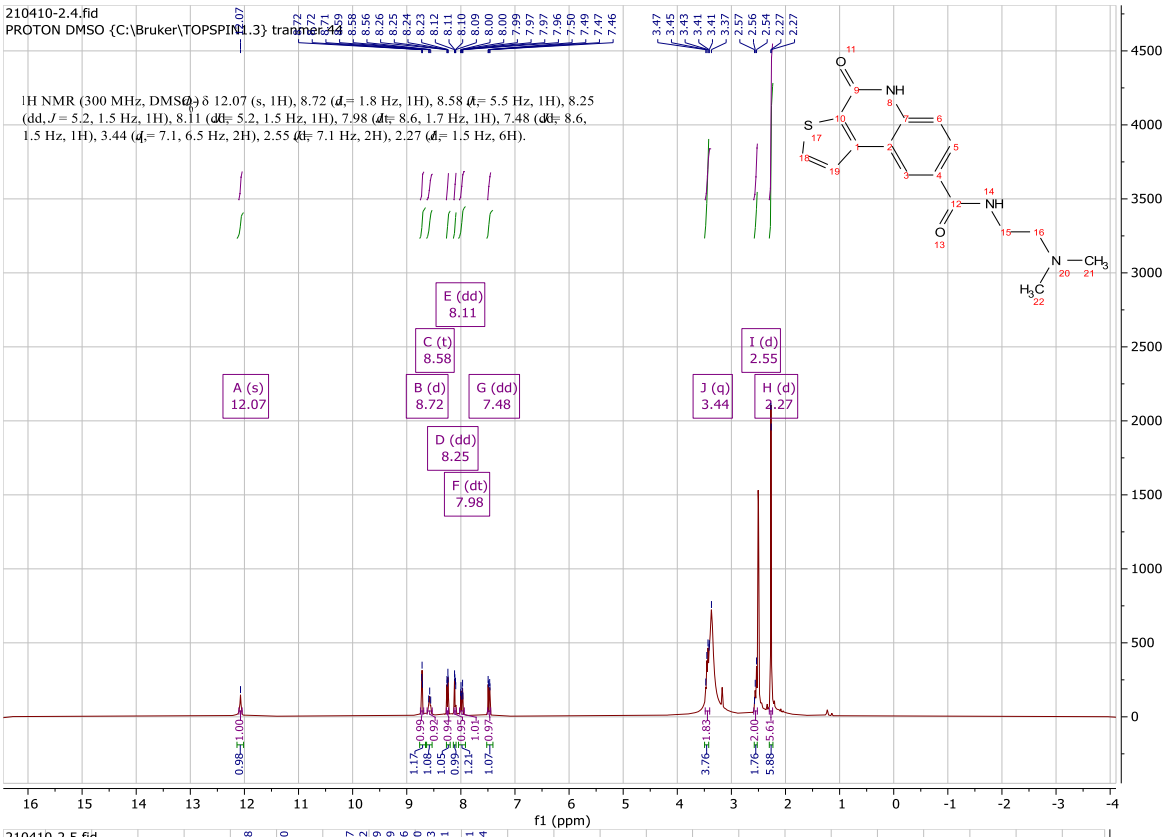
210410-2.4.fid
PROTON DMSO {C:\Bruker\TOPSPIN1.3} tranmer 44
1H NMR (300 MHz, DMSO) δ 12.07 (s, 1H), 8.72 (d, J = 1.8 Hz, 1H), 8.58 (d, J = 5.5 Hz, 1H), 8.25 (dd, J = 5.2, 1.5 Hz, 1H), 8.11 (dd, J = 5.2, 1.5 Hz, 1H), 7.98 (dt, J = 8.6, 1.7 Hz, 1H), 7.48 (dd, J = 8.6, 1.5 Hz, 1H), 3.44 (q, J = 7.1, 6.5 Hz, 2H), 2.55 (d, J = 7.1 Hz, 2H), 2.27 (d, J = 1.5 Hz, 6H).
A (s) 12.07
B (d) 8.72
C (t) 8.58
D (dd) 8.25
E (dd) 8.11
F (dt) 7.98
G (dd) 7.48
H (d) 2.27
I (d) 2.55
J (q) 3.44
f1 (ppm)

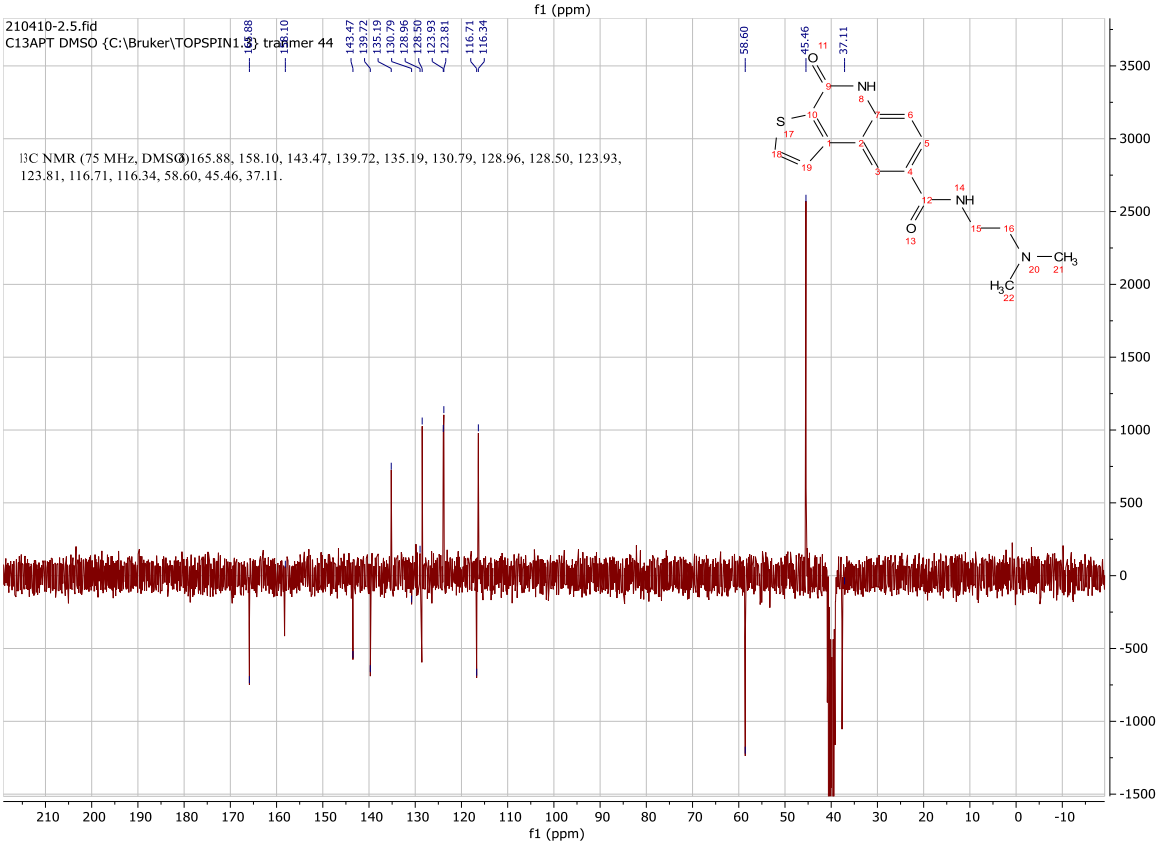
210410-2.5.fid
C13APT DMSO {C:\Bruker\TOPSPIN1.3} tranmer 44
13C NMR (75 MHz, DMSO) δ 165.88, 158.10, 143.47, 139.72, 135.19, 130.79, 128.96, 128.50, 123.93, 123.81, 116.71, 116.34, 58.60, 45.46, 37.11.
f1 (ppm)

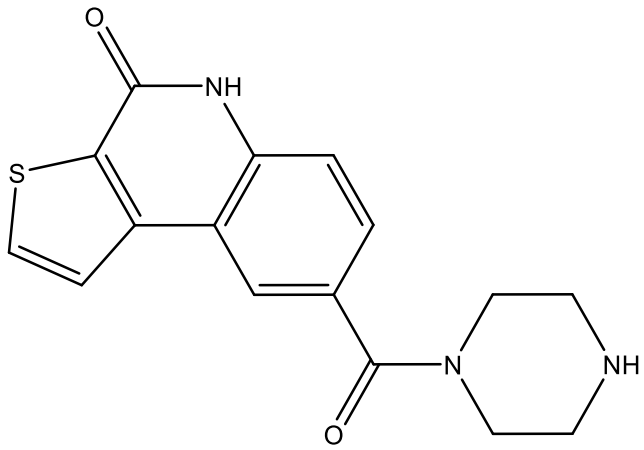

8-(piperazine-1-carbonyl)thieno[2,3-*c*]quinolin-4(*5H*)-one (c4)

Using **Synthesis Method d**, 24.5mg (0.1mmol) **c36** was reacted with 8.8mg (0.1mmol) piperazine to give 23.8mg **c4** (Yield: 76%) and the product was separated as yellowish white solid. ^{1}H NMR (300 MHz, DMSO-d_6) δ 12.00 (s, 1H), 8.19 (dd, *J* = 12.6, 5.3 Hz, 3H), 7.50 (d, *J* = 2.2 Hz, 2H), 3.30 (m, 4H), 2.71 (m, 5H). ^{13}C NMR (75 MHz, DMSO) δ 169.0, 158.2, 143.2, 138.4, 135.0, 130.5, 128.2, 124.3, 123.6, 117.0, 116.5, 49.7, 46.1, 42.5. HRMS m/z (ESI+, M+H): Calcd for C16H15N3O2S: 314.0958, (ESI+, M+H) found: 314.0959

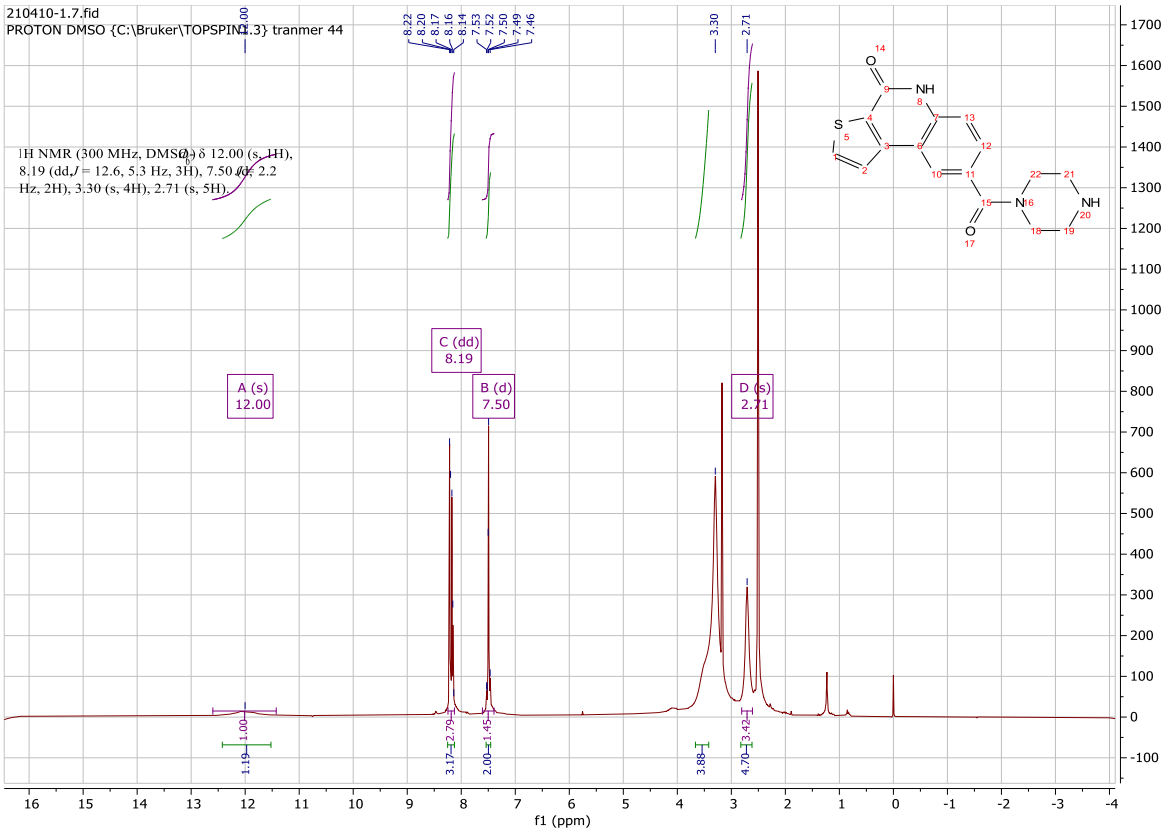
210410-1.7.fid
PROTON DMSO {C:\Bruker\TOPSPIN3.3} tranmer 44
1H NMR (300 MHz, DMSO) δ 12.00 (s, 1H), 8.19 (dd, J = 12.6, 5.3 Hz, 3H), 7.50 (d, J = 2.2 Hz, 2H), 3.30 (s, 4H), 2.71 (s, 5H).
A (s) 12.00
C (dd) 8.19
B (d) 7.50
D (s) 2.71
f1 (ppm)

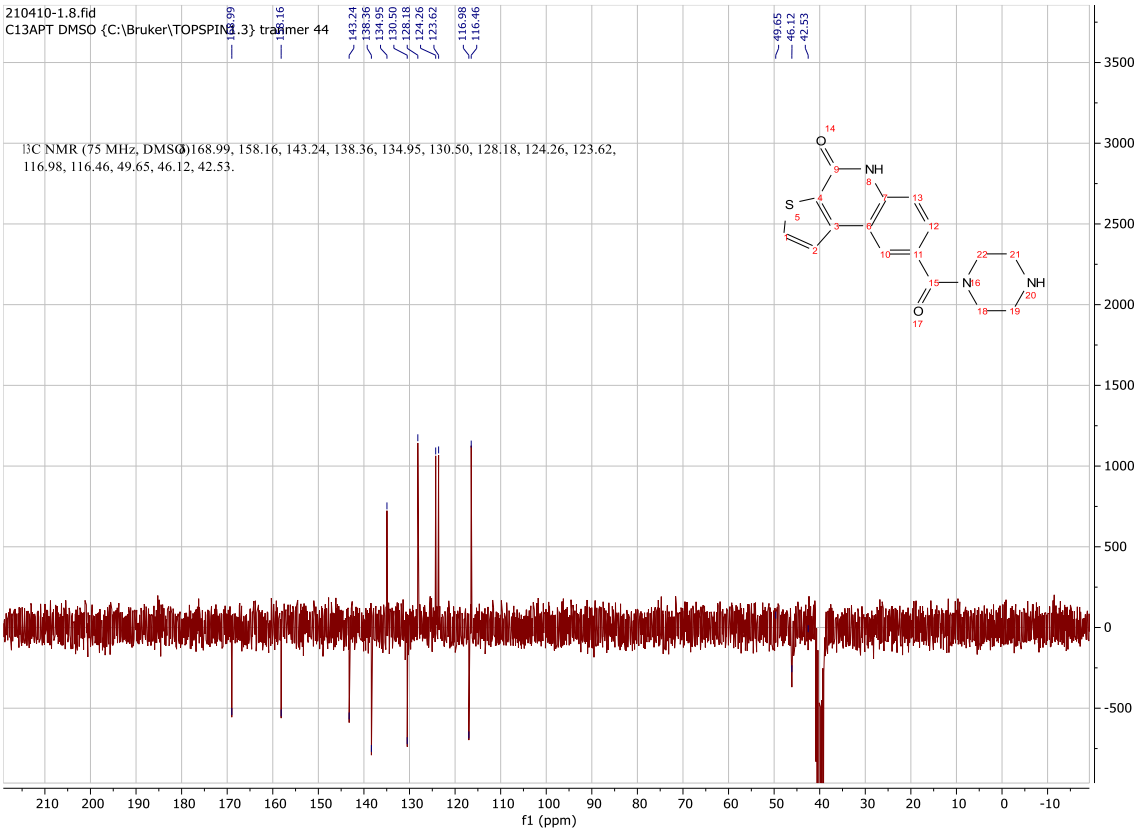
210410-1.8.fid
C13APT DMSO {C:\Bruker\TOPSPIN3.3} tranmer 44
13C NMR (75 MHz, DMSO) 168.99, 158.16, 143.24, 138.36, 134.95, 130.50, 128.18, 124.26, 123.62, 116.98, 116.46, 49.65, 46.12, 42.53.
f1 (ppm)

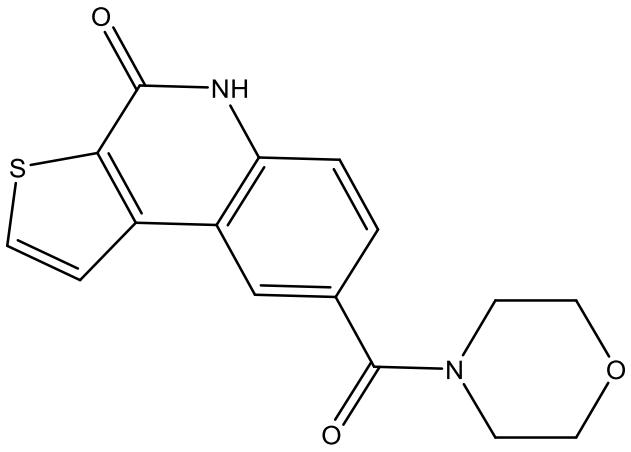

8-(morpholine-4-carbonyl)thieno[2,3-*c*]quinolin-4(5*H*)-one (c5)

Using **Synthesis Method d**, 24.5mg (0.1mmol) **c36** was reacted with 8.8mg (0.1mmol) morpholine to give 22.6mg **c5** (Yield: 72%) and the product was separated as yellowish white solid. ^{1}H NMR (400 MHz, DMSO-d_6) δ 12.01 (s, 1H), 8.24 (d, J = 1.7 Hz, 1H), 8.20 (d, J = 5.2 Hz, 1H), 8.15 (d, J = 5.3 Hz, 1H), 7.54 (dd, J = 8.4, 1.8 Hz, 1H), 7.48 (d, J = 8.4 Hz, 1H), 3.62 (m, 8H).^{13}C NMR (101 MHz, DMSO) δ 169.2, 158.2, 143.2, 138.6, 135.0, 131.0, 129.8, 128.3, 124.2, 123.8, 117.0, 116.5, 66.6, 57.2. HRMS m/z (ESI+, M+Na): Calcd for C16H14N2O3S: 337.0725, (ESI+, M+Na) found: 337.0617

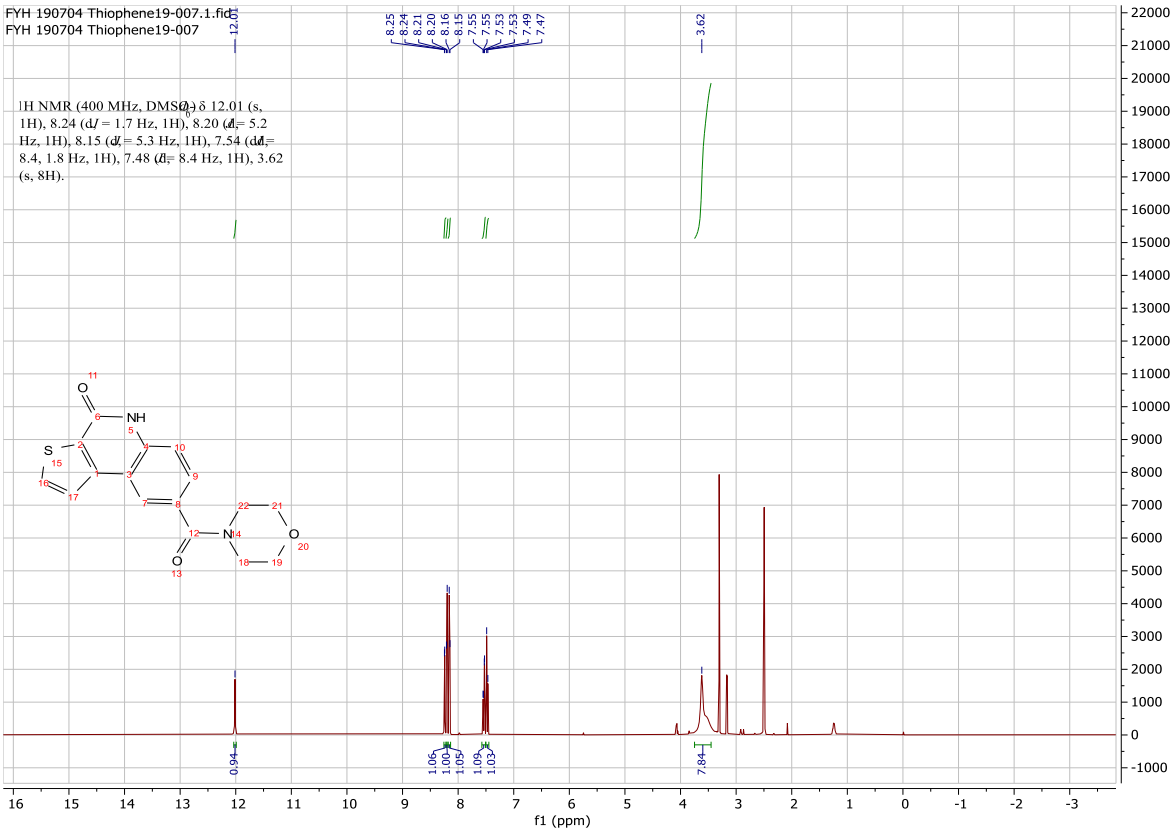
FYH 190704 Thiophene19-007.1.fid
FYH 190704 Thiophene19-007
1H NMR (400 MHz, DMSO) δ 12.01 (s, 1H), 8.24 (d, J = 1.7 Hz, 1H), 8.20 (d, J = 5.2 Hz, 1H), 8.15 (d, J = 5.3 Hz, 1H), 7.54 (dd, J = 8.4, 1.8 Hz, 1H), 7.48 (d, J = 8.4 Hz, 1H), 3.62 (s, 8H).
f1 (ppm)

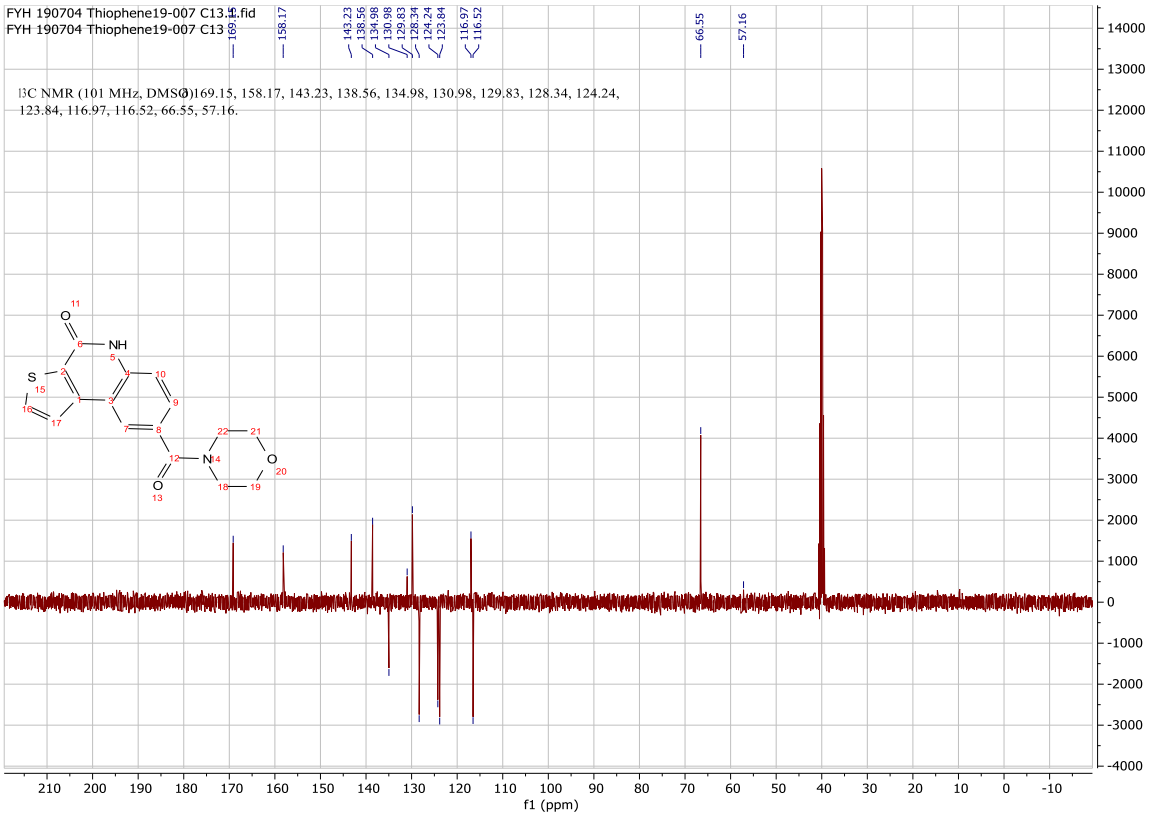
FYH 190704 Thiophene19-007 C13.1.fid
FYH 190704 Thiophene19-007 C13
13C NMR (101 MHz, DMSO) 169.15, 158.17, 143.23, 138.56, 134.98, 130.98, 129.83, 128.34, 124.24, 123.84, 116.97, 116.52, 66.55, 57.16.
f1 (ppm)

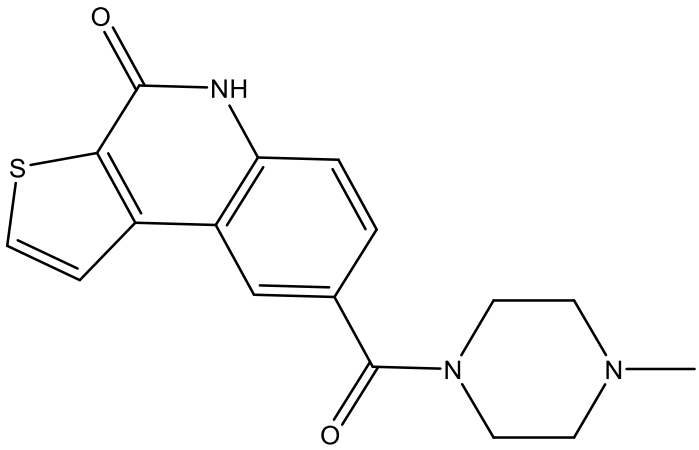

8-(4-methylpiperazine-1-carbonyl)thieno[2,3-*c*]quinolin-4(5*H*)-one (c6)

Using **Synthesis Method d**, 24.5mg (0.1mmol) **c36** was reacted with 10mg (0.1mmol) 1-methylpiperazine to give 20.3mg **c6** (Yield: 62%) and the product was separated as yellowish white solid. ^{1}H NMR (400 MHz, DMSO-d_6) δ 12.03 (s, 1H), 8.23 (d, J = 1.4 Hz, 1H), 8.21 (d, J = 5.2 Hz, 1H), 8.16 (d, J = 5.3 Hz, 1H), 7.52 (dd, J = 8.4, 1.7 Hz, 1H), 7.48 (d, J = 8.3 Hz, 1H), 3.43 (m, 4H), 2.45 – 2.26 (m, 4H), 2.20 (s, 3H). ^{13}C NMR (101 MHz, DMSO) δ 169.0, 158.2, 143.2, 138.5, 135.0, 131.0, 130.3, 128.2, 124.3, 123.7, 117.0, 116.5, 54.9, 46.2, 46.1. HRMS m/z (ESI+, M+H): Calcd for C17H17N3O2S: 328.1114, (ESI+, M+H) found: 328.1117

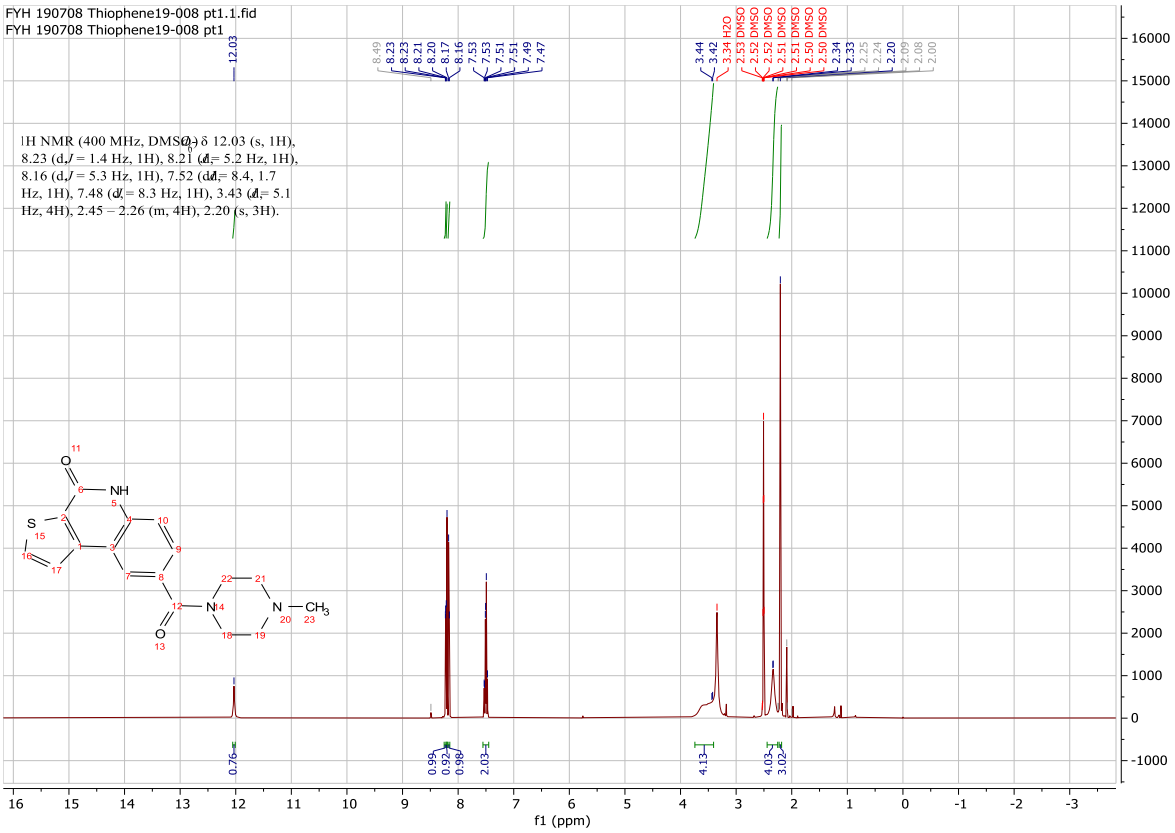
FYH 190708 Thiophene19-008 pt1.1.fid
FYH 190708 Thiophene19-008 pt1
1H NMR (400 MHz, DMSO-d6) δ 12.03 (s, 1H), 8.23 (d, J = 1.4 Hz, 1H), 8.21 (d, J = 5.2 Hz, 1H), 8.16 (d, J = 5.3 Hz, 1H), 7.52 (dd, J = 8.4, 1.7 Hz, 1H), 7.48 (d, J = 8.3 Hz, 1H), 3.43 (d, J = 5.1 Hz, 4H), 2.45 – 2.26 (m, 4H), 2.20 (s, 3H).
f1 (ppm)

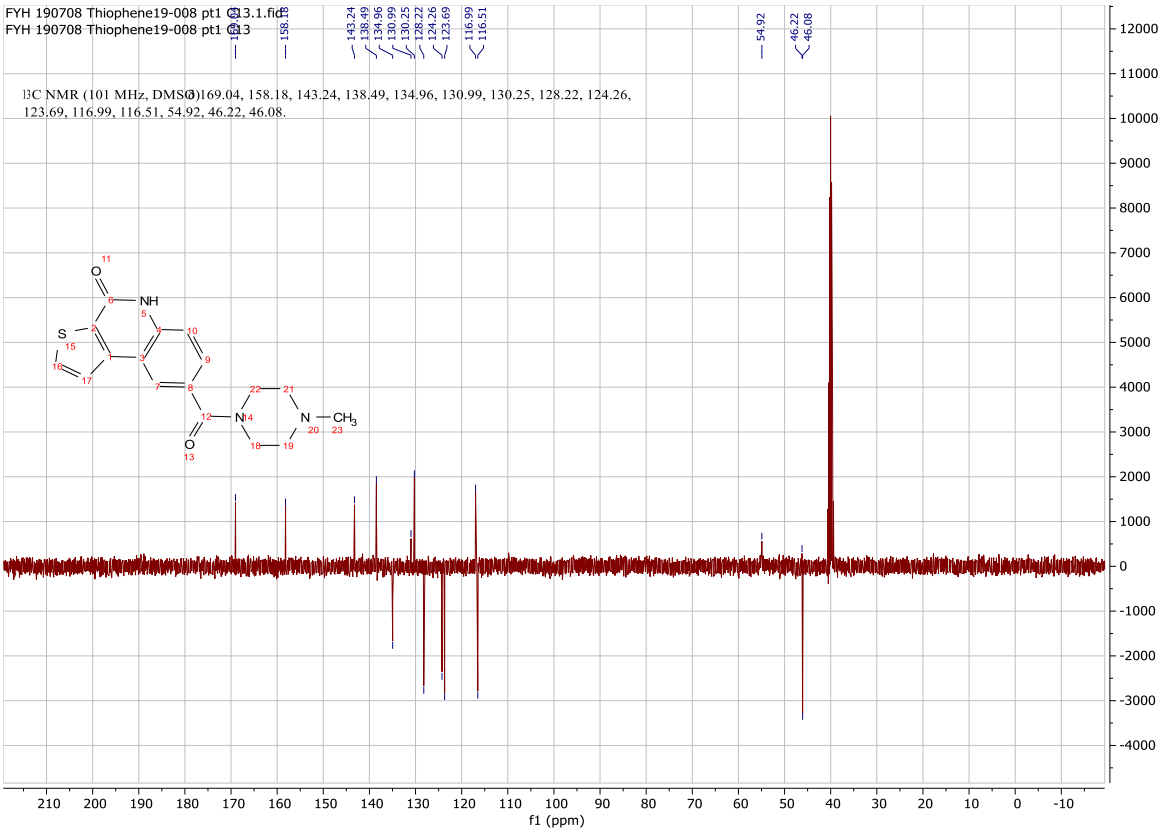
FYH 190708 Thiophene19-008 pt1 C13.1.fid
FYH 190708 Thiophene19-008 pt1 C13
13C NMR (101 MHz, DMSO) 169.04, 158.18, 143.24, 138.49, 134.96, 130.99, 130.25, 128.22, 124.26, 123.69, 116.99, 116.51, 54.92, 46.22, 46.08.
f1 (ppm)

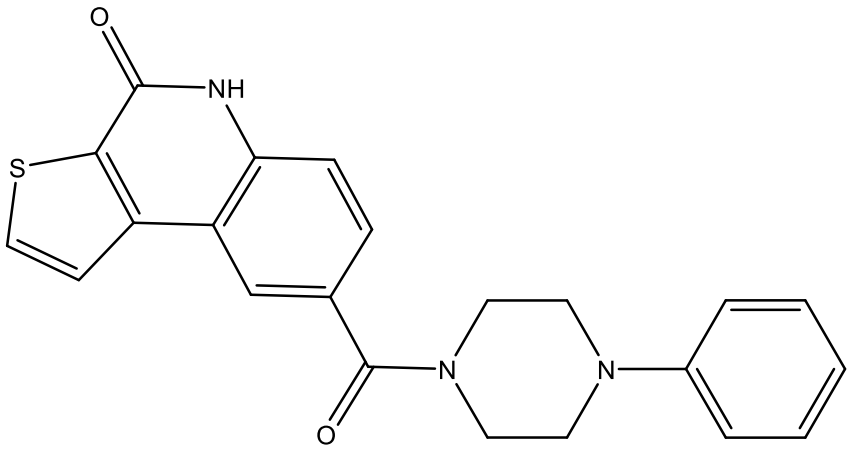

8-(4-phenylpiperazine-1-carbonyl)thieno[2,3-*c*]quinolin-4(5*H*)-one (c7)

Using **Synthesis Method d**, 24.5mg (0.1mmol) **c36** was reacted with 16mg (0.1mmol) 1-phenylpiperazine to give 27.2mg **c7** (Yield: 70%) and the product was separated as yellow solid. ^{1}H NMR (400 MHz, DMSO-d_6) δ 12.03 (s, 1H), 8.28 (s, 1H), 8.23 – 8.14 (m, 2H), 7.60 – 7.54 (m, 1H), 7.49 (d, *J* = 8.4 Hz, 1H), 7.22 (t, *J* = 7.8 Hz, 2H), 6.96 (d, *J* = 8.3 Hz, 2H), 6.81 (t, *J* = 7.2 Hz, 1H), 3.76 (m 4H), 3.20 (m, 4H). ^{13}C NMR (101 MHz, DMSO) δ 169.1, 158.2, 151.2, 143.2, 138.6, 135.0, 131.0, 130.1, 129.5, 128.4, 124.3, 123.8, 119.8, 117.0, 116.5, 116.4, 59.9, 49.0. HRMS m/z (ESI+, M+Na): Calcd for C22H19N3O2S: 412.4628, (ESI+, M+Na) found: 412.1096

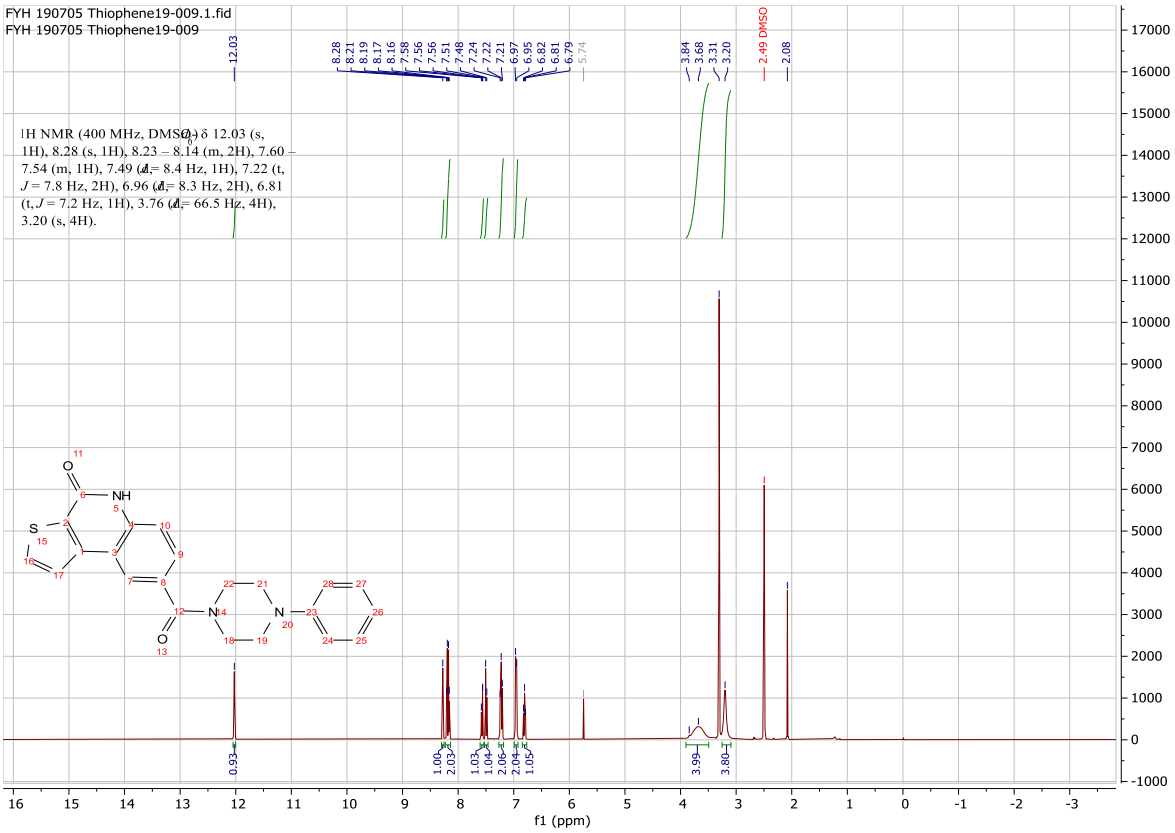
FYH 190705 Thiophene19-009.1.fid
FYH 190705 Thiophene19-009
1H NMR (400 MHz, DMSO-d6) δ 12.03 (s, 1H), 8.28 (s, 1H), 8.23 – 8.14 (m, 2H), 7.60 – 7.54 (m, 1H), 7.49 (d, J = 8.4 Hz, 1H), 7.22 (t, J = 7.8 Hz, 2H), 6.96 (d, J = 8.3 Hz, 2H), 6.81 (t, J = 7.2 Hz, 1H), 3.76 (d, J = 66.5 Hz, 4H), 3.20 (s, 4H).
12.03
8.28
8.21
8.19
8.17
8.16
7.58
7.56
7.56
7.51
7.48
7.24
7.22
7.21
6.97
6.95
6.82
6.81
6.79
5.74
3.84
3.68
3.31
3.20
2.49 DMSO
2.08
f1 (ppm)

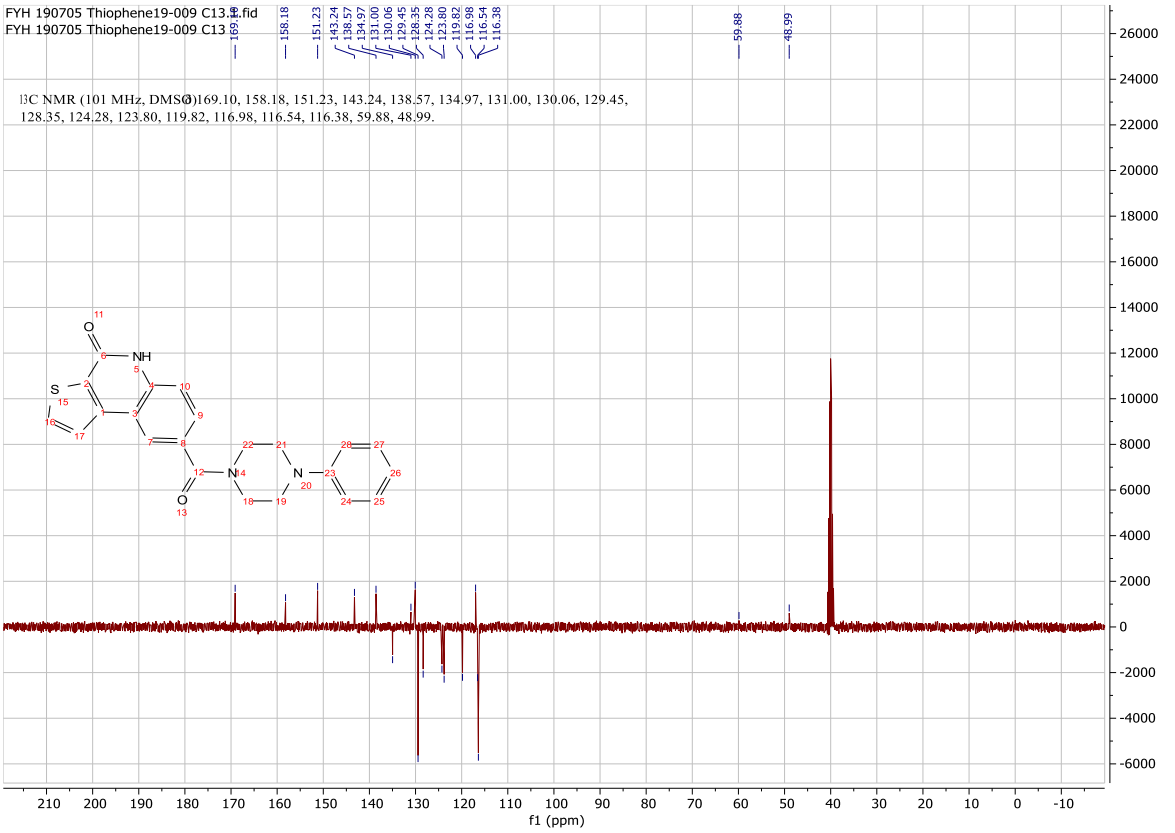
FYH 190705 Thiophene19-009 C13.1.fid
FYH 190705 Thiophene19-009 C13
13C NMR (101 MHz, DMSO) 169.10, 158.18, 151.23, 143.24, 138.57, 134.97, 131.00, 130.06, 129.45, 128.35, 124.28, 123.80, 119.82, 116.98, 116.54, 116.38, 59.88, 48.99.
169.10
158.18
151.23
143.24
138.57
134.97
131.00
130.06
129.45
128.35
124.28
123.80
119.82
116.98
116.54
116.38
59.88
48.99
f1 (ppm)

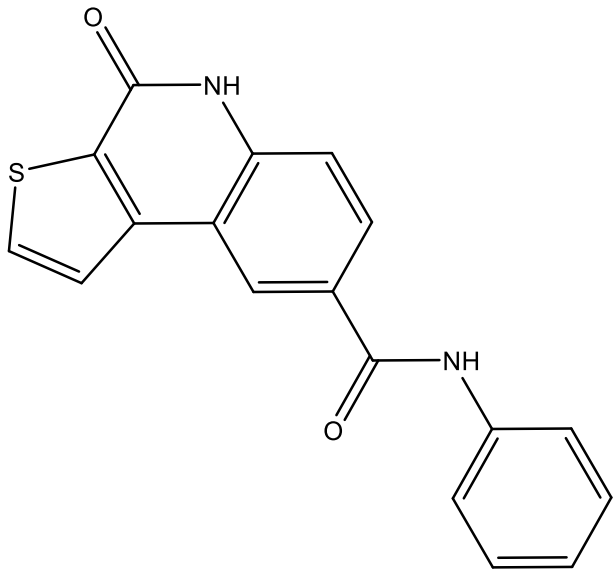

4-oxo-*N*-phenyl-4,5-dihydrothieno[2,3-*c*]quinoline-8-carboxamide (c8)

Using **Synthesis Method d**, 24.5mg (0.1mmol) **c36** was reacted with 9.4mg (0.1mmol) aniline to give 28.8mg **c8** (Yield: 90%) and the product was separated as yellowish white solid. ^{1}H NMR (300 MHz, DMSO-d_6) δ 12.13 (s, 1H), 10.28 (s, 1H), 8.79 (d, J = 2.0 Hz, 1H), 8.27 (d, J = 5.2 Hz, 1H), 8.16 (d, J = 5.2 Hz, 1H), 8.08 (dd, J = 8.6, 2.0 Hz, 1H), 7.84 – 7.76 (m, 2H), 7.54 (d, J = 8.6 Hz, 1H), 7.39 (t, 2H), 7.13 (t, 1H). ^{13}C NMR (75 MHz, DMSO) δ 165.3, 158.3, 143.4, 140.0, 139.6, 135.2, 130.9, 129.1, 128.9, 124.4, 124.2, 124.1, 129.0, 121.0, 116.6, 116.5. HRMS m/z (ESI+, M+Na): Calcd for C18H12N2O2S: 343.0517, (ESI+, M+Na) found: 343.0511

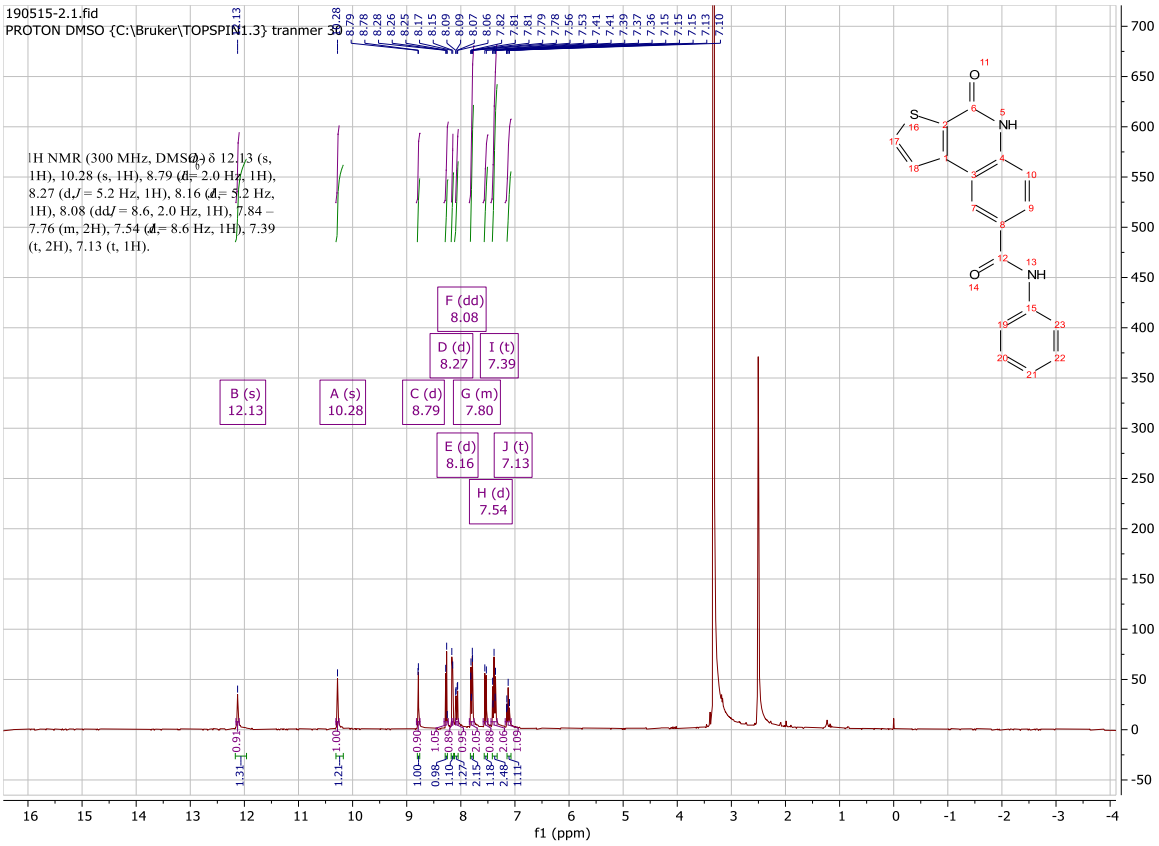
190515-2.1.fid
PROTON DMSO {C:\Bruker\TOPSPIN1.3} tranmer 30
1H NMR (300 MHz, DMSO-d6) δ 12.13 (s, 1H), 10.28 (s, 1H), 8.79 (d, J = 2.0 Hz, 1H), 8.27 (d, J = 5.2 Hz, 1H), 8.16 (d, J = 5.2 Hz, 1H), 8.08 (dd, J = 8.6, 2.0 Hz, 1H), 7.84 – 7.76 (m, 2H), 7.54 (d, J = 8.6 Hz, 1H), 7.39 (t, 2H), 7.13 (t, 1H).
F (dd) 8.08
D (d) 8.27
I (t) 7.39
B (s) 12.13
A (s) 10.28
C (d) 8.79
G (m) 7.80
E (d) 8.16
J (t) 7.13
H (d) 7.54
f1 (ppm)

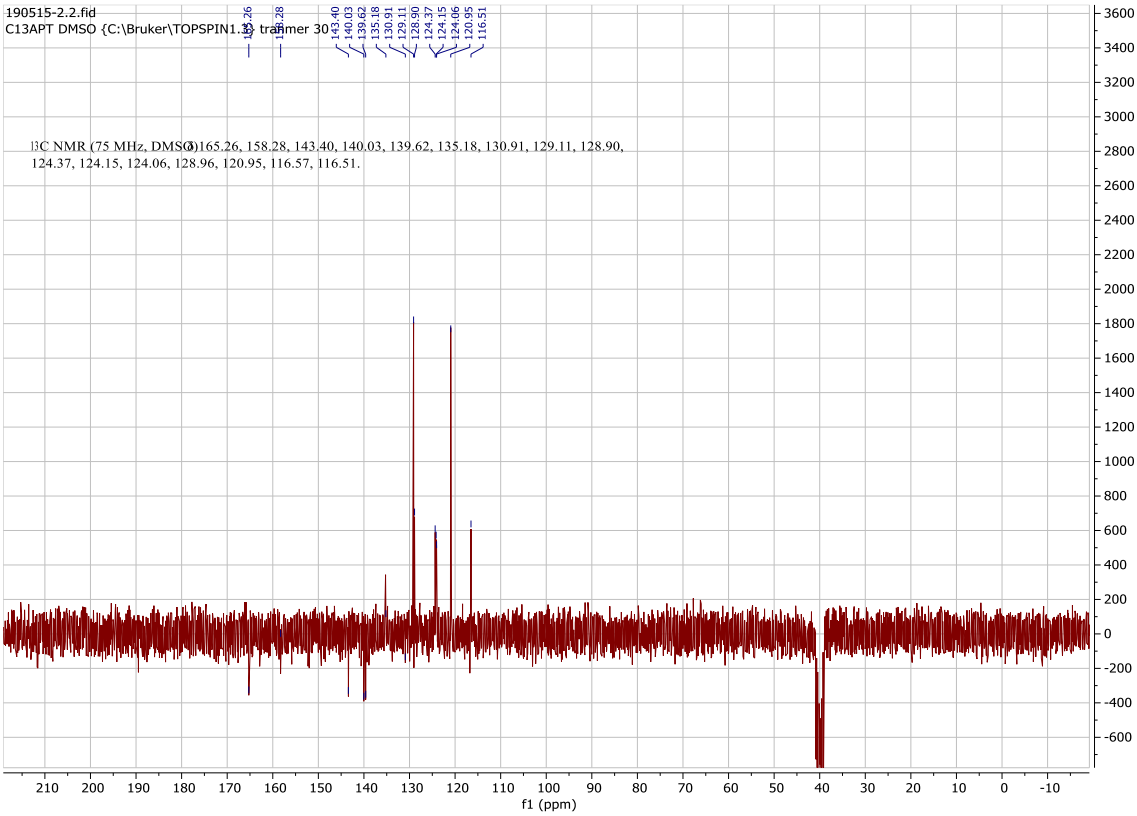
190515-2.2.fid
C13APT DMSO {C:\Bruker\TOPSPIN1.3} tranmer 30
13C NMR (75 MHz, DMSO-d6) 165.26, 158.28, 143.40, 140.03, 139.62, 135.18, 130.91, 129.11, 128.90, 124.37, 124.15, 124.06, 128.96, 120.95, 116.57, 116.51.
f1 (ppm)

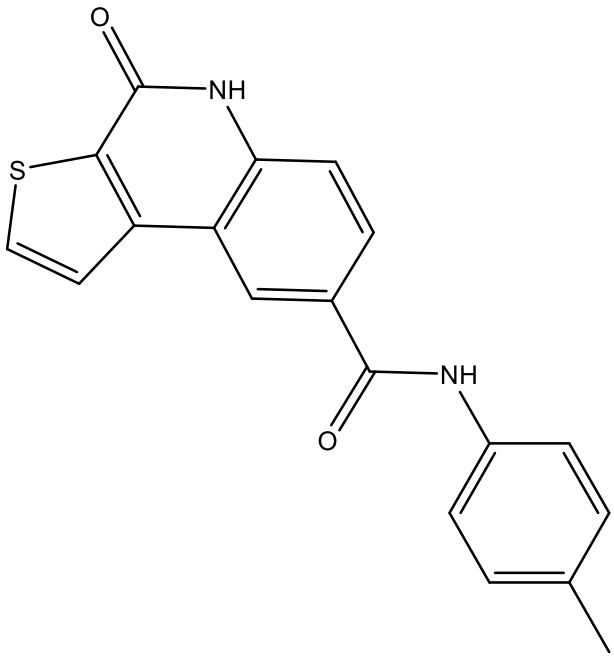

4-oxo-*N*-(*p*-tolyl)-4,5-dihydrothieno[2,3-*c*]quinoline-8-carboxamide (c9)

Using **Synthesis Method d**, 24.5mg (0.1mmol) **c36** was reacted with 10.7mg (0.1mmol) *p*-toluidine to give 25.3mg **c9** (Yield: 76%) and the product was separated as yellowish white solid. ^{1}H NMR (400 MHz, DMSO-d_6) δ 12.11 (s, 1H), 10.19 (s, 1H), 8.77 (d, *J* = 1.9 Hz, 1H), 8.26 (d, *J* = 5.2 Hz, 1H), 8.14 (d, *J* = 5.3 Hz, 1H), 8.06 (dd, *J* = 8.6, 2.0 Hz, 1H), 7.70 – 7.64 (m, 2H), 7.53 (d, *J* = 8.6 Hz, 1H), 7.18 (d, *J* = 8.2 Hz, 2H), 2.29 (s, 3H). ^{13}C NMR (101 MHz, DMSO) δ 165.0, 158.3, 143.4, 140.0 137.1, 135.2, 135.1, 133.1, 129.5, 129.1, 128.9, 124.3, 124.0, 121.0, 116.8, 116.5, 21.0. HRMS m/z (ESI+, M-H): Calcd for C19H14N2O2S: 333.0703, (ESI-, M-H) found: 333.0707

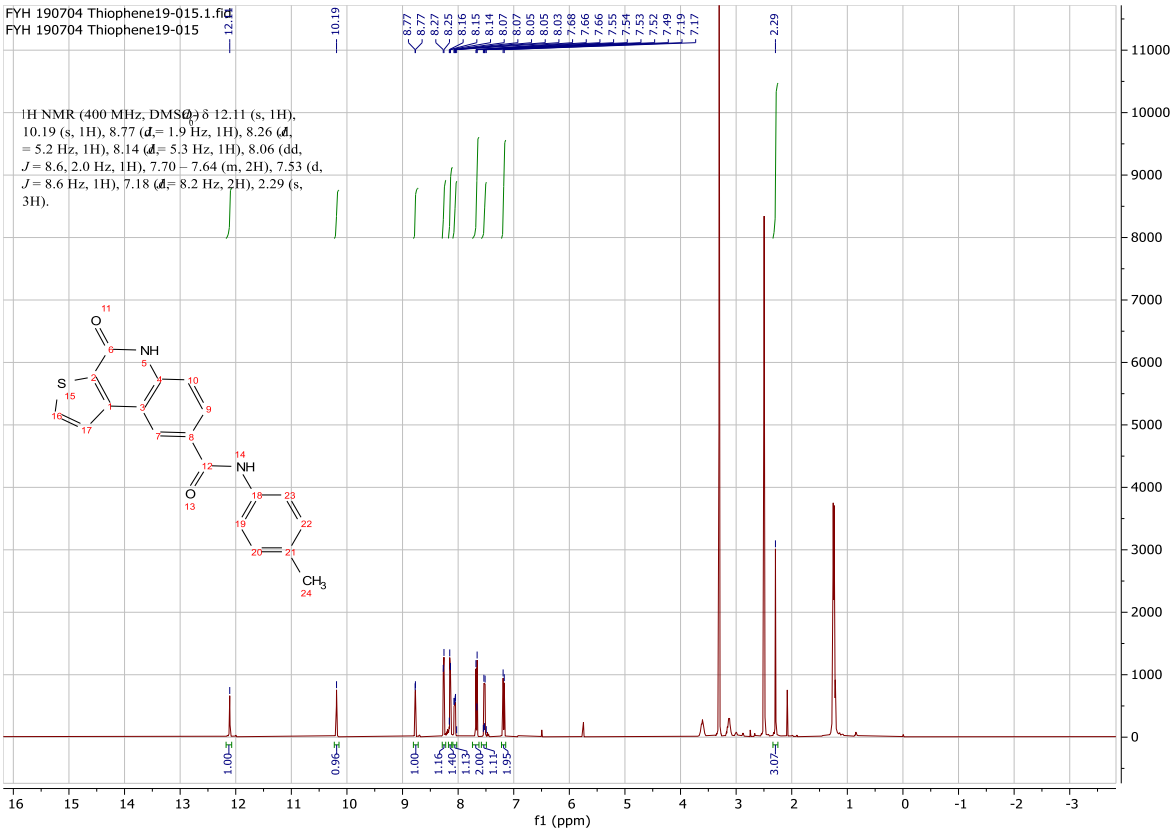
FYH 190704 Thiophene19-015.1.fid
FYH 190704 Thiophene19-015
1H NMR (400 MHz, DMSO-d6) δ 12.11 (s, 1H), 10.19 (s, 1H), 8.77 (d, J = 1.9 Hz, 1H), 8.26 (d, J = 5.2 Hz, 1H), 8.14 (d, J = 5.3 Hz, 1H), 8.06 (dd, J = 8.6, 2.0 Hz, 1H), 7.70 – 7.64 (m, 2H), 7.53 (d, J = 8.6 Hz, 1H), 7.18 (d, J = 8.2 Hz, 2H), 2.29 (s, 3H).
f1 (ppm)

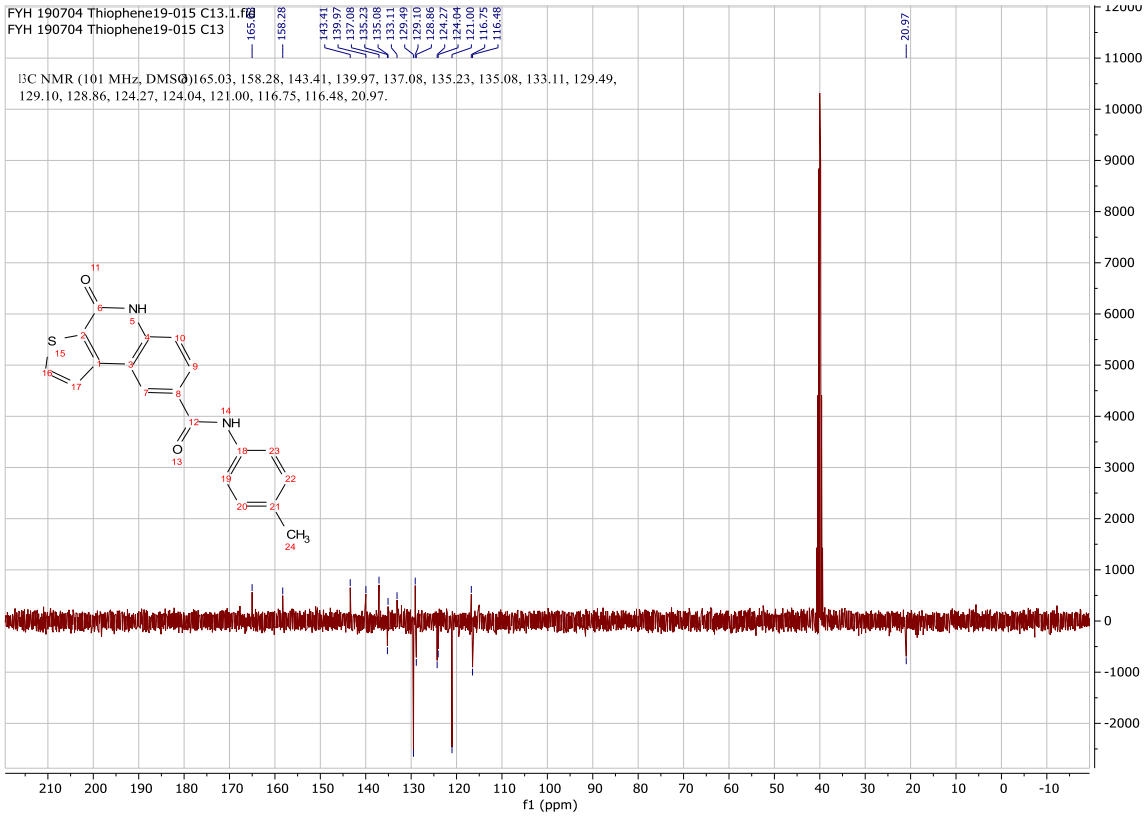
FYH 190704 Thiophene19-015 C13.1.fid
FYH 190704 Thiophene19-015 C13
13C NMR (101 MHz, DMSO-d6) 165.03, 158.28, 143.41, 139.97, 137.08, 135.23, 135.08, 133.11, 129.49, 129.10, 128.86, 124.27, 124.04, 121.00, 116.75, 116.48, 20.97.
f1 (ppm)

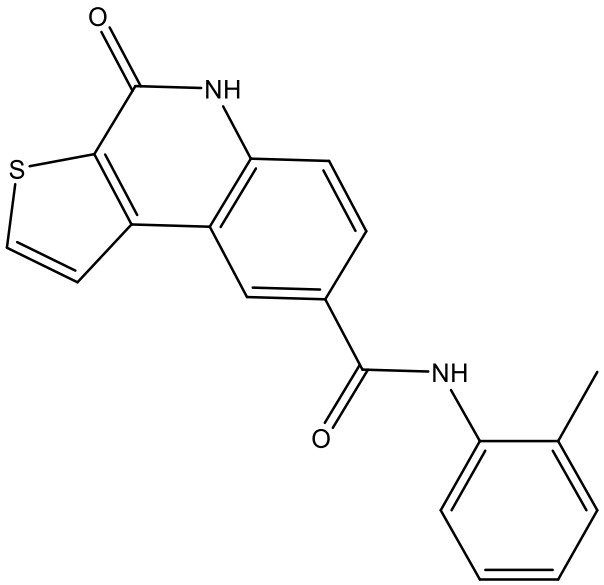

4-oxo-*N*-(*o*-tolyl)-4,5-dihydrothieno[2,3-*c*]quinoline-8-carboxamide (c10)

Using **Synthesis Method d**, 24.5mg (0.1mmol) **c36** was reacted with 10.7mg (0.1mmol) *o*-toluidine to give 24.7mg **c10** (Yield: 74%) and the product was separated as yellowish white solid. ^{1}H NMR (400 MHz, DMSO-d_6) δ 12.12 (s, 1H), 10.19 (s, 1H), 8.79 (d, *J* = 1.9 Hz, 1H), 8.28 (d, *J* = 5.2 Hz, 1H), 8.16 (d, *J* = 5.3 Hz, 1H), 8.08 (dd, *J* = 8.6, 2.0 Hz, 1H), 7.63 – 7.58 (m, 2H), 7.54 (d, *J* = 8.6 Hz, 1H), 7.27 (t, *J* = 7.7 Hz, 1H), 6.95 (d, *J* = 7.5 Hz, 1H), 2.34 (s, 3H). ^{13}C NMR (101 MHz, DMSO) δ 165.1, 158.3, 143.4, 140.0, 139.6, 138.3, 135.3, 130.9, 129.1, 129.0, 128.9, 124.9, 124.3, 124.1, 121.5, 118.1, 116.8, 116.5, 21.7. HRMS m/z (ESI-, M-H): Calcd for C19H14N2O2S: 333.0703, (ESI-, M-H) found: 333.0701

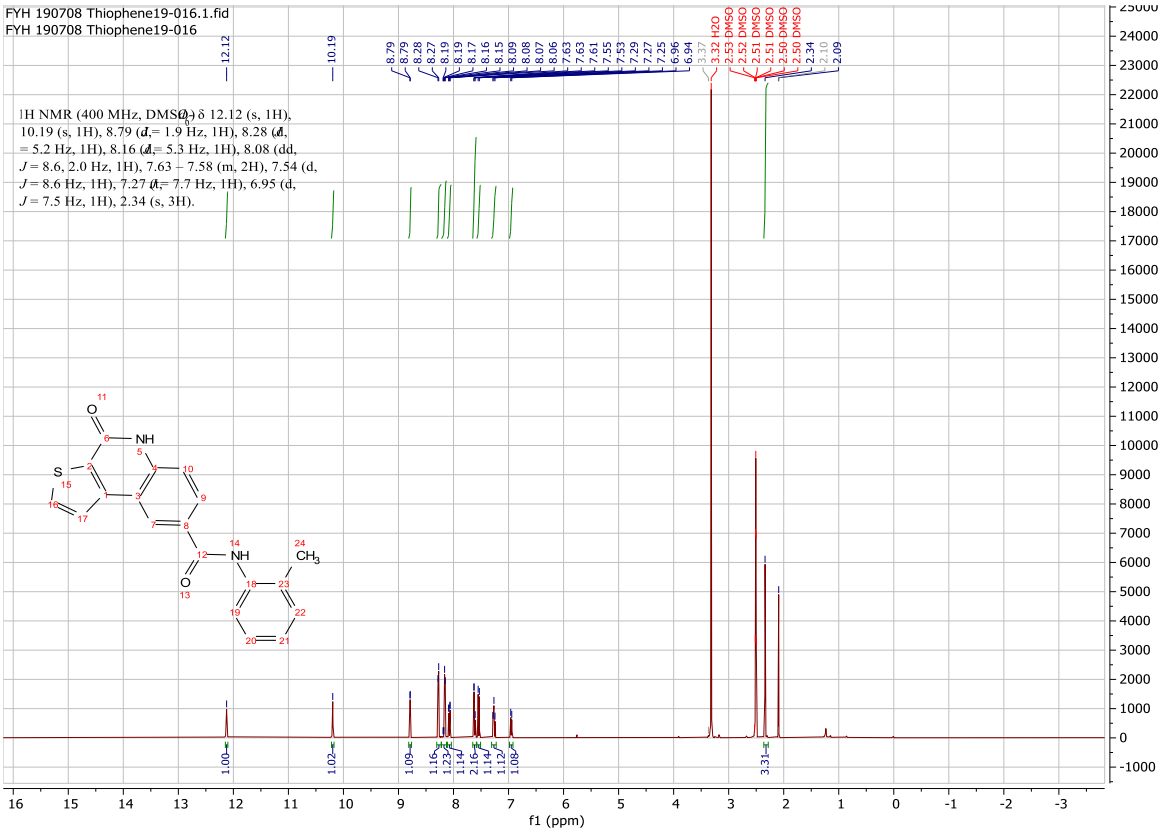
FYH 190708 Thiophene19-016.1.fid
FYH 190708 Thiophene19-016
1H NMR (400 MHz, DMSO-d6) δ 12.12 (s, 1H), 10.19 (s, 1H), 8.79 (d, J = 1.9 Hz, 1H), 8.28 (d, J = 5.2 Hz, 1H), 8.16 (d, J = 5.3 Hz, 1H), 8.08 (dd, J = 8.6, 2.0 Hz, 1H), 7.63 – 7.58 (m, 2H), 7.54 (d, J = 8.6 Hz, 1H), 7.27 (t, J = 7.7 Hz, 1H), 6.95 (d, J = 7.5 Hz, 1H), 2.34 (s, 3H).
f1 (ppm)

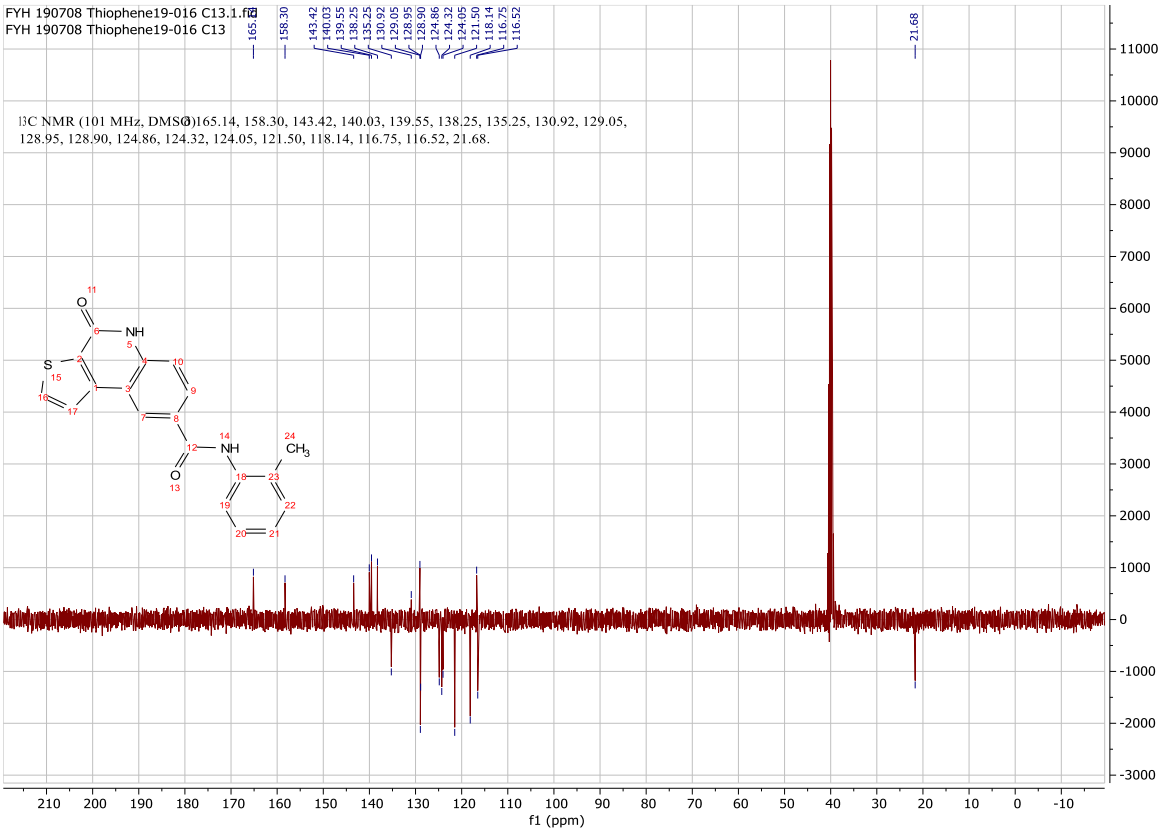
FYH 190708 Thiophene19-016 C13.1.fid
FYH 190708 Thiophene19-016 C13
13C NMR (101 MHz, DMSO-d6) 165.14, 158.30, 143.42, 140.03, 139.55, 138.25, 135.25, 130.92, 129.05, 128.95, 128.90, 124.86, 124.32, 124.05, 121.50, 118.14, 116.75, 116.52, 21.68.
f1 (ppm)

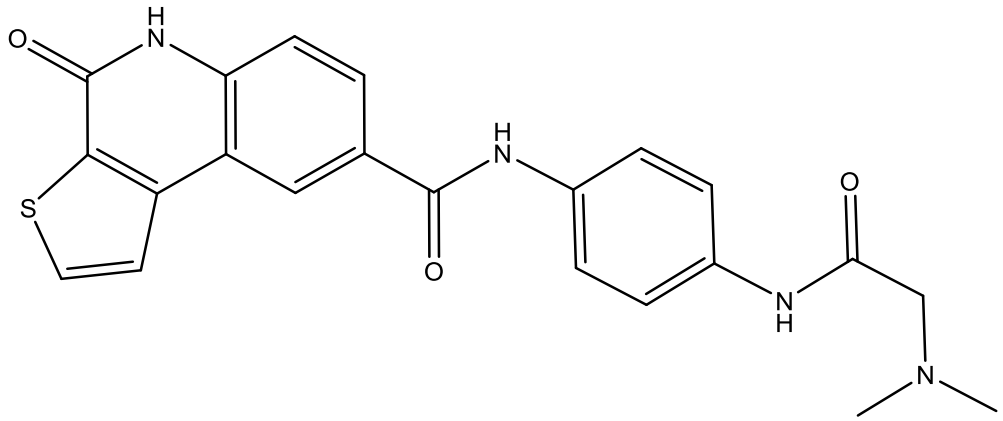

N-(4-(2-(dimethylamino)acetamido)phenyl)-4-oxo-4,5-dihydrothieno[2,3-c]quinoline-8-carboxamide (c11)

Using **Synthesis Method d**, 24.5mg (0.1mmol) **c36** was reacted with 19.7mg (0.1mmol) *N*-(4-aminophenyl)-2-(dimethylamino)acetamide to give 22.7mg **c11** (Yield: 54%) and the product was separated as yellowish white solid. ^{1}H NMR (400 MHz, DMSO-d_6) δ 12.17 (s, 1H), 10.48 (s, 1H), 10.41 (s, 1H), 8.88 (d, *J* = 1.8 Hz, 1H), 8.28 (d, *J* = 5.2 Hz, 1H), 8.21 (d, *J* = 5.3 Hz, 1H), 8.09 (dd, *J* = 8.6, 1.9 Hz, 1H), 7.84 – 7.76 (m, 2H), 7.68 – 7.60 (m, 2H), 7.55 (d, *J* = 8.6 Hz, 1H), 3.84 (s, 2H), 2.71 (s, 6H). ^{13}C NMR (101 MHz, DMSO) δ 165.0, 158.3, 148.8, 143.5, 140.0, 135.7, 135.3, 134.4, 130.9, 128.9, 128.9, 124.4, 124.2, 121.5, 120.2, 116.8, 116.5, 44.4. HRMS m/z (ESI+, M+H): Calcd for C22H20N4O3S: 421.1329, (ESI+, M+H) found: 421.1339

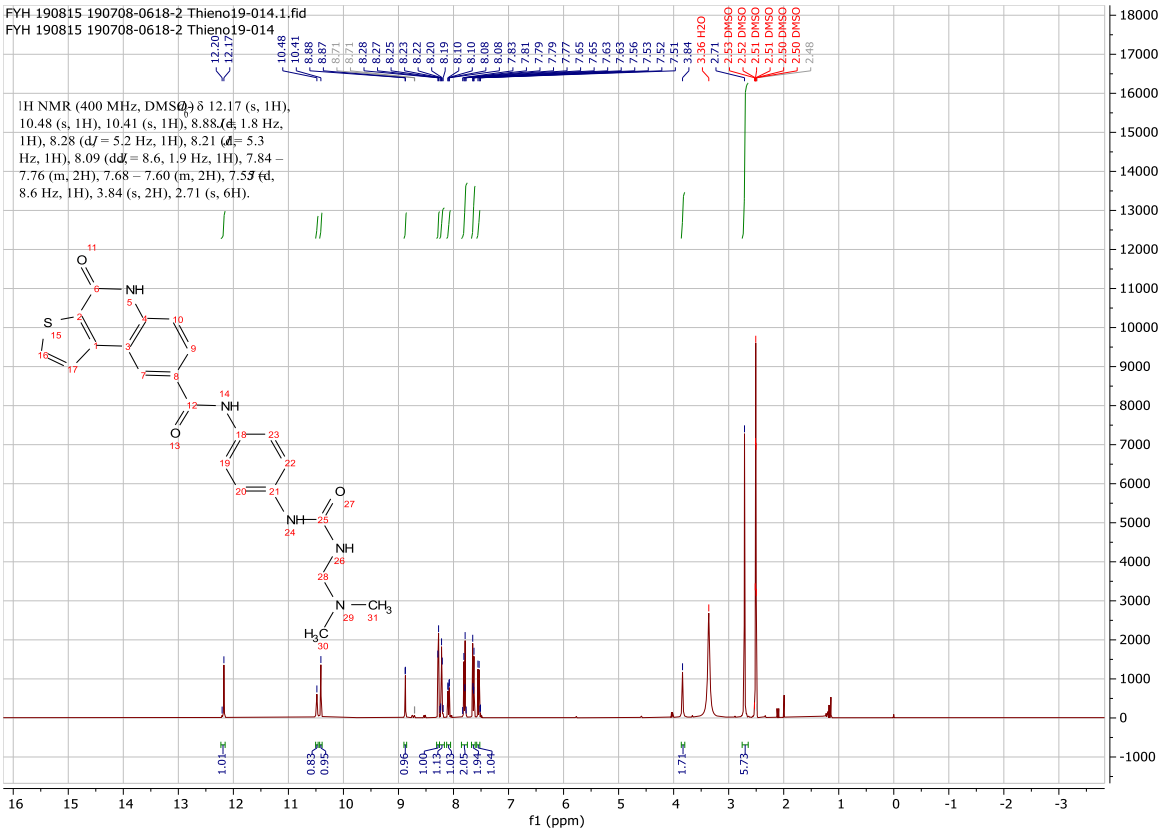
FYH 190815 190708-0618-2 Thieno19-014.1.fid
FYH 190815 190708-0618-2 Thieno19-014
1H NMR (400 MHz, DMSO-d6) δ 12.17 (s, 1H), 10.48 (s, 1H), 10.41 (s, 1H), 8.88 (d, J = 1.8 Hz, 1H), 8.28 (d, J = 5.2 Hz, 1H), 8.21 (d, J = 5.3 Hz, 1H), 8.09 (dd, J = 8.6, 1.9 Hz, 1H), 7.84 – 7.76 (m, 2H), 7.68 – 7.60 (m, 2H), 7.53 (d, 8.6 Hz, 1H), 3.84 (s, 2H), 2.71 (s, 6H).
f1 (ppm)

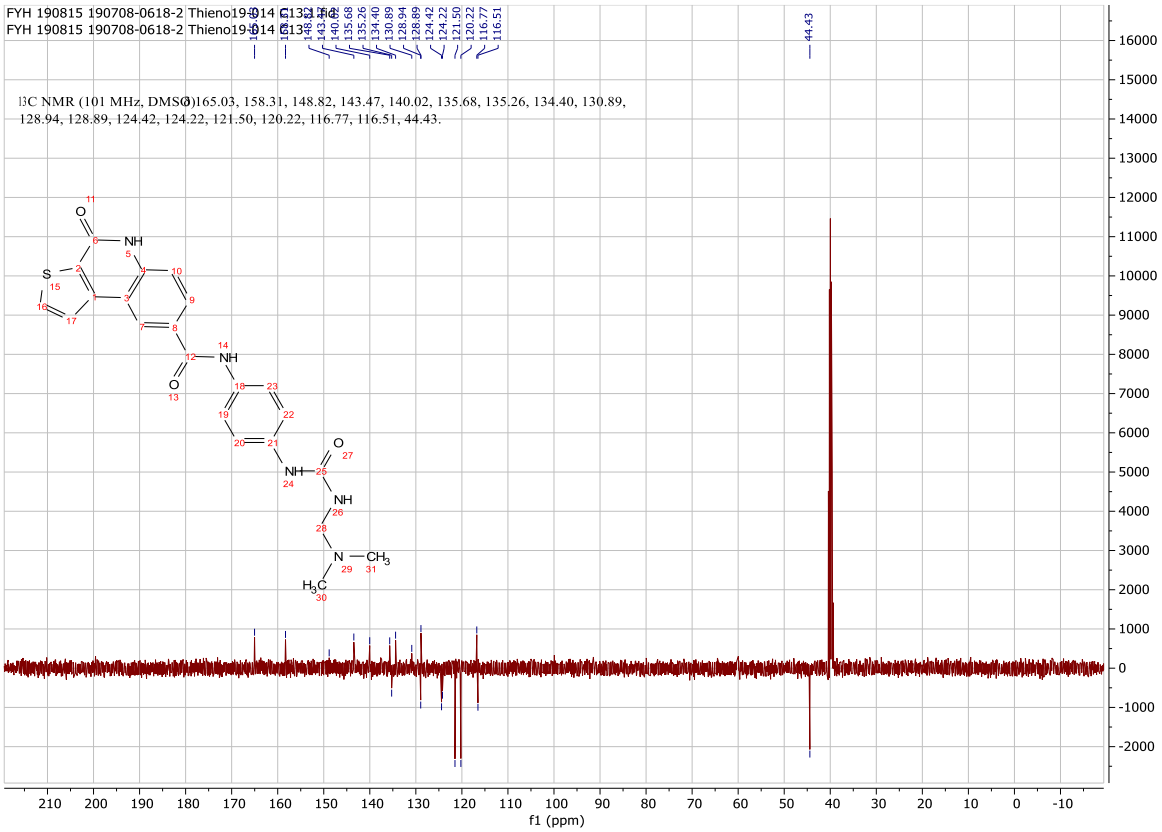
FYH 190815 190708-0618-2 Thieno19-014 C13.1.fid
FYH 190815 190708-0618-2 Thieno19-014 C13.1
13C NMR (101 MHz, DMSO-d6) 165.03, 158.31, 148.82, 143.47, 140.02, 135.68, 135.26, 134.40, 130.89, 128.94, 128.89, 124.42, 124.22, 121.50, 120.22, 116.77, 116.51, 44.43.
f1 (ppm)

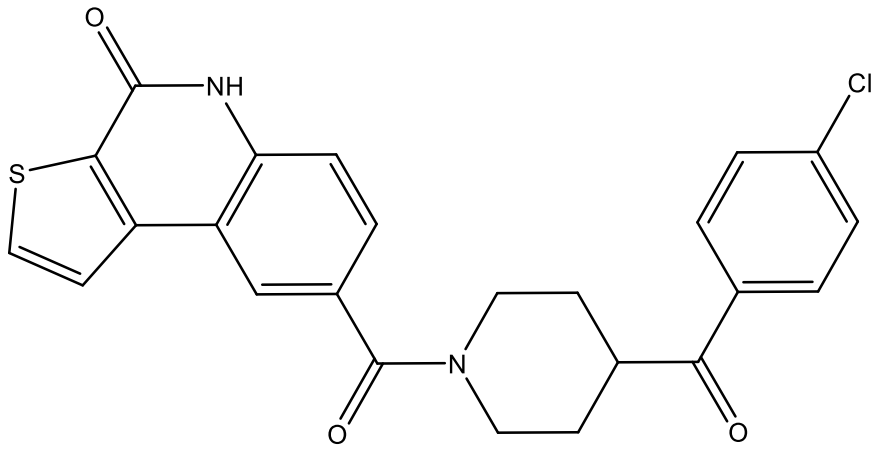

8-(4-(4-chlorobenzoyl)piperidine-1-carbonyl)thieno[2,3-*c*]quinolin-4(5*H*)-one (c12)

Using **Synthesis Method d**, 24.5mg (0.1mmol) **c36** was reacted with 22.4mg (0.1mmol) (4-chlorophenyl)(piperidin-4-yl)methanone to give 26.2mg **c12** (Yield: 58%) and the product was separated as yellowish white solid. ^{1}H NMR (300 MHz, DMSO-d_6) δ 12.01 (s, 1H), 8.25 (d, J = 1.7 Hz, 1H), 8.19 (q, J = 5.2 Hz, 2H), 8.06 – 8.00 (m, 2H), 7.65 – 7.58 (m, 2H), 7.54 (dd, J = 8.4, 1.7 Hz, 1H), 7.48 (d, J = 8.4 Hz, 1H), 3.82 – 3.69 (m, 2H), 1.82 (m, 3H), 1.58 (m, 4H). ^{13}C NMR (75 MHz, DMSO) δ 201.4, 169.2, 158.2, 143.3, 138.6, 138.4, 134.9, 134.6, 130.7, 130.5, 129.4, 128.1, 124.3, 123.6, 117.0, 116.5, 43.0, 28.7. HRMS m/z (ESI+, M+Na): Calcd for C24H19ClN2O3S: 473.0703, (ESI+, M+Na) found: 473.0701

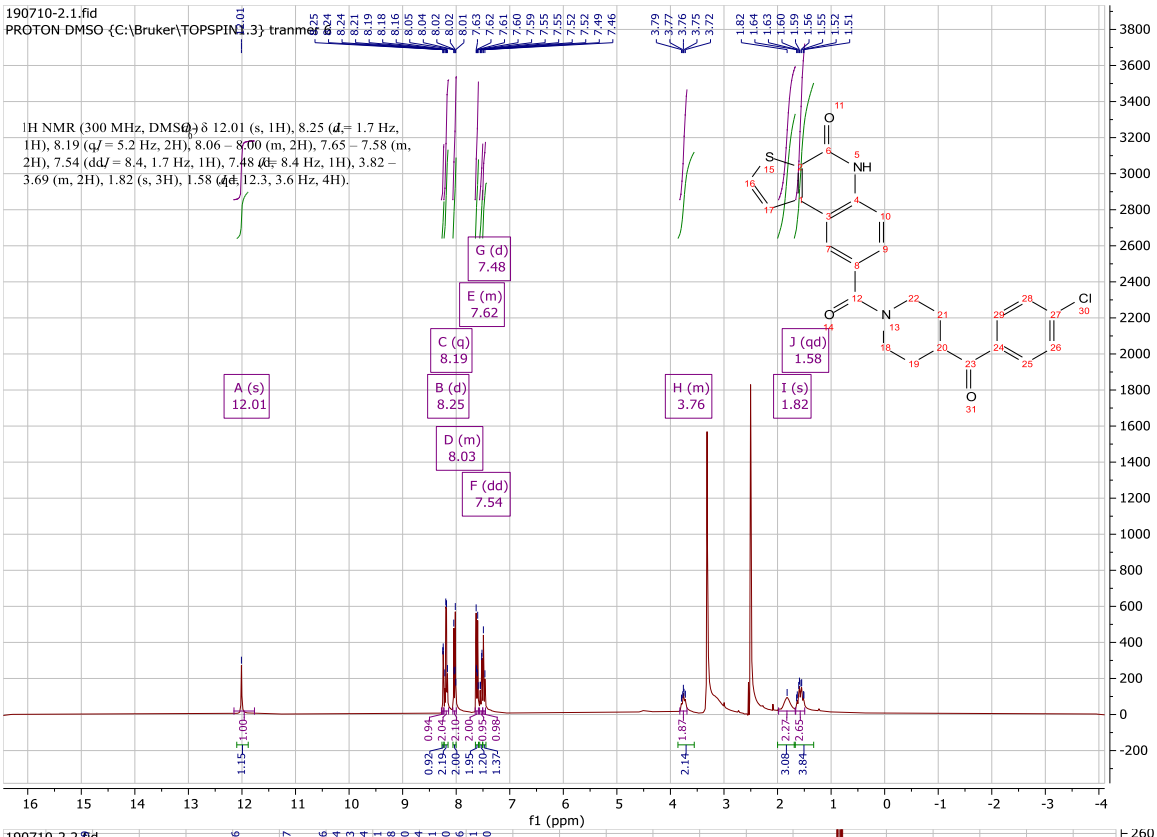
190710-2.1.fid
PROTON DMSO {C:\Bruker\TOPSPIN3.3} tranmer 6
1H NMR (300 MHz, DMSO) δ 12.01 (s, 1H), 8.25 (d, J = 1.7 Hz, 1H), 8.19 (q, J = 5.2 Hz, 2H), 8.06 – 8.00 (m, 2H), 7.65 – 7.58 (m, 2H), 7.54 (dd, J = 8.4, 1.7 Hz, 1H), 7.48 (d, J = 8.4 Hz, 1H), 3.82 – 3.69 (m, 2H), 1.82 (s, 3H), 1.58 (qd, J = 12.3, 3.6 Hz, 4H).
A (s) 12.01
B (d) 8.25
C (q) 8.19
D (m) 8.03
E (m) 7.62
F (dd) 7.54
G (d) 7.48
H (m) 3.76
I (s) 1.82
J (qd) 1.58
f1 (ppm)

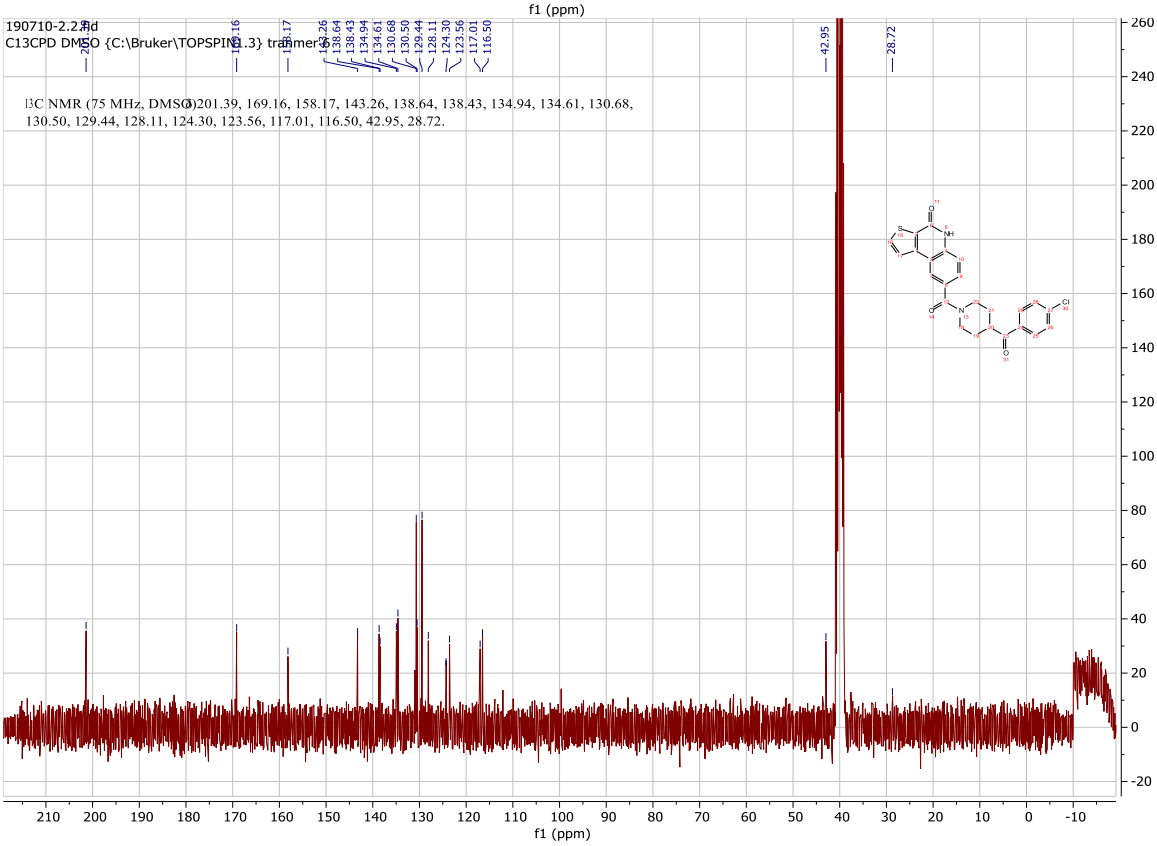
190710-2.2.fid
C13CPD DMSO {C:\Bruker\TOPSPIN3.3} tranmer 6
13C NMR (75 MHz, DMSO) δ 201.39, 169.16, 158.17, 143.26, 138.64, 138.43, 134.94, 134.61, 130.68, 130.50, 129.44, 128.11, 124.30, 123.56, 117.01, 116.50, 42.95, 28.72.
f1 (ppm)

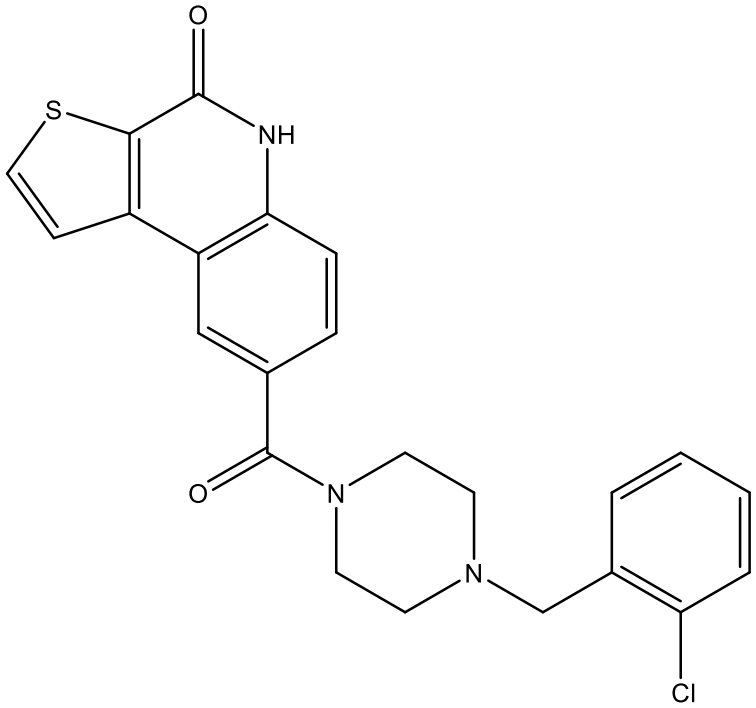

8-(4-(2-chlorobenzyl)piperazine-1-carbonyl)thieno[2,3-*c*]quinolin-4(5*H*)-one (c13)

Using **Synthesis Method d**, 24.5mg (0.1mmol) **c36** was reacted with 21mg (0.1mmol) 1-(2-chlorobenzyl)piperazine to give 24mg **c13** (Yield: 55%) and the product was separated as yellowish white solid. ^{1}H NMR (300 MHz, DMSO-d_6) δ 12.01 (s, 1H), 8.24 (d, J = 1.3 Hz, 1H), 8.23 – 8.12 (m, 2H), 7.56 – 7.40 (m, 4H), 7.31 (pd, J = 7.3, 1.7 Hz, 2H), 3.62 (m, 8H), 2.28 (m, 2H). ^{13}C NMR (75 MHz, DMSO) δ 169.0, 158.2, 143.2, 138.5, 135.8, 135.0, 133.8, 131.4, 131.0, 130.2, 129.8, 129.2, 128.3, 127.5, 124.3, 123.8, 117.0, 116.5, 58.9, 53.0. HRMS m/z (ESI+, M+H): Calcd for C23H20ClN3O2S: 438.1038, (ESI+, M+H) found: 438.1037

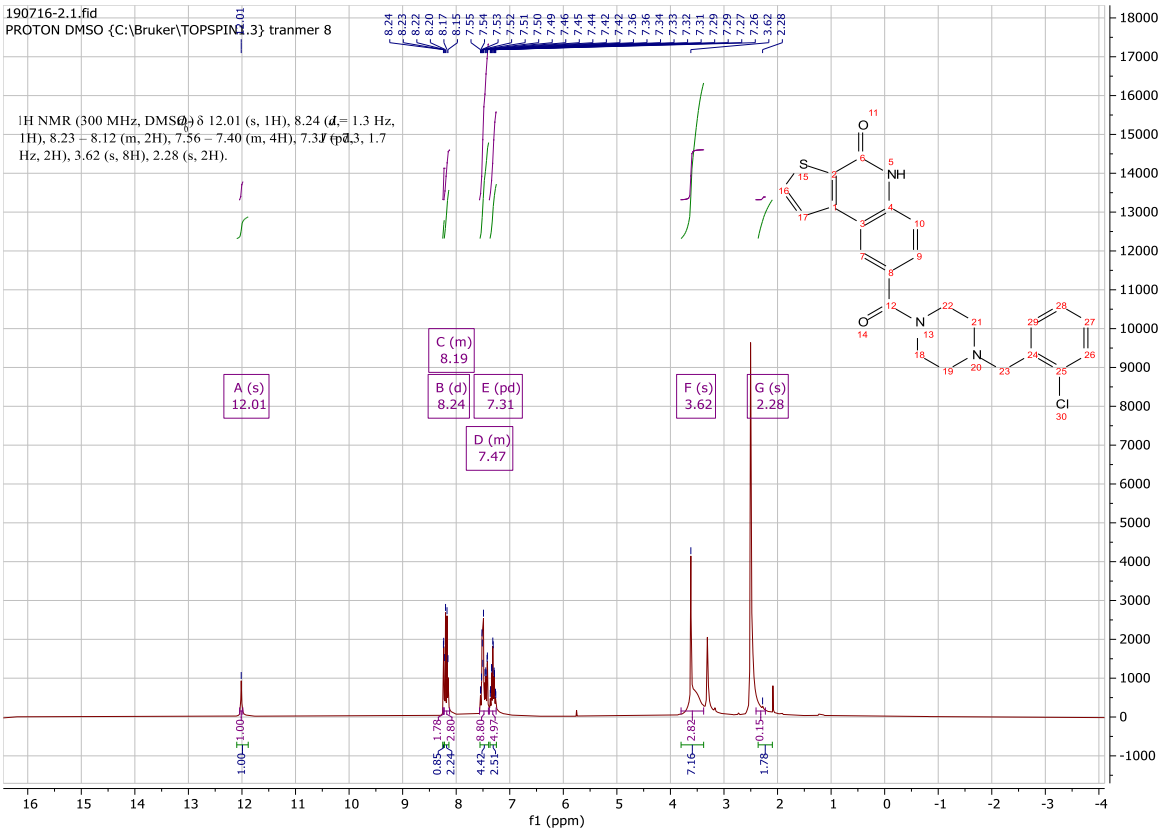
190716-2.1.fid
PROTON DMSO {C:\Bruker\TOPSPIN3.3} tranmer 8
1H NMR (300 MHz, DMSO) δ 12.01 (s, 1H), 8.24 (d, J = 1.3 Hz, 1H), 8.23 – 8.12 (m, 2H), 7.56 – 7.40 (m, 4H), 7.31 (pd, J = 7.3, 1.7 Hz, 2H), 3.62 (s, 8H), 2.28 (s, 2H).
A (s) 12.01
C (m) 8.19
B (d) 8.24
E (pd) 7.31
D (m) 7.47
F (s) 3.62
G (s) 2.28
f1 (ppm)

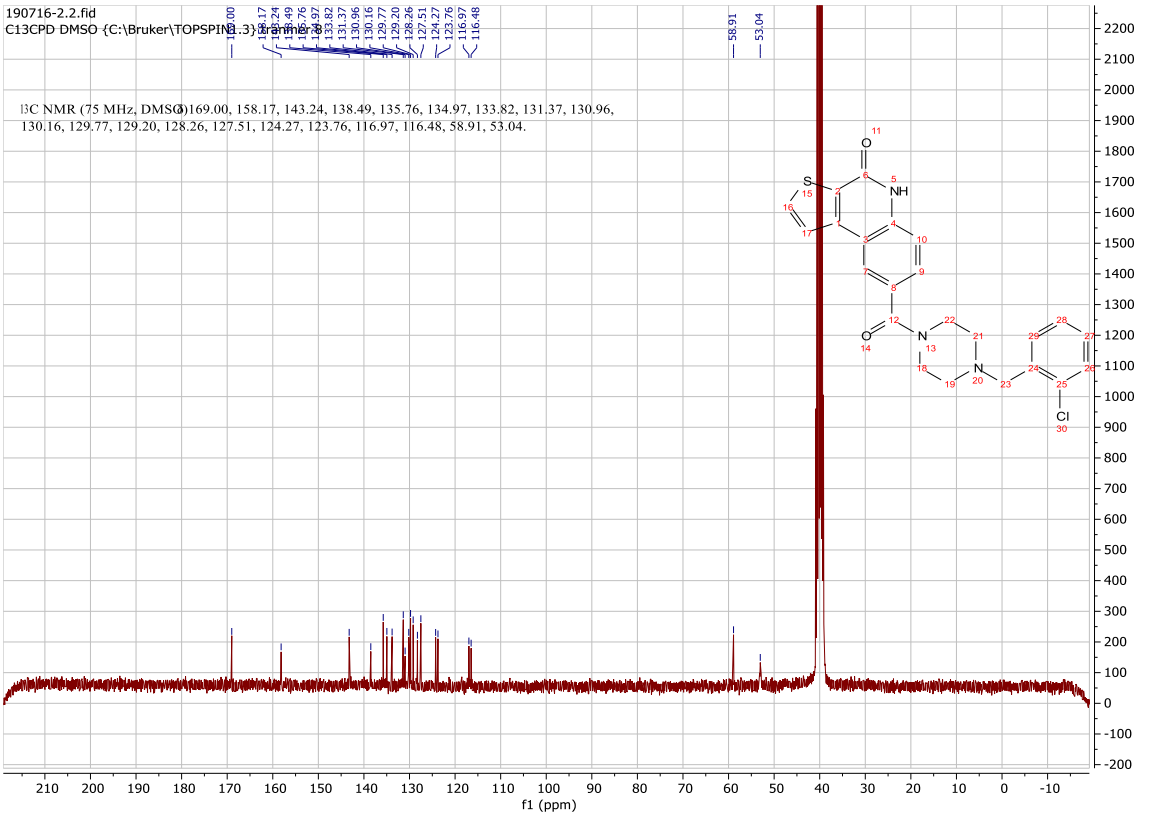
190716-2.2.fid
C13CPD DMSO {C:\Bruker\TOPSPIN3.3} tranmer 8
13C NMR (75 MHz, DMSO) 169.00, 158.17, 143.24, 138.49, 135.76, 134.97, 133.82, 131.37, 130.96, 130.16, 129.77, 129.20, 128.26, 127.51, 124.27, 123.76, 116.97, 116.48, 58.91, 53.04.
f1 (ppm)

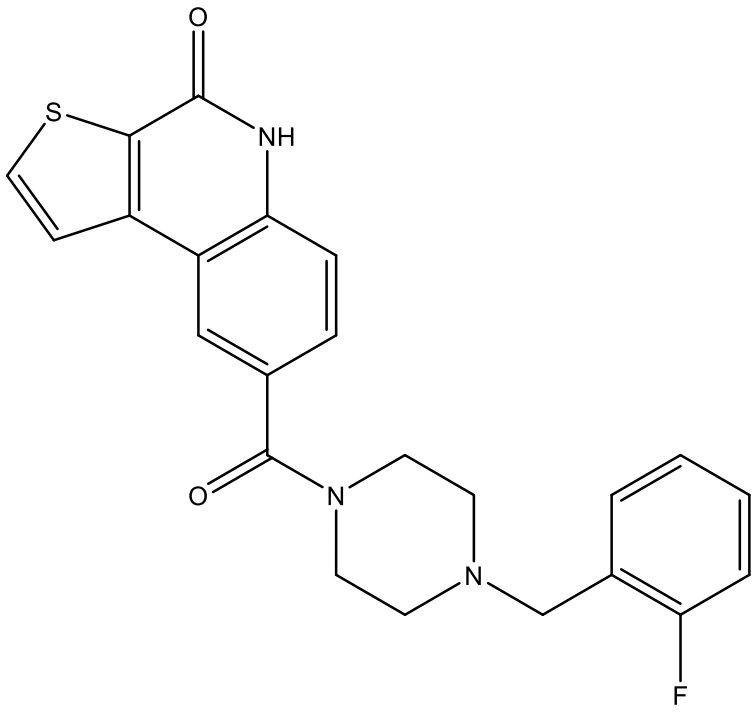

8-(4-(2-florobenzyl)piperazine-1-carbonyl)thieno[2,3-*c*]quinolin-4(5*H*)-one (c14)

Using **Synthesis Method d**, 24.5mg (0.1mmol) **c36** was reacted with 19.6mg (0.1mmol) 1-(2-fluorobenzyl)piperazine to give 20.4mg **c14** (Yield: 49%) and the product was separated as yellowish white solid. ^{1}H NMR (300 MHz, DMSO-d_6) δ 12.01 (s, 1H), 8.23 – 8.11 (m, 3H), 7.59 – 7.26 (m, 4H), 7.22 – 7.09 (m, 2H), 3.58 (m, 6H), 2.44 (m, 4H).^{13}C NMR (75 MHz, DMSO) δ 169.0, 161.3(d, J = 244.4 Hz), 158.2, 143.2, 138.5, 135.0, 132.1(d, J = 4.6 Hz), 131.0, 130.2, 129.7(d, J = 8.4 Hz), 128.2, 124.7 (d, J = 5.4 Hz), 124.6 (d, J = 5.6 Hz), 124.3, 123.8, 117.0, 116.5, 115.7(d, J = 22.1 Hz), 54.9, 52.7. HRMS m/z (ESI+, M+H): Calcd for C23H20FN3O2S: 422.1333, (ESI+, M+H) found: 422.1337

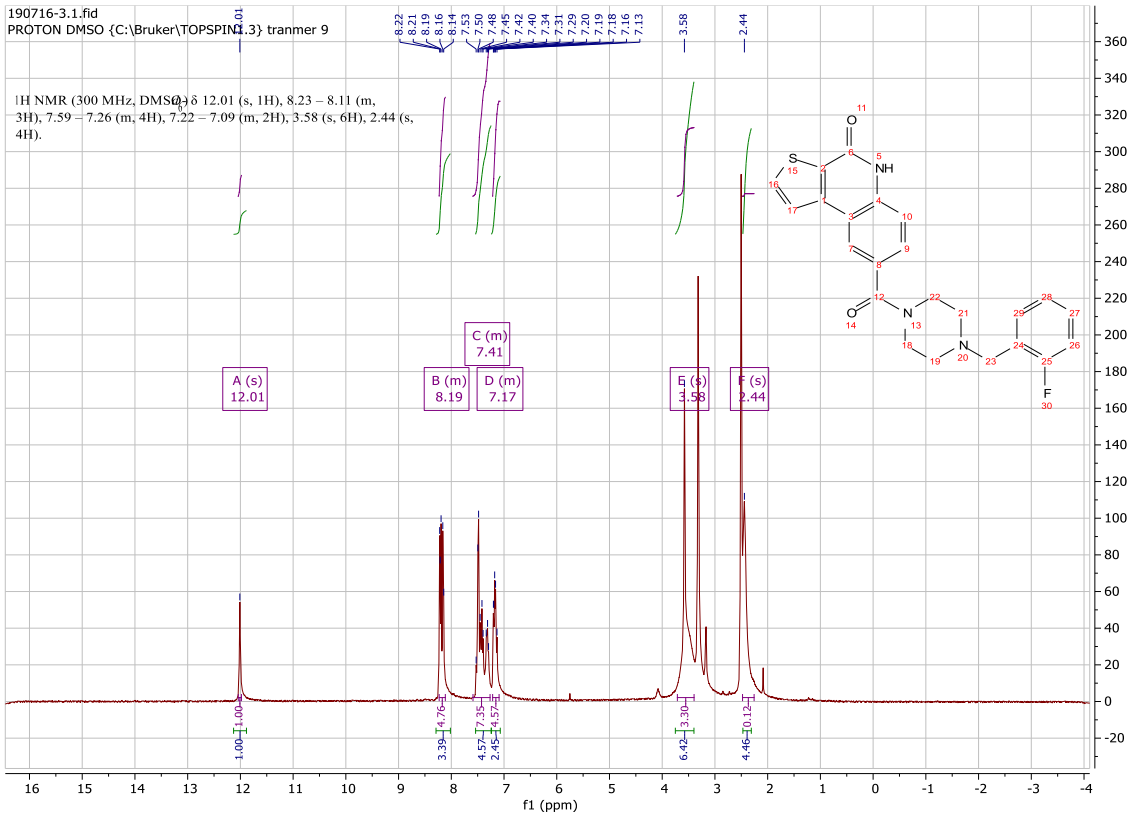
190716-3.1.fid
PROTON DMSO {C:\Bruker\TOPSPIN3.3} tranmer 9
1H NMR (300 MHz, DMSO) δ 12.01 (s, 1H), 8.23 – 8.11 (m, 3H), 7.59 – 7.26 (m, 4H), 7.22 – 7.09 (m, 2H), 3.58 (s, 6H), 2.44 (s, 4H).
A (s) 12.01
B (m) 8.19
C (m) 7.41
D (m) 7.17
E (s) 3.58
F (s) 2.44
f1 (ppm)

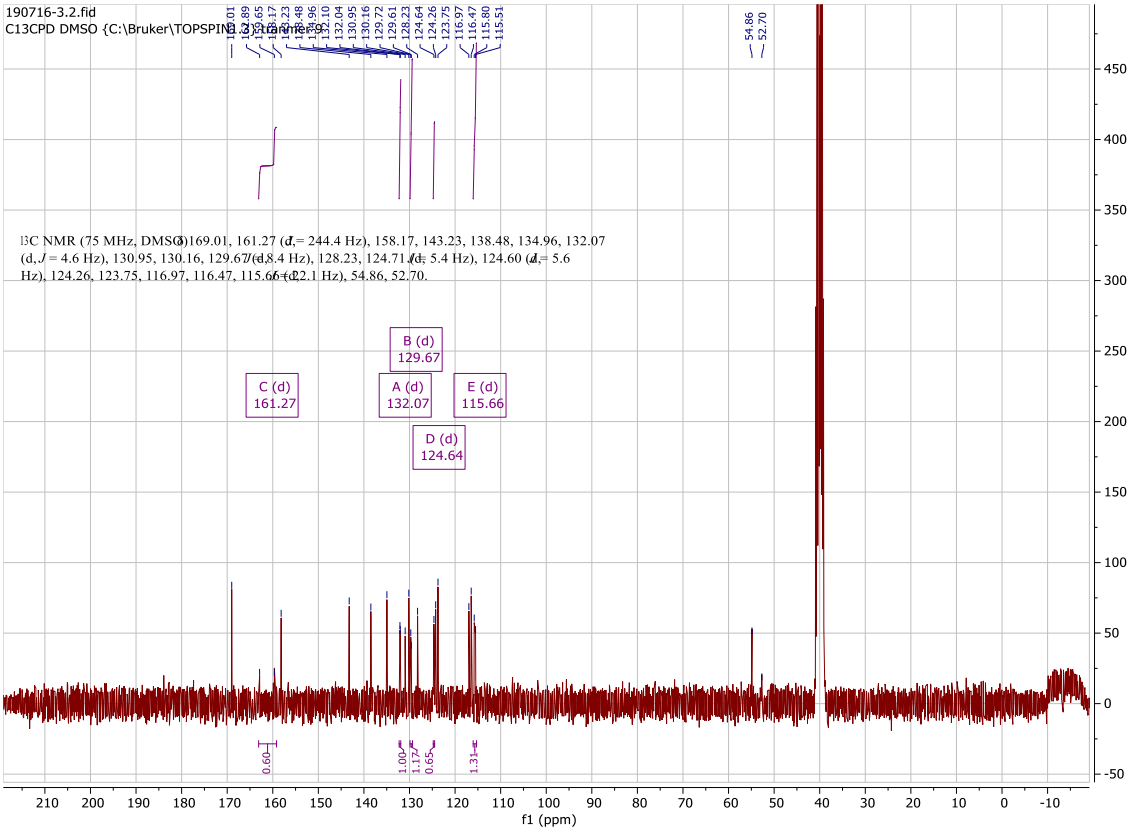
190716-3.2.fid
C13CPD DMSO {C:\Bruker\TOPSPIN3.3} tranmer 9
13C NMR (75 MHz, DMSO) δ 169.01, 161.27 (d, J = 244.4 Hz), 158.17, 143.23, 138.48, 134.96, 132.07 (d, J = 4.6 Hz), 130.95, 130.16, 129.67 (d, J = 8.4 Hz), 128.23, 124.71 (d, J = 5.4 Hz), 124.60 (d, J = 5.6 Hz), 124.26, 123.75, 116.97, 116.47, 115.66 (d, J = 22.1 Hz), 54.86, 52.70.
B (d) 129.67
C (d) 161.27
A (d) 132.07
E (d) 115.66
D (d) 124.64
f1 (ppm)

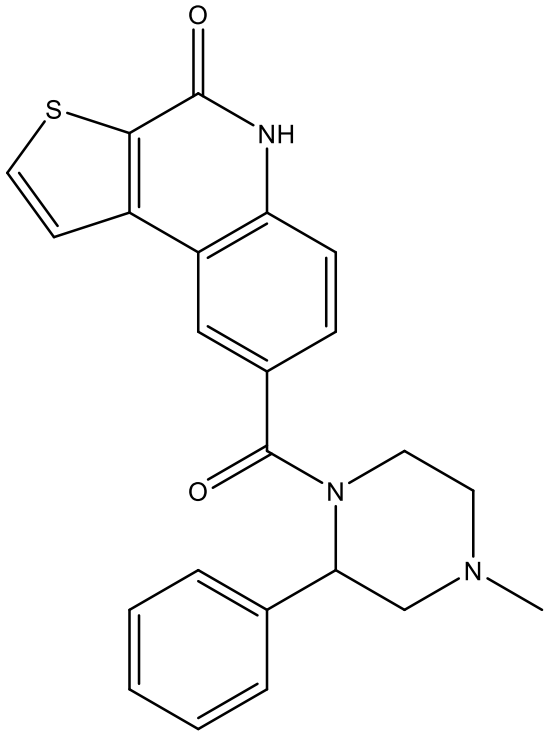

8-(4-methyl-2-phenylpiperazine-1-carbonyl)thieno[2,3-*c*]quinolin-4(5H)-one (c15)

Using **Synthesis Method d**, 24.5mg (0.1mmol) **c36** was reacted with 17.7mg (0.1mmol) 1-methyl-3-phenylpiperazine to give 24.1mg **c15** (Yield: 60%) and the product was separated as yellowish white solid. ^{1}H NMR (300 MHz, DMSO-d_6) δ 12.02 (s, 1H), 8.24 (d, J = 1.8 Hz, 1H), 8.20 (d, J = 5.2 Hz, 1H), 8.10 (s, 1H), 7.54 (dd, J = 8.5, 1.8 Hz, 1H), 7.51 – 7.44 (m, 3H), 7.38 (t, J = 7.5 Hz, 3H), 7.27 (t, J = 7.2 Hz, 1H), 3.44 (d, J = 12.0 Hz, 1H), 2.78 – 2.66 (m, 1H), 2.41 (m, 1H), 2.22 (m, 2H), 2.15 – 2.01 (m, 2H), 1.31 – 1.20 (m, 3H). ^{13}C NMR (75 MHz, DMSO) δ 169.8, 158.1, 143.1, 140.2, 138.5, 135.0, 131.0, 130.2, 128.8, 127.9, 127.7, 127.2, 124.2, 123.4, 117.1, 116.6, 57.5, 55.1, 54.7, 46.2, 18.2. HRMS m/z (ESI+, M+H): Calcd for C23H21N3O2S: 404.1427, (ESI+, M+H) found: 404.1429

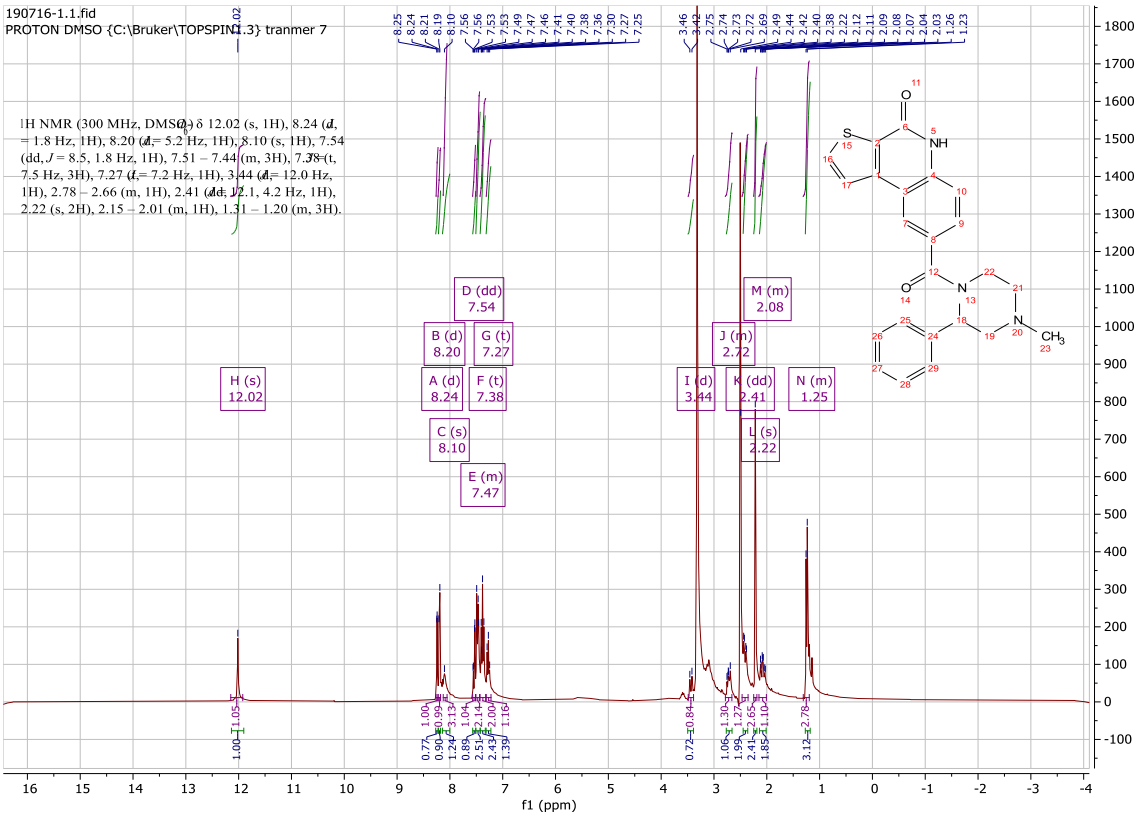
190716-1.1.fid
PROTON DMSO {C:\Bruker\TOPSPIN3.3} tranmer 7
1H NMR (300 MHz, DMSO) δ 12.02 (s, 1H), 8.24 (d, J = 1.8 Hz, 1H), 8.20 (d, J = 5.2 Hz, 1H), 8.10 (s, 1H), 7.54 (dd, J = 8.5, 1.8 Hz, 1H), 7.51 – 7.44 (m, 3H), 7.38 (t, J = 7.5 Hz, 3H), 7.27 (t, J = 7.2 Hz, 1H), 3.44 (d, J = 12.0 Hz, 1H), 2.78 – 2.66 (m, 1H), 2.41 (dd, J = 12.1, 4.2 Hz, 1H), 2.22 (s, 2H), 2.15 – 2.01 (m, 1H), 1.31 – 1.20 (m, 3H).
H (s) 12.02
B (d) 8.20
G (t) 7.27
D (dd) 7.54
A (d) 8.24
F (t) 7.38
C (s) 8.10
E (m) 7.47
I (d) 3.44
K (dd) 2.41
J (m) 2.72
M (m) 2.08
N (m) 1.25
L (s) 2.22
f1 (ppm)

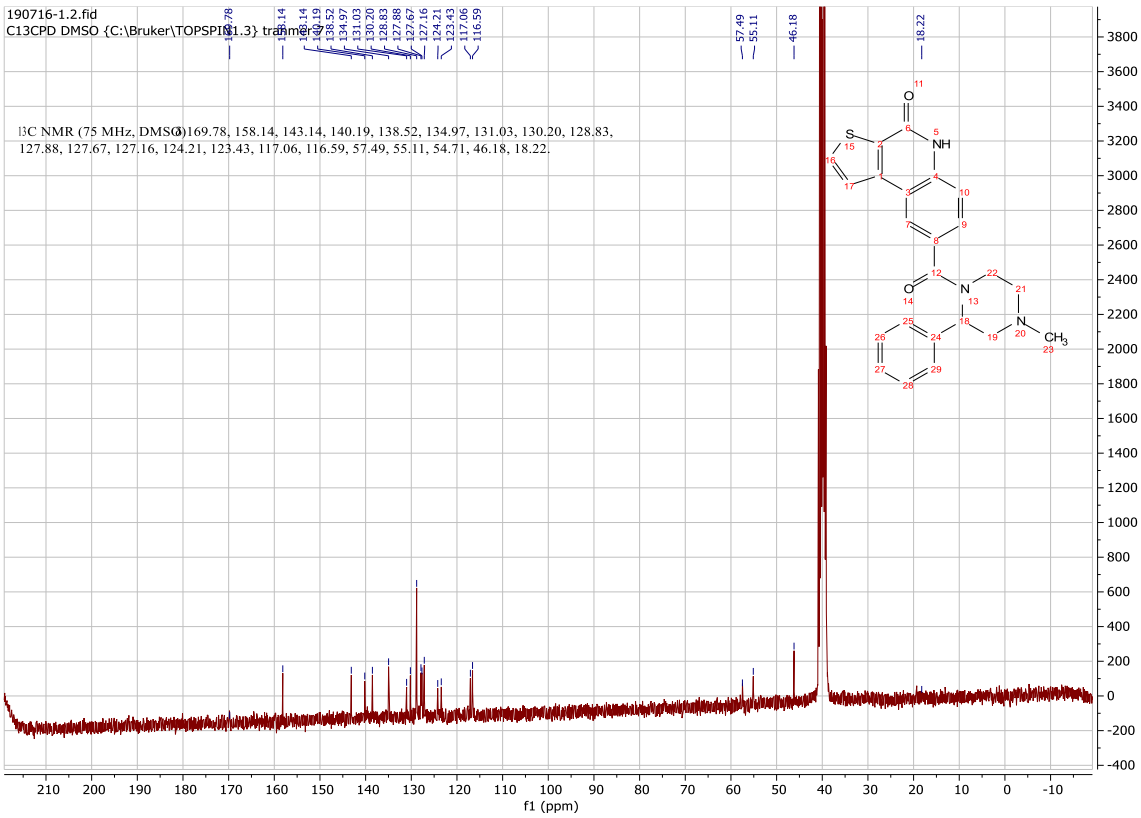
190716-1.2.fid
C13CPD DMSO {C:\Bruker\TOPSPIN3.3} tranmer 7
13C NMR (75 MHz, DMSO) 169.78, 158.14, 143.14, 140.19, 138.52, 134.97, 131.03, 130.20, 128.83, 127.88, 127.67, 127.16, 124.21, 123.43, 117.06, 116.59, 57.49, 55.11, 54.71, 46.18, 18.22.
f1 (ppm)

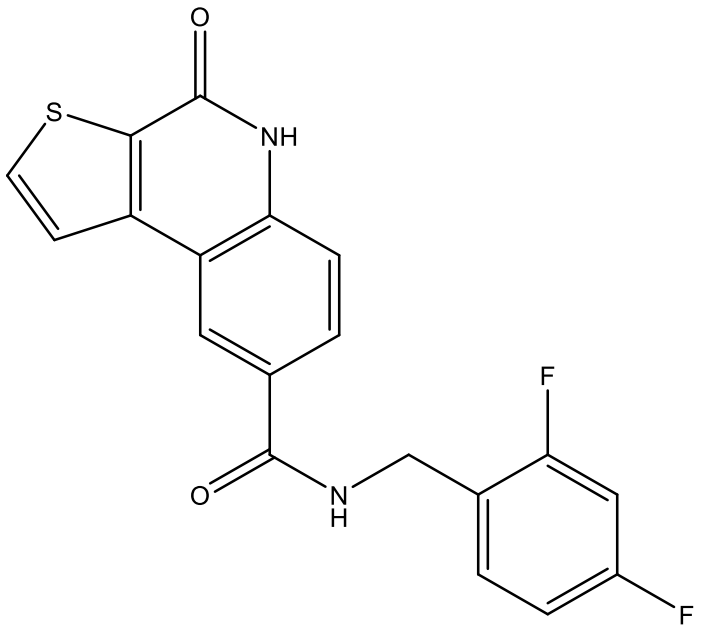

***N*-(2,4-difluorobenzyl)-4-oxo-4,5-dihydrothieno[2,3-*c*]quinoline-8-carboxamide (c16)**

Using **Synthesis Method d**, 24.5mg (0.1mmol) **c36** was reacted with 14.4mg (0.1mmol) (2,4-difluorophenyl)methanamine to give 28.9mg **c16** (Yield: 78%) and the product was separated as yellowish white solid. ^{1}H NMR (300 MHz, DMSO-d_6) δ 12.08 (s, 1H), 9.06 (t, *J* = 5.6 Hz, 1H), 8.72 (d, *J* = 1.8 Hz, 1H), 8.25 (d, *J* = 5.2 Hz, 1H), 8.15 – 7.97 (m, 2H), 7.57 – 7.34 (m, 2H), 7.24 (td, *J* = 10.5, 2.6 Hz, 1H), 7.08 (td, *J* = 8.5, 1.7 Hz, 1H), 4.54 (d, *J* = 5.3 Hz, 2H). ^{13}C NMR (75 MHz, DMSO) δ 168.6 (d, *J* = 225 Hz), 166.1, 158.3, 143.4, 139.9, 135.3, 131.4 (d, *J* = 9.75 Hz), 128.6, 128.1, 123.9, 123.8, 123.1 (d, *J* = 15 Hz), 116.8, 116.4, 111.8(d, *J* = 19.6 Hz), 103.9 (d, *J* = 26.4 Hz), 36.7. HRMS m/z (ESI+, M+Na): Calcd for C19H12F2N2O2S: 393.0485, (ESI+, M+Na) found: 393.0485

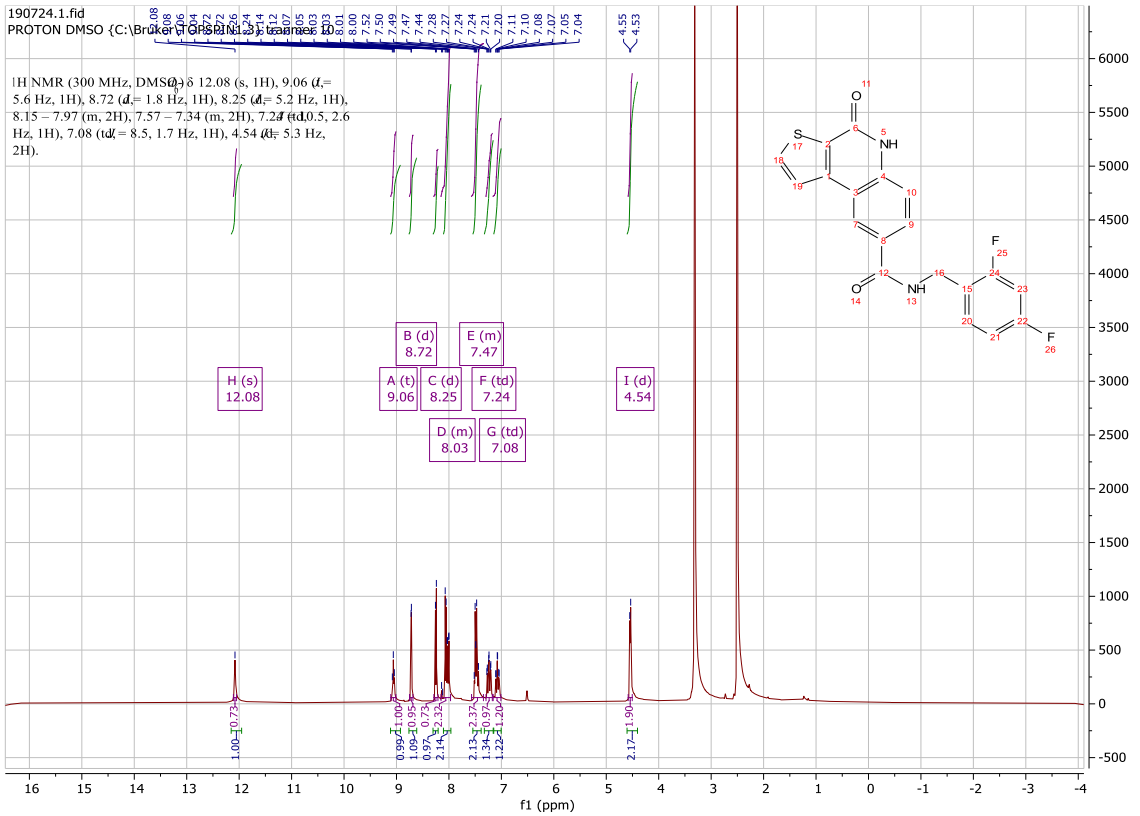
190724.1.fid
PROTON DMSO {C:\Bruker\TOPSPIN4.3.1} trammer 10
1H NMR (300 MHz, DMSO-d6) δ 12.08 (s, 1H), 9.06 (t, J = 5.6 Hz, 1H), 8.72 (d, J = 1.8 Hz, 1H), 8.25 (d, J = 5.2 Hz, 1H), 8.15 – 7.97 (m, 2H), 7.57 – 7.34 (m, 2H), 7.24 (td, J = 10.5, 2.6 Hz, 1H), 7.08 (td, J = 8.5, 1.7 Hz, 1H), 4.54 (d, J = 5.3 Hz, 2H).
H (s) 12.08
A (t) 9.06
B (d) 8.72
C (d) 8.25
D (m) 8.03
E (m) 7.47
F (td) 7.24
G (td) 7.08
I (d) 4.54
f1 (ppm)

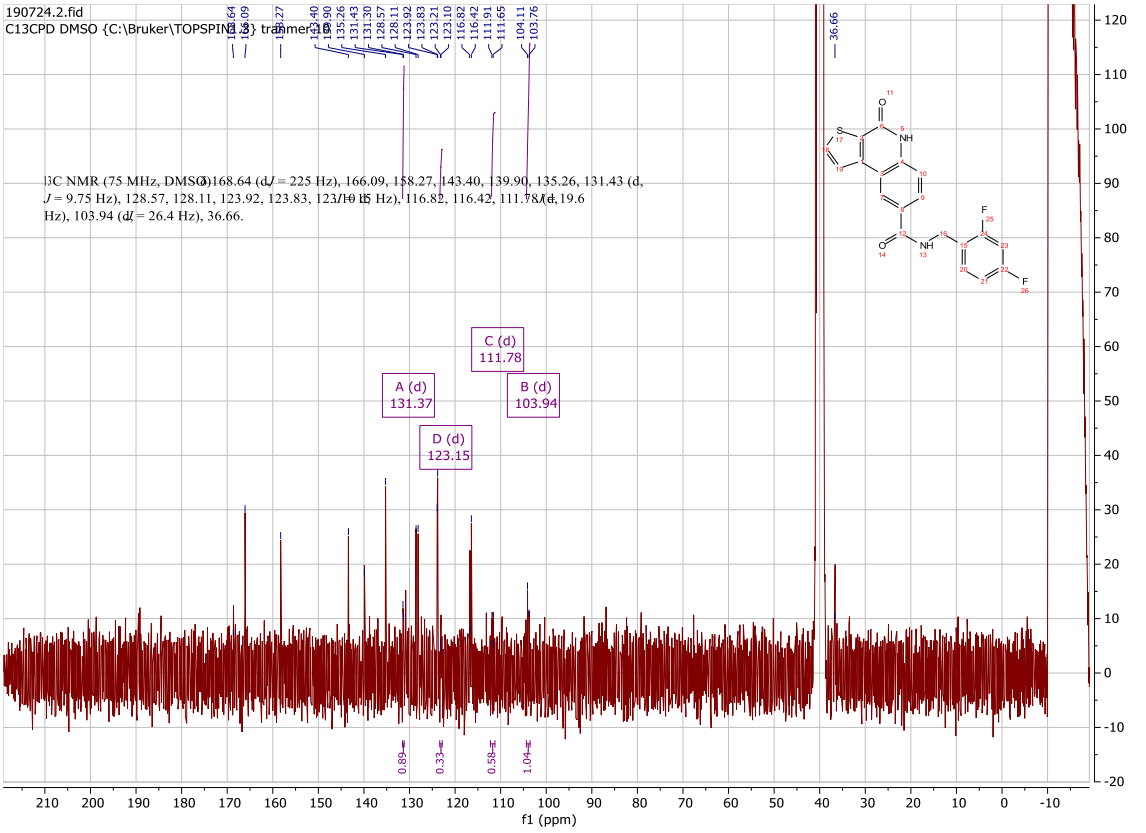
190724.2.fid
C13CPD DMSO {C:\Bruker\TOPSPIN4.3} trammer 10
13C NMR (75 MHz, DMSO-d6) δ 168.64 (d, J = 225 Hz), 166.09, 158.27, 143.40, 139.90, 135.26, 131.43 (d, J = 9.75 Hz), 128.57, 128.11, 123.92, 123.83, 123.10 (d, J = 15 Hz), 116.82, 116.42, 111.78 (d, J = 19.6 Hz), 103.94 (d, J = 26.4 Hz), 36.66.
A (d) 131.37
B (d) 103.94
C (d) 111.78
D (d) 123.15
f1 (ppm)

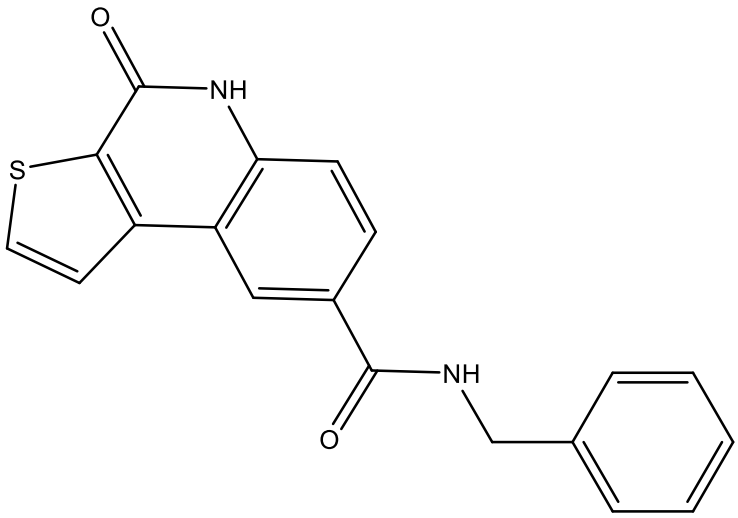

***N*-benzyl-4-oxo-4,5-dihydrothieno[2,3-*c*]quinoline-8-carboxamide (c17)**

Using **Synthesis Method d**, 24.5mg (0.1mmol) **c36** was reacted with 10.7mg (0.1mmol) phenylmethanamine to give 26.3mg **c17** (Yield: 79%) and the product was separated as yellowish white solid. ^{1}H NMR (400 MHz, DMSO-d_6) δ 12.07 (s, 1H), 9.07 (t, J = 5.8 Hz, 1H), 8.73 (s, 1H), 8.24 (d, J = 5.2 Hz, 1H), 8.08 – 7.99 (m, 2H), 7.48 (d, J = 8.6 Hz, 1H), 7.34 (d, J = 6.6 Hz, 4H), 7.25 (t, J = 6.5 Hz, 1H), 4.55 (d, J = 5.9 Hz, 2H). ^{13}C NMR (101 MHz, DMSO) δ 165.9, 158.3, 143.4, 140.1, 139.8, 135.2, 130.8, 128.8, 128.6, 128.4, 127.8, 127.2, 123.8, 123.8, 116.8, 116.4, 43.2. HRMS m/z (ESI+, M+Na): Calcd for C19H14N2O2S: 357.0674, (ESI+, M+Na) found: 357.0670

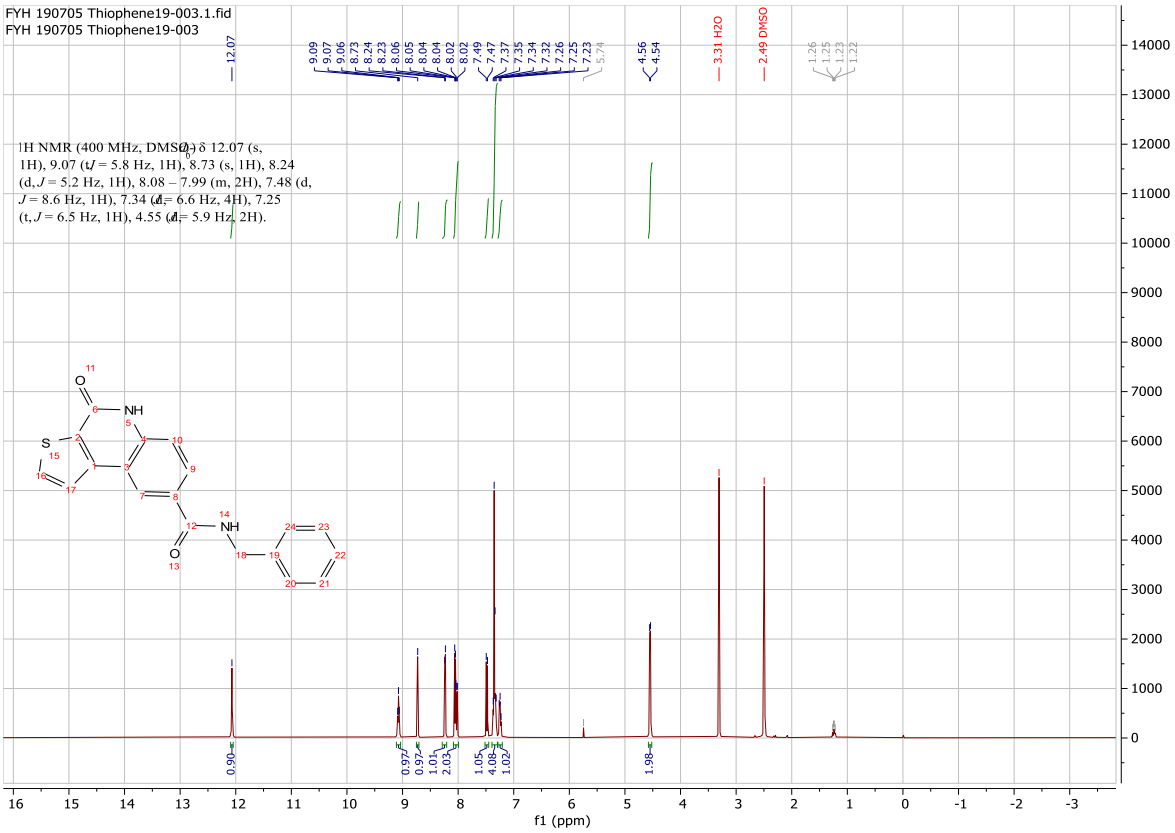
FYH 190705 Thiophene19-003.1.fid
FYH 190705 Thiophene19-003
1H NMR (400 MHz, DMSO-d6) δ 12.07 (s, 1H), 9.07 (t, J = 5.8 Hz, 1H), 8.73 (s, 1H), 8.24 (d, J = 5.2 Hz, 1H), 8.08 – 7.99 (m, 2H), 7.48 (d, J = 8.6 Hz, 1H), 7.34 (d, J = 6.6 Hz, 4H), 7.25 (t, J = 6.5 Hz, 1H), 4.55 (d, J = 5.9 Hz, 2H).
12.07
9.09
9.07
9.06
8.73
8.24
8.23
8.06
8.05
8.04
8.04
8.02
8.02
7.49
7.47
7.37
7.35
7.34
7.32
7.26
7.25
7.23
5.74
4.56
4.54
3.31 H2O
2.49 DMSO
1.26
1.25
1.23
1.22
0.90
0.97
0.97
1.01
2.03
1.05
4.08
1.02
1.98
f1 (ppm)

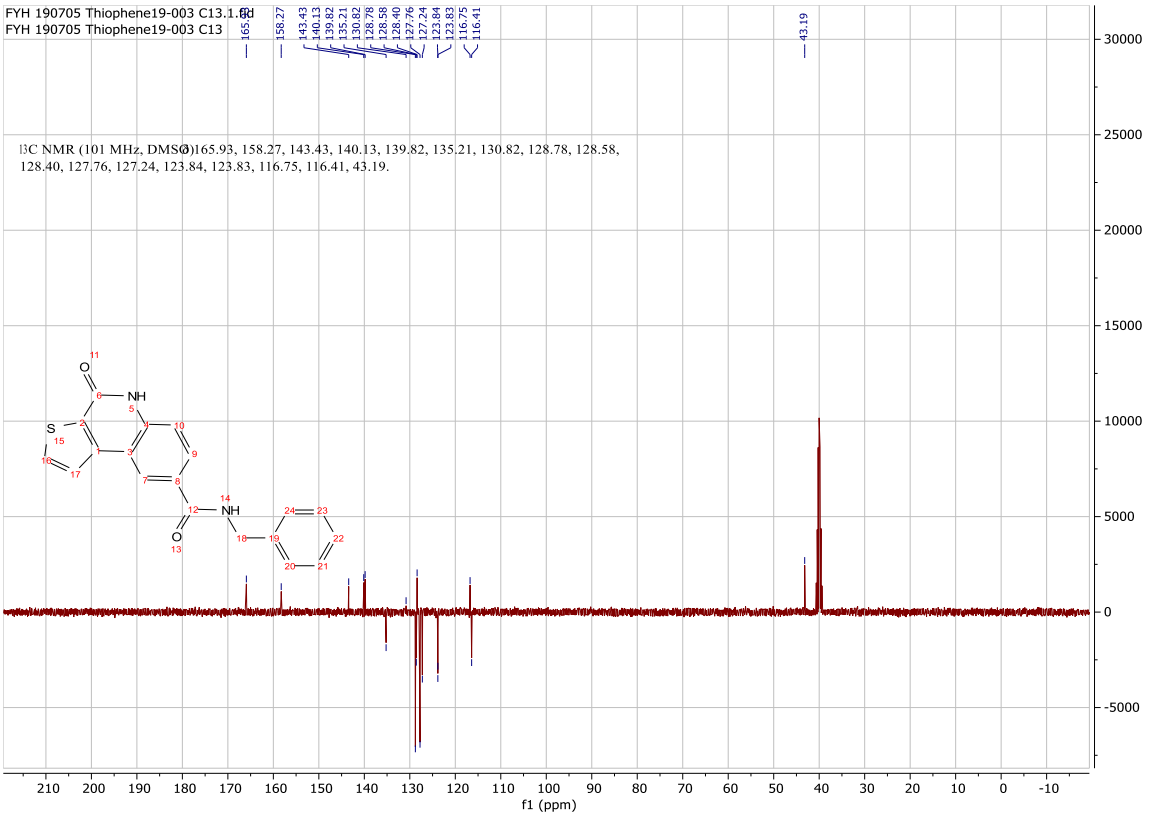
FYH 190705 Thiophene19-003 C13.1.fid
FYH 190705 Thiophene19-003 C13
13C NMR (101 MHz, DMSO-d6) δ 165.93, 158.27, 143.43, 140.13, 139.82, 135.21, 130.82, 128.78, 128.58, 128.40, 127.76, 127.24, 123.84, 123.83, 116.75, 116.41, 43.19.
165.93
158.27
143.43
140.13
139.82
135.21
130.82
128.78
128.58
128.40
127.76
127.24
123.84
123.83
116.75
116.41
43.19
f1 (ppm)

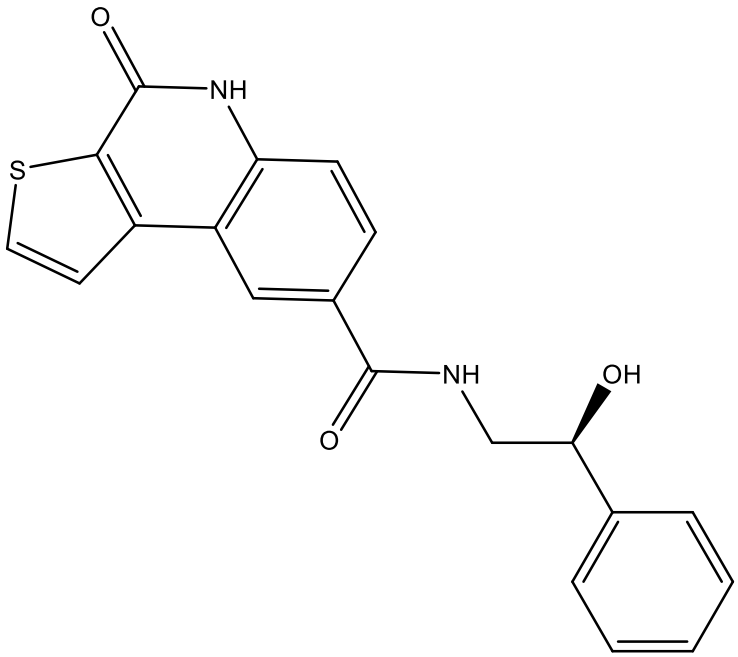

(*S*)-N-(2-hydroxy-2-phenylethyl)-4-oxo-4,5-dihydrothieno[2,3-*c*]quinoline-8-carboxamide (c18)

Using **Synthesis Method d**, 24.5mg (0.1mmol) **c36** was reacted with (*S*)-2-amino-1-phenylethan-1-ol to give 29.8mg **c18** (Yield: 82%) and the product was separated as white solid. ^{1}H NMR (400 MHz, DMSO-d_6) δ 12.06 (s, 1H), 8.70 (d, *J* = 1.9 Hz, 1H), 8.64 (t, *J* = 5.4 Hz, 1H), 8.26 (d, *J* = 5.2 Hz, 1H), 8.07 (d, *J* = 5.3 Hz, 1H), 7.99 (dd, *J* = 8.6, 1.9 Hz, 1H), 7.48 (d, *J* = 8.6 Hz, 1H), 7.44 – 7.31 (m, 4H), 7.32 – 7.23 (m, 1H), 5.57 (s, 1H), 4.82 (dt, *J* = 8.4, 4.3 Hz, 1H), 3.63 – 3.52 (m, 1H), 3.39 – 3.33 (m, 1H). ^{13}C NMR (101 MHz, DMSO) δ 166.2, 158.3, 144.3, 143.5, 139.7, 135.3, 130.8, 128.6, 128.6, 128.5, 127.5, 126.4, 123.9, 123.8, 116.7, 116.3, 71.8, 48.3. HRMS m/z (ESI+, M+Na): Calcd for C20H16N2O3S: 387.0779, (ESI+, M+Na) found: 387.0775

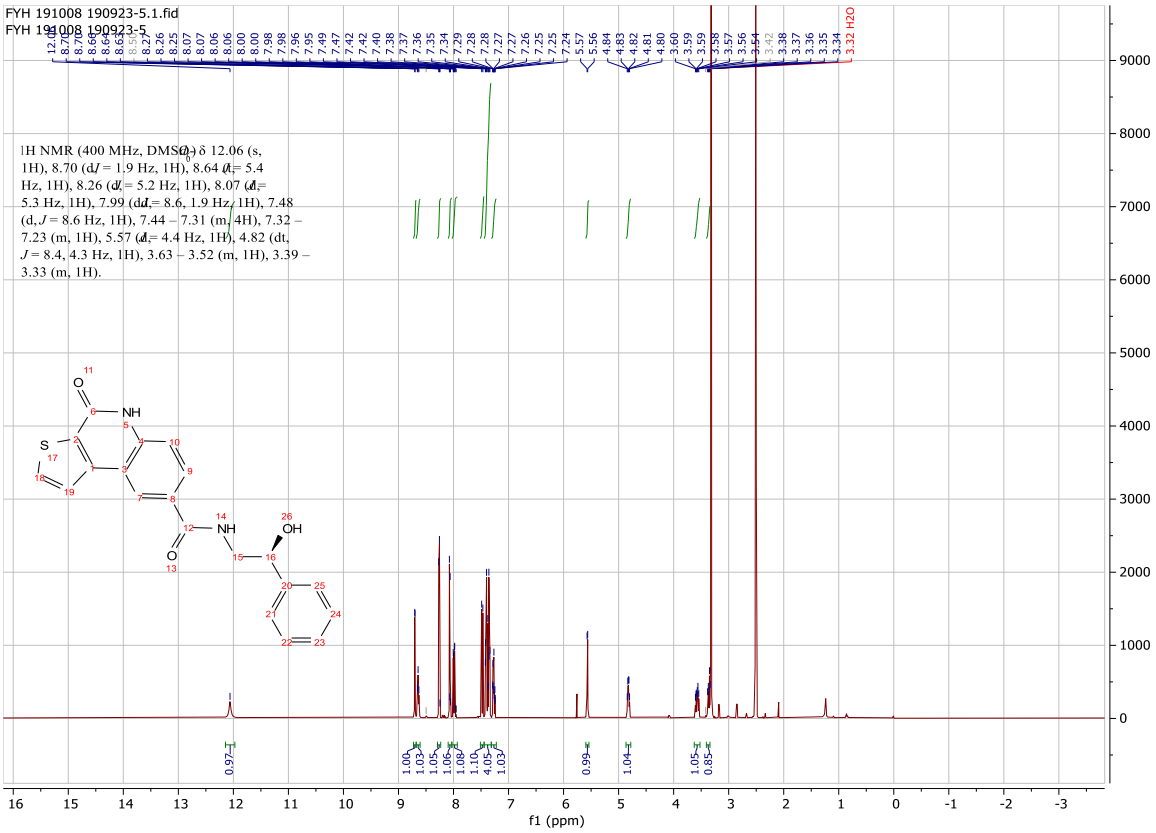
FYH 191008 190923-5.1.fid
FYH 191008 190923-5
1H NMR (400 MHz, DMSO-d6) δ 12.06 (s, 1H), 8.70 (dd, J = 1.9 Hz, 1H), 8.64 (d, J = 5.4 Hz, 1H), 8.26 (dd, J = 5.2 Hz, 1H), 8.07 (d, J = 5.3 Hz, 1H), 7.99 (dd, J = 8.6, 1.9 Hz, 1H), 7.48 (d, J = 8.6 Hz, 1H), 7.44 – 7.31 (m, 4H), 7.32 – 7.23 (m, 1H), 5.57 (d, J = 4.4 Hz, 1H), 4.82 (dt, J = 8.4, 4.3 Hz, 1H), 3.63 – 3.52 (m, 1H), 3.39 – 3.33 (m, 1H).
f1 (ppm)

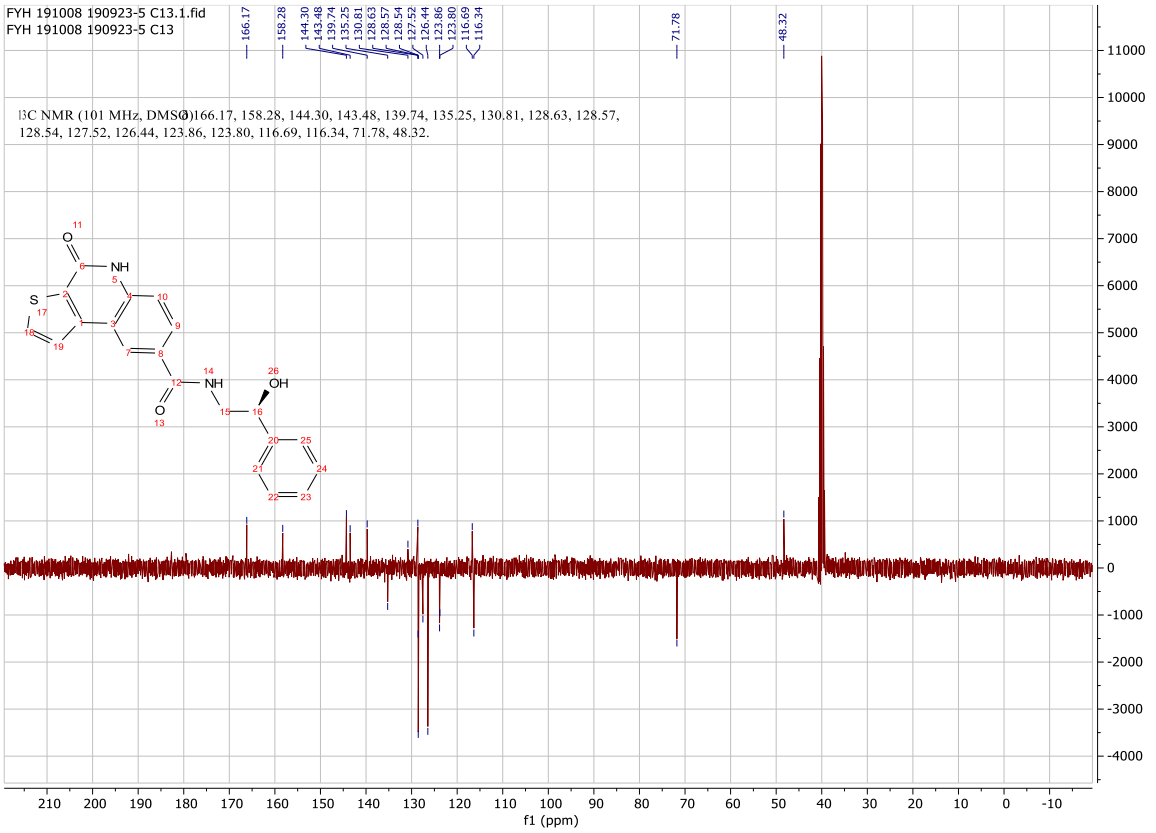
FYH 191008 190923-5 C13.1.fid
FYH 191008 190923-5 C13
13C NMR (101 MHz, DMSO-d6) 166.17, 158.28, 144.30, 143.48, 139.74, 135.25, 130.81, 128.63, 128.57, 128.54, 127.52, 126.44, 123.86, 123.80, 116.69, 116.34, 71.78, 48.32.
f1 (ppm)

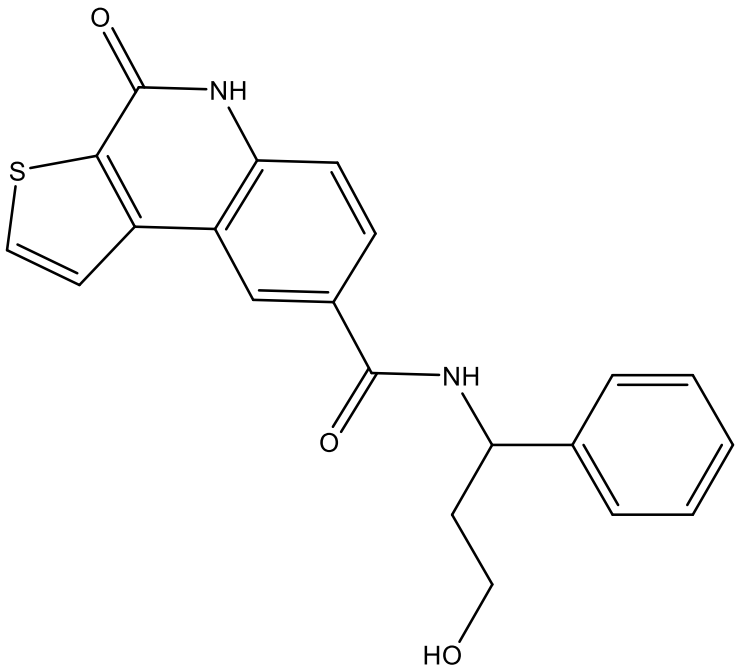

***N*-(3-hydroxy-1-phenylpropyl)-4-oxo-4,5-dihydrothieno[2,3-*c*]quinoline-8-carboxamide (c19)**

Using **Synthesis Method d**, 24.5mg (0.1mmol) **c36** was reacted with 15.1mg (0.1mmol) 3-amino-3-phenylpropan-1-ol to give 26.5mg **c19** (Yield: 70%) and the product was separated as white solid. ^{1}H NMR (300 MHz, DMSO-d_6) δ 12.07 (s, 1H), 8.82 (d, J = 8.1 Hz, 1H), 8.68 (d, J = 1.9 Hz, 1H), 8.26 (d, J = 5.2 Hz, 1H), 8.10 (d, J = 5.2 Hz, 1H), 7.99 (dd, J = 8.6, 1.9 Hz, 1H), 7.49 (d, J = 8.6 Hz, 1H), 7.45 – 7.40 (m, 2H), 7.34 (dd, J = 8.4, 6.7 Hz, 2H), 7.27 – 7.20 (m, 1H), 5.22 (dd, J = 8.4, 7.8 Hz, 1H), 4.61 (s, 1H), 3.63 – 3.40 (m, 2H), 2.15 – 1.89 (m, 2H). ^{13}C NMR (75 MHz, DMSO) δ 165.6, 158.3, 144.6, 143.4, 139.8, 135.2, 130.8, 128.7, 128.7, 128.6, 127.1, 127.0, 124.0, 123.9, 116.7, 116.3, 58.4, 50.8, 39.5. HRMS m/z (ESI+, M+Na): Calcd for C21H18N2O3S: 401.0936, (ESI+, M+Na) found: 401.0931

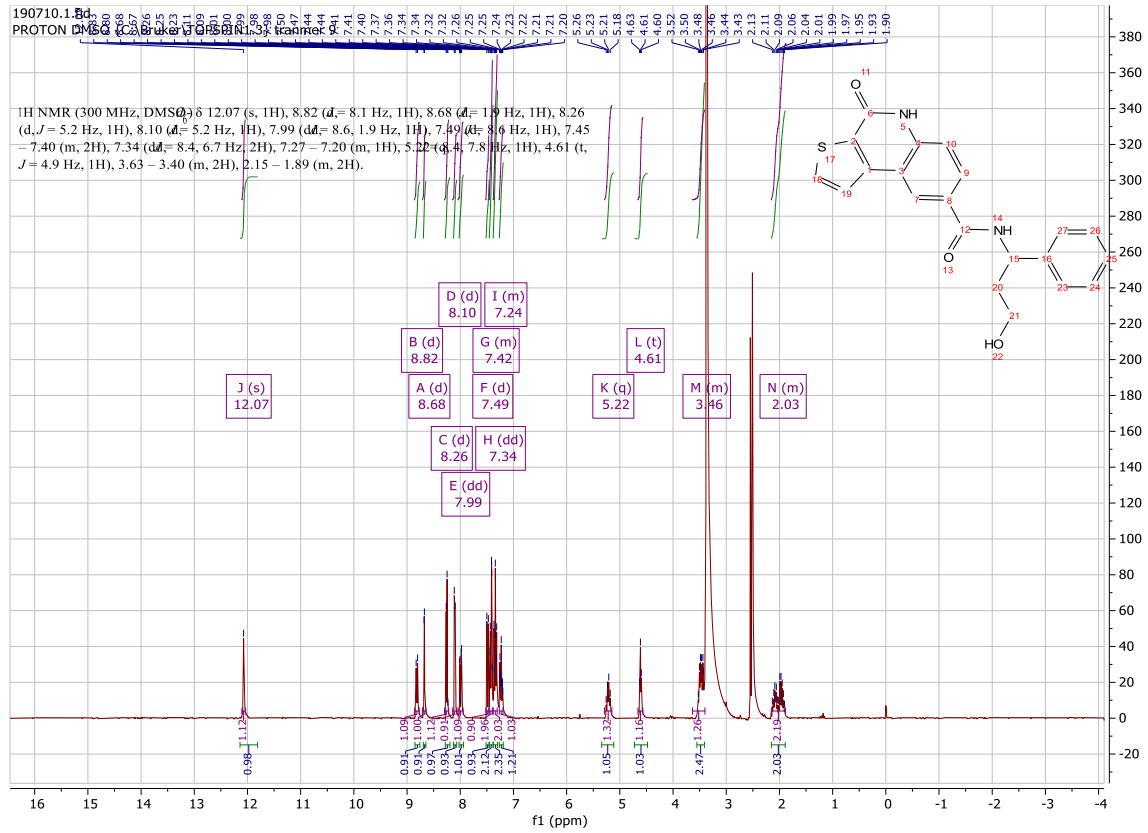
190710.1.fid
PROTON DMSO {C:\Bruker\TOPSPIN1.3} tranmer 9
1H NMR (300 MHz, DMSO) δ 12.07 (s, 1H), 8.82 (d, J = 8.1 Hz, 1H), 8.68 (d, J = 1.9 Hz, 1H), 8.26 (d, J = 5.2 Hz, 1H), 8.10 (d, J = 5.2 Hz, 1H), 7.99 (dd, J = 8.6, 1.9 Hz, 1H), 7.49 (d, J = 8.6 Hz, 1H), 7.45 – 7.40 (m, 2H), 7.34 (dd, J = 8.4, 6.7 Hz, 2H), 7.27 – 7.20 (m, 1H), 5.22 (q, J = 7.8 Hz, 1H), 4.61 (t, J = 4.9 Hz, 1H), 3.63 – 3.40 (m, 2H), 2.15 – 1.89 (m, 2H).
D (d) 8.10
I (m) 7.24
B (d) 8.82
G (m) 7.42
L (t) 4.61
J (s) 12.07
A (d) 8.68
F (d) 7.49
K (q) 5.22
M (m) 3.46
N (m) 2.03
C (d) 8.26
H (dd) 7.34
E (dd) 7.99
f1 (ppm)

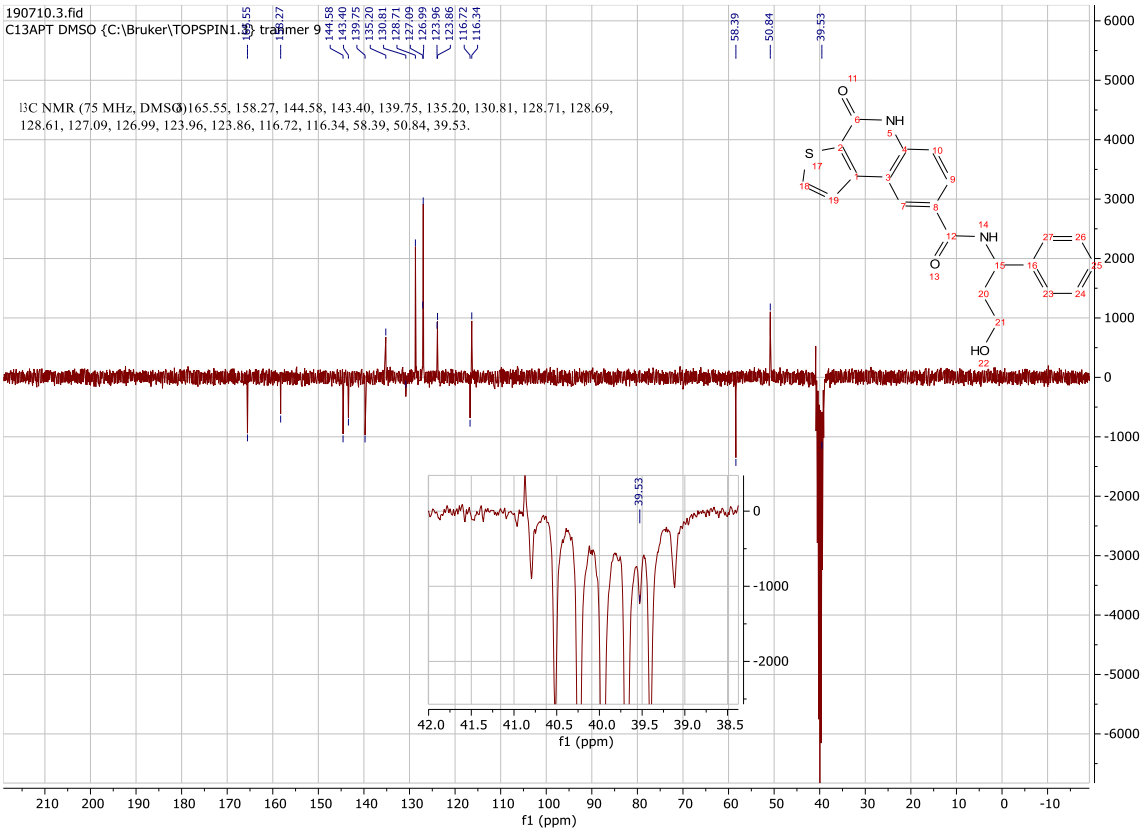
190710.3.fid
C13APT DMSO {C:\Bruker\TOPSPIN1.3} tranmer 9
13C NMR (75 MHz, DMSO) 165.55, 158.27, 144.58, 143.40, 139.75, 135.20, 130.81, 128.71, 128.69, 128.61, 127.09, 126.99, 123.96, 123.86, 116.72, 116.34, 58.39, 50.84, 39.53.
f1 (ppm)

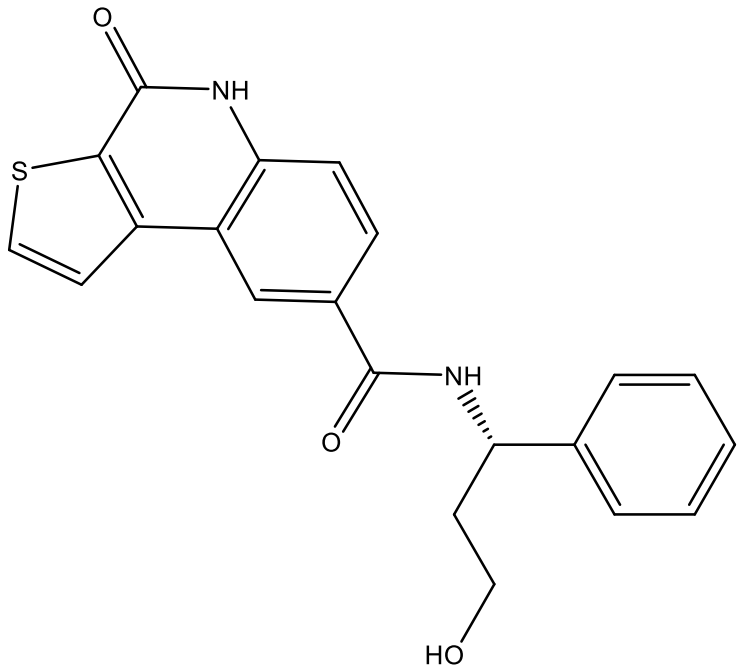

(*S*)-*N*-(3-hydroxy-1-phenylpropyl)-4-oxo-4,5-dihydrothieno[2,3-*c*]quinoline-8-carboxamide (c20)

Using **Synthesis Method d**, 24.5mg (0.1mmol) **c36** was reacted with 15.1mg (0.1mmol) (*S*)-3-amino-3-phenylpropan-1-ol to give 27.2mg **c20** (Yield: 72%) and the product was separated as white solid. ^{1}H NMR (400 MHz, DMSO-d_6) δ 12.09 (s, 1H), 8.82 (d, *J* = 8.1 Hz, 1H), 8.68 (d, *J* = 1.7 Hz, 1H), 8.26 (d, *J* = 5.2 Hz, 1H), 8.11 (d, *J* = 5.2 Hz, 1H), 7.99 (dd, *J* = 8.6, 1.8 Hz, 1H), 7.48 (d, *J* = 8.6 Hz, 1H), 7.42 (d, *J* = 7.4 Hz, 2H), 7.34 (t, *J* = 7.6 Hz, 2H), 7.23 (t, *J* = 7.3 Hz, 1H), 5.21 (dd, *J* = 8.4, 8.0 Hz, 1H), 4.61 (s, 1H), 3.48 (m, 2H), 2.08 − 1.95 (m, 2H). ^{13}C NMR (101 MHz, DMSO) δ 165.5, 158.3, 144.6, 143.4, 139.8, 135.2, 130.8, 128.7, 128.7, 128.6, 127.1, 127, 124.0, 123.9, 116.7, 116.3, 58.4, 50.8, 39.6. HRMS m/z (ESI+, M+Na): Calcd for C21H18N2O3S: 401.0936, (ESI+, M+Na) found: 401.0929

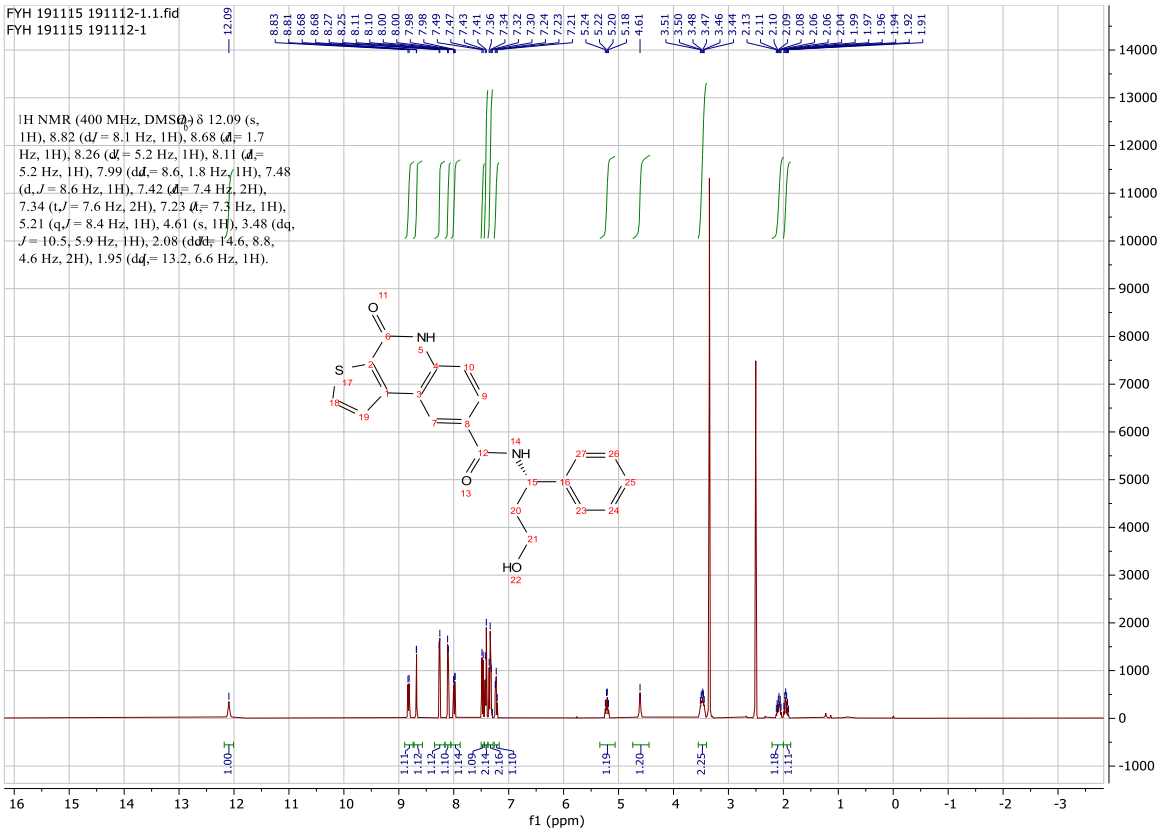
FYH 191115 191112-1.1.fid
FYH 191115 191112-1
1H NMR (400 MHz, DMSO-d6) δ 12.09 (s, 1H), 8.82 (d, J = 8.1 Hz, 1H), 8.68 (d, J = 1.7 Hz, 1H), 8.26 (d, J = 5.2 Hz, 1H), 8.11 (d, J = 5.2 Hz, 1H), 7.99 (dd, J = 8.6, 1.8 Hz, 1H), 7.48 (d, J = 8.6 Hz, 1H), 7.42 (d, J = 7.4 Hz, 2H), 7.34 (t, J = 7.6 Hz, 2H), 7.23 (t, J = 7.3 Hz, 1H), 5.21 (q, J = 8.4 Hz, 1H), 4.61 (s, 1H), 3.48 (dq, J = 10.5, 5.9 Hz, 1H), 2.08 (ddd, J = 14.6, 8.8, 4.6 Hz, 2H), 1.95 (dq, J = 13.2, 6.6 Hz, 1H).
f1 (ppm)

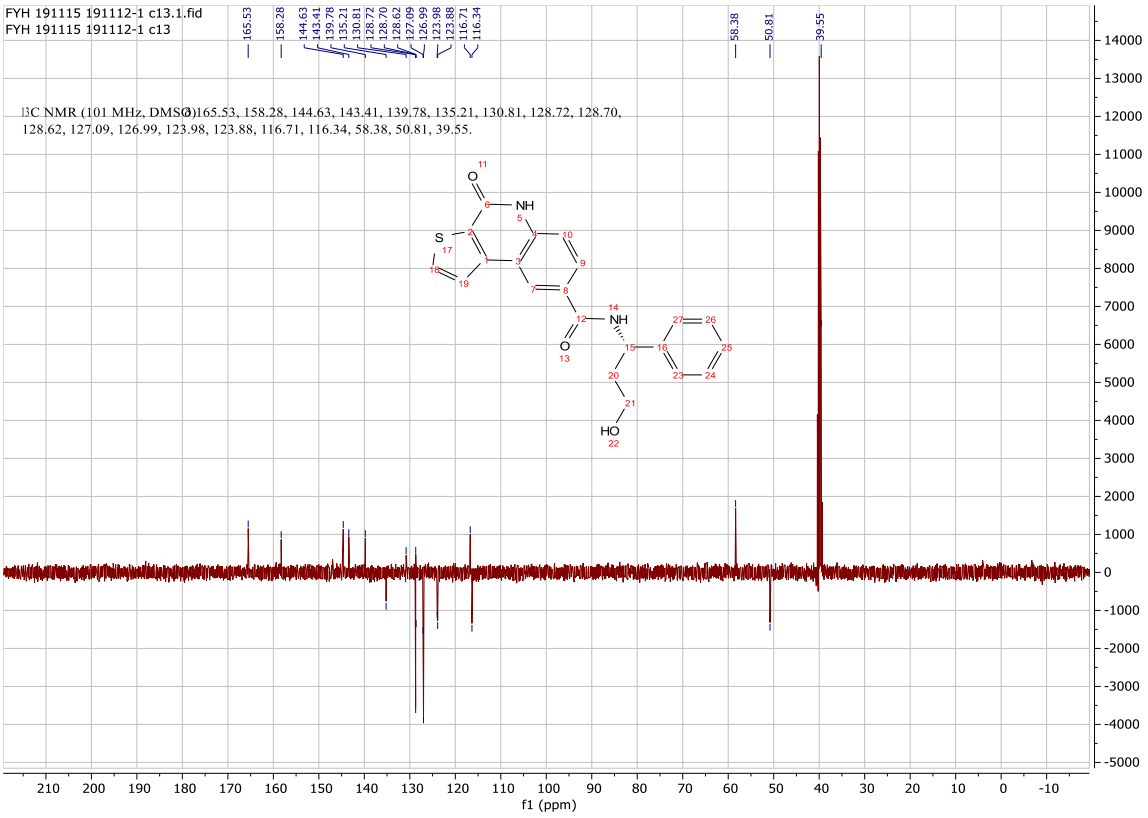
FYH 191115 191112-1 c13.1.fid
FYH 191115 191112-1 c13
13C NMR (101 MHz, DMSO-d6) 165.53, 158.28, 144.63, 143.41, 139.78, 135.21, 130.81, 128.72, 128.70, 128.62, 127.09, 126.99, 123.98, 123.88, 116.71, 116.34, 58.38, 50.81, 39.55.
f1 (ppm)

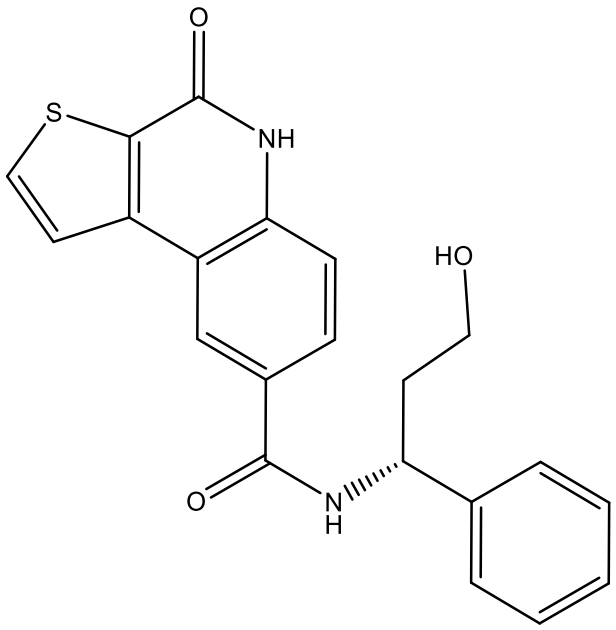

(*R*)-*N*-(3-hydroxy-1-phenylpropyl)-4-oxo-4,5-dihydrothieno[2,3-*c*]quinoline-8-carboxamide (c21)

Using **Synthesis Method d**, 24.5mg (0.1mmol) **c36** was reacted with 15.1mg (0.1mmol) (*R*)-3-amino-3-phenylpropan-1-ol to give 30.6mg **c21** (Yield: 81%) and the product was separated as white solid. ^{1}H NMR (400 MHz, DMSO-d_6) δ 12.08 (s, 1H), 8.82 (d, *J* = 8.1 Hz, 1H), 8.68 (d, *J* = 1.9 Hz, 1H), 8.26 (d, *J* = 5.2 Hz, 1H), 8.10 (d, *J* = 5.2 Hz, 1H), 7.99 (dd, *J* = 8.6, 1.9 Hz, 1H), 7.48 (d, *J* = 8.6 Hz, 1H), 7.45 – 7.39 (m, 2H), 7.34 (dd, *J* = 8.4, 6.9 Hz, 2H), 7.27 – 7.19 (m, 1H), 5.21 (dd, *J* = 8.6, 5.9 Hz, 1H), 4.60 (s, 1H), 3.48 (m, 2H), 2.13 – 1.88 (m, 2H). ^{13}C NMR (101 MHz, DMSO) δ 165.5, 158.3, 144.6, 143.4, 139.8, 135.2, 130.8, 128.7, 128.7, 128.6, 127.1, 127.0, 124.0, 123.9, 116.7, 116.3, 58.4, 50.8, 39.6. HRMS m/z (ESI+, M+Na): Calcd for C21H18N2O3S: 401.0936, (ESI+, M+Na) found: 401.0929

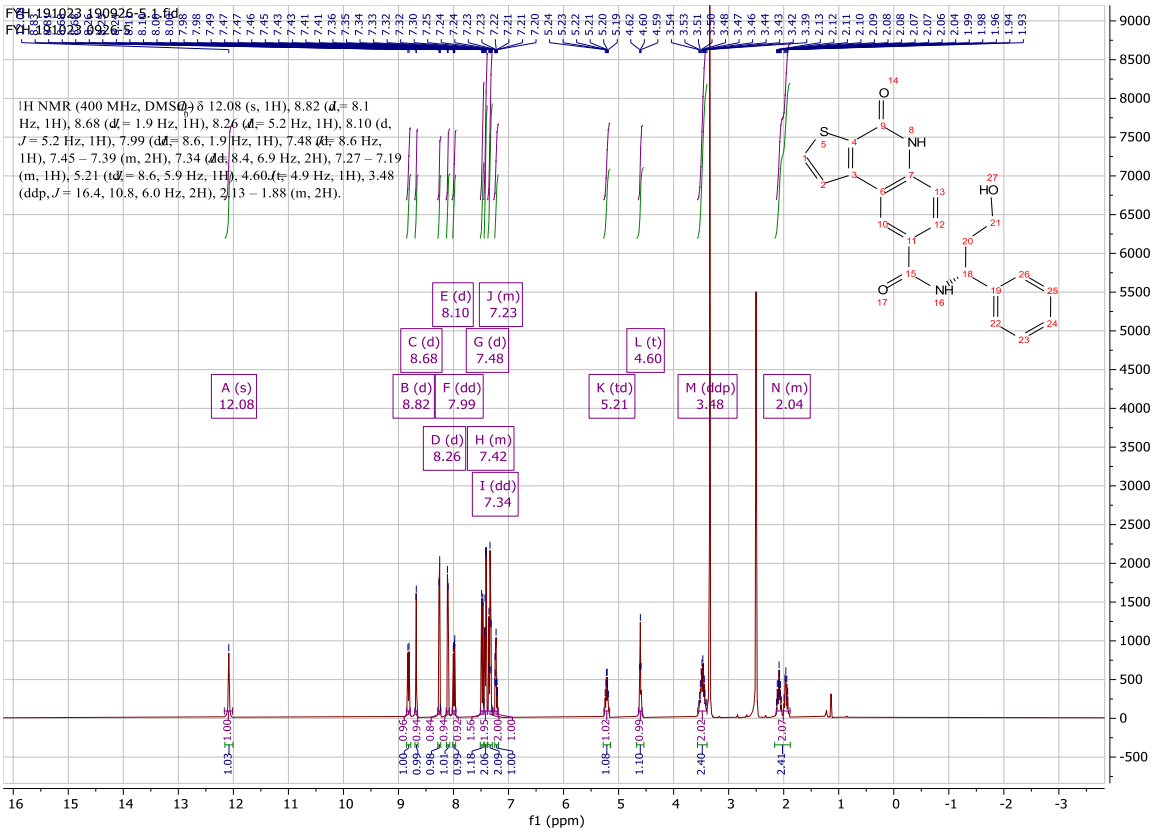
FYH 191023 190926-5 1.fid
FYH 191023 190926-5
1H NMR (400 MHz, DMSO-d6) δ 12.08 (s, 1H), 8.82 (d, J = 8.1 Hz, 1H), 8.68 (d, J = 1.9 Hz, 1H), 8.26 (d, J = 5.2 Hz, 1H), 8.10 (d, J = 5.2 Hz, 1H), 7.99 (dd, J = 8.6, 1.9 Hz, 1H), 7.48 (d, J = 8.6 Hz, 1H), 7.45 – 7.39 (m, 2H), 7.34 (dd, J = 8.4, 6.9 Hz, 2H), 7.27 – 7.19 (m, 1H), 5.21 (td, J = 8.6, 5.9 Hz, 1H), 4.60 (t, J = 4.9 Hz, 1H), 3.48 (ddp, J = 16.4, 10.8, 6.0 Hz, 2H), 2.13 – 1.88 (m, 2H).
A (s) 12.08
B (d) 8.82
C (d) 8.68
D (d) 8.26
E (d) 8.10
F (dd) 7.99
G (d) 7.48
H (m) 7.42
I (dd) 7.34
J (m) 7.23
K (td) 5.21
L (t) 4.60
M (ddp) 3.48
N (m) 2.04
f1 (ppm)

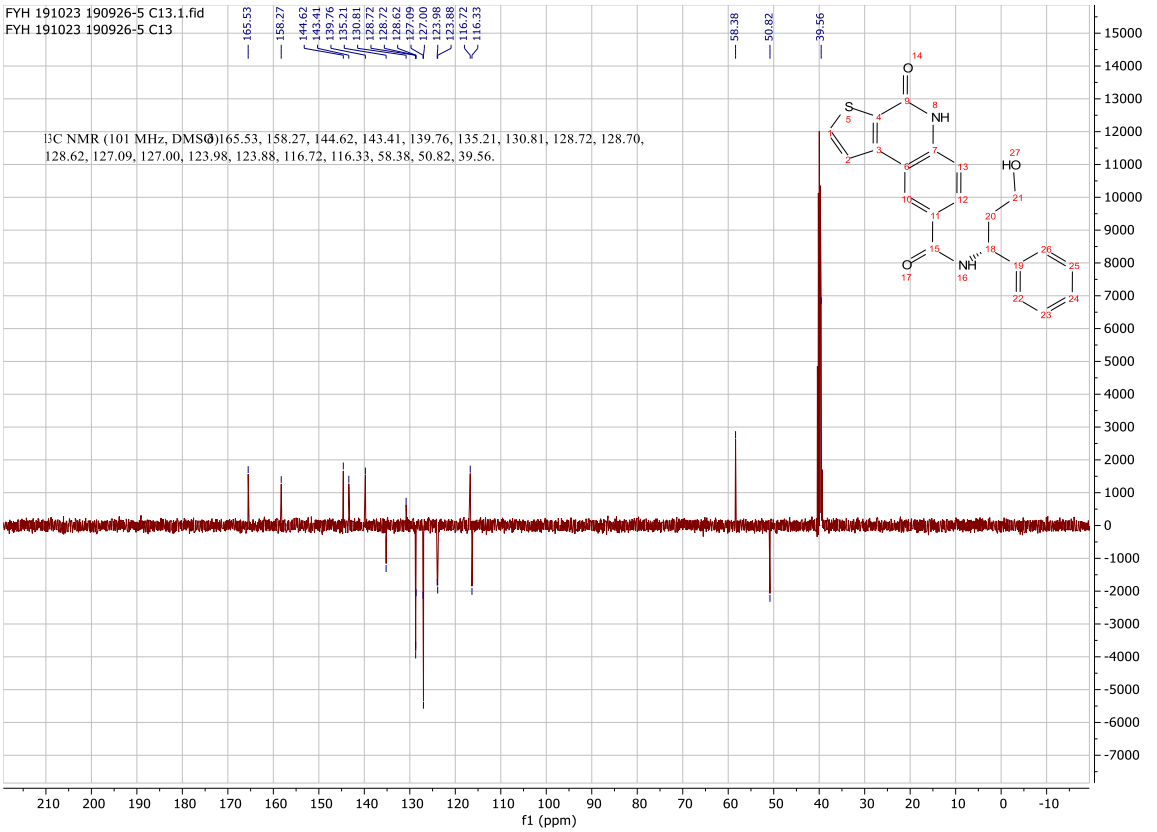
FYH 191023 190926-5 C13.1.fid
FYH 191023 190926-5 C13
13C NMR (101 MHz, DMSO-d6) 165.53, 158.27, 144.62, 143.41, 139.76, 135.21, 130.81, 128.72, 128.70, 128.62, 127.09, 127.00, 123.98, 123.88, 116.72, 116.33, 58.38, 50.82, 39.56.
f1 (ppm)

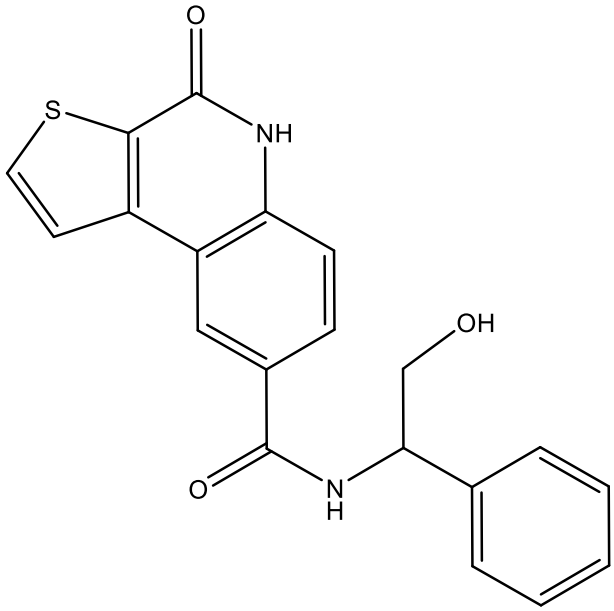

***N*-(2-hydroxy-1-phenylethyl)-4-oxo-4,5-dihydrothieno[2,3-*c*]quinoline-8-carboxamide (c22)**

Using **Synthesis Method d**, 24.5mg (0.1mmol) **c36** was reacted with 13.7mg (0.1mmol) 2-amino-2-phenylethan-1-ol to give 28.4mg **c22** (Yield: 78%) and the product was separated as white solid. ^{1}H NMR (400 MHz, DMSO-d_6) δ 12.07 (s, 1H), 8.78 – 8.70 (m, 2H), 8.27 (d, J = 5.2 Hz, 1H), 8.13 (d, J = 5.3 Hz, 1H), 8.03 (dd, J = 8.6, 1.9 Hz, 1H), 7.49 (d, J = 8.6 Hz, 1H), 7.47 – 7.42 (m, 2H), 7.38 – 7.31 (m, 2H), 7.28 – 7.20 (m, 1H), 5.20 – 5.10 (m, 1H), 4.99 (s, 1H), 3.83 – 3.67 (m, 2H). ^{13}C NMR (101 MHz, DMSO) δ 165.9, 158.3, 143.5, 141.8, 139.8, 135.2, 131.0, 128.8, 128.7, 128.6, 127.5, 127.3, 124.0, 124.0, 116.7, 116.3, 65.0, 56.5. HRMS m/z (ESI+, M+Na): Calcd for C20H16N2O3S: 387.0779, (ESI+, M+Na) found: 387.0777

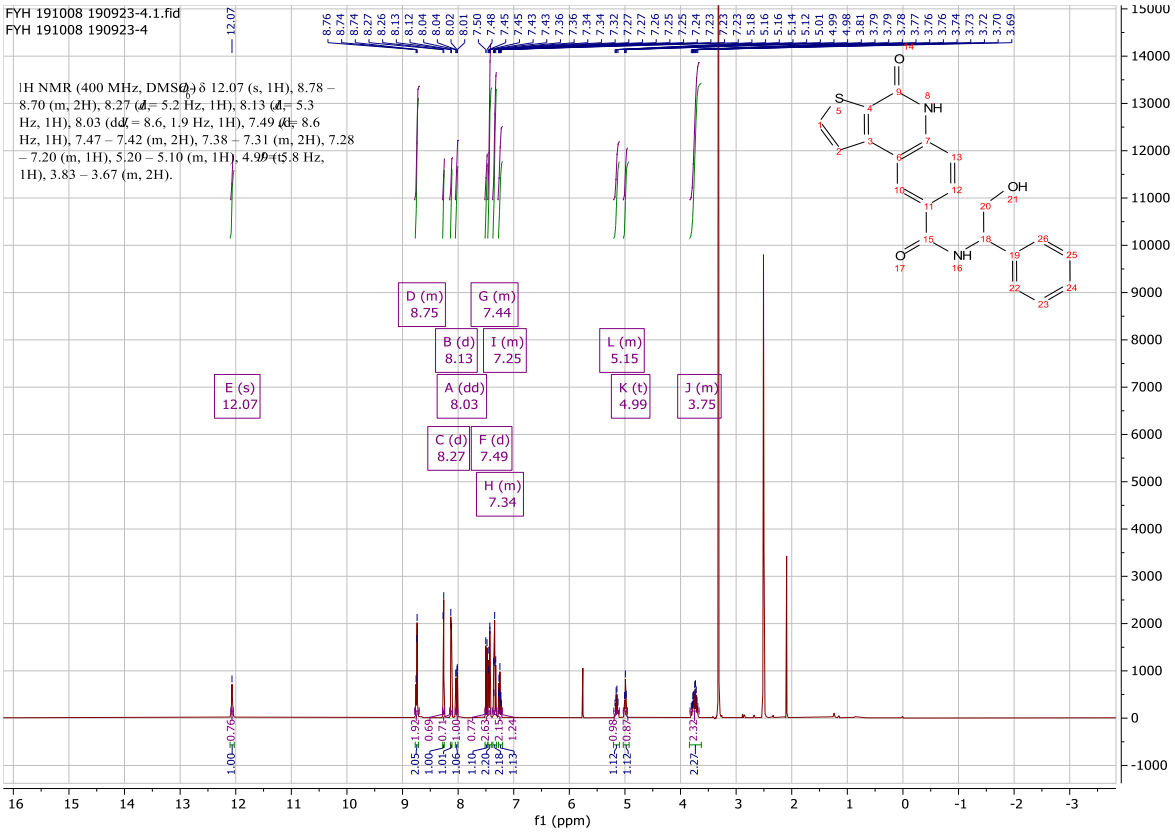
FYH 191008 190923-4.1.fid
FYH 191008 190923-4
1H NMR (400 MHz, DMSO) δ 12.07 (s, 1H), 8.78 – 8.70 (m, 2H), 8.27 (d, J = 5.2 Hz, 1H), 8.13 (d, J = 5.3 Hz, 1H), 8.03 (dd, J = 8.6, 1.9 Hz, 1H), 7.49 (d, J = 8.6 Hz, 1H), 7.47 – 7.42 (m, 2H), 7.38 – 7.31 (m, 2H), 7.28 – 7.20 (m, 1H), 5.20 – 5.10 (m, 1H), 4.99 (t, 5.8 Hz, 1H), 3.83 – 3.67 (m, 2H).
D (m) 8.75
G (m) 7.44
B (d) 8.13
I (m) 7.25
L (m) 5.15
E (s) 12.07
A (dd) 8.03
K (t) 4.99
J (m) 3.75
C (d) 8.27
F (d) 7.49
H (m) 7.34
f1 (ppm)

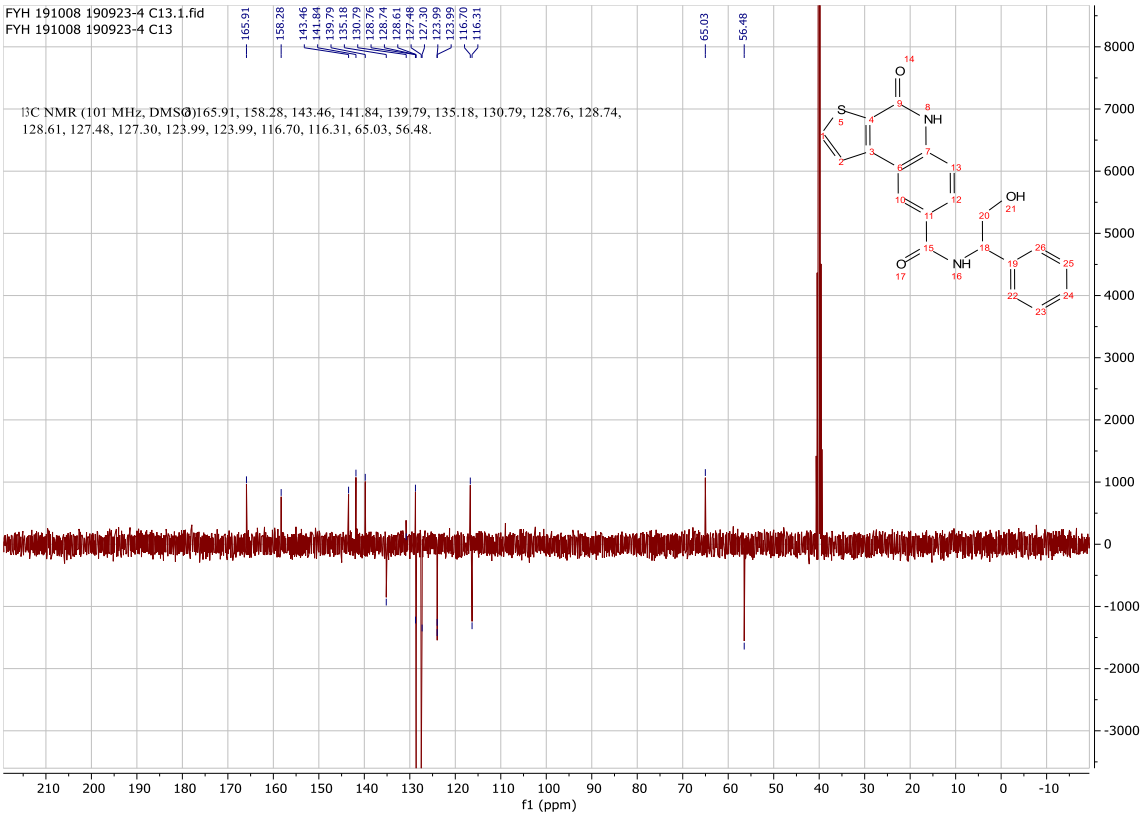
FYH 191008 190923-4 C13.1.fid
FYH 191008 190923-4 C13
13C NMR (101 MHz, DMSO) 165.91, 158.28, 143.46, 141.84, 139.79, 135.18, 130.79, 128.76, 128.74, 128.61, 127.48, 127.30, 123.99, 123.99, 116.70, 116.31, 65.03, 56.48.
f1 (ppm)

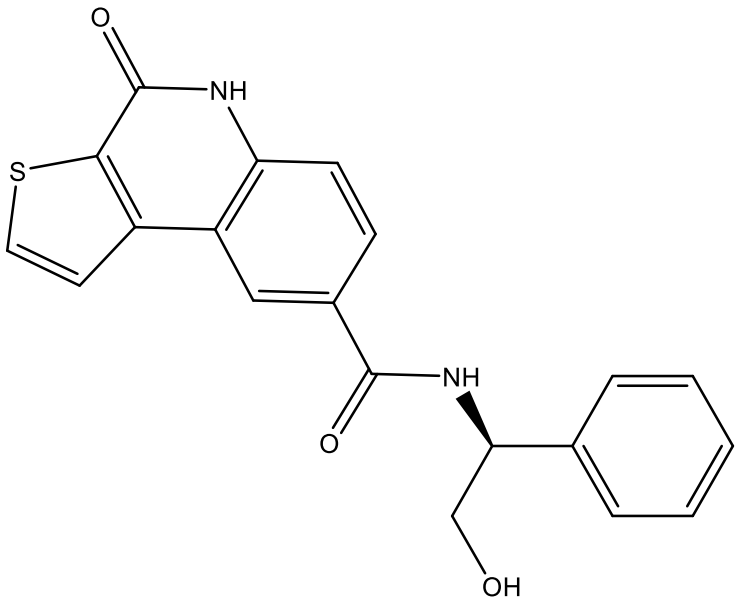

(*S*)-*N*-(2-hydroxy-1-phenylethyl)-4-oxo-4,5-dihydrothieno[2,3-*c*]quinoline-8-carboxamide (c23)

Using **Synthesis Method d**, 24.5mg (0.1mmol) **c36** was reacted with 13.7mg (0.1mmol) (*S*)-2-amino-2-phenylethan-1-ol to give 27.7mg **c23** (Yield: 76%) and the product was separated as white solid. ^{1}H NMR (400 MHz, DMSO-d_6) δ 12.10 (s, 1H), 8.81 – 8.72 (m, 2H), 8.27 (d, *J* = 5.2 Hz, 1H), 8.13 (d, *J* = 5.2 Hz, 1H), 8.03 (dd, *J* = 8.6, 1.8 Hz, 1H), 7.49 (d, *J* = 8.6 Hz, 1H), 7.44 (d, *J* = 7.6 Hz, 2H), 7.34 (t, *J* = 7.5 Hz, 2H), 7.25 (t, *J* = 7.3 Hz, 1H), 5.15 (dd, *J* = 48.0, 7.8 Hz, 1H), 5.02 (s, 1H), 3.72 (m, 2H). ^{13}C NMR (101 MHz, DMSO) δ 165.9, 158.3, 143.5, 141.8, 139.8, 135.2, 130.8, 128.8, 128.7, 128.6, 127.5, 127.3, 124.0, 124.0, 116.7, 116.3, 65.0, 56.5. HRMS m/z (ESI+, M+Na): Calcd for C20H16N2O3S: 387.0779, (ESI+, M+Na) found: 387.0776

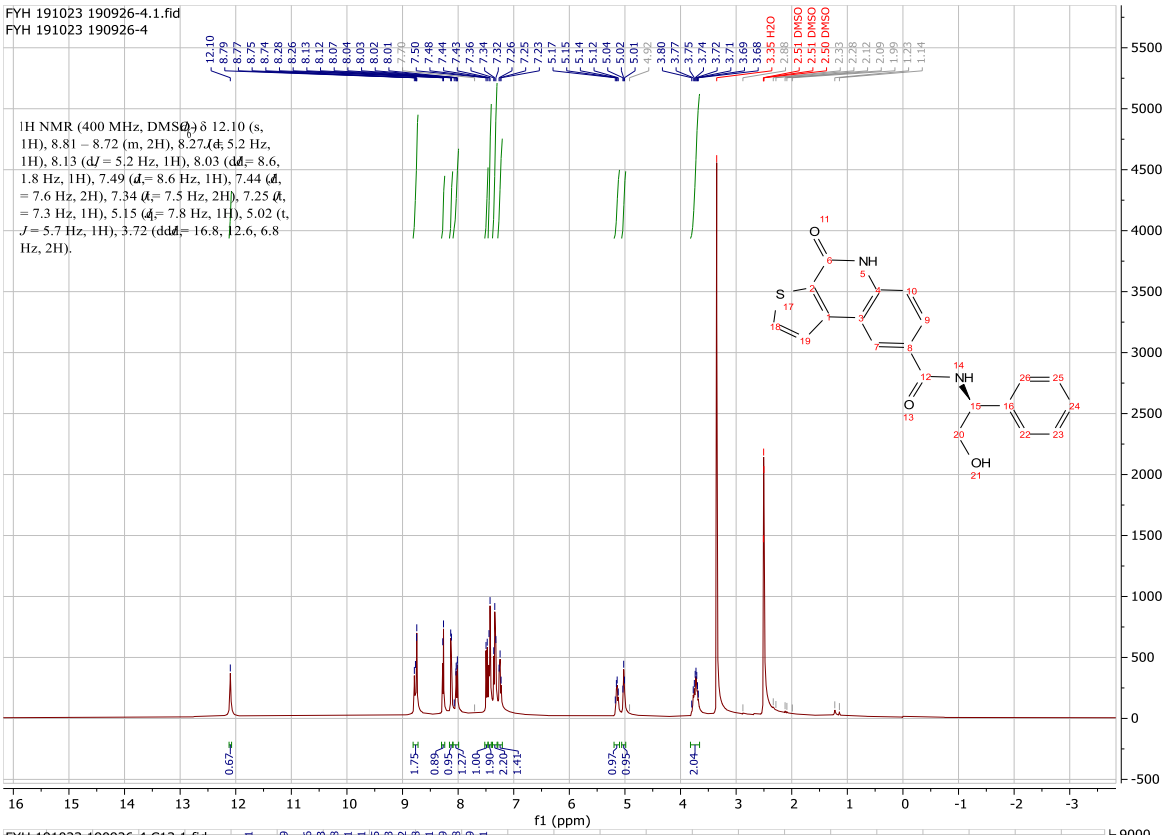
FYH 191023 190926-4.1.fid
FYH 191023 190926-4
1H NMR (400 MHz, DMSO-d6) δ 12.10 (s, 1H), 8.81 – 8.72 (m, 2H), 8.27 (d, J = 5.2 Hz, 1H), 8.13 (d, J = 5.2 Hz, 1H), 8.03 (dd, J = 8.6, 1.8 Hz, 1H), 7.49 (d, J = 8.6 Hz, 1H), 7.44 (d, J = 7.6 Hz, 2H), 7.34 (t, J = 7.5 Hz, 2H), 7.25 (t, J = 7.3 Hz, 1H), 5.15 (d, J = 7.8 Hz, 1H), 5.02 (t, J = 5.7 Hz, 1H), 3.72 (ddd, J = 16.8, 12.6, 6.8 Hz, 2H).
f1 (ppm)

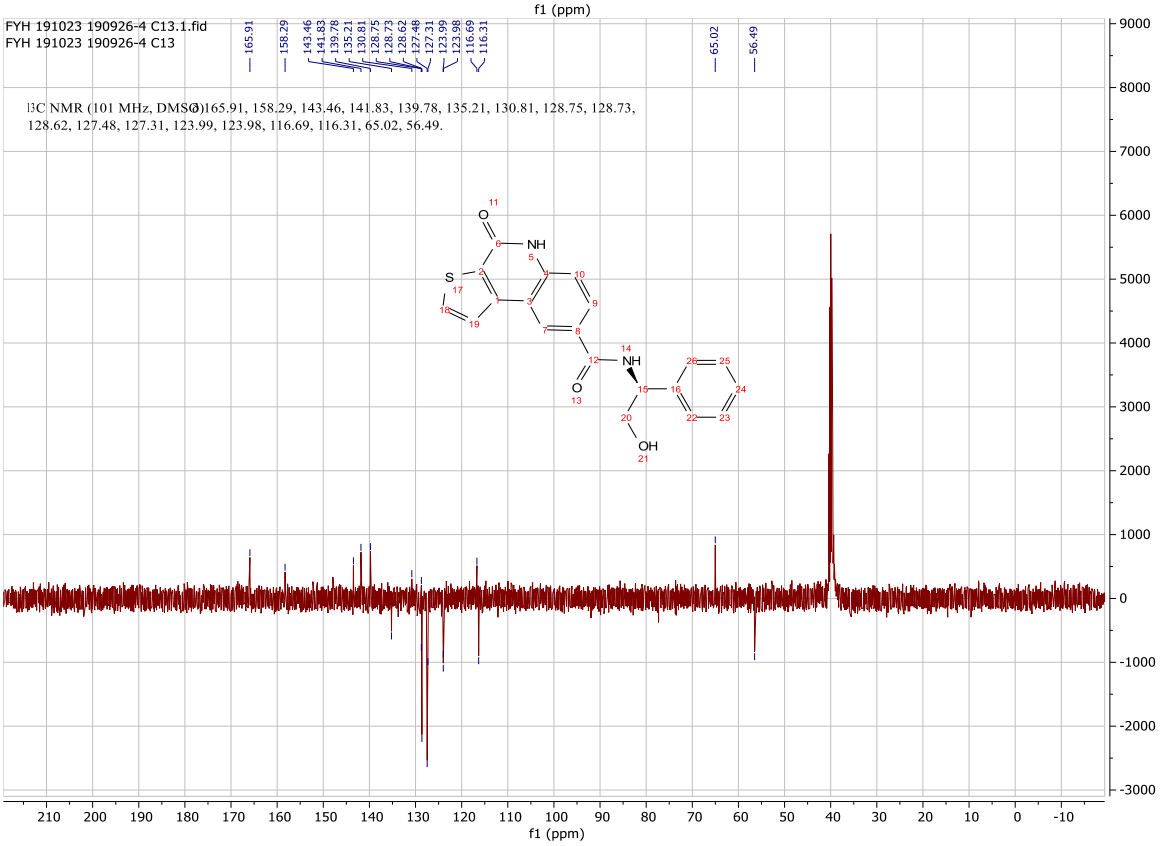
FYH 191023 190926-4 C13.1.fid
FYH 191023 190926-4 C13
13C NMR (101 MHz, DMSO-d6) δ 165.91, 158.29, 143.46, 141.83, 139.78, 135.21, 130.81, 128.75, 128.73, 128.62, 127.48, 127.31, 123.99, 123.98, 116.69, 116.31, 65.02, 56.49.
f1 (ppm)

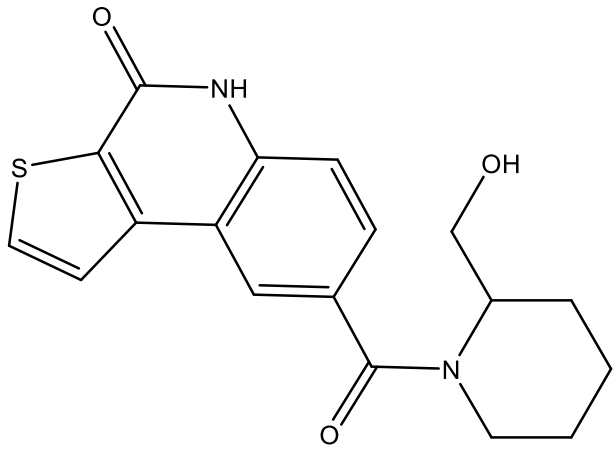

8-(2-(hydroxymethyl)piperidine-1-carbonyl)thieno[2,3-*c*]quinolin-4(5H)-one (c24)

Using **Synthesis Method d**, 24.5mg (0.1mmol) **c36** was reacted with 11.5mg (0.1mmol) piperidin-2-ylmethanol to give 22.7mg **c24** (Yield: 67%) and the product was separated as white solid. ^{1}H NMR (400 MHz, DMSO-d_6) δ 12.02 (s, 1H), 8.21 (d, J = 5.2 Hz, 2H), 8.12 (d, J = 4.6 Hz, 1H), 7.52 (d, J = 8.4 Hz, 1H), 7.46 (d, J = 8.4 Hz, 1H), 4.82 (s, 1H), 4.30 – 2.88 (m, 5H), 1.89 – 1.29 (m, 6H). ^{13}C NMR (101 MHz, DMSO) δ 170.5, 158.2, 143.3, 138.2, 135.0, 131.3, 130.9, 128.2, 124.2, 123.4, 116.9, 116.4, 59.1, 54.9 (C23), 43.9-37.7(C18), 25.7, 19.5. HRMS m/z (ESI+, M+Na): Calcd for C18H18N2O3S: 365.0936, (ESI+, M+Na) found: 365.0931

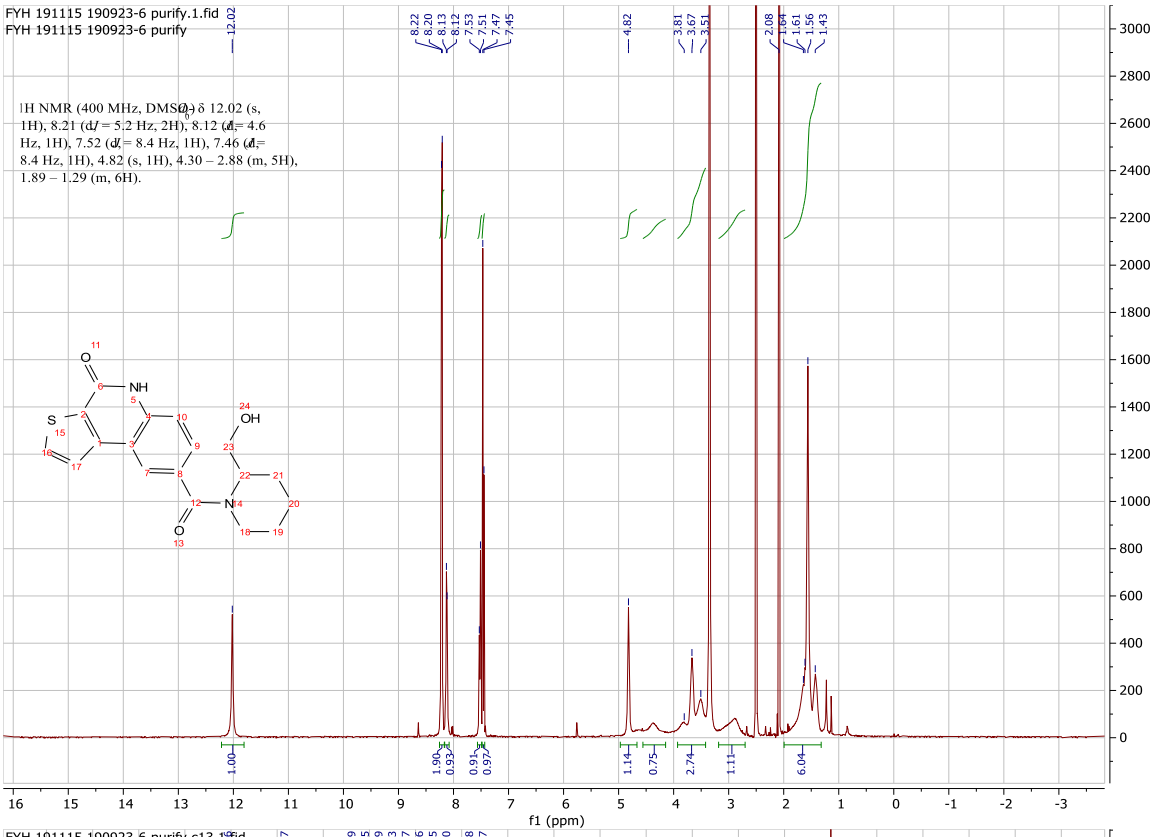
FYH 191115 190923-6 purify.1.fid
FYH 191115 190923-6 purify
1H NMR (400 MHz, DMSO-d6) δ 12.02 (s, 1H), 8.21 (d, J = 5.2 Hz, 2H), 8.12 (d, J = 4.6 Hz, 1H), 7.52 (d, J = 8.4 Hz, 1H), 7.46 (d, J = 8.4 Hz, 1H), 4.82 (s, 1H), 4.30 – 2.88 (m, 5H), 1.89 – 1.29 (m, 6H).
f1 (ppm)

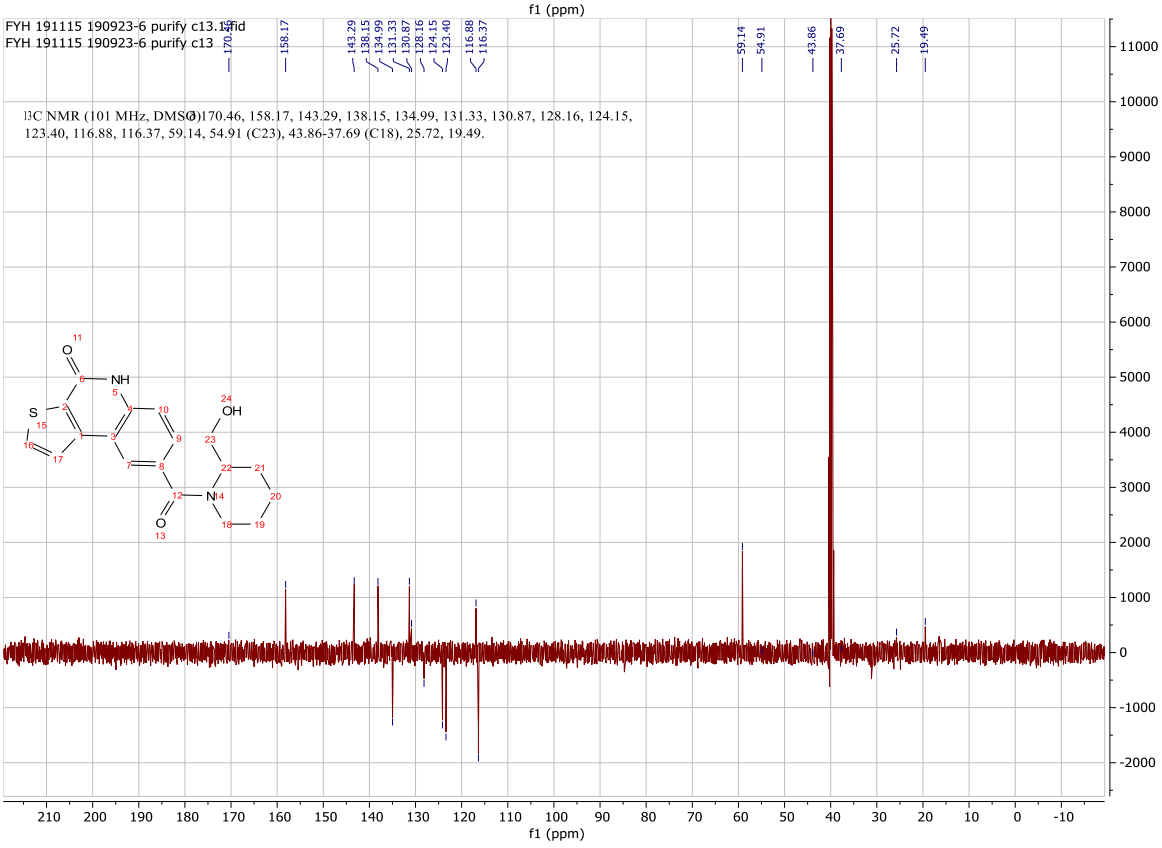
FYH 191115 190923-6 purify c13.1.fid
FYH 191115 190923-6 purify c13
13C NMR (101 MHz, DMSO) 170.46, 158.17, 143.29, 138.15, 134.99, 131.33, 130.87, 128.16, 124.15, 123.40, 116.88, 116.37, 59.14, 54.91 (C23), 43.86-37.69 (C18), 25.72, 19.49.
f1 (ppm)

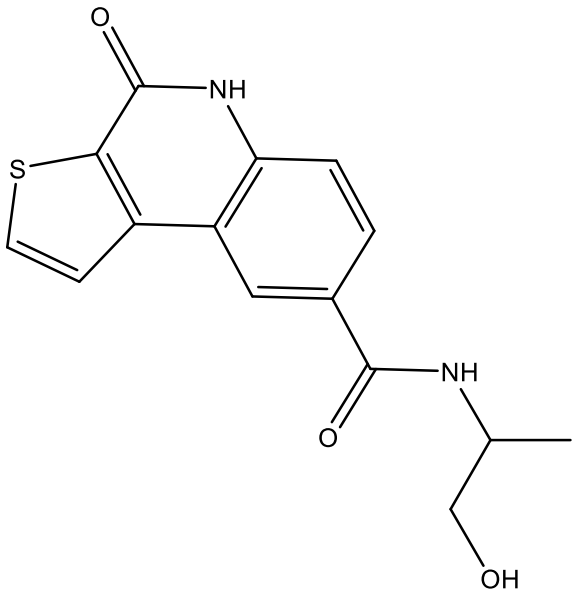

***N*-(1-hydroxypropan-2-yl)-4-oxo-4,5-dihydrothieno[2,3-*c*]quinoline-8-carboxamide (c25)**

Using **Synthesis Method d**, 24.5mg (0.1mmol) **c36** was reacted with 7.5mg (0.1mmol) 2-aminopropan-1-ol to give 22mg **c25** (Yield: 73%) and the product was separated as white solid. ^{1}H NMR (400 MHz, DMSO-d_6) δ 12.09 (s, 1H), 8.68 (d, *J* = 1.9 Hz, 1H), 8.26 (d, *J* = 5.2 Hz, 1H), 8.18 (d, *J* = 7.9 Hz, 1H), 8.11 (d, *J* = 5.2 Hz, 1H), 7.99 (dd, *J* = 8.6, 1.9 Hz, 1H), 7.47 (d, *J* = 8.6 Hz, 1H), 4.79 (s, 1H), 4.08 (m, 1H), 3.51 (ddd, *J* = 11.1, 5.4 Hz, 1H), 3.40 (ddd, *J* = 10.7, 5.4 Hz, 1H), 1.19 (d, *J* = 6.7 Hz, 3H).^{13}C NMR (101 MHz, DMSO) δ 165.5, 158.3, 143.5, 139.7, 135.2, 130.8, 128.9, 128.7, 124.0, 123.8, 116.7, 116.3, 64.9, 47.8, 17.7. HRMS m/z (ESI+, M+Na): Calcd for C15H14N2O3S: 325.0623, (ESI+, M+Na) found: 325.0615

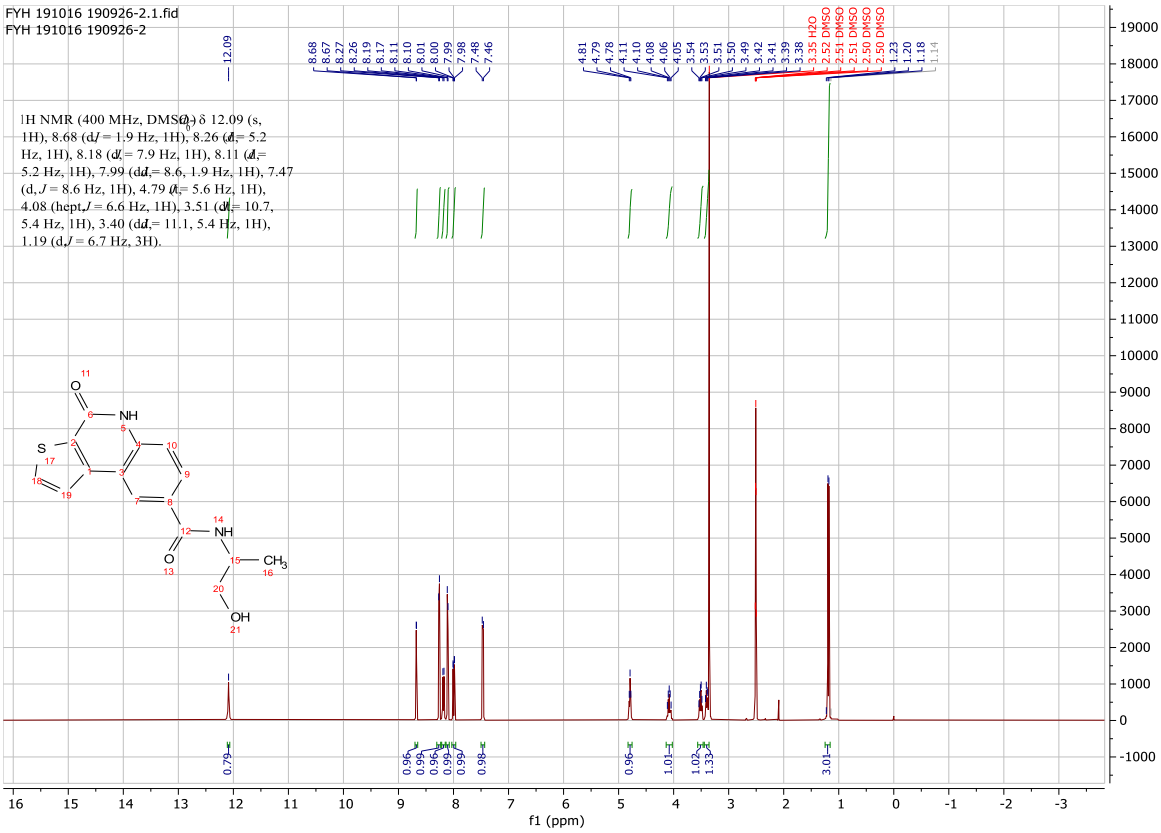
FYH 191016 190926-2.1.fid
FYH 191016 190926-2
1H NMR (400 MHz, DMSO-d6) δ 12.09 (s, 1H), 8.68 (d, J = 1.9 Hz, 1H), 8.26 (d, J = 5.2 Hz, 1H), 8.18 (d, J = 7.9 Hz, 1H), 8.11 (d, J = 5.2 Hz, 1H), 7.99 (dd, J = 8.6, 1.9 Hz, 1H), 7.47 (d, J = 8.6 Hz, 1H), 4.79 (d, J = 5.6 Hz, 1H), 4.08 (hept, J = 6.6 Hz, 1H), 3.51 (dd, J = 10.7, 5.4 Hz, 1H), 3.40 (dd, J = 11.1, 5.4 Hz, 1H), 1.19 (d, J = 6.7 Hz, 3H).
f1 (ppm)

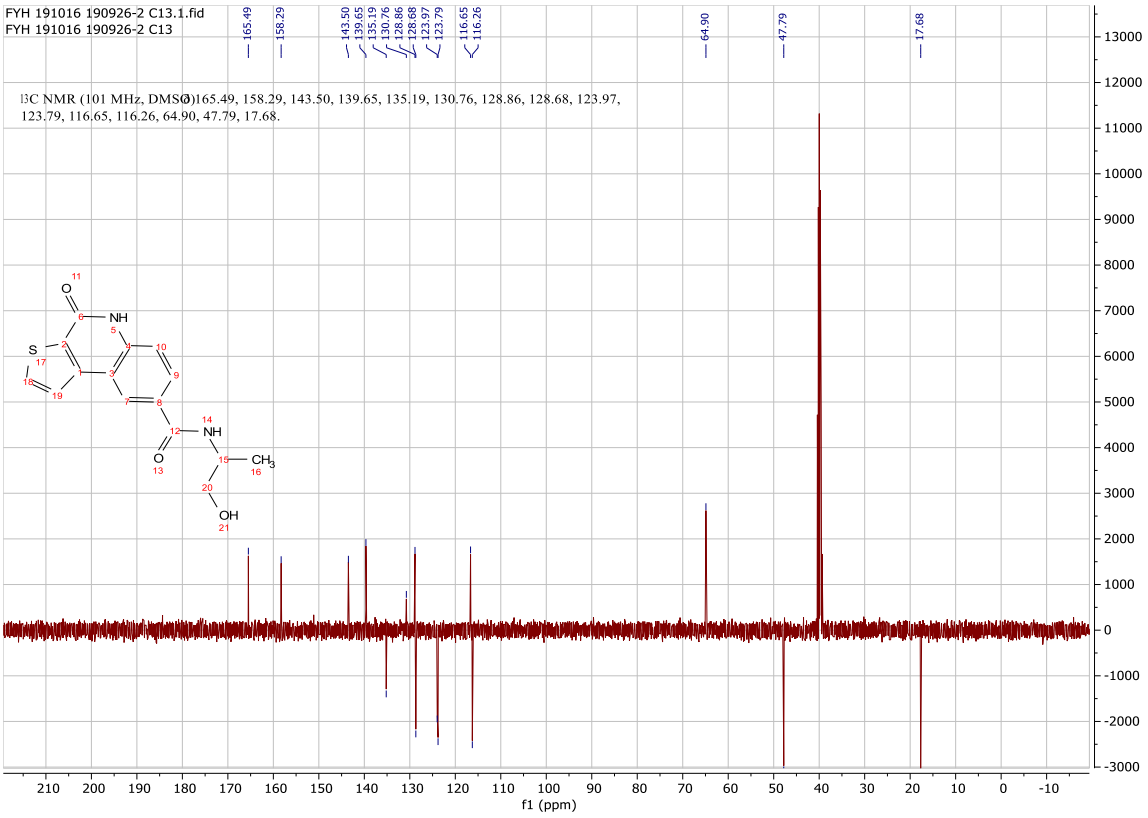
FYH 191016 190926-2 C13.1.fid
FYH 191016 190926-2 C13
13C NMR (101 MHz, DMSO-d6) δ 165.49, 158.29, 143.50, 139.65, 135.19, 130.76, 128.86, 128.68, 123.97, 123.79, 116.65, 116.26, 64.90, 47.79, 17.68.
f1 (ppm)

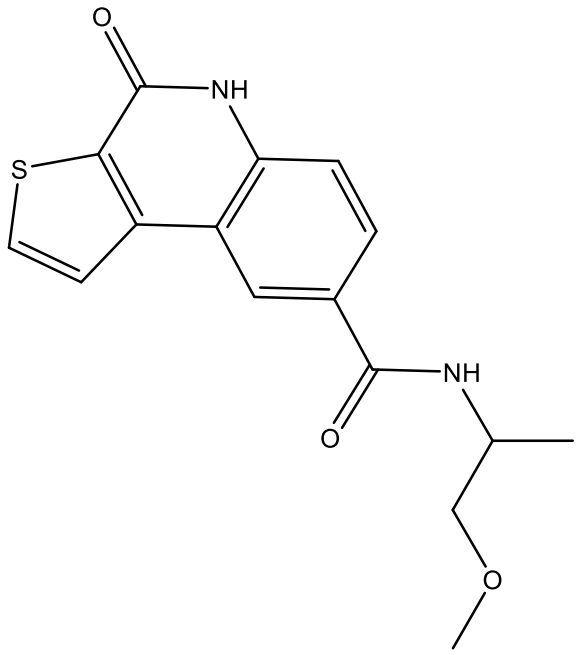

***N*-(1-methoxypropan-2-yl)-4-oxo-4,5-dihydrothieno[2,3-*c*]quinoline-8-carboxamide (c26)**

Using **Synthesis Method d**, 24.5mg (0.1mmol) **c36** was reacted with 8.9mg (0.1mmol) 1-methoxypropan-2-amine to give 24.6mg **c26** (Yield: 78%) and the product was separated as white solid. ^{1}H NMR (400 MHz, DMSO-d_6) δ 12.09 (s, 1H), 8.69 – 8.64 (m, 1H), 8.28 (dd, J = 12.7, 6.6 Hz, 2H), 8.10 (d, J = 5.2 Hz, 1H), 7.99 (dd, J = 8.6, 1.4 Hz, 1H), 7.47 (d, J = 8.6 Hz, 1H), 4.26 (m, 1H), 3.47 (m, 1H), 3.45 (m, 1H), 3.29 (s, 3H), 1.20 (d, J = 6.8 Hz, 3H). ^{13}C NMR (101 MHz, DMSO) δ 165.4, 158.3, 143.5, 139.7, 135.2, 130.8, 128.7, 128.6, 124.0, 123.8, 116.7, 116.3, 75.6, 58.6, 45.0, 17.9. HRMS m/z (ESI+, M+Na): Calcd for C16H16N2O3S: 339.0779, (ESI+, M+Na) found: 339.0773

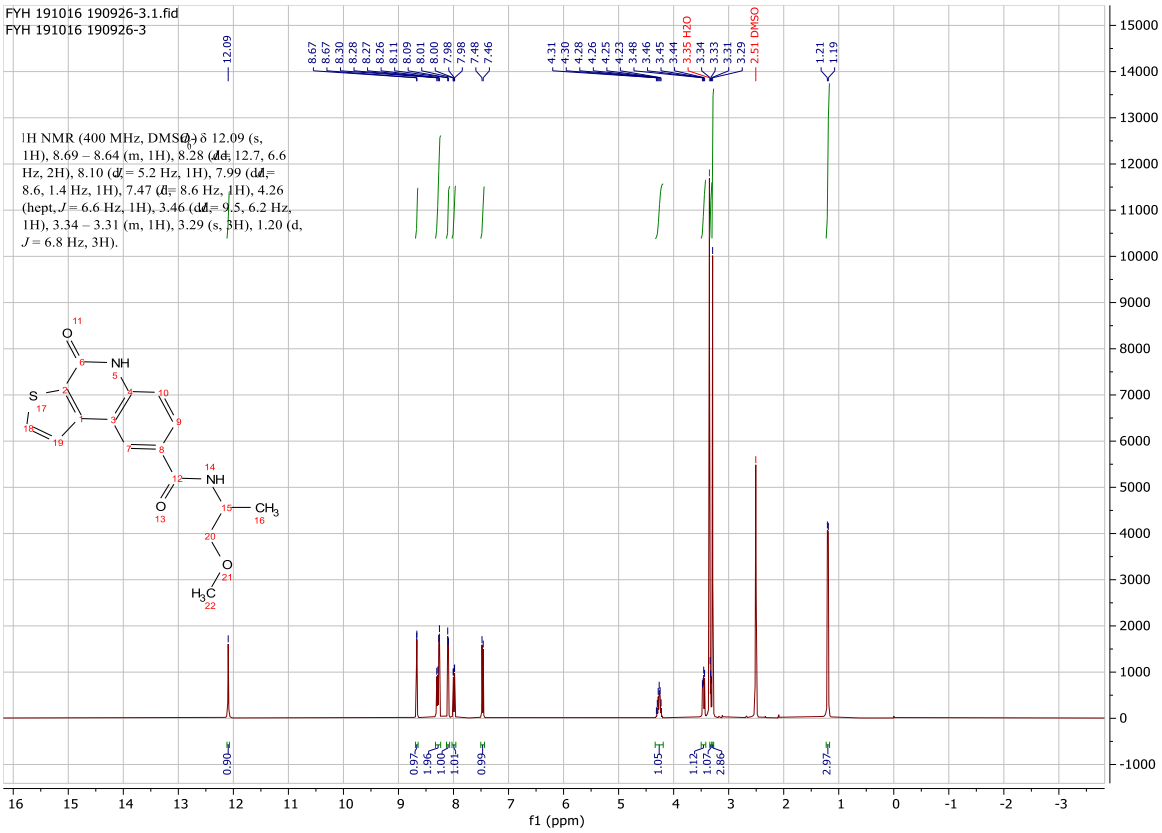
FYH 191016 190926-3.1.fid
FYH 191016 190926-3
1H NMR (400 MHz, DMSO-d6) δ 12.09 (s, 1H), 8.69 – 8.64 (m, 1H), 8.28 (dd, J = 12.7, 6.6 Hz, 2H), 8.10 (d, J = 5.2 Hz, 1H), 7.99 (dd, J = 8.6, 1.4 Hz, 1H), 7.47 (d, J = 8.6 Hz, 1H), 4.26 (hept, J = 6.6 Hz, 1H), 3.46 (dd, J = 9.5, 6.2 Hz, 1H), 3.34 – 3.31 (m, 1H), 3.29 (s, 3H), 1.20 (d, J = 6.8 Hz, 3H).
f1 (ppm)

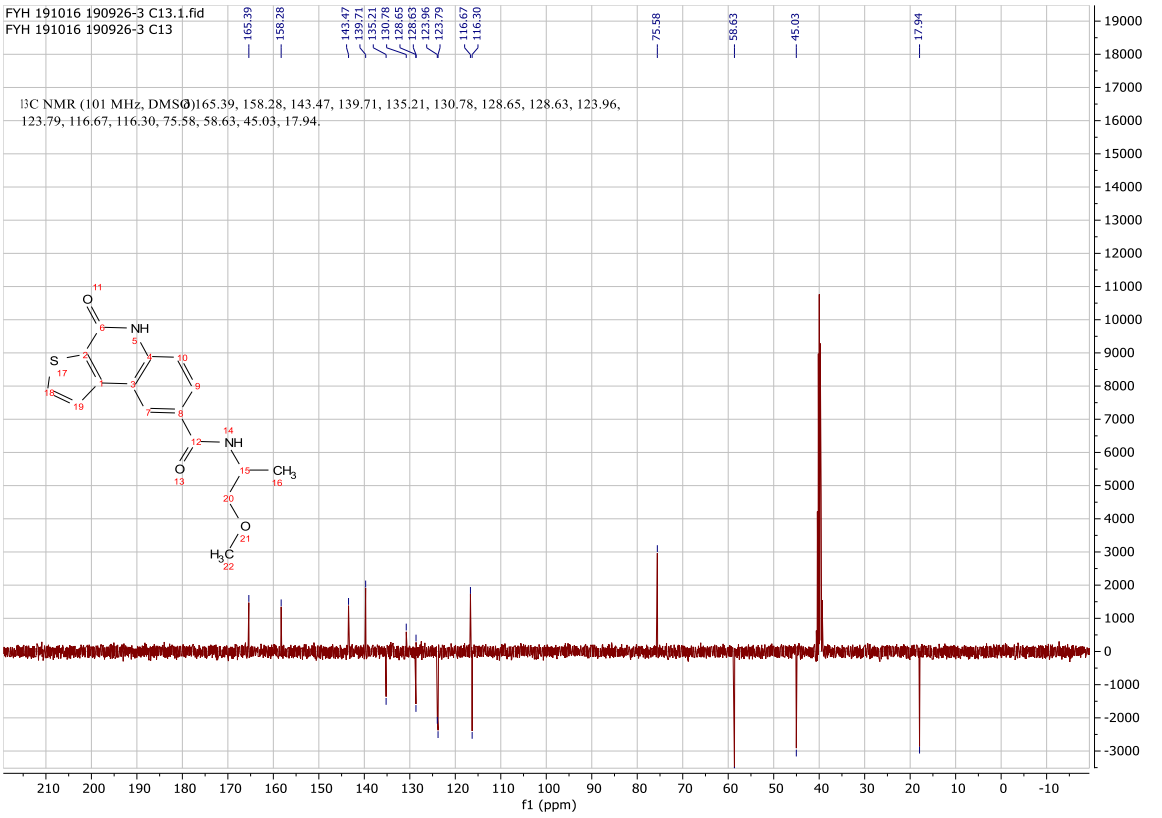
FYH 191016 190926-3 C13.1.fid
FYH 191016 190926-3 C13
13C NMR (101 MHz, DMSO-d6) 165.39, 158.28, 143.47, 139.71, 135.21, 130.78, 128.65, 128.63, 123.96, 123.79, 116.67, 116.30, 75.58, 58.63, 45.03, 17.94.
f1 (ppm)

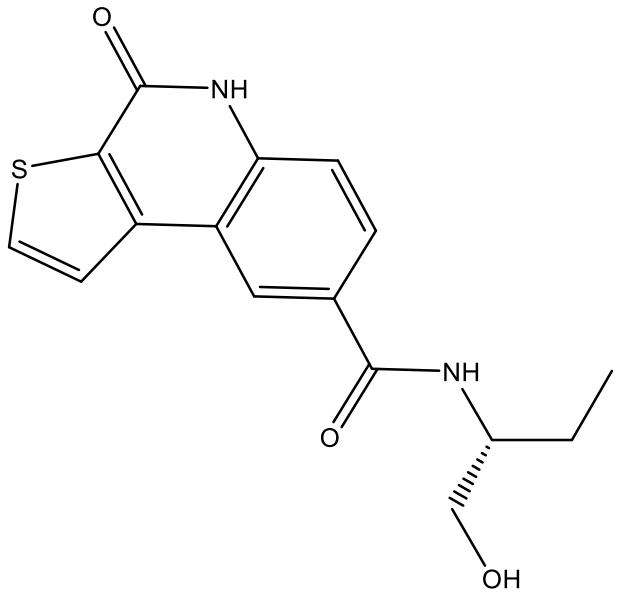

(*R*)-N-(1-hydroxybutan-2-yl)-4-oxo-4,5-dihydrothieno[2,3-*c*]quinoline-8-carboxamide (c27)

Using **Synthesis Method d**, 24.5mg (0.1mmol) **c36** was reacted with 8.9mg (0.1mmol) (*R*)-2-aminobutan-1-ol to give 24.3mg **c27** (Yield: 77%) and the product was separated as white solid. ^{1}H NMR (400 MHz, DMSO-d_6) δ 12.05 (s, 1H), 8.68 (d, *J* = 1.7 Hz, 1H), 8.25 (d, *J* = 5.2 Hz, 1H), 8.11 (d, *J* = 5.2 Hz, 1H), 8.07 (d, *J* = 8.4 Hz, 1H), 8.01 (dd, *J* = 8.6, 1.9 Hz, 1H), 7.48 (d, *J* = 8.6 Hz, 1H), 4.71 (s, 1H), 3.93 (ddt, *J* = 10.9, 5.6, 5.6 Hz, 1H), 3.49 (m, 5.7 Hz, 2H), 1.62 (m, 1H), 0.92 (t, *J* = 7.4 Hz, 3H).^{13}C NMR (101 MHz, DMSO) δ 165.9, 158.3, 143.5, 139.7, 135.1, 130.8, 129.0, 129.0, 124.0, 123.8, 116.7, 116.3, 63.6, 53.6, 24.2, 11.2. HRMS m/z (ESI+, M+Na): Calcd for C16H16N2O3S: 339.0779, (ESI+, M+Na) found: 339.0774

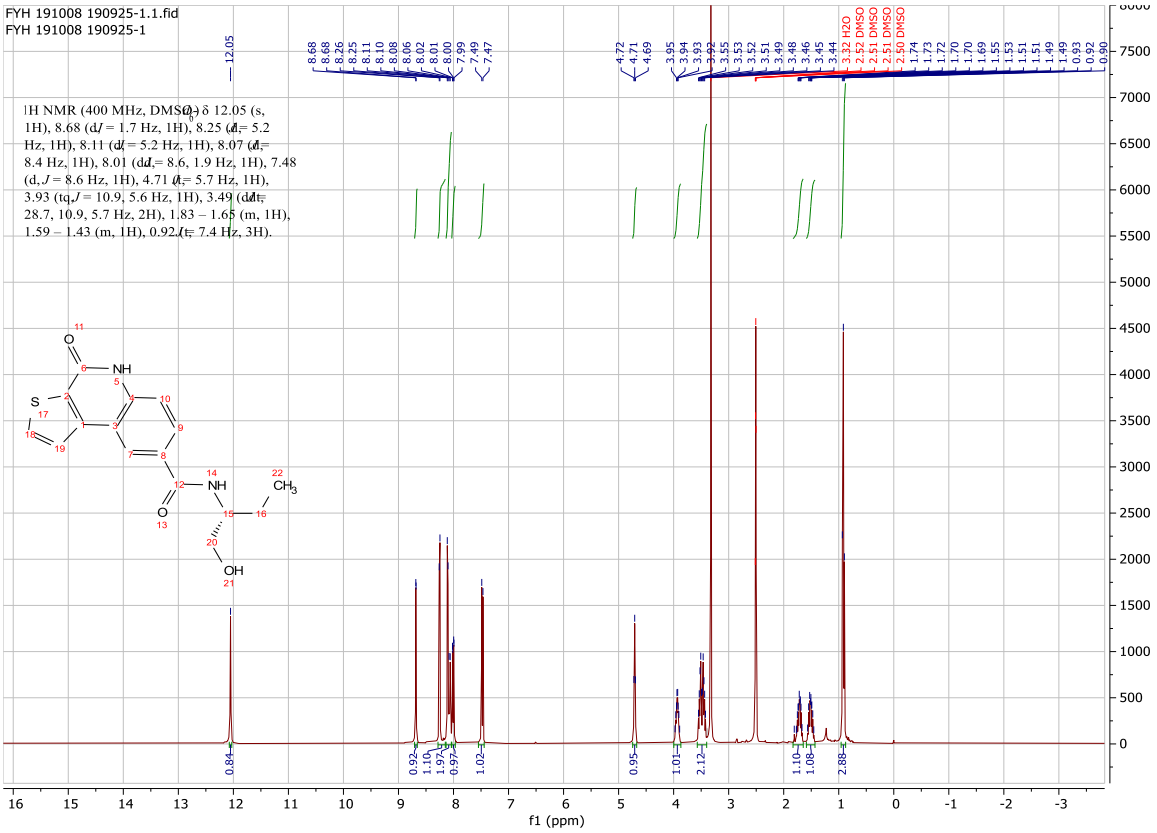
FYH 191008 190925-1.1.fid
FYH 191008 190925-1
1H NMR (400 MHz, DMSO-d6) δ 12.05 (s, 1H), 8.68 (d, J = 1.7 Hz, 1H), 8.25 (d, J = 5.2 Hz, 1H), 8.11 (d, J = 5.2 Hz, 1H), 8.07 (d, J = 8.4 Hz, 1H), 8.01 (dd, J = 8.6, 1.9 Hz, 1H), 7.48 (d, J = 8.6 Hz, 1H), 4.71 (d, J = 5.7 Hz, 1H), 3.93 (tq, J = 10.9, 5.6 Hz, 1H), 3.49 (ddt, J = 28.7, 10.9, 5.7 Hz, 2H), 1.83 – 1.65 (m, 1H), 1.59 – 1.43 (m, 1H), 0.92 (t, J = 7.4 Hz, 3H).
f1 (ppm)

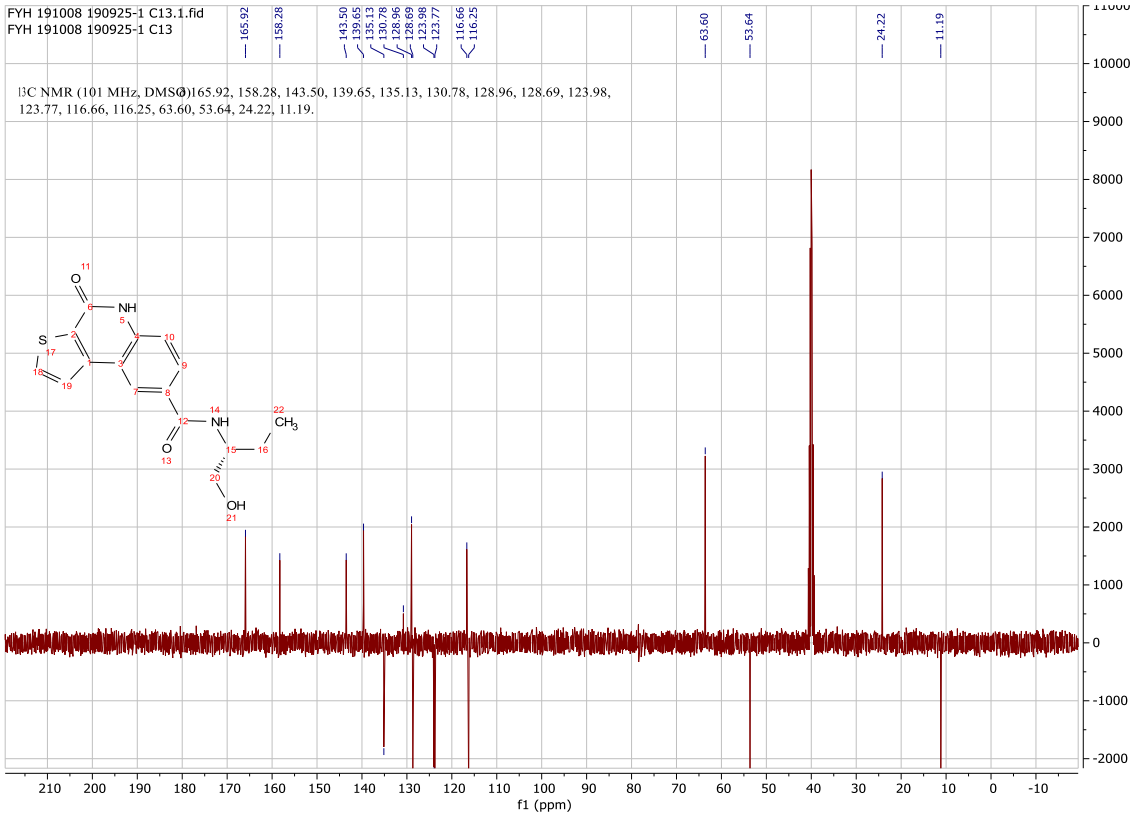
FYH 191008 190925-1 C13.1.fid
FYH 191008 190925-1 C13
13C NMR (101 MHz, DMSO-d6) 165.92, 158.28, 143.50, 139.65, 135.13, 130.78, 128.96, 128.69, 123.98, 123.77, 116.66, 116.25, 63.60, 53.64, 24.22, 11.19.
f1 (ppm)

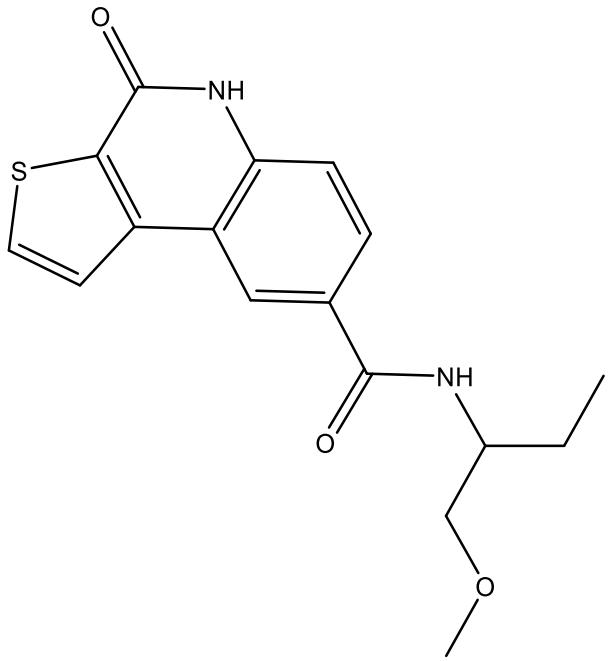

***N*-(1-methoxybutan-2-yl)-4-oxo-4,5-dihydrothieno[2,3-*c*]quinoline-8-carboxamide (c28)**

Using **Synthesis Method d**, 24.5mg (0.1mmol) **c36** was reacted 10.4mg (0.1mmol) 1-methoxybutan-2-amine to give 27.1mg **c28** (Yield: 82%) and the product was separated as white solid. ^{1}H NMR (400 MHz, DMSO-d_6) δ 12.09 (s, 1H), 8.68 (d, J = 1.8 Hz, 1H), 8.26 (d, J = 5.2 Hz, 1H), 8.21 (d, J = 8.4 Hz, 1H), 8.10 (d, J = 5.2 Hz, 1H), 8.00 (dd, J = 8.6, 1.9 Hz, 1H), 7.48 (d, J = 8.6 Hz, 1H), 4.11 (m, 1H), 3.46 − 3.35 (m, 2H), 3.28 (s, 3H), 1.74 – 1.45 (m, 2H), 0.91 (t, J = 7.4 Hz, 3H). ^{13}C NMR (101 MHz, DMSO) δ 165.8, 158.3, 143.5, 139.7, 135.2, 130.8, 128.7, 128.7, 124.0, 123.8, 116.7, 116.3, 74.5, 58.7, 50.8, 24.6, 11.1. HRMS m/z (ESI+, M+Na): Calcd for C17H18N2O3S: 353.0923, (ESI+, M+Na) found: 353.0929

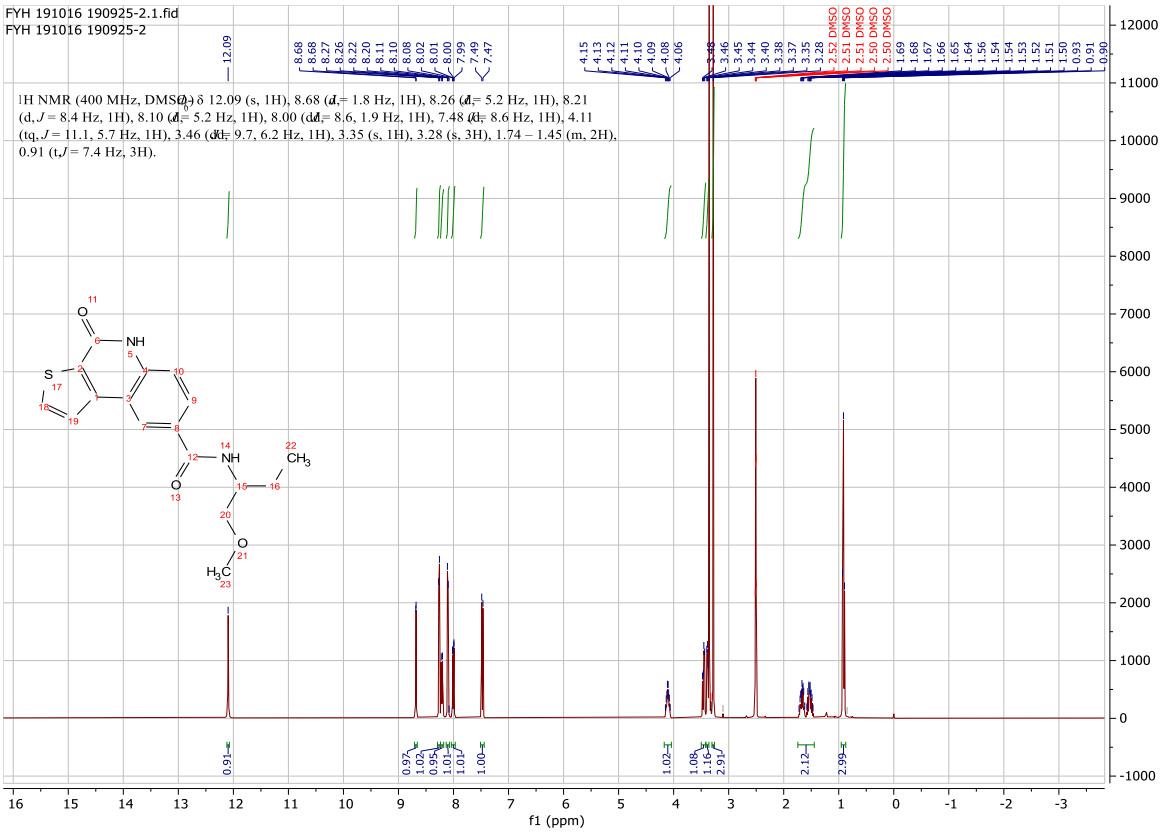
FYH 191016 190925-2.1.fid
FYH 191016 190925-2
1H NMR (400 MHz, DMSO-d6) δ 12.09 (s, 1H), 8.68 (d, J = 1.8 Hz, 1H), 8.26 (d, J = 5.2 Hz, 1H), 8.21 (d, J = 8.4 Hz, 1H), 8.10 (d, J = 5.2 Hz, 1H), 8.00 (dd, J = 8.6, 1.9 Hz, 1H), 7.48 (d, J = 8.6 Hz, 1H), 4.11 (tq, J = 11.1, 5.7 Hz, 1H), 3.46 (dt, J = 9.7, 6.2 Hz, 1H), 3.35 (s, 1H), 3.28 (s, 3H), 1.74 – 1.45 (m, 2H), 0.91 (t, J = 7.4 Hz, 3H).
f1 (ppm)

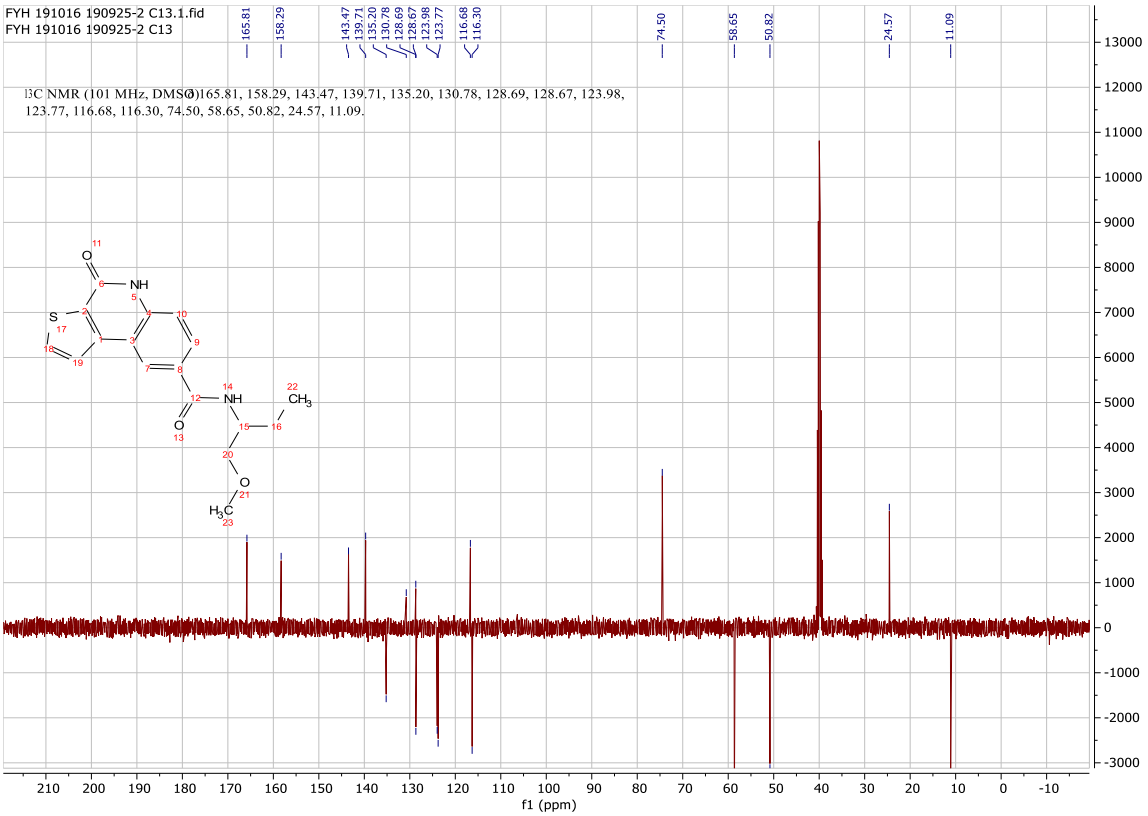
FYH 191016 190925-2 C13.1.fid
FYH 191016 190925-2 C13
13C NMR (101 MHz, DMSO-d6) 165.81, 158.29, 143.47, 139.71, 135.20, 130.78, 128.69, 128.67, 123.98, 123.77, 116.68, 116.30, 74.50, 58.65, 50.82, 24.57, 11.09.
f1 (ppm)

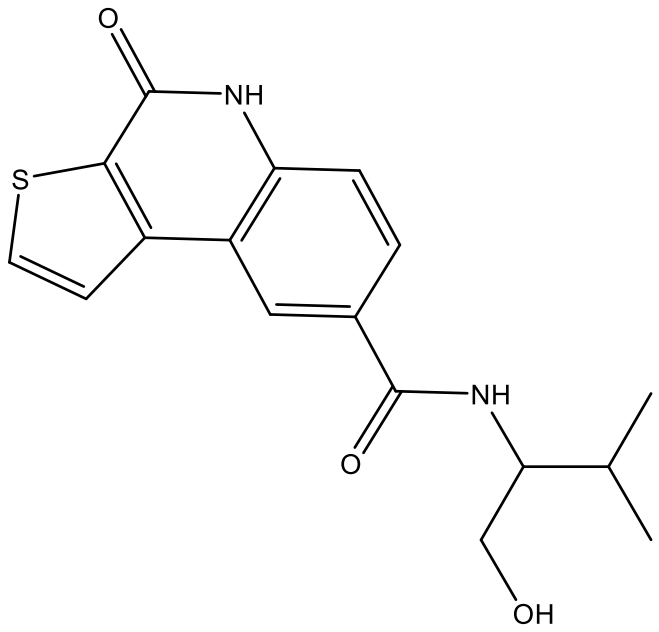

***N*-(1-hydroxy-3-methylbutan-2-yl)-4-oxo-4,5-dihydrothieno[2,3-*c*]quinoline-8-carboxamide (c29)**

Using **Synthesis Method d**, 24.5mg (0.1mmol) **c36** was reacted 10.3mg (0.1mmol) 2-amino-3-methylbutan-1-ol to give 23.4mg **c29** (Yield: 71%) and the product was separated as white solid. ^{1}H NMR (400 MHz, DMSO-d_6) δ 12.08 (s, 1H), 8.70 (d, *J* = 1.8 Hz, 1H), 8.26 (d, *J* = 5.2 Hz, 1H), 8.12 (d, *J* = 5.3 Hz, 1H), 8.07 (d, *J* = 8.8 Hz, 1H), 8.01 (dd, *J* = 8.6, 1.9 Hz, 1H), 7.47 (d, *J* = 8.6 Hz, 1H), 4.65 (s, 1H), 3.86 (ddd, *J* = 13.7, 8.7, 5.5 Hz, 1H), 3.56 (m, 2H), 1.98 (dq, *J* = 13.7, 6.8 Hz, 1H), 0.94 (dd, *J* = 9.3, 6.8 Hz, 6H). ^{13}C NMR (101 MHz, DMSO) δ 166.0, 158.3, 143.5, 139.6, 135.2, 130.8, 129.1, 128.8, 124.1, 123.9, 116.6, 116.2, 61.8, 57.3, 29.1, 20.2, 19.4. HRMS m/z (ESI+, M+Na): Calcd for C17H18N2O3S: 353.0923, (ESI+, M+Na) found: 353.0928

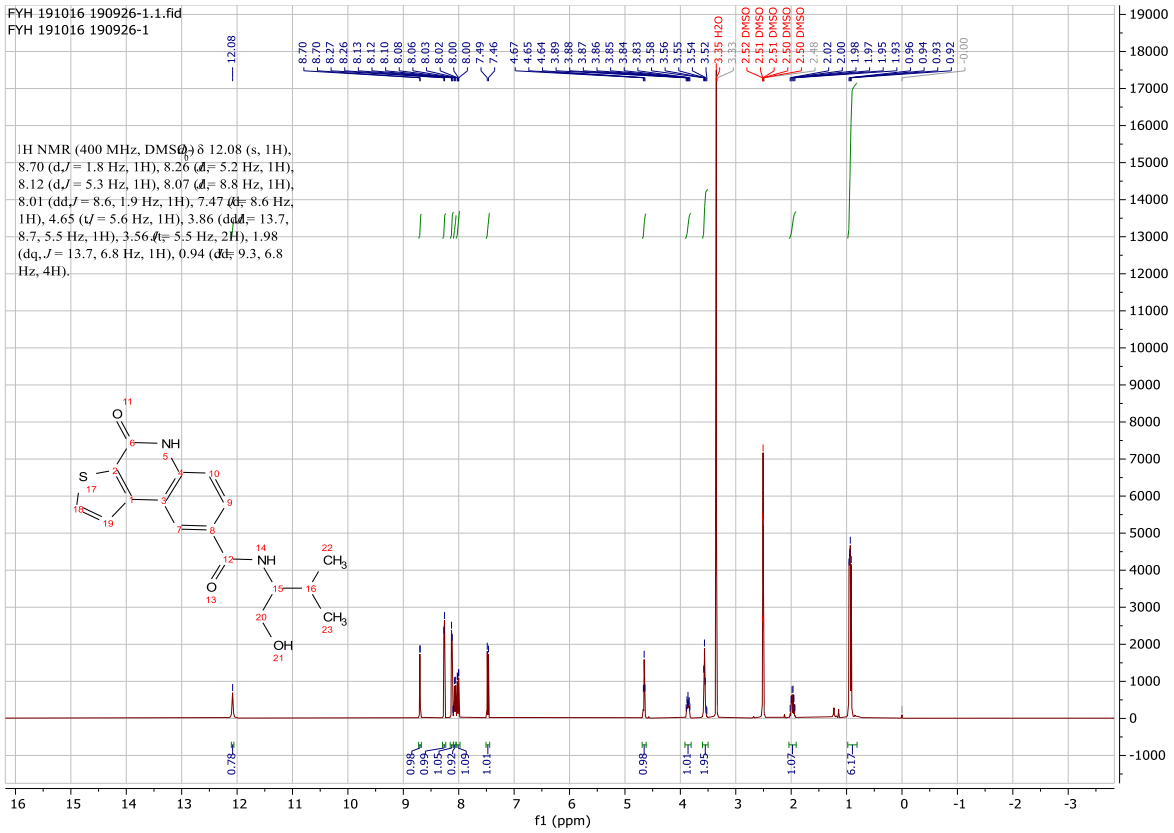
FYH 191016 190926-1.1.fid
FYH 191016 190926-1
1H NMR (400 MHz, DMSO-d6) δ 12.08 (s, 1H), 8.70 (d, J = 1.8 Hz, 1H), 8.26 (d, J = 5.2 Hz, 1H), 8.12 (d, J = 5.3 Hz, 1H), 8.07 (d, J = 8.8 Hz, 1H), 8.01 (dd, J = 8.6, 1.9 Hz, 1H), 7.47 (d, J = 8.6 Hz, 1H), 4.65 (t, J = 5.6 Hz, 1H), 3.86 (ddd, J = 13.7, 8.7, 5.5 Hz, 1H), 3.56 (t, J = 5.5 Hz, 2H), 1.98 (dq, J = 13.7, 6.8 Hz, 1H), 0.94 (d, J = 9.3, 6.8 Hz, 4H).
f1 (ppm)

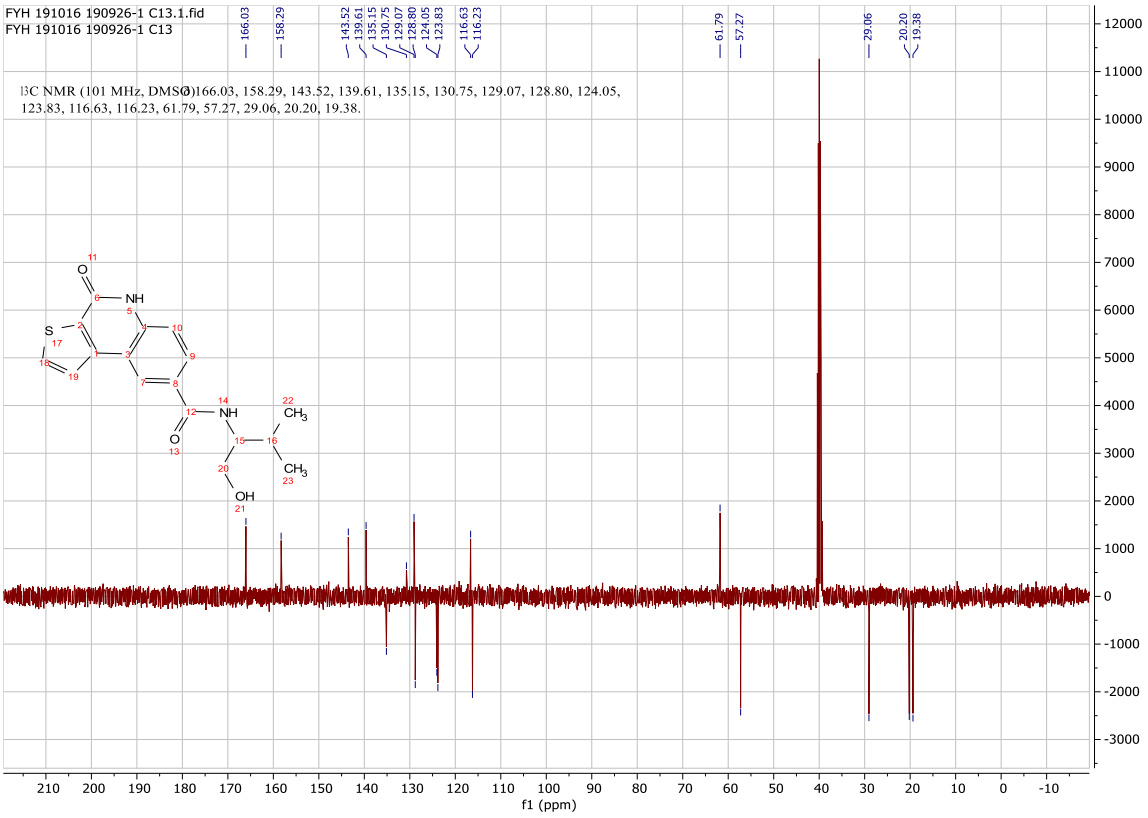
FYH 191016 190926-1 C13.1.fid
FYH 191016 190926-1 C13
13C NMR (101 MHz, DMSO-d6) 166.03, 158.29, 143.52, 139.61, 135.15, 130.75, 129.07, 128.80, 124.05, 123.83, 116.63, 116.23, 61.79, 57.27, 29.06, 20.20, 19.38.
f1 (ppm)

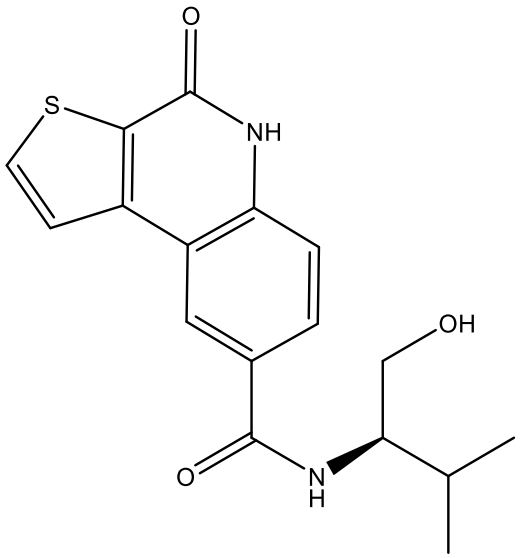

(*R*)-N-(1-hydroxy-3-methylbutan-2-yl)-4-oxo-4,5-dihydrothieno[2,3-*c*]quinoline-7-carboxamide (c30)

Using **Synthesis Method d**, 24.5mg (0.1mmol) **c36** was reacted 10.3mg (0.1mmol) (*R*)-2-amino-3-methylbutan-1-ol to give 22.8mg **c30** (Yield: 69%) and the product was separated as white solid. ^{1}H NMR (300 MHz, DMSO-d_6) δ 12.05 (s, 1H), 8.69 (d, *J* = 1.9 Hz, 1H), 8.25 (d, *J* = 5.2 Hz, 1H), 8.12 (d, *J* = 5.2 Hz, 1H), 8.08 – 7.96 (m, 2H), 7.47 (d, *J* = 8.6 Hz, 1H), 4.62 (s, 1H), 3.86 (m, 1H), 3.56 (m, 2H), 1.98 m, 1H), 0.95 (dd, *J* = 6.9 Hz, 3H), 0.93 (dd, *J* = 6.9 Hz, 3H).. ^{13}C NMR (75 MHz, DMSO) δ 166.0, 158.6, 143.5, 139.6, 135.1, 130.8, 129.1, 128.8, 124.0, 123.8, 116.6, 116.2, 61.8, 57.3, 29.1, 20.2, 19.4. HRMS m/z (ESI+, M+Na): Calcd for C17H18N2O3S: 353.0936, (ESI+, M+Na) found: 353.0930

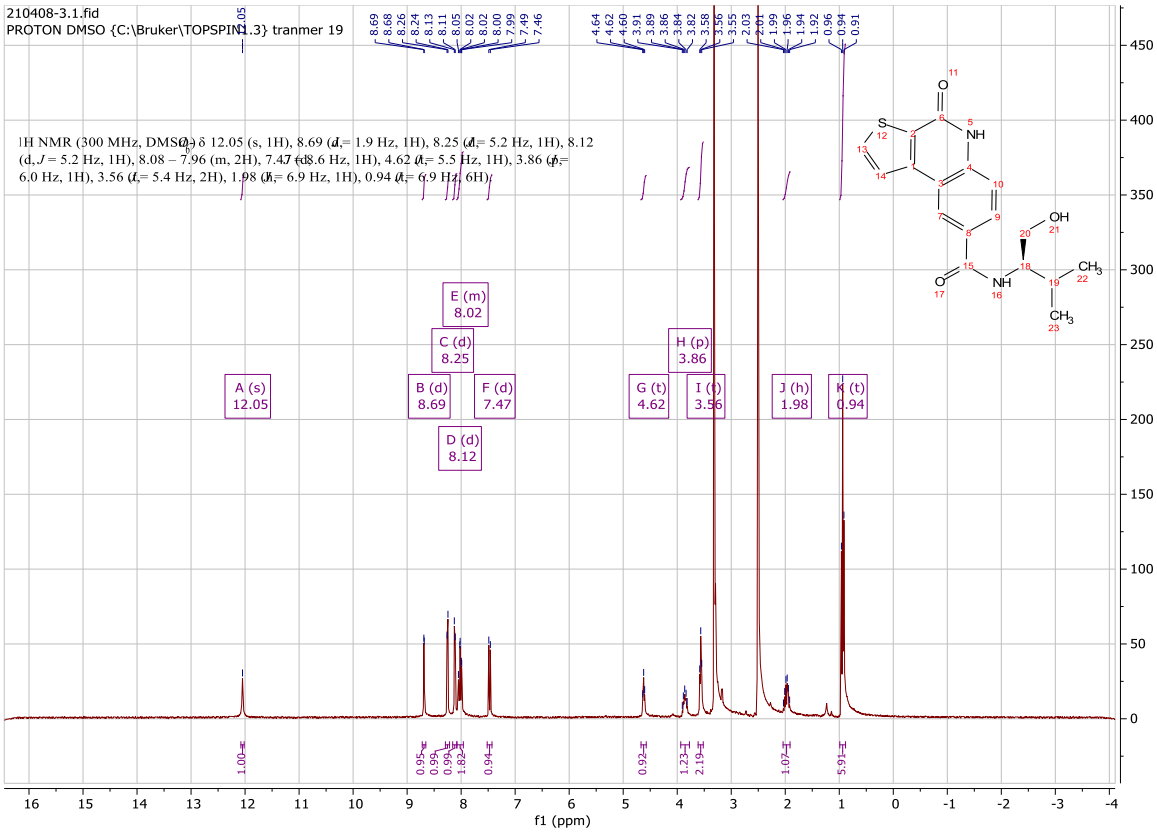
210408-3.1.fid
PROTON DMSO {C:\Bruker\TOPSPIN1.3} tranmer 19
1H NMR (300 MHz, DMSO) δ 12.05 (s, 1H), 8.69 (d, J = 1.9 Hz, 1H), 8.25 (d, J = 5.2 Hz, 1H), 8.12 (d, J = 5.2 Hz, 1H), 8.08 – 7.96 (m, 2H), 7.47 (d, J = 8.6 Hz, 1H), 4.62 (t, J = 5.5 Hz, 1H), 3.86 (p, J = 6.0 Hz, 1H), 3.56 (t, J = 5.4 Hz, 2H), 1.98 (h, J = 6.9 Hz, 1H), 0.94 (t, J = 6.9 Hz, 6H).
A (s) 12.05
B (d) 8.69
C (d) 8.25
D (d) 8.12
E (m) 8.02
F (d) 7.47
G (t) 4.62
H (p) 3.86
I (t) 3.56
J (h) 1.98
K (t) 0.94
f1 (ppm)

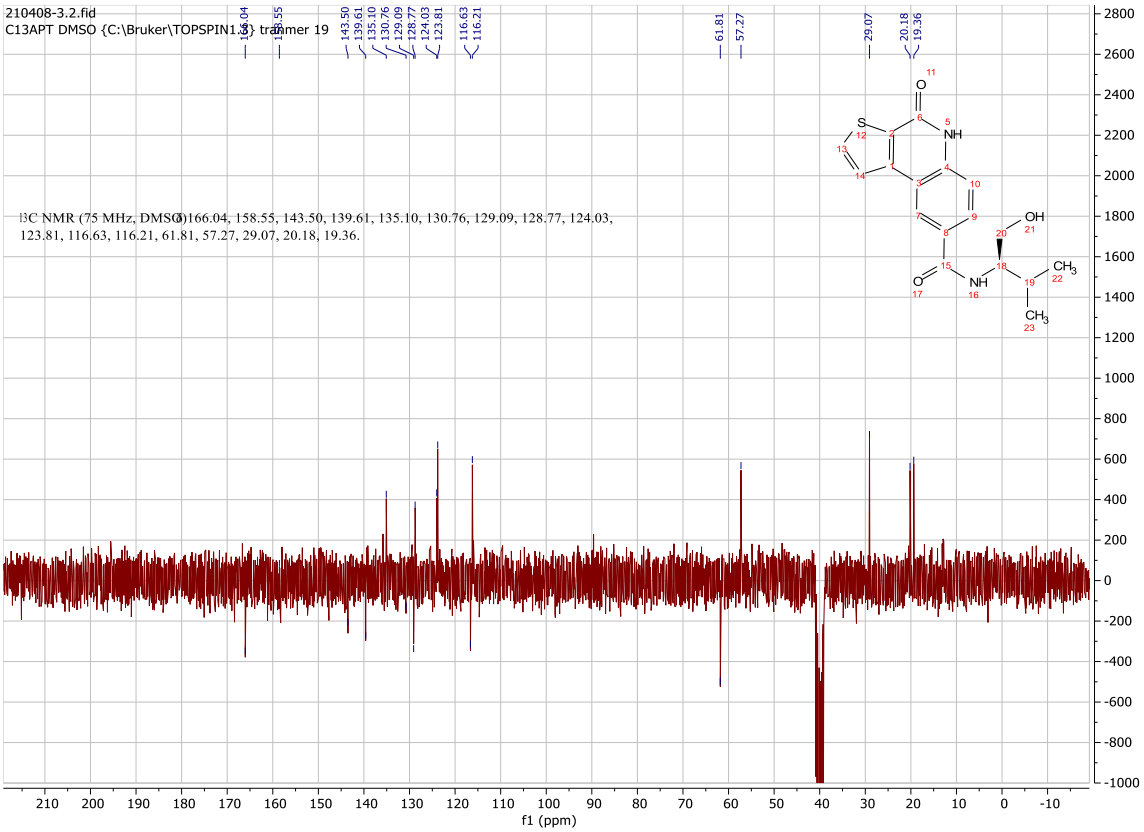
210408-3.2.fid
C13APT DMSO {C:\Bruker\TOPSPIN1.3} tranmer 19
13C NMR (75 MHz, DMSO) δ 166.04, 158.55, 143.50, 139.61, 135.10, 130.76, 129.09, 128.77, 124.03, 123.81, 116.63, 116.21, 61.81, 57.27, 29.07, 20.18, 19.36.
f1 (ppm)

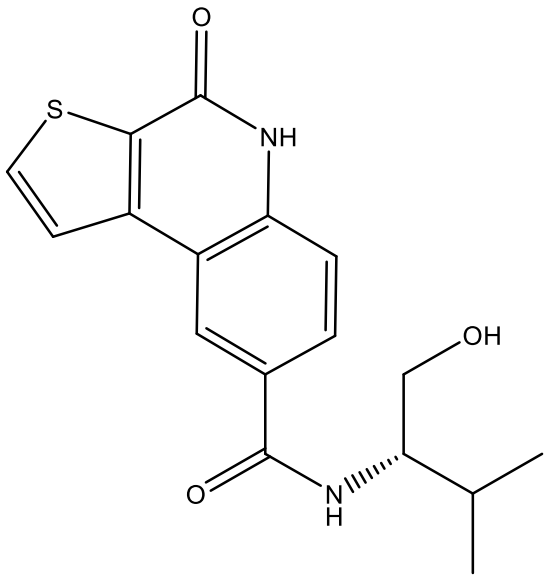

(*S*)-N-(1-hydroxy-3-methylbutan-2-yl)-4-oxo-4,5-dihydrothieno[2,3-*c*]quinoline-7-carboxamide (c31)

Using **Synthesis Method d**, 24.5mg (0.1mmol) **c36** was reacted 10.3mg (0.1mmol) (*S*)-2-amino-3-methylbutan-1-ol to give 23.1mg **c31** (Yield: 70%) and the product was separated as white solid. ^{1}H NMR (300 MHz, DMSO-d_6) δ 12.04 (s, 1H), 8.69 (d, *J* = 1.9 Hz, 1H), 8.25 (d, *J* = 5.2 Hz, 1H), 8.12 (d, *J* = 5.2 Hz, 1H), 8.02 (s, 2H), 7.48 (d, *J* = 8.6 Hz, 1H), 4.62 (s, 1H), 3.86 (dq, *J* = 12.3, 6.0 Hz, 1H), 3.57 (m, 2H), 1.98 (dq, *J* = 12, 6.8 Hz, 1H), 0.94 (d, *J* = 10.0, 6.8 Hz, 6H). ^{13}C NMR (75 MHz, DMSO) δ 166.1, 158.3, 143.5, 139.6, 135.1, 130.8, 129.1, 128.8, 124.0, 123.8, 116.6, 116.2, 61.4, 57.3, 29.1, 20.2, 19.4. HRMS m/z (ESI+, M+Na): Calcd for C17H18N2O3S: 353.0936, (ESI+, M+Na) found: 353.0930

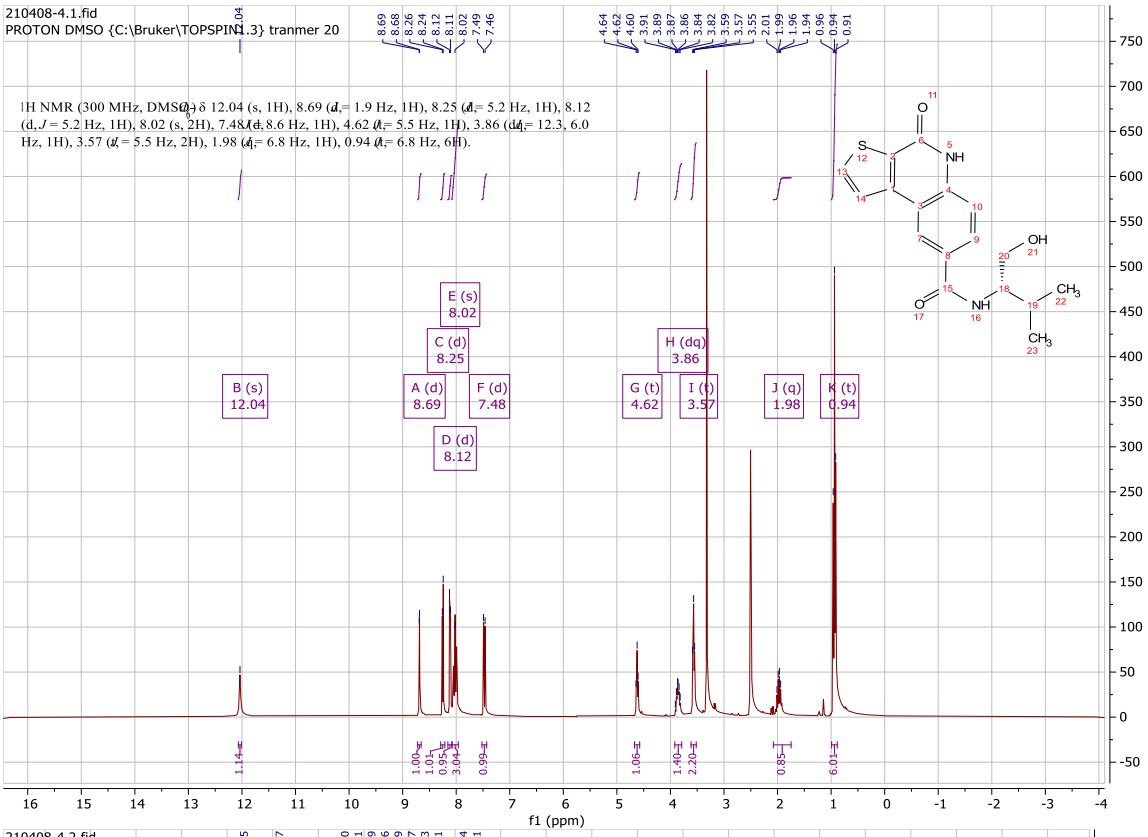
210408-4.1.fid
PROTON DMSO {C:\Bruker\TOPSPIN1.3} tranmer 20
1H NMR (300 MHz, DMSO) δ 12.04 (s, 1H), 8.69 (d, J = 1.9 Hz, 1H), 8.25 (d, J = 5.2 Hz, 1H), 8.12 (d, J = 5.2 Hz, 1H), 8.02 (s, 2H), 7.48 (d, J = 8.6 Hz, 1H), 4.62 (t, J = 5.5 Hz, 1H), 3.86 (dq, J = 12.3, 6.0 Hz, 1H), 3.57 (t, J = 5.5 Hz, 2H), 1.98 (q, J = 6.8 Hz, 1H), 0.94 (t, J = 6.8 Hz, 6H).
B (s) 12.04
A (d) 8.69
C (d) 8.25
D (d) 8.12
E (s) 8.02
F (d) 7.48
G (t) 4.62
H (dq) 3.86
I (t) 3.57
J (q) 1.98
K (t) 0.94
f1 (ppm)


210408-4.2.fid
C13APT DMSO {C:\Bruker\TOPSPIN1.3} tranmer 20
13C NMR (75 MHz, DMSO) 166.05, 158.27, 143.50, 139.61, 135.09, 130.76, 129.09, 128.77, 124.03, 123.81, 116.64, 116.21, 61.37, 57.28, 29.08, 20.18, 19.36.
f1 (ppm)

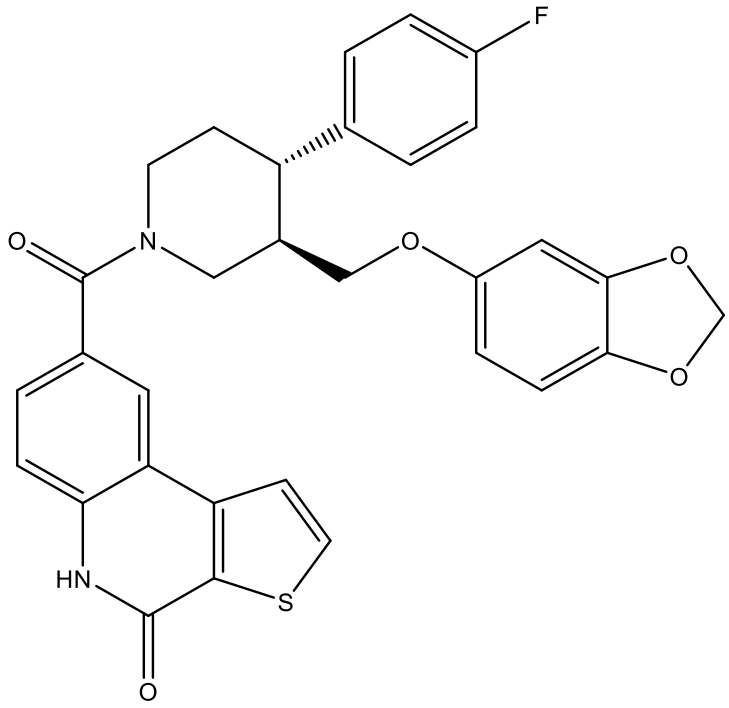

8-((3*R*,4*S*)-3-((benzo[*d*][1,3]dioxol-5-yloxy)methyl)-4-(4-fluorophenyl)piperidine-1-carbonyl)thieno[2,3-*c*]quinolin-4(5H)-one (c32)

Using **Synthesis Method d**, 24.5mg (0.1mmol) **c36** was with 32.9mg (0.1mmol) (3*R*,4*S*)-3-((benzo[*d*][1,3]dioxol-5-yloxy)methyl)-4-(4-fluorophenyl)piperidine to give 23.1mg **c32** (Yield: 70%) and the product was separated as white solid. ^{1}H NMR (300 MHz, DMSO-d_6) δ 12.03 (s, 1H), 8.32 (d, *J* = 1.8 Hz, 1H), 8.22 (d, *J* = 5.2 Hz, 1H), 8.16 (d, *J* = 5.2 Hz, 1H), 7.61 (dd, *J* = 8.4, 1.8 Hz, 1H), 7.51 (d, *J* = 8.4 Hz, 1H), 7.39 (dd, *J* = 8.5, 5.7 Hz, 2H), 7.21 – 7.09 (m, 2H), 6.37 (m, 3H), 5.88 (m, 2H), 3.48 (m, 2H), 2.89 – 2.74 (m, 2H), 2.69 (m, 1H), 2.32 (m, 2H), 1.82 (m, 3H). ^{13}C NMR (75 MHz, DMSO) δ 169.0, 162.4 (d, *J* = 120.3 Hz), 159.8, 158.2, 144.1, 143.3, 140.0, 138.5, 135.0, 130.4, 129.8(d, *J* = 7.2 Hz), 128.2, 124.2, 123.6, 116.9, 116.5, 115.8, 115.5, 108.3, 107.5, 106.0, 101.4, 100.3, 68.4, 44.0, 41.7, 38.0, 34.1. HRMS m/z (ESI+, M+Na): Calcd for C31H25FN2O5S: 579.1366, (ESI+, M+Na) found: 579.1360

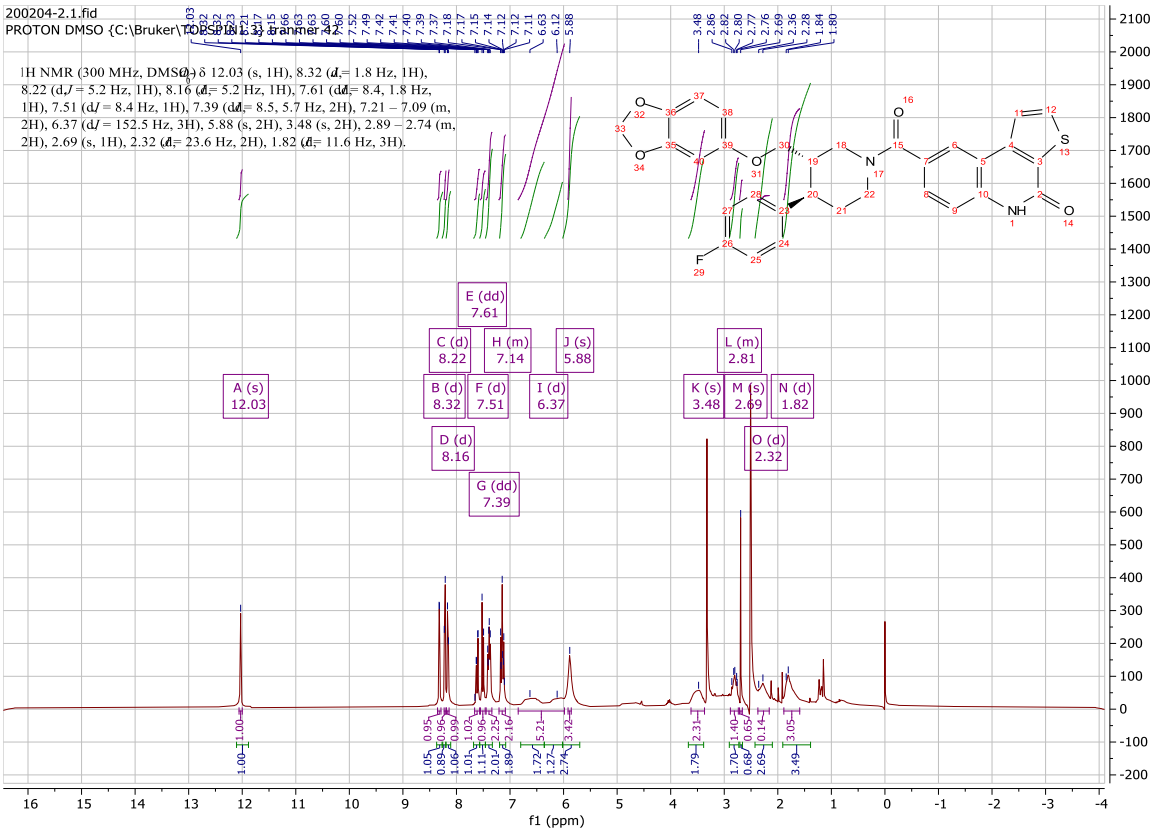
200204-2.1.fid
PROTON DMSO {C:\Bruker\TOPSPIN3.3} tranmer 42
1H NMR (300 MHz, DMSO) δ 12.03 (s, 1H), 8.32 (d, J = 1.8 Hz, 1H), 8.22 (d, J = 5.2 Hz, 1H), 8.16 (d, J = 5.2 Hz, 1H), 7.61 (dd, J = 8.4, 1.8 Hz, 1H), 7.51 (d, J = 8.4 Hz, 1H), 7.39 (dd, J = 8.5, 5.7 Hz, 2H), 7.21 – 7.09 (m, 2H), 6.37 (d, J = 152.5 Hz, 3H), 5.88 (s, 2H), 3.48 (s, 2H), 2.89 – 2.74 (m, 2H), 2.69 (s, 1H), 2.32 (d, J = 23.6 Hz, 2H), 1.82 (d, J = 11.6 Hz, 3H).
A (s) 12.03
B (d) 8.32
C (d) 8.22
D (d) 8.16
E (dd) 7.61
F (d) 7.51
G (dd) 7.39
H (m) 7.14
I (d) 6.37
J (s) 5.88
K (s) 3.48
L (m) 2.81
M (s) 2.69
N (d) 1.82
O (d) 2.32
f1 (ppm)

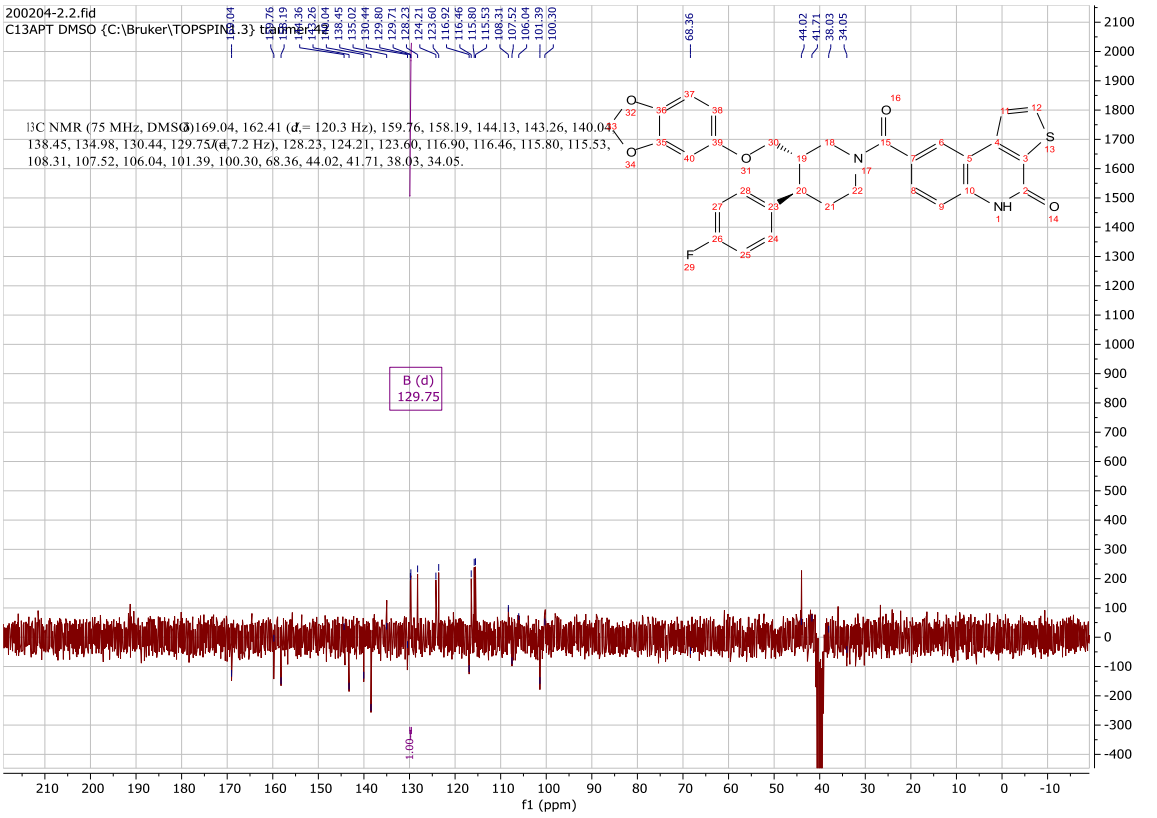
200204-2.2.fid
C13APT DMSO {C:\Bruker\TOPSPIN3.3} tranmer 42
13C NMR (75 MHz, DMSO) δ 169.04, 162.41 (d, J = 120.3 Hz), 159.76, 158.19, 144.13, 143.26, 140.04, 138.45, 134.98, 130.44, 129.75 (d, J = 7.2 Hz), 128.23, 124.21, 123.60, 116.90, 116.46, 115.80, 115.53, 108.31, 107.52, 106.04, 101.39, 100.30, 68.36, 44.02, 41.71, 38.03, 34.05.
B (d) 129.75
f1 (ppm)

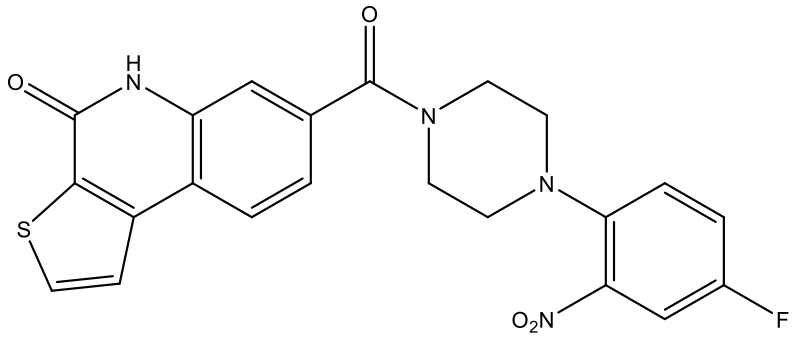

7-(4-(4-fluoro-2-nitrophenyl)piperazine-1-carbonyl)thieno[2,3-*c*]quinolin-4(5H)-one (c33)

1.5g (10mmol) thiophene-2-carbonyl chloride was reacted with 1.7g (10mmol) 3-amino-4-chlorobenzoic acid according to the **Synthesis Method c** to give approximately 34mg impure 4-oxo-4,5-dihydrothieno[2,3-*c*]quinoline-7-carboxylic acid which was difficult to purified. 12mg (~0.05mmol) of them was used to react with 14mg (0.062mmol) 1-(4-fluoro-2-nitrophenyl)piperazine according to **Synthesis Method d** to give crude **c33** 5mg. Failed to get clean product. HRMS m/z (ESI+, M+Na): Calcd for C22H17FN4O4S: 475.0852, (ESI+, M+Na) found: 475.0844

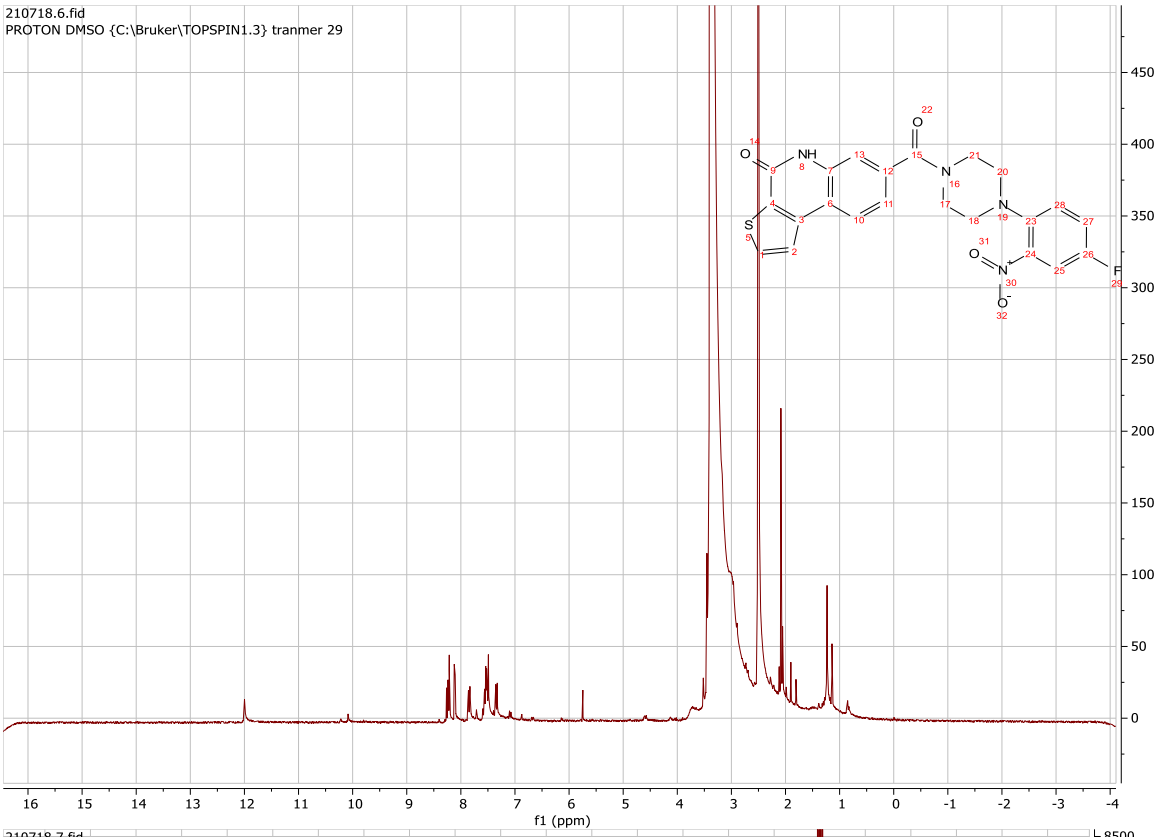
210718.6.fid
PROTON DMSO {C:\Bruker\TOPSPIN1.3} tranmer 29
f1 (ppm)

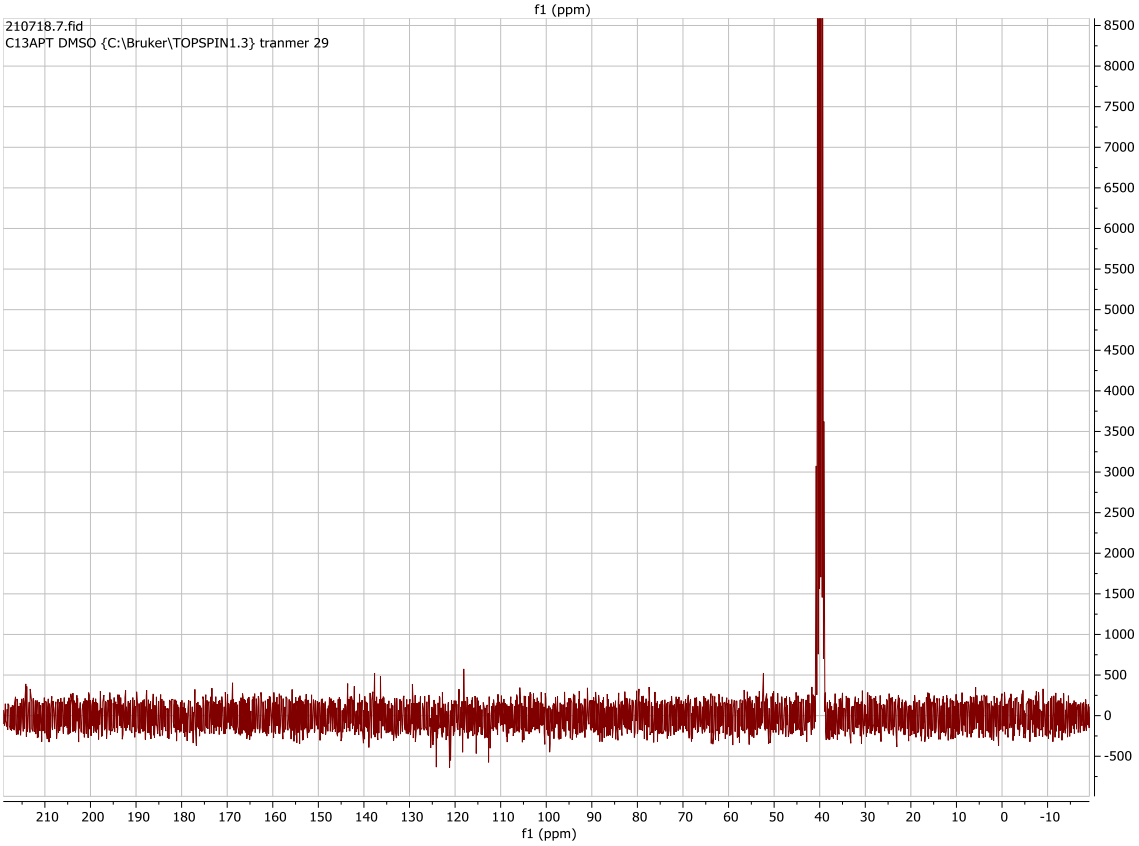
210718.7.fid
C13APT DMSO {C:\Bruker\TOPSPIN1.3} tranmer 29
f1 (ppm)

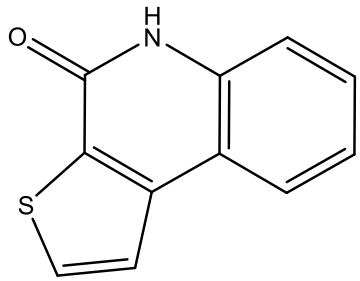

Thieno[2,3-*c*]quinolin-4(5H)-one (c34)

As reported in the M.Sc thesis, 23.8mg (0.1mmol) 3-chloro-*N*-phenylthiophene-2-carboxamide was treated according to the **Synthesis Method b** affording the title compound (17.1 mg, 85%) as white solid. ^{1}H NMR (400 MHz, DMSO-d_6) δ 11.89 (s, 1H, NH), 8.18 (t, *J* =6.8 Hz, 2H), 8.08 (d, *J* =5.2 Hz, 1H), 7.53 – 7.47 (m, 1H), 7.45 (d, *J* =7.8 Hz, 1H), 7.28 (t, *J* =7.4 Hz, 1H). ^{13}C NMR (101 MHz, DMSO-d_6) δ 158.2, 143.5, 137.9, 134.7, 130.5, 129.5, 124.7, 124.0, 122.7, 117.4, 116.6. $C_{11}H_7NOS$. (ESI+, M+H) =202.1. HRMS m/z (ESI+, M+Na): Calcd for C11H7NOS: 224.0146, (ESI+, M+Na) found: 224.0141

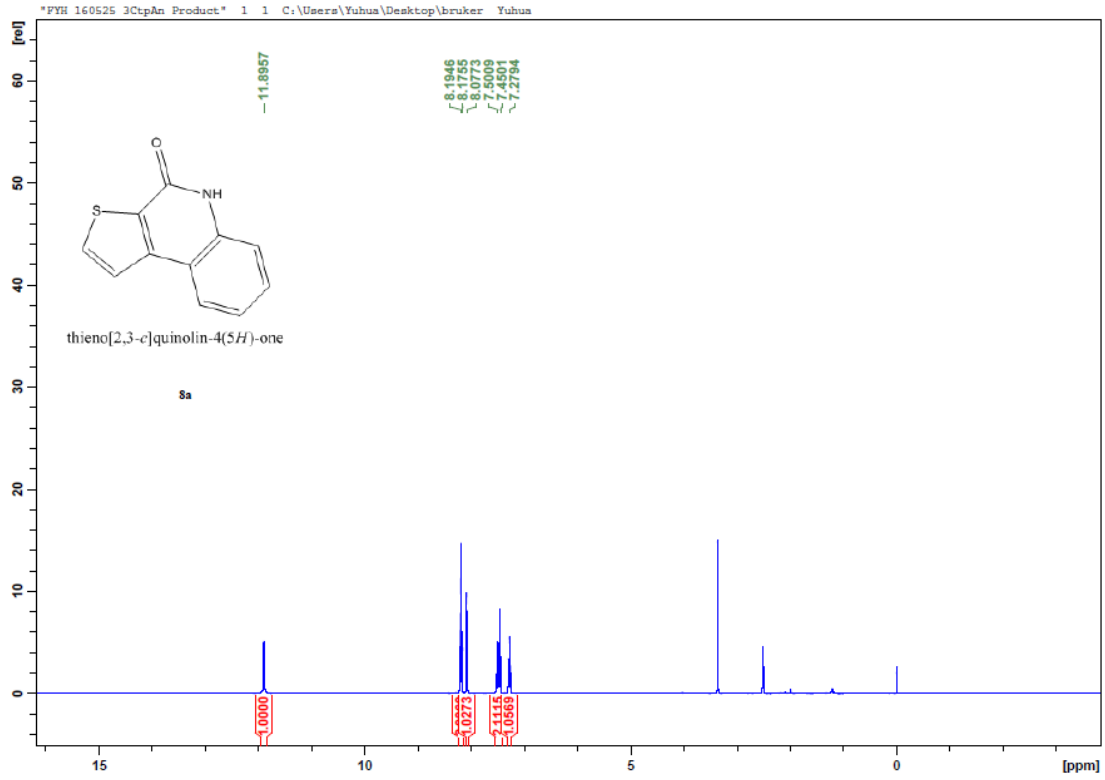
"FYH 160525 3CtpAn Product" 1 1 C:\Users\Yuhua\Desktop\bruker Yuhua
[rel]
11.8957
8.1946
8.1755
8.0773
7.6099
7.4501
7.2794
O
NH
S
thieno[2,3-c]quinolin-4(5H)-one
8a
1.0000
1.0273
2.1115
1.0569
15
10
5
0
[ppm]

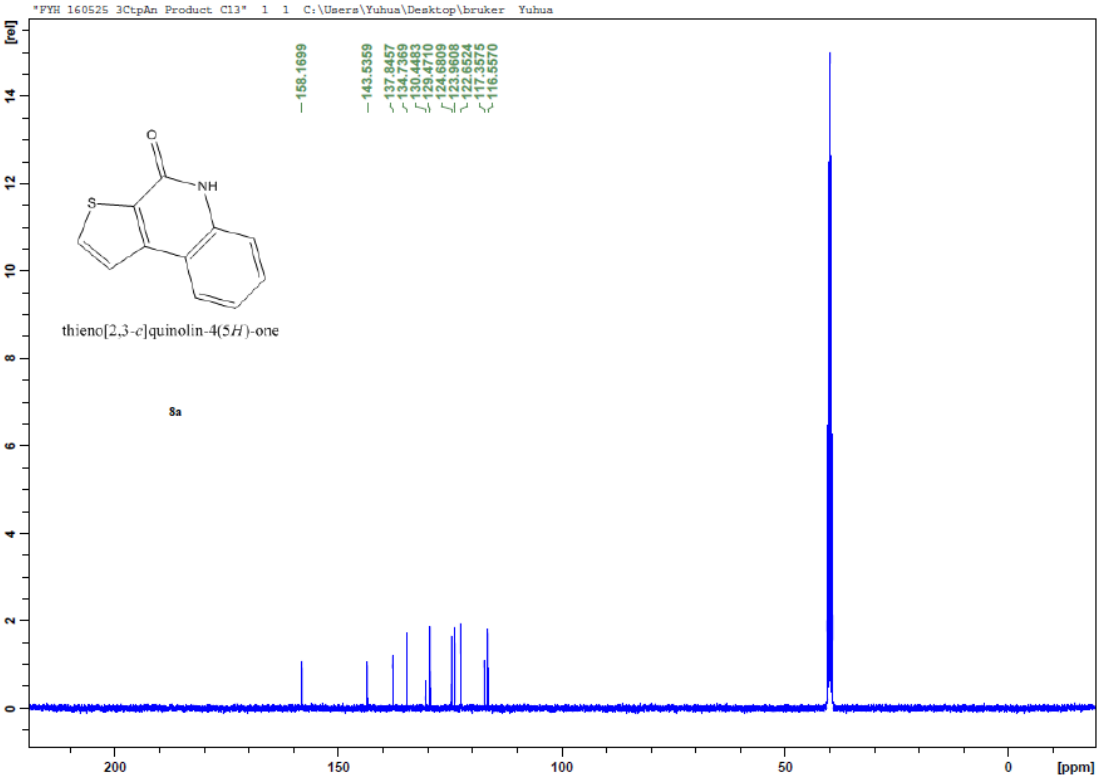
"FYH 160525 3CtpAn Product C13" 1 1 C:\Users\Yuhua\Desktop\bruker Yuhua
[rel]
158.1699
143.5359
137.8457
134.7369
130.4483
129.4710
124.6809
123.9608
122.6524
117.3575
116.5570
O
NH
S
thieno[2,3-c]quinolin-4(5H)-one
8a
200
150
100
50
0
[ppm]

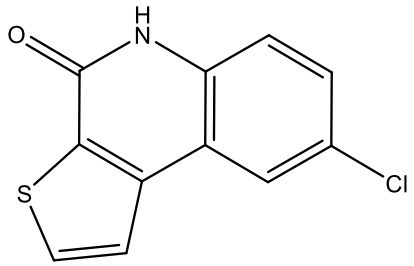

8-chlorothieno[2,3-*c*]quinolin-4(5H)-one (c35)

As reported in the M.Sc thesis, 27.2mg (1mmol) 3-chloro-*N*-(4-chlorophenyl)thiophene-2-carboxamide carboxamide was treated according to the **Synthesis Method b** affording the title compound (21.2 mg, 90%) as white solid. ^{1}H NMR (400 MHz, DMSO-d_6) δ 12.01 (s, 1H, NH), 8.31 (d, *J* =2.2 Hz, 1H), 8.21 (d, *J* =5.2 Hz, 1H), 8.14 (d, *J* =5.2 Hz, 1H), 7.53 (dd, *J* =8.8, 2.2 Hz, 1H), 7.44 (d, *J* =8.8 Hz, 1H). ^{13}C NMR (101 MHz, DMSO-d_6) δ 158.0, 142.5, 136.6, 135.0, 131.4, 129.3, 126.8, 124.3, 124.0, 118.6, 118.4. $C_{11}H_6ClNOS$. (ESI+, M+H) =236.0. HRMS m/z (ESI+, M+Na): Calcd for C11H6ClNOS: 257.9756, (ESI+, M+Na) found: 257.9750

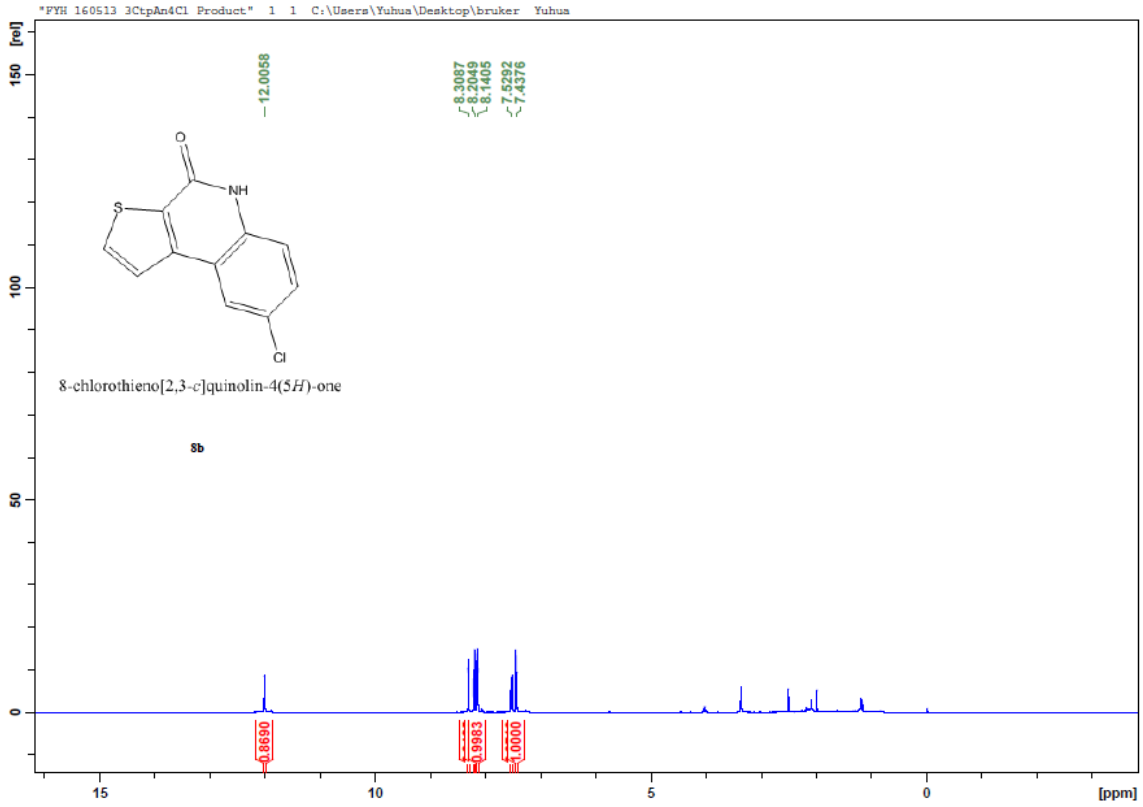
"FYH 160513 3CtpAn4Cl Product" 1 1 C:\Users\Yuhua\Desktop\bruker Yuhua
[rel]
150
100
50
0
12.0058
8.3087
8.2049
8.1405
7.5292
7.4376
O
NH
S
Cl
8-chlorothieno[2,3-c]quinolin-4(5H)-one
8b
0.8690
0.9983
1.0000
15
10
5
0
[ppm]

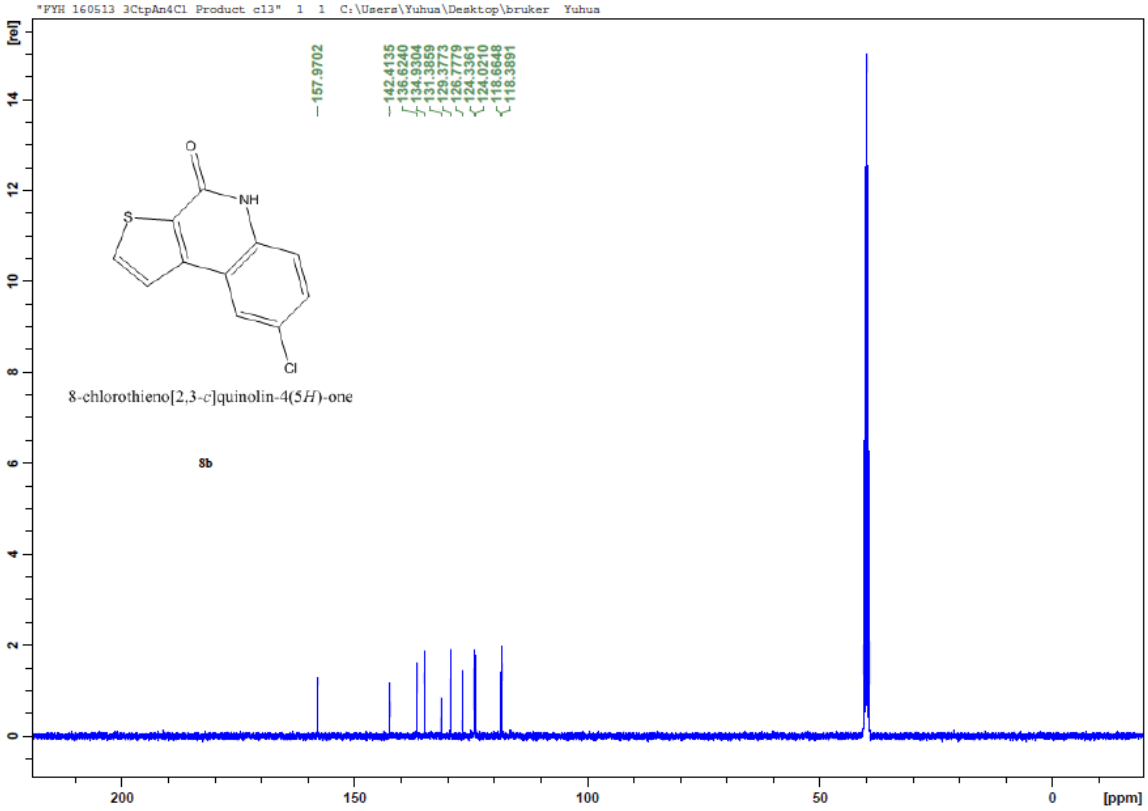
"FYH 160513 3CtpAn4Cl Product c13" 1 1 C:\Users\Yuhua\Desktop\bruker Yuhua
[rel]
14
12
10
8
6
4
2
0
157.9702
142.4135
136.6240
134.9304
131.3859
128.3773
124.4361
124.0210
118.6648
118.3891
O
NH
S
Cl
8-chlorothieno[2,3-c]quinolin-4(5H)-one
8b
200
150
100
50
0
[ppm]

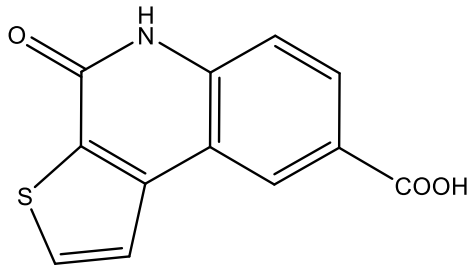

4-oxo-4,5-dihydrothieno[2,3-*c*]quinoline-8-carboxylic acid (c36)

1.8g (10mmol) 3-chlorothiophene-2-carbonyl chloride was reacted with 1.4g (10mmol) 4-aminobenzoic acid according to the **Synthesis Method c** to give approximately 2mg (Yield: 82%) **c36**. ^{1}H NMR (400 MHz, DMSO-d_6) δ 12.97 (s, 1H), 12.16 (s, 1H), 8.70 (d, *J* = 1.8 Hz, 1H), 8.23 (d, *J* = 5.2 Hz, 1H), 8.18 (d, *J* = 5.3 Hz, 1H), 8.05 (dd, *J* = 8.6, 1.9 Hz, 1H), 7.51 (d, *J* = 8.6 Hz, 1H). ^{13}C NMR (101 MHz, DMSO) δ 167.40, 158.3, 143.2, 141.0, 135.3, 130.9, 130.1, 126.4, 125.0, 124.1, 117.0, 116.7. HRMS m/z (ESI+, M+Na): Calcd for C12H7NO3S: 268.0044, (ESI+, M+Na) found: 268.0039

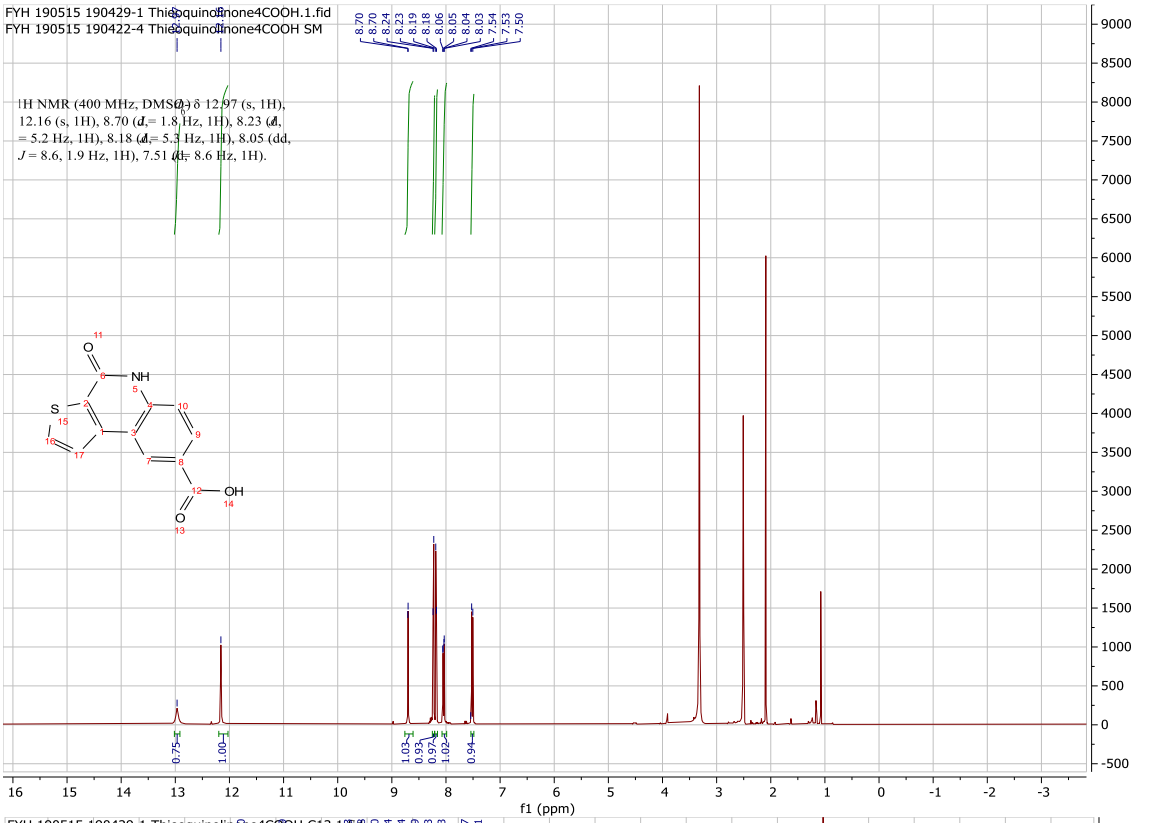
FYH 190515 190429-1 Thieoquinolinone4COOH.1.fid
FYH 190515 190422-4 Thieoquinolinone4COOH SM
1H NMR (400 MHz, DMSO) δ 12.97 (s, 1H), 12.16 (s, 1H), 8.70 (d, = 1.8 Hz, 1H), 8.23 (d, = 5.2 Hz, 1H), 8.18 (d, = 5.3 Hz, 1H), 8.05 (dd, J = 8.6, 1.9 Hz, 1H), 7.51 (d, = 8.6 Hz, 1H).
f1 (ppm)

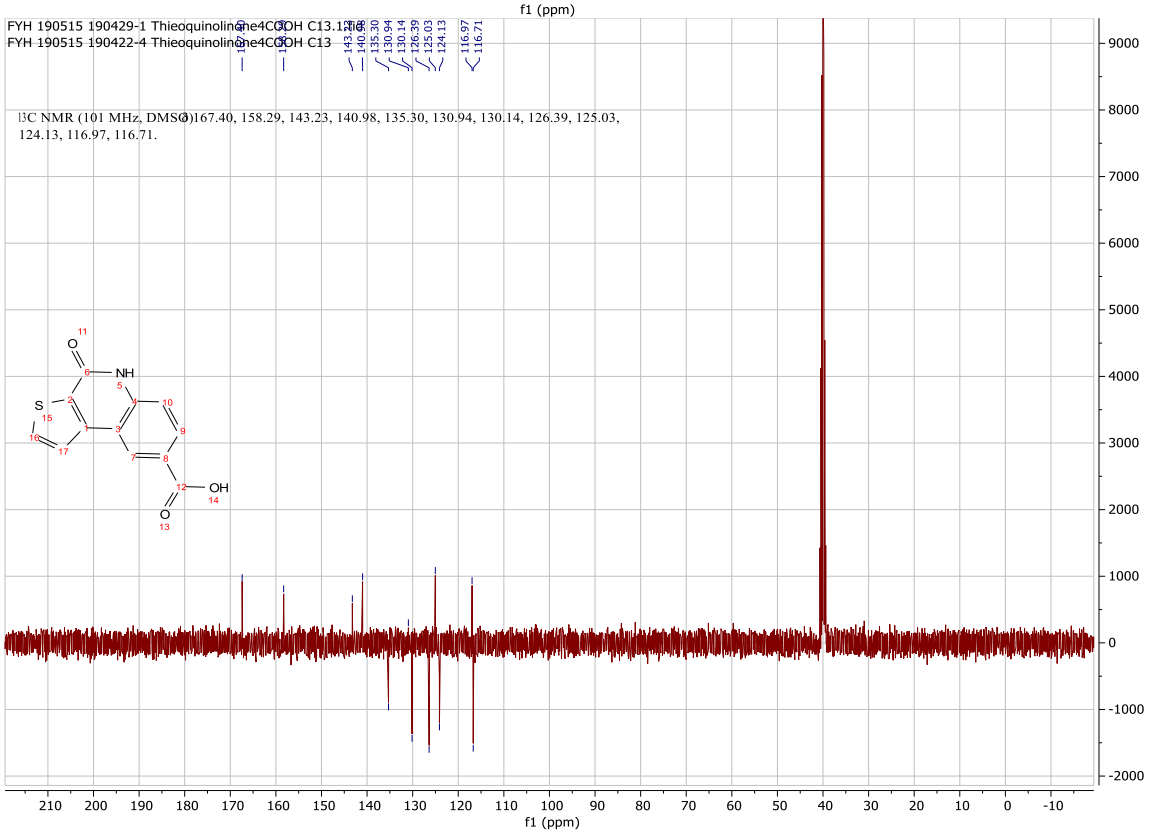
FYH 190515 190429-1 Thieoquinolinone4COOH C13.1.fid
FYH 190515 190422-4 Thieoquinolinone4COOH C13
13C NMR (101 MHz, DMSO) 167.40, 158.29, 143.23, 140.98, 135.30, 130.94, 130.14, 126.39, 125.03, 124.13, 116.97, 116.71.
f1 (ppm)

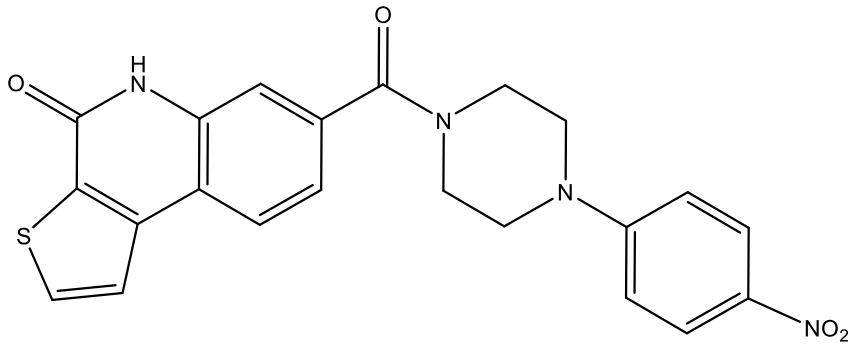

7-(4-(4-nitrophenyl)piperazine-1-carbonyl)thieno[2,3-*c*]quinolin-4(5*H*)-on (c37)

1.5g (10mmol) thiophene-2-carbonyl chloride was reacted with 1.7g (10mmol) 3-amino-4-chlorobenzoic acid according to the **Synthesis Method c** to give approximately 34mg impure 4-oxo-4,5-dihydrothieno[2,3-*c*]quinoline-7-carboxylic acid which was difficult to purified. 12mg (~0.05mmol) of them was used to react with 11.4mg (0.055mmol) 1-(4-nitrophenyl)piperazine according to **Synthesis Method d** to give 8mg **c37**. Overall yield was 14%. ^{1}H NMR (300 MHz, DMSO-d_6) δ 12.01 (s, 1H), 8.27 (d, J = 8.1 Hz, 1H), 8.23 (d, J = 5.2 Hz, 1H), 8.14 – 8.05 (m, 3H), 7.51 (d, J = 1.5 Hz, 1H), 7.36 (dd, J = 8.1, 1.6 Hz, 1H), 7.04 (d, J = 9.5 Hz, 2H), 3.57 (m, 8H). ^{13}C NMR (75 MHz, DMSO) δ 164.4, 154.9, 143.6, 143.0, 137.7, 137.6, 136.3, 135.1, 126.2, 124.9, 124.2, 121.2, 118.2, 116.4, 115.4, 113.2, 53.6, 46.4. HRMS m/z (ESI+, M+Na): Calcd for C22H18N4O4S: 457.0946, (ESI+, M+Na) found: 457.0942

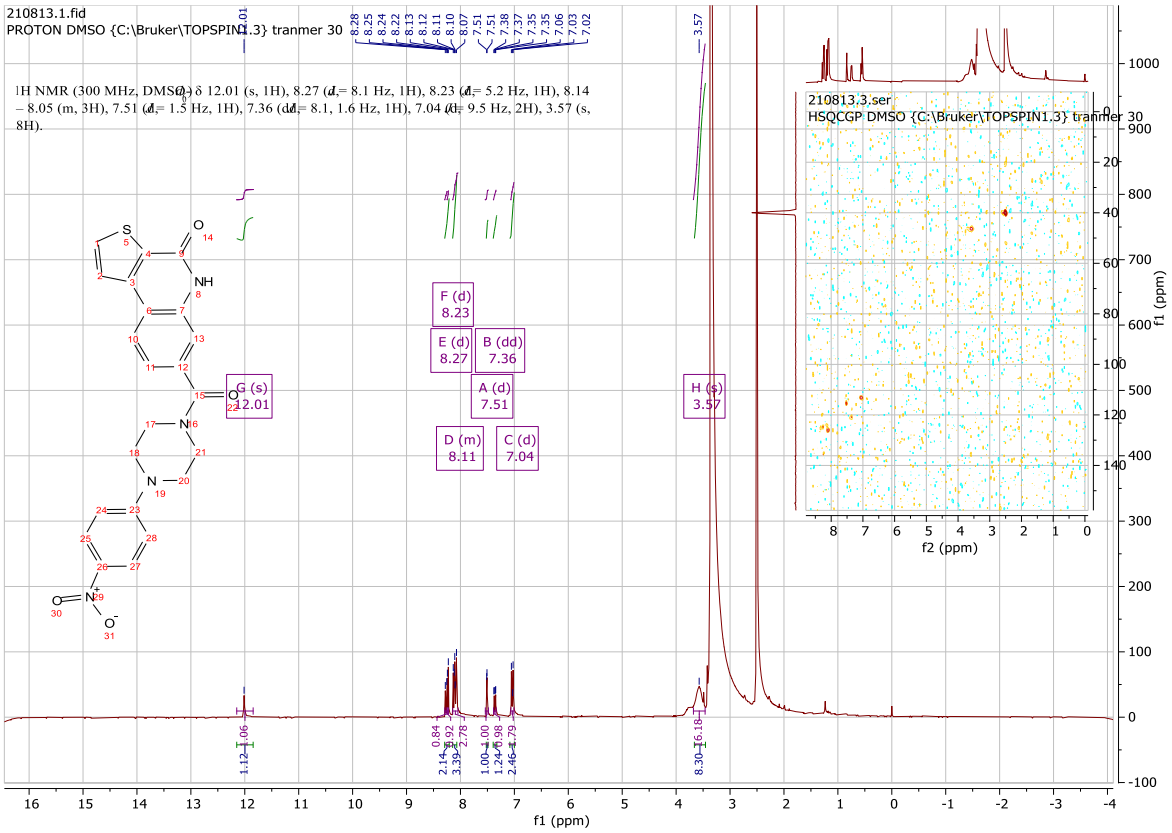
210813.1.fid
PROTON DMSO {C:\Bruker\TOPSPIN1.3} tranmer 30
1H NMR (300 MHz, DMSO) δ 12.01 (s, 1H), 8.27 (d, J= 8.1 Hz, 1H), 8.23 (d, J= 5.2 Hz, 1H), 8.14 – 8.05 (m, 3H), 7.51 (d, J= 1.5 Hz, 1H), 7.36 (dd, J= 8.1, 1.6 Hz, 1H), 7.04 (d, J= 9.5 Hz, 2H), 3.57 (s, 8H).
G (s) 12.01
F (d) 8.23
E (d) 8.27
B (dd) 7.36
A (d) 7.51
D (m) 8.11
C (d) 7.04
H (s) 3.57
210813.3.ser
HSQCGP DMSO {C:\Bruker\TOPSPIN1.3} tranmer 30
f1 (ppm)
f2 (ppm)

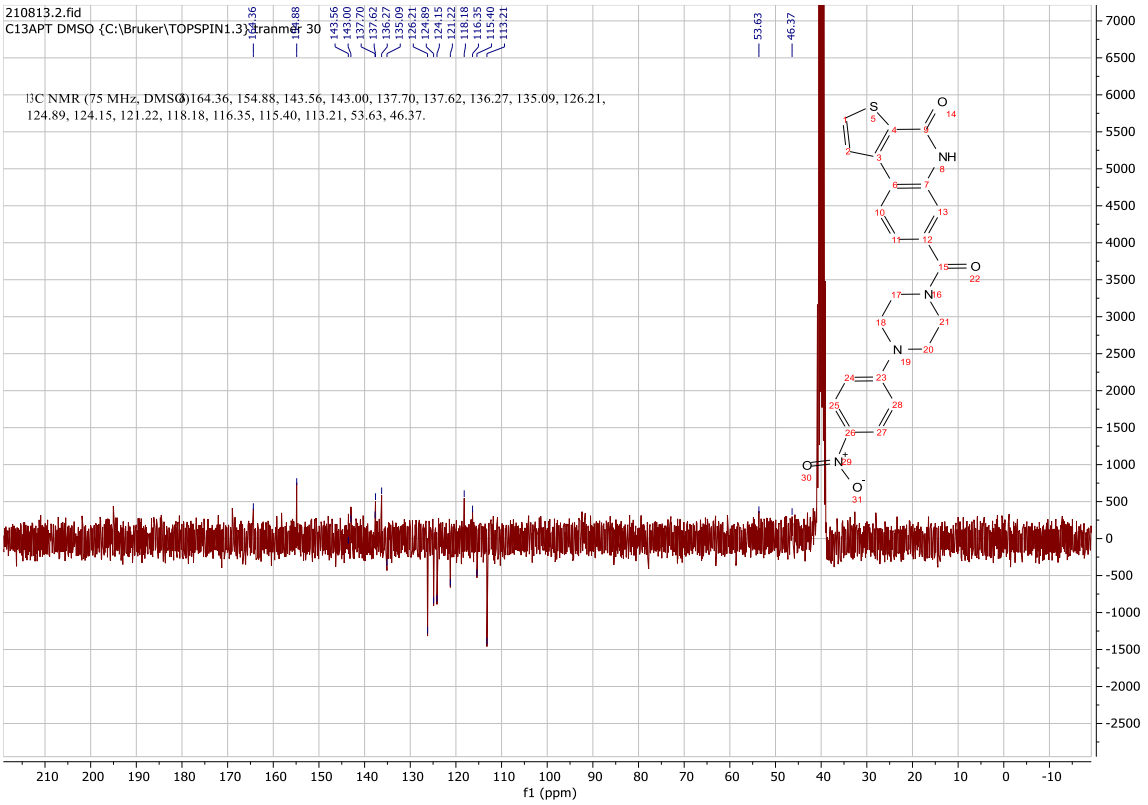
210813.2.fid
C13APT DMSO {C:\Bruker\TOPSPIN1.3} tranmer 30
13C NMR (75 MHz, DMSO) 164.36, 154.88, 143.56, 143.00, 137.70, 137.62, 136.27, 135.09, 126.21, 124.89, 124.15, 121.22, 118.18, 116.35, 115.40, 113.21, 53.63, 46.37.
f1 (ppm)

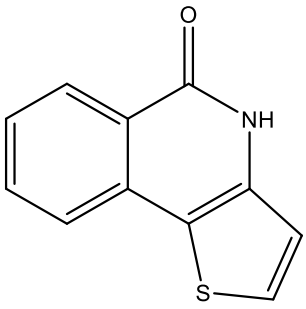

thieno[3,2-*c*]isoquinolin-5(4*H*)-one (d1)

47mg (0.2mmol) **f24** was reacted according to the **Synthesis Method b** to give 15.5mg **d1** (Yield: 39%) and 3.5mg **d2** (Yield: 9%) in the same time as white solid. ^{1}H NMR (300 MHz, DMSO-d_6) δ 11.99 (s, 1H), 8.27 (dd, J = 8.0, 1.0 Hz, 1H), 7.82 – 7.71 (m, 3H), 7.52 (ddd, J = 8.2, 5.6, 2.8 Hz, 1H), 7.06 (d, J = 5.3 Hz, 1H). ^{13}C NMR (75 MHz, DMSO) δ 161.8, 138.9, 133.6, 133.5, 128.7, 128.2, 126.8, 124.1, 122.9, 118.4, 115.5. HRMS m/z (ESI+, M+Na): Calcd for C11H7NOS: 224.0146, (ESI+, M+Na) found: 224.0142

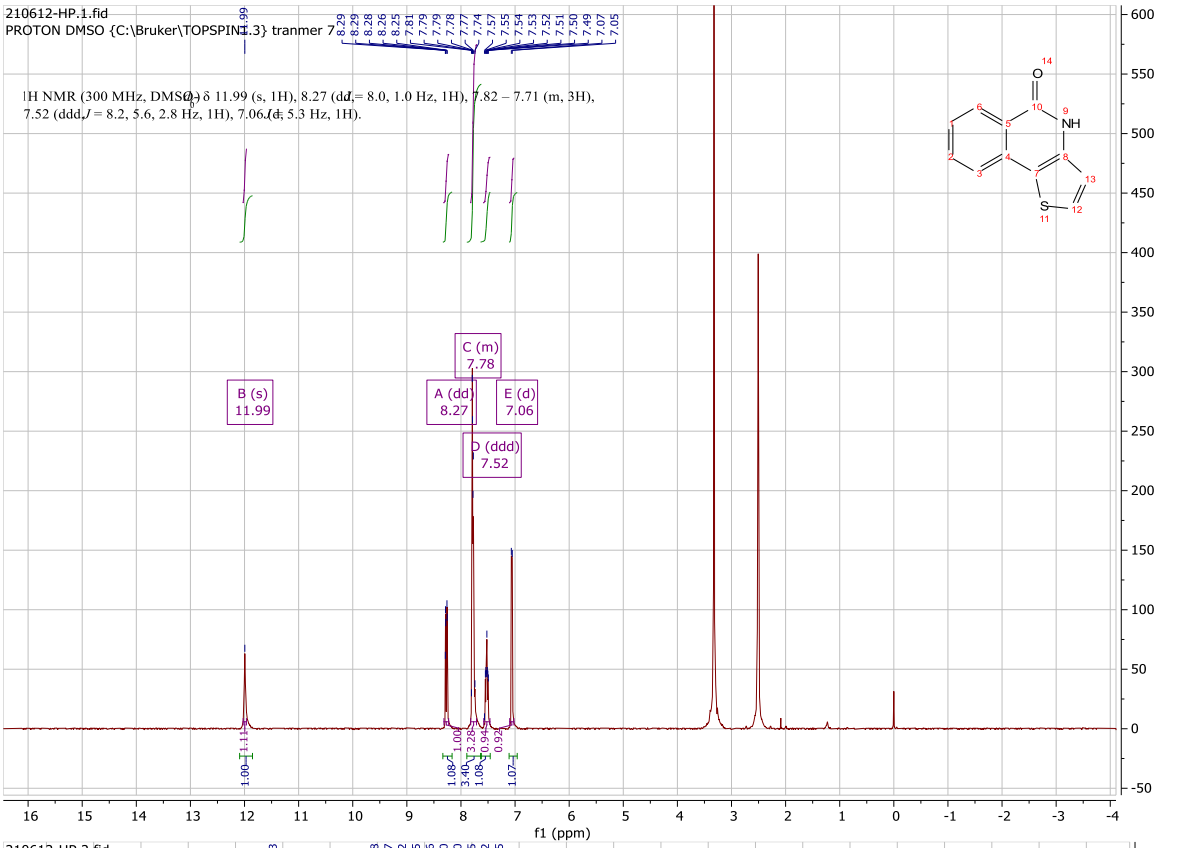
210612-HP.1.fid
PROTON DMSO {C:\Bruker\TOPSPIN1.3} tranmer 7
1H NMR (300 MHz, DMSO) δ 11.99 (s, 1H), 8.27 (dd, J = 8.0, 1.0 Hz, 1H), 7.82 – 7.71 (m, 3H), 7.52 (ddd, J = 8.2, 5.6, 2.8 Hz, 1H), 7.06 (d, 5.3 Hz, 1H).
B (s) 11.99
A (dd) 8.27
C (m) 7.78
D (ddd) 7.52
E (d) 7.06
f1 (ppm)

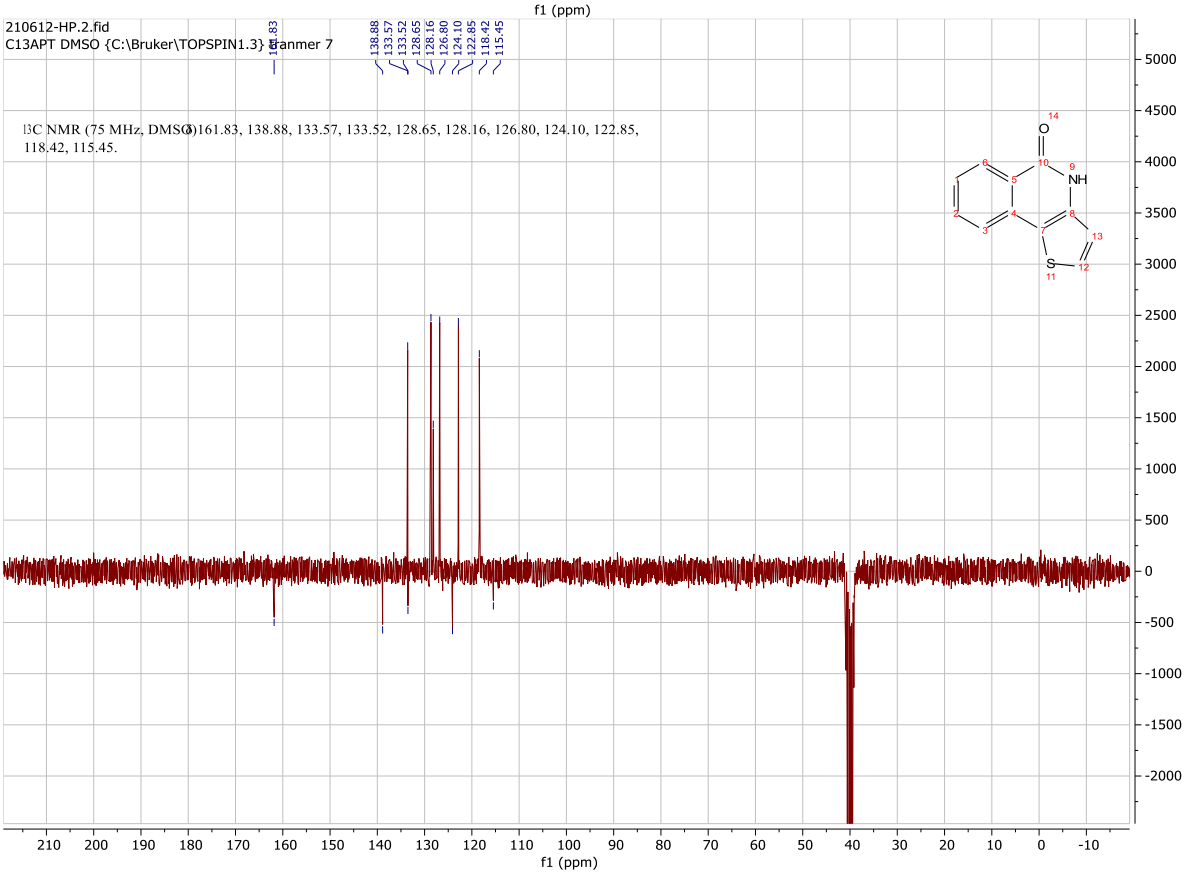
210612-HP.2.fid
C13APT DMSO {C:\Bruker\TOPSPIN1.3} tranmer 7
13C NMR (75 MHz, DMSO) 161.83, 138.88, 133.57, 133.52, 128.65, 128.16, 126.80, 124.10, 122.85, 118.42, 115.45.
f1 (ppm)

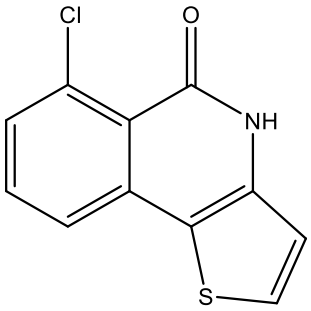

6-chlorothieno[3,2-*c*]isoquinolin-5(4*H*)-one (d2)

47mg (0.2mmol) **f24** was reacted according to the **Synthesis Method b** to give 15.5mg **d1** (Yield: 39%) and 3.5mg **d2** (Yield: 9%) in the same time as white solid. ^{1}H NMR (300 MHz, DMSO-d_6) δ 7.81 (d, *J* = 5.3 Hz, 1H), 7.73 (dd, *J* = 8.0, 1.5 Hz, 1H), 7.67 (t, *J* = 7.7 Hz, 1H), 7.51 (dd, *J* = 7.5, 1.5 Hz, 1H), 7.01 (d, *J* = 5.3 Hz, 1H). ^{13}C NMR (75 MHz, DMSO) δ 160.2, 139.4, 136.5, 135.6, 133.7, 129.9, 129.3, 122.4, 120.0, 118.1, 115.0. HRMS m/z (ESI+, M+Na): Calcd for C11H6ClNOS: 257.9756, (ESI+, M+Na) found: 257.9752

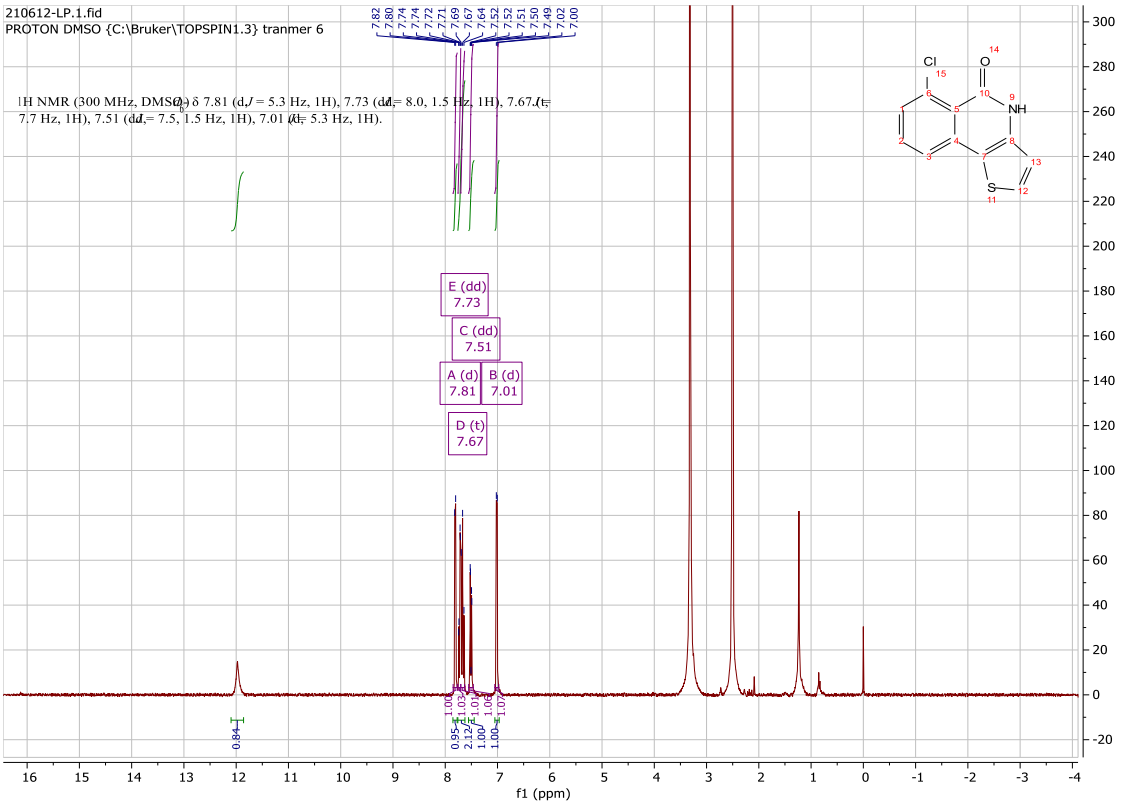
210612-LP.1.fid
PROTON DMSO {C:\Bruker\TOPSPIN1.3} tranmer 6
1H NMR (300 MHz, DMSO-d6) δ 7.81 (d, J = 5.3 Hz, 1H), 7.73 (dd, J = 8.0, 1.5 Hz, 1H), 7.67 (t, J = 7.7 Hz, 1H), 7.51 (dd, J = 7.5, 1.5 Hz, 1H), 7.01 (d, J = 5.3 Hz, 1H).
E (dd) 7.73
C (dd) 7.51
A (d) 7.81
B (d) 7.01
D (t) 7.67
f1 (ppm)

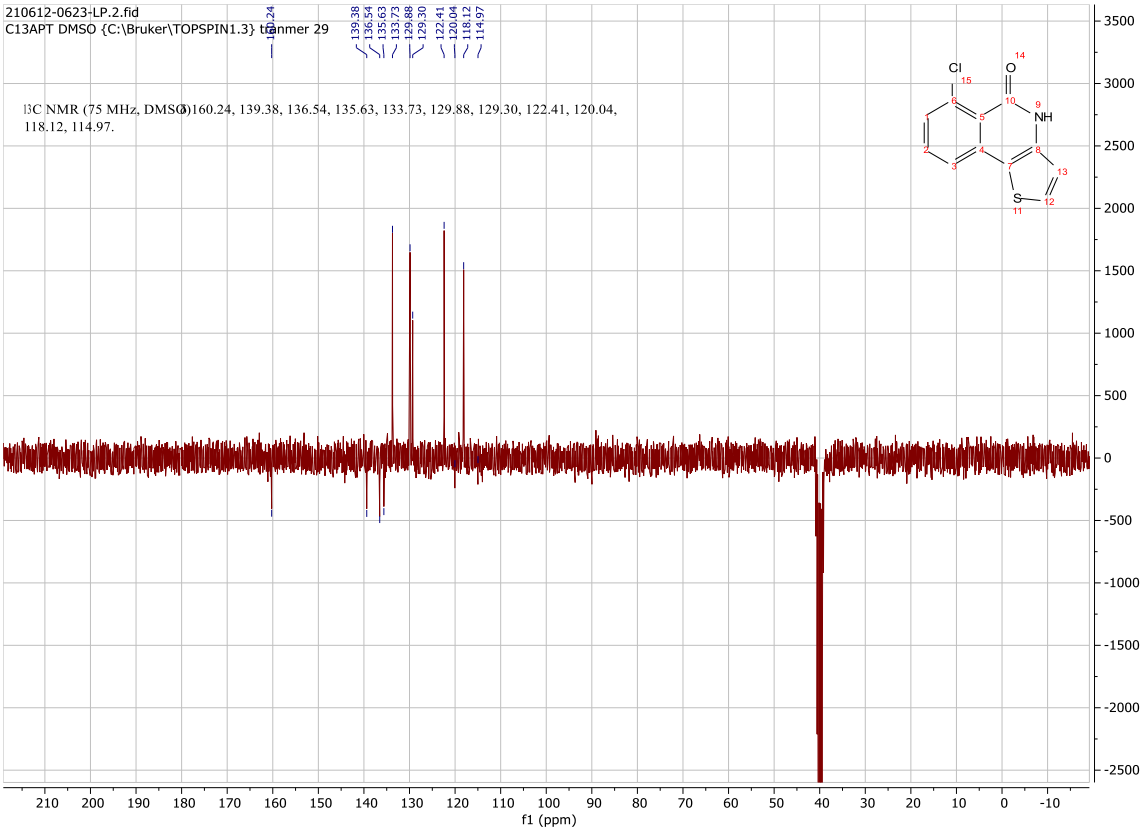
210612-0623-LP.2.fid
C13APT DMSO {C:\Bruker\TOPSPIN1.3} tranmer 29
13C NMR (75 MHz, DMSO-d6) 160.24, 139.38, 136.54, 135.63, 133.73, 129.88, 129.30, 122.41, 120.04, 118.12, 114.97.
f1 (ppm)

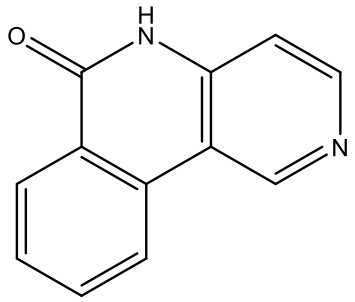

benzo[*c*][1,6]naphthyridin-6(5H)-one (e1)

23.5mg (0.1mmol) **f7** was reacted according to the **Synthesis Method b** to give 7.7mg **e1** (Yield: 39%) as yellow solid. ^{1}H NMR (300 MHz, DMSO-d_6) δ 12.92 (s, 1H), 9.88 (s, 1H), 8.72 (t, J = 7.7 Hz, 2H), 8.36 (d, J = 7.9 Hz, 1H), 8.01 (t, J = 7.7 Hz, 1H), 7.84 (t, J = 7.5 Hz, 1H), 7.72 (d, J = 6.5 Hz, 1H). ^{13}C NMR (75 MHz, DMSO) δ 161.6, 148.0, 140.4, 139.4, 134.5, 131.3, 131.1, 128.2, 126.4, 123.9, 116.0, 112.9. HRMS m/z (ESI+, M+H): Calcd for C12H8N2O: 197.0709, (ESI+, M+H) found: 197.0710

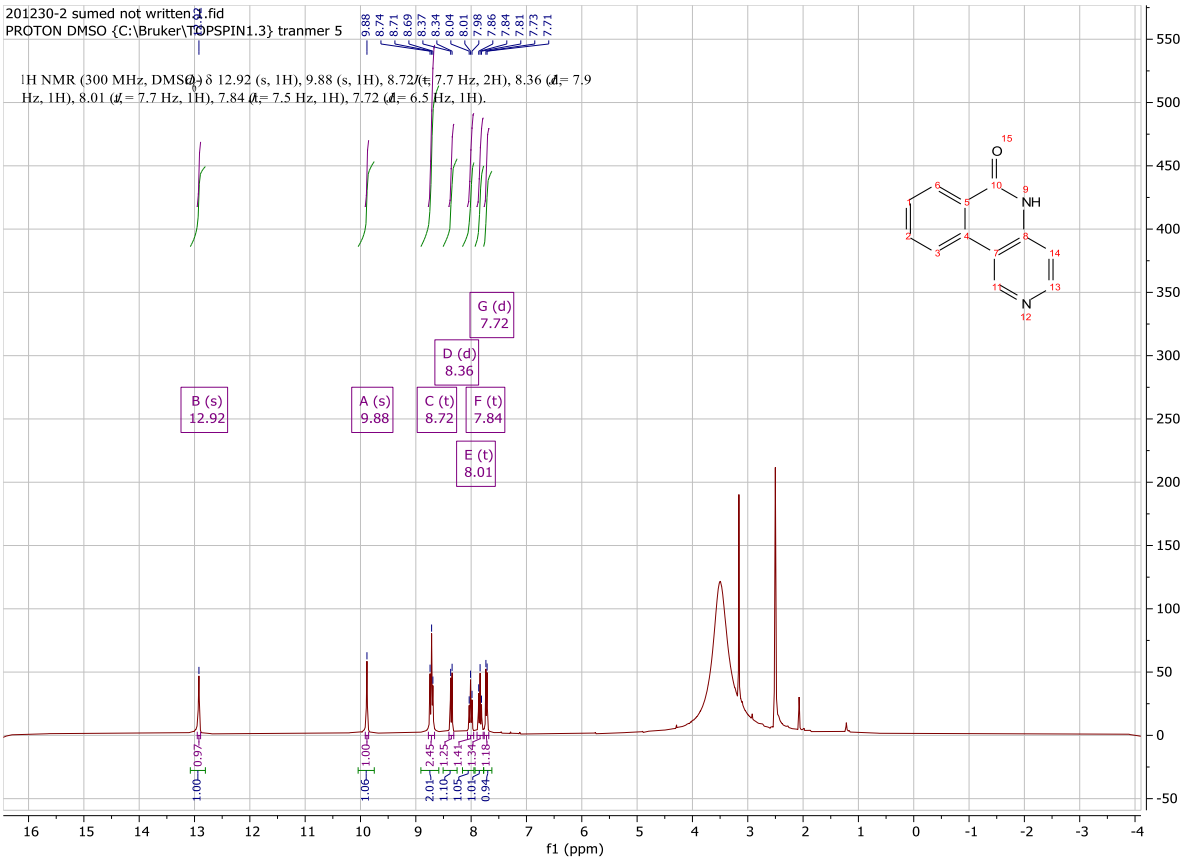
201230-2 sumed not written.1.fid
PROTON DMSO {C:\Bruker\TOPSPIN1.3} tranmer 5
1H NMR (300 MHz, DMSO) δ 12.92 (s, 1H), 9.88 (s, 1H), 8.72 (t, J = 7.7 Hz, 2H), 8.36 (d, J = 7.9 Hz, 1H), 8.01 (d, J = 7.7 Hz, 1H), 7.84 (t, J = 7.5 Hz, 1H), 7.72 (d, J = 6.5 Hz, 1H).
B (s) 12.92
A (s) 9.88
C (t) 8.72
F (t) 7.84
E (t) 8.01
D (d) 8.36
G (d) 7.72
f1 (ppm)

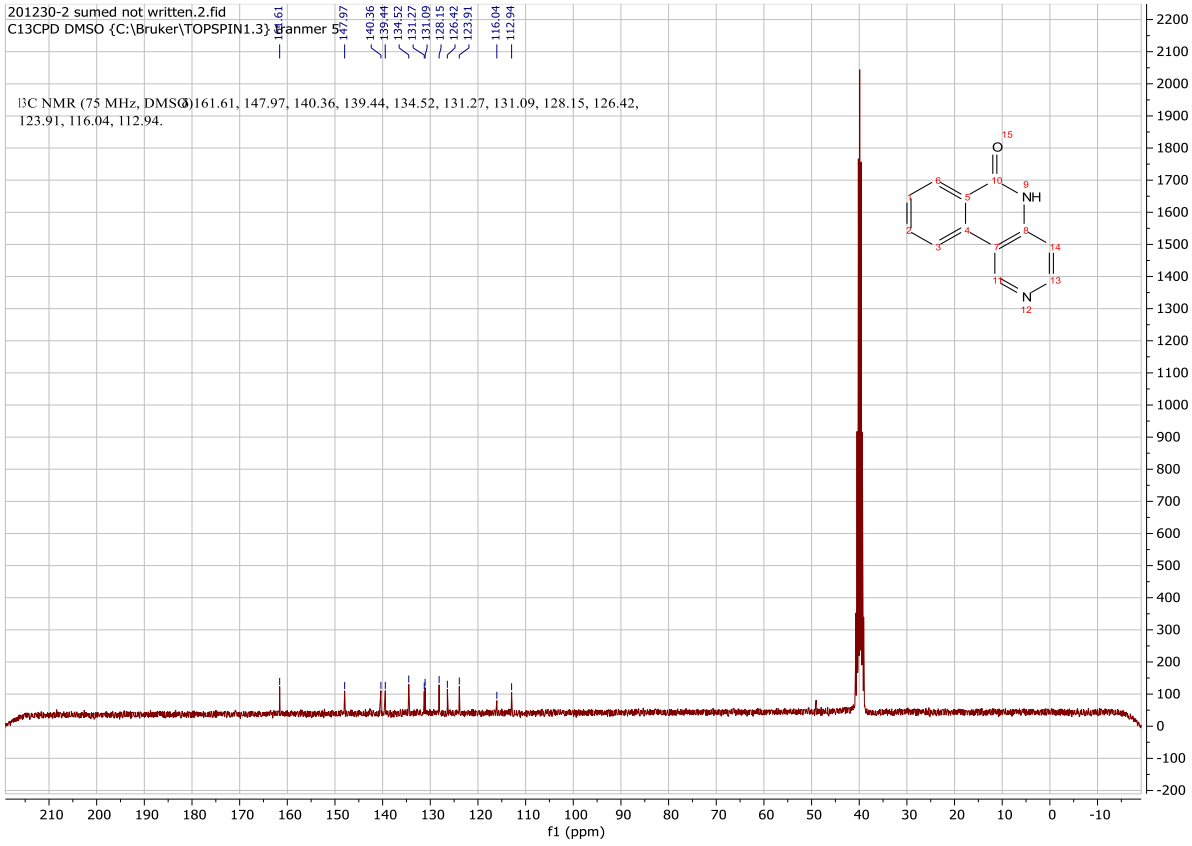
201230-2 sumed not written.2.fid
C13CPD DMSO {C:\Bruker\TOPSPIN1.3} tranmer 5
13C NMR (75 MHz, DMSO) 161.61, 147.97, 140.36, 139.44, 134.52, 131.27, 131.09, 128.15, 126.42, 123.91, 116.04, 112.94.
f1 (ppm)

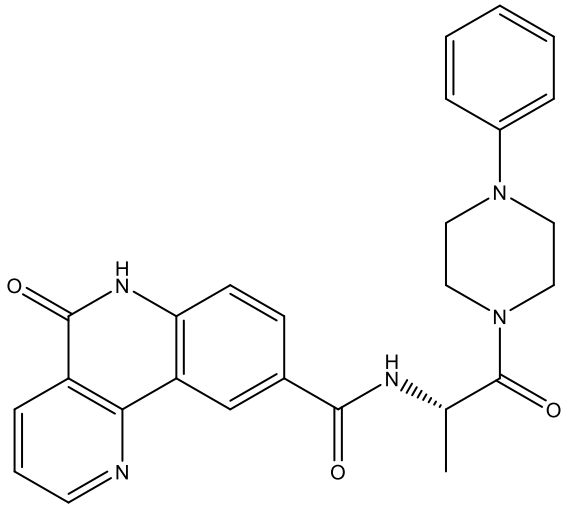

(*S*)-5-oxo-N-(1-oxo-1-(4-phenylpiperazin-1-yl)propan-2-yl)-5,6-dihydrobenzo[*h*][1,6]-naphthyridine-9-carboxamide (**e5**)

2-chloronicotinoyl chloride was reacted with 4-aminobenzoic acid according to the **Synthesis Method c** and the crude product was carried on to react with **f16** according to the **Synthesis Method d** as it cannot be completely purified. The final product was still unable to be purified thoroughly. Analysis with the MS suggested that the target product was synthesized.

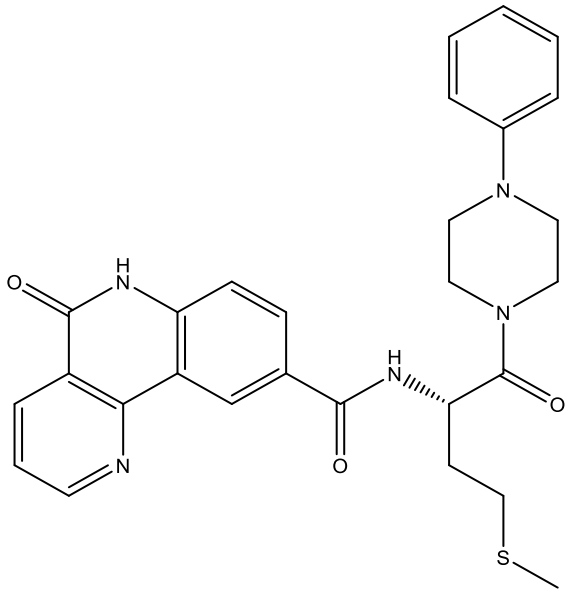

(*S*)-*N*-(4-(methylthio)-1-oxo-1-(4-phenylpiperazin-1-yl)butan-2-yl)-5-oxo-5,6-dihydrobenzo-[*h*][1,6]naphthyridine-9-carboxamide (**e6**)

2-chloronicotinoyl chloride was reacted with 4-aminobenzoic acid according to the **Synthesis Method c** and the crude product was carried on to react with **f20** according to the **Synthesis Method d** as it cannot be completely purified. The final product was still unable to be purified thoroughly. Analysis with the MS suggested that the target product was synthesized.

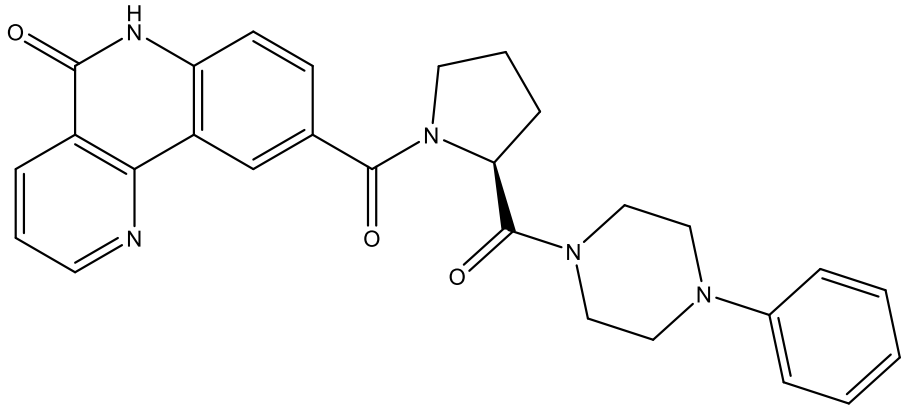

(*S*)-9-(2-(4-phenylpiperazine-1-carbonyl)pyrrolidine-1-carbonyl)benzo[*h*][1,6]-naphthyridin-5(6*H*)-one (**e7**)

2-chloronicotinoyl chloride was reacted with 4-aminobenzoic acid according to the **Synthesis Method c** and the crude product was carried on to react with **f19** according to the **Synthesis Method d** as it cannot be completely purified. The final product was still unable to be purified thoroughly. Analysis with the MS suggested that the target product was synthesized.

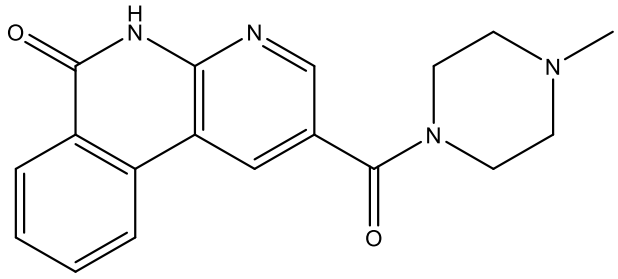

2-(4-methylpiperazine-1-carbonyl)benzo[*c*][1,8]naphthyridin-6(5*H*)-one (**e8**)

2-chlorobenzoyl chloride was reacted with 6-aminonicotinic acid according to the **Synthesis Method c** and the crude product was carried on to react with 1-methylpiperazine according to

the **Synthesis Method d** as it cannot be completely purified. The final product was still unable to be purified thoroughly. Analysis with the MS suggested that the target product was synthesized.

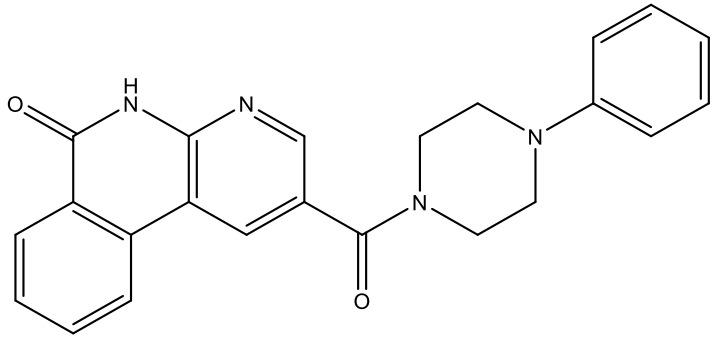

2-(4-phenylpiperazine-1-carbonyl)benzo[*c*][1,8]naphthyridin-6(5*H*)-one (**e9**)

2-chlorobenzoyl chloride was reacted with 6-aminonicotinic acid according to the **Synthesis Method c** and the crude product was carried on to react with 1-phenylpiperazine according to the **Synthesis Method d** as it cannot be completely purified. The final product was still unable to be purified thoroughly. Analysis with the MS suggested that the target product was synthesized.

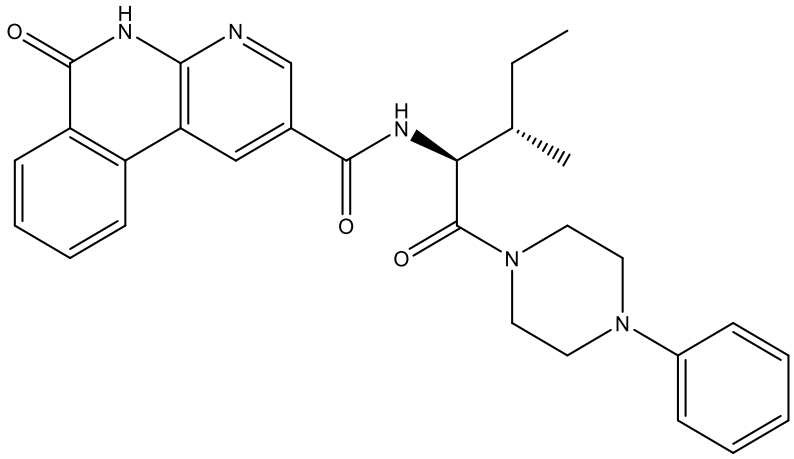

***N*-((2*S*,3*S*)-3-methyl-1-oxo-1-(4-phenylpiperazin-1-yl)pentan-2-yl)-6-oxo-5,6-dihydrobenzo-[*c*][1,8]naphthyridine-2-carboxamide** (**e10**)

2-chlorobenzoyl chloride was reacted with 6-aminonicotinic acid according to the **Synthesis Method c** and the crude product was carried on to react with **f17** according to the **Synthesis Method d** as it cannot be completely purified. The final product was still unable to be purified thoroughly. Analysis with the MS suggested that the target product was synthesized.

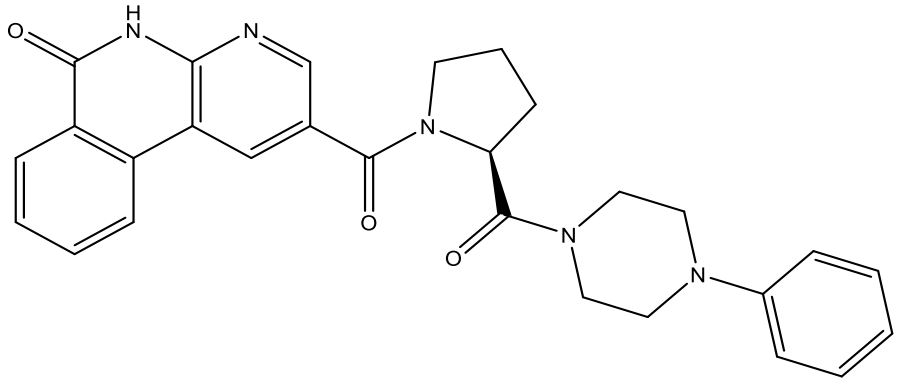

(*S*)-2-(2-(4-phenylpiperazine-1-carbonyl)pyrrolidine-1-carbonyl)benzo[*c*][1,8]-naphthyridin-6(5*H*)-one (**e11**)

2-chlorobenzoyl chloride was reacted with 6-aminonicotinic acid according to the **Synthesis Method c** and the crude product was carried on to react with **f19** according to the **Synthesis Method d** as it cannot be completely purified. The final product was still unable to be purified thoroughly. Analysis with the MS suggested that the target product was synthesized.

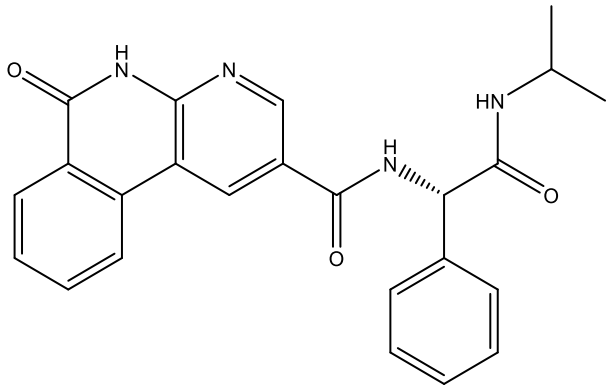

(*S*)-*N*-(2-(isopropylamino)-2-oxo-1-phenylethyl)-6-oxo-5,6-dihydrobenzo[*c*][1,8]-naphthyridine-2-carboxamide (**e12**)

2-chlorobenzoyl chloride was reacted with 6-aminonicotinic acid according to the **Synthesis Method c** and the crude product was carried on to react with (*S*)-*N*-isopropyl-2-(methylamino)-2-phenylacetamide according to the **Synthesis Method d** as it cannot be completely purified. (*S*)-*N*-isopropyl-2-(methylamino)-2-phenylacetamide was synthesized using **Synthesis Method d** with 25mg (0.1mmol) (*S*)-2-((tert-butoxycarbonyl)amino)-2-phenylacetic acid reacting with 6mg (0.1mmol) propan-2-amine, of which the crude product was deprotected using **Synthesis**

Method f. The final product was still unable to be purified thoroughly. Analysis with the MS suggested that the target product was synthesized.

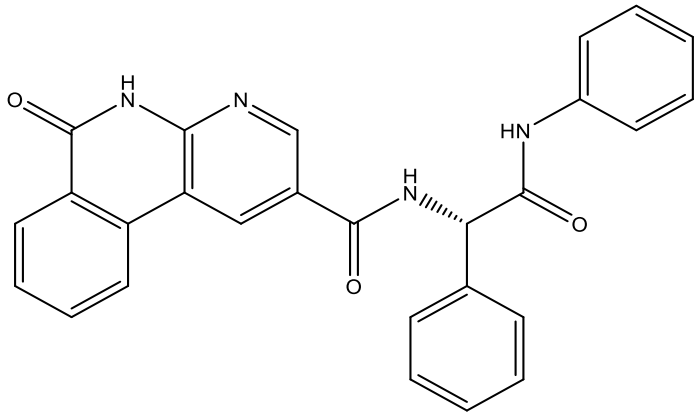

(*S*)-6-oxo-*N*-(2-oxo-1-phenyl-2-(phenylamino)ethyl)-5,6-dihydrobenzo[*c*][1,8]-naphthyridine-2-carboxamide (**e13**)

22-chlorobenzoyl chloride was reacted with 6-aminonicotinic acid according to the **Synthesis Method c** and the crude product was carried on to react with **f22** according to the **Synthesis Method d** as it cannot be completely purified. The final product was still unable to be purified thoroughly. Analysis with the MS suggested that the target product was synthesized.

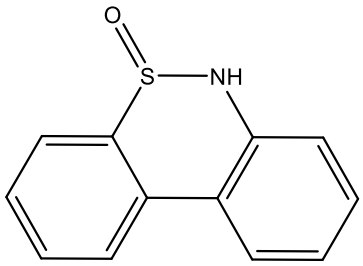

6*H*-dibenzo[*c*,*e*][1,2]thiazine 5-oxide (s1)

51mg (0.2mmol)2-bromobenzenesulfonyl chloride was reacted with 27.5 mg (0.2mmol) (2-aminophenyl)boronic acid according to the **Synthesis Method i & j** to give 12.3 mg **s1** (Yield: 29%) as white solid. ^{1}H NMR (300 MHz, Methanol-d_4) δ 8.27 (dd, *J* = 8.1, 1.2 Hz, 1H), 8.20 (dd, *J* = 8.0, 1.5 Hz, 1H), 7.85 (dd, *J* = 7.7, 1.4 Hz, 1H), 7.76 (td, *J* = 7.7, 1.4 Hz, 1H), 7.59 (td, *J* = 7.6, 1.2 Hz, 1H), 7.46 (td, *J* = 7.6, 1.4 Hz, 1H), 7.27 (td, *J* = 8.6, 1.3 Hz, 2H). ^{13}C NMR (75 MHz, MeOD) δ 135.5, 133.0, 131.9, 129.7, 127.9, 127.7, 126.7, 124.6, 124.3, 123.0, 120.6, 119.4. HRMS m/z (ESI+, M+Na): Calcd for C12H9NOS: 238.0303, (ESI+, M+Na) found: 238.0298

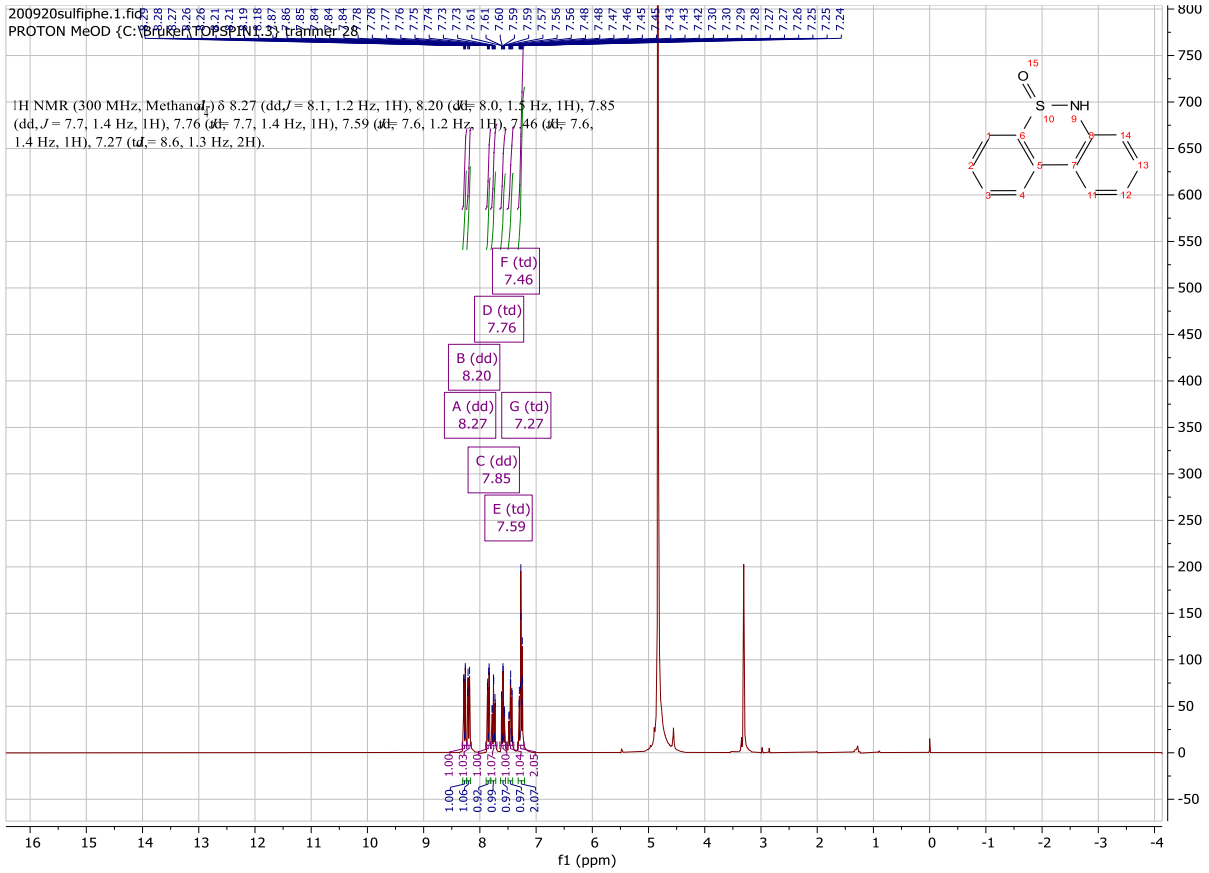
200920sulfiphe.1.fid
PROTON MeOD {C:\Bruker\TOPSPIN1.3} tranmer 28
1H NMR (300 MHz, Methanol-d4) δ 8.27 (dd, J = 8.1, 1.2 Hz, 1H), 8.20 (dd, J = 8.0, 1.5 Hz, 1H), 7.85 (dd, J = 7.7, 1.4 Hz, 1H), 7.76 (td, J = 7.7, 1.4 Hz, 1H), 7.59 (td, J = 7.6, 1.2 Hz, 1H), 7.46 (td, J = 7.6, 1.4 Hz, 1H), 7.27 (td, J = 8.6, 1.3 Hz, 2H).
F (td) 7.46
D (td) 7.76
B (dd) 8.20
A (dd) 8.27
G (td) 7.27
C (dd) 7.85
E (td) 7.59
f1 (ppm)

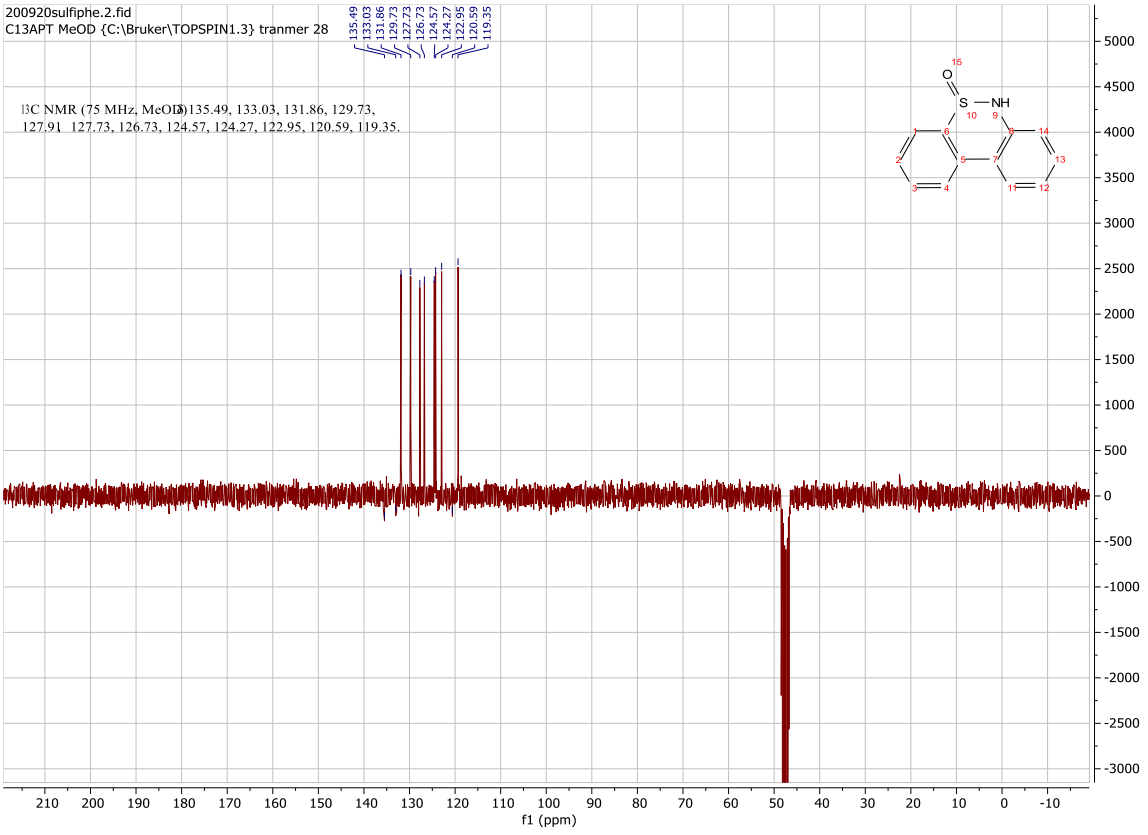
200920sulfiphe.2.fid
C13APT MeOD {C:\Bruker\TOPSPIN1.3} tranmer 28
13C NMR (75 MHz, MeOD) δ 135.49, 133.03, 131.86, 129.73, 127.91, 127.73, 126.73, 124.57, 124.27, 122.95, 120.59, 119.35.
f1 (ppm)

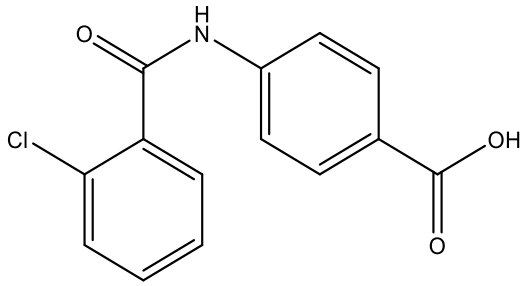

4-(2-chlorobenzamido)benzoic acid (f1)

1.8g (10mmol) 2-chlorobenzoyl chloride was reacted with 1.38g (10mmol) 4-aminobenzoic acid according to the **Synthesis Method a** to give 2.55g **f1** (Yield: 93%) as white solid. ^{1}H NMR (300 MHz, DMSO-d_6) δ 12.73 (s, 1H), 10.81 (s, 1H), 7.97 – 7.91 (m, 2H), 7.84 (d, J = 8.6 Hz, 2H), 7.64 – 7.59 (m, 1H), 7.56 (dd, J = 5.9, 1.8 Hz, 1H), 7.54 – 7.42 (m, 2H). ^{13}C NMR (75 MHz, DMSO) δ 167.4, 165.8, 143.3, 137.1, 131.8, 130.9, 130.4, 130.2, 129.4, 127.8, 126.3, 119.4.

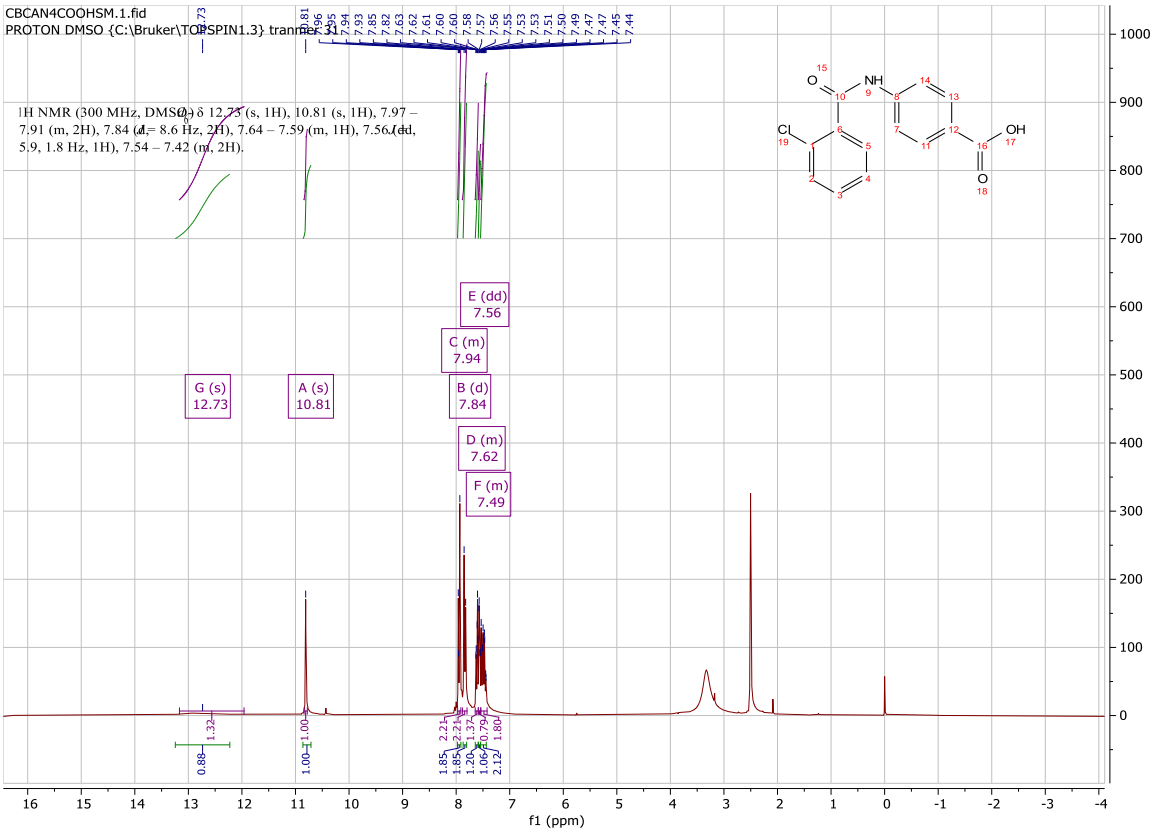
CBCAN4COOHSM.1.fid
PROTON DMSO {C:\Bruker\TOPSPIN1.3} tranner 31
1H NMR (300 MHz, DMSO) δ 12.73 (s, 1H), 10.81 (s, 1H), 7.97 – 7.91 (m, 2H), 7.84 (d, J = 8.6 Hz, 2H), 7.64 – 7.59 (m, 1H), 7.56 (dd, 5.9, 1.8 Hz, 1H), 7.54 – 7.42 (m, 2H).
G (s) 12.73
A (s) 10.81
B (d) 7.84
C (m) 7.94
D (m) 7.62
E (dd) 7.56
F (m) 7.49
f1 (ppm)

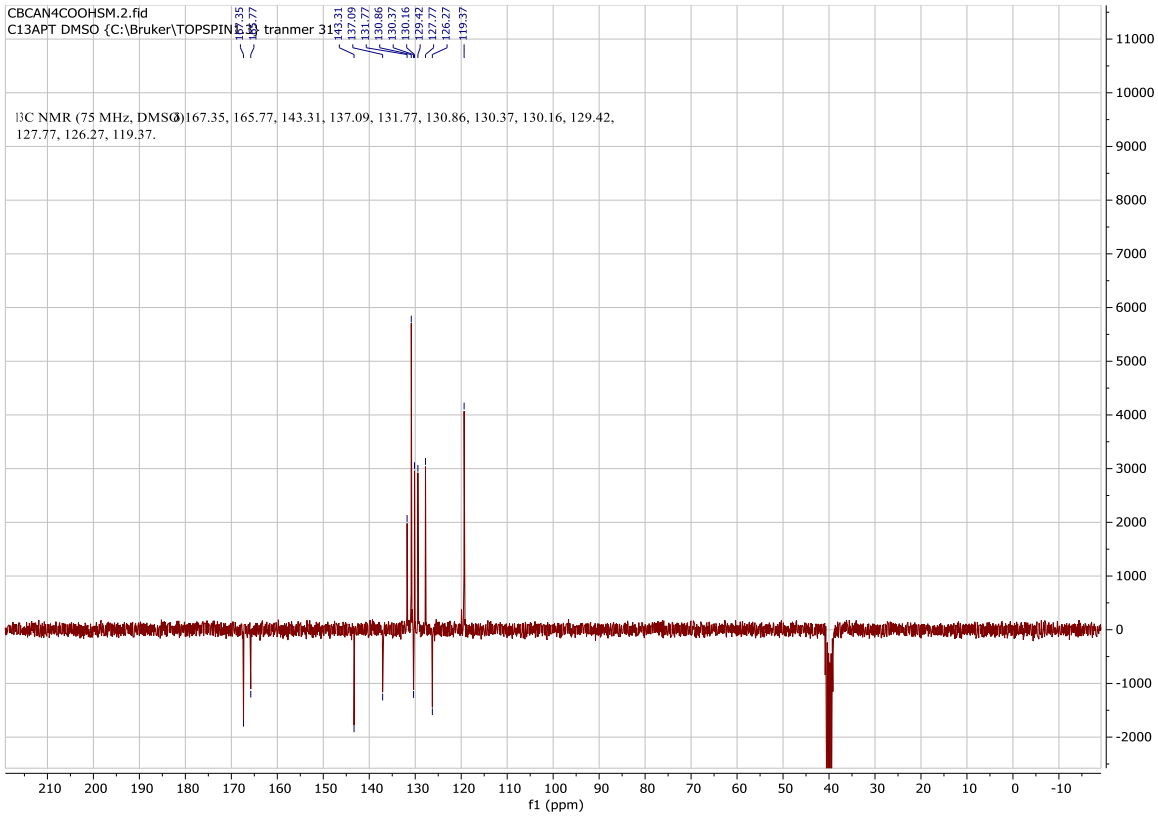
CBCAN4COOHSM.2.fid
C13APT DMSO {C:\Bruker\TOPSPIN1.3} tranner 31
13C NMR (75 MHz, DMSO) δ 167.35, 165.77, 143.31, 137.09, 131.77, 130.86, 130.37, 130.16, 129.42, 127.77, 126.27, 119.37.
f1 (ppm)

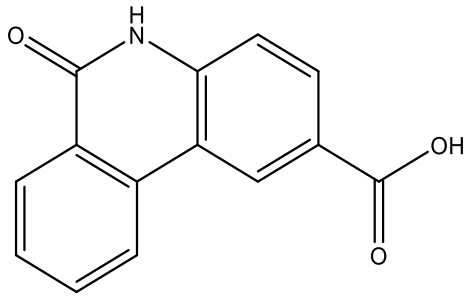

6-oxo-5,6-dihydrophenanthridine-2-carboxylic acid (f2)

278mg (1mmol) **f1** was reacted according to the **Synthesis Method b** to give 178.2mg **f2** (Yield: 74%) as yellow solid. ^{1}H NMR (300 MHz, DMF-d_7) δ 13.33 (s, 1H), 12.39 (s, 1H), 9.30 (d, J = 1.8 Hz, 1H), 8.96 (d, J = 8.2 Hz, 1H), 8.75 (dd, J = 7.9, 1.4 Hz, 1H), 8.46 (dd, J = 8.5, 1.8 Hz, 1H), 8.31 (td, J = 8.2, 7.7, 1.5 Hz, 1H), 8.11 (t, J = 7.5 Hz, 1H), 7.86 (d, J = 8.5 Hz, 1H). ^{13}C NMR (75 MHz, DMF) δ 167.9, 161.9, 140.7, 134.6, 134.1, 131.2, 129.4, 128.4, 126.6, 125.7, 125.5, 123.6, 118.1, 117.2.

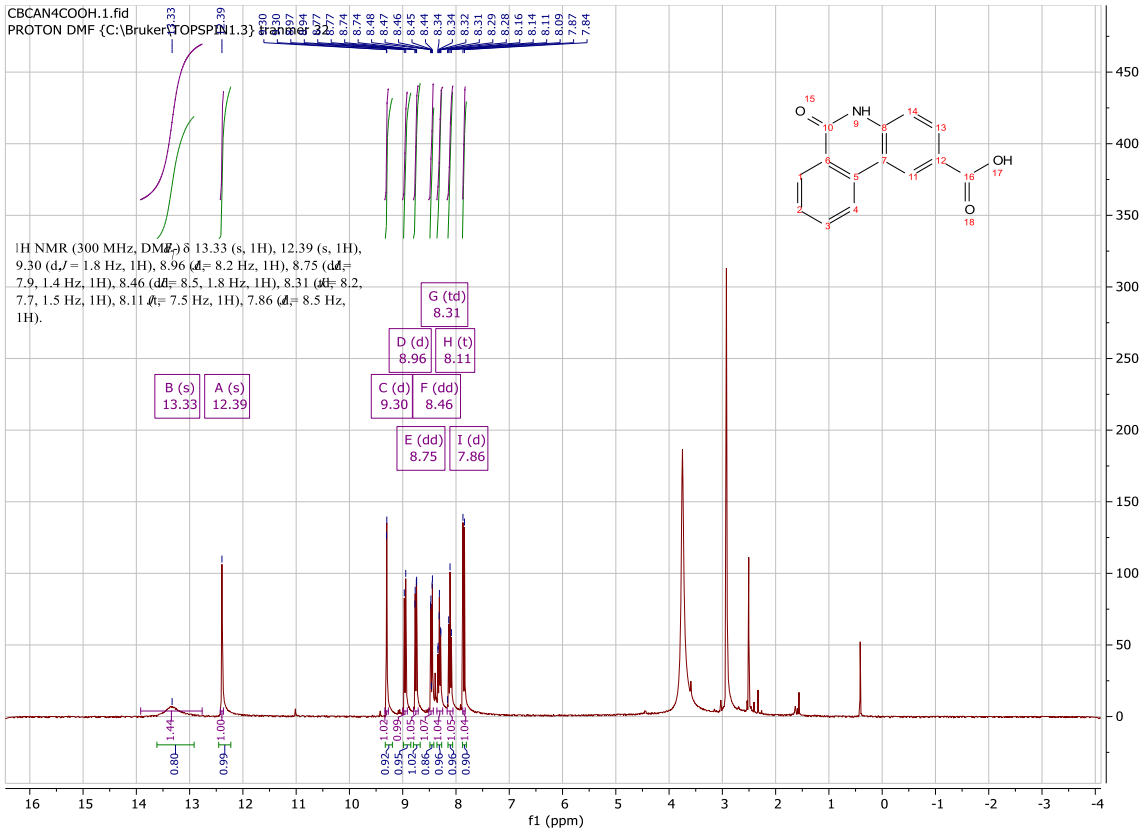
CBCAN4COOH.1.fid
PROTON DMF {C:\Bruker\TOPSPIN1.3} tranmer 32
1H NMR (300 MHz, DMF) δ 13.33 (s, 1H), 12.39 (s, 1H), 9.30 (d, J = 1.8 Hz, 1H), 8.96 (d, J = 8.2 Hz, 1H), 8.75 (dd, J = 7.9, 1.4 Hz, 1H), 8.46 (dd, J = 8.5, 1.8 Hz, 1H), 8.31 (td, J = 8.2, 7.7, 1.5 Hz, 1H), 8.11 (t, J = 7.5 Hz, 1H), 7.86 (d, J = 8.5 Hz, 1H).
B (s) 13.33
A (s) 12.39
C (d) 9.30
F (dd) 8.46
D (d) 8.96
H (t) 8.11
G (td) 8.31
E (dd) 8.75
I (d) 7.86
f1 (ppm)

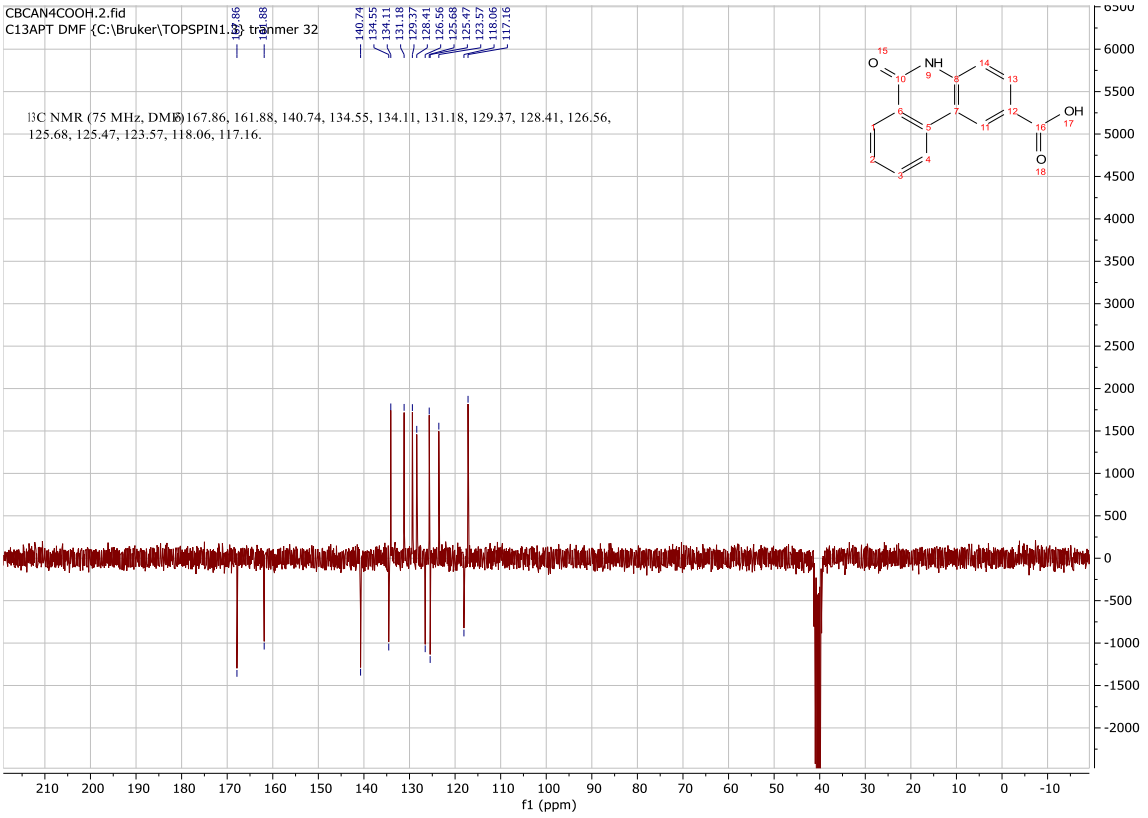
CBCAN4COOH.2.fid
C13APT DMF {C:\Bruker\TOPSPIN1.3} tranmer 32
13C NMR (75 MHz, DMF) δ 167.86, 161.88, 140.74, 134.55, 134.11, 131.18, 129.37, 128.41, 126.56, 125.68, 125.47, 123.57, 118.06, 117.16.
f1 (ppm)

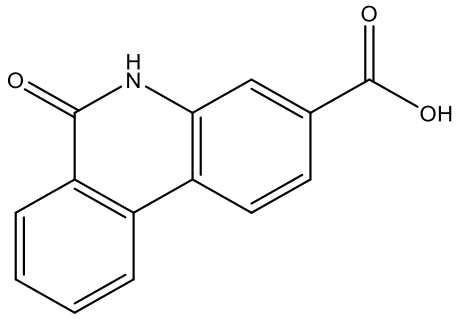

6-oxo-5,6-dihydrophenanthridine-3-carboxylic acid (f3)

142mg (1mmol) benzoyl chloride was reacted with 171mg (1mmol) 3-amino-4-chlorobenzoic acid according to the **Synthesis Method c** to give 102.8mg **f3** (Yield: 43%) as yellow solid. ^{1}H NMR (300 MHz, DMSO-d_6) δ 13.15 (s, 1H) 11.86 (s, 1H), 8.57 (d, J = 8.2 Hz, 1H), 8.51 (d, J = 8.5 Hz, 1H), 8.36 (dd, J = 8.0, 1.4 Hz, 1H), 8.00 (d, J = 1.7 Hz, 1H), 7.91 (td, J = 8.2, 7.7, 1.5 Hz, 1H), 7.79 (dd, J = 8.4, 1.7 Hz, 1H), 7.73 (t, J = 7.5 Hz, 1H). ^{13}C NMR (75 MHz, DMSO) δ 167.2, 161.2, 136.9, 133.9, 133.5, 131.8, 129.5, 128.0, 126.8, 124.1, 123.8, 123.0, 121.5, 117.7. MS m/z (ESI+, M+Na): Calcd for C14H9NO3: 514.64, (ESI+, M+Na) found: 537.19

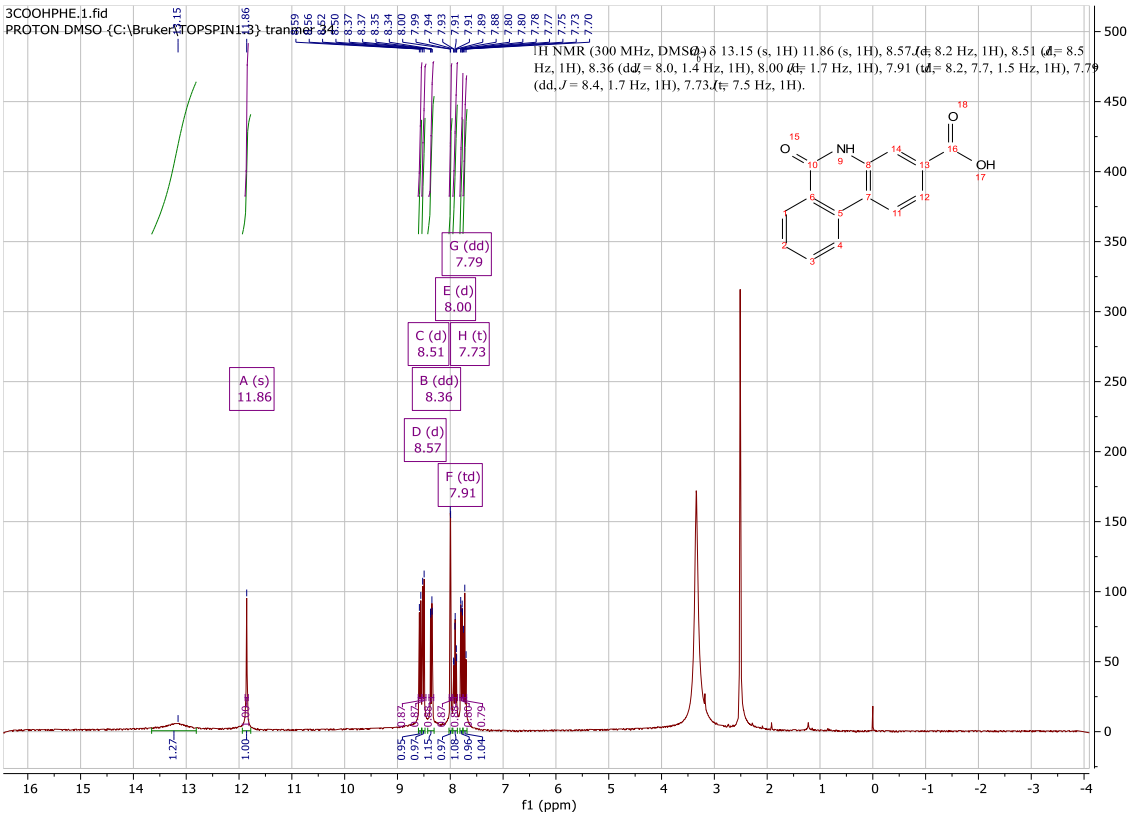
3COOHPHE.1.fid
PROTON DMSO {C:\Bruker\TOPSPIN1.3} tranmer 34
1H NMR (300 MHz, DMSO) δ 13.15 (s, 1H) 11.86 (s, 1H), 8.57 (d, J = 8.2 Hz, 1H), 8.51 (d, J = 8.5 Hz, 1H), 8.36 (dd, J = 8.0, 1.4 Hz, 1H), 8.00 (d, J = 1.7 Hz, 1H), 7.91 (td, J = 8.2, 7.7, 1.5 Hz, 1H), 7.79 (dd, J = 8.4, 1.7 Hz, 1H), 7.73 (t, J = 7.5 Hz, 1H).
G (dd) 7.79
E (d) 8.00
C (d) 8.51
H (t) 7.73
A (s) 11.86
B (dd) 8.36
D (d) 8.57
F (td) 7.91
f1 (ppm)

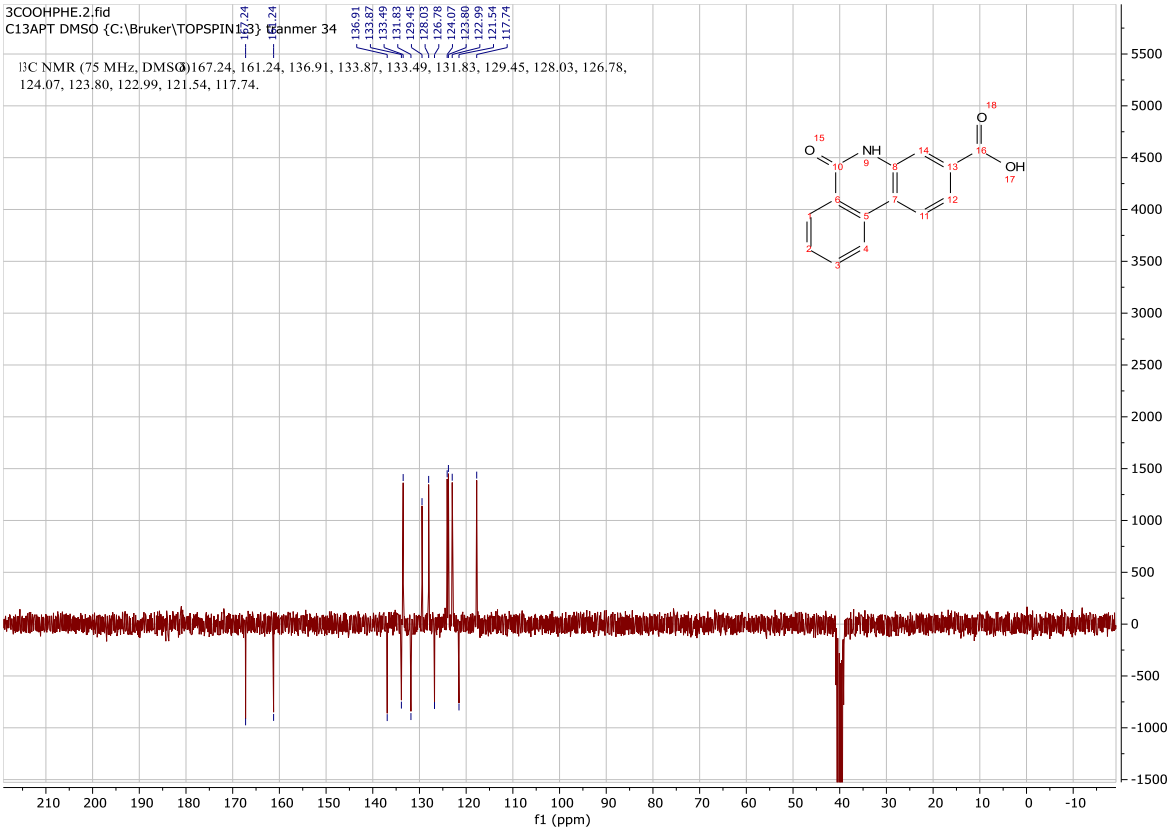
3COOHPHE.2.fid
C13APT DMSO {C:\Bruker\TOPSPIN1.3} tranmer 34
13C NMR (75 MHz, DMSO) δ 167.24, 161.24, 136.91, 133.87, 133.49, 131.83, 129.45, 128.03, 126.78, 124.07, 123.80, 122.99, 121.54, 117.74.
f1 (ppm)

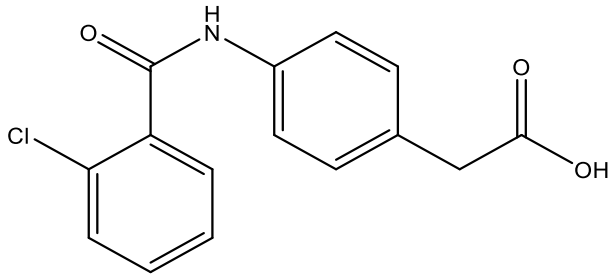

2-(4-(2-chlorobenzamido)phenyl)acetic acid (f4)

177mg (1mmol) 2-chlorobenzoyl chloride was reacted with 151mg (1mmol) 2-(4-aminophenyl)acetic acid according to the **Synthesis Method a** to give 260mg **f4** (Yield: 90%) as white solid. ^{1}H NMR (300 MHz, DMSO-d_6) δ 10.46 (s, 1H), 7.68 – 7.62 (m, 2H), 7.57 (dt, J = 7.6, 2.2 Hz, 2H), 7.48 (dtd, J = 16.0, 7.2, 1.8 Hz, 3H), 7.27 – 7.19 (m, 2H), 3.53 (s, 2H). ^{13}C NMR (75 MHz, DMSO) δ 173.2, 165.3, 137.9, 137.5, 131.5, 131.0, 130.4, 130.1, 130.1, 129.4, 127.7, 120.0, 40.6.

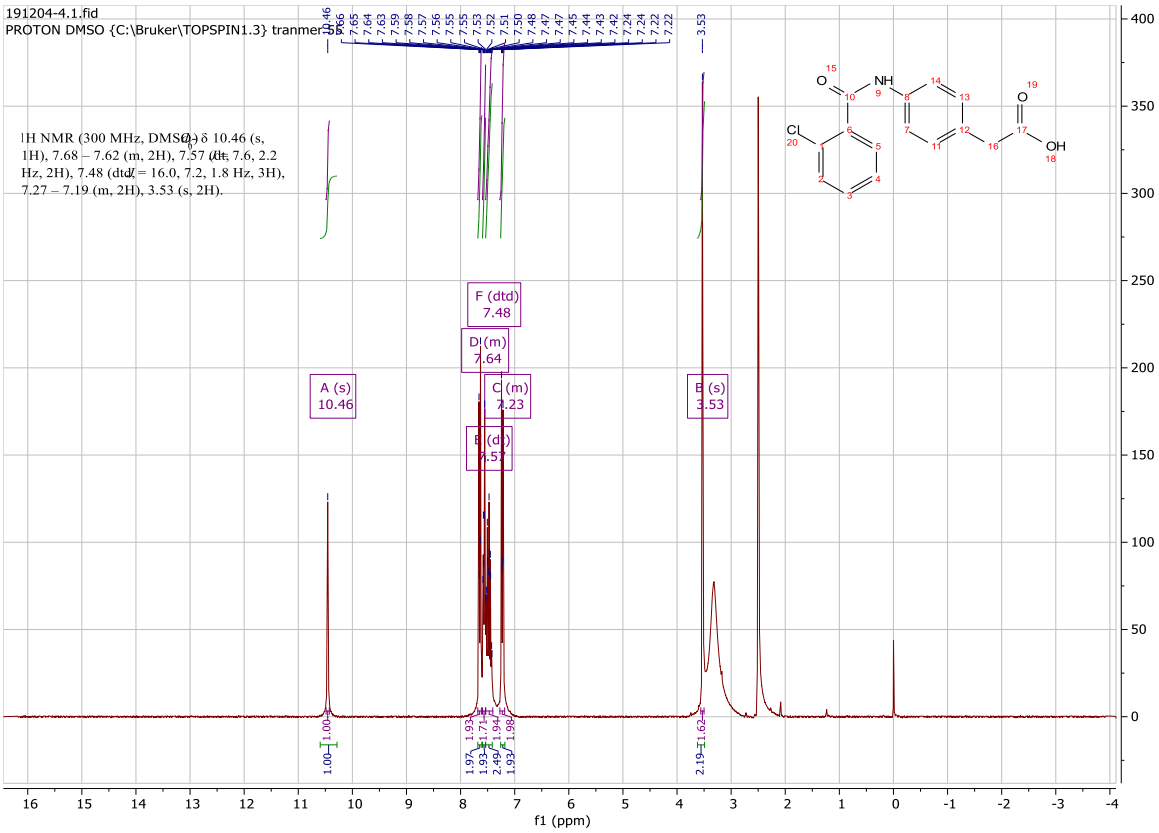
191204-4.1.fid
PROTON DMSO {C:\Bruker\TOPSPIN1.3} tranmer 55
1H NMR (300 MHz, DMSO) δ 10.46 (s, 1H), 7.68 – 7.62 (m, 2H), 7.57 (dt, J = 7.6, 2.2 Hz, 2H), 7.48 (dtd, J = 16.0, 7.2, 1.8 Hz, 3H), 7.27 – 7.19 (m, 2H), 3.53 (s, 2H).
A (s) 10.46
B (s) 3.53
C (m) 7.23
D (m) 7.64
E (dt) 7.52
F (dtd) 7.48
f1 (ppm)

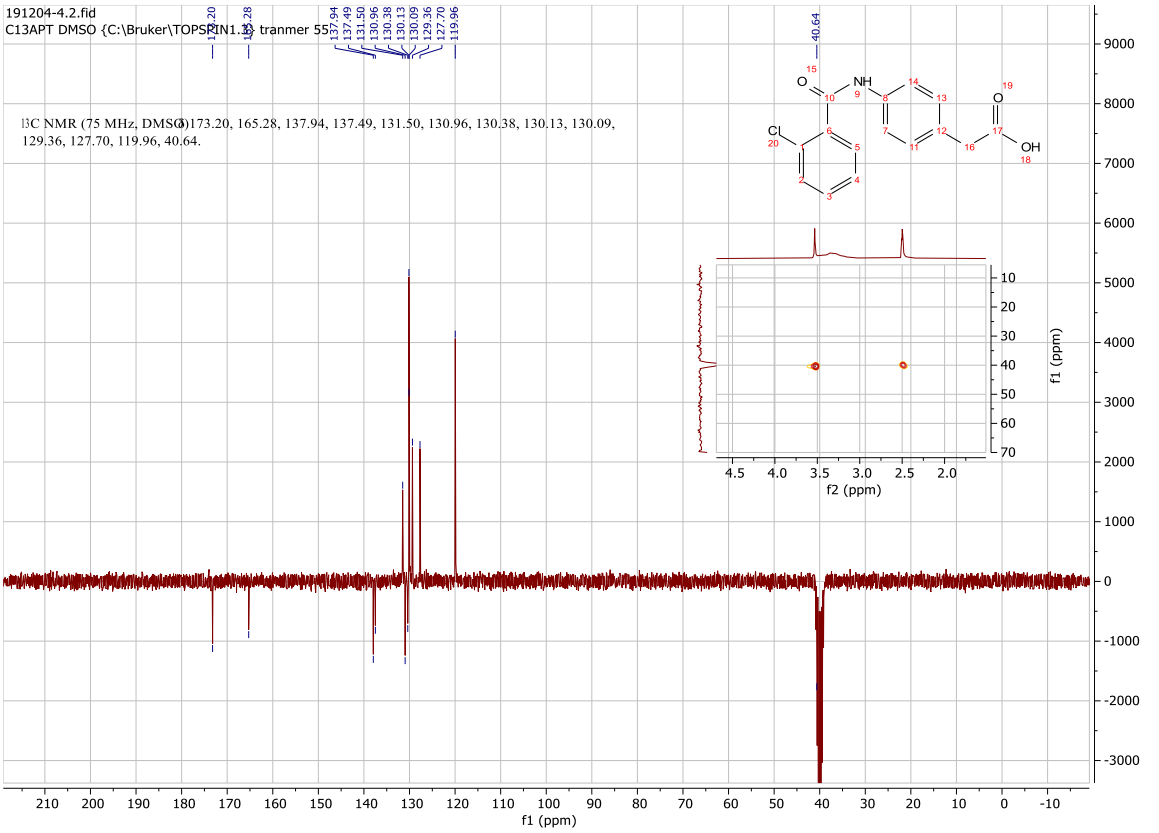
191204-4.2.fid
C13APT DMSO {C:\Bruker\TOPSPIN1.3} tranmer 55
13C NMR (75 MHz, DMSO) 173.20, 165.28, 137.94, 137.49, 131.50, 130.96, 130.38, 130.13, 130.09, 129.36, 127.70, 119.96, 40.64.
f1 (ppm)
f2 (ppm)

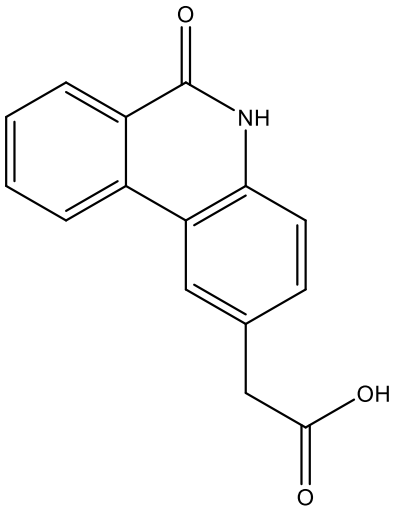

2-(6-oxo-5,6-dihydrophenanthridin-2-yl)acetic acid (f5)

145mg (0.5mmol) **f4** was reacted according to the **Synthesis Method b** to give 96.1mg **f5** (Yield: 76%) as yellow solid. ^{1}H NMR (300 MHz, DMSO-d_6) δ 11.65 (s, 1H), 8.47 (d, J = 8.2 Hz, 1H), 8.32 (dd, J = 7.9, 1.4 Hz, 1H), 8.27 (d, J = 1.7 Hz, 1H), 7.91 – 7.80 (m, 1H), 7.64 (t, J = 7.5 Hz, 1H), 7.39 (dd, J = 8.3, 1.7 Hz, 1H), 7.31 (d, J = 8.3 Hz, 1H), 3.69 (s, 2H). ^{13}C NMR (75 MHz, DMSO) δ 173.4, 161.2, 135.7, 134.6, 133.2, 131.4, 129.7, 128.3, 128.0, 126.2, 124.4, 122.9, 117.8, 116.5, 41.9.

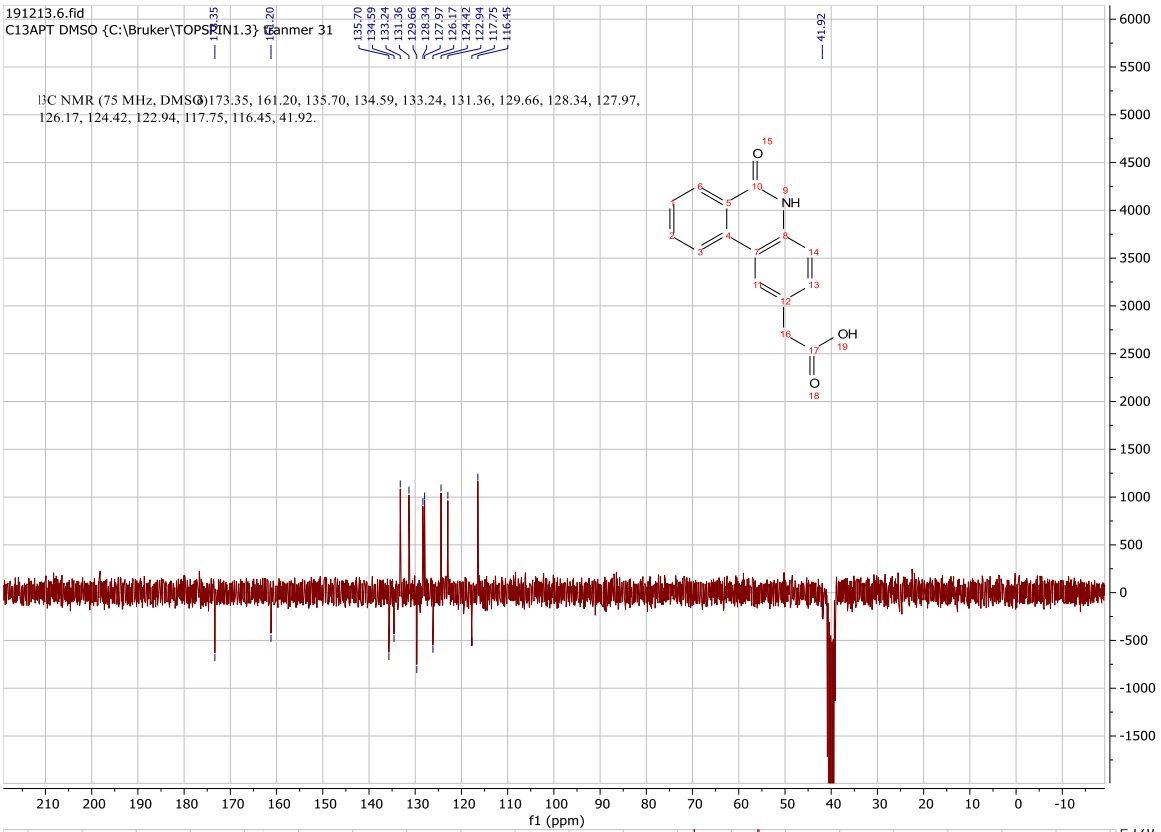
191213.6.fid
C13APT DMSO {C:\Bruker\TOPSPIN1.3} tranmer 31
173.35
161.20
135.70
134.59
133.24
131.36
129.66
128.34
127.97
126.17
124.42
122.94
117.75
116.45
41.92
13C NMR (75 MHz, DMSO) δ 173.35, 161.20, 135.70, 134.59, 133.24, 131.36, 129.66, 128.34, 127.97, 126.17, 124.42, 122.94, 117.75, 116.45, 41.92.
O
NH
OH
f1 (ppm)

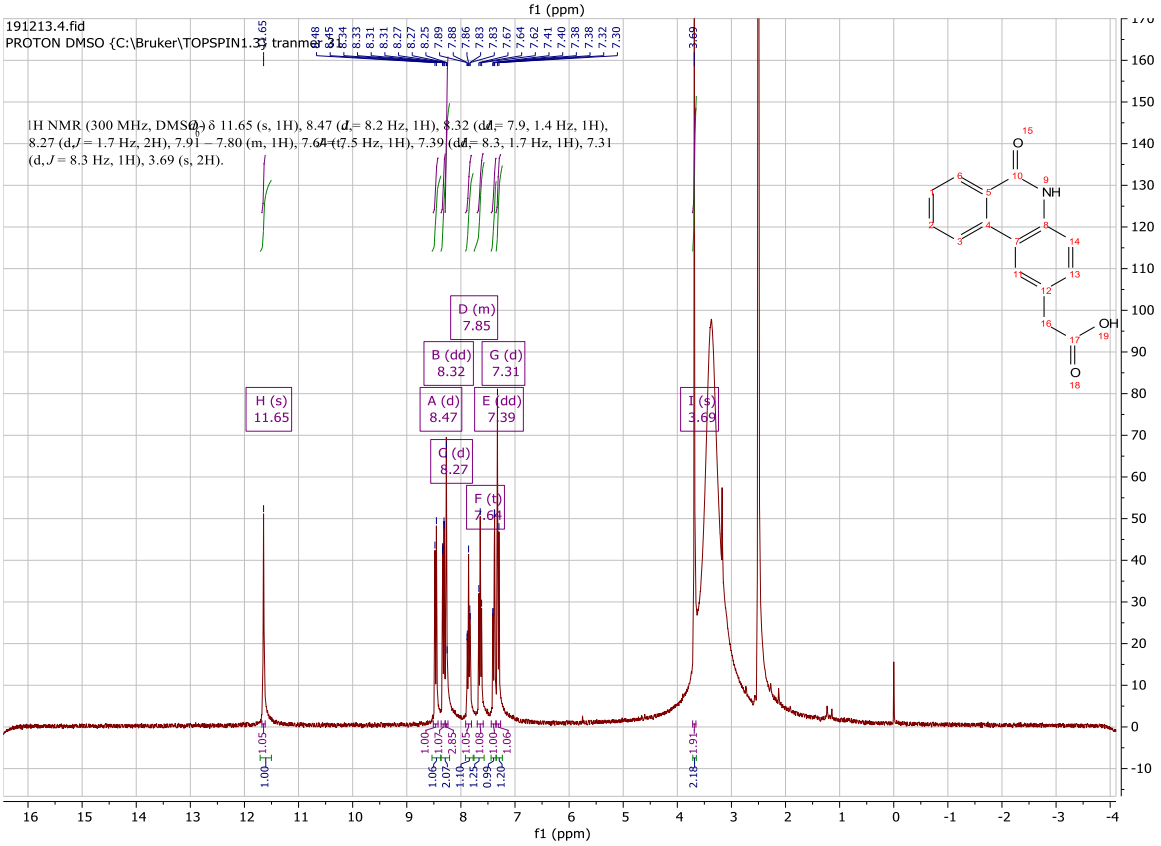
191213.4.fid
PROTON DMSO {C:\Bruker\TOPSPIN1.3} tranmer 31
11.65
8.48
8.47
8.34
8.33
8.31
8.27
8.25
7.89
7.88
7.86
7.83
7.67
7.64
7.62
7.41
7.40
7.38
7.32
7.30
3.69
1H NMR (300 MHz, DMSO) δ 11.65 (s, 1H), 8.47 (d, J = 8.2 Hz, 1H), 8.32 (dd, J = 7.9, 1.4 Hz, 1H), 8.27 (d, J = 1.7 Hz, 2H), 7.91 – 7.80 (m, 1H), 7.64 (t, J = 7.5 Hz, 1H), 7.39 (dd, J = 8.3, 1.7 Hz, 1H), 7.31 (d, J = 8.3 Hz, 1H), 3.69 (s, 2H).
D (m) 7.85
B (dd) 8.32
G (d) 7.31
H (s) 11.65
A (d) 8.47
E (dd) 7.39
I (s) 3.69
C (d) 8.27
F (t) 7.68
O
NH
OH
f1 (ppm)

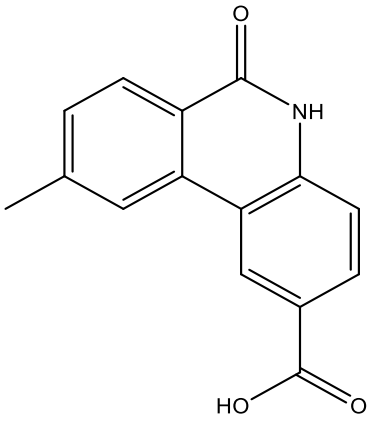

9-methyl-6-oxo-5,6-dihydrophenanthridine-2-carboxylic acid (f6)

154mg (1mmol) 4-methylbenzoyl chloride was reacted with 137mg (1mmol) 34-aminobenzoic acid according to the **Synthesis Method c** to give 164.5mg **f6** (Yield: 65%) as yellow solid. ^{1}H NMR (400 MHz, DMSO-d_6) δ 12.95 (s, 1H), 11.87 (s, 1H), 8.88 (d, J = 2.0 Hz, 1H), 8.35 (d, J = 4.5 Hz, 1H), 8.21 (dd, J = 8.2, 2.2 Hz, 1H), 8.02 (dd, J = 8.5, 1.7 Hz, 1H), 7.50 (d, J = 8.1 Hz, 1H), 7.41 (d, J = 8.5 Hz, 1H), 2.51 (p, J = 1.9 Hz, 3H). ^{13}C NMR (101 MHz, DMSO) δ 167.5, 161.5, 144.1, 140.5, 134.1, 130.6, 130.2, 128.0, 125.3, 124.9, 123.8, 123.0, 117.6, 116.7, 21.9.

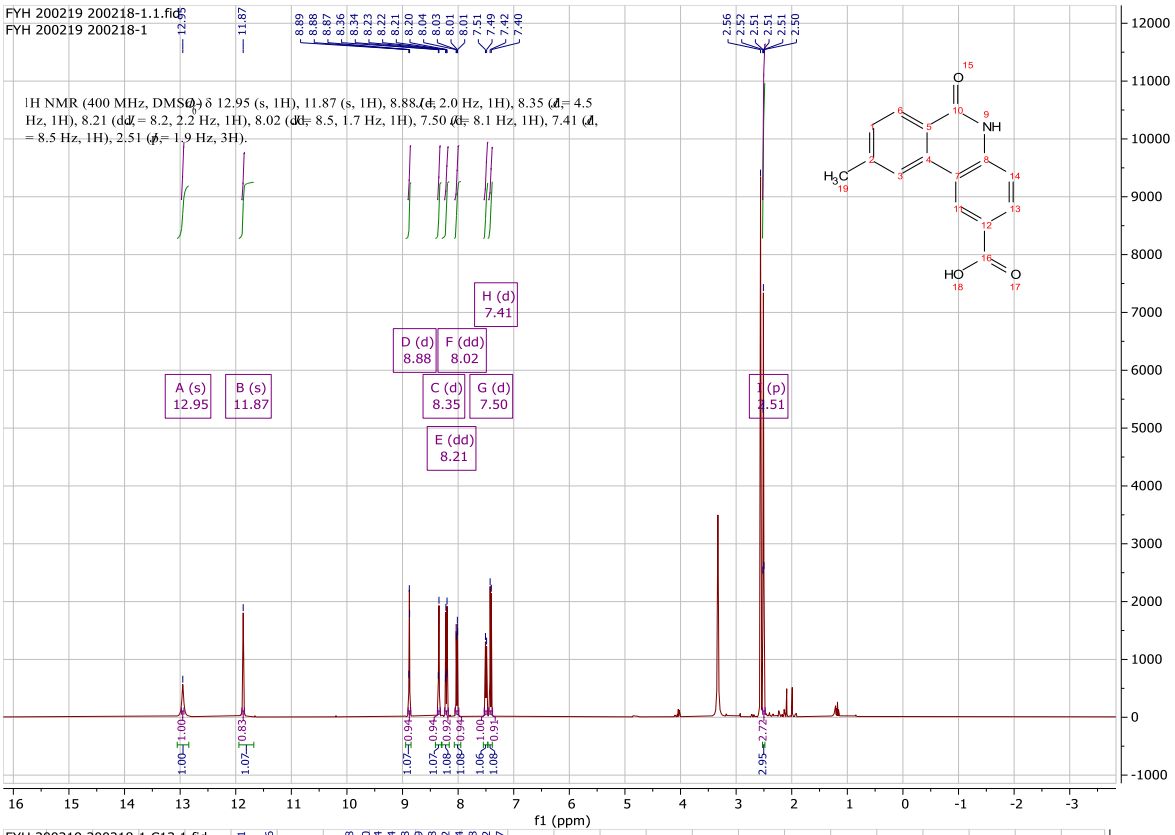
FYH 200219 200218-1.1.fid
FYH 200219 200218-1
12.95
11.87
8.89
8.88
8.87
8.36
8.34
8.23
8.22
8.21
8.20
8.04
8.03
8.01
8.01
7.51
7.49
7.42
7.40
2.56
2.52
2.51
2.51
2.51
2.50
1H NMR (400 MHz, DMSO) δ 12.95 (s, 1H), 11.87 (s, 1H), 8.88 (d, J = 2.0 Hz, 1H), 8.35 (d, J = 4.5 Hz, 1H), 8.21 (dd, J = 8.2, 2.2 Hz, 1H), 8.02 (dd, J = 8.5, 1.7 Hz, 1H), 7.50 (d, J = 8.1 Hz, 1H), 7.41 (d, J = 8.5 Hz, 1H), 2.51 (p, J = 1.9 Hz, 3H).
A (s) 12.95
B (s) 11.87
C (d) 8.35
D (d) 8.88
E (dd) 8.21
F (dd) 8.02
G (d) 7.50
H (d) 7.41
I (p) 2.51
f1 (ppm)

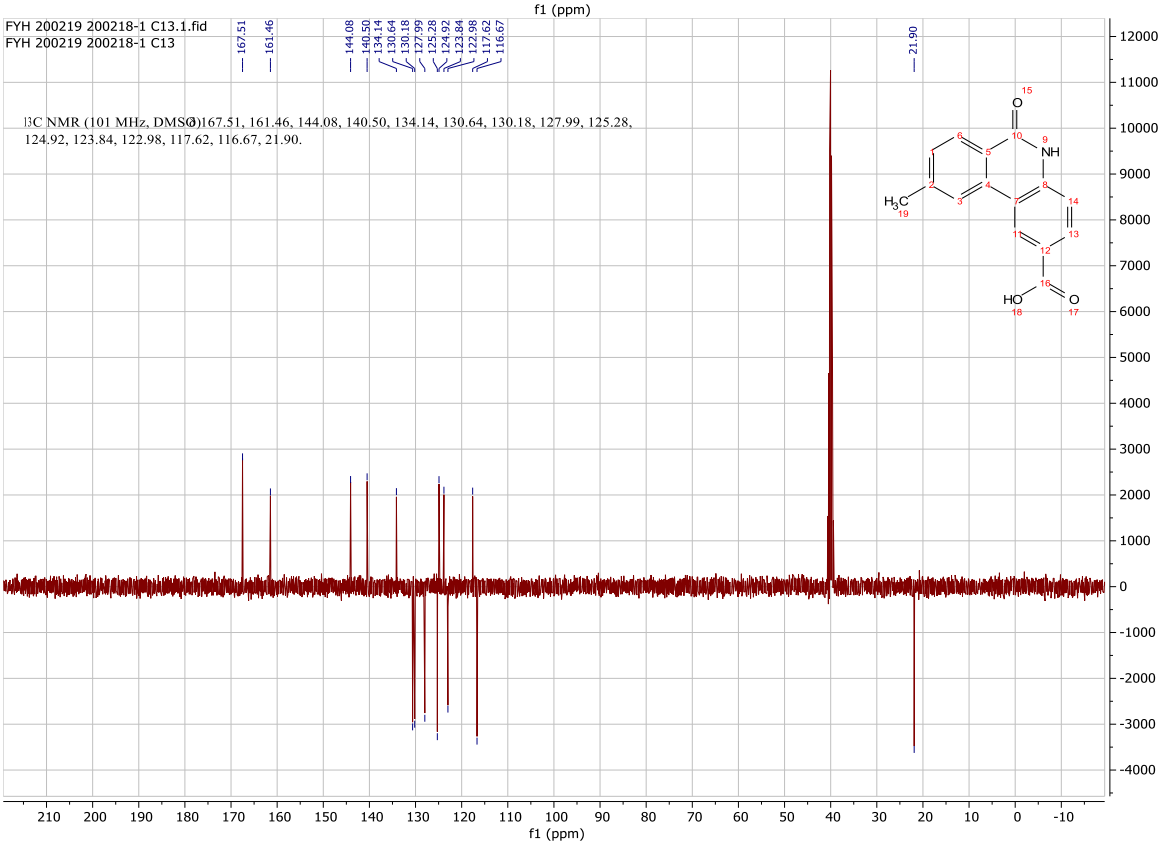
FYH 200219 200218-1 C13.1.fid
FYH 200219 200218-1 C13
167.51
161.46
144.08
140.50
134.14
130.64
130.18
127.99
125.28
124.92
123.84
122.98
117.62
116.67
21.90
13C NMR (101 MHz, DMSO) 167.51, 161.46, 144.08, 140.50, 134.14, 130.64, 130.18, 127.99, 125.28, 124.92, 123.84, 122.98, 117.62, 116.67, 21.90.
f1 (ppm)

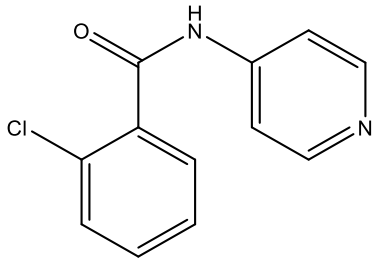

2-chloro-*N*-(pyridin-4-yl)benzamide (f7)

177mg (1mmol) 2-chlorobenzoyl chloride was reacted with 94mg (1mmol) pyridin-4-amineaccording to the **Synthesis Method a** to give 174.2mg **f7** (Yield: 75%) as white solid. ^{1}H NMR (300 MHz, DMSO-d_6) δ 10.93 (s, 1H), 8.49 (d, J = 5.4 Hz, 2H), 7.69 (d, J = 5.1 Hz, 2H), 7.66 – 7.43 (m, 4H). ^{13}C NMR (75 MHz, DMSO) δ 166.4, 151.0, 145.9, 136.6, 132.0, 130.3, 130.2, 129.4, 127.8, 114.0.

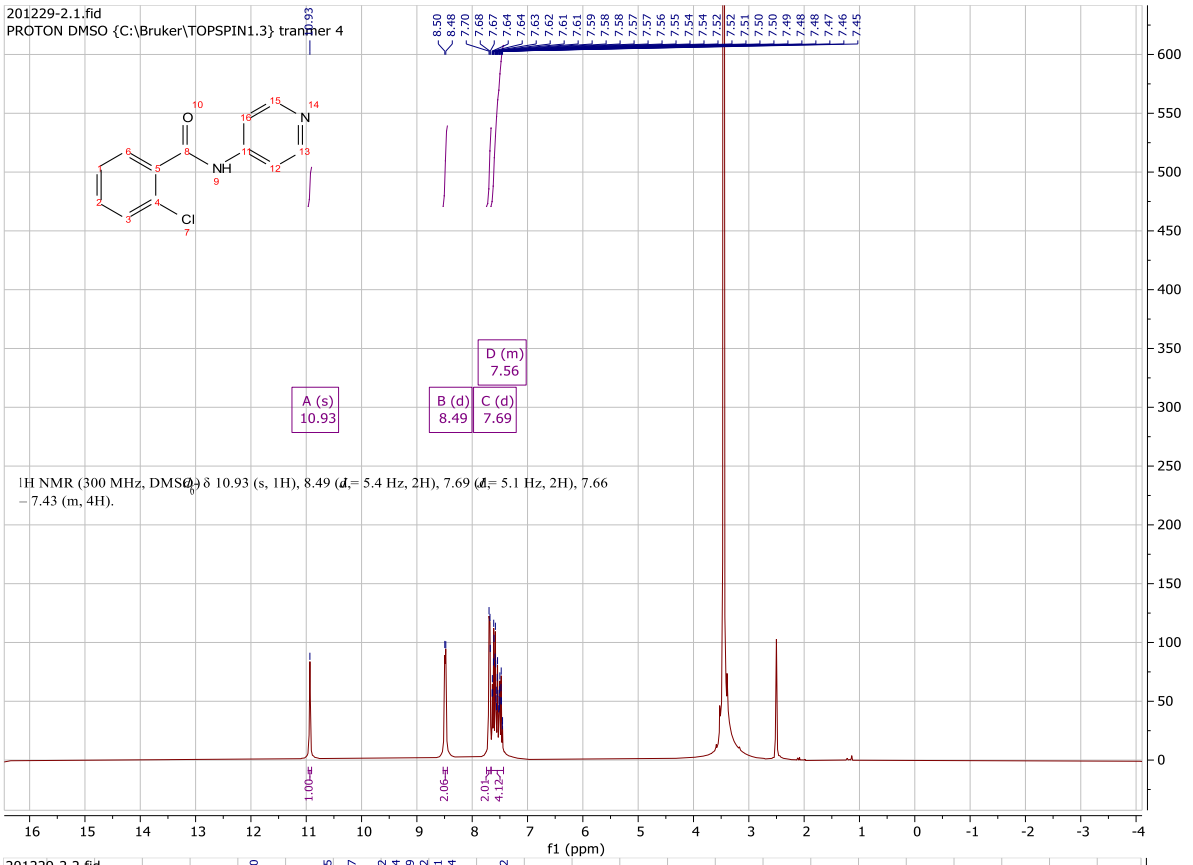

^{1}H NMR (300 MHz, DMSO-d_6) δ 10.93 (s, 1H), 8.49 (*d*, = 5.4 Hz, 2H), 7.69 (*d*, = 5.1 Hz, 2H), 7.66 – 7.43 (m, 4H).

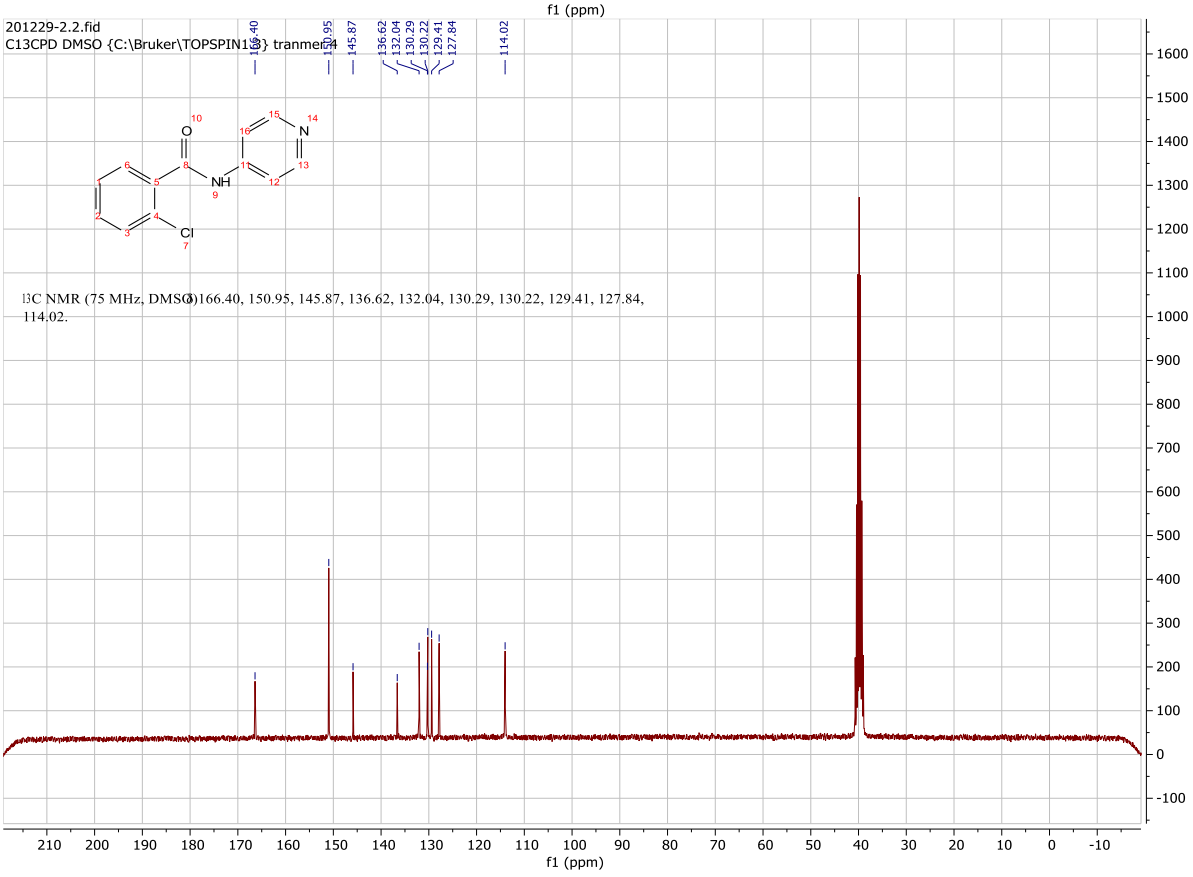

^{13}C NMR (75 MHz, DMSO-d_6) 166.40, 150.95, 145.87, 136.62, 132.04, 130.29, 130.22, 129.41, 127.84, 114.02.

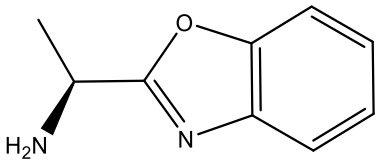

(*S*)-1-(benzo[d]oxazol-2-yl)ethan-1-amine (f8)

According to the **Synthesis Method g**, 140.3mg (0.5mmol) **f9** was converted into Boc-protected **f8**, followed by the **Synthesis Method f** to give unprotected 41.8mg **f8** (Yield: 52%) as orange glue-like product. ^{1}H NMR (300 MHz, DMSO-d_6) δ 8.83 (s, 2H), 7.87 – 7.75 (m, 2H), 7.54 – 7.39 (m, 2H), 4.90 (q, J = 6.6 Hz, 1H), 1.67 (d, J = 6.9 Hz, 3H).^{13}C NMR (75 MHz, DMSO) δ 163.7, 150.6, 140.3, 126.5, 125.6, 120.4, 111.6, 44.7, 17.5.

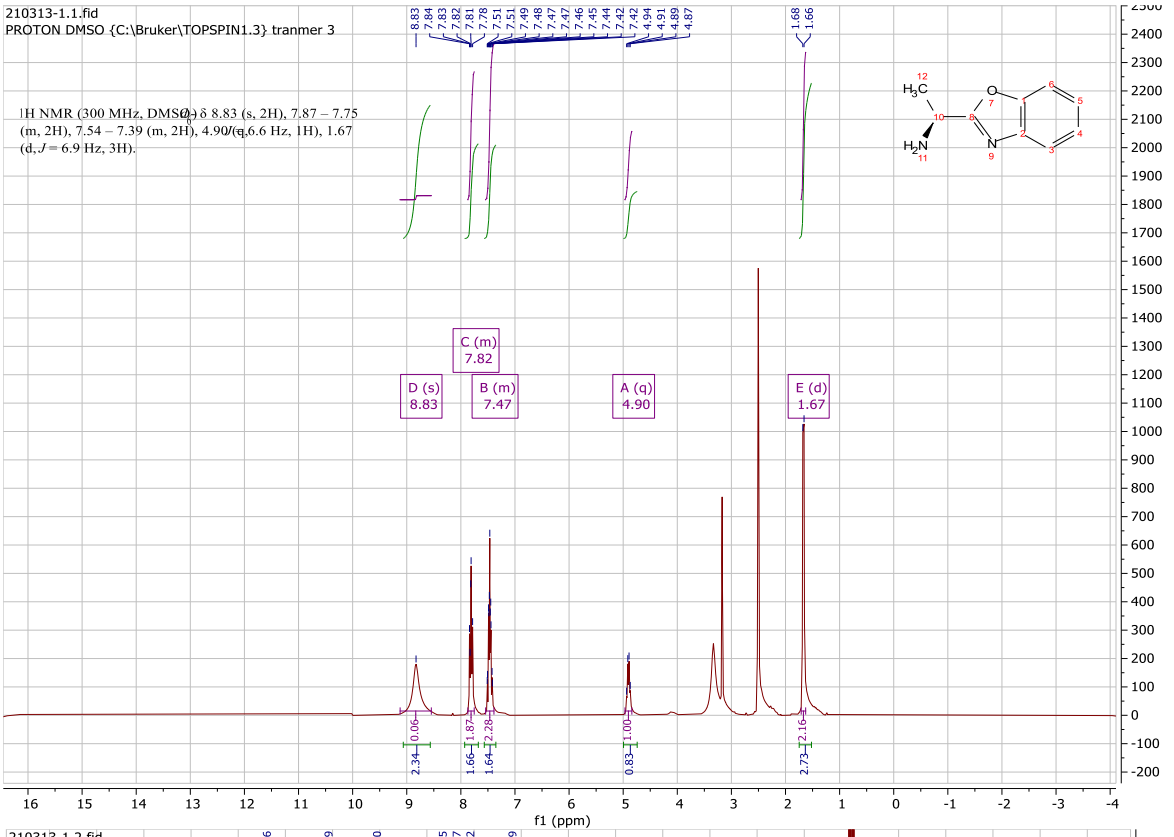
210313-1.1.fid
PROTON DMSO {C:\Bruker\TOPSPIN1.3} tranmer 3
1H NMR (300 MHz, DMSO-d6) δ 8.83 (s, 2H), 7.87 – 7.75 (m, 2H), 7.54 – 7.39 (m, 2H), 4.90 (q, J = 6.6 Hz, 1H), 1.67 (d, J = 6.9 Hz, 3H).
C (m) 7.82
D (s) 8.83
B (m) 7.47
A (q) 4.90
E (d) 1.67
f1 (ppm)

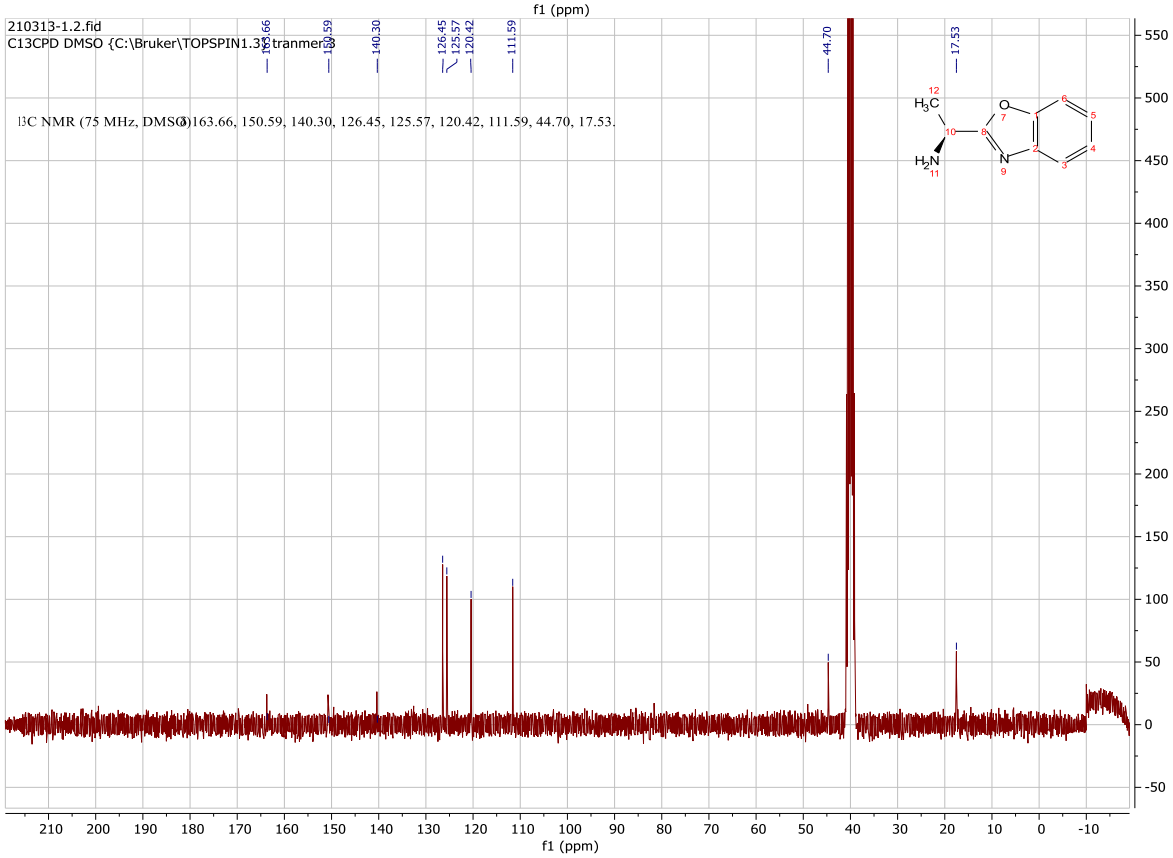
210313-1.2.fid
C13CPD DMSO {C:\Bruker\TOPSPIN1.3} tranmer 3
13C NMR (75 MHz, DMSO-d6) δ 163.66, 150.59, 140.30, 126.45, 125.57, 120.42, 111.59, 44.70, 17.53.
f1 (ppm)

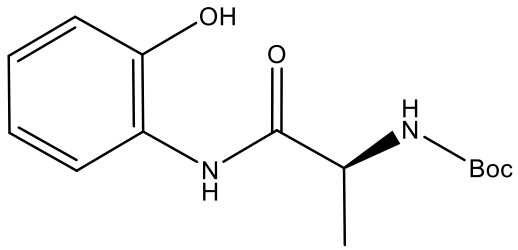

***tert*-butyl (*S*)-(1-((2-hydroxyphenyl)amino)-1-oxopropan-2-yl)carbamate (f9)**

110mg (1mmol) 2-aminophenol was reacted with 190mg (1mmol) (*tert*-butoxycarbonyl)-*L*-alanine according to the **Synthesis Method d** to give 265.8 **f9** (Yield: 95%) as red-orange solid. ^{1}H NMR (300 MHz, Chloroform-*d*) δ 8.73 (s, 2H), 7.13 (d, *J* = 7.8 Hz, 1H), 7.05 (t, *J* = 9.3 Hz, 2H), 6.88 (t, *J* = 7.5 Hz, 1H), 5.06 (m, 1H), 4.45 (m, 1H), 1.52 (s, 9H), 1.49 (m, 3H).^{13}C NMR (75 MHz, $CDCl_3$) δ 172.6, 156.2, 148.7, 127.2, 125.3, 122.4, 120.4, 119.6, 81.0, 50.3, 28.3, 17.1.

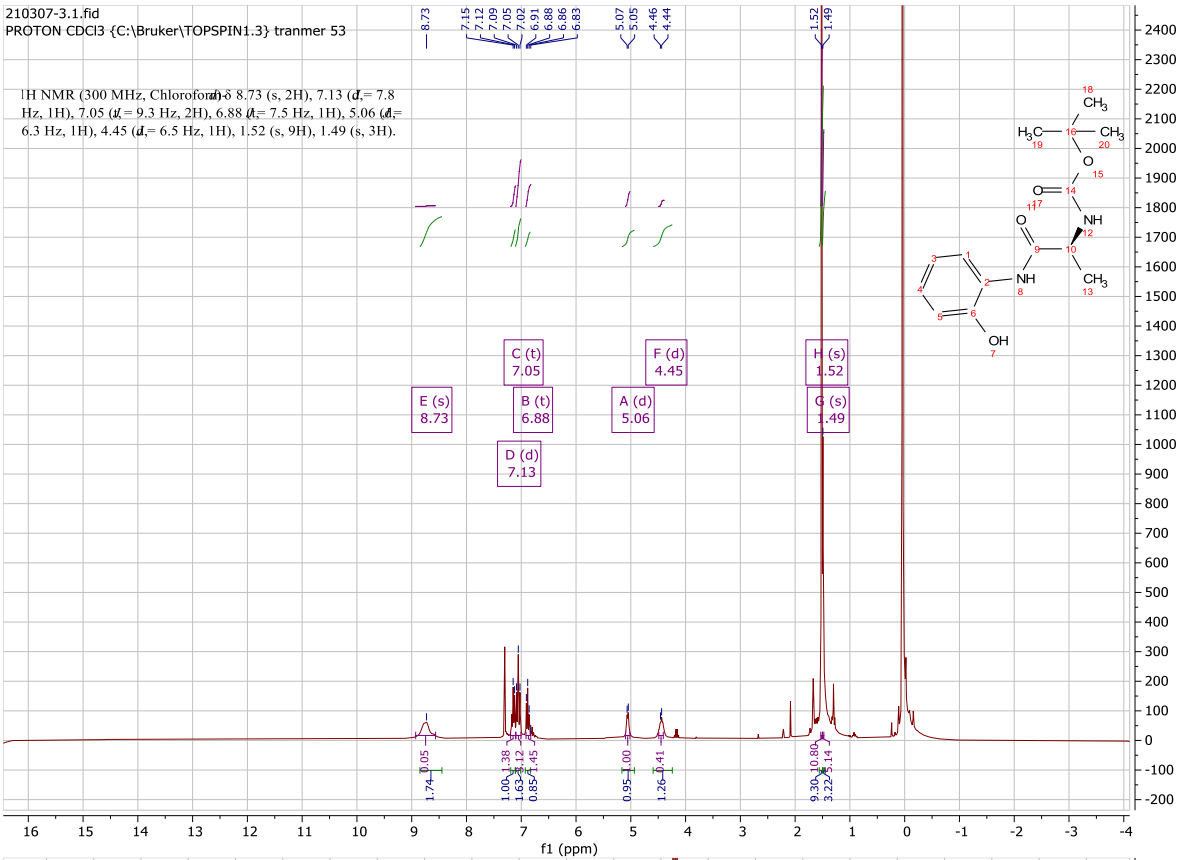
210307-3.1.fid
PROTON CDCl3 {C:\Bruker\TOPSPIN1.3} tranmer 53
1H NMR (300 MHz, Chloroform-d) δ 8.73 (s, 2H), 7.13 (d, J = 7.8 Hz, 1H), 7.05 (d, J = 9.3 Hz, 2H), 6.88 (t, J = 7.5 Hz, 1H), 5.06 (d, J = 6.3 Hz, 1H), 4.45 (d, J = 6.5 Hz, 1H), 1.52 (s, 9H), 1.49 (s, 3H).
E (s) 8.73
C (t) 7.05
B (t) 6.88
D (d) 7.13
A (d) 5.06
F (d) 4.45
H (s) 1.52
G (s) 1.49
f1 (ppm)

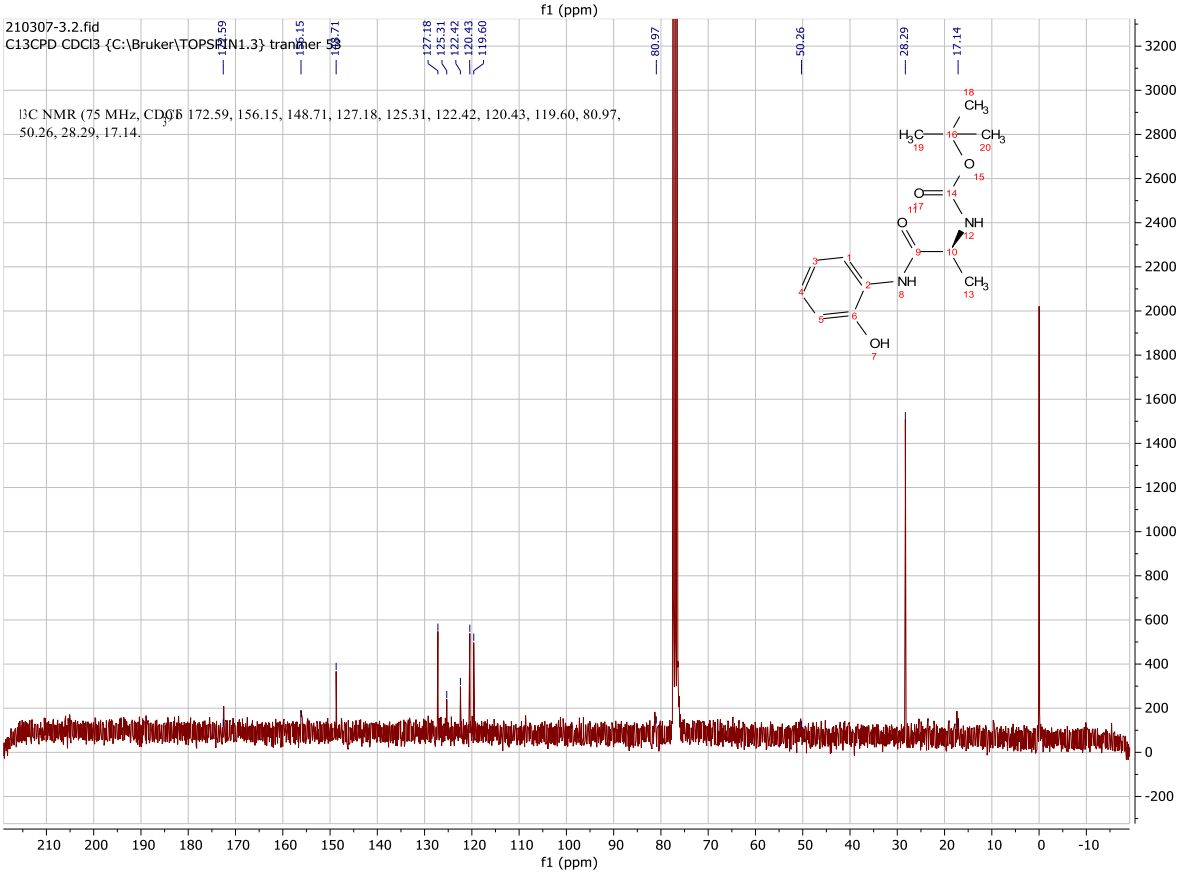
210307-3.2.fid
C13CPD CDCl3 {C:\Bruker\TOPSPIN1.3} tranmer 53
13C NMR (75 MHz, CDCl3) δ 172.59, 156.15, 148.71, 127.18, 125.31, 122.42, 120.43, 119.60, 80.97, 50.26, 28.29, 17.14.
f1 (ppm)

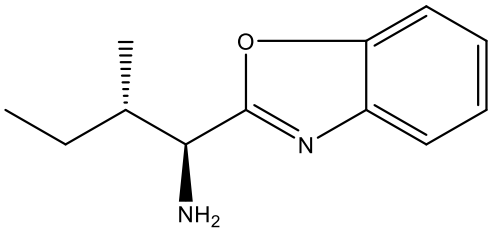

(1*S*,2*S*)-1-(benzo[d]oxazol-2-yl)-2-methylbutan-1-amine (f10)

According to the **Synthesis Method g**, 161mg (0.5mmol) **f11** was converted into Boc-protected **f10**, followed by the **Synthesis Method f** to give unprotected 47.9mg **f10** (Yield: 47%) as orange glue-like product. ^{1}H NMR (300 MHz, DMSO-d_6) δ 8.84 (s, 2H), 7.84 (d, J = 6.8 Hz, 2H), 7.54 – 7.40 (m, 2H), 4.75 (m, 1H), 2.14 (m, 1H), 1.44 (m, 2H), 0.99 – 0.85 (m, 6H). ^{13}C NMR (75 MHz, DMSO) δ 178.4, 149.9, 140.1, 126.49, 125.6, 120.3, 111.7, 53.0, 37.6, 25.6, 14.5, 11.7.

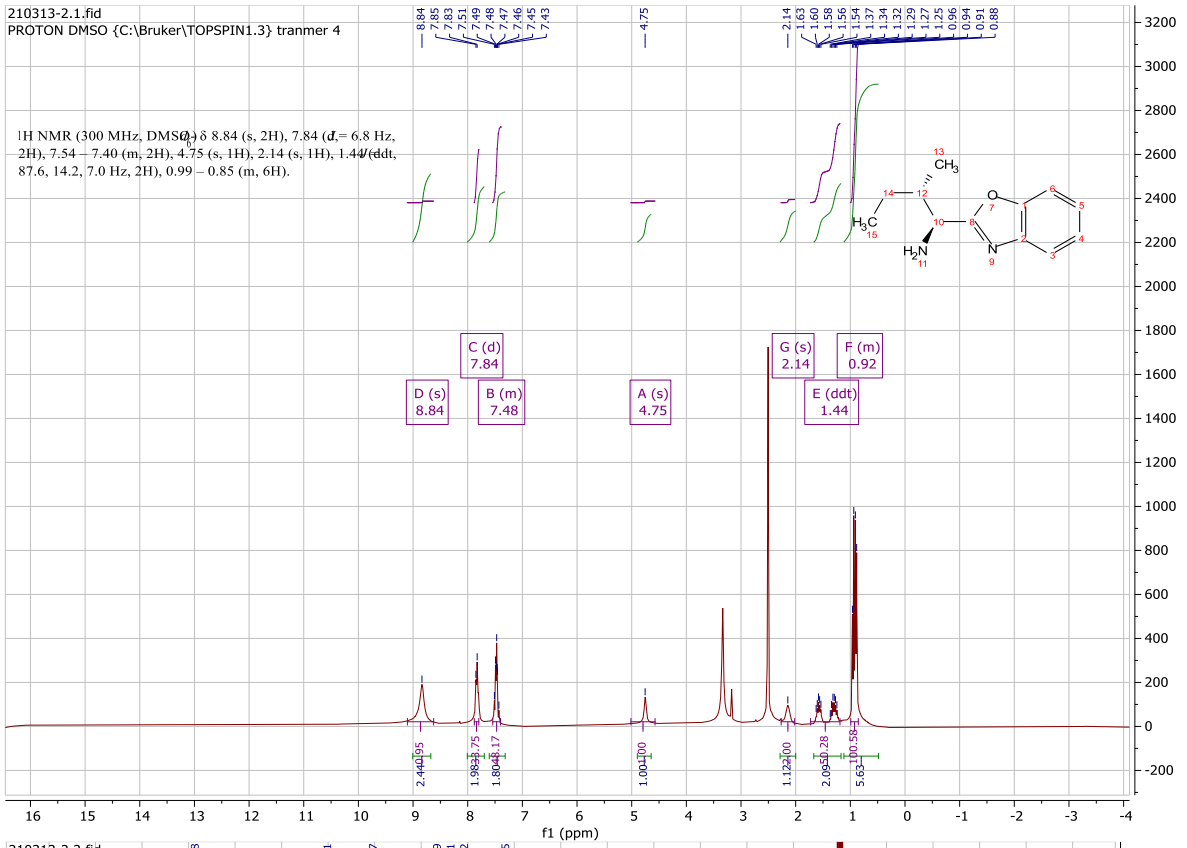
210313-2.1.fid
PROTON DMSO {C:\Bruker\TOPSPIN1.3} tranmer 4
1H NMR (300 MHz, DMSO-d6) δ 8.84 (s, 2H), 7.84 (d, J = 6.8 Hz, 2H), 7.54 – 7.40 (m, 2H), 4.75 (s, 1H), 2.14 (s, 1H), 1.44 (ddt, 87.6, 14.2, 7.0 Hz, 2H), 0.99 – 0.85 (m, 6H).
C (d) 7.84
D (s) 8.84
B (m) 7.48
A (s) 4.75
G (s) 2.14
F (m) 0.92
E (ddt) 1.44
f1 (ppm)

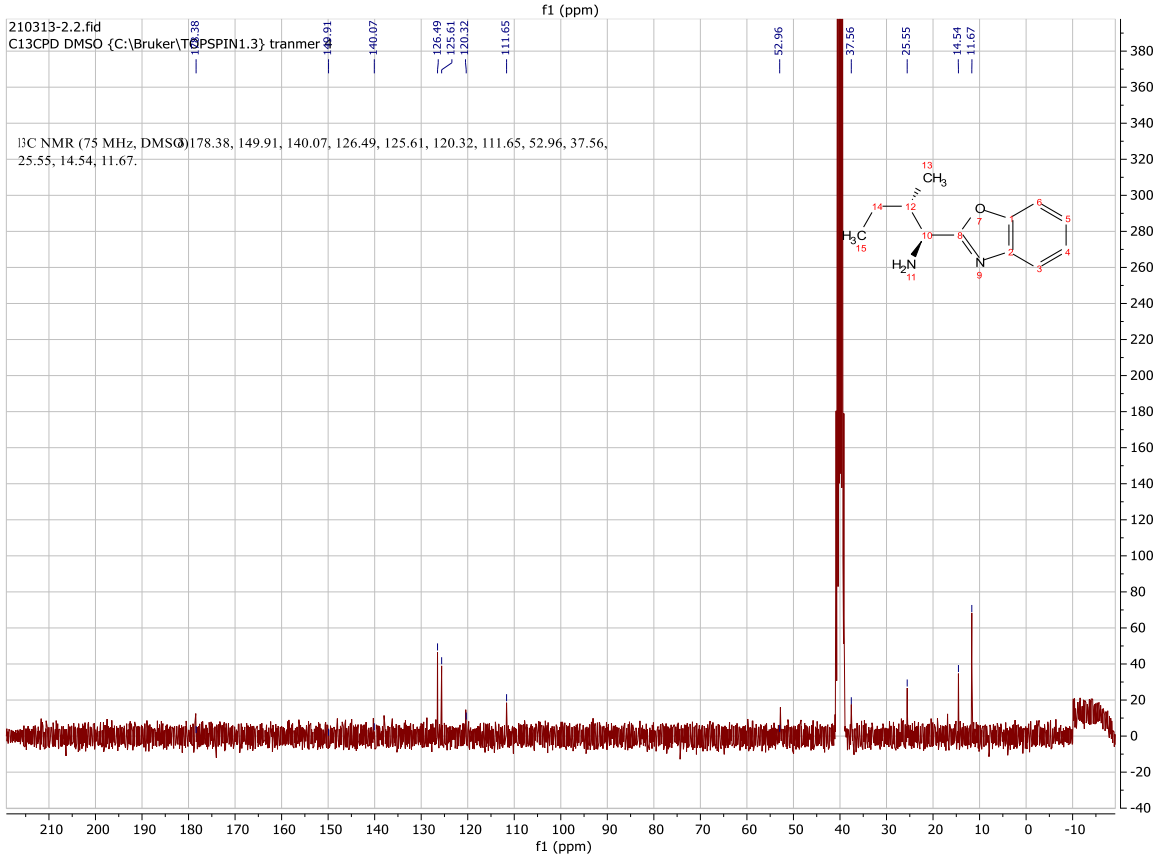
210313-2.2.fid
C13CPD DMSO {C:\Bruker\TOPSPIN1.3} tranmer 3
13C NMR (75 MHz, DMSO-d6) δ 178.38, 149.91, 140.07, 126.49, 125.61, 120.32, 111.65, 52.96, 37.56, 25.55, 14.54, 11.67.
f1 (ppm)

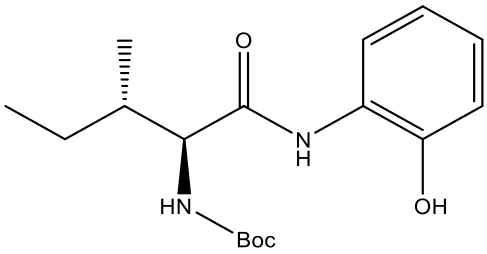

***tert*-butyl ((2*S*,3*S*)-1-((2-hydroxyphenyl)amino)-3-methyl-1-oxopentan-2-yl)carbamate (f11)**

110.1mg (1mmol) 2-aminophenol was reacted with 231.5mg (1mmol) (*tert*-butoxycarbonyl)-*L*-isoleucine according to the **Synthesis Method d** to give 287.3 **f11** (Yield: 89%) as red-orange solid. ^{1}H NMR (300 MHz, Chloroform-*d*) δ 8.71 (s, 1H), 8.53 (s, 1H), 7.20 – 6.99 (m, 3H), 6.87 (t, *J* = 7.5 Hz, 1H), 5.18 (d, *J* = 8.0 Hz, 1H), 4.20 (t, *J* = 7.7 Hz, 1H), 2.04 (m, 1H), 1.50 (s, 9H), 1.34 – 1.14 (m, 2H), 1.06 (m, 3H), 0.98 (m, 3H).^{13}C NMR (75 MHz, $CDCl_3$) δ 172.0, 156.4, 148.8, 127.2, 125.2, 122.5, 120.4, 119.5, 81.2, 69.6, 36.8, 28.3, 24.9, 15.7, 11.2.

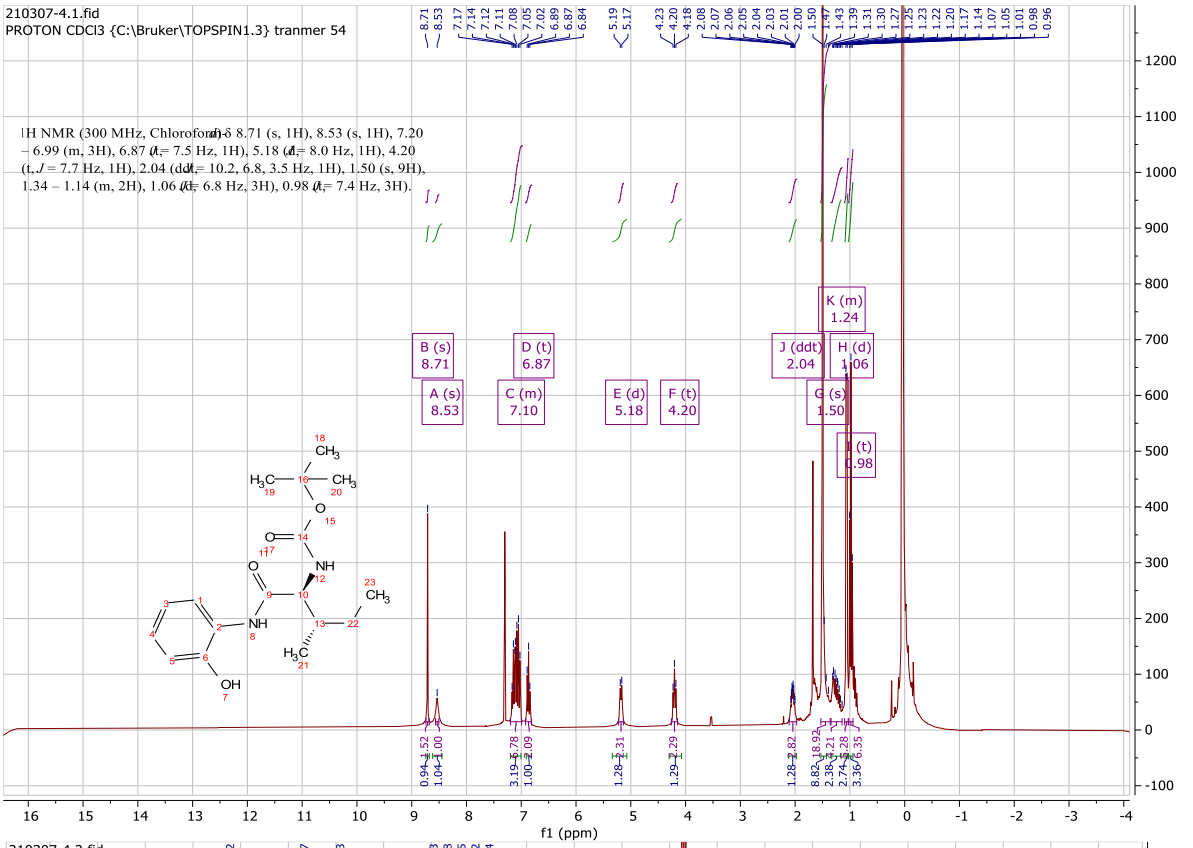
210307-4.1.fid
PROTON CDCl3 {C:\Bruker\TOPSPIN1.3} tranmer 54
1H NMR (300 MHz, Chloroform-d) δ 8.71 (s, 1H), 8.53 (s, 1H), 7.20 – 6.99 (m, 3H), 6.87 (t, J = 7.5 Hz, 1H), 5.18 (d, J = 8.0 Hz, 1H), 4.20 (t, J = 7.7 Hz, 1H), 2.04 (ddt, J = 10.2, 6.8, 3.5 Hz, 1H), 1.50 (s, 9H), 1.34 – 1.14 (m, 2H), 1.06 (d, J = 6.8 Hz, 3H), 0.98 (t, J = 7.4 Hz, 3H).
B (s) 8.71
D (t) 6.87
A (s) 8.53
C (m) 7.10
E (d) 5.18
F (t) 4.20
J (ddt) 2.04
H (d) 1.06
G (s) 1.50
K (m) 1.24
I (t) 0.98
f1 (ppm)

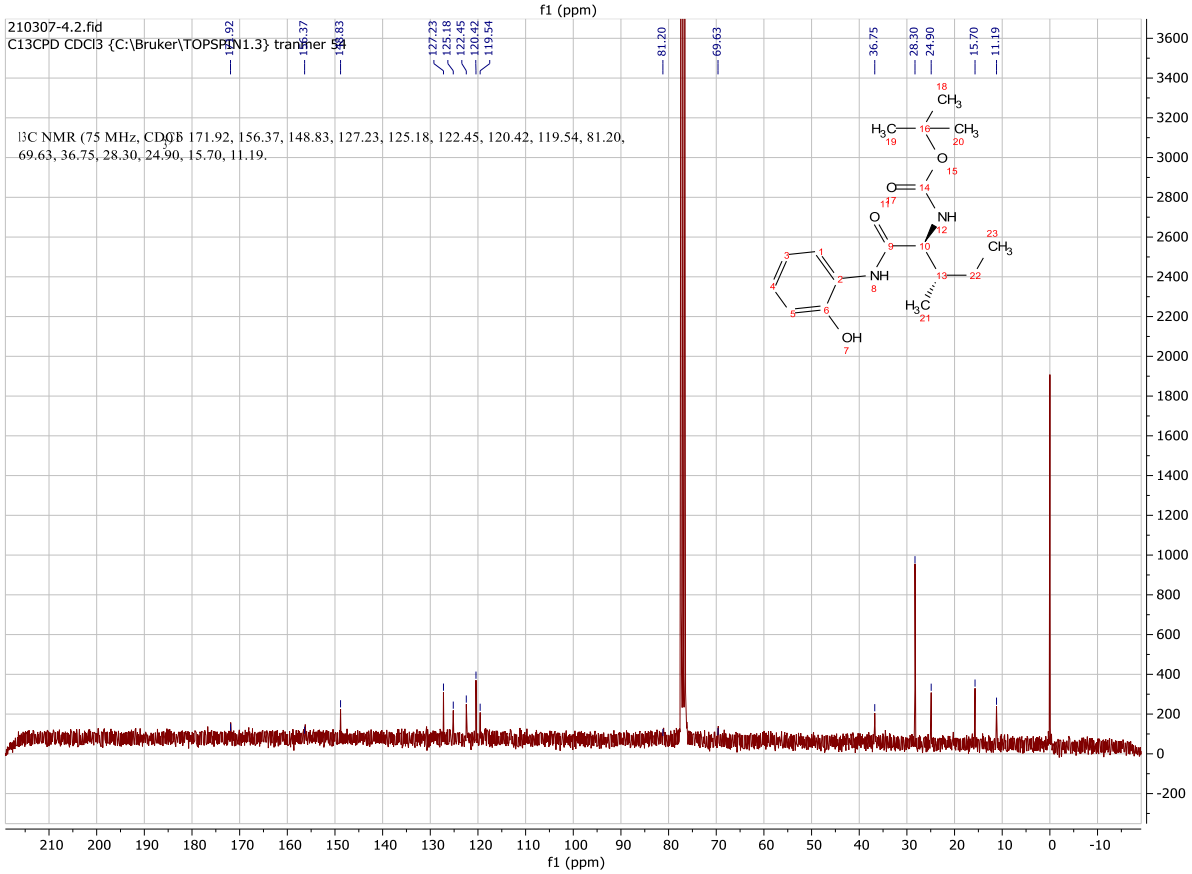
210307-4.2.fid
C13CPD CDCl3 {C:\Bruker\TOPSPIN1.3} tranmer 54
13C NMR (75 MHz, CDCl3) δ 171.92, 156.37, 148.83, 127.23, 125.18, 122.45, 120.42, 119.54, 81.20, 69.63, 36.75, 28.30, 24.90, 15.70, 11.19.
f1 (ppm)

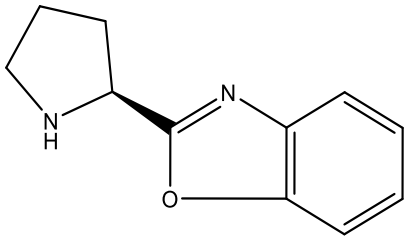

(*S*)-2-(pyrrolidin-2-yl)benzo[*d*]oxazole (f12)

According to the **Synthesis Method g**, 153.2mg (0.5mmol) **f13** was converted into Boc-protected **f12**, followed by the **Synthesis Method f** to give unprotected 52.7mg **f12** (Yield: 56%) as orange glue-like product. ^{1}H NMR (300 MHz, Chloroform-*d*) δ 7.77 – 7.66 (m, 1H), 7.56 – 7.47 (m, 1H), 7.39 (dd, *J* = 6.2, 2.7 Hz, 2H), 5.15 (m, 1H), 3.60 (m, 2H), 2.76 – 2.40 (m, 2H), 2.24 (m, 2H). ^{13}C NMR (75 MHz, $CDCl_3$) δ 160.8, 151.3, 140.0, 126.1, 125.1, 120.4, 111.0, 55.4, 45.8, 29.8, 23.9.

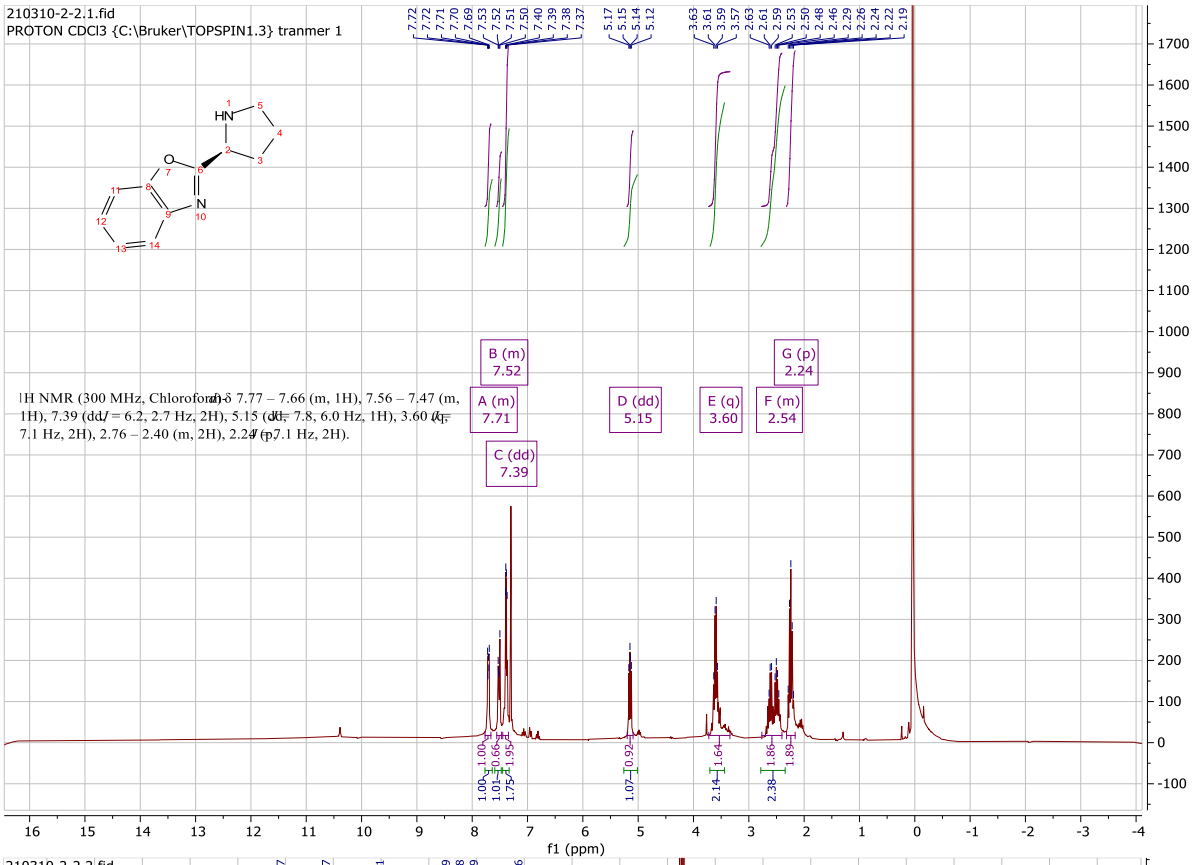

^{1}H NMR (300 MHz, Chloroform-d) δ 7.77 – 7.66 (m, 1H), 7.56 – 7.47 (m, 1H), 7.39 (dd, J = 6.2, 2.7 Hz, 2H), 5.15 (dd, J = 7.8, 6.0 Hz, 1H), 3.60 (q, J = 7.1 Hz, 2H), 2.76 – 2.40 (m, 2H), 2.24 (p, J = 7.1 Hz, 2H).

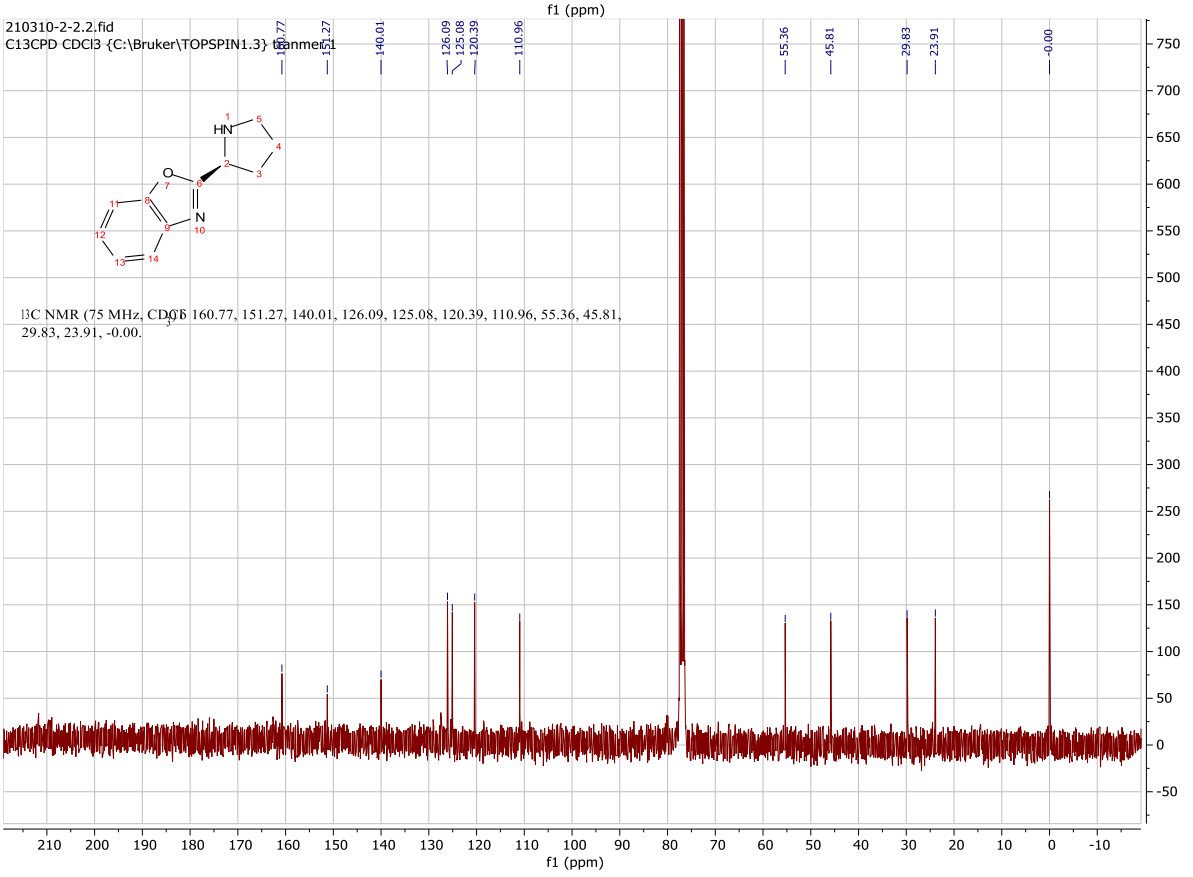

^{13}C NMR (75 MHz, CDCl$_3$) δ 160.77, 151.27, 140.01, 126.09, 125.08, 120.39, 110.96, 55.36, 45.81, 29.83, 23.91, -0.00.

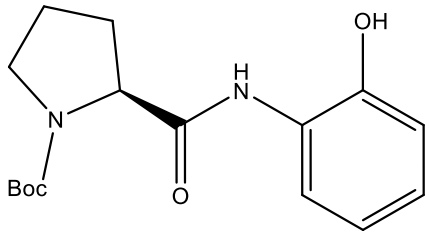

tert-butyl (_S_)-2-((2-hydroxyphenyl)carbamoyl)pyrrolidine-1-carboxylate (f13)

110mg (1mmol) 2-aminophenol was reacted with 215.5mg (1mmol) (*tert*-butoxycarbonyl)-*L*-proline according to the **Synthesis Method d** to give 269.3 **f13** (Yield: 88%) as red-orange solid. ^{1}H NMR (300 MHz, Chloroform-*d*) δ 9.71 (s, 1H), 8.90 (d, *J* = 78.2 Hz, 1H), 7.14 (t, *J* = 8.2 Hz, 1H), 7.04 (d, *J* = 7.8 Hz, 2H), 6.88 (t, *J* = 7.3 Hz, 1H), 4.57 (m, 2H), 3.52 (m, 2H), 2.69 – 2.30 (m, 1H), 2.03 (dd, *J* = 16.3, 10.9 Hz, 2H), 1.52 (d, *J* = 7.5 Hz, 9H). ^{13}C NMR (75 MHz, $CDCl_3$) δ 172.1, 166.1, 148.8, 127.0, 122.4, 122.0, 120.3, 119.6, 81.4, 54.5, 47.3, 42.7, 28.4, 24.7.

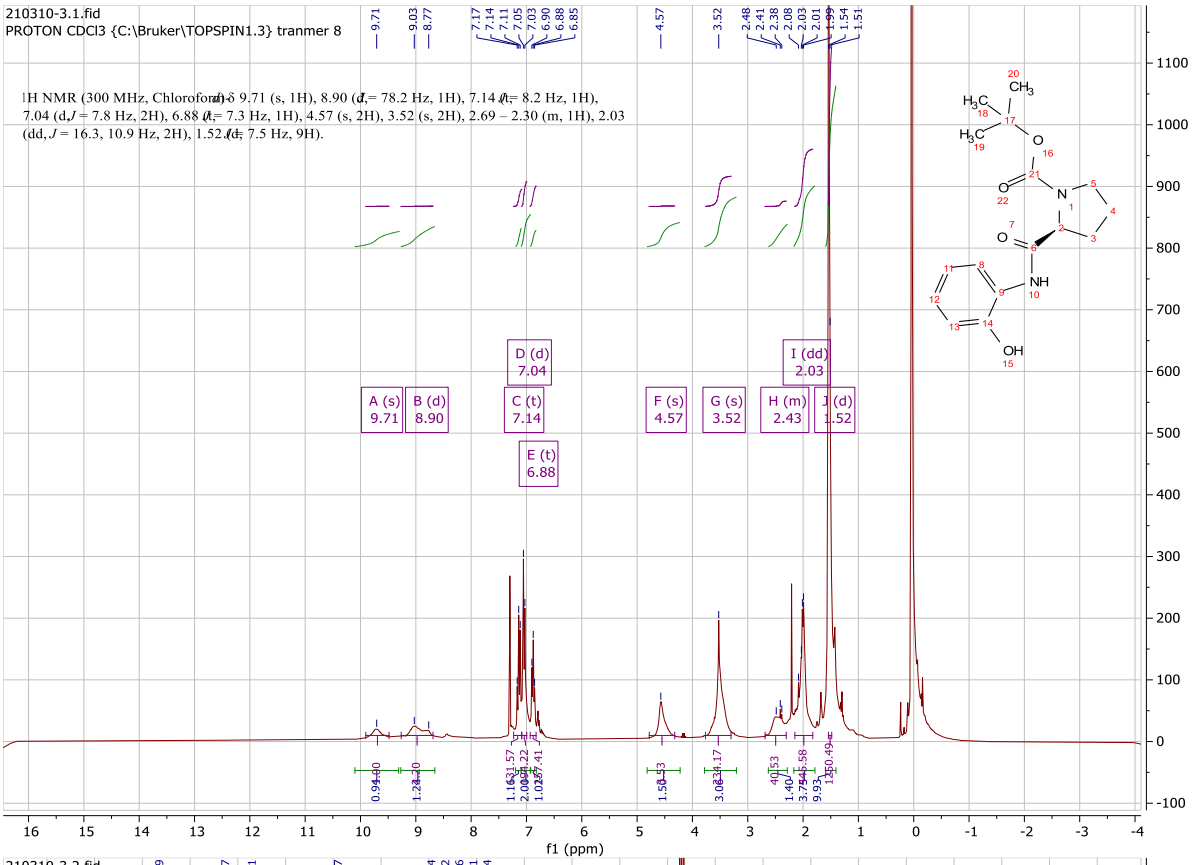
210310-3.1.fid
PROTON CDCl3 {C:\Bruker\TOPSPIN1.3} tranmer 8
1H NMR (300 MHz, Chloroform-d) δ 9.71 (s, 1H), 8.90 (d, J = 78.2 Hz, 1H), 7.14 (t, J = 8.2 Hz, 1H), 7.04 (d, J = 7.8 Hz, 2H), 6.88 (t, J = 7.3 Hz, 1H), 4.57 (s, 2H), 3.52 (s, 2H), 2.69 – 2.30 (m, 1H), 2.03 (dd, J = 16.3, 10.9 Hz, 2H), 1.52 (d, J = 7.5 Hz, 9H).
A (s) 9.71
B (d) 8.90
C (t) 7.14
D (d) 7.04
E (t) 6.88
F (s) 4.57
G (s) 3.52
H (m) 2.43
I (dd) 2.03
J (d) 1.52
f1 (ppm)

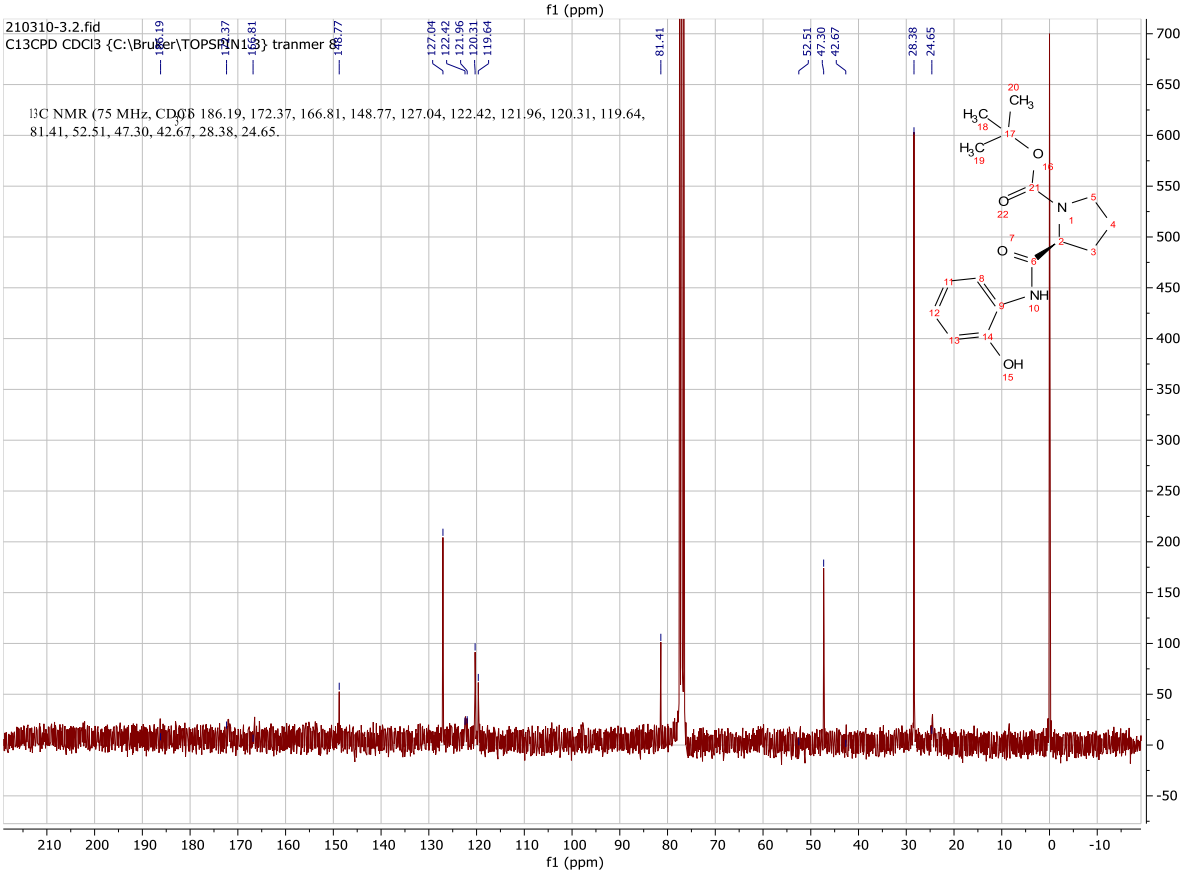
210310-3.2.fid
C13CPD CDCl3 {C:\Bruker\TOPSPIN1.3} tranmer 8
13C NMR (75 MHz, CDCl3) δ 186.19, 172.37, 166.81, 148.77, 127.04, 122.42, 121.96, 120.31, 119.64, 81.41, 52.51, 47.30, 42.67, 28.38, 24.65.
f1 (ppm)

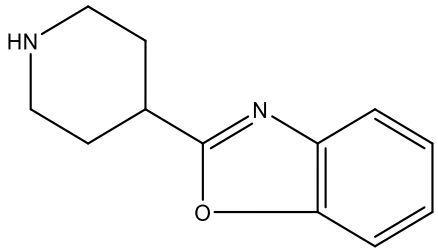

2-(piperidin-4-yl)benzo[*d*]oxazole (f14)

According to the **Synthesis Method g**, 160.2mg (0.5mmol) **f15** was converted into Boc-protected **f14**, followed by the **Synthesis Method f** to give unprotected 54.5mg **f14** (Yield: 54%) as orange glue-like product. ^{1}H NMR (300 MHz, DMSO-d_6) δ 8.64 (s, 1H), 7.77 – 7.65 (m, 2H), 7.38 (m, 2H), 3.39 (m, 3H), 3.11 (m2H), 2.33 – 2.22 (m, 2H), 2.12 – 1.90 (m, 2H). ^{13}C NMR (75 MHz, DMSO) δ 167.9, 150.8, 141.2, 125.5, 124.9, 120.0, 111.2, 42.8, 33.0, 26.4.

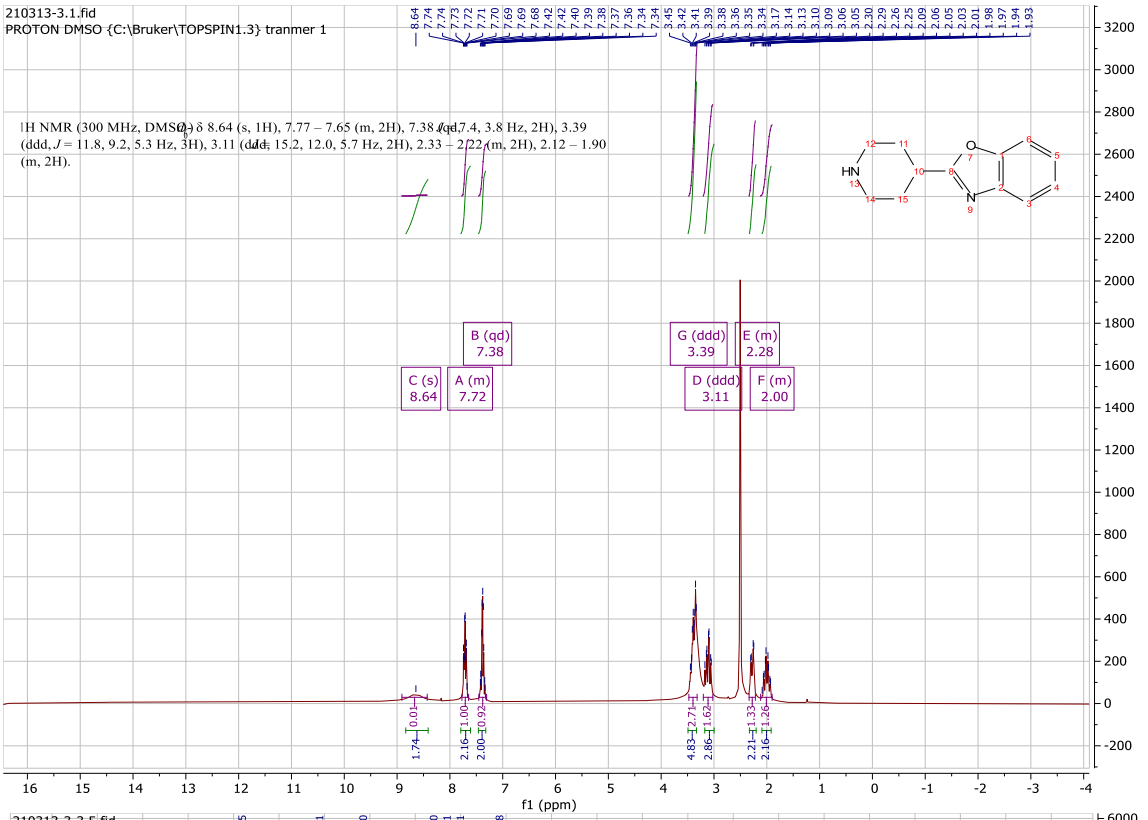
210313-3.1.fid
PROTON DMSO {C:\Bruker\TOPSPIN1.3} tranmer 1
1H NMR (300 MHz, DMSO-d6) δ 8.64 (s, 1H), 7.77 – 7.65 (m, 2H), 7.38 (qd, J = 7.4, 3.8 Hz, 2H), 3.39 (ddd, J = 11.8, 9.2, 5.3 Hz, 3H), 3.11 (ddd, J = 15.2, 12.0, 5.7 Hz, 2H), 2.33 – 2.22 (m, 2H), 2.12 – 1.90 (m, 2H).
B (qd) 7.38
G (ddd) 3.39
E (m) 2.28
C (s) 8.64
A (m) 7.72
D (ddd) 3.11
F (m) 2.00
f1 (ppm)

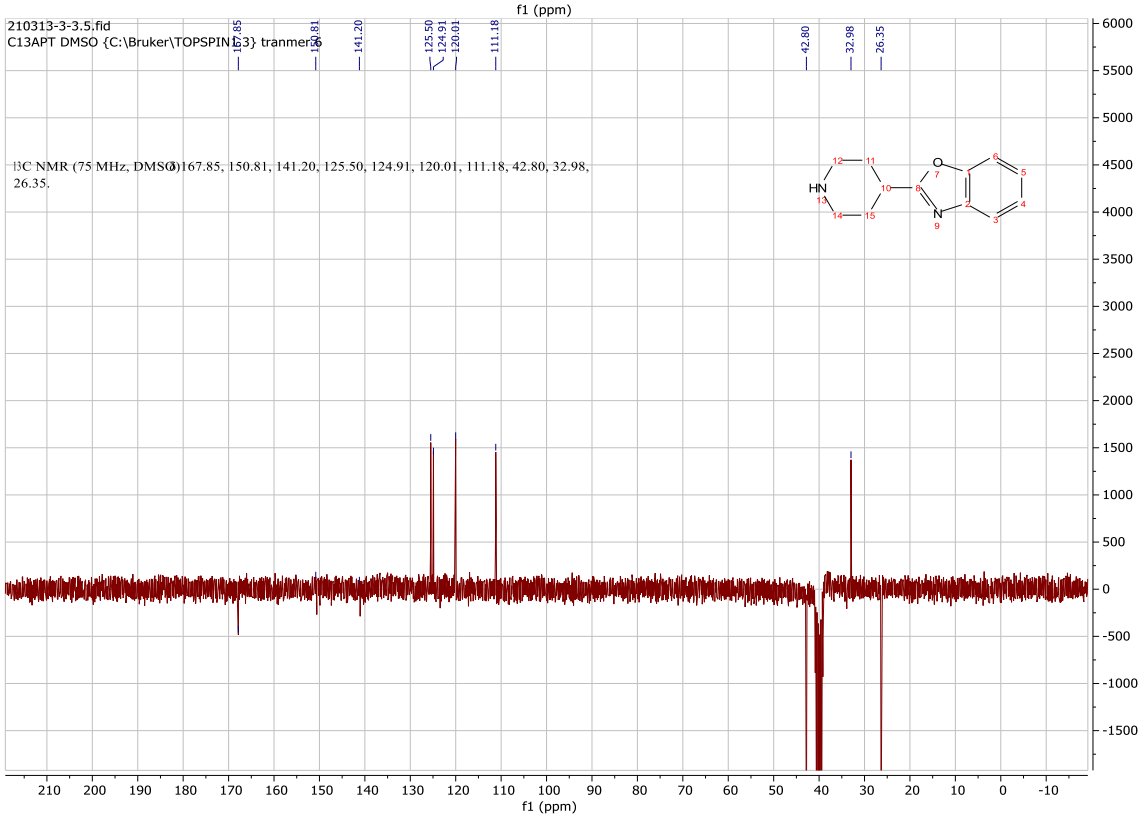
210313-3-3.5.fid
C13APT DMSO {C:\Bruker\TOPSPIN1.3} tranmer 6
13C NMR (75 MHz, DMSO-d6) 167.85, 150.81, 141.20, 125.50, 124.91, 120.01, 111.18, 42.80, 32.98, 26.35.
f1 (ppm)

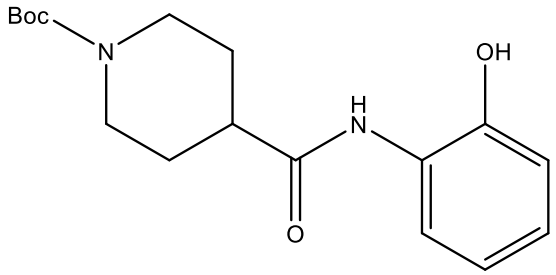

***tert*-butyl 4-((2-hydroxyphenyl)carbamoyl)piperidine-1-carboxylate (f15)**

110mg (1mmol) 2-aminophenol was reacted with 229.5mg (1mmol) *N*-Boc-isonipecotic acid according to the **Synthesis Method d** to give 294.4 **f15** (Yield: 92%) as red-orange solid. ^{1}H NMR (300 MHz, Chloroform-*d*) δ 8.60 (s, 1H), 7.65 (s, 1H), 7.15 (dd, *J* = 7.6, 4.2 Hz, 2H), 7.05 (d, *J* = 7.7 Hz, 1H), 6.91 (t, *J* = 7.6 Hz, 1H), 4.20 (m, 2H), 2.84 (m, 2H), 2.55 (m, 1H), 1.97 (m, 2H), 1.79 (m, 2H), 1.51 (s, 9H). ^{13}C NMR (75 MHz, $CDCl_3$) δ 174.5, 154.7, 148.5, 127.1, 125.5, 122.0, 120.5, 119.6, 79.98, 43.8, 43.1, 28.7, 28.5.

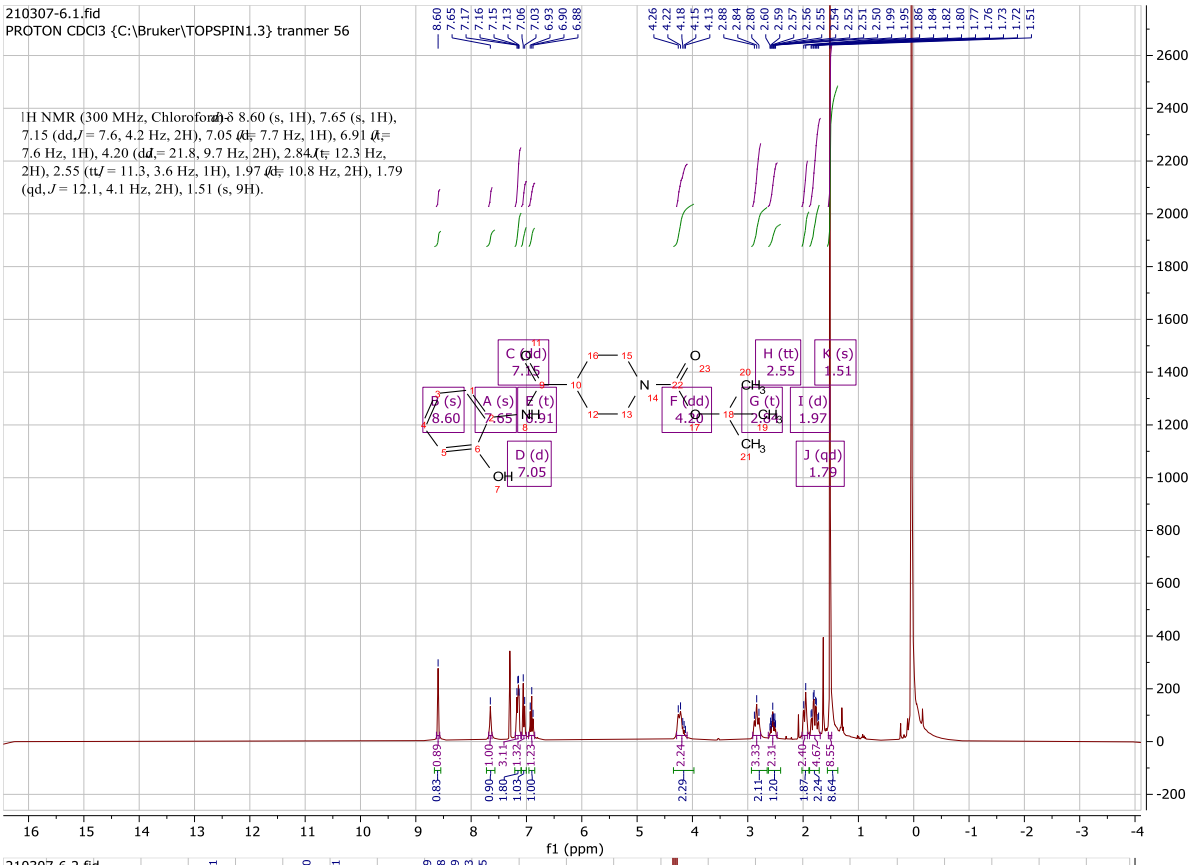
210307-6.1.fid
PROTON CDCl3 {C:\Bruker\TOPSPIN1.3} tranmer 56
1H NMR (300 MHz, Chloroform-d) δ 8.60 (s, 1H), 7.65 (s, 1H), 7.15 (dd, J = 7.6, 4.2 Hz, 2H), 7.05 (d, J = 7.7 Hz, 1H), 6.91 (t, J = 7.6 Hz, 1H), 4.20 (dd, J = 21.8, 9.7 Hz, 2H), 2.84 (t, J = 12.3 Hz, 2H), 2.55 (tt, J = 11.3, 3.6 Hz, 1H), 1.97 (d, J = 10.8 Hz, 2H), 1.79 (qd, J = 12.1, 4.1 Hz, 2H), 1.51 (s, 9H).
B (s) 8.60
A (s) 2.65
Z (t) 2.91
C (dd) 7.15
D (d) 7.05
F (dd) 4.20
G (t) 2.84
H (tt) 2.55
I (d) 1.97
J (qd) 1.79
K (s) 1.51
f1 (ppm)

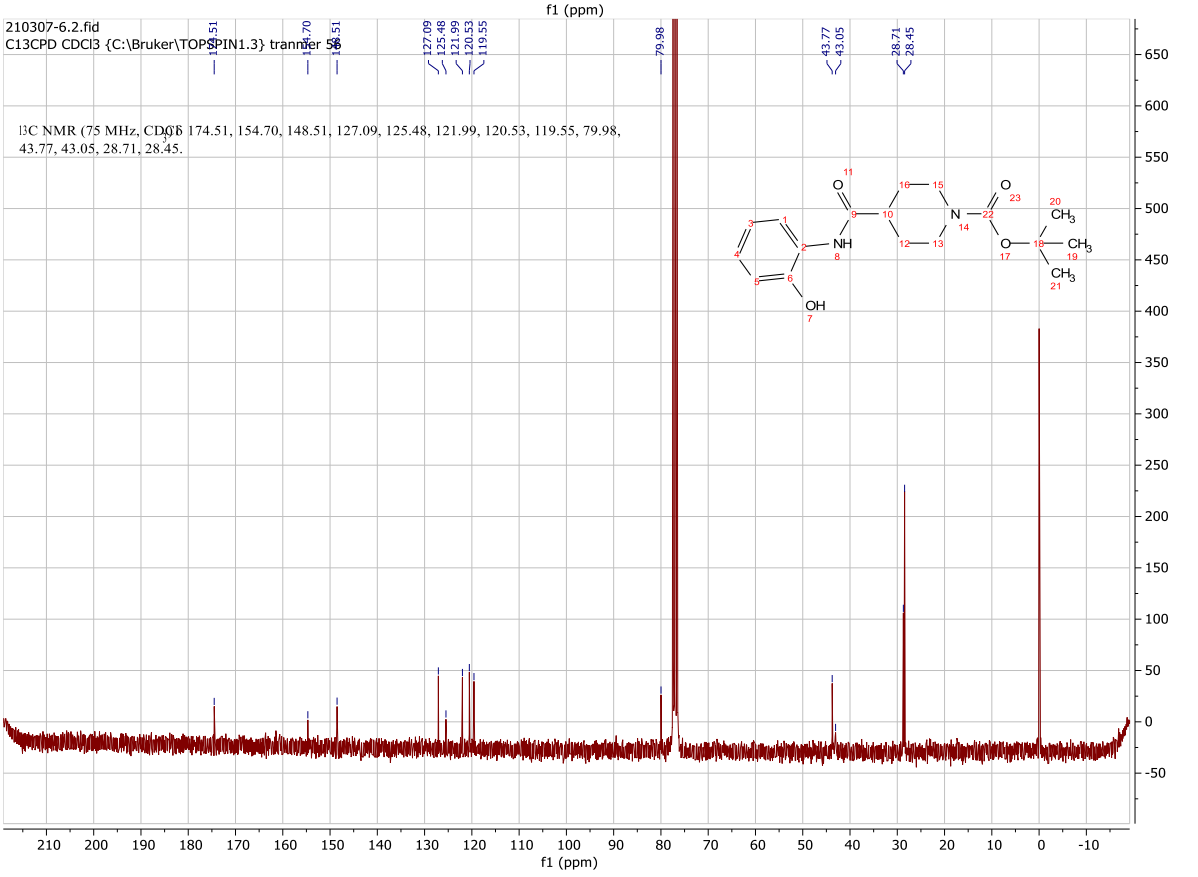
210307-6.2.fid
C13CPD CDCl3 {C:\Bruker\TOPSPIN1.3} tranmer 56
13C NMR (75 MHz, CDCl3) δ 174.51, 154.70, 148.51, 127.09, 125.48, 121.99, 120.53, 119.55, 79.98, 43.77, 43.05, 28.71, 28.45.
f1 (ppm)

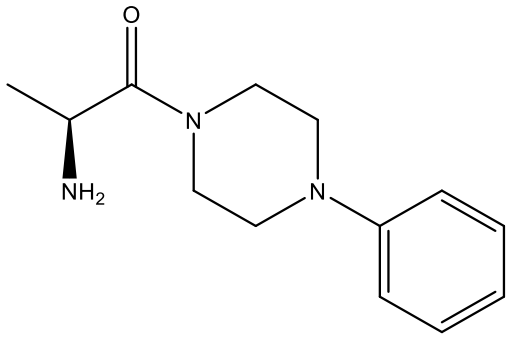

(*S*)-2-amino-1-(4-phenylpiperazin-1-yl)propan-1-one (f16)

189.5mg (1mmol) (*tert*-butoxycarbonyl)-*L*-alanine was reacted with 162.5mg (1mmol) 1-phenylpiperazine according to the **Synthesis Method d** and the crude produce was deprotected according to the **Synthesis Method f** to give 101.4mg **f16** (Yield: 87%) as yellowish white solid. ^{1}H NMR (300 MHz, DMSO-d_6) δ 8.11 (s, 2H), 7.30 – 7.19 (m, 2H), 6.98 (d, J = 8.0 Hz, 2H), 6.83 (t, J = 7.2 Hz, 1H), 4.44 (m, 1H), 3.81 – 3.50 (m, 4H), 3.28 – 3.01 (m, 4H), 1.33 (d, J = 6.9 Hz, 3H). ^{13}C NMR (75 MHz, DMSO) δ 168.5, 151.1, 129.5, 120.0, 116.4, 49.1, 48.7, 46.4, 45.0, 42.0, 16.9.

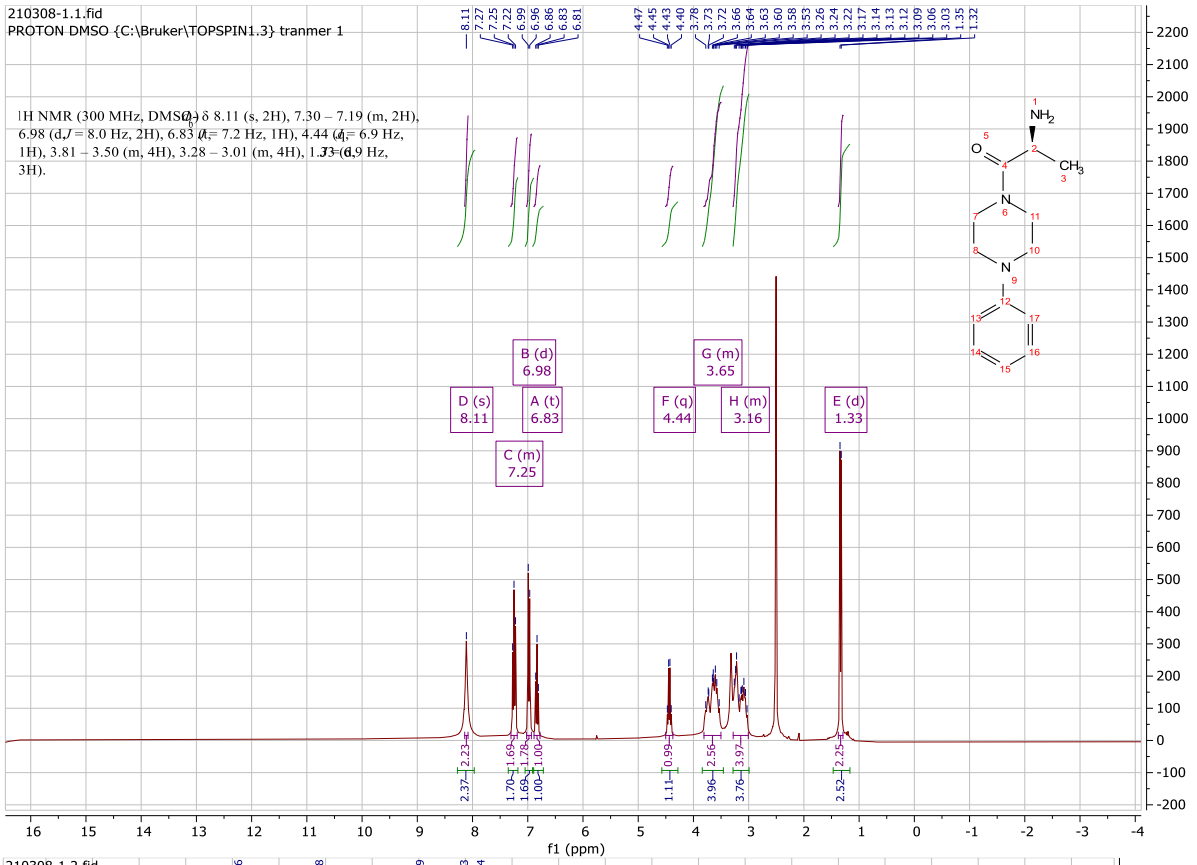

^{1}H NMR (300 MHz, DMSO-d_6) δ 8.11 (s, 2H), 7.30 – 7.19 (m, 2H), 6.98 (d, J = 8.0 Hz, 2H), 6.83 (t, J = 7.2 Hz, 1H), 4.44 (q, J = 6.9 Hz, 1H), 3.81 – 3.50 (m, 4H), 3.28 – 3.01 (m, 4H), 1.33 (d, J = 6.9 Hz, 3H).

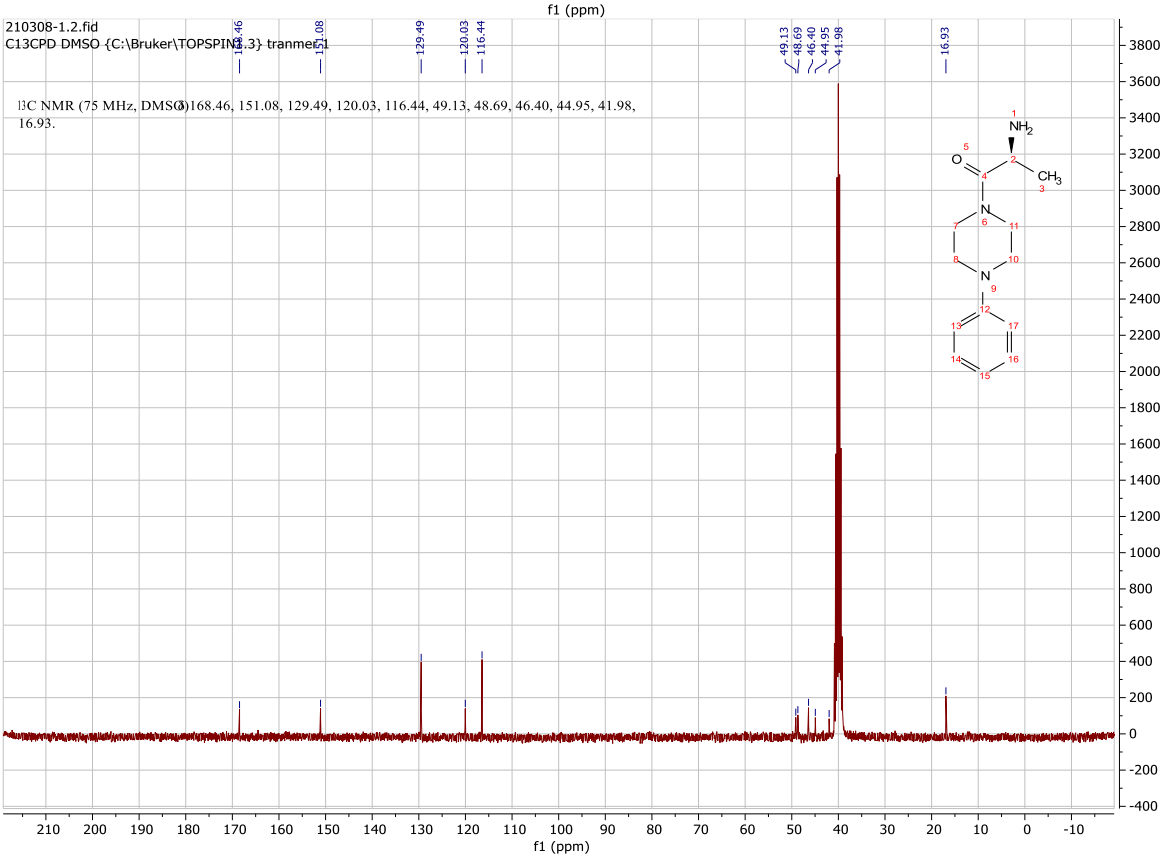

^{13}C NMR (75 MHz, DMSO-d_6) δ 168.46, 151.08, 129.49, 120.03, 116.44, 49.13, 48.69, 46.40, 44.95, 41.98, 16.93.

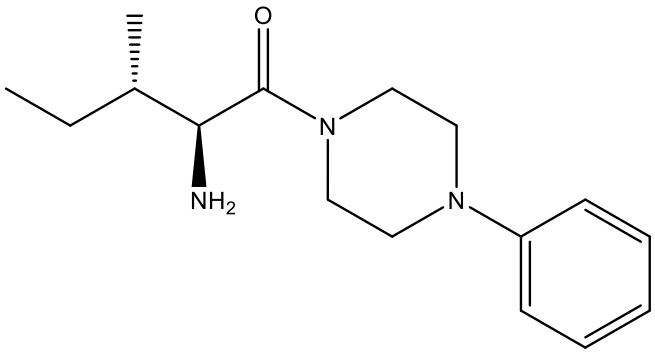

(2*S*,3*S*)-2-amino-3-methyl-1-(4-phenylpiperazin-1-yl)pentan-1-one (f17)

231.5mg (1mmol) (*tert*-butoxycarbonyl)-*L*-isoleucine was reacted with 162.5mg (1mmol) 1-phenylpiperazine according to the **Synthesis Method d** and the crude produce was deprotected according to the **Synthesis Method f** to give 247.5mg **f17** (Yield: 90%) as yellowish white solid. ^{1}H NMR (300 MHz, DMSO-d_6) δ 8.07 (s, 2H), 7.25 (t, J = 7.9 Hz, 2H), 6.98 (d, J = 8.0 Hz, 2H), 6.83 (t, J = 7.2 Hz, 1H), 4.35 (m, 1H), 3.68 (m, 4H), 3.16 (m, 4H), 1.85 – 1.77 (m, 1H), 1.55 – 1.06 (m, 2H), 0.98 (d, J = 6.9 Hz, 3H), 0.87 (t, J = 7.3 Hz, 3H). ^{13}C NMR (75 MHz, DMSO) δ 167.4, 151.1, 129.5, 120.0, 116.4, 54.0, 49.2, 48.7, 45.6, 42.1, 36.4, 23.6, 15.4, 11.8.

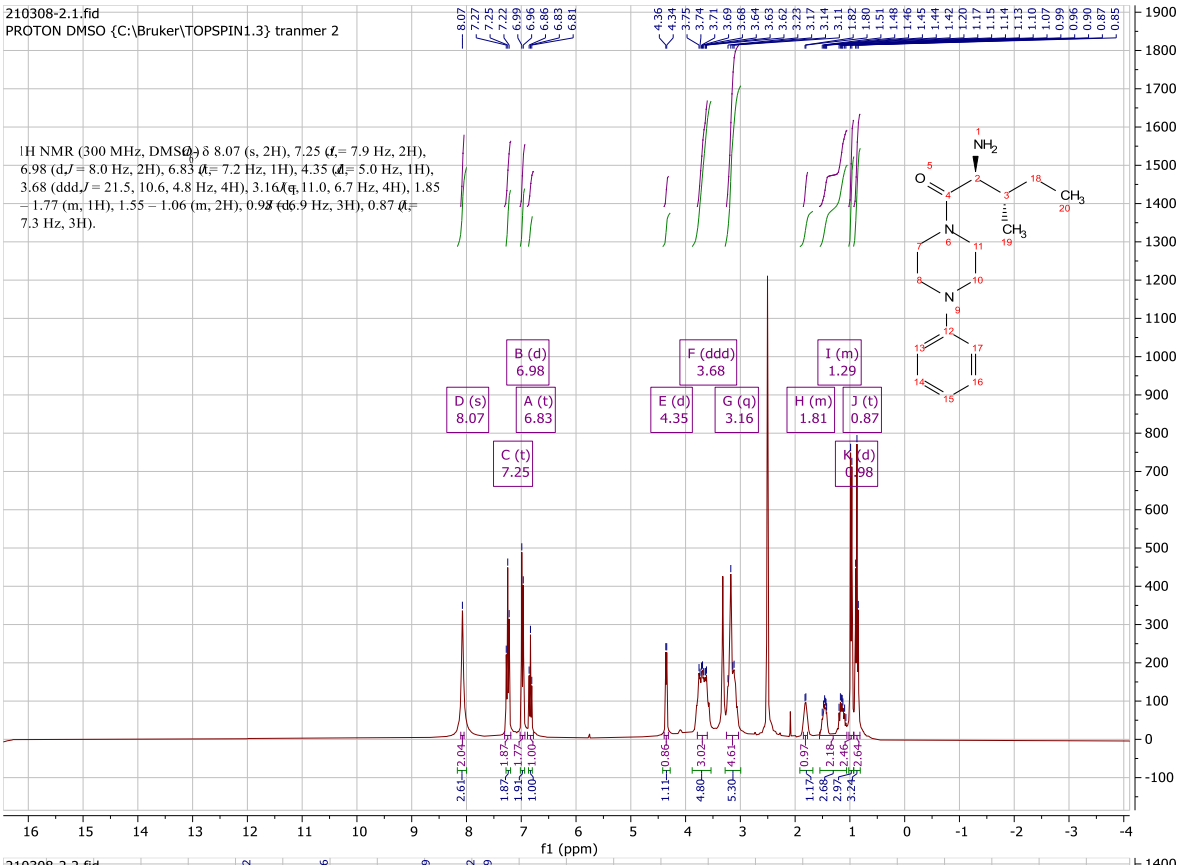
210308-2.1.fid
PROTON DMSO {C:\Bruker\TOPSPIN1.3} tranmer 2
1H NMR (300 MHz, DMSO) δ 8.07 (s, 2H), 7.25 (t, J = 7.9 Hz, 2H), 6.98 (d, J = 8.0 Hz, 2H), 6.83 (t, J = 7.2 Hz, 1H), 4.35 (d, J = 5.0 Hz, 1H), 3.68 (ddd, J = 21.5, 10.6, 4.8 Hz, 4H), 3.16 (q, J = 11.0, 6.7 Hz, 4H), 1.85 – 1.77 (m, 1H), 1.55 – 1.06 (m, 2H), 0.98 (d, J = 6.9 Hz, 3H), 0.87 (t, J = 7.3 Hz, 3H).
D (s) 8.07
B (d) 6.98
A (t) 6.83
C (t) 7.25
F (ddd) 3.68
E (d) 4.35
G (q) 3.16
I (m) 1.29
H (m) 1.81
J (t) 0.87
K (d) 0.98
f1 (ppm)

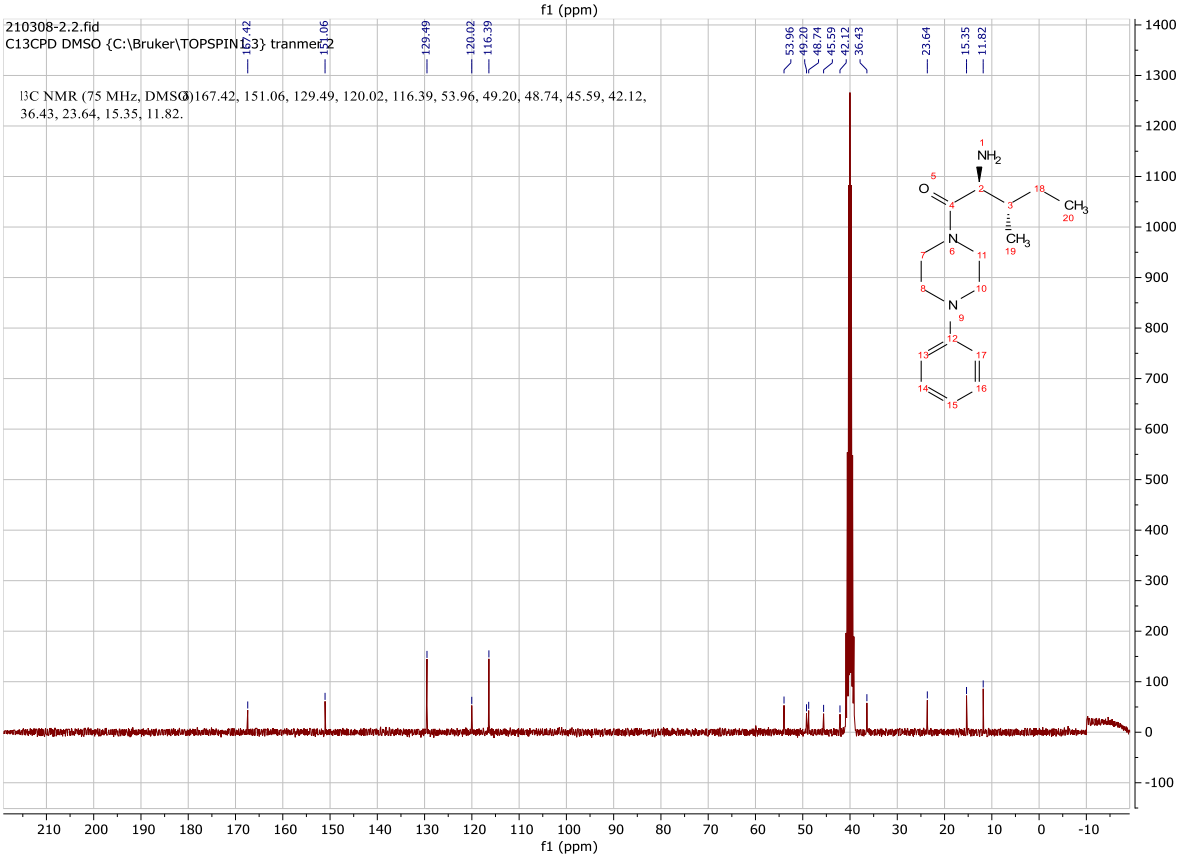
210308-2.2.fid
C13CPD DMSO {C:\Bruker\TOPSPIN1.3} tranmer 2
13C NMR (75 MHz, DMSO) δ 167.42, 151.06, 129.49, 120.02, 116.39, 53.96, 49.20, 48.74, 45.59, 42.12, 36.43, 23.64, 15.35, 11.82.
f1 (ppm)

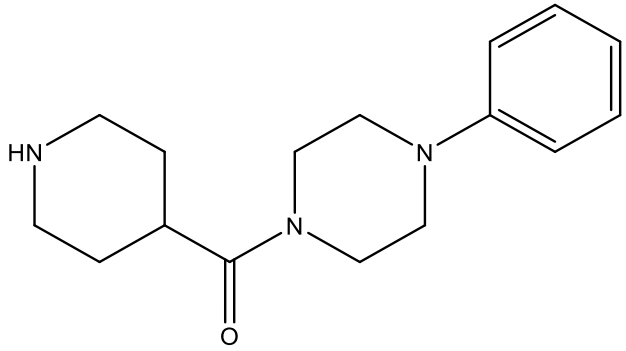

(4-phenylpiperazin-1-yl)(piperidin-4-yl)methanone (f18)

229.5mg (1mmol) *N*-Boc-isonipecotic acid was reacted with 162.5mg (1mmol) 1-phenylpiperazine according to the **Synthesis Method d** and the crude produce was deprotected according to the **Synthesis Method f** to give 200.1mg **f18** (Yield: 73%) as yellowish white solid. ^{1}H NMR (300 MHz, DMSO-d_6) δ 9.04 (s, 1H), 7.25 (t, J = 7.9 Hz, 2H), 6.98 (d, J = 8.0 Hz, 2H), 6.83 (t, J = 7.2 Hz, 1H), 4.72 – 4.61 (m, 1H), 3.79 – 3.57 (m, 5H), 3.21 (m, 5H), 2.47 – 2.32 (m, 1H), 2.02 – 1.72 (m, 3H). ^{13}C NMR (75 MHz, DMSO) δ 167.1, 151.1, 129.5, 120.0, 116.5, 58.1, 48.9, 48.6, 46.2, 45.0, 42.2, 29.1, 24.1.

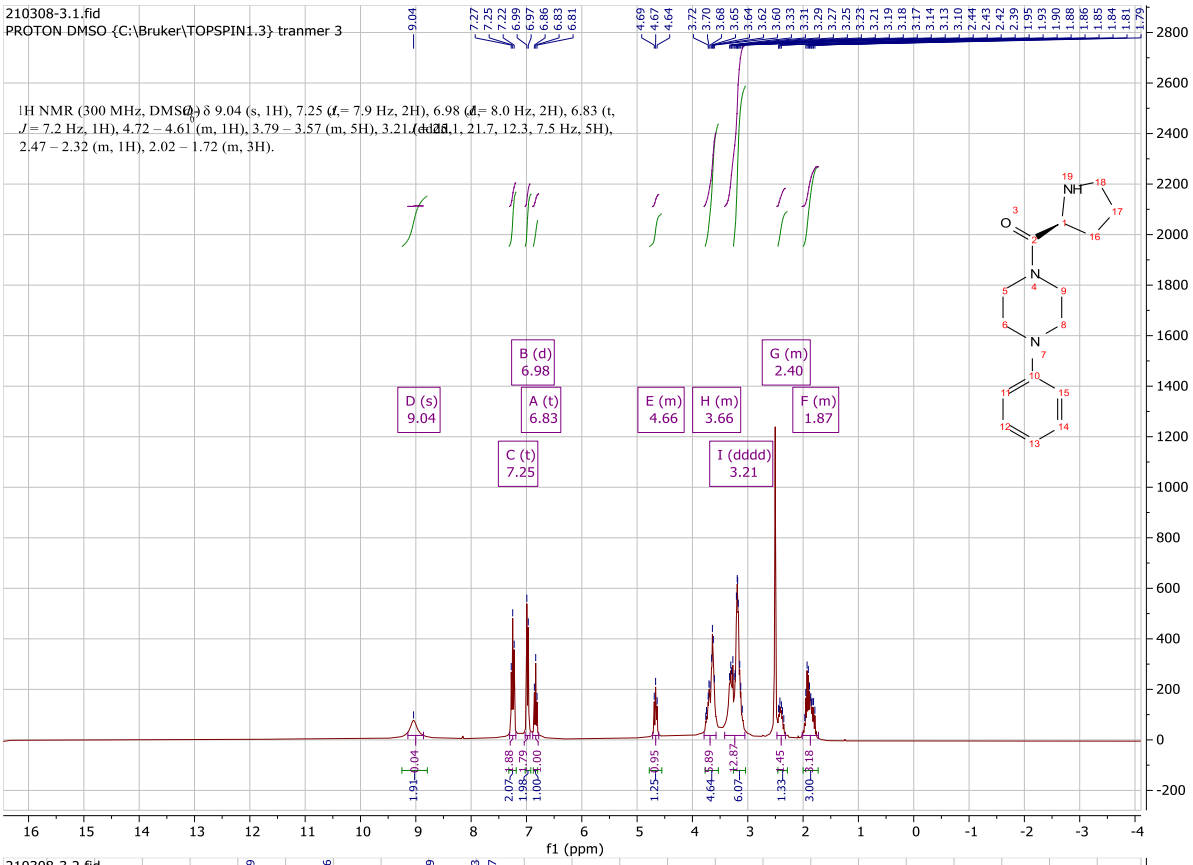
210308-3.1.fid
PROTON DMSO {C:\Bruker\TOPSPIN1.3} tranmer 3
1H NMR (300 MHz, DMSO-d6) δ 9.04 (s, 1H), 7.25 (t, J = 7.9 Hz, 2H), 6.98 (d, J = 8.0 Hz, 2H), 6.83 (t, J = 7.2 Hz, 1H), 4.72 – 4.61 (m, 1H), 3.79 – 3.57 (m, 5H), 3.21 (dddd, J = 28.1, 21.7, 12.3, 7.5 Hz, 5H), 2.47 – 2.32 (m, 1H), 2.02 – 1.72 (m, 3H).
D (s) 9.04
B (d) 6.98
A (t) 6.83
C (t) 7.25
E (m) 4.66
H (m) 3.66
I (dddd) 3.21
G (m) 2.40
F (m) 1.87
f1 (ppm)

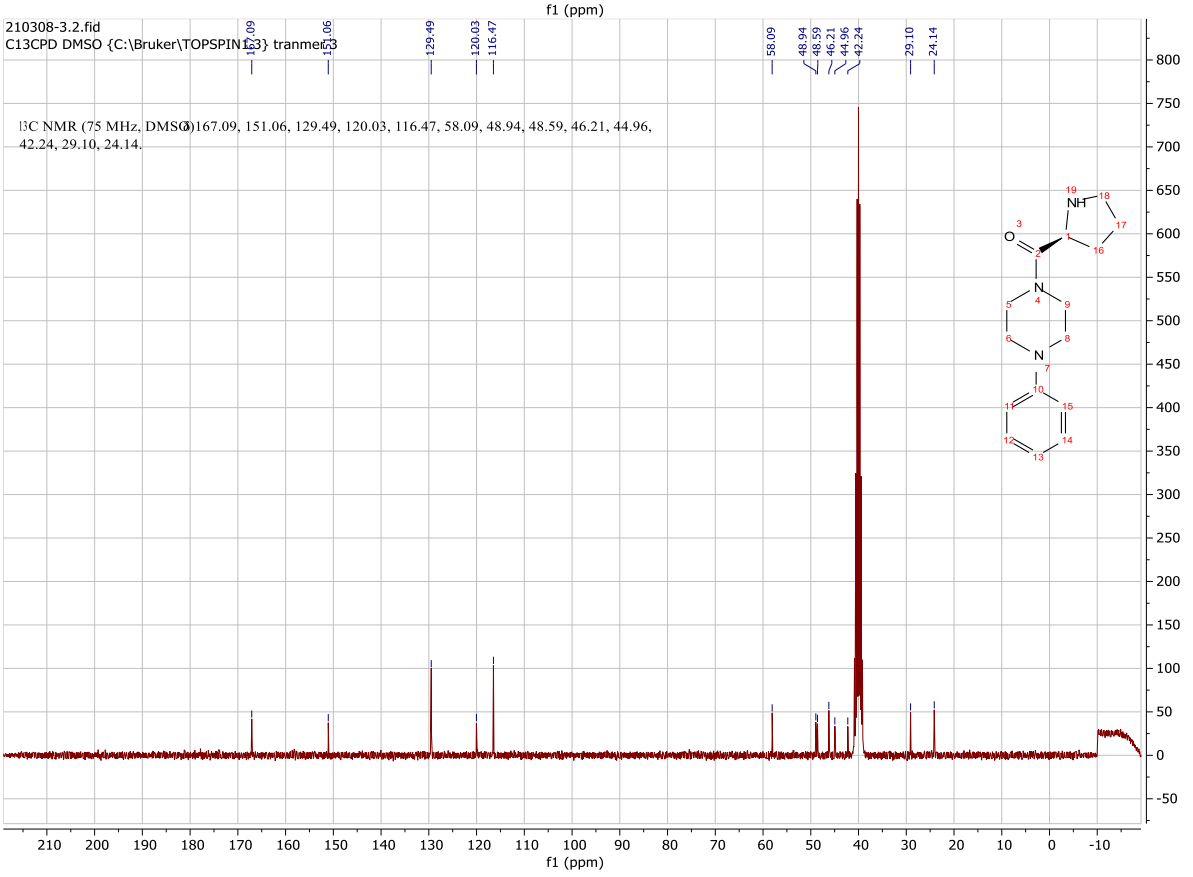
210308-3.2.fid
C13CPD DMSO {C:\Bruker\TOPSPIN1.3} tranmer 3
13C NMR (75 MHz, DMSO-d6) 167.09, 151.06, 129.49, 120.03, 116.47, 58.09, 48.94, 48.59, 46.21, 44.96, 42.24, 29.10, 24.14.
f1 (ppm)

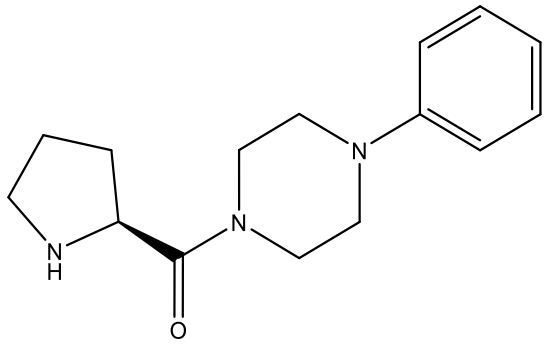

(*S*)-1-phenyl-4-prolylpiperazine (f19)

215.5mg (1mmol) (*tert*-butoxycarbonyl)-*L*-proline was reacted with 162.5mg (1mmol) 1-phenylpiperazine according to the **Synthesis Method d** and the crude produce was deprotected according to the **Synthesis Method f** to give 213.4mg **f19** (Yield: 83%) as yellowish white solid. ^{1}H NMR (300 MHz, DMSO-d_6) δ 9.04 (s, 1H), 7.25 (t, J = 7.9 Hz, 2H), 6.98 (d, J = 8.0 Hz, 2H), 6.83 (t, J = 7.2 Hz, 1H), 4.72 – 4.61 (m, 1H), 3.79 – 3.57 (m, 5H), 3.21 (m, 5H), 2.47 – 2.32 (m, 1H), 2.02 – 1.72 (m, 3H). ^{13}C NMR (75 MHz, DMSO) δ 167.1, 151.1, 129.5, 120.0, 116.5, 58.1, 48.9, 48.6, 46.2, 45.0, 42.2, 29.1, 24.1.

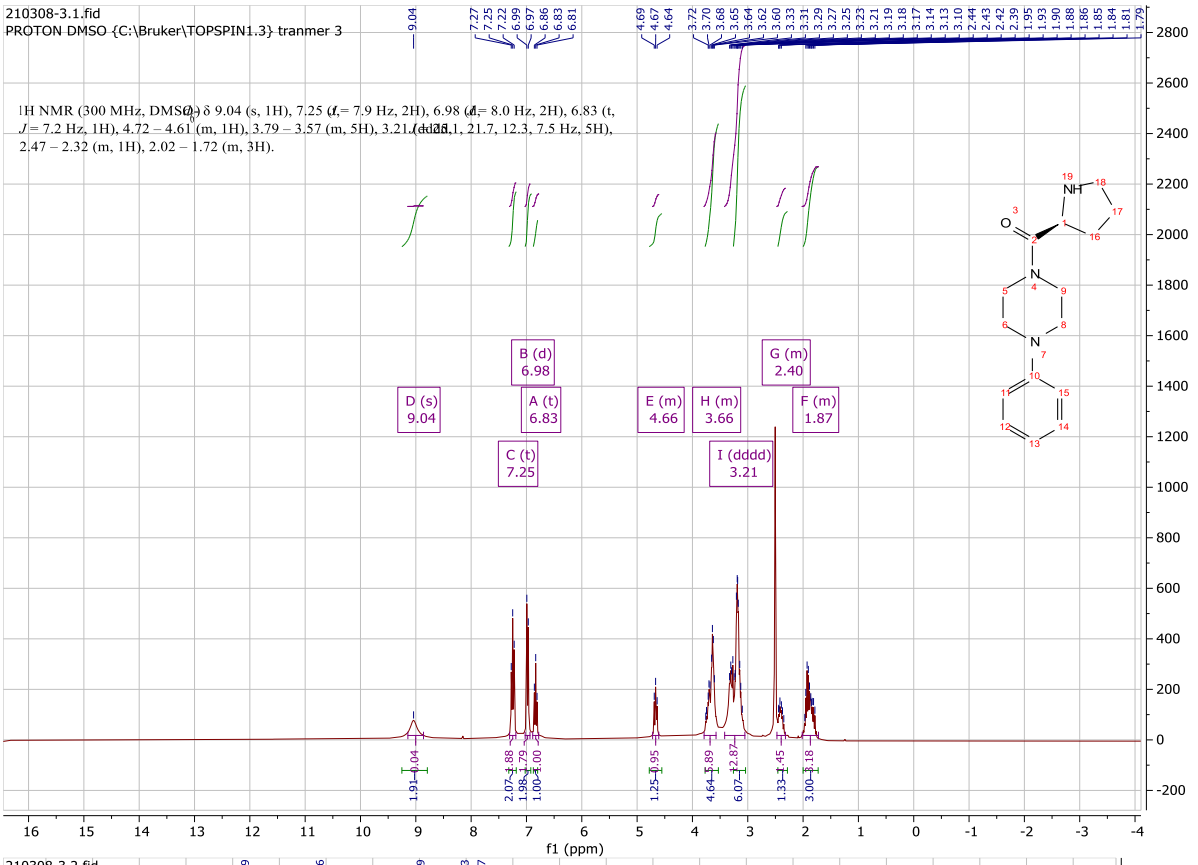
210308-3.1.fid
PROTON DMSO {C:\Bruker\TOPSPIN1.3} tranmer 3
1H NMR (300 MHz, DMSO-d6) δ 9.04 (s, 1H), 7.25 (t, J = 7.9 Hz, 2H), 6.98 (d, J = 8.0 Hz, 2H), 6.83 (t, J = 7.2 Hz, 1H), 4.72 – 4.61 (m, 1H), 3.79 – 3.57 (m, 5H), 3.21 (dddd, J = 28.1, 21.7, 12.3, 7.5 Hz, 5H), 2.47 – 2.32 (m, 1H), 2.02 – 1.72 (m, 3H).
B (d) 6.98
G (m) 2.40
D (s) 9.04
A (t) 6.83
E (m) 4.66
H (m) 3.66
F (m) 1.87
C (t) 7.25
I (dddd) 3.21
f1 (ppm)

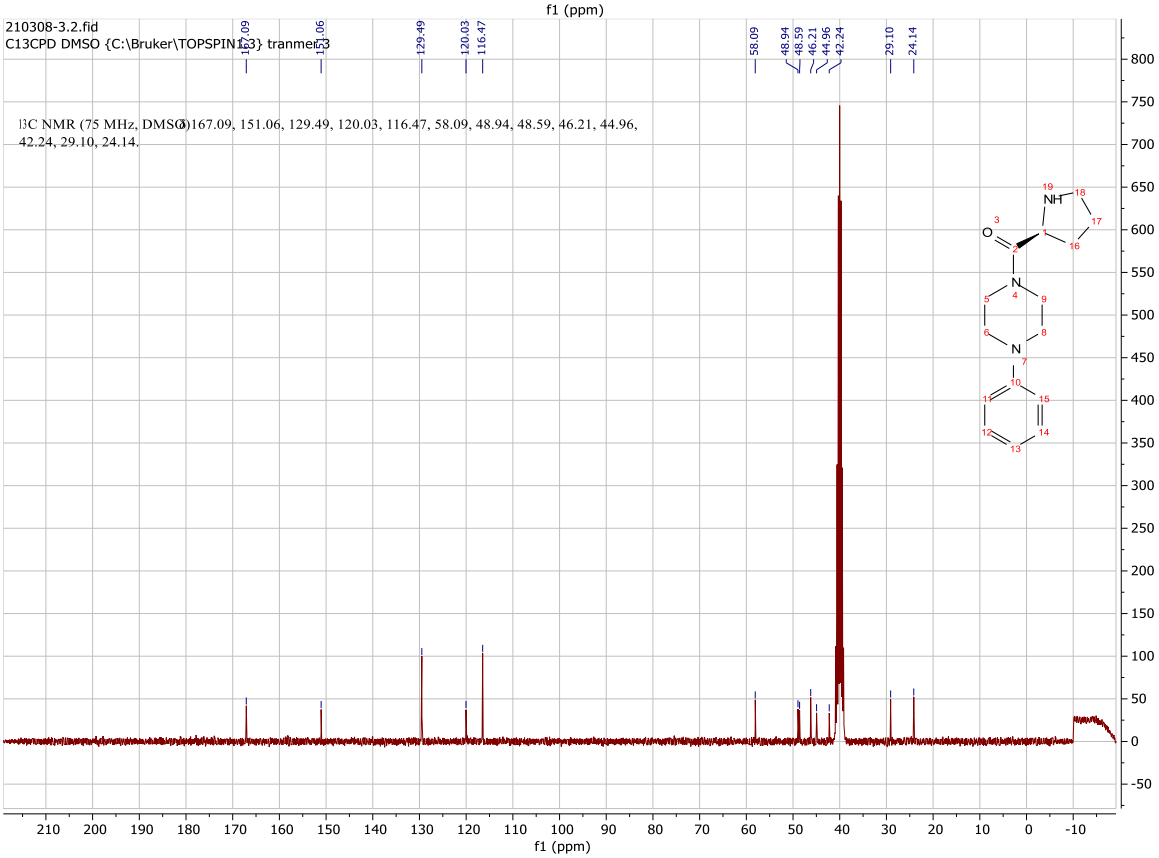
210308-3.2.fid
C13CPD DMSO {C:\Bruker\TOPSPIN1.3} tranmer 3
13C NMR (75 MHz, DMSO) δ 167.09, 151.06, 129.49, 120.03, 116.47, 58.09, 48.94, 48.59, 46.21, 44.96, 42.24, 29.10, 24.14.
f1 (ppm)

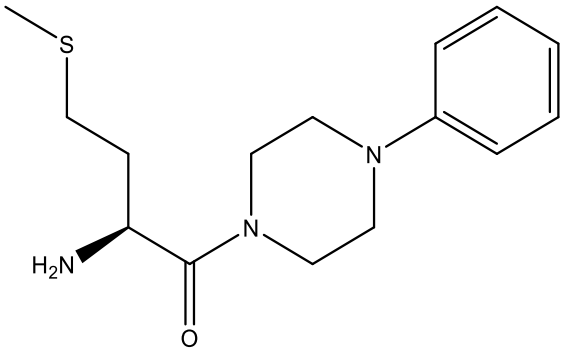

(*S*)-2-amino-4-(methylthio)-1-(4-phenylpiperazin-1-yl)butan-1-one (f20)

249.5mg (1mmol) (*tert*-butoxycarbonyl)-*L*-methionine was reacted with 162.5mg (1mmol) 1-phenylpiperazine according to the **Synthesis Method d** and the crude produce was deprotected according to the **Synthesis Method f** to give 269.7mg **f20** (Yield: 92%) as yellowish white solid. ^{1}H NMR (300 MHz, DMSO-d_6) δ 8.26 (s, 2H), 7.25 (t, *J* = 7.9 Hz, 2H), 6.98 (d, *J* = 7.9 Hz, 2H), 6.83 (t, *J* = 7.2 Hz, 1H), 4.50 (dd, *J* = 6.0, 5.8 Hz, 1H), 3.65 (m, 4H), 3.28 – 3.04 (m, 5H), 2.71 – 2.52 (m, 2H), 2.07 (s, 3H), 1.97 (m, 2H). ^{13}C NMR (75 MHz, DMSO) δ 167.3, 151.0, 129.5, 120.0, 116.4, 49.3, 49.1, 48.6, 45.1, 42.1, 30.7, 28.6, 14.9.

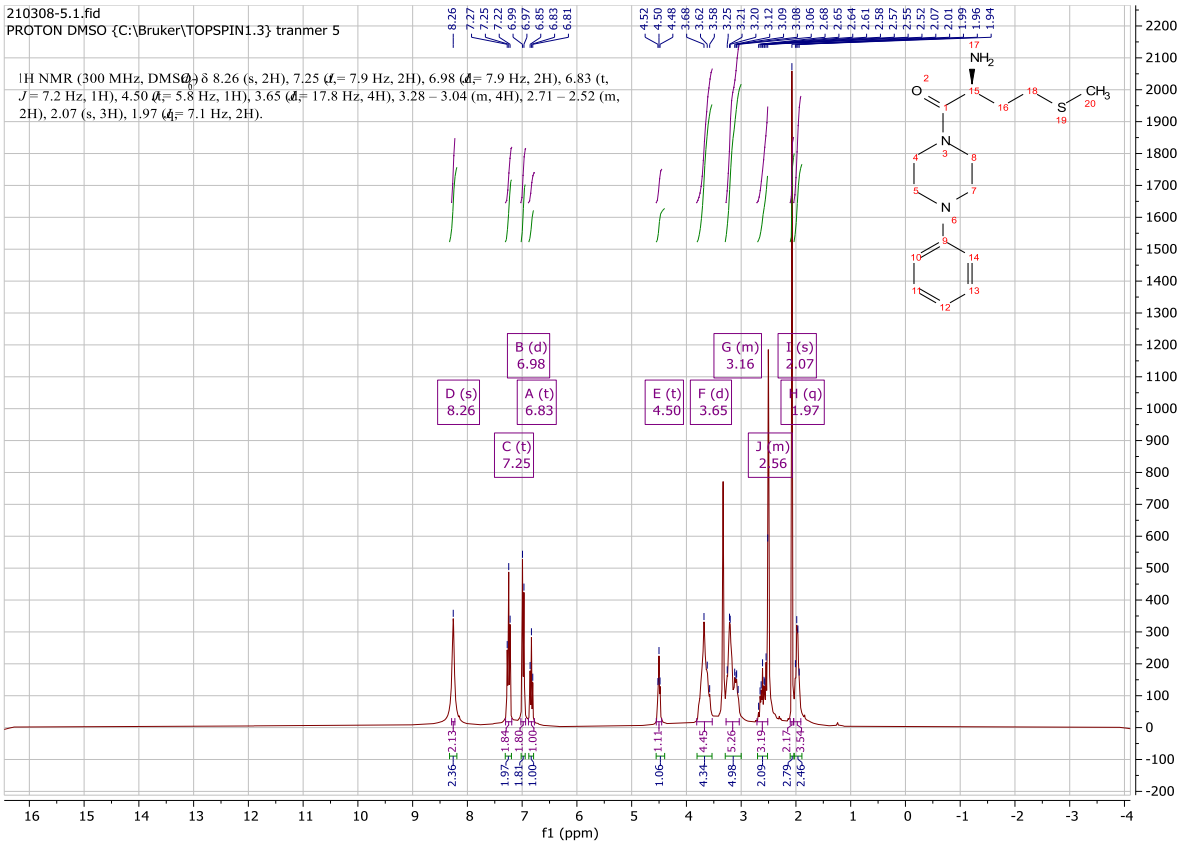
210308-5.1.fid
PROTON DMSO {C:\Bruker\TOPSPIN1.3} tranmer 5
1H NMR (300 MHz, DMSO) δ 8.26 (s, 2H), 7.25 (t, J = 7.9 Hz, 2H), 6.98 (d, J = 7.9 Hz, 2H), 6.83 (t, J = 7.2 Hz, 1H), 4.50 (t, J = 5.8 Hz, 1H), 3.65 (d, J = 17.8 Hz, 4H), 3.28 – 3.04 (m, 4H), 2.71 – 2.52 (m, 2H), 2.07 (s, 3H), 1.97 (q, J = 7.1 Hz, 2H).
B (d) 6.98
G (m) 3.16
I (s) 2.07
D (s) 8.26
A (t) 6.83
E (t) 4.50
F (d) 3.65
H (q) 1.97
C (t) 7.25
J (m) 2.56
f1 (ppm)

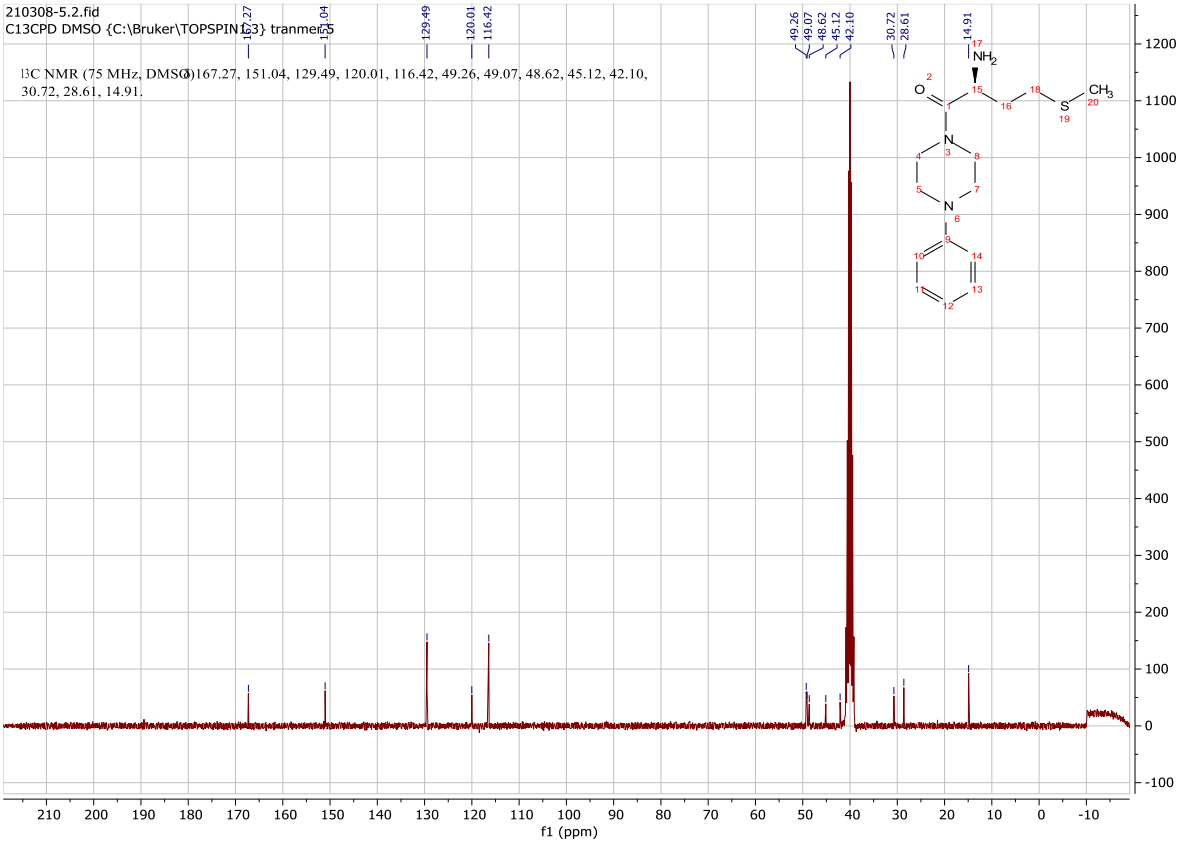
210308-5.2.fid
C13CPD DMSO {C:\Bruker\TOPSPIN1.3} tranmer 5
13C NMR (75 MHz, DMSO) 167.27, 151.04, 129.49, 120.01, 116.42, 49.26, 49.07, 48.62, 45.12, 42.10, 30.72, 28.61, 14.91.
f1 (ppm)

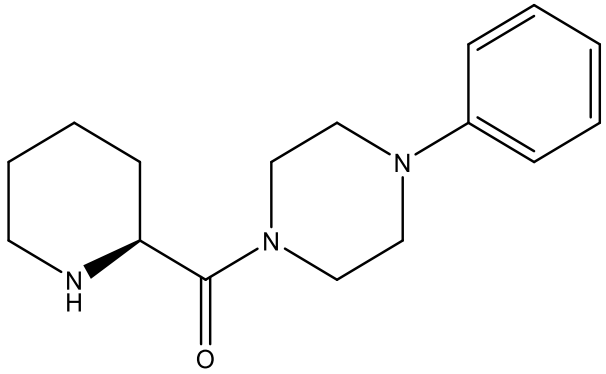

(*S*)-(4-phenylpiperazin-1-yl)(piperidin-2-yl)methanone (f21)

229.5mg (1mmol) (S)-1-(tert-butoxycarbonyl)piperidine-2-carboxylic acid was reacted with 162.5mg (1mmol) 1-phenylpiperazine according to the **Synthesis Method d** and the crude produce was deprotected according to the **Synthesis Method f** to give 242.9mg **f21** (Yield: 89%) as yellowish white solid. ^{1}H NMR (300 MHz, Chloroform-*d*) δ 9.58 (d, *J* = 240.5 Hz, 1H), 7.36 – 7.28 (m, 2H), 6.93 (dd, *J* = 8.0, 5.5 Hz, 3H), 3.71 (dq, *J* = 29.8, 8.7, 6.9 Hz, 4H), 3.39 – 2.97 (m, 8H), 2.14 – 1.67 (m, 5H). ^{13}C NMR (75 MHz, $CDCl_3$) δ 170.6, 150.7, 129.3, 120.8, 116.8, 49.9, 49.4, 45.9, 45.6, 43.8, 41.8, 34.8, 25.8, 21.0.

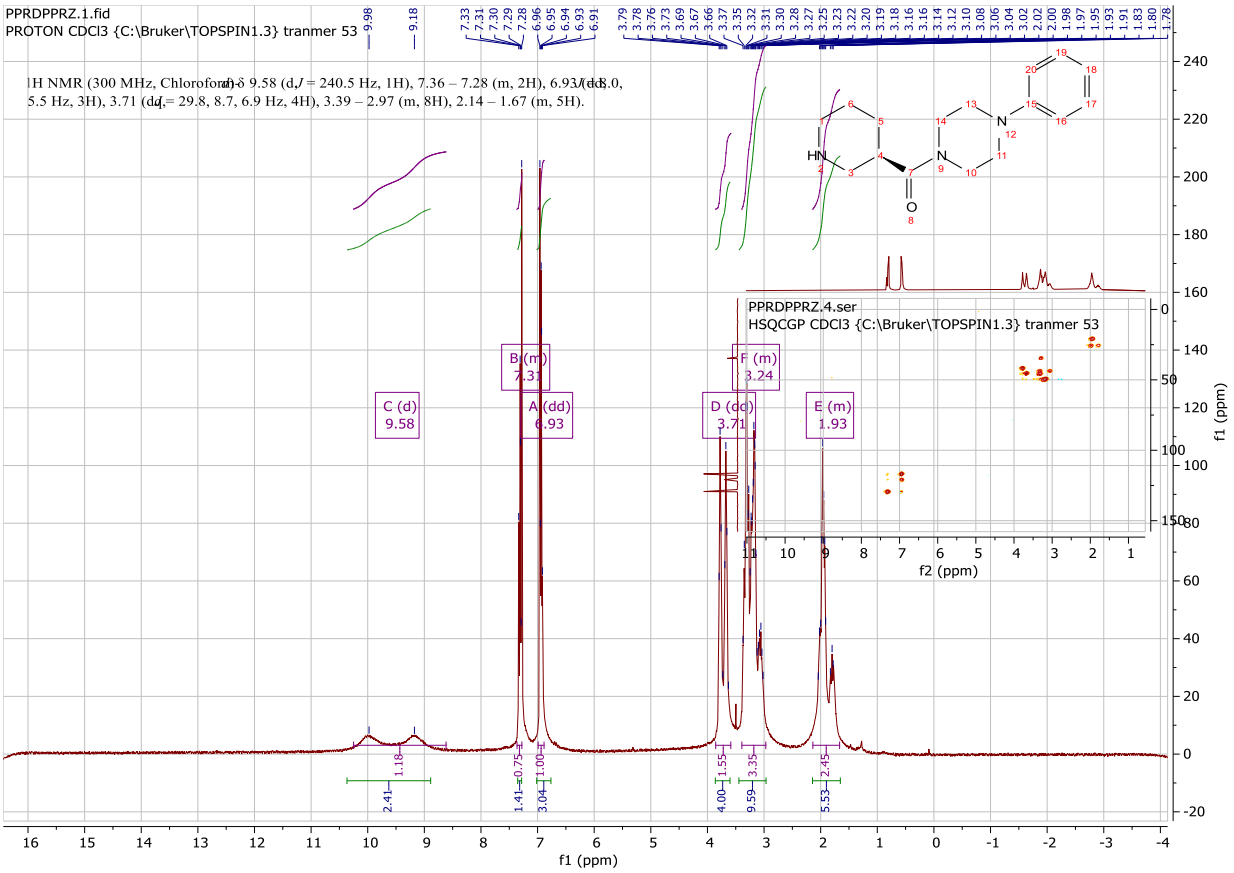

^{1}H NMR (300 MHz, Chloroform-d) δ 9.58 (d, J = 240.5 Hz, 1H), 7.36 – 7.28 (m, 2H), 6.93 (dd, J = 8.0, 5.5 Hz, 3H), 3.71 (dd, J = 29.8, 8.7, 6.9 Hz, 4H), 3.39 – 2.97 (m, 8H), 2.14 – 1.67 (m, 5H).

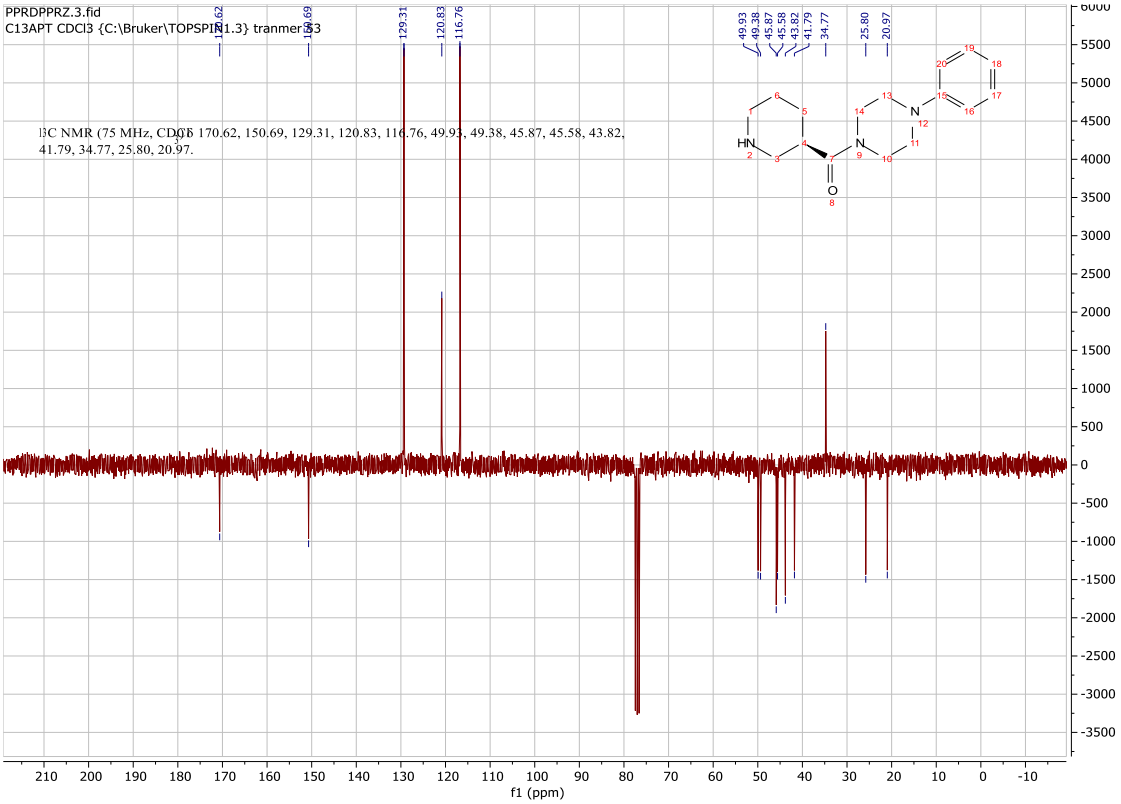

^{13}C NMR (75 MHz, CDCl$_3$) δ 170.62, 150.69, 129.31, 120.83, 116.76, 49.93, 49.38, 45.87, 45.58, 43.82, 41.79, 34.77, 25.80, 20.97.

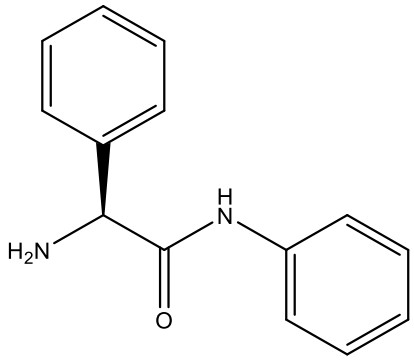

(*S*)-2-amino-N,2-diphenylacetamide (f22)

251.5mg (1mmol) (*S*)-2-((*tert*-butoxycarbonyl)amino)-2-phenylacetic acid was reacted with 93mg (1mmol) aniline according to the **Synthesis Method d** and the crude produce was deprotected according to the **Synthesis Method** f to give 200.2 **f22** (Yield: 89%) as yellowish white solid. ^{1}H NMR (300 MHz, Methanol-d_4) δ 7.63 – 7.45 (m, 9H), 7.30 (t, 2H), 7.12 (t, 1H), 5.07 (s, 1H), 3.35 (s, 1H). ^{13}C NMR (75 MHz, MeOD) δ 153.7, 137.7, 133.0, 129.8, 129.2, 128.6, 127.9, 124.5, 119.8, 57.1.

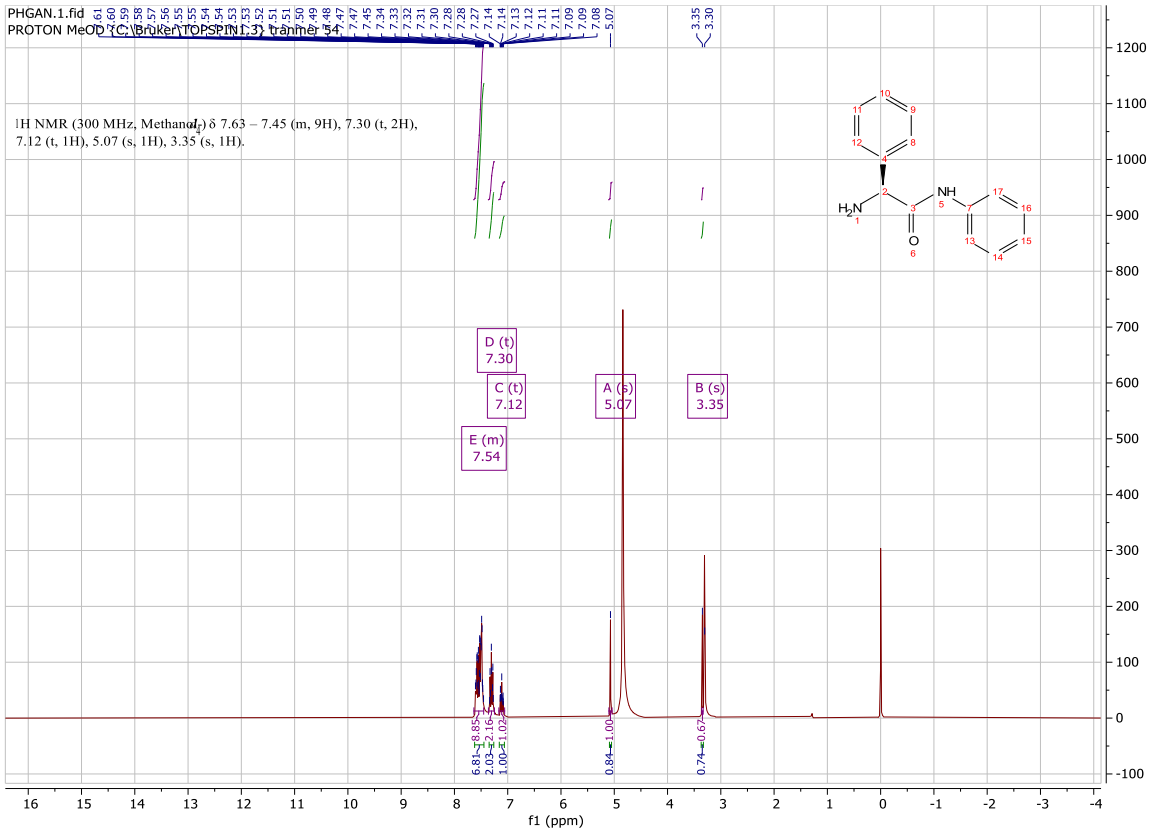
PHGAN.1.fid
PROTON MeOD {C:\Bruker\TOPSPIN1.3} tranmer 54
1H NMR (300 MHz, Methanol-d4) δ 7.63 – 7.45 (m, 9H), 7.30 (t, 2H), 7.12 (t, 1H), 5.07 (s, 1H), 3.35 (s, 1H).
D (t) 7.30
C (t) 7.12
A (s) 5.07
B (s) 3.35
E (m) 7.54
f1 (ppm)

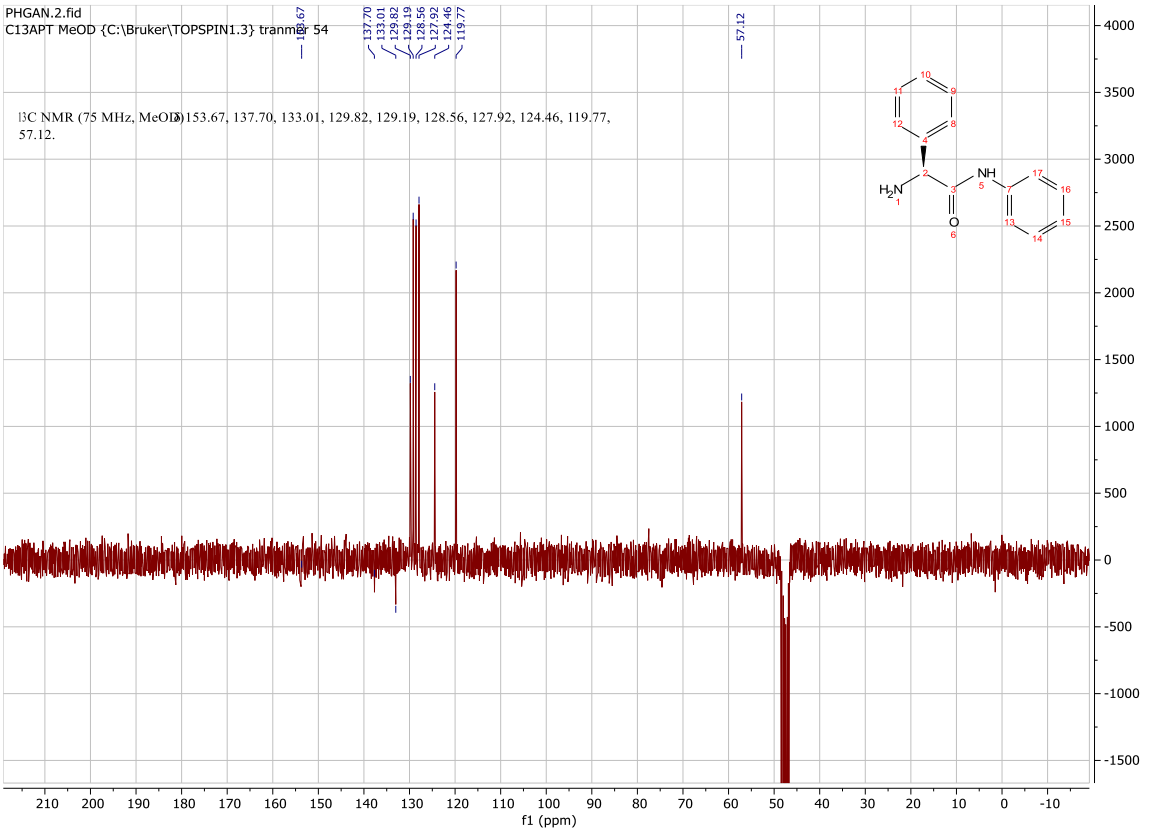
PHGAN.2.fid
C13APT MeOD {C:\Bruker\TOPSPIN1.3} tranmer 54
13C NMR (75 MHz, MeOD) δ 153.67, 137.70, 133.01, 129.82, 129.19, 128.56, 127.92, 124.46, 119.77, 57.12.
f1 (ppm)

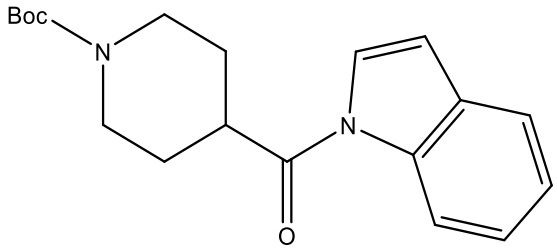

***tert*-butyl 4-(1*H*-indole-1-carbonyl)piperidine-1-carboxylate (f23)**

229.5mg (1mmol) *N*-Boc-isonipecotic acid was reacted with 117mg (1mmol) 1*H*-indole according to the **Synthesis Method d** to give 12.2mg **f23** (Yield 4%) as white solid. ^{1}H NMR (400 MHz, Chloroform-*d*) δ 8.50 (dd, *J* = 8.2, 1.1 Hz, 1H), 7.60 (ddd, *J* = 7.7, 1.4, 0.8 Hz, 1H), 7.51 (d, *J* = 3.8 Hz, 1H), 7.39 (ddd, *J* = 8.4, 7.2, 1.3 Hz, 1H), 7.31 (td, *J* = 7.5, 1.1 Hz, 1H), 6.70 (dd, *J* = 3.8, 0.8 Hz, 1H), 4.24 (s, 2H), 3.19 (tt, *J* = 9.9, 4.3 Hz, 1H), 2.96 (t, *J* = 13.2 Hz, 2H), 2.03 – 1.84 (m, 4H), 1.50 (s, 9H), . ^{13}C NMR (101 MHz, $CDCl_3$) δ 173.2, 154.7, 135.7, 130.4, 125.4, 124.1, 123.9, 120.8, 116.8, 109.5, 79.9, 43.5, 41.7, 28.6, 28.5. HRMS m/z (ESI+, M+Na): Calcd for C19H24N2O3: 514.64, (ESI+, M+H) found: 537.19

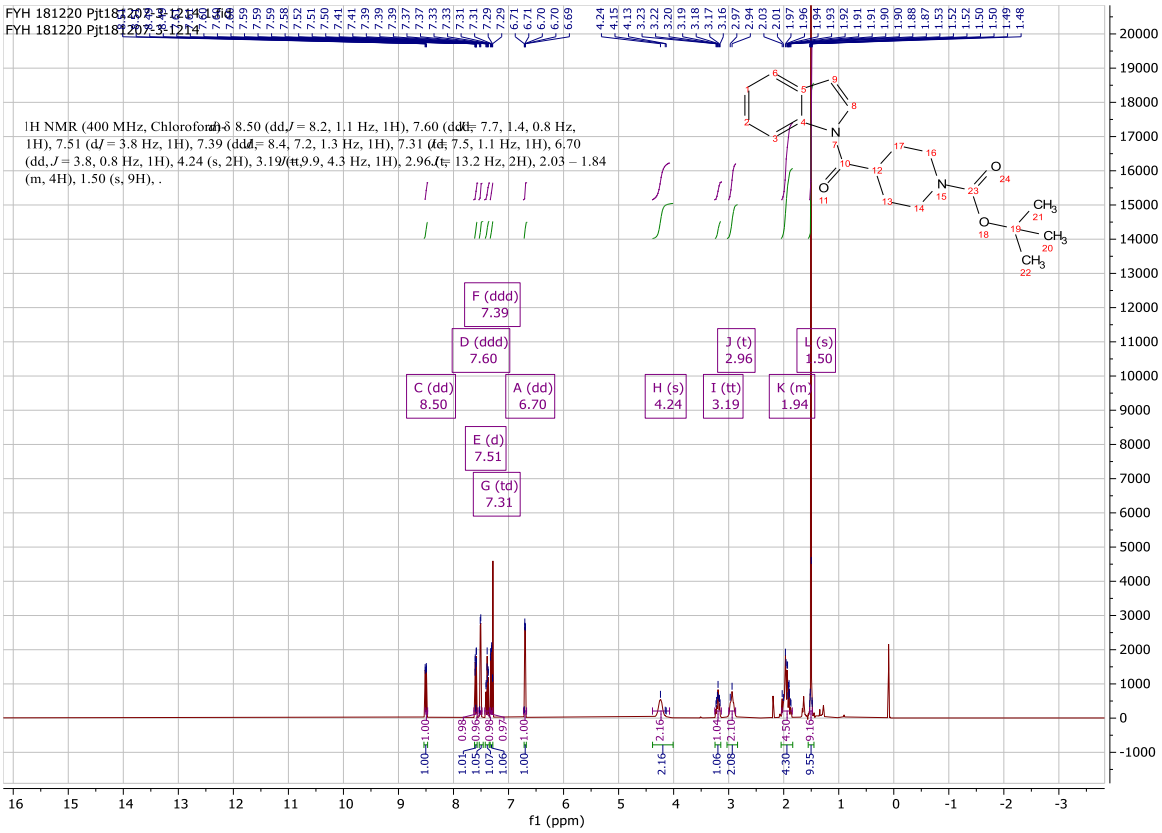
FYH 181220 Pjt181207-3-1214.fid
FYH 181220 Pjt181207-3-1214
1H NMR (400 MHz, Chloroform-d) δ 8.50 (dd, J = 8.2, 1.1 Hz, 1H), 7.60 (ddd, J = 7.7, 1.4, 0.8 Hz, 1H), 7.51 (d, J = 3.8 Hz, 1H), 7.39 (ddd, J = 8.4, 7.2, 1.3 Hz, 1H), 7.31 (td, J = 7.5, 1.1 Hz, 1H), 6.70 (dd, J = 3.8, 0.8 Hz, 1H), 4.24 (s, 2H), 3.19 (tt, J = 9.9, 4.3 Hz, 1H), 2.96 (t, J = 13.2 Hz, 2H), 2.03 – 1.84 (m, 4H), 1.50 (s, 9H), .
F (ddd) 7.39
D (ddd) 7.60
C (dd) 8.50
A (dd) 6.70
E (d) 7.51
G (td) 7.31
J (t) 2.96
L (s) 1.50
H (s) 4.24
I (tt) 3.19
K (m) 1.94
f1 (ppm)

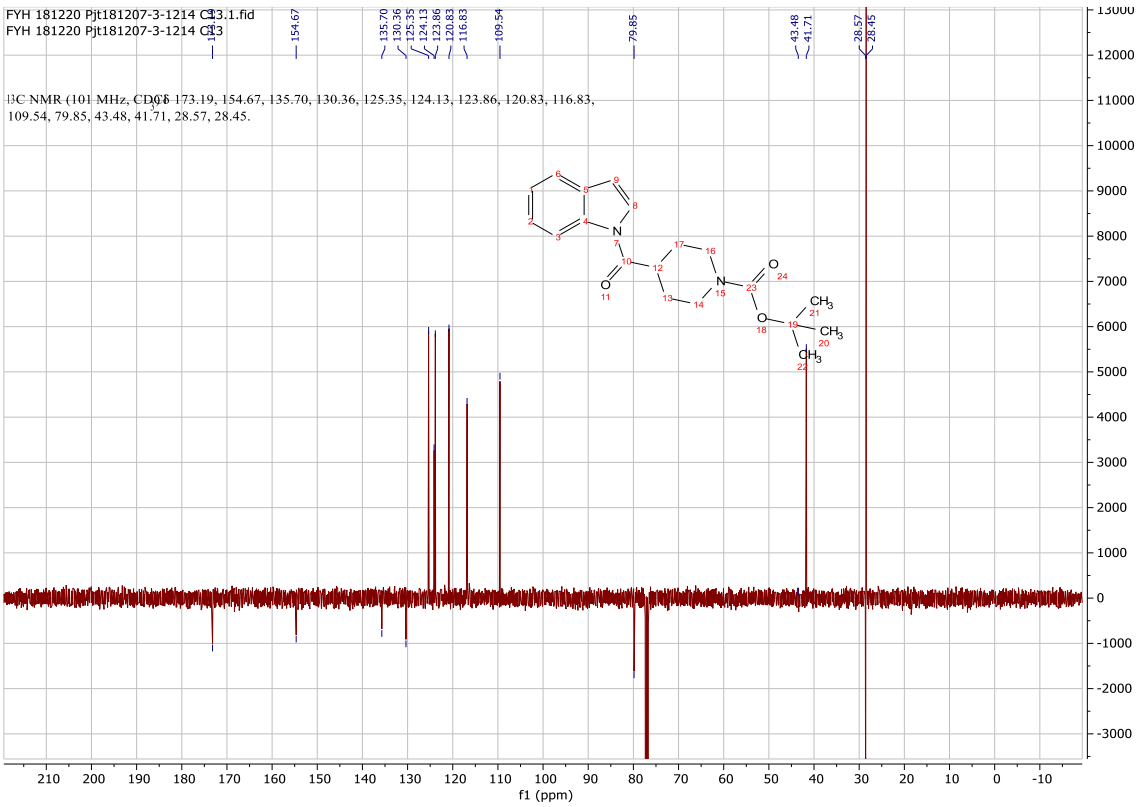
FYH 181220 Pjt181207-3-1214 C13.1.fid
FYH 181220 Pjt181207-3-1214 C13
13C NMR (101 MHz, CDCl3) δ 173.19, 154.67, 135.70, 130.36, 125.35, 124.13, 123.86, 120.83, 116.83, 109.54, 79.85, 43.48, 41.71, 28.57, 28.45.
f1 (ppm)

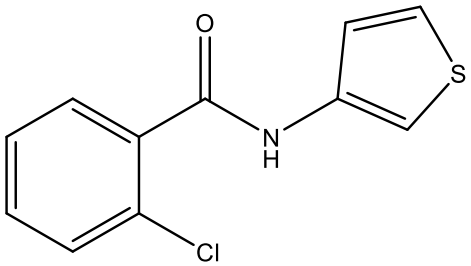

2-chloro-*N*-(thiophen-3-yl)benzamide (f24)

192mg (1.2mmol) 2-chlorobenzoyl chloride was reacted with 136mg (1mmol) thiophen-3-amine according to **Synthesis Method a** to give 213.3mg **f24** (Yield: 90%) ^{1}H NMR (300 MHz, DMSO-d_6) δ 10.80 (s, 1H), 7.72 – 7.64 (m, 1H), 7.61 – 7.39 (m, 5H), 7.21 – 7.13 (m, 1H). ^{13}C NMR (75 MHz, DMSO) δ 164.4, 137.0, 137.0, 131.6, 130.5, 130.2, 129.5, 127.7, 125.3, 122.1, 120.0. HRMS m/z (ESI+, M+Na): Calcd for C19H24N2O3: 237.70, (ESI+, M+H) found: 238.60

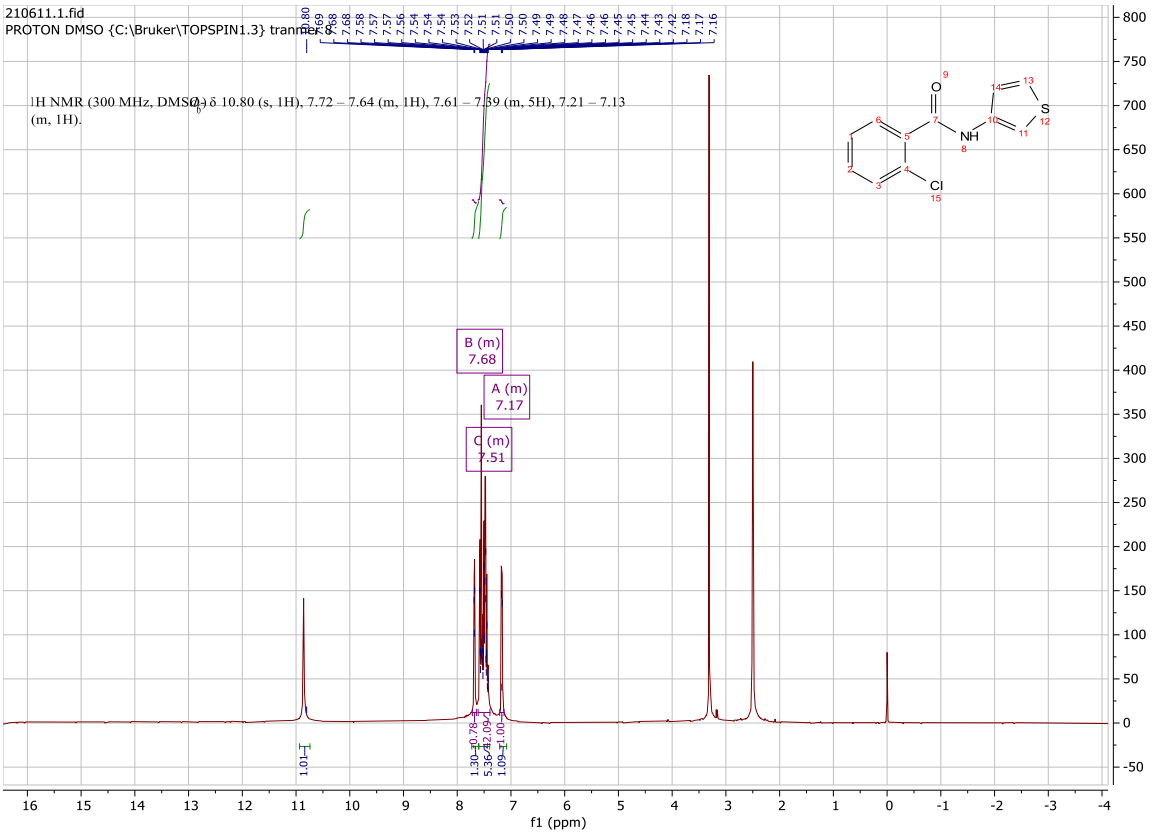
210611.1.fid
PROTON DMSO {C:\Bruker\TOPSPIN1.3} tranmer 8
1H NMR (300 MHz, DMSO-d6) δ 10.80 (s, 1H), 7.72 – 7.64 (m, 1H), 7.61 – 7.39 (m, 5H), 7.21 – 7.13 (m, 1H).
B (m) 7.68
A (m) 7.17
C (m) 7.51
f1 (ppm)

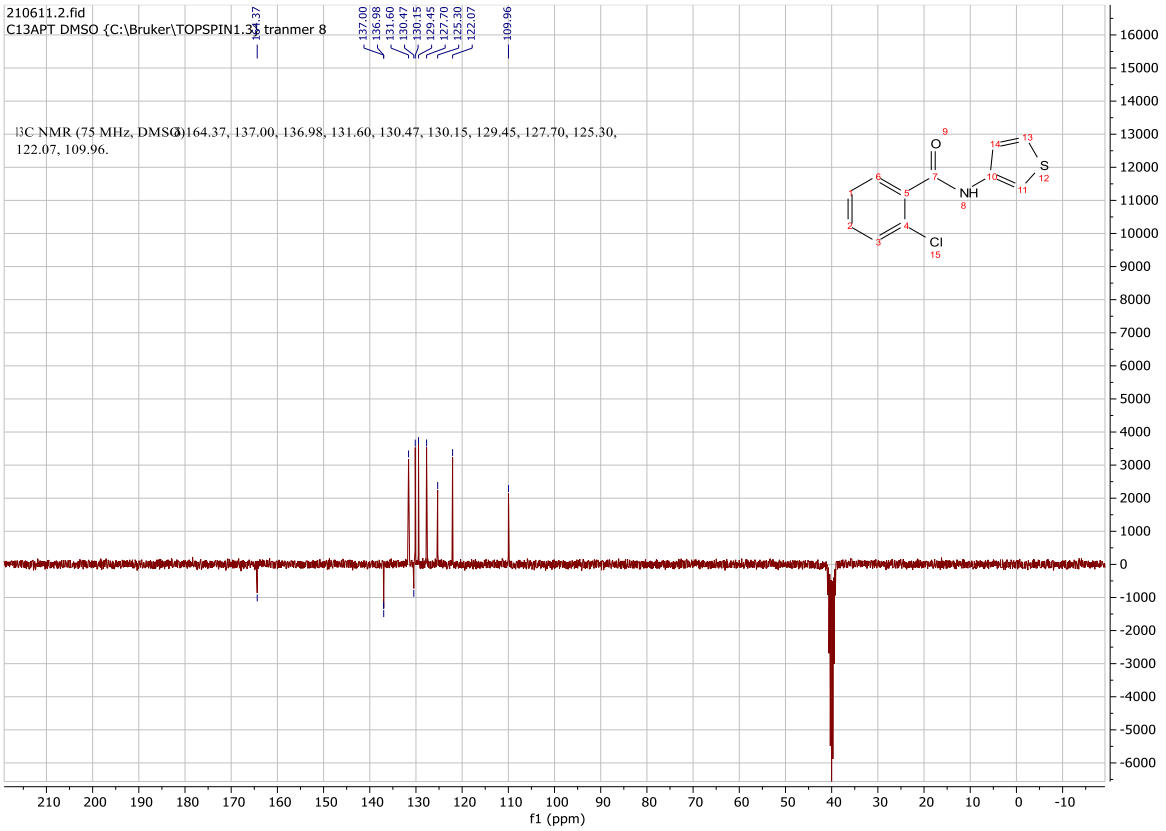
210611.2.fid
C13APT DMSO {C:\Bruker\TOPSPIN1.3} tranmer 8
13C NMR (75 MHz, DMSO-d6) 164.37, 137.00, 136.98, 131.60, 130.47, 130.15, 129.45, 127.70, 125.30, 122.07, 109.96.
f1 (ppm)